

ASTM INTERNATIONAL
Helping our world work better

Supplement to Corrosion Tests and Standards: Application and Interpretation: Second Edition

Edward L. Hibner,
Harvey P. Hack, and
John R. Scully, Editors



Edward L. Hibner, Harvey P. Hack, and John R. Scully, Editors

Supplement to Corrosion Tests and Standards: Application and Interpretation: Second Edition

ASTM Stock Number: MNL20-2ND-SUP

ASTM International
100 Barr Harbor Drive
PO Box C700
West Conshohocken, PA 19428-2959

Printed in the U.S.A.

Library of Congress Cataloging-in-Publication Data

Names: Hibner, Edward L., editor. | Hack, Harvey P., editor. | Scully, John R., 1958- editor.
Title: Supplement to corrosion tests and standards : application and interpretation / Edward L. Hibner, Harvey P. Hack, John R. Scully, editors.
Other titles: Corrosion tests and standards.
Description: Second edition. | West Conshohocken, PA : ASTM International, 2021. | "ASTM Stock Number: MNL 20-2ND-SUP." | Summary: "There is a variety of accelerated exposure tests that have been developed to aid engineers in material selection for corrosion resistance. ASTM tests are probably the most widely used tests for localized corrosion resistance. Thus, an understanding of them can be of great importance in analyzing the results of testing performed in other labs or by manufacturers"– Provided by publisher.
Identifiers: LCCN 2021025326 (print) | LCCN 2021025327 (ebook) | ISBN 9780803171343 (paperback) | ISBN 9780803171350 (ebook)
Subjects: LCSH: Corrosion and anti-corrosives–Testing.
Classification: LCC TA462 .C666 2021 Suppl. (print) | LCC TA462 (ebook) | DDC 620.1/1223–dc23
LC record available at https://lccn.loc.gov/2021025326
LC ebook record available at https://lccn.loc.gov/2021025327

Copyright © 2022 ASTM International, West Conshohocken, PA. All rights reserved. This material may not be reproduced or copied, in whole or in part, in any printed, mechanical, electronic, film, or other distribution and storage media, without the written consent of the publisher.

Photocopy Rights
Authorization to photocopy items for internal, personal, or educational classroom use, or the internal, personal, or educational classroom use of specific clients, is granted by ASTM International provided that the appropriate fee is paid to the Copyright Clearance Center, 222 Rosewood Drive, Danvers, MA 01923, Tel: (978) 646-2600; http://www.copyright.com/

Publisher:
ASTM International
100 Barr Harbor Drive
PO Box C700
West Conshohocken, PA 19428-2959
Phone: (610) 832-9585 Fax: (610) 832-9555

ISBN 978-0-8031-7134-3
ISBN-EB: 978-0-8031-7135-0

ASTM Stock Number: MNL20-2ND-SUP
DOI: 10.1520/MNL20-2ND-SUP-EB

ASTM International is not responsible, as a body, for the statements and opinions advanced in the publication. ASTM International does not endorse any products represented in this publication.

Printed in Hanover, PA
October, 2022

Foreword

THIS PUBLICATION, *Supplement to Corrosion Tests and Standards: Application and Interpretation: Second Edition*, was sponsored by ASTM Committee G01 on Corrosion of Metals and edited by Edward L. Hibner, Special Metals Corporation, Harvey P. Hack, Northrup Grumman Corporation, and John R. Scully, University of Virginia. This publication is a supplement to MNL20-2ND of ASTM's manual series.

Contents

Preface		vii
	Types of Corrosion	
1	Pitting Robert G. Kelly, Ryan M. Katona, and Eric J. Schindelholz	1
2	Crevice Corrosion Mariano Iannuzzi, Edgar Hornus, and Mobin Salasi	15
3	Galvanic Harvey P. Hack, Carol Glover, and Jason Lee	41
4	Hydrogen Damage Kevin Nibur and Brian Somerday	59
5	Microbiological Effects Jason S. Lee and Brenda J. Little	73
6	Tribocorrosion Jeremy L. Gilbert	81
	Analysis, Testing, and Environments	
7	Metallographic Analysis William L. Mankins	93
8	Electrochemical Tests John R. Scully, Carol F. Glover, and Raymond J. Santucci	109
9	Immersion Testing Bradley D. Krantz	141
10	Atmospheric Sheldon W. Dean, Jr.	153
11	Standards and Practices on Corrosion under Insulation John P. Ludman and Bert J. Moniz	169
12	Freshwater Walter T. Young	179
13	Seawater David A. Shifler	187

14 Soils 217
Mike Horton, Lucien Veleva, and Edward Escalante

15 Petroleum Chemistry 241
K. Daniel Efird

16 Organic Liquids 251
C. Sean Brossia

Materials and Applications

17 Titanium 265
Ronald W. Schutz

18 Corrosion Testing of Nonmetallic Coatings 283
William L. Mankins

19 Metal-Matrix Composites 291
L. H. Hihara

20 Water Handling Systems 315
Walter Young

21 Pipeline 325
Abdelmounam M. El-Sherik

22 Highways, Tunnels, and Bridges 345
Stephen R. Sharp and Jason T. Provines

23 Automotive 359
Niamh Hosking

24 Commercial Aircraft 385
Edward L. Colvin

25 Military Aircraft and Associated Equipment 393
Diane Buhrmaster and Nicholas Wilson

26 Industrial Chemicals: Manufacture and Usage 399
Sheldon W. Dean, Jr.

27 Flue Gas Desulfurization 409
James R. Crum and Ralph W. Ross

28 Nuclear Power 419
Barry M. Gordon and George J. Licina

29 Food and Beverage 429
Dipak Negandhi

Index 435

Preface

Corrosion continues to be a problem of worldwide importance, costing roughly 3% of the gross domestic product of any country for which data is available. This supplement has been prepared to address updates to the technology that addresses this form of degradation. Corrosion is often neglected but it not only seriously impacts our economy, but also jeopardizes human health and safety, wastes valuable resources, and impedes technological progress. The most important factors in addressing corrosion and its control are: (1) recognizing and understanding the mechanisms, (2) developing solutions to the problems, and (3) implementing those solutions. Corrosion tests and standards are very significant in addressing each of these factors. Therefore, this manual includes guidelines for recognizing types of corrosion as well as fundamentals of testing and provides the tools required for making calculations, interpretations, and correlations. It serves as a sourcebook of procedures, equipment, and standards used in testing.

The editor and section editors have coordinated this update so that the most recent technologies are included in each section. In some cases, the original authors of chapters have made the revisions. In other cases, new authors have been chosen, or the editors performed that task. In still other cases, the technology described in the chapters has not changed sufficiently since the last edition for those chapters to need updating, in which cases those chapters have not been included in this supplement. Users of the manual will find that chapters in this supplement plus those not revised from the previous edition are an invaluable and instructive tool, as well as a sourcebook on how to conduct corrosion tests, interpret results, and use standards.

The supplement to the manual is the result of a massive effort of planning, writing, reviewing, editing, production, and marketing. It would not have been possible without the outstanding efforts of the ASTM staff and the valuable and competent work of the editors and more than four hundred experts in the field that donated their time as authors and reviewers. They represent industrial, educational, industrial, and government organizations, and their contributions are greatly appreciated.

Edward L. Hibner

Types of Corrosion

Chapter 1 | Pitting

Robert G. Kelly,[1] Ryan M. Katona,[1,2] and Eric J. Schindelholz[3]

Introduction

Pitting corrosion occurs when discrete areas of a material undergo rapid attack, although the vast majority of the surface remains virtually unaffected. This morphology is in sharp contrast to uniform corrosion in which all parts of the exposed surface recede at approximately the same rate. Essentially, all metals and alloys undergo pitting corrosion under some set of experimental conditions, although the relative susceptibility varies widely. The basic requirement for pitting is the existence of a passive state for the material in the environment of interest. Pitting occurs when portions of the metal surface lose their passivity and dissolve rapidly. This loss of passivity often occurs at heterogeneities in the surface (either physical or chemical). Pitting of a given material depends strongly on the presence of an aggressive species in the environment and a sufficiently oxidizing potential (e.g., Cl^- ion in neutral, aerated aqueous solution for Type 304 stainless steel). Many metal–environment combinations can lead to pitting, as extensively reviewed by Szlarska-Smialowska,[1] Frankel,[2] and more recently by Soltis.[3] Additionally, a new framework has been proposed by Frankel, Li, and Scully.[4] In many situations, pitting can severely limit the performance of the material.

Testing for localized corrosion resistance usually aims at meeting one (or more) of four general goals: (1) alloy ranking for selection or development; (2) failure analysis; (3) determination of the effects of changes in process parameters; and (4) prediction of penetration rates. Of the four, the last is by far the most difficult to accomplish, but it is also the most important in many cases. This chapter discusses the different types of tests that have been developed for pitting corrosion. The physical and chemical basis for each test is described, as are some of the practical applications and limitations. The first section describes coupon exposure testing, and the second section describes electrochemical testing.

[1]Dept. of Materials Science and Engineering, University of Virginia, P.O. Box 400745, 295 McCormick Rd., Charlottesville, VA 22904, USA R. G. K. http://orcid.org/0000-0002-7354-0978, R. M. K. http://orcid.org/0000-0001-9158-4651
[2]Sandia National Laboratories, 1515 Eubank Blvd. SE, Albuquerque, NM 87123, USA http://orcid.org/0000-0002-8809-9230
[3]Dept. of Materials Science and Engineering, The Ohio State University, Columbus, Ohio 43210, USA
The authors acknowledge the previous author of this chapter, Robert G. Kelly, University of Virginia, Charlottesville, VA.

DOI: 10.1520/MNL202NDSUP20190041

Coupon Testing

The exposure of test coupons to corrosive solutions to evaluate localized corrosion resistance has a long and successful history. The materials of interest are typically machined into coupon form before being measured, cleaned, weighed, and exposed to the corrosive medium. After a set period of time, the coupons are removed; the surfaces are carefully cleaned and evaluated for attack. General requirements and information on coupon testing can be found elsewhere in this manual as well as in other sources.[5,6] ASTM G1, *Standard Practice for Preparing, Cleaning, and Evaluating Corrosion Test Specimens*, describes the details of the preparation of test coupons. ASTM G4, *Standard Guide for Conducting Corrosion Tests in Field Applications*, details related information on the performance of such tests in plant equipment under operating conditions. The advantages of properly conducted coupon testing include the fact that actual process streams can be used, a large number of coupons can be exposed simultaneously, and various forms of corrosion can be detected. Disadvantages include the inability to monitor the time dependence of the corrosion process and the long exposure times usually required to characterize both the initiation period and the propagation rate.

COUPON PREPARATION AND ANALYSES

Because detailed information on coupon testing is available elsewhere, this section focuses on the aspects of such testing that are specific to the evaluation of pitting corrosion. When performing coupon exposures, it is important to include alloys whose corrosion behavior in the environment of interest is well characterized and reproducible to serve as an internal standard. This protocol is of particular importance when localized corrosion is studied. Because pitting has a stochastic nature, the use of these "controls" increases the confidence with which final material selection choices are made. If the control materials behave as expected, it is probable that the results for the other materials will reflect typical behavior for the environment of interest.

Copyright © 2022 by ASTM International, 100 Barr Harbor Dr., PO Box C700, West Conshohocken, PA 19428-2959
ASTM International is not responsible, as a body, for the statements and opinions expressed in this chapter. ASTM International does not endorse any products represented in this chapter.

Although mass loss characterizes the rate of uniform corrosion well, such measurements can be extremely misleading for pitting corrosion. Badly pitted specimens can exhibit negligible weight loss if the attack is extremely localized. In fact, the more a given amount of attack is localized, the more severe the pitting problem. ASTM G46, *Standard Guide for the Examination and Evaluation of Pitting Corrosion*, describes different methodologies used to evaluate pitting corrosion attack. Visual attack of both cross sections and plane views of pitted specimens can be ranked as shown in the standard. Pit density (number/cm^2) is important, but pit depth measurement is often the most directly applicable measurement.[7] Values for both average pit size and for the deepest pit observed are useful. To quantitatively evaluate the depth of attack, a variety of measurement methods can be used, including depth gages, metallographic examination of cross sections, or change in the focus plane on a metallurgical microscope, depending on the size of the pits. Direct measurement of pit depth using optical profilometry is attractive in that pit depths and distributions can be obtained rapidly. All line-of-sight methods are unable to detect and characterize undercutting pits (i.e., those with "ink-bottle" shapes or those with lacy covers[8]). The pitting factor (PF) is the ratio of the average of the 10 deepest observed pits to the average metal penetration by uniform dissolution, with higher values indicating a greater susceptibility to pitting. Statistical methods also have been applied to the evaluation of pitting corrosion (see ASTM G16, *Standard Guide for Applying Statistics to Analyses of Corrosion Data*, and Shibata and Takeyama[9] and Aziz and Godard[10]). In terms of predictive capability, the use of extreme value statistics is attractive.[10] Plotting the measured maximum pit depths for a large number of small samples has been used to estimate the probability that a pit of a specific depth will occur under the same conditions for a larger area.

EXPOSURE ENVIRONMENTS

Two general types of environments are used in coupon testing for pitting corrosion: those that simulate service conditions and those that seek to accelerate the pitting process. Tests in simulated (or actual) service environments are extremely valuable due to their direct applicability.[11,12] Because time is often of the essence, the long exposure times required usually limit the use of such tests to (1) confirmation of decisions made on the basis of accelerated laboratory tests, and (2) corrosion monitoring. The aim of testing in accelerating environments is usually alloy ranking or screening. Thus, little information is gained on the expected rate of attack in the actual application. The relative susceptibility of different alloy compositions or the effects of heat treatments, welding, or other processing can be assessed rapidly and quantitatively.

A variety of accelerated exposure tests have been developed to aid engineers in material selection for corrosion resistance. This section reviews some of those that are useful for localized corrosion resistance. In addition to a brief description of the test, the scientific reasoning behind it is presented, along with comments concerning the limits of its applicability and alterations to improve the utility of the test for a specific application. An experimenter should not feel bound by the structures of the ASTM standards if the experimenter can justify that by changing the procedure, more relevant information can be gained. Note, however, that these ASTM tests are probably the most widely used tests for localized corrosion resistance. Thus, an understanding of them can be of great importance in analyzing the results of testing performed in other labs or by manufacturers.

ASTM G48, *Standard Test Methods for Pitting and Crevice Corrosion Resistance of Stainless Steels and Related Alloys by the Use of Ferric Chloride Solution*

This test involves exposure of the material to a highly oxidizing, highly acidic, concentrated metal chloride solution. In essence, it is an attempt to simulate very roughly the composition of the environment within a localized corrosion site in a stainless steel. Briefly, a material is exposed to a 10 wt% ferric chloride ($FeCl_3$) solution for a relatively short time (24–72 h) at either ambient or elevated (usually 50°C) temperature. At the end of the test, the sample is examined for weight loss and localized attack (see ASTM G46 for a recommended practice for evaluating the extent of pitting corrosion). If pitting and crevice corrosion are of concern, artificial crevices can be applied by the use of polytetrafluoroethylene (PTFE) blocks held tightly to the sample surface by rubber bands (see ASTM G48). Ferric chloride exposure is commonly used to assess the corrosion resistance of stainless steel weldments (typically per ASTM G48, method A).

The basic concept behind this test is the application of a high potential using a chemical potentiostat in an acidic, concentrated chloride solution. The ferric salt forms an Fe^{3+}/Fe^{2+} redox couple with a potential of approximately +0.45 V(SCE). The high concentration of ferric ion allows the couple to provide a large current without an appreciable change in potential (approaching an ideally nonpolarizable electrode). The cathodic reaction (reduction of ferric to ferrous ion) occurs on the boldly exposed passive surface of the material under test. Thus, the redox couple serves the role of the *chemical* potentiostat. The high potential in turn nearly guarantees that the pitting potential will be exceeded, especially in such a concentrated Cl^- solution (and even more so if the test temperature is raised to 50°C). The low pH of the solution (typically about 1.3) inhibits repassivation and lowers the stability of the passive film. Thus, the $FeCl_3$ test is a test of the resistance of an alloy to propagation of localized corrosion for most alloys, because their pitting potentials are well below +0.45 V(SCE). More highly alloyed materials can resist initiation in this solution, however, the time of the test can be extended to a period of many days or to the increased temperature.

This popular test does have a number of limitations. Few industries operate in 10 wt% $FeCl_3$. Thus, the relation of the results of this test to material performance in real service environments that are profoundly different is questionable, and in fact, reversals in alloy ranking can occur. For nickel-base materials, the use of a ferric ion solution is also of questionable value. Despite these limitations, the $FeCl_3$ test will continue to be an important tool in alloy development and screening for historical, if for no other, reasons.

The $FeCl_3$ test details can be modified and still fall within the spirit of the requirements of the published method. The exposure time and temperature can be altered, as can the surface finish. As mentioned, surface finish can have important impact on the localized corrosion behavior. For example, it can affect the geometry of occluded sites and, in some cases, it can alter the surface area for cathodic reactions. Thus, it is important that the surface finish be chosen with care to simulate the expected conditions of the application.

ASTM B117, *Standard Practice for Operating Salt Spray (Fog) Apparatus*, and ASTM G85, *Standard Practice for Modified Salt Spray (Fog) Testing*

Probably the most widely used test for pitting resistance is salt spray. ASTM B117, *Standard Practice for Operating Salt Spray (Fog) Apparatus*, describes the experimental arrangements to be used and mandates the use of 5 wt% sodium chloride (NaCl) at a slightly elevated temperature (35°C). The test chamber allows the solution to be sprayed within its confines, creating a salt fog environment around the coupons. Such a constantly moist, salty environment is quite aggressive.

ASTM G85, *Standard Practice for Modified Salt Spray (Fog) Testing*, describes modifications to ASTM B117 involving a variety of solution chemistries and exposure regimens that can be used, including acetic acid-NaCl solution, acidified synthetic sea water, NaCl solution with SO_2 gas added, and a 0.05% NaCl + 0.35% ammonium sulfate $[(NH_4)_2SO_4]$ solution. In addition, a variety of cycles (wet/dry) are described that have been found to be more aggressive than the constant moisture of ASTM B117. In general, a spraying period is followed by a longer time at high relative humidity during which the sample can partially dry. Standards such as ASTM G85, however, lack a quantitative specification for relative humidity during dwell periods, which can be strongly affected by the type of test chamber used. Because relative humidity controls both equilibrium salt concentration as well as water layer thickness, localized corrosion rates as well as corrosion damage morphology also will be affected by relative humidity levels.[13,14]

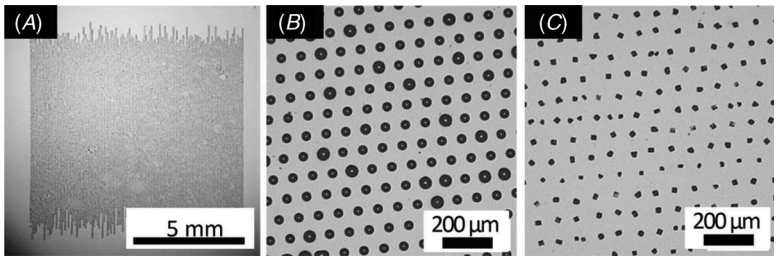
This cyclic type of exposure represents a more aggressive condition for most alloys than does constant, full immersion. Although still the subject of some debate, the generally accepted explanation involves the increased kinetics for oxygen reduction within the thin electrolyte layer that is present. Because of its limited solubility in water, oxygen reduction is usually under mixed or is fully diffusion controlled for most alloys, particularly those undergoing stable pitting. The thin electrolyte layer present during wet/dry cycling increases the rate of delivery of oxygen to the surface by reducing the diffusion boundary layer thickness from about 0.08 cm,[15] which is characteristic of a stagnant solution, to the thickness of the solution layer, which is often between 25 and 100 microns.[16] In addition, the concentration of aggressive ionic species increases dramatically during drying periods to the point of saturation.

Although reams of salt spray data exist, their use must be approached with care. As with $FeCl_3$, few industries actually operate in continuous salt spray (coastal regions and ships being notable exceptions). A number of industries have found that the standard salt spray testing not only fails to reproduce the damage observed in service but also is not particularly accelerating. Thus, the auto industry has developed a more complicated cyclic test, including an increase in the number of test intervals, known as GM 9540.[17] The reasons for the discrepancies between service experience and these laboratory tests are not clear, and users of the test should bear them in mind.

Coupon Exposures after Salt Loading

As salt spray environments often do not to reproduce damage morphologies and rates seen in-service on alloys, coupon exposures under controlled relative humidity and temperature with a known loading density of salt have been used more recently. Multiple methods are used to deposit known salt-loading densities on the surface of the alloys, including a mixture of ethanol and saturated salt solutions[18–20] and inkjet printing.[21–23] When using ethanol, a whitish layer is seen on the surface of the alloy and the error in loading density is within 2 $\mu g/cm^2$.[20] When a salt printer is used, the deposition of the salt is much more precise, as seen in figure 1, with an error in loading of ± 0.1 $\mu g/cm^2$.[22] In both cases, the type of salt and corresponding loading density can be changed to match the environment of interest. After printing, the samples are put into controlled environments for the desired time of exposure. Akin to ASTM G85, cycles of relative humidity can be included in testing to mimic atmospheric conditions. In general, these exposure tests have a smaller water-layer thickness than accelerated tests in ASTM standards and have the possibility to increase the diffusive flux of oxygen to the surface.

FIG. 1 (*A*) printed droplet pattern on steel coupon, (*B*) detail of droplet pattern immediately after printing, and (*C*) detail of crystal pattern immediately after printing.



Droplet Exposures

Along with controlled deposition of salt-loading density, pitting can be studied under the small defined droplets of salt solutions. Micro-pipettes are used to place a small amount of liquid (on the order of microliters) onto the surface of an alloy and result in a droplet with a diameter in the range of a few millimeters. After deposition, the samples can be placed under relative humidity and temperature control and left for a period of time.[24,25] Electrochemical measurements can be made inside the droplets using micro-electrodes to gain insight into the localized corrosion process in thin electrolyte layers.[26] The size and concentration of the salt in the drop is highly dependent upon the relative humidity in which the coupon is exposed in and can affect pitting that is seen on the surface.[25] The droplet can change size and volume through exposures or experimentation, and further affect the results.[26] This needs to be considered when interpreting experimental results. A further consideration of droplet testing is the effect of the area for cathodic reduction reactions. When electrochemical reactions are occurring under the droplet, both the anode and the cathode must be contained in the droplet and thus can affect results from exposure testing.

ASTM G69, *Standard Test Method for Measurement of Corrosion Potentials of Aluminum Alloys*

Aluminum alloys are highly susceptible to localized corrosion, including pitting. For many years, ASTM G69, *Standard Test Method for Measurement of Corrosion Potentials of Aluminum Alloys*, has been used to determine the so-called solution potential of aluminum (Al) alloys. The test solution described in ASTM G69 is a strongly oxidizing, near-neutral pH chloride solution. The oxidizing power originates in the 3 g/L (0.09 M) hydrogen peroxide that is added. In the 1 M NaCl, virtually all precipitation-hardened Al alloys will undergo stable pitting. The solution potential measurement is made over a period of 1 h. It represents a mixed potential between the passive portions of the surface on which peroxide reduction is occurring and the pitting sites. Thus, the potential depends on (1) the cathodic kinetics of peroxide reduction, (2) the pit dissolution kinetics, and (3) the number and size of the pits. As these characteristics vary from alloy to alloy as well as with time, quantitative interpretation of the solution potential is challenging. Mixed potential theory can be used to demonstrate that the solution potential cannot be used to rank the resistance of Al alloys to stable pitting. Nonetheless, it has been used as a type of quality control test to probe batch-to-batch variations within a given alloy. This solution is also specified in ASTM G110, *Standard Practice for Evaluating Intergranular Corrosion Resistance of Heat Treatable Aluminum Alloys by Immersion in Sodium Chloride + Hydrogen Peroxide Solution*.

ALTERATION OF TEST METHODS

When considering how to accelerate a test, the two most commonly applied methods are to increase the temperature and/or increase the concentration of aggressive species (e.g., Cl^- or H^+). Either can be effective, and some of the electrochemical tests described next use the strong temperature dependence of pit stabilization as a parameter to quantify pitting resistance. That said, such changes must be introduced with care to ensure that the mechanism of attack in the accelerated test is the same as that in the actual service environment. Decreased time required for the testing should be balanced against the decreasing relevance of the results, and the consequential increase in the uncertainty in their interpretation. In addition, results from accelerated tests are useful for material selection, but not for life prediction, as no means currently available can connect the rates of pitting corrosion observed in these tests to other environments. This situation can be contrasted with crack growth testing for which the similitude of the stress intensity factor, *K*, has been repeatedly demonstrated. This similitude allows results from laboratory scale test samples to be applied to service structures if the stress and flaw size and shape are known.

Electrochemical Tests

The main advantage of electrochemical testing is the opportunity to investigate corrosion phenomena in the solution of interest rather than in a (possibly) more aggressive and (probably) less relevant environment. In addition, a great deal of information can be gained about the dependence of the phenomena on external variables in a short time. Finally, the determination of critical potentials for initiation and propagation of localized corrosion can be useful in design decisions. For example, the use of mixed potential theory can allow for prediction of the protection (either anodic or cathodic) criteria, as well as provide information on the galvanic couples to avoid.

SPECIMEN MOUNTING

One of the main challenges associated with electrochemical testing for localized corrosion resistance is sample mounting. It can be extremely difficult to mount a sample with an insulated electrical contact and a controlled exposed surface area without introducing a crevice at the sample or mount interface. Because crevice corrosion will occur at lower potentials than pitting, the sample invariably begins to be attacked at the crevice, leading to an underestimation of the resistance of the sample to pitting. Some may argue that for the same reason, this type of testing is not overly conservative, as in service, one wants to know the potential at which any localized corrosion can occur, not just pitting. The flaw in this argument is that most crevices formed during sample preparation are not reproducible either in position or geometry, making comparisons extremely difficult. In addition, there may be applications in which crevice corrosion is not the failure mode of concern, but pitting is. Such testing with crevices present would lead one to choose a more resistant (and therefore more expensive) alloy than one actually would need.

A number of suggested solutions have been made for sample mounting, including the use of "knife-edge" Teflon washers,[27] various mounting compounds and procedures,[28] the use of wire loops,[29] and flag geometries.[30] One experimental design even includes a crevice area that is continually washed with deionized water.[31] All of these solution have limitations, and one must choose the most appropriate method for the particular alloy-environment

combination. The knife-edge PTFE washer, in combination with what has been known as the Stern-Makrides assembly (fig. 2), has been used successfully in a number of applications in which a tight seal can be formed, which (1) prevents ingress of any electrolyte, or (2) causes the voltage drop into the crevice to be so high as to prevent any polarization of the creviced surface away from E_{corr}. Because the latter is unlikely to occur, the prevention of ingress is critical. This prevention of solution ingress is closely related to the quality of the surface finish both in terms of its fineness (i.e., final polishing step particle size) and its uniformity. One large scratch can allow capillary action to draw an electrolyte into an otherwise-impervious crevice and start the crevice corrosion initiation process. This is the prime reason for the failings of this type of approach. In addition, because of the cost of the PTFE washers, many experimenters tend to try to reuse them. After the knife edge is deformed once, however, it will not form a watertight seal again, thus allowing crevice corrosion to occur.

Other methods also have been used to prevent crevice corrosion with varying levels of success. Electroplaters tape can be used as a standalone method[32,33] or in combination with a gasket or PTFE washer. Without the presence of the electroplaters tape, crevice corrosion would occur, whereas when masked with tape, crevice corrosion was not present. This was signified by a higher breakdown potential when an anodic polarization was applied in taped samples compared with non-taped samples.[32] Other lacquers and epoxies also have been used widely to mask off certain areas; however, detailing all types of masks used is beyond the scope of this work. More recently, when a sample has a rough finish, such as printed additively manufactured alloys, quick setting epoxy can be used as a masking technique. In such applications, the epoxy fills rough features present on the surface and helps prevent solution ingress.[34] Although this method has not been extensively tested across multiple materials systems and solutions, it has been proven to be successful over typical flat cell mounting techniques in limited applications.

The cell designed by Ovarfort[31,35] uses a slow flow (4 mL/min) of deionized water into the creviced area to prevent the accumulation of dissolution products inside the occluded area, the hydrolysis of which leads to crevice corrosion. The design has been applied successfully to the study of the pitting of a wide variety of stainless steels at both ambient and elevated temperature.[31,35] This cell, however, can be used only for flat samples. In addition, one must be careful to ensure that the deionized water flow is uniform throughout the crevice. If a dead spot were to develop, crevice corrosion likely would be initiated. Details of the cell can be found in Annex X2 of ASTM G150, *Standard Test Method for Electrochemical Critical Pitting Temperature Testing of Stainless Steels and Related Alloys*.

One example of the effect of crevices is shown in figure 3 for a 18Cr-8Ni stainless steel in a solution in which propagating crevice corrosion will not occur (1 N sulfuric acid [H_2SO_4]).[28] In this case, the higher passive current densities are observed for the insulating materials that perform poorly. In a Cl^- containing solution, this would translate into a lower E_{bd}. As can be seen from figure 3, some mounting materials perform well in this solution, although note that these results cannot be extrapolated to other solutions. For example, the alkyd-varnish is used in electroplating to mask off areas that should not be plated. Although it works well in acid solutions, it performs poorly in neutral or

FIG. 2 Stern-Makrides electrode assembly: (*A*) glass tub that protects threaded steel rod from solution, (*B*) PTFE gasket, and (*C*) specimen. For more details, see ASTM G5, *Standard Reference Test Method for Making Potentiodynamic Anodic Polarization Measurements*.

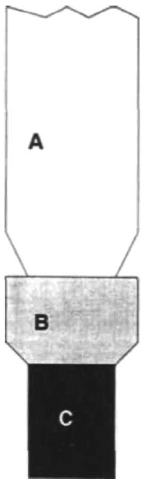
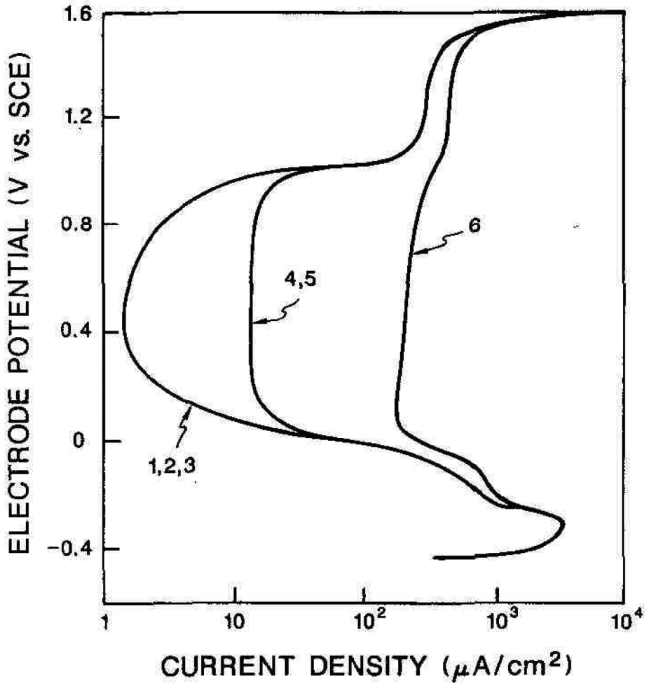


FIG. 3 Polarization curves of stainless steel in 1N sulfuric acid using different specimen mounting methods: (1) Stern-Makrides compression gasket, (2) heat-cured epoxy, (3) alkyd-varnish, (4) phenol-formaldehyde, (5) polymethyl methacrylate, and (6) cold-cured epoxy.[28]

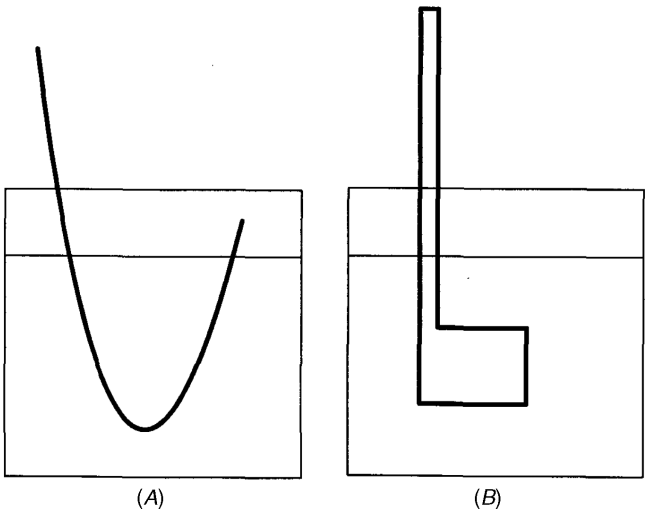


basic solutions, especially on materials with passive films, such as stainless steel.

If mounting cannot be accomplished, three other approaches can be used. The first is the use of a wire loop electrode, as shown in figure 4*A*. Stockert, Hunkeler, and Bohni[29] have used this approach to study pitting without the complications of crevice corrosion. This approach works extremely well if one can get the material in wire form, but there is always the concern of metallurgical differences between material in wire form and that in plate or tube form, which are more likely to be used in engineering applications. A related approach is the use of a flag electrode configuration, as shown in figure 4*B*. This works well with plate material by minimizing the shaft size and thereby minimizing any effects of the waterline. If localized corrosion at the waterline continues to be a problem, deaeration of the solution and the air space above it can be of help. When deaerating, a baffle should be placed between the sample and the bubbler to prevent oscillations of the waterline. Note that flag electrodes can suffer edge attack that is not indicative of the behavior of the flat surface. Thus, post-test inspection of the location of the attack and careful interpretation of the results are important, as is the case for all electrochemical testing.

Suter and Bohni[36] developed a third approach to delineation of the surface area of interest. By using a microcapillary attached to a conventional optical microscope, they were able to define small areas of stainless steel surfaces and generate polarization curves. The area probed is defined by the diameter of the capillary with results demonstrated for capillaries between 2 and 1,000 microns.[37] The cell is of particular use when the behavior of a particular microstructural feature is of interest,[38–40] as the design allows the matrix contribution to be minimized. Another method used to probe local areas on an alloy surface was developed by Policastro et al. in which selective masking by photolithography was used to make electrochemical measurements on individual phases, such as those on duplex steals, and different regions of the alloy.[41] As with many of the newly developed techniques, limited validation is present in literature, and it is important to understand the effects that advanced techniques have on the underlying physical and chemical structure of the material through all processing cycles.

FIG. 4 (*A*) Wire loop configuration for electrochemical testing, and (*B*) flag electrode configuration for electrochemical testing.



CYCLIC POLARIZATION

By far, the most common electrochemical test for localized corrosion resistance is cyclic polarization. ASTM G61, *Standard Test Method for Conducting Cyclic Potentiodynamic Polarization Measurements for Localized Corrosion Susceptibility of Iron-, Nickel-, or Cobalt-Based Alloys*, has been developed to allow experimenters to test their equipment and procedures on systems that are well characterized. The potential is scanned from E_{corr} (or slightly below it) in the anodic direction until localized corrosion initiates as indicated by a large increase in the measured current density. At this point, the direction of the scan is reversed, and the current decreases until it changes polarity (i.e., becomes cathodic). Representative scans are shown in figure 5 for Type 304 SS and Hastelloy C-276. Conventional wisdom states that E_{bd} (the breakdown potential) is the potential above which stable pits are initiated, whereas E_{rp} (the repassivation potential) is the potential below which pits repassivate. The breakdown potential is usually defined as the potential at which there is a large increase in the measured current, whereas the repassivation potential is the potential on the reverse scan at which the measured anodic current becomes zero (i.e., the current changes polarity). Thus, the higher the value of E_{bd}, the more resistant is the alloy to the initiation of localized attack. The higher E_{rp}, the more easily the alloy can repassivate. At potentials between E_{bd} and E_{rp}, sites that have initiated can propagate. On the basis of this argument, one would favor an alloy that had both a high E_{bd} and a high E_{rp}.

Examples of the range of data that can be expected are shown in the standard. The scatter in the data is apparent, especially in the forward scan. This scatter points out the statistical nature of the nucleation of pitting. The average E_{bd} of Type 304 SS was found to be approximately +0.15 V(SCE), whereas the average E_{rp} was found to be approximately -0.21 V(SCE). The reverse scans are much more reproducible, because the local chemistry controls the repassivation. Another example of the inherent scatter in E_{bd} is shown in figure 6 for three variants of Type 304 SS in 1,000 ppm NaCl.[42] The large variation in E_{bd} arises despite the fact that all of the samples of each type were from the same heat of material and were tested under identical conditions.

Numerous attempts have been made to use the amount of hysteresis in the cyclic scan as a measure of localized corrosion susceptibility, with varying degrees of success. In this approach, the larger the hysteresis, the more likely a localized corrosion site will propagate once initiated. In the presence of a well-defined crevice, a good correlation has been found and the relative crevice corrosion susceptibility of alloys can be obtained. Wilde[43] demonstrated this for Hastelloy C, Inconel 825, and Carpenter 20Cb3 in seawater where the amount of hysteresis correlated well with the amount of weight loss (because of crevice

FIG. 5 Representative cyclic potentiodynamic polarization curves (ASTM G61). The average E_{bd} for Type 304SS was approximately +0.15 V_{SCE} while the average E_{rp} was approximately -0.21 V_{SCE}.

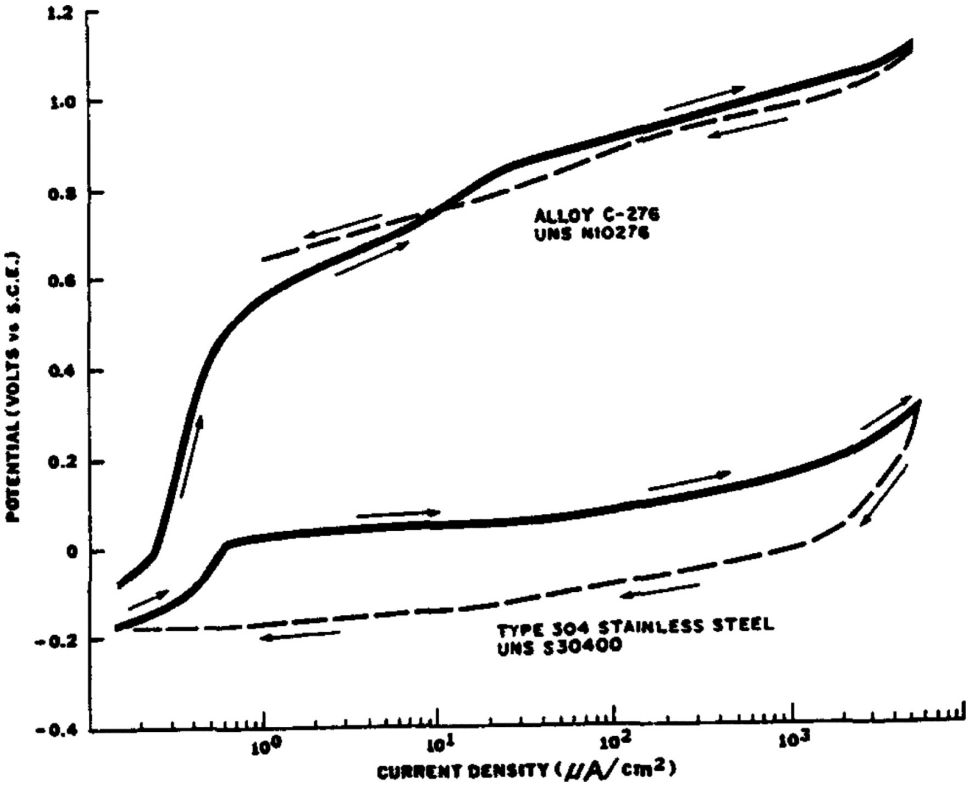
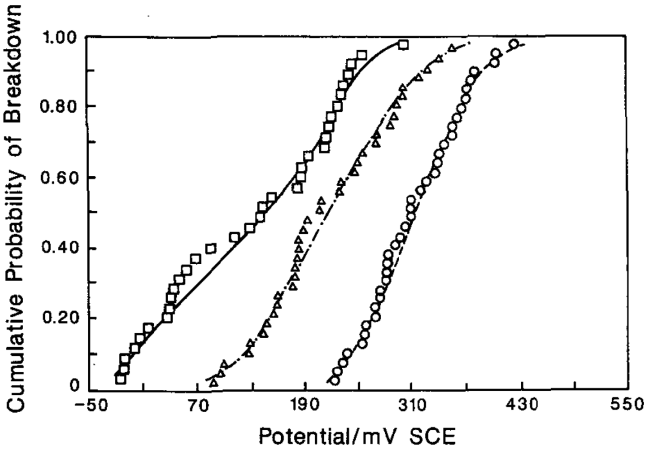


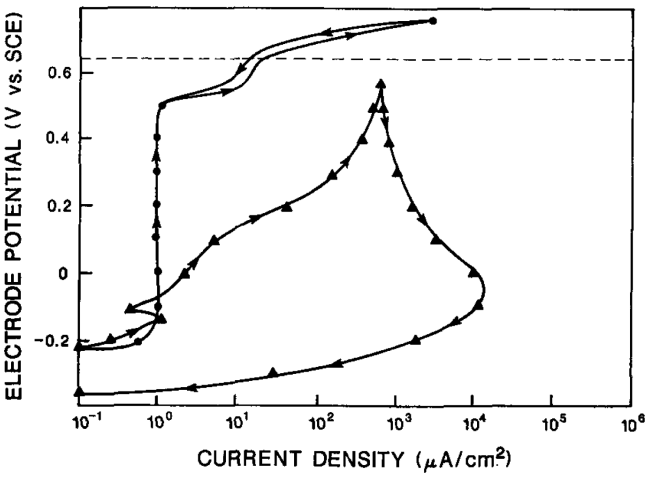
FIG. 6 Cumulative probability distributions of pitting breakdown potentials for three Type 304 stainless steels in 1,000 ppm NaCl with different sulfur contents: high sulfur (□) commercial purity (△), and high purity (○).[42]



corrosion) in a two-year exposure to seawater. There is not a linear correlation, however, so local penetration rates could not be predicted, but the test has been used successfully for alloy selection. In studies that have attempted to explore the relative pitting susceptibility of alloys, it has been found that comparisons are valid only if no crevices are present on any of the specimens tested. An example of the differences that one can observe is shown in figure 7. In the absence of crevices, the Fe-30Cr-3Mo alloy performs well in 1 M NaCl, with a high E_{bd} and a small hysteresis. Microscopic examination showed the attack occurred only at the grain boundaries. When a crevice was intentionally applied, the alloy performed poorly. The possible problems in comparing one specimen that had a crevice with another that did not are obvious; incorrect conclusions concerning the relative resistance of two materials could easily be reached. Independent of the mounting method used, one should always examine the specimen for localized attack after the test is completed. At a minimum, a microscopic examination of likely creviced areas should be performed. Some samples should be broken out of their mounts for more thorough examination.

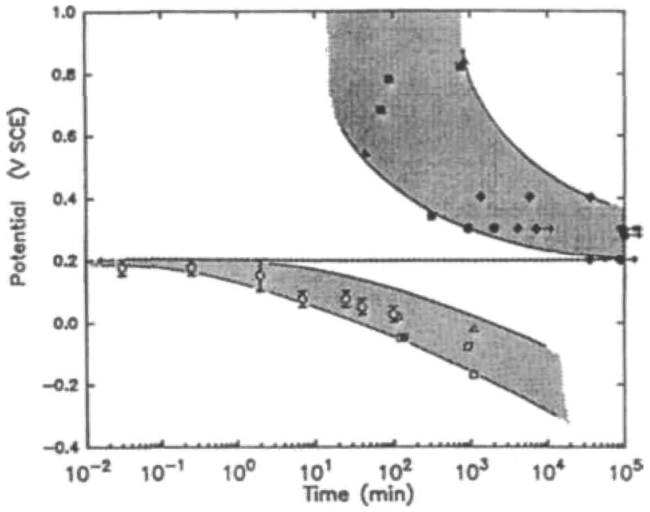
Although the interpretation of breakdown and repassivation potentials remains controversial, progress toward a consensus is being made. The large scatter in the breakdown potential is thought to be due to the sensitivity of pit initiation to the initial conditions. Its dependence on scan rate is most likely the result of the time dependence of the localized corrosion site chemistry development. In addition, it is now generally accepted that corrosion-resistant designs should not use E_{bd} as the important parameter, but should use the appropriate value of E_{rp}, because this is the potential below which pits should repassivate. Under these circumstances, the determination of the proper value of E_{rp} becomes the focus.

FIG. 7 Cyclic polarization curve for Fe-30Cr-3Mo alloy in dearated 1 M NaCl for specimens (a) without a crevice (•), with a crevice (▲).[43]



Thompson and Syrett[44] attempted to address the problem of the proper pitting potential by performing a variety of electrochemical tests on Type 317L and Alloy 825 in simulated flue gas desulfurization environments to determine E_{bd} and E_{rp} as a function of the extent of pitting damage, characterized in terms of the time during which localized attack was allowed to occur. In terms of cyclic polarization, this time would be inversely proportional to the sweep rate on the reverse portion of the scan, with lower sweep rates leading to greater attack. As shown in figure 8 for Type 317L, their results indicate the convergence of E_{bd} and E_{rp} at a single potential of +0.2 V(SCE). This "unique potential" can be interpreted as the potential below which the smallest pit will neither initiate nor grow. Quantifying the size of the "smallest" pit remains an important task. This work is important support for the hope of eventually developing quantitative, engineering-relevant criteria for material selection against pitting.

FIG. 8 Critical potentials (E_{bd} and E_{rp}) for Type 317L stainless steel exposed to a simulated flue gas desulfurization environment as a function of the time during which localized corrosion was allowed to propagate before repassivation occurred. Symbols denote different methods used to determine values: cyclic polarization (filled and open squares and triangles); constant potential tests (filled and open circles and diamonds).[44]



One of the historical controversies with regard to E_{rp} as a "material property" are the results of Wilde[43] in which the repassivation potential was shown to depend to some extent on the amount of localized dissolution that has been allowed to occur, and, therefore, depends on both the scan rate and the current at which the scan is reversed. The more attack that has been allowed to occur, the more negative is the E_{rp}. Other data on stainless steels, however, show a limiting value for large pits (0.05- to 0.5-mm deep),[45,46] complementing the work of Thompson and Syrett,[44] in which a limiting value also was found for small pits.

Despite these problems, polarization testing is useful for comparing alloys with respect to propagation of localized corrosion, although its use gives little information on the initiation time that is necessary for accurate lifetime prediction. One alloy may have superior resistance to propagation, but have much inferior resistance to initiation, and thus result in a shorter application lifetime.

GALVANOSTATIC MEASUREMENTS

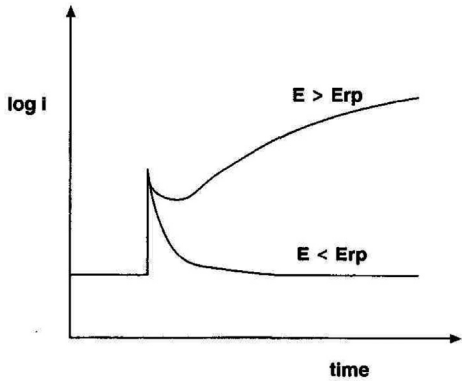
Controlled current tests for pitting are seeing increased popularity. Galvanostatic measurements involve the application of a series of small, step changes in the applied current. The potential is followed as the current is increased as described in ASTM G100, *Standard Test Method for Conducting Cyclic Galvanostaircase Polarization*. In some cases, more reproducible values for E_{rp} can be obtained galvanostatically in some systems, notably aluminum in inhibited water.[47] Potential oscillations at constant current can sometimes occur, which, while of scientific interest, can make interpretation of the results difficult, as the choice of potential becomes almost arbitrary.

POTENTIOSTATIC MEASUREMENTS

By far the most common electrochemical tests used is cyclic polarization. Nonetheless, potentiostatic measurements can be powerful tools in evaluating pitting behavior. Ideally, potentiostatic tests would be conducted over long time periods to avoid being fooled by long initiation times. Potentiostaircase tests can be performed in lieu of potentiodynamic tests, however, at equivalent potential scan rates, the results should be identical. Unfortunately, long-term potentiostatic testing is extremely time-consuming and expensive. In addition, the time frames involved usually are still very short when compared to the projected life. Thus, a number of approaches have been developed for accelerating the process of initiation.

Mechanical scratching is favored by some as a means by which a bare surface can be created. In this technique, one is ascribing no importance to initiation time. The surface is held at a constant potential and then a portion of it is scratched, usually with a diamond-tipped stylus. The current is monitored with time. For potentials below E_{rp}, the surface will repassivate rather

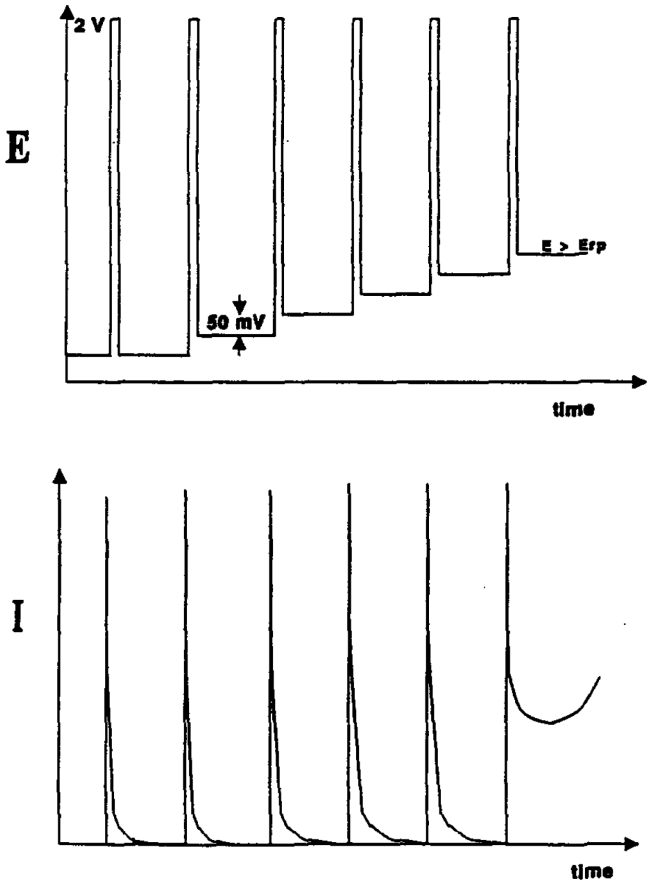
FIG. 9 Scratch test current-time curves for a specimen held potentiostatically above the repassivation potential (E_{rp}) and below E_{bd}.



rapidly, as shown in figure 9. Just above E_{rp}, the surface will try to repassivate, but will fail, and the current eventually will increase. The closer the potential to E_{rp}, the longer is the time before the current increases. Thus, in most cases, the E_{rp} measured by this method is not conservative, as usually no more than 10 min is spent at any one potential. If one had waited long enough at the potential used just before the measured E_{rp}, localized corrosion might have occurred. This, however, does not denigrate its utility as a screening test. One problem with scratching tests of this type is the dependence on the weight of the scratch. For instance, when scratching by hand, the E_{rp} decreases with increasing damage. A mechanical system improves the reproducibility. A more difficult problem concerns the site of pitting. In many cases, pitting occurs at inclusions or second-phase particles of one type or another. Such inclusions are usually present at small volume fractions, so the probability of scratching across one (or more) with a fine diamond tip is extremely small. This paucity of sites can lead to erroneously high values of E_{rp}, which reflect the pitting susceptibility of the matrix material, but ignore the susceptibility of the weakest link, the inclusions.

In addition, purely electrochemical methods can be used to produce a bared surface. In one technique, the entire exposed surface is activated by a large positive voltage excursion, which is followed by a voltage step back to (or toward) E_{corr}. In this way, any potential pitting sites are initiated, and the test measures the ability of the material to resist propagation and to repassivate. One version of this test (fig. 10) involves a step to +2 V for 3 s followed by a step back to E_{corr}, during which time the current is monitored. The potential is held there for 5 min before it is again stepped to +2 V for 3 s to reinitiate localized corrosion. At this point, the potential is stepped back to a potential 50 mV above E_{corr}, and the current is monitored for 5 min. The process is repeated until the current does not decay upon the step in the negative direction. In this way, an estimate of E_{rp} can be made, with better estimates resulting from the use of smaller increments in the test potential (e.g., 25 mV instead of 50 mV). This method is essentially using the potentiostat to "electrochemically

FIG. 10 Schematic E(t) and I(t) for electrochemical scratch method for determining the repassivation potential.



scratch" the specimen surface. A related method is described in ASTM F746, *Standard Test Method for Pitting or Crevice Corrosion of Metallic Surgical Implant Materials*, for determining the pitting and crevice corrosion susceptibility of materials used in medical implants.

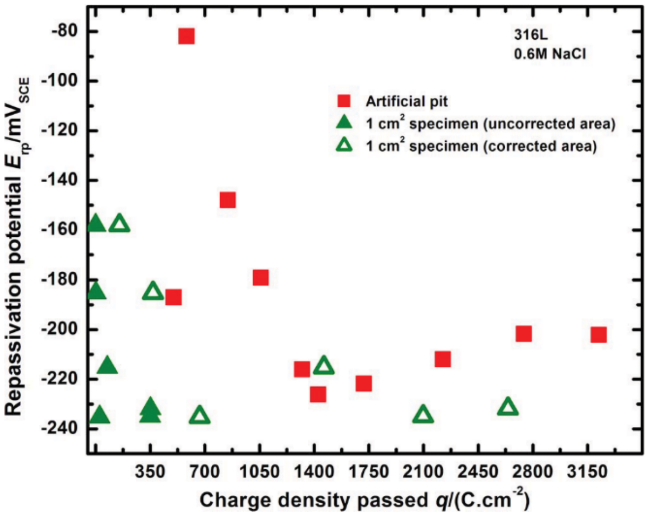
In another electrochemical test that focuses on pit propagation, the potential is scanned at 10 mV/s to a potential E1 between E_{bd} and E_{rp}, where it is held to determine the background passive current density. After 10 min, the potential is scanned anodically past E_{bd} until the current density is 10 mA/cm^2, at which time the potential is stepped back to E1. The current is then monitored for 10 min, after which the potential is held at E_{corr} for 5 min to repassivate the pits. Finally, the potential is stepped back to E1 and the current is monitored to ensure that the background current has not changed appreciably. The amount of charge passed during the propagation stage is compared to the pitted area (determined by optical microscopy) to determine an average pit penetration rate. This test is known as the Pit Propagation Rate (PPR) Test.[48]

Sehgal et al.[49] and Frankel et al.[50] developed a means of testing pit propagation using thin foils. The geometry of the foil restricts the dissolution to two spatial dimensions, allowing optical measurements of changes in diameter to be related to the

measured current, thereby establishing an accurate rate of pit propagation as well as conditions under which such pits repassivate. The method has been applied to sputtered aluminum (Al) thin films[50] as well as Al alloys.[49] The primary experimental challenge is the creation of foils that are sufficiently thin to produce a stable, two-dimensional pit. While sputter deposition is an excellent method, the production of thin foils of engineering alloys provides more of a challenge, although not always an insurmountable one.

Along with two-dimensional dissolution in foils, insights into pit propagation and repassivation can also be made through electrochemical measurements on artificial pits formed by embedding wire (usually on the order of a 50-µm diameter) in an insulating material restricting the geometry to one spatial dimension.[52,53] By leaving a cross-section of the wire exposed to solution, a potentiostatic anodic hold will allow for the entire interfacial area to be active. Dissolution of the wire is in one dimension; therefore, modeling the effects of mass transfer is straight-forward as given by Galvele's original formulism.[53,54] These one-dimensional (1D) electrodes can be used to measure conditions for pit propagation, namely, the pit stability product, $(i \cdot x)$, where i is the current density and x is the pit depth. A critical value of $i \cdot x$ describes the current density needed to continue propagation at any given depth, x; E_{rp} also can be measured with 1D electrodes, as limiting values for E_{rp} are reached at sufficient depth[45,55] (charge passed) as seen in figure 11,[51] further complementing the work of Thompson and Syrett.[44] These E_{rp} values are not affected by the dissolution products created during the 1D pit growth because of the small amount of charge needed, as compared with macro-sized electrodes. Artificial pit electrodes can be used to gain insights into pit propagation and repassivation in different alloys[55,56] as well as to quantify solution and temperature effects.[57–59] Measurements for pit stability generally are made under the presence of a salt film; however, pitting has been shown to occur when a salt film is not present on the surface of a pit, thus a critical value of the fraction of saturation at the pit surface required for propagation is also needed, limiting the direct application of this parameter.[52]

FIG. 11 Repassivation potential of one-dimensional electrodes in comparison to CPP experiments.[51]



CRITICAL TEMPERATURE TESTS

Although ASTM tests use temperature to accelerate attack during exposures, temperature also can be used in combination with electrochemical techniques. One example of this is the determination of critical pitting temperatures (CPT)[35,60,61] for alloy development or selection, or both. An anodic potential is applied to an electrode at low temperature (room temperature or below) in the solution of interest, and the temperature slowly increases to determine the temperature at which initiation of localized corrosion occurs, as signified by an increase in the current above some criterion. Such a method allows for a quantitative ranking of materials in terms of resistance to pitting. Note that CPT does not represent an intrinsic material property but rather a statistically distributed value that is dependent on material surface condition, test exposure area, and test environment.[59]

ASTM G150 describes in detail how to perform such experiments. The solution prescribed is 1 M NaCl, the suggested applied potential is +700 mV(SCE), and the starting temperature is deemed to be 0°C, with the temperature being increased at 1°C/min. The CPT is defined as the temperature at which the current exceeds 100 µA/cm^2 and remains so for more than 1 min. The test method clearly states that alternative potentials can be used if they are within the range for which the CPT is potential independent.

Salinas-Bravo and Newman[62] developed variation on the critical pitting temperature test for welded stainless steels in which a large, unwelded specimen was coupled to a welded sample using a zero resistance ammeter (ZRA). The unwelded specimen polarizes the welded sample to a positive potential. As the temperature is raised, the galvanic current between the two remains low until the CPT is reached. At that point, the welded sample undergoes stable pitting and a large current is observed. The attractiveness of this test is that it probes the inherent galvanic couple that is the essence of localized corrosion: the large, passive cathode, and the small, active pit.

ELECTROCHEMICAL NOISE

Electrochemical noise has seen increased interest as a tool for both corrosion science and corrosion engineering. By carefully monitoring the galvanic current between two nominally identical electrodes or the corrosion potential of a single electrode, metastable pitting can be detected. The localization of the dissolution inherent in localized corrosion implies a separation of the anodic and cathodic reactions that constitute the corrosion couple. This physical separation of reactions distinguishes localized corrosion from uniform corrosion in which it is traditionally thought that the anodic and cathodic sites are in proximity to one another. The majority of the anodic (oxidative dissolution) reaction occurs inside the localized corrosion site, whereas the majority of the cathodic (reduction) reaction occurs on the boldly exposed surface. Thus, a galvanic couple is created. The spatial separation of the processes necessitates the passage of current between the two sites. This passage of current leads to the various electrochemical noise signals measured.

Under open circuit conditions, bursts of dissolution at localized corrosion sites require the generation of bursts of cathodic current from the surrounding boldly exposed surface. This increased demand typically causes a decrease in the measured open circuit potential. Localized corrosion sites are typically very small (<100 μm diameter). The current densities inside these cavities during transient bursts, however, can be on the order of 1 A/cm^2. These rates are possible because of the extremely aggressive environments that develop inside localized corrosion sites. Thus, even though the sites are geometrically small, they can influence the electrochemical potential of the much larger boldly exposed surface on which the electrode kinetics are far slower. This difference in relative current densities on separated anodes and cathodes is what accounts for the ability to detect the electrochemical noise associated with localized corrosion. When the potential of the surface is controlled with an external device, the same burst of dissolution requires the device to supply a burst of current, which can be recorded. Usually, these bursts are transient, with temporary repassivation of the localized corrosion site occurring and allowing the system to return to the previous steady-state condition. On a metal surface of appreciable size (>1 cm^2), there can be many localized corrosion sites. They will usually propagate independently, so that a series of current (or potential) fluctuations is observed because of the summation of the signals from the individual sites. These fluctuations are referred to as "electrochemical noise." Because electrochemical noise often can be observed under open circuit conditions, it has been hailed as the only truly noninvasive electrochemical method. Several methods for *in-operando* corrosion monitoring based on these concepts are overviewed in ASTM G199, *Standard Guide for Electrochemical Noise Measurement*. Changes in the noise signal are often taken as an indication that conditions are favorable for pit initiation to occur. Thus, if one is monitoring a process stream, corrective action can be taken. Numerous data analysis procedures for electrochemical noise signals have been proposed for the identification of pitting conditions, some of which are described in ASTM G199. The theoretical basis for these analysis approaches is often not well defined, and the reliability can be highly variable depending on approach and the conditions of the system being monitored.[63,64] Relatedly, another disadvantage of noise monitoring is that it does not give sufficient information about what level of this metastable pitting is acceptable. For example, there may be literally millions of metastable pits forming and repassivating in a vessel wall, but only one needs to penetrate completely for a leak to develop. It may not be possible to differentiate between conditions that will allow that to develop and those in which the extent of pitting is negligible. Experience and correlations with coupon exposures are critical factors in the use of noise for localized corrosion monitoring. A guide has been provided by Huet and Ngo to improve measurements and data analysis for electrochemical noise measurements.[65]

ACOUSTIC EMISSION MONITORING OF CORROSION

Acoustic emission (AE) testing is a nondestructive technique aimed toward understanding localized corrosion as it occurs. The basics of AE involve the detection of micro-signals from growing corrosion damage by converting very small surface displacement to a voltage, which can be collected as a function of time. The AE signals have been correlated to the number of pits that are present on the surface of the alloy[66] along with other uses detailed in work by Wu, Jung, and Byeon.[67] This technique can be sensitive and allows for detection of very small perturbations; however, it is also a downfall of the technique as deconvolution from ambient vibrations can be rather difficult. There are many sources of vibrations on the surface of a material during corrosion, including the following: (1) bubbling from H_2 evolution, (2) initiation events caused by passive film rupture, and (3) pit propagation. Along with these problems, it is likely that an area under study could have multiple pitting events at different stages of the pitting process and therefore convolute the AE signal.

SCANNING TECHNIQUES APPLIED TO LOCALIZED CORROSION

Although a detailed overview of scanning techniques is beyond the scope of this chapter, a quick summary of advantages and disadvantages to each technique along with the capabilities will be outlined. Various scanning techniques are commonly used to investigate localized corrosion scenarios, including scanning Kelvin probe (SKP), scanning Kelvin probe force microscopy (SKPFM), scanning vibrating electrochemical technique (SVET), and scanning electrochemical microscopy (SECM). SKP is characterized by measuring two-dimensional distributions of the contact potential difference between the tip and the surface of interest. The SKP can be combined with atomic force microscopy to create an SKPFM and results in simultaneous mapping of the surface topography as well as the potential difference.[68] The resolution of these techniques varies and SKPFM can produce measurements on the order of nanometers, while SKP generally is limited by the tip size and distance between the tip and the sample. Because of the small resolution, SKP and SKPFM are useful in determining the propensity for pit initiation sites. SVET measures in solution to map electrochemical currents above the surface of corroding metals and allows for the determination of local cathodic and anodic regions of interest. SVET has a much lower spatial resolution than SKP and SKPFM at about 100–200 μm and has a current density resolution around 1 μA/cm^2.[69] The user should be aware that when using these methods for in-situ measurements, the solution often is stirred, causing mixing of the localized solution and can change diffusion. SECM electrolysis current that flows at a microelectrode immersed in solution is moved above an alloys surface and is used to characterized electrochemical processes.[70] Considering all scanning techniques, localized corrosion is characterized by a stochastic process which can occur on short timescales. When scanning a surface in the presence of an electrolyte, it is possible that these events are either missed or are in the stages of initiation or repassivation and could affect the results.

Predictive Capabilities

With the previous caveats in mind, the study of metastable pitting can be used to assist in lifetime prediction studies. If pitting is truly a stochastic phenomenon, then one can apply statistics to

allow prediction of the likelihood of pit propagation, given sufficient information. The information needed is (1) the probability that a pit will nucleate under a given set of conditions, and (2) the probability that once a pit nucleates, it will survive (i.e., become stable). Such information could be used to estimate component lifetimes, which then could be used to make design decisions based on the consequences of a failure. For example, a 3% chance of perforation may be acceptable for an easily shutdown and repaired vessel if it allows a cheaper alloy to be used, but such a probability would not be acceptable for a critical component in an inaccessible submersible.

Analyses of these current and potential transients caused by metastable pits can provide information regarding the controlling factors and their dependence on environmental, metallurgical, and applied potential conditions. For example, Pride, Scully, and Hudson[71] characterized the metastable pitting behavior of high-purity Al and aged Al-2%Cu. They found that the frequency of pitting events was proportional to both the applied potential and the chloride concentration. The rate of pitting also was found to decrease with increasing exposure time. These kinds of analyses can serve as the basis for the pitting prediction methodologies described next.

Shibata and Takeyama[9] and Williams, Westcott, and Fleischmann[72] have applied such statistical arguments to pitting of stainless steel. To develop these models, a large amount of data that can be treated as an ensemble must be gathered. In other words, variations in results from test to test are expected, even for nominally identical tests. This variation is used to develop the cumulative probability curve for pitting under a certain set of conditions. Both groups used multiple specimen testing apparatus to gather up to 12 data points for critical potentials and metastable pit nucleation rates simultaneously. The results for one set of 30 tests are shown in **figure 6.**[42] This shows that the breakdown potential E_{bd} follows a distribution. Thus, there is a 20% chance that the breakdown potential of commercial 304 SS will be below +160 mV(SCE) in 1,000 ppm NaCl. The argument is that there was nothing "wrong" with those tests whose E_{bd} was less than +160 mV(SCE), but that the variation reflects the stochastic nature of the pitting process. Qualitatively similar data have been developed for Al alloys and their constituent second-phase particles.[73]

The development of commercially available multipotentiostats has made measurements of pitting conditions and the underlying factors more tractable. Lunt et al.[74] used an array of nominally identical electrodes to characterize the strengths and extent of the types of interactions that occur among active pits. In addition, such instrumentation makes the determination of the statistical distribution of pitting potentials through the testing of a large number of specimens much less time intensive, as multiple electrodes (up to 100)[75] can be independently tested simultaneously.

Conclusion

This chapter provided a brief overview of the exposure tests used to determine localized corrosion susceptibility and introduced a variety of electrochemical techniques that can provide important information concerning localized corrosion susceptibility. Although none of the methods is perfect or a panacea, when used judiciously and in combination, a better picture of the localized corrosion process can be gained, even in complicated solutions. This allows for more informed decisions on alloy selection, process alteration, or failure analysis. Although prediction of localized penetration rate remains a goal of electrochemical testing, applications of statistics to the process appear promising.

ACKNOWLEDGMENTS

Sandia National Laboratories is a multimission laboratory managed and operated by National Technology and Engineering Solutions of Sandia, LLC., a wholly owned subsidiary of Honeywell International, Inc., for the U.S. Department of Energy's National Nuclear Security Administration under contract DE-NA0003525. This document is SAND2019-13965 B.

References

1. Z. Szlarska-Smialowska, *Pitting Corrosion of Metals* (Houston, TX: National Assocation of Corrosion Engineers, 1986).
2. G. S. Frankel, "Pitting Corrosion of Metals. A Review of the Critical Factors," *Journal of the Electrochemical Society* 145 (1998): 2186–2198.
3. J. Soltis, "Passivity Breakdown, Pit Initiation and Propagation of Pits in Metallic Materials: Review," *Corrosion Science* 90 (2015): 5–22.
4. G. S. Frankel, T. Li, and J. R. Scully, "Perspective—Localized Corrosion: Passive Film Breakdown vs Pit Growth Stability," *Journal of the Electrochemical Society* 164 (2017): C180–C181.
5. R. Baboian, ed., *Corrosion Tests and Standards: Application and Interpretation,* 2nd Edition (West Conshohocken, PA: ASTM International, 1995).
6. W. H. Ailor, ed., *Handbook On Corrosion Testing and Evaluation* (New York: Wiley, 1971).
7. M. A. Streicher, "Pitting Corrosion of 18Cr-8Ni Stainless Steel," *Journal of the Electrochemical Society* 103 (2007): 375–390.
8. P. Ernst, N. J. Laycock, M. H. Moayed, and R. C. Newman, "The Mechanism of Lacy Cover Formation in Pitting," *Corrosion Science* 39 (1997): 1133–1136.
9. T. Shibata and T. Takeyama, "Stochastic Theory of Pitting Corrosion," *Corrosion* 33 (1977): 243–251.
10. P. M. Aziz and H. P. Godard, "Influence of Specimen Area on the Pitting Probability of Aluminum," *Journal of the Electrochemical Society* 102 (1955): 577–579.
11. *Standard Guide for Conducting Corrosion Tests in Field Applications*, ASTM G4-01 (2014) (West Conshohocken, PA: ASTM International, approved November 1, 2014), 1–10, http://doi.org/10.1520/G0004-01R14
12. *Standard Practice for Conducting Atmospheric Corrosion Tests on Metals 1*, ASTM G50-10 (2015) (West Conshohocken, PA: ASTM International, approved November 1, 2015), 1–11, http://doi.org/10.1520/G0050-10R15

13. M. B. Parker and R. G. Kelly, "Improved Atmospheric Corrosion Testing for Aluminum Alloys Part I: Deconstructing ASTM G85-A2," *Corrosion* 76 (2020): 39–50.

14. M. B. Parker and R. G. Kelly, "Improved Atmospheric Corrosion Testing for Aluminum Alloys Part II: Developing Improved Testing Protocol," *Corrosion* 76 (2020): 51–62.

15. C. Liu, J. Srinivasan, and R. G. Kelly, "Electrolyte Film Thickness Effects on the Cathodic Current Availability in a Galvanic Couple," *Journal of Electrochemical Society* 164 (2017): C845–C855.

16. C. Leygraf and T. E. Graedel, *Atmospheric Corrosion* (New York: Wiley, 2000).

17. S. D. Cramer and B. S. Covino Jr., *Corrosion: Fundamentals, Testing and Protection, ASM Handbook* (Materials Park, OH: ASM International, 2003).

18. R. Lindström, J.-E. Svensson, and L. G. Johansson, "The Influence of Salt Deposits on the Atmospheric Corrosion of Zinc. The Important Role of the Sodium Ion," *Journal of the Electrochemical Society* 149 (2002): B57–B64.

19. S. Li and L. H. Hihara, "Aerosol Salt Particle Deposition on Metals Exposed to Marine Environments: A Study Related to Marine Atmospheric Corrosion," *Journal of the Electrochemical Society* 161 (2014): 268–275.

20. H. Strandberg and L. G. Johansson, "Electrochemical Aspects of Copper Atmospheric Corrosion in the Presence of Sodium Chloride," *Journal of the Electrochemical Society* 145 (1998): 1093–1100.

21. E. J. Schindelholz and R. G. Kelly, "Application of Inkject Printing for Depositing Salt Prior to Atmospheric Corrosion Testing," *Electrochemical and Solid-State Letters* 13 (2010): C29–C31.

22. E. Schindelholz, B. E. Risteen, and R. G. Kelly, "Effect of Relative Humidity on Corrosion of Steel under Sea Salt Aerosol Proxies," *Journal of the Electrochemical Society* 161 (2014): C450–C459.

23. E. Schindelholz, L. K. Tsui, and R. G. Kelly, "Hygroscopic Particle Behavior Studied by Interdigitated Array Microelectrode Impedance Sensors," *Journal of Physical Chemistry A* 118 (2014): 167–177.

24. L. Guo, N. Mi., H. B. Mohammed-Ali, M. Ghahari, A. D. Plessis, A. Cook, S. Street, C. Reinhard, R. Atwood, T. Rayment, and A. Davenport, "Effect of Mixed Salts on Atmospheric Corrosion of 304 Stainless Steel," *Journal of the Electrochemical Society* 166 (2019): C3010–C3014.

25. Y. Tsutsumi, A. Nishikata, and T. Tsuru, "Pitting Corrosion Mechanism of Type 304 Stainless Steel under a Droplet of Chloride Solutions," *Corrosion Science* 49 (2007): 1394–1407.

26. C. M. Hangarter and S. A. Policastro, "Electrochemical Characterization of Galvanic Couples under Saline Droplets in a Simulated Atmospheric Environment," *Corrosion* 9312 (2017): 268–280.

27. M. Stern and A. C. Makrides, "Electrode Assembly for Electrochemical Measurements," *Journal of the Electrochemical Society* 107 (1960): 782.

28. N. D. Greene, W. D. France, and B. E. Wilde, "Electrode Mounting for Potentiostatic Anode Polarization Studies," *Corrosion* 21 (1965): 275–276.

29. L. Stockert, F. Hunkeler, and H. Bohni, "Crevice-Free Measurement Technique to Determine Reproducible Pitting Potentials," *Corrosion* 41 (1985): 676–677.

30. B. Shaw, "Crevice Corrosion of a Nickel-Chromium–Molybdenum-Iron Alloy in Natural and Chlorinated Seawater" (PhD thesis, Johns Hopkins University, 1988).

31. R. Ovarfort, "New Electrochemical Cell for Pitting Corrosion Testing," *Corrosion Science* 28 (1988): 135–140.

32. A. P. Bond and E. A. Lizlovs, "Anodic Polarization of Austenitic Stainless Steels in Chloride Media," *Journal of the Electrochemical Society* 115 (1969): 1130–1135.

33. V. Brusic, M. Russak, R. Schad, G. Frankel, A. Selius, D. DiMilia, and D. Edmonson, "Corrosion of Thin Film Magnetic Disk: Galvanic Effects of the Carbon Overcoat," *Journal of the Electrochemical Society* 136 (1989): 42–46.

34. M. A. Melia, H. D. A. Nguyen, J. M. Rodelas, and E. J. Schindelholz, "Corrosion Properties of 304L Stainless Steel Made by Directed Energy Deposition Additive Manufacturing," *Corrosion Science* 152 (2019): 20–30.

35. R. Ovarfort, "Critical Pitting Temperature Measurements of Stainless Steels with an Improved Electrochemical Method," *Corrosion Science* 29 (1989): 987–993.

36. T. Suter and H. Bohni, "Microelectrodes for Corrosion Studies in Microsystems," *Electrochimica Acta* 47 (2001): 191–199.

37. J. O. Park, T. Suter, and H. Böhni, "Role of Manganese Sulfide Inclusions on Pit Initiation of Super Austenitic Stainless Steels," *Corrosion* 59 (2003): 59–67.

38. L. Staemmler, T. Suter, and H. Böhni, "Glass Capillaries as a Tool in Nanoelectrochemical Deposition," *Electrochemical and Solid-State Letters* 5 (2002): C61–C63.

39. T. Suter and R. C. Alkire, "Microelectrochemical Studies of Pit Initiation at Single Inclusions in Al 2024-T3," *Journal of the Electrochemical Society* 148 (2001): B36–B42.

40. R. R. Leard and R. G. Buchheit, "Electrochemical Characterization of Copper-Bearing Intermetallic Compounds and Localized Corrosion of Al-Cu-Mg-Mn Alloy 2024," *Materials Science Forum* 396–402 (2002): 1491–1496.

41. S. A. Policastro, R. C. Y. Auyeung, F. J. Martin, R. J. Rayne, A. Piqué, A. Lewis, A. Geltmacher, and P. M. Natishan, "An Approach for Determining Microscale Electrochemical Behavior," *Journal of the Electrochemical Society* 159, no. 1 (2012): 15–24.

42. J. Stewart, "Pit Initiation on Austenitic Stainless Steels" (PhD thesis, University of Southampton, 1990).

43. B. E. Wilde, "Passivity and Its Breakdown on Iron and Iron Base Alloys" in *Localized Corrosion*, ed. R. W. Staehle, B. F. Brown, J. Kruger, and A. Agarwal (Houston, TX: National Association of Corrosion Engineers, 1974), 129–142.

44. N. G. Thompson and B. C. Syrett, "Relationship between Conventional Pitting and Protection Potentials and a New, Unique Pitting Potential," *Corrosion* 48 (1992): 649–659.

45. N. Sridhar and G. A. Cragnolino, "Applicability of Repassivation Potential for Long-Term Prediction of Localized Corrosion of

Alloy-825 and Type-316L Stainless-Steel," *Corrosion* 49 (1993): 885–894.

46. T. Hakkareinen, "Repassivation Potential of Corrosion Pits in Stainless Steels," in *Passivity of Metals and Semiconductors*, ed. M. Forment (Amsterdam, The Netherlands: Elsevier Science, 1983), 367–372.

47. S. T. Hirozawa, "Current versus Voltage Hysteresis: Effect on Electrometric Monitoring of Corrosion," in *Laboratory Corrosion Tests and Standards,* ed. G. S. Haynes and R. Baboian (West Conshohocken, PA: ASTM International, 1985), 108–121.

48. B. C. Syrett, "PPR Curves: A New Method of Assessing Pitting Corrosion Resistance," *Corrosion* 33 (1977): 221–224.

49. A. Sehgal, G. S. Frankel, B. Zoofan, and S. Rokhlin, "Pit Growth Study in Al Alloys by the Foil Penetration Technique," *Journal of the Electrochemical Society* 147 (2000): 140–148.

50. G. S. Frankel, R. C. Newman, C. V. Jahnes, and M. A. Russak, "On the Pitting Resistance of Sputter-Deposited Aluminum Alloys," *Journal of the Electrochemical Society* 140 (1993): 2192–2197.

51. J. Srinivasan, M. J. McGrath, and R. G. Kelly, "A High-Throughput Artificial Pit Technique to Measure Kinetic Parameters for Pitting Stability," *Journal of the Electrochemical Society* 162 (2015): C725–C731.

52. N. J. Laycock and R. C. Newman, "Localised Dissolution Kinetics, Salt Films and Pitting Potentials," *Corrosion Science* 39 (1997): 1771–1790.

53. R. C. Newman, M. A. A. Ajjawi, H. Ezuber, and S. Turgoose, "An Experimental Confirmation of the Pitting Potential Model of Galvele," *Corrosion* 28 (1988): 471–477.

54. J. R. Galvele, "Transport Processes and the Mechanism of Pitting of Metals," *Journal of the Electrochemical Society* 123 (1976): 464–474.

55. J. Srinivasan and R. G. Kelly, "On a Recent Quantitative Framework Examining the Critical Factors for Localized Corrosion and Its Impact on the Galvele Pit Stability Criterion," *Corrosion* 73 (2017): 613–633.

56. T. Li, J. R. Scully, and G. S. Frankel, "Localized Corrosion: Passive Film Breakdown vs. Pit Growth Stability: Part III. A Unifying Set of Principal Parameters and Criteria for Pit Stabilization and Salt Film Formation," *Journal of the Electrochemical Society* 165 (2018): C762–C770.

57. J. Jun, G. S. Frankel, and N. Sridhar, "Further Modeling of Chloride Concentration and Temperature Effects on 1D Pit Growth," *Journal of the Electrochemical Society* 163 (2016): C823–C829.

58. M. H. Moayed and R. C. Newman, "The Relationship between Pit Chemistry and Pit Geometry Near the Critical Pitting Temperature," *Journal of the Electrochemical Society* 153 (2006): 330–335.

59. T. Li, J. R. Scully, and G. S. Frankel, "Localized Corrosion: Passive Film Breakdown vs Pit Growth Stability: Part II. A Model for Critical Pitting Temperature," *Journal of the Electrochemical Society* 165 (2018): C484–C491.

60. R. J. Brigham, "Temperature as a Pitting Criterion," *Corrosion* 29 (1973): 33–36.

61. P. Lau and S. Bernhardsson, "Electrochemical Techniques for the Study of Pitting and Crevice Corrosion Resistance of Stainless Steels" in *Electrochemical Techniques in Corrosion Engineering*, ed. R. Baboian (Houston, TX: National Association of Corrossion Engineers, 1986), 281–286.

62. V. M. Salinas-Bravo and R. C. Newman, "An Alternative Method to Determine Critical Pitting Temperature of Stainless Steels in Ferric Chloride Solution," *Corrosion Science* 36 (1994): 67–77.

63. A. M. Homborg, T. Tinga, E. P. M. van Westing, X. Zhang, G. M. Ferrari, J. H. W. de Wit, and J. M. C. Mol, "A Critical Appraisal of the Interpretation of Electrochemical Noise for Corrosion Studies," *Corrosion* 70 (2014): 971–987.

64. H. A. A. Al-Mazeedi and R. A. Cottis, "A Practical Evaluation of Electrochemical Noise Parameters as Indicators of Corrosion Type," *Electrochimica Acta* 49 (2004): 2787–2793.

65. F. Huet and K. Ngo, "Electrochemical Noise: Guidance for Improving Measurements and Data Analysis," *Corrosion* 75 (2018): 1065–1073.

66. H. Mazille, R. Rothea, and C. Tronel, "An Acoustic Emission Technique for Monitoring Pitting Corrosion of Austenitic Stainless Steels," *Corrosion Science* 37 (1995): 1365–1375.

67. K. Wu, W. S. Jung, and J. W. Byeon, "In-Situ Monitoring of Pitting Corrosion on Vertically Positioned 304 Stainless Steel by Analyzing Acoustic-Emission Energy Parameter," *Corrosion Science* 105 (2016): 8–16.

68. C. M. Efaw, T. da Silva, P. H. Davis, L. Li, E. Graugnard, and M. F. Hurley, "Toward Improving Ambient Volta Potential Measurements with SKPFM for Corrosion Studies," *Journal of the Electrochemical Society* 166 (2019): C3018–C3027.

69. A. C. Bastos, M. C. Quevedo, O. V. Karavai, and M. G. S. Ferreira, "Review: On the Application of the Scanning Vibrating Electrode Technique (SVET) to Corrosion Research," *Journal of the Electrochemical Society* 164 (2017): C973–C990.

70. A. J. Bard, F. R. F. Fan, J. Kwak, and O. Lev, "Scanning Electrochemical Microscopy. Introduction and Principles," *Analytical Chemistry* 61 (1989): 132–138.

71. S. T. Pride, J. R. Scully, and J. L. Hudson, "Metastable Pitting of Aluminum and Criteria for the Transition to Stable Pit Growth," *Journal of the Electrochemical Society* 141 (1994): 3028–3040.

72. D. E. Williams, C. Westcott, and M. Fleischmann, "Stochastic Models of Pitting Corrosion of Stainless Steels–II. Measurement and Interpretation of Data at Constant Potential," *Journal of the Electrochemical Society* 132 (1985): 1804–1811.

73. G. O. Ilevbare, J. R. Scully, J. Yuan, and R. G. Kelly, "Inhibition of Pitting Corrosion on Aluminum Alloy 2024-T3: Effect of Soluble Chromate Additions vs. Chromate Conversion Coating," *Corrosion* 56 (2000): 227–242.

74. T. T. Lunt, J. R. Scully, V. Brusamarello, A. S. Mikhailov, and J. L. Hudson, "Spatial Interactions among Localized Corrosion Sites Experiments and Modeling," *Journal of the Electrochemical Society* 149 (2002): B163–B173.

75. N. D. Budiansky, J. L. Hudson, and J. R. Scully, "Origins of Persistent Interaction among Localized Corrosion Sites on Stainless Steel," *Journal of the Electrochemical Society* 151 (2004): B233–B243.

Chapter 2 | Crevice Corrosion

Mariano Iannuzzi,[1] Edgar Hornus,[1] and Mobin Salasi[1]

Introduction

Crevice corrosion is defined in ASTM G193, *Standard Terminology and Acronyms Relating to Corrosion*, as "the localized corrosion of a metal or alloy surface at, or immediately adjacent to, an area that is shielded from full exposure to the environment because of close proximity of the metal or alloy to the surface of another material or an adjacent surface of the same metal or alloy."[1] Crevice corrosion affects most metals and alloys and is among the most damaging forms of corrosion. Crevice geometries can be found on a wide range of structures and components, including flanges, threaded connections, and lap joints, as well as under deposits and damaged coatings.[2]

Metals and alloys that develop a passive film are prone to crevice corrosion. In contrast, those that do not form a surface film tend to corrode uniformly outside the occluded region because of the ready access to the oxidizing species that support the cathodic reactions.[3] Stainless steels, especially those with little to no molybdenum, some nickel-based alloys, and aluminum alloys are particularly susceptible to crevice corrosion.[4] Moreover, materials that have been shown to be highly resistant to pitting corrosion, such as titanium (Ti) and Ti-based alloys, suffer crevice corrosion in specific environments.[5,6]

As will be discussed, pitting and crevice corrosion mechanisms have many similarities. Researchers have argued that for many material-environment combinations, the same mechanism is at play.[7] Although some authors suggest that crevice corrosion is a particular form of pitting corrosion, all pits are crevices as "pits cannot be stable until a crevice-like cavity develops."[8] It is important to emphasize that crevice corrosion resistance is not a property of a material. In this regard, the response of a particular alloy system to a given environment determines the crevice corrosion susceptibility. For example, iron and carbon steels do not suffer crevice corrosion in strong acids because they do not develop a passive film but rather become susceptible in alkaline environments free of aggressive species in which a passive film is thermodynamically stable.[9]

CREVICE GEOMETRY

A crevice is formed when two surfaces, at least one being metallic, are in proximity and are immersed in an electrolyte that can promote crevice corrosion. Examples of materials that can cause crevice corrosion include metals, wood, plastics, ceramics, rubbers, glasses, concrete, asbestos, waxes, sand deposits, marine growth, and coatings.[3,10–12] Figure 1 illustrates an idealized crevice. As seen in figure 1, the crevice geometry is described by the opening or gap (g) and the length (L), measured as the distance from the crevice mouth.[3] The gap has to be wide enough to allow the ingress of the solution, but sufficiently tight to promote the formation of an occluded environment within the cavity. Openings between 0.1 and 100 µm have been found to cause crevice corrosion.[2] Crevice corrosion rarely occurs in wide (e.g., >3 mm) grooves or slots. Thus, the crevice is divided into two regions: the external surface that is freely exposed to the environment and the shielded or creviced area exposed to a stagnant solution.

The gap in a real crevice is not a fixed value. Indeed, at the microscale, the two mating surfaces have a series of ridges and asperities, as shown by the surface profiles in the call-out in figure 1. The surface profiles seen in figure 1 correspond to an ASTM A480, *Standard Specification for General Requirements for Flat-Rolled Stainless and Heat-Resisting Steel Plate, Sheet, and Strip*, surface finish no. 1 with a peak-to-peak distance of approximately 15 µm.[13] As a result, a real crevice has a complex and distributed geometry that cannot be defined rigorously, resulting in "a wide range of crevice gaps, including areas of direct, intimate contact."[2]

OBJECTIVES

Today, a large number of accepted tests are available to study crevice corrosion phenomena. The different methodologies can be used to compare and rank alloys, conduct quality control, assess the effects of changes in manufacturing routes and alloy composition on crevice corrosion resistance, and determine critical temperatures and potentials and induction times.

This chapter describes the various standard test methods available to the corrosion specialist as well as adaptations to

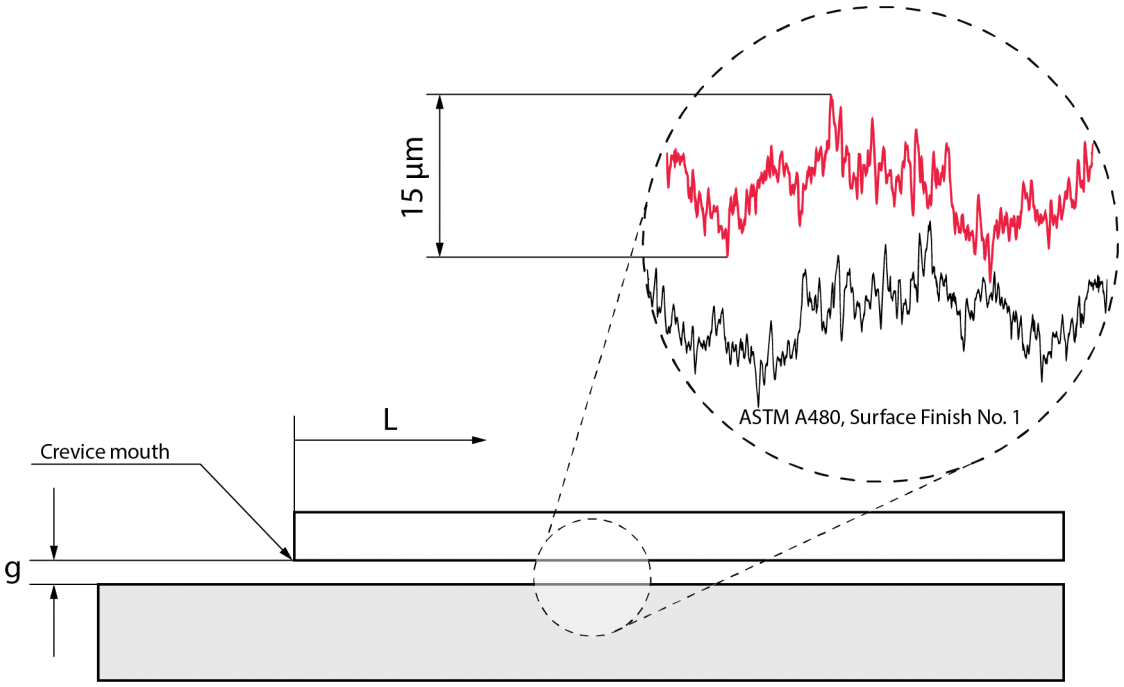
[1]Curtin Corrosion Centre, Curtin University, GPO Box U1987, Perth WA 6845, Australia

The authors acknowledge the previous authors of this chapter, Narsi Sridhar, Darrell S. Dunn, C. S. Brossia, and Gustavo A. Gragnolino, Southwest Research Institute, San Antonio, TX.

DOI: 10.1520/MNL202NDSUP20190034

Copyright © 2022 by ASTM International, 100 Barr Harbor Dr., PO Box C700, West Conshohocken, PA 19428-2959
ASTM International is not responsible, as a body, for the statements and opinions expressed in this chapter. ASTM International does not endorse any products represented in this chapter.

FIG. 1 Geometry of crevice corrosion. In the sketch, the horizontal scale is arbitrary.



study specific crevice corrosion parameters and prevention strategies (e.g., the use of inhibitors). The focus is on test methods developed by the ASTM Committee G-1 on corrosion of metals, but other procedures also are included. Although the test principles have been applied to many alloy systems, the scope of the chapter is on stainless steels and nickel-based alloys.

CREVICE CORROSION MECHANISMS

Differential Aeration and Chloride Concentration

It was realized early on that the metals and alloys that were easily passivated were also those that appeared more susceptible to crevice corrosion.[14] Mears and Evans[10] and Uhlig[15] were the first to propose that oxygen depletion within the crevice was the main driving force leading to the destabilization of the passive film inside the cavity. A mechanism solely based on concentration cells, however, has failed to explain many experimental observations.[16]

In the 1950s, Rosenfeld and Marshakov[17] pioneered crevice corrosion experimental methods. The authors suggested that crevice corrosion occurred through a combination of (1) depletion in oxygen (or a corrosion inhibitor) in the crevice, (2) local acidification, and (3) shift in the potential to more negative values, where active dissolution would take place. Many of the modern crevice corrosion principles are based on these findings by Rosenfeld and Marshakov.

It is now well established that the mechanisms that drive a growing crevice are identical to those promoting a growing pit.[8] In this regard, when a passive metal or alloy (e.g., an austenitic stainless steel, such as UNS S30400), partially covered by a nonmetallic surface is exposed to aerated seawater (pH = 8.0), the electrochemical reactions are the dissolution of the metal and the reduction of dissolved oxygen, equations (1) and (2).[3]

$$\mathrm{Me} \rightarrow \mathrm{Me}^{z+} + ze^{-}, \text{ and} \tag{1}$$

$$\mathrm{O_2} + 2\mathrm{H_2O} + 4e^{-} \rightarrow 4\mathrm{OH}^{-} \tag{2}$$

Initially, these reactions occur inside and outside the crevice. After a given time, oxygen is depleted inside the cavity because of restrictions imposed by convection within the occluded surface. The dissolution of the metal continues within the crevice, resulting in excess of metal cations (e.g., iron [II], chromium [III], aluminum cations). As the corrosion process continues, the concentrated metal cations within the stagnant cavity hydrolyze according to equation (3), which results in the formation of hydrogen ions (H^+).[18–20] The excess of metal cations is necessarily balanced by the migration of anions, such as chloride ions (Cl^-), from the bulk into the cavity, which ensures charge neutrality. As a result, the concentration of metal chlorides increases inside the crevice.

$$Me^{z+} + \mathrm{H_2O} \rightarrow \mathrm{Me}OH^{(z-1)+} + \mathrm{H}^{+}. \tag{3}$$

The formation of a local acidic environment increases the metal dissolution rate in the crevice, producing more protons, and further increasing the Cl^- concentration. This process is often referred to as autocatalytic. Concurrently, the oxygen reduction reaction accelerates on the outer surface to counteract the increased metal dissolution rate within the cavity, cathodically protecting the external surface.[3] Active metal dissolution occurs when the crevice solution concurrently has (1) a sufficiently low pH and (2) a high concentration of Cl^-.[21] The pH at which the passive-to-active transition takes place is referred to as depassivation pH (pHd).[21] Oldfield named the solution that leads to the depassivation of the alloy within the crevice gap "critical crevice

solution" (CCS).[22] The formation of the CCS represents the transition from the initiation to the propagation stage. Although this model phenomenologically explained most experimental observations, it failed to rationalize the existence of a critical potential, above which crevice corrosion develops.[9] In this regard, the primary limitation of Oldfield and Sutton's model is that it considered that the dissolution of cations (and their consequent hydrolysis) was proportional to the passive current density, i_{pass}. Because i_{pass} is constant over a broad potential range, the model is unable to account for the existence of critical potentials, both initiation and repassivation potentials. Moreover, Oldfield and Sutton's description cannot consider the effect of inhibitive species (e.g., fluorides), which increase the passive current density of UNS Alloy 22 (UNS N06022) in hot chloride environments.[23]

The Critical Acidification Model

Galvele[18] and later Oldfield and Sutton[21,24] were the first to consider the transport of species in and out of pits and crevices. These models have since been improved and expanded to provide, in some instances, not just conceptual observations but also numerical solutions.[20,25,26] Galvele proposed that because crevice corrosion is believed to be the result of localized acidification, crevice corrosion could be described by the critical "x·i" parameter (referred to as pitting or crevice stability product) used in his mathematical framework.[9] In the pitting or crevice stability product, *x* represents the diffusion path and *i* the current density of a pit or crevice, as shown in figure 2.[18] Localized corrosion propagates stably above a critical *x·i* value, which is constant for a given material in a specific electrolyte. According to Galvele and later Newman,[8] pitting and crevice corrosion are similar from an electrochemical point of view; the only difference being the geometric characteristics of the sample (i.e., a different diffusion path). Accordingly, the critical potential for stable crevice propagation (E_{Crit}) can be described as follows:

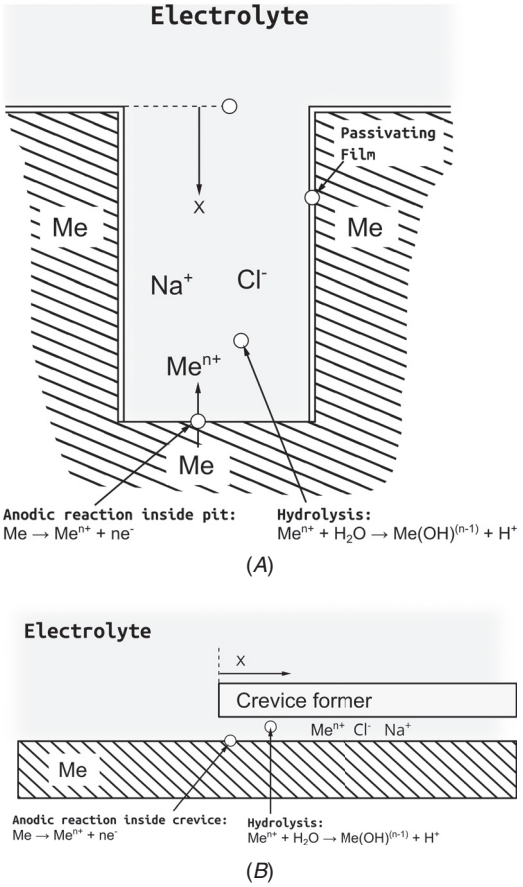
$$E_{Crit} = E^*_{Corr} + \eta + \Phi + E_{inh} \quad (4)$$

where:

E^*_{Corr} = corrosion potential in a simulated crevice electrolyte,
η = polarization needed to reach the critical x·i value,
Φ = electrical potential induced by the migration of the aggressive anions to the crevice (or the bottom of a pit), and
E_{inh} = contribution of the presence of inhibitors in the solution.[16]

However, E_{inh} cannot always be experimentally separated from other factors.[27,28] The validity of equation (4) has been first confirmed by Newman et al.[29] and studied in numerous investigations.[27,30–35] The different parameters in equation (4) can be measured experimentally by conducting anodic polarization experiments in crevice-like solutions.[32–34,36] The effects of alloying elements on the crevice corrosion resistance are reflected in changes in E^*_{Corr} and η.[34,35] Equation (4) also explains why certain metals and alloys are susceptible to crevice corrosion but not to pitting. Indeed, η can be used as a measure of the crevice corrosion resistance of an alloy.[30–34] In this regard, the larger the value of η, the broader the range of potentials in which crevice corrosion would be exclusively observed. For stainless steels and nickel alloys, the values of η range from +470 to +1,000 mV, which explains why crevice corrosion occurs much more readily than pitting.[34]

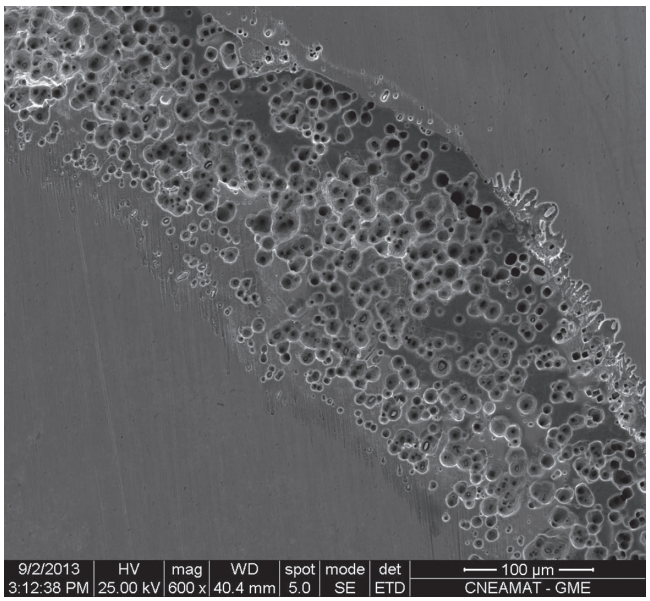
FIG. 2 (*A*) Unidirectional pit and (*B*) crevice model.



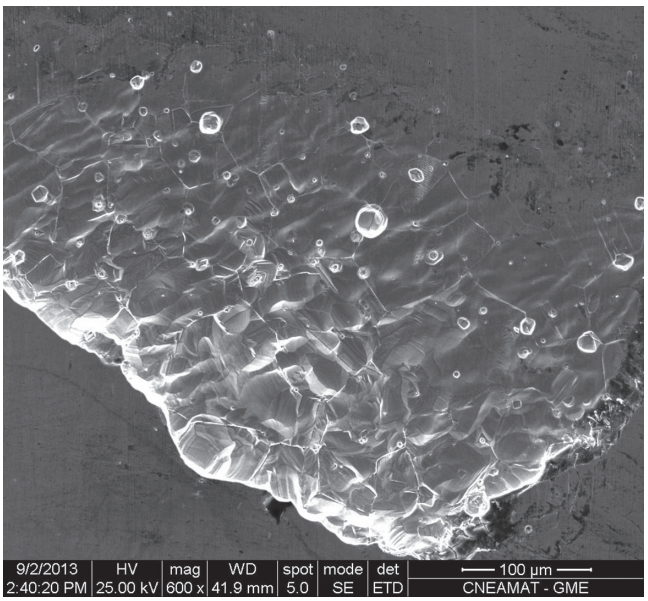
As discussed by Galvele, Wood et al. provided a clear experimental demonstration of the correlation between pitting and crevice corrosion.[37] In their pioneering work, the authors conducted potentiostatic experiments on freely exposed and creviced UNS S30400 stainless steel samples. The crevice was formed using glass microscope covers, leading to *g* values between 50 and 150 μm. The samples were exposed to 5 wt% sodium chloride (NaCl) (pH = 8.0) at room temperature. Wood et al. found that at +600 mV_{SCE}, pitting corrosion initiated not only on the outer surface but also inside the crevice. In contrast, when new samples were polarized at +400 mV_{SCE}, the attack occurred exclusively inside the crevice. Crevice corrosion started as individual pits that spread laterally as the attack progressed, leading the authors to the idea that crevice corrosion is "lateral pitting" within the crevice gap.

Today, it is accepted that the accelerated attack within the crevice can manifest as uniform dissolution, pitting, or both.[24] Figure 3 illustrates three common forms of corrosion attack occurring inside a crevice on different stainless steels. Stockert and Boehni,[38] and later, Laycock, Stewart, and Newman,[8] suggested that pit nucleation within crevices occurs even at small applied potentials, resulting in measurable current noise. The current and, hence, the dissolution rate increase sharply above

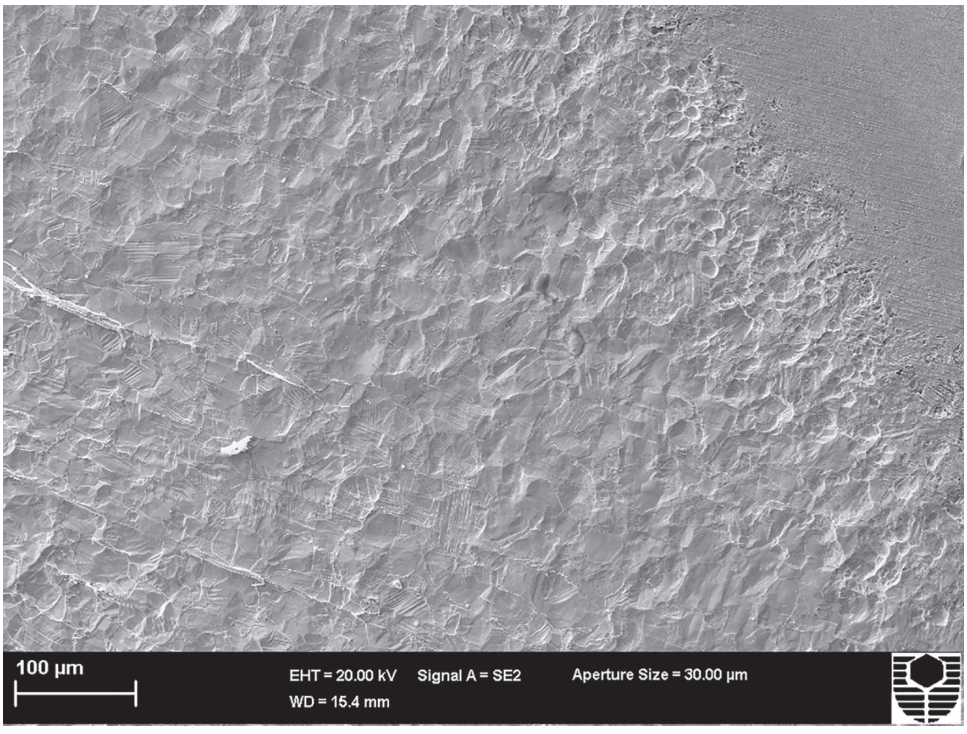
FIG. 3 Different crevice attack morphologies: (*A*) pitting corrosion inside the crevice gap on UNS S30403 in 0.1M NaCl at 60°C, (*B*) pitting and general dissolution with the crevice gap on UNS S31600 in 0.1M NaCl at 30°C, and (*C*) uniform crevice attack on UNS S31603 in 6 wt% $FeCl_3$ at 20°C.



(*A*)



(*B*)



(*C*)

the $E_{Crit,}$ and stable pit propagation takes place and leads to the formation of metal-chloride salts.

OHMIC POTENTIAL DROP

The passage of current from the external surface to the crevice through a solution of finite conductivity results in an ohmic potential drop and, thus, the potential inside the crevice will be lower (i.e., more negative) than at the surface. In systems that exhibit an active-passive behavior in the bulk electrolyte, the ohmic potential drop in the crevice can stabilize pit growth by decreasing the local potential into the active range.[39] This mechanism, proposed by Pickering, does not apply to a system in

which an active-to-passive transition does not occur. Indeed, in systems that show spontaneous passive behavior, a decrease in potential has a negative effect on crevice corrosion stability.

STAGES OF CREVICE CORROSION

The crevice corrosion process, then, can be summarized in four stages, as follows: (1) oxygen consumption within the crevice, (2) increase in H^+ and Cl^- in the crevice, (3) stabilization of a critical H^+ concentration above a threshold x·i value, and (4) propagation. The first stage is key for carbon and low alloy steels in alkaline solutions, which suffer corrosion by differential concentration cells,[40] but it is of less importance for passive alloys. Conversely, the second stage is crucial to explain the depassivation of passive alloys. In this regard, the migration of chlorides supports the reduction in pH resulting in an acidic solution of lower pH than predicted only by cation hydrolysis, because a high concentration of chlorides results in a higher activity coefficient for protons (H^+).[41,42]

Given the similarities between pitting and crevice corrosion discussed earlier, it is reasonable to conceptually adapt the Li-Scully-Frankel (LSF) framework to describe crevice corrosion.[43–46] Thus, the state of a crevice can be fully described in terms of a critical potential (E_{Crit}), a critical temperature (T_{Crit}), and an induction time. The existence of E_{Crit} has been discussed. Temperature has a strong influence on localized corrosion phenomena.[47] Experimentally, pitting and crevice corrosion are observed only above specific temperatures (referred to as critical pitting or crevice temperature, CPT and CCT, respectively) that are usually defined within a narrow 1–2°C range.[48–50] The length of time required to develop a critical crevice solution with a particular crevice geometry, that is, a given "x" in the *x·i* stability product, is referred to as induction time. In this regard, the induction time can be seen as a measure of the effective crevice corrosion resistance of an alloy. Crevice corrosion occurs at lower temperatures and in less time (a shorter induction period) than pitting corrosion.[47,51]

A detailed discussion of the different crevice corrosion mechanisms is outside the scope of this chapter. More information on localized corrosion models and mechanisms can be found in the excellent reviews by Betts and Boulton,[3] Pickering,[52] Frankel et al.,[53] Frankel,[54] and Newman.[55]

Test Methods to Assess Crevice Corrosion Resistance

Different classification schemes could be used to group crevice corrosion test methods. Herein, the tests are divided into two main groups: (1) immersion or nonelectrochemical and (2) electrochemical testing. Electrochemical methods, in turn, are further classified as tests with and without external polarization. Likewise, methods that use an external polarization are subdivided into potentiostatic and potentiokinetic methods. Table 1 to Table 4 summarize the most common standard and custom crevice corrosion techniques. The tables are organized based on the categories described previously. Tables 1 to 4 illustrate the uses, exposure conditions, the type of crevice assembly, the duration, the procedure, and the recommended assessment, among other experimental considerations. For more details, consider some of the excellent works cited in this chapter.[21,22,24,56–59]

THE CREVICE FORMER

Before describing the various crevice corrosion test methods, it is necessary to discuss the use of crevice formers, in particular, the multiple-crevice assembly (MCA) as a means to rank and evaluate crevice corrosion resistance. Described by Anderson in the late 1970s, MCAs were first introduced to study crevice corrosion of stainless steels in seawater.[60] Today, MCAs are used not only on stainless steels, but also nickel, titanium, and aluminum alloys in virtually any process environment.[58,61,62]

An MCA is composed of several grooves and plateaus—typically between 12 and 20 slots—with a depth of approximately 0.5 mm. The purpose of the serrations is to create several crevice initiation sites within a single specimen, which should allow for statistical analysis with a few replicate tests.[58] MCAs are commonly made of polytetrafluoroethylene (PTFE), polychlorotrifluoroethylene (PCTFE), polyvinylidene difluoride (PVDF), ceramic, and PTFE tape-covered ceramic. The contact area of each crevice contact and the total contact area are important variables that need to be reported. Figure 4*A* illustrates the various parts of a typical MCA that complies with ASTM G48, *Standard Test Methods for Pitting and Crevice Corrosion Resistance of Stainless Steels and Related Alloys by Use of Ferric Chloride Solution*.[63] In figure 4*A*, the bolts and nuts are made of highly corrosion-resistant materials, typically titanium grade 2 (UNS R50400) or a nickel-based alloy, such as UNS N10276 or UNS N06022. The bolts and nuts are electrically insulated from the test specimen using, for example, PTFE tape or a polymer insert.[64]

It has long been recognized that the tightness of a crevice former has a profound effect on the crevice corrosion severity, which in the laboratory is usually controlled by the applied torque. Akashi, Nakayama, and Fukuda studied, among other variables, the effect of torque on the crevice repassivation potential ($E_{R,Crev}$).[65] The authors found that if the torque was "too low" (i.e., below 0.98N·m) $E_{R,Crev}$ moved toward higher potentials, indicating a less severe crevice. For torque values between 0.98 and 3.9 N·m, however, $E_{R,Crev}$ became stable and reproducible. Presently, ASTM G48 recommends a torque of 0.28 and 1.54 N·m for nickel alloys and stainless steels, respectively. However, researchers have used torque values from 0.28 to 9.5 N·m with varying degrees of success.[33,66]

Shan and Payer investigated the effect of the crevice former material (i.e., polymer versus ceramic) as well as the influence of the surface finish of the MCA.[66] The authors used potentiokinetic and potentiostatic test methods and evaluated PTFE, PCTFE, ceramic, and PTFE tape-covered ceramic crevice formers on UNS N06022 (Alloy C22). Results showed that PTFE tape-covered MCAs produced systematic and reproducible crevice corrosion of Alloy C22 in all tests. In contrast, as-fabricated ceramic crevice formers were not sufficiently severe. The severity increased as the MCA was polished to 1,200 US-grit before assembly. Polymeric PTFE and PCTFE MCA were also less severe than the PTFE tape-covered formers, possibly because of

TABLE 1 Comparison of Nonelectrochemical Test Methods to Evaluate Crevice Corrosion Resistance

Method	Summary	
ASTM G48 Method B (rubber band)	Uses	• Pitting and crevice resistance in chloride environments. • Rank alloy performance. • Applicable to stainless steels and nickel-base alloys.
	Exposure conditions	• Electrolyte: 6 wt% $FeCl_3$ (unadjusted pH approx. 1.0–2.0) • Recommended test temperatures: • 22 ± 2°C • 50 ± 2°C • Other values could be used.
	Crevice assembly	• Cylindrical TFE-fluorocarbon blocks. • Fluorinated O-rings or rubber bands (low S).
	Test duration	• 72 h (recommended). • Variations are allowed, which depend on the alloy composition. • Periodic extractions are possible (could lead to variations in the rate of attack).
	Assessment	• Visual inspection (ASTM G46 suggested). • Weight loss to 0.001 g or better accuracy.
ASTM G48 Methods D & F	Uses	• Determine the critical crevice temperature (CCT). • Nickel-base and chromium-bearing alloys: Method D. • Stainless steels: Method F. • It can be used to rank alloy performance.
	Exposure conditions	• Electrolyte: 6 wt% $FeCl_3$ + 1 wt% HCl (pH adjusted approx. 1.0). • Start temperature (nearest 5°C): • Method D: (1.5 × %Cr) + (1.9 × %Mo) + (4.9 × %Nb) + (8.6 × %W) – 36.2. • Method F: (3.2 × %Cr) + (7.6 × %Mo) + (10.5 × %N) – 81.0. • Minimum Temperature: 0°C • Maximum recommended temperature: 85°C.
	Crevice assembly	• Multiple-crevice assembly (MCA) • TFE-fluorocarbon segmented washers. • Different materials and geometries are allowed. • Torque • Method D: 0.28 Nm (40 in-oz). • Method F: 1.58 Nm (14 in-lb).
	Test duration	• Method D: 72 h. • Method F: 24 h.
	Assessment	• Visual assessment (could follow ASTM G46): Crevice corrosion is present if local attack >0.025 mm (0.001 in) in depth. • Weigh loss.
ASTM G78	Uses	• Determine the crevice corrosion susceptibility in seawater and other chloride environments. • Applicable to iron- and nickel-base alloys. • It can be used to assess the crevice induction time. • It can be used to determine the critical crevice temperature.
	Exposure conditions	• Seawater, natural waters, and chloride-containing aqueous electrolytes. • Temperature: User-defined and maintained within ± 2°C.
	Crevice assembly	• Many different configurations are allowed, for example, MCA (various geometries and materials), O-rings, gaskets, strips, coatings (for complex geometries).
	Test specimens	• Flat, cylindrical, and complex geometries are allowed. • Specimens should maintain a constant bodily exposed to shielded area ratio.
	Test duration	• 30 days (recommended). • Sampling at different time intervals is allowed.
	Assessment	• Visual assessment: • Maximum crevice depth. • Affected area. • If using MCA, the number of segments showing crevice corrosion. • Weight loss.

TABLE 2 Comparison of Electrochemical Test Methods with No External Polarization to Assess Crevice Corrosion Resistance

Method	Summary
Corrosion Potential Monitoring	• The initiation of pitting and crevice corrosion in stainless steels and nickel-based alloys leads to a sharp decrease in the corrosion potential (E_{Corr}). • E_{Corr} monitoring can be used to determine induction times. • If done as a function of temperature, E_{Corr} monitoring can be used to determine critical temperatures. • Standards such as ASTM G48 and G78 can be modified to include open circuit potential (OCP) monitoring. E_{Corr} measurements during ASTM G48 testing can provide a better pass/fail criterion than visual inspection alone. • Because it is nondestructive, E_{Corr} measurements provide a means for field monitoring.
Zero Resistance Amperometry (ZRA)–Remote Crevice Assembly	• The remote crevice assembly consists of a creviced sample connected to a noncrevice specimen through a zero-resistance ammeter. • The ZRA measures galvanic current and couple potential. • It simulates a real crevice setting. • The initiation of crevice corrosion is associated with a sharp increase in current. • ASTM G71 can be used as a guide. • There is no agreement on a critical current value to define crevice initiation.
ZRA–Electrochemical Noise	• Similar to the remote crevice assembly except that it uses two creviced coupons. • Electrochemical current noise is recorded and analyzed over time. • The start of the crevice attack leads to an increase in current (it can be positive or negative depending on the specimen where the attack initiates). • ASTM G199 can be used as guidance.

TABLE 3 Comparison of Potentiostatic Electrochemical Test Methods to Assess Crevice Corrosion Resistance

Method	Summary	
Chronoamperometry	• Chronoamperometry consists of measuring current (or current density) as a function of time at a constant applied potential. • It can be performed using creviced or crevice-free specimens. • Chronoamperometry is primarily used to determine induction times. • When performed at different temperatures, it can be used to determine critical temperatures. • It can also be used to determine the critical repassivation temperatures ($T_{R,\ Crev}$) by reducing the temperature after crevice initiation.	
ASTM F746	Uses	• Assess the pitting or crevice corrosion resistance of metals and alloys for surgical implants. • Determine the critical potential, E_{Crit}, to initiate pitting, crevice, or both. • Laboratory screening.
	Exposure conditions	• Electrolyte: Phosphate Buffered Saline (PBS) solution ($7.3 < pH < 7.5$). • Temperature: $37 \pm 1°C$
	Test specimen	• Cylindrical coupons: 6.35 mm in diameter and 20 mm in length. • Surface preparation: 600-grit SiC paper.
	Crevice assembly	• Tapered PTFE collar (3.18 mm width). • Force-fit to 10mm from the base of the cylinder
	Procedure	• Step 1: Measure the corrosion potential for 1-h, referred to as E_1. • Step 2: Stimulation • The purpose is to initiate localized corrosion. • The applied potential, E_{App}, is set to $+800\ mV_{SCE}$. • The duration depends on the current response: • If i instantly $> 500\ \mu A \cdot cm^{-2}$ decrease potential to E_1. • If current generally increases, but $i < 500\ \mu A \cdot cm^{-2}$, decrease E_{App} to E_1 after 20 s. • If after 15 min, there is no sharp increase in current, terminate the test. • Step 3: Repassivation • Decrease E_{App} so that $E_{App} = E_1$. • If no repassivation, $E_{Crit} = E_1$. • If repassivation occurs: • After stimulation the new $E_{App} = E_1 + 50$ mV. • Repeat until no repassivation after stimulation.

(continued)

TABLE 3 (*continued*)

Method	Summary	
	Assessment	• E_{Crit} (pitting or crevice) • Visual examination.
Modified ASTM G150	Uses	• Determine the potential independent pitting (or crevice) temperature. • Predict the conditions resulting in stable crevice propagation. • Applicable to stainless steels from UNS S31600 to S31254, but could be extended to other alloys.
	Exposure conditions and procedure	• Electrolyte: Deaerated, 1 M NaCl (unadjusted pH). • Temperature: Start at 0°C, ramp at 1°C/min. • Potentiostatic polarization: • +700 mV_{SCE} (recommended). • Other values are possible. • A test at +800 (or+ 600) mV_{SCE} can be performed to determine changes in CPT
	Test specimen	• Modified to include creviced coupons.
	Assessment	• CCT (CPT) defined as the temperature at which $i > 100\ \mu A \cdot cm^{-2}$ for 60 s. • Visual confirmation.

TABLE 4 Comparison of Potentiokinetic Electrochemical Test Methods to Assess Crevice Corrosion Resistance

Method	Summary	
Modified ASTM G61	Uses	• Determine the relative susceptibility to localized corrosion (pitting and crevice corrosion). • Determine critical potentials, for example, E_{Crev} and $E_{R,Crev}$ if using crevice formers. • If done at different temperatures, determine the critical crevice temperature, often referred to as electrochemical critical temperature. • Check one's experimental technique and instrumentation. • Applicable to Iron, nickel, and cobalt-base alloys, but it could be used for other passive alloys. • It shall not be used to correlate with the rate of propagation.
	Exposure conditions	• Electrolyte: Deaerated 3.56 wt% NaCl (neutral pH), but other solutions can be used. • Temperature: 25 ± 1°C (recommended), but it can be done at different temperatures.
	Test specimens	• Modified to include creviced specimens.
	Procedure	• Step 1: 1-h corrosion potential stabilization. • Step 2: Potentiokinetic polarization: • Scan rate: 0.6 V/h (0.168 mV/s). • Scan reversal at $i = 5\ mA \cdot cm^{-2}$. • Stop test once hysteresis loop closes or once reaching E_{Corr}.
	Assessment	• E_{Crev} and $E_{R,Crev}$ (or E_P and E_{RP} without crevice former). • Hysteresis, $\Delta E = E_{Crev} - E_{R,Crev}$. • Visual confirmation.
ASTM G192 Tsujikawa-Hisamatsu Electrochemical (*THE*) test or PD-GS-PS	Uses	• Determine $E_{R,Crev}$ for corrosion-resistant alloys. • It is understood that an alloy will not develop crevice corrosion below $E_{R,Crev}$ under the tested conditions (i.e., electrolyte composition, pH, temperature). • It can be modified to determine the crevice repassivation temperature ($T_{R,Crev}$). • Applicable to any corrosion-resistant alloy, but developed for UNS N06022.

(continued)

TABLE 4 (*continued*)

Method	Summary	
	Exposure conditions	• Electrolyte: • It can be used with any electrolyte. • Developed using 1 M NaCl (unadjusted pH). • Temperature: • 90°C (UNS N06022). • Lower temperatures can be used for less resistant alloys.
	Procedure	• Step 1 – Potentiodynamic polarization: • 0.6V/h (0.168 mV/s). • Until a preset current is reached (2 $\mu A \cdot cm^{-2}$ for UNS N06022) • Step 2 – Galvanostatic period • The preset current is kept constant for 2 h. • *E* versus *t* is recorded. • The goal is to develop and grow crevice attack (if any develops). • Step 3 – Potentiostatic polarization • The potential is decreased by 10 mV internals. • The duration of each step is 2 h. • *I* versus *t* is recorded at each step.
	Assessment	• $E_{R,Crev}$ is defined as the highest potential for which the current does not increase as a function of time. • $E_{R,Crev}$ and visual confirmation.
PD-GS-PD technique	• The PD-GS-PD technique is a simplification of the *THE* test. • Step 3 is replaced by a potentiodynamic polarization step. • $E_{R,Crev}$ is defined as a crossover potential. • It can be used to determine $T_{R,Crev}$.	

the relaxation of the polymers by creep at the elevated temperature range of the tests. Figure 4*B* illustrates a typical PTFE tape-covered MCA on an Alloy C22 sample.

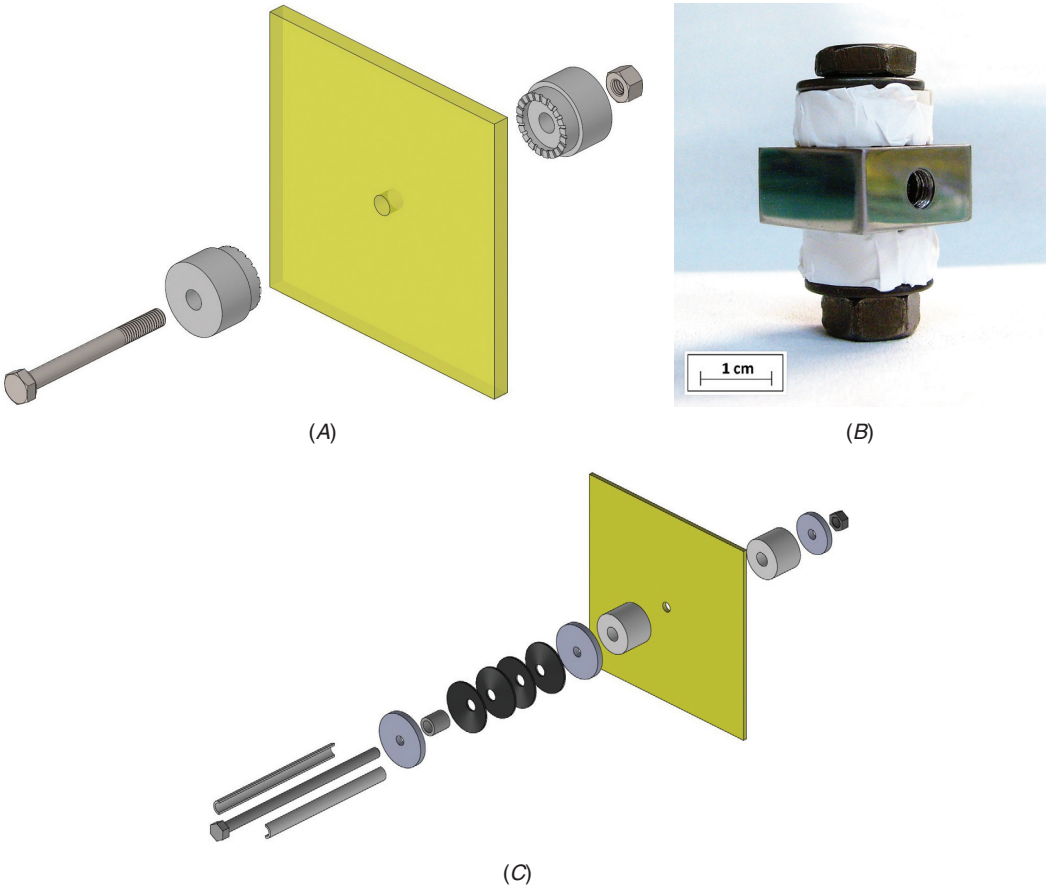
In Europe, research was undertaken as part of the CREVCORR project—funded by the European Community between the years 2000 and 2003 under the Competitive and Sustainable Growth Programme—to develop a crevice corrosion qualification test for stainless steels used in marine environments.[67] The outcome of the CREVCORR project is presented in detail in the European Federation of Corrosion (EFC) Publication No. 60 "Methodology of Crevice Corrosion Testing for Stainless Steels in Natural and Treated Seawaters."[68] Regarding the type of crevice former, the CREVCORR project concluded that a spring-loaded crevice assembly, referred to as disc spring multiple crevice assembly (DSMCA), was the most suitable artificial crevice former.[69] The DSMCA uses a flat polyvinylidene chloride (PVDC) crevice former and employs disc springs to maintain a constant force instead of constant torque during testing, which is especially critical in long-term immersion tests at elevated temperatures.[70] Figure 4*C* details the CREVCORR crevice configuration. The CREVCORR project also adapted the DSMCA configuration to evaluate stainless steel pipes. Finite-element modeling was employed to quantify the clamping force distribution and the uniformity of the crevice condition within the crevice former.[71]

He, Noël, and Shoesmith[72] and Jakupi, Noël, and Shoesmith[73] developed a single crevice array to study crevice corrosion of highly resistant alloys, including titanium grade 2 and Alloy 22 (UNS N06022) at high pressure, high temperature, or both. The crevice electrode consists of a PTFE crevice former of a known area centered and pressed between two flat coupons—one cut from a plate of the metal or alloy of interest and the other cut from a thick polysulfone plate. The crevice assembly is formed by tightening the plates using corrosion-resistant bolts and nuts. The tightness is adjusted with the help of a PTFE "feeler," as described by the authors, using open-faced wrenches.[72] The approach was used by He, Noël, and Shoesmith to construct corrosion damage functions[74] as well as to determine the influence of temperature on crevice corrosion susceptibility.[72] Many other nonstandard methods have been used by researchers to create artificial crevices for different purposes. For a more in-depth explanation, consult the work by Oldfield[22] and Kain.[62]

Nonelectrochemical Test Methods

Nonelectrochemical immersion tests involve immersing a creviced specimen for different lengths of time in solutions that often contain anions that promote crevice corrosion such as chlorides and, in some instances, an oxidizing agent that facilitates the initiation of crevice corrosion (e.g., Fe^{3+} cations). The crevice corrosion resistance, then, is determined based on mass loss and visual observations. Visual characterizations include crevice depth, number of crevice sites, location of the crevice attack within the cavity, and the corrosion morphology.

FIG. 4 Different types of MCAs: (*A*) serrated MCA and Ti Gr. 2 bolts and nuts compliant with ASTM G48, (*B*) assembled PTFE tape-covered ceramic MCA, and (*C*) a CREVCORR DSMCA setup.



ASTM G48 is the most commonly used standard to assess pitting and crevice corrosion resistance of stainless steels and nickel-based alloys and to provide a quantitative ranking of crevice corrosion resistance. The current version of ASTM G48 (2011, reapproved in 2015) has six text methods. Methods A, C, and E cover pitting corrosion resistance, whereas Methods B, D, and F describe different techniques to assess crevice corrosion susceptibility. Additionally, ASTM G78, *Standard Guide for Crevice Corrosion Testing of Iron-Base and Nickel-Base Stainless Alloys in Seawater and Other Chloride-Containing Aqueous Environments*, details guidelines to evaluate the crevice corrosion resistance of iron- and nickel-based alloys in seawater and other chloride environments.

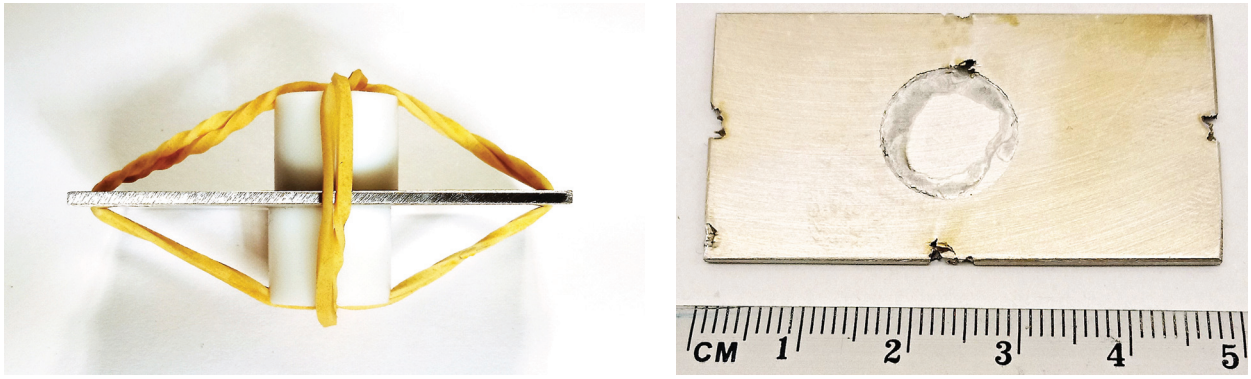
Although ASTM G48 Methods B, D, and F and ASTM G78 are discussed in detail in the following sections, for a comprehensive description, consult the latest versions of these standards.

ASTM G48 METHOD B: THE RUBBER BAND TEST

ASTM G48 Method B is used to assess the pitting and crevice corrosion resistance of stainless steels and nickel-based alloys to chloride-containing environments. The procedure involves immersing a creviced specimen in a 6 wt% iron (III) chloride ($FeCl_3$; equivalent to 10 wt% $FeCl_3 \cdot 6H_2O$) solution (unadjusted pH = 1.0 to 2.0),[75] designed to produce localized corrosion of UNS S30400 (type 304) stainless steel at room temperature. The relative performance of alloys in 6 wt% $FeCl_3$ correlated well with their performance in natural seawater at ambient temperature[76] and strongly oxidizing, low-pH, chloride-containing environments,[22] but exceptions also have been reported.[11,22,77,78]

The standard recommends 22 ± 2 and $50 \pm 2°C$ for the evaluation, but other values could be used depending on the expected corrosion resistance of the alloy. The artificial crevice is formed using two TFE-fluorocarbon blocks, 12.7 mm in diameter and 12.7 mm in height, secured by fluorinated O-rings or rubber bands that should be low in sulfur (i.e., <0.02%). The surface roughness of the crevice formers is not specified. A 25 by 55 mm test specimen is recommended as the standard size, but other dimensions are allowed. According to the standard, both the surface finish and the thickness of the coupons can influence the results. The standard also recommends storing the samples in air for 24-h after grinding or pickling and before testing to restore the naturally occurring passive film. Figure 5*A* illustrates a typical test specimen before exposure.

FIG. 5 ASTM G48 Method B (*A*) type 304 stainless steel creviced specimen before exposure and (*B*) crevice corrosion attack after immersion in 6 wt% $FeCl_3$.



(*A*) (*B*)

After assembling the crevice formers, the coupons are immersed in the electrolyte for 72 h, but other exposure times also are permitted. The standard, likewise, allows for sample removal and inspection; nevertheless, care should be exercised because sample withdrawals could lead to variations in the rate of attack. After the predetermined exposure duration, the samples are removed from the solution, visually inspected, and weighted with a minimum accuracy of 0.001 g. ASTM G46, *Standard Guide for Examination and Evaluation of Pitting Corrosion*, can be used to characterize the extent of the attack.

The rubber band method is inexpensive, easy, fast to assemble, and produces useful comparative results in a short time. The ASTM G48 Method B technique, however, has a few disadvantages and limitations. For example, as shown in figure 5*B*, in certain alloys, particularly the less alloyed materials, such as type 304 stainless steel, crevices can initiate at the contact point between the rubber bands and the specimen. Indeed, similar approaches were used in classical corrosion lectures to demonstrate that stainless steels could be "cut in half" with a rubber band.[16] Likewise, the test is invalid if either rubber band or O-ring breaks during testing, and the compressive pressure exerted by the rubber band onto the crevice formers is not uniform and can be difficult to replicate. Moreover, DeForce has shown that the type of rubber band used affects the results.[79] According to the author, "specifying the rubber band elasticity (or rubber content) can improve the repeatability of ASTM G48 Method B." Last, although the mass loss is recorded after testing, there is currently no acceptance criterion. Producers and end-users have commercially accepted criteria, such as a maximum of 0.038 mm crevice depth and 0.2 mg/cm^2 mass loss. In all cases, the user and the vendor should agree on the pass or fail criteria.

ASTM G48 METHODS D AND F: CREVICE CORROSION TEMPERATURE

ASTM G48 Methods D (nickel- and chromium-bearing alloys) and F (stainless steels) overcome some of the limitations of the rubber band technique and allow the determination of the critical crevice temperature (CCT) of a material. In the standard, the CCT is defined as the minimum temperature, in degrees Celsius, to produce crevice attack at least 0.025-mm deep on the bold surface of a specimen beneath the crevice former, ignoring edge attack. The methods also can be used to rank alloy performance, aid in materials selection, and the design of new materials.[56,80–83]

Methods D and F involve immersing creviced samples in acidified 6 wt% $FeCl_3 + 1$ wt% hydrochloric acid (HCl; pH adjusted to pH = 1.0) for a period of time. Both methods use TFE-fluorocarbon MCA, and various geometries and construction materials are allowed. Method D recommends a torque of 0.28 N·m, whereas Method F suggests 1.58 N·m for stainless steel. Authors also have reported, however, that applied torque values between 2 and 8 N·m were required to produce the most reproducible crevice corrosion results when evaluating highly corrosion-resistant nickel alloys.[84] The recommended duration of the immersion is 72 h (Method D) and 24 h (Method F). The length of the tests has been evaluated by interlaboratory testing.

The initial temperature of the test solution may be estimated using the empirical expressions shown in equations (5) and (6). The minimum temperature is 0°C and the maximum 85°C because of the thermal degradation of the ferric chloride electrolyte.

$$\text{Method D: } (1.5 \times \%\text{Cr}) + (1.9 \times \text{Mo}) + (4.9 \times \%\text{Nb}) + (8.6 \times \%\text{W}) - 36.2. \quad (5)$$

$$\text{Method F: } (3.2 \times \%\text{Cr}) + (7.5 \times \text{Mo}) + (10.5 \times \%\text{N}) + (8.6 \times \%\text{W}) - 81.0. \quad (6)$$

A chief limitation of equations (5) and (6) is that the empirical expressions consider the effects of bulk composition alone, without taking into account the influence of alloy microstructure. For example, sensitized and properly annealed stainless steels will have identical CCT values according to equation (5), yet the actual CCT will be drastically lower in the sensitized samples given the local depletion of chromium and molybdenum adjacent to, for example, chromium carbides.[85,86] Likewise, the

expressions fail to capture the complex and intricate effects of alloying elements. Moreover, the equations were obtained by regression analysis using a limited set of alloys.[86] Interestingly, alloy C-276, which has a nominal composition of 15.5 wt% chromium, 16 wt% molybdenum, and 4 wt% tungsten, would have a predicted CCT = 51.85°C, whereas the more corrosion resistant alloy C22 (22 wt% chromium, 13% molybdenum, and 3 wt% tungsten) should have a CCT of approximately 47°C.

Testing shall begin at the nearest increment of 5°C, estimated based on equations (5) or (6). The temperature shall be recorded and maintained within ±1°C during testing. Only one specimen is permitted per test vessel. The samples are removed at the end of the exposure, rinsed with deionized water, and scrubbed with a nylon brush under running water to remove loosely adhered corrosion products and are dried using compressed air or nitrogen gas.

The specimens are then visually inspected after cleaning, and the weight loss is measured with a precision of 0.001 g. The recommendations of ASTM G46 can be followed to quantify the crevice attack. During the visual examination, the location of the crevice attack shall be determined, as well as the number of MCA sites showing signs of crevice corrosion. A full characterization includes the determination of the greatest depth of attack. As per ASTM G48, crevice corrosion is considered to be present if the local attack is 25 μm or higher in depth, but the standard does not give any weight-loss acceptance criterion.

The CCT obtained by ASTM G48 must be interpreted with caution. Although CCT values are well defined within a narrow range of temperatures, the CCT is not a property of a material, but rather a function of the experimental methodology. The test technique, the composition of the environment, the resulting corrosion potential in the solution, and the presence of inhibiting species all influence CCT results. Indeed, high chloride concentrations, and corrosion potentials, and long exposure times tend to result in lower CCT.[87]

Researchers have shown that the critical pitting temperature (CPT) and the CCT follow a similar trend with alloy composition,[87] which traditionally has been captured in the pitting-resistant equivalent (PRE) expression. Different expressions have been proposed to define the PRE of stainless steels and nickel alloys, and a detailed discussion is outside the scope of the current chapter. For more information, the work of Malik et al.,[87] Lorentz and Medawar,[88] and Jargelius-Pettersson[89] can be consulted. Presently, various international standards, such as NORSOK M-001[90] and ISO 21457,[91] respectively, define PRE as follows:

$$\mathrm{PRE} = \%\mathrm{Cr} + 3.3 \times \%\mathrm{Mo} + 16 \times \mathrm{N}, \quad (7)$$

$$\mathrm{PRE} = \%\mathrm{Cr} + 3.3 \times (\%\mathrm{Mo} + 0.5 \times \mathrm{W}) + 16 \times \mathrm{N}. \quad (8)$$

In equations (7) and (8), the concentrations are given in weight percent. Qualitatively, the higher the PRE, the better the localized corrosion resistance of an alloy. Garner showed that both the CPT and the CCT of various stainless steels and nickel alloys correlated well with their respective PRE, that is, CCT increased with the degree of alloying, especially their molybdenum content.[76] CCT values also were lower than CPT. In this regard, the difference between CCT and CPT was about 20°C for the low-PRE alloys (i.e., PRE = 24) and increased to approximately 50°C for UNS S31254, which has a PRE of about 43. A conclusion that can be drawn from Garner's work is that the more highly alloyed corrosion-resistant alloys (CRAs) can be susceptible to crevice corrosion while maintaining an excellent pitting corrosion resistance, as discussed previously in this chapter. Recently, Klapper et al.[92] produced a comprehensive compilation of CPT and CCT values for a broad range of nickel alloys with PRE values ranging from 25 to approximately 70. Klapper et al.'s results agree well with the work by Garner, with CCT values for alloys with a PRE of 25 being 40°C lower than CPT. The difference between CPT and CCT increased to more than 80°C for alloys with a PRE between 68 and 70. Likewise, the crevice corrosion induction time is typically shorter than that of pitting corrosion.[24,93] Consequently, the duration of pitting tests is longer than a crevice test in the same environment. Last, CPT values are more reproducible than CCT (i.e., 2.5 vs. 10°C).[47,70,94]

Precision and Bias in Critical Temperature Tests

As detailed in ASTM G48, the precision of Methods D and F for measuring the pitting and crevice corrosion resistance was determined in an interlaboratory test program in which seven laboratories carried out triplicate tests on four materials. The results of these tests are given in Table 5. Results were consistent among laboratories, and there were no statistically significant variations between the materials in either repeatability or reproducibility.[95]

ASTM G78: CREVICE CORROSION SUSCEPTIBILITY IN SEAWATER

ASTM G78 is used to determine crevice corrosion susceptibility in seawater and other chloride environments. The scope of the standard is on iron- and nickel-based alloys, but it can be applied to other alloy systems. The standard suggests a multitude of different crevice former geometries, including MCA of various designs, O-rings, gaskets, strips, and coatings, if testing complex geometries. Specimens could be flat or cylindrical or have intricate shapes and be made of different polymers—including transparent acrylics—ceramics, glass, metals, wood, and rubbers. Specimens shall maintain a constant boldly exposed (crevice-free) to shielded (crevice) area ratio to ensure reproducible results that are not restricted by the cathode area.

The exposure temperature is user-defined, and it shall be maintained within 2°C and recorded during testing. As with ASTM G48, tests at different temperatures can be used to determine the CCT. The recommended immersion time is 30 days. Sampling at different time intervals is permitted. A test program can be designed to quantify the crevice induction time by carefully planning frequent extraction intervals.

After immersion, the specimens are visually inspected to determine the maximum crevice depth—measured to the nearest 0.01 mm—and the affected area. When using MCA, the number of segments showing crevice corrosion also should be reported. In addition, samples shall be weighed after exposure to determine weight loss.

TABLE 5 Results of the Second Interlaboratory Test Program

	Method E, CPT Critical Pitting Corrosion Temperature (°C)				Method F, CCT Critical Crevice Corrosion Temperature (°C)			
Alloy/Laboratory	UNS S31603	UNS S31803	UNS S44735	UNS N08367	UNS S31603	UNS S31803	UNS S44735	UNS N08367
1	15/15/[a]	30/30/30	85/85/85	75/[a]	0/0/0	15/[a]/[a]	30/[a]/[a]	30/30/30
2	10/[a]/[a]	25/25/[a]	80/80/80	75/75	0/0/0	15/15/15	30/30/30	25/25/25
3	0/0/0	25/25/[a]	80/80/80	70/70/[a]	0/0/0	20/20/20	35/35/35	30/30/[a]
4	15/15/[a]	30/30/30	75/[a]/[a]	75/75/[a]	0/0/0	20/20/20		20/20/20
5	15/15/15	20/[a]	80/80/80	70/70/70	0/0/0	20/20/20	35/35/35	30/30/30
6		40		75	0/0/0	15	35	25
7	15/15/15	35/35/35	>85/>85/>85	75/75/75	0/0/0	25/25/25	35/[a]/[a]	30/30/30

Note: Minimum temperature (°C) to produce an attack at least 0.025-mm (0.001-in.) deep on the bold surface of the specimen. Edge attack ignored.
[a]Test run but no attack observed.

NATURAL VERSUS SYNTHETIC SEAWATER

It is common to use either a 3.5 wt% NaCl solution or the ASTM D1141, *Standard Practice for the Preparation of Substitute Ocean Water*,[96] artificial seawater composition to simulate natural seawater in the laboratory. Although these methods reproduce the chemical concentration of natural seawater, they do not take into account the influence of microorganisms and biofilm formation that takes place in natural environments. The establishment of biofilms has been shown to increase the corrosivity of seawater drastically.[97–99] Indeed, the corrosion potential increases to about +300 mV_{SCE} upon the development of a biofilm.[100] This increase in potential is often enough to polarize stainless steels above the critical pitting or crevice potential, depending on the PRE of the alloy.[100,101]

A second objective of the CREVCORR program discussed earlier was to develop alternative synthetic seawater chemistry that would better simulate the effect of biofilms during laboratory testing.[102] On the basis of comprehensive electrochemical measurements, the CREVCORR project proposed two possible synthetic seawater compositions. The so-called Chemical Method uses 3.5 wt% NaCl with the addition of 1 mM hydrogen peroxide (H_2O_2) and 1 mM gluconic acid ($C_6H_{12}O_7$). The Biochemical Method involves adding glucose oxidase (GOD) (100 U/L) and 20 mmol/L glucose to either 3.5 wt% NaCl or a simplified version of the ASTM D1141 composition (i.e., NaCl 24.53 $g{\cdot}L^{-1}$, $MgCl_2$ 5.20 $g{\cdot}L^{-1}$, Na_2SO_4 4.09 $g{\cdot}L^{-1}$, $CaCl_2$ 1.16 $g{\cdot}L^{-1}$, KCl 0.695 $g{\cdot}L^{-1}$, $NaHCO_3$ 0.201 $g{\cdot}L^{-1}$) referred to as simplified ASTM-type seawater.[102] Appendix D of the EFC Publication No. 60 details a proposal for an ISO standard specification for synthetic biochemical ocean or seawater. Nevertheless, the standard has yet to be published.[103]

Electrochemical Test Methods

Electrochemical methods are powerful tools to obtain not only a comparative ranking of localized corrosion performance but also quantitative information regarding pitting and crevice mechanisms. Tests can be conducted without an external polarization at the so-called corrosion potential (E_{Corr}) or under different polarization profiles. E_{Corr} is the potential of a corroding surface in a given electrolyte measured under open-circuit conditions versus a reference electrode.[1] At E_{Corr}, the rate of the sum of the anodic reactions equals that of the cathodic reactions and, thus, the net current is zero. Other experiments with no applied polarization employ a zero-resistance ammeter to measure the current flow between two working electrodes, which can be identical or dissimilar.

Tests conducted under an applied current or potential can be used to quantify critical potentials. Critical potentials include the pitting and crevice potentials (E_P or E_{Crev}, respectively) as well as critical repassivation potentials (E_R or $E_{R,Crev}$, depending on whether the experiments are performed using artificial crevices). Potentiostatic tests (i.e., experiments under a fixed potential) also can provide information regarding the induction time, τ. Additionally, the critical pitting or crevice temperatures can be obtained when multiple electrochemical tests—either at E_{Corr} or employing an external polarization—are performed at different temperatures.

This section describes conventional approaches that have been implemented by researchers to quantify localized corrosion resistance, rank alloy families based on performance, and study localized corrosion mechanisms.

ELECTROCHEMICAL TEST METHODS WITH NO EXTERNAL POLARIZATION

Corrosion Potential Measurements

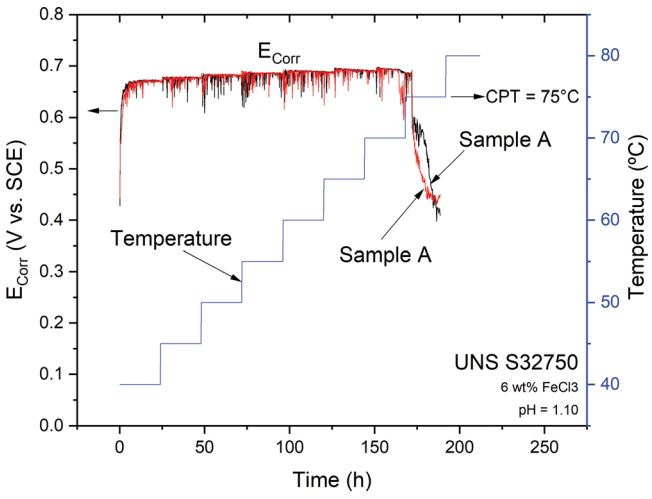
Oldfield and Sutton showed that the initiation of crevice corrosion of stainless steels is accompanied by a sudden decline in E_{Corr} from values within the passive region to low values around the critical potential (i.e., E_{Crev}). The authors showed that the initial drop was associated with the formation of micro-pitting within the crevice gap, followed by pit coalescence and spreading into a well-developed crevice attack.[24] Haugan et al., for example, recently used E_{Corr} to determine induction times of different super-duplex stainless steels (SDSS) as a function of temperature when exposed to natural seawater.[70] Because they are nondestructive, E_{Corr} measurements also could be used to assess the risk of localized corrosion of immersed structures in real-time during field monitoring and, as suggested by Dunn, Cragnolino, and Sridhar,[104] to model the long-term performance of corrosion-resistant alloys.

Standard test methods such as ASTM G48 and G78 can be adapted to include E_{Corr} monitoring to indicate the initiation of localized corrosion.[105] Figure 6 shows the E_{Corr} of UNS S32750 immersed in 6 wt% $FeCl_3$ (pH = 1.10) as a function of time during a stepwise increase in temperature. The temperature was increased by 5°C increments every 24 h if the E_{Corr} remained within typical passive potentials, that is, approximately 0.68 V_{SCE}. The sudden drop in potential at 75°C marked the initiation of localized corrosion, which was confirmed visually after testing. In this example, the CPT was defined as 75°C. Others have suggested the use of E_{Corr} monitoring during ASTM G48 testing, as an additional pass/fail criteria, which may be especially relevant in quality control test methods, such as ASTM A923, *Standard Test Methods for Detecting Detrimental Intermetallic Phase in Duplex Austenitic/Ferritic Stainless Steels*,[106] and to detect sensitized microstructures.[107]

The Remote Crevice Assembly

First used by Lee,[108] the remote crevice assembly implies coupling a creviced specimen to a crevice-free coupon, both made of the same material. The galvanic current flow between specimens is, then, recorded using a zero-resistance ammeter. The coupled potential is monitored concurrently with the net galvanic current as a function of time. The area of the noncreviced sample should be larger than that of the creviced coupon to ensure the cathodic reactions are primarily sustained on the crevice-free side. The choice of area ratio depends on the intended application, and experiments can be conducted with different anode-cathode ratios to study the possible effects of the cathode area. For instance, in a low-conductivity solution, such as the case of condensed water films, the area ratio is expected to be small (e.g., 2:1). In contrast, in full-immersion tests in seawater, the ratio can be quite high (e.g., 300:1).[100]

FIG. 6 E_{Corr} of UNS S32750 as a function of time during immersion in 6 wt% $FeCl_3$ (pH = 1.1) and a stepwise increase in temperature. The duration of each step was 24 h. The sudden drop in E_{Corr} marks the initiation of localized corrosion.



The remote crevice assembly simulates a real crevice in which the crevice-free sample acts as a net cathode and the crevice sample as the net anode. As with any test method based on zero-resistance amperometry (ZRA), both the magnitude and the direction of the current flow carry information about the corrosion process. For this reason, it is crucial to define a sign convention. In this regard, it is common to connect the two working electrodes so that a positive current represents the flow of electrons from the creviced to the crevice-free specimen.[109]

The remote crevice assembly is sensitive to the early stages of crevice corrosion, and it has been used to quantify crevice corrosion initiation and propagation,[110] to model crevice corrosion of UNS N06625,[111] and to determine the effect of biofilms on crevice corrosion of corrosion-resistant alloys.[112] More recently, Martin, Lucas, and Hogan[113] adapted the remote crevice assembly technique to study the crevice corrosion resistance of Ni-Cr-Mo alloys exposed to seawater.

Visual inspection after exposure is paramount to correlate the observed current trends with the degree of crevice corrosion. Likewise, although there is no international standard regulating the methodology and no consensus on a critical current value to define the initiation of crevice corrosion, ASTM G71, *Standard Guide for Conducting and Evaluating Galvanic Corrosion Tests in Electrolytes*,[114] can be used as a guide.

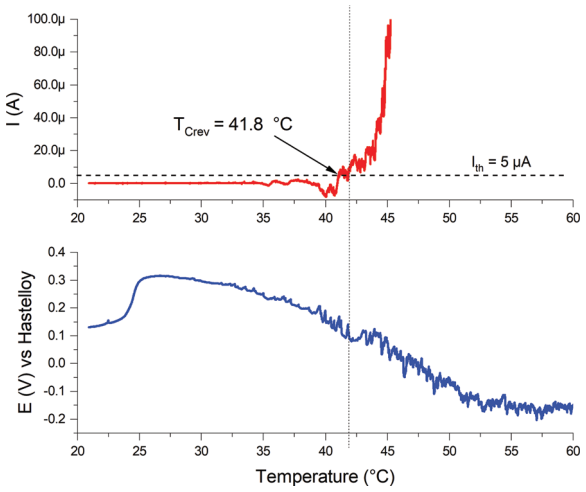
Zero-Resistance Amperometry and Electrochemical Noise

Salinas-Bravo and Newman[115] and Garfias[116–119] popularized the use of ZRA to determine critical pitting temperatures of stainless steels. Later, others employed electrochemical noise (EN) analysis to investigate the crevice corrosion resistance of stainless steels under simulated high-pressure high-temperature oil and gas environments.[109]

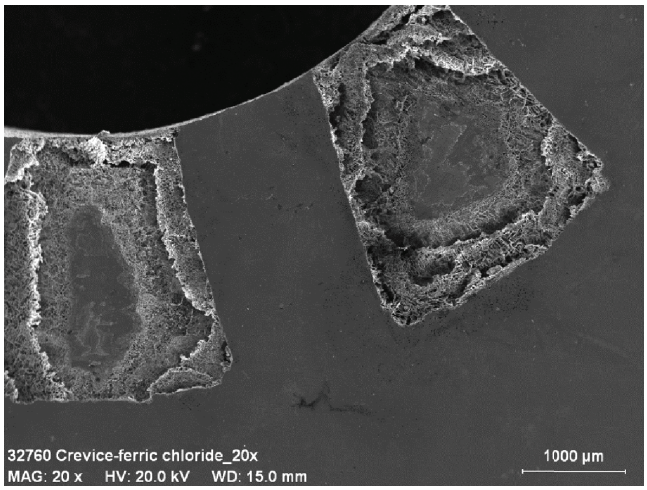
As with the remote crevice assembly, ZRA and EN measure the current flow between two working electrodes. Unlike the remote crevice assembly, ZRA and EN require two identical creviced specimens. During ZRA and EN testing, the start of crevice corrosion leads to an increase in current—which can be either positive or negative depending on the electrode that first developed crevice attack—and a drop in coupled potential. A change in sign indicates a reversal in the net anodic or cathodic behavior versus the defined sign convention. Figure 7*A* shows the coupled current and potential of creviced UNS S32760 specimens in 6 wt% $FeCl_3$ (pH = 1.10) as a function of temperature during ZRA testing. In this case, the temperature was increased at 0.2°C/min. The initiation of crevice corrosion was defined as a sustained current above 5 μA after Salinas-Bravo and Newman.[115] In this case, the critical crevice temperature, T_{Crev}, was 41.8°C. Herein, the nomenclature T_{Crev} is used instead of CCT to indicate the critical temperature was determined using electrochemical means rather than as per ASTM G48.

Unlike ZRA, EN requires a more sophisticated analysis of the results. In this regard, the data can be analyzed in the time domain (i.e., as recorded) or transported to the frequency domain using, for example, a fast Fourier transformation (FFT) algorithm or the maximum entropy method (MEM). Once transformed into the frequency domain, Power Spectral Density (PSD) plots can be constructed to analyze EN current and potentials as well as to

FIG. 7 ZRA testing of UNS S32760 in 6 wt% $FeCl_3$ (pH = 1.1) (*A*) current and potential as a function of temperature and (*B*) crevice corrosion attack.



(*A*)



(*B*)

obtain the EN impedance. For a detailed overview of the EN analysis, consult the work by Cottis[120] as well as ASTM G199, *Standard Guide for Electrochemical Noise Measurement*.[121]

As with the remote crevice assembly technique, visual inspection after exposure is required to correlate the observed current trends with the degree of crevice corrosion, figure 7*B*. The ASTM G199 standard can be used as a guide.

ELECTROCHEMICAL METHODS EMPLOYING AN APPLIED POLARIZATION

The techniques for evaluating crevice corrosion that employ an applied polarization involve holding or incrementally changing, either in steps or at a fixed scan rate, the potential or current. Some of the more common test methods, as defined in the ASTM G193 standard, are as follows:

- Potentiostatic polarization—a technique used to maintain a constant electrode potential. The current response is measured as a function of time. Different samples can be exposed at different applied potentials (E_{App}).
- Galvanostatic technique—a technique wherein an electrode is maintained at a constant current in an electrolyte. The resulting electrode potential is recorded as a function of time. Different samples can be exposed at different applied currents or current densities (I_{App} or i_{App}, respectively).
- Potentiostaircase or potentiostep technique—a potentiostep technique for polarizing an electrode in a series of constant potential steps wherein the time duration and potential increments or decrements are equal for each step. Nevertheless, when studying crevice corrosion, the duration of each step can be varied.
- Galvanostaircase or galvanostep technique—a galvanostep technique for polarizing an electrode in a series of constant current steps wherein the time duration and current increments or decrements are equal for each step.
- Potentiodynamic or potentiokinetic polarization—a technique wherein the potential of an electrode with respect to a reference electrode is varied at a selected rate (e.g., 0.6 V/h) by the application of a current through the electrolyte. When the potential is scanned in a direction so that $E_{App} \geq E_{Corr}$, the result is an anodic polarization curve (i.e., an E-i diagram). Anodic polarization diagrams are used to determine (e.g., E_P and E_{Crev}). ASTM G59, *Standard Test Method for Conducting Potentiodynamic Polarization Resistance Measurements*, describes a method to conduct potentiokinetic anodic polarization measurements on stainless steels and nickel alloys, which also can be applied to other alloy families.[122]
- Cyclic potentiodynamic polarization—a technique in which the applied potential is scanned forward from some low value, typically E_{Corr}, to a high value until reaching a predefined current density (e.g., 5 mA/cm^2) or potential and then is scanned backward to a predetermined potential or current value. The reverse scan continues until the hysteresis loop closes or until a new corrosion potential is reached. The method is described in ASTM G61, *Standard Test Method for Conducting Cyclic Potentiodynamic Polarization Measurements for Localized Corrosion Susceptibility of Iron-, Nickel-, or Cobalt-Based Alloys*.

These techniques are often used alone or combined with varying other environmental factors, such as temperature, pH, and chloride concentration, as discussed previously. It is important to emphasize that, for a given environment, critical potentials and temperatures are not a property of the metal or alloy, as they are influenced by experimental parameters, such as potential and temperature scan rate,[14,123,124] and the selected current at scan reversal.[125] These and other methods are described in more detail in the next section.

POTENTIOSTATIC ELECTROCHEMICAL TEST METHODS

Chronoamperometry

Chronoamperometry involves applying either a constant potential or a series of potential steps and recording the resulting current or current density as a function of time. Tests can be performed using creviced and crevice-free specimens. Chronoamperometry is primarily used to estimate induction times.[126,127] Nevertheless, chronoamperometry can be used to determine critical temperatures (i.e., T_{Pit} or T_{Crev}) when done as a function of temperature. Repassivation temperatures also can be obtained if the temperature is reduced after pitting or crevice corrosion initiation.

Figure 8 shows current density as a function of time of a creviced UNS S39274, that is, a high-W SDSS, immersed in natural seawater during a stepwise increase in temperature followed by a stepped decrease in temperature. The applied potential was +300 mV_{SSE} to simulate the effect of naturally occurring biofilms.[100] During the forward ramp, the temperature was held for 15 days at each step. If no increase in current was observed, the temperature was increased by 5°C. The ramping continued until an apparent increase in current was observed. The critical crevice temperature, T_{Crev}, was adapted after Steinsmo et al.,[101] as the temperature step at which the current density exceeded 25 μA/cm^2 for at least 4 h. This value was chosen because it corresponded to a marked deviation from the passive current density. Once the current density was reached, the temperature was then decreased in a 7-day period at 2.5°C steps, until a stable passive behavior was observed. The repassivation temperature was arbitrarily defined as the temperature at which the current density dropped below the 25 μA/cm^2 threshold and stable passive current density values were observed.

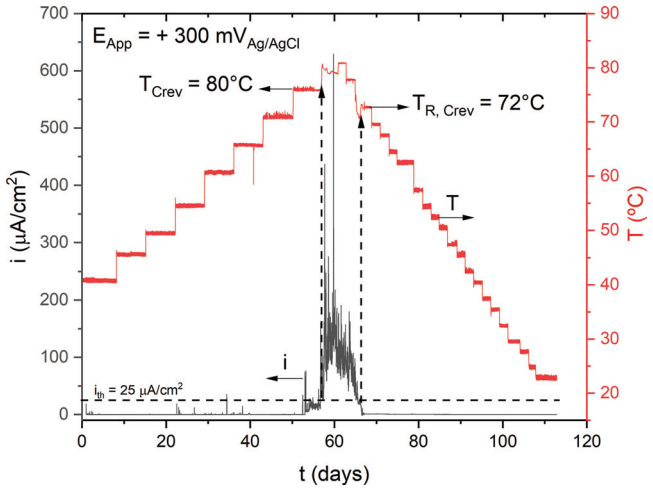
Figure 8 and the work of Steinsmo et al.[101] illustrate well the hysteresis that exists between the temperature at which crevice corrosion starts and repassivates. In their earlier work, Steinsmo et al. applied a +600 mV_{SCE} potential to simulate chlorinated seawater and a temperature scan rate of 4 °C/24h; a technique often referred to as cyclic thermammetry.[128] In the case of UNS N08367, the authors observed an approximately 50°C difference between T_{Crev} and $T_{R,\ Crev}$. The difference between T_{Crev} and $T_{R,Crev}$ (shown in fig. 8) was about 8°C, which was much lower than the values reported by Steinsmo et al. for other corrosion-resistant alloys.[101] The difference in the case of UNS S39274 was attributed to the influence of tungsten.

ASTM F746: Pitting or Crevice Corrosion of Metallic Surgical Implant Materials

ASTM F746, *Standard Test Method for Pitting or Crevice Corrosion of Metallic Surgical Implant Materials,* is used to assess the pitting and crevice corrosion resistance of surgical implant materials.[129–131] The localized corrosion resistance is determined based on the critical potential, E_{Crit}, to initiate pitting, crevice corrosion, or both. The primary purpose of the specification is to perform a laboratory screening of materials. Tests are conducted in phosphate-buffered saline (PBS) solution—8.0 g·L^{-1} NaCl, 0.2 g·L^{-1} KCl, 1.44 g·L^{-1} Na_2HPO_4, and 0.24 g·L-1 KH_2PO_4—with a pH between 7.3 and 7.5. The temperature of the electrolyte is set to 37 ± 1°C to simulate the temperature of the human body. The standard employs cylindrical specimens that are 6.35 mm in diameter and 20 mm in length. The crevice assembly consists of an inert tapered PTFE collar, 3.18 mm in width. The collar is force-fit into the specimen from the base of the cylinder. Figure 9 illustrates the ASTM F746 crevice setup.

The procedure has three steps. Step 1 involves the measurement of a stable corrosion potential for 1 h, referred to as E_1. Step 2 is the stimulation step. The purpose of the stimulation step is to initiate localized corrosion. The applied potential is set at E_{App} = +800 mV_{SCE}, whereas the duration depends on the

FIG. 8 (*A*) Current density and temperature as a function of immersion time of UNS S39274 in natural seawater at an applied potential of E_{App} = +300 mV_{SSE} and (*B*) visual appearance after 110 days of exposure.

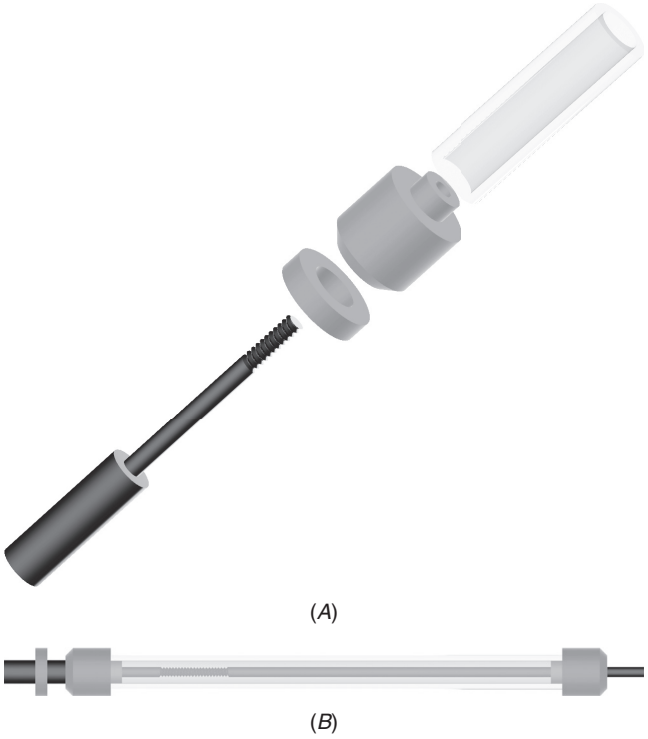


(*A*)



(*B*)

FIG. 9 ASTM F746 crevice assembly (*A*) exploded view and (*B*) assembled working electrode.



current response. If the current density instantly increases above +500 μA/cm^2, the potential is immediately decreased to E_1. If the current generally increases but i < +500 μA/cm^2, the potential is reduced to E_1 after 20 s. The test is terminated if there is no sharp increase in current density after 15 min.

Step 3 is the repassivation step. In Step 3, the applied potential is decreased to $E_{App} = E_1$. If no repassivation is observed, that is, the current remains above the passive current density, E_{Crit} is defined as $E_{Crit} = E_1$. If repassivation occurs, the process is repeated. The new applied potential in Step 3, after the new stimulation step, is set as $E_{App} = E_1 + 50$ mV. The sequence is continued until no repassivation occurs in Step 3. The assessment entails the quantification of E_{Crit} and a visual confirmation after testing.

Modified ASTM G150: Potential-Independent Critical Temperature

ASTM G150, *Standard Test Method for Electrochemical Critical Pitting Temperature Testing of Stainless Steels and Related Alloys,* is used to determine the so-called potential-independent critical pitting temperature. The tests can be modified to determine the potential-independent critical crevice temperature by employing creviced specimens, as described in ASTM G48 or G78 (fig. 4). ASTM G150 also can be used to predict the conditions that would result in stable crevice propagation. The test method applies to stainless steels from UNS 31600 to S31254, but it could be extended to other alloy families. Tests are performed in deaerated 1 M NaCl (unadjusted pH). The technique implies applying a fixed potential and measuring the current response as a function of time. The recommended potential is +700 mV_{SCE}, but other values can be used. A test at +600 or +800 mV_{SCE} can be performed to determine changes in the critical temperature. During testing, the temperature is ramped at 1°C/min. The potential-independent CPT or CCT is defined as the temperature at which i > 100 μA/cm^{-2} for 60 s. Visual confirmation is required at the end of the test to verify the presence of pitting and crevice corrosion. Figure 10 illustrates a modified ASTM G150 test using a PTFE MCA on UNS S32750. The applied potential was +700 mV_{SCE}, and the CCT varied between 61°C and 65°C.

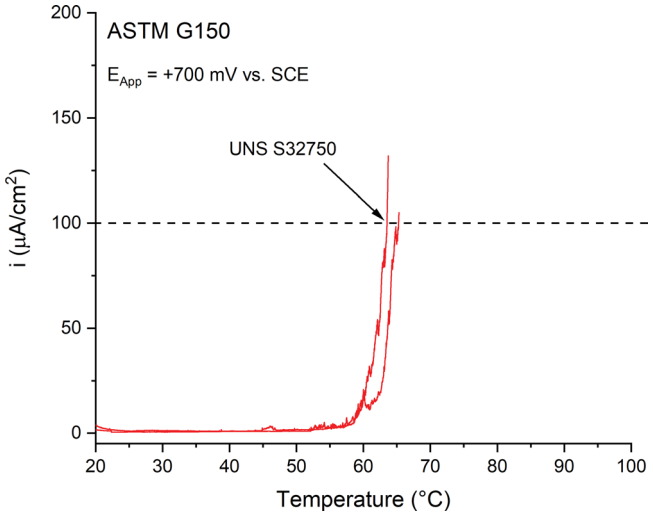
POTENTIOKINETIC ELECTROCHEMICAL TEST METHODS

Modified ASTM G61: Cyclic Potentiodynamic Polarization

ASTM G61 is arguably the most common electrochemical technique used to determine the relative susceptibility to localized corrosion, namely, pitting or crevice, of stainless steels as well as cobalt- and some nickel-based alloys. ASTM G61 focuses on crevice-free specimens, but the standard can be modified to study creviced samples. The crevice former is often an MCA that complies with, for example, ASTM G48. The analysis of the E-i diagrams provides information about the critical crevice and crevice repassivation potentials, E_{Crev} and $E_{R,Crev}$ (E_P and E_R if using crevice-free samples). Likewise, the critical crevice temperature and critical repassivation temperature (T_{Crev} and $T_{R,Crev}$, respectively) can be obtained when multiple experiments are performed at different temperatures. When done on crevice-free specimens, the standard can be used to check one's experimental technique and instrumentation.

As per ASTM G61, experiments are performed in deaerated 3.56 wt% NaCl (neutral pH) at 25 ± 1°C, but other environments and temperatures can be used. The test is divided into two steps. First, the working electrode is exposed at the corrosion potential for 1 h until a stable E_{Corr} is obtained. The

FIG. 10 An example of *i* versus temperature curve of UNS S32750 in 1 M NaCl as per ASTM G150.



potentiodynamic polarization commences immediately after the 1-h stabilization step. The potential is scanned at 0.6 V/h (0.168 mV/s) in the forward direction until reaching a current density threshold of 5 mA/cm^2. Once the current density threshold is met, the direction of the scan is reversed until the hysteresis loop closes or once reaching a new E_{Corr}. Data are plotted in an E-i diagram, where the current density *i* is presented in logarithmic scale.

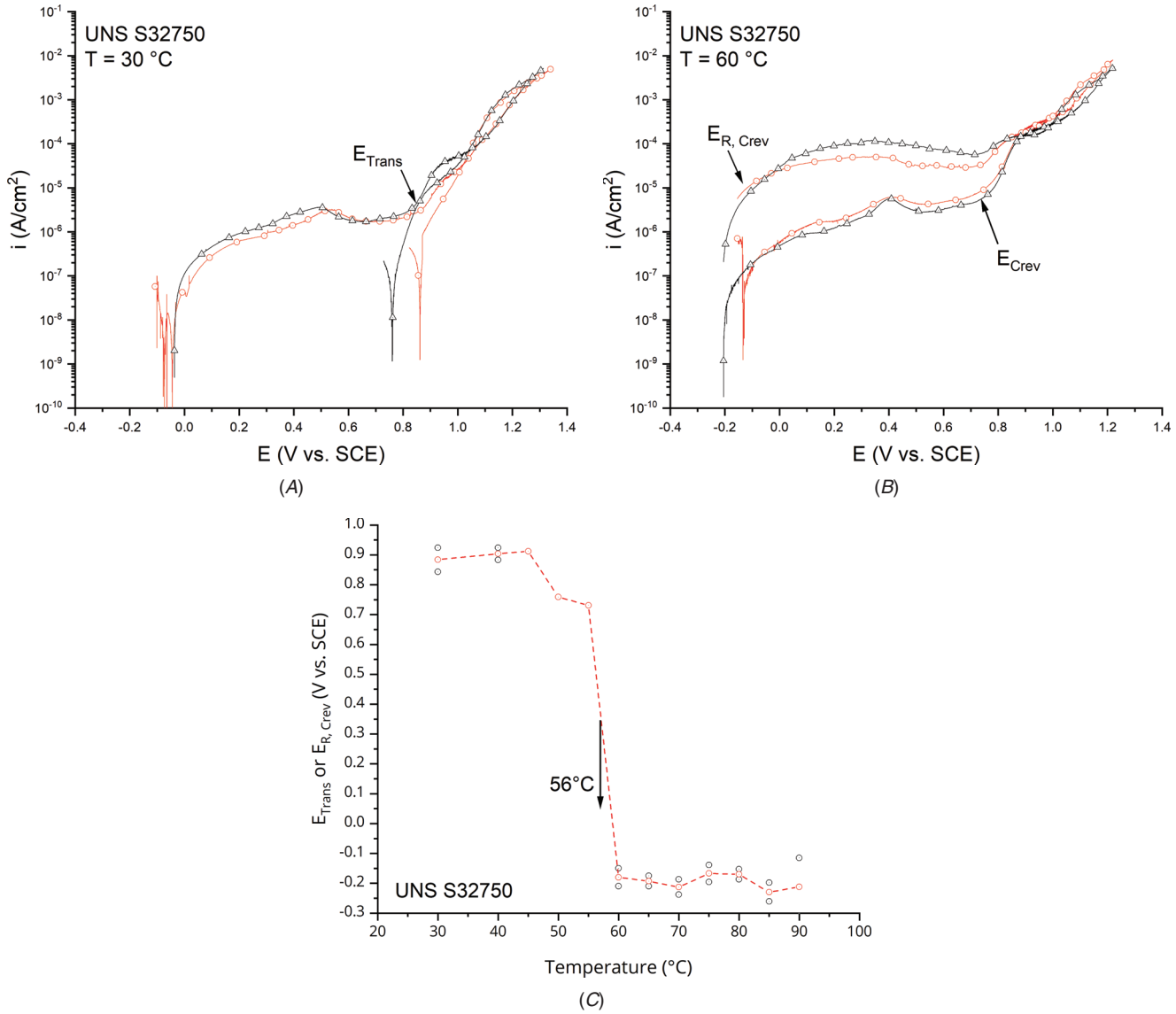
There are different ways to determine pitting, crevice, and repassivation potentials from E-i diagrams. According to Sridhar and Cragnolino,[125] E_P can be measured at the inflection point of the E-i plot, while E_R is defined as the potential, in the backward scan, where the current density reaches 2 μA/cm^2. A similar convention can be applied to tests using MCAs to determine E_{Crev} and $E_{R,Crev}$.[70] For creviced specimens, hysteresis, ΔE, is defined as follows:

$$\Delta E_{Crev} = E_{Crev} - E_{R,Crev}, \quad (9)$$

When evaluating crevice-free samples—where hysteresis is defined as $\Delta E = E_R - E_P$—it is accepted that alloys with large ΔE values are more susceptible to localized corrosion than those with small hysteresis loops.[14]

Figures 11*A* and 11*B* show two potentiokinetic E-i curves of UNS S32750 in 3.56 wt% NaCl at two different temperatures. Each diagram presents two repetitions to illustrate the test-to-test variability. The E-i curves shown in figure 11*A* and figure 11*B* were obtained at 30°C and 60°C, respectively. In Figure 11*A*, the sharp increase in current was associated with the transpassive region and,

FIG. 11 Cyclic anodic polarizations of creviced UNS S32750 samples in 3.56 wt% NaCl at (*A*) 30°C and (*B*) 60°C. (*C*) The critical crevice repassivation temperature is shown in the *E* versus *T* diagram.



thus, the potential was labeled E_{Trans}. The transpassive region represents the "region of an anodic polarization curve, more positive than the passive potential range, in which there is a significant increase in current density (increased metal oxidation) as the potential becomes more positive."[1] In contrast, a large hysteresis loop was obtained at 60°C, figure 11*B*. The forward scan in figure 11*B* also reached high positive values, but crevice corrosion occurred upon scan reversal as confirmed visually. The high ΔE value suggested that the driving force for crevice corrosion was large.[46] Figure 11*C* presents an E versus temperature plot, constructed from a series of cyclic anodic polarization curves performed at different temperatures. The critical crevice repassivation temperature, $T_{R,Crev}$, was 56°C. Figure 11*C* also illustrates that the critical temperature has a well-defined value, as suggested by Brigham and Tozer,[47,48] which in this case was within 5°C and limited by the temperature interval chosen for the tests.

Precision and bias in ASTM G61 testing

ASTM G61 shows the precision of the test method based on interlaboratory testing. An investigator's data should fall within the range of ±2 standard deviations because this includes 95% of all data, provided random variations are the only source of error. No information is available on the repeatability when one laboratory conducts several identical tests. Crevice corrosion under gaskets may lead to erroneous results. Researchers have found that the scatter in E_P and E_{Crev} is much larger than the scatter in E_R and $E_{R,Crev}$.[104,132,133] For example, the limited experimental data suggest a scatter in $E_{R,Crev}$ for type 316L stainless steel, and UNS N09925 of about 100 mV.[104]

ASTM G192: Tsujikawa-Hisamatsu Electrochemical Technique

Adapted from the work of Tsujikawa and Hisamatsu on stainless steels, ASTM G192, *Standard Test Method for Determining the Crevice Repassivation Potential of Corrosion-Resistant Alloys Using a Potentiodynamic-Galvanostatic-Potentiostatic Technique*,[134] is a complex technique that involves potentiodynamic, galvanostatic, and potentiostatic steps.[135] The test has been used to study the crevice[84,136,137] and pitting[138] corrosion susceptibility of highly alloyed nickel alloys. ASTM G192 is used to determine the $E_{R,Crev}$ of corrosion-resistant alloys. It is understood that an alloy will not develop crevice corrosion below $E_{R,Crev}$ under the tested conditions (i.e., electrolyte composition, pH, and temperature). Although ASTM G192 was developed for alloy C22, it applies to any corrosion-resistant alloy. The standard suggests the use of a PTFE tape-covered ceramic MCA and a torque of 3.4 N·m. The test can be modified to measure the critical crevice repassivation temperature, $T_{R,Crev}$, if done at various temperatures.

The tests can be done in any electrolyte, although the method was developed using a deaerated 1 M NaCl. The recommended test temperature for alloy C22 is 90°C, but lower temperatures can be chosen for less corrosion-resistant metals and alloys. The procedure has three steps, as follows. The potentiodynamic (PD) step commences after a 1-h E_{Corr} stabilization period. During the PD step, the potential is scanned in the forward anodic direction at 0.6 V/h (0.168 mV/s) until a pre-set current is reached (e.g., 2 $\mu A/cm^2$ for alloy C22). The galvanostatic (GS) step starts after reaching the current density threshold. In the GS period, the pre-set current is kept constant for 2 h, while the potential is recorded as a function of time. The goal of the GS step is to develop and grow crevice attack if any develops. After the 2-h GS period, the potential is decreased at 10 mV intervals. The duration of each step is 2 h and the current is recorded versus time. $E_{R,Crev}$ is defined as the highest potential for which the current does not increase with time. The presence and extent of crevice corrosion are verified using visual inspection after testing.

Precision and bias in ASTM G192 testing

Under some testing conditions, results from this method may be comparable to results from ASTM G61. The current Tsujikawa and Hisamatsu electrochemical (*THE*) test method is meant to be a complement to ASTM G61. The *THE* test method may produce crevice corrosion in conditions in which cyclic potentiodynamic polarizations have limitations caused by transpassive dissolution.

Results of an interlaboratory program showed that the overall crevice repassivation potential for alloy C22 in 1 M NaCl at 90°C was -107 $mV_{SSE,}$ and the standard deviation was 10.0 mV. This low standard deviation suggests that the measurement of the repassivation potential using the PD-GS-PS test method is highly reproducible. For more details, ASTM G192 should be consulted.

Potentiodynamic-Galvanostatic-Potentiodynamic Technique

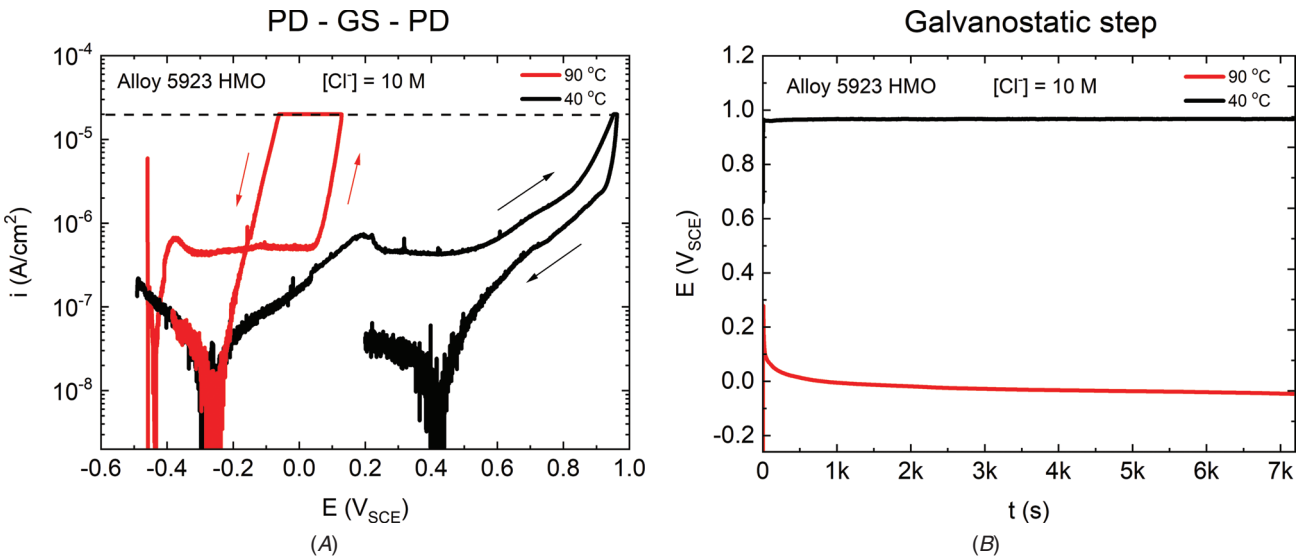
Although the *THE* technique circumvents the limitations of the ASTM G61 method for highly corrosion resistant alloys that would otherwise present transpassive dissolution before crevice corrosion, the method is time consuming and challenging to automate.[136,139] For this reason, Mishra and Frankel developed a simplified version of ASTM G192 that replaces the PS step by a PD polarization.[137] In the so-called PD-GS-PD technique, the potential is first scanned at 0.6 V/h (0.168 mV/s) until the predefined current density threshold. The threshold current density then is applied for 2 h to promote the initiation and propagation of crevice corrosion. After the 2-h GS step, the potential is reverted at a scan rate of 0.6 V/h (0.168 mV/s) until the hysteresis loop closes. The $E_{R,Crev}$ is defined as a crossover potential.

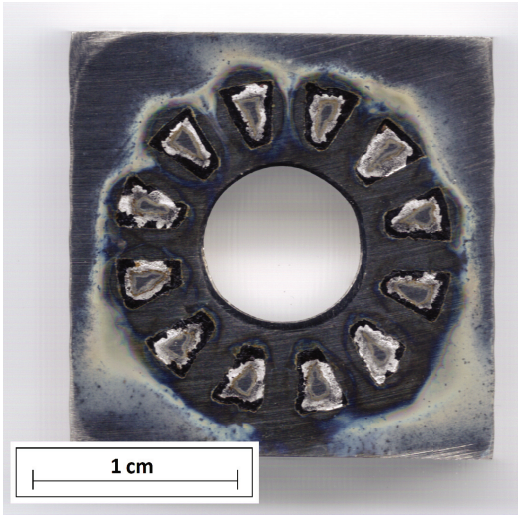
The PD-GS-PD method has been used successfully not only on nickel alloys[64,84,139–142] but also stainless steels with varying degrees of corrosion resistance.[32,33] Figure 12 illustrates an E-i plot as well as the E versus time curve recorded during the GS step of UNS N06059 (alloy 59) in 10 M Cl^- at two different temperatures, as indicated. As seen in figure 12, crevice corrosion did not occur at 40°C, as suggested by the lack of a positive hysteresis loop, which was later confirmed visually (not shown). Crevice corrosion was evident at 90°C, and the hysteresis loop was about ΔE = 200 mV. Figure 12*C* shows the extent of the crevice attack after PD-GS-PD testing.

Crevice Corrosion Repassivation by Cooling

Hornus et al.[30] recently adapted the PD-GS-PD technique to study crevice repassivation by cooling. The authors named the technique PD-GS-PD-(PS + Cooling), which was designed to

FIG. 12 PD-GS-PD test of UNS N06059 in 10 M Cl^- solution at 40°C and 90°C (*A*) *E* versus *I* curve, (*B*) potential versus time during the GS step, and (*C*) crevice corrosion attack after testing at 90°C.



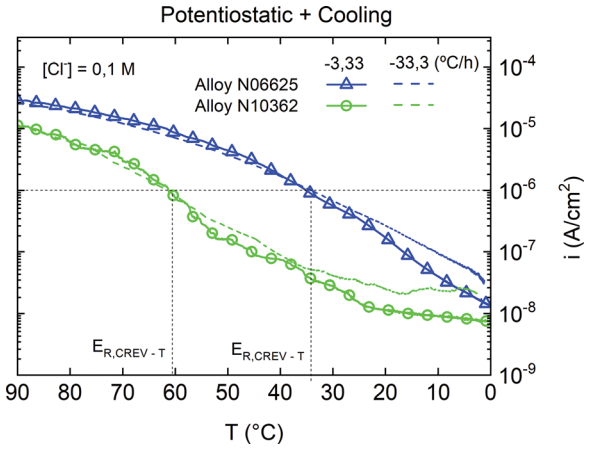


(*C*)

determine $T_{R,Crev}$ values of nickel alloys. First, the temperature of the electrolyte is set to 90°C. After reaching the desired initial temperature, the procedure involves five steps. Step 1 (PD) consists of an anodic potentiodynamic polarization at 0.6 V/h (0.168 mV/s) until the anodic current density reaches 20 μA/cm^2. In Step 2 (GS), the applied current is set at 20 μA/cm^2 for 4-h. Given that the current drops instantaneously upon removal of the GS, Step 3 involves a potentiodynamic polarization at 0.06 V/h (0.0168 mV/s) until the current density reaches ≥20 μA/cm^2. In Step 4 (PS), the last potential of Step 3 is applied for at least 2 h to produce sufficient crevice corrosion to obtain a conservative $T_{R,Crev}$ value. Likewise, Step 4 was designed to ensure a relatively low current density so that the drop in current during Step 5 can be attributed to the cooling effect exclusively. Last, the temperature is decreased while holding the PS polarization at a given cooling rate of, for example, 3.33°C/h or 33.3°C/h, until the current reaches typical passive current density values. The $T_{R,Crev}$ is determined once i = 1 μA/cm^2. Figure 13 illustrates Step 5 applied to UNS N06625 (alloy 625) and N10362 (alloy Hybrid B-C1) in 0.1 M NaCl at two different cooling rates. In this example, the $T_{R,Crev}$ of alloy Hybrid B-C1 was approximately 60°C while that of alloy 625 was approximately 35°C.

Although applying the PD-GS-PD-(PS + Cooling) technique to, for example, stainless steels and nickel alloys with relatively low PRE (e.g., PRE <40[80]) might be excessively complicated, the method can be used to quantify the critical crevice repassivation temperature of highly corrosion-resistant nickel alloys, which cannot be done using other conventional tests methods.

FIG. 13 PD-GS-PD-(PS + Cooling) Step 5 applied to UNS N06625 and N10362 applied potential and cooling rates as indicated.



Depassivation pH and the Critical Crevice Solution

As proposed by Oldfield and Sutton, the depassivation pH (pHd) is defined as the pH at which a metal or alloy does not exhibit any passivity.[21,24] The pHd value is associated with the critically acidic environment that develops inside a crevice, as discussed earlier. In this regard, Oldfield and Sutton referred to the solution that causes the permanent breakdown of the passive film within a crevice and the rapid propagation of the attack as critical crevice solution (CCS).[21,24] According to the authors, the CCS is defined in terms of pH (i.e., the pHd) and chloride concentration. The pHd and CCS can be obtained experimentally using polarization curves in crevice-like environments as a function of solution pH and chloride concentration. Malik et al.[87] and Okayama et al.,[143] for example, determined the CCS of a considerable number of CRAs of increasing PRE. Polarization experiments can be performed adapting ASTM G5 and G61 or by monitoring the potential of a specimen under galvanostatic conditions, while simultaneously decreasing the pH by the addition of HCl. There are, however, no broadly accepted standard procedures to determine CCS.

Conclusion

This chapter summarized the most common electrochemical and nonelectrochemical methods to study crevice corrosion. Other approaches, such as multi-microelectrode array testing and electrochemical methods that can quantify local electrochemical reactions with high spatial resolution, were not covered. It is important to emphasize that the choice of methodology depends on the problem being study. In this regard, all techniques have advantages and disadvantages that need to be considered carefully. Indeed, often short-term accelerated laboratory tests should be combined with long-term exposure evaluations to validate critical parameters, such as induction times, crevice propagation rates, and critical temperatures. The ample literature cited herein can be consulted for more detailed discussions on crevice corrosion mechanisms.

ACKNOWLEDGMENTS

We thank Dr. Ke Wang, Cristian Torres, and Adam Cianfrini for their support in producing the figures for this publication.

Terms and Definitions

CCS	Critical crevice solution
CCT	Critical crevice temperature, as determined by ASTM G48
CPT	Critical pitting temperature, as determined by ASTM G48
CRA	Corrosion-resistant alloy
DSMCA	Disc spring multiple crevice assembly
E_{App}	Applied potential
E_{Crev}	Critical crevice potential (crevice initiation potential)
E_{Crit}	Critical potential as defined by the critical acidification model
E_{Corr}	Corrosion potential
E^*_{Corr}	Corrosion potential in a simulated crevice electrolyte.
E_{ihn}	Overpotential to reflect the contribution of the presence of inhibitors in the solution
EN	Electrochemical noise
E_P	Critical pitting potential (pitting corrosion initiation)
E_R	Repassivation potential
$E_{R,Crev}$	Crevice repassivation potential
FFT	Fast Fourier transformation
g	Crevice gap
I or i	Current or current density
I_{App} or i_{App}	Applied current or current density, respectively
i_{pass}	Passive current density
L	crevice length measured as the distance from the crevice mouth
MCA	Multiple-crevice assembly
MEM	Maximum entropy method
PBS	Phosphate-buffered saline
pHd	Depassivation pH
PCTFE	Polychlorotrifluoroethylene
PRE	Pitting resistant equivalent
PSD	Power spectral density
PTFE	Polytetrafluoroethylene
PVDC	Polyvinylidene chloride
PVDF	Polyvinylidene difluoride
SCE	Saturated calomel electrode
SSE	Silver/silver chloride electrode
T_{Crev}	Critical crevice temperature measured using electrochemical methods
T_{Crit}	Critical temperature (either pitting or crevice)
T_{Pit}	Critical pitting temperature measured using electrochemical methods
$T_{R,Crev}$	Critical crevice repassivation temperature measured using electrochemical methods
x	Diffusion path
x·i	Galvele's pitting or crevice stability product
ZRA	Zero resistance amperometry
	Polarization needed to reach the critical xi value
Φ	The electrical potential induced by the migration of the aggressive anions to the crevice
τ	Induction or incubation time

References

1. *Standard Terminology and Acronyms Relating to Corrosion*, NACE/ASTM G193-12d (West Conshohocken, PA: ASTM International, approved December 1, 2012), http://dx.doi.org/10.1520/G0193-12D
2. R. G. Kelly, "Crevice Corrosion," in *ASM Handbook, Volume 13A: Corrosion: Fundamentals, Testing, and Protection*, ed. S. D. Cramer and B. S. Covino (Metals Park, OH: ASM International, 2003), 242–247.
3. A. J. Betts and L. H. Boulton, "Crevice Corrosion: Review of Mechanisms, Modelling, and Mitigation," *British Corrosion Journal* 28, no. 4 (1993): 279–296.
4. P. Gallagher, R. E. Malpas, and E. B. Shone, "Corrosion of Stainless Steels in Natural, Transported, and Artificial Seawaters," *British Corrosion Journal* 23, no. 4 (1988): 229–233.
5. D. Schlain and C. B. Kenahan, "The Role of Crevices in Decreasing the Passivity of Titanium in Certain Solutions," *Corrosion* 12, no. 8 (1956): 422t–426t.
6. T. E. Standish, M. Yari, D. W. Shoesmith, and J. J. Noel, "Crevice Corrosion of Grade-2 Titanium in Saline Solutions at Different Temperatures and Oxygen Concentrations," *Journal of The Electrochemical Society* 164, no. 13 (2017): C788–C795.
7. B. F. Brown, "Concept of the Occluded Corrosion Cell," *Corrosion* 26, no. 8 (1970): 249–250.
8. N. J. Laycock, J. Stewart, and R. C. Newman, "The Initiation of Crevice Corrosion in Stainless Steels," *Corrosion Science* 39, no. 10–11 (1997): 1791–1809.
9. J. R. Galvele, "Tafel's Law in Pitting Corrosion and Crevice Corrosion Susceptibility," *Corrosion Science* 47, no. 12 (2005): 3053–3067.
10. R. B. Mears and U. R. Evans, "Corrosion at Contact with Glass," *Transactions of the Faraday Society* 30 (1934): 417–423.
11. J. R. Kearns, M. J. Johnson, and J. F. Grubb, "Accelerated Corrosion in Dissimilar Metal Crevices" (paper presentation, Corrosion 1986, NACE International, Houston, TX, 1986).
12. G. S. Frankel and N. Sridhar, "Understanding Localized Corrosion," *Materials Today* 11, no. 10 (2008): 38–44.
13. *Standard Specification for General Requirements for Flat-Rolled Stainless and Heat-Resisting Steel Plate, Sheet, and Strip*, ASTM A480/A480M-18a (West Conshohocken, PA: ASTM International, approved December 1, 2018), http://dx.doi.org/10.1520/A0480_A0480M-18A
14. B. E. Wilde and E. Williams, "The Use of Current/Voltage Curves for the Study of Localized Corrosion and Passivity Breakdown on Stainless Steels in chloride Media," *Electrochimica Acta* 16, no. 11 (1971): 1971–1985.
15. H. H. Uhlig, "Pitting of Stainless Steels," *Transactions of AIME* 140 (1940): 387–432.
16. J. R. Galvele, "Pitting Corrosion," in *Corrosion: Aqueous Processes and Passive Films*, ed. J. C. Scully (London, UK: Academic Press, 1983), 1–57.
17. I. L Rosenfeld and I. S. Danilov, "Electrochemical Aspects of Pitting Corrosion," *Corrosion Science* 7, no. 3 (1967): 129–142.
18. J. R. Galvele, "Transport Processes and the Mechanism of Pitting of Metals," *Journal of The Electrochemical Society* 123, no. 4 (1976): 464–474.
19. J. R. Galvele, "Transport Processes in Passivity Breakdown—II. Full Hydrolysis of the Metal Ions," *Corrosion Science* 21, no. 8 (1981): 551–579.
20. S. M. Gravano and J. R. Galvele, "Transport Processes in Passivity Breakdown—III. Full Hydrolysis Plus Ion Migration Plus Buffers," *Corrosion Science* 24, no. 6 (1984): 517–534.
21. J. W. Oldfield and W. H. Sutton, "Crevice Corrosion of Stainless Steels: I. A Mathematical Model," *British Corrosion Journal* 13, no. 1 (1978): 13–22.
22. J. W. Oldfield, "Test Techniques for Pitting and Crevice Corrosion Resistance of Stainless Steels and Nickel-Base Alloys in Chloride-Containing Environments," *International Materials Reviews* 32, no. 1 (1987): 153–172.
23. R. M. Carranza, M. A. Rodriguez, and R. B. Rebak, "Effect of Fluoride Ions on Crevice Corrosion and Passive Behavior of Alloy 22 in Hot Chloride Solutions," *Corrosion* 63, no. 5 (2007): 480–490.
24. J. W. Oldfield and W. H. Sutton, "Crevice Corrosion of Stainless Steels: II. Experimental Studies," *British Corrosion Journal* 13, no. 3 (1978): 104–111.
25. R. Alkire and D. Siitari, "Initiation of Crevice Corrosion. II—Mathematical Model for Aluminum in Sodium Chloride Solutions," *Journal of The Electrochemical Society* 129, no. 3 (1982): 488–496.
26. J. C. Walton, "Mathematical Modeling of Mass Transport and Chemical Reaction in Crevice and Pitting Corrosion," *Corrosion Science* 30, nos. 8–9 (1990): 915–928.
27. A. D. Keitelman, S. M. Gravano, and J. R. Galvele, "Localized Acidification as the Cause of Passivity Breakdown of High Purity Zinc," *Corrosion Science* 24, no. 6 (1984): 535–545.
28. M. A. Rodriguez, "Inhibition of Localized Corrosion in Chromium Containing Stainless Alloys," *Corrosion Reviews* 30, nos. 1–2 (2012): 19–32.
29. R. C. Newman, M. A. A. Ajjawi, H. Ezuber, and S. Turgoose, "An Experimental Confirmation of the Pitting Potential Model of Galvele," *Corrosion Science* 28, no. 5 (1988): 471–477.
30. E. C. Hornus, M. A. Rodriguez, R. M. Carranza, and R. B. Rebak, "Crevice Corrosion Repassivation of Ni-Cr-Mo Alloys by Cooling," *Corrosion* 75, no. 6 (2019): 604–615.
31. J. Srinivasan and R. G. Kelly, "On a Recent Quantitative Framework Examining the Critical Factors for Localized Corrosion and Its Impact on the Galvele Pit Stability Criterion," *Corrosion* 73, no. 6 (2017): 613–633.
32. M. A. Kappes, M. C. Ortiz, M. Iannuzzi, and R. M. Carranza, "Use of the Critical Acidification Model to Estimate Critical Localized Corrosion Potentials of Duplex Stainless Steels," *Corrosion* 73, no. 1 (2017): 31–40.
33. E. C. Hornus, M. A. Rodriguez, R. M. Carranza, and R. B. Rebak, "Comparative Study of the Crevice Corrosion Resistance of UNS S30400 and UNS S31600 Stainless Steels in the Context of Galvele's Model," *Corrosion* 73, no. 1 (2016): 41–52.

34. J. R. Galvele, J. B. Lumsden, and R. W. Staehle, "Effect of Molybdenum on the Pitting Potential of High Purity 18% Cr Ferritic Stainless Steels," *Journal of The Electrochemical Society* 125, no. 8 (1978): 1204.

35. F. Bocher, R. Huang, and J. R. Scully, "Prediction of Critical Crevice Potentials for Ni-Cr-Mo Alloys in Simulated Crevice Solutions as a Function of Molybdenum Content," *Corrosion* 66, no. 5 (2010): 055002–055002-15.

36. P. A. Martínez, M. A. Rodriguez, E. C. Hornus, R. M. Carranza, and R. B. Rebak, "Crevice Corrosion Resistance of Super-Austenitic and Super-Duplex Stainless Steels in Chloride Solutions" (paper presentation, Corrosion 2015, NACE International, Dallas, TX, March 15–19, 2015).

37. G. C. Wood, "The Role of Flaws in Breakdown of Passivity Leading to Pitting of Aluminum and Crevice Corrosion of Stainless Steel," in *Passivity of Metals*, ed. R. P. Frankenthal and W. H. Sutton (Princeton, NJ: Electrochemical Society, 1978), 973–988.

38. L. Stockert, and H. Boehni, "Metastable Pitting Processes and Crevice Corrosion on Stainless Steels," in *Advances in Localized Corrosion*, NACE-9, ed. H. S. Isaacs (Houston, TX: NACE International, 1987), 467–473.

39. H. W. Pickering, "The Significance of the Local Electrode Potential within Pits, Crevices and Cracks," *Corrosion Science* 29, no. 2 (1989): 325–341.

40. C. S. Brossia and G. A. Cragnolino, "Effect of Environmental Variables on Localized Corrosion of Carbon Steel," *Corrosion* 56, no. 5 (2000): 505–514.

41. T. Suzuki, M. Yamabe, and Y. Kitamura, "Composition of Anolyte within Pit Anode of Austenitic Stainless-Steels in Chloride Solution," *Corrosion* 29, no. 1 (1973): 18–22.

42. J. Mankowski and Z. Szklarskasmialowska, "Studies on Accumulation of Chloride-Ions in Pits Growing during Anodic Polarization," *Corrosion Science* 15, no. 8 (1975): 493–501.

43. T. Li, J. R. Scully, and G. S. Frankel, "Localized Corrosion: Passive Film Breakdown vs. Pit Growth Stability: Part IV. The Role of Salt Film in Pit Growth: A Mathematical Framework," *Journal of The Electrochemical Society* 166, no. 6 (2019): C115–C124.

44. T. Li, J. R. Scully, and G. S. Frankel, "Localized Corrosion: Passive Film Breakdown vs. Pit Growth Stability: Part III. A Unifying Set of Principal Parameters and Criteria for Pit Stabilization and Salt Film Formation," *Journal of The Electrochemical Society* 165, no. 11 (2018): C762–C770.

45. T. Li, J. R. Scully, and G. S. Frankel, "Localized Corrosion: Passive Film Breakdown vs Pit Growth Stability: Part II. A Model for Critical Pitting Temperature," *Journal of the Electrochemical Society* 165, no. 9 (2018): C484–C491.

46. G. S. Frankel, T. Li, and J. R. Scully, "Perspective—Localized Corrosion: Passive Film Breakdown vs. Pit Growth Stability," *Journal of the Electrochemical Society* 164, no. 4 (2017): C180–C181.

47. R. J. Brigham, "Temperature as a Crevice Corrosion Criterion," *Corrosion* 30, no. 11 (1974): 396–398.

48. R. J. Brigham and E. W. Tozer, "Temperature as a Pitting Criterion," *Corrosion* 29, no. 1 (1972): 33–36.

49. J. Kolts and N. Sridhar, "Temperature Effects in Localized Corrosion," in *Corrosion of Nickel-Base Alloys*, ed. R. C. Scarberry (Metals Park, OH: ASM International, 1984): 191–198.

50. R. Qvarfort, "Critical Pitting Temperature-Measurements of Stainless-Steels with an Improved Electrochemical Method," *Corrosion Science* 29, no. 8 (1989): 987–993.

51. A. Garner, "Materials Selection for Bleached Pulp Washers," *Avesta Stainless Bulletin* 1, no. 12 (1982): 3–18.

52. H. W. Pickering, "The Role of Electrode Potential Distribution in Corrosion Processes," *Materials Science and Engineering: A* 198, nos. 1–2 (1995): 213–223.

53. G. Frankel, G. Thornton, S. Street, T. Rayment, D. Williams, A. Cook, A. Davenport, et al., "Localised Corrosion: General Discussion," *Faraday Discussions* 180 (2015): 381–414.

54. G. S. Frankel, "Pitting Corrosion of Metals: A Review of the Critical Factors," *Journal of the Electrochemical Society* 145, no. 6 (1998): 2186–2198.

55. R. C. Newman, "2001 W. R. Whitney Award Lecture: Understanding the Corrosion of Stainless Steel," *Corrosion* 57, no. 12 (2001): 1030–1041.

56. F. P. Ijsseling, "Electrochemical Methods in Crevice Corrosion Testing: Report Prepared for the European Federation of Corrosion Working Party 'Physico-Chemical Testing Methods of Corrosion: Fundamentals and Applications,' " *British Corrosion Journal* 15, no. 2 (1980): 51–69.

57. R. M. Kain, "Electrochemical Measurement of the Crevice Corrosion Propagation Resistance of Stainless Steels: Effect of Environmental Variables and Alloy Content," *Materials Performance* 23, no. 2 (1984): 24–30.

58. R. M. Kain, "Crevice Corrosion Testing in Natural Seawater. Significance and Use of Multiple Crevice Assemblies," *Journal of Testing and Evaluation* 18, no. 5 (1990): 309–318.

59. J. Kruger and K. Rhyne, "Current Understanding of Pitting and Crevice Corrosion and Its Application to Test Methods for Determining the Corrosion Susceptibility of Nuclear Waste Metallic Containers," *Nuclear and Chemical Waste Management* 3, no. 4 (1982): 205–227.

60. D. B. Anderson, "Statistical Aspects of Crevice Corrosion in Seawater," in *Galvanic and Pitting Corrosion—Field and Laboratory Studies*, ed. R. Baboian, W. France, L. Rowe, and J. Rynewicz (West Conshohocken, PA: ASTM International, 1976), 231–242.

61. R. M. Kain, "Seawater Testing to Assess the Crevice Corrosion Resistance of Stainless Steel and Related Alloys," in *Proceedings of the 12th International Corrosion Congress,* Vol. 3B (Houston, TX: NACE International, 1993), 1889–1990.

62. R. M. Kain, "Evaluating Crevice Corrosion," in *ASM Handbook,* Vol. 13A: *Corrosion: Fundamentals, Testing, and Protection*, ed. S. D. Cramer and B. S. Covino, Jr. (Metals Park, OH: ASM International, 2003), 549–561.

63. *Standard Test Methods for Pitting and Crevice Corrosion Resistance of Stainless Steels and Related Alloys by Use of Ferric Chloride Solution*, ASTM G48-11 (2015) (West Conshohocken, PA: ASTM International, approved November 1, 2015), http://dx.doi.org/10.1520/G0048-11R15

64. C. M. Giordano, M. R. Ortiz, M. A. Rodriguez, and R. B. Rebak, "Crevice Corrosion Testing Methods for Measuring Repassivation Potential of Alloy 22," *Corrosion Engineering, Science and Technology* 46, no. 2 (2013): 129–133.

65. M. Akashi, G. Nakayama, and T. Fukuda, "Initiation Criteria for Crevice Corrosion of Titanium Alloys Used for HLW Disposal Overpack," NACE 98185 (paper presentation, Corrosion 1998, San Diego, CA, March 22–27, 1998).

66. X. Shan and J. H. Payer, "Effect of Polymer and Ceramic Crevice Formers on the Crevice Corrosion of Ni-Cr-Mo Alloy 22," *Corrosion* 66, no. 10 (2010): 105005–105005-14.

67. B. Espelid, "Objectives and Background," in *EFC-60: Methodology of Crevice Corrosion Testing for Stainless Steels in Natural and Treated Seawaters*, ed. U. Kivisäkk, B. Espelid, and D. Féron (Wakefield, UK: Maney Publishing, 2010), 8–11.

68. U. Kivisäkk, B. Espelid, and D. Féron, ed., *EFC-60: Methodology of Crevice Corrosion Testing for Stainless Steels in Natural and Treated Seawaters* (Wakefield, UK: Maney Publishing, 2010).

69. B. Espelid, "Crevice Formers for Specimens of Plate Material," in *EFC-60: Methodology of Crevice Corrosion Testing For Stainless Steels in Natural and Treated Seawaters*, ed. U. Kivisäkk, B. Espelid, and D. Féron (Wakefield, UK: Maney Publishing, 2010), 17–20.

70. E. B. Haugan, M. Næss, C. T. Rodriguez, R. Johnsen, and M. Iannuzzi, "Effect of Tungsten on the Pitting and Crevice Corrosion Resistance of Type 25Cr Super Duplex Stainless Steels," *Corrosion* 73, no. 1 (2017): 53–67.

71. U. H. Kivisäkk, "Relation of Room Temperature Creep and Microhardness to Microstructure and HISC," *Materials Science and Engineering: A* 527, nos. 29–30 (2010): 7684–7688.

72. X. He, J. J. Noël, and D. W. Shoesmith, "Temperature Dependence of Crevice Corrosion Initiation on Titanium Grade-2," *Journal of the Electrochemical Society* 149, no. 9 (2002): B440–B449.

73. P. Jakupi, J. J. Noël, and D. W. Shoesmith, "Crevice Corrosion Initiation and Propagation on Alloy-22 under Galvanically-Coupled and Galvanostatic Conditions," *Corrosion Science* 53, no. 10 (2011): 3122–3130.

74. X. He, J. J. Noël, and D. W. Shoesmith, "Crevice Corrosion Damage Function for Grade-2 Titanium of Iron Content 0.078 wt% at 95°C," *Corrosion Science* 47, no. 5 (2005): 1177–1195.

75. T. Mathiesen and A. Anderson, "Challenges in Pre-Qualification Corrosion Testing of CRAs Based on ASTM G48" (paper presentation, Corrosion 2014, San Antonio, TX, March 9–13, 2014).

76. A. Garner, "Crevice Corrosion of Stainless-Steels in Sea-Water-Correlation of Field Data with Laboratory Ferric-Chloride Tests," *Corrosion* 37, no. 3 (1981): 178–184.

77. S. Tsujikawa, K. Kudo, and H. Ogawa, "A New Test for Predicting Pitting Corrosion Resistance of CRAs in Sour Environments" (paper presentation, Corrosion 1988, St. Louis, MO, 1988).

78. D. A. Wensley, R. C. Reid, and H. Dykstra, "Corrosion of Nickel-Based Alloys in Chlorine Dioxide Washer Service" (paper presentation, Corrosion 1990, Houston, TX, 1990).

79. B. S. DeForce, "Comments on ASTM G48: Standard Test Methods for Pitting and Crevice Corrosion Resistance of Stainless Steels and Related Alloys by Use of Ferric Chloride Solution" (paper presentation, Corrosion 2016, NACE International, Vancouver, British Columbia, Canada, March 6–10, 2016).

80. J. I. Skar and S. Olsen, "A Review of Materials Application Limits in NORSOK M-001 and ISO 21457," *Corrosion* 73, no. 6 (2017): 655–665.

81. J. Postlethwaite, "Electrochemical Tests for Pitting and Crevice Corrosion Susceptibility," *Canadian Metallurgical Quarterly* 22, no. 1 (1983): 133–141.

82. M. A. Streicher, "Development of Pitting Resistant Fe-Cr-Mo Alloys," *Corrosion* 30, no. 3 (1974): 77–91.

83. P. Lau and J. Bernhardsson, "Electrochemical Techniques for the Study of Pitting and Crevice Corrosion Resistance of Stainless Steels," in *Electrochemical Techniques for Corrosion Engineering*, ed. R. Baboian (Houston, TX: NACE International, 1977), 281–286.

84. M. Rincón Ortiz, M. A. Rodriguez, R. M. Carranza, and R. B. Rebak, "Determination of the Crevice Corrosion Stabilization and Repassivation Potentials of a Corrosion-Resistant Alloy," *Corrosion* 66, no. 10 (2010): 105002-1-12.

85. A. Garner, "Thiosulfate Corrosion in Paper-Machine White Water," *Corrosion* 41, no. 10 (1985): 587–591.

86. M. Renner, U. Heubner, M. B. Rockel, and D.-I. E. Wallis, "Temperature as a Pitting and Crevice Corrosion Criterion in the FeCl3 Test," *Werkstoffe und Korrosion* 37, no. 1 (1986): 183–190.

87. A. U. Malik, N. A. Siddiqi, S. Ahmad, and I. N. Andijani, "The Effect of Dominant Alloy Additions on the Corrosion Behavior of Some Conventional and High-Alloy Stainless-Steels in Seawater," *Corrosion Science* 37, no. 10 (1995): 1521–1535.

88. K. Lorentz and G. Medawar, "Über das Korrosionsverhalten austenitischer Chrom-Nickel-(Molybd än-) Stähle mit und ohne Stickstoffzusatz unter besonderer Berücksichtigung ihrer Beanspruchbarkeit in Chloridhaltigen Lösungen," *Tyssenforschung* 1, no. 3 (1969): 97–108.

89. R. F. A. Jargelius-Pettersson, "Application of the Pitting Resistance Equivalent Concept to Some Highly Alloyed Austenitic Stainless Steels," *Corrosion* 54, no. 2 (1998): 162–168.

90. *Materials Selection*, NORSOK M-001 (Lysaker, Norway: Standards Norway, 2014).

91. *Petroleum, Petrochemical and Natural Gas Industries—Materials Selection and Corrosion Control for Oil and Gas Production Systems*, ISO 21457:2010 (Geneva, Switzerland: International Organization for Standardization, 2010).

92. H. S. Klapper, N. S. Zadorozne, and R. B. Rebak, "Localized Corrosion Characteristics of Nickel Alloys: A Review," *Acta Metallurgica Sinica (English Letters)* 30, no. 4 (2017): 296–305.

93. R. J. Brigham, "Pitting and Crevice Corrosion Resistance of 18% Cr Stainless Steels," *Materials Performance* 13, no. 11 (1974): 29–31.

94. R. Qvarfort, R., "New Electrochemical Cell for Pitting Corrosion Testing," *Corrosion Science* 28, no. 2 (1988): 135–140.

95. S. W. Dean, *Research Report on Interlaboratory Test Program Results for ASTM G48 Standard Test Method for Pitting and Crevice Corrosion Resistance of Stainless Steels and Related*

Alloys by Use of the Ferric Chloride Solution: Methods E and F (West Conshohocken, PA: ASTM International, 2002).

96. *Standard Practice for the Preparation of Substitute Ocean Water*, ASTM D1141-98 (2013) (West Conshohocken, PA: ASTM International, approved January 1, 2013), http://dx.doi.org/10.1520/D1141-98R13

97. G. Salvago and L. Magagnin, "Biofilm Effect on the Cathodic and Anodic Processes on Stainless Steel in Seawater Near the Corrosion Potential: Part 1—Corrosion Potential," *Corrosion* 57, no. 8 (2001): 680–692.

98. G. Salvago and L. Magagnin, "Biofilm Effect on the Cathodic and Anodic Processes on Stainless Steel in Seawater Near the Corrosion Potential—Part 2: Oxygen Reduction on Passive Metal," *Corrosion* 57, no. 9 (2001): 759–767.

99. L. L. Machuca, S. I. Bailey, and R. Gubner, "Systematic Study of the Corrosion Properties of Selected High-Resistance Alloys in Natural Seawater," *Corrosion Science* 64, no. 1 (2012): 8–16.

100. U. Steinsmo, T. Rogne, and J. Drugli, "Aspects of Testing and Selecting Stainless Steels for Seawater Applications," *Corrosion* 53, no. 12 (1997): 955–964.

101. U. Steinsmo, T. Rogne, J. M. Drugli, and P. O. Gartland, "Critical Crevice Temperature for High-Alloyed Stainless Steels in Chlorinated Seawater Applications," *Corrosion* 53, no. 1 (1997): 26–32.

102. D. Féron, V. l'Hostis, and M. Roy, "Formulation of New Synthetic Seawater for Aerobic Environment," in *EFC-60: Methodology of Crevice Corrosion Testing for Stainless Steels in Natural and Treated Seawaters*, ed. U. Kivisäkk, B. Espelid, and D. Féron (Wakefield, UK: Maney Publishing, 2010), 30–43.

103. U. Kivisäkk, B. Espelid, and D. Féron, ed., "ISO Proposal for Synthetic Biochemical Seawater," in *EFC-60: Methodology of Crevice Corrosion Testing for Stainless Steels in Natural and Treated Seawaters* (Wakefield, UK: Maney Publishing, 2010), 105–109.

104. D. S. Dunn, G. A. Cragnolino, and N. Sridhar, "An Electrochemical Approach to Predicting Long-Term Localized Corrosion of Corrosion-Resistant High-Level Waste Container Materials," *Corrosion* 56, no. 1 (2000): 90–104.

105. C. Torres, R. Johnson, H. Østvold, M. Bernås, and M. Iannuzzi, "Effect of W on Phase Transformation Kinetics and its Correlation with Localized Corrosion Resistance for UNS S39274" (paper presentation, Corrosion 2019, NACE International, Houston, TX, March 24–28, 2019).

106. *Standard Test Methods for Detecting Detrimental Intermetallic Phase in Duplex Austenitic/Ferritic Stainless Steels*, ASTM A923-14 (West Conshohocken, PA: ASTM International, approved March 1, 2014), http://dx.doi.org/10.1520/A0923-14

107. M. Iannuzzi, A. H. Qvale, and A. Fjeldly, *Rapid Non-Destructive Evaluation of the Degree of Sensitization in Stainless Steels and Nickel Based Alloys* (West Conshohocken, PA: ASTM International, 2019).

108. T. Lee, "A Method for Quantifying the Initiation and Propagation Stages of Crevice Corrosion," in *Electrochemical Corrosion Testing*, ed. F. Mansfeld and U. Bertocci (West Conshohocken, PA: ASTM International, 1981), 43–68.

109. M. Iannuzzi, C. Mendez, L. Avila-Gray, G. Maio, and H. Rincon, "Determination of the Critical Pitting Temperature of Martensitic and Supermartensitic Stainless Steels in Simulated Sour Environments Using Electrochemical Noise Analysis," *Corrosion* 66, no. 4 (2010): 411–418.

110. R. M. Kain and T. S. Lee, "Recent Developments in Test Methods for Investigating Crevice Corrosion," in *Laboratory Corrosion Tests and Standards*, ed. G. Haynes and R. Baboian (West Conshohocken, PA: ASTM International, 1985), 299–323.

111. R. S. Lillard and J. R. Scully, "Modeling of the Factors Contributing to the Initiation and Propagation of the Crevice Corrosion of Alloy 625," *Journal of The Electrochemical Society* 141, no. 11 (1994): 3006–3015.

112. H.-J. Zhang and S. C. Dexter, "Effect of Biofilms on Crevice Corrosion of Stainless Steels in Coastal Seawater," *Corrosion* 51, no. 1 (1995): 56–66.

113. F. J. Martin, K. E. Lucas, and E. A. Hogan, "Experimental Procedure for Crevice Corrosion Studies of Ni–Cr–Mo Alloys in Natural Seawater," *Review of Scientific Instruments* 73, no. 3 (2002): 1273–1276.

114. *Standard Guide for Conducting and Evaluating Galvanic Corrosion Tests in Electrolytes*, ASTM G71-81 (2019) (West Conshohocken, PA: ASTM International, approved May 1, 2019), http://dx.doi.org/10.1520/G0071-81R19

115. V. M. Salinas-Bravo and R. C. Newman, "An Alternative Method to Determine Critical Pitting Temperature of Stainless Steels in Ferric Chloride Solution," *Corrosion Science* 36, no. 1 (1994): 67–77.

116. L. F. Garfias-Mesias and J. M. Sykes, "Effect of Copper on Active Dissolution and Pitting Corrosion of 25% Cr Duplex Stainless Steels," *Corrosion* 54, no. 1 (1998): 40–47.

117. L. F. Garfias-Mesias and J. M. Sykes, "Metastable Pitting in 25 Cr Duplex Stainless Steel," *Corrosion Science* 41, no. 5 (1999): 959–987.

118. L. F. Garfias-Mesias, J. M. Sykes, and C. D. S. Tuck, "The Effect of Phase Compositions on the Pitting Corrosion of 25 Cr Duplex Stainless Steel in Chloride Solutions," *Corrosion Science* 38, no. 8 (1996): 1319–1330.

119. T. Tsaprailis, W. Kovacs, III, J. Tuggle, and L. F. Garfias-Mesias, "Corrosion Resistance of Stainless Steels Exposed to Aggressive Environments with Particles and Water" (paper presentation, Corrosion 2009, NACE International, Atlanta, GA, March 22–26, 2009).

120. R. A. Cottis, "Interpretation of Electrochemical Noise Data," *Corrosion* 57, no. 3 (2001): 265–285.

121. *Standard Guide for Electrochemical Noise Measurement*, ASTM G199-09 (2020)e1 (West Conshohocken, PA: ASTM International, approved November 1, 2020), http://dx.doi.org/10.1520/G0199-09R20E01

122. *Standard Reference Test Method for Making Potentiostatic and Potentiodynamic Anodic Polarization Measurements*, ASTM G5-94(2011)e1, (West Conshohocken, PA: ASTM International,

approved November 15, 2011), http://dx.doi.org/10.1520/G0005-94R11E01

123. B. E. Wilde, "A Critical Appraisal of Some Popular Laboratory Electrochemical Tests for Predicting the Localized Corrosion Resistance of Stainless Alloys in Sea Water," *Corrosion* 28, no. 8 (1972): 283–291.

124. B. E. Wilde, "Adaptation of Linear Polarization Techniques for In-Situ Corrosion Measurements in Water Cooled Nuclear Reactor Environments," *Corrosion* 23, no. 12 (1967): 379–384.

125. N. Sridhar and G. A. Cragnolino, "Applicability of Repassivation Potential for Long-Term Prediction of Localized Corrosion of Alloy 825 and Type 316L Stainless Steel," *Corrosion* 49, no. 11 (1993): 885–894.

126. J.-J. Park, S.-I. Pyun, W.-J. Lee, and H.-P. Kim, "Effect of Bicarbonate Ion Additives on Pitting Corrosion of Type 316L Stainless Steel in Aqueous 0.5 M Sodium Chloride Solution," *Corrosion* 55, no. 4 (1999): 380–387.

127. T. Aoyama, Y. Sugawara, I. Muto, and N. Hara, "In Situ Monitoring of Crevice Corrosion Morphology of Type 316L Stainless Steel and Repassivation Behavior Induced by Sulfate Ions," *Corrosion Science* 127 (2017): 131–140.

128. G. T. Burstein and J. J. Moloney, "Cyclic Thermammetry," *Electrochemistry Communications* 6, no. 10 (2004): 1037–1041.

129. C. O. Clerc, M. R. Jedwab, D. W. Mayer, P. J. Thompson, and J. S. Stinson, "Assessment of Wrought ASTM F1058 Cobalt Alloy Properties for Permanent Surgical Implants," *Journal Biomedical Material Research* 38, no. 3 (1997): 229–234.

130. G. Rondelli, B. Vicentini, and A. Cigada, "Localised Corrosion Tests on Austenitic Stainless Steels for Biomedical Applications," *British Corrosion Journal* 32, no. 3 (1997): 193–196.

131. G. Rondelli and B. Vicentini, "Localized Corrosion Behaviour in Simulated Human Body Fluids of Commercial Ni-Ti Orthodontic Wires," *Biomaterials* 20, no. 8 (1999): 785–792.

132. S. Tsujikawa, "Critical Depth for Initiation of Growing Crevice Corrosion," *Critical Factors in Localized Corrosion*, ed. G. S. Frankel and R. Newman (Pennington, NJ: The Electrochemical Society, 1992), 378–388.

133. S. Tsujikawa and S. Okayama, "Repassivation Method to Determine Critical Conditions in Terms of Electrode Potential, Temperature and NaCl Concentration to Predict Crevice Corrosion Resistance of Stainless Steels," *Corrosion Science* 31, no. 1 (1990): 441–446.

134. *Standard Test Method for Determining the Crevice Repassivation Potential of Corrosion-Resistant Alloys Using a Potentiodynamic-Galvanostatic-Potentiostatic Technique*, ASTM G192-08 (2014) (West Conshohocken, PA: ASTM International, approved November 1, 2014), http://dx.doi.org/10.1520/G0192-08R14

135. S. Tsujikawa and Y. Hisamatsu, "On the Repassivation Potential for Crevice Corrosion," *Corrosion Engineering* 29, no. 1 (1980): 37–40.

136. K. J. Evans, A. Yilmaz, S. D. Day, L. L. Wong, J. C. Estill, and R. B. Rebak, "Using Electrochemical Methods to Determine Alloy 22's Crevice Corrosion Repassivation Potential," *Journal of the Minerals, Metals, and Materials Society* 57 (2005): 56–61.

137. A. K. Mishra and G. S. Frankel, "Crevice Corrosion Repassivation of Alloy 22 in Aggressive Environments," *Corrosion* 64, no. 11 (2008): 836–844.

138. K. Evans, S. Chawla, K. M. Sherer, J. Gerst, J. A. Beavers, N. Sridhar, and K. D. Boomer, "The Use of ASTM G192 (Tsujikawa-Hisamatsu Electrochemical Method) to Evaluate the Susceptibility of Hanford Tank Steels to Pitting Corrosion" (paper presentation, Corrosion 2016, NACE International, Vancouver, British Columbia, Canada, March 6–10, 2016).

139. M. A. Rodríguez, R. M. Carranza, and R. B. Rebak, "Effect of Potential on Crevice Corrosion Kinetics of Alloy 22," *Corrosion* 66, no. 1 (2010): 015007-015007-1-14.

140. A. K. Mishra and D. W. Shoesmith, "Effect of Alloying Elements on Crevice Corrosion Inhibition of Nickel-Chromium-Molybdenum-Tungsten Alloys under Aggressive Conditions: An Electrochemical Study," *Corrosion* 70, no. 7 (2014): 721–730.

141. E. C. Hornus, C. M. Giordana, M. A. Rodriguez, R. M. Carranza, and R. B. Rebak, "Effect of Temperature on the Crevice Corrosion of Nickel Alloys Containing Chromium and Molybdenum," *Journal of The Electrochemical Society* 162, no. 3 (2014): C105–C113.

142. M. Rincón-Ortíz, M. A. Rodríguez, R. M. Carranza, and R. B. Rebak, "Determination of the Crevice Corrosion Stabilization and Repassivation Potentials of a Corrosion-Resistant Alloy," *Corrosion* 66, no. 10 (2010): 105002-105002-1-12.

143. S. Okayama, S. Tsujikawa, and K. Kikuchi, "The Effect of Alloying Elements on Depassivation pH for Stainless Steels," *Corrosion Engineering (Jpn.)* 36, no. 11 (1987): 702–709.

Chapter 3 | Galvanic

Harvey P. Hack,[1] Carol Glover,[2] and Jason Lee[3]

Basic Principles

ELECTROCHEMICAL REACTIONS

To be able to properly design and interpret results from galvanic corrosion (also called bimetallic corrosion) tests, it is necessary to have some appreciation of the electrochemical theory behind galvanic corrosion. Metal corrosion consists of at least two reactions. The first is the metal going into solution in the electrolyte:

$$M \rightarrow M^{n+} + ne^{-}. \quad (1)$$

For iron in steel corroding in water at room temperature, this reaction would be

$$Fe \rightarrow Fe^{2+} + 2e^{-}. \quad (2)$$

Because the metal is transformed from an atom with no net charge to an ion in solution with a net positive charge, this type of reaction is called an oxidation reaction, and it generates electrons. Oxidation reactions require a net increase in charge of the metal or ion. The presence of oxygen is not required for an oxidation reaction to occur. The oxidation reaction involved in the corrosion process is also called the anodic reaction.

Because electrons are generated by the oxidation reaction, and because there can be no net accumulation of charge in these reactions, another reaction must be occurring that consumes these electrons. This is the cathodic or reduction reaction, and it always results in some species reducing its charge as it gains electrons. The three common reduction reactions in water follow:

hydrogen reduction, occurring primarily in acids

$$2H^{+} + 2e^{-} \rightarrow H_2(gas), \quad (3)$$

oxygen reduction occurring primarily in acids

$$O_2 + 4H^{+} + 4e^{-} \rightarrow 2H_2O, \text{ and} \quad (4)$$

oxygen reduction occurring primarily in bases or neutral water

$$O_2 + 2H_2O + 4e^{-} \rightarrow 4OH^{-}. \quad (5)$$

The first of these cathodic reactions generates hydrogen gas and is readily observed when zinc or iron are placed in certain strong acids. The last two cathodic reactions use oxygen molecules that are dissolved in the water. Other reduction reactions not illustrated include metal ion reduction, such as electroplating.

All of these reactions generate or consume electrons and, therefore, involve the flow of a current. For this reason, they are called electrochemical reactions, and their rates are influenced by externally applied currents, such as those that control electrode potentials. For example, if electrons are forcibly removed from the anodic corrosion reaction, then the reaction will occur more rapidly. Removing electrons also causes the potential of the corroding metal, as measured relative to a device with a stable potential called a reference electrode, to become more positive. This is plotted in figure 1. The relationship is illustrated as a straight line, where potential is plotted against the log of the reaction rate. This straight-line relationship was first noted by Tafel,[1] and the slope of the line honors him by being called the Tafel slope. Anodic reactions usually have a positive Tafel slope. Ideal reactions frequently yield these straight lines, but in practice, it is common to see curved lines. The process of changing potential by applying a current is called polarization.

The cathodic reactions also can be plotted on the same type of graph. Adding electrons to the hydrogen reduction reaction (or to any cathodic reaction) will increase the rate of that reaction and shift the potential in the negative direction. This is shown in figure 1 as another straight line with a negative Tafel slope. Electrochemical reactions generate or consume electrons, and therefore, the rate of a reaction is equivalent to the electron current generated or used up by that reaction.

GALVANIC SERIES

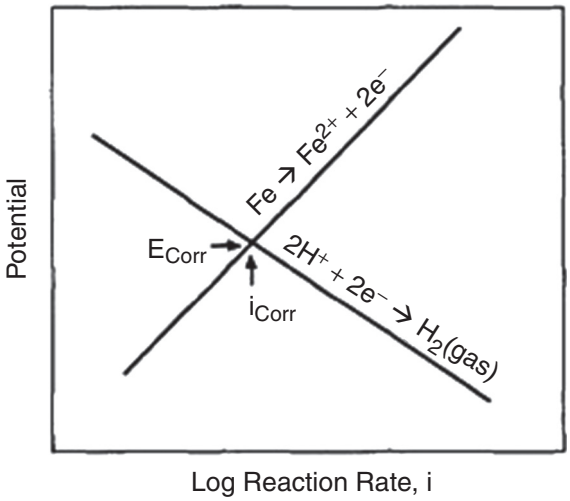
Because no charge can accumulate on any metal surface, the electrons generated by the anodic reaction all must be used up

[1]Northrop Grumman Corp., 895 Oceanic Dr., Annapolis, MD 21409, USA http://orcid.org/0000-0001-9887-2285
[2]Center for Electrochemical Science and Engineering, University of Virginia, 395 McCormick Rd., Charlottesville, VA 22904, USA http://orcid.org/0000-0002-9220-622X
[3]U.S. Naval Research Laboratory, 1008 Balch Blvd., Stennis Space Center, MS 39529, USA http://orcid.org/0000-0002-1079-433X

DOI: 10.1520/MNL202NDSUP20190008

Copyright © 2022 by ASTM International, 100 Barr Harbor Dr., PO Box C700, West Conshohocken, PA 19428-2959
ASTM International is not responsible, as a body, for the statements and opinions expressed in this chapter. ASTM International does not endorse any products represented in this chapter.

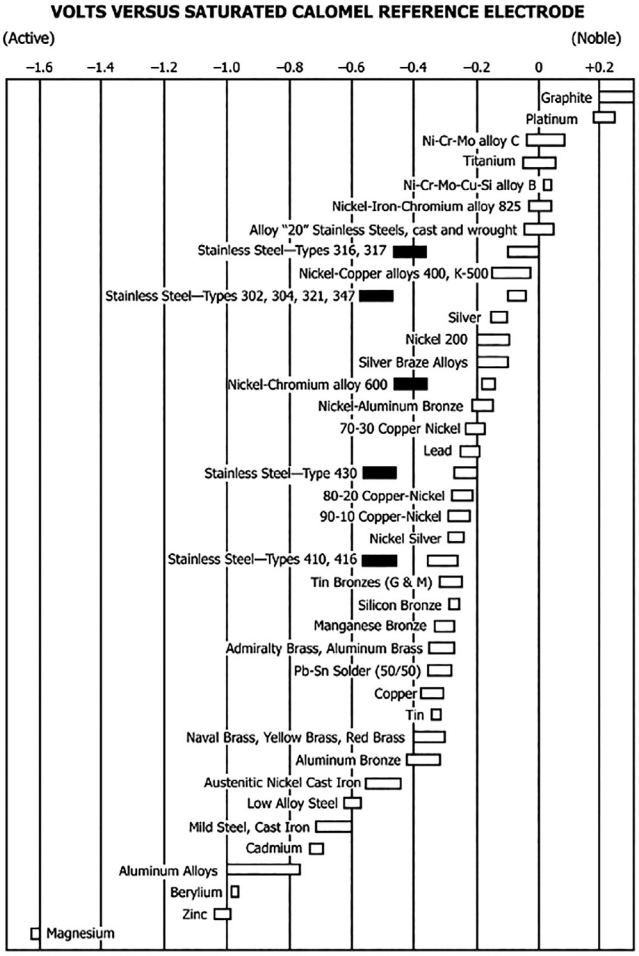
FIG. 1 Evans diagram for iron in an acid.



by the cathodic reaction. This can occur as shown in figure 1 only where the anodic and cathodic reaction lines cross. At this point, the rate of the anodic reaction, the corrosion rate, equals the rate of the cathodic reaction—in this case, hydrogen generation. This rate is called the open-circuit corrosion rate, abbreviated i_{corr}. The potential at which the lines cross is called the open-circuit corrosion potential, abbreviated E_{corr}. This type of plot is called an Evans diagram, after U. R. Evans, a pioneer in corrosion and electrochemistry. Any corroding metal should, under open-circuit conditions, exist at E_{corr} corroding at a rate i_{corr}, which can be predicted from the Evans diagram. The value of E_{corr} will depend on the position of the curves. The anodic curve for metal dissolution is a function of the type of metal and the charge it receives when it goes into solution. The cathodic curve is a function of the type of cathodic reaction, the type of surface on which that reaction takes place, the concentration of reacting species, and other factors, most of which depend on the environment in which the metal sits.

Each metal and environmental combination, therefore, exists at a unique potential. For a given environment, the potentials of various materials can be listed in a form called a galvanic series. Galvanic series can be expressed either as a graph giving the numerical values of the potentials of the materials in the given environment, as in figure 2, or as a list in order of increasing or decreasing potential without the specific values, as in figure 3. The galvanic series is important because it helps to predict what happens when two metals are placed in electrical contact in that environment, called a galvanic couple. For a galvanic couple to exist, there must exist at least two metals with different corrosion potentials, a metal path for electrons to flow between them, and an ionic path through the electrolyte to complete the electronic circuit. The metal that is more negative in the galvanic series will have a driving force to lose electrons to a metal that is in electrical contact that is more positive in the series. This will cause the corrosion rate of the more negative metal to increase when the electrical connection is made. This increase in corrosion of the more negative metal upon contact with a more

FIG. 2 Galvanic series of various metals in flowing seawater at 2.4–4.0 m/x for 5–15 days at 5–30°C. *Source:* Redrawn from original in Isaacs,[21] taken from ASTM G82, *Standard Guide for Development and Use of a Galvanic Series for Predicting Galvanic Corrosion Performance*.



NOTE 1—Dark boxes indicate active behavior of active-passive alloys.

positive metal is called galvanic corrosion. The galvanic series allows for the prediction of which of the metals in contact (i.e., the galvanic couple) will suffer increased corrosion.

MIXED POTENTIAL THEORY

It is tempting to say that the farther apart two metals are in the galvanic series, the more corrosion will occur on the more negative material, or anode. Unfortunately, the galvanic series cannot be used to predict the corrosion rate that may occur. To predict the rate of galvanic corrosion, kinetics of the anodic and cathodic reactions of both materials in a particular environmental exposure condition must be understood. This can be done by considering an Evans diagram of both metals involved. This approach is called Mixed Potential Theory.

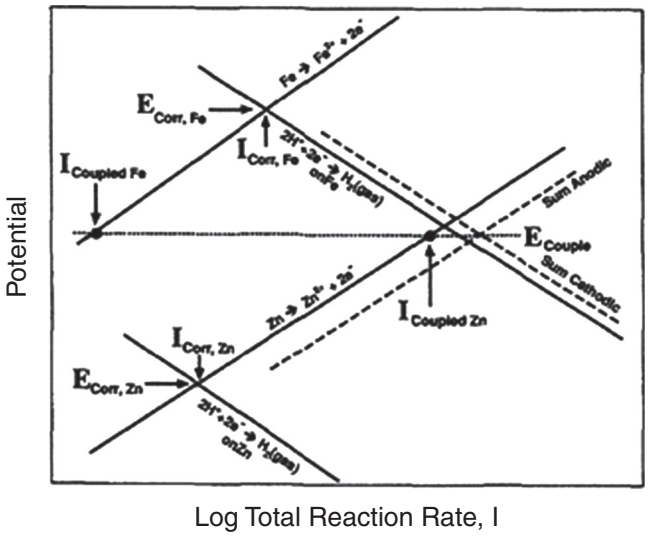
In figure 4, Evans diagrams are shown for two materials of equal surface area that have different potentials on the galvanic series in an acid: iron and zinc. The anodic material, zinc with the more negative $E_{corr,\ Zn}$, corrodes uncoupled at a rate of

FIG. 3 Galvanic series of various metals exposed to seawater. *Source:* Taken from ASTM G82, *Standard Guide for Development and Use of a Galvanic Series for Predicting Galvanic Corrosion Performance*.

ACTIVE END	Magnesium
(–)	Magnesium Alloys
↑	Zinc
I	Galvanized Steel
I	Aluminum 1100
I	Aluminum 6053
I	Alclad
I	Cadmium
I	Aluminum 2024 (4.5 Cu, 1.5 Mg, 0.6 Mn)
I	Mild Steel
I	Wrought Iron
I	Cast Iron
I	13 % Chromium Stainless Steel
I	Type 410 (Active)
I	18-8 Stainless Steel
I	Type 304 (Active)
I	18-12-3 Stainless Steel
I	Type 316 (Active)
I	Lead-Tin Solders
I	Lead
I	Tin
I	Muntz Metal
I	Manganese Bronze
I	Naval Brass
I	Nickel (Active)
I	76 Ni-16 Cr-7 Fe alloy (Active)
I	60 Ni-30 Mo-6 Fe-1 Mn
I	Yellow Brass
I	Admirality Brass
I	Aluminum Brass
I	Red Brass
I	Copper
I	Silicon Bronze
I	70:30 Cupro Nickel
I	G-Bronze
I	M-Bronze
I	Silver Solder
I	Nickel (Passive)
I	76 Ni-16 Cr-7 Fe
I	Alloy (Passive)
I	67 Ni-33 Cu Alloy (Monel)
I	13 % Chromium Stainless Steel
I	Type 410 (Passive)
I	Titanium
I	18-8 Stainless Steel
I	Type 304 (Passive)
I	18-12-3 Stainless Steel
↓	Type 316 (Passive)
(+)	Silver
NOBLE or	Graphite
PASSIVE END	Gold
	Platinum

$I_{corr,\ Zn}$. The cathodic material, iron with the more positive $E_{corr,\ Fe}$, corrodes uncoupled at a rate of $I_{corr,\ Fe}$. When these metals are electrically connected, electrons can flow between them, changing the behavior of each coupled metal. Because there are four reactions to consider, and because electrons can now flow freely between all four reactions, the charge balance must be handled differently than for the individual metals. All of the electrons generated by the anodic reactions must be consumed by the cathodic reactions. Therefore, the sum of the anodic reactions is plotted as a dashed line with a positive Tafel slope, and the sum of the cathodic reactions is plotted as a dashed line with a negative Tafel slope. These two sum lines intersect where all charges balance, and the potential at this intersection is defined as the mixed potential of the galvanic couple, or

FIG. 4 Evans diagram for iron and zinc in acid.



coupled potential, E_{couple}. The mixed potential of the couple is shown as a dotted line in figure 4. The points at which the individual reaction lines cross the mixed potential define the rates of those reactions. The zinc corrosion rate has increased from $I_{corr,\ Zn}$ to $I_{coupled,\ Zn}$. This increase is the galvanic corrosion rate. The iron corrosion rate has decreased from $I_{corr,\ Fe}$ to $I_{coupled,\ Fe}$. This decrease, caused by forcing the metal to act as a cathode, is called cathodic protection and is an important corrosion control method.

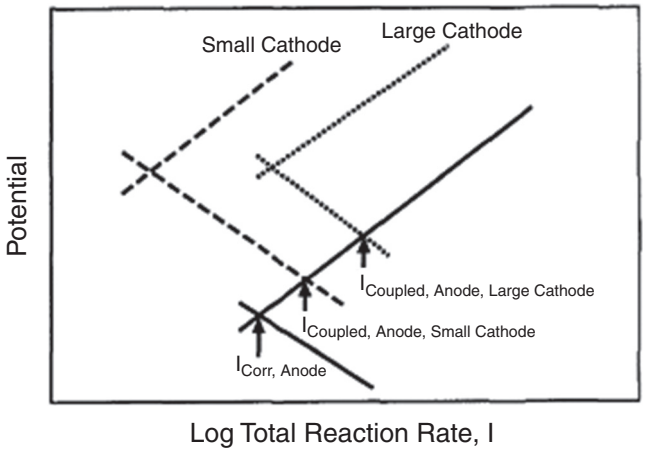
EFFECTS OF ANODE–CATHODE AREA RATIO

The axis labeling shifted between figure 1 and figure 4. Figure 1 expressed the reaction rate as lower case *i*, the reaction current per unit area, which is appropriate for considering single metals. Figure 4 was forced to switch to total reaction current *I*, because it is the total current (summation) from both metals that must be considered. The effect of changing the relative areas of the anode and cathode is illustrated in figure 5. If the exposed surface area of the cathode is small, then the original Evans diagram for the cathodic material must have the current densities multiplied by a small area to obtain total currents. This makes the lines shift far to the left in figure 5, and results in only a small increase in anodic corrosion rate, $I_{coupled,\ anode,\ small\ cathode}$, over $I_{corr,\ anode}$. If the exposed surface area of the cathode is large, then the original Evans diagram for the cathodic material must have the current densities multiplied by a large area to obtain total currents. This makes the lines shift far to the right in figure 5, and results in a large increase in anodic corrosion rate, $I_{coupled,\ anode,\ large\ cathode}$, over $I_{corr,\ anode}$. This illustrates the area ratio effect in galvanic corrosion. A small anode and large cathode result in a large anodic corrosion rate, whereas a large anode and small cathode are far more desirable.

FLOW RATE

Changing the electrolyte flow rate can have significant effects on the reaction kinetics, shifting the curves in the Evans diagram,

FIG. 5 Effect of cathodic area on couple current.



and therefore, can dramatically influence galvanic corrosion rate. The direction of the effect can be predicted only using Evans diagrams, however.

If the cathodic reaction is oxygen reduction rather than hydrogen reduction, then oxygen must be supplied to the metal surface by diffusion in order to react. Diffusion can be a slow process relative to the electron exchange, and this can make the cathodic line in the Evans diagram deviate from a straight line. Oxygen diffusion occurs through a relatively stationary boundary layer, which becomes thinner as flow increases. Diffusion rate therefore increases with flow, and the maximum rate of the oxygen reduction reaction, i_L, increases with flow. This is shown in figure 6. When the diffusion-limited cathodic curve is present in a galvanic couple, the total cathodic current will increase with increasing flow, causing the corrosion rate of the anode to increase with increasing flow.

Flow also can have an effect on the anodic reaction. Many materials exhibit passivity, which causes the anodic reaction to deviate dramatically from a straight line. This is caused by the corrosion products formed during the anodic reaction becoming firmly attached to the metal surface, blocking the reaction from proceeding further. The anodic line in the Evans diagram will be straight until the corrosion product forms, after which the current will rapidly drop even though potential is still increasing. The low current will persist until the potential becomes sufficiently positive to break down the corrosion product or to produce oxygen directly from water by electrolysis. In either event, the current will then rise sharply. This is shown in figure 7. Some of the most protective passivating corrosion products are on stainless steels. These films form more readily in the presence of oxygen, and so are enhanced by flow. This leads to the situation shown in figure 8, where increasing flow increases oxygen delivery, which increases the amount of protective corrosion products, lowering the anodic currents. This can cause corrosion rates in a galvanic couple to decrease with increasing flow, opposite to the oxygen effect on the cathodic reaction discussed previously. Flow also can increase the corrosion rate, as in the case of

FIG. 6 Effect of flow on diffusion-limited current density.

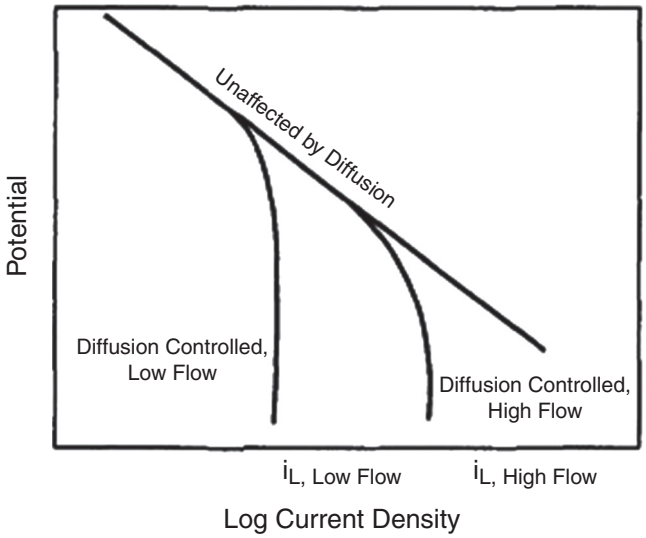
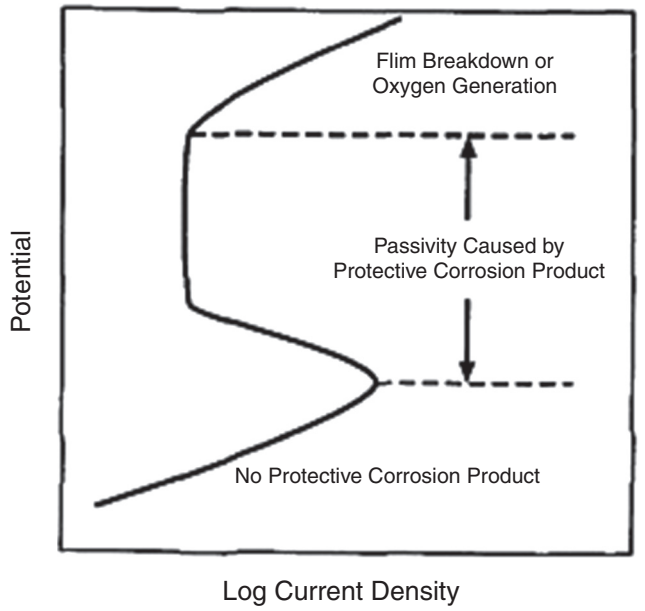


FIG. 7 Effect of passivity on anodic polarization curve.

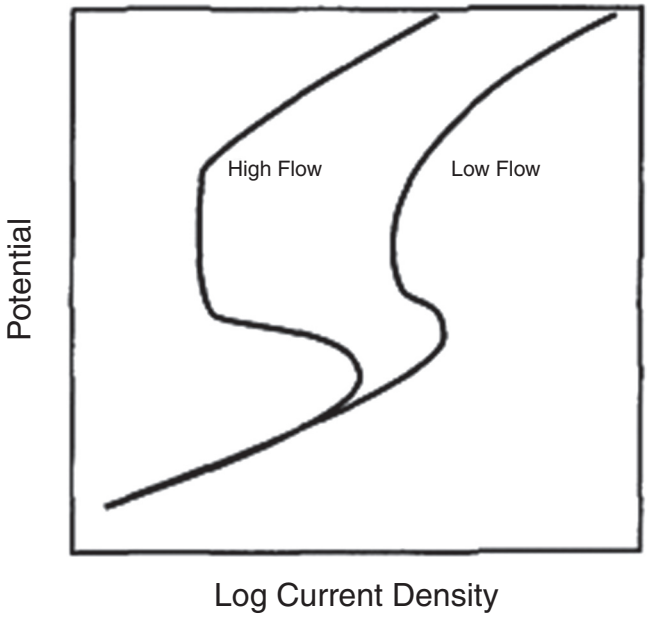


erosion corrosion, or can increase removal of certain less-adherent corrosion products.

MEASURED CURRENTS

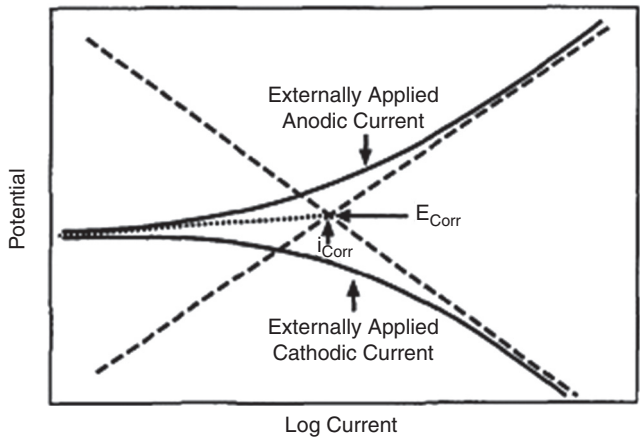
Much of the current that flows between reactions in a galvanic couple will flow between the anodic and cathodic metals, but some also flows within these metals. Internal current is not directly measurable, although it can be inferred from other test methods that use external current that can be measured. Measurable external currents can be predicted from the Evans diagrams as follows. When a metal is corroding by itself, as in figure 9, the

FIG. 8 Effect of flow on passivity.



corrosion current is i_{corr}, which flows entirely between anodic and cathodic sites in the metal and cannot be measured. All electrons produced by the anodic reaction are consumed by the cathodic reaction. If an external source, such as a power supply or another metal electrically connected to the first, removes electrons, then the anodic reaction will increase to supply more electrons, and the cathodic reaction will decrease to use fewer electrons. The externally applied anodic current will be the difference between the anodic and cathodic reaction currents. At very positive potentials, the cathodic current will be negligible, and the applied current will roughly equal to the anodic corrosion rate. At very negative potentials, the anodic current will be negligible, and the applied current will roughly equal the cathodic current. At E_{corr}, the external current will be zero. The externally applied current will follow a shape called a polarization curve, shown in figure 9.

FIG. 9 Creating polarization curves from Evans diagrams.



Galvanic corrosion rate can be roughly predicted by superimposing the polarization curves of the anodic and cathodic materials. This is shown in figure 10. When the open-circuit potentials of the anode and cathode are relatively far apart, more than roughly 120 mV depending on the slopes of the curves, this prediction is fairly accurate. The polarization curves for the anodic and cathodic materials are multiplied by their respective wetted surface areas and placed on the diagram. The intersection of the anodic curve for the anodic material with the cathodic curve for the cathodic material provides an indication of the galvanic corrosion rate, $I_{galvanic}$, and the exact coupled potential, E_{couple}. This technique does have limitations. For example, it does not account for any change in reaction rates that may occur over time.

CURRENT AND POTENTIAL DISTRIBUTIONS

As stated earlier, for galvanic corrosion to occur, there must exist at least two metals with different corrosion potentials, a metal path for electrons to flow between them, and an ionic path through the electrolyte to complete the electronic circuit. The latter is sometimes not considered, but it contributes to the nonuniformity of galvanic current and potential on large structures.

Figure 11 shows two metals electrically connected in an electrolyte that has a significant resistivity, such as tap water. Current I_1 must travel through some small electrolyte resistance R_1 to go the short distance from the anode to the cathode, experiencing a voltage drop according to Ohm's law of I_1R_1. Current I_2 must travel farther, through an increased resistance R_2, and therefore will be smaller than I_1. The voltage drop here is I_2R_2. The largest

FIG. 10 Rough prediction of galvanic current from overlapping polarization curves.

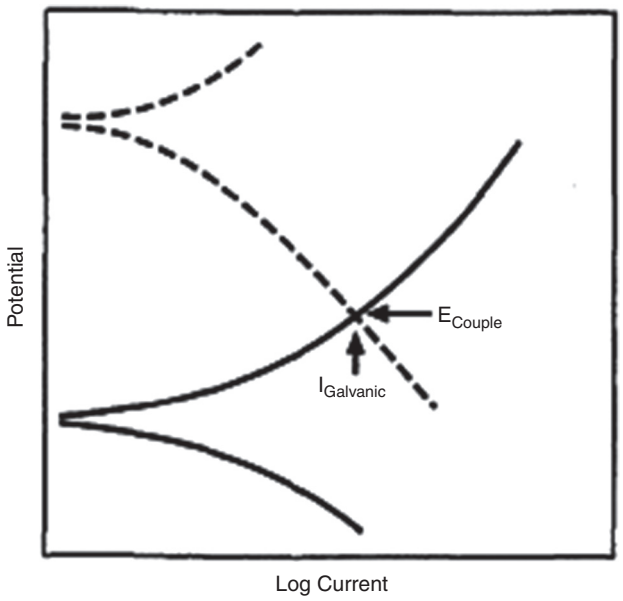
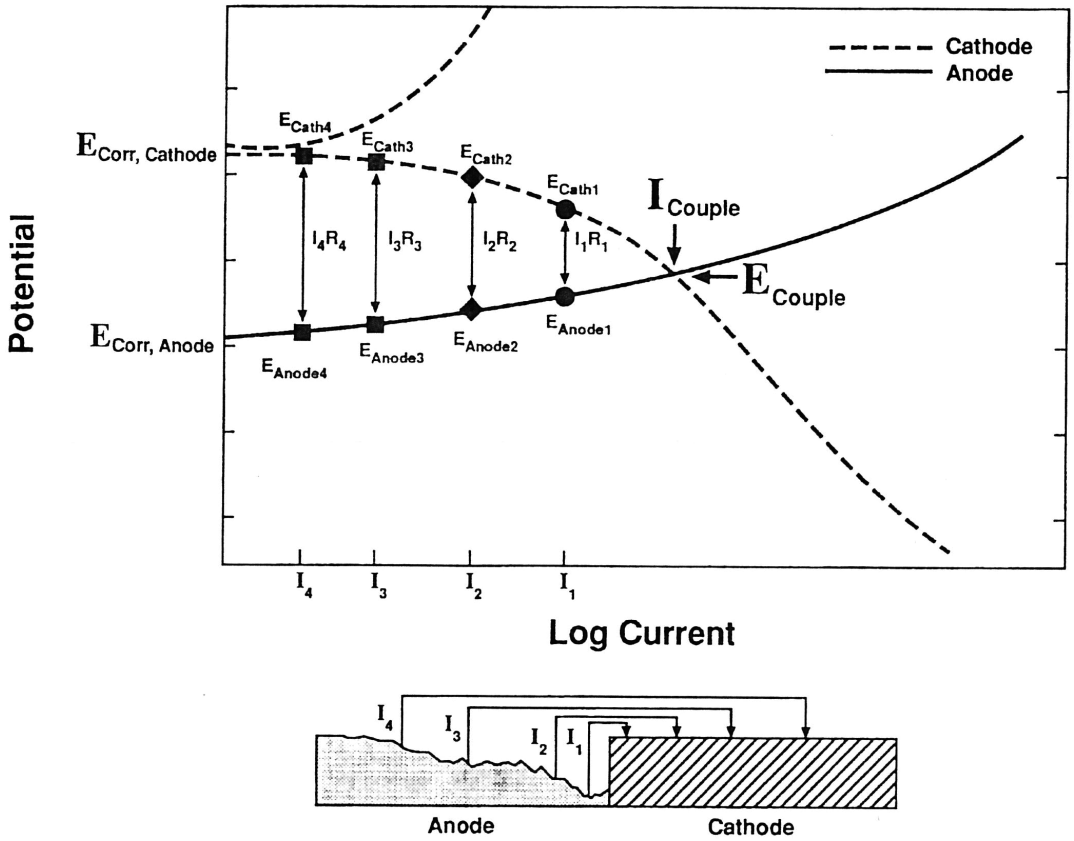


FIG. 11 Effect of distance on IR drop and current density.



distance is traversed by current I_4, through the largest resistance R_4, and therefore will be the smallest current and undergo a voltage drop of I_4R_4. The falloff of current (and corrosion rate) as distance from the second metal increases is a common method for recognizing galvanic corrosion. Although current decreases with distance, the product of current times resistance will increase with distance. The largest voltage drop in this example would be I_4R_4 and the smallest would be I_1R_1. The voltage drops are shown in figure 11. The presence of an IR drop not only decreases the current on the anodic and cathodic materials, but also causes the anode to be at a different potential than the cathode. The potentials will be closest to E_{couple}, where the anode and cathode are closest, and will shift toward E_{corr} for each material as separation distance increases. This creates a potential distribution over the structure that can be measured.

FACTORS CONTROLLING GALVANIC CORROSION

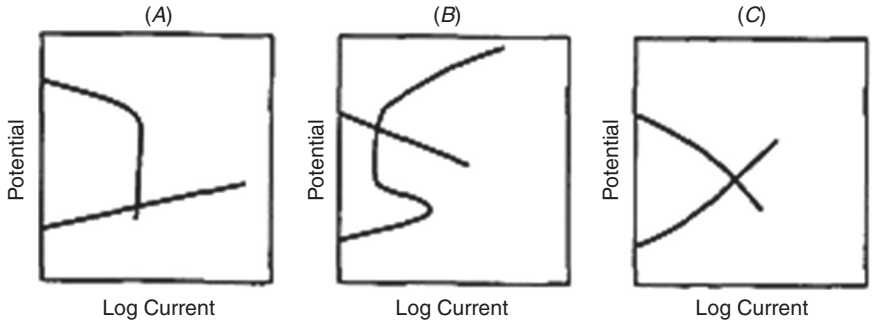
Any factor that controls corrosion of a single metal may control galvanic corrosion by its effect on one or more of the reaction lines on the Evans diagram. In addition to flow and pH, these factors include temperature, electrolyte composition, surface condition of the metals, thermo-mechanical and potential history of the surfaces, and many more too numerous to mention. Factors unique to galvanic corrosion include anode-to-cathode area ratio, electrolyte resistivity, and geometry. Sometimes it is important to know which reactions control or limit galvanic corrosion rates. The polarization curves in figure 12*A* illustrate how a diffusion-limited cathodic reaction will control the rate of galvanic corrosion. Changing the shape of the anodic polarization curve, for example, by the use of an anodic inhibitor, has no effect on galvanic corrosion rate determined by the curve intersection, whereas changes in the cathodic diffusion-limited current result in equivalent changes in galvanic corrosion rate. Similarly, galvanic corrosion of passive materials, as shown in figure 12*B*, is frequently under anodic control, with the shape of the cathodic polarization curve making little difference unless it intersects the active-passive nose of the anodic curve. Mixed control as in figure 12*C* is also possible.

Testing Techniques

EXPOSURE OF GALVANIC COUPLES

The most obvious method of testing for galvanic corrosion is to construct a couple between the materials of interest and place it in the environment of interest. Material condition, environment, and geometry should simulate the application as closely as possible. Care should be taken during assembly to ensure adequate electrical connection, and this connection should be checked

FIG. 12 Type of control of galvanic corrosion reactions: (*A*) cathodic control; (*B*) anodic control; and (*C*) mixed control.



before, after, and occasionally during the exposure using an appropriate ohmmeter. In some cases, it may be possible to electrically isolate the individual metals from each other and connect them through an external wire, which can be used to measure galvanic current during exposure. For small specimens, it is permissible to use a 1-Ω resistor in the line to measure voltage drop and calculate current. Where currents are larger or where corrosion potentials are close for the materials involved, use of a zero-resistance ammeter may be more appropriate for current measurement. The potential of the couple usually can be monitored during the exposure using a suitable reference electrode. More detail on electrochemical potential measurement can be found in ASTM G215, *Standard Guide for Electrode Potential Measurement*, and detail on galvanic corrosion testing in electrolytes can be found in ASTM G71, *Standard Guide for Conducting and Evaluating Galvanic Corrosion Tests in Electrolytes*. In vitro testing information can be found in ASTM F3044, *Standard Test Method for Evaluating the Potential for Galvanic Corrosion for Medical Implants*.

Important material factors to consider when simulating a galvanic corrosion situation include chemical composition, thermal history, and surface condition. Changes in these parameters may change the corrosion behavior of a material when it is not in a galvanic couple without affecting its galvanic corrosion behavior, or changes may affect its galvanic corrosion behavior without a significant effect on its corrosion properties when it is used alone.

Any environmental factor that can influence corrosion also can affect galvanic corrosion. Environmental factors to consider when designing a test include major chemical components, dissolved gases, minor constituents, organic materials, biological organisms and activity, temperature, flow, and electrical conductivity. In atmospheric galvanic couples, atmospheric factors such as time-of-wetness, orientation relative to prevailing winds, sunlight exposure, height above ground, and other unique atmospheric conditions also should be considered. Some important atmospheric factors affecting corrosion are discussed in ASTM G33, *Standard Practice for Recording Data from Atmospheric Corrosion Tests of Metallic-Coated Steel Specimens*; ASTM G50, *Standard Practice for Conducting Atmospheric Corrosion Tests on Metals*; ASTM G84, *Standard Practice for Measurement of Time-of-Wetness on Surfaces Exposed to Wetting Conditions as in Atmospheric Corrosion Testing*; and ASTM G92, *Standard Practice for Characterization of Atmospheric Test Sites*.

The relative geometry of the parts of interest in the galvanic couple also can influence corrosion behavior. In low-conductivity environments, the distance of separation of the dissimilar metals will affect galvanic corrosion rate. Even in high-conductivity environments, it is difficult for galvanic current to travel into long narrow crevices or through narrow tubes. The relative wetted surface areas of the dissimilar metals will dramatically influence galvanic corrosion rate. In atmospheric exposures, geometry can control water trapping and drainage as well as thermal mass, which controls dew retention.

Ensuring adequate electrical contact between the dissimilar metals in a galvanic couple can be difficult. Pressure contact, such as between two plates bolted together, is subject to corrosion products forming between the plates and wedging them apart. Attachment of wires by soldering or brazing will work with some materials, but the use of drilled and tapped holes for screw attachment or through holes for bolting may be required for others. In some cases, spot welding can be used for electrical attachment. Finally, a wire may be inserted into a drilled hole and the hole then peened closed around the wire, although this method is not reliable over long exposure periods. Whatever connection method is used, the connection area and wire are subject to corrosion, which can affect both the electrical contact and the performance of the galvanic couple being tested. For this reason, coatings frequently are used on the connection area, although coatings may result in crevice corrosion. When electrical contact is maintained by physical contact of the dissimilar metals, periodic measurement is desirable to ensure that electrical continuity is maintained. If continuity is checked frequently relative to the length of the exposure, then it will be possible to adjust the materials to regain this continuity without significantly affecting the results. This should be done without disassembly or gross movement, such as by tightening tensioning bolts.

Mounting of galvanic couples for testing should be done carefully using insulator materials to avoid the possibility of establishing electrical continuity with the mounting device or test chamber. Mounting techniques include gasketed seals, rod mounting, epoxy mounting, press-fit, partial immersion, full immersion, and others. The mounting technique chosen is related to the type of corrosion expected, the electrical connection method, the type

of exposure desired, the presence or absence of water-line effects, and the materials chosen.

Duration of exposure is extremely important in galvanic corrosion testing. In many galvanic couples, the amount of corrosion is highly variable with time. Initial high corrosion rates may fall dramatically, initial low rates may suddenly increase, and the relationship between anodic and cathodic materials can even reverse with time. For these reasons, the duration of the test exposure should be of sufficient length to ensure that the corrosion processes have reached steady state if long-term performance is being evaluated. Test duration should be similar to service duration for short-term service. In atmospheric testing, the season of the year when exposure is initiated may influence the test. Multiple exposures of different time periods may be used to give corrosion rate information as a function of time.

Exposures can be conducted on full-scale components or on scaled-down or simplified geometries. Full-scale components have a number of advantages, including not needing to consider details of geometry and ease of relating the results to service performance. Full-scale component testing, however, may be impractical or too expensive, in which case scale modeled components may have to be used. If scale modeling is used, then details of scaling laws must be understood before designing the test. For example, when galvanic corrosion current distribution is important, the conductivity of the electrolyte may need to be scaled by the same factor as the physical size. This procedure, called Dimension and Conductivity Scaling (DACS), involves the use of an electrolyte of one-tenth conductivity for a one-tenth-scale model. DACS scales only primary current distribution, which is controlled by the IR drop in the electrolyte. Secondary and tertiary current distribution are influenced by polarization behavior of the material involved, and are best approximated by the use of full-conductivity electrolytes. Both types of current distributions cannot be modeled simultaneously, so a decision must be made as to which is most important. Small structures in highly conductive electrolytes generally should be tested in full-conductivity electrolytes, whereas DACS should be used primarily for large structures in low-conductivity electrolytes. To date, DACS has been used primarily for ship cathodic protection system design. More information on scaling can be found in previously published work.[2–5]

ELECTROCHEMICAL TESTS

Accelerated testing to get a result in a shorter time period than would be possible naturally should be avoided whenever possible because the mechanism of galvanic corrosion can change if the rate is altered significantly. For this reason, electrochemical tests frequently are chosen to evaluate galvanic corrosion performance. The sensitivity of these tests allows for obtaining results fairly quickly without accelerating the corrosion process.

Electrochemical galvanic corrosion tests can be placed into three categories: sensitive galvanic current measurement, galvanic series determination, and polarization curve measurement. Sensitive current measurement involves an ordinary galvanic couple exposure, but with current between the dissimilar metals forced to flow through an external wire where it can be measured with a zero-resistance ammeter or by voltage drop across a 1-Ω shunt resistor. This type of testing is described in ASTM G71. Galvanic current also can be measured by measuring potential gradients in the electrolyte near the materials of interest. This is discussed in the section "Scanning Electrochemical Testing: Scanning Vibrating Electrode Technique."

Determination of a galvanic series involves placing the materials of interest from the galvanic couple individually in the environment of interest and monitoring their electrochemical potential over time. The material with the more electronegative potential will become the anode and suffer accelerated corrosion when placed in a galvanic couple. Galvanic series are extremely useful during the materials selection process to ensure that the anodic areas are large compared to the cathodic areas in complex structures. The galvanic series is influenced by all of the environmental variables described earlier, so the series should be used only if it is developed in the environment in which the galvanic couple will see service. One disadvantage of the galvanic series is that it is frequently misapplied. A series developed in one environment cannot be used to predict performance in another environment. A second disadvantage of the galvanic series is that it does not predict rate. Separation in potential between dissimilar materials does not relate to the rate of corrosion in a couple. More details of the development and use of galvanic series are given in ASTM G82, *Standard Guide for Development and Use of a Galvanic Series for Predicting Galvanic Corrosion Performance*.

Insight into galvanic corrosion behavior can be gained by overlaying polarization curves, as described earlier. The determination of polarization curves is, therefore, an important method for galvanic corrosion testing, although it may miss important factors that long-term testing may better capture. These curves can be obtained galvanostatically, potentiostatically, or potentiodynamically. Galvanostatic testing is typically used for determining the efficiency of sacrificial anodic materials, such as is done in ASTM G97, *Standard Test Method for Laboratory Evaluation of Magnesium Sacrificial Anode Test Specimens for Underground Applications*, or NACE SP0387, *Metallurgical and Inspection Requirements for Cast Sacrificial Anodes for Offshore Applications*.

The most common method of obtaining polarization curves is potentiodynamically. Potentiodynamic testing is described in Chapter 8, "Electrochemical Tests." For galvanic corrosion, the scan rate for these tests should be as slow as possible, since long-term polarization behavior usually is sought when predicting long-term galvanic corrosion behavior.

Potentiostatic polarization curve generation is advantageous for situations in which polarization is time dependent and prediction of long-term galvanic corrosion performance is desired. This involves exposing a series of individual specimens of each material at a variety of different potentials for a duration sufficient to ensure steady-state behavior. The steady-state current at each potential is obtained, and polarization curves are constructed from the potential–current data pairs.

Using electrochemical tests to predict galvanic corrosion performance has the same caveats as any other type of predictive testing. Conditions must be as close as possible to those being modeled. This includes not only solution chemistry and flow,

but also the surface condition of the samples. Polished samples can behave quite differently from samples with more representative surface conditions and corrosion products developed by preexposure.

More detail on using electrochemical tests for galvanic corrosion can be found in work by Scully[6] and Baboian.[7]

PROBES FOR GALVANIC CORROSION TESTING IN PRODUCTION ENVIRONMENTS

Galvanic probes can be used in a production environment to monitor corrosion. The use of such probes is detailed in NACE TM0416, *Test Method for Monitoring Atmospheric Corrosion Rate by Electrochemical Measurements*, and NACE 1C187, *Use of Galvanic Probe Corrosion Monitors in Oil and Gas Drilling and Production Operations*. Atmospheric time-of-wetness can be determined using a galvanic corrosion probe as detailed in ASTM G84.

COMPUTER MODELING

Although not a laboratory testing technique, computer modeling is an increasingly important tool in understanding and predicting galvanic corrosion performance. As noted, exposure of scaled components of a galvanic couple leads to scaling problems in that the primary current distribution cannot be scaled at the same time as the secondary and tertiary current distributions. Computer modeling is usually best for making accurate predictions of the distribution of galvanic corrosion over a structure in which solution IR drop and polarization behavior both control current distribution. Computer models require the geometry of the structure to be an input. Additional inputs include the electrolyte conductivity and the polarization behavior of the surfaces of all materials, which usually are obtained from laboratory testing. Although finite element analysis and finite difference analysis have both been used to predict the distribution of galvanic currents on structures, the boundary element technique is becoming the computer tool of choice. This technique requires only that the surfaces of the structure be defined, whereas the other methods require that the volume of the electrolyte be divided into a three-dimensional grid, which is a time-consuming and difficult process for complex structures. The disadvantage of the boundary element method is that, at present, some commercially available software for performing this analysis is not user-friendly.

ATMOSPHERIC TESTS

Unlike galvanic corrosion testing in electrolytes, galvanic corrosion testing in the atmosphere has a limited number of test variables, making it easier to conduct standardized tests.

Three factors that are different in atmospheric testing from most other galvanic corrosion testing are the presence of a limited amount of electrolyte, the need for a long duration of exposure, and the importance of specimen orientation. Because rainwater and dew are fairly poor electrical conductors, and because they usually are present only as thin layers on the surfaces of materials exposed to the atmosphere, there is a large IR drop between the anode and the cathode in any atmospheric corrosion exposure. This drop limits the effective distance over which galvanic interactions take place to about 0.5 cm, which in turn means that the effective area ratio of anode to cathode in an atmospheric exposure is almost always about 1:1. The limited electrolyte also makes electrochemical measurements impractical. If atmospheric aerosols are heavy, such as may be the case in coastal conditions, the effective area ratio may not be 1:1 because of the thickness and conductivity of the surface moisture.

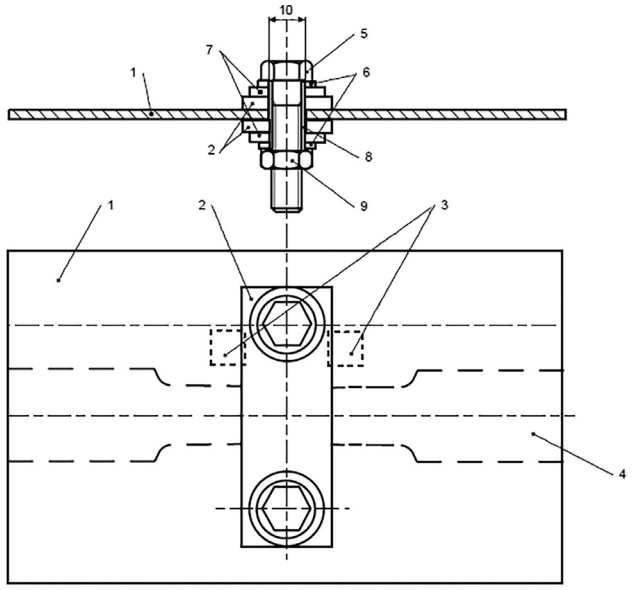
Atmospheric corrosion typically occurs only during a small percentage of the total exposure time, typically when the surfaces are wet from precipitation, dew, or fog, or when hygroscopic compounds on the surface absorb moisture during periods of high humidity. For this reason, atmospheric corrosion occurs slowly, and long exposure durations are usually necessary. Most tests typically involve minimum durations of 1 to 3 years, with 20 years maximum exposure not unusual. Tests of shorter duration than 1 year not only have so little corrosion as to make evaluation of mass loss difficult but also suffer from the effects of seasonal variation of corrosion rate.

Finally, the time that a specimen is wet depends on sunlight heating, prevailing winds, and specimen geometry. Specimen orientation, therefore, is much more critical in atmospheric galvanic corrosion testing. Standard orientations are specified in ASTM G50 as 30° to the horizontal facing south or the nearest source of corrodent (the sea).

Three standardized atmospheric galvanic corrosion tests are the plate test, the wire-on-bolt test, and the disk test. The plate test, described in ISO7441, *Determination of Bimetallic Corrosion in Outdoor Exposure Corrosion Tests*, consists of a large plate of the anodic material sandwiched between two small plates of the cathodic material that are held together with nonmetallic or insulated bolts. Sometimes the crevice area between the plates is coated with an organic material. The two possible configurations are shown in figure 13. Typical exposure durations are 1 to 20 years. At the end of this time, the anodic plate may be evaluated metallographically, visually, by mass loss, or by material property loss (typically using tension testing). The advantages of this test are that materials usually are available in plate form, and a wide range of analyses can be used on the exposed panels. The disadvantages include the need to know which material is the anode beforehand, the long exposure duration, the difficulty of maintaining electrical continuity between panels, and the possibility of confusing crevice effects with galvanic effects. At one time, ASTM also had a standard for this test method, but dropped this standard because of these disadvantages and lack of use.

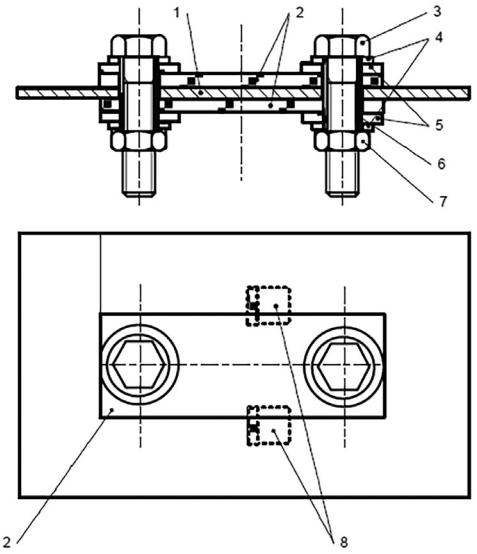
The wire-on-bolt test, described in ASTM G116, *Standard Practice for Conducting the Wire-on-Bolt Test for Atmospheric Galvanic Corrosion*, has been used with standard materials as an atmospheric corrosivity test under the names of the CLIMAT and ATCORR tests. This test consists of wrapping a 1.0-m length of wire of the anodic material around a threaded bolt or rod of the cathodic material. Post-test evaluation typically is done only by mass loss. Because the wire diameter is much smaller than the 0.5-cm galvanic interaction distance in the atmosphere, the effective anode-to-cathode area ratio is well below 1:1, making this a fast test. A typical exposure duration is 90 days. The short duration is a significant advantage to this test. The disadvantages

FIG. 13 Plate test assembly for galvanic corrosion testing (redrawn and simplified from ISO7441).



1 anodic plate
2 cathodic plate
3 microsections
4 tensile test specimen
5 bolt
6 washer
7 insulating washer
8 insulating sleeve
9 nut

test specimen used for evaluations based on criteria other than mass loss



1 anodic plate
2 cathodic plate
3 bolt
4 washer
5 insulating washer
6 insulating sleeve
7 nut
8 microsections

test specimen for evaluation based on criteria other than mechanical properties

include materials needing to be in wire and threaded rod form, the beforehand knowledge of which material is the anode, and the seasonal variations in exposures of such short duration. A diagram of the sizes and forms of the components needed to construct an assembly is given as figure 14, and a completed assembly is shown as figure 15.

The disk test, described in Baboian[8] and Blum[9] and in the now-discontinued ASTM G149, *Standard Practice for Conducting the Washer Test for Atmospheric Galvanic Corrosion* (withdrawn 2004), consists of a set of four washers of alternating anodic and cathodic materials of graduated sizes bolted together with an insulated bolt. Only the center two washers are used for the analysis. A cross-sectional assembly view is shown in figure 16. The duration of this test is usually 1 to 20 years. Post-test evaluation usually consists only of mass loss. Advantages to this test are that material is usually easy to find, the anodic material need not be known beforehand, and it is easy to set up and evaluate. The disadvantages include the long test duration and the lack of information available on corrosion morphology or mechanical property degradation.

COMPUTATIONAL MODELING OF GALVANIC PROCESSES

Computational corrosion models are either empirical or fundamentally deterministic. Models derived from empirical data are inherently linked to the precision and accuracy of the data. Deterministic models are based in the fundamental physics of multivariable processes and therefore are more robust than empirical models. Modeling of corrosion processes allows for the

FIG. 14 Components for making wire-on-bolt atmospheric exposure assemblies. *Source:* Taken from ASTM G116.

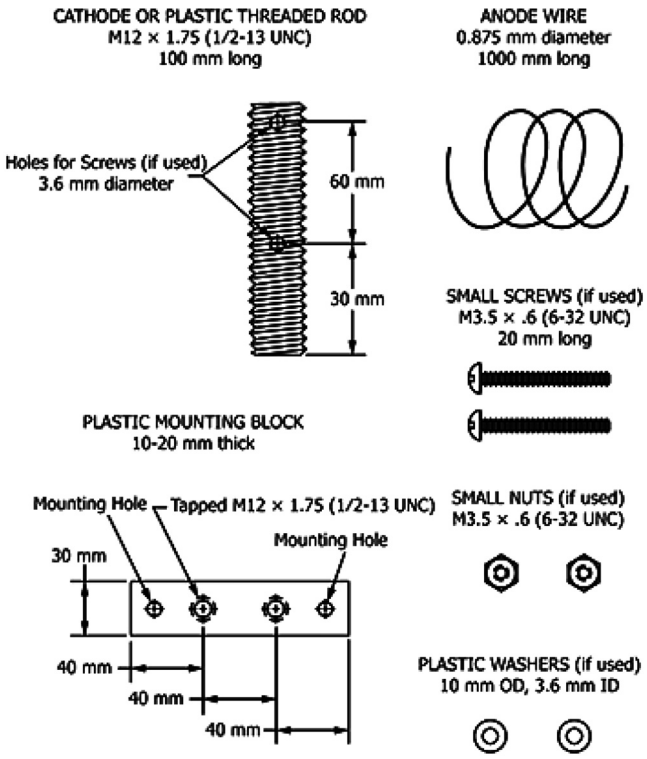


FIG. 15 Schematic of completed wire-on-bolt assemblies mounted for exposure. *Source:* Taken from ASTM G116.

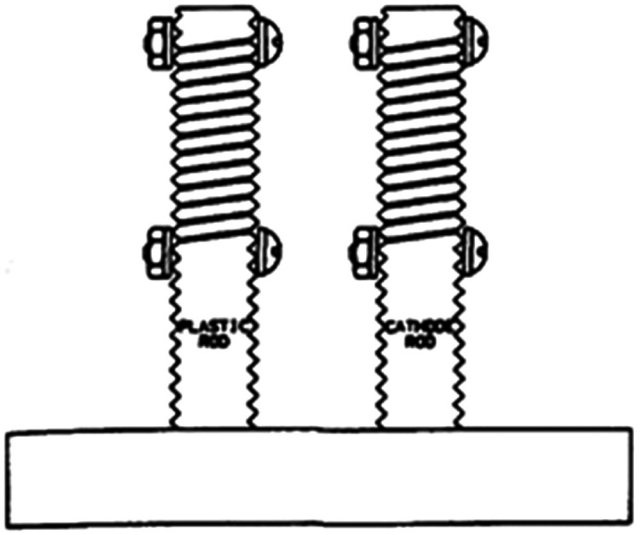
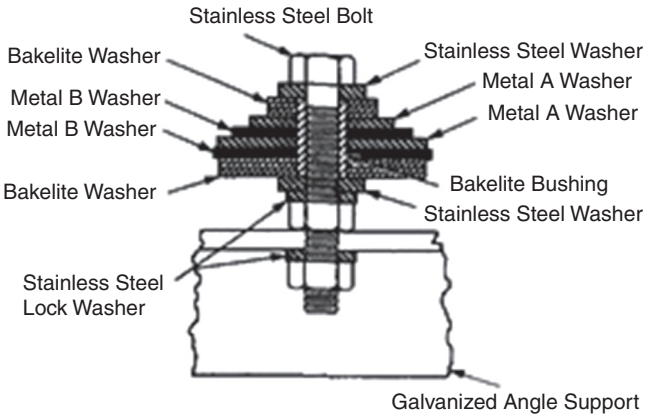


FIG. 16 Cross section of disk test assembly for atmospheric galvanic corrosion.



separation of parameters that cannot be separated in practice (i.e., virtual experiments). Each parameter can be individually probed in computational experiments while holding other parameters to defined values.

Models of corrosion processes have been developed that incorporate a range of chemical and electrochemical reactions with the complex interactions of diffusion and migration. The models often are expressed as differential or other nonexplicit mathematical equations.[10] Numerical methods are used to solve a wide range of partial differential equations based on discretization methods, including the following: (1) finite difference analysis, (2) boundary element analysis, and (3) finite element analysis. The governing equations are based on primary, secondary, and tertiary current distribution equations.[11] The mathematical treatment of the different solver routines is beyond the scope of this work but an overview is provided.

Finite difference modeling involves dividing the region of interest into a grid of points, expressing the governing differential equations as difference equations at each point, and solving the difference equations to determine an approximate solution of the governing equations. Finite difference methods are simple to code, but clumsy when applied to complex geometries. They most often are used for the temporal aspect of a model. Boundary element models translate the differential equations across the geometry volume into integral equations over the surface enclosing the volume and solve these integral equations by dividing up the surface into elements. Boundary element models are most useful when the geometry of interest has a low surface-to-volume ratio. Finite element models divide the region of interest into simple geometric shapes (such as triangles), build equations for the value of the variable of interest at each node on each shape, and then solve the equations for all of the nodes simultaneously. Finite element models have the advantage that they can represent complex geometries. Much of the recent modeling efforts have utilized finite element analysis because of its wide availability in commercial multiphysics frameworks.

As corrosion models add complexity, they become more difficult to solve and require increased computational processing power, speed, and memory. Therefore, assumptions are made to simplify the governing equations that described the underlying physics. The goal is to remove factors that do not play a strong role in the underlying corrosion mechanisms, but not to eliminate too many factors causing the model to lose its predictive behavior. The simplifying assumptions commonly made in corrosion models fall into five different categories, as defined by Stewart:[12]

- Elimination of some thermodynamic variables: Most experiments are performed at a constant temperature and pressure, and the effects of changes to these are often ignored.
- Simplifying chemistry effects: Dilute solution theory is usually assumed; the diffusivity and mobility of a species is independent of its concentration. The precipitation and accumulation of corrosion products is often ignored.
- Simplifying potential effects: As described earlier, the diffusion potential is usually ignored in most models and charge neutrality is maintained by specific species.
- Ignoring some temporal effects: Whereas changes of species concentration over time may be accounted for, the changes in electrode kinetics or generation rates with time are often ignored. The use of a single electrochemical polarization behavior is often used throughout a model. Some models also assume chemical reactions are in equilibrium at all times or also called steady state.
- Simplifying geometry: Models assume that electrodes and the overlying electrolyte have ideal dimensions. This is often not the case, however, of practical systems that often have variations in geometry throughout.

Modeling of galvanic corrosion processes requires the following: (1) dissimilar alloys; (2) electrical contact, either directly or by a secondary, grounding path between the dissimilar alloys; and (3) an electrolyte. Early galvanic corrosion modeling of alloy

surfaces covered by thin electrolytes generally assumed that only the anodic reaction occurred on a single galvanic member and that the cathodic reaction transpired on the other member of the couple.[13–15] When galvanic couples contain more than two individual members, however, there may be anodic and cathodic contributions from more than one member of the couple. Kinetics generally are assumed to follow linear or Butler-Volmer behavior, but this may not be the case in a number of practical cases in which experimentally determined polarization curves may be more appropriate.

Most recently, computational galvanic corrosion models have been employed to examine the corrosion and protection of aluminum. Mizuno and Kelly[16] modeled the galvanic interaction between aluminum-magnesium alloy AA5083 and AISI 4340 steel under atmospheric exposure conditions. The model geometry consisted of co-planar steel and aluminum electrodes covered by a thin electrolyte with a thickness determined from relative humidity and salt loading. A finite element solver was used to calculate the potential distribution over the electrodes based on the tertiary current distribution governing equations. Electrochemical boundary conditions were determined by experimental measurements in the form of polarization curves. The model was validated by correctly predicting that the maximum degree of intergranular corrosion damage of sensitized AA5083 would occur at 90% relative humidity when coupled to AISI 4340 steel.

Murer et al.[17] modeled galvanically coupled co-planar 99.9% aluminum and solid solution aluminum-4% copper electrodes under thin film atmospheric conditions. Electrochemical boundary conditions were determined from experimentally measured polarization curves through microcapillary and bulk solution electrochemical cells. The model framework was based on the finite element method with potential distributions solved through either secondary (LaPlace equation) or tertiary (Nernst-Plank equation) current distribution governing equations. The model was validated against a bimetallic electrode probed by the scanning vibrating electrode technique (SVET). The authors concluded that the model (regardless of current distribution type) qualitatively predicted the experimentally obtained SVET measurements. The model was too overly dependent on the input boundary conditions, however, to be used as a predictive model of microgalvanic coupling.

Liu et al.[18] examined the galvanic interactions of AA7075 anode and austenitic stainless steel 316L cathode under thin films conditions. The finite element model solved the LaPlace governing equation describing the secondary current distribution of the system. Simulated thin film electrochemical boundary conditions were determined from the cathodic kinetics generated experimentally by use of a rotating disk electrode. The model predicted that under thin film conditions, ohmic drop through the electrolyte was the controlling factor for the total galvanic current (corrosion) of the system.

King et al.[19] used the finite element method to examine the throwing power of sacrificial metallic coatings in the cathodic protection of AA2024. The geometry was co-planar electrodes of AA2024 and magnesium rich primer (MgRP) exposed to thin film of salt solution. The model solved the LaPlace equation for secondary current distribution with electrochemical boundary conditions adapted from experimentally determined polarization curves. The model also incorporated thin film resistances mimicking the resistive nature of the MgRP as a heterogeneous structure of metallic Mg particles embedded in an epoxy matrix. The model was validated with a microarray of AA2024 and Mg electrodes exposed to salt solution in humid atmosphere. The model correctly predicted the potential distribution of the galvanic couple interface as a function of electrolyte thickness and solution conductivity. The model also predicted that the inherent resistivity of the MgRP would regulate the cathodic protection throwing power over the AA2024 surface.

Computational modeling is a powerful tool used to examine galvanic systems. Modeling can be used to guide the design of structures to minimize galvanic corrosion or to predict the lifetime of structures exposed in corrosive environments such as seawater. Using computer models to predict the magnitude of galvanic corrosion or the current demand for cathodic protection systems in seawater or other electrolytes requires accurate polarization data for the materials involved.[20] Polarization curves for most structural materials in seawater are exposure-time and scan-rate dependent, however, thus complicating long-term galvanic corrosion predictions.[20]

Because of the need for assumptions to make computational models useful, care must be taken to verify and validate the results after model convergence. Verification can include model result comparisons to an analytically solvable system while validation often requires a proof-of-concept laboratory experiment. In addition, convergence criteria and geometry mesh density interplay between model accuracy and computation time. Specifically for galvanic models, which most often operate under open-circuit conditions, the requirement that the total anodic and cathodic currents sum to zero is a valid verification step.

Evaluation of Test Results

EXPOSURE OF GALVANIC COUPLES

If the different materials can be disassembled after testing, then mass loss measurements can be performed. In some cases, loss of strength also may be of interest. If disassembly is not possible, the specimens still may be examined for pitting, cracking, color, and extent of corrosion products and, in some geometries, thickness loss. Mass loss of an assembly may be useful if corrosion of the cathode was minimal. After exposure, destructive techniques such as metallographic examination may provide information about the extent and morphology of corrosion. Useful standards for cleaning samples after immersion and evaluating mass loss, pitting, and degradation in properties are ASTM G1, *Standard Practice for Preparing, Cleaning, and Evaluating Corrosion Test Specimens*; ISO8407, *Corrosion of Metals and Alloys – Removal of Corrosion Products from Corrosion Test Specimens*; ASTM G46, *Standard Guide for Examination and Evaluation of Pitting Corrosion*; and ASTM G71. Applying the results of a set of measurements designed to generate a galvanic series is described in ASTM G82.

ELECTROCHEMICAL TESTS

When the potentials of two materials in a galvanic couple are widely separated, the majority of the corrosion is driven by the external cathode, in which case Faraday's law can be used to calculate the galvanic corrosion rate from the galvanic current measured between them. This calculation can be done by the procedures in ASTM G102, *Standard Practice for Calculation of Corrosion Rates and Related Information from Electrochemical Measurements*.

Overlaying of polarization curves of the different materials in a galvanic couple must be done by first converting the current densities into total currents by multiplying the polarization curves by the exposed wetted surface area for each material. The curves then may be overlaid, and if IR drop is not important, then the couple current and potential may be predicted. If the coupled potential deviates by more than 50–100 mV from the open-circuit potential of the anode, then the current may be converted by Faraday's law into a corrosion rate. If the coupled potential deviates by less than 50–100 mV from the open-circuit potential of the anode, then it is conservative to add the open-circuit corrosion rate of the anode to the corrosion rate calculated from Faraday's law to get the total anodic corrosion rate. Neither of these methods is exactly accurate, but both will give a reasonable approximation to the true corrosion rate of the anode in the couple.

If the polarization curve for the anode is known, then the coupled potential may be measured to predict corrosion performance. The couple current is the current on the anodic material polarization curve at the measured coupled potential. The corrosion rate may be calculated from the couple current determined in the same way as in the previous paragraph.

SCANNING ELECTROCHEMICAL TESTING: SCANNING VIBRATING ELECTRODE TECHNIQUE

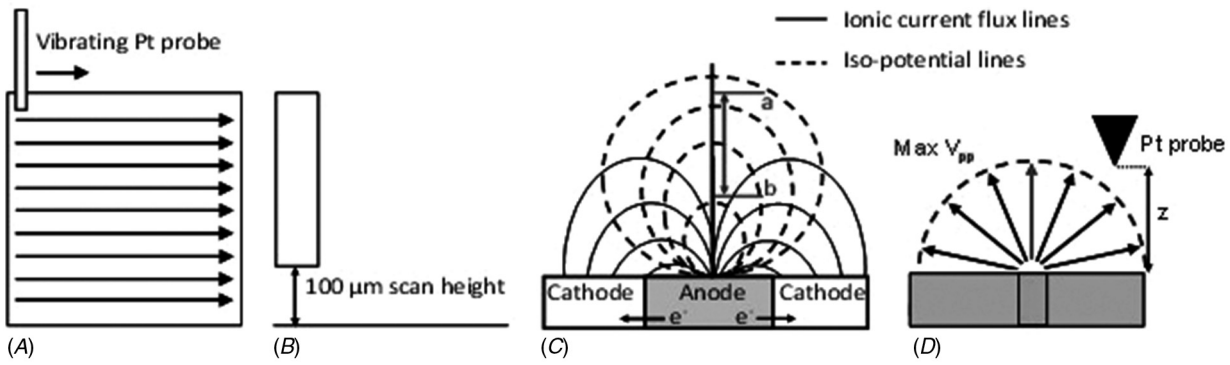
SVET is a well-established tool for in situ assessment of localized corrosion phenomena in full immersion conditions.[21–25] The technique is particularly useful for the study of galvanic corrosion and has been used extensively to study the interface between dissimilar metals.[26–30] A major advantage of the SVET for this application is the ability to measure local internal currents occurring on each metal of a galvanic couple. As such, the efficiency of a sacrificial anode supplying current to a cathodically protected surface can be discerned by differentiating between the current available for cathodic protection or galvanic corrosion and "self-corrosion." Likewise, the distance over which a sacrificial anode can afford protection, termed the "galvanic throwing-power," can be studied by mapping or profiling across an extended length of a cathodically protected surface.[29] Methods for using SVET for the study of dissimilar metal interfaces will be discussed in detail.

The SVET is completely nonperturbing to the corrosion occurring on the metal surface and to the experimental conditions, and thus it enables quantification of corrosion activity over periods of several days. The size, shape, and spatial distribution of anodic (positive) current and cathodic (negative) current above a corroding surface can be measured and a time-resolved data series can be built up to map the progression of electrochemical processes. A vibrating platinum microdisc electrode, typically 5 μm to 150 μm in diameter, is scanned over the surface in a series of lines as shown in figure 17*A*. The probe is held at a fixed height (typically 100 μm) above the corroding metal (fig. 17*B*). In a localized corrosion cell, ionic current flow passes from spatially separated sites of cathodic and anodic activity in the electrolyte solution and electrons flow through the metal from anode to cathode. This is represented schematically in figure 17*C* where lines of ionic current flux and electron flow direction are shown. An ohmic potential gradient is generated that can be represented as lines of isopotential normal to the ionic current flux lines (fig. 17*C*). The vibrating probe measures the peak-to-peak electrochemical potential difference (V_{pp}) between two points in the electrolyte perpendicular to the metal surface, shown as points a and b in figure 17*C*. A matrix of individual data points is collected over the corroding metal surface and each data point is used to build a current density distribution map.

Calibration is necessary to convert the SVET peak-to-peak output voltage signal (V_{pp}) to current flux density along the axis of probe vibration (j_z). These are related as follows:

$$V_{pp} = j_Z(A_{pp}/\kappa), \tag{6}$$

FIG. 17 A series of schematics showing: (*A*) the scanning vibrating Pt probe moving over a metal surface in a series of line scans, (*B*) the probe at a fixed scan height above a metal surface, (*C*) ionic current flux emanating from a dissolving metal surface and the corresponding iso-potential lines, and (*D*) the point-current-source calibration method.



where:
κ = solution conductivity, and
A_{pp} = the peak-to-peak amplitude of vibration.
A quantity G may be defined as the SVET calibration factor,

where:
$G = \kappa/A_{pp}$.

G must be obtained for the specific electrolyte solution of interest and is not linked to the metal being tested. It is recommended that calibration is carried out before every experiment. The most common method for obtaining G is by a "point current source" method,[26,31,32] as demonstrated in figure 17*D*. An applied external galvanostatic current ($i_{applied}$) of known value is set up in the solution and the area that encompasses the emanating current is mapped with the SVET probe at a fixed probe height, z. An even current distribution over the surface of a hemisphere is assumed, and applied current density is calculated by dividing $i_{applied}$ by the surface area of a hemisphere ($2\pi z^2$). The maximum V_{pp} can be obtained from the resulting V_{pp} distribution map. G is then obtained by taking the gradient when plotting the maximum V_{pp} versus $i_{applied}/(2\pi z^2)$ for a range of positive and negative $i_{applied}$. G is applied to equation (6) to obtain j_z.

The maximum test area for a commercial SVET is approximately 30 mm × 30 mm and test samples must be adjusted accordingly, adhering to DACS where necessary. To study a galvanic couple the two metals of interest should be electrically connected either through direct contact or through an external wire connecting them at the back. The most common sample set-up for SVET experiments is by mounting in resin, because the technique requires a smooth, flat surface to ensure a constant probe height when scanning the area of interest. Most commercial instruments are capable of measurement over planar surfaces only; however, height mapping is possible with some in-house instruments.[33] Scan resolution can be calculated using V_{pp} measured during the calibration and is quantified as follows:

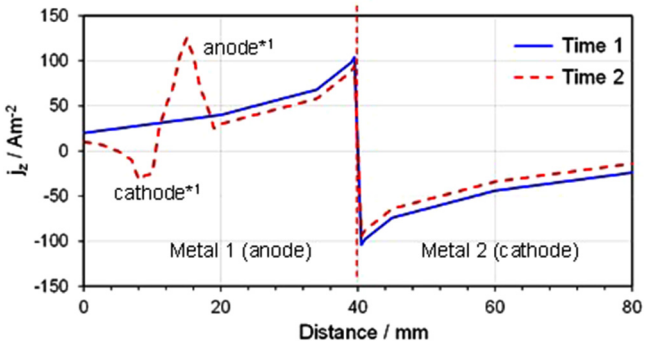
$$V_{pp}/\text{FWHM}, \quad (7)$$

where:
FWHM = full-width at half-maximum signal peak height (μm) and has been shown to be:
FWHM = 1.533 z.[32]

Evaluation of Test Results for a Dissimilar Metal Interface

Data can be plotted either as a series of current density distribution maps or as a series of line profiles across the length of the coupled metals, the latter is shown in the plot given in figure 18. This plot is a representation of data typical of that shown in previous publications.[20,29,34] As described earlier in this chapter, the current (both anodic and cathodic) is at a maximum at the interface between the two coupled metals and gradually diminishes with increasing distance from the interface because of the increased resistance. Line profiles enable inspection of the progression of the current density over time and any localized corrosion occurring on one or both of the predominantly anodic or cathodic metals within the couple can be observed. In figure 18, the labeled anode*1 and cathode*1 pictured on Metal 1 demonstrate areas of local internal corrosion activity at Time 2. A reduction in the overall anodic and cathodic current is typical when some of the current is being supplied to local internal activity, or "self-corrosion," as shown at Time 2 (when compared with Time 1) on Metal 1 and Metal 2, respectively.

FIG. 18 Representation of SVET-derived current density line profiles across the full length and interface of Metal 1 and Metal 2 at Time 1 and Time 2.



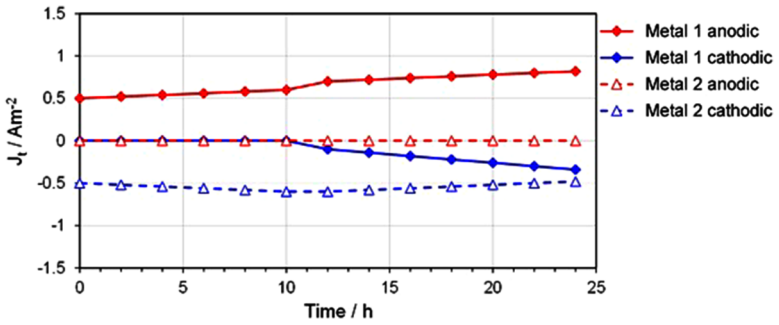
Data from individual current density distribution maps can be converted into time-dependent net anodic (J_{at}) and cathodic (J_{ac}) current density values through area-averaged numerical integration.[35] Compiling all J_{at} values from an experiment and plotting against immersion time enables an estimate of the corrosion rate. For a galvanic corrosion cell in which two metals have been electrically connected, as described here, data from each metal can be integrated separately to monitor the overall currents and local internal currents of each. This is particularly useful for the study of galvanic sacrificial protection systems as "self-corrosion" can be monitored. For any freely corroding surface, J_{at} should be equal to J_{ct} and figure 19 represents an ideal scenario in which the sum of the measured anodic current is equal to the sum of the measured cathodic current in accordance with mixed potential theory,
where:

$$\Sigma I_{anodic} = \Sigma I_{cathodic}.$$

In reality, discrepancies exist between SVET-derived J_{at} and J_{ct} measurements (this is discussed next). Figure 19 illustrates a scenario in which local internal corrosion activity occurs (beyond 10 h) and cathodic activity can be observed on the predominantly anodic Metal 1. Because of the previous equation, the amount of anodic activity on Metal 1 supplying cathode*1 rather than Metal 2 can be discerned.

As with the zero-resistance ammeter experiments described in this chapter, area-averaged current density values can be converted into mass loss by applying Faraday's law to obtain metal dissolution (taken from J_{at} values) or H_2 evolution and O_2 reduction (taken from J_{ac} values).

FIG. 19 Representation of area-averaged integrated SVET-derived anodic and cathodic current density data as a function of time extracted individually for Metal 1 and Metal 2.



Limitations

The SVET has some limitations, and it is typical for complementary measurements to be made to verify quantitative data, such as gravimetric or volumetric measurements. The technique provides only an estimate of current density data as each scan can take several minutes depending on the size of the exposed area to be mapped. The very nature of the scanning probe means that data for the whole surface is not recorded instantaneously. A further limitation of the SVET is low detection efficiency in cases in which the spacing between anodes and cathodes is so small that the current flux lines pass below the plane of scan of the vibrating probe.[27] For localized corrosion with large-spaced anodes and cathodes, however, SVET detection efficiency is high.

Another laboratory method for measuring potential distributions in the vicinity of a galvanic interface is the multielectrode technique, described in ASTM G217, *Standard Guide for Corrosion Monitoring in Laboratories and Plants with Coupled Multielectrode Array Sensor Method*.

ATMOSPHERIC TESTS

Only mass loss information is obtained from the standard atmospheric galvanic corrosion tests, with the exception of the plate test. The plate test specimens also can be evaluated by metallography, visual examination, probe-type attack depth gages, or mechanical tests, such as tensile strength.

Standards

Laboratory testing for galvanic corrosion involves so many variables that it is difficult to write a single standardized test. For this reason, there are no standardized laboratory testing procedures specifically for galvanic corrosion. If another form of corrosion is being studied, then a slight modification to a standardized test for that corrosion form may be used. For example, to study galvanically accelerated stress corrosion testing, ASTM G30, *Standard Practice for Making and Using U-Bend Stress-Corrosion Test Specimens*, may be used, adding only a wire between the specimen and a second material to create the galvanic couple. To study the breaking strength of a piece of metal, a standard mechanical pull test such as that found in ASTM E8, *Standard Test Methods for Tension Testing of Metallic Materials*, may be used. To study the effect of galvanic corrosion on breaking strength, the same test may be used on pieces of metal after exposure to the environment of interest, both with and without galvanic coupling to a second material. Subtracting the strength of the metal with galvanic coupling from that without it will give the effect due to galvanic corrosion. Two guidelines for galvanic corrosion testing are published by ASTM: ASTM G71 and ASTM G82. Specific test standards for atmospheric galvanic corrosion can be found in ASTM G116 and ISO7441, as described earlier.

Additional Information

Additional information and details of galvanic corrosion testing are available in the standards referred in this chapter and in Hack.[36,37] Additional information on the theory of galvanic corrosion is available in several publications.[38–48] A good series of articles summarizing galvanic corrosion theory and application in various industries is available in the edited volume, *Galvanic Corrosion, ASTM STP978*.[49] Galvanic corrosion testing descriptions are written at the level of a corrosion technician following Hack.[37]

References

1. J. Tafel, "On the Polarization during Cathodic Hydrogen Evolution," *Zeitschrift fur Elektrochemie und Angewandte Physikalische Chemie* 50 (1905): 641–712.

2. H. P. Hack, "Scale Modeling for Corrosion Studies," *Corrosion* 45, no. 7 (July 1989): 601–606.

3. D. J. Tighe-Ford, J. N. McGrath, and L. Hodgkiss, "Design Improvements for a Ship's Cathodic Protection System Using Dimension and Conductivity Scaling (DACS)," *Corrosion Prevention and Control* 32, no. 5 (October 1985): 89–91.

4. E. DeCarlo, "Computer Techniques for Offshore Corrosion Protection," *Sea Technology,* September 1981, 25–30.

5. L. Clerbois, E. Heintz, F. P. Ijsselling, J. C. Rowlands, and J. P. Simpson, "Principles for Scaling of Corrosion Tests," *British Corrosion Journal* 20, no. 3 (1985): 107–116.

6. J. R. Scully, "Electrochemical Methods of Corrosion Testing," in *Metals Handbook, Ninth Edition: Volume 13—Corrosion*, (Materials Park, OH: ASM International, 1987), 212–216.

7. R. Baboian, "Prediction of Galvanic Corrosion Using Electrochemical Techniques," *Electrochemical Techniques for Corrosion Engineering,* ed. R. Baboian (Houston, TX: NACE, 1986), 253–258.

8. R. Baboian, "Final Report on the ASTM Study: Atmospheric Galvanic Corrosion of Magnesium Coupled to Other Metals," in *Atmospheric Factors Affecting the Corrosion of Engineering Metals,* ed. S. Coburn (West Conshohocken, PA: ASTM International, 1978), 253–258.

9. W. Blum, *Symposium on Properties, Tests and Performance of Electrodeposited Metallic Coatings* (West Conshohocken, PA: ASTM International, 1956).

10. P. R. Roberge, "Modeling Corrosion Processes," in *ASM Handbook Vol. 13A: Corrosion: Fundamentals, Testing, and Protection*, ed. S. D. Cramer and B. S. Covino (Materials Park, OH: ASM International, 2003), 430–445.

11. J. Newman and K. E. Thomas-Alyea, *Electrochemical Systems,* 3rd ed. (Hoboken, NJ: Wiley, 2004).

12. K. C. Stewart, "Intermediate Attack in Crevice Corrosion by Cathodic Focusing" (PhD thesis, University of Virginia, Charlottesville, VA, 1999).

13. J. T. Waber and B. Fagan, "Mathematical Studies on Galvanic Corrosion IV: Influence of Electrolyte Thickness on the Potential and Current Distributions over Coplanar Electrodes Using Polarization Parameters," *Journal of the Electrochemical Society* 103 (1956): 64–72.

14. R. Morris and W. Smyrl, "Current and Potential Distribution in Thin Electrolyte Layer Galvanic Cells," *Journal of the Electrochemical Society* 136 (1989): 3229–3236.

15. E. McCafferty, "Distribution of Potential and Current in Circular Corrosion Cells Having Unequal Polarization Parameters," *Journal of the Electrochemical Society* 124 (1977): 1869–1878.

16. D. Mizuno and R. G. Kelly, "Galvanically Induced Intergranular Corrosion of AA5083-H131 under Atmospheric Exposure Conditions: Part 2—Modeling of the Damage Distribution," *Corrosion* 69 (2013): 681–692.

17. N. Murer, R. Oltra, B. Vuillemin, and O. Neel, "Numerical Modelling of the Galvanic Coupling in Aluminium Alloys: A Discussion on the Application of Local Probe Techniques," *Corrosion Science* 52 (2010): 130–139.

18. C. Liu, J. Srinivasan, and R. G. Kelly, "Electrolyte Film Thickness Effects on the Cathodic Current Availability in a Galvanic Couple," *Journal of the Electrochemical Society* 164 (2017): C845–C855.

19. A. D. King, J. S. Lee, and J. R. Scully, "Finite Element Analysis of the Galvanic Couple Current and Potential Distribution between Mg and 2024-T351 in a Mg Rich Primer Configuration," *Journal of the Electrochemical Society* 163 (2016): C342–C356.

20. X. G. Zhang, "Galvanic Corrosion," in *Uhlig's Corrosion Handbook*, ed. R. W. Revie (New York: Wiley, 2000), 154–160.

21. H. S. Isaacs, "The Localized Breakdown and Repair of Passive Surfaces during Pitting," *Corrosion Science* 29 (1989): 313–323.

22. M. J. Franklin, D. C. White, and H. S. Isaacs, "A Study of Carbon Steel Corrosion Inhibition by Phosphate Ions and by an Organic Buffer Using a Scanning Vibrating Electrode," *Corrosion Science* 33 (1992): 251–260.

23. H. Krawiec, V. Vignal, and R. Oltra, "Use of the Electrochemical Microcell Technique and the SVET for Monitoring Pitting Corrosion at MnS Inclusions," *Electrochemistry Communications* 6 (2004): 655–660.

24. S. Fajardo, C. F. Glover, G. Williams, and G. S. Frankel, "The Source of Anodic Hydrogen Evolution on Ultra High Purity Magnesium," *Electrochimica Acta* 212 (2016): 510–521.

25. Z. P. Cano, J. R. Kish, and J. R. McDermid, "On the Evolution of Cathodic Activity during Corrosion of Magnesium Alloy AZ31B in a Dilute NaCl Solution," *Journal of the Electrochemical Society* 163 (2016): C62–C68.

26. H. S. Isaacs, "The Measurement of the Galvanic Corrosion of Soldered Copper Using the Scanning Vibrating Electrode Technique," *Corrosion Science* 28 (1988): 547–558.

27. G. Williams, A. J. Coleman, and H. N. McMurray, "Inhibition of Aluminum Alloy AA2024-T3 Pitting Corrosion by Copper Complexing Compounds," *Electrochimica Acta* 55, no. 20 (August 2010): 5947–5958.

28. R. M. Souto, Y. González-García, A. C. Bastos, and A. M. Simões, "Investigating Corrosion Processes in the Micrometric Range: A SVET Study of the Galvanic Corrosion of Zinc Coupled with Iron," *Corrosion Science* 49 (2007): 4568–4580.

29. B. Kannan, C. F. Glover, H. N. McMurray, G. Williams, and J. R. Scully, "Performance of a Magnesium-Rich Primer on Pretreated AA2024-T351 in Full Immersion: A Galvanic Throwing Power Investigation Using a Scanning Vibrating Electrode Technique," *Journal of the Electrochemical Society* 165 (2018): C27–C41.

30. K. B. Deshpande, "Experimental Investigation of Galvanic Corrosion: Comparison between SVET and Immersion Techniques," *Corrosion Science* 52 (2010): 2819–2826.

31. S. Böhm, H. McMurray, S. Powell, and D. Worsley, "Photoelectrochemical Investigation of Corrosion Using Scanning Electrochemical Techniques," *Electrochimica Acta.* 45 (2000): 2165–2174.

32. R. Akid and M. Garma, "Scanning Vibrating Reference Electrode Technique: A Calibration Study to Evaluate the Optimum Operating Parameters for Maximum Signal Detection of Point Source Activity," *Electrochimica Acta* 49 (2004): 2871–2879.

33. J. R. Searle, B. P. Wilson, K. Yliniemi, D. A. Worsley, and H. N. McMurray, "The Use of 3D-SVET for the Examination of Plasticized PVC Coatings: Effect of Deformation and UV Irradiation on Barrier Properties," *ECS Transactions* 64 (2015): 69–80.

34. C. F. Glover, T. W. Cain, and J. R. Scully, "Performance of Mg-Sn Surface Alloys for the Sacrificial Cathodic Protection of Mg Alloy AZ31B0H24," *Corrosion Science* 149 (April 2019): 195–206.

35. G. Williams and H. N. McMurray, "Pitting Corrosion of Steam Turbine Blading Steels: The Influence of Chromium Content, Temperature, and Chloride Ion Concentration," *Corrosion* 62 (2006): 231–242.

36. H. P. Hack, "Evaluation of Galvanic Corrosion," in *Metals Handbook*, *Ninth Edition: Volume 13—Corrosion* (Materials Park, OH: ASM International, 1987), 234–238.

37. H. P. Hack, *Corrosion Testing Made Easy: Galvanic Corrosion Testing Methods*, (Houston, TX: NACE International, 1993).

38. L. C. Rowe and R. L. Chance, "Fundamentals of Corrosion Testing," in *Automotive Corrosion by Deicing Salts,* ed. R. Baboian (Houston, TX: NACE International, 1981), 142–146.

39. H. H. Uhlig, *Corrosion and Corrosion Control* (New York: Wiley, 1985).

40. M. G. Fontana, "Modern Theory—Principles," in *Corrosion Engineering* (New York: McGraw-Hill, 1986), 297–324.

41. D. W. Shoesmith, "Kinetics of Aqueous Corrosion," in *Metals Handbook*, *Ninth Edition: Volume 13—Corrosion* (Materials Park, OH: ASM International, 1987), 29–36.

42. R. Baboian, "Electrochemical Techniques for Predicting Galvanic Corrosion," in *Galvanic and Pitting Corrosion—Field and Laboratory Studies,* ed. R. Baboian, W. France, Jr., L. Rowe, and J. Rynewicz (West Conshohocken, PA: ASTM International, 1976), 5–19.

43. R. Baboian, "New Methods for Controlling Galvanic Corrosion," *Machine Design* 11 (October 1979): 2–9.

44. N. D. Tomashov, *Theory of Corrosion and Protection of Metals* (New York: MacMillan Company, 1966).

45. R. Baboian, "Investigations of Galvanically Induced Localized Corrosion," in *Localized Corrosion—Cause of Metal Failure,* (West Conshohocken, PA: ASTM International, 1972), 145–163.

46. K. G. Compton, "Current Density Distribution on Composite Structures under Cathodic Protection in Seawater," in *Galvanic and Pitting Corrosion—Field and Laboratory Studies,* ed. R. Baboian, W. France, Jr., L. Rowe, and J. Rynewicz (West Conshohocken, PA: ASTM International, 1976), 48–55.

47. H. P. Hack, P. J. Moran, and J. R. Scully, "Influence of Electrolyte Resistance on Electrochemical Measurements and Procedures to Minimize or Compensate for Resistance Errors," in *The Measurement and Correction of Electrolyte Resistance in Electrochemical Tests,* ed. L. L. Scribner and S. R. Taylor (West Conshohocken, PA: ASTM International, 1990), 1–16.

48. F. L. LaQue, *Marine Corrosion, Causes and Prevention* (New York: Wiley, 1975).

49. H. P. Hack, ed., *Galvanic Corrosion,* (West Conshohocken, PA: ASTM International, 1988).

Chapter 4 | Hydrogen Damage

Kevin Nibur[1] and Brian Somerday[2]

Introduction

Hydrogen embrittlement affects virtually every common structural alloy to some degree. Some alloys, notably high-strength steels, are rendered virtually useless by even small concentrations of hydrogen, whereas other alloys, for example, certain austenitic stainless steels, remain quite sound even with large concentrations of dissolved hydrogen. Only sensitive testing methods may detect a degradation of mechanical properties. The variety of mechanical test methods discussed in the chapter can be broadly broken into two categories: those intended to detect only the presence or absence of hydrogen embrittlement and those intended to quantitatively measure the mechanical properties of a material intentionally exposed to hydrogen.

The primary way in which hydrogen alters mechanical properties is by facilitating crack initiation and growth. The influence of hydrogen on fatigue crack growth is covered in the chapter on corrosion fatigue; this chapter emphasizes the influence of hydrogen on quasistatic test methods. Proper selection of test methods and interpretation of the results requires an understanding of hydrogen uptake and transport, trapping, hydrogen-metal interactions, and hydrogen's impact on failure mechanisms.

Hydrogen Uptake, Transport, and Trapping

HYDROGEN UPTAKE

Hydrogen can enter structural metals during exposure to hydrogen-containing or -generating media in gaseous or aqueous form. Prominent sources of hydrogen uptake into structural metals include molecular hydrogen gas and water in either the vapor or liquid phase.

This section first considers hydrogen uptake from gaseous species, focusing on molecular hydrogen as an example. The initial step for hydrogen uptake is the production of atomic hydrogen at the gas–surface interface. This production of atomic hydrogen is catalyzed by transfer of electrons from the structural metal to the hydrogen molecule (H_2), leading to dissociative chemisorption as described by the following reaction:[1]

$$H_2(g) \rightleftarrows H_{ads} + H_{ads}, \tag{1}$$

where:
H_{ads} = atomic hydrogen *ad*sorbed on the surface.

Once adsorbed hydrogen is produced, it can enter the subsurface region *via* interstitial sites between the host metal atoms. This subsurface *ab*sorbed hydrogen can penetrate further into the bulk by diffusion through interstitial sites, as described in an ensuing section.

The concentration of absorbed hydrogen resulting from exposure to H_2 gas is quantified from the relationship:[2,3]

$$C_L = Sf^{1/2} = S_o \exp\left(\frac{-E_s}{RT}\right) f^{1/2}, \tag{2}$$

where:
C_L = the concentration of hydrogen in interstitial lattice sites,
S = the solubility (and S_o is the preexponential factor),
E_s = heat of solution,
R = the gas constant,
T = absolute temperature, and
f = hydrogen fugacity.

The fugacity is related to gas pressure through the following expression:[3]

$$f = P \exp\left(\frac{Pb}{RT}\right), \tag{3}$$

where:
P = pressure, and
b = a constant in the Abel-Noble equation of state.

As the deviation from ideal gas behavior becomes more pronounced at higher pressure, fugacity is the more appropriate parameter to describe hydrogen uptake in equation (2). At lower pressure $f \rightarrow P$, and the relationship between C_L and P in equation (2) becomes the more familiar Sievert's law.

[1]Hy-Performance Materials Testing, LLC, Bend, OR, USA http://orcid.org/0000-0003-0920-3157
[2]Somerday Consulting LLC, 118 Rehoboth Rd., Wayne, PA 19087, USA http://orcid.org/0000-0002-5238-7281

DOI: 10.1520/MNL202NDSUP20190031

Copyright © 2022 by ASTM International, 100 Barr Harbor Dr., PO Box C700, West Conshohocken, PA 19428-2959
ASTM International is not responsible, as a body, for the statements and opinions expressed in this chapter. ASTM International does not endorse any products represented in this chapter.

In aqueous solutions, atomic hydrogen is produced on the structural metal surface through electrochemical reactions. In acidic solutions, the reduction of protons yields surface-adsorbed hydrogen, as described by the following reaction:

$$H^+ + e^- \rightleftarrows H_{ads}. \quad (4)$$

Atomic hydrogen also can be produced in basic solutions by the reduction of water—that is:

$$H_2O + e^- \rightleftarrows OH^- + H_{ads}. \quad (5)$$

Similar to the case of hydrogen gas, the surface-adsorbed hydrogen can then migrate into subsurface lattice sites. The resulting lattice hydrogen concentration can theoretically be quantified from the following relationship:[1]

$$C_L = \frac{\theta_{ads}}{1-\theta_{ads}}\frac{k_{abs}}{k_{des}}, \quad (6)$$

where:
θ_{ads} = the surface coverage of adsorbed hydrogen atoms,
k_{abs} = the rate constant for subsurface hydrogen absorption, and
k_{des} = the rate constant for subsurface hydrogen desorption.

Strictly, this relationship can be derived only when the hydrogen diffusion flux into the bulk is relatively low.[1] In principle, equation (6) also applies to hydrogen uptake in gaseous media, but equation (2) is more practical because the parameters S_o and E_s are readily determined experimentally.

The lattice hydrogen concentration resulting from exposure to gaseous and aqueous media (e.g., equations (2) and (6)) can be amplified by applied stress. The fundamental concept is that an imposed triaxial stress (i.e., mean normal stress) expands the volume of interstitial lattice sites, allowing a higher fraction of these sites to accommodate hydrogen. The magnitude of this effect is a function of mean normal stress (σ_m) and the partial molar volume of hydrogen in solution (V_H), as follows:[2,3]

$$C_{L\sigma} = C_L \exp\left(\frac{\sigma_m V_H}{RT}\right), \quad (7)$$

where:
$C_{L\sigma}$ = the stress-modified lattice hydrogen concentration.

The mean stress can be elevated near features, such as notches and cracks, leading to higher lattice hydrogen concentrations at these locations.

The expressions for lattice hydrogen concentration in equations (2) and (6) tacitly presume that no barriers to hydrogen uptake exist on the surface of the structural metal. One such barrier that realistically forms on the surface of structural metals in both gaseous and aqueous media is an oxide film. In gaseous media, it is essential to recognize that oxide films can form even in high-purity environments, for example, oxide films can result from only part-per-million concentrations of oxygen in hydrogen gas.[4] When oxide films are present on the surface, the lattice hydrogen concentration is reduced according to the following expression:[1]

$$C_L = \frac{\theta_{ads}}{1-\theta_{ads}}\frac{k_{abs}}{k_{des}}\frac{k_o}{k_m}, \quad (8)$$

where:
k_o = the rate constant for hydrogen transfer from the oxide to the metal, and
k_m = the rate constant for hydrogen transfer from the metal to the oxide.

Here, k_{abs} and k_{des} are rate constants for hydrogen absorption and desorption, respectively, at the oxide surface exposed to the environment. When considering bulk hydrogen uptake into structures or laboratory test specimens, equation (8) applies assuming that the oxide is continuous on the surface. It is possible, however, for such oxide barriers to become locally breached, particularly when the structure or test specimen is subjected to stress. In this case, locally elevated plastic strain can mechanically rupture the oxide at specific sites, allowing hydrogen uptake at these locations, following equations (2) and (6).

HYDROGEN TRANSPORT

Once hydrogen enters the subsurface region, it can then diffuse into the bulk *via* interstitial lattice sites. The essential parameter for characterizing this hydrogen transport process is the lattice diffusion coefficient, D_L. The magnitude of the lattice diffusion coefficient depends on the activation energy barrier between adjacent interstitial sites (E_d), the frequency factor (D_o), and temperature according to the Arrhenius relationship:[1–3]

$$D_L = D_o \exp\left(\frac{-E_d}{RT}\right). \quad (9)$$

The flux of hydrogen from the surface into the bulk depends on the lattice diffusion coefficient, as demonstrated through Fick's first law:

$$J = D_L\frac{dC_L}{dx}, \quad (10)$$

where:
flux, J = moles of hydrogen atoms transported through a unit area during a unit time, and dC_L/dx is the hydrogen concentration gradient.

Fick's first law applies to steady-state conditions (i.e., time-independent hydrogen concentration gradient), and the formulation in equation (10) presumes one-dimensional hydrogen transport. As an example, these conditions are designed to prevail in experiments to measure hydrogen permeation through thin membranes.

In the case of an evolving hydrogen concentration gradient from the surface into the bulk (i.e., nonsteady state), the penetration depth of hydrogen can be quantified assuming a constant subsurface concentration and one-dimensional diffusion:

$$x = K\left(2\sqrt{D_L t}\right), \quad (11)$$

where:
x = the penetration distance for a specific hydrogen concentration level in the gradient extending from the surface,
t = time, and
factor, K = parameter dependent on the hydrogen concentration level.

For example, at the level equal to 15% of the surface concentration, K is approximately unity so that the penetration distance for this concentration is $x = 2\sqrt{D_L t}$.

HYDROGEN TRAPPING

As described in the previous section, hydrogen atoms are transported in structural metals by diffusion through interstitial lattice sites. The characteristic volume of these interstitial sites is sufficiently restricted such that occupation by hydrogen perturbs the neighboring host metal atoms. This displacement of the host metal atoms from their equilibrium positions raises the local stored elastic energy. As a result, it is energetically favorable for hydrogen to reside at microstructural sites that have more free volume than interstitial sites. Such lower-energy sites exist at metallurgical features, such as vacancies (point defects), dislocations (line defects), and interfaces (surface defects), and are collectively referred to as hydrogen traps.

One consequence of hydrogen trapping at defects is that the total hydrogen concentration in a structural metal can exceed the lattice concentration. The fraction of a particular trap site type occupied by hydrogen (θ_T) is quantified as follows:[1–3]

$$\frac{\theta_T}{1-\theta_T} = \frac{\theta_L}{1-\theta_L}\exp\left(\frac{E_b}{RT}\right), \tag{12}$$

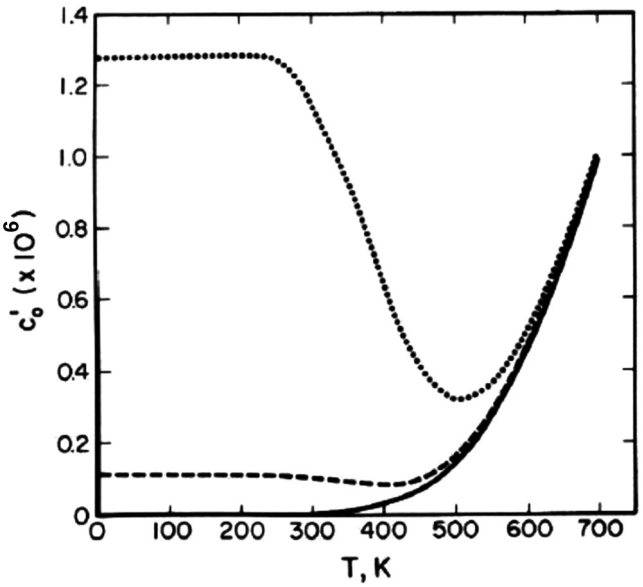
where:
θ_L = the fractional occupancy of lattice sites, and
E_b = the binding energy of hydrogen to the trap site.

The binding energy is the difference in potential energy for hydrogen residing at an interstitial site versus the trap site. Each type of trap site (e.g., point defect, line defect, surface defect) has a characteristic binding energy. The fractional occupancy terms, θ_L and θ_T, are related to hydrogen concentrations through the density of lattice sites or trap sites, that is, $C_L = \theta_L N_L$ and $C_T = \theta_T N_T$, where N_L and N_T are the densities (sites/volume) of lattice sites and trap sites, respectively. The total hydrogen concentration in a structural metal is then the sum of lattice site and trap site concentrations. The relationship in equation (12) presumes equilibrium between hydrogen in lattice sites and hydrogen in trap sites, that is, the rate of hydrogen entering traps from lattice sites equals the rate of hydrogen escaping traps into lattice sites.

For a structural metal in which a lattice hydrogen concentration is established through exposure to a gaseous or aqueous environment (e.g., equations (2) or (6)), figure 1 illustrates how the total hydrogen concentration can vary as a function of temperature.[2] In this figure, the total hydrogen concentration ($C_L + C_T$) is calculated for iron with two different trap site densities ($N_T = 9 \times 10^{15}$ sites/cm^3 and 1×10^{17} sites/cm^3). For the parameters selected in the calculations displayed in figure 1, the trends demonstrate that total hydrogen concentration is dominated by trapped hydrogen at lower temperature. As temperature increases, the trapped hydrogen concentration effectively decreases to zero, and the total hydrogen concentration is dictated solely by lattice hydrogen.

Although trapping can enhance hydrogen uptake, it can have the concomitant effect of hindering hydrogen transport.

FIG. 1 Calculated total hydrogen concentration ($C_L + C_T$ on y-axis) versus temperature for iron.[2] The lattice hydrogen concentration is established from exposure to hydrogen gas at 545 Pa pressure. The total hydrogen concentration is calculated for two trap site densities: $N_T = 9 \times 10^{15}$ sites/cm^3 (dashed line) and 1×10^{17} sites/cm^3 (dotted line). The solid line is the calculated lattice hydrogen concentration. *Source:* Reprinted by permission from Hirth.[2]



This manifestation of hydrogen trapping is characterized by the effective diffusion coefficient, D_{eff}. The magnitude of D_{eff} relative to D_L depends on the fraction of trap sites occupied by hydrogen, θ_T, according to the following expression:[5]

$$D_{eff} = D_L \frac{C_L}{C_L + C_T(1-\theta_T)}. \tag{13a}$$

Similar to equation (12), the relationship in equation (13a) presumes that hydrogen populations in lattice sites and trap sites are in equilibrium. A practical simplification of equation (13a) results at low trap occupancy ($\theta_T \ll 1$), that is:[1,5]

$$D_{eff} = D_L \frac{C_L}{C_L + C_T} = D_L\left[1 + \frac{N_T}{N_L}\exp\left(\frac{-E_b}{RT}\right)\right]^{-1} \tag{13b}$$

Although D_{eff} is typically less than D_L, equations (13a) and (13b) illustrate two cases in which D_{eff} approaches D_L. In equation (13a), one circumstance in which $D_{eff} \to D_L$ occurs when trap sites become fully occupied by hydrogen ($\theta_T \to 1$). Such extensive trap site occupancy can result from hydrogen environments that induce high lattice hydrogen concentrations (e.g., equations (2), (6), and (12)). The diffusion coefficients D_{eff} and D_L similarly converge as temperature increases (equation (13b)). This trend is attributed to the reduced effectiveness of hydrogen trapping at higher temperature (equation (12)). Equivalently, the dwell time of hydrogen in trap sites is reduced as temperature increases.

Implications of Hydrogen Uptake, Transport, and Trapping on Embrittlement

Hydrogen accumulates in structural metals at localized stress fields (equation (7)) and hydrogen traps (equation (12)), and activation of hydrogen embrittlement often is associated with a critical hydrogen concentration at such locations. For this reason, the manifestation of hydrogen embrittlement for components in service and in materials testing is sensitive to variables that affect these local hydrogen concentrations. For both assessing in-service component performance and interpreting materials testing results, temperature is one of the most prominent variables influencing hydrogen embrittlement, and its effects can be rationalized based on hydrogen uptake and trapping. For example, hydrogen embrittlement diminishes at elevated temperature, and this trend has been linked to decreasing hydrogen concentrations in stress fields and traps as temperature increases. Conversely, because these hydrogen populations increase as temperature decreases, it may be expected that hydrogen embrittlement is always exacerbated at lower temperature. The equilibrium relationships between hydrogen concentration and temperature (equations (7) and (12)), however, are satisfied only when transport kinetics are sufficiently high to supply hydrogen to these sites. Thus, there is a temperature-dependent interplay between the hydrogen concentration relationships and hydrogen transport kinetics (e.g., equations (9) and (11)), such that hydrogen embrittlement is often most severe at near-ambient temperatures.

Another aspect that affects hydrogen concentrations in stress fields and traps that must particularly be considered for materials testing methods is the environmental boundary conditions. Specifically, the nature of hydrogen environment exposure (continuous versus discontinuous) coupled with temperature variations can dictate the hydrogen concentrations in stress fields and traps, which in turn determines the severity of hydrogen embrittlement. Two different sets of boundary conditions are common to most testing methods associated with hydrogen embrittlement. First, the open-system boundary condition applies when a test specimen is concurrently exposed to the hydrogen containing or generating environment and subjected to mechanical loading. Second, the closed-system boundary condition applies when a test specimen is first exposed to a hydrogen containing or generating environment to precharge the specimen with hydrogen, and then it is removed from the hydrogen environment and subsequently subjected to mechanical loading.

The temperature-dependent concentration and distribution of hydrogen in a test specimen exposed to the open-system boundary condition are described by equations (2), (6), (7), and (12). Figure 1 illustrates one example of relationships between lattice and trapped hydrogen concentration as a function of temperature for an open system and demonstrates some important aspects of these relationships. Most notably, the lattice concentration of hydrogen (C_L) in metals is small at lower temperature and increases rapidly at elevated temperature, whereas the trapped hydrogen concentration (C_T) is typically largest at lower temperature and decreases with increasing temperature. As the temperature continues to increase, C_T may increase again. This behavior results from the opposing influences of temperature and lattice concentration on trapped hydrogen concentration, as reflected in equation (12).

The concentration and distribution of hydrogen in a test specimen exposed to the closed-system boundary condition is more complicated and often is not intuitive. Although the total hydrogen concentration in the test specimen (C_H) must always be the sum of the trapped and lattice concentrations, that is,

$$C_H = C_T + C_L, \tag{14}$$

under the closed-system boundary condition this total concentration, C_H, is assumed to be fixed by the initial hydrogen-precharging step. Precharging is often conducted at an elevated temperature to exploit the faster diffusivity and larger C_L, which reduces the necessary precharging time and increases C_H, respectively. As the specimen is cooled from the precharging temperature to the test temperature, C_H is assumed to remain constant. Test procedures often involve a short elapsed time between precharging and mechanical loading to enforce this assumption. Figure 1 demonstrates that hydrogen resides predominantly in lattice sites at elevated temperature, so during the precharging step, most hydrogen occupies these sites. As the specimen cools, hydrogen will redistribute between lattice and trap sites according to Equations (2), (6), (7), and (12) but further constrained by equation (14).

When a test specimen microstructure contains multiple trap types, hydrogen preferentially redistributes from lattice sites to trap types with high binding energy, E_b (equation (12)), during cooling. If such high binding energy trap types are also present in high density (N_T), these sites significantly deplete the lattice hydrogen, because the total concentration is fixed according to equation (14).[6] Moreover, high binding energy trap types may not be the locations for activating hydrogen embrittlement, so their primary function is only to limit C_L. In this case, the limited remaining lattice hydrogen concentration cannot sufficiently populate other trap types with lower binding energy, which may serve as locations for hydrogen embrittlement but cannot develop sufficiently high C_T to activate it.

The practical importance is that variations in material microstructure may greatly influence the hydrogen concentration and distribution present during test methods subject to closed-system boundary conditions, potentially leading to substantially different results compared with those from otherwise similar tests conducted under open-system boundary conditions.[7] Moreover, without carefully considering all of the different contributions to hydrogen trapping (e.g., number of trap types and their respective values of E_b and N_T), there is no way to anticipate how test results from the two different types of boundary conditions will compare. When such details are not fully understood, the boundary conditions selected for testing should match, as closely as possible, the service conditions for the application the test is designed to assess.

Note that the closed system condition (fixed total hydrogen concentration) is an idealization that may be tenuous for certain

structural metals. For example, assuming that a fixed total hydrogen concentration is established at elevated temperature, it may not be retained when hydrogen environment exposure is discontinued and temperature is lowered. In structural metals such as ferritic and martensitic steels, the diffusion coefficient for hydrogen is relatively high so that hydrogen egress from the metal is likely, particularly for modest section sizes and slower rates of temperature change. In such situations, the total hydrogen concentration at the lower temperature may be less than the concentration introduced at the higher temperature.

Physics and Micromechanical Elements of Hydrogen Embrittlement

For materials testing characterized by either the open- or closed-system environmental boundary condition, hydrogen in the test specimen concentrates at stress fields and trap sites and interacts with defects at these locations to accelerate material failure. The key serial elements in the failure process include deformation, microcrack formation, and crack growth. Details of the physics and micromechanics of these material responses are described in this section to provide a foundation for the formulation and interpretation of materials test methods.

Structural metals sustain some amount of deformation before microcrack formation. The extent of deformation that precedes microcrack formation is an important contribution to measured fracture resistance. Numerous theoretical and experimental results have demonstrated that hydrogen facilitates the nucleation and motion of dislocations.[8–11] These hydrogen-dislocation interactions can be reflected through modified material properties, such as yield strength and strain hardening, but arguably the most important manifestation that affects material failure is strain localization. Several aspects of hydrogen-dislocation interactions can promote strain localization. In materials with metallurgical characteristics that induce some degree of strain localization, hydrogen concentrates in these regions of localized deformation because it becomes trapped at the dislocations. Hydrogen then enhances the mobility of these dislocations, which further localizes the deformation.[12] In materials that are not metallurgically conditioned toward strain localization, hydrogen still can induce localization by inhibiting cross-slip of dislocations.[9,10] Localized deformation resulting from any material characteristic or environmental effect contributes to material failure by promoting strain incompatibilities. These strain incompatibilities are associated with the impingement of deformation bands on metallurgical features, such as interfaces and boundaries.

Hydrogen-enhanced strain localization can activate or accelerate microcrack formation through several mechanisms. One mechanism that is most directly linked to strain localization is microcrack formation at the intersection of deformation bands.[13–15] The essential role of hydrogen in this mechanism is to promote localized deformation bands, which can then intersect and create strain incompatibilities at these junctions. The stress fields at these incompatibility points then drive the formation of microcracks, where the nucleation site is likely associated with defect structures in the deformation bands. Although the formation of microcracks at deformation band intersections may be uniquely associated with hydrogen exposure, hydrogen-enhanced strain localization alternately can accelerate more conventional microcrack formation mechanisms. For example, hydrogen-enhanced strain localization can expedite stages of the microvoid coalescence mechanism commonly manifested in ductile structural metals.[16] From a physics perspective, the common characteristic of the hydrogen embrittlement mechanisms described earlier is the need to accumulate deformation to activate microcracks. This leads to the deduction that the strain-controlled micromechanical framework[17,18] is most appropriate for quantitatively modeling these types of microcrack formation.

As an alternative to the deformation-dominated forms of hydrogen embrittlement, one of the archetypal signatures of hydrogen embrittlement is microcrack formation along grain boundaries. In this mechanism, it is widely accepted that hydrogen segregates to trap sites on grain boundaries.[19,20] This hydrogen population then weakens the cohesive strength of the interface, leading to microcrack formation. Although there is evidence that trapped hydrogen at grain boundaries is required for microcrack formation,[21] hydrogen-enhanced strain localization may condition these interfaces for failure. Here, one notional role for hydrogen-enhanced localized deformation is to create strain incompatibilities and modify the defect structure at grain boundaries.[14,15,22] Elevated stresses and augmented trapped hydrogen associated with strain compatibilities and modified defect structure promote conditions for microcrack formation. Given these characteristics, the stress-controlled micromechanical framework[18,23] may be the most germane for modeling intergranular microcrack formation.

As a final category of hydrogen embrittlement mechanisms, the mechanistic ingredients of trapped hydrogen and hydrogen-related strain incompatibilities invoked earlier can cause microcracks to form at other interfaces as well (e.g., phase boundaries).[24] Such hydrogen-assisted microcrack formation associated with phase boundaries is often described by the term "quasi-cleavage," but arguably, this is a misnomer because cleavage seldom operates in hydrogen embrittlement failures.[23,25] Generally, these "quasi-cleavage" fracture mechanisms are poorly characterized; however, the role of plastic strain is consistently evident.[17,22] For this reason, quantitative models for this type of microcrack formation may be based on the strain-controlled framework.[18,22]

Although the physics and micromechanics of hydrogen embrittlement are more easily conveyed by describing microcrack formation, materials test methods are not interrogating microcrack formation but rather macroscopic crack extension. Microcrack formation, however, is the fundamental element in macroscopic crack extension given that the repeated nucleation and coalescence of microcracks constitutes crack extension. Thus, the physics and micromechanics of hydrogen embrittlement described previously equally pertain to crack extension. Most important, the difference between strain- and stress-controlled crack extension is critical to the proper selection and

interpretation of materials test methods that assess hydrogen embrittlement. The implications of strain-controlled versus stress-controlled crack extension for materials test methods can be revealed by detailing the following micromechanical modeling frameworks.

The fundamental differences between stress- and strain-controlled fracture mechanisms have been quantified through two similar micromechanical models promulgated by Ritchie. These models describe the relationship between the remotely applied driving force necessary for microcrack formation ahead of an existing macroscopic crack (e.g., the critical value of the linear elastic stress intensity factor, K_i) and the associated fracture resistance expressed as a local stress[18] or strain[26] quantity. The stress-controlled micromechanical framework (fig. 2A) stipulates that microcracks form at the driving force level K_i when a critical value of local stress (σ^*_f) is achieved over a critical length scale ahead of the crack tip (l^*), such that:

$$K_i \propto \left[\left(\sigma^*_f\right)^{(1+n)/2} / (\sigma_o)^{(1-n)/2}\right] l^{*1/2} \tag{15}$$

where:
σ_o = the yield stress, and
n = the strain-hardening exponent.

Similarly, the strain-controlled micromechanical framework (fig. 2B) stipulates that microcracks form at the driving force level K_i when a critical value of local strain (ε^*_f) is achieved over a critical length scale (l^*) ahead of the crack tip, such that:

$$K_i \propto \sqrt{\varepsilon^*_f \cdot l^* \cdot \sigma_o \cdot E}, \tag{16}$$

where:
E = the elastic modulus.

Although the quantitative models for fracture initiation resistance reflected in Equations (15) and (16) were strictly developed by considering microcrack formation, the concepts in the underlying micromechanical frameworks can be applied similarly to model crack growth resistance. One subtlety that is imperative to recognize in the case of strain-controlled crack growth is that the strain field evolves as a function of crack extension. This characteristic of the strain field results because plastically deformed material is transferred from the high-stress region ahead of a loaded crack tip to the crack wake, where it then unloads elastically. This wake of plastically deformed material imparts a residual strain field that interacts with, and alters, the stress and strain fields ahead of the crack tip. This interaction has a negligible effect on the crack tip stress fields but can significantly alter the crack tip strain fields.[28] Because the crack tip strain fields can be affected significantly by the plastic crack wake, these fields are a function of crack growth history. Specifically, a stationary crack with no plastic wake has a strain field described by Hutchinson[29] and Rice and Rosengren,[30] in which the strain (ε) varies with distance from the crack tip (r) as follows:

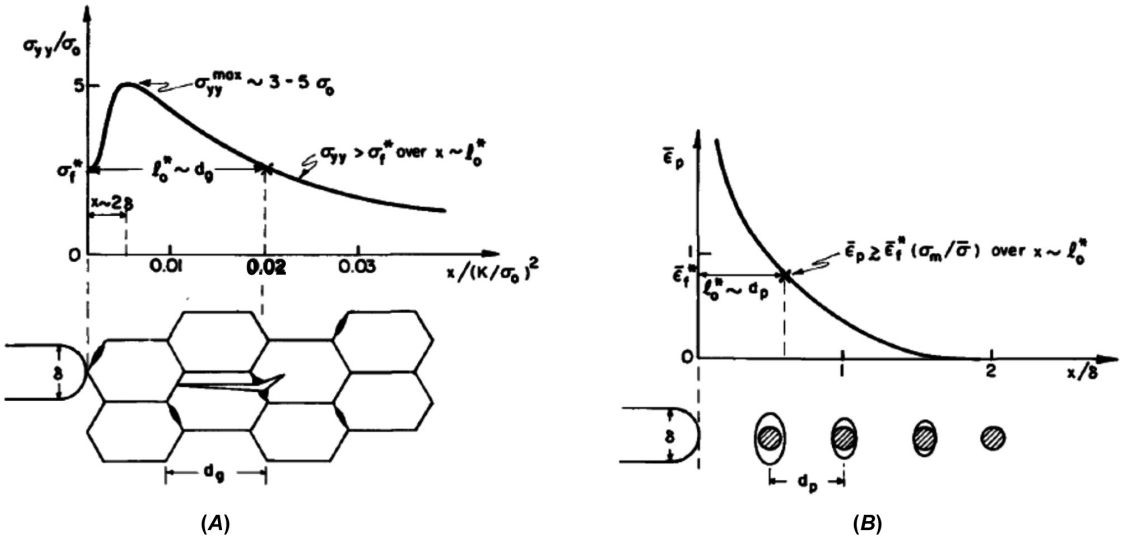
$$\varepsilon \propto (J/r)^{1/2}. \tag{17}$$

Once the crack begins to extend, this relationship between ε and r transitions toward that of a crack propagating under steady state conditions:[28]

$$\varepsilon \propto In(J/r). \tag{18}$$

Compared with equation (17), equation (18) represents a weaker strain singularity at the crack tip, thus at a given relative distance ahead of the crack tip, the strain magnitude will diminish as the crack extends. As a consequence, because the local criterion for strain-controlled fracture (cf. fig. 2B, $\varepsilon = \varepsilon^*_f$ at $r = l^*$) does not change, the driving force level (remotely applied J or K) associated with each successive crack growth increment must

FIG. 2 Schematic of the fracture criteria for (*A*) stress-controlled fracture and (*B*) strain-controlled fracture. *Source:* Reprinted from Ritchie and Thompson.[27]



increase continually. In the limit as crack extension approaches steady state, the crack growth resistance (expressed as remote driving force, J or K) can be quantified by coupling the strain field given by equation (18) with the fracture criterion illustrated in figure 2*B* (i.e., $\varepsilon = \varepsilon^*_f$ at $r = l^*$), as follows:[23]

$$K_R \approx A\sigma_o\sqrt{l^*}exp\left(B * f\left(\varepsilon_f/\varepsilon_0\right)\right). \tag{19}$$

where:
K_R = the predicted crack growth resistance at steady state,
ε_o = the yield strain, and
A and B are undefined constants.

Because the plastic wake does not notably alter the crack tip stress fields, the crack growth resistance, K_R, under stress-controlled conditions is nominally the same as the resistance to microcrack initiation, that is:

$$K_R = K_i \propto \left[\left(\sigma^*_f\right)^{(1+n)/2}/\left(\sigma_o\right)^{(1-n)/2}\right]l^{*(1/2)}, \tag{20}$$

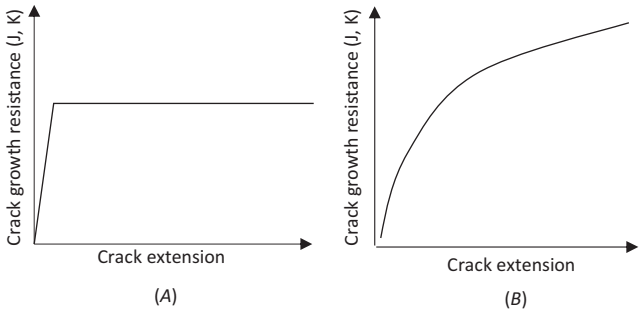
which is simply equation (15) applied to crack extension.

The micromechanical modeling results in equations (16), (19), and (20) are manifested in materials testing through crack growth resistance curve (R-curve) constructions (fig. 3). The conventional crack growth resistance curve concept was born in the ductile fracture domain, in which fracture mechanisms (e.g., microvoid coalescence) are well accepted as strain-controlled. According to the fracture testing of ductile metals, it is well established that the crack growth resistance (as characterized by remotely applied J or K) varies as a function of crack extension (Δa). The fundamental reason for such a relationship is connected to the evolution of the crack tip strain field, as embodied in equations (16) and (19). The crack growth resistance will gradually evolve from that described by equation (16) to that of equation (19) as the crack grows toward steady state. (Practically, most materials test methods do not allow sufficient crack extension to reach steady state conditions.) For any value of ε^*_f greater than ε_o, equations (16) and (19) show that K_R is always greater than K_i, demonstrating that the crack growth resistance increases (fig. 3*B*) as the crack tip strain field gradually evolves from that of a stationary crack (equation (17)) to that of a steady-state propagating crack (equation (18)). In contrast to strain-controlled fracture, stress-controlled fracture is defined by crack tip stress fields that are not significantly modified during crack extension. Hence, the driving force is not dependent on crack growth history and the R-curve has an ideally zero slope (fig. 3*A*).

The evolution of crack growth resistance during crack extension (i.e., the positive slope of the R-curve) is a distinguishing characteristic of strain-controlled fracture and must be recognized in applying materials test methods. The micromechanical models in equations (16) and (19) further illustrate that the local fracture strain, ε^*_f, governs the disparity between K_i and K_R (e.g., for a fixed value of ε_o, lowering ε^*_f reduces the slope of the R-curve). Because ε^*_f dictates the slope of the R-curve, it is essential to revisit the physics of strain-controlled hydrogen embrittlement mechanisms presented earlier. In particular, although the local fracture strain, ε^*_f, is a continuum quantity, its magnitude is related to the severity of hydrogen-induced strain localization. Furthermore, the potential for hydrogen to reduce ε^*_f through strain localization requires that deformation accumulates in the presence of hydrogen—that is, the sequence of hydrogen exposure and deformation is essential. Such history dependence contrasts to stress-controlled hydrogen embrittlement, in which reduced critical fracture stress, σ^*_f, is only a function of the instantaneous hydrogen concentration.

In summary, the physics and micromechanics of hydrogen embrittlement and their connection to crack growth resistance curve behavior have implications for materials test methods. First, the applied driving force (J or K) needed to initiate a microcrack may be different from that needed to sustain crack extension when fracture is strain-controlled and the crack growth resistance curve exhibits a positive slope. In particular, measurements of fracture resistance from materials test methods associated with propagating cracks may be higher than measurements that characterize microcrack initiation. Second, because strain-controlled hydrogen embrittlement is history dependent, materials test methods must consider the sequence of deformation accumulation and hydrogen exposure. It is evident from these two summary points that characterization of strain-controlled hydrogen embrittlement is more complex than characterization of stress-controlled hydrogen embrittlement.

FIG. 3 Schematic crack growth resistance curves (R-curves). (*A*) flat R-curve representative of a material exhibiting ideal stress-controlled fracture and (*B*) rising R-curve typical of higher toughness materials exhibiting strain-controlled fracture.



Testing Methods for Prevention of Hydrogen-Related Failures

Components manufactured from high-strength steel, including high-strength fasteners and certain aircraft components, must be free of internal diffusible hydrogen and often must be coated to prevent corrosive reactions that could generate hydrogen. A variety of standard test methods are available through ASTM to ensure hydrogen embrittlement is precluded following plating procedures. ASTM F1113, *Standard Test Method for Electrochemical Measurement of Diffusible Hydrogen in Steels (Barnacle Electrode)*, and ASTM F326, *Standard Test Method for Electronic Measurement for Hydrogen Embrittlement from Cadmium-Electroplating Processes*, describe methods for directly

monitoring the hydrogen uptake from plating baths; however, this chapter will address only mechanical test procedures.

Two ASTM standards, ASTM F519-18, *Standard Test Method for Mechanical Hydrogen Embrittlement Evaluation of Plating/Coating Processes and Service Environments,* and ASTM F1940-07a, *Standard Test Method for Process Control Verification to Prevent Hydrogen Embrittlement in Plated or Coated Fasteners*, are intended to detect critical levels of hydrogen that may result from processing (e.g., plating or other chemical exposure) of high-strength steel fasteners and components. These standards are not intended to evaluate hydrogen embrittlement resulting from environmental exposure. In both standards, AISI 4340 steel quenched and tempered to high strength (specified as 260–280 ksi in ASTM F519, and 50–52 HRC in ASTM F1940) is selected as a material that is highly susceptible to hydrogen embrittlement. Test specimens fabricated from the high-strength 4340 are to accompany the product during the processing steps of interest. Following processing, these witness specimens are subjected to mechanical testing procedures that evaluate the presence of damaging concentrations of hydrogen. These specimens serve as the conceptual canary in the coal mine to indicate whether the processing steps are leading to hydrogen uptake in the parts. Inherent to these test methods is the assumption that the high-strength 4340 material used for the test specimens has hydrogen embrittlement susceptibility that equals or is more severe than the material used for the components being screened. ASTM F519 is targeted to aerospace applications, whereas ASTM F1940 is targeted to automotive applications.

A variety of specimen geometries are allowed by ASTM F519; the specimens are stressed to an initial force or deflection (typically 75% of notched tensile strength) and held statically for a predetermined period (typically 200 h). The absence of failures within this duration indicates that the process has not resulted in damaging levels of hydrogen uptake. Alternatively, in some cases, ASTM F519 may allow the use of notched bend specimens tested under stepwise increasing displacement (referred to as incremental step loading, or ISL) rather than constant displacement. ASTM F1940 allows only for notched bend specimen testing under stepwise increasing displacement. Both ASTM F519 and ASTM F1940 suggest that the ISL technique yields results that are comparable to sustained load test techniques but in significantly shorter times.

Hydrogen embrittlement of such high-strength steels occurs through intergranular fracture with low crack growth resistance. As such, it is reasonable to consider this as a stress-controlled fracture mechanism, and static loading methods seem appropriate. As discussed in the section "Physics and Micromechanical Elements of Hydrogen Embrittlement," hydrogen-enhanced strain localization has been shown to condition grain boundaries for failure. Thus, even nominally stress-controlled fractures may involve a critical contribution of hydrogen-enhanced plasticity. Speculatively, the use of the ISL test method may allow hydrogen to redistribute to the high-stress region of the notch concomitantly with the application of strain, facilitating hydrogen-enhanced strain localization and accelerating the failure process. Critically, the rate of strain accumulation relative to the rate of hydrogen redistribution will influence the extent of embrittlement so that the loading rate from one step to the next may be as, or more, important than the duration of the step hold. The rate of load increase between steps is not addressed by these standards. Similar active-loading methods using slow rising displacement may be expected to yield similar results, and possibly greater degrees of test acceleration because the rate of strain accumulation is consistently slow during such testing.

Quantitative and Qualitative Measurements of Hydrogen Embrittlement Susceptibility

Numerous applications require materials that maintain structural integrity while exposed to hydrogen environments, including hydrogen pressure vessels, power generation equipment, oil and gas infrastructure, rocket engines, and many others. Design and selection of materials for these applications require knowledge of the impact of hydrogen on the mechanical properties of a given material. Many of the test methods designed to assess the performance of alloys that are intentionally exposed to hydrogen result in qualitative assessments of relative embrittlement. It has been demonstrated (e.g., ISO DTR 10783[31]) that different qualitative assessment tests will not necessarily provide the same quantitative metric. In other words, each specific test method may need to be calibrated against a set of known criteria (i.e., service experience that has demonstrated a set of alloys known to perform acceptably and a set known to perform unacceptably in the presence of hydrogen). ASTM G142-98(2016), *Standard Test Method for Determination of Susceptibility of Metals to Embrittlement in Hydrogen Containing Environments at High Pressure, High Temperature, or Both*; ASTM G129-00(2013), *Standard Practice for Slow Strain Rate Testing to Evaluate the Susceptibility of Metallic Materials to Environmentally Assisted Cracking*; and ASTM F1459-06(2017), *Standard Test Method for Determination of the Susceptibility of Metallic Materials to Hydrogen Gas Embrittlement (HGE)*, are designed to measure the relative susceptibility of an alloy to hydrogen embrittlement.

RELATIVE SUSCEPTIBILITY

Tensile Testing

Tensile testing remains one of the most common methods for assessing material properties because of the relative simplicity of the specimens and test procedures. Hydrogen embrittlement will manifest as a reduction of the tensile ductility. If this reduction in ductility is large enough, it will result in a reduction of the tensile strength as well. When hydrogen causes a reduction of tensile ductility, it also will result in a reduction of other mechanical properties, such as fracture toughness and low-cycle fatigue resistance. For this reason, tensile tests serve as a valuable indicator of relative susceptibility to hydrogen embrittlement. The absence of any degradation in tensile properties, however, does not necessarily mean that hydrogen embrittlement is not present and

may still be realized through fracture or fatigue tests (e.g., Harris and VanWanderham[32] and Stoltz[33]).

Tensile tests conducted in hydrogen-containing or -generating environments usually exhibit surface cracking; specimen failure occurs when one of these surface cracks propagates through the gage section.[16,34] This sequence of events leading to fracture is usually different in inert environment in which failure is often associated with the formation of a plastic instability (necking) followed by microcracking in the interior of the specimen. Some combination of both mechanisms may be present in materials that exhibit moderate resistance to hydrogen embrittlement or when the applied strain rate is too high for hydrogen uptake and transport to keep pace with damage formation mechanisms. Increasing levels of hydrostatic stress enhance hydrogen embrittlement,[33,35] as expected from equation (7); consequently, notched tension specimens may be more sensitive to hydrogen embrittlement.

ASTM G142 provides a standard test method for conducting tensile tests in gaseous hydrogen. This standard issues guidance on the testing apparatus, gaseous hydrogen test environment, test specimen geometry, and loading rates. Specifically, it recommends specimen geometries for smooth and notched tensile specimens. ASTM G142 further recommends displacement rates for testing that, for the specified geometries, correlates to a strain rate of 7×10^{-5} 1/s for smooth specimens and that is 10 times faster for notched specimens. It is unclear why a faster rate would be suggested for the notched specimen because the strain is localized and magnified by the presence of the notch. As such, even for the same applied displacement rate, the effective strain rate at the notch root will be much higher than that in a smooth specimen. It is reasonable to suggest that testing the notched tensile specimens at a slower displacement rate may be appropriate. CSA CHMC1, for example, references ASTM G142 for the slow strain rate tensile test parameters, but it recommends a strain rate of 1×10^{-5} 1/s for smooth specimens and notched specimens should be tested at a displacement rate that corresponds to 1/10 the rate that would produce a strain rate of 1×10^{-5} 1/s in the smooth tensile specimen.

ASTM G129 is a standard practice that provides a method of presenting the property measured in an embrittling environment relative to the corresponding property measured in air or in a nonembrittling environment. Procedures are broadly described for testing smooth, notched and fatigue precracked fracture mechanics specimens. The methods described in ASTM G129 have been applied widely and provide a consistent way to present and compare the relative degree of hydrogen embrittlement based on the particular measured property. This practice is applicable to all alloys, environments, and test types.

Disk Pressure Testing

Another ASTM standard that provides a method to evaluate the relative susceptibility of a given material to hydrogen embrittlement is ASTM F1459. This method subjects a thin disk of material, which is securely clamped into a fixture, to pressurized gas on one side only. The gas pressure is gradually increased until the disk ruptures. This rupture pressure is recorded with hydrogen gas as well as helium or other inert gas, and the ratio of these two rupture pressures is presented in the form of the embrittlement index. This test method is relatively straightforward to perform, and the equipment generally is less complicated than that needed for other types of materials testing in hydrogen gas.

Extensive results have been collected using this test method for pressure vessel steels, and these results have been compared with service history data of hydrogen storage cylinders for many decades.[31] Materials that exhibit a burst pressure in hydrogen that is at least 50% of the burst pressure measured in helium correlate with steels that have reliable service history. This test necessitates that hydrogen pressure continuously increases during the test, so specimens with higher rupture pressures also will be exposed to higher hydrogen pressure. In addition, the stress and strain state at the location of rupture (which is claimed to be a triaxial stress state) cannot be applied easily to design parameters, so this test does not provide any other information about the behavior of the material beyond the embrittlement index.

QUANTITATIVE FRACTURE MECHANICS

Most failures resulting from hydrogen embrittlement are the result of subcritical crack growth. Fracture mechanics-based test methods are necessary to directly measure the effect of hydrogen on subcritical crack growth and, in many cases, offer a preferred way to assess susceptibility to hydrogen embrittlement. ASTM provides several fracture mechanics–based standards, some of which are specific to environment assisted cracking. Standards for measuring conventional fracture toughness (e.g., K_{Ic} and J_{Ic}) are not specific to environment assisted cracking but provide valuable procedures that can be adapted to assess the effects of hydrogen on subcritical crack growth.

Sustained Load Fracture Threshold Test Methods

ASTM E1681-03(2013), *Standard Test Method for Determining Threshold Stress Intensity Factor for Environment-Assisted Cracking of Metallic Materials* (superseded), and ASTM G168-17, *Standard Practice for Making and Using Precracked Double Beam Stress Corrosion Specimens*, describe generally similar test procedures for either constant displacement or constant load testing of precracked specimens in a variety of test environments. Both of these standards describe procedures for applying either a constant load or constant displacement to the test specimens either before or after immersion in the test environment. The specimen is held in the environment for some period of time during which crack extension may or may not occur. The presence or absence of crack extension at various applied K levels can be used to identify the threshold stress intensity factor below which crack extension does not occur. Both standards can be used to assess crack growth velocity and the threshold stress intensity factor for crack arrest if proper instrumentation is applied.

ASTM E1681 and ASTM G168 differ primarily with regards to the specified specimen geometry; ASTM E1681 allows use of any properly characterized fracture mechanics specimen and provides specific guidance for either tension loaded compact specimens (either compact tension or the modified bolt loaded compact specimen) or bend-loaded notched beam specimens. ASTM G168 specifies only the use of double cantilever beam (DCB) specimens. The DCB specimen is known to induce a

positive T-stress*[36] ahead of the crack tip (e.g., Hadj Meliani, Matvienko, and Pluvinage[37]), and positive T-stress has been shown to destabilize straight, in-plane crack paths under mode I loading.[38] The result is that cracks tend to deflect away from the crack plane in the DCB specimen (fig. 4). The use of side grooves may help to constrain the crack to the desired plane; however, the specimen generally must be limited to low K values to prevent out-of-plane cracking.

Sustained load test procedures are relatively easy to execute and have been shown to produce consistent and conservative results when applied to high-strength steels in which the fracture mode was intergranular and nominally stress-controlled.[39] These test procedures, however, are inherently flawed when applied to material-environment combinations that promote strain-controlled hydrogen embrittlement.[23,25] As discussed in the section "Physics and Micromechanical Elements of Hydrogen Embrittlement," two barriers cause sustained load test methods to be nonconservative when the fracture mechanism is strain controlled. First, concurrent hydrogen exposure and slow, active deformation is necessary to stimulate hydrogen-induced strain-controlled fracture mechanisms. Sustained load test procedures often involve load application before environmental exposure, and when load is applied concurrent with environment exposure, the load application is rapid. Either scenario prevents or limits the strain-history dependence of strain-controlled hydrogen-enhanced microcrack formation. Second, constant displacement test methods are designed to identify the threshold stress intensity factor (K_{TH}) as the value of remote driving force at which a small, but detectable, amount of crack growth occurs, or at which a growing crack arrests. The first barrier generally prevents crack growth from occurring unless the applied stress intensity factor is elevated significantly above the threshold stress intensity factor. Large applied stress intensity factors necessarily overestimate the threshold stress intensity factor for the onset of crack extension. The alternative is to measure the threshold stress intensity factor for crack arrest. Testing approaches in which the threshold stress intensity factor is identified based on crack arrest also result in nonconservative measurements when the fracture mechanism is strain controlled because the conditions for arrest of a growing crack are described by equation (19) rather than by equation (16). In other words, the crack will arrest at some position along the R-curve, which is necessarily higher than the K or J value associated with the onset of crack extension.[40] Figure 5 demonstrates the large potential differences in measurements of the threshold stress intensity factor for the onset of crack extension and crack arrest. Figure 5 also demonstrates that this difference diminishes as the critical strain for hydrogen assisted fracture (denoted as ε^H_f) decreases. As ε^H_f decreases toward the yield strain, the fracture mechanism essentially becomes stress controlled and the difference between threshold measurements diminishes.

*The T-stress refers to the uniform stress acting parallel to the crack plane. When the crack tip stress field is expressed as an infinite power series, with K representing the amplitude of the first, singular term, T is the second term.[36]

FIG. 4 Post-test image of a wedge-loaded DCB specimen previously exposed to hydrogen gas showing deflection of the crack away from the crack plane.[25]

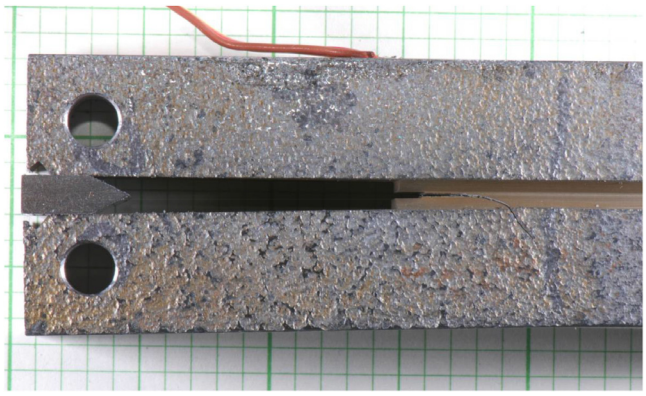
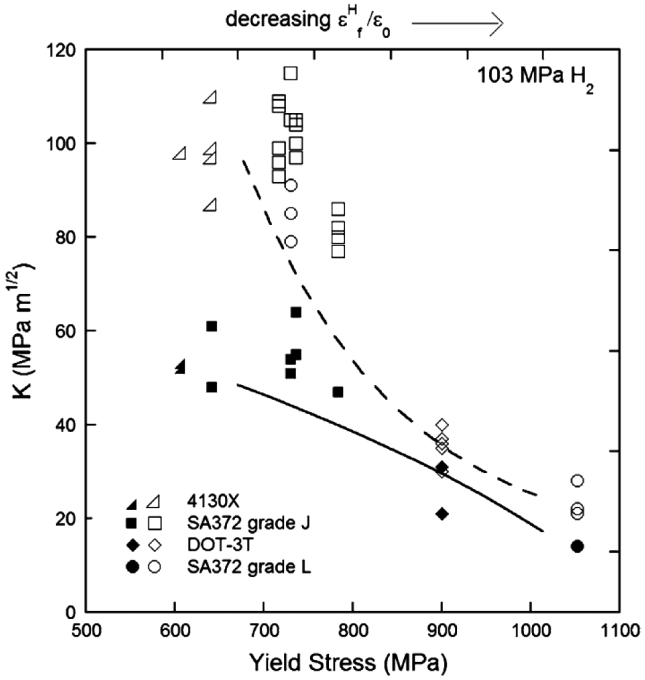


FIG. 5 The relationship between threshold stress intensity factor, K, and yield stress for a variety of low-alloy pressure vessel steels. Filled symbols represent the threshold for the onset of crack extension measured under slow rising displacement whereas open symbols represent the threshold for crack arrest measured under fixed displacement.[23]



Rising Displacement Fracture Threshold Measurement

ASTM E1820-20b, *Standard Test Method for Measurement of Fracture Toughness* (superseded), and ASTM E399-20a, *Standard Test Method for Linear-Elastic Plane-Strain Fracture Toughness of Metallic Materials* (superseded), provide standard methods for measurement of, respectively, the elastic-plastic and linear-elastic

fracture toughness. Neither of these standards are specific to hydrogen embrittlement or environment assisted cracking, but both may easily be adapted to environment-assisted cracking with little modification. In comparison with static-loading test methods, rising displacement tests may produce lower values of the threshold stress intensity factor when the hydrogen embrittlement mechanism is strain controlled (e.g., fig. 5). Conversely, rising displacement methods may produce nonconservative values when the applied loading rate is too high (e.g., Clark and Landes[39] and Nibur and Somerday[41]), because hydrogen uptake and transport kinetics may not be sufficiently accommodated.

Rising displacement test methods utilizing slow, monotonically increasing crack opening displacement ensure that the process zone ahead of the crack tip is continuously exposed to hydrogen throughout the formation of the crack-tip plastic zone. The resulting threshold stress intensity factor will be dependent on the loading rate when the mechanical driving force is applied at rates that truncate the kinetic processes associated with hydrogen uptake and transport. Below some critical loading rate, hydrogen uptake and transport are not limited and threshold stress intensity factor measurements are independent of loading rate. Available data support this concept (fig. 6).[41] Such critical values of loading rate depend on the specifics of the material tested (e.g., the diffusion coefficient) and the severity of the environment (i.e., surface hydrogen concentration) and need to be identified empirically.

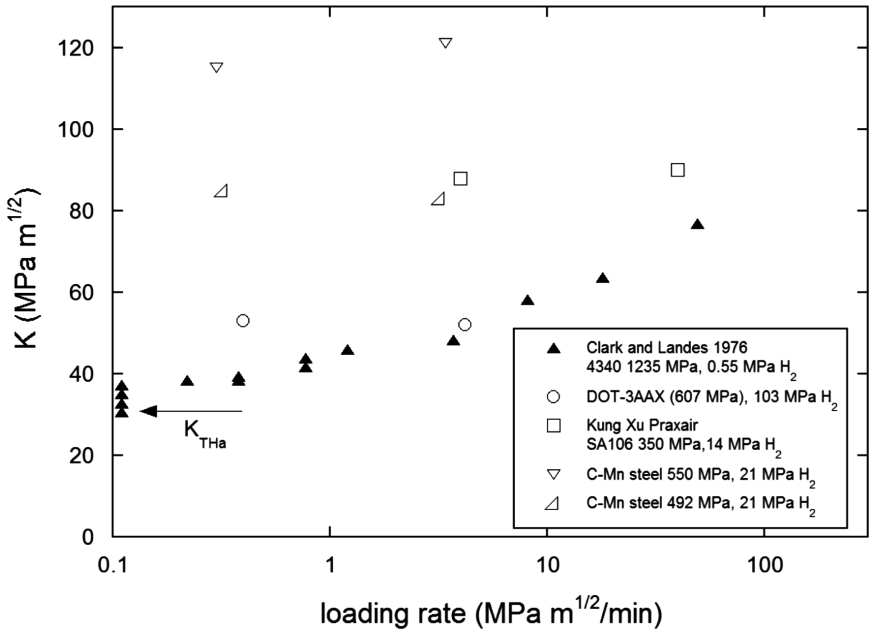
ASTM E1820 describes elastic-plastic fracture mechanics testing procedures that yield a much broader range of applicability and validity compared with linear elastic fracture mechanics methods described in ASTM E399. When compared with ASTM E1820, ASTM E399 requires some combination of larger specimens, higher strength material, and lower threshold stress intensity factors for the measurements to be valid. In addition, any specimen that can yield a valid measure of K_{Ic} from ASTM E399 generally also will yield a valid measure of J_{Ic} from ASTM E1820; however, it is often the case that a specimen capable of yielding a valid measure of J_{Ic} cannot yield a valid measure of K_{Ic}.

Slow-rising displacement methods are the only fracture mechanics tests that address the history dependence of crack tip strain accumulation and therefore provide the only method to accurately measure the threshold stress intensity factor for the onset of crack extension when the hydrogen embrittlement mechanism is strain controlled. In addition, these test methods are fully appropriate for stress-controlled hydrogen embrittlement mechanisms as well. In either case, appropriate selection of loading rate remains necessary.

Rising Step Loaded Measurements

Intermediate between static and rising displacement test methods are the step loading methods described in ASTM F1624, *Standard Test Method for Measurement of Hydrogen Embrittlement Threshold in Steel by the Incremental Step Loading Technique*. Although ASTM F1624 is often used to provide a pass-or-fail criterion for material qualification as an alternative to ASTM F519 or ASTM F1940, this standard is included in the section on fracture mechanics because it also purports to provide an alternative means of measuring the threshold stress intensity factor. This standard specifies that a notched specimen is loaded in either tension or bending through a sequence of displacement increases followed by displacement holds. Crack growth is assumed to occur when load drop is observed during the hold period. The output of this standard is the threshold load, which is the highest load applied to the specimen before the determination of crack extension. It is suggested that this threshold load may be

FIG. 6 Threshold stress intensity factor, K, for the onset of crack extension under rising displacement in hydrogen gas as a function of the applied loading rate. *Source:* Data from Nibur et al.,[23] Clark and Landes,[39] Xu,[42] and San Marchi.[43]



converted to a threshold stress intensity factor, but no guidance for performing this calculation nor any relevant validity criteria are provided in ASTM F1624.

The most consequential difference between static and rising displacement test methods is the sequence of hydrogen exposure and strain accumulation at the crack tip. The effective loading rate utilized in ASTM F1624 is simply the average over the loading portion and hold portion of each step; the rate of increase of displacement during the loading portion of the step is not specified and is typically applied rapidly. The history dependence of strain-controlled hydrogen embrittlement necessitates that the rate of strain accumulation be sufficiently slow to accommodate the kinetics of hydrogen transport to and within the evolving strain field. It is questionable whether the step loading profile fully accommodates these kinetic factors. In fact, direct comparisons between monotonically rising displacement and step-wise increasing displacement using cathodically polarized Monel K-500 in sodium chloride solution at nominally equivalent loading rates (based on total time to reach the final applied displacement) have shown the step load tests to produce much slower crack growth rates and higher threshold stress intensity factors. In addition, the fracture mechanism was intergranular when stressed under monotonically rising displacement but was transgranular with microvoids when stressed using step loading procedures.[44] These results strongly suggest that crack tip strain rate during the active loading segment plays a critical role in full development of the hydrogen embrittlement mechanism.

ASTM F1624 identifies the threshold load based on the assumption that the onset of crack extension will correlate to a load drop during the fixed displacement portion of the loading profile. Implicit to the discussion in the section "Sustained Load Fracture Threshold Test Methods" is the observation that sustained crack growth at fixed displacement is likely to occur only when the R-curve is flat. The presence of a rising R-curve indicates that the driving force must be continually increased to maintain crack growth. For such cases, driving force values significantly greater than the true threshold for the onset of crack extension may be needed to maintain a measurable increment of crack extension under constant displacement conditions.[23,25] Therefore, the use of load drop to indicate crack extension will lead to overestimates of the threshold stress if the fracture mechanism is strain-controlled.

References

1. A. Turnbull, "Hydrogen Diffusion and Trapping in Metals," in *Gaseous Hydrogen Embrittlement of Materials in Energy Technologies*, vol. 2, ed. R. P. Gangloff and B. P. Somerday (Cambridge: Woodhead, 2012), 89–128.
2. J. P. Hirth, "Effects of Hydrogen on the Properties of Iron and Steel," *Metallurgical Transactions A* 11A (1980): 861–890.
3. C. San Marchi, B. P. Somerday, and S. L. Robinson, "Permeability, Solubility and Diffusivity of Hydrogen Isotopes in Stainless Steels at High Gas Pressures," *International Journal of Hydrogen Energy* 32 (2007): 100–116.
4. J. H. Holbrook, H. J. Cialone, E. W. Collings, E. J. Drauglis, P. M. Scott, and M. E. Mayfield, "Control of Hydrogen Embrittlement of Metals by Chemical Inhibitors and Coatings," in *Gaseous Hydrogen Embrittlement of Materials in Energy Technologies*, vol. 2, ed. R. P. Gangloff and B. P. Somerday (Cambridge: Woodhead, 2012), 129–153.
5. R. A. Oriani, "The Diffusion and Trapping of Hydrogen in Steel," *Acta Metallurgica* 18 (1970): 147–157.
6. Z. S. Hosseini, M. Dadfarnia, K. A. Nibur, B. P. Somerday, R. P. Gangloff, and P. Sofronis, "Trapping against Hydrogen Embrittlement," in *Proceedings of the 2016 International Hydrogen Conference: Materials Performance in Hydrogen Environments*, 71–80 (New York: ASME Press, 2017).
7. K. A. Nibur, B. P. Somerday, S. Pillot, and R. P. Gangloff, "The Role of VC Precipitates in Hydrogen Assisted Cracking of Vanadium Modified 2¼ Cr -1Mo Steel," in *Proceedings of the Twenty-Ninth (2019) International Ocean and Polar Engineering Conference*, ISOPE-I-19-405 (International Society of Offshore and Polar Engineers, 2019).
8. H. K. Birnbaum and P. Sofronis, "Hydrogen-Enhanced Localized Plasticity: A Mechanism for Hydrogen-Related Fracture," *Materials Science and Engineering A* A176 (1994): 191–202.
9. I. M. Robertson, M. L. Martin, and J. A. Fenske, "Influence of Hydrogen on the Behavior of Dislocations," in *Gaseous Hydrogen Embrittlement of Materials in Energy Technologies*, vol. 2, ed. R. P. Gangloff and B. P. Somerday (Cambridge: Woodhead, 2012), 166–206.
10. D. Delafosse, "Hydrogen Effects on the Plasticity of Face Centered Cubic (FCC) Crystals," in *Gaseous Hydrogen Embrittlement of Materials in Energy Technologies*, vol. 2, ed. R. P. Gangloff and B. P. Somerday (Cambridge: Woodhead, 2012), 247–285.
11. Y. Z. Chen, X. Y. Ma, X. H. Shi, T. Suo, C. Borchers, K. H. Zhang, F. Liu, and R. Kirchheim, "Hardening Effects in Plastically Deformed Pd with the Addition of H," *Scripta Materialia* 98 (2015): 48–51.
12. Y. Liang, P. Sofronis, and N. Aravas, "On the Effect of Hydrogen on Plastic Instabilities in Metals," *Acta Materialia* 51 (2003): 2717–2730.
13. A. Gysler, G. Lütjering, and V. Gerold, "Deformation Behavior of Age-Hardened Ti-Mo Alloys," *Acta Metallurgica* 22 (1974): 901–909.
14. K. A. Nibur, B. P. Somerday, D. K. Balch, and C. San Marchi, "The Role of Localized Deformation in Hydrogen-Assisted Crack Propagation in 21Cr-6Ni-9Mn Stainless Steel," *Acta Materialia* 57 (2009): 3795–3809.
15. Z. Guo, M. Zhao, C. Li, S. Chen, and L. Rong, "Mechanism of Hydrogen Embrittlement in a Gamma-Prime Phase Strengthened Fe-Ni Based Austenitic Alloy," *Materials Science and Engineering A* A555 (2012): 77–84.
16. C. San Marchi, T. Michler, K. A. Nibur, and B. P. Somerday, "On the Physical Differences between Tensile Testing of Type 304 and 316 Austenitic Stainless Steels with Internal Hydrogen and in External Hydrogen," *International Journal of Hydrogen Energy* 35 (2010): 9736–9745.

17. S. P. Lynch, "Metallographic and Fractographic Techniques for Characterizing and Understanding Hydrogen-Assisted Cracking of Metals," in *Gaseous Hydrogen Embrittlement of Materials in Energy Technologies*, vol. 1, ed. R. P. Gangloff and B. P. Somerday (Cambridge: Woodhead, 2012), 274–346.

18. R. O. Ritchie, J. F. Knott, and J. R. Rice, "On the Relationship between Critical Tensile Stress and Fracture Toughness in Mild Steel," *Journal of the Mechanics Physics of Solids* 21 (1973): 395–410.

19. D. H. Lassila and H. K. Birnbaum, "The Effect of Diffusive Hydrogen Segregation on Fracture of Polycrystalline Nickel," *Acta Metallurgica* 34 (1986): 1237–1243.

20. C. J. McMahon, "The Role of Grain Boundaries in Hydrogen Induced Cracking (HIC) of Steels," in *Gaseous Hydrogen Embrittlement of Materials in Energy Technologies*, vol. 2, R. P. Gangloff and B. P. Somerday, 154–165 (Cambridge: Woodhead, 2012).

21. Z. D. Harris, S. K. Lawrence, D. L. Medlin, G. Guetard, J. T. Burns, and B. P. Somerday, "Elucidating the Contribution of Mobile Hydrogen-Deformation Interactions to Hydrogen-Induced Intergranular Cracking in Polycrystalline Nickel," *Acta Materialia* 158 (2018): 180–192.

22. I. M. Robertson, P. Sofronis, A. Nagao, M. L. Martin, S. Wang, D. W. Gross, and K. E. Nygren, "Hydrogen Embrittlement Understood," *Metallurgical and Materials Transactions A* 46A (2015): 2323–2341.

23. K. A. Nibur, B. P. Somerday, C. San Marchi, J. W. Foulk, III, M. Dadfarnia, and P. Sofronis, *Metallurgical and Materials Transactions A* 44A (2013): 248–269.

24. A. Nagao, C. D. Smith, M. Dadfarnia, P. Sofronis, and I. M Robertson, "The Role of Hydrogen in Hydrogen Embrittlement Fracture of Lath Martensitic Steel," *Acta Materialia* 60 (2012): 5182–5189.

25. K. A. Nibur, B. P. Somerday, C. San Marchi, J. W. Foulk, III, M. Dadfarnia, P. Sofronis, and G. A. Hayden, "Measurement and Interpretation of Threshold Stress Intensity Factors for Steels in High-Pressure Hydrogen Gas," SAND2010-4633 (Sandia National Laboratories, Albuquerque, NM, July 2010).

26. R. O. Ritchie, W. L. Server, and R. A. Wullaert, "Critical Fracture Stress and Fracture Strain Models for the Prediction of Lower and Upper Shelf Toughness in Nuclear Pressure Vessel Steels," *Metallurgical Transactions A* 10A (1979): 1557–1570.

27. R. O. Ritchie and A. W. Thompson, "On Macroscopic and Microscopic Analyses for Crack Initiation and Crack Growth Toughness in Ductile Alloys," *Metallurgical Transactions A* 16A (1985): 233–248.

28. W. J. Drugan, J. R. Rice and T.-L. Sham, "Asymptotic Analysis of Growing Plane Strain Tensile Cracks in Elastic-Ideally Plastic Solids," *Journal of the Mechanics Physics of Solids* 30 (1982): 447–473.

29. J. W. Hutchinson, "Singular Behavior at the End of a Tensile Crack in a Hardening Material," *Journal of the Mechanics and Physics of Solids* 16, no. 1 (1968): 13–31.

30. J. R. Rice and G. F. Rosengren, "Plane Strain Deformation Near a Crack Tip in a Power-Law Hardening Material," *Journal of the Mechanics and Physics of Solids* 16, no. 1 (1968): 1–12.

31. *Testing Methods Used for Hydrogen-Exposed Metallic Materials Selection–Current Knowledge*, ISO DTR 10783, 2010–03–17 (Geneva, Switzerland: International Organization for Standardization, 2010).

32. J. A. Harris, Jr. and M. C. VanWanderham, "Various Mechanical Tests Used to Determine the Susceptibility of Metals to High-Pressure Hydrogen," in *Hydrogen Embrittlement Testing* (West Conshohocken, PA: ASTM International, 1974), 198–220.

33. R. E. Stoltz "Mechanical Property Measurements of Ferritic Steel in Hydrogen," in *Hydrogen Compatibility of Structural Materials for Energy Storage and Transmission*, ed. W. R. Hoover, SAND79–8200 (Livermore, CA: Department of Energy, Sandia National Laboratories, 1976), 47–60.

34. W. T. Chandler and R. J. Walter, "Testing to Determine the Effect of High Pressure Hydrogen Environments on the Mechanical Properties of Metals," in *Hydrogen Embrittlement Testing* (West Conshohocken, PA: ASTM International, 1974), 170–197.

35. R. E. Stoltz, "Plane Strain Tensile Testing for Measuring Environment Sensitive Fracture," *Metallurgical Transactions A* 12A (1981): 543–545.

36. T. L. Anderson, *Fracture Mechanics Fundamentals and Applications*, 3rd ed. (Boca Raton, FL: Taylor and Francis, 2005).

37. M. Hadj Meliani, Y. G. Matvienko, and G. Pluvinage, "Two-Parameter Fracture Criterion ($K_{\rho,\,c}$-$T_{ef,c}$) Based on Notch Fracture Mechanics," *International Journal of Fracture* 167 (2011): 173–182.

38. B. Cotterell and J. R. Rice, "Slightly Curved or Kinked Cracks," *International Journal of Fracture* 16 (1980): 155–169.

39. W. G. Clark and J. D. Landes, "An Evaluation of Rising Load K_{Iscc} Testing," in *Stress Corrosion—New Approaches* (West Conshohocken, PA: ASTM International, 1976), 108–127

40. B. P. Somerday and K. A. Nibur, "Effect of Applied K Level on the Crack-Arrest Threshold in Hydrogen Environments: Mechanics-Based Interpretation," *Corrosion* 75 (2019): 929–937.

41. K. A. Nibur and B. P. Somerday, "Fracture and Fatigue Test Methods in Hydrogen Gas," in *Gaseous Hydrogen Embrittlement of Materials in Energy Technologies*, ed. R. P. Gangloff and B. P. Somerday (Cambridge: Woodhead, 2012), 195–236.

42. K. Xu, "Properties of Linepipe Steels in High Pressure Hydrogen" (paper presentation, ASTM G1 H2 Workshop, Reno, NV, May 17, 2005).

43. C. San Marchi, unpublished results (Sandia National Laboratory, Albuquerque, NM, 2009).

44. R. P. Gangloff, H. M. Ha, J. T. Burns, and J. R. Scully, "Measurement and Modeling of Hydrogen Environment-Assisted Cracking in Monel K-500," *Metallurgical Transactions A* 45 (2014): 3814–3834.

Chapter 5 | Microbiological Effects

Jason S. Lee[1] and Brenda J. Little[2]

Introduction

2010 U.S. Code § 2228, Office of Corrosion Policy and Oversight defines "corrosion" as "the deterioration of a material or its properties due to a reaction of that material with its chemical environment."[1] Similarly, National Association of Corrosion Engineers (NACE) International provides the following definition: "The deterioration of a material, usually a metal, that results from a reaction with its environment."[2] Microbiologically influenced corrosion (MIC) is corrosion that is initiated or aggravated by the direct or indirect activities of microorganisms.

The term "microbiologically influenced corrosion" was first used by Pope et al.[3] and in 1986 was adopted as the term of choice by NACE International. The debate at that time focused on the difference between "influenced" and "induced." "Influenced" was meant to convey multiple direct and indirect effects and mechanisms, whereas "induced" was considered to connotate direct effects. Over time, the word "influenced" has been further interpreted to convey the notion that microorganisms can inhibit corrosion.

The following sections provide information about the microbiological effects that lead to MIC. In all cases, the impact of microorganisms will be determined by the vulnerability of the metal or material on which the microorganisms are growing and the composition of the electrolyte.

Scope of the Problem

Microorganisms produce localized attack, including pitting, dealloying, enhanced erosion corrosion, enhanced galvanic corrosion, stress corrosion cracking, and hydrogen embrittlement. MIC has been documented for the following metals and alloys: carbon steel, low-alloy stainless steels (<6% molybdenum), copper and its alloys, nickel and copper alloys, and aluminum alloys. There are no credible reports of field failures caused by MIC of titanium and high-nickel alloys. In addition, MIC has been reported for metal matrix composites, polymers, paints and coatings, ceramics, glass, sandstone, heritage stone works, sealants caulks, concrete, and fabrics (e.g., tent materials). The industries reporting MIC include oil exploration, refining, transportation, storage, and usage; conventional and nuclear power generation, chemical processing, paper production, and fire protection. MIC has been evaluated as a potential problem in long-term nuclear waste storage. MIC has been documented for materials exposed in water-containing liquids, including ultrapure, distilled, and demineralized waters; natural waters, including marine, estuarine, and fresh; process chemicals; hydrocarbons, including crude oils, and biofuels (i.e., fatty-acid methyl-ester [FAME] fuels); soil; and human plasma, saliva, urine, and sewage.

Corrosion Mechanisms Related to MIC

Corrosion reactions directly related to oxidations (anode) and reductions (cathode) and microbial processes require one- and two-electron transfers (oxidation or reduction reactions). Microorganisms can accelerate rates of partial reactions in corrosion processes or shift the mechanism for corrosion. In all cases, MIC involves a conversion of a metal oxide to a less protective layer (e.g., a sulfide), removal of an oxide layer (e.g., metal oxide reduction or acid production), or localization of an anode or cathode. MIC is not caused by a single mechanism or group of microorganisms.[4] Instead, microorganisms from the three domains of life—that is, archaea (e.g., methnaogens), bacteria, and eucaryotes (e.g., fungi)—can influence corrosion through numerous mechanisms.

Archaea and bacteria are both procaryotes, lacking a membrane-bound nucleus. Archaea are considered the oldest species on Earth. Many are extremophiles, living in waters that are either near boiling (90°C) or freezing (−4°C) and at acidic pH (<2) or a combination of these extremes. In addition to success in extreme environments archaea, "exist in a wide variety of terrestrial, freshwater and marine habitats, sometimes in very

[1]Naval Research Laboratory, 1009 Balch Blvd., Stennis Space Center, MS 39529, USA http://orcid.org/0000-0002-1079-433X
[2]B. J. Little Corrosion Consulting, LLC, 6528 Alakoko Dr., Diamondhead, MS 39525, USA http://orcid.org/0000-0002-9994-791X
The authors acknowledge the previous author of this chapter, Stephen C. Dexter, University of Delaware, Lewes, DE.

DOI: 10.1520/MNL202NDSUP20190005

Copyright © 2022 by ASTM International, 100 Barr Harbor Dr., PO Box C700, West Conshohocken, PA 19428-2959
ASTM International is not responsible, as a body, for the statements and opinions expressed in this chapter. ASTM International does not endorse any products represented in this chapter.

high abundance."[5] Archaea can have the shape and size of bacteria, but the two groups have unique biochemistries. Both bacteria and archaea can be obligate anaerobes, facultative anaerobes, or aerobes, depending on the oxygen requirements for growth. Eucaryotes have a membrane-bound nucleus. Most, but not all, eukaryotes require oxygen to survive (i.e., aerobes).

In aquatic environments, microorganisms attach to solid surfaces. Immobilized (sessile) cells grow, reproduce, and produce extracellular polymeric substances (EPS), forming a structure for microbial growth (i.e., biofilm). Many researchers have investigated biofilm formation on a variety of substrata, and this chapter does not attempt to summarize that body of literature.[6–8] The rate of biofilm formation depends on the characteristics of the substratum and properties of the aqueous medium (e.g., nutrients, flow, temperature) and many other environmental factors. Over time, biofilms form on all substrata exposed to aqueous environments. For many years, biofilms were studied as the preferred habitat for bacteria, allowing the microorganisms to remain stationary within an EPS matrix, protected from biocides and desiccation. During the 1990s, bacterial biofilms were studied in detail and many molecular details were elucidated.[9] During that period, references to "multispecies" biofilms referred to multiple species of bacteria within a biofilm. Biofilms can be formed by a single bacterial or archaeal species, but it is now well established that natural biofilms are mixed communities of archaea and bacteria in varying abundances,[10] suggesting that multispecies biofilms can have representatives from multiple domains.

Biofilm formation is not limited to aqueous environments. All microorganisms require water for growth. Fungi and other microorganisms, however, can survive in humid atmospheric environments (relative humidity >65%) within atmospheric biofilms. Aqueous and atmospheric biofilms have several properties in common. Microorganisms within biofilms tend to stratify for survival. In oxygenated waters, stratification can be related to oxygen concentrations required for growth or survival. Anaerobes are found in anaerobic niches within biofilms, while the aerobes remain at the oxygen-containing water–biofilm interface.[11] As the rate of aerobic respiration increases, the oxygen within the depths of the biofilm decreases. Similarly, biofilms in atmospheric exposures tend to be multidomain, including algae, fungi, and bacteria, forming mutualistic communities with algae located on the outermost layers of biofilms exposed to ultraviolet radiation, whereas bacteria and fungi are located within the inner layers of the biofilm.[12]

Microorganisms within aqueous and atmospheric biofilms maintain environments at the biofilm solid interface that are radically different from the bulk in terms of pH, dissolved oxygen, and organic and inorganic species. Consequently, microorganisms in biofilms produce reactions not predicted by thermodynamic arguments based on the chemistry of the bulk medium. Microbial colonization can change material surface properties, increasing or decreasing the susceptibility to corrosion. Mechanisms and rates of corrosion are microorganism-material-environment specific.

Causative organisms and possible mechanisms for MIC have been described in many reviews.[13] The list of possible MIC-causing microorganisms typically reflects their impact on MIC—for example, acid-producing bacteria (APB) (acid production) and sulfate-reducing bacteria (SRB) (sulfide production). These designations are too simplistic to convey the complexity of microbial reactions within biofilms. For example, any consideration of sulfide production must include sulfate-reducing archaea in addition to SRB and bacteria that can reduce thiosulfate to sulfide. The more inclusive term for the microorganisms that can influence corrosion by sulfide production is sulfide-producing prokaryotes (SPP). Other MIC mechanisms include oxygen concentration cells, metal concentration cells, ammonia production, metal oxidation and deposition, metal reduction, dealloying, and consumption and alteration of corrosion inhibitors.

To clarify mechanisms for the impact of microorganisms, several investigators have invented additional terms. For example, Enning and Garrelfs[14] defined two types of MIC (i.e., chemical and electrical) to describe corrosion damage to iron substrata by SRB. They described chemical microbially influenced corrosion (CMIC) as indirect through a corrosive chemical agent (i.e., hydrogen sulfide) formed by SRB as a dissimilatory product from sulfate reduction with organic compounds or hydrogen. They concluded that other SRB can attack iron by withdrawal of electrons (electrical microbially influenced corrosion, EMIC), directly by metabolic coupling. Gu[15] defined three categories of MIC to distinguish mechanisms (i.e., Types I, II, and III). Gu defined Type I MIC as caused by electrogenic bacteria. The mechanism is based on the assumption that electrogenic bacteria can form pili for electron transfer and energy distribution. The authors claim that electrogenic microorganisms can use carbon steel or other non-noble metals as electron donors because the reduction potentials of the ions of these metals can form thermodynamically favorable redox reactions when coupled with the reduction of an oxidant (e.g., sulfate and nitrate). The supposition is that electrogenic microorganisms use electrons released from elemental metal oxidation and reduce the oxidant intracellularly. Gu defined Type II MIC as corrosion caused by metabolites, such as acids, secreted by APB.[16] Copper MIC caused by SRB is also classified as Type II MIC. According to Gu, Type III MIC is caused by microorganisms that secrete enzymes or other corrosive chemicals and degrade nonmetallic materials containing organic carbon as one of the components. More recently, Gu et al.[17] identified two main types of anaerobic MIC, namely, extracellular electron transfer MIC (EET-MIC) and metabolite MIC (M-MIC). The definitions established by Gu et al.[15–17] and Enning and Garrelfs[14] have not received widespread acceptance. The electron transport mechanisms for both EET-MIC and EMIC are not well described. Blackwood[18] questioned mechanisms for "direct electron" transfer across cell walls (7.5-10 nm) and suggested that electron transfer is more likely mediated by redox intermediates that reside within or on the walls of the microorganisms.

It is obvious that not all materials have the same vulnerabilities and that some specific vulnerabilities can be predicted. For example, SRB are routinely listed as causative microorganisms for MIC. Sulfide can react with some metal oxides to produce metal-sulfide corrosion products. The susceptibility of the oxide

conversion to a sulfide can be predicted.[19] The McNeil and Odom[19] model predicts that titanium and some stainless steels will be immune to sulfide and MIC by SPP, whereas carbon steel and copper alloys will be vulnerable. Similarly, Kovach and Redman[20] predicted that austenitic stainless steels containing more than 6% molybdenum were immune to MIC, despite their extensive use in applications in which lower alloys (i.e., 304 and 316L) were vulnerable.

Researchers at the State Research Center for Microbiology, Moscow, Russian Federation[21] demonstrated that environmental conditions (e.g., electrolyte composition) determined the specific microbiological effects on corrosion processes—not the microorganisms. They demonstrated that a single consortium of microorganisms could both accelerate and inhibit corrosion of carbon steel based on the composition of the electrolyte in which they were growing. Because of this possibility, there are reports of the same microorganism both causing and inhibiting corrosion of the same material. Consequently, lists of causative microorganisms are not useful in the absence of specific information regarding media composition and an evaluation of aggressive:inhibiting anions and electron donors:acceptors.[22,23] Changes in these ratios can dramatically affect the outcome of laboratory experiments.[24,25] For example, *Shewanella* ssp. frequently are cited in lists of MIC-causing bacteria. The mechanism most frequently cited for their involvement is reduction of Fe^{+3} oxides.[26] Philips et al.[27] demonstrated that a *Shewanella* isolate (4t3-1-2LB) could accelerate corrosion using metallic iron (Fe^0) as the sole electron donor and fumarate as the electron acceptor. The authors did not suggest that their observations are applicable to all *Shewanella* ssp. and they provided a careful description of the experimental conditions and medium composition required for their observations.

Corrosion mechanisms requiring microbial growth must account for nutrients, electron donors, and electron acceptors required to support the mechanism. The nutritional requirements of a microorganism include carbon, hydrogen, oxygen, nitrogen, sulfur, phosphorus, potassium, magnesium, iron, calcium, and manganese, and traces of zinc, cobalt, copper, and molybdenum. Microorganisms use assimilatory and dissimilatory pathways to process nutrients and electron acceptors. Assimilatory pathways are methods for moving a nutrient into the cell and using it for biosynthesis of macromolecules. Dissimilatory pathways use electron acceptors to generate energy. Bacteria and archaea have several possible electron donors, including organic molecules, hydrogen, carbon monoxide, ammonia, nitrite, sulfur, sulfide, and ferrous iron. If oxygen is available, it is used as the terminal electron acceptor, because it generates the greatest Gibbs free energy change and produces the most energy. In the absence of oxygen, several electron acceptors can be used (e.g., sulfate [SO_4^{-2}], nitrate [NO_3^-], nitrite [NO_2^-], iron[III] [Fe^{+3}], chromium[VI] [Cr^{+6}], and manganese[IV] Mn^{+4}). Not every donor-acceptor combination is thermodynamically possible. The redox potential of the acceptor must be more positive than that of the donor. Environmental conditions differ from standard conditions used to describe redox potentials. The carbon requirements can be met by organic carbon or carbon dioxide (CO_2).

The relationship between nutrients and MIC is complicated and largely ignored in laboratory experiments. Although oxyanions can serve as nutrients or electron acceptors (e.g., nitrates, phosphates, sulfates), they also can be corrosion inhibitors. Both maintenance and inhibition of localized corrosion require specific ratios of aggressive:inhibiting ions. For example, Webster and Newman[28] demonstrated that an anion ratio of [Cl^-]: Σ [all other anions] of 5:1 was required to consistently produce corrosion in laboratory experiments with SRB and a creviced stainless steel (Fe-15Cr-10Ni).

Critical pitting potentials are the potentials below which pitting and crevice corrosion are not stable. Increasing Cl^- (an aggressive anion) shifts the critical pitting potential to more active (negative) values. Conversely, the potential is shifted to more noble (positive) values by inhibiting anions (e.g., chlorate (ClO_4^-), SO_4^{-2}, NO_3^-, phosphate (PO_4^{-3}), NO_2^-, and hydroxide (OH^-). Kehler, Ilevbare, and Scully[22] developed equations that can be used to predict the corrosiveness of a particular medium/electrolyte to specific metals in the absence of microorganisms. Concentrations and types of anions required for corrosion inhibition in Cl^--containing media are metal-specific. For example, sulfates can inhibit Cl^--induced pitting of stainless steels but are aggressive toward mild steel. Furthermore, inhibitor anions must be maintained in certain minimum concentrations to be fully effective. In many service applications, excursions in solution chemistry, temporary loss of inhibitor, or transient increases in temperature may give rise to localized corrosion in an otherwise inhibited system.[29] Below the critical concentration, inhibitive anions may stimulate breakdown of the oxide films. Microbial activities alter anion ratios through metabolism and respiration,[23] concurrently altering the corrosivity of the electrolyte.

Standards for MIC

There are many motivations for standardized MIC testing in both laboratory and field applications. In the laboratory, testing is used to evaluate the vulnerability of a specific material to a natural source water containing a natural microflora. Alternatively, a range of materials could be ranked as to susceptibility for specific MIC mechanisms in artificial media with an inoculum of microorganisms (pure or mixes cultures). There are no specific standards, however, for MIC laboratory testing. Published experiments have been completed using different test media and electrolytes at differing temperatures with either pure cultures or laboratory-specific consortia. Most important, few experiments have considered aggressive anions–inhibiting anions or electron donor–electron acceptor relationships. Interlaboratory data cannot be compared. Laboratory experiments are routinely conducted in nutrient-rich media inoculated with specific microorganisms. Few researchers verify the identity of the microorganisms at the conclusion of the experiment. Many experiments are conducted in the absence of abiotic controls (i.e., media controls).

The motivations for field testing for MIC typically are related to diagnosing a failure or controlling MIC by establishing pigging intervals or scheduling biocide additions. NACE

International has approved the following test methods for field applications: *TM0106-2016, Detection, Testing, and Evaluation of Microbiologically Influenced Corrosion (MIC) on External Surfaces of Buried Pipelines*;[30] TM0194-2014, *Field Monitoring of Bacterial Growth in Oil and Gas Systems*;[31] and TM0212-2018, *Detection, Testing, and Evaluation of Microbiologically Influenced Corrosion on Internal Surfaces of Pipelines*.[32] These three test methods, designed specifically for oil and gas pipelines, do not consider recent additions to products transported in oil pipelines (e.g., FAME biodiesel and ethanol). The test methods rely on quantification of specific groups of microorganisms, especially bacteria, or some constitutive property of bacteria (e.g., DNA or ATP). There are no NACE International-approved MIC test methods for pipelines in other industries (e.g., drinking water distribution systems).

Diagnosing

The microorganisms responsible for MIC cannot be identified by characterization and quantification of microorganisms in the bulk medium or electrolyte.[33] Kotu, Mannan, and Jayaraman[34] provided a chronological review of the following techniques to investigate microorganisms directly associated with corrosion products or corrosion sites: culture, hybridization, polymerase chain reaction (PCR), sequencing, and metabolomics. The molecular microbiological methods (MMMs; i.e., hybridization, PCR, and sequencing) do not rely on cultivation of microorganisms for diagnosing MIC. Instead, MMMs detect a microbial constituent, such as DNA, RNA, or protein-based markers.[35]

Culture techniques and MMM, related to identification or enumeration of microorganisms associated with corrosion products, have demonstrated the microbial diversity in MIC. For example, Rajasekar et al.[36] reported a phylogenetic analysis of 16S ribosomal RNA (16S rRNA) sequences in samples removed from pitted, diesel-transporting, and naphtha-transporting carbon steel pipelines. They identified *Serratia marcescens, Bacillus subtilis, Bacillus cereus, Pseudomonas aeruginosa, Klebsiella oxytoca, Pseudomonas stutzeri, Bacillus litoralis, Bacillus sp., Bacillus pumilus, Bacillus carboniphilus,* and *Bacillus megaterium*. The dominant species varied between the two pipelines, but SRB were not detected in the samples from either of the pipelines operated under aerobic conditions. Many of these specific microorganisms are not typically associated with MIC. The authors concluded several types of bacteria may be involved in MIC in industrial facilities and that prolonged addition of corrosion inhibitor or biocide resulted in the dominance of the biocide-resistant spore-forming *Bacillus* sp.

All culture techniques underestimate the natural microbial population[37,38] and can produce both false positives and false negatives. There are also inherent limitations to culture techniques and MMM. Hybridization techniques, for example, fluorescence *in situ* hybridization (FISH) and DNA arrays, require probes designed to bind DNA or RNA from specific microorganisms—that is, one can identify only those microorganisms for which probes have been developed. In addition, DNA arrays require "sufficient amounts" of nucleic acids, especially for detection of unstable RNA.[34] Bernstein et al.[39] observed that about 80% of all mRNAs of *Escherichia coli* had half-lives between 3 and 8 min.

PCR can be used to synthesize and amplify a specific section of DNA (e.g., 16S rRNA). Following PCR, the amplified regions are sequenced and used to identify microorganisms in a sample. Design of PCR primers requires prior knowledge about the microorganisms in the sample and amplification bias also has been reported. A further limitation is that no single variable region of 16S rRNA gene can identify all microorganisms in a community. Quantitative information about specific microorganisms requires quantitative PCR (qPCR). Eid, Duncan, and Tanner[40] further demonstrated that "monitoring to single SRB-specific genes such as dsrAB or aprBA or to one SRB genus or species via a technique such as qPCR may be of less utility in detecting microbial communities associated with MIC than measurements that target more than one group or gene." They concluded that simply quantifying the number of *Deltaproteobacteria* (e.g., SRB) or even *Desulfomicrobium* using targeted qPCR "would not be sufficiently predictive."

Extracellular DNA (e-DNA), occurring outside of living organisms, may account for the largest fraction of total DNA in some environments and can include molecules in dead cells as well as organic and inorganic aggregates adsorbed onto mineral matrices.[41] e-DNA undermines the assumption of a direct link between a characterized DNA pool and the actual living microbial cell abundance and diversity in a sample. Makama et al.[42] recently demonstrated e-DNA in corrosion products on carbon steel exposed to sterilized natural seawater. The authors concluded that in a marine environment corrosion deposits on ferrous alloys could harbor bacterial e-DNA. They stressed, "Care must be exercised when using DNA profiling as a sole tool in demonstrating the involvement of biofilms in carbon steel corrosion."[42]

Metabolomics (i.e., identification and characterization of microbial metabolism products [metabolites]) has been advocated as a method to provide information on the functionality of microbial species involved in MIC.[34] Kotu, Mannan, and Jayaraman[34] suggested that identification of key metabolites (e.g., amino acids, fatty acids, carboxylic acids, and their derivatives) produced by microorganisms, in addition to information about community structure, could provide biomarkers for MIC. Bonifay et al.[43] used a combination of metabolomics and metagenomics (16S rRNA gene qPCR and sequencing of 16S PCR products) to demonstrate the fundamental differences between samples from two crude oil production pipelines. The pipelines had similar backgrounds but were experiencing different rates of corrosion. The rates were generalized as high and low. Deposits from the pipeline with the high-corrosion (HC) rate contained SRB and archaea, whereas samples from the pipeline with low-corrosion (LC) rates were dominated by pseudomonads. The abundance of alkylsuccinates and benzylsuccinates, diagnostic for anaerobic hydrocarbon degradation, was an order of magnitude greater in HC samples compared with LC samples. The authors concluded that the differences in metabolic activity and microbial community organization could be used to explain the differences in corrosion rates. Beale et al.[44] reviewed multiple

"omic" approaches for studying MIC, including metabolomics. The approaches demonstrate the possibility for the identification of metabolic networks characteristic for MIC.

Eckert and Skovhus concluded, "A multidisciplinary process for establishing the significance of microbiological data (particularly from molecular methods) in regard to MIC threat identification, mitigation and monitoring has yet to be clearly established. As a result, MMMs will not be embraced by oil and gas asset operators until their significance relative to corrosion management and asset integrity are made more transparent."[35] Kotu, Mannan, and Jayaraman identified two fundamental problems with all identification and enumeration techniques for diagnosing MIC: "all the microorganisms identified at a specific MIC impacted location need not contribute to the observed corrosion at that location."[34] Furthermore, "it is not possible to directly correlate relative abundance of microorganisms to a causative role in MIC."[34]

Care also must be taken when analyzing electrochemical, metallurgical, and chemical data during MIC diagnostics. Electrochemical polarization influences the distribution, number, and types of bacteria associated with the surface. Anodic sites attract microorganisms in the absence of MIC.[45] In addition, MIC does not produce a macroscopic, unique metallographic feature or pit morphology. Metallurgical features previously thought to be unique to MIC, for example, hemispherical pits in 300 series stainless steel localized at welds or tunneling in carbon steel, are consistent with some mechanisms for MIC, but also can be produced by abiotic reactions.[46]

Two microbiological effects on corrosion products can be used as diagnostic tools for MIC—unique mineralogy and isotope fraction. McNeil, Jones, and Little[47] evaluated corrosion product mineralogy using X-ray diffraction data, thermodynamic stability diagrams (Pourbaix), and the simplexity principle for precipitation reactions. They concluded that some sulfides under near-surface natural environmental conditions could be produced only by microbiological activity. Tetragonal mackinawite (FeS_{1-x}) produced by SRB from iron and iron oxides was identified as a mineralogical fingerprint for MIC by SRB (with some exclusions, e.g., industrial water). Alteration of mackinawite depends on Fe^{2+} concentration in the electrolyte. If Fe^{2+} in the electrolyte is low, mackinawite alters to greigite ($Fe^{2+}Fe^{3+}{}_2S_4$), an alteration that is not observed in nonbiological systems. When Fe^{2+} is high, mackinawite is accompanied by green rust 2, a complex ferrosoferric oxyhydroxide. On continued exposure to SRB and continued sulfide production, mackinawite alters to greigite, smythite, and pyrrhotite. Pyrite (FeS_2) is not a typical iron corrosion product, but SRB can produce pyrite from mackinawite in contact with elemental sulfur. Abiotic aqueous synthesis of these minerals, with the possible exception of pyrite, requires hydrogen sulfide (H_2S) pressures higher than those found in shallow waters. Using a similar approach, McNeil and Little[48] reported that djurlelte, spionkopite, and the high-temperature polymorph of chalcocite were mineralogical fingerprints for SRB-influenced corrosion of copper-nickel alloys. Fredrickson et al.[49] indicated that electron donor and acceptor concentrations influenced the microbial reduction of hydrous ferric oxide and the resulting suite of iron minerals formed as a result of the reduction.

Dissimilatory microbial sulfate reduction produces large sulfur isotope fractionation in which the resulting sulfide is deficient in the heavy isotopes (^{33}S, ^{34}S, and ^{36}S) relative to the most abundant isotope ^{32}S.[50,51] Grengg et al.[52] reported sulfur isotope fractionation of up to 13% between sulfate in waste water and newly formed gypsum ($CaSO_4{\cdot}2H_2O$) in a concrete sewer system. In sewer systems, microbial sulfate reduction produces sulfides that are oxidized by sulfur oxidizing bacteria to sulfuric acid (H_2SO_4) that reacts with the concrete to produce gypsum. Little, Wagner, and Jones-Meehan[53] demonstrated sulfur isotope fractionation in sulfide corrosion deposits resulting from activities of SRB within biofilms on copper surfaces. ^{32}S accumulated in sulfide-rich corrosion products, and ^{34}S was concentrated in the residual sulfate in the culture medium.

There is no simple diagnostic test for identifying MIC versus abiotic corrosion.[54] Diagnosing MIC requires a combination of microbiological, metallurgical and chemical analyses. The following are required for an accurate diagnosis of MIC:[13]

- Samples of surface deposits from corroded and unaffected areas that have not been altered by collection or storage.
- Identification of a corrosion mechanism that is consistent with the corroded material and the environment to which it has been exposed.
- Identification of microorganisms capable of growth and maintenance of the corrosion mechanism in the particular environment.
- Demonstration of an association of the microorganisms with the observed corrosion.

The changes introduced by the presence of microorganisms, independent of corrosion-causing reactions, have been largely ignored. Electrochemical techniques cannot separate the biotic and abiotic reactions contributing to the electrochemical parameters being measured. Abiotic control experiments should accompany biotic experiments. It is difficult, however, to maintain a sterile control in nutrient-rich media used to grow microorganisms. Dexter[55] recommended the following three approaches for maintaining an abiotic control: use an artificially prepared water instead of a natural water as the electrolyte,[56] treat the electrolyte to control microbial growth,[57] or manipulate the surface of the working electrode by periodically removing the biofilm.[58] All of these recommendations can have unintended, unmeasured electrochemical consequences. For example, Eid, Duncan, and Tanner[40] demonstrated that 50 ppm glutaraldehyde, a common oil field biocide, in an abiotic experiment was 3.6 times more corrosive than an identical experiment inoculated with SRB. Furthermore, in addition to colonizing the working electrode, microorganisms colonize the Luggin capillary, potentially isolating the reference electrode, and the counter electrode.

Monitoring

There are no industry standards for monitoring MIC. Monitoring techniques have been designed to collect background information

and detect modifications in operating systems that are indicative of MIC.[13] For example, devices can monitor heat-transfer resistance, fluid friction, and galvanic current because of biofilm formation. Weight loss, an indication of general corrosion, can be monitored by periodic removal of witness coupons from operating systems. Electrochemical techniques, including electrochemical noise and linear polarization, are available in commercial instrumentation to provide real-time corrosion rate information. Linear polarization devices measure the polarization resistance (R_p) of a material in a specific environment where the inverse of R_p (R_p^{-1}) is proportional to corrosion rate. Mansfeld et al.[59] compared R_p^{-1} corrosion rate data with weight loss data for copper alloys exposed in artificial and natural seawater, assuming that the difference between the two media was the presence of a natural microflora in natural seawater. Corrosion in abiotic artificial seawater was accurately predicted by the device—that is, the electrochemical R_p^{-1} calculation matched measured weight loss. The calculations based on R_p^{-1} measurements, however, did not match the actual weight loss in natural (i.e., biotic) seawater. Those calculations were two to four times lower than the weight loss measurements. Differences in the absolute measurements may not be significant for monitoring purposes.

Conclusions

Understanding the microbiological effects that result in MIC requires more than the identification of putative microorganisms. The connection between specific microorganisms and metal vulnerabilities is determined by electrolyte composition (e.g., inhibiting anions:aggressive anions). Diagnosis of MIC should begin with identification of a plausible corrosion mechanism, followed by identification of the microorganisms associated with the corrosion products and confirmation that both are consistent with the properties of the electrolyte. State-of-the-art monitoring for MIC is based on detection of changes in electrochemical or microbiological data that may be an indicator of MIC for a particular operating system. Identification of specific minerals or isotope fractionation of elements within corrosion products can provide definitive evidence that the formation of the corrosion product required a microbiological effect.

References

1. 2010 U.S. Code § 2228, Office of Corrosion Policy and Oversight.
2. "What Corrosion Is!" Corrosion Doctors, http://web.archive.org//web/20210429221813/https://corrosion-doctors.org/Principles/What-is.htm
3. D. H. Pope, D. J. Duquette, A. H. Johannes, and P. C. Wayner, *Microbiologically Influenced Corrosion: A State of the Art Review* (Columbus, OH: Materials Technology Institute of the Chemical Process Industries, 1984).
4. C. R. Woese and G. E. Fox, "Phylogenetic Structure of the Prokaryotic Domain: The Primary Kingdoms," *Proceedings of the National Academy of Sciences* 74 (1977): 5088–5090.
5. E. F. DeLong, "Oceans of Archaea," *ASM News* 69, no. 10 (2003): 503–511.
6. W. G. Characklis and K. C. Marshall, *Biofilms* (New York: Wiley, 1990).
7. H. M. Lappin-Scott and J. W. Costerton, *Microbial Biofilms* (Cambridge: Cambridge University Press, 1995).
8. M. Ghannoum and G. A. Toole, *Microbial Biofilms* (Washington, DC: American Society of Microbiology, 2004).
9. M. van Wolferen, A. Orell, and S.-V. Albers, "Archaeal Biofilm Formation," *Nature Reviews Microbiology* 16 (2018): 699–713.
10. S. Fröls, "Archaeal Biofilms: Widespread and Complex," *Biochemical Society Transactions* 41, no. 1 (2013): 393–398.
11. J. Larsen, K. Rasmussen, H. Pedersen, K. Sorensen, T. Lindgaard, and T. L. Skovhus, "Consortia of Bacteria and Archaea Causing Pitting Corrosion in Top Side Oil Production Facilities" (paper presentation, NACE Corrosion 2010, NACE International, San Antonio, TX, March 14–18, 2010).
12. J. S. Lee, B. J. Little, J. M. Sullivan, R. E. Stote, and K. A. Kuehn, "Biodegradation of Expeditionary Temporary Structures and Materials in Tropical Environments" (paper presentation, 2017 Department of Defense, Allied Nations Technical Corrosion Conference, Corrosion Policy and Oversight Office, Birmingham, AL, August 7–10, 2017).
13. B. J. Little, and J. S. Lee, *Microbiologically Influenced Corrosion* (Hoboken, NJ: Wiley, 2007).
14. D. Enning and J. Garrelfs, "Corrosion of Iron by Sulfate-Reducing Bacteria: New Views of an Old Problem," *Applied Environmental Microbology* 80 (2014): 1226–1236.
15. T. Gu, "Theoretical Modeling of the Possibility of Acid Producing Bacteria Causing Fast Pitting Biocorrosion," *Journal of Microbial and Biochemical Technology* 6, no. 2 (2014): 68–74.
16. T. Gu and D. Xu, "Why Are Some Microbes Corrosive and Some Not?" (paper presentation, NACE Corrosion 2013, NACE International, Orlando, FL, March 17–21, 2013).
17. Y. C. Li, D. K. Xu, C. F. Chen, X. G. Li, R. Jia, D. W. Zhang, W. Sand, F. H. Wang, and T. Y. Gu, "Anaerobic Microbiologically Influenced Corrosion Mechanisms Interpreted Using Bioenergetics and Bioelectrochemistry: A Review," *Journal of Materials Science and Technology* 34 (2018): 1713–1718.
18. D. Blackwood, "An Electrochemist Perspective of Microbiologically Influenced Corrosion," *Corrosion and Materials Degradation* 1 (2018): 59–76.
19. M. B. McNeil and A. L. Odom, "Thermodynamic Prediction of Microbiologically Influenced Corrosion (MIC) by Sulfate-Reducing Bacteria (SRB)," in *Microbiologically Influenced Corrosion Testing*, ed. J. R. Kearns and B. J. Little (Philadelphia, PA: ASTM International, 1994), 173–179.
20. C. W. Kovach and J. D. Redman, "High Performance Stainless Steels and Microbiologically Influenced Corrosion" (paper presentation, Stainless Steels '96, Verein Deutscher Eisenhüttenleute, Dusseldorf, Germany, June 3-5, 2006).
21. V. B. Rodin, S. K. Zhigletsova, N. A. Zhirkova, N. V. Alexandrova, G. V. Shtuchnaja, and V. A. Chugunov, "Altering Environmental

Composition as a Potential Method for Reversing Microbilogically Influenced Corrosion" (paper presentation, NACE Corrosion 2005, NACE International, Houston, TX, April 3–7, 2005).

22. B. A. Kehler, G. O. Ilevbare, and J. R. Scully, "Crevice Corrosion Stabilization and Repassivation Behavior of Alloy 625 and Alloy 22," *Corrosion* 57 (2001): 1042–1065.

23. B. J. Little, "A Perspective on the Use of Anion Ratios to Predict Corrosion in Yucca Mountain," *Corrosion* 59 (2003): 701–704.

24. J. S. Lee, R. I. Ray, and B. J. Little, "Comparison of Key West and Persian Gulf Seawater" (paper presentation, NACE Corrosion 2007, NACE International, Nashville, TN, March 11–15, 2007).

25. J. S. Lee, R. I. Ray, and B. J. Little, "Influence of Experimental Conditions on the Outcome of Laboratory Investigations Using Natural Coastal Seawaters," *Corrosion* 66 (2010): 15001–15006.

26. B. J. Little, P. A. Wagner, K. R. Hart, R. I. Ray, D. M. Lavoie, K. Nealson, and C. Aguilar, "The Role of Biomineralization in Microbiologically Influenced Corrosion," *Biodegradation* 9 (1998): 1–10.

27. J. Philips, N. van den Driessche, K. De Paepe, A. Prevoteau, J. A. Gralnick, J. B. A. Arends, and K. Rabaey, "A Novel Shewanella Isolate Enhances Corrosion by Using Metallic Iron as the Electron Donor with Fumarate as the Electron Acceptor," *Applied and Environmental Microbiology* 84, Article e01154-18 (2018): 1–19.

28. B. J. Webster and R. C. Newman, "Producing Rapid Sulfate-Reducing Bacteria (SRB)-Influenced Corrosion in the Laboratory," in *Microbiologically Influenced Corrosion Testing,* ed. J. R. Kearns and B. J. Little (Philadelphia, PA: ASTM, 1994), 28–41.

29. A. Turnbull, D. Coleman, A. J. Griffiths, P. E. Francis, and L. Orkney, "Effectiveness of Corrosion Inhibitors in Retarding the Rate of Propagation of Localized Corrosion," *Corrosion* 59 (2003): 250–257.

30. *Detection, Testing and Evaluation of Microbiologically Influenced Corrosion (MIC) on External Surfaces of Buried Pipes*, NACE Standard TM0106-2016 (Houston, TX: NACE International, 2016).

31. *Field Monitoring of Bacterial Growth in Oil and Gas Systems*, NACE Standard TM0194-2014 (Houston, TX: NACE International, 2014).

32. *Detection, Testing, and Evaluation of Microbiologically Influenced Corrosion on Internal Surfaces of Pipelines*, NACE Standard TM0212-2018 (Houston, TX: NACE International, 2018).

33. T. P. Zintel, D. A. Kostuck, and B. A. Cookingham, "Evaluation of Chemical Treatments in Natural Gas Systems versus MIC and Other Forms of Internal Corrosion Using Carbon Steel Coupons" (paper presentation, NACE Corrosion 2003, NACE International, San Diego, CA, March 16–20, 2003).

34. S. P. Kotu, M. S. Mannan, and A. Jayaraman, "Emerging Molecular Techniques for Studying Microbial Community Composition and Function in Microbiologically Influenced Corrosion," *International Biodeterioration and Biodegration* 144, Article 104722 (2019): 1–11.

35. R. B. Eckert and T. L. Skovhus, "Advances in the Application of Molecular Microbiological Methods in the Oil and Gas Industry and Links to Microbiologically Influenced Corrosion," *International Biodeterioration and Biodegration* 126 (2018): 169–176.

36. A. Rajasekar, B. Anandkumar, S. Maruthamuthu, Y. P. Ting, and P. K. S. M. Rahman, "Characterization of Corrosive Bacterial Consortia Isolated from Petroleum-Product-Transporting Pipelines," *Applied Microbiology and Biotechnology* 85 (2010): 1175–1188.

37. S. J. Giovannoni, T. B. Britschgi, C. L. Moyer, and K. G. Field, "Genetic Diversity in Sargasso Sea Bacterioplankton," *Nature* 345 (1990): 60–63.

38. D. M. Ward, M. J. Ferris, S. C. Nold, and M. M. Bateson, "A Natural View of Microbial Biodiversity within Hot Spring Cyanobacterial Mat Communities," *Microbiology and Molecular Biology Reviews* 62 (1998): 1353–1370.

39. J. A. Bernstein, A. B. Khodursky, P. H. Lin, S. Lin-Chao, and S. N. Cohen, "Global Analysis of mRNA Decay and Abundance in *Escherichia coli* at Single-Gene Resolution Using Two-Color Fluorescent DNA Microarrays," *Proceedings of the National Academy of Sciences* 99 (2002): 9697–9702.

40. M. M. Eid, K. E. Duncan, and R. S. Tanner, "A Semi-Continuous System for Monitoring Microbially Influenced Corrosion," *Journal of Microbiological Methods* 150 (2018): 55–60.

41. A. Torti, M. A. Lever, and B. B. Jørgensen, "Origin, Dynamics, and Implications of Extracellular DNA Pools in Marine Sediments," *Marine Genomics* 24 (2015): 185–196.

42. Z. Makama, S. Celikkol, A. Ogawa, C. Gaylarde, and I. Beech, "The Issue with Using DNA Profiling as a Sole Method for Investigating the Role of Marine Biofilms in Corrosion of Metallic Materials," *International Biodeterioration and Biodegration* 135 (2018): 33–38.

43. V. Bonifay, B. Wawrik, J. Sunner, E. C. Snodgrass, E. Aydin, K. E. Duncan, A. V. Callaghan, A. Oldham, T. Liengen, and I. Beech, "Metabolomic and Metagenomic Analysis of Two Crude Oil Production Pipelines Experiencing Differential Rates of Corrosion," *Frontiers in Microbiology* 8, Article 99 (2017): 1–17.

44. D. J. Beale, A. V. Karpe, S. Jadhav, T. H. Muster, and E. A. Palombo, "Omics-Based Approaches and Their Use in the Assessment of Microbial-Influenced Corrosion of Metals," *Corrosion Reviews* 34 (2016): 1–15.

45. B. J. Little, P. A. Wagner, K. R. Hart, and R. I. Ray, "Spatial Relationships between Bacteria and Localized Corrosion" (paper presentation, NACE Corrosion 96, NACE International, Denver, CO, March 24–29, 1996).

46. Y. Chung and L. K. Thomas, "Comparison of MIC Pit Morphology with Non-MIC Chloride Induced Pits in Types 304/304L/E308 Stainless Steel Base Metal/Welds" (paper presentation, NACE Corrosion 99, NACE International, San Antonio, TX, April 25–30, 1999).

47. M. B. McNeil, J. M. Jones, and B. J. Little, "Mineralogical Fingerprints for Corrosion Process Induced by Sulfate-Reducing Bacteria" (paper presentation, NACE Corrosion 91, NACE International, Cincinnati, OH, March 11–15, 1991).

48. M. B. McNeil and B. J. Little, "Corrosion Mechanisms for Copper and Silver Objects in Near-Surface Environments," *Journal of the American Institute for Conservation* 31 (1992): 355–366.

49. J. K. Fredrickson, S. Kota, R. K. Kukkadapu, C. Liu, J. M. and J. B. Zachara, "Influence of Electron Donor/Acceptor Concentrations on Hydrous Ferric Oxide (HFO) Bioreduction," *Biodegradation* 14 (2003): 91–103.

50. B. A. Wing and I. Halevy, "Intracellular Metabolite Levels Shape Sulfur Isotope Fractionation during Microbial Sulfate Respiration," *Proceedings of the National Academy of Sciences* 111 (2014): 18116–18125.

51. S. Ono, M. Sub Sim, and T. Bosak, "Predictive Isotope Model Connects Microbes in Culture and Nature," *Proceedings of the National Academy of Sciences* 111 (2014): 18102–18103.

52. C. Grengg, F. Mittermayr, A. Baldermann, M. E. Böttcher, A. Leis, G. Koraimann, and M. Dietzel, "Stable Isotope Signatures within Microbial Induced Concrete Corrosion: A Field Study," *Procedia Earth and Planetary Science* 13 (2015): 68–71.

53. B. J. Little, P. A. Wagner, and J. Jones-Meehan, "Sulfur Isotope Fractionation by Sulfate-Reducing Bacteria in Corrosion Products," *Biofouling* 6 (1993): 279–288.

54. E. Hutchens, B. J. Williamson, M. Anand, M. P. Ryan, and R. J. Herrington, "Discriminating Bacterial from Electrochemical Corrosion using Fe Isotopes," *Corrosion Science* 49 (2007): 3759–3764.

55. S. C. Dexter, "Microbial Effects," in *Corrosion Test and Standards: Application and Interpretation*, ed. R. Baboian (West Conshohocken, PA: ASTM International, 2005), 509–522.

56. S. C. Dexter, "Laboratory Solutions for Studying Corrosion of Aluminum Alloys in Seawater," in *The Use of Synthetic Environments for Corrosion Testing*, ed. P. E. Francis and T. S. Lee (Philadelphia, PA: ASTM International, 1988), 217–234.

57. B. Little, S. Gerchakov, and L. Udey, "A Method for Sterilization of Natural Seawater," *Journal of Microbiological Methods* 7 (1987): 193–200.

58. H.-J. Zhang and S. C. Dexter, "Effect of Biofilms on Crevice Corrosion of Stainless Steels in Coastal Seawater," *Corrosion* 51 (1995): 56–66.

59. F. Mansfeld, G. Liu, C. H. Tsai, H. Shih, and B. J. Little, "Evaluation of Polarization Curves for Copper Alloys Exposed to Natural and Artificial Seatwater" (paper presentation, NACE Corrosion 92, NACE International, Nashville, TN, April 27–May 1, 1992).

Chapter 6 | Tribocorrosion

Jeremy L. Gilbert[1]

Basic Principles

REVIEW OF MECHANISMS

Tribocorrosion is a conjoint mechanism of degradation of a metallic surface that involves surface mechanics associated with contact, loading, and motion (tribology) and the increased corrosion that results from such mechanical perturbations. Tribology is the study of wear, friction, and lubrication, whereas tribocorrosion generally is focused on the enhanced corrosion processes that arise when surface mechanical processes are present.[1–3] A more inclusive concept around tribocorrosion is mechanically assisted corrosion,[4–6] wherein enhanced corrosion can arise from surface mechanical processes that are not limited to wear phenomena only and can include other factors like stress corrosion cracking, corrosion fatigue, and strain-enhanced corrosion.

Tribocorrosion processes are focused primarily on passivating alloys that derive corrosion resistance from the kinetic barrier passive oxide films that spontaneously form on such alloy surfaces. These include titanium and its alloys, stainless steels, cobalt-chromium alloys, and others (e.g., Al, Ta, W, Zr, Nb). Low-temperature, high-field-based passive oxide film growth is a central part of such tribocorrosion processes, as are the mechanical factors that affect the adhesion and barrier effects of oxide films, and the fracture and mechanical disruption of the oxides. Much of the research on tribocorrosion has been focused around medical devices and metallic biomaterials, including Ti, CoCrMo, and 316L stainless steel alloys, but these processes are not limited to this field.

Because tribocorrosion is composed of both surface mechanical processes related to deformation, wear, and friction, and processes related to oxidation of metal surfaces when such mechanical effects are present, it requires an understanding of both surface mechanics and electrochemistry. Both the mechanical and electrochemical elements of tribocorrosion will be presented.

[1]Clemson–MUSC Bioengineering Program, Medical University of South Carolina, 68 Presidents St., Charleston, SC 29425, USA; Dept. of Bioengineering, Clemson University, 68 Presidents St., Charleston, SC 29425, USA http://orcid.org/0000-0002-7428-2851

DOI: 10.1520/MNL202NDSUP20190003

The general concern surrounding tribocorrosion is the loss of metal from the surface as a result of tribological and electrochemical processes, and in particular when these two processes interact synergistically.[7] Corrosion in the absence of mechanical effects include oxide film formation (through the already extant film) and ionic dissolution (through the film; so-called passive dissolution[8]). Both processes are typically very slow for intact passive films with current densities typically well below 10 nA/cm^2. These passive corrosion processes are, therefore, of less concern.

When surfaces are tribologically impacted (contact, stress, and motion), several mechanical events occur in tribocorrosion, including plastic deformation of the near-surface alloy, and mechanical removal of metallic materials and passive oxide films resulting from wear processes. The nature of the surface contact between the two tribologically interacting bodies is one of multiple asperity-asperity contacts,[9] in which case the true area of contact, for metal-on-hard interactions, is driven by the normal load and the hardness of the surfaces.[10] That is, the nominal microgeometry (i.e., roughness) of the contacting surfaces has little initial effect on the true area of contact and therefore of extent of abrasion; however, surface topography does affect the locations where contacting asperities interact and the progression of contact as asperities are abraded over time.

In addition to the loss of material from a strictly wear-based phenomenon (without electrochemical processes), dramatically enhanced electrode reactions involve increased currents as well as both charge transfer (Faradaic) and charging (non-Faradaic) processes in the breached region and outside, at least until the oxide film reforms or repassivates, which can take as little as 0.5 ms.[11–15] During this brief period, both ionic dissolution from the bare metal surface and the film reformation (or repassivation) processes generate electrochemical currents that can be monitored and measured. The magnitude of these current densities, when scaled to the breached area, are orders of magnitude greater than those present across intact oxide films. These currents are a highly sensitive measure of the electrochemical processes and can be used as a tool to assess tribocorrosion. In addition, for nonpotentiostatically controlled electrode surfaces, these reactions alter the electrode

Copyright © 2022 by ASTM International, 100 Barr Harbor Dr., PO Box C700, West Conshohocken, PA 19428-2959
ASTM International is not responsible, as a body, for the statements and opinions expressed in this chapter. ASTM International does not endorse any products represented in this chapter.

potential of the surface because of the burst release of electrons from the oxidation processes. Thus, electrode potentials typically become more negative with tribocorrosion processes as corresponding reduction reactions increase to consume these electrons. The balance in reactions is not instantaneous, however, and therefore the capacitive and resistive character of the surface will affect the potential drops observed.[16] Factors including the surface impedance and total electrode area affect the extent of potential change and the time course of the response.[16]

MASS BALANCE DURING TRIBOCORROSION

When assessing material loss from a metal caused by tribocorrosion processes, both mechanical and electrochemical mechanisms contributing to mass loss and mass gain must be accounted for, as shown in equation (1):

$$M_{loss} = M_{wear}^{metal} + M_{wear}^{oxide} + M_{ions} - M_{growth}^{oxide} - M_{adhered}^{debris}. \quad (1)$$

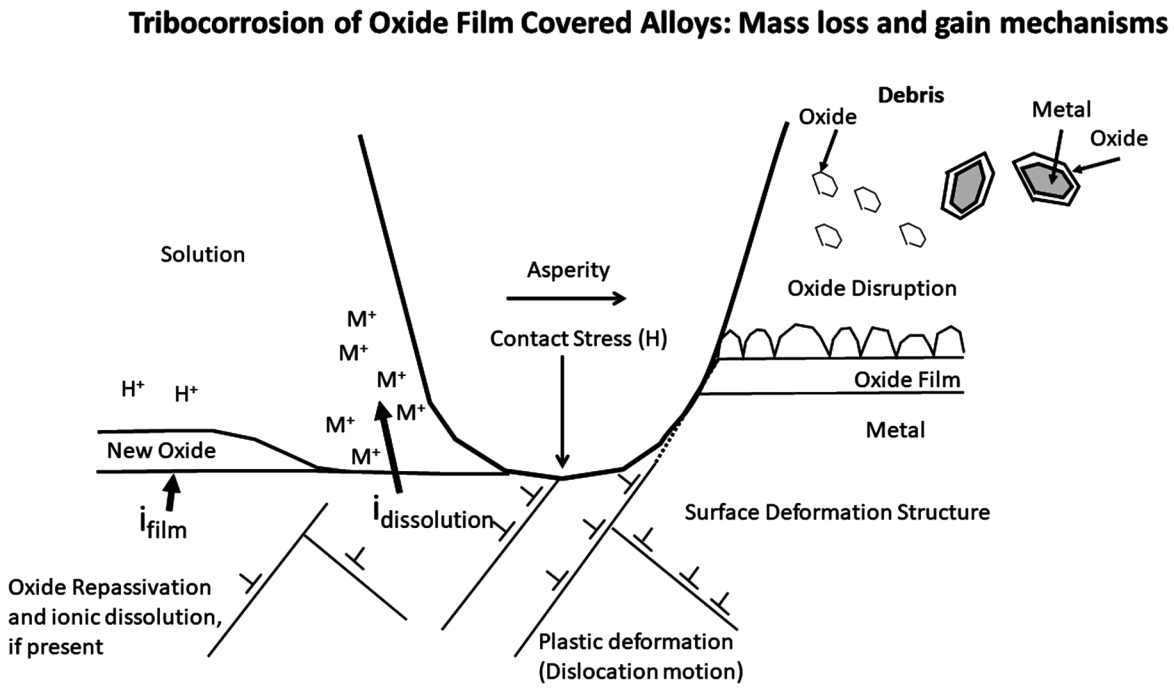
The first mechanism of mass loss is metal mass loss caused by mechanical wear processes only (fig. 1). This mass loss is purely mechanical, with no electrochemical process (or current or voltage dependent mechanism). It results in the generation of metal wear particles leaving the surface by way of the tribological processes of abrasive, adhesive, and fatigue wear. Note, however, that for passivating alloys in an electrolyte, even the purely mechanical removal of metal must be accompanied by repassivation of the freshly exposed metal surfaces. That is, wear of passive alloys in solution *must* include corrosion reactions (and currents) associated with repassivation as oxygen from water and metal combine to form oxide. This includes the metal particle surface as well as the metal substrate surface from which the metal particle comes. In addition, plastic deformation mechanisms (e.g., dislocation motion) intersecting with the metal surface can introduce additional fresh metal (step ledges) for repassivation processes. The details of the surface mechanics will be described in more detail.

The second mechanism of mass loss is wear-based mass loss of the passive oxide film. This is also a mechanical process of oxide removal or disruption from the surface. This releases oxide debris that can accumulate as a solid particle (or agglomerated particles), which can serve both as a lubricant and as an abrasive within the tribocorrosion contact region. The lost passive oxide is replaced by new oxide film repassivation on the freshly exposed metal, the process of which generates currents that can be detected.

The third mechanism of mass loss is the electrochemically based ionic dissolution of metal into metal ions into solution beyond that which normally occurs through the intact oxide. This is ionic dissolution through the instantaneously breached bare metal surface where the charge transfer kinetics are not limited (at least initially) by a passive oxide film. As the surface repassivates, the kinetics of ionic dissolution quickly return to the passive film-based kinetics, and therefore, ionic dissolution is controlled and limited by the repassivation rate of the oxide film. This mass loss is associated with charge transfer and currents across the interface (i.e., Faradaic processes).

The fourth mechanism is mass *gain* resulting from the Faradaic process of metal repassivation, which involves the reaction of metal with water to produce metal oxide (and hydrogen ions

FIG. 1 Schematic of tribocorrosion processes at an asperity-metal contact where an oxide film is being disrupted. Oxide debris, metallic debris, and ions can be released, whereas oxide film can be repassivated and reformed and the metal subsurface material is plastically deformed and damaged.



and electrons). This mass gain of the surface, while small, occurs because of the addition of oxygen anions to the metal cations to form the oxide (i.e., to repassivate the surface); see figure 1 and equation (1). This oxide formation is linked to the oxide film loss and will be nearly identical to, or of similar magnitude as, the oxide reformed. Here, then, the repassivation currents may be reflective of the oxide film loss and is a direct measure of the oxide film reformed after disruption. Note that, while the mass gain per repassivation event is small, the cumulative effect can be significant. For example, a unit volume of titanium (Ti) converted to titanium dioxide (TiO_2) results in a volume of oxide that is 1.75 times the volume of the metal from which it came. Thus, volume loss from the metal and volume of oxide debris are not the same and the difference is significant.

The third and fourth terms of equation (1) both consist of Faradaic processes that are associated with anodic electrochemical currents generated over and above the baseline currents, release of electrons into the metal, and changes in potential that may arise as a result. Examples of ionic dissolution and film growth reactions that result in measurable anodic currents are shown in equations (2) and (3).[13]

$$Ti \rightarrow Ti^{4+} + 4e^{-} \qquad I_{diss} = i_o A(1-\theta)e^{\frac{\eta}{\beta_a}}, \qquad (2)$$

$$Ti + 2H_2O \rightarrow TiO_2 + 4H^{+} + 4e^{-} \qquad I_{Film} = \frac{\rho n F}{M_w} V \frac{d\theta}{dt}. \qquad (3)$$

For ease of representation, these equations are shown for titanium The currents that result from these reactions are also shown, where:

I_{diss} (equation (2)) = the dissolution current;

i_o = the exchange current density for ionic dissolution across a bare metal surface (not the oxide);

A = the area of exposed metal where oxide is removed;

θ = the area (or volume) fraction of the abraded oxide area that has reformed by repassivation;

η = the over potential for ionic dissolution (i.e., the voltage above the equilibrium half-cell potential for ionic dissolution across the bare surface);

βa = the anodic Tafel slope for ionic dissolution across the bare surface;

I_{Film} = the film current that depends on the density, ρ, of the oxide film, the charge per cation, n, Faraday's constant, F, the molecular weight of the oxide, M_w, and the volume of oxide reformed, V; and θ = the volume fraction of oxide formed at any instant after disruption, so the time derivative of θ (i.e., $d\theta/dt$) is the rate of oxide fraction reformed.[13]

Note that the ionic dissolution current directly reflects metal ions lost from the metal. Conversely, the oxide film currents reflect the currents associated with the *formation* of the oxide over the previously breached surface and is related, in fact, to a mass accumulation (resulting from the oxygen addition to the surface; the fourth term in equation (1)). These oxide films are removed in subsequent mechanical disruption processes and reformed in essentially equal amounts. Therefore, although the repassivation reactions increase the mass (and volume) of oxide film on the metal surface, they also reflect the amount of oxide debris removed and generated during the abrasion and the film currents generated. This link between mechanical disruption of the oxide and the film currents associated with reformation of the oxide is an important one for using current as a means of assessing tribocorrosion processes.

Finally, a term is added to account for any accumulated debris (metal or oxide, or other) that occurs over the course of the tribocorrosion process. For example, oxide debris may adhere to the surface and accumulate, thus reducing the overall mass loss into the solution from the tribocorrosion processes.

The various mass terms in equation (1) (and their rates) are not always independent, and indeed, they depend on the interaction of tribology and electrochemistry. For example, the rate of metal mass loss will depend on the nature of the counterface causing the abrasive, adhesive, or fatigue wear process. Generation and accumulation of oxide debris may either enhance or reduce such wear mechanisms as the debris acts either as high-hardness third-body wear particles or as a solid lubricant that limits additional metal wear.

The mass loss from ionic dissolution only represents the increase of ionic dissolution present from bare metal surfaces arising from mechanical disruption of the passive film and exposure of the bare metal. As such, this is a tribologically enhanced ionic dissolution process. Similarly, current arises from repassivation of exposed metal surface. Thus, when one develops a test that measures currents (either potentiostatically, or with an ammeter between abrading electrode and a second electrode), it is important to understand the relative contributions of ionic dissolution and passive film formation to the measured current. These currents, for example, cannot be used as a measure only of ionic loss because most of the current measured goes to oxide formation.

In addition, these terms may be modified over time by local changes in solution chemistry where, for example, proteins of other biologically derived chemical species may alter the surface oxide properties creating oxide film defects, increasing passive dissolution reactions or increasing the oxidizing power of the electrolyte. Recent work has shown, for example, that fretting-initiated crevice corrosion of 316L stainless steel could arise because of the fretting corrosion process generating a local crevice solution chemistry within the fretting contact region that leads to unstable crevice corrosion reactions.[14] Other effects of solution proteins on both the tribological and electrochemical interactions may arise as well. Corrosion in vivo may occur in the presence of significant immune and inflammatory cell reactions, where such biological processes and living systems may induce local changes in solution chemistry and increase the corrosion rates of medical alloys[15,16] and also may alter the tribocorrosion behavior of these alloys.[17] Chemical species involved in reactive oxygen species generation are of particular interest.[18]

The Ambrose model of passive film repassivation[13,19,20] provides a framework around which one can assess the relative contributions of film currents and ionic dissolution currents through bare metal. This model expresses the total current in terms of both ionic and film currents and uses the concept of the fraction

of oxide reformed (θ) starting from an instantaneously removed oxide region.

$$I_{total} = I_{diss} + I_{film}, \tag{4}$$

$$I_{total} = i_o A e^{\frac{\eta}{\beta_a}}(1-\theta) + \frac{\rho n F}{M_w} A h \frac{d\theta}{dt} \tag{5}$$

Experiments on mechanically controlled high-speed single-diamond asperity scratch tests of Ti and cobalt-chromium-molybdenum (CoCrMo) alloys[13,19,21] showed an exponential current transient ($I_{total} = I_o e^{\frac{-t}{\tau}}$), where I_o is the peak current above the baseline current, and τ is the time constant for the repassivation response. The solution of this equation using the previous expression for the total currents follows:

$$\theta = \left(1 - e^{\frac{-t}{\tau}}\right), \tag{6a}$$

$$I_o = i_o A e^{\frac{\eta}{\beta_a}} + \frac{\rho n F V}{M_w \tau}. \tag{6b}$$

Thus, tribocorrosion currents (i.e., currents arising from film formation and ionic dissolution through the breached region) can be assessed based on the parameters outlined. Note that the volume of oxide, V, that reforms depends on the voltage above the onset potential, and the relative amount of ionic current to film current can be assessed by comparing the magnitude of the two terms in equation (6b).

Analysis of the Ambrose model shows, for example, that for a 0.5 ms time constant (typical for Ti/TiO_2 repassivation), the film current density (the second term), is 8.6 A/cm^2 when the film reforming is 2 nm thick.[13] The film currents were significantly larger than the ionic currents in the potential range investigated.

ELECTRODE POTENTIAL EFFECTS ON TRIBOCORROSION

During tribocorrosion, the mechanical disruption of the passive film induces highly energetic oxidation reactions resulting in a burst-like response of ionic dissolution and film repassivation. This results in a buildup of electrons from the oxidation processes that are not instantly reacted (or consumed) by reduction reactions. That is, the mixed-potential theory does not instantaneously hold in the transient response period of oxide disruption. These electrons build up capacitively on the surface, causing electrode potential shifts of the surface that are not solely the result of a balance of anodic and cathodic currents.[22] These potential shifts depend on several characteristics of the surface, including the capacitance of the surface, the reduction reaction kinetics, the surface area, and solution resistance.

The kinetics of electron transfer to consume these excess electrons (i.e., reduction) may be limited compared with the kinetics of oxidation. Thus, a capacitive buildup of electrons at the metal surface will result and the electrode potential will become increasingly more negative. The rate of consumption of these electrons by reduction reactions will be related to the area available for reduction, the solution resistivity, and the polarization resistance of the surface (reflecting the cathodic kinetics). Therefore, the area-dependent impedance (capacitance and polarization resistance) of the electrode surface will affect the extent of the shift in electrode potential from the at-rest open-circuit potential, where in the limit of large areas, the surface acts essentially as a potentiostatically held electrode.

Electrode potential also will affect the repassivation reactions, including the thickness of the oxide reformed. Several studies have shown[13,21,23,24] that the thickness of reformed oxide, after mechanical disruption depends linearly on the electrode potential. There is an onset potential (or passivating potential) below which no oxide repassivation will occur.[25] Thus, the negative excursion in potential that occurs during tribocorrosion is limited by this onset potential (i.e., the electrode potential cannot fall below the onset potential) and thinner films form when the potential is more negative and closer to the onset potential. This is a consequence of the high-field growth model of Gunterschulze and Betz.[22]

It has been documented[13,19,21] in single-asperity scratch or pin-on-disk fretting corrosion tests[25] that the tribocorrosion current increases roughly linearly with potential above the onset potential (for fixed mechanical and tribological conditions; e.g., normal load and sliding speed). In some alloys (CoCrMo, and 316L SS), however, changes in oxide film chemistry, resulting from transitions in the Pourbaix diagram, lead to loss of passivity of the film. This occurs primarily in chromium(III) oxide (Cr_2O_3)–dominant passive films, where above about 300 mV versus silver/silver chloride (Ag/AgCl) in saline, the oxide film begins to transform away from a passive film (Cr_2O_3) to a film with higher valence Cr ions that are much less passive.[26]

CONTACT MECHANICS AND TRIBOCORROSION

The contact mechanics associated with tribocorrosion need to be clearly elucidated. Passive oxide films on metal alloy surfaces are disrupted only when certain specific mechanical conditions hold. For example, oxide disruption arises only when the contact stresses reach or exceed the underlying metal substrates surface plastic deformation limit (i.e., hardness) or when the fracture stress (or strain) of the oxide-metal interface is reached. That is, for the oxide film to be disrupted by mechanical processes, the alloy upon which the film has formed typically must experience localized plastic yielding.[27] Dislocation motion intersecting with the metal surface will disrupt the oxide film and expose underlying metal. Alternatively, the oxide film adhesive strength to the underlying metal must be reached. This, however, is again dominated by the hardness of the underlying alloy. As a result, during tribocorrosion, the metal surface undergoing tribocorrosion processes (i.e., wear, oxide film disruption and repassivation, and ionic dissolution) must be in contact with a counter surface that has specific relevant properties necessary to induce tribocorrosion, which include being capable of inducing localized plastic deformation of the passive oxide covered alloy. Materials with a hardness below the metal surface hardness typically will not induce oxide disruption; however, if such softer materials embed hard oxide particles, then these embedded particles may serve as oxide film disruption counterfaces.

In addition, the contact area between two surfaces, generally, is much smaller than the nominal area available for contact and can be, under some circumstances, only a percent or two of the nominal contact area. Thus, when the tribological conditions are such that a hard-on-hard junction (e.g., ceramic on metal, metal on metal) is present, then contact mechanics show that the true area of contact is basically governed by the normal force across the contact area divided by the effective hardness of the surfaces (the softer one dominating). That is,

$$A_{true} = \frac{F}{H}, \tag{7}$$

where:
F = the force across the interface, and
H = the effective hardness of the softer surface.[10]

This is an upper limit estimate of the contact area because, if elastic contact were present, the stresses in the contact region would be lower than the yield, and hence less area would be in contact.

Of course, this conveys that the details of the surface topography (at least initially) do not affect the tribocorrosion response. It also indicates that the local asperity-based contact stress reaches the hardness of the alloy (i.e., is very high locally) and will induce oxide disruption with sliding because of plastic deformation.

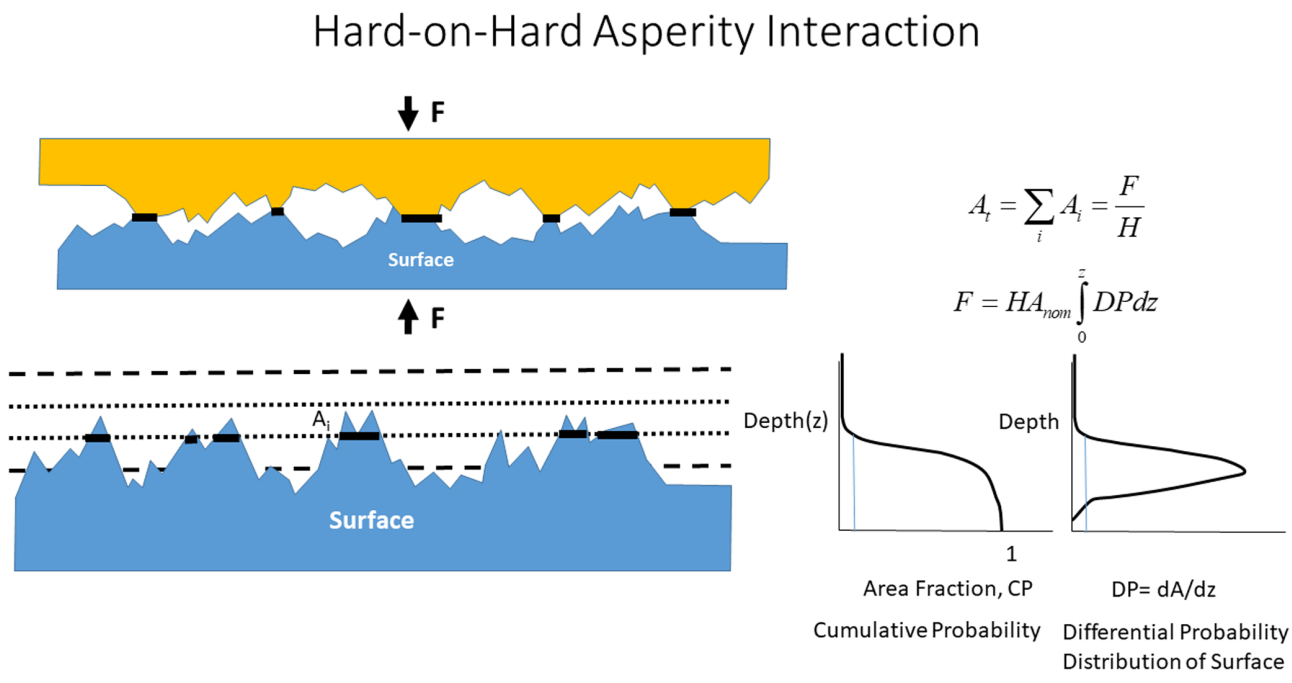
For example, when two Ti-alloy asperity-based surfaces come in contact (fig. 2) with a load of 10,000 N, where the hardness of the titanium is about 3 GPa (3000 N/mm^2), the true area of contact will be 3.3 mm^2 distributed about the area available. How this area is distributed about the nominal area depends on the local topography. When these two surfaces slide relative to one another, the sliding mechanics may rapidly become a complex problem involving coulombic friction (if dry contact is present) or fluid-film lubricated sliding, in which case the environment between the two surfaces may become pressurized and carry a portion (mixed-film lubrication) or all (hydrodynamic lubrication) of the normal load. In some tribocorrosion conditions (e.g., fretting), a dry or mixed lubrication layer is likely and full hydrodynamic lubrication is unlikely.

In each of these regimes (dry contact, mixed lubrication, hydrodynamic lubrication), the frictional interactions and the mechanics of surface film disruption can be affected. The Stribeck curve[10] (coefficient of friction [COF] plotted against the product of the sliding velocity and viscosity divided by the normal load) shows significant transitions in the COF, with a low Stribeck number (low viscosity, slow speed, high normal force) giving rise to Coulombic contact conditions and a "dry" COF. In these and other conditions of mixed lubrication, tribocorrosion conditions lead to significant effects.

Asperity Contact, Surface Roughness, and Friction

The contact mechanics during tribocorrosion are inherently related to asperity-asperity contact mechanics. Regardless of the nominal shape of the contacting surfaces, the true area of contact during tribocorrosion is dominated by the asperity-asperity interactions and local contact stresses. For most tribocorrosion conditions, the surfaces in contact are both high-hardness materials. As the tribocorrosion process continues, abraded debris can remain in the contact region and alter the distribution of stresses and the sliding interaction. It is typical that in long-term

FIG. 2 Asperity-asperity contact schematic. This shows how two randomly rough surfaces would engage (even at the nanometer scale) and how the forces would be distributed over a small true area of contact. In addition, the concept of surface height distributions and how it affects the contact engagement is shown.



fretting corrosion tests, the fretting currents diminish with cycles. This is thought to be the result of debris increasingly carrying the contact load and reducing the amount of oxide surface abrasion taking place.

The surface roughness affects the location and distribution of contact regions. It is useful to conceptualize the surface as containing a distribution of contact that starts at zero above the surface and increases with depth into the surface to 1 (or 100% contact) when a hypothetical plane of intersection is drawn at various depths (see fig. 2). The depth profile or differential distribution (DP; fig. 2) can be used to determine the true area of contact.

Because tribocorrosion of hard-on-metal contacts occurs only at sites where oxide film disruption occurs, it is the sum of the diameters of all asperities in contact times the sliding speed that determines the area disrupted per unit time:

$$\frac{dA}{dt} = \sum_i l_i \frac{d\delta}{dt}, \tag{8}$$

where:
l_i = the diameter of the i_{th} asperity, and
$d\delta/dt$ = the sliding speed.

For many cases, the sum of all asperity diameters for hard-on-metal contacts can be approximated as follows:

$$\bar{l} = 2\sqrt{\frac{F}{\pi H}}, \tag{9}$$

which is assumed to arise from a single small circular contact area.

The link between the contact mechanics during tribocorrosion and the electrochemical currents arises from the relationship between abraded area and oxide film disruption and repassivation. Assuming these correspond to one another, then the area abraded can be linked to the area repassivated (and the associated film current is directly proportional to the abraded area). In addition, from equation (6), if the film currents are assumed to dominate (as they appear to do in many cases), then a link between the abraded area and the currents can be made.

For example, if we used the previous example (i.e., 3.5 mm^2 contact area), which corresponds to a nominal diameter of 2.11 mm, with a sliding speed of 1 mm/s, and an oxide film thickness of 2 nm, then a volume of oxide abraded per second of 0.00422 mm^3/s results. The charge per volume of oxide repassivated ($\rho nF/M_w$), for titanium oxide is: 21,500 C/cm^3 of oxide. This results in a steady-state current of about 90 μA arising from such a process assuming the repassivation rate equals the rate of film removal.

Modeling Tribocorrosion Using Heredity Integrals (Boltzmann Superposition)

A number of modeling approaches have been put forward to help understand tribocorrosion processes. These approaches typically focus on the oxide film currents based on Faraday's law and have attempted to describe several aspects of the tribocorrosion processes present.[2,7] An alternative approach recently advanced is the use of superposition of tribocorrosion events over time and the use of Duhamel integrals (or heredity integrals) to make predictions of both net current and net potential changes during an arbitrary oxide abrasion process.[22,28] In this approach, oxide film removal and repassivation events are discretized into infinitesimal volume elements where the rate of removal of oxide is slow compared with the repassivation rate. Each infinitesimal disruption results in an exponential current transient related to repassivation, and these events are integrated over time for some arbitrary oxide removal path. The net current is then just the integral over time of these summed infinitesimal events.

$$I(t) = A^T(t)V(0) + \int_{\lambda=0}^{t} A^T(t-\lambda)\frac{dV}{d\lambda}d\lambda, \tag{10}$$

where:
A^T = the tribocorrosion admittance, which is a relationship between current generated and the volume of oxide abraded;
V = the volume of oxide abraded and reformed;
I = the current; and
λ = the integration variable for time.

A^T, for the case in which the system is dominated by film currents only, has the following form:

$$A^T(t-\lambda) = \frac{I_o}{V}e^{-\frac{t-\lambda}{\tau}} = \left(\frac{\rho nF}{M_w\tau} + \frac{i_o}{h}e^{\frac{\eta}{\beta_a}}\right)e^{-\frac{t-\lambda}{\tau}} \approx \frac{\rho nF}{M_w\tau}e^{-\frac{t-\lambda}{\tau}}, \tag{11}$$

where:
ρ = the density of the oxide,
n = the valence,
M_w = the molecular weight of oxide, and
τ = the time constant for repassivation.

Note, the second term is very small compared with the first term over most of the potential range. Thus, for any path of volume abrasion ($dV/d\lambda$) the current associated with film formation can be determined and is based primarily on the film currents. A similar type of equation can be developed for how the voltage of the electrode undergoing tribocorrosion currents, I(t), can cause potential shifts. This heredity integral follows:

$$E(t) = Z(t)I(0) + \int_{\lambda=0}^{t} Z(t-\lambda)\frac{dI}{d\lambda}d\lambda, \tag{12}$$

where:
E = the potential away from resting potential,
Z = the time-based impedance response of the surface (which may be modeled using, for example, a Randle's circuit model), and
I = the instantaneous current as a function of time.

Together, these equations for voltage and current can be coupled and integrated over time.

These integrals provide a means to explore the links between the mechanics, electrochemistry, and impedance behavior of tribocorroding systems and could be adapted to more complex analyses (e.g., finite element approaches) to investigate the overall and local responses to tribocorrosion processes.

As an example of how this analysis can be used, figure 3 shows the tribocorrosion currents generated from a known displacement-time movement of a pin on disk, where the area abraded was determined from the contact mechanics, and the thickness was voltage based. The sliding-time behavior is a start-stop cyclic process and the current transients are spike-exponential decay responses. The theory fits the experimental results very well and is based on the vertical load, the sliding speed, the hardness, the potential, and the charge per volume of oxide formed.[28]

Tribocorrosion Testing

The tribocorrosion tests currently in use span a range of applications and test conditions. They all, however, have some basic common instruments and measurements. These include both corrosion testing and mechanical testing. For corrosion testing, current and potential are the two primary tools of analysis and control of the electrochemical portion of testing. Controlled potential (potentiostatic tests) and freely corroding tests can be performed (see fig. 4). Specific conditions for each are necessary (to be explored). In some instances, electrochemical impedance spectroscopy is used before and after tribocorrosion testing to investigate changes in electrode performance.

Solution conditions are also important. These include the overall solution chemistry as well as the local chemistry, which may change if crevices are present.[14]

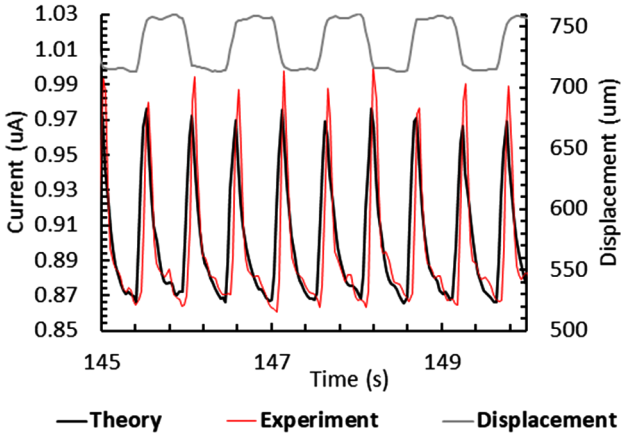
The mechanics of tribocorrosion tests have measurable parameters that include normal loads, friction loads, sliding displacements, contact geometry, and materials. These mechanics may involve fretting motions (cyclic displacements less than 100 um) or other sliding motions. Additionally, measurements can be made on the surface damage, the released solid debris, the ionic species released and adsorption or adhesion of tribocorrosion products. Well-designed tribocorrosion experiments include most of these parameters, which allow for in-depth assessment of performance. Each of these topics will be discussed in more detail.

Electrochemical Conditions

During a tribocorrosion experiment, a number of parameters of both the mechanical and electrochemical systems need to be accounted for and dealt with. From the mechanical perspective, such tribocorrosion experiments typically include a disk and a pin or ball of some specified geometry (radius) and properties (hardness). The normal load, sliding speed, and sliding distance—whether it is reciprocating (oscillatory), linear track (including rotating), or cross patterned—may significantly affect the long-term results as debris entrainment and its effects may be very different. Solution conditions are another consideration. They include the oxidizing conditions, solution resistance, ionic composition, temperature, presence of lubricants, proteins, and pH. In addition, whether the electrode potential is fixed (potentiostatic testing using a three-electrode system) or is allowed to shift with the test conditions will dictate some of the behavior. For freely floating electrode potential tests, the area of the electrode (outside of the contact region) will affect the magnitude of the electrode potential excursions experienced. Test configurations for potentiostatic and freely corroding conditions are shown in figures 4*A* and 4*B* for potentiostatic and freely corroding configurations, and the basic mechanical and electrochemical set up for fretting corrosion is shown in figure 5.

For potentiostatically controlled tests (fig. 4*A*), the role of potential on the electrochemical and mechanical response can be investigated directly. When the potential is held away from the at-rest corrosion potential (or open circuit potential), then a background current representing the sum of all reactions on the intact surface will be present (e.g., net reduction currents, or net oxidation currents). The tribocorrosion currents are then the

FIG. 3 An example of fretting corrosion currents for CoCrMo pin and disk tests. Shown are the sliding displacement-time plot, the experimentally obtained currents under potentiostatic control, and the theoretically obtained currents using the values in table 1 and the sliding displacement-time behavior. Note the excellent fidelity of the theoretical currents to the experimental ones.



$$I(t) = \int_0^t 2\frac{\phi}{\tau}\sqrt{\frac{L}{\pi H}}m(E - E_o)e^{-\frac{t-\lambda}{\tau_1}}\frac{d\delta(\lambda)}{d\lambda}d\lambda$$

CoCrMo Properties

Model Parameters		
hardness	Pa	3.00E+09
load	N	5
w(2a)	cm	0.00461
area	cm^2	1.66667E-05
h	cm	2.00E-07
Φ(pnF/Mw)	C/cm^3	18,020
Tau 1	s	0.1
m	cm/V	2.00E-07
Eo	V	-0.45
Tau	s	0.001

FIG. 4 Schematics of (*A*) potentiostatic three electrode tests and (*B*) freely corroding tests for tribocorrosion experiments. Measurements or control of current and potential are possible in both.

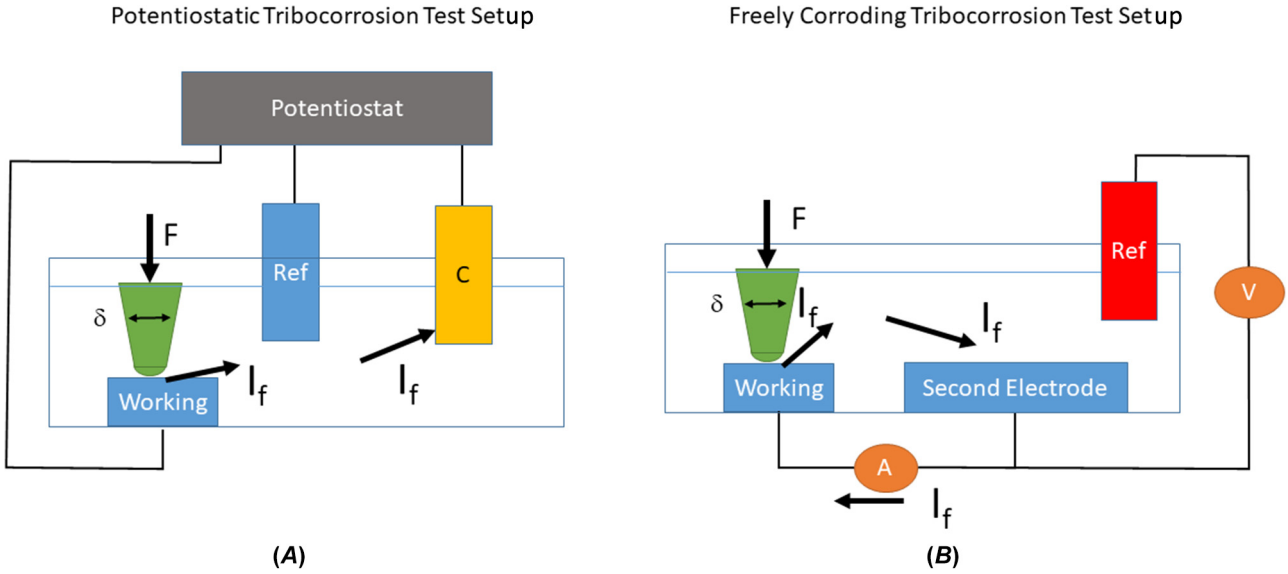
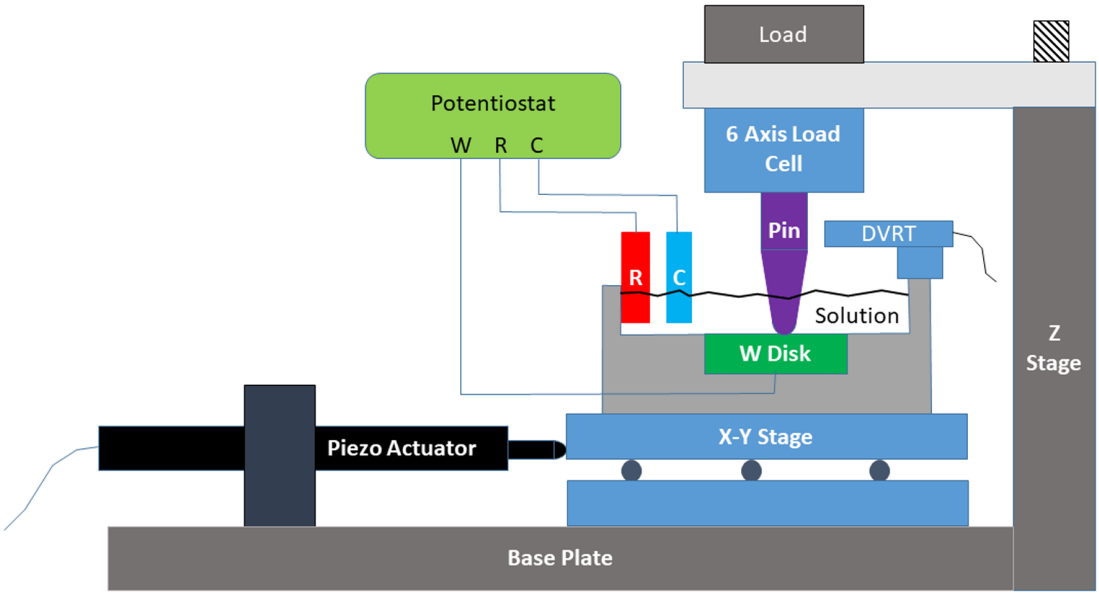


FIG. 5 Schematic of a pin-on-disk fretting corrosion test system used from tribocorrosion testing under fretting mechanics. The test samples, load cell, DVRT displacement sensor, piezoelectric actuator, and movement stage are shown.



deviation away from these background currents as they represent the currents over and above those from nonabrading conditions. For the freely corroding setup (fig. 4*B*), tribocorrosion currents and the shifting electrode potentials can be captured concurrently. The currents and the potential will be affected by the second electrode area and intrinsic impedance. A larger second electrode area will increase the currents (to a plateau) and decrease the potential excursions, whereas a smaller second electrode area will reduce the measured currents and increase the negative potential excursions measured. These second electrode area effects, therefore, affect the measurements of potential and current, and make interpretation of the electrochemistry more indeterminate.

Important results from potentiostatically controlled tribocorrosion tests include the fact that there is a potential (defined as the onset potential or passivating potential) below which no anodic electrochemical currents are generated.[13,21,25] This indicates that even with mechanical perturbation of the surface, there is no driving force for oxide repassivation and therefore no increased anodic tribocurrents. Above the onset potential

average, tribocorrosion currents increase linearly with potential with all other conditions held fixed (e.g., sliding speed, normal force). These results imply that approximately linear increases in oxide thickness are associated with increasing electrode potential above the onset potential.

For freely corroding tests, the potential of the test system will vary with the extent of the tribocorrosion taking place and will depend on the remaining area of the electrode and its properties. This movable potential also will alter the driving potential for film formation, and as a result, the oxide thickness.

Solution Changes in Crevices

During tribocorrosion, especially under fretting crevice corrosion conditions where the interface between the two surfaces remain close and a crevice like geometry is established, alterations in the solution chemistry within the crevice region may alter the results of the tribocorrosion processes. For example, the oxide film reaction (equation (3)) liberates hydrogen ions into the solution, thus altering the local pH in the contact region. In addition, release of cations locally within the crevice will attract chloride ions into the crevice as well. Tight crevices also raise the local solution resistance, resulting in local voltage shifts. These solution changes and others (e.g., deaeration) may alter the stability of the oxide film within the crevice and alter the local electrochemical equilibrium potentials.

When the solutions are complex and contain additional molecules (e.g., proteins, other organic species), the triboelectrochemical interactions that may arise can be similarly complex. There are reports[29] of tribomixing in the surface where proteins mix with tribocorrosion products (e.g., ions and oxides) and become entrained and mixed with surface layers of the material. This results in changes in chemistry of the surface and breakdown of the proteins, otherwise altering the surface chemistry of the tribocorrosion-affected surface.

Mechanical Conditions of Testing

The mechanical factors involved in tribocorrosion testing include the forces normal to and tangential to the interface, the COF, the sliding speed (frequency) and distance (amplitude), the lubrication regime (e.g., sliding speed, fluid viscosity, normal load), and the surface properties of the materials in contact (e.g., modulus, hardness, ductility, fracture resistance). In addition, the test system compliance may affect load-displacement behavior, particularly in cyclic reciprocating tests.

The basic schematic for tribocorrosion testing is shown in figure 5. Tribocorrosion test systems need to control and measure mechanical parameters and electrochemical parameters. For the mechanics of the test, position sensors (e.g., differential variable reluctance transducers, DVRTs), load cells that capture normal and lateral forces, and movement actuators (e.g., piezoelectric actuators) are needed. Typically, the movement control is applied by waveform voltage generators or computer-based data acquisition and control programs. Typical data captured includes normal and tangential loads, displacements versus time, current versus time, potential over time, etc. From these, parameters like COF and work per sliding distance can be determined and correlated on a cycle-by-cycle basis.

Tribocorrosion tests may include variations in normal load, sliding speed (or frequency), sliding amplitude, presence or absence of a crevice geometry, variations in potential, solution chemistry, and temperature. Short-term tests (with relatively few wear cycles) and long-term tests can be performed. When reporting tribocorrosion experiments, all of the test parameters described need to be defined and controlled or measured.

Frictional Load-Displacement Plots

Measurement of forces and displacements during tribocorrosion helps us understand the mechanical conditions present. These include determination of the COF (lateral force divided by normal force). In addition, especially for cyclic type tribocorrosion tests (e.g., fretting corrosion tests), closed-loop friction load versus sliding displacement plots can be obtained (see fig. 6), in which information like COF and work per cycle of load can be determined (i.e., area inside the curve, or hysteresis energy). In addition, the system compliance can be ascertained (i.e., the slope of the friction force versus sliding displacement reversal region) and the conditions of sticking can be determined.

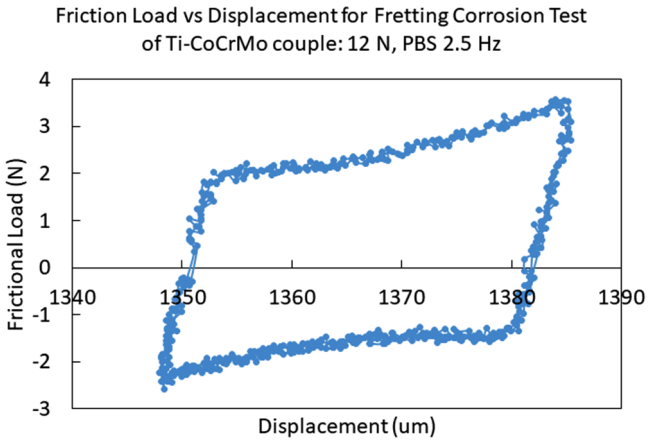
To undertake such load and displacement measurements, appropriately calibrated sensors are needed for displacement and load. These may include noncontact displacement sensors (DVRTs; fig. 4) and normal and lateral (or multi-axis) load cells. All experimental setups must be carefully assessed for machine compliance to ensure that direct analysis of local loads and displacements can be made.

Materials Characterization Post-Testing

SURFACE DAMAGE AND MATERIALS ASSESSMENTS

Tribocorrosion processes, whether they are fretting or sliding based, will result in progressive damage of the surface and near-surface alloy over time. The debris generated (e.g., metal particles, oxide particles, ions, precipitated metal-organic complexes) can remain within the tribocorrosion region or may migrate outward. Indeed, the surface of the alloy may undergo mixing and

FIG. 6 Typical load-sliding displacement plots for fretting corrosion test for Ti-CoCrMo pin-on-disk combination.



incorporation of solution constituents or oxides generated from tribocorrosion. The local solution chemical environment, the local adsorbed tribocorrosion debris layer, and the near-surface metal deformation state can all be altered from the tribocorrosion processes.

It has been documented that a severely plastically deformed surface layer up to 100 nm thick or more can develop from tribocorrosion processes, leading to a range of near-surface metallurgical effects.[27,29–31] There are reports, for example, of tribocorrosion-based mixed layers, in which metal, metal oxide, and organic materials (proteins) can interact and mix to create a surface tribochemical layer that is a consequence of the alloy, oxide, solution, and adsorbed species intermixing. In addition, highly deformed alloy surface layers may result from repeated asperity-asperity interactions. For some alloys, this results in a high dislocation density in the near-surface region resulting in subgrains and in high dislocation density entanglements. In other alloys, particularly those with low stacking fault energies (e.g., CoCrMo alloys), local surface plastic deformation may result in crystallographic transitions (i.e., strain-induced transformations) from hexagonal close packed to face centered cubic and back based on stacking faults. This may result in nano-crystalline grains (or highly deformed subgrains) developing near the surface, which may fracture or egress from the surface as nanoparticles by the mechanism of fatigue wear.

For fretting crevice corrosion processes, the debris generated often will egress from the crevice, in part, but also will adhere to the substrate metals in a zone near the site of generation. These forms of surface and near-surface damage and modification have been assessed primarily using analytical techniques, including X-ray photoelectron spectroscopy, scanning electron microscopy/energy dispersive spectrometry, Fourier-transform infrared spectrometry, and focused ion beam milling and transmission electron microscopy techniques.

Coupling of Electrochemistry and Tribology

In tribocorrosion processes, coupling effects exist between the mechanics and the electrochemistry that may lead to interesting observations that are, as yet, not fully explained. For example, experiments recently conducted have shown that the COF of fretting corrosion pin-on-disk tests of Ti and CoCrMo alloy combinations are highly sensitive to the electrode potential. The COF of Ti-CoCr couples is around 0.2 at potentials near 0 V versus Ag/AgCl in phosphate buffered saline and rise to more than 0.6 at -0.5 V and then fall again as the potential drops to -1V. These variations are not seen for Ti-Ti couples (COF ~0.6 to 0.7) and are less extreme for CoCr-CoCr couples (COF ~0.2–0.25).[17] The mechanism for these variations is not fully elucidated but likely reflects changes in the surface oxide chemistry, thickness, and morphology.

Other material-based effects are observed with potential in tribocorrosion experiments that remain unexplained. Systems and methods under development should provide important new insights into the phenomenon observed. In the biomaterials field, additional studies under development to relate cell response to tribocorroding surfaces[32] are attempting to relate the biological reactions of bone cells and immune cells (e.g., macrophages) to the effects of tribocorrosion. These efforts may elucidate the interplay between this material degradation mechanism and the biological impacts it can have on the living system.

TRIBOCORROSION MAPS AND SYNERGY AND ANTAGONY

A number of efforts have attempted to describe the interplay between wear and corrosion using maps,[33–35] in which the test parameters (e.g., sliding speed, normal load, applied potential) are plotted against one another and different modes of interaction occur, including wear-passivation. Efforts at partitioning the tribocorrosion processes into synergistic effects (wear assists corrosion and corrosion assists wear) and antagonistic effects (wear hinders corrosion and corrosion hinders wear) have been proposed. The challenge in these approaches is in how the various terms are measured and partitioned. Indeed, it is often the case that corrosion is based on measuring currents and the use of Faraday's law. As pointed out, however, currents go to reform passive oxide films as well as toward ionic dissolution. Because the passive oxide current is a formation current, it cannot go toward corrosion-based material loss. It also reflects the oxide that was abraded (by mechanical means), and thus it also contributes to the corrosion-based loss. This shows the challenge of using synergistic or antagonistic analyses, as discussed previously.[36]

Conclusion

This chapter has defined the physics, chemistry, electrochemistry, and mechanics of tribocorrosion to provide insight into the testing methods, parameters, and variations needed to understand tribocorrosion. This mechanism couples a range of disciplines (e.g., tribology, metallurgy, electrochemistry, biology), each of which contribute to the overall observed behavior at tribocorrosion contacts, notably in medically related implant interactions. Test methods to explore such phenomena need to have an ability to control and measure a range of mechanical factors and electrochemical factors to fully explore performance. Post-test analysis of damage is another important approach to explore the materials, transport, and electrochemical factors at play. Tribocorrosion is a complex, interdisciplinary phenomenon with significant consequences in a range of industries and disciplines beyond medical devices and biomaterials. It will continue to be an important element in engineering design and materials performance analysis.

References

1. S. Mischler, S. Debaud, and D. Landholt, "Wear Accelerated Corrosion of Passive Metals in Tribocorrosion Systems," *Journal of the Electrochemical Society* 145, no. 3 (1998): 750–758.

2. P. Jemmely, S. Mischler, and D. Landholt, "Electrochemical Modeling of Passivation Phenomena in Tribocorrosion," *Wear* 237 (2000): 63–76.

3. D. Landholt, S. Mischler, and M. Stemp, "Electrochemical Methods in Tribocorrosion: A Critical Appraisal," *Electrochimica Acta* 46 (2001): 3913–3929.

4. J. L. Gilbert, "Mechanically Assisted Corrosion of Metallic Biomaterials," in *ASM International Handbook, Volume 13C: Corrosion: Environments and Industries*, ed. S. D. Cramer and B. S. Covino, (Materials Park, OH: ASM International, 2006), 826–836.

5. J. L. Gilbert, C. A. Buckley, and J. J. Jacobs, "In-Vivo Corrosion of Modular Hip Prosthesis Components in Mixed and Similar Metal Combinations: The Effect of Crevice, Stress, Motion and Alloy Coupling," *Journal of Biomedical Materials and Research* 27, no. 1 (1993): 1533–1544.

6. J. J. Jacobs, J. L. Gilbert, and R. M. Urban, "Current Concepts Review: Corrosion of Metal Orthopaedic Implants," *Journal of Bone and Joint Surgery* 80-A, no. 2 (1998): 268–282.

7. J. Jiang, M. M. Stack, and A. Neville, "Modelling the Tribo-Corrosion Interaction in Aqueous Sliding Conditions," *Tribology International* 35 (2002): 669–679.

8. K. E. Healy and P. Ducheyne, "The Mechanisms of Passive Dissolution of Titanium in a Model Physiological Environment," *Journal of Biomedical Materials and Research* 26, no. 3 (1992): 319–338.

9. V. Swaminathan and J. L. Gilbert, "Fretting Corrosion of CoCrMo and Ti6Al4V Interfaces," *Biomaterials* 33 (2012): 5487–5503.

10. V. L. Popov, *Contact Mechanics and Friction: Physical Principles and Applications* (New York: Springer, 2010).

11. D. G. Kolman and J. R. Scully, "On the Repassivation Behavior of High-Purity Titanium and Selected α, β, and $\beta+\alpha$ Alloys in Aqueous Chloride Solutions," *Journal of the Electrochemical Society* 143, no. 6 (1996): 1847–1860.

12. D. G. Kolman and J. R. Scully, "Limitations of Potentiostatic Repassivation Techniques and Their Relationship to the Applicability of the High Field Approximation to the Repassivation of Titanium," *Journal of the Electrochemical Society* 142, no. 7 (1995): 2179–2188.

13. J. L. Gilbert, C. A. Buckley, and E. P. Lautenschlager, "Titanium Oxide Film Fracture and Repassivation: The Effect of Potential, pH and Aeration," in *Medical Applications of Titanium and Its Alloys: The Material and Biological Issues*, ed. S. A. Brown and J. E. Lemons (West Conshohocken, PA: ASTM International, 1996), 199–215, https://doi.org/10.1520/STP16080S

14. D. Zhu, Y. Liu, D. Pierre, and J. L. Gilbert, "Fretting Initiated Crevice Corrosion of 316LVM Stainless Steel in Physiological Phosphate Buffered Saline: Potential and Cycles to Initiation," *Acta Biomaterialia* 97 (2019): 565–577.

15. J. L. Gilbert, S. Sivan, Y. Liu, S. Kocagoz, C. Arnholt, and S. M. Kurt, "Direct In Vivo Inflammatory Cell Induced Corrosion of CoCrMo Implant Surfaces," *Journal of Biomedical Materials and Research, Part A* 103, no. 1 (2015): 211–223.

16. Y. Liu and J. L. Gilbert, "The Effect of Simulated Inflammatory Solutions and Fenton Chemistry on the Electrochemistry of CoCrMo Alloy," *Journal of Biomedical Materials and Research, Part B: Applied Biomaterials* 106B (2018): 209–220.

17. Y. Liu and J. L. Gilbert, "The Effect of Simulated Inflammatory Conditions and pH on Fretting Corrosion of CoCrMo Alloy Surfaces," *Wear* 390–391 (2017): 302–311.

18. G. W. Kubacki and J. L. Gilbert, "The Effect of the Inflammatory Species Hypochlorous Acid on the Corrosion and Surface Damage of Ti-6Al-4V and CoCrMo Alloys," *Journal of Biomedical Materials and Research, Part A* 106A (2018): 3185–3194.

19. J. R. Goldberg and J. L. Gilbert, "The Electrochemical and Mechanical Behavior of Passivated and TiN/AlN-Coated CoCrMo and Ti6Al4V Alloys," *Biomaterials* 25, no. 5 (2004): 851–864.

20. J. R. Ambrose, "Repassivation Kinetics," *Treatise on Materials Science and Technology, Corrosion: Aqueous Processes and Passive Films*, ed. J. C. Scully (New York, NY: Academic Press, 1983), 175–204.

21. J. R. Goldberg, E. P. Lautenschlager, and J. L. Gilbert, "Electrochemical Response of CoCrMo to High Speed Fracture of Its Metal Oxide Using an Electrochemical Scratch Test Method," *Journal of Biomedical Materials and Research* 37, no. 2 (1997): 421–433.

22. J. L. Gilbert, S. A. Mali, and Y. Liu, "Area-Dependent Impedance Based Voltage Shifts during Tribocorrosion of Ti-6Al-4V Biomaterials: Theory and Experiment," *IOP Surface Topography: Metrology and Properties, Special Topic Issue: Surfaces and Interfaces in Bioengineering Systems* 034002 (2016): 1–18.

23. A. W. E. Hodgson, S. Kurz, S. Virtanen, V. Fervel, C. O. A. Olsson, and S. Mischler, "Passive and Transpassive Behaviour of CoCrMo in Simulated Biological Solutions," *Electrochimica Acta* 49 (2004): 2167–2178.

24. I. Milosev and H. H. Strehblow, "The Composition of the Surface Passive Film Formed on CoCrMo Alloy in Simulated Physiological Solution," *Electrochimica Acta* 48 (2003): 2767–2774.

25. V. Swaminathan and J. L. Gilbert, "Potential and Frequency Effects on Fretting Corrosion of Ti6Al4V and CoCrMo Surfaces," *Journal of Biomedical Materials and Research, Part A* 101A, no. 9 (2013): 2602–2612.

26. Y. Liu and J. L. Gilbert, "Effect of Simulated Inflammatory Conditions and Potential on Dissolution and Surface Oxide of CoCrMo Alloy: In Situ Electrochemical Atomic Force Microscopy Study," *Electrochimica Acta* 262 (2018): 252–263.

27. R. Buscher, G. Tager, W. Dudzinski, B. Gleising, M. A. Wimmer, and A. Fischer, "Subsurface Microstructure of Metal-on-Metal Hip Joints and Its Relationships to Wear Particle Generation," *Journal of Biomedical Materials and Research, Part B: Applied Biomaterials* 72B (2005): 206–214.

28. J. L. Gilbert and D. Zhu, "A Tribocorrosion Model Linking Fretting Mechanics, Currents and Potentials: Model Development and Experimental Comparison," *Journal of Biomedical Materials Research Part B: Applied Biomaterials*, 108, no. 8 (2020): 3174–3189.

29. M. T. Mathew, C. Nagelli, R. Pourzal, A. Fischer, M. P. Laurent, J. J. Jacobs, and M. A. Wimmer, "Tribolayer Formation in a Metal-on-Metal Hip Joint: An Electrochemical Investigation," *Journal of Mechanical Behavior of Biomedical Materials* 29 (2014): 199–212.

30. R. Pourzal, R. Theissmann, M. M. Morlock, and A. Fischer, "Micro-Structural Alterations within Different Areas of Articulating

Surfaces of a Metal-on-Metal Resurfacing System," *Wear* 267 (2009): 689–694.

31. N. Espallargas, A. Fischer, A. Igual-Munoz, S. Mischler, and M. A. Wimmer, "In-Situ Generated Tribomaterial in Metal/Metal Contacts: Current Understanding and Future Implications for Implants," *Biotribology* 10 (2017): 43–50.

32. G. M. Kubacki, T. Hui, and J. L. Gilbert, "Voltage and Wear Debris from Ti-6Al-4V Interact to Affect Cell Viability during In-Vitro Fretting Corrosion," *Journal of Biomedical Materials and Research, Part A* 106A (2018): 160–167, https://doi.org/10.1002/jbm.a.36220

33. K. Sadiq, M. M. Stack, and R. A. Black, "Wear Mapping of CoCrMo Alloy in Simulated Bio-Tribocorrosion Conditions of a Hip Prosthesis Bearing in Calf Serum Solution," *Materials Science and Engineering C* 46 (2015): 452–462.

34. M. M. Stack, W. Huang, G. Wang, and C. Hodge, "Some Views on the Construction of Bio-Tribo-Corrosion Maps for Titanium Alloys in Hank's Solution: Particle Concentration and Applied Loads Effects," *Tribology International* 44 (2011): 1827–1837.

35. M. M. Stack, "Mapping Tribo-Corrosion Processes in Dry and in Aqueous Conditions: Some New Directions for the New Millennium," *Tribology International* 35 (2002): 681–689.

36. S. Mischler, "Triboelectrochemical Techniques and Interpretation Methods in Tribocorrosion: A Comparative Evaluation," *Tribology International* 41 (2008): 573–583.

Analysis, Testing, and Environments

Chapter 7 | Metallographic Analysis

William L. Mankins[1]

A new door opened into the study of materials in the late-19th century (1863) when a British geologist named Henry C. Sorby learned to polish a piece of steel, etch it with acid, and examine it under a microscope. Since that time, metallographic examinations have been performed on most every engineering metal developed. Metallographic examination is the preparation of specimens for microscopic evaluation and the study of microstructures in relation to the physical and mechanical properties of a particular metal. An etching process reveals the microstructure of the metal. By preparing specimens through a process of cutting (sectioning), grinding mounting, polishing, and etching, skilled metallurgists can examine metal samples on a microscopic level. Using various methods, alloys can be identified and material properties predicted.

Metallography is the study of the physical structure and components of metals, by using microscopy. Metallographic examination is a valuable tool in providing an understanding of structure and property relationships in many metals. The true value in these examinations cannot be obtained without an intimate knowledge of metal thermodynamic phase equilibria, and the effects of environmental factors on that equilibria. Although this knowledge can be gleaned from the numerous technical volumes available, firsthand experience can be a far better teacher.

Sample Selection

The selection of samples can be very important to the outcome of metallographic analysis. If the component is very large, it may require sectioning to provide manageable metallographic samples. The location for removal of metallographic samples should be considered carefully. Samples should contain areas representative of the corroded or fractured component. Samples of unaffected areas can reveal contrasting structures, thus distinguishing damage. Sometimes multiple samples must be taken at different orientations to understand the true nature of failure mechanism.

[1]Metallurgical Services, Inc., Huntington, WV, USA
The author acknowledges the previous author of this chapter, Richard L. Colwell, Bechtel Corp., Houston, TX.

DOI: 10.1520/MNL202NDSUP20190038

When sectioning, care should be taken to keep the sample cool. Elevated temperatures can promote phase transformations and exfoliation of surface deposits and scales. Heat can promote volatilization of chemical species on the surface. Keeping the sample cool may require slow cutting to avoid heat generation. If samples must be cut using a torch, ensure that large areas are removed, thus leaving enough unaffected area for later saw cuts. Recently, the plasma cutting torch has gained much acceptance for use in obtaining samples in steels. The plasma torch transfers very little heat to the steel, thus creating very small heat-affected areas.

Cutting also may require the use of a coolant. One should be careful of liquid coolants, especially if chemical analysis of surface scales and deposits will be required. Introduction of cooling liquids can contaminate areas of metallurgical interest. In addition, chemical species responsible for damage may dissolve and be washed away.

Cutting (Sectioning)

The preferred method of cutting metallographic samples utilizes an abrasive saw with a blade of abrasive particles that do the actual cutting. Rubber or resinoid bonded aluminum oxide or silicon carbide particles of various grits account for the many cutting blades that are available. Various commercially available saws are designed for optimum cutting by saw blade selection, cutting speed, wet or dry cutting, and rate of cutting to ensure that over-heating of the metal does not occur, which can alter the microstructure and mechanical properties. If samples must be cut with a torch, ensure that large areas are removed, thus leaving enough heat-unaffected areas for later saw cuts. A caveat regarding cutting is an old carpenter's saying: "Measure twice, and cut once."

Procedures for Sample Preparation

PREPARING METALLOGRAPHIC SPECIMENS

The surface of a metallographic specimen to be examined is prepared by various methods of grinding, polishing, and etching.

Copyright © 2022 by ASTM International, 100 Barr Harbor Dr., PO Box C700, West Conshohocken, PA 19428-2959
ASTM International is not responsible, as a body, for the statements and opinions expressed in this chapter. ASTM International does not endorse any products represented in this chapter.

Saw cut small or irregular-shaped objects must be metallographically mounted for grinding and polishing if automatic polishing equipment is used. Mounted samples also facilitate etching and performing other metallographic tests and measurements.

FIXTURING AND MOUNTING

Once a sample has been obtained, it can be prepared for metallographic examination. Preparation usually involves taking a representative sample of usable size and fixturing it for easy handling during grinding. The sample may be fixtured in a mechanical assembly by using a clamping load supplied by threaded fasteners. Most often the sample is sandwiched between two pieces of material of similar hardness. This sandwiching promotes good edge retention. One should be sure that the sandwich material is nonreactive with the sample, especially in the presence of water and other fluids. To prevent a capillary draw of fluid into the crevices inherent to the clamping fixture, paraffin can be used to fill the voids and gaps.

Another fixturing technique involves the use of either thermoplastic, or thermosetting polymer granules and powders. These powders and granules have different values of wearability. Mounting resins with high wear resistance promote good edge retention, but slow the material removal rate. Mounting polymers also can be transparent and electrically conductive. Conductive mounts are required to keep the sample from charging when examination using a scanning electron microscope is required.

A systematic preparation method is the easiest way to achieve the true structure. Sample preparation therefore must pursue rules that are suitable for most materials. Different materials with similar properties (hardness and ductility) will respond alike and thus require the same consumables during preparation.

For metals, hot compression mounting is widely used. Phenolics are popular because they are low cost, whereas the diallyphtalates and epoxy resins find applications in which edge retention and harder mounts are required. The acrylic mounting compounds are used because they have excellent clarity.

For cold mounting, castable mounting resins are commonly used for electronic and ceramic materials. They are recommended for brittle and porous materials. These mounting compounds typically have two component systems (1 resin and 1 hardener). Mounting consumables include cold and hot mounting systems and mounting accessories. Mounting instruments includes programmable hot mounting presses.

Formerly, phenolic thermosetting resins were used for mounting specimens, but modern epoxy is becoming more popular because reduced shrinkage during curing results in a better mount with superior edge retention. A typical phenolic (bakelite) mounting cycle will compress the specimen and mounting media to 4,200 psi (~28 MPa) and heat to a temperature of 300°F (~150°C). When specimens are sensitive to temperature, "cold mounts" may be made with a two-part epoxy resin. Mounting a specimen provides a safe, standardized, and ergonomic way by which to hold a sample during the grinding and polishing operations.

Mounting involves inserting a specimen, with the side to be polished face-side down, into a heated mounting press. Next, polymer granules or powder, or both, are carefully added to the cavity, with care being taken to not disturb the sample. Once sufficient material has covered the sample, the ram portion end of the cylinder is secured, and the cylinder is pressurized. Heat and pressure cause the polymer to liquify and then set, thus encapsulating the sample. Thermoplastic polymers should be allowed to cool to near room temperature before releasing pressure. At excessive temperatures above their glass transition, flow will result, causing the polymer to pull away from the sample.

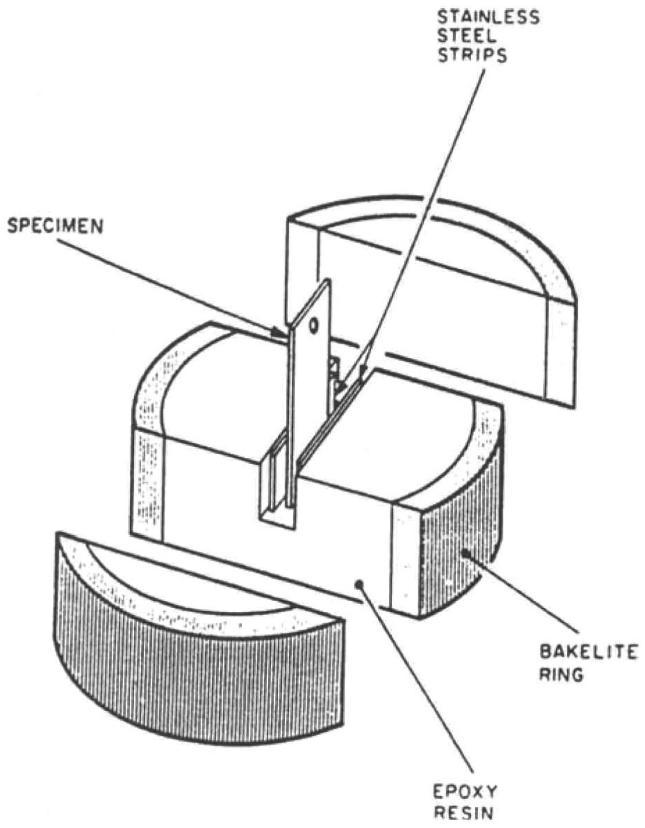
Another means of mounting specimens involves the use of a clear lucite mounting compound, which allows the metallographer to observe the location of cracks, pits, and other anomalies in the mounted specimen, if further polishing and grinding are necessary. When encapsulating samples, it is advisable, if possible, to remove any sharp corners, sharp protrusions, and burrs from the sample edges. Their presence tends to concentrate stresses during polymer cool-down and can promote cracking. Once cool, the sample can be handled easily during grinding and polishing.

Another method of sample fixturing uses cold-set epoxy resins. This method is helpful when samples are large or when cutting affects the physical integrity of the sample. Samples can be mounted in mold release coated metal molds or plastic preforms. Molds or preforms, or both, are then affixed (rubber cement; e.g., Seal-All) to an aluminum foil or polytetrafluoroethylene (PTFE; e.g., Teflon) covered flat surface. The sample is then placed on the flat foil or PTFE surface, in the preform, with the side to be polished down. Mixed, bubble-free epoxy resin is then poured over the sample, filling the mold. When using epoxy resins, it is helpful to have access to a bell jar and vacuum pump. A few minutes under vacuum tends to draw any air and gas bubbles out of the sample. The best method using liquid resins involves introducing it to the sample while under vacuum. Upon venting to atmosphere, resin is actually forced into microcavities. The sample is then placed in the preform mold and resin is added to fill the mold.

The resin reaction is exothermic, raising the temperature significantly and reducing the time required for the resin to cure, but there are some drawbacks. If the temperature is too high, the resin can oxidize, causing discoloration, thus decreasing visibility of the sample. More important, the amount of shrinkage is significantly higher for resins cured at temperatures above room temperature. This shrinkage can lead to cracking of the epoxy resin. Curing at high temperatures also can cause the epoxy to pull away from the sample, which promotes staining during etching.

If metallographic examination of coatings, specifically oxide coatings, is required, the following special techniques are helpful in preserving the integrity of the coating. The basis of coating preservation involves reducing the shrinkage associated with the curing resin. Blank mounts are made by filling bubble-free liquid resin in 1.25-in.-diameter bakelite preforms. After a 24-h cure, two parallel saw cuts are made (approximately 7/8 in. apart) through the sample, creating flats (fig. 1). Next, a thin slot is cut normal to the flats, halfway through the mount thickness. The ends of the slot are dammed up using cellophane tape. The sample is vacuum impregnated and then placed in the slot.

FIG. 1 Mountain arrangement for preserving oxide scales.



The sample is then shimmed up using thin stainless steel strips. According to Hussey, Beaubien, and Caplan, "The strips minimize rounding and reduce the chance of separation at the specimen-resin interface by providing a preferential site for such separation, if any should occur".[1] Other methods are available and the reader is advised to explore them. A good outline of additional mounting methods and materials is given in *Metallography Principles and Practice* by G. VanderVoort (see chap. 2, 60–93),[2] and ASTM E3, *Standard Guide for Preparation of Metallographic Specimens*, sections 7 through 9.

GRINDING

Caution: Before grinding, chamfer the sharp edges of the sample mounting material to prevent cutting the fingers of the person doing the polishing, if hand polishing, and to prevent snagging of the grinding or polishing media. Once the sample is fixtured properly, the surface should be ground smooth and flat. Grinding traditionally is performed using silicon carbide papers, but sometimes diamond impregnated grinding media are used. Grinding can be done manually with stationary abrasive papers, manually using rotating abrasives, or automatically (usually encompassing rotating abrasives, a counterrotating sample platen, and applying downwards pressure of the sample onto the abrasive). The choice between these methods depends on the number of samples and economy.

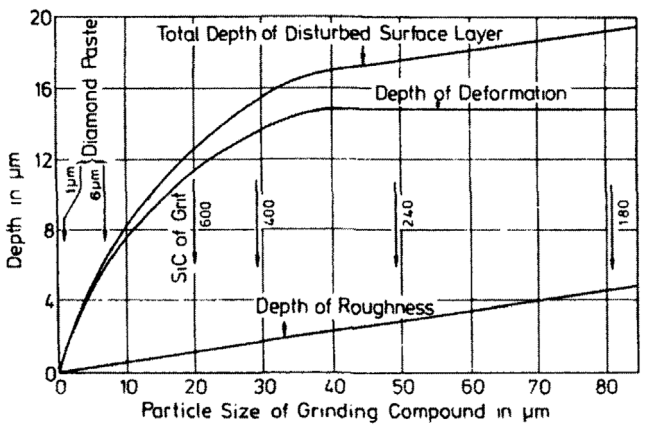
Whatever method is used, the principle is basically material removal. Material is removed for multiple reasons. The initial purpose of grinding is to produce a flat or planar surface. Second, grinding involves removal of gross scratches and deformities from the surface. Finally, it is equally important, especially for softer materials, to remove subsurface damage. During grinding, abrasive particles actually cut microgouges in the sample surface. While cutting, the material just beneath the surface of the gouge is plastically deformed (cold worked). This work-hardened material has a higher dislocation density and is therefore higher in internal strain energy than the material around it. During etching, these higher energy areas are preferentially attacked, thus leaving traces of scratches and etch pits. It is important to not only remove the scratches observed but also remove subsurface damage not visible.

During grinding, the metallographer should keep in mind that increasing the pressure on the sample will result in greater material removal rates, but it will not increase the amount of subsurface damage.[3] The maximum depth of subsurface damage is independent of pressure.[3]

The smoothness of the sample cut surface will decide the grit size of the grinding paper that initially is used. Traditionally, grinding can start at grits as fine as 200 grit, depending on the initial smoothness and flatness of the sample. Grinding should start with the finest grit capable of rendering a flat specimen and removing damage from sectioning. Coarse grinding should be minimized to limit subsurface deformation. If a finer surface finish is required before polishing on a diamond past wheel, polishing 600 grit or finer should be considered. Figure 2 shows the relationship between scratch depth (roughness) and depth of deformation in steels of various grit sizes.[4] Additional grinding is performed using successively finer abrasives, typically using 320, 400, and 600 grit abrasives sequentially. Rinsing of the ground surface with flowing water is imperative between grinding steps to prevent loose abrasive particles from being carried onto the next finer-grade grit paper, which will result in scratching by the larger particles from the coarser paper just used.

During grinding, the sample surface should be kept cool. Cooling usually is provided by use of water, alcohol, or other organic compounds. Methanol or ethanol coolants are used to

FIG. 2 Depth of scratches (roughness) and subsurface deformation in steels as a function of abrasive grit size. *Note:* 1 µm (micrometer = ~4×10^{-4} inches).



inhibit leaching of water-soluble compounds from the sample or oxide scales.

POLISHING

There are basically two methods of polishing metallographic samples: mechanical and electrolytic (electrochemical). Each will be discussed separately.

Mechanical Polishing

Subsequent to grinding and before polishing, the metallographer's hands and the sample should be thoroughly washed. Washing keeps any residual grinding abrasives from contaminating the polishing cloth.

The polishing operation is similar to grinding, but the size of the polishing abrasives is considerably smaller than the size of grinding abrasives. Again, the sample should be washed between each polishing step to inhibit abrasive carryover and contamination of the polishing cloths. Ultrasonic baths are highly recommended for cleaning during polishing. Ultrasonic waves promote superior cleaning by agitating small particles out of cracks and voids. However, metallographers beware: extended use can result in cavitation and pitting on the sample surfaces.

Typically, a sample will first be rough polished using a 6-µm or 3-µm diamond compound. Diamond abrasive can be suspended in an oil-based slurry or paste. Choice of polishing cloth is a function of sample material hardness, polishing rate, desired edge retention, and relief. A typical listing of various polishing cloths and their uses is presented in table 1.

A diamond extender (i.e., fine cutting oil) is used during polishing to minimize the use of expensive diamond polishing compounds and to ensure a uniform distribution of the abrasive over the polishing cloth. Initially, a small amount of diamond compound is distributed on the polishing cloth and polishing begins with the wheel revolving at about 100 to 300 rpm. This oily compound allows diamond particles to adhere to the fibers of the polishing cloths, removes abraded material, and permits dissipation of heat during polishing.

Once the sample has been polished to 3 µm, a final step (fine polishing) usually involving either an alumina slurry or colloidal silica slurry is used. The size of particles in these aqueous slurries can be as small as 0.02 µm. Once finished with this step, the sample is ready for examination as-polished or etching. All samples should be examined in the as-polished condition to evaluate the quality of the polishing, and it is easier to identify very small particles in the microstructure before etching. Procedures such as inclusion measurements (ASTM E45, *Standard Test Methods for Determining the Inclusion Content of Steel*) require assessments be conducted on as-polished samples.

Vibratory Polishing

Vibratory polishing is another method commonly used. Mounted samples are weighted down and allowed to randomly circulate on a cloth-covered vibrating platen. The platen holds an aggressive slurry of polishing abrasives and usually is covered to avoid evaporation and splashing. The downside of vibratory polishing is that it requires much more time than traditional mechanical or electrolytic polishing. Fortunately, this operating time is unattended. Vibratory polishing is very good at producing scratch-free samples for soft metals. Vibratory polishing is also useful for polishing samples having secondary phases in addition to the matrix. Harder phases are more resistant to the abrading action of the polishing media and stand in relief on the polished surface. After polishing, samples should be washed, rinsed in alcohol (and acetone if an oily film is present), and blown dry to avoid staining.

TABLE 1 Polishing Cloth Types and Uses

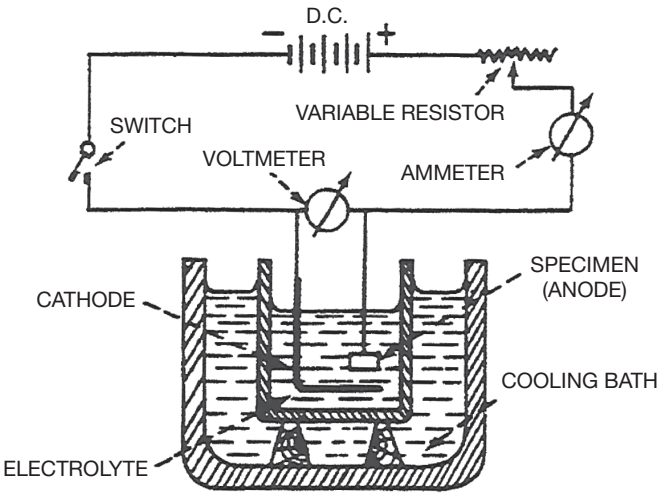
Cloth	Recommended Uses
Canvas	Rough general polishing. Use with coarse grades of silicon carbide (SiC) and aluminum oxide (Al_2O_3).
Billiard Cloth (Sheared Virgin Wool)	Rough general polishing of ferrous-based materials.
Red Felt (Plucked Virgin Wool Pile)	Rough or intermediate polishing.
Cotton-Medium Nap	Intermediate polishing. Commonly used with diamond, Al_2O_3, and colloidal silica
Cotton-Fine Nap	Rough diamond polishing of soft metals. Use with polishing grades ofAl_2O_3, chromium(III) oxide (Cr_2O_3), and silica.
Nylon	Rough polishing with diamond. Helps maintain flatness.
Silk	Use with diamond in rough polishing of extremely friable materials and rough polishing of metals.
Woven Wool	Rough and intermediate polishing of hard materials.
Wool (Short Pile)	Use in all final polishing stages.
Rayon (Flock on Cotton Backing)	Final polishing with diamond, Al_2O_3.
Rayon-Fine	Superior final polishing with diamond, Al_2O_3, and colloidal silica.
Synthetic Velvet	Intermediate and final polishing.
	Minimizes relief and edge rounding.
Synthetic Velvet-Fine	Use in vibratory polisher, especially with soft materials.
Medium Napped Polyurethane Cloth on Polyester	Polishing oxide films. Use with cerium oxide.

Source: Courtesy of South Bay Technology, Inc., San Clemente, CA.

Electrolytic Polishing

Electrolytic polishing is a convenient way to polish metallic samples in the fine ground (600 grit) or machined surface condition. This method requires formation of an electrical circuit in which the sample is the anode (fig. 3). A suitable electrolyte flows across the surface or submerges the sample. The current density is adjusted for the type of material and size of the polished sample to facilitate suitable dissolution of metal ions from the to-be-polished surface. Typically, 30–50 V are applied to the circuit and draw a current of 10–13 amperes. Polishing time is about 10–15 s. As the electrolyte washes over the sample, any perturbations in the surface (high-energy sites) are selectively dissolved. The result is a flat surface with no mechanical damage.

FIG. 3 Diagram of a simple electrolytic polishing cell.



Electrical circuit and arrangement of apparatus suitable for most electrolytic polishing operations. (Source: The Principles of Metallographic Laboratory Practice by George L. Kehl,McGraw-Hill Book Company, Inc., 1949)

Although this method is easy to use, storage and use of potentially dangerous and poisonous electrolytes may limit its use. For example, some solutions of perchloric ($HClO_4$) can become explosive if allowed to evaporate to concentrated solutions or perchlorate salts.

Etching

The final step in sample preparation is etching, which is a controlled corrosion process. Etching exposes the polished surface of a mounted specimen to a suitable environment that reveals particular structural features of the material that are not observable in the as-polished condition. After etching, the various surface constituents must be shown definitively with extreme clarity. Etching is performed to observe microstructural constituents, including grain boundaries, twin planes, slip lines, and second-phase particles. Etching also can reveal a material's propensity toward certain corrosion mechanisms, material defects, and service failures.

Safe laboratory work practices are important. A metallographer is useless without his or her eyes. Use proper protective equipment (e.g., gloves, safety glasses) when using laboratory chemicals.

The basic types of etching mechanisms are chemical etching, electrolytic etching, staining, and optical etching. Chemical etching uses the anisotropy (nonhomogeneity) in a material. The reaction rates of the chemical etchant on a polished sample's surface depend on the energy state of the materials microstructure. The higher the energy state of one region, the faster it will react, and more etching (localized material removal) occurs.

In other words, some microstructural constituents are anodic to others. Grain boundaries and twin boundaries are more energetic (anodic) than the material in the center of a grain. Likewise, regions under elastic tensile strain, or regions that have undergone plastic deformation will etch faster than nonstrained, nondeformed material. In a multiphase material, one phase may be more reactive than another.

Similarly, grain orientation on polished surfaces can affect the degree of etching. Close-packed orientations can etch slightly faster than lesser packed planes.

Microscopic examination of etched samples under reflected light, will show variations in the amount of light reflected to the eyepiece of the microscope as a function of the etching of more or less anodic portion of the surface of the sample. Surface undulations created by etching, reflect light away at different angles. The "off-reflected" light cannot be reflected back through the objective lens of the microscope and therefore appears as regions of darkness (fig. 4).

Some materials etch more easily than others. Grain boundary delineation in aluminum alloys is perhaps one of the most difficult tasks for a metallographer. In aluminum alloys, it is sometimes necessary to experiment with many known etchants to obtain the desired microstructural resolution. Certain alloys are designed for corrosion resistance and therefore are resistant to typically used chemical etchants.

Table 2 lists a number of chemical etchants that have proved useful for a limited number of the more popular engineering alloys. Included are the microstructural characteristics highlighted by the etch.

After chemical etching, samples should be rinsed in water (to terminate the chemical action of the etchant with the metal), followed by alcohol rinse to displace water from the surface (eliminate water staining) and blown dry to avoid further staining. Avoid touching the etched surface of the sample to protect microstructural features or oxidation caused by "finger prints." Samples should be stored in desiccators to inhibit corrosion on the highly polished surfaces. If a desiccator is not available, use of commercial clear-coat spray paints is recommended.

Electrolytic etching is similar to chemical etching and is used to etch corrosion-resistant materials. The electrochemical reaction is supplied by means of an externally applied potential. Etching is accomplished using the electrolytic cell used for electropolishing, as shown in figure 3. Typical operating parameters

FIG. 4 Simplistic representation of the principle of chemical etching.

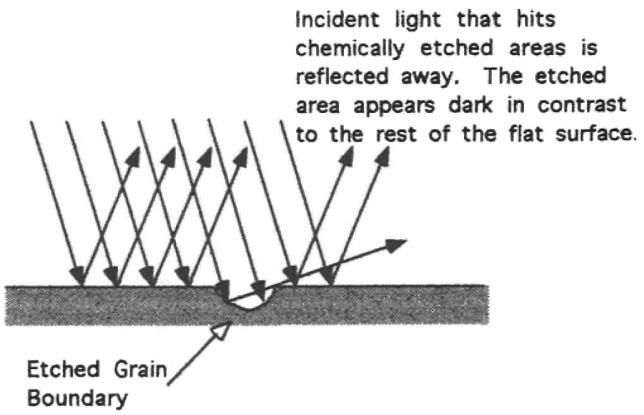


TABLE 2 Typical Chemical Etchants

Alloy	Chemical Etchants	Uses
Aluminum and Al Alloys	0.5–25 g NaOH	General purpose etch.
	1 g zinc chloride	Grain boundary delineation.
	100 mL water	Immerse up to 2 min.
	1 mL HF (48%)	Outlines microconstituents.
	200 mL water	Immerse for 30–40 s.
	12.5 mL HNO_3 (cone.)	General purpose etch.
	2.5 mL HF (48%)	Grain boundary delineation.
	85 mL water	Immerse up to 1 min.
	2 mL HF (48%)	Modified Keller's Rgnt.
	3 mL HCl (cone.)	General purpose etch for Al and Al alloys. Immerse 10-60 s.
	20 mL HNO_3 (cone.)	Wash in warm water, blow dry.
	175 mL water	
Copper and Copper Alloys	10 mL NH_4OH	General purpose etch.
	10 mL H_2O_2 (3%)	Grain boundary delineation.
	Can dilute up to 20 mL water	Use fresh, swab, or immerse up to 1 min.
	10 g $(NH_4)_2S_2O_s$	General purpose etch.
	90 mL water	Grain boundary delineation. Immerse up to 1 min.
	10 g Cr_2O_3	Swab or immerse up to 30 s.
	4 drops HCl	
	75–100 mL water	
Nickel and Nickel Alloys	20 mL HNO_3	Aqua-Regia
	60 mL HCl	Grain boundary, carbide, and a contrast. Use fresh and underhood. Discard after use. Swab or immerse up to 1 min.
	3 parts glycerol	Glyceregia.
	2–3 parts HCl	Popular etch. Use fresh and under hood. Discard after use.
	1 part HNO_3	Swab or immerse up to 1 min.
	10 g $CuSO_4$	Marble's Reagent.
	50 mL HCl	Grain boundary delineation
	50 mL water	Swab or immerse up to 1 min.A few drops of H_2SO_4 increases etch activity.
Iron and Iron Alloys	2 mL HNO_3	Nital.
	98 mL ethanol	Gives good pearlite-ferrite-grain boundary contrast in carbon and low-alloy steels. Swab or immerse up to 1 min.
	4 g picric acid	Picral. Promotes good resolution of pearlite, bainite,
	100 mL ethanol	martensite, and carbides.
	4–5 drops of zephiran	Swab or immerse up to 1 min.
	chloride (wetting agent)	
	100 mL picric acid (sat.)	Reveals prior austenitic grain boundaries in martensitic steels.
	1 g tridecylbenzene	
Stainless Steel	1 part HNO_3	General purpose etch for stainless steels.
	1 part HCl	Promotes grain boundary contrast.
	1 part water	Immerse in a gently stirred solution.
	1 g picric acid	Viella's Reagent.
	5 mL HCl	Outlines carbides, c, and 5.
	100 mL ethanol	Immerse up to 1 min.
	1 part glycerol	Glyceregia for SSs.
	3 parts HCl	Reveals grain structure.
	1 part HNO_3	Outlines *a* and carbides.Use fresh and under hood. Discard after use.Swab or immerse up to 1 min.
	10 g oxalic acid	Electrolytic etch (sample is anode). Use at 1–6 V at 0.1–1.0 A/cm^2.
	100 mL water	Resolves O in 5–10 s. Resolves carbides in 15–30 s. Resolves grain boundaries in 45-60 s.

Note: See VanderVoort,[2] Petzow,[4] and the *ASM Metals Handbook*[5] for extensive listing of etchants.

for electro-etching are as follows: about 100–200 μA, and about 5–10 V, and an etching time of 5–10 s. If the sample is embedded in a polymeric mounting material, provisions for making electrical contact must be made (i.e., prepared mount, drilling through the mount, removal from mount).

A family of chemical etchants known as deposit etchants works slightly differently than chemical etchants. Like electrolytic etchants, deposit etchants promote dissolution of metal on the polished surface. The dissolved metal ions react with agents in the etchant solution, however, thus promoting precipitation of insoluble compounds on the sample surface. The relative thickness of the coating depends on the reaction rate, which again is a variant depending on microstructure and chemical composition.

Commercial electropolishing and etching equipment is also available and is useful for metallographic polishing and etching applications. Electrolytic processes do have some limitations. Alloy specimens that are multiphase, have cracks or voids, or previously have been cold worked may be difficult or even impossible to polish or etch electrolytically. It may be necessary to mechanically polish samples followed by a combination of chemical and electrolytic etches to delineate the actual microstructures. Etching results are a product of the metallographer's experience and patience.

Heat tinting is another type of deposit etch. Exposing a polished sample (not in a plastic mount!) to elevated temperatures in air causes oxidation. On the microscopic level, oxidation rates of microstructural constituents vary according to their reactivity in a given environment.

The second type of etching is more of a staining operation than etching. Staining has been more involved with the identification and differentiation of oxide films than in outlining microstructural constituents.

Optical etching is a nondestructive method. The term optical etching is a misnomer. Optical methods do not involve etching, but they are useful in showing microstructural features in certain alloys. In this method, microstructural contrast, specifically crystallographic contrast of polished samples, is produced by using the Kohler principle of illumination (fig. 5). Modes of illumination including polarized light, differential interference contrast (Nomarski), and dark-field (DF) illumination can produce vivid and sometimes colorful contrast. Microstructural metallurgy has made many technical advances created by metallurgical microscopes utilizing the Kohler system with high-intensity illumination sources, a complex system of diaphragms, and combination lenses.[5]

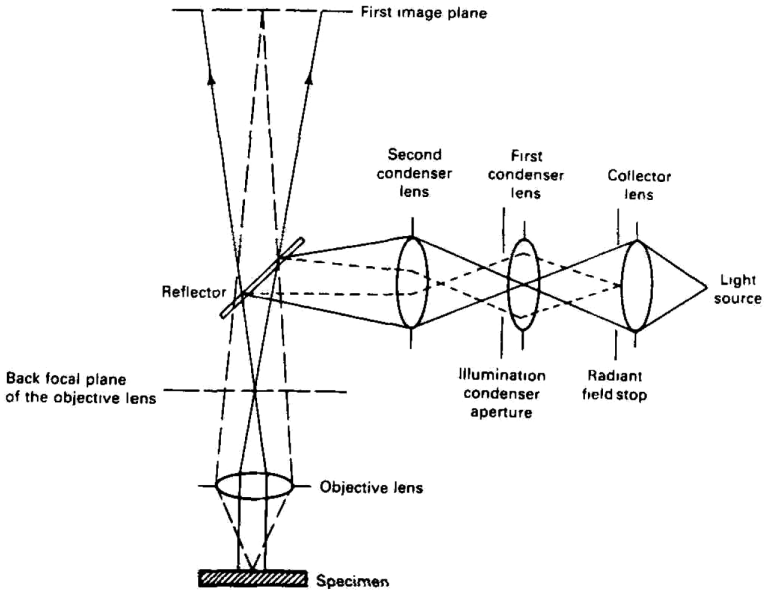
A digital microscope is a more recent development of typical optical microscope that uses both optics and a digital camera to supply an image to a computer coupled monitor. A digital microscope with integral LED lighting differs from an optical microscope in that there is no means to observe the image through an eyepiece. The image is focused on the digital circuitry with the entire system designed for monitor imaging. Digital microscopes provide digitally enhanced three-dimensional in-focus imagery from 20× to 6,000×.

A comprehensive list of electrolytes for electrolytic etching and chemical etchants can be found in VanderVoort,[2] Petzow,[4] and the *ASM Metals Handbook*.[5] Instructions for the preparation of etchants and operating parameters for electrolytic polishing and etching are also referenced.

Metallographic Interpretation

In the preparation of metallographic samples, not only are good hygiene and techniques required but also a good understanding of the sample material and its properties. Most metallographers have been surprised at least once by a structural anomaly that

FIG. 5 The Kohler principle of illumination.



turned out to be an artifact. Experience and an inquisitive nature are necessary for good metallographic interpretation.

Bright- and dark-field microscopy.

Most light optical microscope (LOM) observations are conducted using bright-field (BF) illumination, where the image of any flat feature perpendicular to the incident light path is bright, or appears to be white. But, other illumination methods can be used and, in some cases, may provide superior images with greater detail. DF microscopy is an alternative method of observation that provides high-contrast images and actually greater resolution than BF microscopy. In DF illumination, the light from features perpendicular to the optical axis is blocked and appears dark, whereas the light from features inclined to the surface, which look dark in BF, appear bright, or "self-luminous" in DF. Grain boundaries, for example, are more vivid in DF than BF.[2]

Polarized light microscopy.

Polarized light (PL) is very useful when studying the structure of metals with noncubic crystal structures (mainly metals with hexagonal close-packed (hcp) crystal structures). If the specimen is prepared with minimal damage to the surface, the structure can be seen vividly in cross-polarized light (the optic axis of the polarizer and analyzer are 90 degrees to each other, i.e., crossed). In some cases, an hcp metal can be chemically etched and then examined more effectively with PL. Tint etched surfaces show visible thin films (such as a sulfide, molybdate, chromate, or elemental selenium film) to aid metallographic study. These epitaxial features are grown on the surface to a depth at which interference effects are created when examined with BF producing color images. Microstructural resolution can be improved with PL. If it is difficult to get a good interference film with good coloration, the colors can be improved by examination in PL using a sensitive tint (ST) filter.[2]

Differential interference contrast microscopy.

Another useful imaging mode is differential interference contrast (DIC), which usually is obtained with a system designed by the Polish physicist Georges Nomarski. DIC converts minor height differences on the plane-of-polish, invisible in BF, into visible detail. The detail in some cases can be quite striking and very useful. If an ST filter is used along with a Wollaston prism, color is introduced. The colors are controlled by the adjustment of the Wollaston prism and have no specific physical meaning, however, visibility may be better. DIC capabilities are integral components of numerous commerically available LOM.

DIC has largely replaced the older oblique illumination (OI) technique, which was available on reflected light microscopes before about 1975. In OI, the vertical illuminator is offset from perpendicular, producing shading effects that reveal height differences. This procedure reduces resolution and yields uneven illumination across the field of view. Nevertheless, OI was useful to detect if a second-phase particle was standing above or was recessed below the plane-of-polish, and it is still available on a few microscopes. OI can be created on any microscope by placing a piece of paper under one corner of the mount so that the plane-of-polish is no longer perpendicular to the optical axis.[2]

Scanning electron and transmission electron microscopes.

If a specimen must be observed at higher magnification, it can be examined with a scanning electron microscope (SEM) or a transmission electron microscope (TEM). When equipped with an energy dispersive spectrometer (EDS), the chemical composition of the microstructural features can be determined. The ability to detect low-atomic number elements, such as carbon, oxygen, and nitrogen, depends upon the nature of the detector used. But, quantification of these elements by EDS is difficult and their minimum detectable limits are higher than when a wavelength-dispersive spectrometer (WDS) is used. But quantification of composition by EDS has improved greatly over time. The WDS system has historically had better sensitivity (ability to detect low amounts of an element) and ability to detect low-atomic weight elements, as well as better quantification of compositions, compared with EDS, but it was more time consuming to use. Again, in recent years, the speed required to perform WDS analysis has improved substantially. Historically, EDS was used with the SEM, whereas WDS was used with the electron microprobe analyzer (EMPA). Today, EDS and WDS are used with both the SEM and the EMPA. A dedicated EMPA, however, is not as common as an SEM.[2]

Design, resolution, and image contrast.

Light microscopes are designed for placement of the specimen's polished surface on the specimen stage either upright or inverted. Each type has advantages and disadvantages. Most LOM work is done at magnifications between 50× and 1,000×. With a good microscope, it is possible to perform examination at higher magnifications, for example, 2,000×, and even higher, as long as diffraction fringes are not present to distort the image. The resolution limit of the LOM will not be better than about 0.2–0.3 μm. Special methods are used at magnifications below 50×, which can be helpful when examining the microstructure of cast specimens where greater spatial coverage in the field of view may be required to observe features such as dendrites. In addition to considering the resolution of the optics, one must also maximize visibility by maximizing image contrast. A microscope with excellent resolution may not be able to image a structure, that is there is no visibility, if image contrast is poor. Image contrast depends on the quality of the optics, coatings on the lenses, and reduction of flare and glare; however, it also requires proper specimen preparation and good etching techniques. So, obtaining good images requires maximum resolution and image contrast.[2]

Quantitative metallography.

A number of techniques exist to quantitatively analyze metallographic specimens. These techniques are valuable in the research and production of all metals and alloys and nonmetallic or composite materials. Microstructural quantification is performed on a prepared, two-dimensional plane through the three-dimensional

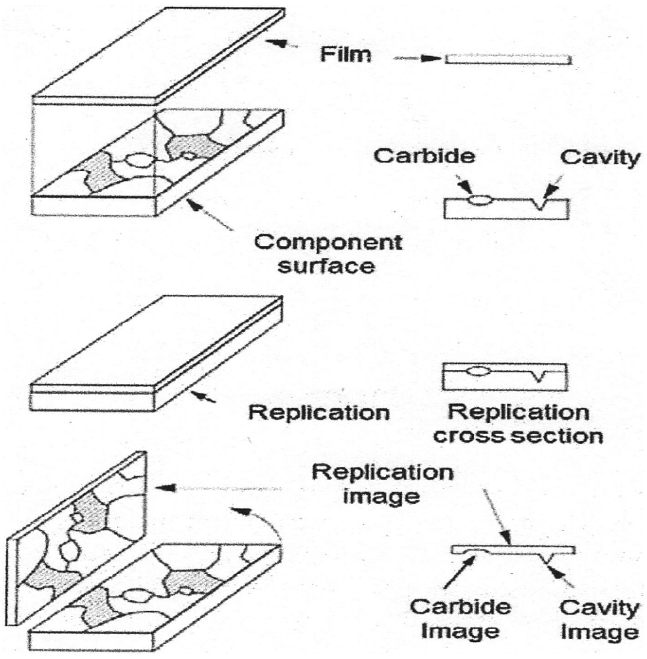
part or component. Measurements may involve simple metrology techniques, for example, the measurement of the thickness of a surface coating, or the apparent diameter of a discrete second-phase particle (e.g., spheroidal graphite in ductile iron). Measurement also may require application of stereology to assess matrix and second-phase structures. Stereology is the field of taking zero-, one-, or two-dimensional measurements on the two-dimensional sectioning plane and estimating the amount, size, shape, or distribution of the microstructure in three dimensions. These measurements may be made using manual procedures with the aid of templates overlaying the microstructure, or with automated image analyzers. In all cases, adequate sampling must be made to obtain a proper statistical basis for the measurement. Efforts to eliminate bias are required. Some of the most basic measurements include determination of the volume fraction of a phase or constituent, measurement of the grain size in polycrystalline metals and alloys, measurement of the size and size distribution of particles, assessment of the shape of particles, and spacing between particles. Standards organizations, including ASTM International's Committee E4 on Metallography and other national and international organizations, have developed standard test methods describing how to characterize microstructures quantitatively. For example, the amount of a phase or constituent, that is, its volume fraction, is defined in ASTM E562, *Standard Test Method for Determining Volume Fraction by Systematic Manual Point Count*; manual grain size measurements are described in ASTM E112, *Standard Test Methods for Determining Average Grain Size* (equiaxed grain structures with a single size distribution) and E1182, *Standard Test Method for Measurement of Surface Layer Thickness by Radial Sectioning (Withdrawn 2002)* (specimens with a bi-modal grain size distribution); ASTM E1382, *Standard Test Methods for Determining Average Grain Size Using Semiautomatic and Automatic Image Analysis*, describes how any grain size type or condition can be measured using image analysis methods. Characterization of nonmetallic inclusions using standard charts is described in ASTM E45, *Standard Test Methods for Determining the Inclusion Content of Steel* (historically, ASTM E45 covered only manual chart methods and an image analysis method for making such chart measurements was described in ASTM E1122, *Standard Practice for Obtaining JK Inclusion Ratings Using Automatic Image Analysis (Withdrawn 2006)*. The image analysis methods are currently being incorporated into ASTM E45). A stereological method for characterizing discrete second-phase particles, such as nonmetallic inclusions, carbides, and graphite, is presented in ASTM E1245, *Standard Practice for Determining the Inclusion or Second-Phase Constituent Content of Metals by Automatic Image Analysis*.

Nondestructive Field Metallography

Field metallography is nondestructive in situ testing of metallurgical conditions of metallic components that are in service wherein the removal of the equipment is either impractical or impossible. This method of nondestructive metallographic testing permits field evaluations without the need to remove equipment from service or production. Metallographic replication is used to assess high-temperature damage of power-generating equipment, chemical-processing units, heat exchangers, high-pressure piping, or other areas where sample removal is not easy.

Field metallographic procedures follow the same procedures used in standard metallography. The surface to be examined is ground and polished with a series of progressively finer abrasive papers and diamond or silica polish is used to achieve a mirror-like scratch-free finish. Pre-mixed etchants are used to swab etch the localized area to be examined. Replication is a nondestructive sampling procedure that records and preserves the topography of a metallographically prepared surface as a negative relief on a plastic film (replica). The replica permits the examination and analysis of the metallographically prepared surface on the LM microscope or the SEM. Enhancement procedures for improving replica contrast for microscopic examination are used and frequently are necessary. ASTM E1351-01, *Standard Practice for Production and Evaluation of Field Metallographic Replicas*, covers recognized methods for the preparation and evaluation of cellulose acetate or plastic film replicas which have been obtained from metallographically prepared surfaces. This procedure describes the evaluation of replicas to ensure that all significant features of a metallographically prepared surface have been duplicated and preserved on the replica with sufficient detail to permit both LM and SEM examination with optimum resolution and sensitivity. Replication involves the application of the acetate sheet on the etched surface to produce a replica of the surface (see fig. 6) Before being applied to the surface, the acetate sheet must be softened using methyl-acetate solution or acetone causing the acetate sheet to adhere to the surface. The softened acetate sheet is pressed firmly onto the etched surface to be replicated. After drying, the acetate sheet is sprayed with a black

FIG. 6 Schematic representation of the replication process (Buehler).



paint to provide an opaque surface to the film and surface contrast before peeling the tape from the component surface. The replica tape is carefully affixed to a glass slide using double-stick adhesive tape.

Care must be taken in handling the fragile replicas. An acetate tape thickness of 20–25 μm is suggested for replication. The contrast of the replica is further improved by applying carbon or metallic coating to the replica through a vacuum deposition sputtering process. Metallic coated replicas will provide exceptional spatial resolution.

The process of acetate sheet replication can be substituted using a silicone-rubber elastomer coating two-part replication process. Commercially available replicating equipment is ideal to measure surface roughness in tribological applications or during the analysis of fracture surfaces of large components. Silicone-based systems provide ideal surfaces and where replicas of low volume are required. The total time for the preparation of a silicone replica is less than the time needed to prepare an acetate replica and the silicone replica is not as fragile when being handled. Once the replicas are prepared, observation procedures are quite similar. Extracted replicas are normally examined with an optical microscope at magnifications of 50× to 1,000× with BF illumination.

Metallographic Examination and Evaluation of Corrosion Mechanisms

STRESS CORROSION CRACKING

The nature of stress corrosion cracking (SCC) can be directly observed by metallographic examination. The distinction between intergranular (IGSCC) and transgranular cracking (TGSCC) is best revealed by etching materials to reveal grain boundaries (fig. 7). In addition, the magnitude of crack branching and crack initiation sites are best revealed by metallographic examination.

Susceptibility of SCC is highly dependent on the metals stress state. Tensile stresses, either applied or residual, above a threshold value (alloy or heat dependent), are required for SCC cracking to occur. Chemical etching of metals can sometimes provide clues into a metal's thermomechanical history. Indications of plastic deformation (deformation twins, slip lines), and thus knowledge of exceeding of material yield strength, can be revealed through etching.

Some stainless steels[6] can be made susceptible to IGSCC by exposure to elevated temperatures 1021°F (550°C) < T < 1963°F (800°C). At these temperatures, carbon atoms migrate to grain boundaries where they combine with chromium atoms to precipitate chromium carbides (see fig. 8). Because chromium atoms are tied up as carbides, they are not available for matrix corrosion resistance, and the near-grain boundary regions are locally depleted in chromium. The 18Cr-8Ni austenitic stainless steels with various modifications in composition are known for corrosion resistance. When these alloys are heated in the temperature range 800°F to 1500°F (425°C to 815°C), for extended periods of time, they become *sensitized,* or susceptible to intergranular corrosion. This depletion renders grain boundary regions susceptible to corrosion, and the alloy is then termed "sensitized." The degree of sensitization is a function of temperature and time at temperature. The commonly accepted explanation for this behavior is the chromium impoverishment or chromium depletion theory. The addition of chromium in the amount of about 12% or more to ordinary steel imparts stainless steel characteristics and corrosion resistance.

In the specified temperature range, carbon migrates (diffuses) to the grain boundaries and precipitates out of solid solution as Cr_3C (in 304SS). Chromium is removed from solid solution, producing metal with lowered chromium content in the areas adjacent to the grain boundaries. Calculations show the composition of these carbides are approximately 93% chromium and 7% carbon, so the area within the grains where chromium is diffused from solution creates a wide corrosion-sensitive band.

FIG. 7 Transgranular stress corrosion cracking (left) and intergranular stress corrosion cracking (right) in 304 stainless steel (200×).

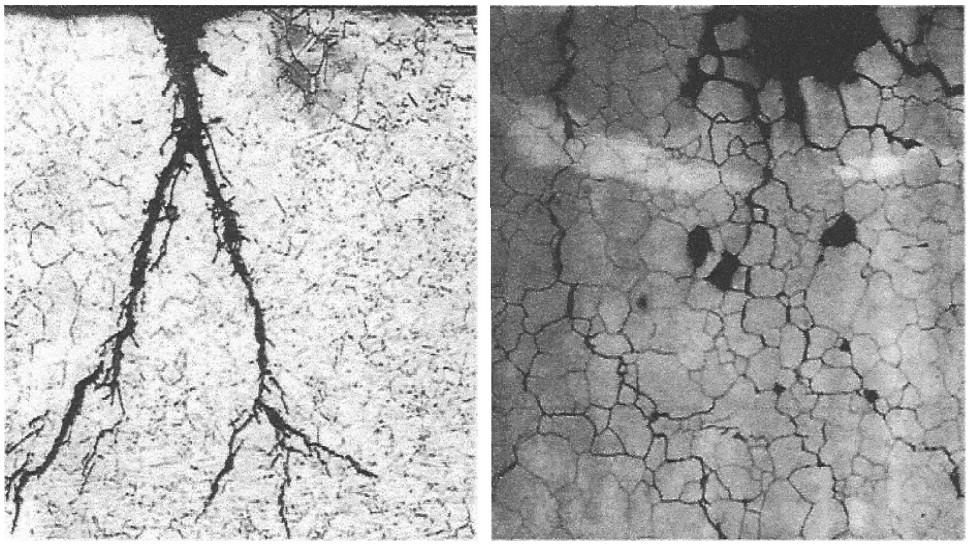
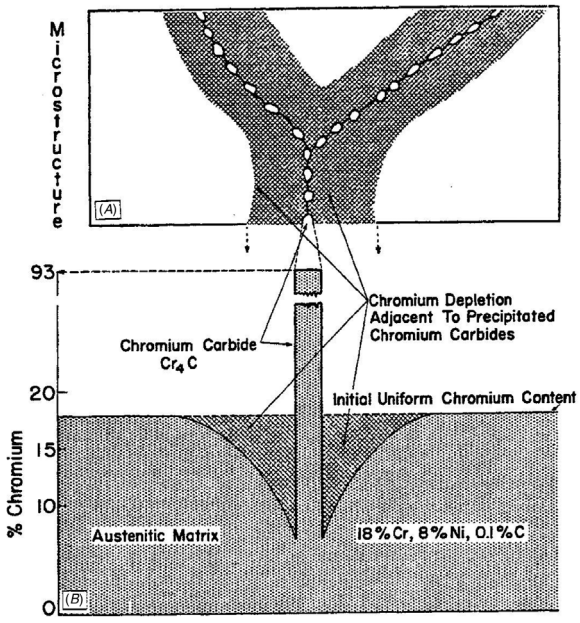


FIG. 8 Schematic diagram illustrating carbide precipitation. (*A*) Microstructure of 18Cr-8Ni stainless steel; white area is austenite of 18-8 composition, white particles in grain boundaries are chromium carbides, and shaded areas are chromium-depleted areas. (*B*) Differences in chromium content caused by carbide precipitation; cross-hatching represents a low-chromium area, which can be severely corroded.



The illustration in figure 8*A* shows chromium as low as 5% at the grain boundary carbide. This produces a chromium gradient which increases to 18% which is the chromium content of the alloy. The chromium-impoverished area of the sensitized layer extends to a width where the chromium is at least 12% and corrosion resistance is restored.

In many cases, a prediction of the susceptibility of austenitic stainless steels to IGSCC can be obtained by a simple electrolytic etch test (ASTM A262, *Standard Practice for Detecting Susceptibility to Intergranular Attack in Austenitic Stainless Steels, Practice A*).

Pitting

Metallographic examination can be quite useful in determining severity of pitting and also can be used to qualify materials for use in specific environments. A procedure for metallographic preparation of pitted samples is cited here, quoting ASTM G46, *Standard Guide for Examination and Evaluation of Pitting Corrosion, Section 5.1.5:* "Select and cut out a representative portion of the metal surface containing pits and prepare a metallographic specimen in accordance to the recommended procedures in ASTM E3. Examine microscopically to determine whether there is a relation between pits and inclusions or microstructure, or whether the cavities are true pits or might have resulted from metal dropout caused by intergranular corrosion, dealloying, etc." Evaluation of the metallographic samples of pitted materials can be performed easily using charts A, B, and C in ASTM G46, Section 7.2.1. (figs. 8 and 9). These charts characterize a sample's pit density, pit size, and pit depths. Metallographic evaluation of pitting is done with the sample in the as-polished condition. These data are convenient ways of relating and illustrating the severity of pitting to the lay person. It is sometimes helpful to reassess a sample after additional grinding and polishing. Material removal can eliminate overly conservative measurements caused by the three-dimensional (3D) travel path of corrosion pits.

Another way to quantify the extent of pitting is to examine the pitted surface of an as-polished sample under a laboratory microscope. By measuring the vertical distance using the micrometer focus knob, focusing on the top surface of the sample and the bottom of the pit, depth can be measured and determined. Care must be exercised because, as seen in figure 10, pits may not be perpendicular to the surface of the sample. Pits may be a continuous path or undercut beneath the surface. An erroneous perceived pit bottom may result in a conservative depth measurement.

DEALLOYING (SELECTIVE LEACHING)

Dealloying is a corrosion mechanism in which one element in a multielement system is selectively leached from the matrix by action of a fluid system. Two alloy systems that are widely known for dealloying are cast iron (graphitic corrosion) and copper-zinc ($Zn > 15$ wt.%) brasses. In gray cast irons (in the presence of sulfate reducing bacteria, salt water, or weak acids), alpha iron is anodic to graphite and corrodes, leaving behind a porous mass of graphite and iron sulfates. In brasses, zinc is

FIG. 9 ASTM G46 pitting chart for density, size, and depth.

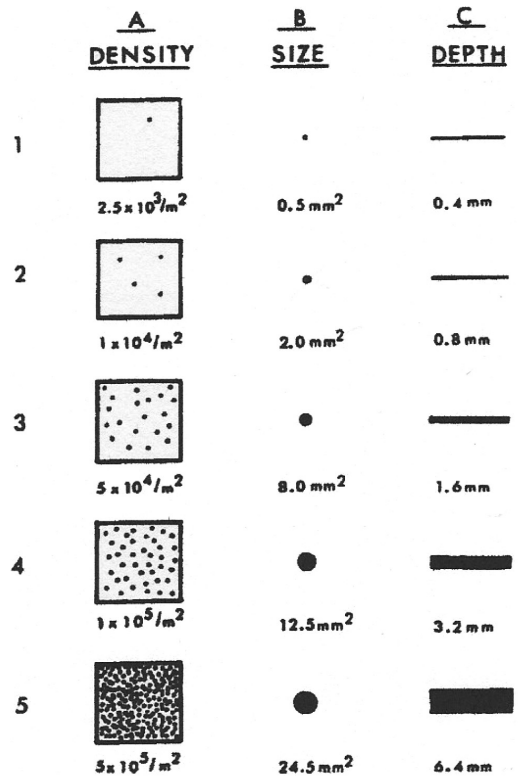
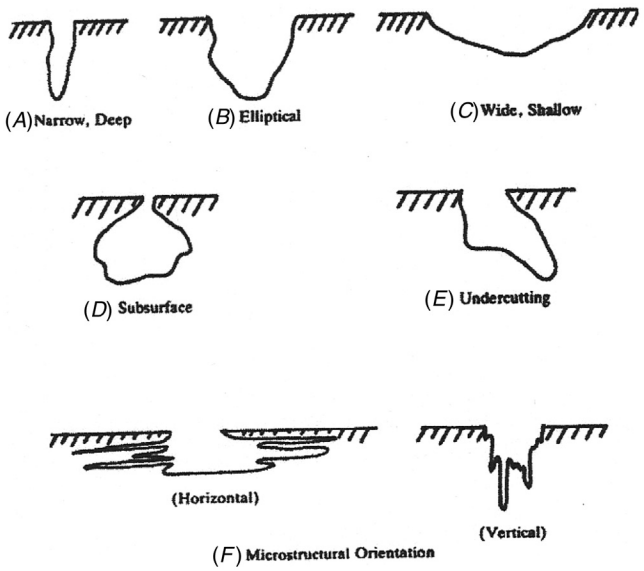


FIG. 10 ASTM G46 pitting chart showing variations in pit shapes.



selectively leached from the matrix, leaving behind a porous mass of copper.[7,8] Dealloying severely reduces the mechanical properties causing complete failure of the affected components. Metallographic examination can confirm visual indications of dealloying (fig. 11).

The zinc-rich grain boundary phase (the dark areas appearing in the grain boundaries at the bottom of fig. 11), can be seen to have dissolved in the top of the photomicrograph leaving grainy copper. Complete dealloying has occurred leaving nearly pure copper after dissolving the zinc. Not only will the microstructure appear changed as one element is selectively leached from the matrix, but also changes in microchemistry can be observed. Dealloying can be observed optically or by analyzing the polished specimen in an SEM (see fig. 12). Backscattered electron images will show contrast in regions of varying atomic number. Another SEM method that graphically displays differences in microstructural elemental composition is the digital X-ray line scan or X-ray dot map. The line scan can show variations in elemental composition along a line (fig. 12). The dot map shows compositional differences over the examined area. Depending on computer capabilities and software, some systems can map out the concentrations of up to 16 elements simultaneously.

FIG. 11 Photomicrograph showing selective dezincification of the continuous alloy phase in an α-β brass (200×).

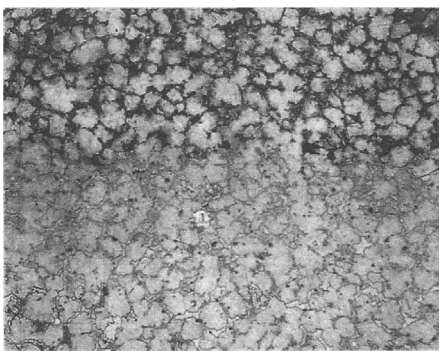
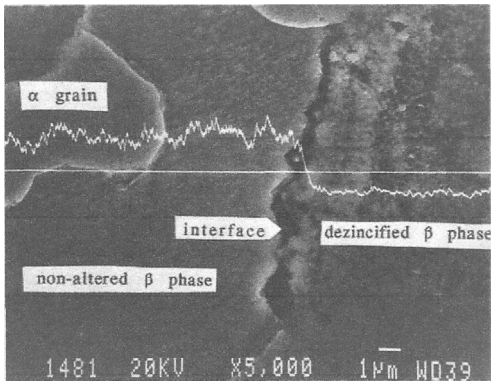


FIG. 12 SEM-EDS utilizing an X-ray dot map shows a reduction in zinc concentration across a de-zincified (de-alloyed) interface in an α-β brass alloy (5000×).



CORROSION DUE TO PHASE CHANGES (σ—SIGMA-PHASE FORMATION IN CR-NI-FE AND FE-CR ALLOYS)

Exposure of certain alloys to elevated temperatures can produce deleterious embrittling phase changes within the alloy. These phase changes sometimes can lead to corrosive attack of the alloy. Corrosion can occur if the phase change alters the formation of protective oxide barriers on the surface. Examples of this mechanism include sensitization of stainless steels (see fig. 8) and sigma-phase (**σ**) formation. Sigma-phase formation occurs in nickel-chromium-iron and chromium-iron alloys containing a minimum of 16.5% Cr exposed to temperatures between 1100°F and 1700°F (593.3°C and 926.7°C) over long periods of time.[9] Sigma phase is an iron chromium–rich phase that precipitates along austenitic grain boundaries and delta ferrite[9] high-temperature grain boundary precipitates (fig. 13). Test results have shown that austenitic stainless steels exhibiting precipitated sigma phase undergo significant intergranular corrosion in boiling 65% HNO_3 and in hot concentrated sulfuric acid solutions.

FIG. 13 Photomicrograph showing (sigma phase σ) precipitate (dark phase in austenitic grain boundaries) of a 310-type stainless steel (500×).



Sigma-phase formation also results in the loss of room temperature base metal ductility.

Sigma-phase formation can be assessed easily by metallographic examination. One of the most definitive ways of determining the presence of sigma phase is by using a 45% aqueous potassium hydroxide solution as an electrolytic etch. Sigma precipitates are revealed as distinct reddish-brown islands in the austenitic matrix.

GENERAL CORROSION

In conditions in which general corrosion occurs, metallographic samples can be used to verify the extent of metal loss through microscopic measurements of sample thickness. The reduction of thickness coupled with weight loss information provides a checks and balances program into the analysis and reveals any corrosion rate differences caused yt anisotropy.

LIQUID METAL EMBRITTLEMENT

Liquid metal embrittlement (LME) is not a common corrosion mechanism. Only a small number of lower melting point liquid metals can cause LME in any given alloy system. LME is an inter- and intragranular cracking mechanism produced by a liquid metal on the surface of a sensitive solid metal in the presence of a tensile stress, either applied or residual. The mechanism occurs only above a threshold stress value and has an incubation period. Table 3 shows a few of the solid and liquid systems exhibiting LME. More alloys systems exhibiting LME are tabulated in the *ASM Metals Handbook*.[10]

Metallographic examination can assist in identifying LME. Liquid metal penetration can be observed readily in mounted, unpolished samples (fig. 14).

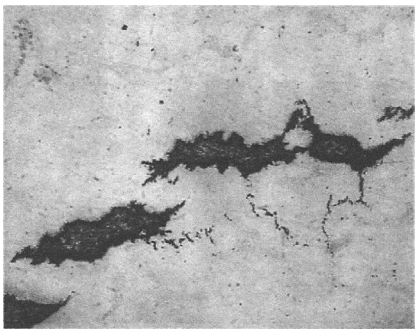
Etching for grain boundaries, however, can distinguish between inter- and intragranular cracking. In addition, SEM/EDS analysis, as discussed in the section covering dealloying, can positively identify the presence of foreign metals at grain boundaries within a matrix. Care should be taken when trying to identify mercury using SEM/EDS. High vacuum and electron beams promote evaporation of mercury. Low kilovolt settings (less than 10 kV) should be used over wide areas to inhibit burning off highly volatile mercury. In addition, mercury X-ray energy peaks (M) and sulfur (Ka) peaks are easily mistaken for each other. Wet chemical spectroscopy is perhaps the best method for absolute identification of liquid metal species.

Radiography can be used as a check for LME in large structures. By virtue of the large difference in liquid and solid metal system densities, cracks can be revealed easily on X-ray film, even when they are not visible on the surface.

TABLE 3 Solid and Liquid Systems Exhibiting

Solid Metal	Liquid Metals Promoting Embrittlement
Aluminum alloys	Mercury, gallium, sodium, indium, tin
Brass (70/30-Cu/Zn)	Mercury, lithium bismuth
Iron or steel	Lithium
Nickel copper alloys	Mercury, lead
Stainless steels	Zinc, cadmium
Ni-Cr-Fe alloys	Lead

FIG. 14 As-polished photomicrograph showing diffusion of Pb/Sb into steel (500×).



HIGH TEMPERATURE CORROSION—METAL DUSTING

Metal dusting of heat-resistant alloys (Ni-Cr-Fe) occurs in carbonaceous atmospheres at temperatures above 800°F (426.7°C), with very high activity in the temperature range of 1450°F to 1550°F (787.7° to 843.3°C) and above 1700°F (926.6°C). In metal dusting environments, a black "sooty" residue (graphite) usually covers the surface in most of the wasted areas. The residual metal is usually thinned and contains multiple rounded pits. The original austenitic matrix transforms to a brittle ferromagnetic material and can be checked with a simple magnet. Metallographic examination reveals an inward diffusion layer of gross carburization and grain "pop out."

SULFIDATION

Metallographic examination of metals that have exhibited wastage because of sulfidation usually show a two-layer scale, the upper layer (surface) being red, the lower being black and shiny. A few drops of aqueous hydrochloric acid on the deposit can release a noticeable H_2S odor and verify the presence of sulfides. In addition, creation of a "sulfur print" can verify sulfidation damage. A sulfur print is produced as follows: A metallographically mounted cross-section sample of thinned metal with surface scale is sanded to a 120 grit finish. Next, wash (immerse) a piece of black and white photographic paper in 2–3% sulfuric acid. Wipe away excess acid with a clean sponge. The sample is placed on the photographic paper for a few seconds. The paper is then stopped (acid neutralized) and fixed (using photographic fixer, sodium, or ammonium thiosulfate, which removes excess unexposed silver halide and a shiny image) as in normal circumstances. An image of the sulfide distribution on the sample will appear.[9]

OXIDATION

Oxidation, perhaps the most visible of all corrosion mechanisms, is responsible for consuming a significant amount of maintenance dollars. Metallography of oxidized metals can provide information about the type of reaction. Types of oxidation

reactions (general, internal [subsurface], intergranular) can be differentiated by microexamination. Knowing the oxide scale thickness and composition can provide data on time-temperature exposure by knowing the oxidation rate laws of the material. In addition, knowledge of the mass ratio of oxide species in the scale can determine exposure temperature.

Metallographic examination of different phases within oxide scales has proven difficult, but some techniques are available. For example, in steels, the scales formed at high temperature generally are composed of three layers: iron oxide (FeO), hematite (Fe_2O_3), and magnetite (Fe_3O_4). The formation of these three oxides can be described by the following reactions:

$$Fe + \tfrac{1}{2}O_2 = FeO$$
$$3Fe + 2O_2 = Fe_3O_4$$
$$2Fe_3O_4 + \tfrac{1}{2}O_2 = 3Fe_2O_3$$

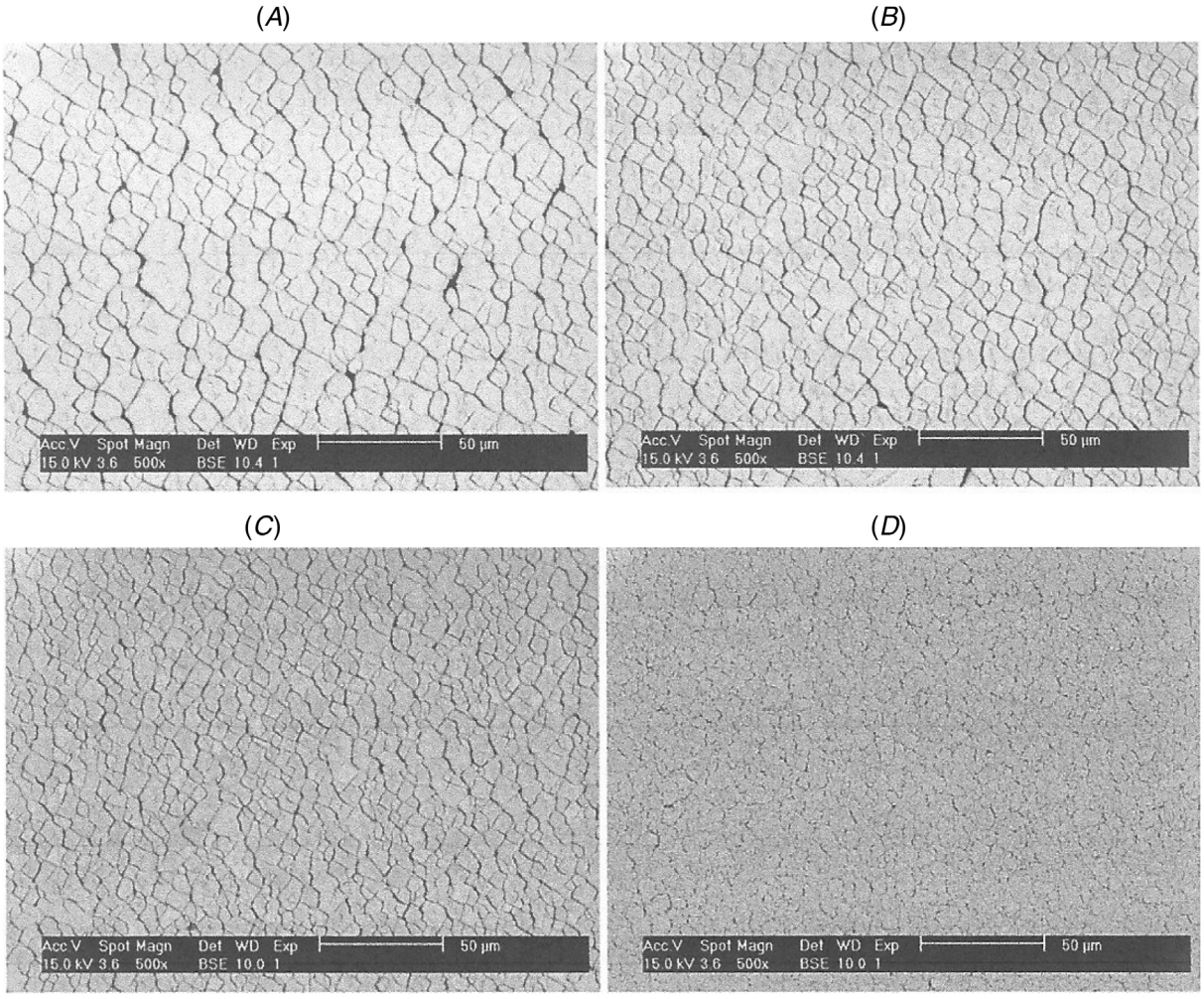
The mineralogical names are used to emphasize their specific physical and chemical properties. Wüstite (from the German name) forms at high temperatures (>565°C, ~1100°F) adjacent to the steel surface. Magnetite is an intermediate layer and hematite is the outer layer. Usually a layer of mixed hematite and magnetite is observed.

An etchant containing 0.5% selenic acid (H_2SeO_4) and 4% hydrochloric acid (HCl) in ethanol can produce a nice contrast between the oxide phases on polished samples after immersion at room temperature.[11] Selected dyes have also been used with various degrees of success. The reader is encouraged to read for further information on dying oxide scales.[12]

THERMAL BARRIER COATINGS

Thermal barrier coatings (TBC)[13] produced by Electron Beam Physical Vapor Deposition (EB-PVD) are primarily applied to critical hot section turbine components. EB-PVD TBC for turbine applications exhibit a complicated structure of porous ceramic columns separated by voids that offers mechanical compliance. Currently, there are no standard evaluation methods for evaluating EB-PVD TBC structure quantitatively. A proposed

FIG. 15 SEM-backscattered scanning electron images of the same sample taken at different positions with respect to the coating thickness. Images (*A*) 150, (*B*) 96, (*C*) 64, and (*D*) 11 μm from the TBC/TGO interface (500×). *Source:* Kelly et al.[13]



metallographic method for preparing samples and evaluating (TBC) techniques quantitatively by measuring the structure is discussed. TBC samples were produced and evaluated with the proposed metallographic technique and digital image analysis for columnar grain size and relative intercolumnar porosity. Incorporation of the proposed evaluation technique will increase knowledge of the relationship between processing parameters and material properties by incorporating a structural link. Application of this evaluation method will directly benefit areas of quality control, microstructural model development, and reduced development time for process scaling.

Modern hot section turbine components are composite systems composed of a metallic structural component, metallic bond coat, thermally grown oxide (TGO) of the bond coat, and a ceramic TBC. The rationale for the layered system design is to reduce thermal conductivity, increase adhesion of the ceramic top layer, reduce sharp changes in thermal expansivity mismatch, improve oxidation resistance, and reduce the diffusion rate of corrosive products to the structural members. TBC produced by either EB-PVD, or thermal spray processes, have been used to protect metallic components in the hot sections of a turbine successfully for more than two decades. TBCs produced by the EB-PVD method typically are described as columnar in nature and offer high lateral mechanical compliance because of the high aspect ratio voids between columns, whereas similar coatings produced by thermal spray techniques offer lower thermal conductivity and lateral compliance because of lamellar formation and discontinuous porosity. Performance of either coating for a particular engineering application is inevitably determined by the coating microstructure dictated by the coating method and process parameters. Understanding the relationships between process parameters for a coating system, coating microstructure, and performance is essential.

References

1. R. J. Hussey, P. E. Beaubien, and D. Caplan, "Metallography of Oxide Scales on Metals," *Metallography* 6 (1973): 27–36.
2. G. VanderVoort, *Metallography Principles and Prentice* (New York: McGraw-Hill, 1984).
3. L. E. Samuels, *Metallographic Polishing by Mechanical Methods* (Materials Park, OH: ASM International, 1982).
4. G. Petzow, *Metallographic Etching* (Materials Park, OH: ASM International, 1978).
5. *ASM Metals Handbook,* 9th ed., Vol. 9 (Materials Park, OH: ASM International, 1985).
6. Robert J. Radebaugh, *Stainless Steel* (Materials Park, OH: ASM International, 1990).
7. H. J. Uhlig, *Corrosion Handbook* (New York: Wiley, 1948).
8. L. L. Shreir, ed., *Corrosion,* Vol. 1 (London: Newnes-Butterworths, 1977).
9. D. J. Gaertner, "Characterization of Sigmatized Austenitic Stainless Steels," *Materials Performance* (January 1985): 18–24.
10. W. R. Warke, *ASM Handbook*, 10th ed., Vol. 11 (Materials Park, OH: ASM International, 2002).
11. B. Chicco and T. Heijkoop, "Metallographic Reagent for the Characterization of Oxide Scales on Iron and Steel," *Praktische Metallographie* 20 (1983): 321–326.
12. B. Chicco, "Dye Adsorption—A New Technique for the Color Metallography of Oxide Scales on Steels," *Metallography* 14 (1981): 319–328.
13. M. Kelly, J. Singh, J. Todd, S. Copley, and D. Wolfe, "Metallographic Techniques for Evaluation of Thermal Barrier Coatings Produced by Electron Beam Physical Vapor Deposition," *Materials Characterization* 59, no. 7 (July 2008): 863–870.

Chapter 8 | Electrochemical Tests

John R. Scully,[1] Carol F. Glover,[1] and Raymond J. Santucci[2]

Introduction

Several textbooks and symposia proceedings cover the application of electrochemical methods in corrosion testing.[1–16] This chapter highlights many of the commonly used laboratory methods after presenting a brief review of thermodynamics and kinetic aspects of electrochemical reactions that describe corrosion processes. Techniques discussed include Tafel extrapolation, polarization resistance, electrochemical impedance spectroscopy (EIS), electrochemical noise (EN) resistance, use of rotating disks, and cylinders to study aspects of corrosion affected by solution flow, polarization methods for assessing susceptibility to localized corrosion, scratch repassivation, potential-step repassivation, EN applied to pitting, potentiodynamic repassivation techniques for assessing sensitization, the barnacle electrode and permeation methods for hydrogen concentration analysis, and methods for evaluating anodized layers and coatings on metals.

ELECTRODE REACTION THERMODYNAMICS AND KINETICS IN CORROSION

Metallic corrosion is usually an electrochemical process. Electrochemical processes require anodes and cathodes in electrical contact, as well as an ionic conduction path through an electrolyte. The electron flow between the anodic and cathodic areas quantifies the rates of the oxidation and reduction reactions. When anodes are physically separated from cathodes, the current can be readily measured by replacing direct electrical contact with a zero-resistance ammeter (ZRA). The conversion of the reaction rate per unit area from units of mol/cm$^{2\text{-s}}$ to electrical current density, i (A/cm^2) is accomplished with Faraday's constant, F, and knowledge of the number of electrons transferred to complete the electrochemical reaction a single time, n, as follows:

$$i = nFJ, \tag{1}$$

where:
n = number of electrons transferred, equivalents/mol, *and*
F = Faraday's constant, 96,484.6 coulombs/equivalent.

Monitoring this current provides the means of assessing the kinetics of the corrosion process, not just the thermodynamic tendencies for corrosion nor merely the mass of metal loss registered after the test. There are three typical half-cell reactions by which a metal (M) may be oxidized in water:

$$\mathrm{M(s) = M^{n+}\,(aq) + ne^-\,(s)}\ \text{Production of metal cations,} \tag{2}$$

$$\mathrm{M(s) + nH_2O = M(OH)_n + \mathit{n}H^+\,(aq) + ne^-(s)}$$
Oxide or hydroxide formation, or (3)

$$\mathrm{M(s) + nH_2O = MOH^-\,(aq) + 2nH^+\,(aq)}$$
$$\mathrm{+ ne^-(s)}\ \text{Anion production.} \tag{4}$$

In all cases, metal atoms in the solid (s) metallic state (in the electronic conductor) are converted to an oxidized state. These species remain either on the metallic surface or are ejected into the aqueous (aq) solution (the ionic conducting phase). Typical cathodic half-cell reactions in aqueous media involve the reduction of oxygen, protons, and water at the interface between the metallic and ionic conducting phases. This process involves consumption of electrons liberated during oxidation:

$$\mathrm{O_2 + 2H_2O + 4e^- = 4OH^-}\ \text{in aerated neutral or alkaline media,} \tag{5}$$

$$\mathrm{O_2 + 4H^+ + 4e^- = 2H_2O}\ \text{in aerated acid media,} \tag{6}$$

$$\mathrm{2H^+ + 2e^- = H_2}\ \text{in acid media, and} \tag{7}$$

$$\mathrm{2H_2O + 2e^- = H_2 + 2OH^-}\ \text{in neutral or alkaline media.} \tag{8}$$

The Nernst equation describes the reversible electrode or equilibrium potential, E_{redox}, associated with the thermodynamic tendency for an electrochemical half-cell reaction to occur spontaneously. At potentials more positive than the equilibrium potential associated with a particular electrochemical half-cell reaction, oxidation proceeds spontaneously, whereas at potentials more negative, reduction occurs. The forms of the Nernst

[1]University of Virginia, 395 McCormick Rd., Charlottesville, VA 22903-2442, USA J. R. S. http://orcid.org/0000-0001-5353-766X, C. F. G. http://orcid.org/0000-0002-9220-622X
[2]U.S. Naval Academy, 121 Blake Rd., Annapolis, MD 21402, USA http://orcid.org/0000-0002-9676-6312

DOI: 10.1520/MNL202NDSUP20190036

Copyright © 2022 by ASTM International, 100 Barr Harbor Dr., PO Box C700, West Conshohocken, PA 19428-2959
ASTM International is not responsible, as a body, for the statements and opinions expressed in this chapter. ASTM International does not endorse any products represented in this chapter.

equation for the oxidation reactions given in equations (2) and (7) are, respectively,

$$E_{\text{redox}} = E_o + (2.303RT/nF)\log(\text{M}^{n+}), \text{ and} \quad (9)$$

$$E_{\text{redox}} = E_o - 2.303RT\text{p}H/F, \quad (10)$$

where:

R = the ideal gas constant, cal/mol-K;
T = temperature, K
n = the number of electrons to complete the half-cell reaction a single time; and
E_0 = the specific standard half-cell potential for the reaction cited at unity activity for dissolved species and 1 atmosphere fugacity for gaseous substances at 25°C.

The standard half-cell potential for the reaction $2H^+ + 2e^- = H_2$ is defined as 0.0 V versus the normal hydrogen electrode at 25°C.

Concerning corrosion in aqueous media, metal oxidation reactions (see equations (2)–(4)) with Nernst or redox potentials more negative than the Nernst or redox potentials associated with typical cathodic reactions given by equations (5)–(8) will occur spontaneously.[4–5] The reaction rate for any single reduction-oxidation process is a function of overpotential E-E_{redox}, where E is the applied potential. For a single charge transfer–controlled redox reaction, i_{net} is described as follows:

$$i_{\text{net}} = i_{\text{ex}}\{\exp[\alpha_a F(E - E_{\text{redox}})/RT] - \exp[-\alpha_c F(E - E_{\text{redox}})/RT]\}, \quad (11)$$

where the exchange current density, i_{ex}, describes the nonzero rate at which the forward (oxidation) and reverse (reduction) reactions occur equally at E_{redox}. Because E_{redox} represents an equilibrium condition, the forward and reverse rates of the reaction must be equal; α is known as the symmetry factor (such that $\alpha_c = 1 - \alpha_a$) in the case of single-step electron transfer processes representing a reduction oxidation process, and α represents a transfer coefficient for a multistep reaction process (in this case, $\alpha_c + \alpha_a \neq 1$). The factor 2.303 $RT/\alpha_a F$ is equal to the anodic Tafel slope, β_a. Similarly, the factor 2.303 $RT/\alpha_c F$ is equal to the cathodic Tafel slope, β_C. If E-E_{redox} is a large positive voltage (i.e., such that the term $[\alpha_a F(E\text{-}E_{redox})/RT]$ is greater than about 2.303 or $(E\text{-}E_{redox})/\beta_a > 1$), then the following simplification known as the Tafel approximation applies for a charge transfer–controlled process:

$$i_{\text{ox}} = i_{\text{ex}}\exp[\alpha_a F(E - E_{\text{redox}})/RT]. \quad (12)$$

Similarly, when E-E_{redox} is a large negative number (i.e., such that $(E\text{-}E_{redox})/\beta_c > 1$), another analogous simplification is applied in the case of a single electrode reaction:

$$i_{\text{red}} = i_{\text{ex}}\exp[-\alpha_c \text{F}(\text{E} - \text{E}_{\text{redox}})/\text{RT}]. \quad (13)$$

Typical corrosion processes occurring under freely corroding conditions involve at least one cathodic and one anodic reaction. The thermodynamics discussed earlier dictate the circumstances in which these reactions will proceed spontaneously. The current density measured during a polarization experiment, i_{app}, involving a single-charge transfer-controlled oxidation and single-charge transfer-controlled reduction reaction follows:

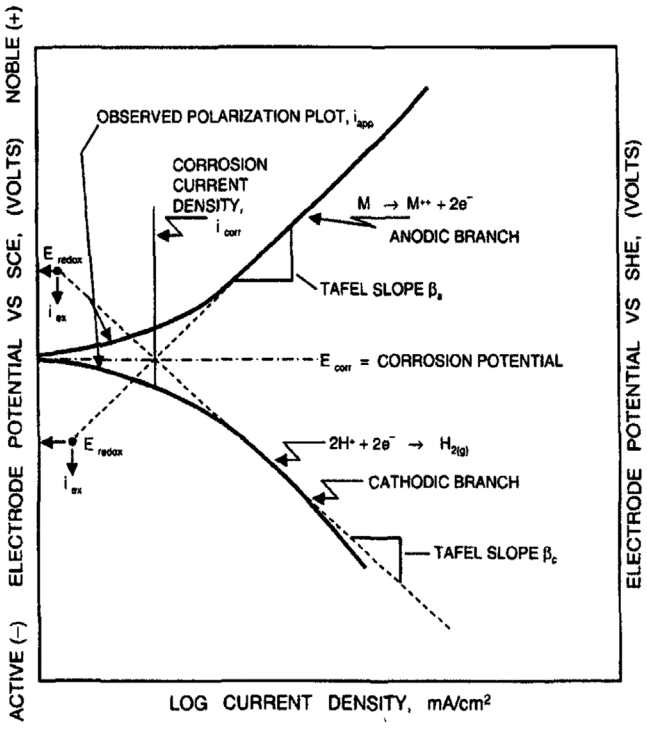
$$i_{app} = i_{corr}\left[\exp\left(\frac{\alpha_a F(E - E_{corr})}{RT}\right) - \exp\left(\frac{\alpha_c F(E - E_{corr})}{RT}\right)\right]. \quad (14)$$

The corrosion potential, E_{corr}, is a kinetically and thermodynamically determined "mixed" potential given by the interception of the lines describing the total anodic and cathodic reaction rates. At E_{corr}, $i_{ox} = i_{red}$ and i_{corr} is described by the magnitude of i_{ox} at E_{corr} as shown in figure 1. Either reaction rate may become mass transport limited under certain circumstances, in which case equations (12)–(14) do not apply.

Obtaining Corrosion Rates from Electrochemical Kinetic Data

According to mixed-potential theory, any overall electrochemical reaction can be algebraically divided into half-cell oxidation and reduction reactions, and there can be no net electrical charge accumulation.[17] For open-circuit corrosion in the absence of an applied potential, the oxidation of the metal and the reduction of some species in solution occur simultaneously at the metal-electrolyte interface, as described by equation (14). Under these circumstances, the net measurable current density, i_{app}, is zero. A finite rate of corrosion defined by i_{corr} occurs at anodic sites on the metal surface, as indicated in figure 1. When the corrosion

FIG. 1 Application of mixed potential theory showing the electrochemical potential-current relationship for a corroding system of a single-charge transfer-controlled cathodic reaction and single-charge transfer-controlled anodic electrochemical reaction. β_c and β_a are Tafel slopes.



potential, E_{corr}, is located at a potential that is distinctly different from the reversible electrode potentials (E_{redox}) of either the corroding metal or the species in solution that is cathodically reduced, the reaction favors reduction and the oxidation of the cathodic reactants or the reduction of any metallic ions in solution becomes extremely small. Because the magnitude of i_{ox} at E_{corr} is the quantity of interest in the corroding system, this parameter must be determined independently of the oxidation reaction rates of other adsorbed or dissolved reactants.

The information obtained in a polarization experiment is i_{app} as a function of the potential, E, as shown by the thick solid line in figure 1, where $i_{app} = i_{ox} - i_{red}$. To obtain i_{app} as a function of E, the applied potential between the reference electrode and working electrode is controlled and scanned at constant rate (potentiodynamic), instantaneously increased a fixed amount (potentiostatic), or stepped at various times (potentiostaircase).[18] I_{app} is measured and normalized with respect to the surface area, A (i.e., $i_{app} = I_{app}/A$). Conversely, i_{app} can be supplied between the working and counterelectrodes under galvanostatic or galvanostaircase control, and the resulting potential between the working and reference electrodes is monitored. Several ASTM standards discuss methods for performing these experiments, including ASTM G5, *Standard Reference Test Method for Making Potentiodynamic Anodic Polarization Measurements*, and ASTM G59, *Standard Test Method for Conducting Potentiodynamic Polarization Resistance Measurements*. Several approaches are available to determine i_{corr} from such experimental information. These methods are discussed in the following section.

Conversion of Corrosion Rates to Mass Loss and Penetration Rate

Determination of I_{ox} at open-circuit potential (OCP) or other potential of interest, where $I_{ox} = i_{ox} \times A$, over a known period of time leads to direct determination of the mass loss:

$$M = \frac{I_{ox} t (A.W.)}{nF}, \tag{15}$$

where:
M = the mass loss, g;
$I_{ox}t$ = the product of current and time, coulombs; and
$A.W.$ = the atomic weight of the electroactive species, g/mol.

This relation is known as Faraday's first law. Rearrangement of equation (15) leads to a straightforward determination of the penetration rate (applicable only when i_{ox} (μA/cm^2) is uniformly distributed over the entire wetted surface area, or where the localized actively corroding area, A, is known), as follows:

$$CR = \frac{K_1 i_{ox} (E.W.)}{\rho}, \tag{16}$$

where:
CR = the corrosion rate, in mm/year;
$E.W.$ = the equivalent weight (considered dimensionless in this calculation); and
P = the metal or alloy density, g/cm^3.

The constant $K_1 = 3.27 \times 10^{-3}$ when i_{ox} is expressed as μA/cm^2. K_1 has units of mm-g/μA-cm-y when CR is desired in mm/yr. ASTM G102, *Standard Practice for Calculation of Corrosion Rates and Related Information from Electrochemical Measurements*, gives other values for this constant when CR is expressed in other units. Expressions are also available to calculate mass loss rate per unit area from knowledge of electrochemical corrosion rate. For instance,

$$MR = K_2 i_{ox} (E.W.), \tag{17}$$

where:
$K_2 = 8.954 \times 10^{-3}$ g-cm^2/ μA m^2 d when MR is expressed as g/m^2 d.

For alloys, the equivalent weight $E.W.$ should be calculated as outlined in ASTM G102:

$$\text{E.W.} = \frac{1}{\sum \left(\frac{n_i f_i}{A.W._i} \right)}, \tag{18}$$

where:
f_i = the mass fraction of the i_{th} component of the alloy (-);
$A.W._i$ = the atomic weight of the ith component element, g/mol;
N_i = the number of electrons transferred or lost when oxidizing the i_{th} component element under the conditions of the corrosion process (equivalents/mol); and
i = the number of component elements in the alloy.

Usually, n is equal to the stable valence of the elements oxidized, or must be determined from either a Pourbaix (potential-pH) diagram or experimentally from an analysis of the ions in the corrosive solution. This expression assumes that all component elements oxidize when the alloy corrodes and that they are all oxidizing at essentially a uniform rate. In some situations, these assumptions are not valid and the calculated corrosion rate will be in error. For example, if an alloy is composed of two or more phases and one phase preferentially oxidizes, the calculation must take this into consideration.

ELECTROCHEMICAL METHODS FOR THE STUDY OF UNIFORM CORROSION: POLARIZATION METHODS

One method for examining the corrosion behavior of a metal is to determine the E-i_{app} relationship by conducting a polarization experiment. The following E-i_{app} relationship is often experimentally observed between applied current and potential. The expression is applicable to charge transfer–controlled corrosion processes, regardless of the exact number of charge transfer–controlled reactions or reaction steps. It provides the basis for the electrochemical polarization technique.[1,2,17,19]

$$i_{app} = i_{corr} \left[\left(\exp \left\{ \left\{ \frac{2.303(E - E_{corr})}{\beta_a} \right\} \right\} \right) - \exp \left\{ \left\{ \frac{-2.303(E - E_{corr})}{\beta_c} \right\} \right\} \right] + C \frac{\partial E}{\partial t}, \tag{19}$$

where:
C = the interfacial capacitance associated with the electrochemical double layer;

B_a and β_c = the anodic and cathodic Tafel slopes ($\partial E/\text{-}\partial\log(i_{app})$) given by the slopes of the polarization curves in the anodic and cathodic Tafel regimes, respectively; and
$\partial E/\partial t$ = the time rate of change in applied potential, or voltage scan rate.

The second term of the expression ($C\ \partial E/\partial t$) approaches 0 at low-voltage scan rates dE/dt. Steady state is desirable, because the goal is to obtain i_{corr} at E_{corr}. Note that i_{app} becomes approximately equal to either i_{ox} or i_{red} at large η, where $\eta = (E\text{-}E_{corr})$. At very large anodic or cathodic overpotentials, equation (19) can be rearranged in the form of the Tafel expression.[1–3,5,7,18,19]

$$\eta_a = \beta_a \log\left(\frac{i_{app}}{i_{corr}}\right), \qquad \eta_c = -\beta_c \log\left(\frac{i_{app}}{i_{corr}}\right), \tag{20}$$

where:
η_a and η_c = the anodic and cathodic overpotentials, respectively.

Equation (20) is strictly valid only for a single anodic or cathodic reaction, although approximately linear behavior can be observed despite several reactions. The linear portion of the solid line describing $E\text{-}i_{app}$ in figure 1 above E_{corr} describes a single anodic reaction that can be described by equation (20). Similarly, the linear portion of the solid line describing $E\text{-}i_{app}$ in figure 1 below E_{corr} describes a single cathodic reaction that can be described by equation (20).

Tafel Extrapolation to Determine Corrosion Rate

In cases in which equation (20) is valid, η can be plotted versus $\log(i_{app})$ over a sufficient range to obtain a linear relationship between the logarithm of current density and potential;[1,5,7,20] i_{corr} can be determined from extrapolation of i_{app} from either the anodic or the cathodic Tafel region to the OCP (zero overpotential). Figure 1 illustrates this method. The method is potentially damaging to the corroding metal, because a large overpotential must be applied. This is true for polarization in either direction but particularly so in the case of anodic polarization, in which the surface is changing because of corrosion and or passivation of the metal. No ASTM standard currently exists for this method.

Complications with the Polarization Method Involving Solution Resistance

Tafel extrapolation, as well as other polarization techniques, can be complicated by several factors. One such factor, ohmic resistance, arises from the resistivity of the solution, cell geometry, location of the reference electrode, and magnitude of applied current.[2,6] Ohmic resistance can contribute a voltage error to the measured potential. This error is summed algebraically with the true interfacial overpotential across the electrochemical interface (the potential usually sought in electrochemical measurements) measured with respect to a reference electrode. Placement of the reference electrode near the working electrode with a Luggin-Haber capillary is used to minimize the solution resistance error, which can be estimated from the product of the applied current density, the solution resistivity, and the perpendicular distance from the Luggin probe to the specimen surface in a planar electrode geometry. The error contributes to the measured overpotential n_{app}:

$$\eta_{app} = \eta_{true\ interfacial} + i_{app} R_s, \tag{21}$$

where:
R_s (Ω-cm^2) = the uncompensated solution resistance between the working electrode and the position at which the reference electrode senses the potential in solution (at the tip of the Luggin-Haber capillary).

Thus, $n_{app} > \eta_{true}$ at high anodic current densities, high R_s, or high cathodic applied current density. $E_{app} > E_{true}$ and the Tafel slope desired from a fit of equations (19) and (20) to E versus i_{app} data cannot be obtained from *E-logi* data. When the dominant term in equation (21) is the second term, a linear relationship between η ($\eta = \eta_{app}$) and i_{app} is obtained instead of the semi-logarithmic relationship discussed earlier. The true scan rate in the potentiodynamic technique also may be altered, because the applied potential (that contains the ohmic component), not the true overpotential, is controlled during the scan. Several excellent reviews are available on the subject of the voltage error introduced from solution resistance.[21–24]

Complications Involving Concentration Polarization Effects

The Tafel relationship established through equations (19) and (20) is valid for pure activation control, or charge transfer control. An additional consideration involves the concept of concentration polarization. In this case, the reaction rate is fast enough that the reacting species is depleted (reduction reaction) or concentrated (oxidation) at the reacting surface. Diffusion through the electrolyte becomes the kinetic limitation which controls the reaction rate. The reaction becomes completely diffusion controlled at the limiting current density, i_L. The deviation from activation control in the case of a cathodic reaction can result in an additional overpotential known as a mass transport overpotential, η_{conc}. This overpotential is described as follows:[4,5]

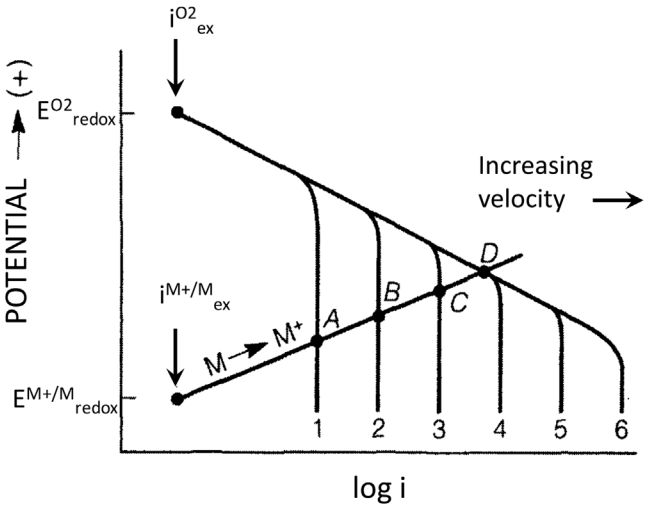
$$\eta_{conc} = \left[\frac{2.303RT}{nF}\right] \log\left[1 - \frac{i_{app}}{i_L}\right], \tag{22}$$

where:
i_L = the mass transfer limiting current density defined by Fick's first law at steady state.

As i_{app} approaches i_L, the concentration overpotential, η_{conc}, becomes very large. The cathodic reaction may be under mixed charged transfer-mass transport or mass transport control for many corrosion situations, particularly if the cathodic reaction is oxygen reduction.[5] The cathodic polarization behavior associated with "mixed" charge transfer–mass transfer control can be described mathematically by the algebraic combination of equations (20) and (22). Tafel extrapolation of cathodic data becomes difficult under these conditions because the Tafel region may not be extensive.

For a completely mass transport– limited corrosion process, the concentration of the cathodic reacting species C_b approaches zero at the electrode interface and $i_{corr} - i_L$ (fig. 2).[2] The diffusional boundary layer thickness, δ, is decreased by increasing

FIG. 2 Application of mixed potential theory showing the electrochemical potential-current relationship for a corroding system consisting of a mass transport–controlled cathodic reaction and a charge transfer–controlled anodic reaction. As the fluid velocity increases from 1 to 4, the corrosion rate increases from *A* to *D*.



solution stirring or rotation rate, Ω (rad/s), in the case of a rotating cylinder or disk electrode.[1] The limiting current density i_L is a linear function of concentration gradient.[15] The concentration gradient (C_b/δ) increases as a function of $\Omega^{0.5}$ or $\Omega^{0.7}$ for the rotating disk and cylinder, respectively.[2,15] For a mass transport controlled cathodic reaction, i_{corr} is increased with flow as shown in figure 2. The governing equation for the rotating cylinder electrode is[15]

$$i_L = 0.079nFC_bD^{0.64}\nu^{-0.34}\Omega^{0.7}r^{0.4}, \quad (23)$$

and for the rotating disk electrode is[2,15]

$$i_L = 0.621nFC_bD^{0.67}\nu^{-0.167}\Omega^{0.5}, \quad (24)$$

where:

C_b = the reacting species concentration in the bulk solution, moles/cm^3;
D = the diffusion coefficient for the reacting species, cm^2/s;
ν = the kinematic viscosity of the solution, cm^2/s; and
r = cylinder or disk radius, cm.

Corrosion engineers often favor the rotating cylinder to simulate flow in turbulent piping systems, because it is readily obtained.[15] In contrast, the rotating disk electrode operates in the laminar flow regime, even at high rotation rates, and does not accurately represent many corrosion situations.[15] No ASTM methods currently exist to examine mass transport controlled corrosion.

Polarization Resistance Methods

Stern and Geary simplified the kinetic expression describing charge transfer–controlled reaction kinetics, as in equation (19), for the case of small overpotentials with respect to E_{corr}.[25,26] Equation (19) can be linearized when $\eta/\beta < 0.1$. This simplified relationship has the following form if the second term describing the capacitive current, $C(dE/dt)$, is negligible:

$$i_{corr} = \left(\frac{\Delta i_{app}}{2.3\Delta E}\right)\left(\frac{\beta_a\beta_c}{(\beta_a+\beta_c)}\right), \quad (25)$$

rearranging

$$i_{corr} = \left(\frac{1}{2.3R_p}\right)\frac{\beta_a\beta_c}{(\beta_a+\beta_c)} = \frac{B}{R_p}, \quad (26)$$

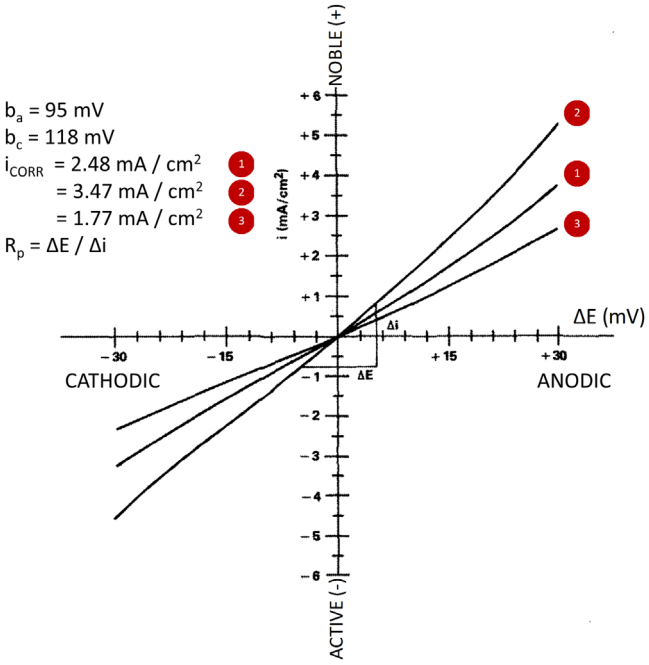
where:

R_p = the polarization resistance (Ω-cm^2) given by dE/di at $t = \infty$, $AE = 0$, and
B = a constant given by the constant terms shown in equation (26).

As shown for AISI 430 stainless steel in sulfuric acid (H_2SO_4), i_{app} is often approximately linear with potential within ± 5-10 mV of E_{corr} (fig. 3). The slope of this plot, $\Delta E/\Delta i$, when determined at E_{corr}, as shown in figure 3, defines the polarization resistance, which is inversely proportional to corrosion rate.[27,28] The surface area of the working electrode must be known. Knowledge of R_p, β_a, and β_c permits direct determination of the corrosion rate at any instant in time using equation (26).[25–29]

ASTM standards G59 and ASTM G96, *Standard Guide for Online Monitoring of Corrosion in Plant Equipment (Electrical and Electrochemical Methods)* describe standard procedures for conducting polarization resistance measurements.[1]

FIG. 3 ASTM G59 polarization curves used for polarization resistance determinations based on the results from eight independent laboratories for AISI-type 430 stainless steel in 1N H_2SO_4. Curve 1 is the mean result, with Curves 2 and 3 showing the 95% confidence limits from the laboratory round robin.



Other techniques rely on exploiting nonlinearity at larger overpotentials; however, this invalidates the approximation given by equation (25).[30] The Oldham-Mansfeld method calculates i_{corr} from nonlinear E versus i_{app} data obtained usually within ± 30 mV of E_{corr}, using tangent slopes and intercepts to calculate corrosion rate without high overpotential determination of β_a and β_c.[31] Computerized curve fitting can exploit nonlinearity to calculate β_a, and β_c from low overpotential data, avoiding the destructive nature of large overpotentials.[32] The Mansfeld technique substitutes equation (26) into equation (19), eliminating i_{corr}.[32] β_a and β_c are determined from the best fit of the resulting expression containing β_a and β_c as unknowns to a nonlinear plot of η versus i_{app} data are obtained within ±30 mV of E_{corr}. R_p is determined from the linear slope of E versus i_{app} within ±5 mV of E_{corr}, and i_{corr} is subsequently determined from equation (25) using R_p, β_a, and β_c.

Complications with Polarization Resistance Measurements

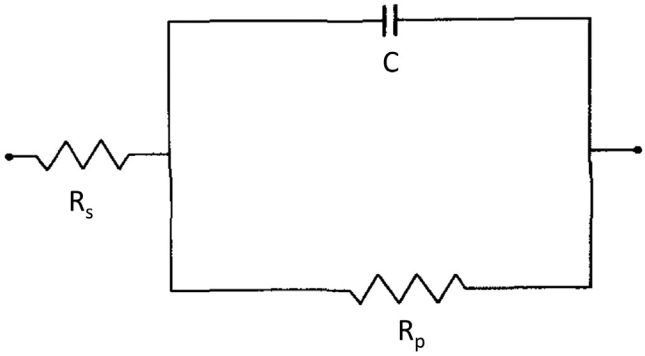
Complications related to the polarization resistance method and possible remedies have been reported in the literature.[30–36] Three of the most common errors involve (1) invalidation of the results through oxidation or reduction of some other electroactive species besides the corroding metal in question; (2) a change in the OCP or corrosion potential during the time taken to perform the measurement; and (3) use of a large η, invalidating the assumption of a linear relationship between i_{app} and E required by equations (25) and (26).

Another source of error involves cases in which both the anodic and cathodic reactions are not charge transfer–controlled processes, as required for the derivation of equation (25). Modifications to equation (25) exist for cases in which pure activation control is not maintained, such as in the case of partial diffusion control or passivation.[37] Other researchers have attempted to calibrate the polarization resistance method using gravimetrically determined mass loss.[38] In fact, polarization resistance data for a number of alloy-electrolyte systems have been compared with the observed average corrosion currents determined from mass loss via Faraday's law.[29] A linear correspondence was obtained over six orders of magnitude in corrosion rates.

Two other frequently encountered complications are the need to correct polarization data for errors that arise from the contribution of solution resistance, R_s, and the addition of capacitive current, $C\ dE/dt$, which occurs with increasing scan rate.[16] Capacitive current gives rise to hysteresis in current-potential plots.[39] Solution resistance contributes to a voltage error, as discussed earlier, as well as a scan rate error. Because the applied potential is increased by an ohmic voltage component, an apparent value of polarization resistance R_p' is obtained, which overestimates R_p by an amount equal to R_s. Consequently, the corrosion rate is underestimated. Hysteresis in the current density-applied potential plot occurs for combinations of a high voltage scan rate and large interfacial capacitances as well as large polarization resistances. Attempting to determine R_p at too fast of a scan rate underestimates its true value, leading to an overestimation of corrosion rate. This error can be minimized by determining the polarization resistance at a slow scan rate or by extrapolating the results at several slow scan rates to zero scan rate. Alternatively, one may take two or more current density measurements from potentiostatic data after long time periods near E_{corr} to minimize fast scan rate effects. These complications and others have been reviewed elsewhere.[40]

Many treatments of this subject have used an electrical equivalent circuit model to simulate the corroding metal-electrolyte interface.*,[40,41] The simplest form of such a model is shown in figure 4. The three parameters discussed earlier (i.e., R_p, R_s, and C) that approximate a corroding electrochemical interface are shown. The algebraic sum of R_s and R_p is measured when a direct current (DC) measurement is performed. The impedance associated with a capacitor approaches infinity as the voltage scan rate approaches zero, and parallel circuit elements are always dominated by the element with the smallest impedance. Therefore, the sum of R_s and R_p is measured and the true corrosion rate will be underestimated when R_s is appreciable. Conversely, any experiment conducted at a fast voltage scan rate causes the algebraic sum of the ohmic resistance and the resultant impedance of the parallel resistive-capacitive network to be measured. This value will be lower than the sum of R_p and R_s determined at an infinitely slow scan rate, as current leaks through the parallel capacitive element at a higher scan rate because of its low impedance at high frequency. This usually will result in an overestimation of the true corrosion rate. These complications can be overcome by using the electrochemical impedance method.

FIG. 4 Electrical equivalent circuit model simulating a simple corroding metal/electrolyte interface. See also figure 5. R_s is the solution resistance. R_p is the polarization resistance. C is the double-layer capacitance.



*This review focuses on corroding systems with different cathodic and anodic half-cell reactions. The concept of polarization resistance, however, applies equally well to reduction-oxidation systems involving a single half-cell reaction. Here, the exchange current density, i_o, may be calculated from the polarization resistance, where R is the ideal gas constant, F is Faraday's constant, T is the temperature, and α_a and α_c are the anodic and cathodic multistep electron transfer coefficients, respectively, for the reduction-oxidation process, as follows:

$$R_n(ohm - cm^2) = \left[\frac{\Delta E}{\Delta i}\right]_{(E-E_{rev})\to 0} = \left(\frac{RT}{i_o F(\alpha_a + \alpha_c)}\right).$$

Electrochemical Impedance Methods

One approach for determining the polarization resistance of a metal involves the electrochemical impedance (sometimes known as alternating current (AC) impedance) method.[2,39–43] ASTM G106, *Standard Practice for Verification of Algorithm and Equipment for Electrochemical Impedance Measurements*, contains an appendix reviewing the technique. In this technique, typically a small-amplitude sinusoidal potential perturbation is applied to the working electrode at a number of discrete frequencies, ω. At each one of these frequencies, the resulting current waveform will exhibit a sinusoidal response that is out of phase with the applied potential signal by a certain amount (Φ) and has a current amplitude that is inversely proportional to the impedance of the interface. The electrochemical impedance, $Z(\omega)$, is the frequency-dependent proportionality factor that acts as a transfer function by establishing a relationship between the excitation voltage signal and the current response of the system:

$$Z(\omega) = V(\omega)/i(\omega), \quad (27)$$

where:
V = the time-varying voltage across the circuit, $V = V_0\sin(\omega t)$;
i = the time-varying current density through the circuit, $i = i_0 \sin(\omega t + \Phi)$;
$Z(\omega)$ = the impedance, Ω-cm^2; and
t = time, s.

$Z(\omega)$ is a complex-valued vector quantity with real and imaginary components whose values are frequency-dependent

$$Z(\omega) = Z'(\omega) + jZ''(\omega), \quad (28)$$

where:
$Z'(\omega)$ = the real component of impedance, $Z'(\omega) = |Z(\omega)|cos(\Phi)$;
$Z''(\omega)$ = the imaginary component of impedance, $Z''(\omega) = |Z(\omega)| sin(\Phi)$;
j^2 = the square of the imaginary number, -1; and
$|Z(\omega)|$ = the impedance magnitude, where $|Z(\omega)| = (Z'(\omega)^2 + Z''(\omega)^2)^{1/2}$.

The electrochemical impedance is a fundamental characteristic of the electrochemical system it describes. A knowledge of the frequency dependence of impedance for a corroding system enables a determination of an appropriate equivalent electrical circuit describing that system. Table 1 shows the transfer functions for resistors, capacitors, and inductors.

TABLE 1 Linear Circuit Elements Commonly Used in Electrochemical Impedance

Circuit Element	Impedance
Resistor	$Z(\omega) = R$
Capacitor	$Z(\omega) = -j/\omega C$
Inductor	$Z(\omega) = j\omega L$

Figure 4 illustrates the equivalent electrical circuit model for an actively corroding metal. The following expression describes the impedance for that system:

$$Z(\omega) = R_s + R_p/(1 + \omega^2 R_p^2 C^2) - j\omega C R_p^2/(1 + \omega^2 R^2 C^2), \quad (29)$$

where:
ω = the frequency of the applied signal where $\omega = 2\pi f$, rad/s;
f = the frequency of the applied signal, Hz (cycles/sec);
R_s = the solution resistance; and
C = the interfacial capacitance, F/cm^2.

The Bode magnitude and phase information of figure 5 and equation (29) show that at very low frequencies,

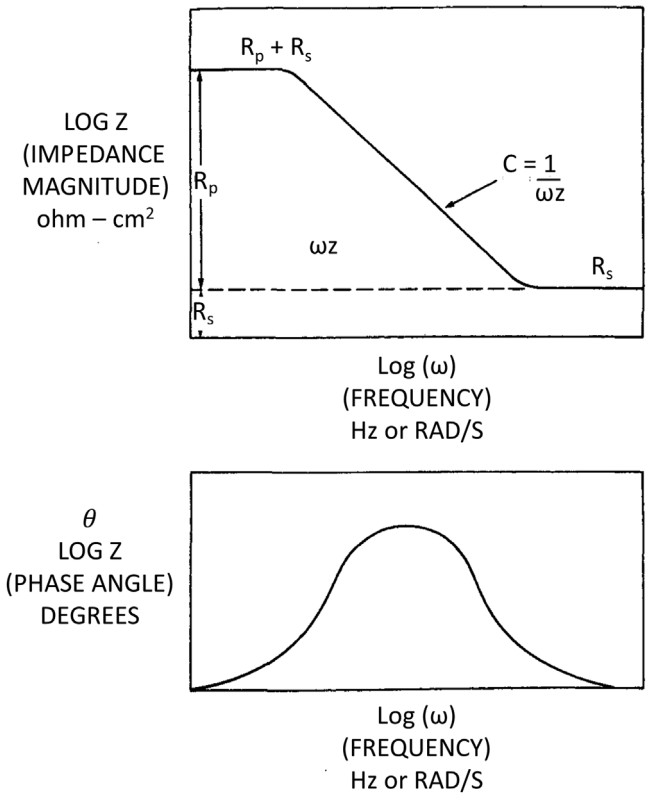
$$Z_{\omega\to 0}(\omega) = R_S + R_p, \quad (30)$$

while at very high frequencies,

$$Z_{\omega\to\infty}(\omega) = R_S. \quad (31)$$

Determination of R_p is attainable in media of high resistivity because R_p can be mathematically separated from R_s by taking the difference between $Z(\omega)$ obtained at low and high ω ($R_p = Z_{\omega\to 0}$ - $Z_{\omega\to\infty}$). Determination of the corrosion rate using equation (25) also requires knowledge of β_a, β_c, and electrode area, A, which are not obtained in the impedance experiment.[44]

FIG. 5 Bode-phase angle and magnitude plots demonstrating the frequency dependence of the electrochemical impedance for the circuit model shown in figure 4.



The minimum applied frequency required to obtain $R_s + R_p$ can be approximated by

$$f_{\min} < f_{bp} = \frac{1}{2\pi C(R_s + R_p)}. \quad (32)$$

where:

f_{bp} = the lower breakpoint frequency approximated by the point on the log | Z(ω) | versus log f plot where the low-frequency plateau dominated by the $R_s + R_p$ and the slope −1 region dominated by the capacitance produce equal values of Z(ω), Hz; and

f_{min} = the minimum required test frequency required according to equation (32), Hz.

Because the magnitudes of C, R_s, and R_p are not known explicitly a priori, prudence dictates that f_{min} be selected as 0.1–0.5 of the estimated f_{bp}. Thus, large values of C, R_s, or R_p dictate that a low f_{min} is required to accurately obtain $R_p + R_s$ at Z(ω)→0. One mHz is typically chosen as a reasonable initial choice of f_{min}, but it is obvious from equation (32) that either a lower frequency may be required or a higher frequency permitted, depending on the circumstances.

Either of the anodic or cathodic half-cell reaction can become mass transport limited and restrict the rate of corrosion at E_{corr}. The presence of diffusion-controlled corrosion processes does not invalidate the EIS method, but this does require extra precaution and a modification to the circuit model shown in figure 4. In this case, the finite diffusional impedance is added in series with the usual charge transfer parallel resistance shown in figure 4. The transfer function for the frequency-dependent finite diffusional impedance, $Z_D(\omega)$, has been described:[45]

$$Z_D(\omega) = R_D\left[\frac{tanh\sqrt{(j\omega s)}}{\sqrt{(j\omega s)}}\right], \quad (33)$$

where:

$s = 1_{eff}^2/D$,

1_{eff} = the actual finite diffusion length, and

D = the diffusivity of the diffusing species that limits the interfacial reaction.

The value of $Z_D(\omega)$ approaches the real component of diffusional resistance, R_D, as ω→0. The frequency required to obtain R_D depends on the value of s. The larger the value of s, such as when l_{eff} is large or D is small, the lower the frequency required. R_p, defined as $[\partial E/\partial Ei_{app}]$ as ω→0, is the sum of the charge transfer–controlled (R_{ct}) and diffusion-controlled (R_D) contributions to the polarization resistance assuming that $R_D + R_{ct} >> R_S$, as follows:

$$R_p = R_{ct} + R_D. \quad (34)$$

A very low frequency or scan rate may be required to obtain R_p defined by equation (34) under circumstances in which reactions are mass transport limited, as indicated by equation (32). Here, a 1_{eff} of 0.1 cm and D = 10^{-5} cm^2/sec requires that a frequency below 0.1 mHz be implemented to obtain R_p from |Z(ω)| at the zero frequency limit. Hence, a common experimental problem in the case of diffusion controlled electrochemical reactions is that extremely low frequency (or scan rates) are required to complete the measurement of R_f. In the case in which R_p is dominated by contributions from mass transport such that equation (33) applies, the Stern approximation of equations (25) and (26) must be modified to account for a Tafel slope for either the anodic or cathodic reaction under diffusion controlled conditions (i.e., β_a or $\beta_C = \infty$). In fact, equation (19) becomes invalid.

Similarly, a frequency above f_{max} must be applied to obtain R_s.

$$f > f_{max} = \frac{1}{2\pi CR_s}, \quad (35)$$

where:

f_{max} = the frequency required such that Z(ω) is dominated by R_s.

Typically, f_{app} must be in the kHz range to determine R_s. These issues equally plague time as well as frequency domain methods for obtaining R_p, because in the time domain measurement, the triangle waveform is simply the Fourier synthesis of a series of sinusoidal signal functions.

The capacitance is also determined from the impedance technique. In many corroding systems, an interfacial capacitance, associated with the electrical double layer, scales linearly with the true electrochemical surface area. An electrochemically based estimate of the surface area may be obtained if the area-specific capacitance is known or determined from the slope of a plot of C versus surface area.[44]

A common issue in the use of impedance-derived capacitance concerns the use of constant phase elements (CPE). The impedance associated with a CPE has been given by the following expression:[46]

$$Z_{CPE}(\omega) = \left(\frac{1}{Y_o(j\omega)^n}\right). \quad (36)$$

Y_0 and n are usually assumed to be frequency-independent parameters. The units for Y_0 are s^n/ohm, and those for capacitance (C) are s/ohm. Hence, in the case of an ideal capacitor or resistor, $n = 1$ or 0, respectively, and either the magnitude of Y_0 equals the magnitude of C with the dimensions s/ohms or $1/Y_0 = R$ (ohms). In the case of $n = 0.5$, an infinite diffusional impedance best describes the constant phase element. At issue is the task of extracting physically meaningful parameters conveyed by the capacitance in the case of impedance data that is best represented in an electrical circuit model by a constant phase element. Examples of such parameters extracted from ideal interfacial capacitance include electrode areas in the case of a double-layer capacitance, surface coverage in the case of an adsorption pseudocapacitance, and dielectric constant or dielectric layer thickness in the case of a coating or oxide with dielectric properties. Other parameters may be extracted from capacitance associated with solid-state impedance experiments, but these are beyond the scope of the present paper. In the case in which $n = 0.8$–0.99, the CPE is often treated as a nonideal capacitance value, and attempts are made to extract physically

meaningful parameters from the CPE data. One equation proposed to convert Y_0 into C follows:[47]

$$C = Y_o(\omega''_{\max})^{n-1}, \quad (37)$$

where:

ω''_{max} = the frequency at which the imaginary component of impedance, Z″, is maximized.

This frequency is independent of n. In an earlier approach, the use of $C = Y_0\ (\omega)^{n-1}V\ \sin(n\pi/2)$ was suggested as a method for extracting capacitance, C, from Y_0, where ω was taken as the frequency at which the phase angle was maximized.[48] This method has the disadvantage that the exact value of ω associated with the phase angle maximum changes with the value of n.

FREQUENCY MODULATION METHODS

Both harmonic and electrochemical frequency modulation (EFM) methods take advantage of nonlinearity in the E-I response of electrochemical interfaces to determine corrosion rate.[49–52] A special application of harmonic methods involves harmonic impedance spectroscopy.[53] The EFM method uses one or more AC voltage perturbations to extract the corrosion rate. The EFM method has been described in the literature[49–52] and recently was reviewed.[54] In the most often used EFM method, a potential perturbation by two sine waves of different frequencies is applied across a corroding metal interface. The E-I behavior of corroding interfaces is typically nonlinear, so that such a potential perturbation in the form of a sine wave at one or more frequencies can result in a current response at the same and at other frequencies. The result of such a potential perturbation is various AC current responses at various frequencies such as zero, harmonic, and intermodulation. The magnitude of these current responses can be used to extract information on the corrosion rate of the electrochemical interface, or, conversely, the reduction-oxidation rate of an interface dominated by redox reactions as well as the Tafel parameters. This is an advantage over linear polarization resistance and EIS methods, which can provide the Z(ω) and, at ω= 0, the polarization resistance of the corroding interface, but that do not uniquely determine Tafel parameters. As such, separate experiments must be used to define Tafel parameters. A special extension of the method involves harmonic impedance spectroscopy in which the harmonic currents are converted to harmonic impedance values at various frequencies through knowledge of the magnitude of the AC perturbation.

In the EFM method, an AC voltage perturbation is applied at two frequencies, ω_1 and ω_2. As an example, the voltage perturbation could be given as follows:

$$\eta = V_0[\sin(\omega_1 t) + \sin(\omega_2 t)], \quad (38)$$

where:

$\eta = E\text{-}E_{corr}$, and

V_0 = the magnitude of the voltage amplitude applied.

Harmonic current responses occur at ω_1, $2\omega_1$, and $3\omega_1$ as well as at ω_1, $2\omega_2$, and $3\omega_2$. Additionally, a current response can be seen at various intermodulation frequencies, such as $2\omega_1 \pm \omega_2$ and $2\omega_2 \pm \omega_1$. Consider the application of this method to a charge transfer–controlled corrosion process with an E-I response that behaves according to equation (19). Under the assumption that $\omega_2 > \omega_1$ and $\beta_a < \beta_C$, the corrosion current density, i_{corr}, and Tafel parameters, b_a (where $b_a = \beta_a/ln\ 10$) and b_c, can be determined from the equations summarized in table 2. The current components at the angular frequency ω_1 or ω_2 can be measured at ω_1 or ω_2. The intermodulation components $\omega_1 \pm \omega_2$ can be determined from the signal response at $\omega_1 + \omega_2$ or ω_1 - ω_2. The method is one of the few that enables extraction of corrosion rate and Tafel parameters directly from a single measurement (see Barnartt[30] and Oldham and Mansfeld[31]). Currently, there are no ASTM standards for this technique.

EN Resistance

EN analysis can provide a parameter called the EN resistance, R_n.[55–61] It is desirable to utilize this parameter in an analogous fashion as the polarization resistance. One electrode configuration that enables such a measurement involves connecting a zero-resistance ammeter (ZRA) between two nominally identical corroding electrodes immersed in the same solution. A third, nominally identical electrode can be immersed in solution and connected to the first two using a high-impedance voltmeter. This electrode serves as a "noisy" psuedoreference electrode. This approach is attractive in field applications because of the

TABLE 2 Governing Equations for Extraction of i_{corr}, as well as b_a and b_c, from Harmonic and Intermodulation Frequency Data[54]

Reaction Type	Governing Equation	Determination of i_{corr}	Determination of Tafel Parameters
Charge transfer control Tafel behavior	Equation (19)	$i_{corr} = \frac{i_{\omega_1,\omega_2}{}^2}{\sqrt[2]{8i_{\omega_1\omega_2}i_{2\omega_2\pm\omega_1} - 3i_{\omega_2\pm\omega_1}{}^2}}$	$b_a = \frac{i_{\omega_1,\omega_2}V_o}{\sqrt[i\omega^2\pm\omega^2]{8i_{\omega_1\omega_2}i_{2\omega_2\pm\omega_1} - 3i_{\omega_2\pm\omega_1}{}^2}}$ Similar expression for b_c
Passive or anodic mass transport control	$i = i_{corr}\left[1 - \exp\left(\frac{-\eta}{b_c}\right)\right]$	$i_{corr} = \frac{i_{\omega_1,\omega_2}{}^2}{2i_{\omega_2\pm\omega_1}}$	$b_c = \frac{i_{\omega_1,\omega_2}}{2i_{\omega_2\pm\omega_1}}V_o$
Cathodic mass transport control	$i = i_{corr}\left[\exp\left(\frac{\eta}{b_a}\right) - 1\right]$	$i_{corr} = \frac{i_{\omega_1,\omega_2}{}^2}{2i_{\omega_2\pm\omega_1}}$	$b_c = \frac{i_{\omega_1,\omega_2}}{2i_{\omega_2\pm\omega_1}}V_o$

Note: $b_a = \beta_a/\ln(10)$, and $b_c = \beta_c/\ln(10)$;
$i_{2\omega_1\pm\omega_2}$ can be evaluated at $i_{2\omega_1+\omega_2}$ or $i_{2\omega_1-\omega_2}$;
$i_{\omega_1\pm\omega_2}$ can be evaluated at $i_{\omega_1+\omega_2}$ or $i_{\omega_1-\omega_2}$; and
i_{ω_1,ω_2} can be evaluated at i_{ω_1} or i_{ω_2}.

more rugged nature of the metallic electrode compared with the laboratory electrodes, but this complicates the analysis because two uncorrelated potential sources (i.e., from the couple and the pseudoreference) are measured in the collection of potential noise, V_n. Because $V_{n(meas)} = (V_{n(couple)} + V_{n(pseudo\text{-}ref)})^{1/2}$, $V_{n(meas)}$ must be divided by 2 to yield $V_{n(couple)}$.[62] Another alternative is a four-electrode arrangement in which the first pair is coupled through a ZRA to monitor current, and the second pair is connected with a high-impedance voltmeter to sample an uncorrelated $V_{n(couple)}$. Alternatively, a less noisy, conventional reference electrode may be utilized in the three-electrode arrangement. In this case, $V_{n(meas)}$ and $I_{n(meas)}$ are correlated. The reference electrode noise can be separately defined as the electrochemical voltage noise between two nominally identical reference electrodes.[63] If the reference electrode noise is low, then the correction factor of 2 is not needed. In either case, the third electrode (reference electrode) is connected to the first two through the high-impedance voltmeter. These arrangements enable simultaneous recording of the galvanic current with time and the galvanic couple potential versus time. The standard deviation of the voltage noise divided by the standard deviation of the current noise has been proposed to yield a statistical parameter called the noise resistance R_n.[55–62,64] Analysis of simulated noise data has led to the conclusion that the ratio of the standard deviations of the current and voltage noises, measured between two identical electrodes, can be normalized by surface area by multiplying by the square root of $A_v A_i$, as follows:[61]

$$R_n(ohm - cm^2) = \left[\frac{\sigma_v(meas)}{\sigma_I(meas)}\right]\sqrt{A_V A_I}, \tag{39}$$

where:

$\sigma_{v(meas)}$ = the standard deviation of the voltage noise;
$\sigma_{I(meas)}$ = the standard deviation of the current noise; and
A_v and A, = the surface areas of the corroding electrodes used for voltage and current measurement, respectively.

Correlations between this parameter and conventionally determined polarization resistance, as well as mass loss–based corrosion rates, have been obtained.[56,62] Unfortunately, experimental confirmation of the area normalization factor has not been extensively performed. Recall that in the case of a polarization resistance determined from E-i_{app} data or EIS data at the zero frequency limit, measured resistance can be multiplied by the electrode area and will yield the same area-normalized polarization resistance over a broad range of electrode areas.

Moreover, the correlation has lacked a rigorous fundamental foundation for correlating R_n with corrosion rate, despite the intuitive connection between σ_v and σ_I given by the proportionality factor R_n. The surface of one freely corroding electrode could be divided into areas that experience fluctuations in interfacial resistance that produce changes in anodic and cathodic half-cell reaction rates in any one patch. The electrode potential must then change in each patch to drive the half-cell reactions, such that the sum of all the anodic half-cell currents from all patches equals the sum of all cathodic half-cell currents, regardless of whether the source of cathodic half-cell current is from capacitive discharge or electrochemical reaction.[60] Some global change in potential also occurs on the electrode. If the first electrode is now connected to a second electrode, whose interfacial properties and global electrode potential do not change on their own at the same instant in time and by the same degree as on the first electrode, then a galvanic cell is momentarily created. This induces a further difference in anodic and cathodic half-cell currents on the first electrode. Current now flows between the first and second electrode, such that the sum of anodic and cathodic half-cell currents over all patches on both electrodes is equal. When the interfacial resistances return to normal values over all patches, the potential difference between the two electrodes is eliminated and so is the measurable current between the two electrodes. Bertocci[60] and Bertocci and Huet[61] argued that the external current fluctuation measured between two identical electrodes is identical to the fluctuation in one electrode.

Theoretical relationships establishing the connection between R_n and R_p have been sought by several researchers,[61,65–68] but their validity has been questioned. A great concern has been that the largest current peaks would occur during the most rapid voltage fluctuations, because the electrode interface contains a capacitance through which current can be shorted.[60,61] Thus, when voltage fluctuations are rapid, the measured noise current will be shorted through the interfacial capacitance. This is assuming a simple electrical equivalent circuit model consisting of a two parallel resistor-capacitor network describing the interface for each electrode connected in series through R_s. This situation would lead to the occurrence of the lowest impedance between the two electrodes during the most rapid voltage fluctuations. This, in turn, would produce the greatest current fluctuations. The theoretical maximum measured current would be given by the voltage fluctuation divided by R_s. The outcome would be a statistical noise resistance parameter that is proportional to, or heavily influenced by, higher frequency data. Indeed, R_n was found to equal an absolute impedance at some frequency that depended on the frequency of the voltage fluctuations and the resistor-capacitor (RC) time constant of the electrode interface in one study of simulated noise.[60] Unfortunately, an R_n value obtained at high frequency would be smaller in magnitude than the R_p obtained at the zero frequency limit. Hence, it would not represent the desired zero frequency limit interfacial resistance, R_p. Indeed, such underestimations in the true value of R_p have been observed experimentally.[62,64]

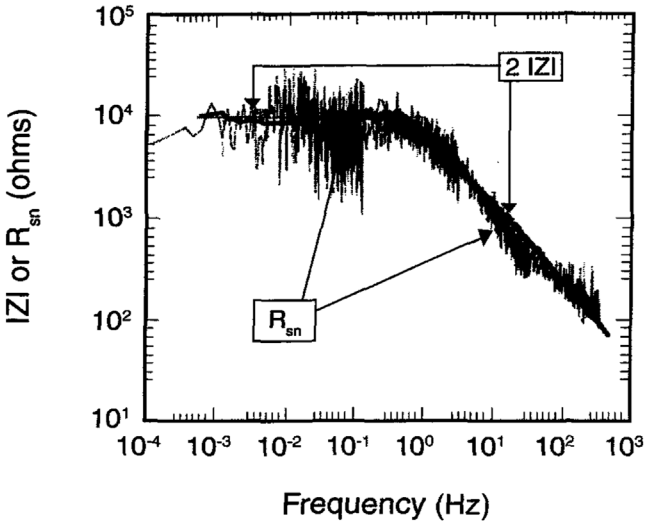
Recently, a more rigorous theoretical and experimental analysis has been made comparing the spectral noise resistance obtained at each frequency with both the polarization resistance obtained from the zero frequency limit of impedance data $|Z(\omega = 0)|$, as well as the frequency-dependent impedance of wo electrodes.[69–72] The spectral noise resistance $R_{sn}(\omega)$ was determined by taking the square root of power spectral density of the voltage noise $(V^2/Hz)^{1/2}$ and dividing it by the square root of power spectral density of the current noise $(A^2/Hz)^{1/2}$ at each frequency using the same two-electrode arrangement as discussed earlier.[72]

$$R_{sn}(\omega) = \frac{\sqrt{(V_{PSD})}}{\sqrt{(I_{PSD})}}, \tag{40}$$

where:
$R_{sn}(\omega)$ = proportional to the magnitude of the cell impedance, $|Z(\omega)|$ in the two electrode arrangement.[72]

The proportionality factor is unity in the case of identically sized electrodes in a two electrode cell with identical impedances and a noiseless reference electrode.[72] Therefore, in the theoretical case of identical electrode impedances (i.e., where R_s is negligible), the spectral noise resistance at the zero frequency limit is equal to the interfacial impedance at the zero frequency limit $|Z(\omega = 0)|$. In this case, $R_{sn}(0) = R_p$. Figure 6 illustrates data for identical Fe electrodes in 1 M aqueous sodium sulfate (Na_2SO_4) solution with an iron reference electrode. Here $R_{sn}(\omega) = \sqrt{3}\,|Z(\omega)|$ because of the noisy RE. Thus, $2|Z(\omega)|$ and $R_{sn}(\omega)$ appear to be similar. For a corroding system, $|Z(\omega = 0)|$ equals R_p and $R_{sn}(0) = R_p$. Even R_n may equal $R_{sn}(\omega = 0) = |Z(\omega = 0)| = R_p$ if $|Z(\omega)|$ equals R_p in the frequency regime dominating the R_n value. The frequency range dominating the R_n value is determined by several factors, but this statement is more likely to be true if $|Z(\omega)|$ and $R_{sn}(\omega)$ both exhibit long low-frequency plateaus over a broad frequency range that encompasses the f_{min} and f_s utilized in the R_n measurement. Here f_{min} is given by the total sampling time, T, where $f_{min} = 1/T$ and f_s equals the data sampling rate. R_n typically varies with f_s and underestimates $|Z(\omega = 0)|$. Unfortunately, $R_{sn}(\omega \rightarrow 0)$ does not equal R_p in the zero frequency limit under many other conditions, such as when $\log (R_s/R_p) > 0$ or in the case of very noisy reference electrodes.[72] Moreover, $R_{sn}(\omega)$ can be dominated by the properties of the high-impedance electrode in the case of dissimilar electrode impedances that are equally noisy, but this is not always the case. For instance, the low-impedance electrode in a two-electrode cell with a third reference electrode can be sensed by $R_{sn}(\omega)$ if the higher impedance electrode is much noisier than the low-impedance electrode.[72] Recent attempts have been made to address circumstances in which $R_{sn}(\omega)$ lies in between $|Z(\omega)|_1$ and $|Z(\omega)|_2$ representing the high- and low-impedance electrodes. Methods have been suggested for sensing the current fluctuations on both electrodes.[73] The reader is referred to these articles for further information.

FIG. 6 $R_{sn}(\omega)$ versus frequency for iron in 1 M Na_2SO_4 at pH 4 with a "noisy" iron reference electrode compared with two times the impedance $|Z(\omega)|$ versus frequency using the EIS method. Impedance measurements were performed in a two electrode cell with two iron electrodes to produce $2|Z(\omega)|$. The value of $R_{sn}(\omega)$ calculated is equal to $\sqrt{3}\,|Z(\omega)|$ for the case of two iron electrodes coupled through a ZRA and a third iron electrode as reference electrode.[72]



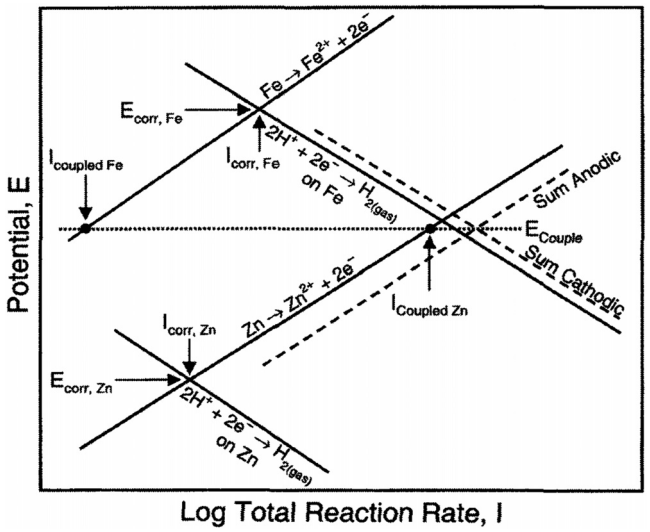
ELECTROCHEMICAL METHODS FOR THE STUDY OF GALVANIC CORROSION

Galvanic corrosion is defined and described in Section IV the "Types of Corrosion" section.

Methods Based on Mixed-Potential Theory

The thermodynamic tendency for galvanic corrosion may be determined from the electromotive series[5] or from the construction of a galvanic series as discussed in ASTM G82, *Standard Guide for Development and Use of a Galvanic Series for Predicting Galvanic Corrosion Performance*. Galvanic corrosion rates can be determined from mixed-potential theory as schematically illustrated in figure 7. In the case of bimetal or multimetal galvanic attack in which two or more metals are electrically in contact with one another, there is in theory a minimum of two cathodic and two anodic reactions. One of each of these reactions is occurring on each metal. In this case, the more noble of the two metals is cathodically polarized, and its anodic reaction rate will thus be suppressed. Conversely, the less noble or anodic material is anodically polarized and the anodic reaction rate is accelerated. The mixed potential (the galvanic couple potential,

FIG. 7 Potential-current relationships for the case of a galvanic couple between two corroding metals. Steel is the more noble metal, and zinc is the less noble metal.[5] The corrosion rate of zinc is increased significantly when coupled, whereas the corrosion rate of steel is decreased.



E_{couple}) of the galvanic couple and the resulting galvanic current can be uniquely determined from the sums of all of the individual anodic and cathodic currents obtained for each material at each potential when the following condition is met:

$$\sum i_a A_a = \sum i_c A_c \text{ at } E_{couple}, \quad (41)$$

where:
i_a, i_c = the anodic and cathodic current densities, uA/cm^2; and
A_a, A_c= the anodic and cathodic areas, cm^2.

The galvanic couple potential is defined by the potential where the sum of the anodic currents equals the sum of the cathodic currents for all reactions on all of the metals in the couple. The galvanic couple potential can be determined either by direct measurement with a reference electrode or from polarization data if:

1. polarization data are available for each material in the galvanic couple,
2. the area of each metal is known, and
3. the current distribution is uniform.

Once E_{couple} is determined, the galvanic corrosion rate may be estimated for the metal of interest in the couple if a relationship such as given in equation (19) is known for that metal. In simple bimetal cases, direct superposition of polarization data (corrected for wetted surface area) can yield E_{couple} and the galvanic corrosion rate.[74] Because applied currents instead of true anodic or cathodic currents are measured in any polarization experiment, the E-log(I) superposition technique will introduce the least error when the cathodic reduction reaction rate on the anode is negligible and the anodic oxidation reaction rate on the cathode is negligible at the galvanic couple potential. Obviously, when the OCPs of the anode and cathode are similar, error is more likely. Fortunately, galvanic corrosion may be less significant in these cases. In addition, special care must be taken in the procedures used to assess the polarization responses,[74] especially if time effects are to be taken into consideration when evaluating long-term galvanic corrosion behavior.

Direct Measurement of Galvanic-Corrosion Rates

A more straightforward procedure involves immersing the two dissimilar metals in an electrolyte and electrically connecting the materials together using a ZRA to measure the resulting galvanic current.[9,75,76] In this method, the galvanic current is directly determined as a function of time. The galvanic corrosion rate so determined is the additional corrosion created with the couple and will not equal the true corrosion rate. This is given by the sum of the galvanic corrosion rate and the corrosion rate under freely corroding conditions, unless the latter is negligible. Recall that the corrosion rate of the uncoupled anode is undetermined by this method, because an equal cathodic reaction rate is occurring on the same surface. A reference electrode connected to the galvanic couple can be used to determine the galvanic couple potential. ASTM standards do not exist for direct measurement of galvanic corrosion or scanning potential probe methods.

Potential Probe Methods

Potential probe methods may be used to determine and map the local ionic currents associated with galvanic corrosion cells between dissimilar metals or heterogeneities on complex alloy surfaces.[75–80] In the most straightforward application, the local potential is mapped over a planar electrode oriented in the x-y plane to give an indication of local current. The basic concept is that the ionic current density in three dimensions can be mapped by either scanning an array of reference electrodes or by vibrating a single electrode. The following equation expresses the orthogonal ionic current flow in terms of solution conductivity and the gradient in potential in the solution above the galvanic couple,

$$i = -\kappa(\nabla E), \quad (42)$$

where:
κ = the solution conductivity; and
$\nabla E = \delta_1\, dE/dx + \delta_2\, dE/dy + \delta_3\, dE/dz$, where x, y, and z, define axes in a coordinate system and δ_1 are unity vectors in the x, y, and z directions.

The advantage of the vibrating technique is that minor differences between the reference potential of separate electrodes is eliminated by using a single vibrating reference electrode. The component of the ionic current density flowing perpendicular to lines of iso-potential in solution is measured. Such lines are generated because of the galvanic couple and the established potential gradient. Therefore, a map of local current can be constructed by scanning over a planar electrode in the x-y plane, where z is the vertical distance in the solution above the electrode. Locations of high local current imply significant galvanic interactions.

SCANNING VIBRATING ELECTRODE TECHNIQUE

The scanning vibrating electrode technique (SVET) has been used widely for the *in situ* study of localized corrosion phenomena in full immersion conditions.[81–94] A full description of SVET is given in chapter 16, which focuses on its use for the study of galvanic corrosion. In brief, SVET records the drop in potential generated by ionic currents in solution originating from a corrosion cell. The technique produces a series of current density distribution maps that provide the size, shape, and location of anodic (positive) current and cathodic (negative) current for a specific area. The nondestructive nature of the test enables repeat scanning of the same corroding surface and a series of time-resolved data is collected, illustrating the evolution of electrochemical processes. Area-averaged integration of all the positive values and all of the negative values enables semiquantitative measurement of the respective anodic and cathodic corrosion activity occurring as a function of time. This technique is particularly useful for studying galvanic corrosion because the current polarity and current intensity can be mapped across two dissimilar metals in electrical contact.[82,95–97] This is of great interest for the study of sacrificial alloys in which self-corrosion of the anode can be isolated and quantified.[98] The spatial resolution is largely controlled by three key factors: the probe-tip diameter, the scan

height, and the number of scanned points per area.[99] Typical probe-tip diameter sizes range from 5 μm to 125 μm depending on the manufacturer.[98,100] Increasing the number of points increases the scan resolution but also the total scan time and, for a metal with a high corrosion rate, certain information can be missed if the scan rate is too slow. The SVET favors the study of localized corrosion occurring because of microgalvanic coupling of phases in which anodes and cathodes are separated by a distance much greater than the plane of scan, which is typically 100 μm. This is demonstrated in the schematic given in figure 8*A*, which illustrates the movement of the vibrating probe through the lines of ionic flux originating from a surface feature, such as an anodic intermetallic-particle coupled to the cathodic matrix phase. A limitation of this technique is poor efficiency, observed when studying uniform corrosion in which the separation distance of highly interspersed anodes and cathodes is much smaller than the plane of scan. The ionic flux lines occur well below the plane of scan and, therefore, are undetected by the vibrating probe.[87,101]

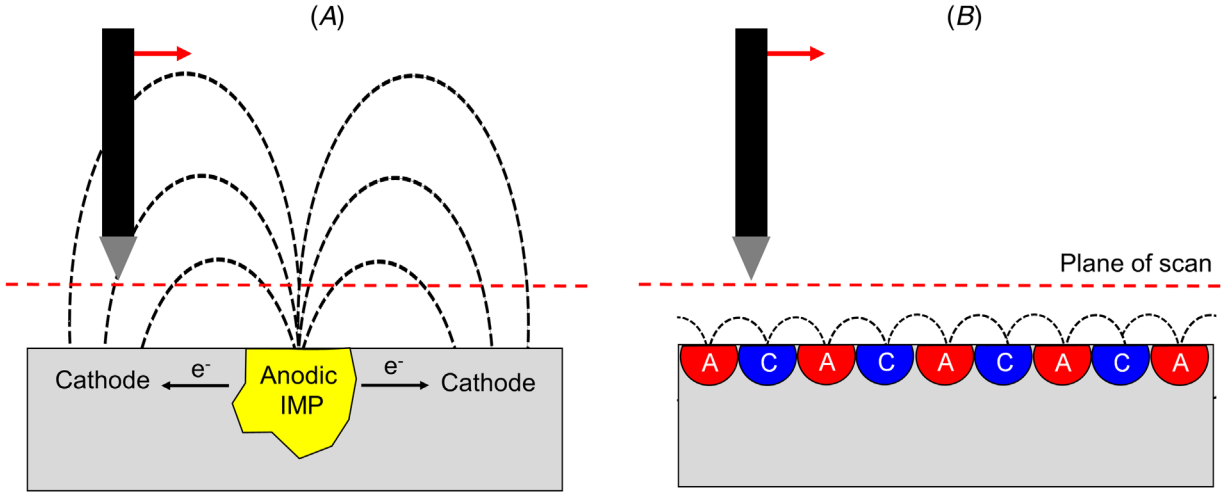
SCANNING ELECTROCHEMICAL MICROSCOPY

Scanning electrochemical microscopy (SECM) is another electrochemical local probe technique that enables time-resolved mapping,[102–104] in this case, of the heterogeneous reactions across a freely corroding surface. The technique has been used extensively for the study of localized corrosion,[105–107] galvanic corrosion of dissimilar metals/metal alloys,[82,108–110] the study of coatings for corrosion protection,[96,111–113] and hydrogen detection.[114–116] SECM is often used as a complementary technique to the SVET as it enables much higher resolution (i.e., on the micrometer length-scale). Payne, Stephens, and Mauzeroll provided a summary of the capabilities of different techniques compared with SECM in a 2017 review article.[117]

SECM operates by scanning a nonvibrating electrochemical mapping micro-electrode (ME) tip over a specimen surface in full immersion conditions. The reaction rate of a redox mediator is used to indirectly sense the local reactivity of the substrate. The mediator typically is used as a supportive reactant added to the electrolyte solution and careful selection can enable control over the specific reactions probed in a particular environment,[109,110,118,119] which will be discussed in more detail. The operation of SECM requires two cells, controlled by a biopotentiostat, in which the ME or the specimen surface act as the working electrodes that share a counter and reference electrode.[120] Electrochemical activity in the solution directly above the corroding substrate is monitored by the oxidation or reduction of dissolved reactants. For example, for the study of galvanic coupling, the typical approach is to monitor the concentration of dissolved oxygen on the cathodic areas.[109] A comprehensive list of metals and alloys studied with each SECM mode and the most common redox mediator and ion of interest is given in a recent publication.[117]

The SECM mode of operation can be adjusted to suit the particular application. The feedback mode is the most commonly used and is particularly useful for studying the corrosion protection of coatings.[96,111,121,122] It can be employed over both conducting and insulating surfaces to enable the distinction between (1) areas of a coating that are defective, (2) areas where reactions at the exposed substrate are detected, and (3) regions where the coating is intact. This allows coating deterioration and self-healing effects to be monitored, as a function of time. In the feedback mode, the ME tip is used as both the current detector and the source.[123,124] A redox mediator, in its reduced form, is added to the electrolyte solution. The SECM measures the current at the ME tip while simultaneously applying a positive potential (to the ME tip) to oxidize the mediator species in the bulk. The rate of this oxidation reaction is governed by the diffusion of the reduced species from the bulk solution to the ME tip. When the tip is positioned above an insulating surface, such as

FIG. 8 Schematic diagrams showing detection efficiency where (*A*) shows an anode-cathode separation distance greater than the scan height where a local anode is surrounded by a distributed cathode and (*B*) shows uniform corrosion with an anode-cathode separation distance less than the scan height.



an intact polymer coating, replenishment of the reduced species at the surface cannot occur and the diffusion of the reduced species from the bulk to the tip will be hindered by the presence of the insulating specimen surface.[125] In such cases, the measured current decreases because of the depleted mediator species at the surface of the substrate, and the SECM will operate in negative feedback mode, as illustrated in the schematic given in figure 9*A*. In the presence of a conducting substrate, the reduced species will be readily replenished at the surface, maintaining a steady-state measured current, and the SECM will operate in positive feedback mode (fig. 9*B*). The redox competition mode is another commonly used mode for corrosion studies and typically is used for the study of galvanic corrosion because, as described earlier, it can be used to monitor the concentration of dissolved oxygen on the cathodic areas.[109] In brief, a specific redox mediator is selected that reacts at both the ME and the specimen surface. When the ME is brought close to the surface, from far away, the ME competes with the substrate for the reduction (or oxidation) of the mediator and the current measured by the ME decreases.

ELECTROCHEMICAL METHODS FOR THE STUDY OF PASSIVITY AND LOCALIZED CORROSION

Pitting and crevice corrosion are associated with the breakdown of passivity.[126] Electrochemical tests for evaluating the susceptibility of a material to pitting and to crevice corrosion include potentiodynamic, potentiostatic, scratch potentiostatic, potentiostaircase, tribo-ellipsometric methods, pit-propagation rate curves, galvanostatic, and EN measurements.[126–128]

Cyclic Potentiodynamic Polarization Methods to Determine E_{bd} and E_{prot}

ASTM G61, *Standard Test Method for Conducting Cyclic Potentiodynamic Polarization Measurements for Localized Corrosion Susceptibility of Iron-, Nickel-, or Cobalt-Based Alloys*, describes a procedure for conducting cyclic potentiodynamic polarization measurements to determine relative susceptibility to localized corrosion. The method is designed for use with iron- or nickel-based alloys in chloride environments. In this experiment, a cyclic anodic polarization scan is performed at a fixed voltage scan rate. Figure 10*A* shows a schematic of the cyclic potentiodynamic method. Particular attention is focused on two features of cyclic polarization behavior (fig. 10*A*). The first is the potential at which the anodic current increases significantly with applied potential (the breakdown potential, E_{bd}). In general, the more noble this potential, obtained at a fixed scan rate in this test, the less susceptible the alloy is to the initiation of localized attack. The second feature of great interest is the potential at which the hysteresis loop is completed during reverse polarization scan after localized corrosion propagation. This potential is often taken as the repassivation potential or protection potential, E_{prot}. In general, once initiated, localized corrosion sites can propagate only at some potential more positive than the potential at which the hysteresis loop is completed (when determined at a fixed scan rate). In other words, repassivation will occur at more negative potentials, even after localized corrosion initiation. Therefore, the more positive the potential at which the hysteresis loop is completed, the less likely that localized corrosion will propagate. Additionally, the difference in potential between E_{corr} and E_{prot} (E_{prot} - E_{corr}) is often taken to indicate relative resistance to local corrosion. ASTM G61 illustrates cyclic polarization behavior for Hastelloy C-276 and 304 stainless steel in 3.5 wt% sodium chloride solution. Based on this criterion, it is evident that Hastelloy C-276 is more resistant to localized corrosion in this environment than AISI 304 stainless steel.

FIG. 9 Schematic diagrams of SECM feedback mode demonstrating (*A*) the negative feedback mode above an insulating surface (intact coating), (*B*) the positive feedback mode above a conducting surface (damaged coating), and (*C*) the redox competition mode used for galvanic corrosion.

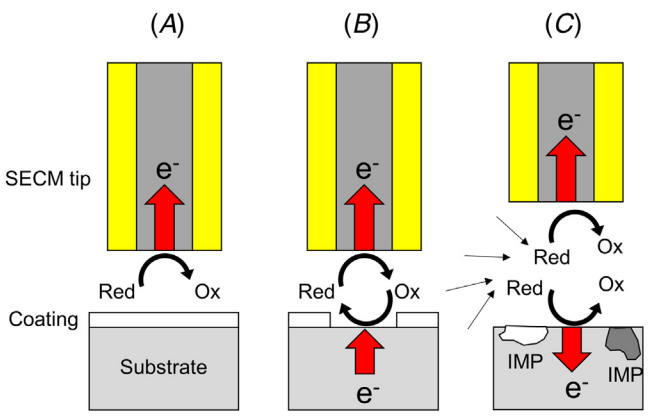
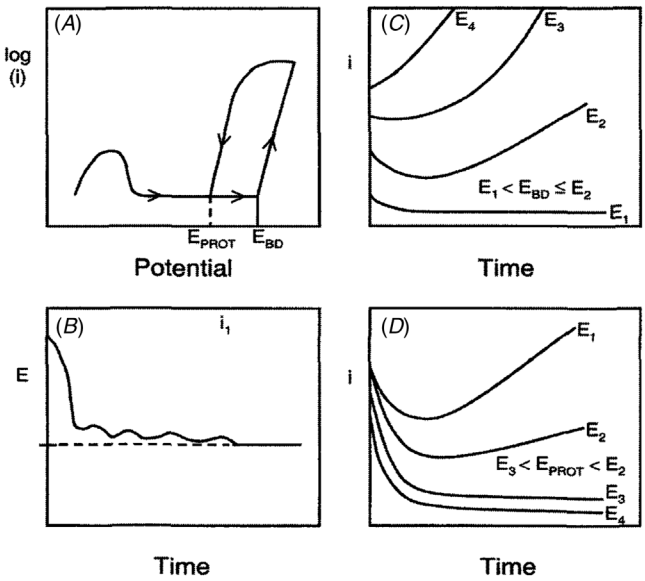


FIG. 10 Schematic representations of experimental data for (*A*) a cyclic potentiodynamic polarization curve; (*B*) galvanostatic potential-time curve for a material; (*C*) potentiostatic current-time curve for a previously passivated surface, which pits at $E_1 < E_{BD} < E_2$; and (*D*) potentiostatic current-time curve for active surface. The protection potential is found as $E_3 < E_{PROT} < E_2$.[125]



Complications with Cyclic Potentiodynamic Polarization Methods

Although the cyclic method is a reasonable method for screening variations in alloy composition and environments, the cyclic potentiodynamic polarization method has been found to have a number of shortcomings.[126–131] One major problem concerns the effect of the potential scan rate. The values of both E_{bd} and E_{prot} are a strong function of the manner in which the tests are performed, particularly the potential scan rate employed. Experimental values of E_{bd} are linked to the induction time required for pitting.[132] Another complication arises from allowing too much pitting propagation to occur before reversing the scan direction. This either alters the localized chemistry in pits, affects pit depth, or both. Pit depth alters the diffusion length associated with the dilution of pit chemistry necessary for repassivation. This factor affects the polarization behavior after the reversal in the direction of scanning and influences E_{prot}. From an engineering standpoint, metal surfaces held at potentials below the repassivation potential of the deepest pits should be safe against stable pit propagation. That is to say, stable pits should not propagate. It has been found that E_{bd} observed after potentiostatic holds, or the slowest scan rates, approaches the protection potential found after minimal pit growth when pits are small.[131] This suggests the existence of a single critical potential, E_c, for pit initiation and growth in the absence of crevices or other occluded sites.[131] If the potential can be maintained below E_c, pitting does not occur.

Potentiostatic and Galvanostatic Methods for Localized Corrosion

The shortcomings of the cyclic potentiodynamic polarization method have become the basis for several other electrochemical techniques. Other methods are schematically illustrated in figure 10. In the galvanostatic or galvanostaircase technique (fig. 10*B*), potential is measured versus time at various constant applied currents that are incrementally increased in steps, then reversed and decreased. In the case of passive materials, a potential rise during galvanostatic testing indicates passive film growth, while a decline indicates breakdown and growth of local corrosion sites. In the galvanostaircase technique, the current is step increased. Potential measurements are made until the time rate of change in potential approaches zero. These forward and reverse potential-current density data are extrapolated to the zero current density to obtain E_{bd} and E_{prot}. The technique is described by ASTM G100, *Standard Test Method of Conducting Cyclic Galvanostaircase Polarization*, as a test method for aluminum (Al) alloys. Potentiostatic methods can overcome the inherent problems involving scan rate. A more conservative estimate of E_{bd} can be obtained by polarizing individual samples for long periods of time at potentials above and below the values of E_{prot} and E_{bd} previously determined from the potentiodynamic method (fig. 10*C*). Eventual initiation is indicated by a current increase. In another approach (fig. 10*D*), initiation of pits is intentionally induced by applying a "stimulation" potential well above E_{bd} and then quickly shifting to a preselected potential below that value. If this second applied potential is above E_{prot}, propagation of the existing pits will continue and the current will increase. At potentials less than E_{prot}, however, the pits eventually will repassivate and the current subsequently will decrease with time. The critical potential for pitting is defined as the most noble potential at which pits repassivate after the stimulation step. This approach is covered in ASTM F746, *Standard Test Method for Pitting or Crevice Corrosion of Metallic Surgical Implant Materials*.

Determination of E_{prot} by Potential Step-down or Scan-down Methods

As stated earlier, E_{bd} and E_{prot} often depend strongly on the method by which they are determined and, therefore, do not uniquely define intrinsic material properties. The E_{prot} values determined from the scanning method can be complicated by scan rate, pit size or depth, vertex potential/current, polarization curve shape, and specimen geometry.[133,134] Investigators have found more consistent E_{prot} values after a critical charge has passed, whereas others report a single critical potential.[131] Often this potential is difficult to choose from E-I data and has been taken at various points on the reverse scan of a cyclic potentiodynamic polarization curve.[134,135]

A method is needed for determination of E_{prot} that defines a conservative value of this potential that likely reflects a true pit or crevice repassivation potential. Tsujikawa has developed a method for determination of E_{prot} from previously grown pits and crevices.[136,137] This method and its variations have been used successfully by several research groups and associates the critical potential for repassivation E_{prot} with the need to grow local corrosion sites to a critical minimum size.[138] The method is an enhancement of the determination of E_{prot}, from potentiodynamic E-I scans that involve scan reversal to the point at which pits are repassivated. In the potential step-down method, the potential is first set at a high enough value to induce and grow stable pits to the specified size. The potential can then be stepped down or scanned downward, while the pit propagation current is recorded. Subsequently, the potential may be held after a pit has been initiated to determine the time until repassivation.[139] Moreover, long potential holds at selected applied potentials enable confirmation of a true repassivation potential, often indicated by an abrupt decrease in current density at the time when the chemical conditions favoring pit stability (often expressed as some fraction of the salt saturation concentration) are no longer maintained. Abrupt transitions in finite repassivation time toward infinity with increasing hold potential may indicate that conditions favorable to pit growth are sustained. Another benefit of determining E_{prot} from controlled growth of pits and crevices is that the repassivation potential can be determined from pits of preselected sizes that can be controlled by the duration of the potential holds. The method has been applied successfully to nickel-base alloys, stainless steels, and Al-base alloys, and is being standardized by the committee for Japanese Industrial Standards. When a one-dimensional pit or pencil electrode is tested, the pit propagation kinetics can be recorded from a single pit.[140] Whether pit growth is ohmic, mass transport, or charge transfer controlled also may be determined. Moreover, the effects of various material and solution parameters (e.g., flow rate, conductivity, and solution composition) on pit propagation rates can be determined.

The Scratch-Repassivation Method for Localized Corrosion

An additional potentiostatic technique to be mentioned in the area of localized corrosion involves the scratch method.[141] In this method, the alloy surface is scratched while being held at a constant potential and the current is measured as a function of time. The potential dependencies of the induction time and the repassivation time are determined by monitoring the current change over a range of different potentials. This is illustrated in figure 11. From this information the critical pitting potential, E_c, thought to be more negative than E_{bd} determined by potentiodynamic scan, can be determined. Other methods of studying localized corrosion are also available.[126] An ASTM standard exists for the critical pitting temperature measurement method under the designation ASTM G150, *Standard Test Method for Electrochemical Critical Pitting Temperature Testing of Stainless Steels and Related Alloys*.

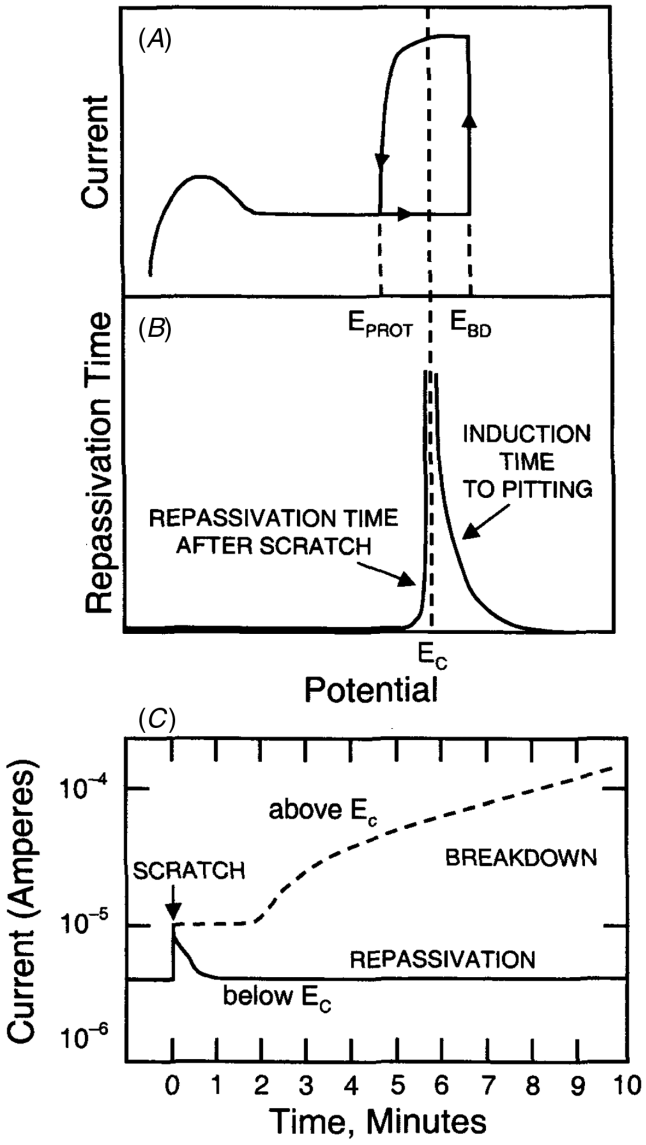


FIG. 11 (*A*) E-log (I) curve showing location of E_{bd} and E_{prot}. (*B*) Time versus applied potential plot from scratch test illustrating a possible location of the critical potential, E_c, as it relates to the induction time and the repassivation time.[125] (*C*) Current versus time plot for a scratched specimen when scratched above and below E_c.

STATISTICAL DISTRIBUTIONS IN CRITICAL POTENTIALS

E_{bd} is typically observed to be a significantly "statistically distributed" property compared with the repassivation potential. This often is observed when critical potentials are determined by potentiodynamic scanning, but also can be observed during potentiostatic tests in which the pit incubation time and subsequent survival probabilities also are seen to be distributed. E_{prot} distributions are often attributed to distributions in pit size. However, E_{prot} is not distributed when pits are uniformly large[142] and may not depend on the depth of corrosion damage at all during crevice corrosion when a crevice former controls mass transport.[143] Statistical distributions in pitting potentials have been observed for AISI 304,[144] Fe-Cr-Z (where x = Nb, Mo, or Ti) alloys,[145] AISI 316,[146] Ti,[147] high purity Al,[148] AA 2024-T3,[149] and amorphous Al-base alloys.[150] These statistical distributions imply that significant variations exist when a number of specimens are tested under identical conditions. These distributions have been attributed to the stochastic nature of pitting,[146] distributions in oxide film cation vacancy transport properties,[151] the effects of potential on the nature of the eligible sites for the metastable pit nucleation process,[144] and the population of fatal flaws or pit-initiating defects on an electrode surface.[152] The possibility that oxide defects at densities exceeding millions of sites/cm^3 produces specimen-to-specimen variations appears unlikely for specimens with surface areas of the order of cm^2. It appears to be more reasonable to expect that sample-to-sample variations, instead, are associated with distributions in the population of micrometer scale defects, such as sulfide inclusions in stainless steel[153] and constituent particles in Al alloys[152] that control the density of pit nucleation sites and produce micropit to micropit variations in growth rates and diffusive transport characteristics (e.g., D_{eff}, pit shape) for a large population of metastable pits grown at a single potential. A statistical distribution of the product $i_{pit} * r_{pit}$ (where i_{pit} is the pit current density and r is pit radius) was observed for a large population of pits at a fixed potential in high purity Al.[148] This product is linearly related to the acid pit chemistry. Although not rigorously proven, it is reasonable to argue that a slightly slower rate of pit transport or slightly larger $i_{pit} * r_{pit}$ product for a given pit might lead to pit stabilization through achievement of the critical acid pit chemistry at different applied potentials on an electrode with a population of pits sites. Moreover, such behavior is likely controlled by micrometer scale defects spaced at tens of micrometer lateral separation distances across planar electrode surfaces. Investigators seeking information on critical potentials for engineering use should consider appropriate specimen sizes relative to critical defect densities and spacings. No ASTM standards address these issues. However, the sizes of test specimens recommended in many ASTM standards are conservatively large so as to include many possible pit sites.

EN Methods

EN methods are used increasingly as a nondestructive tool for evaluating susceptibility to localized corrosion as well as stress-corrosion cracking (SCC), particularly in field or process plant applications.[61,154–158] EN is appealing because it may be conducted at open circuit without perturbing the corroding system. Currently, however, no consensus exists as to the most appropriate test procedure or analysis method, or how well results correlate with coupon exposures. The origins of EN current and potential signals are discussed in more detail in Chapter 1. The transient development of bare metal at newly formed pit or cracking sites as a result of temporary propagation and repassivation can result in potential noise (open-circuit EN), current noise (potentiostatic EN), or both. In the latter case, the current noise is measured with a ZRA used to monitor a galvanic couple consisting of two identical electrodes, while the potential noise comes from the reference electrode (or third metallic electrode) monitoring the couple potential. The noise signal, hereafter referred to as a potential or current time record, is caused by the galvanic couple formed between the very small anode sites corroding at current densities (c.d.) approaching 10 A/cm^2 in pitting corrosion and the much larger remaining cathode surface operating at lower cathodic c.d. (e.g., 10 uA/cm^2). Regarding pitting phenomena, a negative shift in measured potential is observed (OCP and galvanic couple EN), an increase in current is observed for potentiostatic EN, and current fluctuations of either polarity are observed for galvanic couple EN.

Several analysis methods exist, including electrochemical,[159] statistical,[61,158] spectral,[154–157] and autocorrelation.[156] Some of the approaches for determination of spectral noise resistance during uniform corrosion are discussed in the section on polarization resistance. Electrochemical analysis may enable the determination of pit sizes from the charge associated with each pitting event,[148] or from attempting to determine pit current densities. Statistical analyses include determining the root mean square (rms), variance, and standard deviations of the EN voltage or current time records, as well as a noise resistance, R_N, taken as the ratio of the rms or standard deviation of the potential and current time records acquired over various periods of time.[158] Spectral analysis consists of Fourier transformation of EN data acquired in the time domain to create a power spectral density plot.[61,156,157,160] Qualitative assessment of the benefits of inhibitors, or the effects of process stream variations are made possible by comparing statistical or spectral results. Quantitative analysis and predictive capability still require further development.

Coupled Multi-Electrode Arrays

Coupled multi-electrode arrays (CMEA) enable the real-time differentiation of local contributions to net anodic and cathodic currents taking place on an electrode surface on a spatially resolved scale.[161,162] This is of particular interest for engineering components composed of dissimilar materials and complex geometries and service conditions. As such, CMEAs can be designed to satisfy specific corrosion problems that replicate real-life configurations in terms of material, geometry, physical arrangement, and environment, including thin-film and full-immersion conditions, with alternating wet-dry cycling,[163] as well as crevices[164] and recesses.[165–169] Furthermore, CMEAs can be built with either nominally identical electrodes that simulate large planar electrodes or by combining a mix of electrode materials to simulate complex alloys with nonuniform structure and composition.

The net current evolved on a freely corroding surface is always zero, such that the net sum of anodic and cathodic current is equal, as per equation (43), but localized dispersions of excess anodic or cathodic current density may arise on a finely resolved scale:

$$\sum i_{anodic} = \sum i_{cathodic}. \tag{43}$$

Localized distribution of current is dependent on such effects as pitting, crevice corrosion, galvanic pairings, water layer thickness, and microstructural heterogeneities. For this reason, CMEAs have been developed for instantaneous assessment of the spatiotemporal evolution of localized corrosion and current distributions.[161,162]

The CMEA setup incorporates insulated wires of small diameter, typically 0.25 mm, composed of the metal of interest, and flush-mounted with a series of exposed discs embedded within a supporting matrix.[170] The wires are individually connected by a ZRA to individual ports of a multi-electrode analyzer (while remaining insulated from one another) that measures the net current output of each wire, simultaneously and distinctly. In this way, a spatiotemporal map can be constructed of the distribution of local current on the surface of the sample in an MEA in the desired arrangement for any particular experiment.[171–175] Two configurations are common: close-packed configurations simulate specific conditions and elucidate unique corrosion mechanisms as shown in figure 12*A*. In contrast, far-spaced configurations that are optimized for high-throughput experiments are capable of elucidating the statistical distributions of flaws under different variables and their effect on corrosion processes.[163,170] In this case, the separation distance between wires should be large enough that the electrochemical processes taking place on each electrode has no effect on neighboring electrodes during anodic or cathodic polarization. As such, separation distances greater than characteristic transport lengths are used, as demonstrated in the schematic given in figure 12*B*.

Some investigations have demonstrated components that have been designed in a crevice configuration to study the current profiles along the walls of a crevice. This is shown by the dashed line in the schematic given in Figure 12*A* that represents the placement of an artificial crevice.[164,174] Figure 12*C* shows the setup for a simulated rivet that enables measurements to be made throughout the length of the artificial component. Note that the discs have been turned inward for ease and are shown to demonstrate their location. Simulated engineering components can be constructed of dissimilar metals such that the spatial distribution of galvanic current can be monitored as a function of time.[170–172] CMEAs also have been used to investigate the

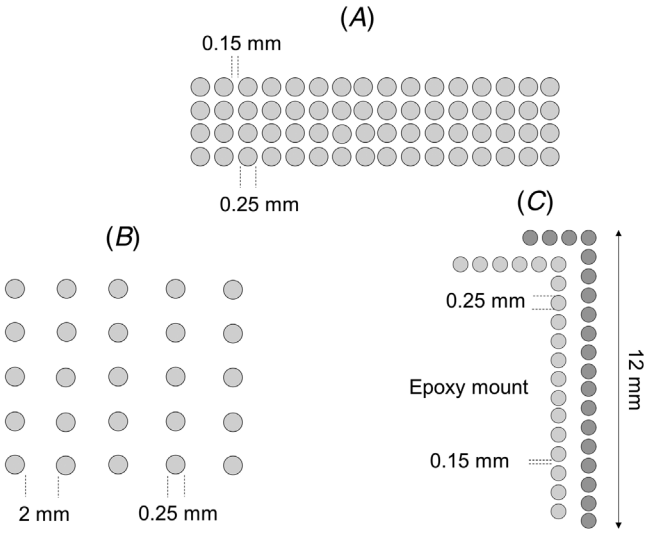


FIG. 12 Schematic diagrams for CMEAs showing (*A*) close-packed, (*B*) far-spaced, and (*C*) rivet electrode configurations. The dashed line in (*A*) demonstrates where an artificial crevice could be placed.

spreading of intergranular corrosion by cooperative interactions in which CMEAs were constructed from sensitized 304 stainless steel to understand the origins of persistent interactions in localized corrosion sites.[161]

By nature of the technique, a reference electrode is not needed, as current can be measured in a two-electrode setup. Small reference electrodes, however, also can be embedded within the array and then connected to individual wires in a three-electrode setup to monitor the potential of individual wires one-at-a-time or even to conduct potential-dependent measurements on individual wires of interest, such as potentiodynamic polarization or EIS.

ENVIRONMENTALLY ASSISTED CRACKING

Several electrochemical techniques can be used to assess susceptibility to environmental cracking. For alloys that are susceptible to SCC by a mechanism of slip-induced passive film rupture and anodic dissolution, electrochemical measurement of the dissolution rate has obvious practical advantages. In this case, the increment of crack growth is defined by the anodic charge associated with each film rupture event. The crack growth rate is defined by this repetitive process. In the case of hydrogen embrittlement (HE) phenomena, determination of the mobile hydrogen concentration in the metallic lattice is an important consideration. Such a determination is possible using an electrochemical approach. Several pertinent methods are discussed in the following sections.

Scratch Repassivation

The scratch repassivation technique discussed earlier may be more useful for studying SCC than it is for pitting.[154] This is because natural pitting is often initiated at defect sites in the passive film that are electronic or chemical in nature. Such sites are not necessarily probed by a mechanical scratch. Scratching can simulate SCC where mechanical film rupture processes are operative and anodic dissolution controls the SCC process. In general, once the passive film is mechanically disturbed at some potential, an electrochemical current can be measured that will decay back to a low level when repassivation has occurred. A measure of the crack growth rate, V (cm/s), can be obtained from these data:

$$V = \frac{E.W.}{\rho F}\left[Q_f \frac{\varepsilon_{ct}}{\varepsilon_f}\right], \tag{44}$$

where:
$E.W.$, p, and F have been defined previously, and
$Q_f = \int_0^t i_{ox} dt$,
Q_f = the anodic charge density (coulombs/cm^2),
ε_f = the fracture strain of the film, and
ε_{ct} = the crack tip strain rate (s^{-1}).

Tribo-ellipsometric Methods

The tribo-ellipsometric method is an advancement of the scratch method and has been used to distinguish between cases in which an alloy is susceptible to localized corrosion, such as pitting or SCC, as opposed to general dissolution. The total anodic current transient following film destabilization consists of the algebraic sum of the repassivation current and the current corresponding to dissolution of the exposed bare metal in lieu of film formation. The electrochemical current measurement is conducted in conjunction with the optical ellipsometric method to measure the rate of film growth and repassivation film thickness. This combination offers a method of separating the two currents (dissolution versus repassivation), assuming that the valence state and density of the oxide are known so that charge can be determined from its volume. Based on the ratio of the charge involved in dissolution and the charge associated with repassivation, a criterion for stress corrosion is established by the parameter R_{scc}:

$$R_{scc} = 1 + Q_d I Q_r, \tag{45}$$

where:
Q_d = the charge involved in dissolution, and
Q_r = the charge associated with repassivation.

For example, a low-carbon steel was not found to be susceptible to SCC in a solution in which R_{scc} was 2.8. In this case, repassivation occurred very rapidly. The steel, however, was found to be susceptible when that ratio was 26, and it was not susceptible again in a solution in which R_{scc} was 75.[172] In the latter case, widespread pitting occurred instead. Hence, a balance between repassivation and widespread dissolution is required for anodically controlled SCC. Only under intermediate conditions is SCC possible.

Potentiodynamic Methods

Parkins devised a slow and rapid potentiodynamic scanning method to determine both the relative susceptibility to slip-film rupture-repassivation SCC susceptibility, as well as possible

ranges of potential where SCC might occur.[62,175] The method applies to metals and alloys whose oxide films can initially be cathodically reduced. The validity of the method relies on the notion that SCC occurs only when crack walls are readily passivated while the crack tip dissolves at a high rate because of continual destabilization of the passive film. In this method, the rapid scan anodic polarization curve provides a measure of the bare dissolution kinetics over a range of anodic potentials. A slow anodic potentiodynamic scan provides a measure of the passive crack flank dissolution kinetics over the same range of potential. Alloy-electrolyte combinations that produce potential ranges in which a difference in dissolution rate of 100–1,000 is observed for the two scan rates are more SCC susceptible. Caution is warranted, however, over concern that the differences in current do not merely reflect capacitive current as indicated in equation (19). All of the techniques mentioned in this section suffer from the need to perform testing in solutions that simulate the relevant crack tip chemistry and at the potentials actually experienced by the crack tip. No ASTM standard exists for these methods.

The Barnacle Electrode Technique for Determination of Diffusible Hydrogen Concentration

The degradation of fracture toughness below levels obtained in dry air or vacuum is a strong function of the internal diffusible hydrogen concentration for alloys prone to HE. Therefore, it is often important to determine this concentration, hereafter referred to as C_H. C_H can be determined by measuring the anodic current density associated with the oxidation of mobile hydrogen, which has diffused to the surface. Of course, precaution must be taken to ensure that i_{ox} is associated only with the reactions given by equations (7) or (8) and does not include a contribution from other oxidation processes, such as metal oxidation. The source of the adsorbed hydrogen is internal hydrogen that exists in a precharged specimen that diffuses to the surface across the concentration gradient created when the surface concentration is lowered to zero as a consequence of hydrogen oxidation and extraction. In the barnacle electrode method, a hydrogen-containing steel part, with initial uniform diffusible hydrogen concentration, C_H, is galvanically coupled to a nickel–nickel oxide electrode in an alkaline electrolyte.[176,177] This couple polarizes the steel to a potential at which the hydrogen is oxidized as it diffuses out while metal oxidation is minimized; i_{ox} is related to mobile hydrogen concentration in the metal by the first term solution to Fick's second law.[176] The appropriate boundary conditions for this equation are $\partial C_H/\partial x = 0$, $x = 0$, $t \geq 0$; $C_H = 0$, $x = L$, $t > 0$; $C = C_H$ $0 < \times < L$, $t < 0$.

$$\frac{i_{ox}}{nF} = C_H \left(\frac{D_H}{\pi t}\right)^{1/2}, \tag{46}$$

where:

C_H = the mobile or diffusible hydrogen concentration (1 gram-mole H/cm^3 Fe = 1.3×10^5 wt. ppm);

D_H = the apparent diffusion coefficient for H (cm^2/s);

t = time, s;

L = one-half the sample thickness so that $x = L$ at the extraction surface and $x = 0$ is the center of the specimen, cm; and

i_{ox} = the current density associated with hydrogen oxidation (A/cm^2).

The first term solution given in equation (46) is valid if $L^2/Dt \geq 4$. The slope of a plot of log(i_{or}) versus *log(t)* should be -0.5. C_H is determined from measured values of i_{ox} and t if D_H is known and the data fit equation (46). If D_H is not known, then the product $C_H D^{1/2}$ is obtained.

The Permeation Method for Determination of Diffusible Hydrogen Concentration

In this method, an electrochemical technique is used to measure the diffusion coefficient, D, and the solubility, C_0, of hydrogen in iron or other metallic foil, under a variety of experimental conditions.[178,179] The advantages of the electrochemical technique are twofold. First, as noted earlier, by adjusting the potential one can apply a wide range of equivalent hydrogen pressures to the charging side of the metal membrane without resorting to high-pressure or high-vacuum techniques. Second, the hydrogen forced through a thin metal foil can be transformed to H^+ ions ($H \rightarrow H^+ + e^-$) when it reaches the solution on the other side of the permeation foil, and thus, the permeation rate will be proportional to the oxidation current required on the exit side of the membrane. Highly accurate and sensitive measurements of the permeation rate can be made, which can be seen from the fact that a current density of 1 |μA cm^{-2} corresponds to a permeation rate of H_2 of about 10^{-7} mL cm^{-2} sec^{-1} at standard temperature and pressure in palladium.

The diffusion equation given by Fick's second law, where $C_H(x,t)$ is the position-dependent diffusible hydrogen concentration, t is time, D is the diffusion coefficient, and x is distance through the foil has been solved for the initial conditions $C_H(x, t = 0) = 0$ and for the boundary conditions $C_H(0, t = \infty) = C_o$, $C_H(L, t = \infty) = 0$. In other words, before the experiment is started, the foil contains no hydrogen and, at any time after the start of the experiment, the hydrogen concentration, C_H, on one side (where $x = 0$) is a constant, C_0, and on the other side (where $x = L$) is equal to zero. The time $t = 0$, in this case, corresponds to the time at which the concentration is switched from 0 to C_0. The solution of equation (47) with the noted initial and boundary conditions yields a series, which, to a good approximation,* can be given by its first term:

$$\frac{i(t)}{i(\infty)} = \left(\frac{2}{\pi^{\frac{1}{2}}}\right)\left(\frac{1}{\pi^{\frac{1}{2}}}\right)\exp\left(-\frac{1}{4_\tau}\right), \tag{47}$$

where:

$i(t)$ and $i(\infty)$ = the measured currents (proportional to the permeation rate of hydrogen) at a time t and at steady state, respectively; and

τ = a dimensionless parameter given by $\tau = Dt/L^2$, where L is the thickness of the membrane.

Figure 13 depicts the relationship between i(t)/i(∞) and τ. The values of τ corresponding to some selected values of γ are given in table 3.

*This approximation is valid for i(t)/i(∞) < 0.96.

FIG. 13 Plot of permeation rise transient *H* oxidation current density expressed as the ratio of the transient current density to the steady-state current density ($\gamma = I(t)/I(\infty)$) versus $\tau = (D/L^2)t$. The constants associated from the breakthrough and lag time methods can be obtained from this plot. Selected values are given in table 3.

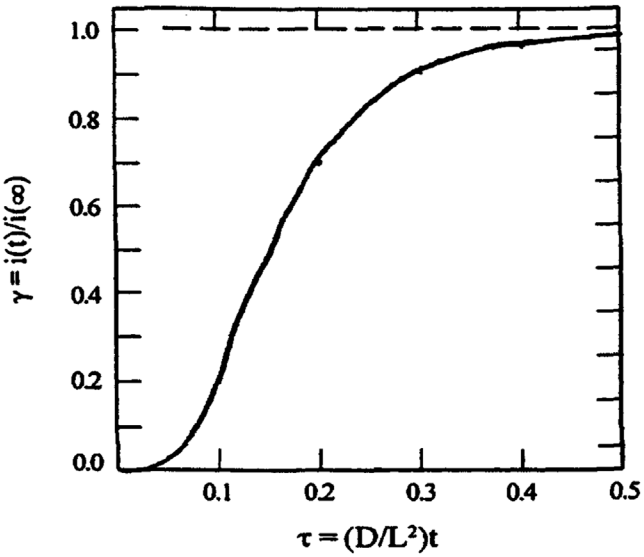


TABLE 3 Selected Values of γ and τ

$\gamma = i(t)/i(\infty)$	$\tau = Dt/L^2$
0.10	0.066
0.30	0.101
0.50	0.138
0.63	0.167
0.70	0.192
0.90	0.304

The diffusion coefficient may be determined from the transient permeation current density at various times and selected foil thickness,

$$D = \tau\ \gamma\ L^2/t\ \gamma\ , \tag{48}$$

where:
$\tau\gamma$ = the time required to reach a current $i(t) = \gamma i(\infty)$, and
$\tau\gamma$ = the corresponding value of τ.

This forms the basis of the lag time and breakthrough time methods discussed in ASTM G148, *Standard Practice for Evaluation of Hydrogen Uptake, Permeation, and Transport in Metals by an Electrochemical Technique*. A test of the validity of the assumptions leading to equation (47) is to calculate D from equation (48) for different values of γ and show that it is independent of γ. An alternative approach facilitates determination of D from a linear regression of many data points, instead of relying on a single data point on the rise transient. Here, the solution given by McBreen for the rise transient is used based on a rearrangement of equation (47):

$$Log\left(i(t)\sqrt{t}\right) = Log\left(\frac{2FC_o\sqrt{D}}{\sqrt{\pi}}\right) - \frac{L^2 Log(e)}{4D} * \frac{1}{t}, \tag{49}$$

such that a plot of $\log\left(i(t)\sqrt{t}\right)$ versus $1/t$ versus $1/t$ is linear and has a slope of

$$-\frac{L^2 Log(e)}{4D}, \tag{50}$$

where:
t = time after start of charging in seconds,
$i(t)$ = the time dependent permeation flux in amps/cm^2,
L = foil thickness in cm, and
D = the diffusion coefficient in cm^2/sec.

This solution assumes that the initial subsurface hydrogen concentration (C_o) is zero. This solution is valid for $0.02 < \tau < 0.9$. This method has been used to determine the effective diffusion coefficient in high-strength steels.[180]

For steady-state conditions we have

$$i(\infty) = \frac{nFDC_o}{L}, \tag{51}$$

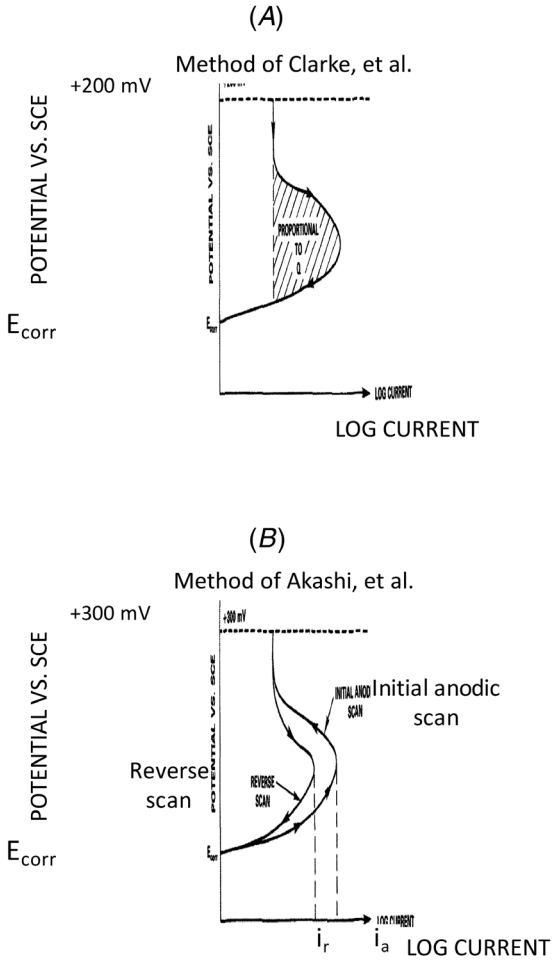
and knowing the value of D from the transient, the concentration $C_0 = C(0, t)$ at $t = \infty$ can be calculated.

This is the diffusible hydrogen concentration under the conditions of interest. HE severity is often proportional to this steady-state diffusible hydrogen concentration when specimens are charged at the same hydrogen overpotential as used in the permeation experiment. ASTM G148 describes this method.

Evaluation of Alloy Sensitization

Measurement of the coulombs generated during the electrochemical polarization of a material from the passive range to the active corrosion potential can be used to quantify the susceptibility to intergranular attack associated with the precipitation of chromium carbides and chromium nitrides at grain boundaries.[181–183] The method is described by ASTM G108, *Standard Test Method for Electrochemical Reactivation (EPR) for Detecting Sensitization of AISI Type 304 and 304L Stainless Steels*. A modification of this procedure, called the double-loop electrokinetic repassivation test,[184,185] involves a potentiodynamic polarization of the metal surface initially from the OCP in the active region to a potential in the passive range. This is immediately followed by reverse polarization in the opposite direction back to the OCP. The second method is less dependent on surface finish and precise knowledge of the grain size. Both variations of the method are illustrated in figure 14. In the latter method, the degree of sensitization is determined by the ratio, (I_r/I_a), of the maximum current generated in the reactivation, I_r, or reverse scan compared with that generated in the initial anodic scan, I_a. The procedure is contingent on the presence of anodic current during the reactivation scan that results mainly from incomplete passivation of the zone adjacent to the grain boundaries that is depleted of

FIG. 14 Schematics of two procedures for anodic reactivation polarization testing. (*A*) The Clarke method involves a downward reactivation scan;[180,181] and (*B*) the Akashi method involves an upward scan to the passive state followed by a reverse scan.[182,183]



chromium because of carbide precipitation at grain boundaries. For nonsensitized material, the passive film remains essentially intact during the reverse scan and the magnitude of the reactivation polarization peak remains small. For the same reasons, the charge, *Q*, obtained from integration of current versus potential for a known voltage scan rate in the single-loop method is small for nonsensitized material. As a refinement to the method, the charge is normalized by the grain-boundary area (GBA) because this is the area from which most of the current arises in the single reactivation scan:[183]

$$P = Q/GBA, \tag{52}$$

$$GBA = A_s[5.09544 \times 10^{-3} \times \exp(0.34696 \times GS)], \tag{53}$$

where:

P = the reaction charge density associated with the sensitized area, coulombs/cm^2,

A_s = the wetted specimen surface area, *GBA*, and

GS = the ASTM grain size in accordance with ASTM E112, *Standard Test Methods for Determining Average Grain Size*.

The same procedure can be used to normalize the ratio I_r/I_a.[185] The current peak, I_r, for the reactivation scan is normalized for the GBA, while the initial anodic current peak remains normalized to A_s, as follows:

$$\frac{i_r}{i_a} = \left[\frac{I_r}{I_a \times [5.09544 \times 10^{-3}\exp(0.34696 \times GS)]}\right]. \tag{54}$$

I_r/I_a ratios approaching 1 imply sensitization. A number of investigators have correlated this electrochemically derived ratio with optical metallographic evaluations of the degree of material sensitization, such as those outlined in ASTM A262, *Standard Practices for Detecting Susceptibility to Intergranular Attack in Austenitic Stainless Steels*. This has been accomplished for several different iron-nickel-chromium alloys.[186–188] The technique is nondestructive to the underlying metal and can be applied in the field.

ELECTROCHEMICAL EVALUATION OF PROTECTIVE COATINGS AND FILMS

Numerous AC and DC electrochemical methods have been used to study the performance and the quality of protective coatings, which include passive films on metallic substrates, and to evaluate the effectiveness of various surface pretreatments. Several are discussed in the following sections.

Anodized Aluminum Corrosion Test

The Ford anodized aluminum corrosion test (FACT)[189] involves the cathodic polarization of the anodized Al surface by using a small cylindrical glass clamp-on cell and a special 5% sodium chloride (NaCl) solution containing cupric chloride ($CuCl_2$) acidified with acetic acid. A large voltage is applied across the cell by using a platinum auxiliary electrode. The alkaline conditions created by the cathodic polarization promote dissolution at small defects in the anodized Al. As the coating resistance is decreased, more current begins to flow, and the voltage decreases. The cell voltage (auxiliary electrode to test specimen voltage) is monitored for 3 min and the cell voltage multiplied by time is recorded. Former standard ASTM B538-70, *Method of FACT (Ford Anodized Aluminum Corrosion Test) (Withdrawn 1986)*, described this method. This standard has been withdrawn because some Al alloys failed the test but still performed well in service. A similar test, known as the cathodic breakdown test, involves cathodic polarization to -1.6 V versus saturated calomel electrode (SCE) for a period of 3 min in acidified NaCl.[190] Again, the test was designed for anodized Al alloys because the alkali created at the large applied currents will promote the formation of corrosion spots at defects in the anodized film. Today, EIS provides a more informative approach to examining anodized Al.

The Electrolytic Corrosion Test

The electrolytic corrosion test was designed for electrodeposits of nickel and chromium on less noble metals, such as zinc or steel.[20,191–192] Special solutions are used, and the metal is polarized

to +0.3 V versus the standard calomel electrode. The metal is taken through cycles of 1 min anodically polarized and 2 min unpolarized. An indicator solution is then used to detect the presence of pits that penetrate to the substrate. Each exposure cycle attempts to simulate one year of exposure under atmospheric-corrosion conditions. Former standard ASTM B627, *Test Method of Electrolytic Corrosion Testing (EC Test) (Withdrawn 1998)*, described the method.

The Paint Adhesion on a Scribed Surface Test

This involves the cathodic polarization of a small portion of painted metal. The area exposed contains a scribed line that exposes a line of underlying bare metal. The sample is cathodically polarized for 15 min in 5% NaCl. At the end of this period, the amount of delaminated coating is determined from an adhesive tape pulling procedure.

THE SINGLE-FREQUENCY IMPEDANCE TEST FOR ANODIZED ALUMINUM

The method described by ASTM B457, *Standard Test Method for Measurement of Impedance of Anodic Coatings on Aluminum*, is used to study the seal performance of anodized Al.[193,194] This method uses a 1-V rms 1-kHz signal source from an impedance bridge to determine the sealed anodized Al impedance. The test area is again defined with a portable cell, and a platinum or stainless steel auxiliary electrode is typically used. The sample is immersed in 3.5% NaCl (see ASTM B457).

EIS Methods

The EIS method offers an advanced method of evaluating the performance of metallic-based coatings (passive film forming and/or conversion coatings) and the barrier properties of organic coatings and corrosion rates under paints.[195–203] The method does not accelerate the corrosion reaction and is nondestructive. The technique is quite sensitive to changes in the resistive-capacitive nature of coatings as well as the electrochemical interface. It is possible to monitor the polarization resistance of the corroding interface under the coating with this technique. In this respect, the electrochemical impedance technique offers several advantages over DC electrochemical techniques in that resistances related to the corrosion rate can be separated from the high DC resistance of the dielectric coating. This is not possible with the DC methods. Because a large frequency bandwidth is used for the applied signal (usually from the mHz range to the kHz range), the electrochemical impedance technique is "spectroscopic" and surpasses the capabilities of single-frequency impedance methods. The reason for this lies in the capability of the electrochemical impedance technique to discriminate between the resistive properties of the coating or passive film, which arise because of its ionic or electronic conductivity and the capacitive nature of the passive film or coating, which result from its dielectric constant, area, and thickness. Although impedance circuit models for coatings (fig. 15) contain more elements than the model shown in figure 4 for bare metals, frequency regimes in which impedance information is primarily due to the coating capacitance or coating resistance can be separated from one another and analyzed independently by using a broad frequency bandwidth. If the coating or passive film capacitance can be determined by impedance analysis and if the dielectric constant is known, then the film thickness can be estimated for a given exposed area, as follows:

$$C = \frac{\varepsilon \varepsilon_0 A}{d}, \tag{55}$$

where:

A = the surface area, cm^2;
d = the dielectric thickness, cm;
ε_0 = the electric permittivity of a vacuum (8.854×10^{-12} F/m); and
ε = the dielectric constant for the passive film or coating.

In addition to this relationship between thickness and area of dielectric and capacitance, the uptake of water in an organic coating can be monitored because the dielectric constant for water is more than an order of magnitude greater than the dielectric constant for the dry organic coating. The quantity of water absorbed in the organic coating can be estimated as follows:[196,198]

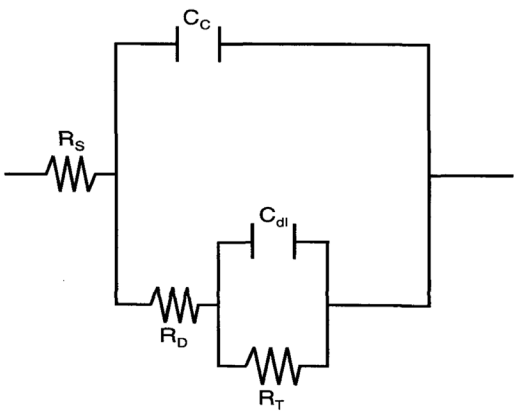
$$vol.\%H_2O = \left[\frac{100 \log\left(\frac{C_t}{C_0}\right)}{\log(79)}\right], \tag{56}$$

where:

C_t = the coating capacitance after some exposure time, and
C_0 = the initial coating capacitance at time zero when the exposure begins.

The coating resistance also can be monitored as a function of exposure time. Large decreases signify permeation of ionic species through the coating or the presence of defects in the coating.[202,203] The breakpoint frequency is a useful method for estimating the area fraction of physical defects in an organic coating.[201–204] The following expression describes the dependency

FIG. 15 Electrical equivalent circuit to simulate a coated steel panel with a defect.[196,197,199] R_D is the coating defect resistance, R_T is a charge transfer resistance (similar to R_D) at the metal interface where water has penetrated, and C_c is the coating capacitance.



between the high-frequency breakpoint frequency and defect area:

$$f_{bpt} = \left(\frac{1}{2\pi\varepsilon\varepsilon_0\rho}\right)\left(\frac{A_d}{A}\right), \quad (57)$$

where:
A_d = the defect area where electrochemical reactions operate,
A = the total painted surface area, and
ρ = the resistivity of the coating at defects.

Thus, f_{bpt} can track with change in defect area provided that decreases in p over time and increase in e with electrolyte uptake do not dominate. Under such circumstances, the term preceding the ratio (A_d/A) remains constant. In this case, increases in f_{bpt} occur mainly as a function of the increases in the defective area. Circumstances may exist, however, in which small increases A_d in ε and very large decreases in p occur so that f_{bpt} does not relate linearly to defect area.

Moreover, bare metal under delaminated coating regions may not be detected under all circumstances, especially if the coating resistivity over the delaminated area and dielectric constant are identical to those in regions where the coating is not delaminated. The hypothetical relationship between f_{bp}, and the open defect area is shown in figure 16.[204] No ASTM standard currently exists for conducting impedance measurements on coated metals.

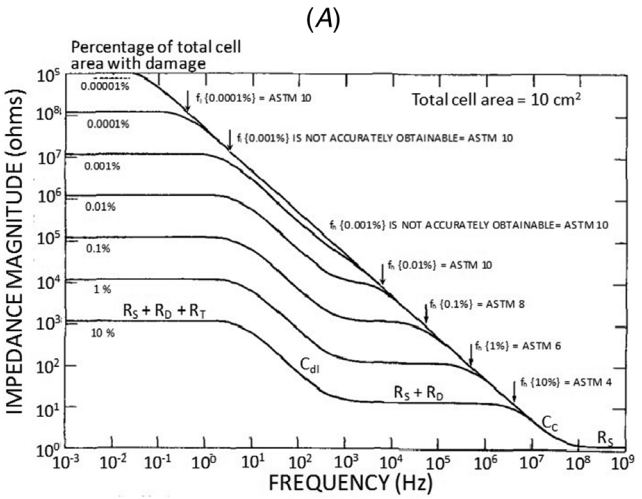
Electrochemical Noise Methods for Organic Coating Evaluation

Electrochemical noise (EN) methods also have been explored as a method to analyze the degradation of polymer-coated metals.[205–209] A variety of methods have been used. A common method involves the use of a cell with two identical working electrodes connected through a ZRA. The entire galvanic couple is coupled through a high impedance voltmeter to an ideally noiseless reference electrode. Two samples often experience drastically different behavior; for instance, if one electrode has a coating defect and the other does not, then asymmetrical electrode behavior results. The spectral noise impedance obtained is equivalent to the geometric mean of the moduli of individual electrode impedances. Instrument noise should be carefully considered when this approach is used to analyze high-resistance coatings. No ASTM standard currently exists for conducting EN tests on coated metals.

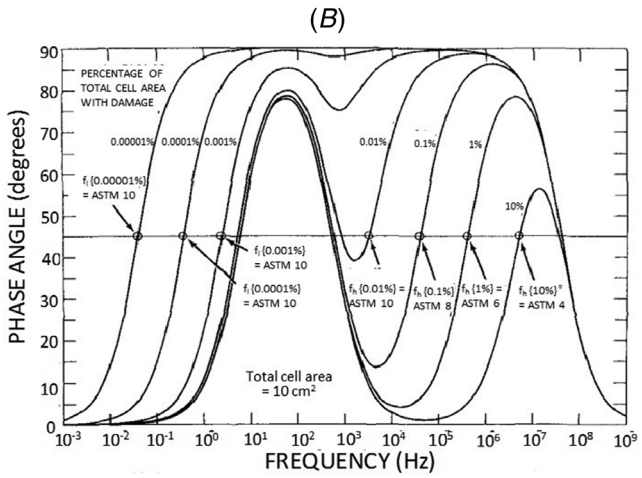
CHARACTERIZATION OF ANODIZED SURFACES AND CONVERSION COATINGS ON METALS

The impedance technique also provides a useful approach for characterizing anodization,[210–212] conversion coatings, sealing of anodized layers, and passivity.[213] ASTM *STP1188*, *Electrochemical Impedance: Analysis and Interpretation*, covers some of these applications.[214] EIS methods also have been applied to the study of conversion coatings.[215–217] In the case of conversion coatings, an impedance modulus of 1–2 megaohm-cm^2 at the DC limit is a threshold value required for the conversion coating to pass an ASTM B117, *Standard Practice for Operating Salt Spray (Fog) Apparatus*, salt spray test.[218] This value must be passed after a 24-h exposure to aerated 0.5 M NaCl solution.[219] EIS studies of synthesized bulk copper-based intermetallic compounds have improved insight on the role of conversion coatings in affecting the electrochemical properties of intermetallic compounds.[220] Such phases are often responsible for microgalvanic corrosion of Al-base alloys.

FIG. 16 Theoretical Bode Magnitude and Phase Angle Plots for various known electrochemically active defect areas for a coating containing a cylindrical defect penetrating to the metal substrate and no delaminated regions: (*A*) Bode magnitude, and (*B*) Bode Phase Angle. ASTM visual ratings with the percent of area damaged as blisters or rust spots according to standards ASTM D610, *Standard Practice for Evaluating Degree of Rusting on Painted Steel Surfaces*, and ASTM D714, *Standard Test Method for Evaluating Degree of Blistering of Paints*, are included for comparison.[202]



(2) Effect of Defect Area Percentage on Impedance Magnitude Behavior of a Coated Steel Equivalent Circuit. Total Cell Area Assumed is 10 cm².



(3) Effect of Defect Area Percentage on Impedance Phase Behavior of a Coated Steel Equivalent Circuit. Total Cell Area Assumed is 10 cm².

Scanning Kelvin Probe (SKP)

The scanning Kelvin probe (SKP) technique is a local electrochemical technique used for atmospheric-condition investigations of under-film cathodic delamination[221–226] and anodic filiform corrosion[227–233] on polymer-coated surfaces as well as hydrogen permeation[234–237] and the corrosion underneath a water droplet.[238] The technique is completely nonperturbing and enables the temporal and spatial resolution of corrosion potential distributions beneath intact and delaminated organic coatings. A lateral resolution of 0.1 mm (depending on the probe diameter and probe-specimen distance[239]) is typical and a limitation if a study of features on a smaller length scale is required. The higher-resolution scanning Kelvin probe force microscope (SKPFM) is recommended for such requirements.[233] The setup and calibration of the SKP is well documented[224] and will be described here in brief. A thin (typically between 5 μm and 125 μm) gold probe is rastered above a specimen surface at a height of approximately 100 μm. An external circuit creates an electrical connection between the specimen and the probe and the potential required to nullify the resultant current flows is measured giving the Volta potential difference, or Kelvin probe potential (E_{KP}). This can be converted to corrosion potential (E_{corr}) via the following equation:

$$E_{corr} = E_{kp} + \text{constant}, \quad (58)$$

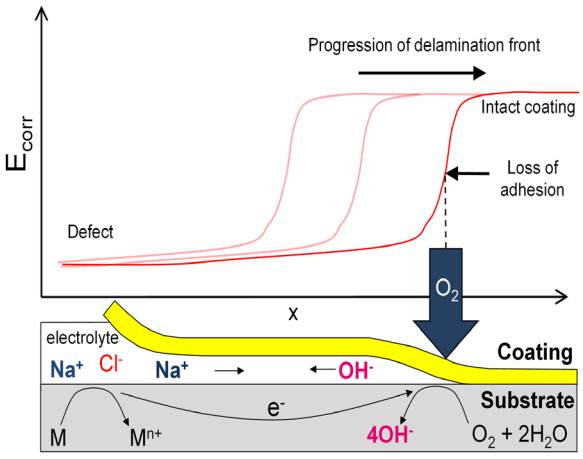
where the constant is obtained from an offset measured by taking an SKP measurement of a redox couple (typically Cu/Cu^{2+}) and comparing it to a known or potentiostat-measured value. The effect of a polymer film must be taken into account in cases in which a free-standing film is laid over the aqueous media in the redox couple while the SKP measurement is taken. Furthermore, in the case of a delaminated polymer film, where a layer of electrolyte is present through an ingress between the substrate metal and the polymer layer, a so-called Donnan potential ($\Delta\varphi_D$) must be taken into consideration. $\Delta\varphi_D$ can be described as the Galvani potential difference established between the polymer layer and the electrolyte solution (i.e., $\varphi_{El} - \varphi_{Pol}$[240,241]). $\Delta\varphi_D$ can be minimized, such that it is considered negligible, by using model coatings that are chemically unlikely to develop a fixed charge density (such as polyvinyl-butyral[224]) and electrolytes with high salt content (i.e., 0.86 M NaCl (aq)).[224] Experiments are conducted inside a Faraday cage that also enables control of the humidity, which must be maintained at a consistently high level.

The most common use for the SKP in corrosion studies is to monitor cathodic delamination, which will be discussed herein. Investigations of this nature were pioneered by Stratmann,[242,243] who developed a now well-utilized method for assessing cathodic delamination occurring at coating defects. The method is particularly useful for assessing the performance and inhibition mechanism of in-coating corrosion inhibitors.[244,245–246] After the introduction of an electrolyte to the defect, the progression of a cathodic delamination front is monitored periodically using line profiles that extend across the intact coating from the edge of the defect, the schematic diagram given in figure 17 illustrates this. The point at which coating adhesion is lost is taken as the midpoint of a sharp drop in potential that connects the potential in the remaining intact region (E_{intact}) to the delaminated region. The latter is polarized by the anodic reaction, which typically occurs exclusively in the defect, depending on the metallic substrate.[224] The build-up of OH^- in the underfilm region results in base-catalyzed hydrolysis of the interfacial bonds, resulting in loss of coating adhesion.[229] Cathodic delamination of an uninhibited coating usually will initiate within several hours depending on the substrate and proceed with parabolic kinetics where the limiting factor is the migration of sodium cations from the defect to the delamination front. The mode of inhibition can be determined by analysis of the rate kinetics, the E_{intact} values, and the time for delamination to occur. A transformation from parabolic to linear kinetics is typically a result of, but not limited to, one of the two following conditions:

1. The formation of a passive layer during coating deposition (typical of an etch primer) such that electron transfer at the substrate/coating interface becomes the rate limiting step.
2. The addition of pigments to the coating can act as a barrier to oxygen permeation such that the vertical diffusion of oxygen becomes the rate limiting step.

Retention of parabolic kinetics with a reduced rate is typically a result of a noncontinuous blocking layer that increases the tortuosity of the pathway of migrating sodium cations. A phenomenon has been reported on conducting polymer and graphene-based coatings where parabolic kinetics are accompanied by an elevated E_{intact}, which has been shown to be the displacement of the cathodic reaction from the substrate–coating

FIG. 17 Schematic diagrams showing the cathodic delamination and the progression of SKP-measured corrosion potentials where the midpoint of the sharp drop in potential represents the point of coating adhesion failure.[222,240]



interface into the coating, which prevents the increase in local pH at the interface and, hence, loss of adhesion.[222,223] The inhibitory effect of inhibitor leaching can be detected by a delay in the onset of delamination and a change in the measured potential near the defect. This can be demonstrated with an experiment with an uninhibited coating and the addition of the inhibitor into the defect electrolyte.[224,230]

References

1. J. O'M. Bockris and A. K. N. Reddy, *Modern Electrochemistry,* vol. 2 (New York: Plenum Press, 1970).
2. E. Gileadi, *Electrode Kinetics for Chemists, Chemical Engineers and Materials Scientists* (New York: VCH Publishers, 1993).
3. N. D. Tomashov, *Theory of Corrosion and Protection of Metals* (New York: Macmillan, 1966).
4. D. A. Jones, *Principles and Prevention of Corrosion* (New York: Macmillan, 1992).
5. M. G. Fontana and N. D. Greene, *Corrosion Engineering* (New York: McGraw-Hill, 1978).
6. J. Newman, *Electrochemical Systems* (New York: Prentice-Hall, 1973).
7. H. H. Uhlig and R. W. Revie, *Corrosion and Corrosion Control* (New York: Wiley, 1985).
8. J. O'M. Bockris, B. E. Conway, E. Yeager, and R. E. White, ed., *Electrochemical Materials Science*, vol. 4, *Comprehensive Treatise of Electrochemistry* (New York: Plenum Press, 1981).
9. R. Baboian, ed., *Electrochemical Techniques for Corrosion* (Houston, TX: National Association of Corrosion Engineers, 1977).
10. U. Bertocci and F. Mansfeld, ed., *Electrochemical Corrosion Testing,* (West Conshohocken, PA: ASTM International, 1979).
11. G. Haynes and R. Baboian, ed., *Laboratory Corrosion Tests and Standards,* (West Conshohocken, PA: ASTM International, 1985).
12. G. C. Moran and P. Labine, ed., *Corrosion Monitoring in Industrial Plants Using Nondestructive Testing and Electrochemical Methods* (West Conshohocken, PA: ASTM International, 1986).
13. R. Baboian, ed., *Electrochemical Techniques for Corrosion Engineers* (Houston, TX: National Association of Corrosion Engineers, 1986).
14. R. Baboian, W. D. France, Jr., L. C. Rowe, and J. F. Rynewicz, ed., *Galvanic and Pitting Corrosion-Field and Laboratory Studies* (West Conshohocken, PA: ASTM International, 1974).
15. B. Poulson, *Electrochemical Measurements in Flowing Solutions*, *Corrosion Science* 23, no. 4 (1983): 391–430.
16. D. D. MacDonald, *Transient Techniques in Electrochemistry* (New York: Plenum Press, 1977).
17. C. Wagner and W. Z. Traud, "On the Interpretation of Corrosion Processes through the Superposition of Electrochemical Partial Processes and on the Potential of Mixed Electrodes," *Electrochem* 44, (1938): 843–855.
18. W. D. France, Jr., "Controlled Potential Corrosion Tests, Their Applications and Limitations," *Materials Research Standardization* 9, no. 8 (1969): 21.
19. Z. Tafel, "About the Polarization in Cathodic Hydrogen Evolution," *Physical Chemistry* 50 (1904): 641.
20. R. L. Saur and R. P. Basco, "An Accelerated Electrolytic Corrosion Test and a Corrosion Analysis Procedure for the Nickel-Chromium Plating System," *Plating* 53 (1966): 35–38.
21. D. Britz, "iR Elimination in Electrochemical Cells," *Journal of Electroanalytical Chemistry* 88 (1978): 309–352.
22. M. Hayes, J. Kuhn, and W. Patefield, "Techniques for the Determination of Ohmic Drop in Half-Cells and Full Cells: A Review," *Journal of Power Sources* 2 (1977–1978): 121–136.
23. F. Mansfeld, "The Effect of Uncompensated Resistance on the True Scan Rate in Potentiodynamic Experiments," *Corrosion* 38, no. 10 (1982): 556–559.
24. L. L. Scribner and S. R. Taylor, ed., *The Measurement and Correction of Electrolyte Resistance in Electrochemical Tests* (West Conshohocken, PA: ASTM International, 1990).
25. M. Stern and A. L. Geary, "Anodic Behavior of Iron in Acid Solutions," *Journal of the Electrochemical Society* 104 (1957): 56–63.
26. S. Evans and E. L. Koehler, "Use of Polarization Methods in the Determination of the Rate of Corrosion of Aluminum Alloys in Anaerobic Media," *Journal of the Electrochemical Society* 108 (1961): 509–514.
27. M. Stern and R. M. Roth, *Anodic Behavior of Iron in Acid Solutions, Journal of the Electrochemical Society* 104 (1957): 390–392.
28. M. Stern, "The Mechanism of Passivating-Type Inhibitors," *Journal of the Electrochemical Society* 105 (1958): 638–647.
29. M. Stern and E. D. Weisert, *Proceedings of the American Society of Testing and Materials*, vol. 59 (West Conshohocken, PA: ASTM International, 1959).
30. S. Barnartt, "Two-Point and Three-Point Methods for the Investigation of Electrode Reaction Mechanisms," *Electrochimica Acta* 15 (1970): 1313–1324.
31. K. B. Oldham and F. Mansfeld, "Corrosion Rates from Polarization Curves: A New Method," *Corrosion Science* 13 (1973): 813–819.
32. F. Mansfeld, "Simultaneous Determination of Instantaneous Corrosion Rates and Tafel Slopes from Polarization Resistance Measurements," *Journal of the Electrochemical Society* 120 (1973): 515–518.
33. F. Mansfeld and M. Kendig, "Concerning the Choice of Scan Rate in Polarization Measurements," *Corrosion* 37, no. 9 (1981): 545–546.
34. R. Bandy and D. A. Jones, "Analysis of Errors in Measuring Corrosion Rates by Linear Polarization," *Corrosion* 32 (1976): 126–134.

35. M. J. Danielson, "Analysis of Errors in Using the Two Electrode and Three Electrode Polarization Resistance Methods in Measuring Corrosion Rates," *Corrosion* 36, no. 4 (1980): 174–178.

36. J. C. Reeve and G. Bech-Nielsen, "The Stern-Geary Method. Basic Difficulties and Limitations and a Simple Extension Providing Improved Reliability," *Corrosion Science* 13 (1973): 351–359.

37. I. Epelboin, C. Gabrielli, M. Keddam, and H. Takenouti, "Alternating-Current Impedance Measurements Applied to Corrosion Studies and Corrosion-Rate Determination," in *Electrochemical Corrosion Testing*, ed. F. Mansfeld and U. Bertocci (West Conshohocken, PA: ASTM International, 1981), 150–166.

38. A. C. Makrides, "Corrosion in Dilute Acids. Part I. A Modified Linear Polarization Technique," *Corrosion* 29, no. 9 (1973): 148–152.

39. D. D. MacDonald and M. C. H. McKubre, "Electrochemical Impedance Techniques in Corrosion Science," in *Electrochemical Corrosion Testing,* ed. F. Mansfeld and U. Bertocci (West Conshohocken, PA: ASTM International, 1981), 110–149.

40. J. R. Scully, "Polarization Resistance Method for Determination of Instantaneous Corrosion Rates," *Corrosion* 56, no. 2 (2000): 199–218.

41. A. J. Bard and L. R. Faulkner, *Electrochemical Methods: Fundamentals and Applications* (New York: Wiley, 1980).

42. F. Mansfeld, "Recording and Analysis of AC Impedance Data for Corrosion Studies," *Corrosion* 36, no. 5 (1981): 301–307.

43. F. Mansfeld, M. W. Kendig, and S. Tsai, "Recording and Analysis of AC Impedance Data for Corrosion Studies," *Corrosion* 38 (1982): 570–580.

44. J. N. Murray, P. J. Moran, and E. Gileadi, "Utilization of the Specific Pseudocapacitance for Determination of the Area of Corroding Steel Surfaces," *Corrosion* 44, no. 8 (1988): 533–538.

45. D. R. Franceschetti and J. R. Macdonald, "Diffusion of Neutral and Charged Species under Small-Signal A.C. Conditions," *Journal of Electroanalytical Chemistry* 101 (1979): 307–316.

46. B. A. Boukamp, "A Nonlinear Least Squares Fit Procedure for Analysis of Immittance Data of Electrochemical Systems," *Solid State Ionics* 20 (1986): 31–44.

47. C. H. Hsu and F. Mansfeld, "Technical Note: Concerning the Conversion of the Constant Phase Element Parameter Y0 into a Capacitance," *Corrosion* 57 (2001): 747–748.

48. S. F. Mertens, C. Xhoffer, B. C. De Cooman, and E. Temmerman, "Short-Term Deterioration of Polymer-Coated 55% Al-Zn — Part 1: Behavior of Thin Polymer Films," *Corrosion* 53 (1997): 381–388.

49. J. Devay and L. Meszaros, "Study of the Rate of Corrosion of Metals by a Faradaic Distortion Method," *Acta Chimica Academy of Sciences Hungary* 100 (1979): 183–202.

50. J. S. Gill, M. Callow, and J. D. Scantlebury, "Corrosion Measurements Derived from Small Perturbation Non-Linearity—Part 1: Harmonic Analysis," *Corrosion* 39 (1983): 61–66.

51. G. P. Rao and A. K. Mishra, "A.C. Techniques to Evaluate the Kinetics of Corrosion Reactions," *Journal of Electroanalytical Chemistry* 77 (1977): 121–125.

52. L. Meszaros and J. Devay, "Study of the Rate of Corrosion of Metals by a Faradaic Distortion Method," *I Acta Chimica Academy of Sciences Hungary* 105 (1980): 183–202.

53. M. C. H. McKubre and B. C. Syrett, "Harmonic Impedance Spectroscopy for the Determination of Corrosion Rates in Cathodically Protected Systems," in *Corrosion Monitoring in Industrial Plants Using Nondestructive Methods,* ed. G. C. Moran, and P. Labine (West Conshohocken, PA: ASTM International, 1986), 433–458.

54. R. W. Bosch, J. Hubrecht, W. F. Bogaerts, and B. C. Syrett, "Electrochemical Frequency Modulation: A New Electrochemical Technique for Online Corrosion Monitoring," *Corrosion* 57 (2001): 60–70.

55. D. A. Eden, A. N. Rothwell, and J. L. Dawson, Paper No. 444, in *Proceedings of the Corrosion Conference* (Houston, TX: National Association of Corrosion Engineers, 1991).

56. J. L. Dawson, "Electrochemical Noise Measurement: The Definitive In-Situ Technique for Corrosion Applications?," in *Electrochemical Noise Measurement for Corrosion Applications,* ed. J. R. Kearns, J. R. Scully, P. R. Roberge, D. L. Reichert, and J. L. Dawson (West Conshohocken, PA: ASTM International, 1996), 3–35.

57. D. A. Eden, K. Hladky, D. G. John, and J. L. Dawson, Paper No. 276, in *Proceedings of the Corrosion Conference* (Houston, TX: National Association of Corrosion Engineers, 1986).

58. D. A. Eden and A. N. Rothwell, Paper No. 292, in *Proceedings of the Corrosion Conference* (Houston, TX: National Association of Corrosion Engineers, 1992).

59. A. N. Rothwell and D. A. Eden, Paper No. 223, in *Proceedings of the Corrosion Conference* (Houston, TX: National Association of Corrosion Engineers, 1992).

60. U. Bertocci, "A Comparison of Electrochemical Noise and Impedance Spectroscopy for the Detection of Corrosion in Reinforced Concrete," in *Electrochemical Noise Measurement for Corrosion Applications,* ed. J. R. Kearns, J. R. Scully, P. R. Roberge, D. L. Reichert, and J. L. Dawson (West Conshohocken, PA: ASTM International, 1996), 39–58.

61. U. Bertocci and F. Huet, "Noise Analysis Applied to Electrochemical Systems," *Corrosion* 51 (1995): 131–144.

62. D. L. Reichert, "Electrochemical Noise Measurement for Determining Corrosion Rates," in *Electrochemical Noise Measurement for Corrosion Applications,* ed. J. Kearns, J. R. Scully, P. R. Roberge, D. L. Reichert, and J. L. Dawson (West Conshohocken, PA: ASTM International, 1996), 79–89.

63. P. C. Searson and J. L. Dawson, "Analysis of Electrochemical Noise Generated by Corroding Electrodes under Open-Circuit Conditions," *Journal of the Electrochemical Society* 135, no. 8 (1988): 1908–1915.

64. F. Mansfeld and H. Xiao, "Electrochemical Noise and Impedance Analysis of Iron in Chloride Media," in *Electrochemical Noise Measurement for Corrosion Applications,* ed. J. Kearns, J. R. Scully, P. R. Roberge, D. L. Reichert, and J. L. Dawson (West Conshohocken, PA: ASTM International, 1996), 59–78.

65. G. P. Bierwagen, "Calculation of Noise Resistance from Simultaneous Electrochemical Voltage and Current Noise Data," *Journal of the Electrochemical Society* 141 (1994): L155–L157.

66. F. Mansfeld and H. Xiao, "Evaluation of Coating Degradation with Electrochemical Impedance Spectroscopy and Electrochemical Noise Analysis," *Journal of the Electrochemical Society* 141 (1994): 2332–2337.

67. F. Huet, "Comment on 'Calculation of Noise Resistance from Simultaneous Electrochemical Voltage and Current Noise Data,'" *Journal of the Electrochemical Society* 142 (1995): 2861–2863.

68. J. F. Chen and W. F. Bogaerts, "The Physical Meaning of Noise Resistance," *Corrosion Science* 37 (1995): 1839–1842.

69. H. Xiao and F. Mansfeld, "Evaluation of Coating Degradation with Electrochemical Impedance Spectroscopy and Electrochemical Noise Analysis," *Journal of the Electrochemical Society* 141 (1994): 2332–2337.

70. F. Mansfeld and H. Xiao, "Electrochemical Noise Analysis of Iron Exposed to NaCl Solutions of Different Corrosivity," *Journal of the Electrochemical Society* 140 (1993): 2205-2209.

71. F. Mansfeld, L. T. Han, and C. C. Lee, "Analysis of Electrochemical Noise Data for Polymer Coated Steel in the Time and Frequency Domains," *Journal of the Electrochemical Society* 143 (1996): L286–L289.

72. U. Bertocci, C. Gabrielli, F. Huet, and M. Keddam, "Noise Resistance Applied to Corrosion Measurements: I. Theoretical Analysis," *Journal of the Electrochemical Society* 144 (1997): 31–37.

73. A. Bautista and F. Huet, "Noise Resistance Applied to Corrosion Measurements: IV. Asymmetric Coated Electrodes," *Journal of the Electrochemical Society* 146 (1999): 1730–1736.

74. H. Hack and J. R. Scully, "Galvanic Corrosion Prediction Using Long- and Short-Term Polarization Curves," *Corrosion* 42, no. 2 (1986): 79–90.

75. R. Baboian, "Electrochemical Techniques for Predicting Galvanic Corrosion," in *Galvanic and Pitting Corrosion—Field and Laboratory Studies,* ed. R. Baboian, W. D. France Jr., L. C. Rowe, and J. F. Rynewicz (West Conshohocken, PA: ASTM International, 1974), 5–19.

76. F. Mansfeld and J. Kenkel, "Laboratory Studies of Galvanic Corrosion of Aluminum Alloys," in *Galvanic and Pitting Corrosion—Field and Laboratory Studies,* ed. R. Baboian, W. D. France Jr., L. C. Rowe, and J. F. Rynewicz (West Conshohocken, PA: ASTM International, 1974), 20–47.

77. R. G. Kasper and C. R. Crowe, "Comparisons of Localized Ionic Currents as Measured from 1-D and 3-D Vibrating Probes with Finite-Element Predictions for an Iron-Copper Galvanic Couple," in *Galvanic Corrosion,* ed. H. P. Hack (West Conshohocken, PA: ASTM International, 1988), 118–135.

78. R. G. Kasper and C. R. Crowe, "Ionic Current Densities in the Nearfield of a Corroding Iron-Copper Galvanic Couple," *Journal of the Electrochemical Society* 33 (1986): 879–887.

79. H. S. Isaacs, "The Measurement of the Galvanic Corrosion of Soldered Copper Using the Scanning Vibrating Electrode Technique," *Corrosion Science* 28 (1988): 547–558.

80. V. S. Voruganti, H. B. Huft, D. DeGeer, and S. A. Bradford, "Scanning Reference Electrode Technique for the Investigation of Preferential Corrosion of Weldments in Offshore Applications," *Corrosion* 47, no. 5 (1991): 343–351.

81. H. S. Isaacs, "The Localized Breakdown and Repair of Passive Surfaces during Pitting," *Corrosion Science* 29 (1989): 313–323.

82. A. M. Simões, A. C. Bastos, M. G. Ferreira, Y. González-Garcıá, S. González, and R. M. Souto, "Use of SVET and SECM to Study the Galvanic Corrosion of an Iron–Zinc Cell, *Corrosion Science* 49 (2007): 726–739.

83. G. Williams, N. Birbilis, and H. N. McMurray, "Controlling Factors in Localised Corrosion Morphologies Observed for Magnesium Immersed in Chloride Containing Electrolyte," *Faraday Discussions* 180 (2015): 313–330.

84. P. A. Dick, G. H. Knörnschild, and L. F. P. Dick, "Anodising and Corrosion Resistance of AA 7050 Friction Stir Welds," *Corrosion Science* 114 (2017): 28–36.

85. J. Lin, D. Battocchi, and G. P. Bierwagen, "Inhibitors for Prolonging Corrosion Protection of Mg-Rich Primer on Al Alloy 2024-T3," *Journal of Coatings Technology and Research* 14 (2017): 497–504.

86. R. M. Souto, Y. González-García, A. C. Bastos, and A. M. Simões, "Investigating Corrosion Processes in the Micrometric Range: A SVET Study of the Galvanic Corrosion of Zinc Coupled with Iron," *Corrosion Science* 49 (2007): 4568–4580.

87. G. Williams, A. J. Coleman, and H. N. McMurray, "Inhibition of Aluminium Alloy AA2024-T3 Pitting Corrosion by Copper Complexing Compounds," *Electrochimica Acta* 55 (2010): 5947–5958.

88. G. Williams, K. Gusieva, and N. Birbilis, "Localized Corrosion of Binary Mg-Nd Alloys in Chloride-Containing Electrolyte Using a Scanning Vibrating Electrode Technique," *Corrosion* 68 (2012): 489–498.

89. R. Zlatev, B. Valdez, M. Stoytcheva, R. Ramos, and S. Kiyota, "Solution Conductivity Influence on Pitting Corrosion Studies by SVET," *International Journal of Electrochemical Science* 6 (2011): 2746–2757.

90. H. S. Isaacs and Y. Ishikawa, *Proceedings of the Corrosion Conference* (Houston, TX: NACE Corrosion, 1985).

91. H. S. Isaacs, "The Measurement of the Galvanic Corrosion of Soldered Copper Using the Scanning Vibrating Electrode Technique," *Corrosion Science* 28 (1988): 547–588.

92. Y. Ishikawa and H. S. Isaacs, "Electrochemical Behavior of Pits Developed on Aluminum in a Dilute Chloride Solution," *Corrosion Engineering* 33 (1984): 147–152.

93. S. Fajardo, C. F. Glover, G. Williams, and G. S. Frankel, "The Source of Anodic Hydrogen Evolution on Ultra High Purity Magnesium," *Electrochimica Acta* 212 (2016): 510–521.

94. C. F. Glover and G. Williams, "Inhibition of Localized Corrosion of Hot Dip Galvanized Steel by Phenylphosphonic Acid," *Journal of the Electrochemical Society* 164 (2017): C407–C417.

95. K. B. Deshpande, "Effect of Aluminium Spacer on Galvanic Corrosion between Magnesium and Mild Steel Using Numerical Model and SVET Experiments," *Corrosion Science* 62 (2012): 184–191.

96. A. M. Simões, D. Battocchi, D. Tallman, and G. Bierwagen, "Assessment of the Corrosion Protection of Aluminium Substrates by a Mg-Rich Primer: EIS, SVET and SECM Study," *Progress in Organic Coatings* 63 (2008): 260–266.

97. A. M. Simões, D. Battocchi, D. Tallman, and G. Bierwagen, "SVET and SECM Imaging of Cathodic Protection of Aluminium by a Mg-Rich Coating," *Corrosion Science* 49 (2007): 3838–3849.

98. C. F. Glover, T. W. Cain, and J. R. Scully, "Performance of Mg-Sn Surface Alloys for the Sacrificial Cathodic Protection of Mg Alloy AZ31B-H24," *Corrosion Science* 149 (2019): 195–206.

99. A. C. Bastos, M. C. Quevedo, O. V. Karavai, and M. G. S. Ferreira, "Review—On the Application of the Scanning Vibrating Electrode Technique (SVET) to Corrosion Research," *Journal of the Electrochemical Society* 164 (2017): C973–C990.

100. J. R. Kish, N. Birbilis, E. B. McNally, G. F. Glover, X. Zhang, J. R. McDermid, and G. Williams, "Corrosion Performance of Friction Stir Linear Lap Welded AM60B Joints," *Journal of Materials* 69 (2017): 2335–2344.

101. H. N. McMurray and D. A. Worsley, "Scanning Electrochemical Techniques for the Study of Localised Metallic Corrosion," *Research in Chemical Kinetics* 4 (1997): 149.

102. H. Luo, X. G. Li, C. F. Dong, and K. Xiao, "Effect of Solution Treatment on Pitting Behavior of 2205 Duplex Stainless Steel," *Arabian Journal of Chemistry* 10 (2017): S90–S94.

103. Y. González-Garcia, G. T. Burstein, S. González, and R. M. Souto, "Imaging Metastable Pits on Austenitic Stainless Steel In Situ at the Open-Circuit Corrosion Potential," *Electrochemistry Communications* 6 (2004): 637–642.

104. J. Izquierdo, L. Nagy, I. Bitter, R. M. Souto, and G. Nagy, "Potentiometric Scanning Electrochemical Microscopy for the Local Characterization of the Electrochemical Behaviour of Magnesium-Based Materials," *Electrochimica Acta* 87 (2013): 283–293.

105. E. Völker, C. G. Inchauspe, and E. J. Calvo, "Scanning Electrochemical Microscopy Measurement of Ferrous Ion Fluxes during Localized Corrosion of Steel," *Electrochemistry Communications* 8 (2006): 179–183.

106. D. O. Wipf, "Initiation and Study of Localized Corrosion by Scanning Electrochemical Microscopy," in *Colloids and Surfaces A: Physicochemical and Engineering Aspects* 93, no. 5 (1994): 251–261.

107. K. Fushimi and S. Masahiro, "An SECM Observation of Dissolution Distribution of Ferrous or Ferric Ion from a Polycrystalline Iron Electrode," *Electrochimica Acta* (2001): 121–127.

108. F. Andreatta, H. Terryn, and J. H. W. De Wit, "Effect of Solution Heat Treatment on Galvanic Coupling between Intermetallics and Matrix in AA7075-T6," *Corrosion Science* 45 (2003): 1733–1746.

109. P. Marcus and V. Maurice, "Applications of Scanning Tunneling Microscopy to Corrosion Research," *Materials Science Forum* 192–194 (1995): 765–778.

110. R. M. Souto, Y. G. Garcia, D. Battistel, and S. Daniele, "On the Use of Mercury-Coated Tips in Scanning Electrochemical Microscopy to Investigate Galvanic Corrosion Processes Involving Zinc And Iron," *Corrosion Science* 55 (2012): 401–406.

111. A. C. Bastos, A. M. Simões, and M. G. Ferreira, "Corrosion of Electrogalvanized Steel in 0.1 M NaCl Studied by SVET," *Electrochimica Acta* 21 (2003): 371–387.

112. R. M. Souto, Y. González-García, J. Izquierdo, and S. González, "Examination of Organic Coatings on Metallic Substrates by Scanning Electrochemical Microscopy in Feedback Mode: Revealing the Early Stages of Coating Breakdown in Corrosive Environments," *Corrosion Science* 52 (2010): 748–753.

113. Y. González-García, J. M. C. Mol, T. Muselle, I. De Graeve, G. Van Assche, G. Scheltjens, B. Van Mele, and H. Terryn, "SECM Study of Defect Repair in Self-Healing Polymer Coatings on Metals," *Electrochemistry Communications* 13 (2011): 169–173.

114. R. Unwin and A. J. Bard, "Scanning Electrochemical Microscopy. 14. Scanning Electrochemical Microscope Induced Desorption: A New Technique for the Measurement of Adsorption/Desorption Kinetics and Surface Diffusion Rates at the Solid/Liquid Interface," *Journal of the American Chemical Society* (1992): 5035–5045.

115. R. F. Schaller, S. Thomas, N. Birbilis, and J. R. Scully, "Spatially Resolved Mapping of the Relative Concentration of Dissolved Hydrogen Using the Scanning Electrochemical Microscope," *Electrochemistry Communications* 51 (2015): 54–58.

116. U. M. Tefashe, M. E. Snowden, P. D. Ducharme, M. Danaie, G. A. Botton, and J. Mauzeroll, "Local Flux of Hydrogen from Magnesium Alloy Corrosion Investigated by Scanning Electrochemical Microscopy," *Journal of Electroanalytical Chemistry* 720–721 (2014): 121–127.

117. N. A. Payne, P. I. Stephens, and J. Mauzeroll, "The Application of Scanning Electrochemical Microscopy to Corrosion Research," *Corrosion* 73 (2017): 759–780.

118. L. Bland, R. F. Schaller, and J. R. Scully, "Utilization of a Partially Non-Aqueous Electrolyte for the Spatial Mapping of Mg Corrosion Using a Model Mg–Al Electrode," *Magnesium Technology* (2017): 421–428.

119. P. Dauphin-Ducharme, R. M. Asmussen, U. M. Tefashe, M. Danaie, W. J. Binns, P. Jakupi, G. A. Botton, D. W. Shoesmith, and J. Mauzeroll, "Local Hydrogen Fluxes Correlated to Microstructural Features of a Corroding Sand Cast AM50 Magnesium Alloy," *Journal of the Electrochemical Society* 161, no. 12 (2014): C557–C564.

120. J. Kwak and A. J. Bard, "Scanning Electrochemical Microscopy. Theory of the Feedback Mode," *Analytical Chemistry* 61 (1989): 1221–1227.

121. X. Lu, Y. Zuo, X. Zhao, and Y. Tang, "The Improved Performance of a Mg-Rich Epoxy Coating on AZ91D Magnesium Alloy by Silane Pretreatment," *Corrosion Science* 60 (2012): 165–172.

122. G. Bierwagen, R. Brown, D. Battocchi, and S. Hayes, "Active Metal-Based Corrosion Protective Coating Systems for Aircraft Requiring No-Chromate Pretreatment," *Progress in Organic Coatings* 67 (2010): 195–208.

123. A. J. Bard, F. R. F. Fan, J. Kwak, and O. Lev, "Scanning Electrochemical Microscopy in Electroanalytical Chemistry: A Series of Advances," *Analytical Chemistry* 61 (1989): 132–138.

124. A. J. Bard, F.-R. F. Fan, and M. V. Mirkin, "Scanning Electrochemical Microscopy," in *Electroanalytical Chemistry, vol: A Series of Advances*, ed. A. J. Bard, vol. 18 (New York: Marcel Dekker, 1994): 243–373.

125. J. Kwak and A. J. Bard, "Scanning Electrochemical Microscopy. Apparatus and Two-Dimensional Scans of Conductive and Insulating Substrates, *Analytical Chemistry* 61 (1989): 1794–1799.

126. Z. Szklarska-Smialowska, *Pitting Corrosion of Metals* (Houston, TX: National Association of Corrosion Engineers, 1986).

127. B. E. Wilde, "A Critical Appraisal of Some Popular Laboratory Electrochemical Tests for Predicting the Localized Corrosion Resistance of Stainless Alloys in Sea Water," *Corrosion* 28 (1972): 283–291.

128. B. C. Syrett, "PPR Curves—A New Method of Assessing Pitting Corrosion Resistance," *Corrosion* 33 (1977): 221–224.

129. N. Pessall and C. Liu, "Determination of Critical Pitting Potentials of Stainless Steels in Aqueous Chloride Environments, *Electrochimica Acta* 16 (1971): 1987–2003.

130. B. E. Wilde and E. Williams, "The Relevance of Accelerated Electrochemical Pitting Tests to the Long-Term Pitting and Crevice Corrosion Behavior of Stainless Steels in Marine Environments," *Journal of the Electrochemical Society* 118 (1971): 1057–1062.

131. N. G. Thompson and B. C. Syrett, "Relationship between Conventional Pitting and Protection Potentials and a New, Unique Pitting Potential," *Corrosion* 48, no. 8 (1992): 649–659.

132. R. Revie, *Uhlig's Corrosion Handbook*, 2nd ed. (New York: Wiley, 2000).

133. B. E. Wilde and E. Williams, "The Use of Current/Voltage Curves for the Study of Localized Corrosion and Passivity Breakdown on Stainless Steels in Chloride Media," *Electrochemica Acta* 16 (1971): 1971–1975.

134. K. K. Starr, E. D. Verink, Jr., and M. Pourbaix, "The Significance of the Protection Potential for Fe-Cr Alloys at Room Temperature," *Corrosion* 2 (1976): 47–51.

135. M. Yasuda, F. Weinburg, and D. Tromans, "Pitting Corrosion of Al and Al-Cu Single Crystals," *Journal of the Electrochemical Society* 137 (1990): 3708–3715.

136. S. Tsujikawa, T. Hasamatsu, and G. Boshoku, "On the Repassivation Potential for Crevice Corrosion," *Corrosion Engineering* 29 (1980): 37–40.

137. T. Shinohara, S. Tsujikawa, and G. Boshoku, "In-situ Measurement for Crevice Corrosion of High Purity 18Cr-14Ni Steel under Optical Glass in 3% NaCl Solution," *Corrosion Engineering* 39 (1990): 238–246.

138. S. Tsujikawa, Z. Heng, Y. Hisamatsu, and G. Boshoku, "Critical Potentials for Crevice Corrosion of Type 444 Steel in NaCl Solutions at 80°C," *Corrosion Engineering* 32 (1983): 149–156.

139. D. Dunn and N. Sridhar, *Proceedings of the Electrochemical Society,* vols. 95–15 (Pennington, NJ: Electrochemical Society, 1996), 79–90.

140. G. T. Gaudet, W. T. Mo, T. A. Hatton, J. W. Tester, J. Tilly, H. S. Isaacs, and R. C. Newman, "Mass Transfer and Electrochemical Kinetic Interactions in Localized Pitting Corrosion," *American Institute of Chemical Engineers Journal* 32, no. 60 (1986): 949–958.

141. J. R. Ambrose and J. Kruger, "Tribo-Ellipsometric Study of the Repassivation Kinetics of a Ti 8Al-1Mo-1V Alloy," *Journal of the Electrochemical Society* 121 (1974): 599–604.

142. N. Sridhar and G. A. Cragnolino, "Applicability of Repassivation Potential for Long-Term Prediction of Localized Corrosion of Alloy 825 and Type 316L Stainless Steel," *Corrosion* 49 (1993): 885–894.

143. B. A. Kehler, G. O. Ilevbare, and J. R. Scully, "Crevice Corrosion Stabilization and Repassivation Behavior of Alloy 625 and Alloy 22," *Corrosion* 57, no. 12 (2001): 1042–1065.

144. P. C. Pistorius and G. T. Burstein, "Metastable Pitting Corrosion of Stainless Steel and the Transition to Stability," *Philosophical Transactions of the Royal Society of London* 341 (1992): 531–559.

145. T. Shibata, "Stochastic Approach to the Effect of Alloying Elements on the Pitting Resistance of Ferritic Stainless Steels, *Transactions ISIJ* 23 (1983): 785–788.

146. T. Shibata and T. Takeyama, "Stochastic Theory of Pitting Corrosion," *Corrosion* 33 (1977): 243–251.

147. T. Shibata and Y.-C. Zhu, "The Effect of Film Formation Potential on the Stochastic Processes of Pit Generation on Anodized Titanium," *Corrosion Science* 36, no. 1 (1994): 153–163.

148. S. T. Pride, J. R. Scully, and J. L. Hudson, "Metastable Pitting of Aluminum and Criteria for the Transition to Stable Pit Growth," *Journal of the Electrochemical Society* 141 (1994): 3028–3040.

149. G. O. Ilevbare, J. R. Scully, J. Yuan, and R. G. Kelly, "Inhibition of Pitting Corrosion on Aluminum Alloy 2024-T3: Effect of Soluble Chromate Additions vs Chromate Conversion Coating," *Corrosion* 56, no. 3 (2000): 227–242.

150. J. E. Sweitzer, G. J. Shiflet, and J. R. Scully, "Localized Corrosion of Al90Fe5Gd5 and Al87Ni8.7Y4.3 Alloys in the Amorphous, Nanocrystalline and Crystalline States: Resistance to Micrometer-Scale Pit Formation," *Electrochimica Acta* 48 (2003): 1223–1234.

151. D. D. Macdonald, *Critical Factors in Localized Corrosion*, vol. 92-9, Electrochemical Society Proceedings Series, ed. G. S. Frankel and R. C. Newman (Pennington, NJ: Electrochemical Society, 1992), 144.

152. T. Suter and R. C. Alkire, "Microelectrochemical Studies of Pit Initiation at Single Inclusions in Al 2024-T3," *Journal of the Electrochemical Society* 148, no. 1 (2001): B36–B42.

153. G. T. Burstein and G. O. Ilevbare, "The Effect of Specimen Size on the Measured Pitting Potential of Stainless Steel," *Corrosion Science* 38 (1996): 2257–2265.

154. K. Hladky and J. L. Dawson, "The Measurement of Corrosion Using Electrochemical Noise," *Corrosion Science* 22 (1982): 231–237.

155. K. Hladky and J. L. Dawson, "The Measurement of Localized Corrosion Using Electrochemical Noise," *Corrosion Science* 21 (1982): 317–322.

156. H. S. Bertocci, *Proceedings of the 2nd International Conference on Localized Corrosion*, NACE-9, ed. H. Isaacs, U. Bertocci, J. Kruger, and S. Smialowska (Houston, TX: National Association of Corrosion Engineers, 1990).

157. H. S. Bertocci and J. Kruger, "Studies of Passive Film Breakdown by Detection and Analysis of Electrochemical Noise," *Surface Science* 101 (1980): 608–618.

158. D. A. Eden and A. N. Rothwell, Paper No. 92, in *Proceedings of the Corrosion Conference* (Houston, TX: National Association of Corrosion Engineers, 1992).

159. D. E. Williams, J. Stewart, and B. H. Balkwill, *Proceedings of the Symposium on Critical Factors in Localized Corrosion*, vol. 92-9, ed. G. S. Frankel and R. C. Newman (Pennington, NJ: Electrochemical Society, 1992), 36.

160. S. T. Pride, J. R. Scully, and J. L. Hudson, "Analysis of Electrochemical Noise from Metastable Pitting in Aluminum, Aged Al-2%Cu, and AA 2024-T3" in *Electrochemical Noise Measurement for Corrosion Applications,* ed. J. R. Kearns, J. R. Scully, P. R. Roberge, D. L. Reichert, and J. L. Dawson (West Conshohocken, PA: ASTM International, 1996), 307–331.

161. N. D. Budiansky, F. Bocher, H. Cong, M. F. Hurley, and J. R. Scully, "Use of Coupled Multi-Electrode Arrays to Advance the Understanding of Selected Corrosion Phenomena," *Corrosion Journal* 63 (2007): 537–554.

162. L. Yang, N. Sridhar, O. Pensado, and D. S. Dunn, "An In-Situ Galvanically Coupled Multielectrode Array Sensor for Localized Corrosion," *Corrosion Journal* 58 (2002): 1004–1014.

163. F. Bocher, F. J. Presuel-Moreno, N. D. Budiansky, and J. Scully, "Couple Multi-Electrode Investigation of Crevice Corrosion of 316 Stainless Steel and NiCrMo Alloy 625," *ECS Transactions* 3 (2007): 105–123.

164. F. Bocher, F. Presuel-Moreno, and J. R. Scully, "Investigation of Crevice Corrosion of AISI 316 Stainless Steel Compared to Ni–Cr–Mo Alloys Using Coupled Multielectrode Arrays," *Journal of the Electrochemical Society* 155 (2008): C256–C268.

165. A. D. King, J. S. Lee, and J. R. Scully, "Galvanic Couple Current and Potential Distribution between a Mg Electrode and 2024-T351 under Droplets Analyzed by Microelectrode Arrays," *Journal of the Electrochemical Society* 162 (2015): C12–C23.

166. N. D. Budiansky, F. Bocher, H. Cong, M. F. Hurley, and J. R. Scully, "Use of Coupled Multi-Electrode Arrays to Advance the Understanding of Selected Corrosion Phenomena," *Corrosion Journal* 63 (2007): 537–554.

167. H. Cong and J. R. Scully, "Use of Coupled Multielectrode Arrays to Elucidate the pH Dependence of Copper Pitting in Potable Water," *Journal of the Electrochemical Society* 157 (2010): C36–C46.

168. N. Budiansky, J. L. Hudson, and J. R. Scully, "Origins of Persistent Interaction among Localized Corrosion Sites on Stainless Steel," *Journal of the Electrochemical Society* 151 (2004): B233–B243.

169. Z. Fei, R. G. Kelly, and J. L. Hudson, "Spatiotemporal Patterns on Electrode Arrays," *Journal of Physical Chemistry* 100 (1996): 18986–18991.

170. V. N. Rafla, A. Davenport, and J. R. Scully, "Determination of Cathodic and Anodic Charge from Operando X-Ray Tomography Observation of Galvanic Corrosion of Aluminum Alloy 7050-T7451 and 304 Stainless Steel in a Simulated Fastener," *Corrosion* 71 (2015): 1300–1303.

171. V. N. Rafla, A. Davenport, and J. R. Scully, "Operando Assessment of Galvanic Corrosion between Al-Zn-Mg-Cu Alloy and a Stainless Steel Fastener Using X-Ray Tomography," *Corrosion* 74 (2017): 5–23.

172. V. N. Rafla, A. D. King, S. Glanvill, A. Parsons, A. Davenport, and J. R. Scully, "Operando Observation of Galvanic Corrosion between Aluminum Alloy 7050-T7451 and 304 Stainless Steel in a Simulated Fastener Arrangement Using X-Ray Tomography," *Corrosion* 71 (2015): 1171–1176.

173. B. D. Chambers, S. R. Taylor, and M. W. Kendig, "Rapid Discovery of Corrosion Inhibitors and Synergistic Combinations Using High-Throughput Screening Methods," *Corrosion Journal* 61 (2005): 480–489.

174. F. Bocher and J. R. Scully, "Stifling of Crevice Corrosion and Repassivation: Cathode Area versus Controlled Potential Decreases Assessed with a Coupled Multi-Electrode Array," *Corrosion Journal* 71 (2015): 1049–1063.

175. R. N. Parkins, "Predictive Approaches to Stress Corrosion Cracking Failure," *Corrosion Science* 20 (1990): 147–166.

176. J. J. DeLuccia and D. A. Berman, "An Electrochemical Technique to Measure Diffusible Hydrogen in Metals (Barnacle Electrode)," in *Electrochemical Corrosion Testing,* ed. F. Mansfeld and U. Bertocci (West Conshohocken, PA: ASTM International, 1981), 256–273.

177. D. A. Berman and V. S. Agarwala, "The Barnacle Electrode Method to Determine Diffusible Hydrogen in Steels," in *Hydrogen Embrittlement: Prevention and Control,* ed. L. Raymond (West Conshohocken, PA: ASTM International, 1988), 98–104.

178. M. A. V. Devanathan and Z. Stachurski, "The Adsorption and Diffusion of Electrolytic Hydrogen in Palladium," *Proceedings of the Royal Society, A* 270 (1962): 90–102.

179. J. McBreen, J. Nanis, and W. Beck, "A Method for Determination of the Permeation Rate of Hydrogen through Metal Membranes," *Journal of the Electrochemical Society* 113 (1966): 1218–1222.

180. J. R. Scully and P. J. Moran, "The Influence of Strain on Hydrogen Entry and Transport in a High Strength Steel in Sodium Chloride Solution," *Journal of the Electrochemical Society* 135, no. 6 (1988): 1337–1348

181. P. Novak, R. Stefec, and F. Franz, "Testing the Susceptibility of Stainless Steel to Intergranular Corrosion by a Reactivation Method," *Corrosion* 31, no. 10 (1975): 344-347.

182. W. L. Clarke, V. M. Romero, and J. C. Danko, Paper No. 180, in *Proceedings of the Corrosion Conference* (Houston, TX: National Association of Corrosion Engineers, 1977).

183. W. L. Clarke, R. L. Cowan, and W. L. Walker, "Comparative Methods for Measuring Degree of Sensitization in Stainless Steel," in *Intergranular Corrosion of Stainless Alloys,* ed. R. F. Steigerwald (West Conshohocken, PA: ASTM International, 1978), 99–132.

184. M. Akashi, T. Kawamoto, and F. Umemura, "Evaluation of IGSCC Susceptibility of Austenitic Stainless Steels Using Electrochemical Reactivation Method," *Corrosion Engineering* 29 (1980): 163–169.

185. A. P. Majidi and M. A. Streicher, "The Double Loop Reactivation Method for Detecting Sensitization in AISI 304 Stainless Steels," *Corrosion* 40, no. 11 (1984): 584–593.

186. J. B. Lee, "A New Electrochemical Potentiokinetic Reactivation Test for Determining Degree of Sensitization in Ferritic Stainless Steels," *Corrosion* 42, no. 2 (1986): 106–110.

187. A. Roelandt and J. Vereecken, "A Modified Electrochemical Technique (Electrochemical Potentiokinetic Reactivation) for Evaluating the Susceptibility of Inconel 600 to Intergranular Corrosion," *Corrosion* 42, no. 5 (1986): 289–298.

188. J. R. Scully and R. Kelly, "An Electrochemical Test for Detecting the Intergranular Corrosion Susceptibility of a Duplex Stainless Steel," *Corrosion* 42, no. 9 (1986): 537–542.

189. J. Stone, H. A. Tuttle, and H. N. Bogart, "Ford Anodized Aluminum Corrosion," *Plating* 43 (1965): 877–888.

190. C. E. Michaelson, S. W. Dean, and Strousky, *CORROSION/69, Proceedings of the 25th Conference* (Houston, TX: National Association of Corrosion Engineers, 1969), 648.

191. R. L. Saur and R. P. Basco, "Corrosion of Triplex Nickel Systems in Service and in the EC and CASS Tests," *Plating* 53 (1966): 981–985.

192. R. L. Saur and R. P. Basco, "Correlation of 'EC' and CASS Tests to Service Using Duplex Nickel Systems," *Plating* 53 (1966): 320–325.

193. E. T. Englehart and G. Sowinski, Jr., *Society of Automotive Engineers Journal* 72 (1974): 51.

194. E. T. Englehart and D. J. George, *Materials Protection* 3 (1964): 25.

195. J. D. Scantlebury, K. N. Ho, and D. A. Eden, "Impedance Measurements on Organic Coatings on Mild Steel in Sodium Chloride Solutions," in *Electrochemical Corrosion Testing,* ed. F. Mansfeld and U. Bertocci (West Conshohocken, PA: ASTM International, 1981), 187–197.

196. S. Narian, N. Bonanos, and M. G. Hocking, "AC Impedance Measurements on Thick Organic Coatings on Mild Steel Substrates," *Journal of Oil Colour Chemical Association* 66, no. 2 (1983): 48–52.

197. T. A. Strivens and C. C. Taylor, "An Assessment of A/C Impedance as a Basic Research and Routine Testing Method for Studying Corrosion of Metals under Paint," *Materials Chemistry* 7 (1982): 199–220.

198. F. Mansfeld, M. W. Kendig, and S. Tsai, "Evaluation of Corrosion Behavior of Coated Metals with AC Impedance Measurements," *Corrosion* 38, no. 9 (1982): 478–485.

199. M. Kendig, F. Mansfeld, and S. Tsai, "Determination of the Long Term Corrosion Behavior of Coated Steel with A.C. Impedance Measurements," *Corrosion Science* 23, no. 4 (1983): 317–329.

200. R. Touhsaent and H. Leidheiser, "A Capacitance-Resistance Study of Polybutadiene Coatings on Steel," *Corrosion* 28, no. 12 (1972): 435–440.

201. S. Haruyama, M. Asari, and T. Tsuru, in *Corrosion Protection by Organic Coatings*, ed. M. Kendig and H. Leidheiser, Jr., Electrochemical Society Proceedings Series (Pennington, NJ: Electrochemical Society, 1980), 197.

202. J. R. Scully, "Electrochemical Impedance of Organic-Coated Steel: Correlation of Impedance Parameters with Long-Term Coating Deterioration," *Journal of the Electrochemical Society* 136, no. 4 (1989): 979–990.

203. M. W. Kendig and J. R. Scully, "Basic Aspects of Electrochemical Impedance Application for the Life Prediction of Organic Coatings on Metals," *Corrosion* 46, no. 1 (1990): 22–29.

204. H. P. Hack and J. R. Scully, "Defect Area Determination of Organic Coated Steels in Seawater Using the Breakpoint Frequency Method," *Journal of the Electrochemical Society* 138, no. 1 (1991): 33–40.

205. R. Mansfeld and C. C. Lee, "The Frequency Dependence of the Noise Resistance for Polymer-Coated Metals," *Journal of the Electrochemical Society* 144 (1997): 2068–2071.

206. F. Mansfeld, L. T. Han, C. C. Lee, C. Chen., G. Zhang, and H. Xiao, "Analysis of Electrochemical Impedance and Noise Data for Polymer Coated Metals," *Corrosion Science* 39 (1997): 255–279.

207. H. Xioa, L. T. Han, C. C. Lee, and F. Mansfeld, "Collection of Electrochemical Impedance and Noise Data for Polymer-Coated Steel from Remote Test Sites," *Corrosion* 53 (1997): 412–422.

208. D. E. Tallman and G. P. Bierwagen, Paper No. 380, in the *Proceedings of the Corrosion Conference* (Houston, TX: National Association of Corrosion Engineers, 1998).

209. A. Aballe, A. Bautista, U. Bertocci, and F. Huet, "Measurement of the Noise Resistance for Corrosion Applications," *Corrosion* 57 (2001): 35-42.

210. J. P. Hoar and G. C. Wood, "The Sealing of Porous Anodic Oxide Films on Aluminium," *Electrochimica Acta* 7 (1962): 333–353.

211. J. Hitzig, K. Juttner, W. J. Lorenz, and W. Paatsch, "AC-Impedance Measurements on Corroded Porous Aluminum Oxide Films," *Journal of the Electrochemical Society* 133 (1986): 887–892.

212. F. Mansfeld and M. Kendig, "Evaluation of Anodized Aluminum Surfaces with Electrochemical Impedance Spectroscopy," *Journal of the Electrochemical Society* 135 (1988): 828-833.

213. D. G. Kolman and J. R. Scully, "Electrochemistry and Passivity of a Ti-15Mo-3Nb-3Al Beta-Titanium Alloy in Ambient Temperature Aqueous Chloride Solutions," *Journal of the Electrochemical Society* 140 (1993): 2771–2779.

214. J. R. Scully, D. Silverman, and M. W. Kendig, ed., *Electrochemical Impedance: Analysis and Interpretation* (West Conshohocken, PA: ASTM International, 1993).

215. F. Mansfeld, V. Wang, and H. Shih, "Development of "Stainless Aluminum" *Journal of the Electrochemical Society* 138 (1991): L74–L75.

216. H. Shih and F. Mansfeld, "Passivation in Rare Earth Metal Chlorides—A New Conversion Coating Process for Aluminum Alloys," in *New Methods for Corrosion Testing of Aluminum Alloys*, ed. V. S. Agarwala and G. M. Ugiansky (West Conshohocken, PA: ASTM International, 1992), 180–195.

217. F. Mansfeld, S. Lin, and H. Shih, "Corrosion Protection of Al Alloys and Al-Based Metal Matrix Composites by Chemical Passivation," *Corrosion* 45 (1989): 615–630.

218. S. Kendig, M. Jeanjaquet, and M. Cunningham, *Final Report to Rockwell International Space Systems Division and the South Coast Air Quality Management District* (Ventura, CA: Rockwell International Space System, September 1993).

219. R. G. Buchheit, M. Cunningham, H. Jensen, M. W. Kendig, and M. A. Martinez, "A Correlation between Salt Spray and Electrochemical Impedance Spectroscopy Test Results for Conversion-Coated Aluminum Alloys," *Corrosion* 54 (1998): 61–72.

220. G. O. Ilevbare and J. R. Scully, "Mass-Transport-Limited Oxygen Reduction Reaction on AA2024-T3 and Selected Intermetallic Compounds in Chromate-Containing Solutions," *Corrosion* 57 (2001): 134–152.

221. J. L. Davies, C. F. Glover, J. Van De Langkruis, E. Zoestbergen, and G. Williams, "The Effect of Mg Concentration on the Resistance of PVD Zn-Mg Coatings to Corrosion Driven Organic Coating Delamination," *Corrosion Science* 100 (2015): 607–618.

222. C. F. Glover, C. A. J. Richards, G. Williams, and H. N. McMurray, "Evaluation of Multi-Layered Graphene Nano-Platelet Composite Coatings for Corrosion Control Part II–Cathodic Delamination Kinetic," *Corrosion Science* 136 (2018): 304–310.

223. G. Williams, A. Gabriel, A. Cook, and H. N. McMurray, "Dopant Effects in Polyaniline Inhibition of Corrosion-Driven Organic Coating Cathodic Delamination on Iron," *Journal of the Electrochemical Society* 153 (2006): B425-B433.

224. G. Williams and H. N. McMurray, "Chromate Inhibition of Corrosion-Driven Organic Coating Delamination Studied Using a Scanning Kelvin Probe Technique," *Journal of the Electrochemical Society* 148 (2001): B377–B385.

225. G. Williams, H. N. McMurray, and D. A. Worsley, "Cerium(III) Inhibition of Corrosion-Driven Organic Coating Delamination Studied Using a Scanning Kelvin Probe Technique," *Journal of the Electrochemical Society* 149 (2002): B154–B162.

226. V. Shkirskiy, M. Uebel, A. Maltseva, G. Lefèvre, P. Volovitch, and M. Rohwerder, "Cathodic Driven Coating Delamination Suppressed by Inhibition of Cation Migration along Zn|Polymer Interface in Atmospheric CO2," *NPJ Materials Degradation* 3 (2019): 1–10

227. M. Fedel, F. Deflorian, and S. Rossi, "Correlations between the Volta Potential and Filiform Corrosion on Painted AA2024 Aluminum Alloy," *Surface and Interface Analysis* 42 (2010): 199–204.

228. H. N. McMurray, A. Holder, G. Williams, G. M. Scamans, and A. J. Coleman, "The Kinetics and Mechanisms of Filiform Corrosion on Aluminium Alloy AA6111," *Electrochimica Acta* 55 (2010): 7843–7852.

229. G. Williams and H. N. McMurray, "The Mechanism of Group (I) Chloride Initiated Filiform Corrosion on Iron," *Electrochemistry Communications* 5 (2003): 871–877.

230. G. Williams and H. N. McMurray, "Polyaniline Inhibition of Filiform Corrosion on Organic Coated AA2024-T3," *Electrochimica Acta* 54 (2009): 4245–4252.

231. G. Williams and H. N. McMurray, "Inhibition of Filiform Corrosion on Polymer Coated AA2024-T3 by Hydrotalcite-Like Pigments Incorporating Organic Anions," *Electrochemical and Solid-State Letters* 7 (2004): B13–B15.

232. G. Williams, H. N. McMurray, D. Hayman, and D. C. P. Morgan, "Time-Lapse Potentiometric Imaging of Active Filiform Corrosion Using a Scanning Kelvin Probe Technique," *Physical Chemical Communications* 4 (2001): 1–6.

233. H. N. McMurray and G. Williams, "Under Film/Coating Corrosion," in *Shreir's Corrosion, Vol. 2: Corrosion in Liquids, Corrosion Evaluation*, ed. T. A. J. Richardson (Oxford, UK: Elsevier, [2009] 2016), 988–1004.

234. R. F. Schaller and J. R. Scully, "Measurement of Effective Hydrogen Diffusivity Using the Scanning Kelvin Probe," *Electrochemistry Communications* 40 (2014): 42–44.

235. G. Schimo, W. Burgstaller, and A. W. Hassel, "Rolling Direction Dependent Diffusion Coefficients of Hydrogen in Ferritic Steel by SDCM Charging and SKP Probing," *ISIJ International* 56 (2016): 487–491.

236. G. Schimo, W. Burgstaller, and A. W. Hassel, "Potentiodynamic Hydrogen Permeation on Palladium-Kelvin Probe Compared to 3D Printed Microelectrochemical Cell," *Electrochemistry Communications* 60 (2015): 208–211.

237. G. Williams, H. N. McMurray, and R. C. Newman, "Surface Oxide Reduction by Hydrogen Permeation through Iron Foil Detected Using a Scanning Kelvin Probe," *Electrochemistry Communications* 27 (2013): 144–147.

238. S. C. Morton and G. S. Frankel, "Atmospheric Pitting Corrosion of AA7075-T6 under Evaporating Droplets with and without Inhibitors," *Materials and Corrosion* 65 (2014): 351–361.

239. H. N. McMurray and G. Williams, "Probe Diameter and Probe–Specimen Distance Dependence in the Lateral Resolution of a Scanning Kelvin Probe," *Journal of Applied Physics* 91 (2002): 1673–1679.

240. W. Furbeth and M. Stratmann, "The Delamination of Polymeric Coatings from Electrogalvanised Steel–A Mechanistic Approach," *Corrosion Science* 43 (2001): 207–227.

241. A. Leng, H. Streckel, and M. Stratmann, "The Delamination of Polymeric Coatings from Steel. Part 1: Calibration of the Kelvinprobe and Basic Delamination Mechanism," *Corrosion Science* 41, no. 3 (1998): 579–597.

242. M. Stratmann, A. Leng, W. Fürbeth, H. Streckel, H. Gehmecker, and K.-H. Groβe-Brinkhaus, "The Scanning Kelvin Probe: A New Technique for the In Situ Analysis of the Delamination of Organic Coatings," *Progress in Organic Coatings* (1996): 261–267.

243. W. Furbeth and M. Stratmann, "Scanning Kelvin Probe Investigations on the Delamination of Polymeric Coatings from Metallic Surfaces," *Progress in Organic Coatings* 39 (2000): 23–29.

244. C. F. Glover, R. Subramanian, and G. Williams, "In-Coating Phenyl Phosphonic Acid as an Etch-Primer Corrosion Inhibitor System for Hot Dip Galvanized Steel," *Journal of the Electrochemical Society* 162 (2015): C433–C441.

245. C. F. Glover, C. Richards, J. Baker, G. Williams, and H. N. McMurray, "In-Coating Graphene Nano-Platelets for Environmentally-Friendly Corrosion Protection of Iron," *Corrosion Science* 114 (2017): 169–172.

246. M. Rohwerder, S. Isik-Uppenkamp, and C. A. Amarnath, "Application of the Kelvin Probe Method for Screening the Interfacial Reactivity of Conducting Polymer Based Coatings for Corrosion Protection," *Electrochimica Acta* 56 (2011): 1889–1893.

Chapter 9 | Immersion Testing

Bradley D. Krantz[1]

Introduction

Most chemical plant processes are complex. Materials of construction for process equipment and piping must be selected with care to ensure adequate corrosion resistance during operation of those plants. Sustainable operation is critical to plant safety and business vitality. In a well-designed plant, materials selection should be based on as much information as is available. The information on which materials selection is based can include the following, in the relative order of usefulness: prior service history, in-plant monitoring and testing, pilot plant evaluations, and laboratory corrosion tests.

As is usually the case, not all of the desired data are available. In many cases, actual service history regarding materials performance is not available or in-plant corrosion studies were not performed. Plant personnel are rarely trained to evaluate corrosion failures thoroughly and detailed failure analysis may not have been performed or sufficiently documented. New processes naturally will not have a service history or corrosion studies that can be utilized. In such instances, pilot plant studies are critical. For practical and economic reasons, however, such studies usually are conducted for short test periods and thus long-term corrosion performance data are unavailable.

When various factors have eliminated other data sources, laboratory corrosion tests are often the only reliable source of corrosion data for screening candidate materials. If these tests are well planned, they can provide the information necessary for intelligent plant design and proper selection of materials of construction. Laboratory tests also offer unique advantages over in-plant tests: for example, many test parameters can be varied and evaluated, and exposure conditions can be controlled or accelerated to simulate worst-case scenarios. In contrast, poorly designed or improperly run and interpreted corrosion tests can give misleading information that can lead to costly materials selection errors.

[1]Corrosion Testing Laboratories, Inc., 60 Blue Hen Dr., Newark, DE 19713, USA
http://orcid.org/0000-0003-3299-4508
The authors acknowledge the previous author of this chapter, Richard A. Corbett, Corrosion Testing Laboratories, Inc., Newark, DE.

DOI: 10.1520/MNL202NDSUP20190004

The following discussion is focused on immersion testing of metals. Similar procedures can be utilized for nonmetallic materials with some modifications to methods of evaluation but are not included in this discussion.

Basic Principles

For any given chemical process, it is not always possible to predict which forms of corrosion will occur, or even which chemical or parameter will dominate the corrosion scenario. Process flow diagrams define certain chemicals and "normal" operating conditions, but they frequently overlook effects of trace elements (impurities), transient conditions, or chemical intermediates. Such factors can have a major effect on corrosion and hence materials performance. Subtle changes in pH can shift electrochemical potentials, for example, from a passive range into a pitting range. Certain ionic species, while having little effect in the bulk environment, can act as accelerating charge carriers when concentrated inside a pit or crevice. Such factors must be considered when designing a laboratory corrosion test.

Laboratory corrosion test parameters usually are separated into two groups: chemical and physical. Chemical parameters include not only the concentration of various compounds but also such factors as dissociation, pH, phase equilibrium (especially vapor phase chemistry), dissolved gases, conductivity, and degradation reactions caused by the candidate test materials themselves. Relevant physical parameters include temperature (including temperature gradients and heat transfer), pressure, flow velocity, surface area effects (such as ratio of volume-to-surface area of corrosion test coupons), and time (i.e., test duration). Also important are cyclical changes in these parameters. It is often cost and time prohibitive to conduct a full factorial study to determine the effects of all variables, so educated decisions must be made as to which variables might be important in a particular process and how many variations of each parameter should be included in the corrosion test program.

Depending on the expected mechanism of corrosion (i.e., general or localized pitting, crevice, environmentally assisted cracking or galvanic attack), different tests are usually required to determine the susceptibility to attack. Table 1 summarizes

Copyright © 2022 by ASTM International, 100 Barr Harbor Dr., PO Box C700, West Conshohocken, PA 19428-2959
ASTM International is not responsible, as a body, for the statements and opinions expressed in this chapter. ASTM International does not endorse any products represented in this chapter.

TABLE 1 Common Forms of Corrosion and Laboratory Evaluation Tests

Mode of Attack	Occurrence in Industry (Typical)	Evaluation Tests	ASTM Std. (Typical)
General Corrosion	28%	Total Immersion Tests (Atmospheric & Autoclave)	G31, *Standard Guide for Laboratory Immersion Corrosion Testing of Metals*
		Multiphase (liquid, vapor, condensate, interface) Tests	G31
		Hot Wall	
		Electrochemical Polarization	G5, *Standard Reference Test Method for Making Potentiodynamic Anodic Polarization Measurements*
		Electrochemical Impedance	G106, *Standard Practice for Verification of Algorithm and Equipment for Electrochemical Impedance Measurements*
Stress Corrosion Cracking	24%	Boiling Chloride U-Bend Tests	G36, *Standard Practice for Evaluation Stress-Corrosion-Cracking Resistance of Metals and Alloys in a Boiling Magnesium Chloride Solution* G123, *Standard Test Method for Evaluating Stress-Corrosion Cracking of Stainless Alloys with Different Nickel Content in Boiling Acidified Sodium Chloride Solution*
		Wick Test	C692, *Standard Test Method for Evaluating the Influence of Thermal Insulations on External Stress Corrosion Cracking Tendency of Austenitic Stainless Steel*
		Polythionic Acid Cracking Test	G35, *Standard Practice for Determining the Susceptibility of Stainless Steels and Related Nickel-Chromium-Iron Alloys to Stress-Corrosion Cracking in Polythionic Acids*
		Caustic Solution Cracking Tests	
		Custom Process Solution Testing	
Pitting Corrosion	15%	Ferric Chloride Immersion Test	G48, *Standard Test Methods for Pitting and Crevice Corrosion Resistance of Stainless Steels and Related Alloys by Use of Ferric Chloride Solution*
		Cyclic Potentiodynamic Polarization (Hysteresis)	G61, *Standard Test Method for Conducting Cyclic Potentiodynamic Polarization Measurements for Localized Corrosion Susceptibility of Iron-, Nickel-, or Cobalt-Based Alloys*
		Critical Pitting/Crevice Temperature Determination	G48
		Seawater/Marine Exposure Testing	G78, *Standard Guide for Crevice Corrosion Testing of Iron-Base and Nickel-Base Stainless Alloys in Seawater and Other Chloride-Containing Aqueous Environments*
		Surgical Implant Test	F2129, *Standard Test Method for Conducting Cyclic Potentiodynamic Polarization Measurements to Determine the Corrosion Susceptibility of Small Implant Devices* F3044, *Standard Test Method for Conducting Cyclic Potentiodynamic Polarization Measurements to Determine the Corrosion Susceptibility of Small Implant Devices*
		Green Death Test	
		Critical Pitting Potential Test (Potentiostatic)	G5
Crevice Corrosion	2%	Critical Pitting/Crevice Temperature Determination	G48, G150, *Standard Test Method for Electrochemical Critical Pitting Temperature Testing of Stainless Steels and Related Alloys*
		Multi-Crevice Washer/Process Solutions	G48, G78
Intergranular	15%	Electrolytic Oxalic Acid Screening Test	A 262[A], *Standard Practices for Detecting Susceptibility to Intergranular Attack in Austenitic Stainless Steels*
		Ferric Sulfate-Sulfuric Acid (Stretcher Test)	A 262[B]
		Nitric Acid (Huey Test)	A 262[C]
		Copper Sulfate-Sulfuric Acid Test	A 262[D]
		EPR Test (Electrochemical Potentiokinetic Reactivation)	G108, *Standard Test Method for Electrochemical Reactivation (EPR) for Detecting Sensitization of AISI Type 304 and 304L Stainless Steels*
Erosion Corrosion	7%	Miller Test	G75, *Standard Test Method for Electrochemical Reactivation (EPR) for Detecting Sensitization of AISI Type 304 and 304L Stainless Steels*
		Rotating Spindle, Cage, or Disk Tests	
De-alloying	2%	Total Immersion Testing for De-alloying	G31
		Galvanic Couple Test	G71, *Standard Guide for Conducting and Evaluating Galvanic Corrosion Tests in Electrolytes*
		Electrochemical Tests	G5
		Exfoliation of Aluminum Tests	G34, *Standard Test Method for Exfoliation Corrosion Susceptibility in 2XXX and 7XXX Series Aluminum Alloys (EXCO Test)*

(continued)

TABLE 1 (*continued*)

Mode of Attack	Occurrence in Industry (Typical)	Evaluation Tests	ASTM Std. (Typical)
Galvanic	1%	Dissimilar Metal Couple Immersion Test	G31
		Galvanic Couple Test	G71
		Zero Resistance Ammeter	G3, *Standard Practice for Conventions Applicable to Electrochemical Measurements in Corrosion Testing*
		Electrochemical Tests	

some of the more common forms of corrosion and the appropriate laboratory tests used to evaluate the susceptibility of a material to a specific mode of attack.[1] Many of these tests are accelerated rather than simulating service conditions and are performed routinely to provide information for use in

- fundamental corrosion evaluation,
- failure analysis,
- corrosion prevention or control,
- acceptance for quality assurance,
- environmental issues involving corrosion, and
- new alloy/nonmetallic or product process development.

Customized and unique test setups to evaluate heat transfer, thermal shock, velocity, fatigue, or abrasion and wear effects also are used to determine the susceptibility of a material to a specific environment or process.

TEST CONDITIONS

The selection of conditions for a laboratory corrosion test should be determined by the expected results and the purpose of the test. If the test is to be a guide for the selection of a material for a particular application, then the limits of the controlling factors under service conditions must be determined. Normally these factors include, but are not limited to, service temperature ranges, process fluid flow rates, pH, atmosphere—for example, air, carbon dioxide (CO_2), hydrogen sulfide (H_2S), ammonia (NH_3), nitrogen (N_2), and mixed gases—aqueous or organic phases, and other characteristics of the bulk solution (e.g., impurities or contaminants). There should be an effort to ensure duplication of the service conditions in the laboratory corrosion test, with conditions adequately controlled during the entire test duration to ensure reproducible results.

Experience has shown that, at a minimum, duplicate test specimens should be exposed in each test. Under laboratory tests, corrosion rates of duplicate specimens are usually within ± 10% of each other, when the attack is uniform. Occasional exceptions, in which a large difference is observed, can occur under conditions of borderline passivity of alloys that depend on a passive film for their resistance to corrosion. If the rate difference exceeds 10%, re-testing should be considered, unless it is observed that a localized attack is predominant. Corrosion rates are calculated assuming a uniform loss of metal; therefore, when specimens are attacked nonuniformly, the calculated corrosion rates only indicate the relative severity of attack and should not be used to predict the performance of an alloy to the test solution. In such cases, weight loss per unit of surface area and the depth of the nonuniform attack may be used to avoid implying a uniform penetration rate.

Ideally, laboratory tests should use actual solutions from plant processes. This often can be impractical. In these instances, test solutions are prepared from reagent grade chemicals and using reagent water (ASTM D1193, *Standard Specification for Reagent Water*, Type IV or better) to simulate the environment as closely as possible. No matter what the source of the test solution, its composition should be controlled accurately and described in the test report as completely as possible. Minor constituents should not be overlooked because they can affect the corrosion rate. Chemical content may be reported as percentage by weight, molarity, or normality. The composition of the test solution can be checked before and after testing to determine the extent of change in composition. Evaporation losses should be controlled by a constant level device, by frequent additions of the evaporating solution, or by use of cooled condensers to maintain the original volume within ±1%. Sometimes, an environmental sampling plan is necessary to ensure that the solution components of interest remain within the desired range.

In some situations, the composition of the test solution may change as a result of the build-up of corrosion products in the solution, catalytic decomposition, or reaction with the test specimens. If these changes are expected to occur, consideration should be given to periodic solution adjustments or replacement with fresh solution. Sometimes it may be of interest to measure the metal ion content as a method of measuring corrosion.

Wherever possible, only one type of alloy or family of nonmetallics should be exposed in a given test apparatus. If several alloys or nonmetallics are exposed in the same apparatus the corrosion products from one material may affect the corrosion behavior of other materials. For example, copper corrosion products can inhibit corrosion of stainless steels but accelerate corrosion of aluminum and its alloys.

If different alloys are galvanically coupled in a particular process, these dissimilar metal couples must be reproduced in the laboratory test. For example, in ASTM D1384, *Standard Test Method for Corrosion Test for Engine Coolants in Glassware*; ASTM D2570, *Standard Test Method for Simulated Service Corrosion Testing of Engine Coolants*; or D2758, *Standard Test Method for Engine Coolants by Engine Dynamometer*, copper, brass, and solder found in the radiator and heaters in automobiles are electrically connected and tested in the same laboratory apparatus.

PHYSICAL PARAMETERS

Temperature

The temperature of the test solution should be controlled within ±1°C and should be stated as such in the report of test results. When the test temperature is well above ambient, some form of stirring may be necessary to avoid temperature gradients in the test solution. If no specific temperature, such as boiling, is required or if a temperature range is selected, this also should be reported. For processes that are conducted under ambient conditions, the laboratory tests should be conducted at the highest temperature anticipated, for example, outdoor stagnant storage during the summer months. This temperature may be as high as 55°C (131°F). When testing at or near boiling, the use of reflux condensers is highly recommended.

Laboratory tests conducted at the temperature of a process solution may provide misleading results when compared with the heat transfer surfaces within an actual in-service vessel where heated surfaces can be 10°C (18°F), or more, hotter than the bulk process solution. If this condition is expected, it may be necessary to test at higher temperatures than the bulk solution temperature or, preferably, employ specialized test apparatus to simulate the heat transfer effect.

Gas Sparging of Solution

Most laboratory tests used to replicate process equipment should be controlled with the natural atmosphere inherent under process conditions, such as the vapors of the boiling solution. Some applications may require aeration or deaeration, whereas others may require sparging with a particular gas or gas mixture. If gas sparging is used, the test specimens should not be located in the direct stream of the gas sparge tube. Undesirable effects can be encountered if the gas stream impinges on the test specimens.

Complete removal of oxygen from a test vessel may require special procedures to obtain and prevent subsequent ingress of oxygen (O_2). Certain gasses—for example, hydrogen sulfide (H_2S), carbon monoxide (CO), chlorine (Cl_2)—may have additional safety considerations inherent to them or in combination with the test solution or test conditions.

Test Solution Flow

The effect of process solution flow is not usually determined in normal laboratory tests, although specific tests have been designed for this purpose. Tests under boiling conditions should be conducted with minimal heat input, and inert boiling chips should be used to avoid excessive turbulence and bubble impingement. For tests conducted below the boiling point, thermal convection generally is the only source of liquid agitation in the laboratory test, which may or may not be adequate. Test solutions with high viscosities or multiple phases may require supplemental controlled stirring with a magnetic stirrer or a gas sparge to maintain a uniform environment.

Test Solution Volume

The volume of the test solution should be large enough to avoid any appreciable change in its corrosiveness, either through depletion of the corrodent or accumulation of corrosion products that may affect further corrosion. The preferred minimum solution volume-to-specimen surface area ratio is 20 mL/cm^2 (130 mL/in^2).

When the test objective is to determine the influence of a metal or alloy on the test solution, it may be desirable to reproduce the solution volume-to-surface area ratio that exists in practice. The time of contact also should be replicated in this type of application.

On occasion, a low volume-to-surface area ratio is unavoidable. In these instances, periodic replenishment of the corrodent or complete replacement of the test solution should be considered.

Methods of Supporting Test Specimens

It is important that the supporting device and the test apparatus should not be affected by or cause contamination of the test solution. The method of supporting test specimens will vary with the apparatus used for conducting the test, but they should be designed to insulate the specimens from each other physically and electrically (unless the purpose of the test is to evaluate galvanic corrosion) and to insulate the specimens from any metallic container or supporting device used with the apparatus. Support systems that hold the test specimens tightly may induce crevice corrosion, which may be an undesirable result unless crevice corrosion is part of the study. The shape and form of the specimen support should ensure free contact of the specimen with the test solution, the liquid or vapor interface, or the vapor phase, whichever is applicable. Common supports include glass or ceramic rods or hooks; glass cradles, fluorocarbon plastic thread, or string; and various insulated or coated metallic supports.

Test Duration

The duration of any laboratory test should be determined by the nature and purpose of the experiment. The amount of corrosion attack under any given test condition will depend directly on the duration of the test. Materials that experience severe corrosion usually do not require long exposure duration to obtain accurate corrosion rates, with testing periods typically 24–240 h. Results from short duration tests can be used to determine whether a longer duration exposure is warranted. Experience suggests that laboratory tests of longer duration are considerably more realistic. This is particularly important if localized corrosion such as pitting, crevice, or environmentally assisted cracking are being investigated.

Relying solely on short-term tests can yield misleading results. For example, aluminum exposed to solutions of sodium hydroxide corrodes at an extremely high rate, often in excess of an inch per year, while it is building up a protective corrosion product film. Afterward, the rate decreases dramatically so that further corrosion is almost negligible, provided the film is not damaged. Conversely, the passive films that form on stainless steels may be broken down under prolonged exposure leading to rapid localized corrosion. Long-term tests, however, should not proceed to the point at which the original specimen size or the exposed area is drastically reduced or the material is perforated or dissolved.

Corrosion rates determined from a single exposure period assumes that metal loss is linear with time. This may not be the case in practice, however, as many factors can affect corrosion reactions over time. A corrosion rate is really an average of the

varied rate measured over a defined period of time. In some instances, the variation of the rate is insignificant and the assumption of linearity is appropriate. In other cases, this assumption can be misleading. A prime example is in materials that rely on a passive film for corrosion resistance. These materials may experience a very high corrosion rate until a protective layer has developed, significantly decreasing further corrosion as described for aluminum in sodium hydroxide. Conversely, some materials may require an initiation period before discernible corrosion initiates and then proceeds more rapidly once initiated as described for stainless steels. Changes in the test solution can cause a similar effect either through depletion of the corrodent or concentration of a corrosive by-product. The "Planned Interval Test"[2] is an excellent procedure for evaluating the effect that time has on metal corrosion and solution corrosivity. This technique and evaluation of the results are presented in table 2.[2]

TABLE 2 Planned Interval Test

Specimen #	0	1	t	t+1
1	→			
2	→			
3	→			
4			→	
5	Calculated Specimen #3 - #2		→	

Four test specimens (#1 through #4) are exposed and a fifth (#5) is a calculated value. All test specimens are exposed in the same test vessel. The test conditions are held constant throughout the test. The parameter being evaluated is the penetration rate,[a] as defined in the table note.

Interpretation		Criteria
Liquid Corrosiveness:	Unchanged if	1 = 4
	Decreases if	1 > 4
	Increases if	1< 4
Metal Corrodibility	Unchanged if	4 = 5
	Decreases if	4 > 5
	Increases if	4 < 5

Other Combinations of Interpretation

	Liquid Corrosiveness	Metal Corrodibility	Criteria
1.	Unchanged	Unchanged	1 = 4 =5
2.	Unchanged	Decreases	1 = 4 > 5
3.	Unchanged	Increases	1 = 4 < 5
4.	Decreases	Unchanged	1 > 4 = 5
5.	Decreases	Decreases	1 > 4 > 5
6.	Decreases	Increases	1 > 4 < 5
7.	Increases	Unchanged	1< 4 = 5
8.	Increases	Decreases	1< 4 > 5
9.	Increases	Increases	1< 4 < 5

Specimen	Duration	Mass Loss	Penetration[a]		Apparent Corrosion rate[b]	
#	Days	mg	mm	mils	mm/y	mpy
1	0–1	1495	0.064	2.4	23	880
2	0–4	2240	0.095	3.6	8.7	330
3	0–5	2280	0.097	3.7	7.1	270
4	4–5	95	0.004	0.15	1.5	55
5 calc.	3–2	40	0.002	0.06	0.7	22

[a] $\text{Penetration} = \dfrac{(\text{mass loss in mg})(\text{C-factor})}{(\text{Area in mm}^2 \text{ or in}^2)(\text{density in g/cm}^2)}$

where:
C = 1 for mm; or
C = 0.061 for mils.

[b] $\text{Apparent Corrosion Rate} = \dfrac{(\text{Penetration in mm or mils})365}{\text{Time in days}}$

From penetration information: Specimen 1 > 4 > 5
Based on the interpretation criteria, the liquid has decreased its corrosiveness during the test, and suggests the formation of a protective film owing to a decrease in metal corrodibility.

Types of Tests

The type of laboratory test that should be used is dictated by the environmental conditions that are being simulated. For example, if the equipment is immersed in service, then the test specimens should be immersed in the laboratory test; if the exposure alternates between immersion and atmospheric exposure, because of cyclic exposure to wet/dry conditions, an alternate immersion test designed to replicate these cycles should be used.

Another factor that dictates test setup is the allowable test duration to obtain the necessary results. This determines the degree to which the test method must be accelerated. The principal reason for accelerated testing is the need to obtain results sooner than can be obtained under field conditions. Acceleration may be achieved in a number of ways. A common way to accelerate a corrosion test is to intensify the test conditions by increasing the solution acidity, corrodent concentration, temperature, or other parameters. The test specimen configuration may be altered, for example, by increasing stress intensity (SCC tests), adjusting crevice geometry or tightness (crevice corrosion tests), or increasing cathode-anode area ratio (galvanic tests). In specific cases, the contact or exposure time may be increased. For example, if a vessel is to be batch processed with a chemical for 24 h, then a laboratory corrosion exposure of 240 h should be considered. Care should be taken when accelerating the exposure conditions. Overly aggressive conditions may alter corrosion mechanisms, disqualify materials that otherwise would be acceptable for the intended exposure or both. For example, some materials may exhibit a critical temperature above which they will experience rapid corrosion (such as SCC or pitting on stainless steels) but little attack below the critical temperature.

Electrochemical corrosion tests may be employed to obtain rapid results. These tests typically have a short duration, and most can be completed in a matter of hours versus weeks or months for immersion testing. These tests also can provide additional information that may not be readily evident from immersion testing. For instance, immersion testing of several stainless steel alloys in a salt solution may indicate little or no corrosion on any of the alloys even after several weeks. The results from electrochemical potentiodynamic polarization tests, however, can rapidly screen susceptibility to pitting and crevice corrosion of candidate test alloys.

Both immersion tests and electrochemical tests have their pros and cons. Immersion tests are time weighted and evaluated based on mass loss and visual evidence of corrosion. Electrochemical tests provide information on metal-environment interactions and corrosion mechanisms based on electrical measurements taken at a given point in time. Immersion test methods may be employed in any environment, whereas most electrochemical methods are limited to electrically conductive environments. Many times it is beneficial to use both testing methods in the materials selection process. A more detailed description of electrochemical test methods may be found in other chapters of this book that deal specifically with electrochemical corrosion testing.

Once the service conditions of the test have been determined, and evaluation tests for all forms of corrosion that might occur have been designed, they should be repeated a sufficient number of times to determine whether it meets the desired reliability standard for reproducibility. Changes in test procedures may be required if the reliability is not satisfactory.

If the test procedure is to be used by other laboratories, either to qualify on the basis of a specification or simply to compare results among laboratories, then it is important that reproducibility of results be determined. This is accomplished through round-robin (interlaboratory) tests conducted by interested laboratories to develop standard test procedures, such as those by ASTM International, International Organization for Standardization (ISO), Japanese Standards Association (JSA), Materials Technology Institute (MTI) of the Chemical Process Industries, and the Association for Materials Protection and Performance (AMPP, formerly NACE International).

It is not unusual to use a laboratory test procedure for which there is no direct correlation with service or field results. Sometimes correlation cannot be obtained immediately because service results are either not available or are not practical to obtain in a reasonable time frame. For example, suppose a company wishes to offer a lifetime warranty of a coating exposed to an industrial environment but needs data to back up their claim. Humidity chamber tests plus ultraviolet light exposure can give "best guess" results in a matter of weeks rather than years of actual exposure to the elements. Long-term behavior in actual service environments, however, still serves as the gold standard for materials performance. For example, many vendors conduct long-term atmospheric corrosion-performance studies by exposing large numbers of test specimens (e.g., coated panels, fasteners, hardware, non-metallics) in marine, industrial, and rural environments over many years, sometimes decades. This provides information on such effects as climate, salts, pollutants, ultraviolet, and solar radiation on material performance. Test results from many previous long-term studies have been reported widely in the published literature, such as ASTM Selected Technical Papers, ASM Metals Handbooks, and government-funded research.

Laboratory tests are normally designed around a synthesized or contrived environment; however, it is important that the results provide reliable information that can be used to screen candidate materials of construction.

SIMPLE IMMERSION TESTS

There are many variations in a laboratory immersion test. NACE/ASTM G31, *Standard Guide for Laboratory Immersion Corrosion Testing of Metals*, provides general guidelines on how these tests may be performed (see table 3 for these and other standard corrosion test procedures). Basically, small pieces (i.e., 2.5 cm by 5 cm by 0.3 cm thick) of the candidate material are exposed to the test medium, and the loss of weight of the material is measured for a given period of time. Immersion testing remains the best relatively quick method to screen candidate materials for corrosion resistance. The most serious disadvantage of this method of corrosion study is the assumed average-time weight loss. The corrosion rate could be high initially and then decrease with

TABLE 3 Standard Corrosion Test Procedures

NACE STANDARDS	
No.	**Title**
TM-0169	*Laboratory Corrosion Testing of Metals at Atmospheric Pressure*
TM-0174	*Laboratory Methods for the Evaluation of Protective Coatings Used as Lining Materials for Immersion Service*
TM-0177	*Testing of Metals for Resistance to Sulfide Stress Cracking at Ambient Temperatures*
TM-0196	*Chemical Resistance of Polymeric Materials by Periodic Evaluation*
TM-0284	*Test Method for Evaluation of Pipeline Steels for Resistance to Stepwise Cracking*
TM-0286	*Cooling Water Test Units Incorporating Heat Transfer Surfaces*
TM-0416	*Test Method for Monitoring Atmospheric Corrosion Rate by Electrochemical Measurements*
ASTM STANDARDS	
No.	**Title**
A262	*Standard Practices for Detecting Susceptibility to Intergranular Attack in Austenitic Stainless Steels*
A763	*Standard Practices for Detecting Susceptibility to Intergranular Attack in Ferritic Stainless Steels*
C692	*Standard Test Method for Evaluating the Influence of Thermal Insulations on External Stress Corrosion Cracking Tendency of Austenitic Stainless Steel*
D1384	*Standard Test Method for Corrosion Test for Engine Coolants in Glassware*
D2570	*Standard Test Method for Simulated Service Corrosion Testing of Engine Coolants*
F2129	*Standard Test Method for Conducting Cyclic Potentiodynamic Polarization Measurements to Determine the Corrosion Susceptibility of Small Implant Devices*
F3044	*Standard Test Method for Evaluating the Potential for Galvanic Corrosion for Medical Implants*
G1	*Standard Practice for Preparing, Cleaning, and Evaluating Corrosion Test Specimens*
G3	*Standard Practice for Conventions Applicable to Electrochemical Measurements in Corrosion Testing*
G4	*Standard Guide for Conducting Corrosion Tests in Field Applications*
G5	*Standard Reference Test Method for Making Potentiostatic and Potentiodynamic Measurements*
G28	*Standard Test Methods of Detecting Susceptibility to Intergranular Attack in Wrought Nickel-Rich, Chromium-Bearing Alloys*
G31	*Standard Guide for Laboratory Immersion Corrosion Testing of Metals*
G34	*Standard Test Method for Exfoliation Corrosion Susceptibility in 2XXX and 7XXX Series Aluminum Alloys (EXCP Test)*
G35	*Standard Practice for Determining the Susceptibility of Stainless Steels and Related Nickel-Chromium-Iron Alloys to Stress-Corrosion Cracking in Polythionic Acids*
G36	*Standard Practice for Evaluating Stress-Corrosion-Cracking Resistance of Metals and Alloys in a Boiling Magnesium Chloride Solution*
G44	*Standard Practice for Exposure of Metals and Alloys by Alternate Immersion in Neutral 3.5% Sodium Chloride Solution*
G46	*Standard Guide for Examination and Evaluation of Pitting Corrosion*
G48	*Standard Test Methods for Pitting and Crevice Corrosion Resistance of Stainless Steels and Related Alloys by Use of Ferric Chloride Solution*
G49	*Standard Practice for Preparation and Use of Direct Tension Stress-Corrosion Test Specimens*
G50	*Standard Practice for Conducting Atmospheric Corrosion Tests on Metals*
G60	*Standard Practice for Conducting Cyclic Humidity Exposures*
G61	*Standard Test Method for Conducting Cyclic Potentiodynamic Polarization Measurements for Localized Corrosion Susceptibility of Iron-, Nickel-, or Cobalt-Based Alloys*
G71	*Standard Guide for Conducting and Evaluating Galvanic Corrosion Tests in Electrolytes*
G75	*Standard Test Method for Determination of Slurry Abrasivity (Miller Number) and Slurry Abrasion Response of Materials (SAR Number)*
G78	*Standard Guide for Crevice Corrosion Testing of Iron-Base and Nickel-Base Stainless Alloys in Seawater and Other Chloride-Containing Aqueous Environments*
G106	*Standard Practice for Verification of Algorithm and Equipment for Electrochemical Impedance Measurements*
G108	*Standard Test Method for Electrochemical Reactivation (EPR) for Detecting Sensitization of AISI Type 304 and 304L Stainless Steels*
G157	*Standard Guide for Evaluating Corrosion Properties of Wrought Iron- and Nickel-Based Corrosion Resistant Alloys for Chemical Process Industries*
G162	*Standard Practice for Conducting and Evaluating Laboratory Corrosion Tests in Soils*
G170	*Standard Guide for Evaluating and Qualifying Oilfield and Refinery Corrosion Inhibitors in the Laboratory*
G189	*Standard Guide for Laboratory Simulation of Corrosion Under Insulation*
G205	*Standard Guide for Determining Emulsion Properties, Wetting Behavior, and Corrosion-Inhibitory Properties of Crude Oils*
G210	*Standard Practice for Operating the Severe Wastewater Analysis Testing Apparatus*

(continued)

TABLE 3 (*continued*)

MTI METHODS

No.	Title
MTI 1	*Laboratory Testing of Wrought Iron and Nickel Based Alloys for Relative Resistance to Corrosion in Selected Media*
MTI 2	*Laboratory Testing of Wrought Iron and Nickel Based Alloys for Relative Resistance to Crevice Corrosion in a Standard Ferric Chloride Solution*
MTI 3	*Laboratory Testing of Wrought Iron and Nickel Based Alloys for Relative Resistance to Stress Corrosion Cracking in a Boiling Magnesium Chloride Solution*
MTI 4	*Laboratory Testing of Wrought Iron and Nickel Based Alloys for Relative Resistance to Crevice Corrosion in Sodium Chloride Solutions*
MTI 5	*Laboratory Testing of Wrought Iron and Nickel Based Alloys for Relative Resistance to Stress Corrosion Cracking in a Sodium Chloride Drop Evaporation System*

time. In other cases, the rate of corrosion might increase gradually with time, could cycle, or could undergo some combination of these scenarios. No single corrosion test will address every situation. The investigator must be aware of the limitations of the selected test methods and test conditions to obtain meaningful results.

Besides the full immersion test, several variations could be used to accentuate certain types of exposure conditions. For example, the test specimen can be immersed partially in an electrolyte (liquid or solid) to create an oxygen concentration cell at the vapor-liquid-solid interface (as opposed to an occluded cell).

ALTERNATE IMMERSION TESTING

Another variation of the immersion test is the cyclic test procedure in which a test specimen is immersed for a period of time in the test environment, is removed and dried (either air dry or with heat lamps), and then is re-immersed to continue cyclic exposure. Normally, hundreds of such cycles are performed during the course of the test program. In ASTM G60, *Standard Practice for Conducting Cyclic Humidity Exposures*, test specimens are dipped in a test solution before being exposed to atmospheres varying in relative humidity. The intent of the test is to develop a layered corrosion product similar to that found on sheltered outdoor exposure test specimens. These tests can be manually performed or conducted in apparatus equipped for automatic cycling.

SIMULATED SERVICE TESTING

Simulated service testing, sometimes called "customized testing," is an attempt by the investigator to replicate actual service conditions in a laboratory setting. This type of test usually requires a special apparatus to study particular conditions, such as heated vapors, condensate exposure, heat transfer, or flow velocity. Occasionally, this may be accomplished simply by building a scaled-down model of a particular operation. If the service operation is not too large, actual parts of the system can be modified to a laboratory bench-top set-up to permit a better simulation of the actual process. The simulation also may include exposure to varying conditions or chemicals that occur in the process environment. The investigator may find it useful to employ a mix of test methods, such as electrochemical monitoring or stimulation, cabinet tests, atmospheric exposure, or high temperature exposure along with immersion testing.

There are many examples where this approach has been applied. An excellent example is depicted in figure 1 of a circulating brine cooling/heating heat exchanger system. The effect of brine corrosion, and inhibitors, in the piping system is simulated by using full-size pipe spool pieces of different alloy composition. The test model further incorporates the use of small test specimens and electrochemical monitoring probes.

ACCEPTANCE TESTING

Acceptance tests expose samples taken from the final products to a corrosive environment to evaluate the materials susceptibility to a particular type of corrosion or susceptibility in a particular simulated environment or as a quality control test for the material being supplied. Many acceptance tests have been developed by standards organizations mentioned previously. Typically, these tests have undergone lengthy studies to affirm their applicability to the desired outcome and are continually being reviewed and revised, usually every five years. Acceptance criteria for some tests are stated in the test procedure, whereas others may not provide specific criteria, leaving the details to be specified by the end-user or some other authority. A classic example is the use of acceptance testing for susceptibility of stainless steel alloys to intergranular corrosion using the test methods described in ASTM A262, *Standard Practices for Detecting Susceptibility to Intergranular Attack in Austenitic Stainless Steels*. Another example is simulation of sour gas or sour oil environments in NACE International TM0284 and TM0177 procedures for hydrogen-induced cracking susceptibility and resistance to sulfide stress cracking.

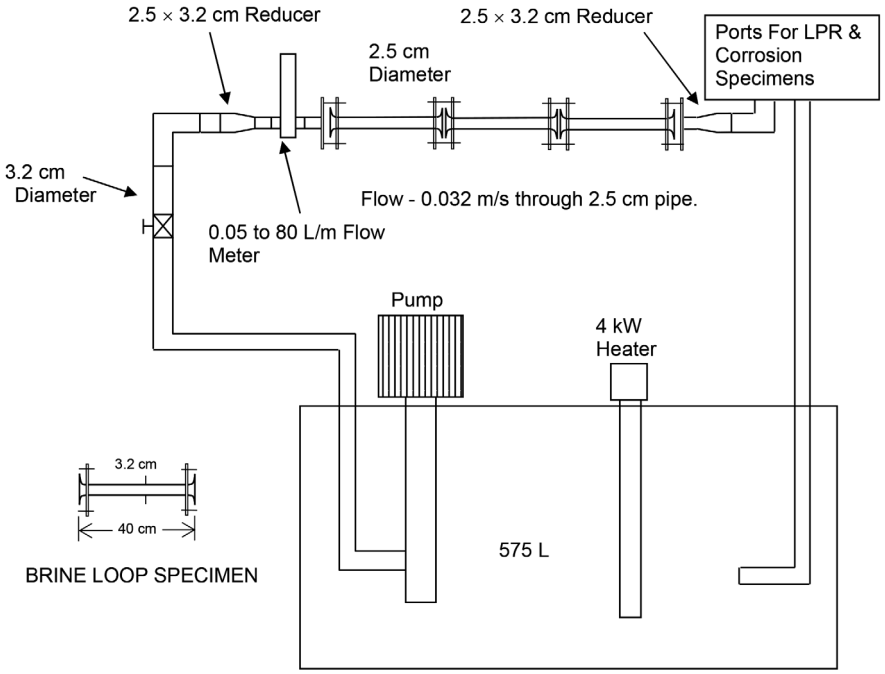
Test Specimen Preparation, Cleaning, and Evaluation

PREPARATION

One of the most important aspects of corrosion testing is the preparation of test specimens or parts to be tested. It is desirable to use the same test specimen surface condition as found in service, although this is not always possible

Test specimens should have as many of the characteristics of the material that will be used for the service application as possible. This includes composition (elemental chemistry), mechanical properties (strength, ductility, hardness), form (sheet,

FIG. 1 Scaled-down model for a circulating brine cooling and heating heat-exchanger system.



plate, bar, cast), size and shape (surface-area-to-corrodent-volume ratio, flat-stock, end-grain exposure), metallurgical treatment (heat treatment, welding, presence or absence of weld heat-tints, hot or cold working), and surface finish (die-cut, sheared, saw-cut, mill scale, ground and polished, electropolished). All of these factors can influence the corrosion resistance of the material. Care should be taken in the selection of identification procedures (stamped, engraved) and cleaning procedures (passivated, degreased, water washed) because these also can have an impact on the performance of the material.

Although the size and shape of the specimen will depend on the purpose of the test, rectangular specimens of the dimensions 2.5 cm by 5 cm by 0.3 cm thick are common. A typical variation in test specimen geometry is found when a corrosion test requires the specimen to be mechanically stressed as part of the evaluation procedure. Stressed test specimens can be prepared as U-bends, C-rings, bent beams, tensile specimens, or some other form that induces a mechanical tensile stress in the material. Standards organizations have developed procedures for preparation of many types of stressed specimens. Other examples include the use of disk-shaped specimens for rotational erosion tests or the use of special (e.g., serrated) washers to evaluate resistance to crevice corrosion.

Holes can be drilled in the test specimen for sturdy mounting or to provide crevice formers to simulate crevice conditions on tight-fitting parts or under shielding deposits on the metal surface. The placement of the crevice formers, or washers, should include contact with the weld, heat-affected zone, and base metal on welded test specimens. This typically requires machining or grinding the weld bead flat for the crevice washer to seat properly. Crevice forming washers typically are fabricated from polymeric materials, although ceramic and metal washers may be more appropriate in specific applications. ASTM G48, *Standard Test Methods for Pitting and Crevice Corrosion Resistance of Stainless Steel and Related Alloys by Use of Ferric Chloride Solution*, and G78, *Standard Guide for Crevice Corrosion Testing of Iron-Base and Nickel-Base Stainless Alloys in Seawater and Other Chloride-Containing Aqueous Environments,* provide examples on the use and assembly of crevice forming washers. For surfaces that cannot be ground flat for seating of the washers, crevices can be simulated using O-rings or by applying an inert (e.g., epoxy) paint coating at the desired local areas.

A reproducible surface finish is desirable for repetitive testing. A common final surface finish for test specimens is No. 120 grit abrasive paper or cloth, or their equivalent. Whenever possible or known, the same metallurgical treatment should be used for the test specimen as for the service part, because heat treatment or cold work can change the surface composition, grain size and structure, and residual stresses. Mechanical operations can affect the material's surface condition. Cutting, shearing, grinding, and polishing operations should be performed in a manner to avoid excessive work-hardening or stresses, overheating, and embedding grinding or blasting-media particles in the surface—all of which can adversely affect corrosion resistance. Similarly, test specimens should be tested with or without heat tints to simulate post fabrication surface conditions in service.

There are many ways to identify test specimens, such as marking with ink or paint, engraving, or stamping numbers or letters on the surface. Precautions should be observed to avoid excessive stresses, the creation of sites for pit initiation, or the use of materials that will be reactive with the metal. It is important that the identification endures the duration of the test, so

some of these problems may have to be tolerated. Alternatively, small identification tags prepared from a corrosion-resistant nonmetallic material (e.g., polytetrafluoroethylene), can be attached to the test specimen using fluoropolymer thread.

CLEANING SPECIMENS BEFORE TESTING

After the test specimens have been prepared for testing, they must be cleaned to remove oil, soil, and fingerprints. Either chemical or electrochemical means can be used for the final cleaning, but the effects of cleaning on surface topography must be considered. A recommended procedure involves scrubbing with a nylon toothbrush and a nonchlorinated scouring powder, followed by thorough rinsing with distilled or deionized water and a suitable solvent (such as acetone or methanol) and warm air-drying. For relatively soft metals (such as aluminum, magnesium, and copper) scrubbing with abrasive powder may be objectionable as it can mar the surface of the test specimens. Ultrasonic cleaning techniques may be used, if necessary. Air drying is preferred over towel drying, as towels may introduce contaminates that can influence corrosion behavior. Cleaned test specimens should be handled and stored in a manner that prevents contamination of the surfaces by foreign matter, including fingerprints.

If coatings are to be evaluated, it is important that the metal surface be prepared for coating application in a similar manner to that used in the service application. This step may involve the use of commercial production facilities to apply coatings.

After cleaning, the test specimens are weighed on an analytical balance with a resolution of 0.1 mg, and dimensional measurements are made to ±0.01 mm to permit accurate calculation of the exposed surface area.

CLEANING SPECIMENS AFTER TESTING

The effect that corrosion and the resulting corrosion products have on the test specimen should be determined to evaluate the severity of the attack. Locations of deposits or corrosion products are important in evaluating localized attack, such as pitting, crevice attack, or cracking. Therefore, before cleaning, the exposed specimens should be examined carefully (using a binocular microscope, if necessary) and the appearance documented photographically. Although this method is qualitative, it can be helpful in assessing the nature and extent of corrosion.

Corrosion rate calculations are based on weight (mass) loss incurred during the test. Therefore, cleaning the specimens to remove corrosion products is a vital step in the test protocol. Generally, the cleaning procedure should remove all corrosion products from the specimen with minimum metal loss of the base material. Procedures for specimen cleaning vary depending on the type of the material being cleaned and on the adherence of corrosion products. Cleaning methods are divided into three general categories: mechanical, chemical, and electrolytic. Detailed procedures are described in ASTM G1, *Standard Practice for Preparing, Cleaning, and Evaluating Corrosion Test Specimens*, and ISO 8407. After cleaning, the specimens are reweighed. The weight loss during the test duration is used as the principal measure of corrosion (i.e., the corrosion rate). Corrosion rates determined in this manner assume that the mass loss has been uniform over the entire exposed surface area. When corrosion is nonuniform or localized (i.e., pitting), the calculated corrosion rate is not representative of the metal penetration rate and additional means of evaluation should be considered, such as depth of penetration.

EVALUATION OF RESULTS

Even though each step of the corrosion test procedure is important, proper evaluation of the results is critical to avoid erroneous data and conclusions. It is important to remember that the corrosion rate is often based on the extrapolation of results from relatively short-term tests. For example, corrosion rates may be reported in terms of mils per year (mpy, where 1 mil = 0.001 inch = 25.4 μm) or in millimeters per year (mm/y where 1 mm = 1,000 μm = 39.7 mils) on the basis of results obtained from exposure of one month, one week, or one day. The degree of extrapolation ranges from a multiple of 12 to 365. Because corrosion is rarely linear, with initial rates frequently being extremely high and tending to moderate over time, it is important that the extent of extrapolation be considered in the evaluation phase of the test program.

After the specimens have been re-weighed, they should be carefully examined visually and under low-power magnification for the presence of localized attack. This is very important as localized corrosion can penetrate the material thickness at a much higher rate than indicated by the calculated corrosion rate based on mass loss. If there are pits or creviced areas, the depth of attack can be measured with a pit gauge or a calibrated microscope, which is first focused on the bottom of the pit and then the specimen surface edge. For localized attack, reported data can include the depth of the deepest pit, average of the five deepest pits, and pit distribution (for details, see ASTM G46, *Standard Guide for Examination and Evaluation of Pitting Corrosion*). Pitting rates should not be reported (e.g., in mpy or mm/y) based on sparse data because pit growth rates can be notoriously nonlinear with time. In some cases, pitting rates decrease with time, whereas in others they accelerate with time.

If the test material is suspected of being subject to dealloying (such as dezincification), intergranular corrosion, or environmental cracking, a metallographic cross-section of the specimen should be prepared and microscopically examined. If embrittlement is suspected, simply bending the specimen may indicate this susceptibility. Sometimes it may be desirable to perform additional tests to compare mechanical properties of the exposed test specimens versus unexposed specimens.

Precautions and Validity of Results

Many metals and alloys are thermodynamically unstable and therefore tend to revert back to their native stable state (e.g., red rust or ferric oxide in the case of iron and steel). The rate at which this reversion (corrosion) occurs varies with the particular alloy and the environment to which it is exposed. The purpose of laboratory corrosion tests is to best simulate the service conditions, determine corrosion rates, and assess the various modes of

attack. Although each data point is important, the results can be misinterpreted and lead to false conclusions if they are not carefully evaluated. Therefore, a laboratory corrosion test can be most useful if the test results can be correlated with actual plant or process service experience.

The precautions mentioned throughout this section focus on the planning and execution of laboratory corrosion tests and particularly the interpretation of test results. These precautions are not intended to suggest that corrosion tests are inherently unreliable. Rather, they are intended to emphasize that when corrosion test procedures are executed carefully and results are interpreted intelligently, the knowledge of corrosion is enhanced, which makes for better materials selection decisions.

Standards

Reference is made throughout this section to standards and test methods issued regularly by technical societies, such as ASTM International and AMPP (formerly NACE International). Other organizations that also issue standards for the many types of corrosion tests include, but are not limited to, ISO, British Standards Institution (BSI), JSA, *Deutsches Insitut für Normung* (DIN, the German Institute for Standardization), and MTI. These professional organizations have produced industry-accepted recommended practices and test procedures that allow for the comparison of results with others through direct interaction or published data. Numerous corrosion test procedures have been standardized; a partial listing is presented in table 3.

References

1. R. A. Corbett, "Using Corrosion Tests Effectively," *Chemical Processing* 50, no. 12 (1987): 28–32.

2. A. Wachter and R. S. Treseder, "Corrosion Testing Evaluation of Metals for Process Equipment," *Chemical Engineering Progress* 43 (June 1947): 315–326.

Chapter 10 | Atmospheric

Sheldon W. Dean, Jr.[1]

Introduction

Atmospheric corrosion occurs with many metals used in architectural, industrial and other services. In outdoor exposures, the primary cause of the corrosion process is the development of a film of moisture on the surface. This film results from either direct contact with liquid water, or from condensation (i.e., dew deposition). Extensive experience, together with many exposure programs, has shown that atmospheric corrosion is a phenomenon that varies greatly from location to location.[1] Studies throughout the world have revealed that the rate of atmospheric corrosion is a function of the metal being tested, the location, the climate, the proximity to pollutants, and a variety of other factors. Most people understand that atmospheric corrosion can occur in outdoor exposures, but more recent experience has shown that corrosion can occur from indoor atmospheres under certain circumstances.[2]

Outdoor atmospheric exposure tests have been carried out for a variety of purposes.[3] ASTM International has sponsored 11 symposia with resulting compilations of technical papers on atmospheric corrosion for almost a century. Alloy producers have used this type of testing to evaluate the performance of new alloys in a variety of atmospheric conditions. Atmospheric corrosion testing also has been used to test both metallic and nonmetallic coatings to demonstrate their performance in atmospheric conditions.[4] Manufacturers of items designed to be used in outdoor conditions sometimes expose components to various atmospheres to demonstrate their performance and develop data on the service life that may be expected from such components. In some cases, atmospheric exposure programs are run to evaluate the corrosivity of specific atmospheres. This type of information can be helpful in selecting coatings or other corrosion protection systems to be used at specific sites.

[1]Dean Corrosion Technology, Inc., 306 Marshall Landing, Glen Mills, PA 19342, USA
http://orcid.org/0000-0003-0611-7384

DOI: 10.1520/MNL202NDSUP20190006

Basic Principles

KINETICS OF ATMOSPHERIC CORROSION

In most cases, the kinetics of static atmospheric corrosion follows a power law function of the form shown in equation (1):

$$D = At^b, \quad (1)$$

where:

D = the total damage usually expressed as mass loss per unit area or penetration;
t = the total time the metal has been exposed, usually in years;
A = the amount or depth of attack experienced in a unit of time (e.g., one year); and
b = the time exponent, usually but not always, less than 1.0.

This power law relationship distinguishes atmospheric corrosion from other forms of corrosion where the rate is constant throughout the exposure.

Static exposures have been carried out by several organizations around the world. The ISO CORRAG program was sponsored by ISO TC156/WG4, at 53 exposure sites located in 14 countries. This program included both flat panels and wire helix specimens of unalloyed steel, rolled zinc, copper, and aluminum materials, for exposures of 1, 2, 4, and 8 years. The A values represent the initial period mass loss or penetration that occurred during the exposure. In most cases, this is a 1-year period, but in the information shown in ASTM G101, *Standard Guide for Estimating the Atmospheric Corrosion Resistance of Low-Alloy Steels*, a 1-month period was reported. These results are strongly dependent on exposure conditions and the specimen variables, including surface finish and alloy composition. More detailed information on numerous exposures has been reported in ISO 9223 and is covered later in this chapter.

The results from the ISO CORRAG program were used to calculate average b values for each of the metals.[5] The results of these calculations are shown in table 1.

In the case of steels, the protectiveness of the rust layer is largely determined by the alloying elements in the steel, but the microstructure does not appear to affect the corrosion rate. Weathering steels have specific alloying additions that promote

Copyright © 2022 by ASTM International, 100 Barr Harbor Dr., PO Box C700, West Conshohocken, PA 19428-2959
ASTM International is not responsible, as a body, for the statements and opinions expressed in this chapter. ASTM International does not endorse any products represented in this chapter.

TABLE 1 Average Time Exponent Values for Flat Panels in the ISO CORRAG Program

Metal	b	Std. Dev.
Carbon steel	0.523	0.026
Rolled zinc	0.813	0.030
Unalloyed copper	0.667	0.029
Unalloyed aluminum	0.728	0.039

Note: The number of sites used for these calculations was 22.

the development of a protective rust layer. For these steels, testing has shown that the microstructure (i.e., ferrite-perlite or tempered martensite) does not affect their corrosion performance in atmospheric exposures.[6] Other types of carbon steels and low-alloy steels vary significantly in their performance. The steel used in the ISO CORRAG program had the following composition: 0.056% carbon, 0.06% silicon, 0.012% sulfur, 0.013% phosphorous, 0.02% chromium, 0.01% molybdenum. 0.04% nickel, 0.03% copper, 0.01% niobium, 0.01% titanium, 0.01% vanadium, 0.02% aluminum, 0.005% tin, 0.004% nitrogen, and 0.39% manganese.[5]

In cases in which the steel composition is known, the following formula can be used to estimate the b value for use in equation (1).

$$b = 0.569 + \sum a_i x_i, \quad (2)$$

where:
a_i = the multiplier for the *i*th element, and
x_i = the mass percent of that element.

This equation is based on data taken from ASTM G101. The a_i values for equation (2) are shown in table 2.

The 0.569 value in equation (2) is the average of b values for pure iron in three non-marine exposures. The standard error of the regression that produced equation (2) was 0.029.

In marine atmospheres, chloride deposition reduces the protectiveness of the rust layer that develops on steels. The extent of this effect can be estimated if the rate of chloride deposition is known. Equation (3) shows the magnitude of this effect on the b exponent, based on wet candle measurements:

$$\Delta = 0.844[Cl]^{0.26}, \quad (3)$$

TABLE 2 Alloying Element Multipliers for Equation (2)

Element	Multiplier, a_i
C	−0.084
P	−0.490
S	+1.440
Si	−0.163
Ni	−0.066
Cr	−0.124
Cu	−0.069

where:
Δ = the increase in b value, and
Cl = the chloride deposition rate in mg Cl/m^2.

The data used to develop equation (3) were taken from studies in which 19 different steel materials were exposed at nine marine sites that had different chloride deposition rates.[7–10]

Note that steels hardened to the point at which their tensile strengths exceed 1,000 MPa may suffer environmentally assisted cracking if they are subjected to sufficient tensile stress.

Weathering steels are steel alloys that have compositions designed to give good long-term performance in non-marine outdoor exposures. There are many applications in which these alloys offer significant benefits as they do not need to be painted and maintenance costs are minimal. These include building curtain walls, lamp poles, and guard rails. These alloys conform to ASTM A242, *Standard Specification for High-Strength Low-Alloy Structural Steel*, or ASTM A588 *Standard Specification for High-Strength Low-Alloy Structural Steel, up to 50 ksi [345 MPa] Minimum Yield Point, with Atmospheric Corrosion Resistance*. Note, however, that designs using these alloys may experience higher corrosion rates in crevices or sheltered areas not exposed to direct rain impingement. Crevices may develop deformations from corrosion product wedging, and significant rust staining may occur on concrete, stone, masonry, and other porous surfaces exposed to rain run-off from steels, including weathering steels.

To evaluate the atmospheric corrosion resistance of weathering steels, two corrosion indices have been created to provide a single value that incorporates all of the relevant composition information. The original concept was to use the data generated in a major study of the effect of composition on the atmospheric corrosion of steels. The data then were analyzed using a statistical regression approach to yield a b value for these steels. This analysis was carried out by Lagault and Leckie.[11] The equation that they generated was modified to create the corrosion index shown in ASTM G101. The second corrosion index was developed to expand the composition range covered and eliminate some of the anomalous behavior of the earlier version.[12] This version is somewhat more complicated. It is based on calculation the times required for pure iron to suffer a 254-µm loss at three sites (i.e., Bethlehem, PA, Columbus, OH, and Pittsburgh, PA).

These times then are used to determine the material losses for the alloy composition in question and then these losses are converted to thousandths of an inch and subtracted from 10. Then they are averaged to produce the corrosion index for the alloy. This index is also covered in ASTM G101. In this system, a corrosion index of 0 represents pure iron while weathering steels meeting the ASTM A588 specification exceed 5.5 or 5.0 depending on which index is used. For example, the steel used in the ISO CORRAG program has a corrosion index of 1.3 when calculated by either method. A calculator program available on the ASTM Committee G01 website to carry out the calculations.

The ASTM A588 specification was developed for steels in atmospheric exposures. The ASTM A242 specification was developed for steels used in coal-fired power plants in their economizer sections where the flue gases have significant sulfur dioxide contents.

Stainless steels (i.e., steels with chromium contents greater than 10%) are usually considered resistant to atmospheric corrosion. They may, however, experience superficial rust staining in marine atmospheres. Austenitic stainless steels also may exhibit chloride stress corrosion cracking in marine atmospheres if the metal temperature exceeds 60°C for extended periods, and the item is under significant tensile stress.

Zinc alloys also vary significantly in their atmospheric performance. The b value shown in table 1 was obtained from commercially available pure rolled zinc, but other zinc alloys have shown higher b values in atmospheric exposures. Electroplated zinc coatings, mechanically plated zinc coatings, and hot dipped zinc coatings all have unique behaviors in atmospheric exposures. Die cast zinc material are unique in their performance. Chromate conversion coatings are commonly applied to zinc surfaces to prevent water staining and white rust development, but such surfaces have shown b values in excess of 1.0.[13] Sulfur dioxide pollution in the atmosphere occurs when sulfur-containing fuels are burned, and this compound will accelerate the atmospheric corrosion of zinc alloys. In cases in which the life of zinc coatings has to be estimated, it may be reasonable to use a linear relationship (i.e., the b value is 1.0).

Painted steel is commonly used in atmospheric exposures. This material provides all of the benefits of steel construction along with the aesthetic appeal of a painted surface. A major drawback of this approach is that holidays in the coating (i.e., areas where the coating has been damaged or is missing) will cause both rust staining and loss of paint adhesion. One approach to minimizing these problems has been to apply a zinc coating between the paint and the steel. This has been shown to be effective in minimizing both problems in automotive applications.[14] In this case the extent of damage was evaluated by measuring the creep or peel back of the paint from the scribe line after the exposure, and the extent of rust staining was also evaluated.

Copper alloys, such as brasses, bronzes, nickel silvers, and cupronickels, have atmospheric corrosion rates similar to pure copper. Brasses with zinc contents above 20% may suffer dezincification in aggressive atmospheres, especially if sulfur dioxide is present. Two-phase brass alloys (i.e., those with zinc content greater than 30%) are most susceptible to this form of attack. Strain-hardened copper alloys may experience environmentally assisted cracking in atmospheric exposures, especially if ammonia is present in the atmosphere.

Aluminum alloys generally experience pitting in natural environments. As a result, the damage predicted from equation (1) may seriously underestimate the penetration that corrosion causes on these alloys. In addition, high-strength, age-hardening aluminum alloys containing significant copper or copper plus zinc levels, may show exfoliation in atmospheric exposures, especially in marine environments. Alclad materials generally have better corrosion resistance in these situations. Specific tempers have been developed to minimize the possibility of environmentally assisted cracking of high-strength aluminum alloys.

Equation (1) has been observed to be valid for most metals up to 20 years. In cases in which the b value is less than 1.0, however, the validity of this relationship is based on the fact that the corrosion product layer that develops becomes more protective as the exposure continues. This may occur because the layer is thicker or denser, or both. In any event, it seems likely that the layer will stabilize at some point, and the rate will become linear (i.e., the b value becomes 1.0). Unfortunately, no data currently exist that allows a prediction of when this may occur.

TYPES OF EXPOSURES

Probably the most common type of atmospheric exposure is conducted in a static location—that is, racks or holding devices are fixed in a location and specimens are exposed for a test period at that site. This type of exposure can be carried out in sheltered sites or boldly exposed sites. A wide variety of different types of specimens may be employed in long-term tests.

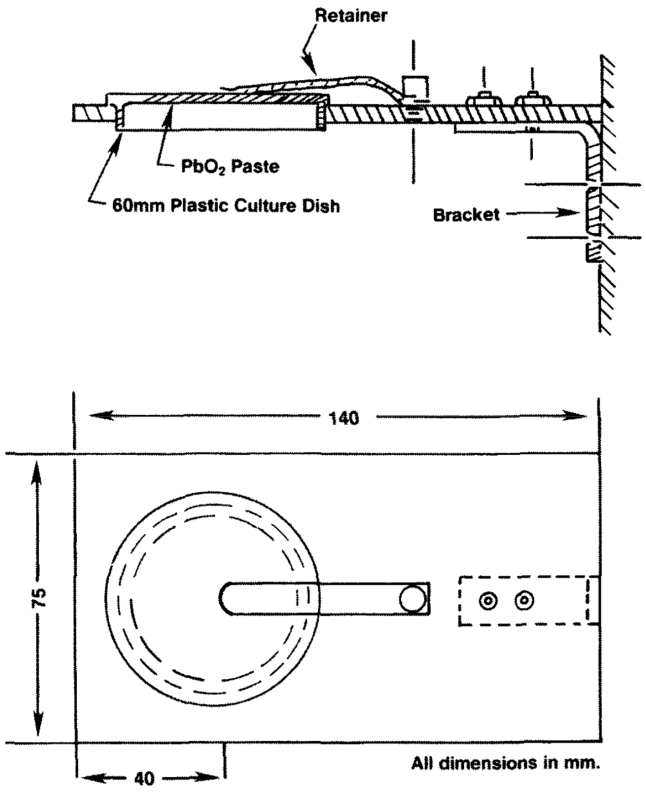
Another type of test is the dynamic or mobile test in which panels are mounted on vehicles to simulate the service conditions of cars or trucks. Vehicles are exposed to significant amounts of spray and splash from the road surface and, as a consequence, this environment is significantly different from that normally seen in the static exposures. In some cases, panels have been mounted on the sides of trucks to allow a larger number of panels to be mounted in approximately the same type of environment.[15] Panels mounted on automobiles generally are mounted in locations in which they are not visible, although in some cases bumper-mounted panels have been used.[16] Variability in dynamic tests is substantial because no two vehicles see exactly the same environment. A similar situation exists for oceangoing vessels. The atmospheric corrosion that occurs on aircraft carriers, for example, is distinct because it incorporates both marine spray from the ocean and flue gases from the engines.

Because of the rather substantial variability in dynamic tests, coupled with the problem of having limited numbers of panels on each vehicle, some investigators have employed an approach of spraying static panels with simulated road splash solutions, for example, mixtures of sodium and calcium chloride. This is, of course, a much more severe environment than normal static atmospheric exposure. It does have the advantage, however, of being more reproducible than a vehicular exposure while allowing many panels to be exposed at the same time under the same conditions. Such an approach also allows for the natural wetting and drying that is normally seen in atmospheric exposures. These conditions are difficult to simulate in cabinet-type tests.

MONITORING ATMOSPHERIC VARIABLES

A conventional weather station approach often has been used to monitor atmospheric variables regarding atmospheric corrosion.[17] Temperature and relative humidity may be recorded continuously, and these data are used to produce average temperatures for periods of time such as days, weeks, or months. Electrical monitoring sensors have been developed to measure when wetness exists on the surface by means of detecting a potential difference between dissimilar metals.[18] A standard device is shown in ASTM G84, *Standard Practice for Measurement of Time-of-Wetness on Surfaces Exposed to Wetting Conditions as in Atmospheric Corrosion Testing*. The information on

FIG. 1 Sulfation plate in holder (see ASTM G91).



time of wetness is usually reduced to a percentage or fraction of time a surface is wet in a month or in a year.

Atmospheric sulfur, usually in the form of sulfur dioxide, is measured by means of a volumetric sampling approach in which samples of the air are passed through a detector that directly measures the sulfur dioxide concentration. Another approach is to use a sulfation plate or sulfation candle (fig. 1).[19] These devices rely on lead dioxide to react with the sulfur compounds in the atmosphere to form lead sulfate. At the conclusion of a fixed exposure period, usually 30 days, the sulfation plate or candle is removed from exposure and analyzed for the presence of lead sulfate. ASTM G91, *Standard Practice for Monitoring Atmospheric SO_2 Using the Sulfation Plate Technique*, describes the sulfation plate method. Sulfation plates are exposed in a horizontal downward-facing position so that the lead dioxide reagent is not exposed to rainwater. ASTM D2010, *Standard Test Methods for Evaluation of Total Sulfation Activity in the Atmosphere by the Lead Dioxide Technique*, describes the sulfation candle, which is a similar type of collector except that it employs a vertical cylinder rather than a flat disk. Again, the sulfation candle must be protected from exposure to rain or snow. Neither the sulfation plate nor the sulfation candle is specific for sulfur dioxide. They will respond to reduced sulfur species, such as hydrogen sulfide and carbonyl sulfide. The presence of these gases is relatively rare, however, and usually a source of such reduced species would be apparent to investigators at the site. These gases dramatically enhance the corrosion of some alloys but are not equivalent to sulfur dioxide.

Note that the volumetric measurement of sulfur dioxide by means of infrared absorption and the deposition rate measurement measure different phenomena. The transfer from the gas phase to the solid surface requires both convective diffusion and surface adsorption steps.[20]

Air movement assists the convection process while the adsorption step is accelerated by the presence of condensed moisture. As a result, correlations between volumetric concentration and deposition rate are approximate and may not necessarily apply from site to site. For corrosion correlation purposes, the deposition rate is a more relevant phenomenon. As a practical matter, however, the mass transfer rate that occurs on a sulfation plate or candle probably is not equivalent to what would occur on a flat surface or a wire. Therefore, the results obtained from devices such as sulfation plates provide a reasonable measure of the concentration of sulfur in the atmosphere but not an accurate measure of what deposits are on test samples or structures. The volumetric concentration monitoring instruments are clearly the preferred technique because they require less labor to expose and retrieve samples and can provide much more detailed information about how the sulfur dioxide concentration varies with time.

Sulfur dioxide deposition and chloride deposition have been designated dry depositions in studies concerned with the effects of acid precipitation in spite of the fact that these processes do occur when the specimen is physically wet with dew or rain. The term *wet deposition* refers to acidity delivered to the specimen during periods of rain or snow.[21] The reason for this distinction is that the source of acidity in precipitation is probably different from the source of either atmospheric sulfur dioxide or chloride. To monitor wet deposition, it is necessary to collect and analyze precipitation samples. In general, the damage to metals from acid precipitation is relatively small compared with the damage caused by significant levels of sulfur dioxide or chloride on most engineering metals.[22]

Several techniques have been used to monitor chloride in the atmosphere. The wet candle method, ASTM G140, *Standard Test Method for Determining Atmospheric Chloride Deposition Rate by Wet Candle Method*, has been used in marine sites and consists of a fabric-wrapped tube in which the fabric is kept wet with water (fig. 2).[23] The wet fabric acts as a collector for chloride particulates or droplets. Exposure periods of 1 week or up to 1 month have been used. The longer time periods can be a problem because the water source must not be allowed to dry. It is important to protect the wet candle from rain exposure so that wet candle assemblies are usually mounted with a cover over them.

With the wet candle method, it is necessary to employ an antifreeze solution in cold climates when freezing can occur. Glycerin has been used for this purpose, but if glycerin is used, it is necessary to add an inhibitor to prevent biological growth in the solution. Another technique that has been used is the dry plate method. In this case, a vertical assembly is used with fabric stretched over a frame. Chloride-containing particles adhere to the dry fabric and are extracted from the fabric and analyzed at the end of the exposure period. Figure 3 shows the relationship

FIG. 2 Wet candle apparatus with holder (see ISO 9225).

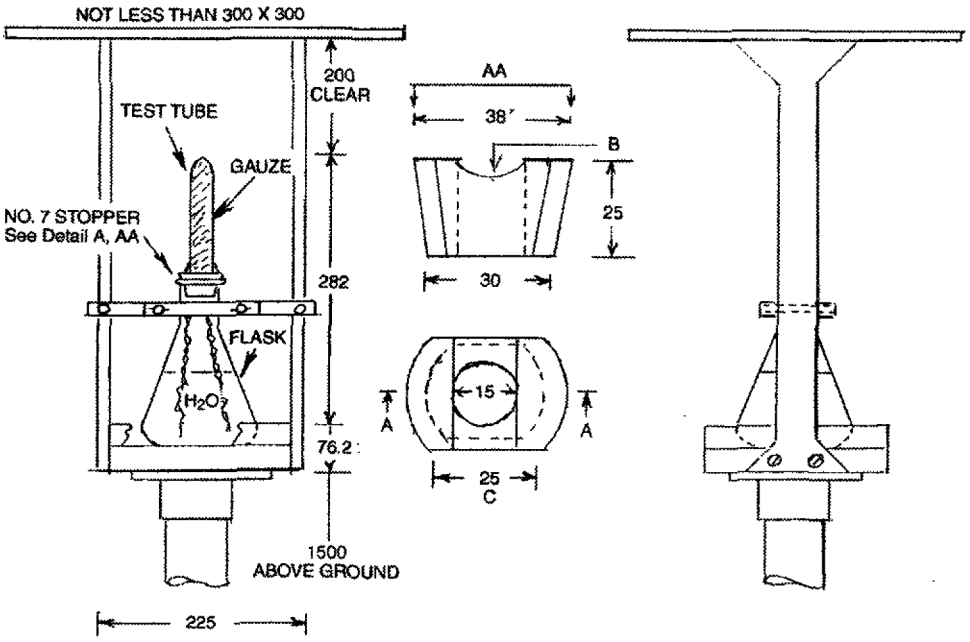
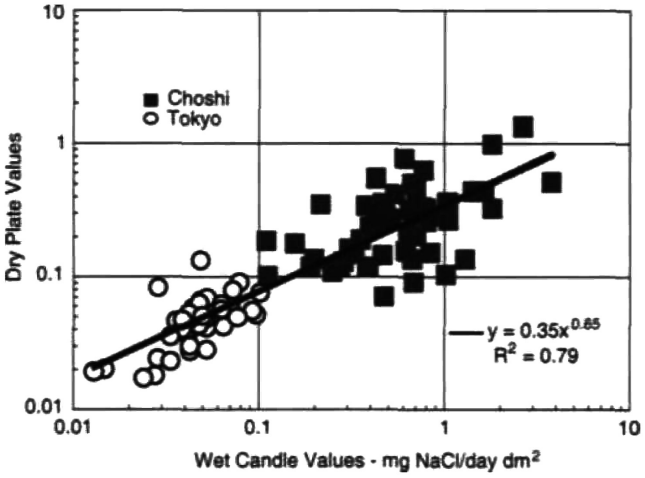


FIG. 3 Comparison of wet candle and dry plate results for atmospheric deposition at two sites (see ISO/TC156/WG4/N236).



between chloride deposition rates measured by both methods at two sites.

Atmospheric chlorides generally originate from marine sources. Surf is a major contributor to atmospheric chlorides. The spray from surf is entrained in the air and carried inland by the wind. As a result, spray droplets tend to settle out and dry out as they move inland, becoming smaller and more concentrated in an almost exponential decay as they move. Chloride particles are very water soluble so that areas washed by rain tend to retain much less chloride than protected areas. Large smooth surfaces are much poorer collectors of salt particles than small diameter wires. As a result, devices such as the chloride candle or dry plate collector give only rough approximations of actual chloride depositions on test samples or structures exposed to the atmosphere. Note that seawater also contains sulfate, so that any finding of sulfur compounds in marine locations does not necessarily indicate the presence of sulfur dioxide. The ratio of sulfate to chloride in most seawater on a mass basis is 0.103.[24]

In cases in which both chloride and sulfate are found, only the excess sulfate above this ratio should be designated as sulfur dioxide. This is important because sulfur dioxide is a much more aggressive contributor to atmospheric corrosion than is sulfate. Chlorine and hydrogen chloride are sometimes found in industrial atmospheres. These compounds can cause serious corrosion, but they are not covered by the ISO standards.

CLASSIFICATION OF THE ATMOSPHERE—ISO APPROACH

The International Organization for Standardization Technical Committee on Corrosion of Metals and Alloys, ISO/TCI56, has developed a systematic approach to classification of atmospheric corrosivity. This approach is based on two different methods. The first method involves exposure of standard coupons of steel, zinc, copper, or aluminum to the atmosphere at the site where the classification is to be made. The selection of which metal is to be used will depend on the purpose of the test. Panels are exposed for a one-year period, and then they are retrieved, and a mass loss per unit area measurement is obtained. This mass loss value can then be used to determine the corrosivity of the atmosphere at that location. Table 3 shows the corrosivity classes based on mass loss results.

The second method involves measurement of the temperature, time of wetness, amount of sulfur in the atmosphere, and the amount of chloride in the atmosphere. Temperature and

TABLE 3 ISO Corrosion Classes for Metals Based on 1-Year Exposure Results

			Mass Losses	
Steel, g/m	Copper, g/m^2	Aluminum, g/m	Zinc, g/m^2	Corrosion Category
<10	<0.9	~0	<0.7	CI
10–200	0.9–5	<0.6	0.7–5	C2
201–400	5.01–12	0.6–2	5.01–15	C3
401–650	12.01–25	2.01–5	15.01–30	C4
651–1,500	25.01–50	5.01–10	30.01–60	C5

Note: Based on ISO 9223.

TABLE 4 ISO Wetness Class Based on Time of Wetness

	Wetness	
Class	Time Wet, %	Examples of Occurrence, hours wet/year
TI	<0.1	<10 indoor
T2	0.1–3	10–250 indoor—unheated
T3	3–30	250–2,500 shed storage—cold climate
T4	30–60	2,500–5,500 outdoor temperate climate
T5	60	5,500 tropical outdoor or surf

Note: Based on ISO 9223.

TABLE 5 Sulfur Dioxide and Chloride Classes

	Sulfur Dioxide		Chloride	
SO_2 Class	Deposit Rate, mg/m^2 day	Concentration, mg/m^3	Cl Class	Deposit Rate, mg/m^2 day
P0	<10	<12	S0	<3
PI	10–35	12–40	S1	3–60
P2	36–80	41–90	S2	61–300
P3	81–200	91–250	S3	301–1,500

Note: Based on ISO 9223.

humidity information can be used to estimate the time of wetness. This estimation is based on the percentage of time that the temperature is above freezing, 0°C, and the relative humidity is at the same time above 80%. Once the time of wetness is known, it is then possible to determine a time of wetness class (table 4). Sulfur dioxide content of the atmosphere can be estimated either by measurement of the concentration in the atmosphere over some period of time or by means of the sulfation plate or candle. This information is then used to develop a sulfur dioxide class or P class (table 5). The chloride dry plate or wet candle method is used to obtain the chloride deposition rate of the atmosphere, which is then converted to a chloride class or S class (table 5). The corrosion class or C class can be obtained for the time of wetness, chloride, and sulfur dioxide classes (table 6). Once the corrosion class is known, it is possible to estimate the corrosion damage that will occur in either short-term or long-term exposures for the five metals, steel, weathering steel, aluminum, copper, and zinc (table 7). The detailed information on this method is discussed in tables 4–7. The ISO procedure for estimating long term damage assumes a linear rate after the first year of exposure shown in table 7 as LT rates.

This system of atmospheric classification is now being revised to create a new approach based on dose-response functions for steel, copper, and zinc. Because the corrosion of aluminum occurs by a pitting or localized mechanism, the traditional approach of using mass loss to determine severity of attack is often misleading. Atmospheric corrosion problems with aluminum alloys are most frequently a result of metallurgical conditions rather than environmental conditions, and the behavior of aluminum may be excluded in the upcoming revision of the ISO 9223-6 documents.

INDOOR ATMOSPHERES

Although the ISO approach to classification of the atmosphere was envisioned to cover both indoor and outdoor atmospheres, the classification range on indoor atmospheres was too broad to be useful for many applications. The corrosion concerns for

TABLE 6 Corrosion Classes for Environmental Classes

	T2			T3			T4			T5		
	S0-S1	S2	S3	S0-S1	S2	S3	S0-S1	S2	S3	S0-S1	S2	S3
Unalloyed Steels												
PO-PI	1	2	3-4	2-3	3	4	3	4	5	3-4	5	5
P2	1-2	2-3	3-4	4	3-4	4-5	4	4	5	4-5	5	5
P3	2	3	4		4-5	5	5	5	5	5	5	5
Zinc and Copper												
PO-PI	1	1-2	3	3	3	3-4	3	4	5	3-4	5	5
P2	1-2	2	3	3	3-4	4	3-4	4	5	4-5	5	5
P3	2	3	3-4	3	3-4	4	4-5	5	5	5	5	5
Aluminum												
PO-PI	1	2-3	4	3	3-4	4	3	3-4	5	4	5	5
P2	1-2	3-4	4	3	4	4-5	3-4	4	5	4-5	5	5
P3	3-4	4	4	3-4	4-5	5	4-5	5	5	5	5	5

Note: T = wetness class, P = SO_2 class, S = chloride class. Based on ISO 9223.

TABLE 7 Atmospheric Corrosion Rates for Corrosion Class

	Steel		Copper, µm/year		Zinc, µm/year		Aluminum, µm/year		Weathering Steel, µm/year	
Class	ST	LT	ST	LT	ST	LT	ST	LT	ST	LT
1	<0.5	<0.1	<0.01	<0.01	<0.1	<0.05		<0.01	<0.1	<0.1
2	0.5–5	0.1–1.5	0.01–0.1	0.01–0.1	0.1–0.5	0.05–0.5	0.01–0.025	0.01–0.02	0.1–2	0.1–1
3	5–12	1.5–6	0.1–1.5	0.1–1.0	0.5–2	0.5–2	0.02–0.2	0.02–0.2	2–8	1–5
4	12–30	6–20	1.5–3	1.0–3	2–4	2–4			8–15	5–10
5	30–400	20–90	3–5	3–5	4–10	4–10			15–80	10–80

Note: ST = average corrosion rate during the first 10 years of exposure. LT = steady state corrosion rate for long-term exposures. Based on ISO 9224.

indoor atmospheres covered three different categories. One major area of concern was storage of metallic parts and components in warehouses. The concern is that the storage conditions do not stain or damage the parts. The second area of concern is the use of metallic materials in indoor atmospheres where corrosive conditions can occur, for example, plumbing fixtures in humid environments such as kitchens and bathrooms. A third area of concern is for electronic components.[25] There have been serious problems with failures of measuring devices, computers, and related equipment in control rooms, and even in offices, that have been attributed to corrosion. The ISO system is adequate to deal with the concerns of warehouse storage but has not been adequate to deal with the concerns of electronic materials degradation. The reason for this is that the mechanism of corrosion that causes problems in electronic circuitry is quite different from that encountered by engineering materials in atmospheric outdoor exposure. The problems that occur in electronics include the development of resistive films that interfere with switch operation and the migration of corrosion products causing short circuits or related problems. Two specific problems have been noted. One is the development of pore corrosion. This phenomenon has been observed on gold surfaces in the form of black spots distributed over the gold surface. The second problem is film creep, which refers to a rapid diffusion of corrosion products across the gold surface. Other problems also have been noted.

In the case of corrosion in storage areas and the protection of materials in humid indoor atmospheres, conventional techniques that apply to outdoor corrosion are suitable. The primary mechanism seems to be the development of moisture films on the metallic surfaces that then promote corrosion. In the case of electronic components corrosion, the critical moisture contents are at substantially lower values than are normally seen in outdoor corrosion. In addition, the critical pollutants seem to be reduced sulfur species such as hydrogen sulfide, and also acid chloride species such as hydrogen chloride. These species are present in indoor atmosphere at very low levels, typically 0.1–10 ppb (table 8).

TABLE 8 Gaseous and Solid Materials Affecting Indoor Atmospheric Corrosion

Substance	Concentration, µg/m^3	Comments
SO_2	1–100	30–50% lower than outdoors
NO_2	2–150	Similar to outdoors
H_2S Cl_2	1–3 <0.1	Higher in some situations
HCl NH	0.1–20 20	Usually very low
SootO_3	5 2–25	Higher when fires are used Usually lower than outdoors

Atmospheric Testing

PROGRAM DEVELOPMENT

The first step in an atmospheric testing program is to develop a program that will provide answers to the question: What is the purpose of this program?[26] If the purpose of the program is to characterize the atmospheric performance of a new material, it is important to determine what time interval is relevant and what reference materials should be included so that a definite comparison can be made. It also is important to determine what type of exposure will be used and what the specimens should look like. Furthermore, it is important to determine at this time how the results of the program will be evaluated. Understanding these issues at the beginning of the process is helpful in determining later how many specimens are needed and what types of materials are required and, ultimately, what the cost of the exposure program will be. Table 9 lists the key issues that need to be decided at the beginning of any atmospheric testing program.

EXPOSURE PROGRAM

The simplest type of exposure program is a fixed material program in which a set of specimens is exposed for a fixed time period. At the conclusion of this period, the specimens are retrieved and evaluated. A variation on this approach is to

TABLE 9 Program Development Issues

- Purpose of the program?
- Exposure time to achieve purpose?
- Reference materials?
- Results evaluation?
- Replication needed?
- Coating for the ground facing surface of panel?
- Edge preparation or masking?

inspect the specimens at the exposure site at intervals during the exposure period and report results.

A somewhat different approach is to expose a group of specimens initially and then retrieve portions of the group at intervals (e.g., 1 year, 3 years, 5 years, 10 years, and 20 years). This approach allows the investigator to estimate the kinetics of the process if an assumption can be made about the constancy of the environment. A variation of this approach is to replace each specimen removed with an unexposed specimen to be retrieved at the conclusion of the test. This approach allows for variations in the environment to be averaged out or at least acknowledged (fig. 4).

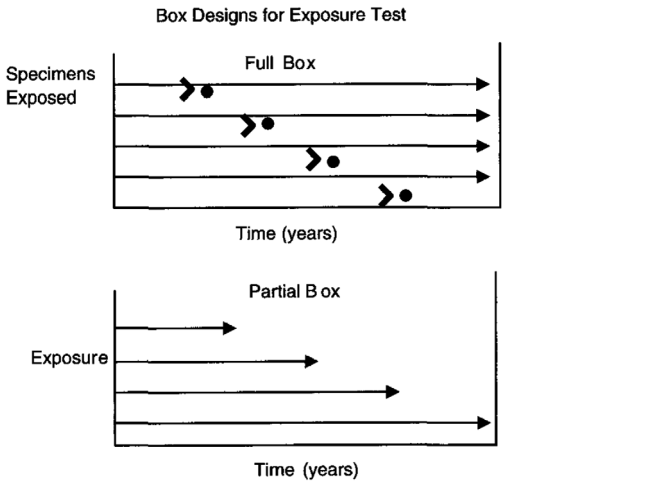
An important issue in exposure tests is the question of replication. It is desirable to use at least duplicate specimens in corrosion tests. In atmospheric tests, however, it is good practice to use a larger degree of replication, preferably five specimens for statistical analysis. Three specimens are generally considered the minimum acceptable in most cases to avoid problems from damage, loss, and unexpected events.

In general, indoor exposures usually are made for relatively short periods. In most cases, 30 days and 90 days are typical, although occasionally a 1-year exposure is used. Because the purpose of these exposures is generally to evaluate the environment, it is usually necessary to obtain results rapidly to determine what protective measures are necessary.

SPECIMEN TYPES

Once the purpose of the program is decided, the next question is: What type of specimen should be used? Some typical specimen types are listed in table 10. Probably the most widely used specimen in atmospheric exposure programs is a 100-mm by 150-mm panel. This type of panel is suitable for mass loss measurements. It is also used to evaluate coatings and is convenient to handle. For nonferrous metals, investigators have preferred to use larger panels, for example, 100 mm by 200 mm.[27] Larger sizes do lose some convenience and ability to fit on some balances.

FIG. 4 Example of exposure program designs.[15] *Source:* Reprinted from Materials Performance. © 1988 by NACE International. All rights reserved by NACE; reprinted with permission.



Specimens exposed at dots and retrieved for evaluation at arrow head
Full box allows atmospheric corrosivity change estimate as well as specimen corrodibility estimate Partial box estimates only specimen changes

TABLE 10 Types of Specimens

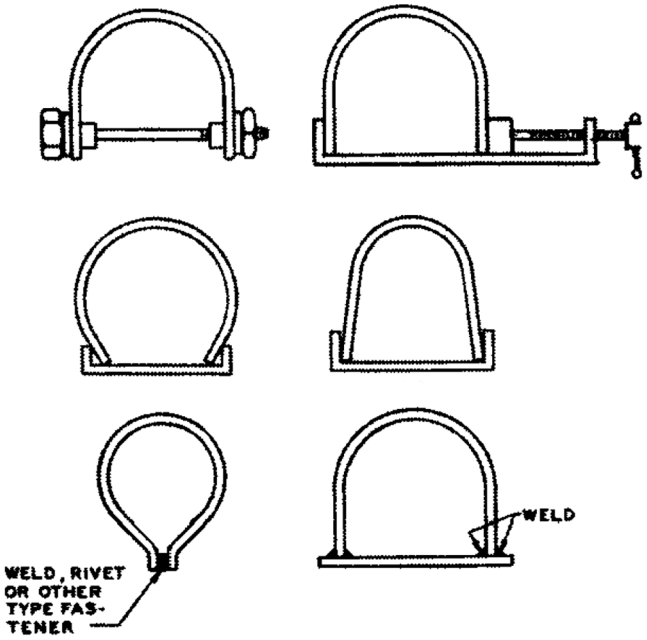
Type	Standards
Flat Panel	ASTM G50
100 × 150 mm	
100 × 200 mm	
100 × 300 mm	
Helix Wire	
Stress Corrosion	
Bent Beam	ASTM G39
C Ring	ASTM G38
U Bend	ASTM G30
Direct Tension	ASTM G49
Welded	ASTM G58
Galvanic	
Plate on Plate	ISO 7441
Disk on Disk	ASTM G149
Wire on Bolt	ASTM G116
Coated Specimen	ASTM D1654
Fabricated Items such as fasteners, hardware, beams, etc.	

Wire helix specimens have been used to monitor atmospheric corrosivity.[28] Note that this type of specimen tends to show higher corrosion rates than flat panels of the same material. For this reason, it is likely that helix specimens will be dropped for the purpose of site monitoring. Wire samples show higher corrosion rates because of the increased collection efficiency of small diameter cylinders in gathering other gaseous or solid particles, and these materials tend to stimulate the corrosion process.[29]

Atmospheric stress corrosion tests are frequently run with U-bend specimens or two-point loaded specimens. U-bend specimens are used when the stress level is not a variable, but it is desired to determine if an alloy is susceptible to cracking (fig. 5). Two-point loaded specimens have the advantage of being held at points of low stress and at locations where a crevice will do the least damage. It is relatively simple to construct racks to hold two-point loaded specimens. A two-point loaded specimen can be designed to cover a wide range of maximum stresses.[30] Other types of standard stress specimens also may be used, for example, direct tension specimens, C-ring specimens, and other bent beam configurations (fig. 6). Table 10 lists standard stressed specimens that may be used in atmospheric corrosion.

It is occasionally desirable to evaluate galvanic corrosion effects from atmospheric exposures (see ASTM G116, *Standard Practice for Conducting Wire-on-Bolt Test for Atmospheric Galvanic Corrosion*, and ASTM G149, *Standard Practice for Conducting the Washer Test for Atmospheric Galvanic Corrosion* [*Withdrawn 2004*]). Several different types of specimens have been used for this purpose.

FIG. 5 U-bend specimen designs (see ASTM G30).



One approach is to use washers bolted together as shown in figure 7.[31] At the end of the test, it is possible to measure the depth of corrosive attack associated with the region of galvanic corrosion by means of mass loss measurements. Other types of galvanic exposure specimens that have been used have included plates of different metals bolted together and the helix wire-on-bolt type of specimen (see ASTM G116).[32] In this latter case, the test specimen is usually a wire that is wrapped around a bolt of a different material to evaluate the galvanic corrosion that may occur from this couple. Mass loss measurements are usually used to evaluate the loss of metal from the wire specimen.

Atmospheric exposure programs are often run to evaluate coating performance. This is true for both organic coatings and for inorganic coatings, including metallic coatings such as electroplated coatings,[33] flame-sprayed coatings,[34] and hot-dipped coatings.[35] The key issue in the case of organic coatings is the adhesion of the coating and particularly the ability of the coating to maintain adhesion and protection even in the face of mechanical damage. Consequently, it is often desirable to scribe an x-shaped mark on the surface of the panel after the coating process. The scribe should penetrate to the basis metal.

At various times during the exposure, the panel is evaluated by noting how far the corrosion of the basis metal has proceeded under the paint or coating. In the case of metallic coatings, visual examinations usually are conducted during the life of the exposure to look for penetration of rust through the coating, spalling, or other degradation of the coating itself. It is often desirable to expose fabricated items, such as roofing panels, automotive trim parts, wire ropes, wire specimens, and a host of other hardware items. This type of program allows the performance of a finished

FIG. 6 Bent beam specimen designs (see ASTM G39).

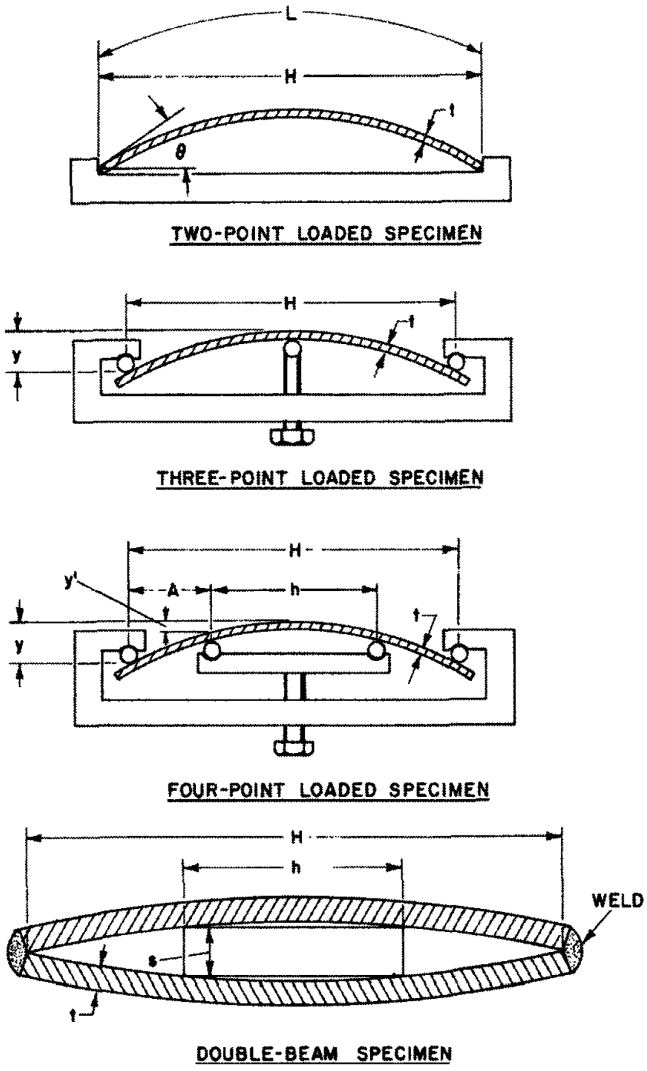
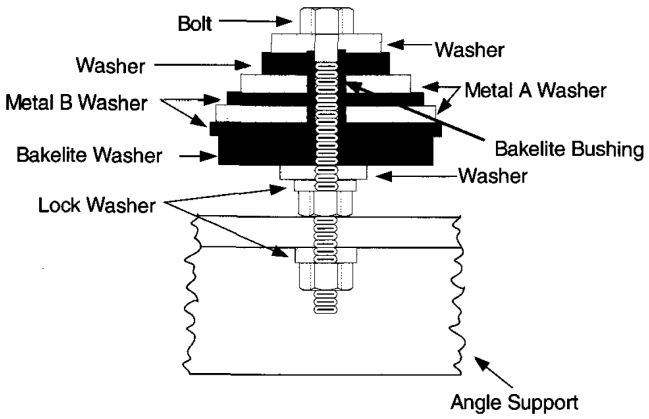


FIG. 7 Cross section of washer bimetal assembly (see ASTM G149).



product to be evaluated in a controlled exposure program. It is especially good for evaluating differences in finishes to determine if the difference in the finishing process has caused a change in the coating performance.

SPECIMEN PREPARATION

The type of preparation that a specimen will require depends very much on purposes of the exposure program.[3] In cases in which bare metals are to be exposed to the atmosphere, a somewhat arbitrary decision must be made on what type of surface finish will be tested. Typical steps in an atmospheric exposure program are given in table 11.

Characteristically for ferrous metals, it is generally desirable to employ a mechanical finishing technique that removes the mill scale. Surface grinding with 120-grit abrasive is a typical finish. Such finishes are rather active, and consequently, panels must be wrapped with an inhibiting paper or protected by other means so that the surface rust does not develop during shipment. In this case, it is necessary to remove any traces of inhibitor that might have transferred to the metal surface. A solvent cleaning step immediately before exposure is frequently used.

It is also necessary to place an identifying mark on the panels before exposure (table 12). In the case of ferrous metals where heavy corrosion occurs, it is necessary to use techniques, such as drilling holes in the panels in specific locations or milling notches in the side of the panel, so that it will be possible to identify the panel even after extensive corrosion has occurred.[28] In the case of materials that do not suffer such extensive corrosion in atmospheric exposures, techniques such as stencil stamping may be used. It is desirable to use clean, sharp stencils and to avoid transferring foreign metals from the stencil stamps to the metal surface. In the case of coated samples, stencil stamping may not be acceptable. Other approaches may be used, such as writing the panel identification on the back of the panel with a weather-resistant paint or attaching a tag to the panel with the panel identification stamped on it.

The panels should be carefully weighed and measured before exposure. This should be the last step before the panel leaves the laboratory. In the case of coated samples, an important issue is the edge protection. In some cases, specimens are sheared from larger sheets and, consequently, the edges are left uncoated. In this case, it is essential that measures be applied to edges to prevent edge damage from confusing the results. For short-term exposures, vinyl tape is sometimes used to protect the edges. It also may be necessary to carry out preliminary evaluations of the surface of coated samples, including reflectivity measurements, color measurements, or related optical measurements before placing them on exposure.

For indoor exposures, the metals used are usually copper, silver, or steel. Typical exposure panels are 10 mm by 50 mm by 0.5 mm thick. These panels are usually abraded with a fine silicon carbide abrasive paper; 1,200 grit for copper and silver and 500 for steel. After polishing, the specimens should be cleaned in ethanol in an ultrasonic bath before exposure. Occasionally, nickel or zinc specimens may be used in special circumstances in which these metals are to be used.

TABLE 11 Specimen Preparation Steps

- Mechanical preparation
  - Cut to size
  - Finish edges
  - Finish faces
- Identification and cleaning
- Initial measurement
  - Mass
  - Size
  - Optical
  - Photographic
- Shipment
- Final cleaning and edge protection, if necessary
- Exposure

TABLE 12 Specimen Identifying Systems

Type of Panel	Appropriate System
Steel	Drilled holes according to matrix
	Mill or saw edge notches
Nonferrous and stainless steel alloys	Stencil stamping
Metallic coated	Stencil stamping
	Plastic or nonferrous tags
	Paint on back side

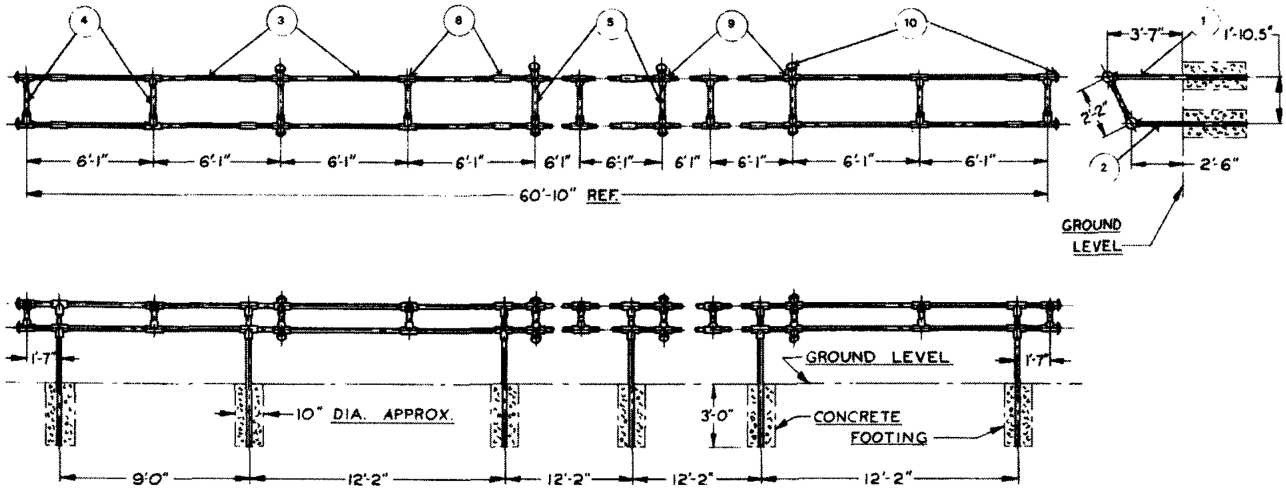
OUTDOOR EXPOSURE

Most outdoor exposures are carried out in static situations with the specimens mounted on racks. A standard system has been developed in the United States whereby racks are mounted on stands with the panels exposed at an angle of 30° to the horizontal.[28] In Europe, the exposure angle is generally 45° to the horizontal (fig. 8).[36] Exposure racks have been designed so that panels can be placed in the rack without disturbing adjacent panels.

It is general practice to have the panel racks facing south in the northern hemisphere. In the case of panels with organic coatings, the top surface will receive the greatest sun exposure if the panel is mounted at an angle to the horizontal equal to the latitude of the site. When panels are mounted in locations where sources of atmospheric-borne corrodents are present, generally it is desirable to have the racks face the source of the corrodent species. For example, at seacoast locations, panels should face the surf. In cases adjacent industrial sites, it may be desirable to orient the panels so that they face the source of the pollutants from the industrial source.[3]

At the time panels are exposed, the weather should be recorded. It is also important to record the location of each panel on the rack and the rack identification and location at the site.

FIG. 8 Atmospheric exposure text rack support design (see ASTM G50).



Plans should be made at this time to retrieve the panels or specimens. For short-term exposures, this may not be a problem. For programs that go for many years, however, maintenance of the site can be a problem.

In the case of exposure programs where visual examination of the specimens is to be made at intervals during the program at the exposure site, it is important to set up an evaluation form so that the information desired is recorded along with the specimen identification (see ASTM G33, *Standard Practice for Recording Data from Atmospheric Corrosion Tests of Metallic-Coated Steel Specimens*). In the case of tests on stress corrosion specimens, it is desirable to remove specimens at regular intervals during the exposure period so that they may be examined for cracking. This is especially true for specimens that develop thick corrosion product films on their surface because such films often obscure the cracks. It is also desirable to retrieve broken specimens in stress corrosion programs so that the specimen may be evaluated for mode of cracking and presence of secondary cracks. For two-point loaded specimens, it is desirable to wire both ends to the holder in case the specimen fails by total fracture.

INDOOR EXPOSURE

Indoor exposure sites generally employ vertical panels hung from hooks or wires through a hole near the top of the specimen. In some cases, a plastic enclosure is used to protect the specimens from direct exposure to air currents and to shield the specimens from falling dust. In general, it is desirable to avoid locating the panels near walls and corners where unusual air currents may circulate. It is important that the site location be chosen to be representative of the conditions in question, but more important, that they not be damaged or disturbed by the activities in the area.

Indoor specimens may be evaluated by several techniques, including mass gain, mass loss, electrochemical reduction (coulometric measurement), and electrical resistance increase. Microbalance measurements of mass gain after removal of particulates is probably the most popular method because it requires the least specimen handling. It will detect dust and particulates on the surface that adhere strongly, however, and may overestimate the corrosion damage in cases in which this condition occurs.

Another approach to the microbalance concept is to deposit a thin layer of the metal in question on a quartz crystal and monitor the mass change due to oxidation by means of the change in resonance frequency of the crystal. Applying an AC potential across the thickness of the crystal and detecting the resonance frequency in the shear direction can activate the quartz crystal. By selecting a crystal orientation that has minimal temperature dependence on the resonance frequency, it is possible to obtain a device that can monitor mass changes on a continuous basis.[37] This technique can detect mass changes as low as 10^{-6} g/cm^2. The metal chosen for the test is typically deposited by vacuum evaporation onto the quartz surface.

SITE MONITORING AND EVALUATION OF ENVIRONMENT

One of the distinguishing characteristics of atmospheric exposure programs is that the environment is not under the investigator's control. Sites may be selected to have specific properties or characteristics; however, unpredictable variations occur in weather patterns in both short- and long-term exposures. Furthermore, the presence of corrosive materials in the environment is often the function of activities that go on at some distance from the exposure site and, as such, are entirely outside the control of the investigator. Consequently, it has long been a desire of investigators to develop techniques to evaluate the corrosivity of sites where exposure programs are taking place. One approach to measuring site corrosivity is to expose a set of standard panels of a known material that can be used as a control. Steel panels have been widely used for this purpose (see ASTM G92, *Standard Practice for Characterization of Atmospheric Test Sites*); however, zinc, copper, and aluminum also have been used.[28] The test material performance can be compared to the standard panel material performance and conclusions drawn from that. This

important approach should be practiced as much as possible because we may never be able to measure all of the variables that affect atmospheric corrosion.

The standard panel approach, however, does not provide information as to what caused corrosivity of the environment. To understand the factors that contribute to corrosivity, it is desirable to obtain data on the temperature, relative humidity, time of wetness, time during which precipitation occurred, and wind velocities.[27] It is also desirable to obtain samples of precipitation at various times during the exposure period and have it evaluated for acidity and the presence of ionic species. Another factor is the presence of sulfur species in the air, especially sulfur dioxide. The sulfation plate or actual volumetric sampling may be used. In addition, in marine locations, it is desirable to have some estimate of the airborne salinity, either through a chloride candle or the dry plate method.[38] Another variable that is important, but seldom measured, is the temperature during the period which panels are wet. Corrosion occurs mainly during periods of wetness, so that the temperature during this period is most important in terms of determining the corrosion kinetics. Table 13 lists atmospheric variables that are often monitored.

In the case of indoor corrosion, several parameters can be measured to determine the corrosivity of the atmosphere. Unfortunately, there are no standards currently available that relate the corrosivity of the atmosphere to the concentrations of corrosive components, but the measurement of such components may be helpful in determining the cause of problems with an indoor environment.

For gaseous components, two types of measurements can be used: active sampling and passive sampling. Active sampling requires a pump to draw a specific quantity of air into a measurement chamber. The gaseous components are measured by a specific method (e.g., infrared absorption) and are recorded. Passive samplers use either a diffusion cell or a direct deposition method. The diffusion cell employs a stagnant tube through which the components must diffuse and then be absorbed and measured. The deposition method eliminates the stagnant tube and relies solely on natural convection to transport the species in question to the reactive surface. The following gases have been monitored using diffusions cells: SO_2, NO_2, H_2S, NH_3, and O_3. Particulates are more difficult to monitor and require different methods. Again, active sampling requires a pump to draw a specific volume of air through a filter or onto impingement plates that is then analyzed. Collection plates also may be used together with microscopic methods of analysis and evaluation. Temperature and humidity measurements are also important to measure for evaluation of the environment.

The corrosivity of indoor atmospheres must be determined by standard panel exposures.

TABLE 13 Atmospheric Variables for Exposure Programs

Variable Measurement Frequency	Report	Typical Units
Temperature, hourly	30 day A&R	°C
Temperature when wet, hourly	30 day A	°C
Relative humidity, hourly	30 day A	%
Time of wetness, hourly	30 day T	h or %
Dew point temperature, hourly	30 day A	°C
Insolation time, hourly	30 day A	h
Insolation, hourly	30 day A	J/m^2h
Precipitation time, hourly	30 day	T h
Precipitation, daily	30 day	T mm
Precipitation pH, daily	30 day A&R	
SO_2 concentration, hourly	30 day A	ppb (vol)
SO_2 deposition, 30 day	30 day T	mg SO_2/m^2day
Chloride deposition, 30 day	30 day T	mg Cl/ m^2day

Note: A = average, R = range (high and low value), T = total, Insolation time = time during sun exposure, Insolation = solar heating.

Atmospheric Exposure Standards

ASTM Committee G01 has written a number of atmospheric exposure standards, which are listed in table 14. ASTM G50, *Standard Practice for Conducting Atmospheric Corrosion Tests on Metals*, provides a recommended practice for atmospheric corrosion test programs. ASTM G33 covers visual examination of panels with metallic coatings. such as galvanized or aluminized panels.

TABLE 14 ASTM Committee G01 Atmospheric Exposure Standards

Designation	Title
G30	*Standard Practice for Making and Using U-Bend Stress—Corrosion Test Specimens*
G33	*Standard Practice for Recording Data from Atmospheric Corrosion Tests of Metallic-Coated Steel Specimens*
G38	*Standard Practice for Making and Using C-Ring Stress—Corrosion Test Specimens*
G39	*Standard Practice for Preparation and Use of Bent-Beam Stress—Corrosion Test Specimens*
G49	*Standard Practice for Preparation and Use of Direct Tension Stress—Corrosion Test Specimens*
G50	*Standard Practice for Conducting Atmospheric Corrosion Tests on Metals*
G58	*Standard Practice for Preparation of Stress-Corrosion Specimens for Weldments*
G84	*Standard Practice for Measurement of Time-of-Wetness on Surfaces Exposed to Wetting Conditions as in Atmospheric Corrosion Testing*
G91	*Standard Practice for Monitoring Atmospheric SO_2 Deposition Rate for Atmospheric Corrosivity Evaluation Using the Sulfation Plate Technique*
G92	*Standard Practice for Characterization of Atmospheric Test Sites*
G101	*Standard Guide for Estimating the Atmospheric Corrosion Resistance of Low-Alloy Steels*
G116	*Standard Practice for Conducting Wire-on-Bolt Test for Atmospheric Galvanic Corrosion*
G149	*Standard Practice for Conducting the Washer Test for Atmospheric Galvanic Corrosion (Withdrawn 2004)*

ASTM Committee G01 has written several standards on stress corrosion specimens shown in table 14. In addition, several standards describe galvanic specimen design, sulfation plate, time of wetness, and characterization of atmospheric test sites. ASTM Committee B08 has published a standard on evaluating electroplated samples and atmospheric exposures. This standard, ASTM B537, *Standard Practice for Rating of Electroplated Panels Subjected to Atmospheric Pressure*, includes charts showing pit densities.

ISO Technical Committee 156 has written six standards that apply to atmospheric exposures, which are shown in table 15. One standard covers galvanic corrosion specimens, one is a general procedure for atmospheric exposures, and four cover the subject of classification of atmospheres for corrosivity. ISO/TCI56 is now considering the question of indoor atmospheric corrosivity classification and will be preparing standards in this area.

NACE International has written several standards related to atmospheric corrosion, which are shown in table 16. These standards apply mainly to coating systems to protect from corrosion. The Instrument Society of America (ISA) has established a classification system for indoor corrosivity[39] that applies mainly to electronic devices.

TABLE 15 ISO Standards Relating to Atmospheric Corrosion.

Designation	Title
ISO 4540	*Metallic Coating—Coatings Cathodic to the Substrate—Rating of Electroplated Test Specimen Subjected to Corrosion Tests*
ISO 4542	*Metallic and Other Non-organic Coatings—General Rules for Stationary Outdoor Exposure Corrosion Tests*
*ISO 7441	*Corrosion of Metals and Alloys—Determination of Bimetallic Corrosion in Outdoor Exposure Corrosion Tests*
*ISO 8565	*Corrosion of Metals and Alloys—Atmospheric Corrosion Testing—General Requirements*
ISO 8994	*Anodized Aluminum and Aluminum Alloys—Rating System for Evaluation of Pitting Corrosion Grid Method*
*ISO 9223	*Corrosion of Metals and Alloys Classification of the Corrosivity of Atmospheres*
*ISO 9224	*Corrosion of Metals and Alloys Guiding Values for the Corrosivity Categories of Atmospheres*
*ISO 9225	*Corrosion of Metals and Alloys—Aggressivity of Atmosphere-Methods of Measurement of Pollution Data*
*ISO 9226	*Corrosion of Metals and Alloys—Corrosivity of Atmospheres—Methods of Determination of Corrosion Rate of Standard Specimens for the Evaluation of Corrosivity*
ISO 11303	*Specification of Protection Methods on the Basis of Atmospheric Corrosivity Classification*

*Standards developed by ISO Technical Committee TCI56 on corrosion of metals and alloys.

TABLE 16 NACE International Standards Relating to Atmospheric Exposure Tests

Designation	Title
RPO172-72	*Surface Preparation of Steel and Other Hard Materials by Water Blasting Prior to Coating or Recoating—Item #53008-P*
RP0176-83	*Corrosion Control of Steel, Fixed Offshore Platforms Associated with Petroleum Production—Item #53031-P*
RP0281-86	*Method for Conducting Coating (Paint) Panel Evaluation Testing in Atmospheric Exposure—Item #21026-P*
RP0591-91	*Coating for Concrete Surfaces in Non-immersion and Atmospheric Service—Item #21052-P*
RP0692-92	*Application of a Coating System to Exterior Surfaces of Steel Rail Cars—Item #21058-P*
TM0170-70	*Visual Standard for Surfaces of New Steel Air-blast Cleaned with Sand—Item #21201-P*
TM0175-75	*Visual Standard for Surfaces of New Steel Centrifugally Blast Cleaned with Steel Grit and Shot—Item #21209-P*

ACKNOWLEDGMENT

The author is grateful to Air Products and Chemicals, Inc. for permission to publish this paper.

References

1. H. Guttman and P. J. Sereda, "Measurement of Atmospheric Factors Affecting the Corrosion of Metals," in *Metal Corrosion in the Atmosphere,* ed. W. Ailor and S. Coburn (West Conshohocken, PA: ASTM International, 1968), 326–359, https://doi.org/10.1520/STP34097S

2. D. Knotkova-Cermakova and K. Barton, "Corrosion Aggressivity of Atmospheres (Derivation and Classification)," in *Atmospheric Corrosion of Metals,* ed. S. W. Dean, Jr. and E. C. Rhea (West Conshohocken, PA: ASTM International, 1982), 225–249.

3. S. W. Dean, Jr., "Planning Instrumentation and Evaluation of Atmospheric Corrosion Tests and a Review of ASTM Testing," in *Atmospheric Corrosion,* ed. W. H. Ailor (New York: Wiley, 1982), 195–216.

4. S. W. Dean, "Corrosion Testing of Materials with Metallic and Inorganic Coatings," in *Testing of Metallic and Inorganic Coatings,* ed. W. B. Harding and G. A. DiBari (West Conshohocken, PA: ASTM International, 1987), 177–192.

5. D. Knotkova, K. Kreislova, and S. W. Dean, Jr., *ISO CORRAG, International Atmospheric Exposure Program: Summary of Results* (West Conshohocken, PA: ASTM International, 2010).

6. H. E. Townsend, "Atmospheric Corrosion Performance of Quench- and Tempered-, High-Strength Weathering Steel," *Corrosion* 56, no. 9 (2000): 883–886.

7. H. E. Townsend, "Effects of Silicon and Nickel Contents on the Atmospheric Corrosion Resistance of ASTM A588 Weathering Steel," in *Atmospheric Corrosion,* ed. W. W. Kirk and H. H. Lawson (West Conshohocken, PA: ASTM International, 1995), 85–100, https://doi.org/10.1520/STP14914S

8. S. K. Coburn, M. E. Komp, and S. G. Lore, "Atmospheric Corrosion Rate of Weathering Steels at Test Sites in the Eastern United States—Effect of Environments and Test Panel Orientation," in *Atmospheric Corrosion,* ed. W. W. Kirk and H. H. Lawson (West Conshohocken, PA: ASTM International, 1995), 101–113.

9. D. Knotkova and J. Vlckova, "Atmospheric Corrosion of Bolted Lap Joints Made of Weathering Steels," in *Atmospheric Corrosion,* ed. W. W. Kirk and H. H. Lawson (West Conshohocken, PA: ASTM International, 1995), 114–136.

10. M. Morcillo, J. Simaneas, and S. Feliu, "Long Term Atmospheric Corrosion in Spain: Results after 13-16 Years of Exposure and Comparison with World Wide Data," in *Atmospheric Corrosion,* ed. W. W. Kirk and H. H. Lawson (West Conshohocken, PA: ASTM International, 1995), 195–214.

11. R. A. Legault and H. P. Leckie, "Effect of Alloy Composition on the Atmospheric Corrosion Behavior of Steels Based on a Statistical Analysis of the Larrabee-Coburn Data Set," in *Corrosion in Natural Environments,* ed. W. Ailor, S. Dean, and F. Haynie (West Conshohocken, PA: ASTM International, 1974), 334–347, https://doi.org/10.1520/STP32171S

12. H. E. Townsend, "Estimating the Atmospheric Corrosion Resistance of Weathering Steels," in *Outdoor Atmospheric Corrosion,* ed. H. E. Townsend (West Conshohocken, PA: ASTM International, 2002), 292–300.

13. H. E. Townsend, "Atmospheric Corrosion Resistance of Skyward and Groundward Exposure of Exposed Surfaces of Zinc and 55% Al-Zn Alloy Coated Steel Sheets," *Corrosion* 54, no. 7 (1998): 561–565.

14. H. E. Townsend, M. W. Simpson, W. B. van der Linde, and D. C. McCune, "License Plate Corrosion Test of Automotive Coated Steel Sheet Steel," *Corrosion* 55, no. 4 (1999): 406–411.

15. H. Black and L. Lherbier, "A Statistical Evaluation of Atmospheric, In-Service, and Accelerated Corrosion of Stainless Steel Automotive Trim Material," in *Metal Corrosion in the Atmosphere,* ed. W. Ailor and S. Coburn (West Conshohocken, PA: ASTM International, 1968): 3–32, https://doi.org/10.1520/STP34077S

16. J. D. Palmer, "Atmospheric Corrosion and the Automobile," in *Atmospheric Corrosion,* ed. W. H. Ailor (New York: Wiley, 1982): 705–710.

17. S. W. Dean, Jr., "Planning Instrumentation and Evaluation of Atmospheric Corrosion Tests (Part 3)," *Materials Performance* 27, no. 12 (December 1988): 35–37.

18. P. J. Sereda, "Weather Factors Affecting Corrosion of Metals," in *Corrosion in Natural Environments,* ed. W. Ailor, S. Dean, and F. Haynie (West Conshohocken, PA: ASTM International, 1974), 7–22, https://doi.org/10.1520/STP32153S

19. B. Levadie, "Sampling and Analysis of Sulfur Dioxide with the Lead Dioxide Plate (Huey Plate)," *Journal of Testing and Evaluation* 7, no. 2 (March 1979): 61–67.

20. J. W. Spence and F. H. Haynie "Derivation of a Damage Function for Galvanized Steel Structures: Corrosion Kinetics and Thermodynamic Considerations," in *Corrosion Testing and Evaluation: Silver Anniversary Volume,* ed. R. Baboian and S. W. Dean (West Conshohocken, PA: ASTM International, 1990), 208–224.

21. F. H. Haynie, "Environmental Factors Affecting the Corrosion of Galvanized Steel," in *The Degradation of Metals in the Atmosphere,* ed. S. W. Dean and T. S. Lee (West Conshohocken, PA: ASTM International, 1988), 282–289.

22. M. R. Foran, E. V. Gibbons, and J. R. Wellington, "The Measurement of Atmospheric Sulfur Dioxide and Chlorides," *Chemistry in Canada* 10, no. 5 (May 1958): 33–41.

23. S. W. Dean, "Corrosion Testing of Metals under Natural Atmospheric Conditions," in *Corrosion Testing and Evaluation: Silver Anniversary Volume,* ed. R. Baboian and S. W. Dean (West Conshohocken, PA: ASTM International, 1990): 163–176.

24. *Standard Practice for the Preparation of Substitute Ocean Water,* ASTM D1141-98(2013) (West Conshohocken, PA: ASTM International, approved January 1, 2013), http://doi.org/10.1520/D1141-98R13

25. W. H. Abbott, "Field vs. Laboratory Experience in the Evaluation of Electronic Components and Materials," *Materials Performance* 24, no. 8 (August 1985): 46–50.

26. S. W. Dean, Jr., "Planning Instrumentation and Evaluation of Atmospheric Corrosion Tests (Part 1)," *Materials Performance* 27, no. 10 (October 1988): 56–59.

27. K. L. Money, "Corrosion Testing in the Atmosphere," *Metals Handbook Ninth Edition,* Vol. 13, *Corrosion* (Materials Park, OH: ASM International, 1987), 204–206.

28. S. W. Dean, "ISO CORRAG Collaborative Atmospheric Exposure Program: A Preliminary Report," in *Degradation of Metals in the Atmosphere,* ed. S. W. Dean and T. S. Lee (West Conshohocken, PA: ASTM International, 1988), 385–431.

29. S. W. Dean and D. B. Reiser, "Comparison of the Atmospheric Corrosion Rates of Wires and Flat Panels," *Corrosion 2000,* Paper 00455 (Houston, TX: NACE International, March 2000).

30. S. W. Dean and H. R. Copson, "Stress Corrosion Behavior of Maraging Nickel Steels in Natural Environments," *Corrosion* 21, no. 3 (March 1965): 95–103.

31. R. Baboian, "Final Report on the ASTM Study: Atmospheric Galvanic Corrosion of Magnesium Coupled to Other Metals," in *Atmospheric Factors Affecting the Corrosion of Engineering Metals,* ed. S. K. Coburn (West Conshohocken, PA: ASTM International, 1978), 17–29.

32. D. P. Doyle and H. P. Godard, "Rapid Determination of Corrosivity of an Atmosphere to Aluminum" *Proceedings of the Third International Congress on Metallic Corrosion,* vol. 4 (Moscow, Russia: MIR Publishers, 1969), 429–437.

33. G. A. DiBari, G. Hawk, and E. A. Baker, "Corrosion Performance of Decorative Electrodeposited Nickel and Nickel Iron Alloy Coating," in *Atmospheric Corrosion of Metals,* ed. S. W. Dean, Jr. and E. C. Rhea (West Conshohocken, PA: ASTM International, 1982), 186–213.

34. K. J. Altorfer, "Service Evaluation of Zinc Thermal Spraying Systems," in *Atmospheric Corrosion,* ed. W. H. Ailor (New York: Wiley, 1982), 645–650.

35. G. German, "Behavior of Zinc-Coated Steel in Highway Environments," in *Atmospheric Factors Affecting the Corrosion of Engineering Metals,* ed. S. K. Coburn (West Conshohocken, PA: ASTM International, 1978), 74–82.

36. V. H. Kucera, S. Haagenrud, L. Atteraas, and J. Gullman, "Corrosion of Steel and Zinc in Scandinavia with Respect to Classification of the Corrosivity of Atmospheres," in *Degradation of Metals in the Atmosphere,* ed. S. W. Dean and T. S. Lee (West Conshohocken, PA: ASTM International, 1988), 264–281.

37. M. Seo, "Application of Quartz Crystal Microbalance to Corrosion Research," *Corrosion Engineering* 48 (1999): 809–828.

38. B. S. Phul and W. W. Kirk, "Monitoring the Corrosivities of Atmospheric Exposure Sites," *Journal of Protective Coatings and Linings* 8, no. 10 (October 1991): 152–162.

39. *Environmental Conditions for Process Measurement and Control Systems: Airborne Contaminants*, ISA-S 71-04-1985 (Durham, NC: Instrument Society of America, 1985).

Chapter 11 | Standards and Practices on Corrosion under Insulation

John P. Ludman[1] and Bert J. Moniz[2]

Introduction

Corrosion under insulation (CUI) occurs on the external surfaces of hot, thermally insulated carbon steel or austenitic stainless steel process equipment and piping systems within appropriate temperature ranges when moisture penetrates the insulation. Cold thermally insulated carbon steel surfaces may become wet and corrode when water condenses from ambient air as the temperature falls below the dew point, as with piping that carries cold liquids or gases.[1]

CUI is a serious problem because it usually is unnoticed and, by the time it is noticed, the consequences are potentially harmful. Because carbon steel and stainless steel are the most common construction materials used on chemical process plants, refineries, offshore structures, and power plants, CUI has far-reaching implications.[2]

CUI mechanisms (damage mechanisms) are not unique. They consist of pitting and general corrosion of carbon and alloy steels, and external chloride stress corrosion cracking (ECSCC) of austenitic stainless steels. Lately, pitting of aluminum and ECSCC of duplex stainless steels have been included as CUI damage mechanisms, but these problems are less common.

Insulation systems simply do not remain dry in the long run. Water enters because the systems are relatively fragile and vulnerable to mechanical damage and deterioration. Insulation provides an annular space where moisture can be retained on the metal surface. Depending on the source of moisture, contaminants may be present and concentrate, but the principal harmful species is the chloride ion.

It may take several years for CUI to develop and cause equipment or piping rupture or leakage. To combat the problem, a great deal of effort has gone into the development of managing systems for CUI to prevent it from becoming a maintenance headache or the cause of an incident.

An important rule to embrace is, "Don't insulate if it's not needed for thermal conservation." For example, protective cages made of steel mesh with standoffs around equipment and piping may be used when insulation is needed only for personnel protection.[3]

A wealth of industry standards, guidelines, and literature has been developed relating to CUI. The purpose of this chapter is to compile them and show how they complement each other. Three broad guidelines have been assembled on CUI, representing the work of specialists in thermal insulation, risk-based inspection, nondestructive testing (NDT), process engineering, maintenance engineering, protective coatings, and materials engineering. The guidelines are American Petroleum Institute Recommended Practice (API RP) 583, *Corrosion under Insulation and Fireproofing*; National Association of Corrosion Engineers Standard Practice (NACE) SP0198-2016, *Standard Practice Control of Corrosion under Thermal Insulation and Fireproofing Materials*; and European Federation for Corrosion (EFC) 55, *Corrosion-under-Insulation (CUI) Guidelines*. The first two standard practices are extensively cited in this chapter. Note that NACE International and SSPC, the Society for Protective Coatings have merged to form AMPP, The Association for Materials Protection and Performance.

API RP583, *Corrosion under Insulation and Fireproofing.*[4]

API RP583 covers design, maintenance, inspection, and mitigation practices for CUI of pressure vessels, piping, storage tanks, and spheres. The standard examines factors that affect damage mechanisms and provides guidelines for prevention, maintenance practices, and inspection practices to detect and assess damage. It also provides guidelines for conducting risk assessments on equipment or structural steel subject to CUI.

AMPP SP0198-2016, *Standard Practice Control of Corrosion under Thermal Insulation and Fireproofing Materials.*[5]

SP0198-2016 provides current technology and industry practices for CUI and fireproofing materials. The standard contains sections organized by function on corrosion mechanisms, mechanical design, protective coatings, insulation materials, and inspection and maintenance.

[1]DuPont Company, Dupont Chestnut Run Plaza, 974 Centre Rd., Wilmington, DE 19805, USA
[2]Retired, 2201 W 16th St., Wilmington, DE 19806, USA

DOI: 10.1520/MNL202NDSUP20190026

Copyright © 2022 by ASTM International, 100 Barr Harbor Dr., PO Box C700, West Conshohocken, PA 19428-2959
ASTM International is not responsible, as a body, for the statements and opinions expressed in this chapter. ASTM International does not endorse any products represented in this chapter.

EFC-55, *Corrosion-under-Insulation (CUI) Guidelines.*[6]

These guidelines represent the output of working parties in major European oil refining, petrochemical, and offshore companies. Appendices amplify topics such as cost analysis, quality assurance, insulation techniques, coatings and application methods, cladding, and inspection techniques. The guidelines include a risk-based inspection methodology for CUI and recommended best practices for various topics.

Corrosion under fireproofing is a related problem. It is not covered in this chapter.[7]

INCIDENTS

A symposium was held in 1983 to discuss experience with CUI. It was sponsored by the American Society for Testing and Materials (ASTM), NACE (now AMPP), and the Materials Technology Institute of the Chemical Process Industries (MTI). The proceedings were published as an ASTM Special Technical Publication, *Corrosion of Metals under Insulation*, in 1985 and contain a number of case histories.[8]

Since that symposium, numerous presentations have been made and several articles has been published describing failures that highlight the significance of CUI.[9–12]

MECHANISM

Insulation systems have the potential to collect and transmit moisture-containing corrosive ions to the metal substrate and concentrate them as the water evaporates with temperature. The chloride ion present in moisture and some insulation is the principal corrosive ion responsible for CUI, although other halides also may assist.

Carbon steels.

Carbon steels suffer general corrosion and pitting under wet insulation. The corrosion rate increases at elevated temperature.[13]

CUI continues when insulated carbon steel plant equipment and piping is idled (mothballed) for an extended time. The insulation should be stripped and the equipment and piping painted if required to prevent atmospheric rusting.[14]

Austenitic stainless steels.

Austenitic stainless steels suffer ECSCC under wet insulation, especially in the presence of oxygen.[15] Specially formulated insulation materials, however, can inhibit ECSCC in the short term.

Although less commonly used, aluminum alloys may suffer chloride pitting,[16] and duplex stainless steels may suffer ECSCC under wet insulation under applicable conditions.[16] Caustic attack also has been reported on aluminum components in cold boxes filled with perlite during warm-up periods when moisture has entered the cold box during operation, has frozen into ice balls, and then melted (Sheldon Dean, pers. comm.).

SUSCEPTIBLE TEMPERATURE RANGES FOR CUI

The optimum temperature range for CUI depends on the alloy and the corrosion mechanism. For example, for ECSCC of austenitic stainless steels to occur, the temperature must be high enough to concentrate chloride ions on the surface, but not so high that the system is essentially dry. Cycling through the susceptible temperature range reduces crack incubation time.

Surface versus operating temperature.

It is necessary to consider whether the operating temperature is within the boundaries for CUI, but it is the actual surface temperature of the piece of equipment or piping that is relevant. Many factors can influence how closely the exposed metal surface temperature approaches the service temperature, including the type, condition, and thickness of the insulation. Although the range of susceptibility is relatively wide, there is an optimum temperature range for each type of metal affected.

NACE SP0198-2016 and EFC-55 suggest the following temperature ranges of susceptibility for CUI:

- Carbon steel operating continuously between -4°C and 175°C
- Austenitic stainless steel operating continuously between 50°C and 175°C
- For both types of alloy, intermittent operation within the temperature range

API RP583 encourages consideration of a wider temperature ranges to account for variability in insulation and operating conditions. For example the recommended carbon steel temperature range for CUI susceptibility is extended to from -12°C to 175°C.[17,18]

MOISTURE ENTRY SOURCES

It is important to identify the most vulnerable areas in a plant as well as the most vulnerable locations on process equipment and piping systems. For example, areas adjacent to a chlorine-producing facility or downwind of a cooling tower mist are likely to accelerate CUI. A protected area inside a building is likely to have no problem. In vulnerable areas, features that exhibit warning signs of CUI must be dealt with promptly, such as open insulation terminations or mechanically abused insulation jacketing.[19]

Susceptible locations on process equipment.

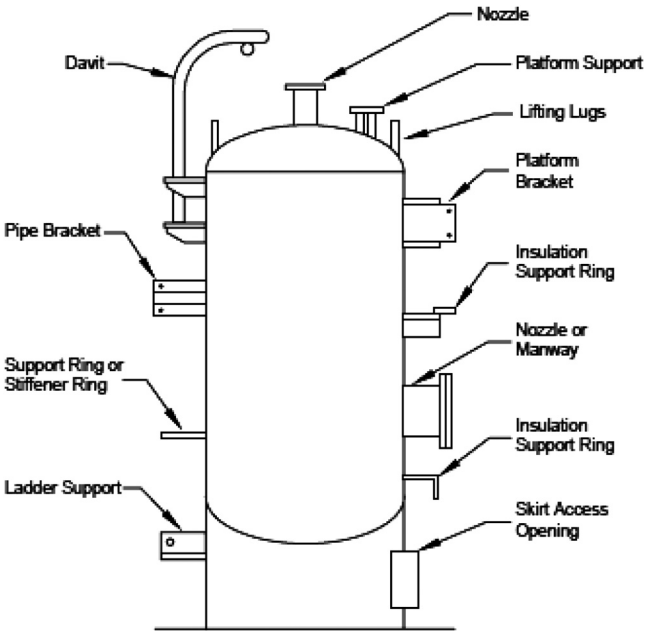
The design of vessel attachments can significantly affect CUI susceptibility. Improved designs can help prevent moisture penetrating the insulation boundary. Some methods include providing sealing discs on nozzles and other attachments, ensuring that nozzle length is adequate to permit effective sealing, and designing insulation rings that can either shed water or drain any water that enters.[20,21]

Susceptible locations on equipment are shown in figure 1.

Susceptible locations on piping systems.

Piping systems are the items that usually are most susceptible to CUI.[24] Locations include pipe hangers and other supports, dead legs, valves and fittings, bolt-on pipe shoes, steam and electric tracer tubing penetrations, termination of insulation at flanges and other piping components, damaged or missing insulation jacketing, insulation jacketing seams located on the top of horizontal piping or improperly lapped or sealed insulation jacketing,

FIG. 1 Vulnerable locations on a vessel.[22,23]



termination of insulation in a vertical pipe, and locations where caulking has deteriorated or is missing.

CUI damage on flanged assemblies can be accelerated in services such as chlorine, anhydrous hydrochloric acid, and sulfuric acid, as well as areas where fugitive emission from bolted assemblies combine with atmospheric moisture or wet insulation to accelerate corrosion. The insulation can "trap" the fugitive emission at these locations. It is usually advisable to inspect these locations.

The design, installation, and location of piping systems have a big impact on susceptibility to CUI. Design details such as the piping material, presence of tracing, and type of protective coating influence CUI. The quality of the installation, including the integrity of seals and caulking at penetrations, also will have a significant impact on the level of moisture intrusion and subsequent CUI. The location of piping relative to moisture sources (e.g., deluge systems, cooling towers) also can affect the susceptibility to CUI.[25]

LABORATORY TESTS THAT SIMULATE CUI

All insulation materials support corrosion, although the type of material affects the extent of corrosion. Accelerating factors include the following:

- Content of damaging water-soluble salts (especially chloride)
- Presence of inhibiting salts that can delay attack
- Capacity to absorb or retain water and dry again
- Tendency of some organic insulations to produce acid during aging.

Several ASTM standards have been developed to detect and measure the extent of corrosion produced by insulation materials or the tendency to produce harmful by-products when wet.

Standards relating to ECSCC of austenitic stainless steels. ASTM standards focused on simulating ESCC of austenitic stainless steel and the potential of insulation materials to cause corrosion include ASTM C692, *Standard Test Method for Evaluating the Influence of Thermal Insulations on External Stress Corrosion Cracking Tendency of Austenitic Stainless Steel*; ASTM C871, *Standard Test Methods for Chemical Analysis of Thermal Insulation Materials for Leachable Chloride, Fluoride, Silicate, and Sodium Ions*; ASTM C795, *Standard Specification for Thermal Insulation for Use in Contact with Austenitic Stainless Steel*; and ASTM C929, *Standard Practice for Handling, Transporting, Shipping, Storage, Receiving, and Application of Thermal Insulation Materials for Use in Contact with Austenitic Stainless Steel.*

> ASTM C692, *Standard Test Method for Evaluating the Influence of Thermal Insulations on External Stress Corrosion Cracking Tendency of Austenitic Stainless Steel.*[26]

Adopted in 1971, ASTM C692 was originally entitled *Evaluating the Influence of Wicking Type Thermal Insulations on the Stress Cracking Tendency of Austenitic Stainless Steels*,[26] and was based on a test method developed by Dana and DeLong. Wicking of leachable chlorides to the surface was then considered the primary concentration mechanism.[27]

The standard currently covers two types of 28-day laboratory test procedures to determine which thermal insulations contribute to stress corrosion cracking of sensitized austenitic stainless steel caused by soluble chlorides in the insulation.

The procedures are intended primarily as a preproduction test for qualification of the basic chemical composition of a particular manufacturer's lot. They are not intended as routine tests for quality assurance or production lot compliance. ASTM C871, however, is used to confirm acceptable chemical properties of subsequent lots of insulation previously found acceptable by ASTM C692.

> ASTM C871, *Standard Test Methods for Chemical Analysis of Thermal Insulation Materials for Leachable Chloride, Fluoride, Silicate, and Sodium Ions.*[28]

This is the second of a series of standards, first issued in 1977. It covers procedures for determining water-leachable chloride, fluoride, silicate, and sodium ions in thermal insulation materials in the parts per million range. Fluoride ions can contribute to the chloride stress corrosion cracking of austenitic stainless steels. Sodium and silicate ions in insulation have been found to inhibit ECSCC.[29]

> ASTM C795, *Standard Specification for Thermal Insulation for Use in Contact with Austenitic Stainless Steel.*[30]

This is the third of a series of standards, first issued in 1992. It covers basic material requirements for thermal insulation for use in contact with austenitic stainless steel piping and equipment. It includes physical and chemical requirements and preproduction corrosion test and chemical analysis, which shall be performed to conform to the requirements.

The insulation materials also must pass the preproduction test requirements of ASTM C692 for stress corrosion effects on austenitic stainless steel and the confirming quality control chemical requirements of ASTM C871.

> ASTM C929, *Standard Practice for Handling, Transporting, Shipping, Storage, Receiving, and Application of Thermal Insulation Materials for Use in Contact with Austenitic Stainless Steel.*[31]

Insulating materials must be protected from exposure to water-soluble, corrosive ion-containing compounds at all stages of manufacture, handling, shipping, storage, and application.

The standard provides guidance and direction on the handling, transporting, shipping, storage, receiving, and application of thermal insulating materials to be used as a surface treatment or as part of the thermal insulation system in contact with austenitic stainless steel.

Standards relating to general and localized corrosion of carbon steel.

Relevant standards are ASTM G189, *Standard Guide for Laboratory Simulation of Corrosion under Insulation*; and ASTM C1617, *Standard Practice for Quantitative Accelerated Laboratory Evaluation of Extraction Solutions Containing Ions Leached from Thermal Insulation on Aqueous Corrosion of Metals.*

> ASTM G189, *Standard Guide for Laboratory Simulation of Corrosion under Insulation.*[32]

Describes a method of simulating CUI on insulated specimens cut from carbon or low-alloy steel pipe sections exposed to a corrosive environment, usually at elevated temperature under wet-dry conditions. Temperature simulation may be isothermal or cyclic. It is based on a method developed by W. G. Ashbaugh.[33]

The test apparatus includes (1) an idealized annular geometry between piping and surrounding thermal insulation, (2) internal heating to produce a hot-wall surface on which CUI can be quantified, (3) introduction of ionic solutions into the annular cavity between the piping and thermal insulation, (4) control of the temperature to produce either isothermal or cyclic temperature conditions, and (5) control of the delivery of the control or solution to produce wet or wet-dry conditions.

> ASTM C1617, *Standard Practice for Quantitative Accelerated Laboratory Evaluation of Extraction Solutions Containing Ions Leached from Thermal Insulation on Aqueous Corrosion of Metals.*[34]

Covers procedures for determining the corrosive or inhibiting effect of ions extracted from thermal insulation materials. Corrosion rates are calculated for metals exposed on a hot plate for four days to the leached solutions and the type and depth of localized corrosion recorded.

Ions may be added to the extracted solutions to simulate contamination from an external source. Expected corrosion-inhibiting ions also can be added to investigate their effect. Other liquids can be tested for their potential corrosiveness, such as cooling tower water, boiler feed, and chemical feed stocks. Chemical inhibitors also can be evaluated.

INSULATION MATERIALS

The selected type of insulation affects CUI. For example, some types are more prone to mechanical damage; some are more likely to leach chlorides and other salts; and some contain potential inhibitors.

Insulation materials are covered by ASTM standards, as given in table 1.

PROTECTIVE COATINGS

The first line of defense for the metal surface is a protective coating. Various factors influence coating selection, such as maximum and minimum surface temperature and single coat dry film thickness. For example, indoor equipment that is not exposed to external moisture sources may require something less conservative than an immersion grade coating. The substrate must be prepared according to the manufacturer's guidelines for any type of coating. Inadequate surface preparation reduces anticipated coating life and increases the likelihood of coating failure.

Carbon steel.

Commonly used coatings on carbon steel are immersion-grade organic coatings, fusion bonded coatings, thermal spray aluminum (TSA),[36] and petrolatum wax tape (for dew point corrosion).[37]

Austenitic stainless steel.

Commonly used coatings on austenitic stainless steel are immersion-grade organic coatings, TSA,[38] and loose wrapped with aluminum foil[39] are used.

Austenitic stainless steel coating systems shall not contain free, soluble chlorides or other halides after curing to prevent ESCC. Similarly, the coating shall not contain zinc, lead, copper, or their compounds because of the risk of liquid metal cracking, for example, from the heat effect of a fire.

Inorganic coatings.

High-temperature inorganic coatings also are available (see fig. 2).

Standards for mastics and coatings and their properties.

Relevant standards include ASTM C461, *Standard Test Methods for Mastics and Coatings Used with Thermal Insulation*; and ASTM C647, *Standard Guide to Properties and Tests of Mastics and Coating Finishes for Thermal Insulation.*

> ASTM C461, *Standard Test Methods for Mastics and Coatings Used with Thermal Insulation.*[41]

This standard covers test methods and procedures for sampling and testing mastics and coatings for use as weather and vapor barrier finishes on thermal insulations and for other accessories. Properties include uniformity and storage, stability, stability under freezing, density and weight per gallon, consistency, solids content, coverage, sag resistance drying time, and flash point.

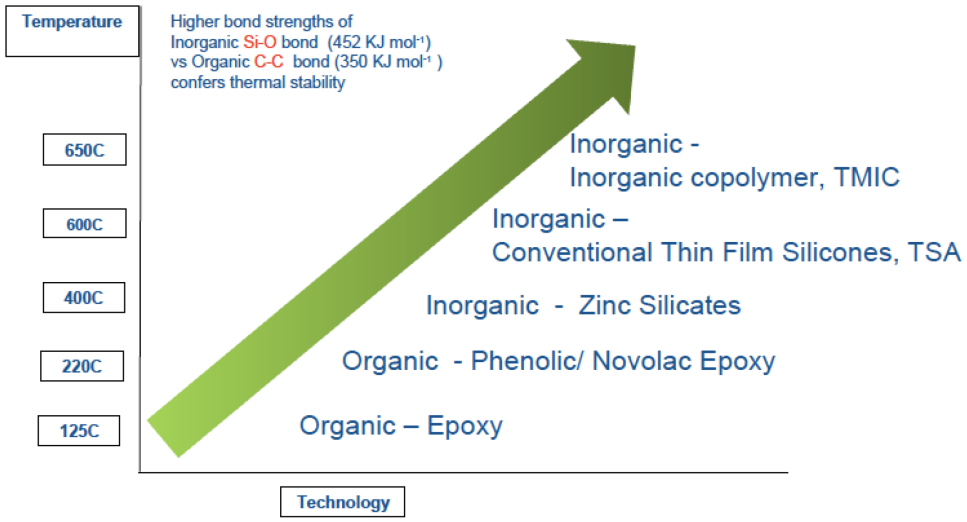
> ASTM C647, *Standard Guide to Properties and Tests of Mastics and Coating Finishes for Thermal Insulation.*[42]

This standard is a key to specific properties of mastics and coating finishes that characterize their performance in application or

TABLE 1 ASTM Insulation Standards[35]

ASTM	Type	Kind	Form	Components
C533, *Standard Specification for Calcium Silicate Block and Pipe Thermal Insulation*	Calcium silicate	Homogeneous inorganic	Block and pipe	Hydrous calcium silicate usually with fibrous reinforcement
C552, *Standard Specification for Cellular Glass Thermal Insulation*	Cellular glass	Homogeneous inorganic	Block and shapes	Foamed when molten to form a closed cell structure.
C610, *Standard Specification for Molded Expanded Perlite Block and Pipe Thermal Insulation*	Expanded perlite	Homogeneous inorganic	Block and pipe cover	Expanded perlite, inorganic silicate binders, fibrous reinforcement, and silicone water-resistant additions
C553, *Standard Specification for Calcium Silicate Block and Pipe Thermal Insulation*	Mineral fiber	Blanket	Fiber	Rocks, slag, or glass processed from a molten state into a fibrous form and including organic binders.
C892, *Standard Specification for High-Temperature Fiber Blanket Thermal Insulation*	Ceramic fiber	Blanket	Fiber	Man-made vitreous alumino-silicate fiber
C534, *Standard Specification for Preformed Flexible Elastomeric Cellular Thermal Insulation in Sheet and Tubular Form*	Elastomeric	Organic foam	Sheet and tube	Flexible, closed-cell foam formed by extrusion
C578, *Standard Specification for Rigid, Cellular Polystyrene Thermal Insulation*	Polystyrene	Organic foam	Rigid block and extruded	Closed-cell foam formed by either an extrusion or molding
C591, *Standard Specification for Unfaced Preformed Rigid Cellular Polyisocyanurate Thermal Insulation*	Polyisocyanurate	Organic foam	Rigid block and preform	Closed-cell foam formed by a controlled chemical reaction and may contain leachable chlorides, fluorides, silicate, and sodium ions
C1029, *Standard Specification for Spray-Applied Rigid Cellular Polyurethane Thermal Insulation*	Polyurethane	Organic foam	Rigid spray-applied	Closed-cell foam formed by a chemical reaction at the time of application
C1126, *Standard Specification for Faced or Unfaced Rigid Cellular Phenolic Thermal Insulation*	Phenolic	Organic foam	Rigid board or tubular	Closed-cell foam formed by a controlled chemical reaction
C1728, *Standard Specification for Flexible Aerogel Insulation*	Silica	Aerogel	Blanket	Air-filled foam

FIG. 2 Temperature limitations of protective coatings.[40]



service. Properties include consistency, coverage, build, wet flammability, toxicity, temperature and humidity range, surface wetting and adhesion, gap filling and bridging, sizing and sealing, drying time and curing time, shrinkage, storage stability, freeze-thaw stability, outdoor durability, temperature limits, chemicals and water resistance, mold and mildew resistance, surface flammability, water-vapor transmission rate, adhesion, impact resistance, abrasion resistance, flexure, elongation, color, and odor.

INSPECTION PLANNING

Developing an effective strategy for detecting CUI starts with planning. During the inspection planning process, essential considerations such as operating conditions (temperature, cycles), material systems (insulation, equipment), environmental conditions, risk tolerance, and operational requirements are brought together to establish the type, extent, and frequency of the inspections selected to achieve the appropriate level of confidence that CUI will not trigger a loss of containment.

The type of inspection technique used for monitoring CUI is driven primarily by operation and economic considerations, while the extent and frequency of CUI inspection will be driven by likelihood and consequence considerations. For example, techniques that do not require insulation removal (e.g., profile radiography, guided wave) may be considered in cases in which insulation removal creates operational issues or is expensive. Similarly, insulation systems located on equipment that is likely to have CUI and could result in significant consequences require more extensive and frequent inspection than systems not as likely to have CUI or that result in relatively lower consequences.

Inspection methods.

The methods of inspecting for CUI range from visual inspection following insulation removal to various remote examination techniques that do not need insulation removal. In general, inspection methods are complementary and more than one may be required to provide an accurate assessment of condition. See table 2 for a summary.

Inspection standards and codes.

API inspection codes and recommended practices provide requirements and guidance on important considerations when establishing an inspection plan for evaluating CUI. These codes and recommended practices are often referred to as Recognized and Generally Accepted Good Engineering Practices (RAGAGEPs).

In addition to providing susceptible temperature ranges for various material systems and defining susceptible locations, these documents detail the extent of examination needed and which nondestructive examination (NDE) methods should be considered. A description of each RAGAGEP is provided in the following paragraphs. Table 3 shows which RAGAGEP may be applicable to a given equipment type.

API 510, *Pressure Vessel Inspector Program.*[44]

This code covers the in-service inspection, repair, alteration, and rerating activities for pressure vessels and pressure relieving devices protecting them. API 510 provides guidance on important considerations when establishing an inspection plan for evaluating CUI. In addition to providing susceptible temperature ranges for various material systems and defining susceptible locations (described earlier), this API Code gives practical guidance on if and how much insulation to remove. Some of these considerations include insulation type, insulation condition, consequence of leakage, and age of the vessel.

API RP572, *Inspection of Pressure Vessels.*[45]

This recommended practice supplements API 510 with reasons for inspection, causes of deterioration, frequency and methods of inspection, methods of repair, and preparation of records and reports. CUI is discussed.

TABLE 3 Inspection RAGAGEPs Covering CUI Requirements/ Guidance

Equipment	Codes	Guidance Documents
Pressure Vessels	API 510, NB-23	API RP583, API RP572, API RP571, API RP580/API RP581
Piping	API 570	API RP583, API 574, API RP571, API RP580/API RP581
Storage Tanks	API 653	API RP583, API RP575, API RP571, API RP580/AP RP581

TABLE 2 Summary of CUI Inspection Methods[43]

Acronym	Name	Feature	Disadvantage
VT	Visual examination	Qualitative	Requires complete or partial insulation removal
PT	Penetrant testing	Detects ECSCC	Requires complete or partial insulation removal
GWT	Guided wave	For remote inspection of piping	Cannot detect pitting
RT	Profile radiography	For general corrosion	Radiation safety hazard
RT	Film density radiography	Can locate pitting	Radiation safety hazard
RT	Flash radiography	Can detect waterlogged insulation	Poorer image contrast and resolution
RT	Radiometric profiling	Very portable	Cannot differentiate between ID and OD corrosion
RTR	Real-time radiography	Easily viewed digital images	Wet insulation hampers testing
CR	Computed radiography	Image is digitized	Plates must be scanned
DR	Digital radiography	Image electronically stored for distribution	Panel detectors prone to damage
PEC	Pulsed eddy current	Averages corrosion over small areas	May not detect pitting
NBS	Neutron backscatter	Detects wet insulation	Does not detect corrosion
IR	Infrared thermography	Can be done remote from equipment	Can only detect wet or damaged insulation

API 570, Piping Inspection Code. Inspection, Repair, Alteration and Re-rating of In-Service Piping Systems.[46]

This code provides guidance on the frequency and extent of inspection based on several factors including the severity of the service (toxicity/flammability) and the likelihood of CUI. Some of the likelihood factors include the pipe material system, operating temperature, insulation type, external environment, and insulation condition.

API 570 also includes guidance on determining which piping systems are most susceptible to CUI, as well as some of the most common locations for CUI on those systems determined to be susceptible to it.

API 574, *Inspection Practices for Piping System Components.*[47]

This recommended practice supplements API 570 by providing piping inspectors with information to improve skill and increase basic knowledge of inspection practices. It covers piping, tubing, valves, and fittings used in petroleum refineries and chemical plants. It does not cover inspection of specialty items, including instrumentation, furnace tubulars, and control valves.

API 653, *Tank Inspection, Repair, Alteration, and Reconstruction (5th ed., addendum 1, April 2018).*[48]

This code covers external inspection requirements for storage tanks, including computation of frequency based on wall thickness measurements. CUI aspects are discussed.

API RP575, *Inspection Practices for Atmospheric and Low Pressure Storage Tanks.*[49]

This recommended practice supplements API 653 and covers the inspection of atmospheric and low-pressure storage tanks (fabricated to API RP620 or API RP650) that have been designed to operate at pressures from atmospheric to 15 psig. It includes reasons for inspection, frequency and methods of inspection, methods of repair, and preparation of records and reports. It also includes CUI guidance.

NB-23, National Board Inspection Code.[50]

This code provides limited guidance on inspection for CUI.

API RP571, *Damage Mechanisms Affecting Fixed Equipment in the Refining Industry.*[51]

This standard provides an in-depth description of more than 60 different damage mechanisms (a general term referring to any cause of problems or failures that can occur to process equipment in refineries).

The standardized format includes a general description of the damage mechanism, susceptible materials of construction, critical factors, inspection methods, selection guidelines, and control factors. This standard supplements API RP580, *Risk-Based Inspection*; and API RP581, *Risk-Based Inspection Technology*.

Risk-based inspection (RBI).

RBI is a complex program that requires support and cooperation of the entire organization, from senior management to field-unit operators. The initial setup of an RBI program requires extensive in-house work, a generous budget, and time to implement. Operation of a successful RBI program also requires a multiyear commitment, because scheduled major maintenance programs on insulated equipment and piping can be at 10- to 15-year intervals.

API RP580, *Risk-Based Inspection.*[52]

Outlines and explains the basic elements for developing, implementing, and maintaining a credible RBI program. It is a generic document on RBI that can be used as a measuring stick by which the quality of any and all RBI methods and work processes could be evaluated to determine if they meet the level of quality prescribed in the RP.

API RP581, *Risk-Based Inspection Technology.*[53]

Provides a methodology for establishing an inspection program for fixed equipment based on risk. The likelihood of various damage mechanism occurring is estimated through calculation of a "damage factor." The magnitude of these damage factors facilitates assignment of a relative likelihood (1–5) that a particular damage mechanism will occur.

Part 2 of API RP581 provides specific criteria for calculating damage factors for insulated carbon steel and stainless steel equipment. The assessment requires consideration of many factors, including complexity of the installation (number of penetrations or protrusions, condition, coating quality, inspection history, and system design (type of insulation, temperature).

Producing a risk assessment evaluation requires identification of potential events and their potential consequences, estimating their potential severity and likelihood, and then estimating the level of risk based on the combination of severity and likelihood of the event happening. A risk assessment evaluation is required for every location. See Annex A, API RP583 for Qualitative Likelihood Assessment, Tables A3 and A4.

References

1. *Corrosion under Insulation and Fireproofing*, API RP583, Section 5.4.2 (Washington, DC: American Petroleum Institute, 2014).
2. R. King, "Does Insulation Cause Corrosion," in *Insulation Outlook*, June 2009, updated May 2019, http://web.archive.org/web/20220720204408/https://insulation.org/io/articles/does-insulation-cause-corrosion/
3. *Corrosion under Insulation and Fireproofing*, API RP583, Section 11.5.6 (Washington, DC: American Petroleum Institute, 2014).
4. *Corrosion under Insulation and Fireproofing*, API RP583 (Washington, DC: American Petroleum Institute, 2014).
5. *Standard Practice Control of Corrosion under Thermal Insulation and Fireproofing Materials*, NACE SP0198-2016 (Houston, TX: AMPP, 2016).
6. *Corrosion-under-Insulation (CUI) Guidelines*, EFC-55, 2nd ed., ed. S. Winnik (Cambridge, UK: European Federation for Corrosion, 2015).
7. *Corrosion under Insulation and Fireproofing*, API RP583, Section 4.4 (Washington, DC: American Petroleum Institute, May 2014).

8. W. I. Pollock and J. M. Barnhart, eds., *Corrosion of Metals under Insulation*, (West Conshohocken, PA: ASTM International, 1985).

9. R. Sampaio and A.L. M. V. Leite, "More Lessons 'Re-Learned' from Corrosion under Insulation" (Dow Chemical Company, Midland, MI, 2009), http://www.penderlo.com/doc/Dow_CUI.pdf

10. H. Ahluwalia, "The Hidden Enemy: Corrosion under Insulation" (paper presentation, Georgia Tech Renewable Bioproducts Institute (RBI) 2014 Corrosion Symposium, 2014), https://rbi1.gatech.edu/sites/default/files/documents/Presentations/2014 Corrosion Symposium - Ahluwalia.pdf

11. A. A. Al-Beed, "Engineering Approach to Control Corrosion under Thermal Insulation (CUTI) in Petrochemical Industries" (paper presentation, Petrotech 2001, 12th Industrial Security Symposium, Saudi Petrochemical Company [SADAF], Jubail, KSA, 2001), http://www.ndt.net/article/mendt2009/papers/AlBeed-1.pdf

12. W. G. Ashbaugh, "Corrosion of Steel and Stainless Steel under Thermal Insulation," in *Process Industries Corrosion—The Theory and Practice*, ed. B. J. Moniz and W. I. Pollock (Houston, TX: AMPP, 1986), 768–795.

13. *Standard Practice Control of Corrosion under Thermal Insulation and Fireproofing Materials*, NACE SP0198-2016, Section 2.1 Corrosion Mechanisms, Carbon Steel (Houston, TX: AMPP, 2016).

14. R. J. Twigg, *Guidelines for Mothballing of Process Plants*, Publication 34 (St. Louis, MO: Materials Technology Institute, 2002).

15. *Standard Practice Control of Corrosion under Thermal Insulation and Fireproofing Materials,* NACE SP0198-2016, Section 2.2 Austenitic and Duplex Stainless Steel (Houston, TX: AMPP, 2016).

16. *Corrosion under Insulation and Fireproofing*, API RP583, Section 4.5 (Washington, DC: American Petroleum Institute, May 2014).

17. *Corrosion under Insulation and Fireproofing*, API RP583, Section 4.2.1 (Washington, DC: American Petroleum Institute, May 2014).

18. *Corrosion under Insulation and Fireproofing*, API RP583, Section 4.2.2 (Washington, DC: American Petroleum Institute, May 2014).

19. *Corrosion under Insulation and Fireproofing*, API RP583, Section 5.2 (Washington, DC: American Petroleum Institute, May 2014).

20. *Corrosion under Insulation and Fireproofing*, API RP583, Section 9.5.3 (Washington, DC: American Petroleum Institute, May 2014).

21. *Pressure Vessel Inspector Program*, API 510, 10th ed., (Washington, DC: American Petroleum Institute, March 2018).

22. Association for Materials Performance and Protection, "Figure 2. Typical Vessel Attachments Where Water May Bypass Insulation," in *Standard Practice Control of Corrosion under Thermal Insulation and Fireproofing Materials*, NACE SP0198-2016 (Houston, TX: AMPP, 2016).

23. American Petroleum Institute, "Figure 20" in *Corrosion under Insulation and Fireproofing*, API RP583, Section 9.4.2 (Washington, DC: American Petroleum Institute, May 2014).

24. B. J. Fitzgerald and S. Winnik, "A Strategy for Preventing Corrosion under Insulation on Pipeline in the Petrochemical Industry," Exxon Mobil Chemical Company, 2004, http://web.archive.org/web/20220720214326/https://cupdf.com/document/xom-strategy-for-preventing-cui.html?page=1

25. *Corrosion under Insulation and Fireproofing*, API RP583, Section 5.4 (Washington, DC: American Petroleum Institute, May 2014).

26. *Standard Test Method for Evaluating the Influence of Thermal Insulations on External Stress Corrosion Cracking Tendency of Austenitic Stainless Steel*, ASTM C692-13(2018) (West Conshohocken, PA: ASTM International, approved November 1, 2018), http://doi.org/10.1520/C0692-13R18

27. A. W. Dana and W. B. DeLong, "Stress Corrosion Cracking Test," in *Corrosion*, vol. 12 (Houston, TX: AMPP, 1956), 309t–310t.

28. *Standard Test Methods for Chemical Analysis of Thermal Insulation Materials for Leachable Chloride, Fluoride, Silicate, and Sodium Ions*, ASTM C871-95(2000) (West Conshohocken, PA: ASTM International, approved June 15, 1995), http://doi.org/10.1520/C0871-95R00

29. K. M. Whorlow, E. Woolridge, and F. Hutto, "Effect of Halogens and Inhibitors on the External Stress Cracking of Type 304 Austenitic Stainless Steel," in *Insulation Materials: Testing and Applications*, ed. R. S. Graves and R. R. Zarr (West Conshohocken, PA: ASTM International, 1997), 485–497.

30. *Standard Specification for Thermal Insulation for Use in Contact with Austenitic Stainless Steel*, ASTM C795-08(2018) (West Conshohocken, PA: ASTM International, approved November 1, 2018), http://doi.org/10.1520/C0795-08R18

31. *Standard Practice for Handling, Transporting, Shipping, Storage, Receiving, and Application of Thermal Insulation Materials for Use in Contact with Austenitic Stainless Steel*, ASTM C929-2014 (West Conshohocken, PA: ASTM International, approved March 15, 2014), http://doi.org/10.1520/C0929-14

32. *Standard Guide for Laboratory Simulation of Corrosion under Insulation*, ASTM G189-07(2013) (West Conshohocken, PA: ASTM International, approved August 1, 2013), http://doi.org/10.1520/G0189-07R13

33. D. Abayarathna, W. G. Ashbaugh, R. D. Kane, N. McGowan, and B. Heimann, "Measurement of Corrosion under Insulation and Effectiveness of Protective Coatings," in *Corrosion 97,* Paper No. 266 (Houston, TX: AMPP, 1997).

34. *Standard Practice for Quantitative Accelerated Laboratory Evaluation of Extraction Solutions Containing Ions Leached from Thermal Insulation on Aqueous Corrosion of Metals*, ASTM C1617-19 (West Conshohocken, PA: ASTM International, approved May 1, 2019), http://doi.org/10.1520/C1617-19

35. *Standard Practice Control of Corrosion under Thermal Insulation and Fireproofing Materials*, Section 5, *Insulation, Fireproofing and Accessory Materials*, NACE SP0198-2016 (Houston, TX: AMPP, 2016).

36. O. Doble and G. Pryd, "Use of Thermally Sprayed Aluminum in the Norwegian Offshore Industry," *Protective Coatings Europe* 2, no. 4 (April 1997), http://www.wermac.org/pdf/corrosion12.pdf

37. *Thermal Insulation of Pipework, Ductwork, Associated Equipment and Other Industrial Installations in the Temperature Range of*

−100°C to +870°C, BS 5970:2012, Code of Practice, British Standards Institution (New York: American National Standards Institute, 2012).

38. P. Bock, "Preventing CUI with Thermal-Spray Metal Coating: New Use for a Traditional Process," *JPCL* (February 2015), https://www.paintsquare.com/library/articles/(062-70)Bock.pdf

39. *Standard Practice Control of Corrosion under Thermal Insulation and Fireproofing Materials* NACE SP0198-2016, Section 4.2.3 Protective Coatings (Houston, TX: AMPP, 2016).

40. M. O'Donoghue and V. Datta, "From Trauma to Transcendence: CUI and Coatings of Choice," AkzoNobel, SSPC Webinar, 2016, http://web.archive.org/web/20220720212645/https://www.paintsquare.com/webinars/view/?272

41. *Standard Test Methods for Mastics and Coatings Used with Thermal Insulation*, ASTM C461-17 (West Conshohocken, PA: ASTM International, approved September 1, 2017), http://doi.org/10.1520/C0461-17

42. *Standard Guide to Properties and Tests of Mastics and Coating Finishes for Thermal Insulation*, ASTM C647-19 (West Conshohocken, PA: ASTM International, approved March 1, 2019), http://doi.org/10.1520/C0647-19

43. *Standard Practice Control of Corrosion under Thermal Insulation and Fireproofing Materials*, NACE SP0198-2016, Section 6. Nondestructive Moisture and Corrosion Detection Techniques (Houston, TX: AMPP, 2016).

44. *Pressure Vessel Inspector Program*, API 510, 10th ed., Addendum 2 (Washington, DC: American Petroleum Institute, March 2018).

45. *Inspection of Pressure Vessels*, API RP572, 4th ed. (Washington, DC: American Petroleum Institute, December 2016).

46. *Piping Inspection Code: In-Service Inspection, Rating, Repair and Alteration of Piping Systems,* 4th ed. (Washington, DC: American Petroleum Institute, February 2016).

47. *Inspection Practices for Piping System Components*, API 574, 4th ed. (Washington, DC: American Petroleum Institute, 2016).

48. *Tank Inspection, Repair, Alteration, and Reconstruction*, API 653, 5th ed., Addendum 1 (Washington, DC: American Petroleum Institute, 2018).

49. *Inspection Practices for Atmospheric and Low Pressure Storage Tanks*, API RP575, 3rd ed., Section 8.2.7 (Washington, DC: American Petroleum Institute, 2014).

50. *National Board Inspection Code*, NB-23 (Columbus, OH: National Board of Pressure Vessel Inspectors, 2019).

51. *Damage Mechanisms Affecting Fixed Equipment in the Refining Industry*, API RP571, 2nd ed. (Washington, DC: American Petroleum Institute, 2011).

52. *Risk-Based Inspection*, API RP580, 3rd ed. (Washington, DC: American Petroleum Institute, 2016).

53. *Risk-Based Inspection Technology*, API RP581, 3rd ed. (Washington, DC: American Petroleum Institute, 2019).

Chapter 12 | Freshwater

Walter T. Young[1]

Introduction

Corrosion testing in freshwater environments is performed to determine the corrosion characteristics of water, evaluate the behavior of various materials when exposed to water, and evaluate various corrosion mitigation methods. For example, waters in cooling systems often are analyzed to determine how much and what forms of corrosion might occur on a given metal. Screening tests are used to select the most appropriate metal for use as piping material. Various water treatment alternatives can be tested in the laboratory or in a pilot plant. Tests are used to monitor the selected treatment scheme. Laboratory screening tests, detailed simulations, pilot plant studies, and system monitoring are typical corrosion testing methods. In any event, the selection of the appropriate test method will depend on the objectives of the test, details of the system, and process parameters (e.g., flow, temperature, and chemistry). Test design and analysis are covered elsewhere in this book as well as in the referenced documents. This chapter discusses the causes and types of corrosion common in freshwater systems and the standardized tests used for evaluation. Freshwater can be defined as either water with a salinity between 0.5 and 17 parts per thousand or water having less salt than seawater but still undrinkable.[1,2] Then freshwater can be further defined as water with a salinity less than 0.5 parts per thousand. For the purposes of this chapter, freshwater systems include potable water, heating/cooling, condensate, rivers, streams, and lakes.

The Freshwater Environment

In designing an effective laboratory test program, it is important to consider factors that influence corrosion in a freshwater environment. The following discussion summarizes these factors, but the complexity of the topic does not permit a detailed discussion in this chapter. Details on corrosion processes affecting metals in freshwaters are found in the references provided at the end of this chapter.[1–6]

WATER CHEMISTRY

Although water has a definite molecular structure, freshwater is not a pure substance and may contain numerous ions, dissolved minerals, and gasses. Examples of dissolved solids include combinations of calcium, magnesium, manganese, nitrates, iron, copper, lead, chlorides, sulfates, carbonates, and bicarbonates. Water chemistry is one of the most important factors affecting the corrosion of metals in water. Dissolved salts, such as chlorides and sulfates, not only can increase the aggressiveness of the water but also can affect the ability of the water to form protective deposits. Generally, waters with higher dissolved salt contents are more corrosive. Dissolved gases also affect the corrosivity of water. Oxygen and carbon dioxide concentrations can increase corrosivity, as does hydrogen sulfide. Not all metals are affected the same in a given water composition.

Acidity and alkalinity affect the corrosion rate. Generally, alkaline conditions favor lower corrosion rates; however, some metals, such as aluminum and zinc show increased corrosion rate at pH above 9 because of the adhered aluminum oxide and zinc oxide. For iron alloys, the corrosion rate is relatively steady between a pH of 4 and 10 at ambient temperature and where oxygen reduction is the primary cathodic corrosion reaction; however, the corrosion rate increases rapidly below pH 4.[5] Iron passivates and the corrosion rate decreases rapidly above a pH of 10 at ambient temperature, except at very high pH levels at which the corrosion rate again can increase.

The solubility of elements in freshwater is limited and the solubility of calcium and magnesium carbonates are of particular importance in freshwaters. The solubility of carbonates is inversely proportional to the temperature of the water. In other words, as the water temperature increases, calcium and magnesium carbonates become less soluble. If the solubility decreases sufficiently, carbonates will precipitate and form a scale on the surfaces of the system. This scale can provide a protective barrier to prevent corrosion of the metallic elements in a system. Excessive scale deposits can interfere with water flow and heat transfer. The quality of

[1]Corrpro Companies, Inc., 470 Lapp Rd., Malvern, PA 19355, USA
http://orcid.org/0000-0003-4670-8066
The authors acknowledge the previous authors of this chapter, Walter T. Young and Philippa Fairer, Corrpro Companies, Inc. West Chester, PA.

DOI: 10.1520/MNL202NDSUP20190016

Copyright © 2022 by ASTM International, 100 Barr Harbor Dr., PO Box C700, West Conshohocken, PA 19428-2959
ASTM International is not responsible, as a body, for the statements and opinions expressed in this chapter. ASTM International does not endorse any products represented in this chapter.

the scale depends on the quantity of calcium that can precipitate as well as water flow and the chloride and sulfate content of the water. The tendency of water to precipitate a carbonate scale is estimated from corrosion indices such as the Langelier Saturation Index (LSI) and Caldwell-Lawrence calculations,[7–9] which use calcium, alkalinity, total dissolved solids, temperature, and pH properties of the water. Other indices, such as the Ryznar Index, purport to indicate corrosivity directly using the same elements as the LSI.[7] Manganese in excess of 0.50 mg/L can cause pitting of copper in hot water systems.[1] Copper in excess of 0.1 mg/L causes pitting of zinc galvanized steel and aluminum if the zinc and aluminum are downstream of the copper.[1] The reversal of the potential between zinc galvanizing and steel can occur in some water, resulting in the steel becoming the anode in a bimetallic couple. This normally occurs in hot water with relatively high carbonates, bicarbonates, phosphates, and silicates relative to sulfate and chlorides.

PROCESS CONDITIONS

Water velocity and turbulence can damage protective films and deposits on metal surfaces, causing increased corrosion. Soft metals, such as copper, are particularly susceptible to erosion corrosion, but steel and other metals are also susceptible if the water velocity is sufficiently high. The critical velocity for erosion-corrosion of copper in freshwater is about 5 fps (1.52 m/s), but this critical velocity can drop sharply as the chemical corrosivity of the water increases. Suspended solids in the water can increase the erosion characteristics of the water.[1] Deposits can result in accelerated corrosion from the formation of oxygen differential concentration corrosion cells.

Generally, higher temperatures cause an increase in corrosion activity and a corresponding increase in metal loss, particularly in a closed (pressurized) system. A closed system does not allow oxygen and other gasses to leave the water. If the system is open, increasing the temperature beyond 91°C causes a decrease in corrosion because oxygen is removed from the water. Higher temperatures also can cause the solids in a system (where evaporation occurs) to concentrate, which can lead to increased corrosion rates. Alternately, increased temperature can cause an increase in the scaling tendency of the water resulting in lower corrosion rates.

The use of water treatment can increase or decrease corrosion rate. Excessive amounts of chlorine (used as a biocide) can increase corrosion. Water softening is the reduction of hardness, alkalinity, and other constituents by the use of chemicals or resin exchange to reduce scaling. Water softening can lead to increased corrosion rates. Conversely, the addition of caustic, soda ash, or corrosion inhibitors are used to decrease corrosion rates. Aeration can decrease corrosion rates when used to remove carbon dioxide. Deaeration also is used to decrease corrosion rates in some systems.

BIOLOGICAL FACTORS

Biological activity can increase corrosion rate either by increasing the occurrence of concentration cell corrosion beneath the biomass or by producing corrosives from metabolic processes. Corrosion occurs as one of the common forms discussed in the following sections. Bacteria can survive under most conditions found in water systems and are either aerobic or anaerobic. *Desulfovibrio desulfricans* is an anaerobic sulfate-reducing bacterium that can be found in cooling towers and potable water piping. *Thiobacillus thioxidans* (an acid producer) is another anaerobic bacterium known to influence corrosion. An example of aerobic bacteria is iron bacteria (*Gallionella*), which are found in some water wells. Slimes also influence corrosion by promoting concentration cell corrosion.[3] Anaerobic metal reducing bacteria cause pitting of stainless steel. Manganese in the presence of anaerobic manganese fixing bacteria (e.g., *Gallionella*, *Sphaerotilus*) and chloride can cause pitting corrosion of stainless steel in fresh water.

METALLURGY

In gray cast iron, the iron can be selectively removed leaving the graphite matrix, a process called graphitic corrosion, also known as graphitization. High-zinc brasses and aluminum-bronzes are susceptible to selective leaching of specific elements in the alloy. In brass, the zinc selectively corrodes, leaving behind a weak, spongy, porous copper-rich matrix. The process, dezincification, generally occurs in relatively corrosive, soft, and acidic waters. Aluminum bronzes can undergo selective leaching of aluminum (dealuminification) under conditions similar to dezincification. Stainless steels can undergo intergranular corrosion at welds and elsewhere caused by the effective removal of chromium from the metal matrix in combination with carbides under high-temperature exposure. Denickelification is the selective removal of nickel from copper-nickel alloys, which has been found in fresh waters under conditions of high heat flux and low water velocity.[10] Brass is also subject to stress corrosion cracking in water where tensile stress and a corrosion species, such as nitrate or ammonia, are present in the water.

OTHER FACTORS

Poor workmanship and defective materials can increase corrosion. Water turbulence effects can be increased by poor workmanship, such as the failure to ream burrs from the cut ends of copper pipe. This increases the turbulence at the joints and results in erosion of the copper. Excessive and corrosive flux used in soldered coppers joints results in pitting corrosion along the flux runs. Incomplete longitudinal welds in electric resistance welded (ERW) steel pipe result in concentration cell corrosion and metal loss.

Contamination of the water system can increase the corrosion rate. In cooling tower systems, water corrosivity is increased by the absorption of sulfur gases from the atmosphere. Airborne salts can contaminate open water systems. Process water systems can be contaminated with process debris, such as fibers and chemicals that can increase the corrosion rate.

Test Methods

Table 1 shows the most common forms of corrosion that affect metals in the freshwater environment. These corrosion forms are described in ASTM G15, *Standard Terminology Relating to Corrosion and Corrosion Testing*.

TABLE 1 Corrosion Forms Affecting Common Engineering Metals in Freshwater

Metal	Corrosion Form
Steel	Uniform
	Pitting
	MIC
	Erosion
	Galvanic
	Fretting
	Concentration cell
Galvanized steel	Uniform
	Pitting
	Galvanic
	MIC
	Concentration cell
Cast and ductile iron	Uniform
	Pitting
	MIC
	Concentration cell
Copper	Uniform
	Pitting
	Crevice
	Erosion corrosion
	Cavitation
	Galvanic
	Concentration cell
Bronze	Pitting
	De-alloying
	Cavitation
	Concentration cell
Brass	Pitting
	Cavitation
	De-alloying
	Stress corrosion cracking
	Concentration cell
Aluminum	Pitting
	Galvanic
	Bacterial
	Concentration cell
Stainless Steel	Pitting
	MIC
	Stress corrosion cracking
	Crevice
	Intergranular corrosion
	Concentration cell

Note: MIC = microbiologically influenced corrosion

This section, "Test Methods," provides information about the use and applicability of various corrosion tests. Details of performing the tests are provided in the cited references and in the section "Analysis, Testing, and Environments." Tables 2 through 10 list the test methods applicable to the various tests.

ELECTROLYTE CHEMISTRY

In designing a test program, it is important to know the chemistry of the system water to accurately simulate the environment of interest. Knowledge of the water chemistry will not provide quantitative corrosion data but will provide insight into the corrosivity of the water. The chemical constituents of importance in corrosion are pH, conductivity (or resistivity), total dissolved solids, chlorides, sulfates, suspended solids, alkalinity, carbonates, bicarbonates, hardness, carbon dioxide, oxygen, sulfur dioxide, nitrates, manganese, and heavy metals. Also, the scaling tendency of the water should be determined by either the LSI or Caldwell-Lawrence diagrams.[8,9] A computer program for calculating the scale-forming tendencies is available from the American Water Works Association, Denver, CO.

Applicable test methods are found in the following:

- *ASTM Annual Book of Standards*[11]
- American Public Health Association's *Standard Methods for the Examination of Water and Wastewater*[12]
- NACE TM0374, *Laboratory Screening Tests to Determine the Ability of Scale Inhibitors to Prevent the Precipitation of Calcium Sulfate and Calcium Carbonate from Solution*[13]

UNIFORM CORROSION

Uniform corrosion is metal that is both evenly distributed over the metal surface and uniform in the rate of penetration. Uniform corrosion is readily measured with standard test procedures. Weight loss testing, polarization resistance, Tafel extrapolation, resistance change measurements, and AC impedance all measure the average corrosion rate of a sample surface. Each test is conducted by immersing the sample in the environment and averaging the corrosion losses, current flows, or volume changes over the entire surface area. Nonuniform corrosion, however, will provide inaccurate corrosion rates because the results are averaged over the surface area. Specimens must be visually examined for signs of pitting, crevice corrosion, stress-corrosion cracking (SCC), or other localized corrosion. When using electrochemical or resistance tests, parallel immersion testing should be conducted to determine if localized corrosion will occur.

Weight loss is the easiest and least expensive method because that method requires only test specimens, the solution, a container, and the appropriate environmental parameters. Weight loss tests can be conducted in low-conductivity solutions, even in the atmosphere. An analytical balance is required for both before and after weight measurements. Multiple specimens must be used sequentially when evaluating the change in corrosion rate over time. Specimens cannot be reused for corrosion rate versus time measurements after first exposed and cleaned because high initial corrosion rates will occur each time the specimen is used. This will lead to artificially high corrosion rate data.

Weight loss testing is widely used both in the laboratory and for in-plant testing. For in-plant tests, racks of corrosion samples or single coupons are inserted at locations where corrosion rates are desired. Test specimens can be inserted in pipes or other structures using "hot-tap" devices and in bypass loops. Weight loss testing is slow (especially in systems with low corrosion rates) and does not allow instantaneous measurement. Extreme care must be exercised in designing weight loss tests because velocity, crevice, stagnation, and heat transfer conditions will influence the results.

DC polarization measurements, both polarization resistance and Tafel extrapolation, provide the ability to measure instantaneous corrosion rates and corrosion rate variation over time.[14,15] Standard polarization techniques assume a uniform corrosion rate. Special techniques as discussed in the following discussion and provided in tables 3 to 10 can be used to evaluate localized corrosion. The solution must have sufficient conductivity to perform this test. Solutions with low conductivity require correction factors or special techniques to account for the effect of voltage drops on the measured specimen potential caused by current flow through the solution (IR drop). Tafel extrapolation requires relatively large changes to the electrochemical potential that can damage the specimen. In addition, relatively long test times are required. Corrosion reactions that are not under activation control will obscure the Tafel slope. In contrast, significant information on the corrosion process can be obtained from full anodic and cathodic polarization curves. Polarization resistance requires only small changes in specimen electrochemical potential; therefore, this method is fast and does less damage to the specimen compared with Tafel extrapolation. Polarization can be applied to field testing and monitoring. Computerized equipment is available for both types of tests. Instruments based on the polarization resistance technique are widely used for process monitoring.

Resistance probes are used for in-plant corrosion testing. As a metal corrodes, its volume decreases with a corresponding increase in resistance. Resistance probe instruments are commercially available on the market. Probes can be made from many different metals and alloys. The probes are inserted into the environment and the loss of cross-sectional area of the probe element is detected by its increase in electrical resistance with time. The data obtained by plotting resistance against time of exposure provide a graphic history of corrosion rate. Resistance probes can be used in low-conductivity solutions. Visual inspection is necessary to differentiate between pitting and general metal loss. Pitting can result in the appearance of a low corrosion rate followed by rapid increases in corrosion. The method is not sensitive either to very low or to rapid changes in corrosion rate. The positions of the probe in the environment, the fluid velocity, and heat transfer have a pronounced effect on the results. ASTM G96, *Standard Guide for Online Monitoring of Corrosion in Plant Equipment (Electrical and Electrochemical Methods)*, provides the details about conducting this test.

Electrochemical impedance spectroscopy (EIS) provides detailed information on the corrosion reaction by determining the equivalent electrical circuit of a corroding system. The method requires low potential changes in the system and can be used in low-conductivity solutions. Complex equipment is needed to conduct the tests and specialized knowledge needed to interpret the data.[16,17]

Table 2 provides information on standard test methods for evaluating uniform corrosion.

TABLE 2 Test Methods for Evaluating Uniform Corrosion

Test Method	Test Title	Application
ASTM D2688	*Standard Test Method for Corrosivity of Water in the Absence of Heat Transfer (Weight Loss Method)*	Provides weight loss methods to evaluate corrosion directly in piping systems.
ASTM G1	*Standard Practice for Preparing, Cleaning, and Evaluating Corrosion Test Specimens*	Provides methods for cleaning and evaluating weight loss coupons.
ASTM G3	*Standard Practice for Conventions Applicable to Electrochemical Measurements in Corrosion Testing*	Provides information on reporting and displaying polarization measuring techniques, including both DC and AC methods.
ASTM G4	*Standard Guide for Conducting Corrosion Tests in Field Applications*	Provides guidelines for in-plant testing: weight loss coupons, specimen racks, reporting.
ASTM G31	*Standard Practice for Laboratory Immersion Corrosion Testing of Metals*	Describes procedures for conducting laboratory weight loss tests. Provides information on reporting and factors to be aware of.
ASTM G59	*Standard Test Method for Conducting Poteniodynamic Polarization Resistance Measurements*	Provides details on how to conduct DC polarization resistance tests.
ASTM G96	*Standard Guide for Online Monitoring of Corrosion in Plant Equipment (Electrical and Electrochemical Methods)*	Provides details on conducting polarization resistance and electrical resistance tests.
ASTM G102	*Standard Practice for Calculation of Corrosion Rates and Related Information from Electrochemical Measurements*	Describes practice for converting corrosion current data from electrochemical polarization measurements to corrosion rate.
NACE TM-01-71 (Test Method)	*Autoclave Testing of Metals in High Temperature Water*	Methods for testing water at temperatures greater than 100°C but less than 360°C. Test is weight loss method, but could be modified for electrochemical techniques.
NACE TM-02-74	*Dynamic Corrosion Testing of Metals in High Temperature Water*	Similar to TM-01-71, but uses circulating loop and heat exchangers; discusses the weight loss method.
NACE TM-01-69	*Laboratory Corrosion Testing of Metals for the Process Industries*	Discusses factors of concern for laboratory testing. Discusses planning tests and evaluation. Emphasizes weight loss methods
NACE RP-0775-87 (Recommended Practice)	*Preparation and Installation of Corrosion Coupons and Interpretation of Test Data in Oilfield Operations*	Discusses the use of weight loss coupons, interpretation of data, and analysis. Principals are applicable to freshwater systems.

PITTING CORROSION

Pitting corrosion is localized corrosion of a metal surface that is a surface cavity with a depth equal to or greater than the minimum dimension at the opening. Pitting corrosion is difficult to evaluate because it can initiate at random locations on a metal surface. Large areas of a surface can be corrosion-free with pits only at a few locations. Small corrosion coupons might not show pitting or might not provide enough pit depth data for a reliable analysis. Conversely, the surface can have a large number of pits over a given area.

Immersion testing using specimens of sufficient size and number should be used to measure corrosion rate accurately. The depth of pitting follows the normal probability distribution. Extreme value statistical analysis provides a useful tool to evaluate pitting.[18,19] Pit depths can be measured using calipers, micrometer, or metallurgical microscope with a calibrated focus.

Cyclic anodic polarization curves are used to provide relative susceptibility to pitting corrosion. This method does not provide specific corrosion rate data. Some corrosion rate devices that are based on the polarization resistance method use a technique involving monitoring electrochemical noise to determine a metal's resistance to pitting or localized corrosion, sometimes called the pitting index. The pitting index is qualitative and does not provide a corrosion rate. Another factor is the Pitting Resistance Equivalent Number (PREN) and might be useful for stainless steel alloys. The PREN, also not quantitative, is calculated using a weighted formula typically based on the chromium, molybdenum, nitrogen, and tungsten content of the alloy, developed to rank the pitting and crevice corrosion resistance of stainless steels and some nickel-based alloys.[20]

Table 3 provides the standard test methods for evaluating pitting corrosion.

CREVICE AND CONCENTRATION CELL CORROSION

Crevice corrosion and concentration cell corrosion susceptibility can be measured directly by exposing test specimens to the environment. ASTM F746, *Standard Test Method for Pitting or Crevice Corrosion of Metallic Surgical Implant Materials*; ASTM G48, *Standard Test Methods for Pitting and Crevice Corrosion of Stainless Steels and Related Alloys by Use of Ferric Chloride Solution*; and ASTM G78, *Standard Guide for Crevice Corrosion Testing of Iron-Base and Nickle-Base Stainless Alloys in Seawater and Other Chloride-Containing Aqueous Environments*, can be used to evaluate these forms of corrosion. These methods were designed to measure crevice corrosion in severe electrolytes, such as salt solutions, but can be modified for freshwaters.

Electrochemical polarization also can be used by conducting cyclic anodic polarization scans. This technique, described in ASTM G61, *Standard Test Method for Conducting Cyclic Potentiodynamic Polarization Measurements for Localized Corrosion Susceptibility of Iron-, Nickel-, or Cobalt-Based Alloys*, provides a qualitative approach to evaluate crevice corrosion. Polarization can be used to provide a more quantitative analysis by applying a graphical technique. This approach uses the same general method as described under galvanic corrosion in ASTM G82, *Standard Guide for Development and Use of a Galvanic Series for Predicting Galvanic Corrosion Performance*. Its use requires knowledge of the solution chemistries inside and outside of the crevice and the ability to simulate these environments for the anodic and cathodic tests.

Table 4 provides information on standard test procedures for evaluating crevice corrosion.

GALVANIC (BIMETALLIC) CORROSION

The galvanic series may be used to predict the possibility of galvanic corrosion, but it cannot be used to predict the quantity of corrosion that can occur. Most published galvanic series apply only to the seawater environment and some metals behave differently in different environments. For example, stainless steels can behave either in the active state or in the passive state depending on the environment and the metals to which they are connected. Sometimes the behavior of a galvanic couple in a particular environment can be the reverse of that shown in most published galvanic series. Metals also polarize (change potentials as a result of current flow) when connected to each other in an electrolyte. This will affect the corrosion behavior and cannot be predicted from the galvanic series. The area ratio of the two metals has a marked influence on the corrosion rate of the bimetallic couple. The solution operating conditions (e.g., aeration, movement) also can have significant effects.

Two test methods can be employed to determine the susceptibility of two metals to galvanic corrosion in an electrolyte. In the first method, the two metals are immersed in the electrolyte and the current flow between them is measured using a zero resistance ammeter. The corrosion current is calculated according to the following relationship: $I_{tl} = I_g + I_{la}$, where I_{tl} is the total

TABLE 3 Test Methods for Evaluating Pitting Corrosion

Test Method	Test Title	Application
ASTM F746	*Standard Test Method for Pitting or Crevice Corrosion of Metallic Surgical Implant Materials*	Discusses measurement of pitting or crevice tendency by measuring repassivation tendency after polarization at noble potential. Applicable only to passive alloys.
ASTM G16	*Standard Guide for Applying Statistics to Analysis of Corrosion Data*	Discusses statistical analysis methods of corrosion data.
ASTM G46	*Standard Guide for Examination and Evaluation of Pitting Corrosion*	Provides information needed for collecting and interpreting pitting data.
ASTM G61	*Standard Test Method for Conducting Potentiodynamic Polarization Measurements for Localized Corrosion Susceptibility of Iron-, Nickel-, or Cobalt-Based Alloys*	Provides information on conducting cyclic anodic polarization tests. Useful procedure for evaluating pitting and crevice corrosion susceptibility. Can be modified for other alloys that exhibit passive behavior.

TABLE 4 Test Methods for Evaluating Crevice Corrosion

Test Method	Test Title	Application
ASTM F746	*Standard Test Method for Pitting or Crevice Corrosion of Metallic Surgical Implant Materials*	Measurement of pitting or crevice tendency by measuring repassivation tendency after polarization at noble potential. Applicable only to passive alloys.
ASTM G48	*Standard Test Methods for Pitting and Crevice Corrosion Resistance of Stainless Steels and Related Alloys by the Use of Ferric Chloride Solution*	Method for characterizing crevice and pitting resistance of metals. Specific to chloride containing environment, but useful for any environment where ion concentration or oxygen differential corrosion can occur.
ASTM G61	*Standard Test Method for Conducting Potentiodynamic Polarization Measurements for Localized Corrosion Susceptibility of Iron-, Nickel-, or Cobalt-Based Alloys*	Provides information on conducting cyclic anodic polarization tests. Useful procedure for evaluating pitting and crevice corrosion susceptibility. Can be modified for other alloys that exhibit passive behavior.
ASTM G78	*Standard Guide for Crevice Corrosion Testing of Iron-Base and Nickel-Base Stainless Alloys in Seawater and Other Chloride-Containing Aqueous Environments*	Useful for evaluating crevice corrosion susceptibility in any environment where ion or oxygen concentration cells can occur.

current, I_g is the measured galvanic corrosion current, and I_{la} is the local action corrosion current measured by another technique. The galvanic corrosion rate is calculated using Faraday's law. ASTM G71, *Standard Guide for Conducting and Evaluating Galvanic Corrosion Tests in Electrolytes*, describes the method.

The galvanic corrosion behavior can be predicted using polarization behavior. Electrochemical potential measurements are used to predict which metal is the anode and which is the cathode. Anodic and cathodic polarization curves are produced for the anticipated environments then superimposed on each other at the known initial potential difference. The corrosion current is graphically determined. ASTM G82 describes the method as does Jones.[21]

Table 5 provides information on standard test methods for evaluating galvanic corrosion.

EROSION CORROSION

Immersion testing and impinging an electrolyte flow onto the metal of interest measure erosion corrosion resistance. ASTM G73, *Standard Test Method for Liquid Impingement Erosion Using Rotating Apparatus*, provides standardized methods for performing these erosion tests. For a detailed discussion about various erosion tests, see Rowe.[22]

Table 6 provides standard tests for evaluating erosion corrosion.

CAVITATION

ASTM G32, *Standard Test Method for Cavitation Erosion Using Vibratory Apparatus*, provides a standardized method of conducting a cavitation test. Another nonstandard method is to construct a flow channel and mount the specimens in such a manner as to produce cavitation on the downstream side of the specimen. For a detailed discussion about various cavitation tests, see the ASM *Corrosion Handbook*.[10]

Table 7 provides information on ASTM G32.

STRESS-CORROSION CRACKING

SCC susceptibility is directly evaluated by immersing stressed specimens in water, and then evaluating the specimens for cracks using high-magnification metallographic or low-magnification macrographic examination. ASTM G30, *Standard Practice for Making and Using U-Bend Stress-Corrosion Test Specimens*; ASTM G38, *Standard Practice for Making and Using C-Ring Stress-Corrosion Test Specimens*; ASTM G39, *Standard Practice for Preparation and Use of Bent-Beam Stress-Corrosion Test Specimens*; ASTM G47, *Standard Test Method for Determining*

TABLE 5 Test Methods for Evaluating Galvanic (Bimetallic) Corrosion.

Test Method	Test Title	Application
ASTM G71	*Standard Guide for Conducting and Evaluating Galvanic Corrosion Tests in Electrolytes*	Evaluation of galvanic corrosion using two dissimilar metals in an electrolyte connected through a zero resistance ammeter.
ASTM G82	*Standard Guide for Development and Use of a Galvanic Series for Predicting Galvanic Corrosion Performance*	Procedure for development of a galvanic series in an electrolyte.

TABLE 6 Test Methods for Evaluating Erosion Corrosion.

Test Method	Test Title	Application
ASTM G40	*Standard Terminology Relating to Wear and Erosion*	Definition of terms for erosion and wear.
ASTM G73	*Standard Practice for Liquid Impingement Erosion Testing*	Resistance to erosion from impacts of liquid drops or jets.

TABLE 7 Test Method for Evaluating Cavitation Corrosion

Test Method	Test Title	Application
ASTM G32	*Standard Test Method for Cavitation Erosion Using Vibratory Apparatus*	Test for comparing cavitation resistance of different alloys.

Susceptibility to Stress-Corrosion Cracking of 2XXX and 7XXX Aluminum Alloy Products; ASTM G49, *Standard Practice for Preparation and Use of Direct Tension Stress-Corrosion Test Specimens*; ASTM G58, *Standard Practice for Preparation of Stress-Corrosion Test Specimens for Weldments*; and ASTM G64 *Standard Classification of Resistance to Stress-Corrosion Cracking of Heat-Treatable Aluminum Alloys* provide methods of preparing specimens and conducting immersion tests. ASTM E3, *Standard Guide for Preparation of Metallographic Specimens*, and ASTM E407, *Standard Practice for Microetching Metals and Alloys*, provide methods of metallurgical examination.

SCC susceptibility is more readily detected using slow strain rate techniques than normal tension testing. This is because the slow straining procedure allows the corrosion effects to occur.[17]

Table 8 provides information on standard test methods for evaluating SCC.

DEALLOYING

Dealloying is a localized phenomenon that can be evaluated through the use of immersion testing and metallographic techniques (ASTM E3 and ASTM E80, *Recommended Practice for Dilatometric Analysis of Metallic Materials [Withdrawn 1986]*). Energy dispersive X-ray spectroscopy (EDS) and wavelength dispersive X-ray spectroscopy (WDS) are used to detect small amounts of dealloying. Using EDS and WDS, the surface chemistry of the sample is examined to detect losses in the active elements and enrichment in the noble alloying elements.

INTERGRANULAR CORROSION

Because intergranular corrosion is limited to corrosion at or immediately adjacent to grain boundaries and is detectable at the microstructural level, simple corrosion rate calculations using weight loss measurements provide no information. Standard ASTM tests, such as the oxalic acid etch test (ASTM A262, *Standard Practice for Detecting Susceptibility to Intergranular Attack in Austenitic Stainless Steels*) provide relative susceptibility only for austenitic stainless steels. These tests have little usefulness in freshwater environments. A metallographic analysis performed after test samples are exposed provides the most useful information about susceptibility to intergranular corrosion (ASTM E3 and E80).

Cyclic polarization measurements provide relative information about susceptibility as described in ASTM G61. ASTM G108, *Standard Test Method for Electrochemical Reactivation (EPR) for Detecting Sensitization of AISI Type 304 and 304L Stainless Steels*, provides a test method applicable to type 304 stainless steel.

Table 9 provides information on standard test methods.

FRETTING CORROSION

Fretting corrosion can occur between two metal parts having an electrolyte and slight vibratory movement. Although ASTM F897, *Standard Test Method for Measuring Fretting Corrosion of Osteosynthesis Plates and Screws*, is intended specifically for surgical implants, it can be modified for use in other environments.

Table 10 provides information on ASTM F897.

TABLE 8 Test Method for Evaluating Stress Corrosion Cracking

Test Method	Test Title	Application
ASTM E3	*Standard Guide for Preparation of Metallographic Specimens*	Techniques for preparing metal samples for metallographic examination.
ASTM E407	*Standard Practice for Microetching Metals and Alloys*	Techniques for preparing metal samples for metallographic examination.
ASTM G30	*Standard Practice for Making and Using U-Bend Stress Corrosion Test Specimens*	Procedures for preparing and testing strip specimens for stress corrosion testing.
ASTM G38	*Standard Practice for Making and Using C-Ring Stress-Corrosion Test Specimens*	Procedures for preparing and testing tube samples or ring samples from thick solid material for stress corrosion cracking immersion testing. For testing above the elastic limit of the alloy.
ASTM G39	*Standard Practice for Preparation and Use of Bent-Beam Stress-Corrosion Test Specimens*	Testing strip specimens from sheet or plate for stress corrosion cracking immersion tests. For testing below the elastic limit of the alloy.
ASTM G47	*Standard Test Method for Determining Susceptibility to Stress-Corrosion Cracking of 2XXX and 7XXX Aluminum Alloy Products*	Procedure for using ring or strip samples for testing 2xxx and 7xxx series aluminum alloys.
ASTM G49	*Standard Practice for Preparation and Use of Direct Tension Stress-Corrosion Test Specimens*	Procedures for testing axially loaded specimens. Specimens may be straight, or joined (welded, riveted or other means).
ASTM G58	*Standard Practice for Preparation of Stress-Corrosion Test Specimens for Weldments*	Procedures for producing welded test specimens for use in other stress corrosion tests.
ASTM G64	*Standard Classification of Resistance to Stress-Corrosion Cracking of Heat-Treatable Aluminum Alloys*	

TABLE 9 Test Method for Evaluating Intergranular Corrosion

Test Method	Test Title	Application
ASTM G61	*Standard Test Method for Conducting Potentiodynamic Polarization Measurements for Localized Corrosion Susceptibility of Iron-, Nickel-, or Cobalt-Based Alloys*	Provides information on conducting cyclic anodic polarization tests. Useful procedure for evaluating pitting and crevice corrosion susceptibility. Can be modified for other alloys that exhibit passive behavior.
ASTM G108	*Standard Test Method for Electrochemical Reactivation (EPR) for Detecting Sensitization of AISI Type 304 and 304L Stainless Steels*	Describes cyclic polarization technique for evaluation of sensitivity to intergranular corrosion. Specific to 300 series stainless steel, but might be adaptable to other passive alloys with laboratory evaluation.

TABLE 10 Test Method for Evaluating Fretting Corrosion

Test Method	Test Title	Application
ASTM F897	*Practice for Fretting Corrosion of Osteosynthesis Plates and Screws*	This test provides a screening test for determining the amount of metal loss from plates and crews used in medical implants but might also be useful to evaluate materials and environments where relative motion between parts could create fretting such as bearings and fasteners.

References

1. *Internal Corrosion of Water Distribution Systems*, 2nd ed. (Denver, CO: AWWA Research Foundation, 1996).
2. J. R. Davis, ed., *ASM Materials Engineering Dictionary* (Materials Park, OH: ASM International, 1992).
3. H. M. Herro and R. D. Port, *Cooling Water Systems Failures* (New York: McGraw-Hill, 1993).
4. M. Fontana and N. Greene, *Corrosion Engineering* (New York: McGraw-Hill, 1967).
5. H. H. Uhlig, *Corrosion and Corrosion Control* (New York: Wiley, 1967).
6. R. W. Lane, *Control of Scale and Corrosion in Building Water Systems* (New York: McGraw-Hill, 1993).
7. *Prevention and Control of Water Caused Problems in Building Potable Water Systems*, 2nd ed., NACE TPC Publication No. 7 (Houston, TX: NACE International, 1995).
8. S. T. Powell, *Water Conditioning for Industry* (New York: McGraw-Hill, 1954).
9. *Corrosion Control by Deposition of $CaCO_3$ Films* (Denver, CO: AWWA Research Foundation, 1978).
10. *Corrosion Handbook*, vol. 13, *Corrosion* (Materials Park, OH: ASM International, 1987).
11. *Annual Book of ASTM Standards* (West Conshohocken, PA: ASTM International, 2022).
12. *Standard Methods for the Examination of Water and Wastewater*, 23rd ed. (Washington, DC: American Public Health Association, 2017).
13. *Laboratory Screening Tests to Determine the Ability of Scale Inhibitors to Prevent the Precipitation of Calcium Sulfate and Calcium Carbonate from Solution*, NACE TM0374, (Houston, TX: NACE International, 2016).
14. M. Stern and A. L. Geary, "Electrochemical Polarization I. A Theoretical Analysis of the Shape of Polarization Curves," *Journal of the Electrochemical Society* 104 (1957): 56–63.
15. M. Stern, "A Method for Determining Corrosion Rates from Linear Polarization Data," *Corrosion* 14, no. 9 (1958): 60–64.
16. F. Mansfeld, "Recording and Analysis of AC Impedance Data for Corrosion Studies, Part I. Background and Analysis," *Materials Performance* 37, no. 5 (1981): 301–307.
17. F. Mansfeld, M. Kendig, and M. W. Tsai, "Recording and Analysis of AC Impedance Data for Corrosion Studies, Part II. Experimental Approach and Results," *Corrosion* 38, no. 11 (November 1982), 301–307.
18. P. M. Aziz, "Application of Statistical Theory of Extreme Values to the Analysis of Maximum Pit Depth Data for Aluminum," *Corrosion* 12, no. 10 (1956): 35–46.
19. L. C. Rowe, "Measurement and Evaluation of Pitting Corrosion," in *Galvanic and Pitting Corrosion—Field and Laboratory Studies* (West Conshohocken, PA: ASTM International, 1976), 203–216.
20. *Petroleum and Natural Gas Industries—Materials for Use in H_2S-Containing Environments in Oil and Gas Production*, NACE MR0175/ISO 15156 (Houston, TX: NACE International, 2015).
21. D. A. Jones, "Polarization Studies of Brass-Steel Galvanic Couples," *Corrosion* 40, no. 4 (1984): 181–185.
22. G. M. Ugiansky and J. H. Payer, eds., *Stress Corrosion Cracking—The Slow Strain Rate Technique* (West Conshohocken, PA: ASTM International, 1979).

Chapter 13 | Seawater

David A. Shifler[1]

Introduction

Seawater is an aggressive, complex fluid that affects nearly all common structural materials to some extent.[1] Two competing processes operate simultaneously in seawater environments: (1) the chloride ion activity, which tends to destroy the passive film, and (2) dissolved oxygen, which acts to promote and repair the passive film on metallic materials of construction.[2] Metals and alloys that develop protective films by the formation of thin metal oxides can have the formation of passive films delayed or have films destroyed by chloride ions in seawater.[3]

The type of corrosion testing required depends on the extent and type of information desired and the environmental conditions expected in service for the alloy component. Seawater corrosion depends on a number of factors, including, but not limited to, alloy composition, water chemistry, pH, biofouling, microbiological organisms, pollution and contamination, alloy surface films, geometry and surface roughness, galvanic interactions, fluid velocity characteristics and mode, ocean depth, oxygen content, salinity, heat transfer rate, temperature, type of exposure, time, and the seawater environmental zone to which the material is exposed. Understanding how these factors may interact and affect experimental results can help the design of seawater corrosion testing to best simulate service conditions.

Description of the Seawater Environment

COMPOSITION

Seawater, the Earth's most abundant resource, covers 71% of the Earth's surface. This electrolyte approximates a 3.5 wt% sodium chloride (NaCl) solution, but it is much more complex, containing almost all naturally occurring elements.[4,5] The major chemical constituents of seawater, listed in table 1, are consistent throughout the world.[1] The minor constituents, including dissolved trace elements and gases, can vary substantially because of seasonal changes, storms, or tidal cycles. Biological organisms, combined with the minor constituents, often control the rate of the corrosion reactions occurring on metals in seawater.[1,5,6] In addition, the concentration of seawater can vary from full-strength ocean water to coastal seawater or brackish conditions. The type of corrosion and the corrosion rate occurring on metals and alloys in seawater depend on numerous variables in the specific seawater composition, its salinity, and the environmental zone to which the material is exposed.

TABLE 1 Major Seawater Constituents at (35 ppt salinity) and 25°C[1]

	Concentration	
Ion or Molecule	mmol/kg	g/kg
Na^{+}	468.5	10.77
K^{+}	10.21	0.399
Mg^{+2}	53.08	1.290
Ca^{+2}	10.28	0.4121
Sr^{+2}	0.090	0.0079
Cl^{-}	545.9	19.354
Br^{-}	0.842	0.0673
F^{-}	0.068	0.0013
HCO_3^{-}	2.30	0.140
SO_4^{-2}	28.23	2.712
$B(OH)_3$	0.416	0.0257

Seawater is a unique environment that cannot be duplicated in the laboratory. Throughout the world, seawater can vary widely in terms of its specific chemical composition, geography, oxygen content, temperature, salinity, pH, and biological activity. At a given location, seawater is also prone to variations from seasonal influences. All of these variables, combined with the long-term time dependence of many metal reactions, affect the corrosion occurring on metals and alloys in seawater. In addition, the composition of corrosion products and of calcareous deposits formed under cathodic polarization conditions will influence metal corrosion.

[1]Office of Naval Research, Naval Materials Division, 875 N. Randolph St., Arlington, VA 22203-1995, USA http://orcid.org/0000-0002-3709-7825
The author acknowledges the previous authors of this chapter, Denise Aylor and David A. Shifler.

DOI: 10.1520/MNL202NDSUP20190001

Copyright © 2022 by ASTM International, 100 Barr Harbor Dr., PO Box C700, West Conshohocken, PA 19428-2959
ASTM International is not responsible, as a body, for the statements and opinions expressed in this chapter. ASTM International does not endorse any products represented in this chapter.

Seawater pH ranges from 7.5 to 8.3. This narrow pH range is due to reactions that cause the interchange of carbon dioxide in the air with seawater and photosynthesis. Changes in the pH of seawater are buffered by the carbonate system and the presence of undissociated boric acid.[7] The buffering capacity and the constancy of natural waters, such as seawater, are discussed in Stumm and Morgan.[8]

ENVIRONMENTAL ZONES

Materials are exposed to marine environments in numerous applications, such as ships and submarines, offshore platforms, subsea pipelines and telecommunications cables, oceanographic instruments, dock bulkheads; heat exchangers, piping, pumps and valves in seawater-cooled power, chemical, and desalination plants; and ferries, yachts, pleasure boats, fishing gear, and oceanfront buildings. Marine environments typically are classified in terms of "zones" to which materials are exposed in given situations. Environmental zones involving seawater include marine atmosphere, splash-spray, tidal, submerged/shallow ocean, deep ocean, and mud. Figure 1 illustrates the relative corrosion rates of steel pilings in the different environmental zones.[9] The marine environment generally is considered to be a highly aggressive environment.

Atmospheric

Atmospheric corrosion is responsible for a large fraction of the total corrosion in the world. Factors that affect the atmospheric corrosion of materials in a marine environment are the time of wetness, temperature, material, atmospheric contaminants and pollutants, solar radiation, composition of the corrosion products, wind velocity, and biological species.[10] Deposition velocities can vary as much as two orders of magnitude for particles of different diameters.[11,12] Atmospheric corrosion of a passive alloy tends to be localized. For electrochemical processes related to corrosion to occur, an electrolyte must be present to allow current to pass through the diffusion and electrochemical migration of cations and anions. Seawater is a conductive electrolyte. The severity of corrosion in an atmospheric environment is related to the time of wetness during which electrochemical processes and corrosion take place. A direct relationship also exists between atmospheric salt content and measured corrosion rates.[13]

Atmospheric corrosion rates tend to increase with winds directly from the ocean to the site, at lower elevations, and the closer the ocean is to the specimen, as shown in table 2. The direction and velocity of the wind can affect the accumulation of entrained seawater–related particles on specimen surfaces. Generally, the closer the site is to the ocean in the face of a prevailing wind, the greater the corrosion rate of metals and alloys. Magnesium and calcium chlorides are hydroscopic and tend to keep surfaces wet or moist. Sulfur dioxide lowers the critical humidity required to activate corrosion[10] and increases the aggressiveness of the marine atmospheric environment, such as found in an industrial marine environment versus a rural marine environment (table 2). The dew-point temperature and the component or specimen temperature also will influence the rate of corrosion. Details on the factors affecting the degree of corrosion at atmospheric locations can be found in Leygraf and Graedel[11] and Leygraf, Wallinder, Tidblad, and Graedel.[12]

Solar radiation tends to degrade the performance of organic coatings and plastics, and stimulates biological formation and photosensitive electrochemical-corrosion reactions on copper or iron. Ultraviolet (UV) radiation can embrittle polymers unless UV stabilizers are added.[13]

FIG. 1 Corrosion profile of steel piling in seawater. Curve (a) represents behavior of uncoated piling; curve (b) represents steel piling corrosion at coating defect coated with organic, insulating substance.[18]

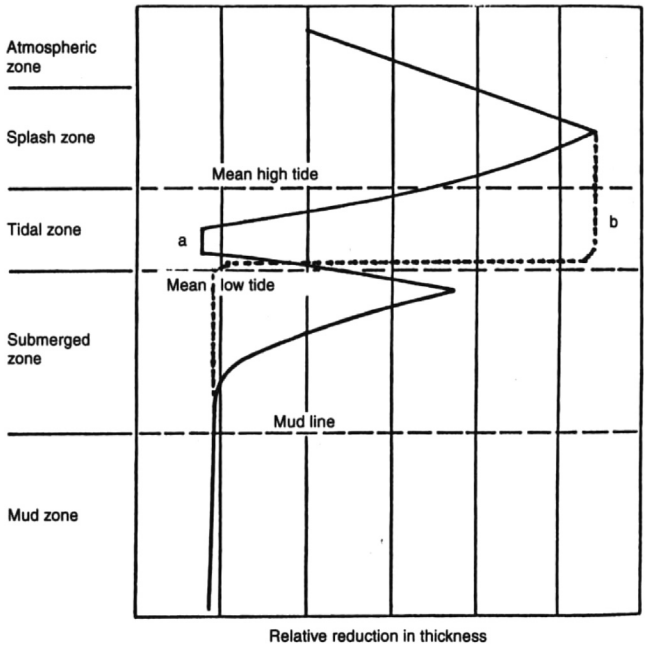


TABLE 2 Corrosion Rates of Uncoupled Steel Panels after Two Years at Different Atmospheric Test Sites

Location	Distance from Ocean, m	Steel Corrosion Rate 2-year test	
		mpy	mm/y
Cape Canaveral ground level	55	17.37	0.44
Cape Canaveral 9 m elevation	55	6.48	0.165
Cape Canaveral 18 m elevation	55	5.17	0.131
Cape Canaveral	800	3.39	0.086
Point Reyes, CA	400	19.71	0.50
Kure Beach, NC	25	21.00	0.53
Kure Beach, NC	250	5.73	0.145
Dungeness, England	Industrial Marine	19.22	0.49
Pilsey Island, England	Industrial Marine	4.04	0.013
Durban, Salisbury I., S. Africa	10	2.20	0.056
Esquimalt, B.C.	Rural Marine	0.53	0.013

Source: Data compiled from Dexter et al., table 13.[6]

Splash-Spray Zone

The splash-spray zone can be characterized as an aerated seawater environment where exposed metals are almost continually wet and biofouling organisms do not attach.[13,14] In an excessively windy seawater environment, the corrosion of metals can be increased as a result of seawater impinging on their surfaces. The aerated condition of the splash-spray environment is detrimental to many metals, such as steel, where its corrosion rate is higher than in any of the other marine environments. This is because dissolved oxygen is easily accessible for electrochemical reactions and chlorides can concentrate during drying of moist films created by spray and condensation.[15] As illustrated by curve (a) in figure 1, the most severe corrosion occurs in the splash-spray zone for uncoated steel pilings. The splash-spray environment is also destructive to protective coatings, such as organic coatings. Passive film-forming alloys, such as stainless steels and titanium, have good resistance in this well-aerated environment.[14]

Tidal Zone

The tidal zone is an environment where metals are alternately submerged in seawater and exposed to the splash-spray zone as the tide fluctuates. In the submerged condition, metals are exposed to well-aerated seawater and biofouling occurs.[13,14] A continuous cover of biofouling organisms protects some metal surfaces, such as steel, while the presence of biofouling on stainless steel surfaces can accelerate localized corrosion. Metals or alloys such as steel are influenced by tidal flow, where increased movement resulting from tidal action causes an increased steel corrosion rate.[14] Curve (b) in figure 1 shows that steel corrosion at exposed coating defect sites is as severe in the tidal zone as it is in the splash-spray zone.

Submerged/Shallow Ocean

The submerged/shallow ocean environmental zone usually is characterized by well-aerated water combined with marine biofouling organisms of both the plant and animal variety. As in the tidal zone, the biofouling can either protect the metal surface from attack or can accelerate localized corrosion at the site of the attachment.[13,14] The temperature of the seawater in this environmental zone depends on seasonal and specific geographic location but, other than in the polar regions, it is substantially warmer than in the deep ocean environment. The corrosion rate of metals in the shallow ocean varies. Titanium exhibits excellent corrosion resistance in this environment, while the corrosion resistance of steel largely depends on the availability of oxygen to be transported to cathodic sites on steel surfaces.[14]

Deep Ocean

The deep ocean environment is very different from the ocean at the surface. At sites in the North Atlantic and North Pacific oceans, oxygen, temperature, and salinity vary with depth. At the ocean surface, the oxygen concentration in the North Pacific is 1.4 times the oxygen content in the North Atlantic. In addition, both the surface temperature and surface salinity are lower in the North Pacific than in the North Atlantic. Below about 1,500 m, however, temperature and salinity levels are approximately the same at these two ocean sites.[1,6]

The oxygen concentration also varies with seawater depth, as shown in figure 2. This figure compares the concentration level with depth at sites in both the North Atlantic and North Pacific Oceans. As the depth is increased to an intermediate level, the oxygen concentration decreases at both sites; however, the reduction in oxygen is much greater in the Pacific Ocean than in the Atlantic. As the depth is then increased even farther, and the concentration of oxygen increases once again at both ocean sites.[6]

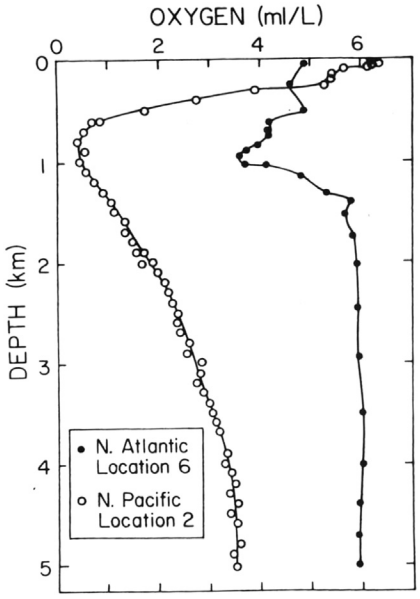
As a general rule, the pH varies with the change in dissolved oxygen content. Both variables decrease with depth and reach a minimum value before increasing again (as shown in fig. 2 for oxygen content). The dissolved oxygen and carbon dioxide concentrations are related to pH in the ocean according to the following reaction:[16,17]

$$\begin{gathered} \leftarrow \text{(photosynthesis)} \\ CH_2O_n + nO_2 \Longleftrightarrow nCO_2 + nH_2O \\ \text{(biochemical oxidation, respiration)} \rightarrow \end{gathered}$$

As organic matter decomposes, the dissolved oxygen content decreases and carbon dioxide is produced. The production of carbon dioxide, a weak acid, results in a pH reduction in seawater. With photosynthesis, the previous reaction is reversed.[1,6]

Beyond a depth of 18–30 m, plant biofouling ceases because of the lack of solar radiation, and any biofouling present is entirely due to animal life sources. In general, the degree of fouling decreases substantially as the depth is increased, an effect that is independent of the distance from the shoreline.[14] In contrast, at a given depth, as one moves away from the shoreline where breeding of macroorganisms takes place, significantly less fouling on metal surfaces is observed.

FIG. 2 Variation in oxygen concentration with depth at sites in the northwest Atlantic (36°44′ N, 64°28′ W) and northeast Pacific (38°21′ N, 133°38′W).[3]



Mud

The bottom sediments of the ocean comprise the mud zone. Anaerobic sediments contain bacteria that develop gases such as ammonia (NH_3), hydrogen sulfide (H_2S), and methane (CH_4). Sulfides present in the mud zone can attack metals, such as steels and copper alloys. The corrosion rate of low-carbon steel (as shown in fig. 1) in this environment, however, usually is lower than that in the other seawater environmental zones just described, predominantly because of the reduced supply of oxygen.[14]

UNIQUENESS

Seawater is a unique environment that cannot be duplicated in the laboratory. A recent worldwide test program recently was completed by ASTM Task Group G1.09.02.03 to evaluate the corrosivity of seawater at a number of sites.[18] Although these results indicated the uniqueness of natural seawater, corrosivity was site specific and influenced by numerous factors. Seawater can vary widely in terms of chemical composition, dissolved oxygen content, temperature, salinity, pH, carbonate levels, flow, degree of fouling, biological activity, and pollution.[19]

Environmental Variables Affecting Corrosion Rates in Seawater

TEMPERATURE

As a general rule, the corrosion reaction rate in seawater increases as the temperature is increased. This applies only when the effect of temperature alone is a factor. Other variables such as oxygen concentration, diffusion rates, salinity, calcareous deposit formation, and biological activity vary as a function of temperature and also must be considered as to how it affects the corrosion rate of a material, component, or system.

Surface water temperatures vary mainly by latitude, with the temperature ranging from approximately –2°C in the arctic to about 35°C in the tropics.[19] Table 3 shows the variation of surface temperatures in selected oceans as a function of latitude in the northern and southern hemispheres.[6] The data suggest that for a given latitude, corrosion tests results may vary slightly depending on the ocean location chosen. Also, metal corrosion rates are usually higher at the surface where temperatures are warmer than in the deep ocean where the temperatures are colder.[6,14] The effect of temperature as a function of ocean depth for low-carbon steel alloys is presented in figure 3.

Metal corrosion rates are similar at different locations throughout the world because of a number of controlling factors that compensate for one another.[20] Increasing seawater temperatures increase diffusion rates but decrease oxygen solubility. Although increasing temperatures tend to increase corrosion rates, temperature increases also promote the formation of calcareous deposits[6,14] and microbiological colonization, which form barrier layers that often throttle corrosion attack.[20] Bacteria may participate in anaerobic corrosion reactions that replace the cathodic oxygen-reduction reaction.

Temperature variations resulting from seasonal changes also may affect corrosion rates in seawater. For many copper and iron alloys, the corrosion rates increase during the warmer months of the year. The start of the corrosion test, therefore, may be affected by the time that a corrosion test is initiated, and the tendency is for corrosion rates to slow down with increased times of exposure to the natural seawater environment, depending on the actual environmental zone.

Some of the highest corrosion rates in the world, however, are found in cold-weather climates. Corrosion rates in Alaska are reported to be twice as high as those in the North Sea and six times greater than the rates reported in the Gulf of Mexico. The high corrosion rates are caused by the high dissolved oxygen levels, abrasion from glacial silts, tidal changes of more than 30 feet (9.1 m) and the action of ice floes in winter.[21] Corrosion rates on steel in the splash zones on docks are estimated to be as high as 30–35 mpy (761–889 µm/y) in the Aleutians.[22]

DISSOLVED OXYGEN

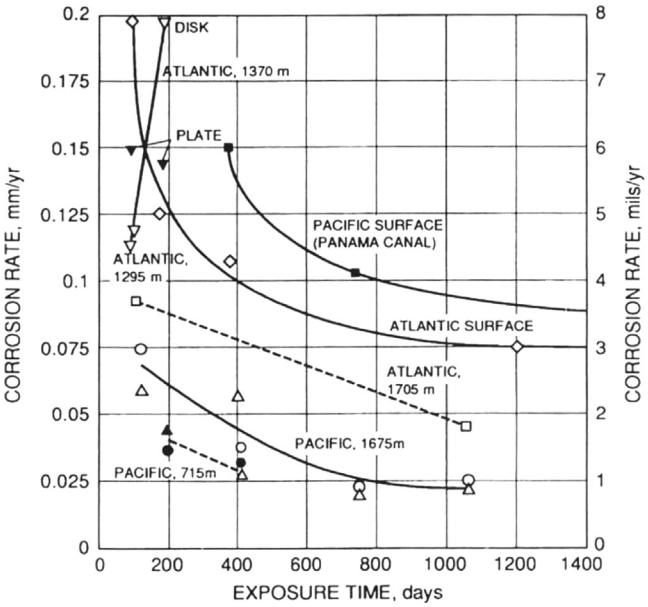
Dissolved oxygen in seawater has a major influence on corrosivity because oxygen is the principal reactant involved in the cathodic reaction and is involved in the passivation reactions that occur for most metals and alloys in seawater. The solubility of oxygen decreases as the temperature is increased. The oxygen content in surface seawater can be as high as 11–12 ppm in the arctic as compared with 6 ppm in the tropics. Oxygen solubility in surface seawater can become supersaturated by as much as 200% of its equilibrium concentration because of photosynthesis by marine plants[19] and by wave action.[19,23,24] The change in the degree of saturation of the surface waters, with respect to the major atmospheric gases, depends on the aerosol productivity of

TABLE 3 Average Surface Temperature (°C) of the Oceans as a Function of Latitude

North Latitude	Atlantic Ocean	Indian Ocean	Pacific Ocean	South Latitude	Atlantic Ocean	Indian Ocean	Pacific Ocean
70°–60°	5.60	–	–	70°–60°	–1.30	–1.50	–1.30
60°–50°	8.66	–	5.74	60°–50°	1.76	1.63	5.00
50°–40°	13.16	–	9.99	50°–40°	8.68	8.67	11.16
40°–30°	20.40	–	18.62	40°–30°	16.90	17.00	16.98
30°–20°	24.16	26.12	23.38	30°–20°	21.20	22.53	21.53
20°–10°	25.81	27.23	26.42	20°–10°	23.16	25.85	25.11
10°–0°	26.66	27.88	27.20	10°–0°	25.18	27.41	26.01

Source: Data courtesy Prentice Hall.

FIG. 3 Corrosion rate of low carbon steels at varying ocean depths.[14]



an individual whitecap.[23] As the level of dissolved oxygen increases from 100% saturation to 130% supersaturation, the production of aerosol droplets by the whitecap waves generated by a standard laboratory breaking wave was found to increase by a factor of 2.4 in the case of submicron radius droplets, whereas the generation of larger droplets ($r > 2.5$ μm) was observed to increase by at least a factor of 4.0. Conversely, the dissolved oxygen concentration can decrease and become undersaturated because of oxygen consumption created by the decomposition of organic matter.

The combined influence of these natural cycles on the dissolved oxygen content can vary as a function of seasonal changes and the ocean depth at any given location.[14] Oxygen solubility in seawater goes through a minimum at intermediate ocean depths: the depth of minimum oxygen solubility ranges from 400 m in the equatorial eastern Pacific to 2400 m in the Central Pacific Ocean. The minimum oxygen concentration at these ocean depths ranges from 0.16 to 6.4 ppm.[6]

Seawater temperature and salinity also affect the dissolved oxygen content, with temperature having a larger influence on the oxygen solubility. The general rule is that as either the temperature or the salinity is decreased, the dissolved oxygen content increases.[1,6] The equilibrium concentration of dissolved oxygen in seawater as a function of salinity and temperature is shown in table 4.[6]

The effect of the dissolved oxygen level on corrosion depends on the metal or alloy. For metals or alloys that form passive films like stainless steel and aluminum, a high oxygen content is favorable in that it helps to delay the initiation of pitting on the metal surface. Once pitting is initiated, however, the propagation rate is increased with high oxygen content in the seawater. For common steels and copper alloys, the effect of

TABLE 4 Equilibrium Concentration of Oxygen in Seawater as a Function of Temperature and Salinity

	Salinity (ppt)					
	0	8	16	24	31	36
Temperature, °C	Oxygen Solubility (ppm) at Specific Salinity Levels					
0	14.6	13.9	13.1	12.4	11.8	11.4
5	12.5	11.9	11.3	10.7	10.2	9.9
10	10.9	10.4	9.8	9.4	8.9	8.7
15	9.5	9.1	8.7	8.2	7.9	7.7
20	8.5	8.1	77.7	7.3	7.0	6.8
25	7.6	7.2	6.9	6.6	6.3	6.2
30	6.8	6.5	6.2	6.0	5.7	5.6

Source: Calculated based on data from Dexter et al.[6]

dissolved oxygen depends on the seawater flow velocity. The oxygen concentration has a negligible effect on copper alloy corrosion rates in quiescent seawater, while at a seawater flow rate of 1.8 m/sec, an increasing oxygen content accelerates the copper corrosion rate. For metals such as iron and steel, the corrosion rate increases linearly with an increasing oxygen concentration at a constant temperature.[14,25]

Oxygen concentration cells can be created from deposits on a metal's surface or may be due to improper component design, which introduces crevices. Differences in oxygen content due to discrete films or deposits randomly scattered along a metal surface can cause pitting or crevice corrosion at these localized sites. In contrast, complete coverage of a surface by a film or a deposit can provide an effective barrier and reduce corrosion of the metal.[6,26]

SALINITY

Salinity in marine atmospheres accelerates metallic corrosion and varies within broad limits, ranging from extremely high values close to surf to low values near calm waters. The concentration of marine aerosol in the atmosphere depends on several factors, such as altitude, distance from the sea, land geography, land topography, direction, and velocity of prevailing winds.[27]

Salinity is defined as the total weight of solids dissolved in 1,000 g of water. For example, 35 parts per thousand ($^{o}/_{oo}$) salinity is equivalent to 35 g of solids dissolved in 1,000 g of water or a dissolved matter content of 35,000 ppm.[14] Salinity usually is determined by measuring chlorinity and then deriving the salinity from the following relation:

$$S = 1.80655\ Cl, \quad (1)$$

where S (salinity) and Cl (chlorinity) are measured in parts per thousand.[1,6]

The salinity of open ocean water at the surface typically varies from 32 to 37.5$^{o}/_{oo}$. Generally, this degree of variation does not alter metal corrosion rates. Some of the more isolated seas, such as those shown in table 5, can have large variations in salinity, which may influence metal corrosion rates. Salinity variations can affect a metal's uniform corrosion rate. For example, in areas with high evaporation rates, the salinity can be very

TABLE 5 Total Solids in Different Seawater Locations

Body of Water	Total Dissolved Solids, ppm
Baltic Sea	8,000
Caspian Sea	13,000
Black Sea	22,000
Irish Sea	32,500
Atlantic Ocean	37,000
Mediterranean Sea	41,000
Arabian Sea(Doha, Kuwait)	39,000–47,000
Dead Sea	260,000

Source: Compiled from various sources.

high. Conversely, at the mouth of a river, seawater salinity is more dilute than in open ocean water.

Variations in salinity also alter the localized corrosion resistance of metals in seawater. As the salinity is increased, the chloride ion activity increases and can result in increased pit and crevice corrosion initiation and propagation.[6]

pH AND CARBONATES

The pH of open ocean water varies from approximately 7.5 to 8.3 and is buffered by a complex carbonate system. This variation in pH does not affect the corrosion of most metals, except for aluminum. As the pH decreases from 8.3 at the surface to 7.5–7.7 in deep water, the initiation of pitting and crevice corrosion in aluminum alloys is accelerated.[1,6]

Depending on various conditions, calcareous deposits form when the solubility of calcium and magnesium ions is exceeded. Calcareous deposits form at pH levels between 8 and 10 and consist mainly of calcium carbonate ($CaCO_3$), magnesium carbonate ($MgCO_3$), and magnesium hydroxide ($Mg(OH)_2$).[14] Although changes in pH do not directly alter the corrosion behavior of most metals, pH variations can influence the formation of protective calcareous scales that subsequently can affect the corrosion rate of the substrate alloy. Spontaneous calcareous deposits are more likely to occur at higher pH values, but the function of these deposits is limited because of the presence of organic matter and seawater salinity.[16]

At the surface, the ocean waters throughout most of the world are 200 to 500% supersaturated in $CaCO_3$ and precipitation of these carbonate scales will influence the corrosion reaction occurring at the metal surface.[6] The buildup of protective calcareous deposits by cathodic protection can lower the subsequent current demand in natural seawater.[28–30]

Dilute seawater is undersaturated in carbonates, which reduces the likelihood of forming protective calcareous films on a metal surface. In deep ocean waters, the calcareous deposits are not spontaneously formed in an ambient environment and often are not precipitated under cathodic protection conditions.[6] In the cold waters of the deep ocean environmental zones, the precipitation and dissolution of the calcareous deposits is controlled mainly by the $CaCO_3$ saturation level, Ω:[31]

$$\Omega = [Ca^{+2}][CO_3^{-2}]/K'_{sp}, \quad (2)$$

where:

$[Ca^{+2}]$, $[CO_3^{-2}]$ = calcium, carbonate measure concentrations, respectively;

K'_{sp} = apparent solubility product; and

$\Omega = CaCO_3$ saturation value.

The calcareous deposits formed by cathodic protection will be stable when the degree of saturation is $\Omega > 0.6$ as in most ocean areas down to depths of 3,000 m.[31] At depths greater than 3,000 m, however, the $CaCO_3$ formation may be unstable. At $\Omega = 0.6$, the dissolution rate of $CaCO_3$ may be at around 1 µm/y.

BIOLOGICAL ORGANISMS

Seawater is a living medium sustaining a wide variety of organisms.[32] Marine biological organisms consist of either micro (bacterial) and macro (algae, barnacles) speciation. These organisms can affect the corrosion behavior of metals and alloys in a number of ways, including the following: (1) influencing one or both of the anodic and cathodic reactions occurring, (2) influencing the formation or maintenance of protective films, (3) producing deposits on metal surfaces, and (4) creating a corrosive environment. The previous factors can act singly or can be combined to alter a metal's corrosion behavior.[26]

One of the keys to the alteration of the condition at the metallic surface, and the subsequent delay or acceleration of corrosion, is the formation of a biofilm. The exact sequence of events leading to biofilm formation depends on the environment and the organisms present.[32] Biological organisms can attach and multiply on any solid surface in seawater. Within 2 h of immersion, a nonliving organic conditioning film develops on a solid surface. Within the first 1–2 days, a bacterial slime film develops over the conditioning film. The slime film creates a partial barrier to diffusion between the liquid–metal interface and the bulk seawater environment. Slime films usually are not continuous and can create oxygen or chemical concentration cells on the metal surface, which can result in accelerated localized corrosion.

Biofilms are structured, but complex assemblages of microorganisms embedded in exopolymers (extracellular material produced by microorganisms that define their shape, their ability to adhere to solid surfaces, and their ability to trap particulate nutrients).[32] Biofilms include communities of colonies, consortia, newly created cells, dying cells, extracellular products, polymers, and trapped inorganic material. Biofilms and individual organisms that are contained within the biofilm interact with external influences originating from the substratum and the bulk medium to cause oxygen or chemical concentration gradients and other localized effects related to mitigating or accelerating corrosion.[32,33]

Ammonia and sulfides also can be produced from the decay of organic matter within the slime film, resulting in increased corrosion of some alloys.[34] Sulfur-oxidizing organisms produce sulfuric acid from sulfur or other reduced sulfur species.[34] The presence of ammonia is known to cause stress corrosion cracking (SCC) of copper alloys, whereas sulfides may lead to an accelerated attack on copper alloys and steel. The presence of the slime film on the metal surface can locally change the local environment at the liquid–metal interface such that the corrosion behavior of a metal can be considerably altered from one that

normally displays low corrosion rates in seawater to conditions in which corrosion is accelerated.[6]

The reduction or complete elimination of marine organisms in dilute seawater reduces the probability of forming protective biofilms and could result in increased metal corrosion caused by a different mechanistic pathway.[14]

Macrofouling films begin to develop over the conditioning and slime films within 2–3 days after immersion in seawater.[6] If the macrofouling is continuous along the solid surface, the film can decrease the amount of dissolved oxygen present at the surface and thus decrease the overall metal corrosion rate. If, however, the macrofouling is discontinuous, the film acts in the same manner as discontinuous slime films in which case oxygen or chemical concentration cells can be formed and result in localized corrosion of the metal.[6]

The macrofouling organisms attach in embryonic form to the slimed solid surfaces. Once attached, they metamorphose and mature. The most common sessile fouling organisms in seawater include the following: (1) organisms with hard shells, annelids, barnacles, encrusting bryzoa, mollusks, and corals; and (2) organisms without hard shells, such as marine algae, filamentous bryzoa, coelenterates or hydroids, tunicates, and calcareous and siliceous sponges.[14] The accumulation of these biological organisms depends on specific environmental conditions. Conditions that are most conducive to their development are (1) relatively shallow water such as in a harbor, (2) warm temperatures, (3) low seawater flow, and (4) smooth hard surfaces.[26]

Both macro- and microfouling can have a major impact on the performance of marine components.[6,14,26] Macro- and microfouling organisms can break down protective paint films on a component surface. On ship hulls, these organisms increase drag and power requirements. In heat exchangers, fouling limits the heat transfer and seawater flow, and severe fouling can cause complete blockage.[26] Fouling also shields the component surface from any oxygen supply, thereby creating the possibilities that differential aeration cells can develop. Fouling can cause catalytic effects.[7] Fouling, in addition to causing drag or blockage, can cause localized turbulence. Plant decay or secretion products from animal life can accelerate corrosion processes.[7]

FLOW VELOCITY OF SEAWATER

Fluid velocity can significantly affect metal corrosion rates in seawater by increasing anodic or cathodic species to the metal surface. Flow-assisted corrosion depends on variables such as water chemistry, pH, component geometry, surface roughness, biofouling, microbiologically influenced corrosion, pitting and crevice corrosion, water pollution and contamination, alloy composition and surface films, galvanic interaction, fluid velocity and mode, oxygen content, heat transfer rate, and temperature.[35]

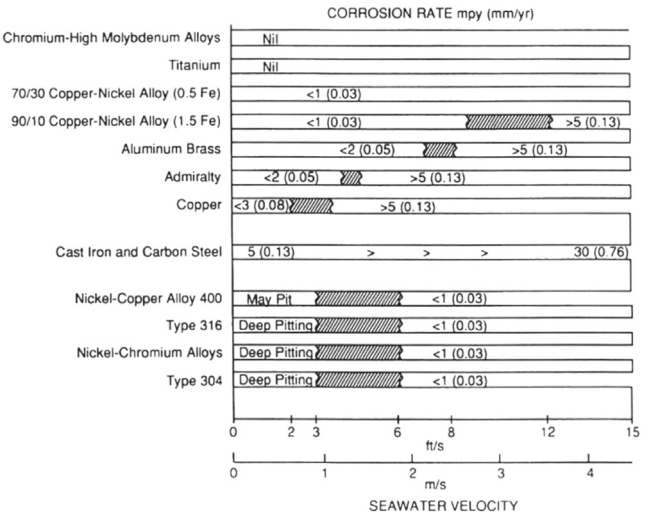
Corrosion rates and the type of corrosion often depend on environmental factors such as fluid flow and the availability of appropriate species required to drive electrochemical reactions.[36] A change in the motion of a corroding metal or alloy relative to its environment by fluid flow can increase corrosion rates by removing protective films or by increasing the diffusion or migration of deleterious species. An increase in fluid flow, however, can decrease corrosion rates by eliminating aggressive ion concentration or enhancing passivation or inhibition by transporting the protective species to the fluid–metal interface.[26]

Under high flow conditions, corrosion may take the form of impingement, erosion corrosion, or cavitation.[14] In any given velocity domain, different local velocities may exist over diverse areas of the component because of factors such as geometry or mode of fabrication.[2] The effect of seawater velocity on a metal's corrosion rate varies with the particular alloy. Alloys such as 304 and 316 stainless steel or nickel-chromium-molybdenum alloys exhibit deep pitting in static and low-flow conditions, yet at high seawater velocities, their corrosion rate decreases to less than 25 μm per year. Contrary to this, iron and copper show significantly lower corrosion rates at low flow velocities than under high seawater flow conditions.[37] The corrosion rates for various metals as a function of seawater velocity are included in figure 4.

Seawater velocity for immersed samples may decrease to a lower value as the seawater depth is increased; this decrease typically begins at depths of 18–30 m. Lack of flow can exacerbate crevice corrosion, which takes place with passive oxide film formers, such as stainless steels. When occluded, stagnant areas become oxygen-deficient anodic sites as compared with outer cathodic, oxygenated regions.[26,38]

Removal of the corrosion product or oxide layer by excessive flow velocities leads to increased corrosion rates of the metallic material, particularly when bounded in a piping or tubing system. Although corrosion rates often depend on fluid flow and the availability of appropriate species required to drive electrochemical reactions, surface shear stress is a measure of the force applied by fluid flow to the corrosion product film. For seawater, this takes into account changes in seawater density and kinematic viscosity with temperature and salinity.[39] Accelerated corrosion of copper-based alloys under velocity conditions occurs when the shear surface stress exceeds the binding force of the corrosion product film. Alloying elements, such as chromium, improve the adherence of the corrosion product film on

FIG. 4 Corrosion rate of metals and alloys in seawater as a function of flow velocity.[137] denotes critical range.



copper alloys in seawater based on measurements of the surface shear stress. The critical shear stress for C72200 (297 N/m^2, 6.2 lb_f/ft^2) far exceeds the critical shear stresses of both C70600 (43 N/m^2, 0.9 lb_f/ft^2) and C71500 (48 N/m^2, 1.0 lb_f/ft^2) copper-nickel alloys.[39]

Seawater turbulence can substantially alter the flow rates and subsequent corrosion rate of metals. Consider, for example, a seawater piping system that operates at a 1.8 m/sec velocity. Increases of pipe diameter will increase the thickness of the velocity boundary layer and the diffusion boundary layer. The thicker velocity boundary layer leads to a decreased velocity gradient and reduced shear stresses at the piping wall. For design purposes, a single-velocity value marking the initiation of erosion corrosion can provide misleading service life prediction.[35] Factors that affect erosion in pipe bends include the degree of internal ellipticity and asymmetry, sudden changes in cross-section, and a reduction in cross-sectional area.[40] As the radii of directional change are reduced, the erosion corrosion rates are expected to increase. Ledges, crevices, deposits, and other obstructions disturb laminar flow and result in turbulence at sometimes significant velocities.[26] In a turbulent area, such as downstream of a valve, velocities far exceeding the 1.8 m/sec nominal velocity may occur and cause accelerated corrosion of the metal. In testing piping systems, turbulent areas should be accounted for and mitigated by choosing appropriate erosion and cavitation-resistant materials[37] and by implementing a proper design.[41]

SULFIDES

Sulfides, sulfur, and other sulfur compounds can produce pitting, crevice corrosion, dealloying, SCC, and stress-assisted hydrogen-induced cracking of susceptible metals and alloys.[34] Polluted waters, like those found in coastal harbors and estuaries, contain hydrogen sulfide and sulfur-containing compounds. Sulfides can be generated in several ways: (1) bacterial reduction of naturally occurring sulfates in seawater; (2) rotting vegetation; and (3) industrial waste discharge.[35] Hydrogen sulfides are known to adversely affect the corrosion rate of various metals and alloys. Sulfates themselves are not usually harmful; however, sulfates can be reduced to harmful sulfides by sulfate-reducing bacteria. These sulfide pollutants can contribute to the corrosion of steels, stainless steels, copper, and aluminum alloys.[6]

Sulfide corrosion has been found to occur on a number of different copper-base alloys. Wrought 90/10 copper-nickel can exhibit sulfide-induced attack in the form of accelerated pitting with as little as 0.01 ppm sulfide concentration, whereas 70/30 copper-nickel is susceptible at sulfide concentrations of 0.05 ppm or greater.[42] The presence of sulfide-modified films interfered with the formation of normal passivating films of copper nickel alloys found in unpolluted waters.[43,44] Sulfide-modified films generally are more loosely adherent than the normal cuprous oxide films; turbulence tends to selectively remove the sulfide-modified films. The accelerated corrosion rates of copper-nickel alloys in aerated sulfide-containing seawater remain high because the sulfides prevent protective corrosion product layers from forming.[45]

A number of variables, including duration of sulfide exposure, system operating velocity, and degree of turbulence, must be assessed in conjunction with the sulfide concentration to accurately predict the sulfide susceptibility of copper-nickel alloys. Other research[14] on copper-base alloys has found that 3-ppm hydrogen sulfide significantly increases the corrosion rates of several copper alloys as indicated in table 6.

HEAVY METALS

Concentrations of copper in seawater can cause accelerated corrosion of metallic components. In unpolluted seawater, the copper concentration is 0.2 ppb, which typically is not high enough to influence a metal's corrosion behavior. If, however, the copper concentration is increased above approximately 30 ppb, corrosion of aluminum alloys can occur. The copper concentration may be increased because of a number of factors, including copper leaching from antifouling paints, pollutants containing copper, or nearby copper alloy corrosion. If the copper deposits onto aluminum alloy surfaces, a galvanic couple is formed, resulting in localized pitting of the aluminum.[6]

The corrosion products generated from iron and steel also have been known to cause corrosion of aluminum alloys in desalination plants. The iron contamination effects, however, are less and are not as consistent as they are for copper.[6]

Corrosion Mechanisms

Seawater is an aggressive, complex aqueous medium that has unique properties that affects most common structural materials somewhat differently than in most other natural media. As stated earlier, two competing processes operate simultaneously in seawater environments: (1) the chlorinity in seawater tends to destroy alloy passive films, while (2) dissolved oxygen acts to promote and repair passive films on metallic materials.[2] Although oxygen is the reactant involved in the major cathodic (oxygen reduction) reaction that occurs in seawater, species such as hydrogen (involved with cathodic protection applications), sulfates, nitrates, or ammonium compounds (related to reactions via bacteria or other microorganisms in polluted waters) can be involved in other cathodic reactions in seawater. Seawater is also

TABLE 6 Corrosion of Copper-Base Alloys in Clean and Polluted Seawater[14]

Seawater Velocity, 7.5 fps (2.3 m/sec), Test Duration, 64 Days

Alloy	CDA No.	Corrosion Rate, mpy (mm/yr)	
		Clean Seawater	Seawater (3 ppm H_2S)
90/10 Cu-Ni	706	3 (0.08)	34 (0.86)
70/30 Cu-Ni	715	5 (0.13)	26 (0.66)
2% Al Brass	687	3 (0.08)	22 (0.56)
6% Al Brass	608	5 (0.13)	21 (0.53)
As-inhibited admiralty brass	443	13 (0.33)	35 (0.89)
Phosphor copper	122	14 (0.36)	105 (2.67)

a conductive medium because of its inherent electrolyte content, leading to reactions detrimental to alloy performance.

Corrosion can occur by numerous pathways. Fontana and Greene.[46] list eight forms of corrosion: (1) uniform corrosion, (2) pitting, (3) crevice corrosion, (4) galvanic corrosion, (5) intergranular corrosion, (6) selective leaching or dealloying, (7) erosion corrosion, and (8) stress corrosion. Some of these "classic" forms of corrosion are somewhat simplistic and are discussed in more detail.[47] Some additional background information on these corrosion mechanisms is discussed in "Corrosion Testing."

Uniform corrosion is characterized by an electrochemical–corrosion reaction that proceeds over an entire surface area. This form of corrosion can be measured easily and is conducive to prediction of component failure.

Pitting is a mode of localized dissolution leading to the formation of cavities within a passivated surface that is boldly exposed.[47] Pitting is a probabilistic or stochastic corrosion mechanism that depends on electrochemical potential, alloy chemical composition and microstructure, electrolyte composition, and temperature.[47] Natural seawater, with a relatively high concentration of chlorides, contributes to the development of pitting of passive alloys, such as stainless steels.

Pitting corrosion usually initiates at surface inhomogeneities, such as intermetallic phases, nonmetallic inclusions, grain boundaries, dislocations, defects, or mechanically damaged sites.[47] At low potentials, pitting is followed by repassivation; this is termed metastable pitting. Above a certain potential or potential range, a transition from metastable pitting to stable pitting formation occurs. If the environmental conditions do not change in the anodic pit site(s), the pit continues to grow, in part, because of the large cathode (where oxygen reduction occurs)-to-anode ratio over the specimen or component surface.

Crevice corrosion is localized corrosion that occurs within crevices or at shielded surfaces where a stagnant solution exists. To develop as a corrosion site, a crevice must be wide enough to permit entry of a corrodent but sufficiently narrow to cause and maintain a stagnation environment. Crevices can be formed at metal-metal or nonmetal-metal junctions or at holidays that form in coatings on metals or alloys. The parameters leading to geometries that will cause crevice corrosion of an alloy are difficult to quantify.[46] Like pitting, crevice corrosion involves both initiation and propagation processes. During the initiation stage, discrete areas develop within the crevice.[48,49] In a creviced site exposed to a seawater environment, the crevice becomes oxygen deficient. The increasing concentration of metal cations causes an associated migration and buildup of chloride ions within the crevice to maintain electroneutrality. Metal chlorides then are hydrolyzed by water to form an insoluble metal hydroxide and free acid (in the case of chloride environments, HCl) thus creating overall acidification of the crevice site. The loss of oxygen, chloride ion buildup, and acidification, and a large IR drop between the boldly exposed cathodic sites outside of the crevice and the anodic crevice propagate crevice corrosion.[50]

Under-deposit attack or "poultice" corrosion may occur when a metal is locally covered by foreign, absorbent (organic or inorganic) materials.[46,51] In this case, attack can proceed even when the bulk of the system is dry due to retention of moisture in the poultice. The corrosion mechanism is similar to crevice corrosion in that the deposits act to limit the migration of oxygen to the covered area. This leads to acidic shifts in pH, concentration of Cl^- ions in the shielded area, and a shift to a more active corrosion potential under the deposit. Local corrosion rates can be extremely high because of the large cathode-to-anode area ratio.

The coupling of dissimilar alloys in conductive, corrosive solutions, such as seawater, is called galvanic corrosion and can lead to accelerated corrosion of the more anodic, electronegative alloy and protection of the more cathodic, electropositive alloy. The extent of galvanic corrosion depends on the following factors: (1) the effective area ratio between the anodic and cathodic members of the couple; (2) solution conductivity; (3) flow characteristics of the solution; (4) temperature; (5) system geometry; (6) the potential difference of the dissimilar alloys; (7) solution composition and environment; and (8) the cathodic efficiency of the more noble metal or alloy.[52–54] Galvanic corrosion and erosion corrosion can synergistically attack the passive films of susceptible alloys. Galvanic action between dissimilar metals can destroy the passive film of the more anodic member exposing the bared substrate to possible erosion corrosion. The removal of the protective films on copper-nickel alloys by flow may promote dissolution of the bare, exposed areas by galvanic interaction with the surrounding surfaces covered by corrosion product scales.

Under certain conditions, grain boundary interfaces are quite reactive, causing intergranular corrosion. Intergranular corrosion can be caused by impurities at the grain boundaries, or enrichment or depletion of one of the alloying elements in the grain boundary region.[43] Iron segregation at the grain boundaries of aluminum alloys can initiate intergranular corrosion. Depletion of chromium makes sensitized, unstabilized, austenitic stainless steels susceptible to intergranular corrosion.[46] A form of intergranular corrosion called knife-line attack may occur on welded, stabilized austenitic stainless steels if proper post-weld heat treatment is not implemented.[46]

Dealloying is the selective removal of one element from an alloy by corrosion processes. Dealloying, also called selective leaching, parting, and selective corrosion, is a type of corrosion found in some solid solution alloys. When in suitable conditions, a component of the alloys is preferentially leached from the material leaving a modified residual microstructure.[55,56] The most common example is the selective removal (dezincification) of zinc in brass alloys. Dezincification may either be plug-type or uniform. In other alloy systems, aluminum, iron, cobalt, nickel, chromium, and other elements may be selectively removed.[57] The less noble metal is removed from the alloy by a microscopic-scale galvanic corrosion mechanism. Little work has been done in differentiating susceptibility of selective leaching of alloys in synthetic seawater (this usually refers to ASTM D1141, *Standard Practice for the Preparation of Substitute Ocean Water*) and natural seawater.[6]

A change in the motion of a corroding metal or alloy relative to its environment by fluid flow can increase corrosion rates

by removing protective films or by increasing the diffusion or migration of deleterious species. An increase in fluid flow also can decrease corrosion rates by eliminating aggressive ion concentration or enhancing passivation or inhibition by transporting the protective species to the fluid–metal interface. Accelerated corrosion resulting from flow has been termed flow-assisted, flow-influenced, flow-induced, or flow-accelerated corrosion. Several mechanisms are described by the conjoint action of flow and corrosion that result in flow-influenced corrosion: (1) mass transport–controlled corrosion; (2) phase transport–controlled corrosion; (3) erosion corrosion; and (4) cavitation.[58–59]

Mass transport–controlled corrosion implies that the rate of corrosion depends on the convective mass transfer processes at the metal–fluid interface. Mass transfer can have a significant effect on corrosion rates of metals and alloys depending on factors, such as bulk solution chemistry, temperature, flow conditions, surface roughness, and geometry.

Phase transport–controlled corrosion suggests that the wetting of the metal surface by a corrosive phase is flow dependent. This may occur because one liquid phase separates from another or because a second phase forms from a liquid. The distribution and morphology of the corrosive attack will be related to the distribution of the corrosive phase; the corroded sites will frequently display rough, irregular surfaces and be coated with or contain thick, porous corrosion deposits.[35]

Erosion corrosion is associated with a flow-induced mechanical removal of the protective surface film that results in subsequent corrosion rate increases through either electrochemical or chemical processes. It is often accepted that a critical fluid velocity must be exceeded for a given material. The mechanical damage by the impacting fluid imposes disruptive shear stresses or pressure variations on the material surface or the protective surface film. Erosion corrosion may be enhanced by particles (solids or gas bubbles) and affected by multi-phase flows.[35] Increased flow stream velocities and increases of particle size, sharpness, density, and concentration increase the erosion corrosion rate. Increases in fluid viscosity, density, target material hardness, or pipe diameter tend to decrease the corrosion rate. The morphology of surfaces affected by erosion corrosion may be in the form of shallow pits or horseshoes or other local phenomena related to the flow direction.

Factors that affect erosion in pipe bends include the degree of internal ellipticity and asymmetry, sudden changes in cross-section, and reduction in cross-sectional area.[40] As the radii of directional change are reduced, the erosion corrosion rate is expected to increase. Ledges, crevices, deposits, and other obstructions disturb laminar flow and result in turbulence at significant velocities.[46] Short distances less than 10 diameters after directional changes or obstructions do not allow turbulence to dissipate.[60] Above a critical Reynolds (Re) number, a given surface roughness increases mass transfer and the critical Re number decreases with increasing roughness.[61] During testing, Poulson[61] observed that failures that occurred on the bend intrados about 45° into an 180° copper pipe bend were associated with possible flow separation, whereas surface roughening occurred only at high Re numbers.

Copper-based alloys are susceptible to a critical surface shear stress in seawater where the corrosion product film begins to break down and is removed from the alloy surface, subsequently causing accelerated attack.[62] The generally accepted critical velocity for 70/30 copper-nickel in unpolluted seawater is about 15 fps (4.5 m/s).[62] Copper-based alloys are susceptible to a critical surface shear stress in seawater where the corrosion product film begins to break down and is removed from the alloy surface, thereby initiating accelerated attack.[62] The generally accepted critical velocity for 90/10 copper-nickel (C 70600) is about 12 fps (3.6 m/s)[63] for large piping sizes before erosion corrosion becomes a problem. This corresponds to a critical shear stress of 43 N/m^2 (0.9 lb_f/ft^2). Erosion corrosion rates also depend on parameters such as pH, dissolved oxygen content or other entrained gases, and temperature.

Cavitation sometimes is considered a special case of erosion corrosion and is caused by the formation[64] and collapse of vapor bubbles in a liquid near a metal surface. Cavitation is a process by which a liquid is ruptured by decreasing the pressure at roughly constant liquid temperature. Cavitation removes protective surface scales by the implosion of gas bubbles in a fluid; calculations have shown that the implosions produce shock waves with pressures approaching 60 ksi.[46] Cavitation damage often appears as a collection of closely spaced, sharp-edged pits or craters on the surface. It has been suggested[64] that the corrosion rate by cavitation can be influenced by surface roughness that permits a large number of nuclei for bubble formation. Under this condition, the concentration of deleterious ions in solution next to the metal surface will be greater, and the observed corrosion damage indicates that the steam bubbles may provide crevices or enhanced possibilities for dissolution at the solution-metal-steam interface.

Environmental cracking can take several forms: (1) SCC, (2) corrosion fatigue, and (3) hydrogen embrittlement. SCC is caused by the presence of a tensile stress and a specific corrosion medium to a susceptible alloy. Failures from corrosion fatigue of alloys occur with time after the application of repeated cyclic stresses below the yield stress in a corrosive environment. It is generally considered that steels stressed below a fatigue limiting stress will endure an infinite number of cycles without fracture in noncorrosive environments.[46] Corrosion fatigue is influenced by the corrosive medium, pH, temperature, oxygen content, and the presence of any contaminants. In seawater, aluminum bronzes and austenitic stainless steels retain about 70% and 80% of the normal fatigue resistance, whereas high-chromium alloys retain only 30% to 40% of normal fatigue resistance.[46]

Hydrogen embrittlement lowers the yield stress and the ultimate tensile stress of a metal or alloy from the penetration of atomic hydrogen into susceptible alloys. This may occur in seawater for high-strength steels subjected to overprotection from cathodic protection systems. The term hydrogen embrittlement is used to characterize the near-room-temperature effects of hydrogen on materials. Hydrogen can have a considerable effect on susceptible alloys when it enters into the atomic structure and causes embrittlement. Embrittlement phenomena, including the acceleration of crack formation and growth,

are well known, and hydrogen, generated from cathodic protection can be a considerable problem in areas of stress corrosion or corrosion fatigue. The effects increase as the strength of the steel increases and absorbed hydrogen has been a major cause of failure of components, structures, pipelines, and pressure vessels.[65] The amount of hydrogen available to enter the steel, and the ease with which it moves into the steel, is influenced by the nature of the environment in which the steel is placed. In seawater, where structures are protected from corrosion by cathodic protection, hydrogen is available at the metal surface, particularly in anaerobic (oxygen free) environments, because of the cathodic electrochemical reactions The main bacteria responsible for the enhancement of hydrogen entry are the sulphate-reducing bacteria (SRB).[66]

More recently, attention has been directed to the "ninth" form of corrosion, biologically influenced corrosion, which include studies on an area referred to as "ennoblement." The presence of biofilms on metals and alloys immersed in natural seawater produces a complex, heterogeneous chemistry along the metallic surface. It usually has been observed that passive alloys, such as aluminum, stainless steels, nickel-base alloys, or titanium, show an increase to more noble (electropositive) potentials or ennoblement of several hundred millivolts with exposure time in natural seawater, thus magnifying the potential differences that may exist between dissimilar alloys.[32,67–76] Ennoblement is likely caused by the formation of microbiological films, which increase the kinetics of the cathodic reaction.[67–75]

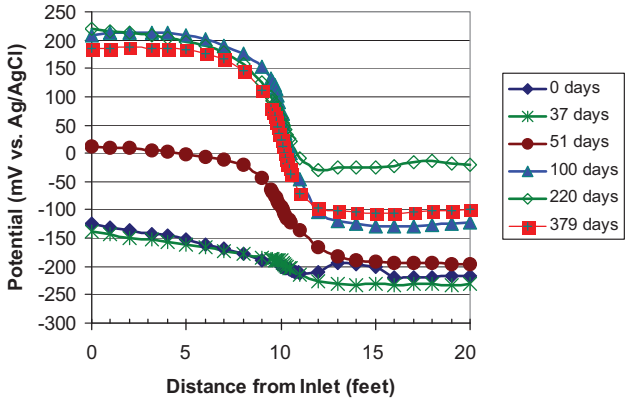
The ennoblement of these passive alloys by biofilms has been attributed to increasing the kinetics of the oxygen reduction reaction, or by the introduction of alternative redox reactions, such as peroxide production or heavy metal (Mn or Fe) reduction.[71] The ennoblement caused by the influence of cathodic reactions occurring on these passive alloys results in increasing the initiation and propagation of crevice corrosion,[29,73] pitting,[73] and galvanic corrosion.[75,76] However, if natural seawater is heated above 50°C to 60°C, the biofilm ceases to form and ennoblement does not occur.[77]

Figure 5 illustrates that the ennoblement of Alloy 625 occurred between 37 and 51 days of exposure to flowing natural seawater.[75,76] This ennoblement of Alloy 625 increased the driving force for increased galvanic corrosion of the 70/30 copper-nickel pipe.[76] Continued buildup of the microbiological film thickness gradually decreased the potential difference between the Alloy 625 and the copper-nickel alloy.[76]

Corrosion Testing

Corrosion testing is important in evaluating materials in seawater and related marine environments. Such tests can ascertain the performance of different materials, measure the degradation processes, and evaluate alternative materials and designs that optimize service life for given marine environments. Marine environments may include high-temperature oxidizing or reducing conditions found in marine gas turbines or waste incinerators; testing also may be done in the marine environmental zones discussed earlier. High-temperature testing for marine

FIG. 5 Alloy 625/70:30 copper-nickel piping couple. Potential profile shown as a function of time and location along the pipe (junction between the dissimilar alloys is located 10 feet [3 m] from inlet). *Source:* Courtesy of U.S. Navy.[76]



applications must consider the presence of seawater salts contained in the air intake of the turbines or waste incinerators because such electrolytes enhance the high-temperature corrosion processes of hot corrosion, sulfidation, and carburization.

Testing should be properly planned. Tests should be relevant and correlate with actual field use. Accelerated tests often provide useful information, but degradation processes in such tests may not reflect the actual corrosion mechanisms by which the materials naturally deteriorate. Testing may require laboratory, field, simulated service evaluations, or a combination of the tests. Specific test methods are discussed in the following sections.

Before testing components in most practical applications, one should be knowledgeable of the corrosion properties of possible candidate materials, an idea of the type and complexity of testing desired, and have a sufficient level of experience to comprehend possible materials interactions that a component may have with other material components and be able to interpret and translate the test results into the requirements of the service application.[6]

The objective for performing a corrosion test should be identified during the initial phase of designing the testing procedure. The test conditions, including specimen size, test environment versus service environment, geometry, sample preparation, temperature, flow velocity, potential, and type of corrosion test (e.g., general, crevice, pitting resistance, galvanic, stress-related, dealloying) should be considered.

LABORATORY EVALUATION

The corrosion behavior of metals or coatings is often evaluated in the laboratory rather than in an actual service environment because of time or budget limitations. Laboratory evaluation is generally of relatively short duration and is often used to study environmental effects on a metal's corrosion behavior because the specific environmental conditions can be controlled. The major disadvantage of testing in the laboratory is that the actual service environment and conditions may not be fully duplicated.

Service conditions are being simulated, which involves accepting certain assumptions. It is important when testing in the laboratory to correlate field data with laboratory data so that the validity of the laboratory information can be assessed.[78]

Natural seawater is the preferred environment for laboratory testing, but synthetic seawater solutions are often utilized. The term natural seawater refers to fresh seawater that is pumped directly into the laboratory, rather than seawater that has been stored and possibly shipped to an onshore location for the testing. Once seawater is removed from its natural environment, its composition changes, and this can have a large impact on the resultant metal corrosion rate. Synthetic seawater solutions that typically are used include 3.5-wt% NaCl and substitute ocean water per ASTM D1141.[79] The substitute ocean water can be used either with or without heavy metals added according to ASTM D1141.[79] Both 3.5% NaCl and substitute ocean water solutions do not contain the same organic and biological components as natural seawater. Substitute ocean water with heavy metals most nearly approximates the actual composition of natural seawater. The disadvantage in using any of the synthetic solutions is that, like the stored natural seawater, the composition varies from that of fresh, natural seawater and thus the corrosion behavior of the metals evaluated can be considerably affected. One advantage of using 3.5% NaCl is that calcareous deposits will not form under cathodic polarization conditions in this solution. This is extremely useful in fracture surface evaluation of metal specimens, where the presence of calcareous deposits often prohibits examination of the surfaces unless the deposits are dissolved or mechanically removed, which could alter the original fracture surface.

A primary goal of accelerated testing is to be able to perform tests over a short time period that can then be used to predict long-term performance (e.g., service life). To do this, two things must be determined. For example, in atmospheric corrosion testing, the rate of atmospheric corrosion must be quantified in both the field conditions being simulated and the accelerated test conditions. Direct measurements of the atmospheric corrosion rate typically are not available, making it necessary to derive the atmospheric corrosion rate from an indirect measurement, such as weight loss, corrosion product thickness, or, for laboratory tests, contaminant consumption rate. Second, the corrosion mechanisms (and resulting corrosion products) must be determined to be nominally identical for the two conditions—in other words, it must be established that the more aggressive conditions are accelerating the same mechanisms that exist under field exposure in such a manner that the final result is comparable to what is observed in the field. As such, it must be determined that new corrosion processes are not activated, or that the correct mechanisms are not altered in a manner such that the final result is different than field exposure. There are examples throughout the literature in which acceleration factors have been properly determined. Consider, as an example, the work of Pednekar[80] in evaluating the marine corrosion of AISI 1020 steel at Kure Beach, NC, and comparing those results with ASTM B117, *Standard Practice for Operating Salt Spray (Fog) Apparatus*, neutral salt spray exposure.[81] In their evaluation, researchers found that the nature and extent of corrosion after one-year exposure from 800 feet from the shore at Kure Beach, NC, was equivalent to 24 days' salt spray exposure.[80] Care must be taken in the interpretation and use of this data, however. The acceleration factor (approximately a factor of 15) applies only to the specific set of environmental conditions that were evaluated. When materials are exposed closer to the shore or at higher elevations from the shore, it was clearly demonstrated that the acceleration factor would be different.

IMMERSION TESTING

Immersion testing usually is performed on panel specimens or small component parts, such as fasteners. Specimens are exposed to the seawater environment in fully immersed, partially immersed, or alternately wetted and dried in a cyclic pattern. Sample weight loss, physical surface changes, visually assessed modifications, and surface compositional changes can be documented. For example, long-term uniform corrosion testing usually is performed in test racks or in test loops. Immersion testing is useful to examine different variables, such as environmental compositions, alloying elements, coating type, surface condition, and controlled defects. Immersion testing may be done in either natural or synthetic seawater. Natural seawater for laboratory immersion testing is often filtered to prevent macrofouling on the specimen surfaces. The filtering can be accomplished by passing seawater through a sequence of coarse to fine filters, with final filtering through 5- to 10-μm pore-size filter cartridges. Stagnant natural seawater solutions are not recommended for testing because of decay of the marine biological organisms, which will alter the seawater composition and can affect the resultant corrosion behavior.[71]

NACE/ASTM G31, *Standard Guide for Laboratory Immersion Corrosion Testing of Metals*,[82] describes accepted procedures for and factors that influence laboratory immersion corrosion tests. Factors that may influence test results may include sample preparation, apparatus, test conditions, methods of cleaning samples, evaluation of results, and calculation and reporting of corrosion rates. Natural seawater for laboratory immersion testing is often filtered to prevent macrofouling on the specimen surfaces. The filtering can be accomplished by passing seawater through a sequence of coarse to fine filters, with final filtering through 5- to 10-μm pore-size filter cartridges. Stagnant natural seawater solutions are not recommended for testing because of the decay of the marine biological organisms, which will alter the seawater composition and can affect the resultant corrosion behavior.[13]

During the alternative immersion corrosion test, ASTM G44, *Standard Practice for Exposure of Metals and Alloys by Alternate Immersion in Neutral 3.5% Sodium Chloride Solution*,[83] the specimen is immersed for a specified time period in a test environment then removed and dried before being re-immersed to continue the cycle. Normally, hundreds of these immersion-drying cycles are completed during the course of a test program. This standard is intended for alloy development for applied protective coatings on alloys and for applications where the alternate immersion test is to serve as a control test on the quality of successive lots of the same material. Alternative immersion would help distinguish performance of alloys or coated alloys exposed

to the marine tidal zone. Artificial seawater can replace the 3.5% NaCl solution, and although ASTM G44 often has been used to evaluate resistance to stress corrosion, it also has been used for uniform, pitting, crevice, and galvanic corrosion evaluations. In field testing, specimen racks may be placed between low-tide and high-tide levels with the objectives to observe performance of materials in the tidal zone.

SALT SPRAY/SALT FOG TESTING

Salt spray (fog) testing is an accelerated laboratory method for assessing the corrosion behavior of coated and uncoated metals. The generally accepted methods in the United States for salt spray testing are discussed in ASTM B117;[81] ASTM G85, *Standard Practice for Modified Salt Spray (Fog) Testing* (superseded);[84] and GM9540P.[85] These tests have been used successfully used to screen both coated and uncoated metals as well as to evaluate coating performance as shown in figure 6, particularly in terms of thickness uniformity and porosity. Cyclically acidified salt spray tests also have been used to determine the exfoliation corrosion resistance of aluminum alloys.[86]

A common atmospheric corrosion laboratory test, particularly when exploring the behavior of a material or an applied coating on alloys in marine environments, is the salt spray, or salt fog test. The environmental safety and health concerns associated with the salt spray technique are readily mitigated in most laboratory environments, and as such, this technique is appealing in an industrial setting. This procedure is of most use when evaluating materials for exposure to high-chloride environments, such as marine exposure. Because of its widespread use, and hence, the large body of data available for different materials acquired under nominally identical conditions, salt fog testing often is used as a generic metric for coating and material performance, irrespective of its applicability to any specific set of environmental conditions. In this test, as the name implies, the materials under test are exposed to a mist or fog of a salt solution for a period of time, and the degree of attack is used as a metric to gauge performance. Assessment of performance is typically qualitative in nature, assessing the total extent of corrosion, rather than making specific measurements as to the depth of attack.

FIG. 6 Example of salt fog cabinet capable of ASTM B117 and G85 of coated and uncoated alloys. *Source*: U. S. Navy.



A typical salt spray system consists of two basic components: the exposure chamber, and the salt spray/fog delivery system, both of which have a number of key features. The salt fog delivery system consists of a reservoir for the salt solution, a source of a compressed carrier gas, typically air, and one or more spray nozzles. The salt fog is created by feeding the compressed gas alongside the salt solution into the spray nozzles, where the solution is atomized and driven into the system. The chemistry of the salt solution (i.e., concentration, pH) varies depending on the specific environmental conditions being evaluated, but generally consists either of a simple sodium chloride solution or artificial seawater.

The second component of a salt spray system is the test chamber itself. The chamber is relatively simple in design, its key requirements being that it allow for the maintenance of the desired target temperature, that it deliver the salt fog, and that it provide an appropriate means to secure the specimens and ensure they are exposed only to the salt fog, and not condensate or corrosion product from other samples. Achieving proper exposure requires that the roof of the chamber, as well as all of the internal components, must be designed such that no liquid or condensation may fall on the specimens under test. Furthermore, the specimen racks are positioned such that condensation from one sample cannot fall onto another sample. Finally, a collection and removal system must be present to collect and remove condensed salt solution from the chamber such that it does not build up and allow the samples to be exposed to a bulk liquid phase.

Types of Salt Spray Environments

The solution used to generate the salt spray or fog generally is selected based on the material being investigated, and the environmental conditions in which the material or the applied organic coating on an alloy will be used. Although virtually any salt solution can be used, some standard solutions are described in a series of ASTM and ISO specifications, as well as in the literature.

5 wt% NaCl solution (ASTM B117;[81] ISO 9227, Section 3.2.2).[87] The standard solution for salt fog testing does not correspond to any particular set of environmental conditions. The test temperature is typically 35°C, and the solution pH is approximately neutral. This environment generally selected as a standard solution for comparing materials and generally is not used to ascertain specific performance characteristics in other environments.

Acetic acid-salt spray test (continuous or variable) (ASTM G85, Annex 1+2;[84] ISO 9227, Section 3.2.3).[87] This test solution consists of 5 wt% NaCl that has been pH adjusted to approximately 3 using acetic acid. Exposure is

performed at a temperature of 35°C. This test has been applied successfully to evaluate the impact that process parameters have on deposit quality for decorative chromium plating on steel or die-cast zinc, as well as for the evaluation of the overall quality of the plated deposit.

Seawater acidified test, cyclic (SWAAT) (ASTM G85, Annex 3).[84] The test solution in this exposure is ASTM artificial ocean water that has been pH adjusted to 2.8 to 3 with acetic acid. The test temperature is selected based on the material or property being assessed. This variant of the salt fog test has been applied to assess the performance of 2000, 5000, and 7000 series aluminum alloys, as well as to evaluate the performance of organic coatings on a variety of substrates.

SO_2 salt spray test, cyclic (ASTM G85, Annex 4).[84] The test solution consists of either a 5 wt% NaCl solution or ASTM artificial ocean water, and testing is performed at a temperature of 35°C. SO_2 is added periodically at a flow rate of 1 cm^3/min per cubic foot of cabinet volume (35 cm^3/min per m^3 of cabinet volume). The test is cyclic in nature, with specimens exposed to a series of cycles, the nature of which is dictated by the environmental conditions the test is attempting to probe. The test will consist of periods when the samples are exposed to salt fog, periods when they are exposed to SO_2, and a drying period. An example cycle might consist of 30-min exposure to salt spray, followed by 30-min exposure to the SO_2, and then finally a 2-h thermal soaking and drying period.

Dilute electrolyte cyclic fog dry test (ASTM G85, Annex 5).[84] In this test, the exposure solution is an 0.05 wt% sodium chloride and 0.35 wt% ammonium sulfate solution. Each cycle consists of 1-h salt fog exposure followed by 1-h dry-off period. During the fog portion of the cycle, the temperature is ambient/unheated. During the dry-off period, the chamber is heated to 35°C and specimens must be dry within 45 min. The cycling from wet to dry subjects the specimens to a range of solution concentrations varying from very dilute during the fog period to very concentrated just before the water dries off completely.

Copper-accelerated acetic acid-salt spray (CASS) ASTM B368, *Standard Test Method for Copper-Accelerated Acetic Acid-Salt Spray (Fog) Testing (CASS Test)*;[88] **ISO 9227 section 3.2.4).**[87] In this test, the test solution is made from 5 wt% NaCl to which 0.25 g of copper chloride ($CuCl_2 \cdot 2H_2O$) is added to each liter of the salt solution. The solution pH is then adjusted to between 3.1 and 3.3 using acetic acid. This test method is applicable to evaluating the corrosive performance of decorative copper/nickel/chromium or nickel/chromium coatings on steel, zinc alloys, aluminum alloys, and plastics designed for severe service. It is also applicable to the testing of anodized aluminum.

Accelerated Corrosion Tests GM9540P.[85] Test procedure provides combination of cyclic conditions (salt solution, various temperatures, humidity, and ambient environment) to accelerate metallic corrosion. The procedure is effective for evaluating several corrosion mechanisms, such as uniform, galvanic, and crevice. The test duration can be individually tailored to achieve any desired level of corrosion exposure. Synergistic effects resulting from temperature, mechanical, and electrical cycling can be comprehended by this test. The test method is composed of 1.25% g (0.9% sodium chloride, 0.1 o/o calcium chloride and 0.25% sodium bicarbonate) salt mist applications coupled with high temperature and high humidity and moderately high temperature dry-off.

Limitations of Salt Spray Testing

Although salt spray testing is simple to use, is readily accessible, and enables the ready differentiation between materials in terms of their relative corrosion performance in high chloride conditions, care must be taken to avoid over-interpretation of the results. There are only a few environmental conditions for which a salt fog experiment accurately reproduces the relevant corrosion mechanisms. Furthermore, there can be considerable variability in the test results as demonstrated in the work of Sterling,[89] in which a wide variety of copper alloys were exposed to several variations of the salt spray technique, resulting in considerable variability in weight change observations and no discernable trends in corrosion behavior. As such, careful consideration must be given to the nature and extent of corrosion that results from salt spray exposure. Because of the severe nature of the test, it is possible that the observed response does not probe degradation mechanisms relevant to field exposure. Therefore, before interpreting and assigning meaning to the results of a salt spray exposure, it must be determined whether the nature of the resulting corrosion damage is relevant to the intended application for which corrosion testing is being performed.

Another limitation of the salt spray test is that the coupons are not instrumented and not typically monitored throughout the test. It generally is not possible to measure electrochemical variables such as the open circuit potential or the polarization behavior of the surface during salt spray testing. Information is acquired by interrogating materials after the test has been completed, rather than continuously throughout the experiment. Interrupted testing is possible; however, removing and cleaning a material under evaluation can have a significant impact on the observed corrosion behavior and, as such, is not recommended.

Outdoor corrosion is influenced by a number of variables, including corrosive atmospheres, UV light, wet/dry cycling, and temperature cycling that can occur to varying degrees in environmental zones discussed earlier. ASTM D5894, *Standard Practice for Cyclic Salt Fog/UV Exposure of Painted Metal, (Alternating Exposures in a Fog/Dry Cabinet and A UV/Condensation Cabinet)*,[90] alternatively exposes samples to UV light with ASTM G85 salt fog exposures. Although salt spray testing is commonly used as a screening test, this method is not reliable for accurately predicting the corrosion rate of a metal in its service environment.[6]

ELECTROCHEMICAL TESTING

Electrochemical techniques utilize mixed-potential theory.[91] The corrosion potential, E_{corr}, or the open-circuit potential is the mixed potential in which the anodic and cathodic reactions are exactly equal. Applying a potential or a current to a sample in a

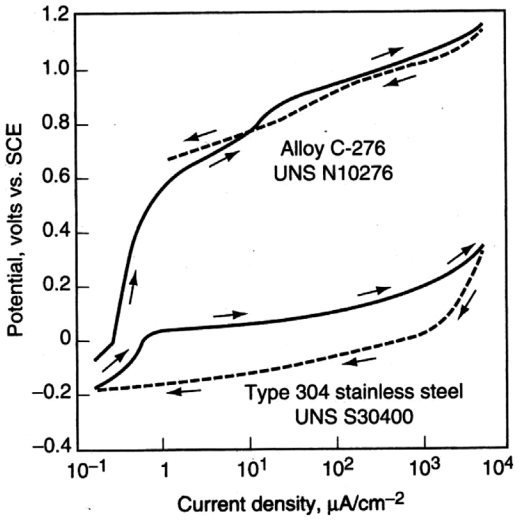
conducting electrolyte alters the relative balance of the anodic and cathodic reactions. Raising the potential in an electropositive direction relative to a reference electrode like a saturated calomel electrode (SCE) or a Ag/AgCl electrode will increase the anodic reaction on the sample relative to the cathodic reaction (electrochemical conditions become more oxidizing in place of preparing a more oxidizing solution chemically). Likewise, lowering the potential in an electronegative direction, lowers the anodic reaction leading to reducing conditions. The idealized potential versus log current density plots tend to show a linear relationship of potential versus current density termed the cathodic and anodic Tafel slopes, respectively. Raising or lowering the applied potential or applied current and then keeping it fixed as a function of time is a potentiostatic or galvanostatic polarization that commonly is used in electrochemical testing.

The electrochemical test setup generally consists of the usual three-electrode test cell, a potentiostat, and a computer loaded with the software to run various types of electrochemical tests. Specific methods include potentiodynamic polarization, potentiostatic polarization, galvanostatic polarization, Tafel extrapolation, and polarization resistance determinations that reproduce data and investigator check techniques.[92] In seawater, passive film-forming alloys like aluminum alloys or stainless steel require an induction time for pitting to occur, and thus the scan rate in a potentiodynamic test can significantly influence the results obtained. Also, the dynamic nature of these test methods may preclude the natural formation of films on a metal or alloy surface, which can cause the distorted results. Potentiostatic and galvanostatic polarization methods often are applied in studying localized corrosion. Electrochemical methods to measure the susceptibility of alloys to pitting corrosion are reviewed elsewhere.[93,94] The disadvantages associated with selecting the proper scan rate in the potentiodynamic method do not apply to the potentiostatic and galvanostatic methods.[86]

The Tafel extrapolation test is capable of determining very low metal corrosion rates in a short period of time. When conditions are ideal, its accuracy is equivalent to or better than weight loss measurements.[95–98] To maintain accuracy, however, the Tafel regions must encompass at least one order of magnitude of current. Also, this method can be applied only to systems that have one reduction process or the Tafel region may be distorted and corrosion rate determinations will be inaccurate. Finally, the Tafel method yields only an average, uniform corrosion rate and is not sensitive to localized corrosion. Therefore, use of this technique in seawater is considered to be limited primarily to obtaining an indication of the corrosion rate within an order of magnitude.[99,100] Tafel slope extrapolations are complicated by ohmic resistance from low conductivity solutions, cell geometry, and the magnitude of the applied current as well as from mass-transport, concentration polarization rather than activation control, charge-transfer processes.[101]

Laboratory tests involving electrochemical testing may provide instantaneous corrosion rates and ways to characterize corrosion thresholds before the onset of high corrosion rates or cabinet tests that provide a mean mass loss. Techniques may include Tafel extrapolation, polarization resistance, electrochemical impedance spectroscopy, electrochemical noise resistance, rotating disk, or cylinder electrodes to characterize corrosion affected by flow, polarization (either current- or potential-driven) methods for assessing susceptibility to localized corrosion (polarization, potential-step repassivation or scratch repassivation, electrochemical noise applied to pitting, and potentiodynamic repassivation for assessing sensitization.[102] ASTM G61, *Standard Test Method for Conducting Cyclic Potentiodynamic Polarization Measurements for Localized Corrosion Susceptibility of Iron-, Nickel-, or Cobalt-Based Alloys*, presents a standard for conducting cyclic potentiodynamic polarization measurements to determine relative susceptibility to localized corrosion (pitting and crevice corrosion) for iron-, nickel-, or cobalt-based alloys in a chloride environment.[103] An indication of the susceptibility to initiation of localized corrosion in this test method is given by the potential at which the anodic current increases rapidly, generally termed E_{bd} (E_{bd} depends on the scan rate of the potentiodynamic test, a higher scan rate will tend to have a higher E_{bd}).[104] The more noble E_{bd}, observed at a fixed scan rate during this test, the less susceptible the alloy is to the initiation of localized corrosion. When the scan is reversed, the localized corrosive stops when repassivation occurs at E_{prot}. The hysteresis loop forms from the resulting electrochemical behavior of the alloy of the corresponding forward and reverse potentiodynamic scans. The cyclic potentiodynamic test results are not intended to correlate in a quantitative manner with the rate of propagation that one might observe in service when localized corrosion occurs, but the size of the hysteresis is a qualitative measure of the localized corrosion susceptibility of the alloy; the larger the hysteresis, generally the more susceptible the alloy is to localized corrosion as shown in figure 7 for 304 stainless steel vice C-276.[102]

FIG. 7 Cyclic potentiodynamic polarization scans for 304 stainless steel and Alloy C-276 in 3.5% NaCl. The area of the hysteresis of the 304 SS cyclic is much larger than that generated from the cyxlic scan of C-276, indicating that 304 stainless steel is more susceptible to localized corrosion than C-276.[104]



ASTM G150, *Standard Test Method for Electrochemical Critical Pitting Temperature Testing of Stainless Steels and Related Alloys*,[104] determines the potential independent critical pitting temperature (CPT) by way of a potentiostatic technique using a temperature scan and a specimen holder that is designed to eliminate the occurrence of crevice corrosion in 1 M NaCl solution After an initial temperature stabilization period, a potential is applied to the test specimen that is above the pitting potential range and the solution is heated at a rate of 1°C/min. The current is monitored during the temperature scan, and the CPT is defined as the temperature at which the current increases rapidly, which for practical reasons is defined as the temperature at which the current density exceeds 100 $\mu A/cm^2$ for 1 min.

ASTM G192, *Standard Test Method for Determining the Crevice Repassivation Potential of Corrosion-Resistant Alloys Using a Potentiodynamic-Galvanostatic-Potentiostatic Technique* (superseded),[105] is a laboratory anodic polarization test method that measures the crevice repassivation potential by combining potentiodynamic, galvanostatic, and anodic polaotentiostatic polarization techniques. ASTM G192 is more time-consuming than the already well-established cyclic potentiodynamic polarization (CPP) described under ASTM G61. The crevice repassivation potential is the highest potential during potentiostatic control for which current density does not increase as a function of time. It is understood that at a potential below the crevice repassivation potential, an alloy will not develop crevice corrosion under the tested conditions. This test method may be used to rank several alloys by using the same testing electrolyte and temperature.

Many of the disadvantages discussed for the Tafel extrapolation method can be eliminated by using the polarization resistance technique. This nondestructive method can be used on systems that have either activation or diffusion controlled reactions. A comprehensive review of the polarization resistance method was compiled by Mansfeld.[106] Very low corrosion rates can be determined accurately and quickly and can be monitored as a function of time. Polarization resistance also can be used to measure the corrosion rate of a component, such as a seawater tank or piping system, where inspections and weight loss tests are difficult if not prohibitive. The major disadvantage with this technique is that, like the Tafel extrapolation method, the calculated corrosion rate represents a uniform value and does not indicate localized corrosion. Corrosion rates can be underestimated in low-conductivity solutions or when very high corrosion rates are experienced.[102]

Nondestructive Electrochemical Methods

Electrochemical impedance spectroscopy (EIS) has become a tool for practical corrosion prediction. EIS uses an applied small-amplitude, sinusoidal potential perturbation to the material in question and is useful for examining the corrosion behavior of both coated and uncoated metals and alloys.[100,107–118] EIS techniques record impedance data as a function of the frequency of the applied perturbation at a fixed potential. A large frequency range (1 mHz to 65 kHz) is needed to obtain a complete impedance spectra. This method is nondestructive and does not cause any acceleration of the corrosion reaction. The EIS technique can be used to monitor corrosion of a system or coating resistance as a function of time. EIS has demonstrated its usefulness for corrosion measurements involving: (1) rapid estimation of corrosion rates (within 30 min to 24 h); (2) estimation of extremely low corrosion rates and metal contamination rates ($<10^{-4}$ mm/yr, 0.01 mpy); (3) estimation of corrosion rates in low-conductivity media; (4) rapid evaluation of corrosion inhibitor performance in aqueous and nonaqueous media; and (5) rapid evaluation of coatings.[119] Decreases in the measured coating resistance suggest that an electrolyte has permeated through the coating, that there are defects in the coating, or that corrosion has initiated.[86] Reducing the distance between the working and counter electrodes to approximately 50 μm allows local EIS measurements to be done over uncoated and coated metal and alloy surfaces to discern surface inhomogeneities that may lead to corrosion initiation before corrosion is visually observed.[117,118]

Electrochemical noise (ECN) involves the nondestructive measurement of electrochemical transients or noise generated during corrosion processes without disturbing the system. Measurements are made by (1) monitoring potential noise through measurement of potential difference between two identical electrodes, (2) monitoring the current noise by assessing the current fluctuations between two short identical electrodes through a zero resistance ammeter, or (3) monitoring both potential and current perturbations. No external potential or current signal is applied during ECN measurements. The current noise is associated with discrete dissolution events. Electrochemical noise has been used to evaluate localized corrosion, SCC, or uniform corrosion in laboratory or field applications.[120–125] Electrochemical voltage or current noise can determine the onset of pitting or crevice attack.[126,127] ASTM G199, *Standard Guide for Electrochemical Noise Measurement* (superseded),[128] covers the procedure for conducting online corrosion testing and monitoring of metals using the ECN technique. ECN can be used to detect localized corrosion activity and to estimate corrosion rate on a continuous basis without removal of the monitoring probes from the plant or an experimental cell.[128] This guide covers zero-resistance ammeter-based current and potential measurements, potentiostatic current measurement with standard reference electrode, and galvanostatic potential measurements.

Direct Current Methods

Laboratory test methods include a number of direct current measurement techniques that are commonly used in electrochemical testing. Specific methods include potentiodynamic polarization, potentiostatic polarization, galvanostatic polarization, Tafel extrapolation, and polarization resistance determinations. In seawater, passive film-forming alloys like aluminum or stainless steel require an induction time for pitting to occur, and thus the scan rate in a potentiodynamic test can significantly influence the results obtained. Also, the dynamic nature of these test methods may preclude the natural formation of films on a metal or alloy surface, which can cause the distorted results. Potentiostatic and galvanostatic polarization methods often are applied when studying localized corrosion. Electrochemical methods to measure the susceptibility of alloys to pitting corrosion are reviewed

elsewhere.[118,119] The disadvantages associated with selecting the proper scan rate in the potentiodynamic method do not apply to the potentiostatic and galvanostatic methods.[117]

The Tafel extrapolation test is capable of determining very low metal corrosion rates in a short period of time. When conditions are ideal, its accuracy is equivalent to or better than weight loss measurements. To maintain accuracy, however the Tafel regions must encompass at least one order of magnitude of current. Also, this method can be applied only to systems that have one reduction process or the Tafel region may be distorted and corrosion rate determinations will be inaccurate. Finally, the Tafel method yields only an average, uniform corrosion rate and is not sensitive to localized corrosion. Therefore, use of this technique in seawater is considered to be limited primarily to obtaining an indication of the corrosion rate within an order of magnitude.[21,95]

HIGH VELOCITY FLOW TESTING

A variety of high velocity tests have been designed to simulate and evaluate cavitation and erosion properties in seawater environments. Specific tests are as follows: (1) high velocity flow tests, which include venturi tubes, rotating disks, and ducts with specimens positioned in the throat sections; (2) high-frequency vibration tests that utilize magnetostriction or piezoelectric devices (described in ASTM G32, *Standard Test Method for Cavitation Erosion Using Vibratory Apparatus*);[129] and (3) impinging jet tests where rotating or stationary specimens are exposed to a high-velocity jet or droplet impact described in ASTM G73, *Standard Test Method for Liquid Impingement Erosion Using Rotating Apparatus*).[130,131] A test loop using flowing artificial seawater and 1 wt% sand was able to evaluate the relative erosion resistance of materials under consideration for valves in a piping system.[132] ASTM G134, *Standard Test Method for Erosion of Solid Materials by Cavitating Liquid Jet*,[133] which can compare the cavitation erosion resistance of solid materials provides an alternative to ASTM G32. In ASTM, cavitation is induced by vibrating a submerged specimen at high frequency (20 kHz) at a specified amplitude. In ASTM G134, cavitation is generated in a flowing system so that both the jet velocity and the downstream pressure (which causes the bubble collapse) can be varied independently. This test method covers a test that can be used to compare the cavitation erosion resistance of solid materials. A submerged cavitating jet, delivering from a nozzle, impinges on a test specimen placed in its path so that cavities collapse on it, thereby causing erosion. ASTM G134 is carried out under specified conditions in a specified liquid, usually water.[133]

The test may deviate from actual service conditions. For example, do single or multi-phase (liquid-gas, liquid-solid particle, or liquid-gas-solid) conditions exist in marine environments that could affect the life of a material or corrosion control application? Is the flow laminar or turbulent? How is the fluid dynamics characterized? Are there contaminants or corrodents in the fluid that alone could cause degradation of passive films? Erosion-type tests should attempt to simulate disturbed turbulent flow conditions with sudden changes in flow geometry, such as bends, tube inlets, orifice plates, valves, fittings, pumps, compressors, or propellers. Fluid flow interactions with material surfaces should be defined in terms of wall shear stress or mass transfer coefficient.[134] LaQue developed several in-house apparati to evaluate mass transfer phenomena and wall shear stresses from relatively low velocity regimes to very high fluid flows over 100 fps.[135]

High velocity flow laboratory testing has a number of disadvantages. First, the results from these tests can vary widely because of differences in test technique, specimen size and shape, and environmental conditions like salinity, pH, temperature, and oxygen content. Second, these tests are designed to expose small specimens to high intensity flow conditions; however, the edges of the small specimens utilized can alter turbulent flow conditions in such a manner that the results do not simulate the actual service environment. The flow dynamics and conditions produced by the different high velocity techniques vary significantly. Although these high velocity laboratory tests may not accurately simulate the desired service condition, they are still useful in ranking different metals according to their resistance to velocity effects. For reproducibility among test laboratories, it is important to run a standard control material along with the candidate test materials so that the data can be normalized with respect to the control standard.[86,131]

ENVIRONMENTAL CRACKING TEST METHODS

A wide variety of SCC, corrosion fatigue, and hydrogen embrittlement tests to study environmental cracking phenomena have been developed. These tests, which employ either a static or a dynamic load, can vary widely in terms of specimen configuration, cost, and test duration. These tests may include the effects of cathodic protection on the susceptibility of materials to environmental cracking. In general, they fall into three major categories:

1. Constant displacement techniques include bent-beam, U-bend, wedge-open loading, and proving ring tests. In these tests, specimens are loaded to some fixed displacement and are exposed to the corrosive environment. Initiation of cracking causes the stress to be relieved, thus causing crack arrest. These tests tend to be plagued by a high degree of data scatter and, in many cases, do not result in providing useful design parameters. ASTM G30, *Standard Practice for Making and Using U-Bend Stress-Corrosion Test Specimens*,[136] describes the procedures for making and using U-bend specimens in metals and alloys for the evaluation of stress-corrosion cracking.[92] ASTM G38, *Standard Practice for Making and Using C-Ring Stress-Corrosion Test Specimens*, describes the essential features of the design and machining, and procedures for stressing, exposing, and inspecting C-ring type of stress-corrosion test specimens.[137] The C-ring, as generally used, is a constant-strain specimen with tensile stress produced on the exterior of the ring by tightening a bolt centered on the diameter of the ring. Preparation and use of bent-beam stress-corrosion test specimens are covered under ASTM G39, *Standard Practice for Preparation and Use of Bent-Beam Stress-Corrosion Test Specimens*.[138] ASTM G49, *Standard Practice for Preparation and Use of Direct*

Tension Stress-Corrosion Test Specimens (superseded), describes procedures for designing and preparing standard tension test specimens for investigating susceptibility to stress-corrosion cracking. Axially loaded specimens may be stressed quantitatively with equipment for application of either a constant load, constant strain, or with a continuously increasing strain.[139]

ASTM G36, *Standard Practice for Evaluating Stress-Corrosion-Cracking Resistance of Metals and Alloys in a Boiling Magnesium Chloride Solution*,[140] is an accelerated test method, using boiling magnesium chloride, to evaluate the relative ranking of stress corrosion susceptibility for stainless steels and related alloys in aqueous chloride-containing environments. ASTM G44[83] and ASTM G47, *Standard Test Method for Determining Susceptibility to Stress-Corrosion Cracking of 2xxx and 7xxx Aluminum Alloy Products* (superseded),[141] evaluate the stress corrosion susceptibility of stressed 2xxx and 7xxx aluminum alloy test specimens under alternative immersion in 3.5% NaCl solution. This test provides an environment for assessing the SCC resistance of materials similar to natural outdoor marine environments. Uniaxial direct tension SCC tests by alternate immersion in 3.5% NaCl (ASTM G44 and ASTM G49) show that during uniaxial loading, 5xxx alloys, when sensitized, are particularly susceptible to SCC when tested in the short-transverse orientation but are not susceptible to SCC when tested in the long-transverse orientations unless the alloy is fully recrystallized.[83,139]

Rising load techniques include the slow strain rate (SSR) test.[142] In this technique, axially loaded tension test specimens or fatigue precracked (fracture mechanics) specimens are subjected to a rising stress, typically applied by a screw-driven testing machine. SSR tests deliver a result in a reasonably short time, usually within 1–2 days. The dynamic straining reduces incubation time to the onset of cracking in susceptible materials and sustains the cracking process. The SSR method allows for evaluation of the effects of metallurgical variables, such as alloy composition, heat treatment, and processing and or environmental parameters in shorter times than is usually possible with constant load or stress specimens.[143] SSR evaluation of materials through environmentally assisted cracking (EAC) is generally obtained through the comparison of test results conducted in a corrosive environment versus corresponding SSR results obtained in an inert environment.[143] ASTM G129, *Standard Practice for Slow Strain Rate Testing to Evaluate the Susceptibility of Metallic Materials to Environmentally Assisted Cracking*,[144] describes steps for the design, preparation, and use of axially loaded, tension test specimens and fatigue precracked (fracture mechanics) specimens for use in SSR tests to investigate the resistance of metallic materials to EAC. Strain is imposed by an external means on the gauge section or notch tip of a uniaxial tension specimen or crack tip of a fatigue precracked specimen for materials evaluation. The slow constant extension produces a gauge section strain rate, which is usually in the range from 10^{-4} to $10^{-7}/s^{-1}$. The SSR test is used for relatively rapid screening or comparative evaluation, or both, of environmental, processing or metallurgical variables, or both, which can affect the resistance of a material to EAC.[142] SSR tests tend to produce conservative results (i.e., materials that show susceptibility in these tests may not show susceptibility in service) in a relatively short period of time. This conservatism may result from the fact that engineering structures are rarely loaded in this fashion. As such, these tests typically are used only to relatively rank susceptibility of materials to different environments.[143]

2. Load-controlled techniques include methods such as the cantilever beam test. In these tests, specimens are deadweight loaded to produce the desired stress. Any cracks that initiate then grow into an increasing stress field, resulting in failure of the specimen. Unfortunately, these tests are time-consuming and costly. A critical linear elastic stress intensity factor can be obtained from these tests, however, and this parameter subsequently can be used in design or to determine the flaw tolerance of an engineering structure. ASTM G139, *Standard Test Method for Determining Stress-Corrosion Cracking Resistance of Heat-Treatable Aluminum Alloy Products Using Breaking Load Method*,[145] evaluates SCC resistance using residual strength as the gauge of damage evolution through EAC by the breaking load test method. In this test, tensile bars or direct tension sheet specimens are exposed to 3.5 wt% aqueous sodium chloride solution, are removed before they fail, and are tension tested to determine the amount of corrosion damage that has occurred. This test method[145] was developed for use with high-strength, heat-treatable aluminum alloys (2xxx and copper-containing 7xxx).

   ASTM G168, *Standard Practice for Making and Using Precracked Double Beam Stress Corrosion Specimens*,[146] is a standard practice covers procedures for fabricating, preparing, and using precracked double-beam stress corrosion test specimens. This specimen configuration as formerly designated the double cantilever beam specimen. Guidelines are given for methods of exposure and inspection. The precracked double-beam specimen is conducive for evaluating a wide variety of metals exposed to corrosive environments. It is particularly suited to evaluation of products having a highly directional grain structure, such as rolled plate, forgings, and extrusions, when stressed in the ST direction. The precracked double-beam specimen may be stressed in constant displacement by bolt or wedge loading or in constant load by use of proof rings or dead weight loading. The precracked double beam specimen is amenable to exposure to aqueous or other liquid solutions by specimen immersion, by periodic drop-wise addition of solution to the crack tip, or exposure to the atmosphere.[146]

ASTM E1681, *Standard Test Method for Determining Threshold Stress Intensity Factor for Environment-Assisted Cracking of Metallic Materials* (superseded),[147] provides a standard method for determining a threshold stress intensity factor for EAC of metallic materials under constant load using a cantilever beam. The cantilever-beam technique utilizes long-term static load testing of fatigue precracked, single-edge notched beam specimens manufactured according to guidelines designed to produce plane-strain SCC data.[148] Test durations range from several hours to more than 10,000 h. The 10,000-h runout time is preferred to ensure sufficient time for crack incubation (hydrogen entry and transport to the crack tip region in the case of hydrogen embrittlement) without being excessively long. The threshold stress intensity (K_{Iscc}) obtained from these tests subsequently can be used in design or to determine the flaw tolerance of an engineering structure.

Two concepts are central to understanding the effects of mechanical, metallurgical, and chemical variables to corrosion fatigue. First, many variables, such as electrolyte composition and pH, are governed by mass transport and electrochemical reaction conditions within the crack. Second, corrosion fatigue can be time dependent.[149,150] The most common apparatus for conducting corrosion fatigue tests in seawater is the rotating beam type using a specimen machined to distribute stress uniformly along the gauge section when loaded. High-cycle fatigue specimens are loaded in uniaxial tension or bending (three-point, four-point, or cantilevered).[151,152] ASTM E466, *Standard Test Method for Conducting Force Controlled Constant Amplitude Axial Fatigue Tests of Metallic Materials*,[151] covers a standard procedure for the performance of axial force controlled fatigue tests to obtain the fatigue strength of metallic materials in the fatigue regime where the strains are predominately elastic, both upon initial loading and throughout the test. This practice is limited to the fatigue testing of axial unnotched and notched specimens subjected to a constant amplitude, periodic forcing function in air at room temperature. This standard was intended to evaluate steels and aluminum alloys in aqueous chloride solutions.[153,154]

For low-cycle fatigue ($<10^4$ cycles), tests are conducted with controlled cycles of elastic plus plastic total strain range rather than controlled load or stress cycles. ASTM E606, *Standard Test Method for Strain-Controlled Fatigue Testing* (superseded),[155] determines the fatigue properties of nominally homogeneous materials by the use of test specimens subjected to uniaxial forces. It is intended as a guide for fatigue testing performed in support of such activities as materials research and development, mechanical design, process and quality control, product performance, and failure analysis. Although this practice is intended primarily for strain-controlled fatigue testing, some parts of the standard test method may provide useful information for force-controlled or stress-controlled testing.

For a given material, the fatigue strength, or fatigue life at a given value of maximum stress, generally decreases in the presence of an environment that is aggressive to the material. The environment affects the fatigue crack initiation, the fatigue crack growth rate, or both.[156] ASTM E647, *Standard Test Method for Measurement of Fatigue Crack Growth Rates*,[157] determines fatigue crack growth rate (da/dN) from near-threshold to K_{max} (maximum stress intensity controlled instability).[158] Results are expressed in terms of the crack-tip stress-intensity factor range (ΔK), defined by the theory of linear elasticity. ASTM E647[159] is divided into two main parts. The first part gives general information concerning the recommendations and requirements for fatigue crack growth rate testing. The second part is composed of annexes that describe the special requirements for various specimen configurations, special requirements for testing in aqueous environments, and procedures for nonvisual crack size determination. In addition, appendices cover techniques for calculating da/dN, determining fatigue crack opening force, and measuring the growth of small fatigue cracks. This method is applicable in marine atmosphere and seawater.[157,168]

ASTM F1624, *Standard Test Method for Measurement of Hydrogen Embrittlement Threshold in Steel by the Incremental Step Loading Technique*,[159] establishes a procedure to measure the susceptibility of steel to a time-delayed failure caused by hydrogen. It does so by measuring the threshold for the onset of subcritical crack growth using standard fracture mechanics specimens, irregular-shaped specimens such as notched round bars, or actual product such as fasteners (threaded or unthreaded), springs, or components.[159] It also can be used to test the effect of hydrogen introduced into the steel caused by external environmental sources of hydrogen, such as excessive cathodic protection or galvanic coupling, in a marine aqueous environment.

Field Evaluation

IN-SERVICE TESTING

In-service testing provides the advantage of examining the corrosion behavior of a metal in the actual service environment. The advantages and disadvantages of some of these tests are briefly described below. More detail can be found in NACE/ASTM G31.[82] Guides for conducting corrosion testing under field conditions can be found under ASTM G4, *Standard Guide for Conducting Corrosion Tests in Field Applications*,[160] and ASTM G50, *Standard Practice for Conducting Atmospheric Corrosion Tests on Metals* (superseded).[161]

Small-Specimen Testing

Small-specimen testing allows a large number of variables to be evaluated at minimal cost. Small specimens can be designed to determine specific types of corrosion; for example, creviced specimens can be exposed to assess localized corrosion.[86] ASTM G16, *Standard Guide for Applying Statistics to Analysis of Corrosion Data* (superseded),[162] provides guidance for establishing the number of replicate samples required for the desired reliability of the test results.

Although small-specimen testing allows for examination in the actual service environment, the corrosion rate determined on a small specimen usually is not consistent with the corrosion rate of a large-scale piece of equipment primarily because it is difficult to duplicate all of the metallurgical conditions of the large equipment on a small specimen. In addition, it is difficult to

simulate erosion-corrosion by small-specimen testing, because small specimens can shield each other from turbulence, thus providing inaccurate results.[86] The use of spool pieces for piping and tubing may provide useful test information related to in-service performance for similar components.

Electrical Resistance Probes

Electrical resistance probes are small in size and can be installed easily in the service environment; however, the walls of the test equipment must be penetrated for the probes to be installed and, consequently, care must be taken to avert leakage in the system. The usefulness of the probes is limited in that they provide a measurement of uniform corrosion and can be continuously monitored, but they provide no information on localized corrosion, such as pitting or crevice corrosion. In addition, errors can result in the probe data if the temperature is varied during the time of the measurement.[86] ASTM B826, *Standard Test Method for Monitoring Atmospheric Corrosion Tests by Electrical Resistance Probes* (superseded),[163] describes a test method that employs a resistance monitor probe fabricated from a chosen metal conductor, with one conductor segment uncovered to permit exposure of the chosen metal conductor to the corrosive gas mixture and the second conductor segment covered to insulate the metal conductor of this segment from exposure to the corrosive gas mixture. The covered conductor segment provides a reference for evaluating changes in the uncovered segment. ECN can be utilized to conduct online corrosion monitoring of metals within the limitations of the ASTM G199 guidance.[128]

Ultrasonic Measurements

The ultrasonic thickness measurement method is quite popular for in-service corrosion testing. The major advantage of this method is that the equipment is portable and easy to use. The major disadvantage is that a bare metal surface is required for accurate measurements. The presence of coatings or corrosion products can introduce errors into the thickness measurements.[86] Curved surfaces such as piping bends and small tubing diameters require special attention.

SIMULATED SERVICE TESTING

Like in-service testing, simulated service testing provides the advantage of exposure to the actual environment. Fluctuations in the weather, the influence of geographical location, and bacteriological influences are part of the simulated service test environment and are factors that cannot be simulated in the laboratory.[86] Simulated service testing in seawater typically consists of panel specimens exposed on test racks suspended from a pier or a float.[13] Testing in this environment is discussed in ASTM G52, *Standard Practice for Exposing and Evaluating Metals and Alloys in Surface Seawater* (superseded).[164] Specimens may be exposed in full immersion, splash-spray, or tidal conditions. The disadvantage of exposing panel specimens in the full seawater immersion environment is the occurrence of extensive macrofouling on the panel surfaces. The presence of these organisms prohibits inspection of the test panels during the exposure period and can result in the difficult task of removing the macrofouling after testing to obtain accurate weight loss measurements. For coated specimens, removal of the macrofouling after testing could cause partial removal of the coating as well, making an accurate corrosion assessment impossible. For this reason, simulated service testing in the full immersion testing is often conducted using filtered natural seawater to eliminate microorganisms.

Standards for Seawater Testing

The following standards are specific to testing in seawater:

- ASTM G52, *Standard Practice for Exposing and Evaluating Metals and Alloys in Surface Seawater*
- ISO/CD 23226, *Corrosion of Metals and Alloys: Guidelines for Corrosion Testing of Metals and Alloys Exposed in Deep Sea Water*

The following standards apply only to artificial seawater environments:

- ASTM D1141, *Standard Practice for the Preparation of Substitute Ocean Water*
- ASTM D5894, *Standard Practice for Cyclic Fog/UV Exposure of Painted Metal, (Alternating Exposures in a Fog/Dry Cabinet and a UV/Condensation Cabinet)*
- ASTM E1524, *Standard Test Method for Saltwater Immersion and Corrosion Testing of Photovoltaic Modules for Marine Environments*
- ASTM G44, *Standard* Practice for *Exposure of Metals and Alloys by Alternate Immersion in Neutral* 3.5% *Sodium Chloride Solution*
- ISO 4623, *Paints and Varnishes—Filiform Corrosion Test on Steel*
- ISO 7384, *Corrosion tests in Artificial Atmosphere—General Requirements*
- ISO 16539, *Corrosion of metals and alloys—Accelerated cyclic corrosion tests with exposure to synthetic ocean water salt-deposition process—"Dry" and "wet" conditions at constant absolute humidity*

The standards listed below describe corrosion testing and data evaluation in natural seawater or artificial seawater environments:

- ASTM E606, *Standard Test Method for Strain-Controlled Fatigue Testing*
- ASTM E647, *Standard Test Method for Measurement of Fatigue Crack Growth Rates*
- ASTM E1681, *Standard Test Method for Determining a Threshold Stress Intensity Factor for Environment-Assisted Cracking of Metallic Materials*
- ASTM E739, *Standard Practice for Statistical Analysis of Linear or Linearized Stress-Life (S-N) and Strain-Life (ε-N) Fatigue Data*
- ASTM E1049, *Standard Practices for Cycle Counting in Fatigue Analysis*

- ASTM G1, *Standard Practice for Preparing, Cleaning, and Evaluating Corrosion Test Specimens*
- ASTM G3, *Standard Practice for Conventions Applicable to Electrochemical Measurements in Corrosion Testing*
- ASTM G4, *Standard Guide for Conducting Corrosion Tests in Field Applications*
- ASTM G5, *Standard Reference Test Method for Making Potentiostatic and Potentiodynamic Anodic Polarization Measurements*
- ASTM G16, *Standard Practice for Applying Statistics to Analysis of Corrosion Data*
- ASTM G30, *Standard Practice for Making and Using U-Bend Stress-Corrosion Test Specimens*
- NACE/ASTM G31, *Standard Guide for Laboratory Immersion Corrosion Testing of Metals*
- ASTM G32, *Standard Test Method for Cavitation Erosion Using Vibratory Apparatus*
- ASTM G38, *Standard Practice for Making and Using C-Ring Stress-Corrosion Test Specimens*
- ASTM G39, *Standard Practice for Preparation and Use of Bent-Beam Stress-Corrosion Test Specimens*
- ASTM G46, *Standard Practice for Examination and Evaluation of Pitting Corrosion*
- ASTM G47, *Standard Test Method for Determining Susceptibility to Stress-Corrosion Cracking of 2xxx and 7xxx Aluminum Alloy Products*
- ASTM G49, *Standard Practice for Preparation and Use of Direct Tension Stress-Corrosion Test Specimens*
- ASTM G59, *Standard Practice for Conducting Potentiodynamic Polarization Resistance Measurements*
- ASTM G61, *Standard Test Method for Conducting Cyclic Potentiodynamic Polarization Measurements for Localized Corrosion Susceptibility of Iron-, Nickel-, or Cobalt-Based Alloys*
- ASTM G69, *Standard Test Method for Measurement of Corrosion Potentials of Aluminum Alloys*
- ASTM G71, *Standard Guide for Conducting and Evaluating Galvanic Corrosion Tests in Electrolytes*
- ASTM G73, *Standard Test Method for Liquid Impingement Erosion Using Rotating Apparatus*
- ASTM G78, *Standard Guide for Crevice Corrosion Testing of Iron-Base and Nickel-Base Stainless Alloys in Seawater and Other Chloride-Containing Aqueous Environments*
- ASTM G82, *Standard Guide for Development and Use of a Galvanic Series for Predicting Galvanic Corrosion Performance*
- ASTM G100, *Standard Test Method for Conducting Cyclic Galvanostaircase Polarization*
- ASTM G102, *Standard Practice for Calculation of Corrosion Rates and Related Information from Electrochemical Measurements*
- ASTM G107, *Standard Guide for Formats for Collection and Compilation of Corrosion Data for Metals for Computerized Database Input*
- ASTM G129, *Standard Practice for Slow Strain Rate Testing to Evaluate the Susceptibility of Metallic Materials to Environmentally Assisted Cracking*
- ASTM G139, *Standard Test Method for Determining Stress-Corrosion Cracking Resistance of Heat-Treatable Aluminum Alloy Products Using Breaking Load Method*
- ASTM G150, *Standard Test Method for Electrochemical Critical Pitting Temperature Testing of Stainless Steels and Related Alloys*
- ASTM NACE/ASTM G193, *Standard Terminology and Acronym Relating to Corrosion*
- ASTM G199, *Standard Guide for Electrochemical Noise Measurement*
- GM9540P, *Accelerated Corrosion Test*
- ISO 1462, *Metallic Coatings—Coatings Other Than Those Anodic to the Basis Metal—Accelerated Corrosion Tests—Method for the Evaluation of the Results*
- ISO 4540, *Metallic Coatings—Coatings Cathodic to the Substrate—Rating of Electroplated Test Specimens Subjected to Corrosion Tests*
- ISO 7539, *Corrosion of Metals and Alloys—Stress Corrosion Testing, Parts 1–7*
- ISO 8993, *Anodized Aluminum and Aluminum Alloys—Rating System for the Evaluation of Pitting Corrosion—Chart Method*
- ISO 8994, *Anodized Aluminum and Aluminum Alloys—Rating System for the Evaluation of Pitting Corrosion—Grid Method*
- ISO 9591, *Corrosion of Aluminum Alloys—Determination of Resistance to Stress Corrosion Cracking*
- ISO 11306, *Corrosion of Metals and Alloys—Guidelines for Exposing and Evaluating Metals and Alloys in Surface Sea Water*
- ISO 11463, *Corrosion of Metals and Alloys—Evaluation of Pitting Corrosion*
- ISO 11782-1, *Corrosion of Metals and Alloys—Corrosion Fatigue Testing, Part 1: Cycles to Failure Testing*
- ISO 11782-2, *Corrosion of Metals and Alloys—Corrosion Fatigue Testing, Part 2: Crack Propagation Testing Using Precracked Specimens*
- ISO 11845, *Corrosion of Metals and Alloys—General Principles for Corrosion Testing*
- NACE RP0173-73, *Collection and Identification of Corrosion Products*

The following standards apply to atmospheric environments:

- ASTM B117, *Standard Practice for Operating Salt Spray (Fog) Apparatus*

- ASTM G33, *Standard Practice for Recording Data from Atmospheric Corrosion Tests of Metallic-Coated Steel Specimens*
- ASTM G50, *Standard Practice for Conducting Atmospheric Corrosion Tests on Metals*
- ASTM G84, *Standard Practice for Measurement of Time-of-Wetness on Surfaces Exposed to Wetting Conditions as in Atmospheric Corrosion Testing*
- ASTM G91, *Standard Practice for Monitoring Atmospheric SO2 Deposition Rate for Atmospheric Corrosivity Evaluation*
- ASTM G140, *Standard Test Method for Determining Atmospheric Chloride Deposition Rate by Wet Candle Method*

Corrosion Performance of Specific Materials

Metals and alloys commonly used in the seawater environment include carbon steels, stainless steels, nickel (Ni) alloys, copper (Cu) alloys, titanium (Ti) alloys, and aluminum (Al) alloys. All of these alloys exhibit differing degrees of corrosion resistance in seawater, and in general, coatings and cathodic protection often are applied to decrease the corrosion of these metals. The corrosion resistance within a class of alloys also may depend on metallurgical differences caused by fabrication and processing or heat treatments. Joining processes, such as welding, brazing, and soldering, use of adhesives or coatings, surface roughness, and proximity to dissimilar metals or alloys, also will cause changes in the corrosion resistance of materials.

Carbon steels corrode in aerated seawater conditions. Their corrosion rate decreases with time as protective barrier films are formed on the carbon steel surfaces. These protective films may be a rust layer, calcareous deposits, or biofouling. The corrosion rate of carbon steels increases in high-velocity seawater because the protective barrier layer is either not allowed to form or is stripped away under the flow conditions. Also, the available oxygen at the metal surface is increased in flowing seawater, which promotes a higher carbon steel corrosion rate. A 2.5-year study showed that immersion corrosion mass loss as a function of time for mild steel exhibits a characteristic monotonic bi-modal behavior, both for natural and for sterile seawater. The bimodal behavior can be explained as arising from a change from localized cathodic oxygen reduction to localized cathodic hydrogen reduction. This change is the direct result of the decreasing ability of oxygen to diffuse through the increasing thickness and reducing the permeability of rust layers as corrosion proceeds. The cathodic hydrogen reduction reaction is rate controlled by the outward diffusion of hydrogen through the rust layers.[165]

Stainless steels are used in a variety of applications in marine service. Stainless steels may be chosen for corrosion resistance, strength, resistance to flow velocity, weight savings, and fabricability. Stainless steels are susceptible to localized corrosion in quiet seawater but maintain good corrosion resistance in seawater flow conditions because of the increased oxygen supply, which promotes passivity of these alloys. Biofouling is also minimized in high-velocity conditions, and this in turn minimizes the number of sites for crevice or poultice attack.[81] Type 304 and 316 stainless steels are not recommended in flow conditions less than approximately 1.5 m/sec because of the deep pitting of these alloys from crevices created by biofouling.[25] Surface roughness had a pronounced effect on the pitting corrosion of stainless steels in chloride solutions. A smoother surface finish reduced the incidence of metastable pitting substantially by reducing the number of sites capable of being activated into metastable pit growth. Once growing, however, a metastable pit on a smoother surface had a greater probability of achieving stable pit growth. The origin of the observations was in the geometry of the sites, particularly in the openness. A more deeply recessed pit site (expected on a rougher surface) had a greater probability of being activated into diffusion-controlled dissolution, but because it was more deeply recessed, it grew at a smaller current density.[166]

Nickel and Ni alloys owe their corrosion resistance partly to the inherent lower reactivity of nickel relative to iron as measured by its more noble oxidation potential in the EMF series. Similar to stainless steels, chromium-containing Ni alloys have the capability to passivate (i.e., to spontaneously form an ultrathin but tenacious surface oxide that functions as an effective corrosion barrier). Types of corrosion-resistant nickel and Ni alloys: (1) commercial nickel; (2) Ni-Cu alloys; (3) Ni-Fe-Cr-Mo alloys, such Incoloy alloy 825; (4) Ni-Cr-Mo alloys, such as Hastelloy C-276; and (5) Fe-Ni-Cr alloys, such Incoloy alloy 800. Ni-Cu and Ni-Cr-Mo alloys are the nickel-base alloys that typically are used in seawater. The Ni-Cu alloys have good corrosion resistance in high-velocity seawater, but they do exhibit localized corrosion in quiescent seawater.[25]

Ni-Cr-Mo alloys generally have high resistance to localized corrosion. Alloy 625 was developed for high-temperature service, but it was observed that it also had high resistance to localized corrosion in aqueous chloride. Alloy 625, a Ni-Cr-Mo alloy, is susceptible to crevice corrosion in both quiescent and flow conditions.[167–169] Further alloy development to maximize the levels of Cr, Mo, and W has led to Ni-Cr-Mo alloys (UNS N06059, N06022, N06686, N06200) with vastly increased resistance to pitting and crevice corrosion as suggested by their respective pitting resistance equivalence number (PRENW; see equation (3)), ranging from 67 to 76. Equation (3) includes nitrogen, but the solubility of nitrogen is very low and is not included by some researchers.[170] The higher the PRENW, the greater resistance of an alloy to pitting and crevice corrosion, though it is not absolute predictor of resistance in all seawater applications.

$$\mathrm{PRENW} = \%\mathrm{Cr} + 3.3(\%\mathrm{Mo} + \%\mathrm{W}) + 16(\%\mathrm{N}). \qquad (3)$$

These Ni-Cr-Mo alloys are strong, weldable, and highly resistant to localized corrosion and also can be used for weld overlays.[162]

Cu alloys exposed to seawater depend on the alloy and water composition. In unpolluted seawater, a loosely adherent porous cupric hydroxy-chloride ($Cu_2(OH)_3Cl$) corrosion product scale forms over a thin, tightly adherent layer of cuprous oxide (Cu_2O) that increases corrosion resistance with increased exposure times.[171,172] The iron and nickel from the Cu-Ni alloy are concentrated in the inner portion of the porous layer.[173] Iron,

if present in solid solution, also increases the corrosion resistance of Cu-Ni alloys by assisting in the formation of the protective film.[174] The initial corrosion rate of Cu-Ni alloys is relatively high but quickly decreases as the oxide film and the corrosion product layers are formed.

A variety of Cu alloys are used in seawater applications. Their generally good resistance is due to the formation of a protective film of cuprous oxide on the metal surface. Additional deposits such as Cu-containing compounds and calcareous materials often form on top of this film, which can further increase their corrosion resistance.[12] Cu-30Ni (C71500) and Cu-10Ni (C70600) generally have excellent uniform and pitting corrosion resistance in seawater.[14,25] Copper and some Cu alloys do exhibit erosion corrosion under high-velocity conditions. Their corrosion resistance depends on the growth and maintenance of the protective layers formed on the metal surface. The maximum velocity recommended for Cu in seawater is 0.9 m/sec. Alloying with nickel, aluminum, or chromium increases the resistance of Cu alloys to impingement attack.[14,25] Cu-Zn alloys (brasses) with more than 15% zinc are susceptible to a type of dealloying called dezincification. Some aluminum bronze (Cu-Al) alloys, especially those containing more than 8% aluminum, are also susceptible to dealloying. The dealloying in Cu-Al alloys can be prevented by adding more than 3.5% nickel or by heat treating to obtain an $\alpha + \beta$ microstructure.[25]

Hack and Gudas[175] showed that 90/10 Cu-Ni was susceptible to sulfide-induced pitting in natural, flowing seawater containing 0.01 ppm or more sulfides. Similarly, 70/30 Cu-Ni was susceptible to sulfide-induced pitting but required higher sulfide concentrations. Sulfide-modified films generally were more loosely adherent than the normal cuprous oxide films; turbulence tended to selectively remove the sulfide-modified films. The exposed surfaces are anodic to the surfaces covered by the films and localized corrosion at the exposed sites is promoted. Depending on water quality, additional sulfide-modified films may form and the process becomes cyclic.

Al alloys are susceptible to localized corrosion in seawater under both low- and high-velocity conditions. However, these alloys, particularly 5000 series and 6061 Al alloy, are commonly used in marine applications.[14,25] In most freshwater applications, crevice corrosion of aluminum is negligible. In seawater, however, crevice corrosion can be quite active and takes the form of pitting. Unlike steel, localized corrosion of aluminum is primarily determined by the properties, size, and distribution of intermetallic precipitates and less so by the properties of the solid-solution matrix. Resistance to crevice corrosion in Al alloys parallels its resistance to pitting. The pitting–crevice corrosion resistance of Al-Mg alloys (5xxx) is higher than observed in Al-Mg-Si (6xxx) alloys.[176] The corrosion potential of Al 1100 in natural and synthetic seawater is more positive than its repassivation potential and consequently aluminum would be expected to suffer localized corrosion.[177]

Ti alloys have the best corrosion resistance of the metals and alloys typically used in seawater. Titanium is a passive film-forming alloy and retains excellent resistance in both low and high velocity seawater. Some Ti alloys, specifically the all alpha and near-alpha alloys, do exhibit a susceptibility to stress corrosion cracking.[12]

Titanium and Ti alloys continue to see increased usage in naval and commercial and marine applications for many reasons. It is unsurpassed in its corrosion immunity in marine service, its low density provides for significant weight reductions, it has a high strength–to–weight ratio, has high erosion resistance, and is highly shock resistant. All these factors allow design engineers the opportunity to provide systems that significantly reduce (or eliminate) maintenance time and costs while providing unexcelled performance and a practically unlimited service life. It is available as fittings, flanges, pipe, tube, plate, sheet, and fasteners and is formable into most all required forms. It has a long history in heat exchanger service (shell and tube and plate and frame), in piping systems, and in components.

Titanium's exceptional corrosion resistance is derived from its protective oxide film, TiO_2, which has motivated extensive applications in seawater, marine, brine, and aggressive industrial and chemical service over the past 50 years. Today, titanium and its alloys are extensively used for the following applications: desalination; offshore, marine deep sea applications; and Navy ship components, such as seawater piping. Ti alloy forms form a protective oxide scale under different environmental conditions studied at both low and higher temperatures. The corrosion rate evaluated in different environments and at different temperatures was correlated. Pitting corrosion studies in different environments revealed that the alloy is resistant to pitting and crevice corrosion in marine environments at 25–50°C.[178] Titanium and its alloys are extremely resistant to pitting attack in seawater and other chloride-containing solutions at ambient and moderately elevated temperatures. The pitting potential is well above that associated with naturally occurring environments. Ti alloys typically have poorer resistance to pitting than commercially pure titanium.[179] When iron, low-alloy steel, or carbon steel are gouged, smeared, or embedded on the surface, penetrating the Ti oxide film, pitting of unalloyed titanium occurs in hot brines. This pitting may also be viewed as a special case of crevice corrosion.[180]

Mg alloys are starting to see limited applications in marine applications. A new alloy system, high entropy alloys (also called multiple principal element alloys) are compositionally complex alloys that were first developed in 2004, but their complexity has kept them largely in the experimental stage at this writing. In addition to metals and alloys, organic composites, such as graphite-reinforced epoxy, are gaining increasing use in the marine environment. The advantage of these composites over conventional materials is in their high strength-to-weight and stiffness-to-weight ratios. These composites also offer excellent marine corrosion resistance.[181,182] but may be susceptible to attack from the alkaline environment produced by cathodic protection techniques.

References

1. S. C. Dexter and C. Culberson, "Global Variability of Natural Sea Water," *Materials Performance* 19, no. 9 (1980): 16–28.

2. G. J. Danek, "The Effect of Sea-Water Velocity on the Corrosion Behavior of Metals," *Journal of Naval Engineers* 78 (1966): 763–769.

3. T. P. Hoar, "Electrochemical Principles of the Corrosion and Protection of Metals," *Journal of Applied Chemistry* 11, no. 4 (April 1961): 121–130.

4. R. A. Horne, *Marine Chemistry* (New York: Wiley-Interscience, 1969).

5. J. C. Rowlands, "Seawater," in *Corrosion: Metal/Environment Reactions*, 3rd ed., ed. L. L. Sheir, G. T. Jarman, and G. T. Burnstein (Oxford, UK: Butterworths-Heinemann, 1994): 60–71.

6. S. C. Dexter, R. B. Griffin, J. A. Montemarano, J. A. Smart III, and R. H. Heidersbach, "Corrosion in Specific Industries and Environments: Marine Corrosion," in *Metals Handbook: Corrosion*, 9th ed., vol. 13 (Metals Park, OH: ASM International, 1987), 893–926.

7. F. P. Ijsseling, "General Guidelines for Corrosion Testing of Materials for Marine Applications," *British Corrosion Journal* 24 (1989): 53–78.

8. W. Stumm and J. P. Morgan, *Aquatic Chemistry: An Introduction Emphasizing Chemical Equilibria in Natural Waters*, 2nd ed. (New York: Wiley, 1981), 556–580.

9. H. A. Humble, "The Cathodic Protection of Steel Piling in Sea Water," *Corrosion* 5 (1949): 292–302.

10. R. B. Griffin, "Marine Atmosphere," in *Metals Handbook: Corrosion*, 9th ed., vol. 13 (Materials Park, OH: ASM International, 1987), 902–906.

11. C. Leygraf and T. E. Graedel, *Atmospheric Corrosion* (New York: Wiley-Interscience, 2000).

12. C. Leygraf, I. O. Wallinder, J. Tidblad, and T. Graedel, *Atmospheric Corrosion*, 2nd ed. (New York: Wiley-Interscience, 2016).

13. K. G. Compton, "Seawater Tests," in *Handbook on Corrosion Testing and Evaluation*, ed. W. H. Ailor (New York, 1971), 507–514.

14. W. K. Boyd and F. W. Fink, *Corrosion of Metals in Marine Environments* (Columbus, OH: Metals and Ceramics Information Center, 1978).

15. D. A. Jones, *Principles and Prevention of Corrosion*, 2nd ed. (Upper Saddle River, NJ: Prentice Hall, 1996).

16. R. A. Horne, *Marine Chemistry* (New York: Wiley-Interscience, 1969).

17. W. Stumm and J. P. Morgan, *Aquatic Chemistry: An Introduction Emphasizing Chemical Equilibria in Natural Waters*, 2nd ed. (New York: Wiley, 1981).

18. B. S. Phull, S. J. Pikul, and R. M. Kain, "Seawater Corrosivity around the World: Results from Five Years of Testing," in *Corrosion Testing in Natural Waters*, ed. R. M. Kain and W. T. Young (West Conshohocken, PA: ASTM International, 1997), 34–73.

19. I. Matsushima, "Carbon Steel–Corrosion by Seawater," in *Uhlig's Corrosion Handbook*, 2nd ed., ed. R. W. Revie (New York: Wiley, 2000), 545–553.

20. F. L. LaQue, "Specific Topics in Corrosion: Corrosion by Sea Water," in *Corrosion Handbook*, ed. H. H. Uhlig (New York: Wiley, 1948), 383–430.

21. L. D. Perrigo, "An Overview of Corrosion in Cold Climates" (paper presentation, Corrosion/2001, paper 306, NACE International, Houston, TX, March 2001).

22. J. P. Talkington and L. D. Perrigo, "Special Aspects of Corrosion Control in the Artic and Subarctic," in *Proceedings of the International Conference of Offshore Mechanics and Artic Engineering* (New York: American Society of Mechanical Engineers, 1994), 337–344.

23. M. Stramska, R. Marks, and E. C. Monahan, "Bubble-Mediated Aerosol Production as a Consequence of Wave Breaking in Supersaturated (Hyperoxic) Seawater," *JGR Oceans* 95 (1990): 18281–18288.

24. A. Y. Benilov, "Air Sea Interactions: Surface Waves," in *Encyclopedia of Atmospheric Sciences*, 2nd ed., ed. G. R. North, F. Zhang, and J. Pyle (London: Elsevier, 2015).

25. J. R. Davis, ed., "Corrosion of Specific Alloy Systems," in *Metals Handbook: Corrosion*, 9th ed., vol. 13 (Metals Park, OH: ASM International, 1987).

26. M. G. Fontana, *Corrosion Engineering*, 3rd ed. (New York: McGraw-Hill, 1986).

27. M. Morcillo, B. Chico, L. Mariaca, and E. Otero, "Salinity in Marine Atmospheric Corrosion: Its Dependence on the Wind Regime Existing in the Site," *Corrosion Science* 42, no. 1 (2000): 91–104.

28. K. P. Fischer and J. E. Finnegan, "Cathodic Protection Behavior of Steel in Sea Water and the Protective Properties of the Calcareous Deposits" (paper presentation, Corrosion/89, paper 582, NACE International, New Orleans, LA, April 17–21, 1989).

29. J. S. Luo, R. U. Lee, T. Y. Chen, W. H. Hartt, and S. W. Smith, "Formation of Calcareous Deposits under Different Modes of Cathodic Polarization," *Corrosion* 47 (1991): 189–196.

30. K. E. Mantel, W. H. Hartt, and T. Y. Chen, "Substrate, Surface Finish, and Flow Rate Influences on Calcareous Deposits," *Corrosion* 48 (1992): 489–500.

31. K. P. Fischer, B. Espelid, and B. Schei, "A Review of CP Demand and Anode Performance for Deep Water" (paper presentation, Corrosion/2001, paper 13, NACE International, Houston, TX, March 2001).

32. H. A. Videla, *Manual of Biocorrosion* (New York: CRC Press, 1996).

33. S. C. Dexter, "Role of Biofilms in Determining the Rate of Localized Marine Corrosion," in *Critical Factors in Localized Corrosion III*, PV 98–17, ed. R. G. Kelly, G. S. Frankel, P. M. Natishan, and R. C. Newman (Pennington, NJ: Electrochemical Society, 1999), 339–352.

34. B. J. Little, R. I. Ray, and R. K. Pope, "The Relationship between Corrosion and the Biological Sulfur Cycle" (paper presentation, Corrosion/2000, paper 00394, NACE International, Orlando, FL, March 26–31, 2000).

35. D. A. Shifler, "Environmental Effects in Flow-Assisted Corrosion of Naval Systems" (paper presentation, CORROSION/99, paper 99619, NACE International, San Antonio, TX, April 25–30, 1999).

36. B. Poulson, "Electrochemical Measurements in Flowing Solutions," *Corrosion Science* 23 (1983): 391–430.

37. A. H. Tuthill and C. M. Schillmoller, *Guidelines for Selection of Marine Materials* (New York: International Nickel, 1971).

38. L. L. Sheir, "Localized Corrosion," in *Corrosion: Metal/Environment Reactions*, 3rd ed., vol. 1, ed. L. L. Shreir, R. A. Jarman, and G. T. Burnstein (Oxford, UK: Butterworths-Heinemann, 1994), 151–212.

39. K. D. Efird, "Effect of Fluid Dynamics on the Corrosion of Copper-Based Alloys in Seawater," *Corrosion* 33, no. 1 (1977): 3–8.

40. B. Poulson and R. Robinson, "The Local Enhancement of Mass Transfer at 180° Bends," *International Journal of Heat and Fluid Flow* 31, no. 6 (1988): 1289–1297.

41. B. Chexal, J. Horowitz, R. Jones, B. Dooley, C. Wood, M. Bouchacourt, F. Remy, Nordmann, and P. St. Paul, *Flow-Accelerated Corrosion in Power Plants* (Palo Alto, CA: EPRI and Electricite′ de France, 1996).

42. J. P. Gudas and H. P. Hack, "Sulfide Induced Corrosion of Copper Nickel Alloys" (paper presentation, Corrosion/77, paper 93, NACE International, San Francisco, CA, March 14, 1977).

43. D. D. MacDonald, B. C. Syrett, and S. S. Wing, "The Corrosion of Cu-Ni Alloys 706 and 715 in Flowing Seawater. II," *Corrosion* 35, no. 8 (1979): 367–378.

44. B. C. Syrett, "The Mechanism of Accelerated Corrosion of Copper-Nickel Alloys in Sulphide-Polluted Seawater," *Corrosion Science* 21 (1981): 187–209.

45. L. E. Eiselstein, B. C. Syrett, S. S. Wing, and R. D. Caligiuri, "The Mechanism of Accelerated Corrosion of Cu-Ni Alloys in Sulphide-Polluted Seawater: Mechanism No. 2," *Corrosion Science* 23 (1983): 223–239.

46. M. G. Fontana and N. D. Greene, *Corrosion Engineering*, 2nd ed. (New York: McGraw-Hill, 1978).

47. R. W. Revie, ed., *Uhlig's Corrosion Handbook*, 2nd ed. (New York: Wiley, 2000).

48. J. W. Oldfield and W. H. Sutton, "Crevice Corrosion of Stainless Steels: I. Mathematical Model," *British Corrosion Journal* 13 (1978): 13–22.

49. G. S. Eklund, "On the Initiation of Crevice Corrosion on Stainless Steel," *Journal of the Electrochemical Society* 123, no. 2 (1976): 123–170.

50. A. J. Sedriks, *Corrosion of Stainless Steels*, 2nd ed. (New York: Wiley, 1996), 176–230.

51. C. H. Hare, "Corrosion Phenomena: Specific Forms," *Journal of Protective Coatings and Linings* 15, no. 1 (1998): 67.

52. J. W. Oldfield, "Electrochemical Theory of Galvanic Corrosion," in *Galvanic Corrosion*, ed. H. P. Hack (West Conshohocken, PA: ASTM International, 1988), 5–22.

53. R. Francis, "Galvanic Corrosion of High Alloy Stainless Steels in Sea Water," *British Corrosion Journal* 29, no. 1 (1994): 53–57.

54. H. P. Hack, "Galvanic Corrosion of Piping and Fitting Alloys in Sulfide-Modified Seawater," DTNSRDC/SME-79-31 (Carderock Division, Naval Surface Warfare Center, West Bethesda, MD, May 1979).

55. R. H. Heidersbach, Jr., "Dealloying," in *Forms of Corrosion: Recognition and Prevention*, ed. C. P. Dillion (Houston, TX: NACE International, 1982), 99–104.

56. R. H. Heidersbach, "Clarification of the Mechanism of the Dealloying Phenomenon," *Corrosion* 24, no. 2 (1968): 38–44.

57. R. Steigerwald, "Metallurgically Influenced Corrosion," in *Metals Handbook: Corrosion*, 9th ed., vol. 13 (Materials Park, OH: ASM International, 1987), 123–135.

58. E. Heitz, "Chemo-Mechanical Effects of Flow on Corrosion," *Corrosion* 47 (1991): 135–145.

59. E. Heitz (paper presentation, Corrosion/90, paper 1, NACE International, Las Vegas, NV, April 23–27, 1990).

60. N. S. Hirota, "Erosion-Corrosion in Wet Steam Flow," in *Metals Handbook: Corrosion*, 9th ed, vol. 13 (Materials Park, OH: ASM International, 1987), 964–971.

61. B. Poulson, " Mass Transfer from Rough Surfaces," *Corrosion Science* 30 (1990): 743–746.

62. K. D. Efird, "Effects of Fluid Dynamics on the Corrosion of Copper-Base Alloys in Sea Water," *Corrosion* 33 (1977): 3–8.

63. G. Kuiper, *Cavitation and Multiphase Flow Forum*, ed. J. W. Hoyt and O. Furuya (New York: ASME, 1985).

64. G. Butler and H. C. K. Ison, *Proceedings of 1st International Congress on Metallic Corrosion* (London: Butterworths, 1961).

65. A. Turnbull, ed., *Hydrogen Transport and Cracking in Metals* (London: Institute of Materials, 1995).

66. R. G. J. Edyvean, J. Benson, C. J. Thomas, I. B. Beech, and H. A. Videla, "Biological Influences on Hydrogen Effects in Steel in Seawater" (paper presentation, Corrosion/97, paper 97206, NACE International, New Orleans, LA, March 1997).

67. V. Scotto, R. D. Cintio, and G. Marcenaro, "The Influence of Marine Aerobic Microbial Film on Stainless Steel Corrosion Behaviour," *Corrosion Science* 25 (1985): 185–194.

68. S. C. Dexter and G. Y. Gao, "Effects of Seawater Biofilms on Corrosion Potential and Oxygen Reduction of Stainless Steel," *Corrosion* 44 (1988): 717–723.

69. F. Mansfield and B. J. Little, "The Application of Electrochemical Techniques for the Study of MIC: A Critical Review" (paper presentation, Corrosion/90, paper 108, NACE International, Las Vegas, NV, April 23–27, 1990).

70. F. Mansfield, R. Tsai, H. Shih, B. J. Little, R. Ray, and P. Wagner, "Results of Exposure of Stainless Steel and Titanium to Natural Seawater" (paper presentation, Corrosion/90, paper 109, NACE International, Las Vegas, NV, April 23–27, 1990).

71. H. J. Zhang and S. C. Dexter, "Effect of Biofilms on Crevice Corrosion of Stainless Steels in Coastal Seawater," *Corrosion* 51 (1995): 56–66.

72. S. C. Dexter, "Effects of Biofilms on Marine Corrosion of Passive Alloys," in *Bioextraction and Biodeterioration of Metals*, ed. C. C. Gaylarde and H. A. Videla (Cambridge, UK: Cambridge University Press, 1995), 129–168.

73. H. J. Zhang and S. C. Dexter, "Effect of Biofilms on Critical Pitting Potentials for Stainless Steels S30400 and S31600 in Seawater," in *International Conference on Microbiologically Influenced Corrosion*, ed. P. Angell (Houston, TX: NACE International, 1995), 70–71.

74. V. Scotto and M. E. Lai, "The Ennoblement of Stainless Steels in Seawater: A Likely Explanation Coming from the Field," *Corrosion Science* 40 (1998): 1007–1018.

75. S. C. Dexter and J. P. LaFontaine, "Effect of Natural Marine Biofilms on Galvanic Corrosion," *Corrosion* 54, no. 11 (1998): 851–861.

76. D. A. Shifler, *Advanced Measures to Control Galvanic Corrosion in Piping Systems*, CARDIVNSWC-TR-61-99-18 (Carderock Division, Naval Surface Warfare Center, West Bethesda, MD, September 1999).

77. R. Francis, *Galvanic Corrosion: A Practical Guide for Engineers* (Houston, TX: NACE International, 2001).

78. R. S. Treseder, "An Engineering View of Laboratory Corrosion Tests," in *Laboratory Corrosion Tests and Standards*, ed. G. S. Haynes and R. Baboian (Philadelphia, PA: ASTM International, 1985), 5–13.

79. *Standard Practice for the Preparation of Substitute Ocean Water*, ASTM D1141-98(2013) (West Conshohocken, PA: ASTM International, approved January 1, 2013), https://doi.org/10.1520/D1141-98R13

80. S. P. Pednekar, "The Salt Spray Test as an Alternative to Long-Term Marine Exposure," in *1997 Tri-Service Conference on Corrosion*, vol. 1 (Bethesda, MD: Naval Surface Warfare Center, 1997), 4.70–4.76.

81. *Standard Practice for Operating Salt Spray (Fog) Apparatus*, ASTM B117-18 (West Conshohocken, PA: ASTM International, approved August 1, 2018), https://doi.org/10.1520/B0117-18

82. *Standard Guide for Laboratory Immersion Corrosion Testing of Metals*, NACE/ASTM G31-12a (West Conshohocken, PA: ASTM International, approved July 1, 2012), https://doi.org/10.1520/G0031-12A

83. *Standard Practice for Exposure of Metals and Alloys by Alternate Immersion in Neutral 3.5 % Sodium Chloride Solution*, ASTM G44-99(2013) (West Conshohocken, PA: ASTM International, approved May 1, 2013), https://doi.org/10.1520/G0044-99R13

84. *Standard Practice for Modified Salt Spray (Fog) Testing*, ASTM G85-11 (West Conshohocken, PA: ASTM International, approved May 1, 2011), https://doi.org/10.1520/G0085-11

85. *Accelerated Corrosion Test, General Motors Engineering Standards: Materials and Processes-Procedures*, GM9540P (Detroit, MI: General Motors Corporation, December 1997).

86. J. R. Davis, ed., "Corrosion Testing and Evaluation," in *Metals Handbook: Corrosion*, vol. 13 (Metals Park, OH: ASM International, 1987).

87. *Corrosion Tests in Artificial Atmospheres—Salt Spray Tests*, ISO 9227:2012 (Geneva, Switzerland: International Organization for Standardization, 2012).

88. *Standard Test Method for Copper-Accelerated Acetic Acid-Salt Spray (Fog) Testing (CASS Test)*, ASTM B368-09(2014) (West Conshohocken, PA: ASTM International, approved May 1, 2014), https://doi.org/10.1520/B0368-09R14

89. A. Sterling, A. Atrens, and I. O. Smith, "Accelerated Atmospheric Corrosion of Copper and Copper Alloys," *British Corrosion Journal* 25, no. 4 (1991): 271–278.

90. *Standard Practice for Cyclic Salt Fog/UV Exposure of Painted Metal, (Alternating Exposures in a Fog/Dry Cabinet and A UV/Condensation Cabinet)*, ASTM D5894-16 (West Conshohocken, PA: ASTM International, approved April 1, 2016), https://doi.org/10.1520/D5894-16

91. *Standard Reference Test Method for Making Potentiostatic and Potentiodynamic Anodic Polarization Measurements*, ASTM G5-14e1 (West Conshohocken, PA: ASTM International, approved November 1, 2014), https://doi.org/10.1520/G0005-14E01

92. Z. Szlarska-Smialowska, *Pitting Corrosion of Metals* (Houston, TX: NACE International, 1986).

93. A. J. Sedriks, *Corrosion of Stainless Steels*, 2nd ed. (New York: Wiley, 1996), 104–111.

94. M. G. Fontana and N. D. Greene, *Corrosion Engineering* (New York: McGraw-Hill, 1967).

95. J. O'M. Bockris and A. K. N. Reddy, *Modern Electrochemistry*, vol. 2 (New York: Plenum Press, 1970).

96. P. R. Roberge, *Corrosion Engineering: Principles and Practice* (New York: McGraw-Hill, 2008).

97. H. H. Uhlig and R. W. Revie, eds., *Corrosion and Corrosion Control* (New York: Wiley, 1985).

98. J. Tafel, "The Polarization during Cathodic Hydrogen Evolution," *Zeit, Physik, Chemie* 50, (1905): 641–712.

99. O. W. Siebert, "Laboratory Electrochemical Test Methods," in *Laboratory Corrosion Tests and Standards*, ed. G. S. Haynes and R. Baboian (Philadelphia, PA: ASTM International, 1985), 65–90.

100. E. Gileadi, *Electrode Kinetics for Chemists, Chemical Engineers, and Material Scientists* (New York: VCH Publishers, 1993).

101. W. L. Clarke, V. M. Romero, and J. C. Danko (paper presentation, Corrosion/77, paper 180, NACE International, San Francisco, CA, March 14, 1977).

102. *Standard Test Method for Conducting Cyclic Potentiodynamic Polarization Measurements for Localized Corrosion Susceptibility of Iron-, Nickel-, or Cobalt-Based Alloys*, ASTM G61-86(2018) (West Conshohocken, PA: ASTM International, approved May 1, 2018), https://doi.org/10.1520/G0061-86R18

103. B. J. Little, R. I. Ray, and J. S. Lee, "Diagnosing, Measuring, and Monitoring Microbiological Influenced Corrosion," in *Uhlig's Corrosion Handbook*, 3rd ed., ed. R. W. Revie (New York: Wiley, 2011), 1202–1212.

104. *Standard Test Method for Electrochemical Critical Pitting Temperature Testing of Stainless Steels and Related Alloys*, ASTM G150-18 (West Conshohocken, PA: ASTM International, approved May 1, 2018), https://doi.org/10.1520/G0150-18

105. *Standard Test Method for Determining the Crevice Repassivation Potential of Corrosion-Resistant Alloys Using a Potentiodynamic-Galvanostatic-Potentiostatic Technique*, ASTM G192-08(2014) (West Conshohocken, PA: ASTM International, approved November 1, 2014), https://doi.org/10.1520/G0192-08R14

106. F. Mansfeld, M. W. Kendig, and S. Tsai, "Evaluation of Corrosion Behavior of Coated Metals with AC Impedance Measurements," *Corrosion* 38, no. 9 (1982): 478–485.

107. J. D. Scantlebury, K. Ho., and D. Eden, "Impedance Measurements on Organic Coatings on Mild Steel in Sodium Chloride Solutions," in *Electrochemical Corrosion Testing,* ed. F. Mansfeld and U. Bertocci (Philadelphia, PA: ASTM International, 1981), 187–197.

108. J. N. Murray and H. P. Hack, "Testing Organic Architectural Coatings in ASTM Synthetic Seawater Immersion Conditions Using EIS," *Corrosion* 48, no. 8 (1992): 671–685.

109. J. R. Scully, *Electrochemical Impedance of Organic Coated Steel: Correlation of Impedance Parameters with Long Term Coating Deterioration*, DTRC/SME-86/108 (Annapolis, MD: David Taylor Research Center, April 1988).

110. D. D. MacDonald and M. C. H. McKubre, "Electrochemical Impedance Techniques in Corrosion Science," in *Electrochemical Corrosion Testing,* ed. F. Mansfeld and U. Bertocci (Philadelphia, PA: ASTM International, 1981), 110–149.

111. J. R. Scully, D. C. Silverman, and M. W. Kendig, eds. *Electrochemical Impedance: Analysis and Interpretation* (West Conshohocken, PA: ASTM International, 1993).

112. F. Mansfeld, L. T. Han, and C. C. Lee, "Analysis of Electrochemical Impedance and Noise Data for Polymer Coated Metals," *Corrosion Science* 39 (1997): 255–279.

113. J. N. Murray and H. P. Hack, *Electrochemical Impedance of Organic Coated Steel: Final Report–Correlation of Impedance Parameters with Long Term Coating Deterioration*, DTRC/SME-89/76 (Annapolis, MD: David Taylor Research Center, September 1990).

114. F. Mansfeld, "Use of Electrochemical Impedance Spectroscopy for the Study of Corrosion Protection by Polymer Coatings," *Journal of Applied Electrochemistry* 25, no. 3 (1995): 187–202.

115. K. Itagda, M. Noaki, M. Endou, K. Watanabe, H. Katayama, and H. Masuda, "Corrosion Monitoring in Marine Environments Using Electrochemical Impedance," in *Corrosion in Marine and Saltwater Environments II*, PV2004-14, ed. D. A. Shifler, T. Tsuru, P. M. Natishan, and S. Ito, (Pennington, NJ: Electrochemical Society, Pennington, 2005), 1–12.

116. R. S. Lillard, J. Kruger, and W. S. Tait, "Using Local Impedance Spectroscopy for Monitoring Coating Performance in Condensing Environments," *Corrosion* 51 (1995): 251–259.

117. F. Zou and D. Thierry, "Localized Electrochemical Impedance Spectroscopy for Studying the Degradation of Organic Coatings," *Electrochimica Acta* 42, no. 20–22 (1997): 3293–3301.

118. D. C. Silverman, "Practical Corrosion Prediction Using Electrochemical Techniques," in *Part V: Testing for Corrosion Resistance*, *Uhlig's Corrosion Handbook*, 3rd ed., ed. R. W. Revie (New York: Wiley, 2011), 1150–1166.

119. U. Bertocci, "Electrochemical Noise and Its Analysis to Corrosion" (paper presentation Corrosion/89, paper 24, NACE International, New Orleans, LA, April 17–21, 1989).

120. U. Bertocci, "Statistics of Localized Breakdown Noise," in *Proceedings of the 2nd International Conference on Localized Corrosion*, NACE-9, ed. H. Isaacs, U. Bertocci, J. Kruger, and S. Smialowska (Houston, TX: NACE International, 1990), 127–136.

121. D. A. Eden, A. N. Rothwell, and J. L. Dawson, "Electrochemical Noise for Detection of Susceptibility to Stress Corrosion Cracking" (paper presentation, Corrosion/91, paper 444, NACE International, Cincinnati, OH, March 11–15, 1991).

122. B. C. Syrett and W. M. Cox, "Electrochemical Noise Measurement for Corrosion Applications," in *Proceedings of the First International Symposium on Electrochemical Noise Measurements for Corrosion Applications*, ed. J. R. Kearns, J. R. Scully, P. R. Roberge, D. L. Reichert, and J. L. Dawson (West Conshohocken, PA: ASTM International, 1996), 173–185.

123. F. Mansfeld, Z. Sun, E. Speckert, and C. H. Hsu, "Electrochemical Noise Analysis (ENA) for Active and Passive Systems" (paper presentation, Corrosion/2000, paper 418, NACE International, Orlando, FL, March 26–31, 2000).

124. G. L. Edgemon and E. E. Barr, "Applications of Electrochemical Noise: Real Time Plant and Field Challenges" (paper presentation, Corrosion/2001, paper 283, NACE International, Houston, TX, March 2001).

125. F. Mansfeld, Z. Sun, C. H. Hsu, and A. Nagiub, "Electrochemical Impedance (EIS) and Electrochemical Noise Analysis (ENA) for Active and Passive Systems in Chloride Media," in *New Trends in Electrochemical Impedance (EIS) and Electrochemical Noise Analysis*, PV2000-24, ed. F. Mansfeld, E. Huet, and O. R. Mattos (Pennington, NJ: Electrochemical Society, 2001), 165–187.

126. R. A. Cottis, G. Bagley, A. A. Alawadhi, H. Al-Mazeedi, and P. J. Laycock, "Electrochemical Parameters for the Identification of Localized Corrosion," in *New Trends in Electrochemical Impedance (EIS) and Electrochemical Noise Analysis*, PV2000-24, ed. F. Mansfeld, E. Huet, and O. R. Mattos (Pennington, NJ: Electrochemical Society, 2001), 247–258.

127. G. Berthome and B. Baroux, "Crevice Corrosion of Stainless Steel: Electrochemical Noise Analysis at Rest Potential," in *New Trends in Electrochemical Impedance (EIS) and Electrochemical Noise Analysis*, PV2000-24, ed. F. Mansfeld, E. Huet, and O. R. Mattos (Pennington, NJ: Electrochemical Society, 2001), 259–264.

128. *Standard Guide for Electrochemical Noise Measurement*, ASTM G199-09(2014) (West Conshohocken, PA: ASTM International, approved May 1, 2014), https://doi.org/10.1520/G0199-09R14

129. *Standard Test Method for Cavitation Erosion Using Vibratory Apparatus*, ASTM G32-16 (West Conshohocken, PA: ASTM International, approved February 1, 2016), https://doi.org/10.1520/G0032-16

130. *Standard Test Method for Liquid Impingement Erosion Using Rotating Apparatus*, ASTM G73-10 (2017) (West Conshohocken, PA: ASTM International, approved July 15 2017), https://doi.org/10.1520/G0073-10R17

131. J. Z. Lichtman, D. H. Kallas, and A. Rufolo, "Evaluating Erosion (Cavitation) Damage," in *Handbook on Corrosion Testing and Evaluation*, ed. W. H. Ailor (New York: Wiley, 1971), 453–472.

132. R. L. Ruedisueli and D. M. Aylor, "Erosion Resistance Testing for Candidate Seawater Valve Materials" (paper presentation, Corrosion/2001, paper 468, NACE International, Houston, TX, March 2001).

133. *Standard Test Method for Erosion of Solid Materials by Cavitating Liquid Jet*, ASTM G134-17 (West Conshohocken, PA: ASTM International, approved November 1, 2017), https://doi.org/10.1520/G0134-17

134. D. Efird, "Flow Effects on Corrosion," in *Part I: Basics of Corrosion Science and Engineering*, *Uhlig's Corrosion Handbook*, 3rd ed., ed. R. W. Revie (New York: Wiley, 2011), 203–213.

135. F. L. LaQue, "Marine Corrosion Testing," in *Marine Corrosion* (New York: Wiley, 1975), 56–69.

136. *Standard Practice for Making and Using U-Bend Stress-Corrosion Test Specimens*, ASTM G30-97(2016) (West Conshohocken, PA: ASTM International, approved May 1, 2016), https://doi.org/10.1520/G0030-97R16

137. *Standard Practice for Making and Using C-Ring Stress-Corrosion Test Specimens*, ASTM G38-01(2013) (West Conshohocken, PA: ASTM International, approved May 1, 2013), https://doi.org/10.1520/G0038-01R13

138. *Standard Practice for Preparation and Use of Bent-Beam Stress-Corrosion Test Specimens*, ASTM G39-99(2016) (West Conshohocken, PA: ASTM International, approved May 1, 2016), https://doi.org/10.1520/G0039-99R16

139. *Standard Practice for Preparation and Use of Direct Tension Stress-Corrosion Test Specimens*, ASTM G49-85(2011) (West Conshohocken, PA: ASTM International, approved March 1, 2011), https://doi.org/10.1520/G0049-85R11

140. *Standard Practice for Evaluating Stress-Corrosion-Cracking Resistance of Metals and Alloys in a Boiling Magnesium Chloride Solution*, ASTM G36-94(2018) (West Conshohocken, PA: ASTM International, approved October 1, 2018), https://doi.org/10.1520/G0036-94R18

141. *Standard Test Method for Determining Susceptibility to Stress-Corrosion Cracking of 2xxx and 7xxx Aluminum Alloy Products*, ASTM G47-98(2011) (West Conshohocken, PA: ASTM International, approved September 1, 2011), https://doi.org/10.1520/G0047-98R11

142. R. N. Parkins, "Slow Strain Rate Testing—25 Years' Experience," in *Slow Strain Rate Testing for the Evaluation of Environmentally Induced Cracking, Research and Engineering Applications,* ed. R. D. Kane (Philadelphia, PA: ASTM International, 1993), 7–21.

143. R. D. Kane, "Testing for Environmentally Assisted Cracking," in *Uhlig's Corrosion Handbook*, 2nd ed., ed. R. W. Revie (New York: Wiley, 2000), 1117–1128.

144. *Standard Practice for Slow Strain Rate Testing to Evaluate the Susceptibility of Metallic Materials to Environmentally Assisted Cracking*, ASTM G129-00(2013) (West Conshohocken, PA: ASTM International, approved May 1, 2013), https://doi.org/10.1520/G0129-00R13

145. *Standard Test Method for Determining Stress-Corrosion Cracking Resistance of Heat-Treatable Aluminum Alloy Products Using Breaking Load Method*, ASTM G139-05(2015) (West Conshohocken, PA: ASTM International, approved November 1, 2015), https://doi.org/10.1520/G0139-05R15

146. *Standard Practice for Making and Using Precracked Double Beam Stress Corrosion Specimens*, ASTM G168-17 (West Conshohocken, PA: ASTM International, approved November 1, 2017), https://doi.org/10.1520/G0168-17

147. *Standard Test Method for Determining Threshold Stress Intensity Factor for Environment-Assisted Cracking of Metallic Materials*, ASTM E1681-03(2013)e1 (West Conshohocken, PA: ASTM International, approved October 15, 2013), https://doi.org/10.1520/E1681-03R13E01

148. S. R. Novak and S. T. Rolfe, "Comparison of Fracture Mechanics and Nominal Stress Analyses in Stress Corrosion Cracking," *Corrosion* 26, no. 4 (1970): 121–130.

149. R. P. Gangloff, in *Environment Induced Cracking in Metals*, ed. R. P. Gangloff and M. B. Ives (Houston, TX: NACE International, 1990), 55–109.

150. R. P. Wei and R. P. Gangloff, "Environmentally Assisted Crack Growth in Structural Alloys: Perspectives and New Directions," in *Fracture Mechanics: Perspectives and Directions (20th Symposium),* ed. R. P. Wei and R. P. Gangloff (West Conshohocken, PA: ASTM International, 1989), 233–264.

151. *Standard Practice for Conducting Force Controlled Constant Amplitude Axial Fatigue Tests of Metallic Materials*, ASTM E466-15 (West Conshohocken, PA: ASTM International, approved May 1, 2015), https://doi.org/10.1520/E0466-15

152. E. J. Czyryca, in *Metals Handbook: Mechanical Testing*, 9th ed. (Materials Park, OH: ASM International, 1985), 366–375.

153. R. A. Cottis, A. Markfield, A. Boukerrou, and P. Haritopoulos, "Crack Initiation and Short Crack Growth during the Corrosion Fatigue Steels in Saline Solutions," in *Environment Induced Cracking in Metals*, ed. R. P. Gangloff and M. B. Ives (Houston, TX: NACE International, 1990), 223–227.

154. W. J. Derrick Jones and A. P. Blackie, "Cyclic Tension Corrosion Fatigue of High Strength Steels in Seawater," in *Environmentally Assisted Cracking: Science and Engineering,* ed. B. Lisagor, T. W. Crooker, and B. N. Leis (West Conshohocken, PA: ASTM International, 1990), 447–462.

155. *Standard Test Method for Strain-Controlled Fatigue Testing*, ASTM E606/E606M-12 (West Conshohocken, PA: ASTM International, approved June 1, 2012), https://doi.org/10.1520/E0606-04E01

156. B. Phull, "Evaluating Corrosion Fatigue," in *ASM Handbook* vol. 13A, *Corrosion: Fundamentals, Testing, and Protection* (Materials Park, OH: ASM International, 2003), 625–638.

157. *Standard Test Method for Measurement of Fatigue Crack Growth Rates*, ASTM E647-15e1 (West Conshohocken, PA: ASTM International, approved May 1, 2015), https://doi.org/10.1520/E0647-15E01

158. T. W. Crooker, F. D. Bogar, and G. R. Yoder, "Standard Method of Test for Constant-Load-Amplitude Fatigue Crack Growth Rates in Marine Environments" (Naval Research Laboratory Report 4594, Washington, DC, 1981).

159. *Standard Test Method for Measurement of Hydrogen Embrittlement Threshold in Steel by the Incremental Step Loading Technique*, ASTM F1624-12(2018) (West Conshohocken, PA: ASTM International, approved November 1, 2018), https://doi.org/10.1520/F1624-12R18

160. *Standard Guide for Conducting Corrosion Tests in Field Applications*, ASTM G4-01(2014) (West Conshohocken, PA: ASTM International, approved November 1, 2014), https://doi.org/10.1520/G0004-01R14

161. *Standard Practice for Conducting Atmospheric Corrosion Tests on Metals*, ASTM G50-10(2015) (West Conshohocken, PA: ASTM International, approved November 1, 2015), https://doi.org/10.1520/G0050-10R15

162. *Standard Guide for Applying Statistics to Analysis of Corrosion Data*, ASTM G16-13 (West Conshohocken, PA: ASTM International, approved December 1, 2013), https://doi.org/10.1520/G0016-13

163. *Standard Test Method for Monitoring Atmospheric Corrosion Tests by Electrical Resistance Probes*, ASTM B826-09(2015) (West Conshohocken, PA: ASTM International, approved May 1, 2015), https://doi.org/10.1520/B0826-09R15

164. *Standard Practice for Exposing and Evaluating Metals and Alloys in Surface Seawater*, ASTM G52-00(2016)e1 (West Conshohocken, PA: ASTM International, approved November 1, 2016), https://doi.org/10.1520/G0052-00R16E01

165. R. E. Melchers, "The Changing Character of Long Term Marine Corrosion of Mild Steel," Research Report No. 277.04.2010 (Centre for Infrastructure Performance and Reliability, University of Newcastle, 2010).

166. G. T. Burstein and P. C. Pistorius, "Surface Roughness and the Metastable Pitting of Stainless Steel in Chloride Solutions," *Corrosion* 51, no. 5 (1995): 380–385.

167. P. A. Klein, R. J. Ferrara, and R. M. Kain, "Crevice Corrosion of Nickel-Chromium-Molybdenum Alloys in Natural and Chlorinated Seawater" (paper presentation, Corrosion/89, paper 112, NACE International, New Orleans, LA, April 17–21, 1989).

168. D. M. Aylor, R. J. Ferrara, R. A. Hays, and R. M. Kain, "Crevice Corrosion Performance of Candidate Naval Ship Seawater Valve Materials in Quiescent and Flowing Natural Seawater" (paper presentation, Corrosion/99, paper 329, NACE International, San Antonio, TX, April 25–30, 1999).

169. R. M. Kain and P. A. Klein, "Crevice Corrosion Propagation Studies for Alloy N06625: Remote Crevice Assembly Testing in Flowing Natural and Chlorinated Seawater" (paper presentation, Corrosion/90, paper 158, NACE International, Las Vegas, NV, April 23–27, 1990).

170. C. A. Powell and D. Jordan, "Nickel Alloys" in *The Corrosion Performance of Metals for the Marine Environment: A Basic Guide*, European Federation of Corrosion and NACE International, ed. C. A. Powell and R. Francis, Joint Publication 63 (Leeds, UK: Maney Publishing, 2012), 42–50.

171. H. P. Hack, H. Shih, and H. W. Pickering, "Role of the Corrosion Product Film in the Corrosion Protection of Cu-Ni Alloys in Saltwater," in *Surfaces, Inhibition, and Passivation*, PV86-7, ed. E. McCafferty and J. Brodd (Pennington, NJ: Electrochemical Society, 1986), 355–367.

172. H. P. Hack, "Role of the Corrosion Product Film in the Corrosion Protection of Cu-Ni Alloys in Saltwater," DTNSRDC SME-87-22 (Carderock Division, Naval Surface Warfare Center, West Bethesda, MD, November 1987).

173. C. Kato, J. E. Castle, B. G. Ateya, and H. W. Pickering, "On the Mechanism of Corrosion of Cu-9.4Ni-1.7Fe in Air Saturated Aqueous NaCl Solution," *Journal of the Electrochemical Society* 127 (1980): 1897–1902.

174. C. Pearson, "Role of Iron in the Inhibition of Corrosion of Marine Heat Exchangers," *British Corrosion Journal* 7 (1972): 61–68.

175. J. P. Gudas and H. P. Hack, "Sulfide Induced Corrosion of Copper-Nickel Alloys," *Corrosion* 35 (1979): 67–73.

176. H. P. Godard, ed., *Corrosion of Light Metals* (New York: Wiley, 1967).

177. N. Sridhar, C. S. Brossia, D. S. Dunn, and A. Anderko, "Predicting Localized Corrosion in Seawater," *Corrosion* 60, no. 10 (2004): 916–936.

178. I. Gurrappa, "Characterization of Titanium Alloy Ti-6Al-4V for Chemical, Marine and Industrial Applications," *Materials Characterization* 51 (October 2003): 131–139.

179. F. H. Froes, *Titanium: Physical Metallurgy, Processing, and Applications* (Materials Park, OH: ASM International, 2015).

180. L. C. Covington, "Pitting Corrosion of Titanium Tubes in Hot Concentrated Brine Solutions," *Galvanic and Pitting Corrosion—Field and Laboratory Studies* (West Conshohocken, PA: ASTM International, 1976), 147–154.

181. S. R. Brown and J. J. Deluccia, "Corrosion Characteristics of Naval Aircraft Metals and Alloys in Contact with Graphite-Epoxy Composites," in *Proceedings of the Environmental Materials Conference* (Blacksburg, VA, October 1977), 277–288.

182. G. L. Lubin, ed., *Handbook of Composites* (New York: Van Nostrand Reinhold, 1982), 699–702.

Chapter 14 | Soils

Mike Horton,[1] Lucien Veleva,[2] and Edward Escalante[3]

Description of Soils

DEFINITION AND CLASSIFICATION

Soil as a corrosive environment is probably of greater complexity than any other environment.[1–6] The corrosion process of buried metal structures is extremely variable and can range from rapid to negligible. In fact, some pipes in corrosive soils can be perforated within a few years, presenting very localized or uniform corrosion attack (fig. 1). Other pipe in nonaggressive soils may serve for decades or even centuries, such as sections of a more-than-350-year-old cast iron pipeline installed in 1664 providing water to the fountains at the Palace of Versailles (fig. 2). With background knowledge of the principal soil specifics and their influence on metal corrosion, the most serious corrosion problems can be prevented. In discussion of the soil as an environment for corrosion, no strict definitions exist. The origin of soil is in the earth's crust and the following four main classes of soil have been proposed:

1. soils formed *in situ* from soft rocks, such as chalk and volcanic ash;
2. soils formed *in situ* from hard rocks, such as granite, limestone, and marble;
3. soils transported from their place of origin before weathering to form soils, including those moved by water, such as marine and beach sediments, and also those moved by wind, such as sands, and those moved by glacial drift; and
4. soils formed *in situ* from organic material, such as peat.

Soils are commonly named and classified according to the size range of their particulate matter. For example, *sand*, *silt*, and *clay* derive their name from the predominant size range of their inorganic constituents. Particles between 0.02 and about 2 mm are classed as fine (0.02–0.2 mm) and coarse (0.20–2.00 mm) sands. Silt particle sizes range from 0.002 to 0.02 mm and clay particles have a mean diameter of <0.002 mm down to colloidal matter. Table 1 presents the terminology for different soils according to ASTM D2488, *Standard Practice for Description and Identification of Soils (Visual-Manual Procedures)*. The United States and more than 50 other countries now use a more detailed classification of their soils, which includes 11 major orders and 47 suborders.

FIG. 1 Buried pipe with detected corrosion failure. *Source:* Photo courtesy of Corrpro, an Aegion Company.



FIG. 2 350-plus-year-old cast iron pipeline furnishing water to the fountains at the Palace of Versailles. *Source:* Photo courtesy of the Ductile Iron Pipe Research Association.



[1]U.S. Pipe and Foundry, 2023 St. Louis Ave., Bessemer, AL 35020, USA
[2]Applied Physics Department, CINVESTAV-IPN, Unidad Merida, Yucatan, C.P. 97310, Mexico
[3]National Institute of Standards and technology, Gaithersburg, MD, USA
The authors acknowledge the previous author of this chapter, Edward Escalante, NIST, 100 Bureau Dr., Gaithersburg, MD 20899.

DOI: 10.1520/MNL202NDSUP20190009

Copyright © 2022 by ASTM International, 100 Barr Harbor Dr., PO Box C700, West Conshohocken, PA 19428-2959
ASTM International is not responsible, as a body, for the statements and opinions expressed in this chapter. ASTM International does not endorse any products represented in this chapter.

TABLE 1 ASTM D2488, Terminology for Soils

Term		Description
Clay		<0.75 μm (passes No. 200 sieve)
Gravel		<75 mm and >4.75 mm (No. 4 sieve)
Organic	clay	Clay, except that its liquid limit values after oven drying are <75% of its liquid limit value before oven drying.
Organic	silt	Silt, except that its liquid limit values after oven drying are −75% of its liquid limit value before oven drying.
Peat		Soil, primarily vegetable tissue, in various stages of decomposition, usually with organic odor, dark brown or black, spongy consistency, with fibrous to amorphous texture.
Sand		Rock particles passing No. 4 sieve (4.75 mm) and retained on a No. 200 (75 μm).
Silt		Soil passing No. 200 sieve; nonplastic or very slightly plastic, and exhibiting little or no strength when air-dried.

Variation of the proportion of soil size groups determines many of the properties of the soil. Terms commonly used for soil classification include sandy clay, clay loam, silt loam, loamy sand, silty clay loam, sandy loam, and gravel. The clays are plastic mixtures with high moisture content and are considered to be the most important inorganic constituents of the soil. Often the clays are grouped depending on the weathering conditions (e.g., montmorillonite, illite, kaolinite). Soils of fine texture, because of their high clay content, present more packed particles and have less pore capacity for moisture and gas (oxygen) diffusion than an open-type soil such as sand. The clay mineralogy and properties are closely related to the corrosion aggressiveness of soil, and this fact needs attention.

Soil has a specific gravity from 1.1 to 1.7, which is measured as described in ASTM D2937, *Standard Test Method for Density of Soil in Place by the Drive-Cylinder Method*. The main chemical constituent of soils, such as loam, clay, and silt is silicon dioxide (SiO_2), usually along with aluminum oxide (Al_2O_3). Commonly dissolved species in wet soils are H^+, Cl^-, sulfate (SO_4^{-2}), bicarbonate (HCO_3^-) ions. The soil mineralogy and chemistry determine the corrosion aggressiveness of soil. Soils with the poorest drainage, like clay, silt, and loam, are generally the most corrosive, whereas soils with excellent and good drainage (gravel and sand, respectively) are generally the least corrosive.

Because of the complex content of the soil (including organic matter and organisms, gases, mineral particles, moisture), the relative size range does not represent the whole nature of the soil. In fact, most soils consist of aggregates of particles, which give the possibility for moisture penetration, less erosion by water and wind, and generally great aeration and biological activity. The destruction of this structure by mechanical action or chemical alteration (such as excess alkali or salt accumulation) can alter the physical nature of the soil. To understand the corrosion behavior of buried metal, it is also important to have information about the soil profile (section through the soil showing the various layers). Complex physical, chemical, and biological nature; corrosion aggressiveness; and dynamic interactions with the environment distinguish the soil.

Climatic changes of sun irradiation; air temperature and relative humidity; rainfall, winds, and mechanical action of natural forces; various physical, chemical, and biological factors; and human manipulation can alter soil properties, which directly affect the corrosion rate of metals buried in the soil. The amounts of moisture and rainfall are considered to be of primary importance in soil evolution. They affect the type of soil that forms, the weathering process, and all changes taking place within the soil. Plant and animal life with their soil-building action, acid or base reactions in the parent material, dissolution of soluble components, the leaching out of alkaline minerals of the weathering rock, and other phenomena are strictly influenced by changes in these factors.

The conditions in soils can range from atmospheric to completely immersed metal, depending on the soil compactness (existence of capillaries and pores) and moisture content. The corrosiveness of a soil depends on an interaction between climate and soil reactions. The variation in soil composition and structure can create distinct corrosive environments, which results in different metal activities and oxygen concentrations (differential aeration) at the metal–soil interface.

Characteristics and Testing of Soils Related to Corrosion

The metal corrosion in soils is determined primarily by such factors as moisture content and its level of electrical (ionic) conductivity, aeration and oxygen content, relative acidity or alkalinity, bacterial activity, and amount of dissolved salts.[1–6,8–13,23,29] The two primary conditions necessary to initiate metal corrosion in soil are water (moisture) and oxygen. After these factors, a number of variables can affect the corrosion process.

SOIL MOISTURE

Principally, three types of water provide the soil moisture: free ground water, gravitational water, and capillary water. They have a significant influence on the metal and environmental characteristics and on the determination of the corrosion rate. The amount of moisture in a soil can be determined by the method described in ASTM D2216, *Standard Test Methods for Laboratory Determination of Water (Moisture) Content of Soil and Rock by Mass*.

The *free ground water* is present in the soil at some depth (a few meters to hundreds of meters) below the surface, and usually only river-crossing pipelines are surrounded by ground water. In such a situation, metal corrosion occurs in an aqueous environment (e.g., on a fully immersed metal structure). The principal sources of the *gravitational water* are rainfall, snow, flood, and irrigation. This water enters and flows through the soil, governed by its physical structure, including pore and capillary spaces at various zones in the soil profile, and usually percolates to the level of permanent ground water. A measure of the compactness

of mineral soils is the *apparent specific gravity index*. The amount of organic matter influences this value markedly. Some impervious soils, such as clay and water-resistant materials, act as effective barriers to the passage of gravitational water and cause zones of water accumulation and saturation. The tendency of the soil to crack on drying and swell when wetted is defined by the term *volume shrinkage*, and it is an indicator of the colloidal nature of the clay and loam particles in a soil. In drying, the soil forms cracks that allow oxygen to flow freely to buried metals.

The *capillary water* represents an important reservoir of water in soil. A considerable amount is held in the capillary spaces of silt and clay particles. The term *moisture equivalent of soil* is a measure of the retentiveness or water holding capacity of the soil. The water retained by a soil is a consequence of equilibrium between capillary and gravitational forces. The permeability and moisture retention of granular soils can be measured by the method described in ASTM D2434, *Standard Test Method for Permeability of Granular Soils (Constant Head)*. For the water-holding capacity of peat, one can use ASTM D2980, *Standard Test Method for Saturated Density, Moisture-Holding Capacity, and Porosity of Saturated Peat Materials*. The existence of moisture in good conductivity soil indicates high ion content and the possibility for very strong corrosion attack.

SOIL RESISTIVITY

The *soil resistance (R)* to passage of electrical current is the most used parameter as an indicator of corrosion aggressivity of soils. It is related to three terms in the following equation:

$$R = \rho I/A, \quad (1)$$

where:

ρ = *specific resistivity* of the particular soil,
I = a length of the electrical path, and
A = the cross-sectional area of the electrodes.

Soil resistivity is normally reported in the units ohm-cm (i.e., Ω·cm).

The resistivity indicates the probable corrosivity of the soil. Its value depends on the soil water content on the layers and on types of soils underneath (e.g., sand, rock, gravel, clay, mud). Vertically homogeneous soils are virtually nonexistent. Thus, it is convenient to consider a nonuniform soil to consist of different layers or strata.[13] Electron flow will deflect downward in the case of a high-resistivity strata over a low-resistivity one, and vice versa, as shown in figure 3 and figure 4. The electrical resistivity of the surface strata has a greater influence on test results than does that of deeper strata. Also, the soil resistivity decreases with increasing water content and with increasing water salinity because of high contents of ions. Thus, nonporous soils exhibit relatively high values of resistance, because the water content is small. These include nearly all of the igneous and metamorphic rocks, such as granite, plus many sedimentary rocks, such as dense limestone or sandstone. The resistivity of bedrock can vary considerably depending on the type of bedrock and the extent of weathering and fracturing.

FIG. 3 Low-resistivity layer over high-resistivity layer.

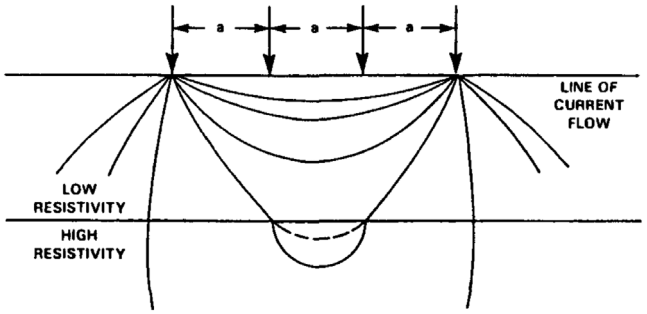
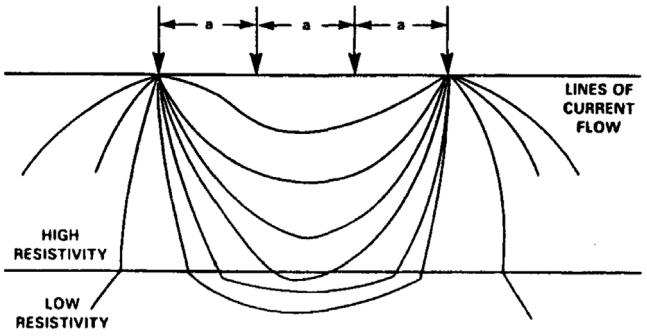


FIG. 4 High-resistivity layer over low-resistivity layer.



The resistivity of sand and gravel deposits is generally high and uniform, whereas many bedrock formations have high but erratic resistivity. Table 2 gives typical resistivity values of various minerals and soils.

Along the length of the pipe, variations in soil resistivity may stimulate localized metal corrosion and can cause long line currents; in the area of *lower resistivity* soil, the buried metal surface is usually *anodic*, with a more negative potential, compared with that in the soil of higher resistivity. Table 3 relates soil resistivity values with corrosion.[11]

Field soil resistivity measurements are normally carried out by the *Wenner technique, four-pin method,* with or without the Barnes method, according to ASTM G57, *Standard Test Method for Measurement of Soil Resistivity Using the Wenner Four-Electrode Method*. (The Barnes method is a mathematical procedure for calculating the resistivity of the soil in each incremental layer.) Four steel electrodes, each spaced an equal distance from the next, are driven into the ground. The depth of soil being evaluated depends on the pin spacing. An alternating current (ac) or direct current (dc) is passed between the outer two pins, and the corresponding potential drop (voltage AV) is measured between the inner pins, as shown in figure 5. The resistance $R = AV/I$, where I is the applied current.

The average resistivity value depends on how many measurements are taken in the area and when they were taken. Measurements should be made at various times and under various weather conditions (e.g., dry or rainy seasons, summer or winter). It is impossible, therefore, to give any precise assessment as to the rate at which corrosion will occur under any particular

TABLE 2 Electrical Resistivity of Various Minerals and Soils

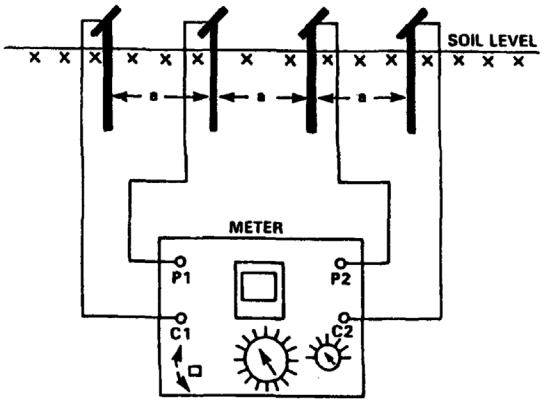
Minerals and Soils	Resistivity, ohm-cm
Minerals	
Pyrite magnetite	0.1 0.6–1.0
Graphite	0.03
Rock salt (impure)	3,000–500,000
Serpentine	20,000
Sederite	7,000
Igneous Rock	
Granite	500,000–100,000
Diorite	1,000,000
Gabbro	10,000,000–1,400,000,000
Diabase	310,000
Metamorphic Rocks	
Garnet gneiss	20,000,000
Mica chist	130,000
Biotite gneiss	100,000,000–600,000,000
Slate	64,000–6,500,000
Sedimentary Rock	
Chattanooga shale	2,000–130,000
Michigan shale	200,000
Calumet and hecla conglomerates	200,000–1,300,000
Muschelkalk sandstone	7,000
Ferruginous sandstone	18,000
Muschelkalk limestone	18,000
Marl	7,000
Glacial till	50,000
Type of Soil	
Sand	10,000–500,000
Oil sand	400–22,000
Gravel	20,000–400,000
Loam	3,000–20,000
Clay	500–2,000
Silt	1,000–2,000

TABLE 3 Soil Resistivity versus Degree of Corrosivity

Soil Resistivity (ohm-cm)	Degree of Corrosivity
0–500	Very corrosive
500–1,000	Corrosive
1,000–2,000	Moderately corrosive
2,000–10,000	Mildly corrosive
Above 10,000	Negligible

condition, and the results of any survey must be taken as giving only a general indication of the probability of corrosion. Chemical and other forms of industrial contamination of the soil can significantly influence soil resistivity and corrosivity. In real life, the soil is not homogeneous and layers are not always horizontal. In fact, as the spacing between Wenner pins changes, soil resistivity readings also may change.

FIG. 5 Four-electrode method for the electrical soil resistance measurement.



Several *commercial meters* allow measurement of soil resistivity. A commonly used resistance meter is shown in figure 6. One reliable and widely used instrument uses an alternating current 97-Hz square wave. It offers several advantages, such as eliminating the effect of polarization that can affect the measurements when using dc, and eliminating interference by 60-Hz sinusoidal currents.

Soil resistivity can be measured under either field or laboratory conditions. In the laboratory, the soil sample is placed and compacted to the same amount as the soil at the site in a *soil box*. The resistivity is measured by applying low voltage dc or ac. Errors could result from polarization when using a dc or ac current of too low a frequency. The soil box measurement (representing a specific soil sample) is a point measurement, not an average soil resistivity as is the Wenner method.

Soil resistivity testing using a soil box may be conducted with a four-electrode soil box as described in ASTM G57 (fig. 6) or a two-electrode soil box method (fig. 7 and fig. 8) as described in ASTM G187, *Standard Test Method for Measurement of Soil Resistivity Using the Two-Electrode Soil Box Method*. ASTM G57

FIG. 6 General view of four-pin soil resistance meter and four-pin soil box. *Source:* Photo courtesy of U.S. Pipe and Foundry.



FIG. 7 ASTM G187, two-electrode soil box.

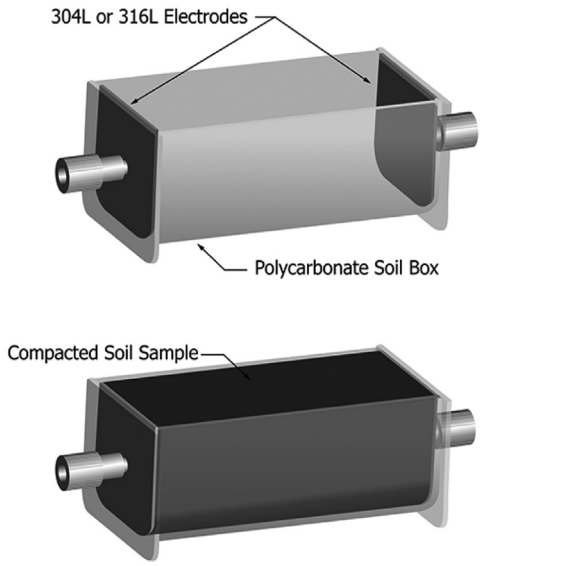
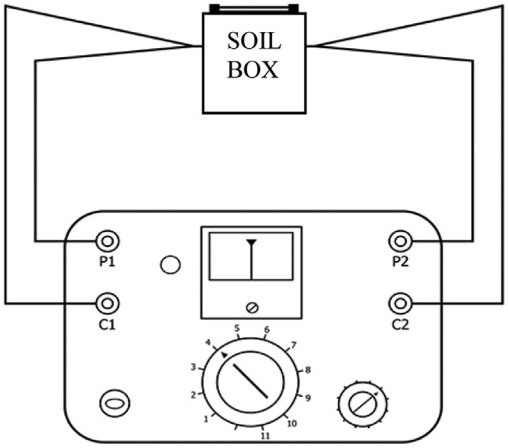


FIG. 8 Typical connections for use of two-electrode soil box with soil resistance meter.



emphasizes an *in situ* measurement commonly utilized in the design of a buried structures' corrosion control system (e.g., cathodic protection systems, ground bed design) and also includes information and procedures on a four-pin soil box method. The two-electrode soil box method is an accurate and more expeditious method than the four-pin soil box and often complements the four-pin *in situ* soil resistivity method.

In laboratory tests, the soil resistivity also can be measured at 100% water saturation using distilled water, which gives a value that could correspond to that of rainy climatic periods, when a lot of salts may be dissolved and cause a decrease of the soil resistivity. The temperature changes have only a slight effect on the soil resistivity value until total freezing of soil moisture occurs. The ice resistance, however, increases sharply as temperature drops. ASTM G57 includes a correction chart for resistivity based on temperature.

AERATION AND OXYGEN CONTENT

The percentage of the volume of the soil occupied by air at a certain moisture content is determined by *air-pore space* and is used for permeability characterization of the soil. High values of air-pore space could provide a dry soil environment, which may not permit the electrochemical development of corrosion. The aeration and oxygen content in soil moisture are important for the corrosion process, because the oxygen is the principal oxidizing agent in the cathodic (electron consumption) corrosion reaction. It is generally assumed that the gases of the upper layers of soil are similar in composition to the atmosphere above the soil, except for a higher carbon dioxide content. By the fact that the plant roots require oxygen to penetrate a soil, it may be assumed that gases in some soils at depths of 6 m or more contain a significant amount of oxygen. For soils with coarse texture, such as sand and gravel, the circulation of air is relatively free and the corrosion rate may reach that in the atmosphere.

From a corrosion perspective, the solubility of oxygen in soil moisture (electrolyte) is one of the most significant effects. The dissolved oxygen concentration increases until the saturation limit is reached. The solubility of oxygen in water is a function of temperature and the oxygen solubility decreases as soil temperature increases. The temperature, however, also increases the corrosion kinetics, even at lower levels of oxygen concentration. Some specific climates, such as warm and tropical humid (and their daily temperature variations), may cause expansion and contraction of the surface-soil gases. The oxygen content also depends on the biological activity within the soil and the consumed oxygen can be replaced with gases from metabolic activity, such as carbon dioxide.

Differences in oxygen concentration in layers of soils can result in the development of oxygen concentration corrosion cells. When the concentration of dissolved oxygen at two points on a metal surface is different, the surfaces in contact with the solution or soil containing the higher concentration of dissolved oxygen will become cathodic to the surfaces in contact with the solution or soil containing the lower concentration of dissolved oxygen. These surfaces exposed to the lowest O_2 concentration will suffer accelerated corrosion as anodes in an oxygen concentration cell. For example, on a buried pipe, an oxygen concentration corrosion cell may be set up between the pipe in contact with nonaerated undisturbed soil (i.e., bottom of a pipeline trench), and areas of the pipe in contact with aerated disturbed soil (i.e., backfill around a pipe). Corrosion will occur preferentially on the bottom of the pipe in contact with the low-oxygen-content nondisturbed soil.

OXIDATION-REDUCTION POTENTIAL

Oxidation-reduction potential (also called redox potential or ORP) for soil is defined by ASTM G200, *Standard Test Method for Measurement of Oxidation-Reduction Potential (ORP) of Soil*, as an "electrical potential measurement to determine the tendency of a soil to transfer electrons between its chemical species. It is the measured potential of an inert metal electrode (generally platinum) with respect to a reference electrode such as silver/silver chloride." In soils, redox potential can be used as an

indication of aeration, corrosivity, and the potential for microbiologically influenced corrosion (MIC) by sulfate-reducing bacteria (SRB). The use of redox potentials as one of the methods to predict soil corrosivity is presented in table 4.

Soil test procedures described in Appendix X1 of ASTM A674, *Standard Practice for Polyethylene Encasement for Ductile Iron Pipe for Water or Other Liquids*, states the following: "The oxidation- reduction (redox) potential of a soil is significant because the most common SRB can live only under anaerobic conditions. A redox potential greater than +100 mV shows the soil to be sufficiently aerated so that it will not support sulfate reducers. Potentials of 0 to +100 mV may or may not indicate anaerobic conditions; however, a negative redox potential definitely indicates the anaerobic conditions in which sulfate reducers thrive." Conditions under which SRB could grow do not prove that SRB are present.

RELATIVE ACIDITY (pH) OF SOIL

The soil moisture (electrolyte) can be described as acidic (pH < 7), neutral (pH = 7), or alkaline (pH > 7), based on the relative ratio of hydrogen ions (H^+) to hydroxyl ions (OH^-). When H^+ ions predominate over OH^- ions, the soil is acidic and vice versa. In a neutral solution, both ions are in balance. (The value of pH indicates only the hydrogen ion concentration.) Fresh water and seawater typically have a near-neutral pH. Concrete environments are strongly alkaline (pH ~13). The corrosion effect of soil moisture acidity or alkalinity depends very much on the specific metal of interest.

Acidity in soils is the result of processes of weathering under humid conditions, such as mineral leaching, decomposition of acidic plants, industrial wastes, acid rain, and certain forms of microbiological activity. Most soils range from pH 4.5 to pH 8. In this range, pH generally is not considered to be a problem for buried iron, steel, or concrete pipelines and steel tanks. Corrosion causing SRB, which are anaerobic and live in poorly drained soils, require a near-neutral pH environment from 6 to 8. More acidic soils (pH lower than 4.5) can cause rapid metal corrosion and serious risk to common construction materials, including some stainless steel (SS) grades. In areas with moderate rainfall, soluble salts accumulate only where the water concentrates in depressions. In areas with considerable rainfall, soluble salts and bases may be removed, potentially resulting in increased acidity.

Soil acidity, or its pH, is an important measured parameter. Details for conducting field and laboratory measurements of soil pH for use in corrosion testing are covered in ASTM G51, *Standard Test Method for Measuring pH of Soil for Use in Corrosion Testing*. Two electrodes, glass and calomel (or other reference electrode), of a standard pH meter are pressed into the soil and the value of their potential difference is linearly related to pH. A combination electrode consisting of a reference electrode and a glass electrode combined as a single electrode also is used commonly. By the nature of the measurement, pH is determined for a small volume of soil at each reading, and it is important that three measurements at different locations be made and that a simple average is calculated.

The pH of soil may be sampled *in situ*, from disturbed samples in the field brought to the surface, or in the laboratory. Of these three methods, the least desirable is that which is based on a soil sample transported to a laboratory for evaluation. If this must be done, it is recommended to make the pH measurement as quickly as possible after the soil is taken from the field.

In the case of soils rich in sulfide, the pH value could be more acidic because of the oxidation of sulfides to sulfates as the soil dries out. The treatment of the soil before pH measurement remains an open issue. Drying of soil samples and addition of distilled water are two of the treatments used. The soil pH value, however, is not sufficient to unambiguously indicate soil corrosivity. For example, a neutral soil (pH 6.6–7.3) could be corrosive because of the presence of chloride ions or the presence of SRB bacteria.

In some cases, a determination of the *total acidity* may be desirable. Additional measurement requires a soil treatment by mixing the soil with a solution of neutral salts like potassium chloride (KCl) or calcium dichloride ($CaCl_2$) to determine the *exchange* or *total acidity* of the soil, which includes the hydrogen ions loosely bonded to soil minerals. This extraction method is practically unaffected by fertilizers or other salts that may be present in the soil.

TABLE 4 Soil Redox Potentials as an Indicator for Soil Corrosivity

Redox Potential versus SHE[a]	Aeration	Soil Corrosivity Indicator
Negative	Not aerated	Extremely severe
0–100 mV	None to weak	Severe
100–200 mV	Weakly aerated	Moderate
200–400 mV	Aerated	Slight
Above 400 mV	Strongly aerated	Noncorrosive

[a]SHE, standard hydrogen electrode, conventionally accepted to be 0.00.

DISSOLVED SALTS AND CORROSION AGENTS

The soil water is a good solvent for salts of the soil, which dissociate to form cations and anions and render the soil conductive. In moderate rainfall areas, the soil solution is relatively dilute (80 to 1,500 ppm total dissolved salts). Lower salt concentrations characterize regions with extensive rainfall as a result of leaching action. Soils in arid regions usually are quite high in salts, because of surface evaporation.

The most common *cations* in the soil electrolyte are potassium and sodium in alkaline soils, magnesium and calcium in basic (calcareous) soils. Salts containing the four cations, K^+, Na^+, Mg^+, and Ca^{2+}, can accelerate metal corrosion. In nonacid soils, however, calcium and magnesium tend to form insoluble metal oxides or carbonates, which act as an effective barrier against corrosion. The corrosion rate in these soils may diminish significantly. From a corrosion point of view, the important anions found in soil and moisture are chloride (Cl^-), sulfate (SO_4^{-2}), nitrate (NGy), phosphate (PO_4^{-3}), carbonate (CO_3^{-2}), and bicarbonate (HCOy). These *anions* play an important role in the corrosion process because if they react with metal ions, produced during the anodic corrosion reaction, and form an insoluble salt precipitate on the metal surface, this layer could act as an

effective barrier against corrosion. This is the case of corrosion of lead sheathing for power and communications cables in a soil solution that contains SO_4^{-2}. This protective effect also has been reported for metallized zinc coatings on ductile iron pipe in which a protective layer was formed consisting of zinc carbonate, oxy-chloride of zinc, and other complex combinations.[14]

The most corrosive anion for metals is the chloride ion (Cl^-), which usually is naturally present in soils and sands of the marine-coastal regions, or it may be present as a result of external sources, such as de-icing salts applied to roadways. Its attack is localized and more dangerous than the uniform corrosion, because the formed pits could perforate the metal surface. The chloride ion concentration in corrosive soil electrolytes (moisture) varies as soil conditions alternate between wet and dry, and can significantly affect the soil resistivity. ASTM D512, *Standard Test Methods for Chloride Ion in Water*, may be used to analyze for chloride ions in water.

Sufficient chloride ion concentration can destroy the passivation of steel embedded in concrete and initiate corrosion if oxygen is also present at the steel surface. Where concrete cylinder pipe are to be buried in soils with resistivity readings below 1,500 ohm-cm and the water soluble chloride contents exceed 400 ppm at those same locations, corrosion protection in the form of a moisture barrier, silica fume addition, or cathodic protection (CP) is recommended.[15]

Compared with the corrosion aggressivity of chloride ions, sulfate ions generally are considered to be less aggressive for iron and steel. They can be converted, however, into highly corrosive sulfide ions by anaerobic SRB. Soil test procedures in Appendix IX of ASTM A674 includes a quantitative sodium azide-iodine test for sulfides as an indicator of the presence of SRB.

According to American Water Works Association (AWWA) Manual M9, *Concrete Pressure Pipe*,

> Instances of sulfate attack on concrete or mortar are generally limited to partially buried structures in soils containing high concentrations of sodium, magnesium, or calcium sulfate. For buried concrete pipe installations in soils with more than 2,000 ppm sulfate, cement with a tricalcium aluminate (C_3A) content not exceeding 5 percent should be specified. For installations of mortar-coated pipe in soils with more than 5,000 ppm water-soluble sulfates, use of both low C_3A cement and a barrier material should be considered.[15]

In some cases, the presence of sulfides such as hydrogen sulfide (H_2S) also should be determined. The ion concentration is measured in a water soil extract using various analytical techniques. Slightly alkaline ground water usually contains Na^+, Ca^{2+}, Mg^{2+}, SO_4^{2-}, and HCO_3^- ions, as part of the dissolved salts (<1,000 mg/L or in a higher range of 1,000–10,000 mg/L). In slightly acidic water, the principal ions are Na^+, Ca^{2+}, Mg^{2+}, and HCCV, with a lower concentration of total dissolved solids of <100 mg/L.

The salt content of soil may be altered by several human activities, such as fertilizer use in heavy doses, industrial wastes, deicing salts on road and walkways, salt brines from petroleum production, and many others. Another important relationship between the salt in the soil and corrosion has to do with biological activity. Because the growth of plants and microorganisms depend on the proper inorganic mineral nutrients, the action of these forms of life varies with the salt content of the soil.

MICROBIOLOGICAL ACTIVITY

The role of microbes or bacteria in the corrosion of metals is due to the chemical activities associated with their metabolism, growth, and reproduction. For example, the MIC of metals by SRB is a recognized problem in pipelines. These bacteria are anaerobic and live in poorly drained wet soils, with a pH from 6 to 8, that contain sulfate ions, organic compounds, and minerals in the absence of oxygen and temperature from 20°C to 30°C. In well-aerated soils, the anaerobic bacteria cause no problem. During metabolism of the bacteria, oxygen is extracted from the sulfate ions, and this reaction converts the soluble sulfates to sulfides, which attack the metal surface, forming, for example, iron sulfide (FeS). Numerous studies have established the relationship of sulfides and sulfates to bacterial activity in microbiologically induced metal corrosion.[16–22]

The corrosive microbial effect on metals can be attributed to removal of electrons from the metal and formation of corrosion products principally by the following:

- Direct chemical action of metabolic products, such as sulfuric acid, inorganic or organic sulfides, and chelating agents, such as organic acids; and
- Changes in oxygen content, salt concentration, and pH that increase the possibilities for differential diffusion and concentration gradients, which establish local electrochemical corrosion cells.

Anaerobic bacteria have been reported to accelerate the normal corrosion process and convert noncorrosive soil to an aggressive environment (fig. 9). The environmental conditions under which the microorganisms normally operate are as follows: temperature from 20°C to 30°C, pH from 6 to 8, and soil

FIG. 9 Localized corrosion attack on a buried pipe accelerated by the presence of SRB.



resistivity from 500 to 20,000 ohm-cm. Rate and extent of corrosion are related directly to bacterial growth in contact with the metallic surface. Bacteria have been found that are capable of growing on many kinds of coating materials, including hydrocarbons. One survey reported that MIC was responsible for 27% of the corrosion deposits on the exterior of line pipe.[12]

National Association of Corrosion Engineers (NACE) TM0106-2016, *Detection, Testing, and Evaluation of Microbiologically Influenced Corrosion (MIC) on External Surfaces of Buried Pipelines*, states the following:

> Microbiologically influenced corrosion (MIC) is corrosion caused by the presence or activity (or both) of microorganisms in biofilms on the surface of the corroding material. Many materials, including most metals and some nonmetals, can be degraded in this manner. Microbiologically mediated reactions can alter both rates and types of electrochemical reactions in a corrosion cell. These reactions influence pitting, crevice corrosion, differential aeration cells, concentration cells, de-alloying, and galvanic corrosion. Therefore, MIC investigations require microbiological, chemical, and metallurgical testing for proper diagnosis. The conclusion that MIC has taken place should be based on the preponderance of circumstantial evidence.
>
> MIC typically takes place in the presence of microbial consortia that are comprised of more than one physiological type of microorganism. Depending on the environment, these microbes may include metal-oxidizing bacteria, sulfate-reducing prokaryotes (SRP), acid-producing bacteria (APB), metal-reducing bacteria (MRB), and methanogens that interact in complex ways within the structure of the biofilm. MIC does not produce a unique form or morphology of corrosion. Instead, MIC can result in pitting, crevice corrosion, underdeposit corrosion (UDC), and de-alloying, in addition to galvanic corrosion.[12]

Test methods and procedures for evaluating external MIC include but are not limited to the following: microbiological culture testing, general microscopy, epifluorescent microscopy, adenosine triphosphate photometry (ATP), hydrogenase measurements, adenosine phosphosulfate reductase (APS), molecular microbiological methods (MMM; also referred to as genetic methods), organic acid analysis, and chemical analysis. See also chapter 35, "Microbiological Effects," of this manual for additional information.

DISTURBANCE OF NATURAL SOILS

Experience shows that the pipeline ditch markedly disturbs natural soil. The operation of ditching and backfilling create several zones around the metal structure. The soil in the ditch is less compact and sometimes the disturbed soil is a mixture of surface and subsurface soils. This new heterogeneous soil environment may have higher moisture content, increased aeration, and microbial population, which may result in differential aeration or concentration corrosion cells developing. Contact with organic matter in coatings applied over the pipeline and the previous factors may create conditions for accelerated localized corrosion attack.

Corrosion in Soils

The metal corrosion in soils is *aqueous* (in an electrolyte) and its mechanism is *electrochemical*.[1–6,8,9,11,23] It is generally accepted that four elements are necessary for the formation and operation of an electrochemical corrosion cell: an anode, a cathode, an electrolyte, and a metallic path. The terms are defined by NACE/ASTM G193, *Standard Terminology and Acronyms Relating to Corrosion*, as follows:

Electrochemical cell: an electrochemical system consisting of an anode and a cathode in metallic contact and immersed in an electrolyte.

Anode: the electrode of an electrochemical cell at which oxidation occurs. (Electrons flow away from the anode in the external circuit. It is usually the electrode where corrosion occurs and metal ions enter solution.)

Cathode: the electrode of an electrochemical cell at which reduction is the principal reaction. (Electrons flow toward the cathode in the external circuit.)

Electrolyte: a chemical substance containing ions that migrate in an electric field.

The electrochemical corrosion of metals buried in wet soils is based on the creation of multiple corrosion cells, formed by coupled anodes and cathodes. The cathodes are characterized by metal areas with a higher level of potential energy (Gibbs free energy) and the anodes have a lower potential energy. This energy difference between anodes and cathodes sites usually is due to the heterogeneity of composition of the metal structure. The soil in which the metal resides also could contribute to corrosion cell formation.

The metal corrosion is an oxidation process and it occurs at the anode areas where the metal goes into soil moisture as metal cation (ion), leaving electrons. The principal anodic reaction is as follows:

$$M \rightarrow M^{n+} + ne^{-}$$
$$(\text{i.e., } Fe_{steel} \rightarrow Fe^{2+} + 2e^{-})$$

The generated free electrons flow through the metal to the *cathode* areas, where they are accepted by oxidizing agents, such as air oxygen dissolved in the moisture. The oxidizing agents undergo a reduction process in the cathodic reaction:

$$O_2 + 2H_2O + 4e^{-} \rightarrow 4OH^{-}$$

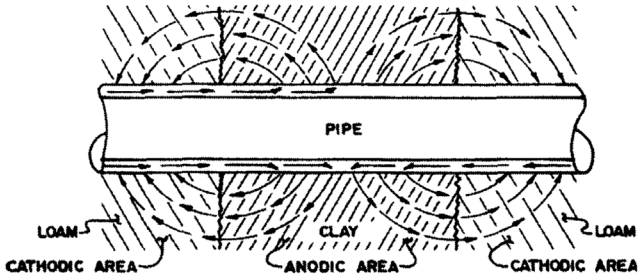
In weak acid soils, the cathodic reaction involves the participation of oxygen molecules and hydrogen ions (H^{+}):

$$O_2 + 4H^{+} + 4e^{-} \rightarrow 2H_2O$$

In strong acid soil the principal oxidizing agent is the hydrogen cation:

$$2H^{+} + 2e^{-} \rightarrow H_2 \uparrow$$

FIG. 10 A metallic pipe is anodic in wet soil with a lower oxygen content and cathodic in better oxygenated soil.



Different oxygen contents in the soil moisture at the metal surface can create local oxygen concentration cells. Wet soil with lower oxygen usually gives rise to anodic areas, whereas well-aerated soils form cathodic areas on the metal surface (fig. 10). In most cases, when the metal structure is exposed to different temperatures, the areas at higher temperatures become anodes and those at lower temperatures become cathodes. Because soils usually are a mixture of different kinds of soils, they often provide no uniform environment for the metal structure. This heterogeneous environment creates different and local aeration zones on the metal surface, and as a consequence, can cause serious localized corrosion attack (fig. 11 and fig. 12).

FIG. 11 Oxygen concentration corrosion cells caused by a mixture of different soils.

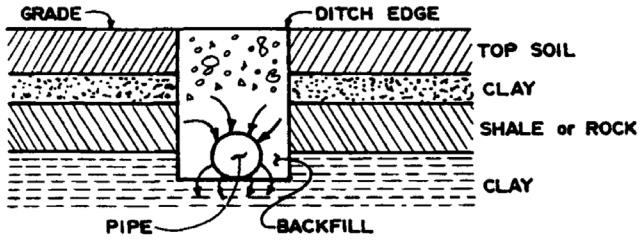


FIG. 12 General view of corrosion attack in soil at local aeration zones.



Sometimes pipes are buried with mill scale (FeO and Fe_3O_4 gray oxide layer) that is formed on their surface as a product of high-temperature chemical corrosion during hot-rolling production and thermal treatments. This layer is an efficient protective coating for the metal, because it is resistant to corrosion and it is quite adherent. It is brittle, however, and its structure presents a lot of heterogeneity and cracks that contribute to creation of local corrosion cells at the interface metal or scale. The scale oxides are electronic semiconductors, and they can serve as cathodes. Areas covered with scale are more cathodic than those in which the metal is not covered and open to the environment. Such bare area can be a perfect anode for a corrosion cell (fig. 13).

If the buried metal structure involves contact between different metals (e.g., mild steel, copper, bronze, brass, aluminum, zinc, lead, SS, cast iron), it is possible that local galvanic cells can form in the contact areas (fig. 14 and fig. 15). Each metal has its own tendency to corrode. An alternative way to express the metal reactivity is to look at the excess of its free energy (standard electrochemical metal potential) and predict the electromotive force (emf) between metals in contact, as a general indication for the corrosion process (table 5). The metal that has a more positive potential is nobler in the galvanic cell, and it is a cathode. The metal with a more negative potential is more active and acts as an anode in the corrosion cell (e.g., it suffers corrosion).

As corrosion proceeds, the steel changes its surface physical-chemical properties because of the formed corrosion layer. Insoluble corrosion products partially act as a physical barrier against the corrosion process. In this case, when a new

FIG. 13 Corrosion cell created on metal surface due to the presence of heterogeneity in the formed corrosion layer.

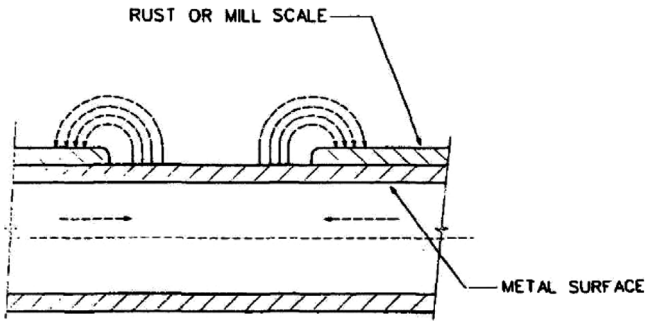


FIG. 14 Galvanic corrosion caused by contact of dissimilar metals. Steel is the anode, which suffers corrosion, and brass is the cathode. Electrons leave the steel and flow to brass.

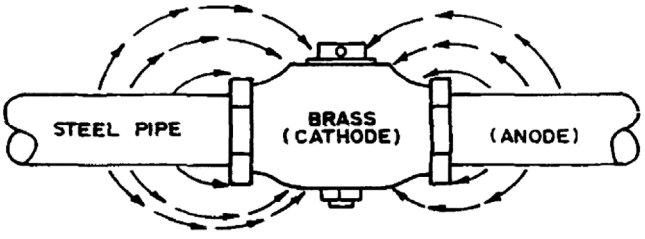


FIG. 15 Galvanic corrosion attack produced on the surface of buried pipe.



TABLE 5 Electromotive Series of Metals

Metal	Metal / Formed Ion	Potential, V[a]
Lithium	Li / Li +	−2.96
Rubidium	RbRb +	−2.93
Potassium	K/K +	−2.92
Strontium	Sr/Sr ++	−2.92
Barium	Ba/Ba ++	−2.90
Calcium	Ca/Ca ++	−2.87
Sodium	Na / Na +	−2.71
Aluminum	Al / Al +++	− 1.70
Beryllium	Be/Be ++	−1.69
Manganese	Mn/Mn++	−1.10
Zinc	Zn / Zn ++	−0.76
Chromium	Cr/Cr ++	−0.56
Iron (Ferrous)	Fe/Fe ++	−0.44
Cadmium	Cd / Cd ++	−0.40
Indium	In / In +++	−0.34
Thallium	Tl *m* +	−0.33
Cobalt	Co / Co ++	−0.28
Nickel	Ni/Ni ++	−0.23
Tin	Sn / Sn ++	−0.14
Lead	Pb/Pb ++	−0.12
Iron (ferric)	Fe / Fe +++	−0.04
Hydrogen	H2/H +	0.00
Antimony	Sb/Sb +++	+ 0.10
Bismuth	Bi / Bi +++	+ 0.23
Arsenic	As /As +++	+ 0.30
Copper (cupric)	Cu / Cu ++	+ 0.34
Copper (cuprous)	Cu/Cu +	+ 0.47
Tellurium	Te / Te ++++	+ 0.56
Silver	Ag/Ag +	+ 0.80
Mercury	Hg/Hg++	+ 0.80
Platinum	Pt/ Pt ++++	+ 0.82

(continued)

TABLE 5 Electromotive Series of Metals (*continued*)

Metal	Metal / Formed Ion	Potential, V[a]
Palladium	Pd/Pd ++++	+ 0.86
Gold (auric)	Au / Au +++	+ 1.36
Gold (auras)	Au / Au +	+ 1.50

[a]The metal that has a more positive potential is more noble in a galvanic cell between two metals, and it is the cathode. A more negative potential corresponds to the more active anodic metal. The state of oxidation of the metal ion (cation) is equal to the number of electrons liberated by the metal during the anodic corrosion process, for example: $Ni => Ni^{2+} + 2e$.

repaired part of steel is connected to old steel, which has been in the soil for a relatively long time, the new section suffers corrosion because it is anodic with respect to old steel, even when the steel composition is identical.

STRAY CURRENT CORROSION

Stray currents, picked up by a buried structure, also can cause metal corrosion. They are usually direct electric currents (dc) deflected from their principal service. Sources of stray currents could be direct current equipment and systems, such as electric railway systems, grounded dc power supplies, electric welders, CP systems for underground natural gas pipelines, and electroplating plants that are not well insulated from the earth. The metal structure suffers severe stray current corrosion at the area where the stray current discharges and leaves the metal, as it seeks for a new low resistance path. As shown in figure 16, when tracks are laid at ground level and not insulated well from the earth, some part of the load current enters the ground where the tracks are most positive (at the load) and follows an earth path back to the substation. The stray current corrosion looks like pitting on an otherwise-smooth surface where the stray current is discharged. Figure 17 is a photo of stray current corrosion on a ductile iron pipe joint. Corrosion occurred at the rubber gasketed joint, which increased resistivity of the pipeline and caused the current to seek an alternate lower resistivity return path. Stray current prevention measures include corrective design

FIG. 16 Stray current in street railways. The area near the substation, where a current flowing in a pipeline leaves its surface to return to the negative bus, can suffer severe corrosion attack.

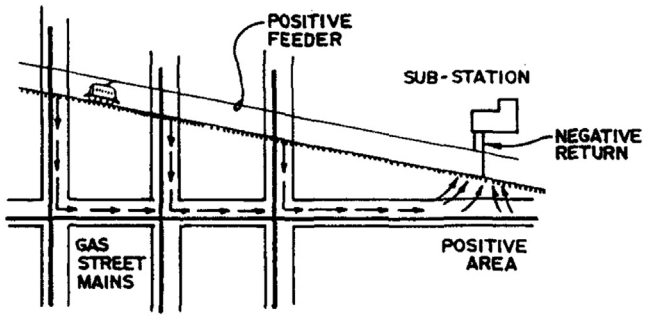


FIG. 17 Stray current corrosion failure on ductile iron pipe joint. Corrosion occurred where dc currents left the pipe and entered the soil. *Source:* Photo courtesy of U.S. Pipe and Foundry.



modifications, repair of electrical systems, corrective drainage, and good insulation. Lead pipelines and lead cable sheathing also can suffer severe stray current corrosion caused by minor earth currents.

PITTING CORROSION

In certain specific soil chemistries, the metal corrosion may be nonuniform, concentrated in relatively small areas that form sharply defined local holes called *pits* (fig. 18) that grow deep into the metal and can cause failure by perforation. The pits are usually small in diameter, isolated from each other, and occur in more anodic metal areas with respect to the rest of the surface. The pitting corrosion is a dangerous form of localized metal attack and sometimes cannot be detected by simple visual examination.

For example, when pitting corrosion occurs along with slight or moderate general corrosion, the corrosion products often mask the pits. Soils in marine-coastal environments containing relatively high concentrations of chloride ions (active anions) cause chloride-induced pitting corrosion on the metal structure. Once a pit initiates, an active corrosion cell is set up as shown in figure 19. The rapid dissolution of metal in the pit produces an excess of positive metal ions, which hydrolyze in the water solution, causing a high concentration of hydrogen ions. The cause of pitting could be associated with local inhomogeneity on the metal surface, mechanical or chemical defects (holidays) in a protective organic or oxide coating (Fig. 20), galvanic corrosion, or the presence of biological organisms. Pitting corrosion occurs most commonly in buried metals and alloys.

Some specific corrosion environments, in the presence of applied tensile stress on the metal surface (above some threshold value), can cause stress-corrosion cracking (SCC). The source of stresses can be external, but residual stresses can also cause SCC failures. Specific corrosive pollutants, which may contribute to the SCC of carbon steels, are for example, the carbonates in water. Sulfide stress cracking (SSC) commonly occurs on the

FIG. 18 General view of localized pitting corrosion on an underground pipe surface. *Source:* Photo courtesy of Corrpro, an Aegion Company.



FIG. 19 Pit action and active pitting cell.

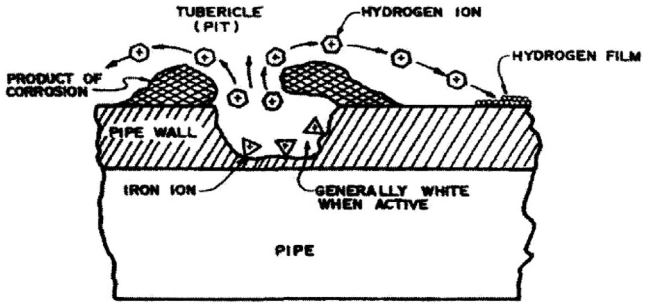


FIG. 20 Localized corrosion on buried metal structure, concentrated at holidays (defects) of the coated surface. *Source:* Photo courtesy of Corrpro, an Aegion Company.



outside of a pipe where SRB are present at a soil pH of 3–7. Because of the produced FeS, which adsorbs readily on the steel surface, hydrogen atoms generated during the cathodic corrosion reaction cannot combine to form molecular hydrogen, and therefore, enter into the iron crystal, causing hydrogen embrittlement and initiating microcracks.

GENERAL METHODS FOR CORROSION PROTECTION

The electrochemical corrosion of metals occurs at the metal–corrosive electrolyte (metal–soil moisture) interface. Consequently, the first group of methods for corrosion protection aims to create an efficient separation of the metal from the aggressive environment, using metallic, organic, and inorganic coatings.

Organic and inorganic coatings often are used in conjunction with CP. From the thermodynamic point of view, some metals can be polarized in a range of potentials where the metal enters into an immune (no corrosion) or passive state (creation of resistant oxides). These states could be achieved, respectively, by cathodic and anodic electrochemical methods of protection, applying external polarization (potential) using dc. Pourbaix diagrams provide useful thermodynamic information on the possible metal states using metal potential-pH of water solution coordinates.

When it is economically and technically feasible, a third method includes modification or chemical treatment of the corrosive environment, to decrease its aggressiveness, by changing its pH, salt, and moisture content; oxygen content; existing microbes; and existing bacteria. An example of environment modification which is described in ASTM G218, *Standard Guide for External Corrosion Protection of Ductile Iron Pipe Utilizing Polyethylene Encasement Supplemented by Cathodic Protection* is the use of a corrosion inhibitor and antimicrobial enhanced polyethylene encasement film to wrap ductile iron pipe in corrosive soils.[7]

A fourth method is decreasing the metal activity, by alloying with metals, like chromium, nickel, molybdenum, cobalt, titanium, and copper, that usually form passive oxide layers and that are resistant in a given environment.

STEELS IN SOILS

One of the most frequently used materials for buried metal structures is carbon steels. For prevention of their corrosion the most recommended method is CP, which normally is used in conjunction with coatings. The use of CP is now standard procedure for long-term corrosion protection of underground regulated pipelines, oil and gasoline tanks, and other structures. With a shift of the metal potential to more of a negative value of -0.85 V versus a copper/copper sulfate ($Cu/CuSO_4$) reference electrode, it is possible to make the metal surface a cathode, which ensures an immune state of the carbon steel. Cathodic polarization is achieved by dc, which can be supplied either by sacrificial anodes in galvanic contact with the steel structure, or by impressed current from a rectifier.

Some organic coatings like polymers, plastics, and rubbers, other than paint, are used to advantage along with CP of steels. Coatings of coal tar, coal tar/epoxy, extruded polyethylene, tape wraps, polyurethane, or fusion-bonded epoxy powders are used to ensure a passive metal protection, isolating the metal from the soil environment, and also to decrease the current required for CP. Several references provide a more detailed discussion of CP and coatings for carbon steel.[9,11,25,26]

SS also is used as a material for buried metal structures. In principle, the SS should be in the passive state in soils, because of the naturally formed resistive oxide layer on its surface, composed of oxides of different alloying elements (nickel, chromium, molybdenum, copper) and iron. The presence of chloride in the soil, however, can cause SS to pit or corrode in crevices, so this material should be avoided in chloride-containing soils. It is also known that SS can be attacked by certain species of microbes, contributing to MIC. An increase in chromium content of steel decreases the observed weight loss in a variety of soils, but above 6% chromium, the depth of pitting increases.

DUCTILE IRON PIPE IN SOILS

Ductile iron piping is used primarily in water and wastewater service. The primary method of external corrosion control is polyethylene encasement installed in accordance with ASTM A674. In Europe, the primary method for corrosion protection for ductile iron pipe has been metallic zinc coatings for typical soils supplemented with polyethylene encasement for aggressive soils. Recently in the United States, an enhanced polyethylene encasement infused with corrosion inhibitor and antimicrobial additives has become commercially available. CP, with and without coatings and polyethylene encasement, also has been used. Several references provide a more detailed discussion of corrosion protection methods for ductile iron pipe in soils.[7,9,10,14,26,27]

CONCRETE PRESSURE PIPE IN SOILS

Concrete pressure piping is used primarily in water and wastewater service. Types include pre-stressed concrete cylinder pipe (AWWA C301), reinforced concrete cylinder pipe (AWWA C300), reinforced concrete noncylinder pipe (AWWA C302), and concrete bar-wrapped cylinder pipe (AWWA C303). Various corrosion control recommendations are given based on pH, carbon dioxide content, chloride content, and sulfate content of the soils. Corrosion control recommendations include moisture barrier, bonded joints, a system to monitor corrosion activity, CP, silica fume addition equal to 8–10% of concrete, membrane, sealer, barrier coating, consolidated limestone, and consolidated clay. Several references provide a more detailed discussion of corrosion protection methods for concrete pressure pipe.[9,15,24,26]

LEAD IN SOILS

Another metal with a successful service record in soils is lead. Thousands of kilometers of lead-sheathed power and communication cables and lead pipes have shown good performance underground. They are directly buried in the ground or installed in ducts or conduits. Lead corrodes less on the average than does steel. Most of the initially formed corrosion products of lead are relatively insoluble salts, such as carbonates, silicates, or sulfates.

They are deposited on the lead surface and ensure compact and dense protective layers for the metal. The formation of such a layer is responsible for the high resistance of lead to corrosion. Because of its less negative potential (table 5), the lead is cathodic when connected to steel (except for strongly alkaline environments), aluminum, zinc, or cadmium, and thus will accelerate the corrosion process of these metals. Only in galvanic contact with copper, SS, and titanium, will lead be an anode in the formed corrosion cell and suffer corrosion attack. In poorly aerated soils or soils high in organic acids, the corrosion rate may be four to six times higher than the average. Other factors that may accelerate the corrosion of lead are stray currents, microorganisms (like SRB), a high concentration of hydroxides (e.g., up to 1,000 ppm in a wet concrete tunnel), and contact with acetic acid (in a wooden duct). CP criteria and test methods are given in NACE RP0194, *Criteria and Test Methods for Cathodic Protection of Lead Sheath Cable*.[28]

COPPER IN SOILS

Copper is another metal used for underground cables and it usually has very good corrosion resistance. Copper, on average, corrodes at about one-sixth the rate of iron, but in tidal marsh, the rate is higher than in most other soils (i.e., about half that of iron). When connected to buried steel or iron, the copper will be a cathode of the galvanic cell and will not suffer any corrosion.

Laboratory Corrosion Testing in Soils

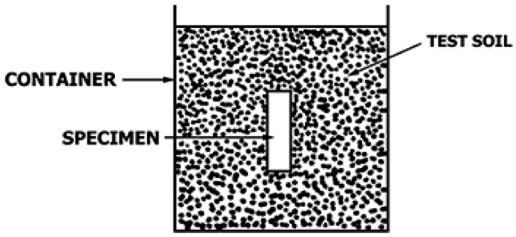
LABORATORY SOIL BOX CORROSION TESTING

ASTM G162, *Standard Practice for Conducting and Evaluating Laboratory Corrosion Tests in Soils*, covers procedures for conducting laboratory corrosion tests in soils to evaluate the corrosive attack on engineering materials.[29–31] The test is conducted under laboratory ambient temperature unless the effect of temperature is being evaluated. It does not include provisions for MIC testing, nor its influence on results. Structures and components may be made of several different metals; therefore, the practice may be used in conjunction with ASTM G71, *Standard Guide for Conducting and Evaluating Galvanic Corrosion Tests in Electrolytes*, to evaluate galvanic corrosion effects. This practice also may be used in conjunction with ASTM G46, *Standard Guide for Examination and Evaluation of Pitting Corrosion*, to evaluate pitting corrosion. A minimum of 40 cm^3 soil is specified to be used for each 1 cm^2 of exposed metal surface area (fig. 21). This practice is used to determine corrosion rates based on weight loss, pitting corrosion, galvanic corrosion effects, effect of defective metallic coatings, effect of defective or incompletely covering coatings and jackets, and the effect of multiple types of soils on specific materials.

ELECTROCHEMICAL LABORATORY TESTS

Several electrochemical tests have been used successfully over the years to estimate the corrosion behavior of a given metal in soil

FIG. 21 Apparatus for conducting ASTM G162.



or to determine the soil corrosivity.[32–36] These tests can be carried out in water extract of soil or in water-saturated soil, when all dissolved salts (ions) are present.

Electrochemical test methods and practices are described in several of the following ASTM Tests Methods and Practices:

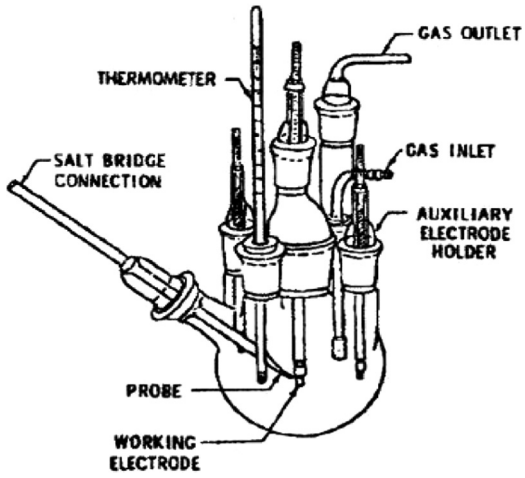
- ASTM G3, *Standard Practice for Conventions Applicable to Electrochemical Measurements in Corrosion Testing*
- ASTM G5, *Standard Reference Test Method for Making Potentiostatic and Potentiodynamic Anodic Polarization Measurements*
- ASTM G59, *Standard Test Method for Conducting Potentiodynamic Polarization Resistance Measurements*
- ASTM G61, *Standard Test Method for Conducting Cyclic Potentiodynamic Polarization Measurements for Localized Corrosion Susceptibility of Iron-, Nickel-, or Cobalt-Based Alloys*
- ASTM G71, *Standard Guide for Conducting and Evaluating Galvanic Corrosion Tests in Electrolytes*
- ASTM G102, *Standard Practice for Calculation of Corrosion Rates and Related Information from Electrochemical Measurements*
- ASTM G106, *Standard Practice for Verification of Algorithm and Equipment for Electrochemical Impedance Measurements*
- ASTM G148, *Standard Practice for Evaluation of Hydrogen Uptake, Permeation, and Transport in Metals by an Electrochemical Technique*

These standard methods and practices provide the necessary information for electrochemical potentiostatic and potentiodynamic anodic measurements, calculation of corrosion rate from electrochemical measurements, and conducting potentiodynamic polarization resistance measurements. Recently, electrochemical impedance spectroscopy (EIS) has been introduced for corrosion measurements of steel structures corroding in soils. These tests can be performed using a commercial potentiostat, appropriate computer software for analysis of the results, a standard electrochemical cell, a platinum or carbon counter electrode (CE), a reference electrode, and a sample of the metal as a working electrode (WE). Figure 22 presents a general view of equipment in use for electrochemical measurements, figure 23 shows a standard electrochemical test cell as described in ASTM G5, and figure 24 shows a test cell specially constructed to conduct

FIG. 22 General view of equipment for electrochemical measurements. *Source: Photo* courtesy of U.S. Pipe and Foundry.



FIG. 23 Standard electrochemical test cell as described in ASTM G5.



electrochemical corrosion testing in soils and horizontal directional drilling fluids.[36]

Field Burial Corrosion Testing

Underground corrosion is particularly insidious in that, generally, we are not aware of its progress until a failure occurs. Physical and electrochemical techniques are available, however, that will provide information on corrosion processes.[29–31,37–54] Physical measurements furnish cumulative corrosion information obtained at the final removal stage, while monitoring and electrochemical measurements supply data during the period of exposure to soil.

This section on field testing will concentrate on the types of underground corrosion measurements that can be made in controlled and uncontrolled conditions, with an emphasis on

FIG. 24 Special electrochemical test cell constructed to conduct testing in soil and drilling fluids.[36] *Source:* Photo courtesy of U.S. Pipe and Foundry.



controlled site testing. At a controlled exposure site, metal samples are intentionally exposed so that control of variables such as specimen surface area and size, depth of burial, minimum electrical and mechanical interference, and site accessibility are maximized. The design of this type of site allows for retrieval of specimens from the ground without interrupting services, as may be the case with a real structure. In an uncontrolled exposure site, these variables may be in question, and this situation usually applies to any real underground structure. For example, the surface area of an underground pipeline is difficult to determine, because from the standpoint of electrochemical polarization measurements, the pipeline is of infinite length. In addition, electrical isolation from other structures or services may not be possible with an underground system in use. In general, techniques for measuring corrosion are the same for controlled and uncontrolled sites, but some precautions and limitations must be kept in mind when these techniques are applied to real structures, and these will be discussed where appropriate. Assessing the corrosion of buried steel tanks is complicated by the presence of internal corrosion as well as external wall deterioration. This special case is addressed in ASTM G158, *Standard Guide for Three Methods of Assessing Buried Steel Tanks.*

MAINTAINING RECORDS

Determining corrosion performance of metals in underground environments generally requires long-term testing, sometimes exposures of several years or even decades. Such long-term studies make it imperative that information be maintained in a readable, accessible, permanent system. Experience has shown that a bound notebook with numbered pages is one format that has

proven successful for keeping these records. These data must include the exact location of the test site and its configuration. Identifying the location of the site with reference to survey markers or other reliable long-term features may be warranted, and this becomes more important as the length of exposure is increased. Computer files are invaluable for organizing and examining data, but they are a poor format for long-term storage of data. Changes in computer equipment, software, or damage may make it difficult or impossible to access old data files. For this reason, hard paper copies of burial plots and records are recommended to supplement electronic records. The importance of maintaining good records cannot be overemphasized.

Using global positioning satellite (GPS) technology, a point on the surface of the earth can be identified with an error of less than ± 1 m, making it an attractive means of identifying the location of buried specimens. One test site out of the direct control of this author was paved over for parking motorized equipment, and survey information allowed for successful retrieval of the specimens. Specimen surface treatment, heat treatment, and identification marks must be carefully described in these records. Photographic records during all phases of preparation and burial are useful for future site and specimen evaluation.

SPECIMEN DESIGN

The design of specimens is determined by several factors, such as the form of corrosion expected (e.g., uniform corrosion, pitting), the type of structure in question (e.g., pipe, tank), and the measurements necessary for obtaining the data. Measurement requirements for determining the loss in a cross section of a structural H-pile are different from measurements designed to examine pitting of a pipeline material. In general, the larger the sample exposed, the better the data, but a size limitation may be imposed by the measurements. Weight loss data requires weighing a specimen before and after exposure, and for this type of data, the size and weight of a sample is limited by the capabilities of the weighing equipment. Surface preparation of a sample must be considered. If the sample is a simulation of a real structure, then care should be taken to ensure that the specimen surface is representative of that structure. Thus, chemical cleaning, abrading, and polishing of the specimen surface may be undesirable if the real structure is not subjected to the same surface treatment. For evaluation of pipeline materials, a segment of the pipe with endcaps to protect the interior may be the most suitable design for a test specimen. It is also common practice to use sheet material for specimens, where sheet metal is used to produce containers such as holding tanks. Where welds are encountered, it is valuable to include specimens with welded sections in the burial test. Coated panels and coated panels with intentional breaks in the coating may be desirable. Galvanic coupling of specimens is also a consideration, where two unlike metals are expected to be in contact. Stressed U-bend or C-ring type specimens are used for studies of stress corrosion failures. Specimen identification marks stamped or scribed must be easy to read. Thus, the design of the specimen is tailored to meet the needs of the study.

CONSIDERATIONS FOR PHYSICAL MEASUREMENTS

Weight loss, pit depth, or wall thickness determinations are physical measurements used as a reference to correlate nondestructive electrochemical techniques. Physical measurements are considered destructive because, generally, the specimen must be removed from the site and cleaned. The process of extraction and preparation for examination changes the surface condition of the specimen, effectively destroying the possibility of continuing the exposure test with that particular specimen. Nevertheless, to rely solely on electrochemical measurements can result in misleading information, and it is strongly recommended that the test design include some form of physical verification of nondestructive measurements. To obtain corrosion data from physical measurements during long-term exposures, it is common practice to place enough samples in the ground to allow for removals at intervals of time. The most meaningful data are obtained when duplicate samples are used for each removal, allowing for data averaging and providing a better representation of material performance.

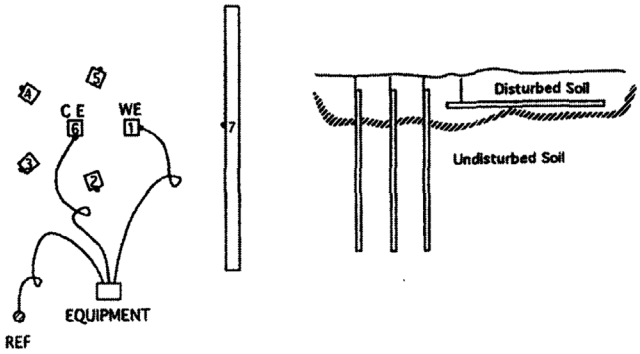
BURIAL SITE

Choosing the correct burial site is important, because the environment will have a direct effect on the performance of buried materials. This choice must take into account more than just characteristics of a soil and long-term availability; it also must include consideration of local conditions of temperature, rainfall, and location. For example, a soil located in a valley near a stream provides a different environment to the same soil on a nearby hill. In general, the best test site is near the structure in question. Such a site has the added advantage that measurements can be made on the real structure, which then can be compared to data obtained from controlled specimens nearby. Where a variety of soils are encountered, several soil sites may be needed. If only one site is chosen, then the site with the worst-case conditions will provide the most conservative data. Where anaerobic bacterial corrosion is of concern, redox potential measurements of the soil can identify the sites where these bacteria are most likely to be present.[44] Soil characterization and testing methods are discussed in other sections of this chapter.

SPECIMEN EMPLACEMENT

The manner in which a sample is buried is influenced by the configuration of the specimens. For example, steel piling specimens are driven into the ground with pile drivers, whereas small specimens will most likely be buried in trenches dug with a back hoe. A typical steel pile test site involves the placement of five pilings in a 2-m radius circle around a sixth centrally located pile, as illustrated in figure 25.[45] The central pile was used as a CE during electrochemical polarization measurements of the other piles, as will be explained later. The top of each pile was 0.6 m below ground level, and a steel rod that extended to just below the surface of the ground was welded to the top of each pile. A removable concrete marker, extending above ground, was placed over the rod to help locate the steel rod. Because the study included an examination of the effect of disturbed soil, a seventh pile was buried horizontally in a nearby trench.

FIG. 25 Typical view of steel pile placement at an underground test site.



Small specimens can be buried in a long, narrow excavation made by a backhoe, as shown in figure 26. Such a trench is typically 1–2 m deep and is as wide and long as necessary to accommodate the specimens placed along the length of the trench. In cases in which several retrievals are to be made over a period of time, specimens for a given removal can be grouped together in one section of the trench, so that when a group is retrieved, those remaining are not disturbed during digging (fig. 27). In cases in which electrical wires from specimens extend above ground, commercially available test stations, as shown in figure 28, are commonly used. Wood posts also may be used to serve as markers and hold the wires. Untreated wood is recommended, because leaching of chemicals from treated wood will modify the surrounding soil and possibly affect the results of the corrosion test. It is especially important to avoid placing wood treated with copper salts near aluminum specimens, because it is known that copper ions accelerate the corrosion of aluminum. Retrieval of specimens without wires may be simplified by tying specimens together with a small-diameter plastic cord and attaching the cord to wood posts. In this way, finding the cord or one

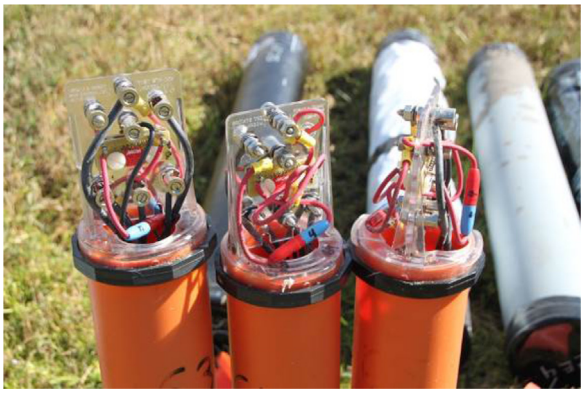
FIG. 26 Long narrow trench used for burial of corrosion test specimens. *Source:* Photo courtesy of U.S. Pipe and Foundry.



FIG. 27 Specimens for a given removal can be grouped together in one section of the trench, so that when a group is retrieved, those remaining are not disturbed during digging. *Source:* Photo courtesy of U.S. Pipe and Foundry.



FIG. 28 Commercially available test stations used for aboveground monitoring wire attachment. *Source:* Photo courtesy of U.S. Pipe and Foundry.



specimen allows retrieval of all other specimens in a group. Wooden posts can be used as trench markers to delineate groups of specimens, or metal markers can be located just below the ground surface and later can be found using a metal detector.

More than one system of specimen identification should be incorporated in the test. For example, stamping identification characters on the specimen and on an attached plastic label reduces problems of identification in the future. In addition, specimens can be buried in a known sequence for further verification of identity.

SPECIMEN RETRIEVAL

Immediately after excavation, a rapid superficial cleaning of specimens with a scrubbing brush and water allows for easy removal of oxides and soil–oxide conglomerates that harden as they dry, making later cleaning difficult. An immediate cursory examination of specimens on initial removal, coupled with photographic documentation, has several advantages. This examination can become important in those unfortunate cases in which

specimens are lost or damaged in transit. Furthermore, although identification of a specimen may be obvious on removal, it may be difficult later if tags are separated or lost, and thus documentation with photographs or notes becomes crucial for identification. In cases in which specimens have corroded to the point of separation, it is important to tag the parts for later identification, and this may include placing specimens in envelopes or bags. In some cases, metal specimens undergo surface changes after retrieval, especially if there is a long period of time between removal and final examination, and photographs help identify those instances in which this happens, allowing the examiner to differentiate between burial damage and damage from subsequent handling. This can be especially important in cases in which coatings are involved in the test. Thus, the employment of some precautions and documentation on initial removal of specimens will save time and effort in subsequent examination procedures.

Some information can be obtained from the soil at the time of sample extraction. For example, soil conditions may vary along the length of a trench, resulting in a variation in the corrosion performance of similar samples, and these soil differences should be noted. In some cases, where warranted, local measurements of soil pH, resistivity, and redox at the depth of the specimens can provide insight to material performance. When *in situ* pH measurements as described in ASTM G51 cannot be performed, the use of pH paper is an excellent method of obtaining a rapid reading on a soil. Unusual conditions of pH found with pH paper can be verified with more traditional pH electrodes. The resistivity of small samples of soil can be measured using a soil cup or soil box. The use of these techniques is an excellent way of getting information on localized soil conditions in the vicinity of the specimens. Always be aware that local, small soil sample readings can change dramatically from place to place in the same trench, and these readings must not be assumed to be representative of the soil as a whole.

CLEANING AND EXAMINATION OF SPECIMENS

Examination of specimens at the time of excavation is a critical step in the process of obtaining information from underground exposure studies. As has already been suggested, it is instructive to examine and characterize the condition of specimens before the final cleaning process. The presence or absence of an oxide on a corroded surface, the color of an oxide, and its location on the metal surface provide clues to the mechanism of attack. This initial examination is followed by removal of all corrosion products from the specimen. Fortunately, information on this difficult process, including the removal of oxide layers with minimum substrate attack, has been published by ASTM Committee G01 on Corrosion of Metals, in ASTM G1, *Standard Practice for Preparing, Cleaning, and Evaluating Corrosion Test Specimens*. This publication describes reagents and detailed chemical and electrochemical methods for cleaning ferrous and nonferrous metallic specimens.

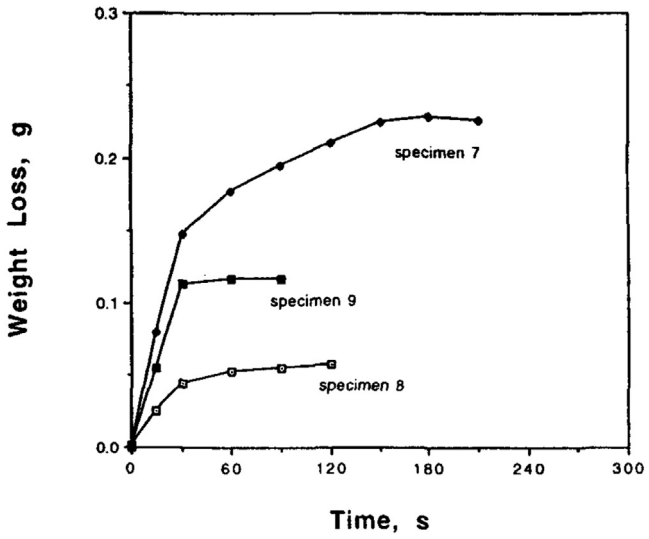
PHYSICAL MEASUREMENTS

Weight Loss

Determining weight loss resulting from exposure to soil is a common technique used to measure corrosion rate. This type of data is most meaningful when corrosion is uniform over the surface of the specimen, because normally the entire exposed surface area of the specimen is used for calculating corrosion rate. If corrosion attack is localized and the total exposed surface area is used for the corrosion rate calculation, then the result will underestimate penetration. One possible way around this problem is to measure the area where the localized attack has occurred and use this corrected area in the calculation of corrosion rate. Possible sources of error in weight loss determinations are (1) excessive removal of metal during cleaning, (2) inadequate cleaning of specimen, and (3) using the total surface area for calculating corrosion rate when the attack is localized.

A typical approach that has been used to determine weight loss of specimens through physical measurements is as follows. Small steel coupons, weighing approximately 200 g, were exposed to a soil environment. The samples were weighed before and after exposure. Prior to the "after exposure" weighing, the samples were cleaned using the ASTM solution designation C.3.1, which is an inhibited hydrochloric acid solution described in detail in ASTM G1. To determine the immersion time necessary for the removal of the oxide, the specimens were cleaned and weighed repeatedly, until weight loss stabilized, indicating that the cleaning reaction had gone to completion. Figure 29 shows an example of these data. Note that specimen 9 required immersion of only 30 s to remove the oxide, whereas specimen 7 took approximately 2.5 min to clean. This cleaning and weighing procedure allows for monitoring of the chemical process and reduces the likelihood of error from removing too much base metal. ASTM G1 also provides information on the mathematical procedure for calculating corrosion rate from weight loss in terms of a variety of units, both English and metric.

FIG. 29 A plot of weight loss versus time for three steel coupons in inhibited hydrochloric acid, showing the initial rapid oxide removal and the slower dissolution of metal as a function of time.



Pit Depth

Obtaining information of the degree of pitting involves some form of visual inspection, so that the shape, depth, and density of pitting can be determined. Large shallow pits are relatively easy to evaluate, compared with small, narrow, deep pits. The degree of pit penetration of wide pits can be measured with a pit depth micrometer or by the use of a microscope that allows for measuring the change in movement of the stage when focusing between the bottom of the pit and the surface of the metal. Determining the shape and depth of a narrow, deep pit is more challenging and may involve a metallographic cross-sectional examination of the pitted area. This same metallographic technique may be the most effective way of examining pits that get wider with depth. A crude but effective way of measuring the depth of relatively straight-line pits is to insert a small diameter wire into the pit and measuring the length of penetration by the wire. In some cases, the rate of wall penetration is critical, as for pipeline material, and identifying and measuring the deepest pit is important, along with information on the average penetration of the 10 deepest pits. Density of pitting can be obtained by counting pits in a known area or by comparing the pitted surface to standard charts as described in the ASTM G46.

STRESS INDUCED FAILURE

Determining susceptibility of a material to SCC or hydrogen embrittlement in a soil environment has been studied using buried U-bend specimens.[46] This approach provides information on whether or not a specimen failed, but it will not reveal when, during the exposure period, the failure occurred. One novel method for the application of stress allows for monitoring the condition of the specimen from the surface, using a steel ring located above ground level to apply the stress to a tubular tensile specimen in the soil via a steel rod.[47] By monitoring the load on the steel ring, the failure of the tensile specimen is detected. Another technique that provides a remote indication of failure is the aboveground monitoring of gas pressure used to apply a hoop stress to small containers buried in the ground. The ASTM committee on the corrosion of metals has developed and published standard methods for the use of U-bend (ASTM G30, *Standard Practice for Making and Using U-Bend Stress-Corrosion Test Specimens*) and C-ring specimens (ASTM G38, *Standard Practice for Making and Using C-Ring Stress-Corrosion Test Specimens*) for the application of stress.

Corrosion Monitoring in Soils

DIRECT AND INDIRECT CORROSION MEASUREMENTS AND TECHNIQUES FOR USE

The corrosion behavior of a buried metal structure needs to be indirectly controlled or monitored to determine the time for direct examination when repairs may be necessary.[29–35,37–43,55–58] Looking at the corroded surface is usually expensive and is acceptable only for a special corrosion situation. Direct external surface assessment, however, may be imperative, for example, to verify some indirect measurements or for visual examination of the coating for damage. Direct assessment also gives a possibility for direct mechanical or ultrasonic measurement of pit depth and wall thickness change due to the corrosion. X-ray radiography can be used to inspect welds. This technique also can show SCC and corrosion pits in the weld area where the coating has failed to seal the metal structure. The following NACE Standard Practices (SPs), Recommended Practices (RPs), Test Methods (TMs), and other publications discuss direct and indirect measurements and techniques for corrosion monitoring in soils:

- SP0104, *The Use of Coupons for Cathodic Protection Monitoring Applications*
- SP0169, *Control of External Corrosion on Underground or Submerged Metallic Piping Systems*
- SP0207, *Performing Close-Interval Potential Surveys and DC surface Potential Gradient Surveys on Buried or Submerged Metallic Pipelines*
- TM0497, *Measurement Techniques Related to Criteria for Cathodic Protection on Underground or Submerged Metallic Piping Systems*
- RP0174, *Corrosion Control of Underground Residential Distribution Systems*
- RP0177, *Mitigation of Alternating Current and Lightning Effects on Metallic Structures and Corrosion Control Systems*
- RP0194, *Criteria and Test Methods for Cathodic Protection of Lead Sheath Cable*
- RP0274, *High-Voltage Electrical Inspection of Pipeline Coatings*
- RP0285, *Corrosion Control of Underground Storage Tank Systems by Cathodic Protection*
- RP0286, *Electrical Isolation of Cathodically Protected Pipelines*
- RP0375, *Wax Coating Systems for Underground Piping Systems*
- RP0502, *Pipeline External Corrosion Direct Assessment Methodology*
- Pub. 05107, *Report on Corrosion Probes in Soil or Concrete*
- Pub. 07037, *Use of CP Coupons and Soil corrosion Probes in Application of Pipeline Cathodic Protection Criteria*

POTENTIAL MEASUREMENT IN SITU

This measurement establishes the corrosion potential of buried metal in a given soil. Its value is an indication of the degree and extent of corrosion attack and the efficiency of applied CP. The metal potential usually shifts with time to less negative values if the corrosion products form an inert and compact layer on the metal surface. As a result, it is possible to observe more positive potential values on an old structure than those measured on a new metal surface. A new, coated steel pipe may have a potential of -0.7 V versus a $Cu/CuSO_4$ reference electrode, whereas an old pipe surface is generally more positive (-0.1 to -0.3 V). The surface areas where the potential is less negative will be more cathodic, and as a consequence, they will suffer less corrosion.

Stray currents or interference from foreign CP systems may cause potential fluctuations and have to be taken into account.

The *in situ* CP test criteria for full protection of steel is that all measured points are more negative than -0.85 V versus a $Cu/CuSO_4$ reference electrode. For long pipelines, passing through different types of soil, the potential is usually measured every 30 m or less (often at 1.5 m).

Experience indicates that the corrosion potential value of buried copper cable correlates with its corrosion behavior (table 6). A potential value of -0.50 V or more negative, versus a $Cu/CuSO_4$ reference electrode, indicates full CP of this metal, typically provided by a connection to a steel structure.

Potential measurements of metal in soil require the use of some assistance tools, such as insulated wire, reels, alligator clips, terminal connectors, hand tools, a reference electrode (RE), and specialized equipment like voltmeters and ammeters. The saturated $Cu/CuSO_4$ RE is the most used in soils (+ 0.316 V versus SHE standard potential). This RE has poor reproducibility and needs to be frequently checked and renewed. In high chloride environments, the most appropriate electrode is a silver/silver chloride RE (Ag/AgCl/KCl (0.1N) +0.288 V versus SHE standard potential). Usually it provides reproducible and reliable values. The lead sulfate RE ($Pb/Pb0_2/PbS0_4/ H_2S0_4$ (0.1M), + 1.565 V versus SHE standard potential) is connected to lead-sheathed cables for measurement of their potential. Very dry soils may be wetted or a shallow hole may be dug to establish good electrical contact between the electrode and the soil moisture. The RE should be placed near the metal structure, auguring a hole down to near the pipeline surface, to minimize ohmic potential drop (IR) resulting from the soil and coating resistance. The tester must avoid any damage to the coating or protective scale on the metal. The potentials over well-coated pipelines do not vary much over distance.

Factors affecting the potential measurements are broken test leads, corroded contact points, inaccurate RE, and defective insulation of test leads. The existence of vegetation or of other metals may introduce errors of more than 100 mV. An improperly calibrated RE can also be an important source of errors. ASTM G215, *Standard Guide for Electrode Potential Measurement*, and Appendix A of NACE TM0497 contain information regarding calibration, care, and maintenance of reference electrodes.

The metal potential can be measured using voltmeters with more than 10 $M\Omega$ input impedance. Ammeters are used to measure electric current passing through the structure protected by CP and are relatively low-resistance instruments.

TABLE 6 Copper Potential and Corrosion Behavior

Potential vs. Cu/CuSO	Corrosion Behavior
Positive to -0.1 V	Probably corroding
−0.1 to -0.25 V	Possibly corroding
−0.25 to -0.50 V	Probably not corroding
−0.50 V or more negative	Full protection

POTENTIAL MAPPING

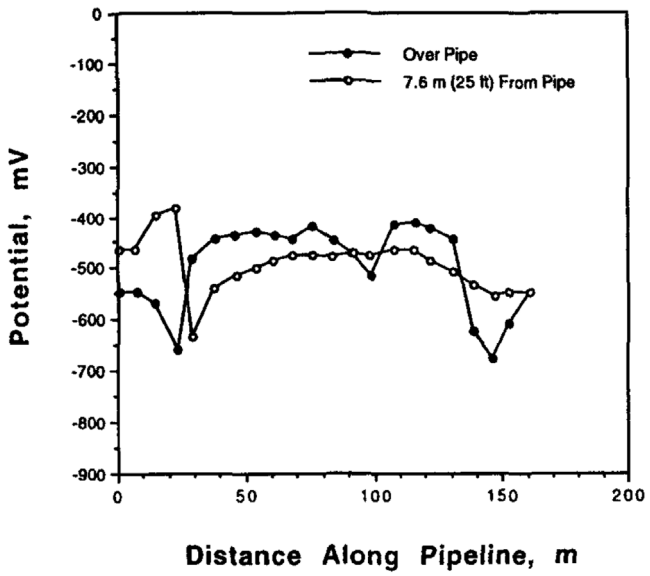
Measured potentials at the soil surface above a utility, such as a pipeline, are often used to evaluate the effectiveness of CP systems and coatings. One technique that has been applied for many years uses two sets of measurements where one of the electrodes is positioned over the pipeline and the second electrode is placed several meters to the side. The data from this approach provide a comparison of the local potential to the more distant potential made to the side of the pipeline, as illustrated in figure 30. Regions where the "over pipe" potential are more positive than the "25 ft from pipe" potential are cathodic to other sections of the pipe line. Potential effects of stray currents, galvanic currents, and CP interference are identified from this information.[52]

Another technique relies on a set of potential measurements between the pipeline and an RE, where the electrode is positioned directly over the pipeline, and measurements are made along its length at intervals. Computerized data logging permits a detailed analysis of discontinuities in potentials that reveal areas of active corrosion.[54] Improvements in programming and equipment permit elimination of IR error from CP potential measurements and also incorporate use of "over the pipe" and "beside the pipe" potential data.

POLARIZATION

The technique of electrochemical polarization is a useful tool for obtaining corrosion rate data nondestructively during exposure, with a minimum of disruption to the test. The polarization resistance measurement is especially attractive because its use is well documented, and it requires a minimal amount of equipment, some of which is commercially available. The measurement involves applying current to a specimen from a second electrode,

FIG. 30 A plot of potential over a pipeline and to the side of the pipeline versus distance, illustrating the presence of cathodic regions where "over the pipe" potentials are more positive than "beside the pipe" potentials.

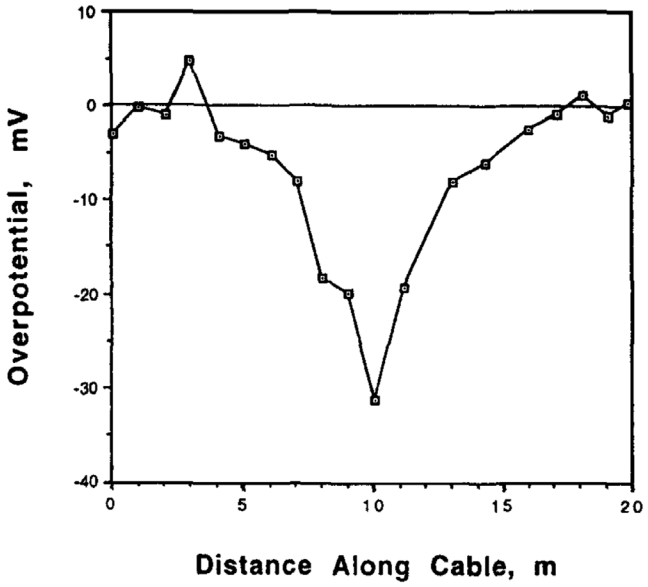


changing the potential of the specimen by approximately 10 mV versus an RE, and noting the amount of current needed to make that change. The slope of the change in potential versus the applied current is inversely related to the corrosion current of the specimen.[48] With information on the Tafel slope of the material in that environment, the corrosion current can be determined. This approach uses (1) a specimen as the WE, (2) a reference potential electrode (REF), and (3) a CE to apply the polarizing current. Additional information on polarization is available in ASTM G59, the previous section in this chapter on electrochemical testing, and chapter 8 of this manual, "Electrochemical Tests."

Corrosion current density, and corrosion rate, can be calculated when the entire specimen is polarized and its surface area is known. This is the case for finite area specimens, as illustrated in figure 25 for steel piling. The reference electrode is located at the soil surface approximately 30 m from the WE. For these measurements, each of the seven piles was polarized using the centrally located pile as the CE with the REF at a fixed location. In this way, measurements could be duplicated from year to year and the results compared.[45] From this corrosion current measured over a period of time, in this case 14 years, an estimate of weight loss can be calculated.

In some situations, the polarized area of the specimen is not known, as is the case where the WE is a long structure such as a pipeline or electric power utility. In this situation, the WE is essentially infinitely long, and the CE can only supply current to a portion of the structure. An estimate of how much of the structure is polarized when current is applied can be made by measuring the potential of the structure in the vicinity of the CE, as illustrated in figure 31.[24] In this example, the polarization region extends from the 4 m mark to the 18 m mark. From this information, the approximate polarized area can be calculated.

FIG. 31 A plot of over-potential versus distance, illustrating the distribution of current on an underground cable when 1.5 mA is applied from a rod placed 1 m to the side of the cable.



CORROSION COUPONS AND PROBES

Direct measurement of metal corrosion rate can be achieved using pre-weighed metal coupons. They are buried in the pipeline trench and are unconnected or connected to the structure at a controlled test post. Periodically, they can be removed and processed for weight loss resulting from corrosion. A simple calculation can give the corrosion rate value, expressed, for example, in g/m^2 year. This method is time consuming, especially when a large number of samples are needed for removal at consistent intervals.

The buried coupons can be made in a wide variety of sizes and shapes and are made of the same metal as the structure. Comparing the mass loss of connected and unconnected coupons may provide information about the effectiveness of CP. Electrical resistance (ER) probes and linear polarization resistance (LPR) probes are designed to measure corrosion in soil, without the necessity to be dug up for examination. This is an advantage over the coupons. These probes also give indirect information about the soil corrosivity and its changes with time.[49]

Special probes with associated measuring equipment that provide a means of determining the corrosion rate of a material in soil are commercially available. An attractive feature of this equipment is that the data read out directly in terms of corrosion rate or can be readily converted to corrosion rate. The biggest concern is that the specimen in the probe may not be representative of the structure of interest because of the small size of the probe specimen or its isolation from the structure. Corrosion probes and coupons are discussed in the following NACE Publications: Publication 05107, *Report on Corrosion Probes in Soil or Concrete*; NACE SP0104 (formerly RP0104), *The Use of Coupons for Cathodic Protection Monitoring Applications*; and NACE Publication 07037, *Use of CP Coupons and Soil Corrosion Probes in Application of Pipeline Cathodic Protection Criteria*.

ER Probe

ER probes, also known as soil corrosion probes, measure a change in the resistance of a metallic sensing element, made of the material of interest or a representative alloy. The resistance changes as a function of metal loss in the cross section of the sensing element. This reading is then converted to corrosion rate. Several types of ER probes are shown in figure 32.

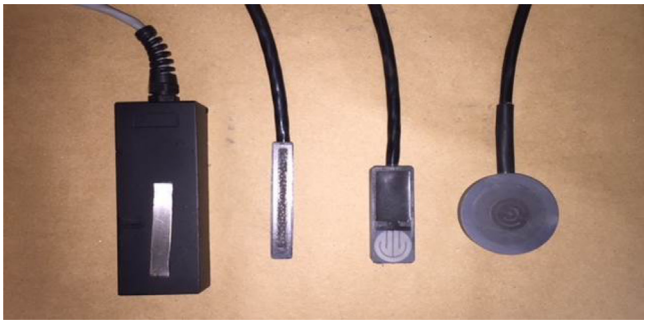
LPR Probe

An LPR probe determines the corrosion rate on its metal electrode or electrodes by measuring the polarization resistance under the application of a small applied potential, typically 10 to 20 mV, above the free corroding potential of the electrode or electrodes.

Cathodic Protection Coupons

CP coupons have been shown to be a simple tool for determining the level of polarization of a cathodically protected pipeline and to confirm the IR drop in a potential measurement. CP coupons

FIG. 32 Several types of commercially available ER corrosion probes. *Source:* Photo complements of U.S. Pipe and Foundry.



are installed in the soil or electrolyte near the pipeline and then are connected to it through a test station. The CP coupon can be easily disconnected from the pipeline for periodic monitoring of "instant off" and depolarization potential measurements.

Other types of probes use electrochemical polarization techniques and two or three electrodes to measure the corrosion rate of the WE in the probe.[50,51] Details on calculating corrosion rate from electrochemical data are discussed in ASTM G102.

In the laboratory, the technique of ac impedance is supplementing polarization resistance because it provides additional information on mechanisms of the processes involved. Guidance on performing corrosion tests in the laboratory in liquids or in soils is provided in ASTM G31, *Standard Guide for Laboratory Immersion Corrosion Testing of Metals*. Although ac impedance systems are now commercially available, these units generally are limited to low polarization currents of 1 A or less, making them unsuitable for most field applications in which larger current capabilities (>1 A) are needed.

GALVANIC CORROSION

The galvanic coupling of unlike metals in soil is an all too common occurrence, and the need to obtain information on the consequences of this condition is recognized. Copper ground rods and copper mesh ground beds are typically connected to steel piling supported structures and underground telephone, water, and fuel utilities to the detriment of the less noble steel. Burial of galvanically coupled metals in soil provides information on the degree of corrosion and the possibility of hydrogen embrittlement. The effect of relative surface area of the coupled metals and the spacing between them are important.[52]

Measuring the galvanic current of the coupled metals during the exposure period allows for monitoring of changes in the magnitude of the current and direction of current flow. This can be accomplished by attaching insulated wire conductors that extend above the surface of the soil where they are connected together. Periodically, an ammeter is inserted in the circuit and the current is measured. To reduce the possibility of affecting the current during the measurement, which may involve currents in the milliamp range or less, the use of a zero-resistance ammeter is recommended.[46]

FIELD SOIL TESTS

A number of soil tests are used to correlate soil corrosion aggressivity to its physical and chemical properties. These tests are discussed in previous sections of this chapter. Sampling errors are the most common errors encountered in soil analysis, because of the extreme heterogeneity of the material. In the laboratory, grinding and mixing can minimize such errors, but the largest sampling error occurs in field measurements. In field measurements of soils, each of the different types of soil in contact with the structure (i.e., organics, sand, clays) should be tested individually. For resistivity, this can be performed with either a four-pin or a two-pin resistivity soil box as described in ASTM G57 and G187. The most desirable measurements of redox potential, pH, and resistivity are those conducted in the field adjacent to the structure of interest. If it is not possible to conduct redox and pH measurements in the field, soil samples should be collected in air-tight containers and tested as soon as possible when received at the laboratory.

FIELD BIOLOGICAL ACTIVITY TEST

Testing for MIC has been discussed in a previous section of this chapter. As specified in NACE TM0106-2016, *Detection, Testing, and Evaluation of Microbiologically Influenced Corrosion (MIC) on External Surfaces of Buried Pipelines*, "MIC investigations require microbiological, chemical, and metallurgical testing for proper diagnosis. The conclusion that MIC has taken place should be based on the preponderance of circumstantial evidence."[12]

Chemical analysis of the water source and the soil is helpful in determining the critical nutrients necessary to support microbiological activity. These tests should be conducted under the direction of a microbiologist who has experience in microbiologically influenced corrosion. Field test kits are currently available that employ an antibody tagging technique to identify and that facilitate the determination of the population of microbes.[56,57] MIC can be studied using field survey and other techniques, such as electrochemical polarization curves, polarization resistance, EIS, thin-film ER probe, galvanic current measurement, scanning electron microscopy, and energy-dispersive X-ray spectroscopy surface analysis.[22]

EXTERNAL CORROSION DIRECT ASSESSMENT (ECDA) OF BURIED PIPELINES

As a result of regulatory changes in the United States, the pipeline industry needed an alternative method to pressure testing on in-line tool inspection to assess buried pipelines.[55,58] External corrosion direct assessment (ECDA) is a four-step process consisting of the following:

- *Pre-assessment:* assesses pipe data, construction data, soil/environmental conditions, corrosion protection data, and operating parameters/history
- *Indirect inspection:* identifies the locations of coating faults, insufficient CP, and electrical shorts (close-interval, on/off potential surveys, electromagnetic current attenuation surveys, alternating current voltage gradient surveys), interference,

geological current surveys, and other anomalies along the pipeline.

- *Direct examination:* excavates the pipe and performs physical inspections and tests on the pipe surface and the surrounding soil/water electrolytes, to assess the degree of corrosion
- *Post-assessment:* assesses the overall effectiveness of direct assessment and to define reassessment intervals based on remaining-life calculations

The ECDA process incorporates standard techniques for compiling historical information, pipeline and soil surveys, external pipeline inspections, and data analysis. The procedure includes no new measurement techniques, but it does allow for the future addition of such techniques. New advances in satellite technology may soon help pipeline operators and utilities observe encroachments and ground movements near their assets with unprecedented details.[55] Some rules and information about ECDA are present in NACE RP0502, *Pipeline External Corrosion Direct Assessment Methodology*.

Summary

As discussed in the beginning of this chapter, soil as a corrosive environment is probably of greater complexity than any other environment. The corrosion process of buried metal structures is extremely variable and can range from rapid to negligible. With background knowledge of the principal soil characteristics and their influence on metal corrosion, the most serious corrosion problems can be prevented. ASTM Committee G01 on Corrosion of Metals and other ASTM committees have prepared test methods, recommended practices, guides, and other documents to aid in the testing and identification of corrosive soils. Many of these are listed in Appendix A. The NACE, AWWA, Societies of Protective Coatings (SSPC), and other organizations have prepared documents to aid in the protection and monitoring of buried structures. The information presented in this chapter, and in this manual, will assist the reader not only in identifying corrosive environments but also aid in preventing corrosion of our valuable infrastructure.

References

1. L. L. Shreir, R. A. Jarman, and G. T. Burstein, eds., *Corrosion,* vol. 1, *Metal/Environment Reactions* (London: Butterworth Heinemann, 1994).
2. M. Romanoff, *Underground Corrosion* (Houston, TX: NACE International, 1989).
3. H. H. Ulig, *Corrosion and Corrosion Control* (New York: Wiley, 1985).
4. J. R. Davis, ed., *Corrosion, Understanding the Basics* (Materials Park, OH: ASM International, 2000).
5. M. E. Parker, *Corrosion by Soils*, NACE Basic Corrosion Course (Houston, TX: NACE International, 1975).
6. E. E. Stansbury and R. A. Buchanan, *Fundamentals of Electrochemical Corrosion* (Materials Park, OH: ASM International, 2000).
7. DIPRA/CORRPRO, *Advancements in Pipe Longevity–The Design Decision Model* (Birmingham, AL: Ductile Iron Pipe Research Association, 2018).
8. J. H. Fitzgerald, III, "The Future as a Reflection of the Past," in *Effect of Soil Characteristics on Corrosion,* ed. V. Chaker and J. D. Palmer (West Conshohocken, PA: ASTM International, 1989), 1–4.
9. *External Corrosion Control for Infrastructure Sustainability*, 3rd. ed., AWWA Manual M27 (Denver, CO: American Water Works Association, 2014).
10. *Ductile Iron Pipe and Fittings*, 3rd. ed., AWWA Manual M41 (Denver, CO: American Water Works Association, 2009).
11. A. W. Peabody and R. L. Bianchetti, *Control of Pipeline Corrosion*, 2nd ed. (Houston, TX: National Association of Corrosion Engineers, 2001).
12. *Detection, Testing, and Evaluation of Microbiologically Influenced Corrosion (MIC) on External Surfaces of Buried Pipelines*, NACE TM0106-2016 (Houston, TX: National Association of Corrosion Engineers, 2016).
13. Earth Resistivity Manual (Evanston, IL: Soiltest Inc., 1968).
14. A. M. Horton, "Zinc Metallizing for External Corrosion Control of Ductile Iron Pipe" (paper presentation, ASCE Pipelines Conference, American Society of Civil Engineers, Reston, VA, 2014).
15. *Concrete Pressure Pipe*, 3rd. ed., AWWA Manual M9 (Denver, CO: American Water Works Association, 2008).
16. E. G. Pont, "Association of Sulfate Reduction in the Soil with Anaerobic Iron Corrosion," *Journal of Australian Institute of Agricultural Science* 5, no. 5 (1939): 170–171.
17. G. Seelmeyer, "Biological Corrosion of Iron and Steel," *Werkstoffe und Korrosion* 4 (1953): 241–247.
18. J. C. Senez, "Investigation in Biological Corrosion in Anaerobic Soils by Sulfate-Reducing Bacteria," *Corrosion and Anti-Corrosion* 1 (1953): 131–132.
19. J. O. Harris, "Bacterial Activity at the Bottom of Back-Filled Pipe-Line Ditches," *Corrosion* 16 (1960): 149–154.
20. W. P. Iverson, "Biological Corrosion," *Advanced Corrosion Science and Technology* 2 (1972): 1–42.
21. N. Prakash, K. Srivastava, and S. Gupta, "Corrosion of Mild Steel by Soil Containing Sulfate-Reducing Bacteria," *Microbiological Biotechnology* 3, no. 2 (1988): 79–84.
22. S. Y. Li, Y. G. Kim, K. S. Jeon, Y. T. Kho, and T. Kang, "Microbiological Influenced Corrosion of Carbon Steel Exposed to Anaerobic Soil," *Corrosion* 57, no. 9 (2001): 815–828.
23. E. Escalante, "Concepts of Underground Corrosion," in *Effects of Soil Characteristics on Corrosion,* ed. V. Chaker and J. D. Palmer (West Conshohocken, PA: ASTM International, 1989), 81–94.
24. *Standard Practice–Cathodic Protection to Control External Corrosion of Concrete Pressure Pipelines and Mortar-Coated Steel Pipelines for Water or Waste Water Service*, NACE SP01-00 (Houston, TX: National Association of Corrosion Engineers, 2014).

25. *Steel Water Pipe—A Guide for Design and Installation*, 5th ed., AWWA Manual M11 (Denver, CO: American Water Works Association, 2017).

26. *Control of External Corrosion on Underground or Submerged Metallic Piping Systems*, NACE SP0169 (Houston, TX: National Association of Corrosion Engineers, 2016).

27. *Corrosion and Corrosion Control for Buried Cast and Ductile Iron Pipe*, NACE TG014 (Houston, TX: National Association of Corrosion Engineers, 2013).

28. *Criteria and Test Methods for CP of Lead Sheath Cables*, NACE RP0194 (Houston, TX: National Association of Corrosion Engineers).

29. S. A. Bradford, *Practical Handbook of Corrosion Control in Soils* (West Conshohocken, PA: ASTM International, 2000).

30. V. Chaker, "Corrosion Testing in Soils—Past, Present, and Future," in *Corrosion Testing and Evaluation: Silver Anniversary Volume,* ed. R. Baboian and S. W. Dean (West Conshohocken, PA: ASTM International, 1990), 95–111.

31. E. Escalante, "Measuring the Corrosion of Metals in Soils," in *Corrosion Testing and Evaluation: Silver Anniversary Volume,* ed. R. Baboian and S. W. Dean (West Conshohocken, PA: ASTM International, 1990), 112–124.

32. J. R. Scully and K. J. Bundy, "The Use of Electrochemical Techniques for Measurement of Pipe Steel Corrosion Rates in Soil Environments" (paper presentation, Corrosion/83, paper 253 NACE International, Houston, TX, March 1983).

33. E. Levlin, "Aeration Cell Corrosion of Carbon Steel in Soil: In Situ Monitoring Cell Current and Potential," *Corrosion Science* 38, no. 12 (1996): 2083–2090.

34. K. Kasahara and F. Kajiyama, "Application of AC Impedance Measurements to Underground Monitoring," *Corrosion* 39 (June 1983): 296–302.

35. J. C. Murphy, G. Hartong, R. F. Cohn, P. J. Moran, K. Bundy, and J. R. Scully, "Magnetic Field Measurement of Corrosion Processes," *Electrochemical Science and Technology* 135, no. 2 (February 1988): 310–313.

36. A. M. Horton, *Corrosion Rates of Ductile Iron Pipe in Drilling Fluids: A Comparison of ASTM Electrochemical Test Standards G59, G102, AND G106 to ASTM Weight Loss Standard G162*, (West Conshohocken, PA: ASTM International, 2018).

37. J. B. Bushman and T. E. Mehalick, "Statistical Analysis of Soil Characterization to Predict Mean Time to Corrosion Failure of Underground Metallic Structures," in *Effects of Soil Characteristics on Corrosion,* ed. V. Chaker and J. D. Palmer (West Conshohocken, PA: ASTM International, 1989), 107–118.

38. C. P. Dillon, *Corrosion Control in the Process Industries* (New York: McGraw-Hill, 1986).

39. V. Chaker, "Simplified Method for Electrical Soil Resistivity Measurement," in *Underground Corrosion,* ed. E. Escalante (West Conshohocken, PA: ASTM International, 1981), 61–91.

40. E. Escalante, "The Effect of Soil Resistivity and Soil Temperature on the Corrosion of Galvanically Coupled Metals in Soil," *Galvanic Corrosion,* ed. H. P. Hack (West Conshohocken, PA: ASTM International, 1988), 193–202.

41. W. P. Iverson, "An Overview of the Anaerobic Corrosion of Underground Metallic Structures, Evidence for a New Mechanism," in *Underground Corrosion* (West Conshohocken, PA: ASTM International, 1981).

42. J. D. Palmer, "Environmental Characteristics Controlling the Soil Corrosion of Ferrous Piping," in *Effects of Soil Characteristics on Corrosion,* ed. V. Chaker and J. D. Palmer (West Conshohocken, PA: ASTM International, 1989), 5–17.

43. J. D. Palmer, "Field Soil Corrosivity Testing—Engineering Considerations," in *Corrosion Testing and Evaluation: Silver Anniversary Volume,* ed. R. Baboian and S. W. Dean (West Conshohocken, PA: ASTM International, 1990), 125–138.

44. G. H. Booth, A. W. Cooper, and P. M. Cooper, "Criteria of Soil Aggressiveness towards Buried Metals, I. Experimental Methods," *British Corrosion Journal* 2 (1967): 104–108.

45. E. Escalante, "Measuring the Underground Corrosion of Steel Piling at Turcot Yard, Montreal, Canada: A 14 Year Study," in *Corrosion Forms and Control for Infrastructure,* ed. V. Chaker (West Conshohocken, PA: ASTM International, 1992), 339–355.

46. E. Escalante and W. F. Gerhold, "Galvanic Coupling of Some Stressed Stainless Steels to Dissimilar Metals Underground," in *Galvanic and Pitting Corrosion: Field and Laboratory Studies,* ed. R. Baboian, W. D. France, Jr., L. C. Rowe, and J. F. Rynewicz (West Conshohocken, PA: ASTM International, 1976), 81–93.

47. E. Escalante, E., "Corrosion Testing In Soil," in *Corrosion,* ed. J. R. Davis (Materials Park, OH: ASM International, 1987), 208–211.

48. F. Mansfeld, "The Polarization Resistance Technique For Measuring Corrosion Currents," in *Advances in Corrosion Science and Technology,* ed. M. G. Fontana and R. W. Staehle (New York: Plenum Press, 1976), 163–262.

49. A. M. Horton and G. A. Ash, "Corrosion Monitoring of Ductile Iron Pipe in 'Uniquely Severe Environment' " (paper presentation, American Water Works Association Annual Conference and Exposition, Atlanta, GA, June 8–12, 2008).

50. J. M. Kilpatrick, "Measuring Corrosion Rate—Now," *Oil and Gas Journal* (March 1964): 155–157.

51. G. A. Marsh, "The Measurement of Instantaneous Corrosion Rates," in *2nd International Congress on Metallic Corrosion* (Houston, TX: NACE International, 1963), 936–941.

52. M. G. Fontana and N. D. Greene, *Corrosion Engineering* (New York: McGraw-Hill, 1978).

53. B. Husock, "Use of Pipe-to-Soil Potential in Analyzing Underground Corrosion Problems," *Corrosion* 17, no. 8 (1961): 97–101.

54. D. Kroon and K. W. Nicholas, "Computerized Potential Logging: Results on Transmission Pipelines" (paper presentation, Corrosion/82, NACE International, Houston, TX, 1982).

55. M. V. Veazey and S. Writer, "The Next Big Thing in Pipeline Monitoring," *Materials Performance* 42 (June 2003): 16–21.

56. D. H. Pope, "Discussion of Methods for the Detection of Microorganisms Involved in Microbiologically Influenced Corrosion," in *Biologically Induced Corrosion—Proceedings of the International Conference* (Houston, TX: NACE International, 1986), 275.

57. J. G. Stoecker, "Guide for the Investigation of Microbiological Induced Corrosion," *Materials Performance* 23, no. 8 (1984): 48–55.

58. D. H. Kroon, "External Corrosion Direct Assessment of Buried Pipelines: The Process," *Materials Performance* 42 (June 2003): 28–32.

Appendix A. ASTM Standards Related to Soil Corrosion and Soil Testing

ASTM A674, *Standard Practice for Polyethylene Encasement for Ductile Iron Pipe for Water or Other Liquids*, Appendix XI (Soil Tests)

ASTM D512, *Standard Test Methods for Chloride Ion in Water*

ASTM D516, *Standard Test Method for Sulfate Ion in Water*

ASTM D653, *Standard Terminology Relating to Soil, Rock, and Contained Fluids*

ASTM D1452, *Standard Practice for Soil Exploration and Sampling by Auger Borings*

ASTM D1586, *Standard Test Method for Standard Penetration Test (SPT) and Split-Barrel Sampling of Soils*

ASTM D2216, *Standard Test Method for Laboratory Determination of Water (Moisture) Content of Soil and Rock by Mass*

ASTM D2434, *Standard Test Method for Permeability of Granular Soils (Constant Head)*

ASTM D2487, *Standard Practice for Classification of Soils for Engineering Purposes (Unified Soil Classification System)*

ASTM D2488, *Standard Practice for Description and Identification of Soils (Visual-Manual Procedures)*

ASTM D2937, *Standard Test Method for Density of Soil in Place by the Drive-Cylinder Method*

ASTM D2980, *Standard Test Method for Saturated Density, Moisture-Holding Capacity, and Porosity of Saturated Peat Materials*

ASTM D4083, *Standard Practice for Description of Frozen Soils (Visual-Manual Procedure)*

ASTM D4427, *Standard Classification of Peat Samples by Laboratory Testing*

ASTM E11, *Standard Specification for Woven Wire Test Sieve Cloth and Test Sieves*

ASTM G1, *Standard Practice for Preparing, Cleaning, and Evaluating Corrosion Test Specimens*

ASTM G3, *Standard Practice for Conventions Applicable to Electrochemical Measurements in Corrosion Testing*

ASTM G5, *Standard Test Method for Making Potentiostatic and Potentiodynamic Anodic Polarization Measurements*

ASTM G16, *Standard Guide for Applying Statistics to Analysis of Corrosion Data*

ASTM G30, *Standard Practice for Making and Using U-Bend Stress-Corrosion Test Specimens*

ASTM G31, *Standard Guide for Laboratory Immersion Corrosion Testing of Metals*

ASTM G38, *Standard Practice for Making and Using C-Ring Stress-Corrosion Test Specimens*

ASTM G46, *Standard Guide for Examination and Evaluation of Pitting Corrosion*

ASTM G51, *Standard Test Method for Measuring pH of Soil for Use in Corrosion Testing*

ASTM G57, *Standard Test Method for Measurement of Soil Resistivity Using the Wenner Four-Electrode Method*

ASTM G59, *Standard Test Method for Conducting Potentiodynamic Polarization Resistance Measurements*

ASTM G61, *Standard Test Method for Conducting Cyclic Potentiodynamic Polarization Measurements for Localized Corrosion Susceptibility of Iron-, Nickel-, or Cobalt-Based Alloys*

ASTM G71, *Standard Guide for Conducting and Evaluating Galvanic Corrosion Tests in Electrolytes*

ASTM G102, *Standard Practice for Calculation of Corrosion Rates and Related Information from Electrochemical Measurements*

ASTM G106, *Standard Practice for Verification of Algorithm and Equipment for Electrochemical Impedance Measurements*

ASTM G158, *Standard Guide for Three Methods of Assessing Buried Steel Tanks*

ASTM G148, *Standard Practice for Evaluation of Hydrogen Uptake, Permeation, and Transport in Metals by an Electrochemical Technique*

ASTM G162, *Standard Practice for Conducting and Evaluating Laboratory Corrosion Tests in Soils*

ASTM G187, *Standard Test Method for Measurement of Soil Resistivity Using the Two-Electrode Soil Box Method*

NACE/ASTM G193, *Standard Terminology and Acronyms Relating to Corrosion*

ASTM G200, *Standard Test Method for Measurement of Oxidation-Reduction Potential (ORP) of Soil*

ASTM G215, *Standard Guide for Electrode Potential Measurement*

ASTM G218, *Standard Guide for External Corrosion Protection of Ductile Iron Pipe Utlizing Polyethylene Encasement Supplemented by Cathodic Protection*

Chapter 15 | Petroleum Chemistry

K. Daniel Efird[1]

Introduction

The petroleum production environment provides a unique challenge for corrosion testing in that it is not a controlled chemistry, as a chemical process environment, but is an environment provided by nature, with all the potential variability in phase distribution and chemical composition this implies. Petroleum environments are always complex, and often change during production from a formation, or they may change because of production from formations that were not included or anticipated in the original planning for field exploitation. The corrosion test program for petroleum environments, therefore, must account for the environment nature has created with little ability to alter or control it. In a very real sense the petroleum chemistry environment is a case of, "what you see is what you get." The primary concern with corrosion testing in petroleum environments is to ensure that what you test is, in fact, what really exists in the actual production environment.

The effect of petroleum chemistry on corrosion lies primarily in its influence on the formation, chemical composition, and characteristics of a liquid water phase, because liquid water in contact with the containing material is a necessary condition for corrosion to occur for the operating temperatures and pressures encountered in petroleum production. This fact dictates the direction of the discussion on the influence of petroleum chemistry in corrosion testing. This chapter deals solely with the effects of naturally occurring petroleum chemistry on corrosion testing and methods to deal with the effects of petroleum chemistry in corrosion testing. It does not elaborate on the actual test techniques except as they are affected by the petroleum chemistry considerations, and it does not consider refinery operations or alterations to the petroleum chemistry used to control corrosion.

[1]Stress Engineering Services, Inc., Houston, TX 77041, USA

DOI: 10.1520/MNL202NDSUP20190029

Chemical and Physical Characterization of Petroleum Environments

Petroleum production is generally classified on the basis of existing phases in the production stream, the relative proportions of these phases, and the presence or absence of hydrogen sulfide (H_2S). Carbon dioxide (CO_2), H_2S, hydrocarbons and organic compounds (gas and liquid), water, and dissolved salts are the primary constituents of the petroleum environment, and provide the basis for additional characterization. The acid gases, CO_2, and H_2S, have the primary effect on corrosion, and hence, provide a primary basis of classification.

The term "sweet" is commonly applied to petroleum production environments containing CO_2 and no H_2S. These environments generally are defined for corrosion purposes on the basis of the partial pressure of CO_2 in the gas phase. This grossly defines the level of dissolved CO_2 in the water phase and, according to many sources, roughly defines the relative aggressiveness of the water phase.

The term "sour" is applied to petroleum production environments containing H_2S. Sour environments generally contain CO_2 as well as H_2S. The concentration of H_2S required to consider an environment "sour" is not well defined. The currently accepted definition is found in Specification ANSI/NACE MR0175/ISO 15156,[1] which in Part 1 defines "sour service" as exposure to oilfield environments that contain sufficient H_2S to cause cracking of materials by the mechanisms addressed in the standard. This definition is based on safety considerations and the susceptibility of materials to sulfide stress corrosion cracking and is not related to general or localized corrosion. The term "sour" also can be defined as an environment containing sufficient H_2S to produce a primarily iron sulfide corrosion product on steel. The H_2S concentration in the water phase required for this to occur is not well defined; however, a concentration of more than 50 ppm H_2S in the water phase is sometimes used as a criteria for a sour environment.

The physical phases in a petroleum environment—including gas, liquid hydrocarbon (gas condensate or crude oil), and liquid water phases—may occur singly or in combination in a wide range

Copyright © 2022 by ASTM International, 100 Barr Harbor Dr., PO Box C700, West Conshohocken, PA 19428-2959
ASTM International is not responsible, as a body, for the statements and opinions expressed in this chapter. ASTM International does not endorse any products represented in this chapter.

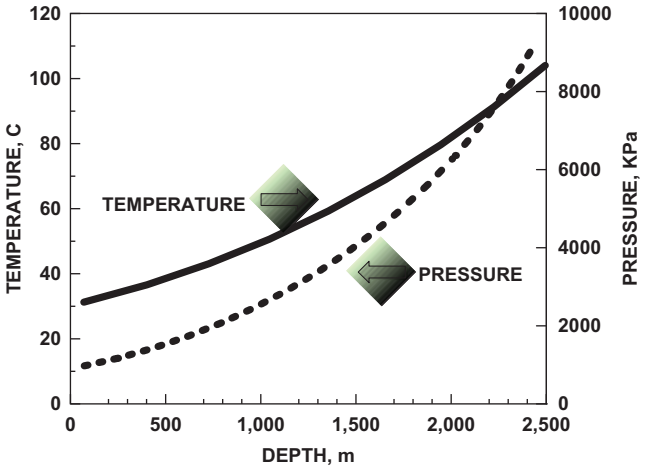
of phase ratios, and these phase ratios and compositions may change during production. Producing fields and individual wells are broadly classified as gas or oil fields or as wells depending on the primary phase produced. Other types of wells or systems for which corrosion testing may be considered are used for subsurface injection (e.g., CO_2, water or gas injection wells, and produced water disposal wells). A gas well is defined as one whose production consists primarily in a a gas phase with possibly some gas condensate, condensed water, or produced water, but no crude oil. An oil well is defined as one whose production consists of crude oil with varying amounts of gas and produced water. The relative proportion of gas and crude oil in the well production is expressed as the gas-to-oil ratio in units of volume of gas at standard conditions per volume of crude oil at 20°C (68°F).

TEMPERATURES AND PRESSURES ENCOUNTERED

The temperatures and pressures encountered in oil and gas production can vary widely. In general, high pressures and high temperatures go together for gas wells, but this is not necessarily the case for crude oil wells. The total bottom hole pressure in gas wells can range from a low of 40 to 60 bar to a high of more than 1,500 bar. Bottom hole temperatures can range from 50°C to well over 150°C. The temperatures and pressures normally encountered in surface production facilities are generally significantly lower.

Changes in temperature and pressure occur along the length of a tubing string during well production. The temperature and pressure variations for a typical well are shown in figure 1.[2] The significance of the change in temperature and pressure is that the phases present in the formation can change in the tubing string during production and in surface facilities. This can result in the formation of liquid water and gas condensate that were not present in the original produced fluid, which can dramatically affect corrosion. A valid corrosion test procedure must account for this effect.

FIG. 1 Subsurface variation in temperature and pressure in a well as a function of depth from downhole surveys.[2]



GAS PHASE AND GAS CONDENSATE PHASE

The gas phase is composed of various combinations and ratios of methane (CH_4), heavier hydrocarbons (e.g., ethane, propane), acid gases (e.g., CO_2 and H_2S), water (H_2O), dinitrogen (N_2), and helium (He). The primary gas is usually CH_4. A typical gas analysis for a producing well is given in table 1. The gases of greatest importance to corrosion are the acid gases CO_2 and H_2S. The other gases in the well stream are important to corrosion primarily because of their influence on the concentration of the acid gases dissolved in a liquid water phase.

The gas condensate phase is composed of C_3 and heavier alkanes and alkenes, present in the gas phase at reservoir conditions, that condense as a result of the temperature and pressure drop in the well string during production or in flowlines and production facilities. The gas condensate phase can occur in gas wells, flowlines, and in crude oil well gas processing facilities after the separation of gas from the crude oil. The primary effect of gas condensate on corrosion is the result of the displacement of liquid water from the metal surface by the gas condensate, thus inhibiting corrosion of the metal by the water phase. This relative condensation of liquid hydrocarbon and liquid water is difficult to simulate in laboratory tests, but the effect on corrosion must be accounted for in assessing the corrosivity of production from a well. At this time, there is no simple answer to the problem. Calculations of relative condensation from well data are about the only recourse.

LIQUID WATER PHASE

The liquid water phase in petroleum production can consist of either produced water, injected water, or condensed water, and combinations of these in varying proportions. Produced water is present in the reservoir as a liquid water phase and is produced along with the gas, gas condensate, or crude oil. Condensed water is liquid water condensed directly from gaseous H_2O in the gas phase.

Condensed water is condensed from H_2O in the gas phase as a result of changes in temperature and pressure along the length of a tubing string during production and in flowlines and surface facilities. The condensed water contains dissolved acid gases (CO_2 and H_2S) and low levels of dissolved corrosion

TABLE 1 Typical Gas Analysis for a Producing Well

Compound	Mole, %
Methane (CH_4)	81.5%
Ethane (C_2H_6)	3.6%
Propane (C_3H_8)	2.0%
Butane (C_4H_{10})	0.4%
Pentane (C_5H_{12})	0.2%
$> C_5$	1.0%
CO_2	4.6%
H_2S	1.4%
N_2	5.2%
He	0.04%

product from the well tubing. It can be corrosive. Condensed water is the fluid studied by de Waard and Milliams in their landmark work on the effects of CO_2 on steel corrosion in gas transmission lines, and the equations developed apply to condensed water.[3] The equation has since been modified to account for additional variables.[4]

A special case of corrosion by condensed water occurs in the vapor phase of pipelines and vessels. This condensed water can be corrosive and must be accounted for in designing a corrosion test program, if the phenomenon is anticipated in the specific production system being studied. Extensive discussion of vapor phase corrosion by water condensation and possible remedies are given by Dugstad, Lunde, and Olsen,[5] Olsen and Dugstad,[6] and Nyborg, Dugstad, and Lunde.[7]

Produced water is an extremely complex chemical solution, composed of liquid water, minerals dissolved from formation rocks, and water-soluble organics from the hydrocarbon phase, because it originates within the formation source rocks. The most important inorganic compounds with corrosion implications are chlorides and buffering compounds (e.g., bicarbonate, borate, silicate). The presence of buffering compounds reduces corrosion by raising the solution pH, countering the effect of dissolved acid gases. An accurate, detailed analysis of the produced water is essential so it can be accurately reproduced for corrosion testing, and accurate simulation of the produced water is essential for realistic laboratory corrosion test results. The basic analytical detail needed for produced water is given in table 2. This degree of detail is necessary to allow the required simulation of the produced water for the laboratory corrosion experiments. Research into the effects of produced water chemistry have been reported by Crolet and Bonis,[8,9] Schmitt,[10] Murata,[11] and Videm.[12]

The original produced water chemistry can be altered during production by dilution with condensed water in the tubing string and in production facilities. The effect of this dilution is to reduce the concentration of buffering compounds in the produced water, resulting in potentially lower pH and increased corrosion.

CRUDE OIL PHASE

The crude oil phase is the most chemically complex phase in the petroleum environment. Crude oil contains alaphatic and aromatic hydrocarbons, heterocyclic and metal organic compounds, high-molecular-weight organic compounds, and a broad assortment of nitrogen-, sulfur-, and oxygen-containing organic compounds.

TABLE 2 Recommended Analysis for Produced Waters

Anions	Cations	Additional
Na	Cl	pH[a]
K	SO_4	TDS
Ca	HCO_3	CO_2[a]
Mg	CO_3	H_2S[a,b]
Ba	F	O_2[a,b]
Sr	NO_3	
Fe	CH_3COO	

[a]Analysis at the time of taking the sample is preferred.
[b]Sampling technique must prevent iron contamination.

Chemical and Physical Characterization of Crude Oil

Crude oils are generally classified according to API gravity (inversely proportional to the crude oil density), sweet or sour, and asphaltenic or parafinic (hydrocarbon characteristics). A so-called heavy crude oil has a low API gravity (<20), a medium crude oil has an intermediate density (20 to 34), and a light crude oil has a high API gravity (>34). These ranges are not absolutely defined, but they serve as a general reference. All crude oils are composed of some or all of eight basic classes of organic compounds as given in table 3. Another way to classify crude oils is based on the nature of the organic compounds that make up the crude oil, specifically the proportions of paraffins, aromatic compounds and naphthenic compounds, as shown in figure 2.[13]

The recommended physical and chemical analyses for determination of the general characteristics of a crude oil are given in table 4 and table 5. Results of these analyses provide a solid basis for comparison of crude oils from different formations and fields. The crude oil components that have the greatest

TABLE 3 Basic Organic Compound Groups for Crude Oils

1. n-alkanes
2. iso-alkanes
3. mono- and poly-nuclear naphthenes
4. mono- and poly-nuclear aromatics
5. mono- and poly-nuclear naphthenoaromatics
6. hetero-compounds
7. asphaltenes
8. carbenes

FIG. 2 Classification of crude oils based on petroleum fractions.[8]

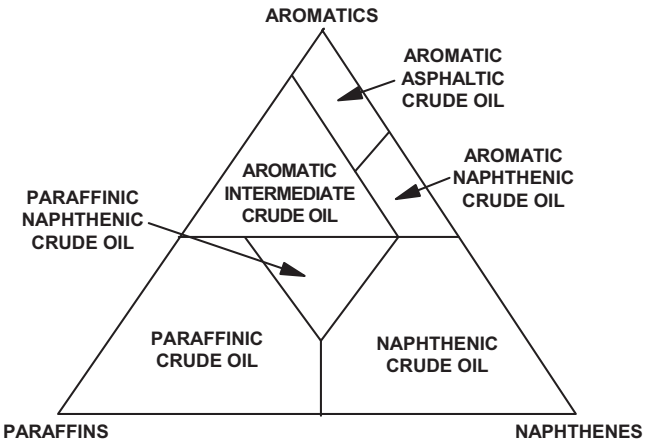


TABLE 4 Recommended Analysis for Crude Oils

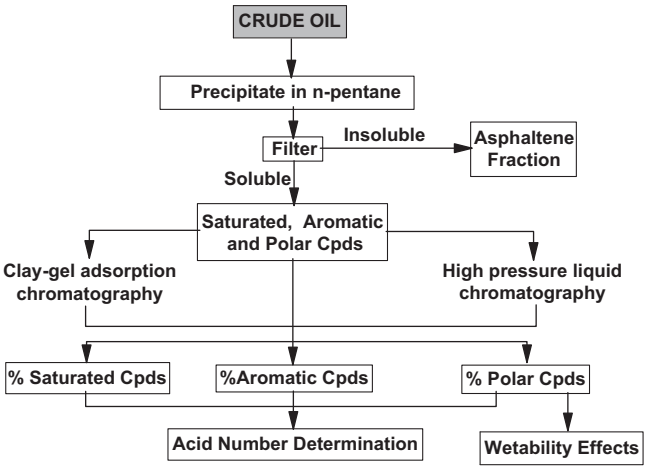
1. Gravity, API @ 15°C		2. Pour point, °C (°F)
3. Flash point, Pensky-Martens		4. Base sediment and water, vol%
5. Carbon residue, Conradson		6. Salt content, ptb
7. Ash content, wt%		8. Wax content, wt%
9. Neutralization number, mg/g		10. N-heptane insoluble, wt%
11. Toluene insoluble, wt%		12. Colloid content (ethyl acetate pptn), wt%
13. Bubble point pressure		
14. Element analysis:	Sulfur, wt%	Nitrogen (total), wt%
	Copper, ppm	Iron, ppm
	Nickel, ppm	Vanadium, ppm
	Calcium, ppm	Magnesium, ppm
	Sodium, ppm	

TABLE 5 True Boiling Point Crude Oil Distillation

Crude Oil	True Boiling Point
Light ends	to 32°C (90°F), vol%
Light naphtha	32°C to 171°C (90°F to 340°F), vol%
Kerosene	171°C to 260°C (340°F to 500°F), vol%
Diesel	260°C to 353°C (500°F to 700°F), vol%
Light distillate	353°C to 409°C (700°F to 800°F), vol%
Medium distillate	409°C to 464°C (800°F to 900°F), vol%
Heavy distillate	464°C to 520°C (900°F to 1,000°F), vol%
Residue	>520°C (>1,000°F), vol%

potential effect on corrosion are the polar organic compounds, because the polar organic compounds are the most water soluble components in the crude oil and are surface active. A procedure for the extraction of the polar components of a crude oil published by Donaldson is diagrammed in figure 3.[14]

FIG. 3 Schematic diagram of chromatographic separation procedures for extraction of polar compounds from crude oil.[9]



CHEMICAL CONSTITUENTS OF CRUDE OIL THAT AFFECT CORROSION

As stated earlier, the effect of petroleum chemistry on corrosion lies primarily in its influence on the formation, composition, and characteristics of a liquid water phase. This discussion deals with the chemical constituents in crude oil that affect the chemical composition of the liquid water phase. The water soluble constituents in crude oil are primarily the heterocyclic and metal organic compounds, and the nitrogen-, sulfur-, and oxygen-containing organic compounds. These include pyridines, indoles, benzofurans, phenols, amines, organic acids, thiols, ketones, and .aldehydes. All are organic compounds that are water soluble and surface active to varying degrees.[14–16]

The effect of these organic compounds on the corrosivity of the water phase is not well understood, but it probably results from either direct chemical interaction with the metal surface in the manner of a chemical corrosion inhibitor, or their effect on wetability. An example of the effect of the crude oil acid number on crude oil wetability is shown in figure 4.[14] The relative wetability of the crude oil and water phases determines whether the metal surface will be oil wet or water wet, with significant effects on corrosion.[17] Data also correlate with the corrosion rate of steel in crude oil–brine mixtures with the total nitrogen and acid content of the crude oil as shown in figure 5.[18]

VARIABILITY OF CRUDE OIL

The problem with corrosion testing for crude oil environments is the wide variability in the composition of the crude oils and the resulting variability in their effect on corrosion. Examples of the variability in composition are shown for 10 crude oils in figure 6 and figure 7.[14] Differences in aromatic and polar organic content for the 10 crude oils are shown in figure 6, and differences in the acid numbers for these crude oil fractions are shown in Figure 7.

These differences in composition result in wide variability in corrosion for various crude oils. The effect of specific crude oils on the corrosion rate of carbon steel as a function of the

FIG. 4 Effect of acid number and interfacial tension of the crude oil water interface on crude oil wetability.[9]

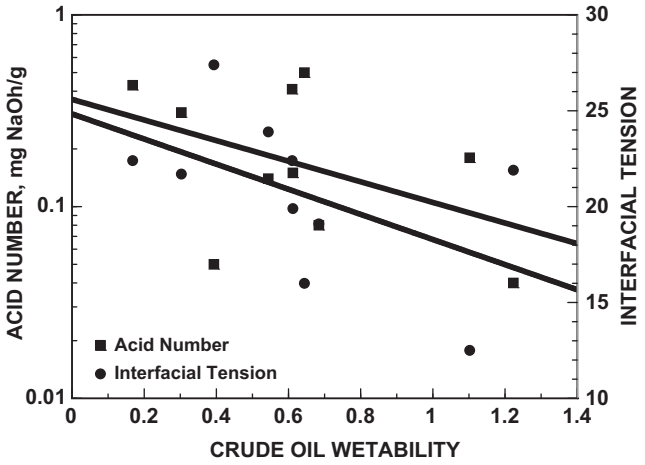


FIG. 5 The relationship of the acid content (acid number) and organic nitrogen content of crude oil on steel corrosion rate in crude oil/brine mixtures (4% NaCl brine at 5.2 MPa CO_2 pressure and 85°C).[13]

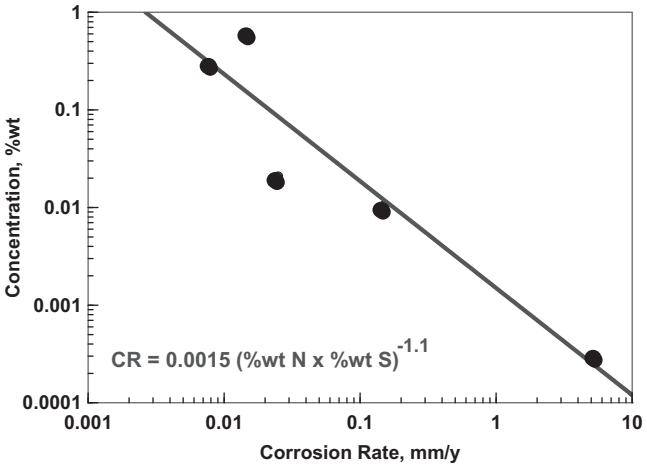
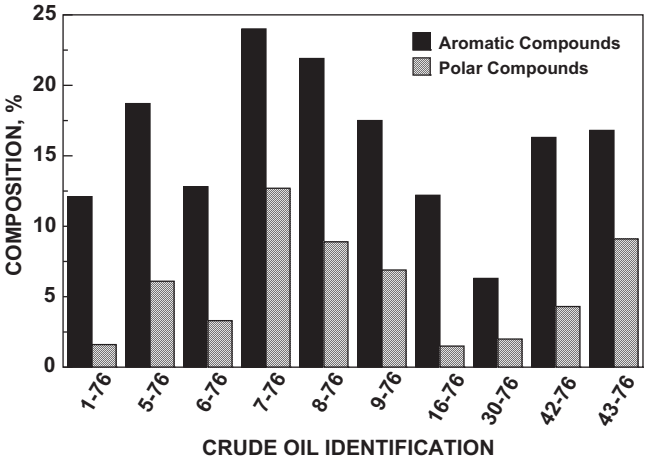


FIG. 6 Chromatographic analysis of 10 crude oils for aromatic and polar organic compounds, with the balance saturated organic compounds.[9]



produced water content for a constant produced water composition is shown in figure 8 and figure 9.[18] This compositional variation also results in differences in the way the amount of brine in a crude oil stream affects corrosion, as shown in figure 10.[19]

Laboratory Corrosion Testing

The unique characteristics of petroleum chemistry have a major effect on corrosion test methodology, experimental techniques, and considerations. The most important step preliminary to conducting corrosion tests is to ensure that the actual petroleum chemistry that occurs in the production system is the one investigated. This requires accurate field data and rigorous sampling techniques. No corrosion test in the petroleum environment can be more precise than the accuracy of the production temperature

FIG. 7 Acid number for 10 crude oils and the aromatic and polar organic fractions. Acid number as mg NaOH/g of sample.

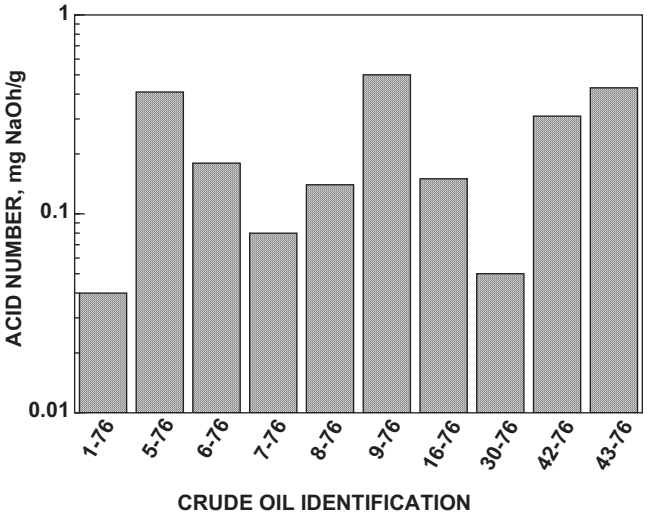
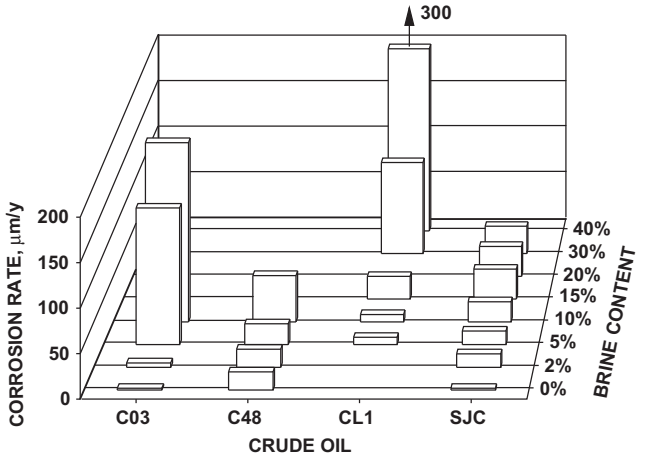


FIG. 8 Steel corrosion rate on a logarithmic scale for crude oil–brine mixtures using different crude oils with the same brine composition (4% NaCl solution).[13]



and pressure data, the gas composition data, and the fluid sample analyses. The well fluids composition, particularly the gas, crude oil, and produced water analysis, must be correct.

Six fundamental test principles must be followed to preserve the petroleum chemistry for corrosion testing and to allow for valid laboratory corrosion tests in petroleum environments:

1. A representative production environment for the area of interest, or the most potentially corrosive or highest risk area in a production system, should be duplicated as nearly as possible for all corrosion testing, and its composition should not be altered, except for the purpose of investigating specific field or composition variables, for example, changes in produced water level, CO_2 partial pressure, and H_2S partial pressure (field souring).

FIG. 9 Steel corrosion rate on a linear scale for crude oil/brine mixtures using different crude oils with the same brine composition (4% NaCl solution), showing different effects of increasing brine content.[13]

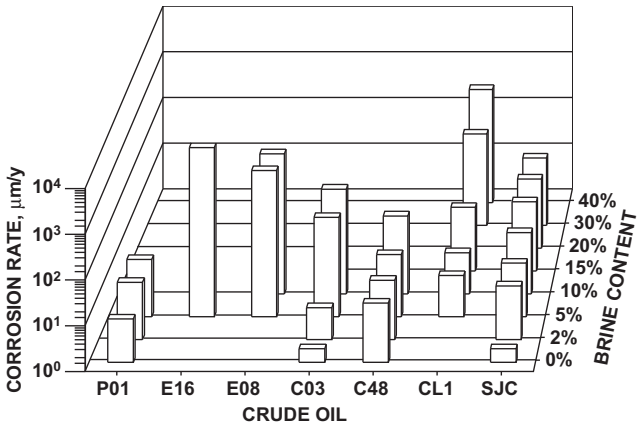
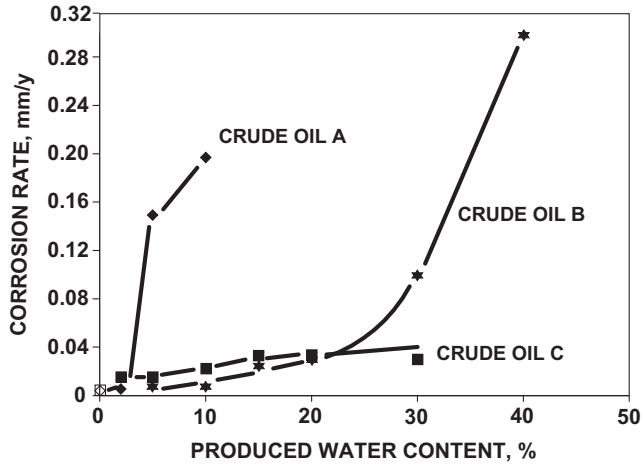


FIG. 10 The change in corrosion rate of steel in crude oil–produced water mixtures with increasing produced water content showing the three general types of behavior observed.[13]



2. The composition of corrosive gases in the test solution should be calculated on the basis of gas fugacity not partial pressure for correlation with the production environment. The higher the total pressure of the production environment, the more important this becomes.
3. For crude oil corrosion tests, the actual production crude oil should be used for all corrosion testing, and oxygen must not be allowed to contact the crude oil at any time before corrosion testing.
4. Artificially produced water may be used. If, however, crude oil is produced in service, the artificially produced water must be intimately contacted with the crude oil before testing to ensure that the soluble organics from the crude oil are present in the test solution.
5. Great care must be taken to prevent oxygen contamination during corrosion testing, unless oxygen is one of the test variables.
6. Each individual corrosion test must be completed before the chemistry of the water phase in the test environment is changed significantly by the corrosion process, or a flow-through system must be used to maintain the solution chemistry.

CORROSION TESTING FOR HYDROCARBON GAS SYSTEMS

The following discussion applies to corrosion testing of hydrocarbon gas systems and to the gas phase used for produced or condensed water and crude oil system corrosion testing.

Accurately reproducing the composition of the concurrently produced water phase is the primary concern with corrosion testing for hydrocarbon gas systems. The concentration of corrosive gases in the water phase must be accurately simulated, and simple equalizing of the partial pressure with the production environment is not sufficient. As stated previously, gas production wells are generally at high pressure. It is the high pressure that causes the error with the use of partial pressure as the determinant of acid gas concentration in the liquid water phase. This error is not as great for surface facilities operating at much lower pressures.

Using equality of gas fugacity rather than partial pressure to reproduce the production environment in the corrosion test accounts for the effect of nonideality in the solubility of the gas in the water phase at increasing total pressure. For example, a test conducted at 20 psi total pressure of pure CO_2 will not result in the same CO_2 concentration in the water phase as 20 psi CO_2 partial pressure in a well with a total pressure of 5,000 psi with CH_4 as the other gas. Significantly less CO_2 is dissolved in the water phase at the high-pressure well than in the low-pressure test, even though the partial pressures are the same. This can have a major effect on the application of corrosion test results to the operating system, because the concentration of acid gas dissolved in the water phase strongly affects its corrosivity.

Care is required to ensure that unwanted oxygen is removed from the gas phase to prevent it from being introduced into the water phase. Oxygen contamination in the water phase, even at a level of 50 ppb, can result in significant errors in the test results. Anaerobic gases should be used wherever possible. If oxygen removal from the test gas is required, this can be accomplished by passing the gas through commercial oxygen removal cartridges, with final oxygen removal being accomplished by passing the prescrubbed gas through a nickel chloride ($NiCl_2$)–catalyzed 10,000 ppm solution of hydrazine chloride.

When H_2S or gas mixtures containing H_2S are used, the supplied gas has rarely any oxygen. These situations do require removal of oxygen from the test solution and the test cell gas space before introduction of the H_2S-containing test gas. Oxygen remaining in the test cell can react with the H_2S to form oxysulfide compounds, which can greatly affect corrosion.

CORROSION TESTING FOR PRODUCED WATER SYSTEMS

The following discussion applies to corrosion testing in produced or condensed water systems and to the liquid water phase used for hydrocarbon gas and crude oil system corrosion testing.

Produced water is an extremely complex chemical solution that can include minerals dissolved from formation rocks, and water-soluble organics from the hydrocarbon phase. Simulated produced water used in corrosion testing must reproduce this complexity. Good initial analysis of the produced water to be tested is essential for success of the test program.

Complete removal of unwanted oxygen from the solution before testing is vital, because oxygen contamination can result in significant errors in the test results. The test solution is best deaerated by purging with the test gas. Purging times must be sufficient to lower the oxygen concentration to less than 20 ppb. The actual purge time required will vary with the solution concentration and temperature. A hydrazine salt solution can be added to the test solution before its use to remove any residual oxygen and maintain the solution in a reducing condition for the duration of the test period, if this is required.

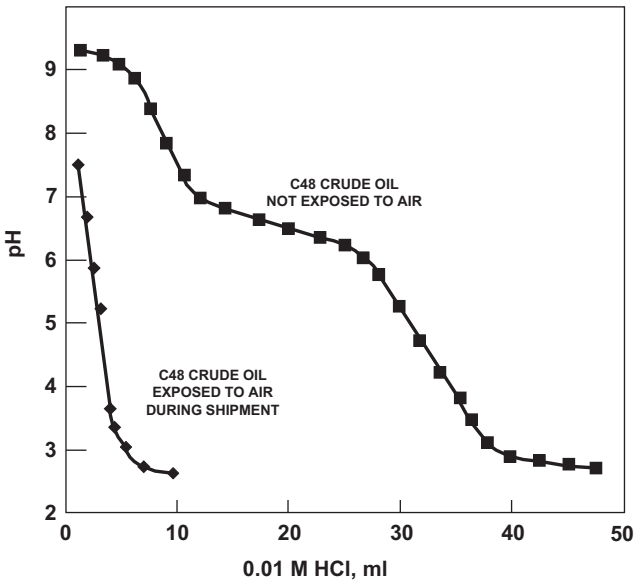
The test gas must be in equilibrium with the test solution before corrosion testing begins. Because chemical equilibrium between the gas phase and the water phase, particularly for CO_2, can require 4 to 8 h, purging overnight before testing begins is recommended. If the gas and water phases are not at equilibrium, errors in the corrosion test results are possible. Caution must be exercised, however, if volatile components in the test solution could be stripped out by the purge gas. The primary goal is to generate a test solution that accurately simulates the production environment.

CORROSION TESTING FOR CRUDE OIL SYSTEMS

The actual production of crude oil must be used for all testing to evaluate corrosion in crude oil, and oxygen must never be allowed to contact the crude oil at any time. The crude oil samples used in corrosion tests must be obtained in a manner designed to prevent contact of the crude oil with air. The sample container must be purged with inert gas before filling with crude oil, and the crude oil must be shipped under positive inert gas pressure. The sample container construction must be type 316 stainless steel or a material of greater corrosion resistance, or the container must be lined with an inert material. The crude oil sample must be stored under an inert gas blanket. The crude oil must be transferred from its shipping container into the test cell using inert gas pressure or vacuum.

The extreme measures to ensure the complete exclusion of oxygen are needed because oxygen can react with some crude oils to form organic acids that were not present in the original crude oil, and could alter the test results. Figure 11 shows the effect air exposure (oxygen) can have on the concentration of acid compounds in a crude oil. Acids in the crude oil sample were extracted with 0.06 M sodium hydroxide (NaOH), which was then titrated with 0.01 M hydrochloric acid (HCl). The crude oil sample not exposed to air shows a titration curve that implies that carbonate–bicarbonate is the titrated species, which

FIG. 11 The effect of exposure to air on the titration curve for acidic compounds extracted from 200 mL of a crude oil with 10 mL of 0.06 M NaOH using 0.01 M HCl as the titrant.



probably originated from the CO_2 in the crude oil reacting with the NaOH. The crude oil sample that was exposed to air contains 1.5 milliequivalents per liter of acidic compounds that are not present in the unexposed sample. This phenomenon does not occur for all crude oils, but it is not possible at this time to know which crude oils will be affected.

PREVENTING CHANGES IN SOLUTION CHEMISTRY

Contamination of the test solution with corrosion products is a very real problem, particularly for corrosion testing with carbon and alloy steel. In designing the corrosion test program, calculations using an estimated corrosion rate should be made to determine the solution volume and maximum exposure time for the test. During the test, and at test termination, solution samples should be taken and analyzed to ensure that no significant changes in solution chemistry occurred that could affect the results. The formation of one mole of ferrous ion will generate two moles of bicarbonate in a sweet environment. For many produced water compositions, this is not necessarily a problem. For condensed water, however, the bicarbonate can result in a significant increase in solution pH. As a general guide iron concentrations should not be allowed to exceed 10 ppm during a test.

This assumes that there is no dissolved iron in the produced water, however, in which case the requirement becomes to not allow significant changes in the iron concentration during the test period. Many produced waters do contain dissolved iron, but care must be exercised to ensure that the iron concentration analyzed is actually contained in the produced water and is not an extraneous artifact resulting from tubular corrosion.

Maintaining the dissolved acid gas concentration in the solution during the test period can be a problem, particularly

when testing carbon and alloy steel for periods of more than 30 days. This is generally overcome by rapid stirring and sparging gas below the liquid surface. Autoclave testing is a particularly difficult problem in that the liquid volumes are small. One effective method for maintaining the solution dissolved acid gas concentration is to recirculate the test solution and allow it to fall through the gas phase when it reenters the autoclave.

Application of Corrosion Testing to New Production

An approach utilizing corrosion testing for application to new production is given in the logic diagram shown in figure 12.[20] Steels, including corrosion testing of steels, are appraised before any consideration is given to alloys. This is done because the very heavy cost penalty for alloys dictates that steels generally should be used if technically feasible.

The first step is to obtain valid field production data and samples. As discussed previously, no corrosion test is any more accurate than the accuracy of the temperature, pressure, and composition data, and the sampling methodology. The well fluid composition, particularly the gas analysis and produced water analysis, must be reasonably accurate. The crude oil samples for use in the corrosion tests must be obtained as previously described.

The field data are evaluated as they relate to known corrosion information and corrosion prevention practices. At this point, a decision is made on the possibility of sulfide stress corrosion cracking, including consideration of the possibility for future H_2S occurrence, even though it is not presently contained in the produced fluids. If sulfide stress corrosion cracking is a concern, only resistant steels are passed to the corrosion testing phase.

The corrosion tests are conducted to determine the corrosion rate break produced water level for steel, which is defined as the sudden increase in the corrosion rate between two produced water levels when testing in a series of produced water levels.[20] Generally, only one or two of the steels will need to be tested, because there is no significant difference in the corrosion rate break produced water level measured for the various carbon and low alloy steels commonly used in crude oil service. The corrosion rate break produced water level is determined from corrosion tests conducted at 10% by volume produced water increments starting with 100% crude oil until a high corrosion rate is obtained or the expected produced water limit for the field is reached, or to 90% produced water level. If a corrosion rate break is observed, additional corrosion tests are conducted at 2% produced water increments between the two produced water levels that form the break.[20] An example of the results from this type of test sequence is shown in figure 13.[20]

FIG. 12 The logic diagram for new field corrosion testing to determine the corrosion rate break produced water level for steel corrosion, corrosion inhibitor application, and alloy selection.

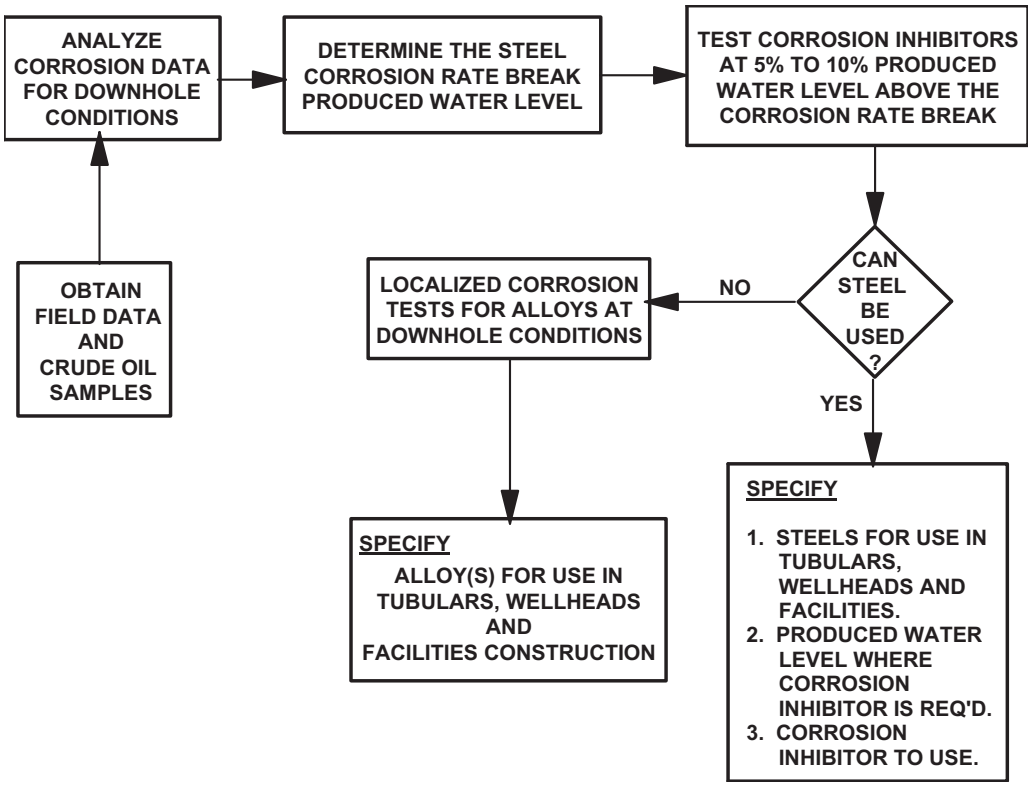
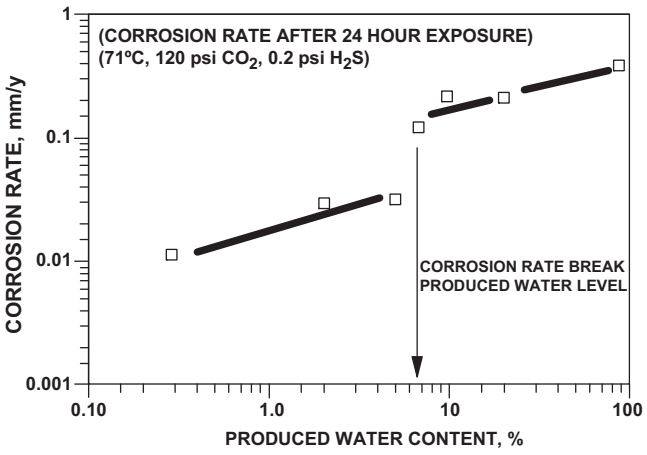


FIG. 13 Change in the corrosion rate of steel in crude oil–produced water mixtures with increasing produced water content, showing a corrosion rate break at approximately 7% produced water.



The corrosion rate break tests are followed by tests for corrosion inhibitor effectiveness at a produced water content above the corrosion rate break level. At this point, the decision is made on whether or not steel can be used, based on the corrosion rate data and corrosion inhibitor effectiveness coupled with estimates of future produced water levels during the life of the field.

If steel can be used, the corrosion rate break data are employed to specify:

- the steels to use for tubulars, wellheads, and facilities;
- the produced water level at which the injection of corrosion inhibitor is required; and
- the corrosion inhibitor to use when the corrosive produced water level is reached.

If steel cannot be safely used, alloys must be evaluated. The consideration of sulfide stress corrosion cracking must be made for the alloys in the same manner as for steels. The production environment must be duplicated in alloy corrosion tests in the same manner as for steels. Standard corrosion tests modified to use the production environment are conducted for the alloys with due consideration given to the probable failure modes—for example, crevice and pitting corrosion for stainless steels. On completion of this test sequence, the alloy or alloys to use for tubulars, wellheads, and facilities construction are specified.

Summary

Petroleum chemistry is complex and sensitive to error when translated to the laboratory. Great care must be taken when designing and conducting corrosion tests for the petroleum environment to ensure that the corrosion measurements made are relatable to the intended service environment. Following the six basic principles given here will aid immensely in obtaining successful results. The preventive corrosion engineering technique to determine the corrosion rate break produced water level for steel, corrosion inhibitor treatment requirements, and alloy selection can be used to minimize the cost of corrosion protection while also maximizing its effectiveness.

References

1. *Petroleum and Natural Gas Industries—Materials for Use in H_2S-Containing Environments in Oil and Gas Production*, ANSI/NACE MR0175/ISO 15156, ISO-ANSI-NACE International Standard, 2nd ed. (Houston, TX: NACE International, 2009).
2. D. A. Shock and J. D. Sudbury, "Prediction of Corrosion in Oil and Gas Wells," in *Carbon Dioxide Corrosion in Oil and Gas Production*, ed. L. E. Newton et. al. (Houston, TX: NACE International, 1984), 394–401.
3. C. de Waard and D. E. Milliams, "Carbonic Acid Corrosion of Steel," *Corrosion* 31, no. 5 (1975): 177–181.
4. C. de Waard, U. Lotz, and D. E. Milliams, "Predictive Model for CO_2 Corrosion Engineering in Wet Natural Gas Pipelines" (paper presentation, Corrosion/91, paper 577, NACE International, Cincinnati, OH, March 11–15, 1991).
5. A. Dugstad, L. Lunde, and S. Olsen, "Dewing Corrosion: A Possible Problem Area for Pipelines Transporting Unprocessed Gas over Long Distances" (paper presentation, 5th International Conference on Mulitphase Production, British Hydrodynamics Research Group, Cranfield, UK, 1991).
6. S. Olsen and A. Dugstad, "Corrosion under Dewing Conditions" (paper presentation, paper 472, NACE International, Cincinnati, OH, March 11–15, 1991).
7. R. Nyborg, A. Dugstad. and L. Lunde, "Top-of-the-Line Corrosion and Distribution of Glycol in a Large Wet Gas Pipeline" (paper presentation, Corrosion/93, paper 77, NACE International, Houston, TX, 1993).
8. J.-L. Crolet and M. R. Bonis, "A Tentative Method for Predicting the Corrosivity of Wells in New CO_2 Fields," *Advances in CO_2 Corrosion* (Houston, TX: National Association of Corrosion Engineers, 1985), 2:23–38.
9. J.-L. Crolet and M. R. Bonis, "pH Measurements in Aqueous CO_2 Solutions under High Temperature and Pressure," *Carbon Dioxide Corrosion in Oil and Gas Production*, ed. L. E. Newton et. al. (Houston, TX: NACE International, 1984), 178–184.
10. G. Schmitt and D. Engels, "SEM/EDX Analysis of Corrosion Products for Investigation of Metallurgy and Solution Effects in CO_2 Corrosion" (paper presentation, Corrosion/88, paper 149, NACE International, St. Louis, MO, March 21–25, 1988).
11. T. Murata, E. Sato and R. Matsuhashi, "Factors Controlling Corrosion of Steels in CO_2-Saturated Environments," *Advances in CO_2 Corrosion* (Houston, TX: NACE International, 1985), 1:64–71.
12. K. Videm and A. M. Koren, "Corrosion, Passivity, and Pitting of Carbon Steel in Aqueous Solutions of HCO_3^-, CO_2, and Cl^-," *Corrosion* 49, no. 9 (1993): 746–754.

13. H.-J. Neumann, B. Paczynska-Lahme, and D. Severin, *Geology of Petroleum,* vol. 5, *Composition and Properties of Petroleum* (New York: Halsted Press, 1985).

14. E. C. Donaldson, "Characterization of the Crude Oil Polar Compound Extract" (U.S. Department of Energy Publication DOE/BETC/RI-80/5, Washington, DC, October, 1980).

15. L. R. Snyder, "Petroleum Nitrogen Compounds and Oxygen Compounds," *Accounts of Chemical Research* 3, no. 9 (1970): 290–299.

16. H. H. Hasiba and F. W. Jessen, "Film Forming Compounds from Crude Oils, Interfacial Films and Paraffin Deposition," *Journal of Canadian Petroleum Technology* 7, no. 1 (1968): 1–12.

17. J. S. Smart, "Wetability: A Major Factor in Oil and Gas System Corrosion" (paper presentation, Corrosion/93, New Orleans, LA, March 7–12, 1993).

18. K. D. Efird and R. J. Jasinski, "Effect of the Crude Oil on Corrosion of Steel in Crude Oil/Brine Production," *Corrosion* 45, no. 2 (1989): 165–171.

19. K. D. Efird, "Predicting Corrosion of Steel in Crude Oil Production," *Materials Performance* 30, no. 3 (1991): 63–66.

20. K. D. Efird, "Preventive Corrosion Engineering in Crude Oil Production" (paper presentation, Offshore Technology Conference, Houston, TX, May 6–9, 1991).

Chapter 16 | Organic Liquids

C. Sean Brossia[1]

Description of Environment

OVERVIEW

Organic liquids are used in a wide variety of industrial applications. They can be characterized as liquids that consist of one or more carbon atoms joined to other atoms through covalent bonds. Common atoms included in organic molecules are hydrogen, oxygen, nitrogen, sulfur, and halogens. Both the rate and yield of certain reactions have been found to greatly increase when performed in organic liquids. Thus, they are widely used in the chemical process industry for synthesis. With an increase in the use of organic liquids, increases in observed corrosion problems associated with the exposure of materials to them also have occurred. In some cases, failures involve an unacceptably large loss of metal or degradation of material properties. In many other cases, however, the major issue is discoloration, contamination, or degradation of the organic solution resulting from corrosion of the processing vessel, as the solution is the product of commercial interest. For example, many pharmaceuticals are synthesized in organic solutions in large vessels. For these applications, the corrosion resistance requirements for materials used are stringent. The introduction of metals into a product can lead to rapid degradation of the product as well as to health and safety concerns.

Although corrosion in pure organic liquids can occur, many corrosion problems in organic liquids involve solutions with multiple components. For example, Schindelholz et al.[1] examined unusually high corrosion rates of Alloy 22 in organic solutions at room temperature and found that the prime cause was due to hydrogen chloride (HCl) formation from a reaction between ethyl aluminum dichloride and ethanol when combined with a 2,3-dichloro-5,6-dicyano-1,4-benzoquinone. Furthermore, a solution containing ethanol, water, oxygen, and HCl contains four components. Some of the components may be present at small concentrations, but these can have dramatic effects. This often is the case with water because of its low molecular mass compared with many organic liquids. Small mass percentages of water can represent significant concentrations in moles/L (e.g., 100 ppm water in acetonitrile results in a water concentration of more than 4 mM).

Organic liquids are classified in a variety of ways. A common classification scheme is based on the nature of the bonding between molecules during solvation. Using this classification approach, three general categories exist: protic liquids, nonpolar aprotic liquids, and dipolar aprotic liquids. Protic liquids (e.g., alcohols, carboxylic acids, amines, amides) are those that can provide protons to other molecules. Solvation in protic organic solvents occurs through dipole-dipole interaction, ion-dipole interaction, and hydrogen bonding. These liquids are generally miscible with water (another protic liquid) and can solvate both organic and inorganic acids. Nonpolar, aprotic liquid molecules (e.g., aromatic and aliphatic hydrocarbons) interact through weak van der Waals bonds and have little solvating ability. The protons in these liquids do not dissociate to any measurable extent. Dipolar, aprotic liquid molecules (e.g., acetonitrile, aldehydes, esters, ethers, dimethyl sulfoxide, tetrahydrofuran, dimethylformamide) interact through ion-dipole and dipole-dipole forces and usually strongly solvate cations and tend to be poor acceptors of electrons and poorly solvate anions in solution. Organic solvents also may have functional groups that are either hydrophobic, which repel water molecules, or hydrophilic, in which case the functional groups readily react with water. It has been shown that the predominant interaction of a metal with an organic adsorbate is through its functional groups.[2]

The wide variety of organic liquids leads to complexity in the analysis of corrosion problems. In addition, the large number of different liquids leads to difficulties because of the limited physical and chemical data on specific liquids. This has ramifications both for the recording of corrosion data and for the development of a broad-based understanding of the important corrosion processes. The lack of physical and chemical information is a limiting factor in any broad description of behavior, such as found in this chapter. Also, while many testing considerations can be generalized for organic liquids, the corrosion behavior of materials in nonaqueous solvents is not nearly as well understood as in aqueous solutions. As a result, appropriate testing and accurate interpretation of the results obtained can be challenging.

[1]INVISTA, 16945 Northchase Dr., Houston, TX 77060, USA http://orcid.org/0000-0002-0522-1123

DOI: 10.1520/MNL202NDSUP20190024

Copyright © 2022 by ASTM International, 100 Barr Harbor Dr., PO Box C700, West Conshohocken, PA 19428-2959
ASTM International is not responsible, as a body, for the statements and opinions expressed in this chapter. ASTM International does not endorse any products represented in this chapter.

TYPES OF CORROSION

The types of corrosion (i.e., the morphology of attack and the oxidation process) that can be encountered in organic liquids are essentially the same as those observed in aqueous solutions. The solution chemistry and solution electrochemistry may be different, but the types of fundamental corrosion processes that can occur remain the same. An excellent review of examples of corrosion in various organic solutions can be found in the work of Heitz.[3] In addition to a review of the fundamental principles involved, Heitz critically evaluates the literature published before 1973 and describes a number of industrial case histories of component failures due to corrosion in organic solutions. Kelly and Moran[4] summarized much of the work in aprotic liquids and put forth a general description of the effect of water on passivation processes. That said, many organic liquids are noncorrosive, particularly to carbon steel.

LIMITS ON COVERAGE OF SECTION

Because of the wide variety of organic liquids, specific information relevant to each one cannot be covered in limited space. The focus of this chapter will be primarily on corrosion of metals in the liquid phase, although many of the comments are applicable to nonmetals as well as vapor phase attack. Because corrosion in organic liquids is not fundamentally different than corrosion in aqueous solution, testing procedures for types of corrosion generally are similar. Thus, only unique considerations with respect to testing in organic liquids will be considered.

VARIABLES THAT AFFECT CORROSION

Corrosion in organic liquids is not fundamentally different from corrosion in aqueous solutions, and therefore, all of the variables that affect corrosion in aqueous solutions can affect corrosion in organic solutions. These include temperature; redox potential; presence and concentration of salts, acids, and bases; and fluid velocity. A number of variables (that are not possible in aqueous solution), however, can be important in organic solutions. The most important of these will be covered in the next section.

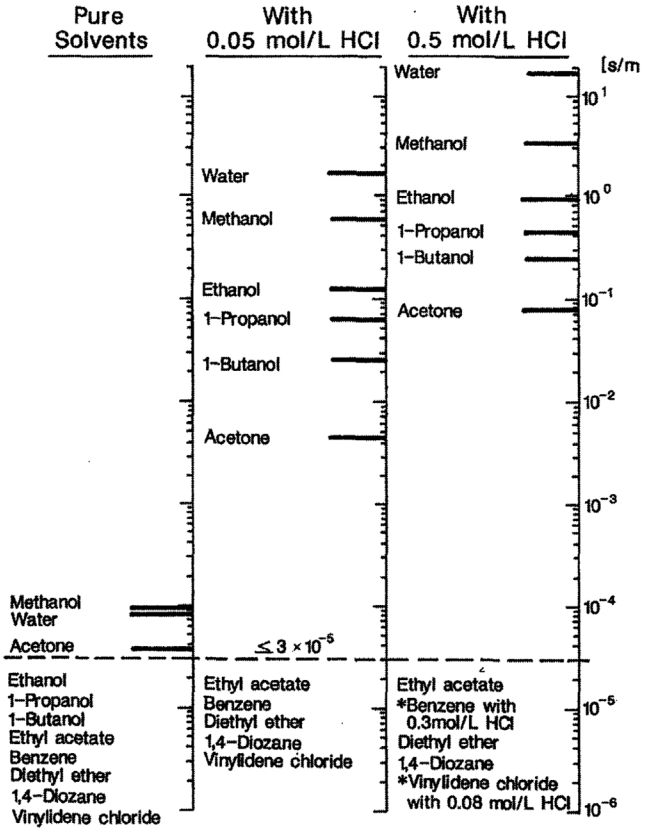
Aspects Making Testing Unique

Several aspects to conducting electrochemical tests in organic liquids often are not encountered or important while testing in aqueous solutions. These include effects resulting from low solution conductivities, the importance of the water concentration in the solution, the existence of an extremely wide variety of liquid compositions, the complexity of products from electroactive organic liquids, and a lack of thermodynamic data.

The low conductivity associated with most organic liquids can give rise to experimental problems with conducting electrochemical experiments. During electrochemical experiments in which a current is applied, the potential measured is the sum of the actual potential difference between the working and the reference electrodes plus the ohmic potential developed in the solution resulting from the passage of current through the solution, which exhibits a finite resistance. This ohmic potential is also known as IR_S, where I is the current passing, and R_s is the solution resistance between the reference electrode and the working electrode. The conductivity of organic liquids is often less than that of pure water,[5] as shown in figure 1. The resulting high solution resistance can result in the development of large ohmic potentials during the passage of even small currents. These ohmic potentials reduce the amount of the applied potential at the metal–solution interface and can affect the current–potential distribution on an electrode. Because the amount of the error changes as the applied current changes, a distorted current–potential relationship can result. More information on ohmic drop and ways to minimize or compensate for its effects can be found in chapter 8, "Electrochemical Tests," in this manual.[6] One common method used to minimize ohmic drop in organic liquids is to add a supporting electrolyte. The ideal supporting electrolyte is a substance that substantially increases the conductivity of the solution without affecting the reactions that occur. Because organic liquids do not solvate many salts in high concentrations, often only a small amount of supporting electrolyte can be added before reaching saturation. Supporting electrolytes are discussed in more detail in the section "Important Experimental Variables."

Another approach that has been used with some success has been through the utilization of microelectrodes. Gui and Sridhar[7] and Gui, Sridhar, and Beavers[8] utilized microelectrodes to interrogate the electrochemistry of steel in fuel-grade ethanol in an

FIG. 1 Comparison of electrolyte conductivity (S/m) of various liquids with HCl added as a supporting electrolyte.[5]



attempt to elucidate the underlying mechanisms responsible for observed stress corrosion cracking (SCC) behavior. The use of microelectrodes attempts to reduce the ohmic potential drop (IR_S) by reducing the area of the electrodes. Thus, at a given current density, the absolute current is lower, thereby making the error due to the ohmic potential drop smaller. Gui et al.[8] used this approach primarily to avoid using a supporting electrolyte, which was thought to alter the polarization behavior that was of interest. In addition, the authors also moved the reference electrode as close as possible to the working electrode to help minimize R. By using this combination of approaches, the authors were able to explore the effects of different environmental variables on the polarization behavior of carbon steel in ethanol-gasoline mixtures. A summary of the key potentials (i.e., open circuit, repassivation, and pitting potentials) from these measurements is shown in figure 2.

Gui and Sridhar[7] and Gui, Sridhar, and Beavers[8] as well as Cao, Frankel, and Sridhar[9,10] also utilized electrochemical impedance spectroscopy (EIS) to measure the solution resistance to perform a correction to the observed polarization behavior for ohmic drop. In particular, Cao, Frankel, and Sridhar[9,10] found that using EIS measurements before and after cyclic polarization tests to estimate IR drop tended to result in overcompensation at higher currents. As is shown in figure 3, at current densities above approximately 100 μA/cm^2 the shown polarization behavior curves downward, thus making the data unreliable. Although the correction was not perfect, this approach was successful in helping to identify the effect of aeration on the polarization behavior of steel in simulated fuel grade ethanol. The results were able to better delineate in what ways that aeration resulted in lower pitting damage compared with the deaerated case.

Water concentration in organic liquids is difficult to control and measure at low levels. Even small amounts of water, however, can have dramatic effects on the corrosion behavior, as shown in table 1. In this case, the corrosion rate of aluminum decreases by three orders of magnitude because of a 0.3 mass % increase in the water concentration. Thus, even though each acid would be considered commercially pure, dramatic differences in corrosion rates resulting from small water additions are observed. This also can be true for other impurities that often are present in organic liquids. Thus, the measurement and control of water levels can be a key aspect to corrosion testing in organic liquids.

FIG. 2 Effect of oxygen concentration in the gas phase on the key potentials of carbon steel as a microelectrode measured against an ethanol-based silver–silver chloride reference electrode using the cyclic potentiodynamic polarization method in simulated fuel grade ethanol.[8]

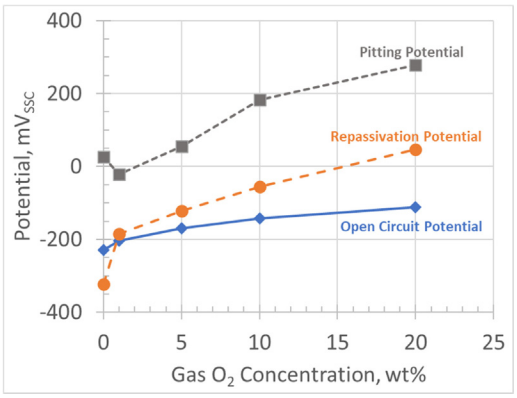


FIG. 3 Effect of applying IR correction based on electrochemical impedance spectroscopy results to polarization data for steel in simulated fuel grade ethanol.[9]

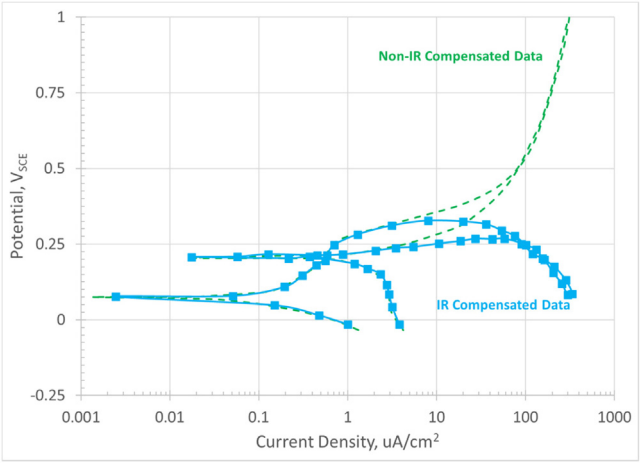
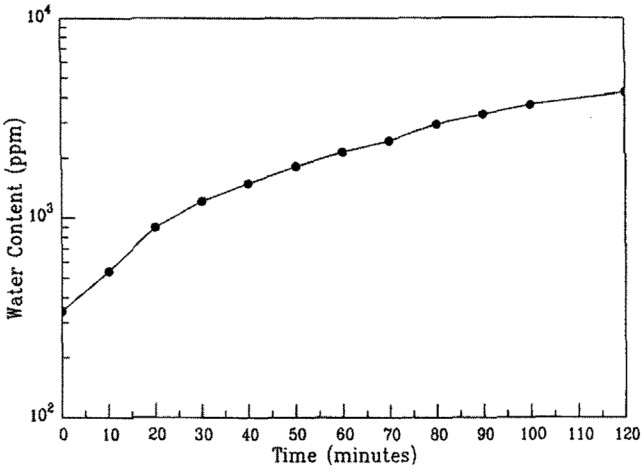


TABLE 1 Weight Loss of Aluminum in Organic Acids[5]

Acid	Acid Concentration, % (Remainder Water)	Mass Loss, g/m^2 day
Acetic	99.5	**0.4**
Acetic	99.94	**990.0**
Propionic	99.5	**2.0**
Propionic	99.4	**2,650**

A popular technique to measure water content is the Karl Fischer titration method.[11] This method can reliably analyze water contents as low as 100 ppm (0.01 mass %). Aliquots of solution can be taken before, during, and after an experiment to follow any changes in water content. Such changes can occur because of the tendency of some organic liquids to absorb water from the ambient atmosphere. For example, it has been found that the water content of a 100 mL sample of methanol, exposed to laboratory air at 25°C with a relative humidity of approximately 55%, increased from 0.035 mass % to 0.42 mass % in 2 h, as shown in figure 4.[12] This illustrates the need for incorporating a sealed experimental cell or a dry glove box when working at low water levels. By using one or both of these, water absorption can be minimized and water levels of 100 ppm and below can be realized in the pure organic liquid. Care must be taken when adding other components to the anhydrous liquid, as most salts as well as electrodes also can add appreciable amounts of water to the solution, which then is difficult to remove. Also, extremely dry solutions can sometimes pose a safety hazard if suddenly exposed to air or water.

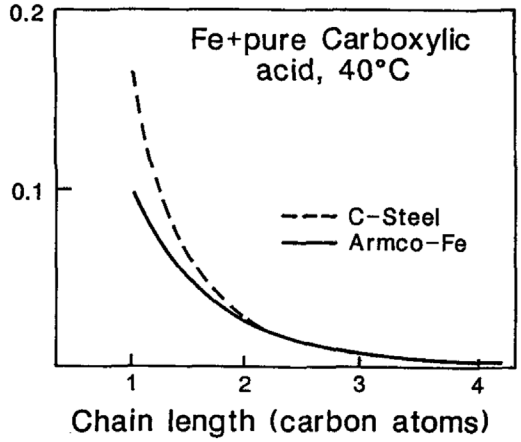
FIG. 4 Increase in water concentration in methanol due to absorption from the atmosphere at ambient conditions.[12]



Organic liquids encompass an extremely wide variety of compounds. They can be classified into two main categories: aprotic (which are generally water insoluble) and protic (which are generally water soluble). Many solution properties, such as solvating power, depend on the primary functional groups of the organic liquid. Thus, the protic nature of a given organic liquid will determine the solubility of various impurities and corrosion products. Even within a type of organic liquid, important differences emerge among individual liquids. For example, the corrosion rate of iron decreases in monocarboxylic acids as the chain length increases (fig. 5).[3] These differences among similar organic liquids add another layer of complexity to the corrosion phenomena as compared with aqueous solution.

Cosolvent interactions are related to liquid composition effects. In many applications, a mixture of liquids (organic/organic, organic/inorganic) is of interest. Several aspects need to be considered when testing in such organic liquid mixtures, which typically are not considered in aqueous solutions. First, the possibility exists that when two or more liquids are combined, they are either immiscible or have limited miscibility. This results in the formation of multiple liquid phases (phase separation) in which the properties of each phase could be significantly different from others. The net result is that testing in mixtures can be difficult. The difficulty arises in trying to determine which phase or composition is detrimental to material behavior and also may involve partitioning of dissolved species between the various phases present. The possibility also exists that it is not an individual phase, but rather the interface between two phases in solution that is deleterious. Multiphase solutions cause special problems, such as concentrations of aggressive species into one phase (e.g., HCl into the aqueous phase of a HCl/water/dioxane mixture),[3] specific adsorption of one phase at the metal surface, and preferential attack at the phase boundary (akin to waterline attack). Additional discussion of multiphase attack is outside the scope of this chapter but can be found in Heitz's review.[3]

FIG. 5 Corrosion rate (mm/y) of iron in mono-carboxylic acids of different chain lengths (i.e., formic, acetic, propionic, butyric).[3]



One important complication for the study of corrosion in a large variety of organic liquids is the paucity of thermodynamic data. Thus, an equivalent to Pourbaix diagrams,[13] used widely in aqueous solutions, has not been extensively developed for organic liquids. In fact, pH in organic liquids is not relevant in aprotic organic solvents because there is no readily available hydrogen. In nonaqueous solutions, however, it is possible to generate more powerful proton donors than the hydronium ion found in aqueous solutions by way of the following reaction:

$$B + H^+ \leftrightarrow BH^+. \quad (1)$$

The strength of these possibly extremely strong acids in nonaqueous solutions is measured by the Hammett acidity function,[14] which is defined as follows:

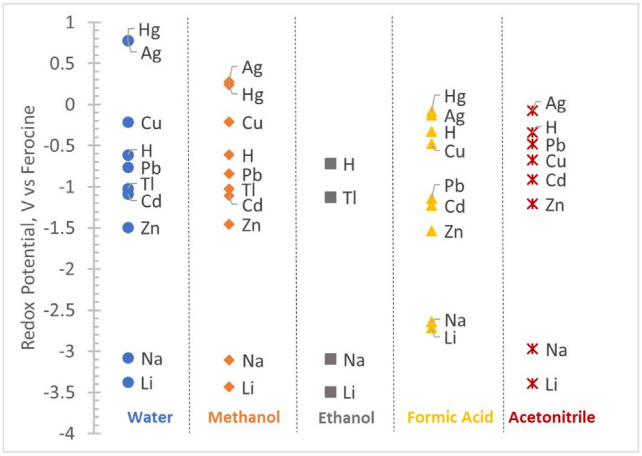
$$H_0 = pK^+_{BH} - \log\frac{[BH^+]}{[B]}, \quad (2)$$

where:
B = the nonaqueous solvent.

No standard metal–solution potential difference has been defined for all liquids. Some of the behavior in organic liquids can be explained by using the concept of Lewis acids and bases employed in aqueous chemistry. A Lewis acid is an electron pair acceptor, and a Lewis base is an electron pair donor. All the usual ligands can be considered to be Lewis bases and metal ions can be considered to be Lewis acids.

Because of these complications, thermodynamic data in the literature pertaining to specific material–aqueous solution systems (e.g., Pourbaix diagrams) may not necessarily be valid for the same material in organic liquids. Some efforts have been made to develop electromotive series in different liquids, as shown in figure 6. The reference point is given by the ferrocene/ferricinium$^+$ couple. The selection of a reference electrode is discussed later in this chapter. In general, the order of reversible potentials is maintained from aqueous solutions, although the

FIG. 6 Electromotive series for the redox reactions associated with different materials in water and organic media.



numerical values can change appreciably. That is, in most environments, the redox potential for silver, given by

$$Ag \leftrightarrow Ag^{+} + e^{-} \tag{3}$$

typically will be at more positive potentials than the corresponding redox reaction for hydrogen, given by

$$H_2 \leftrightarrow 2H^{+} + 2e^{-}. \tag{4}$$

The absolute value and the relative difference between different redox reactions, however, are not constant and can vary significantly.

Finally, as is the case for water, organic liquids have a limited range of electrochemical stability. The products of electrochemical reactions involving organic liquids often are electroactive and can become involved in the electrochemical or chemical reactions that are of interest. Although solution oxidation or reduction also can occur in aqueous solutions, the products are simple bases or acids (i.e., H^{+} and OH^{-}). The products resulting from electroactive organic liquids, however, usually are a mixture of complex organic acids. These complex organic acids can combine with other ions in solution and form other chemicals that could be even more aggressive than the acid from which they were derived. This has been shown to be an issue in methanol by Smialowska and Mankowski,[15] who found that galvanostatic polarization of stainless steel in pure methanol resulted in the formation of formic acid as follows:

$$CH_3OH \rightarrow CH_2O + 2H^{+} + 2e^{-}, \tag{5}$$

$$CH_2O + H_2O \rightarrow HCOOH + 2H^{+} + 2e^{-}, \text{ and} \tag{6}$$

$$HCOOH \rightarrow CO_2 + 2H^{+} + 2e^{-}. \tag{7}$$

The observed oxidation current was a mixture of metal dissolution and methanol oxidation, complicating comparisons of material loss and charge passed based on Faraday's second law.

Important Environmental Variables

The environmental variables that influence corrosion testing in organic liquids include metal, alloy, or nonmetallic material in contact with the organic solution, solution conductivity, solution acidity, water content of the solution, presence and stability of oxide or other preexisting films, type and concentration of surface contaminants or inclusions, functional group and concentration of organic solvent, solvent oxidation or reduction products, type and concentration of supporting electrolyte, applied potential, possible mechanistic paths for passivation, and temperature. As in all corrosion testing, matching the test environment to the actual service environment is critical for obtaining useful information. In addition, by studying the effects of these variables on the corrosion processes, better insight into the controlling mechanisms, as well as the sensitivity of the corrosion processes to changes in the service environment, can be gained.

As noted, the high resistances often associated with organic solutions can distort electrochemical measurements. To minimize these ohmic losses, supporting electrolytes are often used. Ideally, supporting electrolytes dissociate and increase the solution conductivity without altering the corrosion process under study. A commonly used electrolyte is lithium perchlorate ($LiClO_4$) in concentrations ranging from 10 to 500 mM. The perchlorate anion is thought to be inert in most solutions and is weakly adsorbing to surfaces. Thus, $LiClO_4$ is not expected to affect the electrochemical reactions considered in most organic liquids. The addition of 0.1 M $LiClO_4$ as a supporting electrolyte to methanol can increase the conductivity from 10^{-6} S/cm[5] to 6×10^{-3} S/cm, thereby reducing the ohmic resistance by a factor of 200. This reduction allows the experimenter to more easily compensate for the ohmic drop. For fundamental studies of corrosion in organic liquids, the addition of a well-chosen supporting electrolyte is a reasonable approach to allow electrochemical information to be gathered. For more applied measurements, the addition of any supporting electrolyte salt should be considered carefully and comparison tests (e.g., coupon exposures) should be performed to verify the absence of an effect of the supporting electrolyte on the corrosion process. If a supporting electrolyte is not added, caution must be used in the gathering and interpretation of electrochemical data. In some cases, if a supporting electrolyte cannot be added and the solution resistance is high, the performance of meaningful electrochemical measurements is extremely difficult.

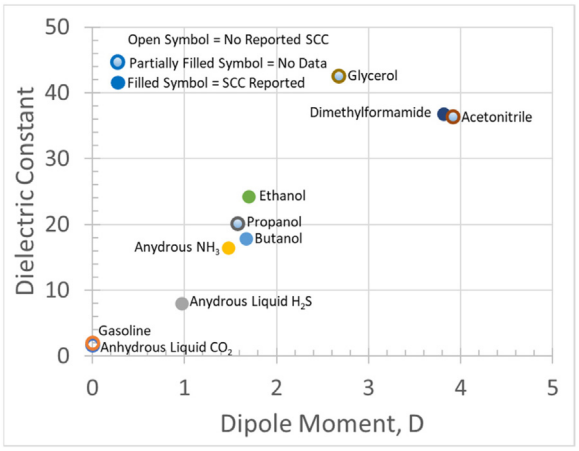
Acids have often been used as supporting electrolytes.[5] Strong acids—for example, sulfuric acid (H_2SO_4), HCl, and nitric acid (HNO_3)—generally enhance the conductivity of organic solutions greatly. Some organics, however, are susceptible to degradation in acids. When water is present, acid hydrolysis becomes an additional degradation pathway.[16] Also, the acidity of the solution can have a controlling effect on the corrosion behavior of metals in organic solutions. For example, a recent review[4] of the literature on the corrosion of metals in aprotic liquids has shown that corrosion behavior, and more specifically, the mechanisms of passivity, are affected by the acidity of the solution. The mechanisms of passivation were classified into four

types: (1) air-formed film, (2) salt film, (3) chemisorption of the liquid, and (4) oxide/oxyhydroxide formation. Acidity is deleterious to all four passivation mechanisms in organic solutions. Hence, control of acidity is important. In addition to H^+, acidity also implies the presence of a corresponding anion. Its presence can alter material behavior by adsorbing to the surface in addition to increasing the solution conductivity.

Thus, acids should not be considered as supporting electrolytes, because they influence the behavior observed, unless the service environment contains acids, in which case they should be included in the test solution. An additional passivation mechanism has been proposed by Shifler, Moran, and Kruger involving the formation of a passive electro-polymerized film (polymer films in which the polymerization process is electrochemically activated) on bare steel surfaces in dimethoxyethane (DME)/$LiAsF_6$ solutions at potentials above the oxidation potential of DME.[17] The complex electropolymerization mechanism for carbon steel in DME/propylene carbonate mixtures with $LiAsF_6$ as the supporting electrolyte depends on the following: (1) DME concentration, (2) cationic intermediate adsorbed concentration and degree of coverage, (3) $LiAsF_6$ concentration, (4) applied potential, (5) rate of iron cation dissolution, and (6) water concentration. Decreases in any of these factors will either decrease the rate of electropolymerization or may prevent electropolymerization entirely.[18] Numerous other investigators also have examined the role of electro-polymerized films as a means of metal passivation in dioxolane,[19,20] ether,[21–24] pyrrole,[25,26] and carbazoles/dicarbazoles with polyether chain substitution,[27] and phenol.[28] For clarification, table 2 contains the physical data for many solvents commonly encountered. Table 2 is not intended to be a complete list, but rather to provide the reader with a sense of the range of physical properties of organic solvents.

Interestingly, Sridhar[29] put forth an argument that the physical properties of the nonaqueous liquid, in particular the dielectric constant and the dipole moment, may provide some ability to predict when SCC of carbon steel might take place. As shown in figure 7, nonaqueous systems that have higher dielectric constants also coincide with observed cracking behavior. The

FIG. 7 Plot of dielectric constant versus dipole moment for different nonaqueous environments illustrating in which environments SCC has been observed.[29]



dielectric constant is a measure of ionic species dissociation in the given solvent. It was further argued that the dipole moment can be related to the dielectric constant through the following:

$$\frac{(\varepsilon-1)(2\varepsilon+1)}{9\varepsilon}=\frac{4\pi N}{3\nu}\left(\alpha+\frac{\mu^2 g}{3kT}\right), \quad (8)$$

where:
ε = the dielectric constant,
N = Avogadro's constant,
υ = the molar volume,
μ = the dipole moment,
g = a correlation factor that relates how neighboring molecules are orientated with each other,
k = Boltzmann's constant, and
T = temperature.

Environments that have low dielectric constants and low dipole moments, thus, are less likely to cause cracking because of the low amount of dissociation of any ionic species present as well as low polarity (dipole moment). This at least sets the foundational

TABLE 2 Some Typical Physical Properties of Selected Solvents at 25°C

Solvent	M.W., g/mole	Density, g/cm^3	Dielectric constant, e	Viscosity, cP Dipole	Moment (Debye)	Formula
Water	18.0152	0.997044	78.30	0.8904	1.87	H_2O
Methanol	32.042	0.7864	32.66	0.5513	2.87	CH_4O
Propylene carbonate	102.090	1.1951	64.92	2.53	4.94	$C_4H_6O_3$
Dimethoxyethane	76.95	0.859	7.20	0.455	1.07	$C_3H_8O_2$
Tetrahydrofuran	72.12	0.880	7.58	0.46	1.71	C_4H_7O
Dioxolane (1,3-D)	74.079	1.0640 (20°C)	7.13	0.589	1.47	C_3HA
Acetonitrile	41.052	0.88649	35.95	0.341	3.53	C_2H_3N
Dimethysulfoxide	78.129	1.09537	46.45	1.991	4.06	C_2H_6OS
Dimethylformamide	73.094	0.94873	36.71	0.802	3.24	C_3H_7ON
Pyrrole	67.09	0.9691 (20°C)	7.5 @ 17°C			C_4H_5N
Phenol	94.11	1.07	4.3 @ 10°C			C_6H_5OH

stage from which different systems exhibit differences in cracking behavior.

As noted, when mixtures of nonaqueous liquids have been combined, unexpected corrosion results have occurred. Schindelholz et al.[1] investigated why high corrosion rates for Alloy 22 where observed during pharmaceutical production. To determine what was causing this, the authors systematically varied each main compositional variable in different combinations. In addition, they also conducted controlled negative tests to prove that other combinations and variables did not cause corrosion rates as high as 25 mm/y at room temperature. Because of this disciplined approach, they identified that the key was a reaction between ethyl aluminum dichloride and ethanol when combined with a 2,3-dichloro-5,6-dicyano-1,4-benzoquinone. As this work illustrates, when investigating mixed solvents, it is critically important to examine each component in isolation as well as in combination, which requires a more complex and rigorous testing approach than typically is needed in aqueous environments.

The supporting electrolyte, which frequently is added, also may play an integral role in passivation processes. In supporting electrolytes, increasing the size of the counter-ions may lead to a decreased film mobility and polyvalent ions, acting as stronger acids, may enhance the formation of cross-links between chains and electrolyzed films.[30] It has also been observed that AsF_6-, added as a supporting electrolyte, can be an integral component of the polymerization process on iron[24] and carbon steel[17] in DME. The use of either tetrabutylammonium perchlorate (TBAP) or $LiClO_4$ as supporting electrolytes leads to alloy breakdown around the solvent oxidation potential.[31] The oxidation of aluminum was found to be influenced by the nature of the passivation mechanisms in nonaqueous solutions, which depended on the kind of electrolyte salt.[32]

The water concentration in the experimental testing solution should duplicate as accurately as possible the water concentration found in the actual service solution. This is because the concentration of water present in the testing environment affects material behavior and the solvating ability of the solution. The presence of water in minimal concentrations (0.1–0.5 mass %) in acidified protic organic liquid solutions leads to the passivation of several materials. For example, iron, stainless steel, and nickel exhibit this behavior in methanol,[33–35] as shown in figure 8. Water concentrations outside this range generally lead to increased corrosion rates.[34,35] In neutral aprotic organic solutions, water in any concentration, except in high concentrations (i.e., 80 + mass %), tends to be deleterious. For example, iron and nickel in neutral dimethylsulfoxide were passive only when the water content was low (0.02 mass % for iron and 0.01 mass % for nickel).[36,37] Iron in neutral propylene carbonate solutions exhibits similar behavior,[38,39] as shown in figure 9. For other materials and liquids, for example, molybdenum and chromium in methanol and dimethylformamide, and iron in acidified dimethylformamide, no clear dependence upon water content is observed.[35,40] Additionally, water can decrease the solvation ability of organic liquids, thus inhibiting the solvation of impurities and corrosion products. In contrast, anhydrous ethers cannot form hydrogen bonds, but the small additions of water allow

FIG. 8 The effect of water content on the anodic polarization of nickel in methanol containing 1 M H_2SO_4.[35]

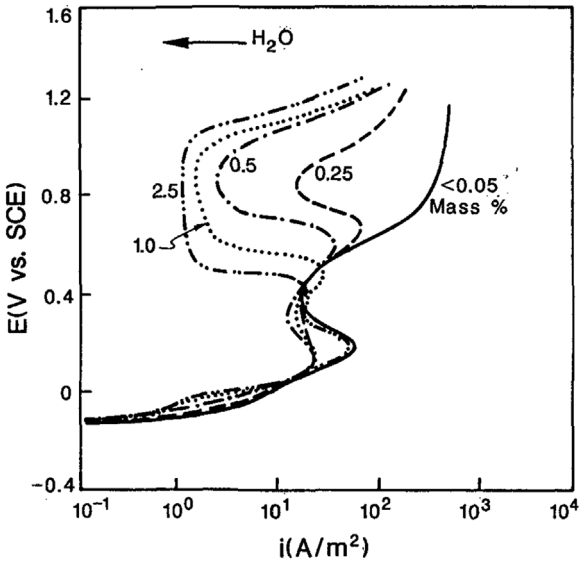
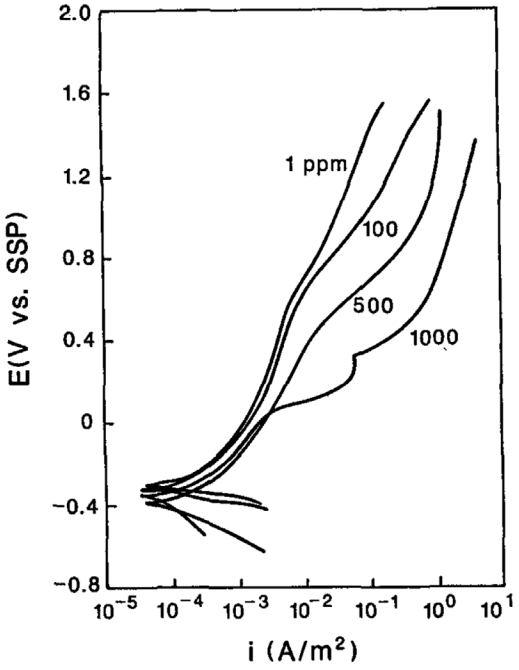


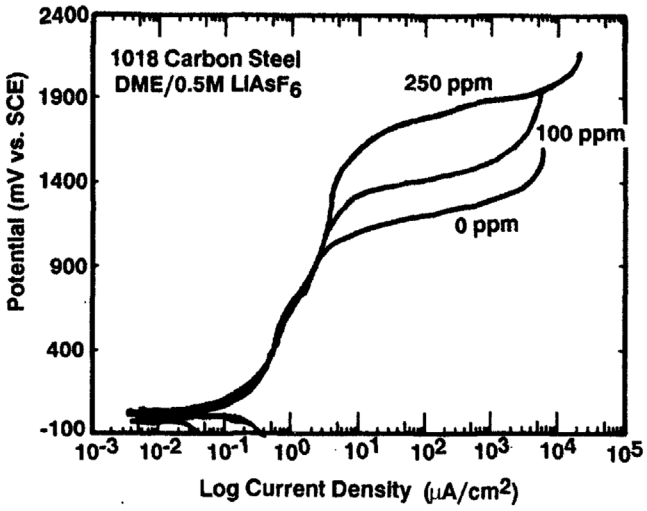
FIG. 9 The effect of water content on the anodic polarization of iron in propylene carbonate at 25°C.[39]



hydrogen bonds to form between the water hydrogen and the ether oxygen. Water added to DME increases the passive range of steel, as shown in figure 10, by several hundred millivolts[17] and of iron by contributing to hydrogen bonding or as a Lewis acid.[41] Thus, as stated earlier, water content needs to be closely monitored and controlled.

The preexistence of a surface film can affect testing in organic solutions in several ways. In the absence of aggressive species, an air-formed film can be protective even under anodic

FIG. 10 The effect of water content on the anodic polarization of carbon steel in DME at 25°C.[17]



polarization. Examples of this include iron in propylene carbonate[38,39] and ferritic stainless steel (Fe-18%Cr) in methanol.[42] The presence of competing mechanisms may also contribute to breakdown of metals and alloys in multicomponent organic mixtures as observed for steel in PC-DME mixtures.[43] Propylene carbonate interferes with DME electro-polymerization by solvating organic cations or cationic radical, or by contaminating the polymer to form pores that allow charge and ionic species to pass through. Adding water to PC-DME mixtures allows for the possibility of aqueous passivating mechanisms that further complicate solvent interactions and competition.[18] Even if aggressive species are present in the solution, however, the air-formed film may be protective until sufficient anodic polarization is achieved. This creates the need for a testing technique that permits removal of the film, enabling examination of the base metal. This can be accomplished by using a stylus to scratch the surface, thereby removing any preexisting protective film to expose new metal. By monitoring the current over time, the corrosion behavior of the material in the absence of any preexisting film can be observed. The long-term stability of air-formed oxides in organic solutions is not known, and thus, the corrosion processes that occur on bared surfaces may be the most relevant to the service conditions. In aqueous solution, cathodic polarization often is used to remove air-formed films. Extensive work in the literature on iron and ferrous alloys,[44] as well as other materials,[45] support the idea that this approach leads to an oxide-free surface. Such information does not exist for oxide reduction in organic liquids. Many workers, however, cathodically polarize their samples before performing electrochemical measurements.[34,46–49]

Because the composition and purity of the organic liquid can strongly affect the corrosion process, a key feature to testing is the choice of an appropriate experimental testing solution. This solution should be as close in composition and impurity concentrations to the service solution as possible, unless accelerated testing is desired. The composition of organic liquids can influence the corrosion rate. For example, the corrosion rate of iron in monocarboxylic acids of different chain lengths was studied and showed that as the chain length increased, the corrosion rate decreased.[3] Often, organic liquids contain impurities, such as water, acids, and metal ions. Although these impurities generally have low concentrations in commercially purchased organic liquids, these concentrations could still be significant. For example, nickel in dimethylsulfoxide was passive only when the water concentration was below 100 ppm. Therefore, the testing solution may need to be purified such that the experimental testing solution closely matches the service solution. In contrast, some corrosion problems develop because of the presence of impurities, so that an initially pure liquid may need to have impurities added to mimic the attack observed. Additionally, if accelerated testing is desired, care should be taken to ensure that the corrosion mechanisms and the location of the corrosion attack (e.g., vapor phase, immersed phase, etc.) accurately mimic in-service observations.

In most organic solutions, the nature of the cathodic process is unclear. In aqueous solutions, water reduction is the most common cathodic reaction, with the reduction of dissolved oxygen also being very important. The electrochemical reduction of many organics is very sluggish, however, and usually poorly characterized. Often, the reduction of residual water is assumed to be the predominant cathodic reaction. The role of molecular oxygen on the corrosion process in organic solutions has not been characterized. Its solubility, however, is nearly 10 times higher in methanol than in water,[3,50] making it a potentially much more influential oxidant. Additionally, aliphatic ethers are slowly converted to unstable peroxides when in contact with oxygen or air, leading to an unsafe condition that could induce a violent explosion during distillations.[16] Deaeration by the passage of an inert gas through the solution must be performed with care to avoid the selective evaporation of the liquid. For low-boiling-point liquids, such as methanol, this is of particular importance. For high-boiling-point liquids, such as propylene carbonate, the passage of ultrahigh-purity nitrogen through the solution for extended times can be used to selectively evaporate the water, leading to higher purity solutions, even after the addition of electrolytic salts.[39] The study of solution electrochemistry on platinum often can give insight into the nature of the cathodic as well as anodic reactions.

Temperature affects corrosion testing in organic liquids in that the reaction rates, charge transport diffusional coefficient, and rate of liquid evaporation are increased and the potential for ignition or explosion is greater. The effect of temperature on reaction kinetics, in general, follows the same principles that hold true for other heterogeneous chemical reactions.[3] Corrosion rates of iron in monocarboxylic acids increase by a factor of 8 to 20 by increasing the temperature from 25°C to 80°C. Although this behavior is not unique to organic liquids, it is important to realize that deviations in testing temperature compared with service temperature could lead to erroneous conclusions. Elevated temperatures also may lead to alternative reaction pathways, leading to other organic intermediate species. Temperature may result in hysteresis in macroscopic polymer properties, such as

swelling, elasticity, and turbidity.[30] If testing at elevated temperatures is called for, caution and appropriate safety preparations are needed.

Laboratory Testing

The two types of laboratory testing are coupon testing and electrochemical testing. This section discusses the special considerations for each type of testing when organic liquids are involved.

COUPON TESTING

Exposure of coupons to the solution of interest with post-test evaluation according to accepted standards, such as ASTM G31, *Standard Guide for Laboratory Immersion Corrosion Testing of Metals*, is the most directly applicable method of testing in organic liquids. Because of the general lack of data on corrosion in organic liquids, coupon testing often takes on additional importance. Although standard test practices have been developed mostly for aqueous solutions, the protocols are essentially independent of the chemical nature of the environment, with minor exceptions. More detailed information on laboratory coupon testing can be found in ASTM G31. One of the most important caveats for such testing in organic solutions is the need to check that the materials that make up the test apparatus are not affected by the liquid. Many nonmetallics are degraded by or preferentially absorb organic liquids, leading to dimensional and mechanical property changes. If such materials are used as spacers in a coupon exposure rack, unexpected experimental variability can result. For example, the nonmetallics may act as getters for aggressive species, produce aggressive species that normally would not be present, or produce inhibiting agents that bias the results. Compounds that have been used as mounting materials successfully in aqueous solution often do not perform well in either completely organic solutions or in mixed organic–aqueous solutions. Thus, a first step in coupon testing is careful selection of the exposure rack and spacer materials. Often, information of this sort is available from the material manufacturer. For example, many nonmetallics have been tested for weight loss or gain and mechanical properties after exposure to a range of different types of organics (e.g., alcohols, aliphatics, aromatics) at ambient and elevated temperature. Although these data can provide general guidance, accelerated tests in the environment of interest often may be warranted.

A second important aspect of laboratory coupon testing in organics is the possibility of an evolution of the solution composition during the test. These changes can be severe, especially at elevated temperatures used to accelerate the corrosion process. Elevated temperature also will accelerate many organic liquid degradation processes, including oxidation by ultraviolet (UV) light. This can be severe in some instances. Thus, it is important to run solution blanks simultaneously. In these tests, no coupon is added to the solution under test, so its composition can be checked both before and after the testing to see whether any significant changes in composition have occurred. Degradation reactions for many organics are well studied and available in the organic chemistry literature. This allows for an identification of the expected by-products. Analysis of solutions after the exposure will allow for a quantitative measurement of the degradation rate of the liquid in the absence of any interaction with the corroding materials. Comparison of the results with analyses of the liquid exposed to metal coupons also may give insight into the nature of the cathodic reaction that occurs.

Water ingress during coupon testing must be monitored if it is suspected that water concentrations are important in the system under study. During testing, seals can develop minute leaks, allowing water levels to increase. Constant purging with an inert gas is an option if the boiling point of the solution is high. For many organics, this is the case. For example, the boiling point of propylene carbonate is more than 200°C. For low-boiling-point liquids, such as methanol (b.p. = 64.9°C), constant purging will drive off liquid, increasing the concentration of the dissolved nonvolatile species with time.[51]

ELECTROCHEMICAL TESTING

For the most part, electrochemical testing in organic solutions is no different than such testing in aqueous solutions, The same experimental arrangements are used, and the appropriate standards, such as ASTM G5, *Standard Test Method for Making Potentiostatic and Potentiodynamic Anodic Polarization Measurements*; ASTM G59, *Standard Test Method for Conducting Potentiodynamic Polarization Resistance Measurements*; and ASTM G61, *Standard Test Method for Conducting Cyclic Potentiodynamic Polarization Measurements for Localized Corrosion Susceptibility of Iron-, Nickel-, or Cobalt-Based Alloys*, are still applicable (see section "Relevant ASTM Standards" in this chapter). Chapter 8 in this manual, "Electrochemical Tests," should be consulted for other information on that subject. This section focuses on the special considerations in electrochemical testing in organic solutions.

The most central difficulty in electrochemical testing of materials in organics is the choice of a suitable reference electrode. Aqueous reference electrodes, such as saturated calomel (SCE), have been widely used in such studies,[34,40,42,46,49,51,52] but can suffer from three types of problems. Because these reference electrodes are in contact with the test solution, water can diffuse from the reference electrode into the test solution, thereby changing the concentration of water during the test. The organic liquid also will diffuse into the reference electrode, and may foul the interface, leading to irreversible changes in its potential. Such a change cannot be detected easily, as it would be superimposed on any change in the potential of the working electrode. A second difficulty with using aqueous reference electrodes is the development of a liquid junction potential. This potential develops at the interface of the aqueous solution and the nonaqueous solution because of the large difference in composition. Such potentials are extremely difficult to measure or calculate and vary with time because of the interdiffusion of the two solutions. The third possible difficulty that may be encountered is reference electrode plugging. This is particularly troublesome when potassium chloride–based reference electrodes are used in perchlorate solutions. As the potassium diffuses out of the reference

electrode, precipitation of potassium perchlorate ($KClO_4$) may occur.

Some research exists on organic liquid–based reference electrodes that have been successfully used in electrochemical studies.[1,7–10,53–55] These include the $Ag/AgClO_4$ (propylene carbonate),[53] Ag/AgCl (multiple),[1,7–10,54] and numerous others, as detailed in Ives and Janz.[55] The $Ag/AgClO_4$ reference electrode developed by Kirowa-Eisner and Gileadi[53] is easy to prepare, stable over time, highly reproducible, and easily stored. This electrode has been used successfully in conducting electrochemical experiments in propylene carbonate solutions. Similarly, the Ag/AgCl (methanol) reference electrode developed by Brossia and Kelly[54] has similar characteristics and has been successfully employed in electrochemical experiments conducted in methanol, ethanol,[7–10] and other organic solutions.[11] Using a reference electrode in which the electrolyte is based on the testing solution will minimize contamination of the testing solution as well as fouling of the reference electrode and the liquid junction potential.

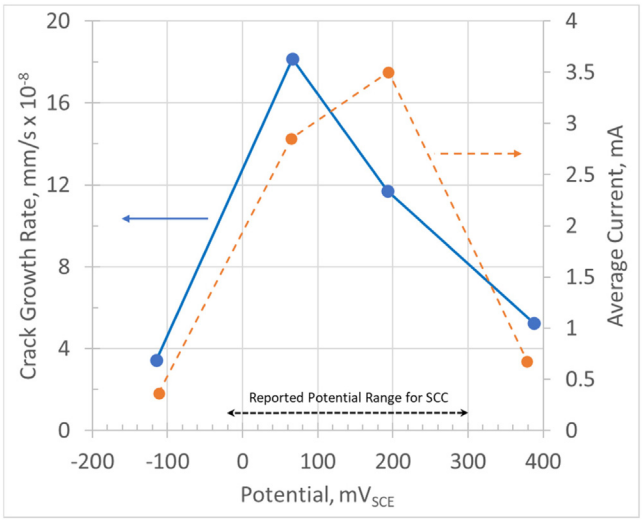
Another aspect of electrochemical testing in organic solutions is the isolation of the counter-electrode from the working electrode. In aqueous solutions, this is often ignored, because the predominant reactions at the counter-electrode are either oxygen evolution (producing H^+) or hydrogen evolution (producing OH^-) during cathodic and anodic polarization of the working electrode, respectively.

Especially in a buffered solution, these reaction products have little effect. In an organic solution, however, the products of the reactions at the counter-electrode are often more complex, and usually unknown. Thus, it is usually good practice to isolate the counter-electrode from the working electrode with porous frits. This will minimize, but not eliminate, any effects of those reaction products.

STRESS CORROSION CRACKING TESTING

Similar to what has been deployed to investigate SCC in aqueous environments, SCC testing in organic liquids also has been performed[7–10,56–62] and in some cases, it has been combined with electrochemical measurements to better elucidate the interaction between key electrochemical parameters and cracking behavior.[7–10,58–59,62] An example of the types of results that have been generated are shown in figure 11.[10] Cao et al.[10] were able to determine that the rate of dissolution of carbon steel in simulated fuel-grade ethanol seemed to track similarly with potential as the measured crack growth rate from compact tension SCC tests. Both crack growth rate and anodic dissolution rates peaked in the same potential range as that observed for SCC in slow strain rate tests. These various test methods were deployed following the same guidelines found for tests in aqueous systems but accounted for complications such as IR drop arising from testing in ethanol. In this case, the authors used EIS to correct for the IR drop in their measurements.

FIG. 11 Effect of potential on measured carbon steel stress corrosion crack growth rate and anodic dissolution in simulated fuel grade ethanol.[10]



Relevant ASTM Standards

- ASTM E203, *Standard Test Method for Water Using Volumetric Karl Fischer Titration*
- ASTM E1064, *Standard Test Method for Water in Organic Liquids by Coulometric Karl Fischer Titration*
- ASTM G1, *Standard Practice for Preparing, Cleaning, and Evaluating Corrosion Test Specimens*
- ASTM G5, *Standard Test Method for Making Potentiostatic and Potentiodynamic Anodic Polarization Measurements*
- ASTM G30, *Standard Practice for Making and Using U-Bend Stress-Corrosion Test Specimens*
- ASTM G31, *Standard Guide for Laboratory Immersion Corrosion Testing of Metals*
- ASTM G38, *Standard Practice for Making and Using C-Ring Stress-Corrosion Test Specimens*
- ASTM G39, *Standard Practice for Preparation and Use of Bent-Beam Stress-Corrosion Test Specimens*
- ASTM G59, *Standard Test Method for Conducting Potentiodynamic Polarization Resistance Measurements*
- ASTM G61, *Standard Test Method for Conducting Cyclic Potentiodynamic Polarization Measurements for Localized Corrosion Susceptibility of Iron-, Nickel-, or Cobalt-Based Alloys*
- ASTM G100, *Standard Test Method for Conducting Cyclic Galvanostaircase Polarization*
- ASTM G102, *Standard Practice for Calculation of Corrosion Rates and Related Information from Electrochemical Measurements*
- ASTM G129, *Standard Practice for Slow Strain Rate Testing to Evaluate the Susceptibility of Metallic Materials to Environmentally Assisted Cracking*
- ASTM G168, *Standard Practice for Making and Using Precracked Double Beam Stress Corrosion Specimens*

- ASTM G192 *Standard Test Method for Determining the Crevice Repassivation Potential of Corrosion-Resistant Alloys Using a Potentiodynamic-Galvanostatic-Potentiostatic Technique*

LABORATORY TESTING USING CORROSION MONITORING TOOLS

Corrosion monitoring tools can offer a sensitive way in which to study corrosion reactions in organic systems under controlled laboratory conditions. Corrosion monitoring typically includes the exposure of coupons and the use of electrochemically and non-electrochemically-based probes. Corrosion coupons and electrochemical test methods were discussed previously. One of the most commonly used non-electrochemically-based corrosion monitoring probes is the electrical resistance method. Corrosion monitoring probes changes in electrical resistance have been in use since the mid- to late-1950s.[63,64] Because the sensing element made of the material of interest is exposed to the environment and experiences corrosion, its cross-sectional area will decrease, resulting in an increase in the measured resistance. If this resistance is monitored in real time and depending on the sensing element shape and size, very small changes in corrosion rate can be observed. Because no electron transfer occurs through the environment, electrical resistance probe measurements are not hindered by high-resistivity media, such as organic liquids. In fact, these probes often are used in the oil and gas industry and also often are deployed to monitor corrosion under atmospheric conditions in which only an intermittent thin film electrolyte layer is formed.

Figure 12 and figure 13 show data obtained in a set of organic liquids consisting of nitriles and long-chain carboxylic acids. In figure 12, the corrosion rate for carbon steel and 316 stainless steel are compared over the temperature range of 70°C to 300°C using electrical resistance probes. As can be seen, in this system, the corrosion rate of carbon steel is initially on the order of 1–2 mm/y until the temperature reaches approximately 125°C, at which point it begins to increase significantly ultimately reaching values over 100 mm/y at 300°C. In contrast, the corrosion rate of the 316 stainless steel remains relatively constant over the entire temperature range varying from 0.51 to 0.77 mm/y. Figure 13 shows the effect of temperature on the corrosion rate of carbon steel in an organic liquid with three different compositions. In the case of composition A, the corrosion rate was observed to steadily increase from 3.5 to 360 mm/y as the temperature increased from 50°C to 200°C. In composition B, the corrosion rate remained relatively low (on the order of 1 mm/y) up to a temperature of 120°C, at which point the corrosion rate suddenly increased dramatically increasing to 854 mm/y at 125°C. In composition C, the corrosion rate increased steadily with increasing temperature similar to composition A; however, the corrosion rates measured were considerably lower. At 50°C, the corrosion rate in composition C was 1.5 mm/y and then increased to 4.1 mm/y at 200°C. As these results indicate, a reasonable picture of corrosion behavior of different materials and the effect of composition and temperature can be obtained using this approach.

FIG. 12 Effect of temperature on measured corrosion rates for carbon steel and 316 stainless steel in an organic liquid obtained using electrical resistance corrosion probes.[65]

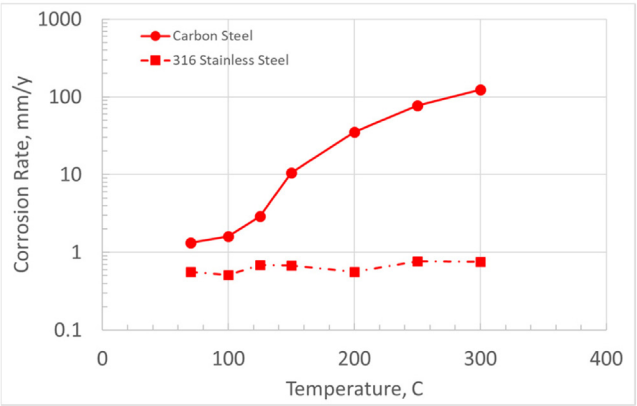
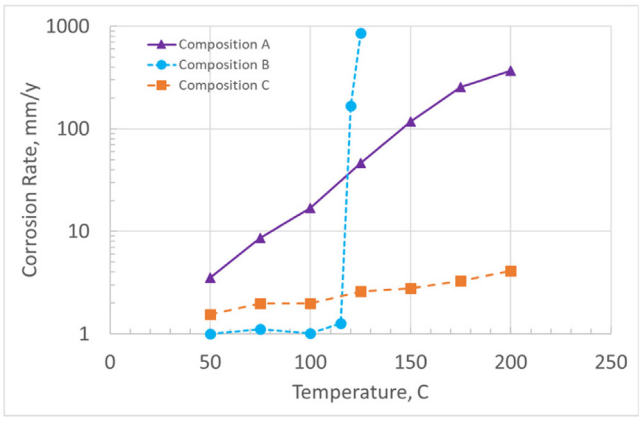


FIG. 13 Effect of temperature on measured corrosion rates for carbon steel in three organic liquids of slightly different composition obtained using electrical resistance corrosion probes.[65]



Electrical resistance probes, however, do experience issues and confounding effects. If conductive surface scales or deposits form, the resistance of the sensing element will tend to decrease, providing a negative corrosion rate. Compensating for the change in metal resistance as a function of temperature also must be performed if tests are conducted at elevated temperatures.

Field Testing

The approach to field studies of corrosion in organic liquids is no different than that used for aqueous corrosion. The choice of coupon size, rack design, test length, and other variables is more strongly influenced by the goals of the testing than by the testing medium. Safety concerns also must be addressed. Different organic liquids have different properties and safety issues, and appropriate references and experts should be consulted. More guidance on the general topic of field testing can be found in ASTM G4, *Standard Guide for Conducting Corrosion Tests in Field Applications*. The concerns expressed in the previous

section on laboratory coupon testing with regard to the effects of the organic liquid on the nonmetallic components of the mounting hardware should be considered.

Because the corrosion behavior of materials in organic liquids can be influenced by low levels of water, minimizing the introduction of water from the ambient atmosphere during the introduction of samples or probes should be carefully considered. For long-term testing at sites where there is a constant turnover of solution, these effects may be small for a one-time insertion of coupons. If, however, a retractable electrochemical probe is used, the solution with which it comes into contact should be flushed to allow it to sample the most relevant environment.

In all field testing, the effects of variability in the composition of the stream being studied on the corrosion processes must be considered. Because small changes in the composition in organic solutions can have dramatic effects on the corrosion rate as well as the stability of passive films, large transients in corrosion rate may be experienced. Thus, it is important to complement the corrosion measurements with solution composition measurements to develop an understanding of the role of stream composition on the corrosion behavior. In addition to ionic composition, water concentrations and the level of liquid byproducts should be monitored.

Summary

Corrosion testing in organic liquids has taken on greater importance in recent years because of the increase in the use of nonaqueous and mixed liquids in material and chemical synthesis as well as energy production. Although the basic types of corrosion processes are similar in both aqueous and organic liquid environments, special attention must be given to the direct application of testing tools to organic testing because of the complexity of organic systems. The wide variety of organic liquids and mixtures increases the number of experimental variables that need to be considered and controlled.

References

1. E. J. Schindelholz, M. A. Christie, S. P. Allwein, and R. G. Kelly, "Extremely High-Rate, Uniform Dissolution of Alloy 22 in Anhydrous Organic Solutions at Room Temperature," *Corrosion* 72 (2016): 1292–1299.
2. S. Trasatti, "Interfacial Behaviour of Non-Aqueous Solvents," *Electrochimica Acta* 32 (1987): 843–850.
3. E. Heitz, "Corrosion of Metals in Organic Solvents," in *Advances in Corrosion Science and Technology*, vol. 4, ed. M. G. Fontana and R. W. Staehle (New York: Plenum, 1974).
4. R. G. Kelly and P. J. Moran, "Passivity of Metals in Organic Solvents," *Corrosion Science* 30 (1990): 495–509.
5. P. Hronsky, *Corrosion* 137 (1981): 161.
6. J. R. Scully, "Electrochemical Tests," in *Corrosion Tests and Standards: Application and Interpretation*, 2nd ed., ed. R. Baboian (West Conshohocken, PA: ASTM International, 2006), 107–130.
7. F. Gui and N. Sridhar, "Conducting Electrochemical Measurements in Fuel-Grade Ethanol Using Microelectrodes," *Corrosion* 66 (2010): 045005-1.
8. F. Gui, N. Sridhar, and J. A. Beavers, "Localized Corrosion of Carbon Steel and Its Implications on the Mechanism and Inhibition of Stress Corrosion Cracking in Fuel-Grade Ethanol," *Corrosion* 66 (2010): 125001-1–125001-12.
9. L. Cao, G. S. Frankel, and N. Sridhar, "Effect of Oxygen on Ethanol Stress Corrosion Cracking Susceptibility: Part 1. Electrochemical Response and Cracking-Susceptible Potential Region," *Corrosion Science* 69 (2013): 768–780.
10. L. Cao, G. S. Frankel, and N. Sridhar, "Effect of Oxygen on Ethanol Stress Corrosion Cracking Susceptibility: Part 2. Dissolution-Based Cracking Mechanism," *Corrosion Science* 69 (2013): 851–862.
11. R. F. Milton and W. A. Waters, eds., *Methods of Quantitative Micro-Analysis*, 2nd ed. (London: Edward Arnold, 1955).
12. C. S. Brossia, "Iron Corrosion in Methanol Solutions" (M.S. thesis, University of Virginia, Charlottesville, VA, 1994).
13. M. Pourbaix, *Atlas of Electrochemical Equilibria in Aqueous Solutions* (Houston, TX: NACE International, 1974).
14. C. H. Rochester, "Acidity Functions," in *Organic Chemistry, Monographs* Series 17 (New York: Academic Press, 1970).
15. Z. Szklarska-Smialowska and J. Mankowski, *Corrosion Science* 22 (1982): 1105.
16. R. T. Morrison and R. N. Boyd, *Organic Chemistry* (Boston, MA: Allyn and Bacon, 1973).
17. D. A. Shifler, P. J. Moran, and J. Kruger, *Electrochimica Acta* 38 (1993): 881.
18. D. A. Shifler, P. J. Moran, and J. Kruger, in *Proceedings of the Symposium on Passivity and Its Breakdown*, PV 97-26, ed. Natishan et al. (Pennington, NJ: Electrochemical Society, 1998), 432.
19. P. G. Glugla, in *Power Sources for Biomedical Implantable Applications and Ambient Temperature Lithium Batteries*, ed. B. B. Owens and N. Margalit (Pennington, NJ: Electrochemical Society, 1980).
20. X. S. Foos and S. M. Erker, *Journal of the Electrochemical Society* 134 (1987): 1724.
21. V. R. Koch, *Journal of the Electrochemical Society* 126 (1979): 181.
22. K. M. Abraham, J. L. Goldman, and D. L. Natwig, *Journal of the Electrochemical Society* 129 (1982): 2404.
23. M. Odziemkowski, M. Krell, and D. E. Irish, *Journal of the Electrochemical Society* 139 (1992): 3052.
24. J. F. Scanlon, P. J. Moran, and J. Kruger, in *Critical Factors in Localized Corrosion*, PV92-9, ed. G. S. Frankel and R. C. Newman (Pennington, NJ: Electrochemical Society, 1992), 525.
25. J. Prejza, I. Lundstrom, and T. Skotheim, *Journal of the Electrochemical Society* 129 (1982): 1685.
26. F. Beck, M. Oberst, and R. Jansen, *Electrochimica Acta* 35 (1990): 1841.

27. P. Marrec, C. Dano, N. Gueguen-Simonet, and J. Simonet, *Synthetic Metals* 89 (1997): 171.

28. G. Mengoli and M. M. Musiani, *Journal of the Electrochemical Society* 134 (1987): 643C.

29. N. Sridhar, "2017 Frank Newman Speller Award: Knowledge-Based Predictive Analytics in Corrosion," *Corrosion* 74, no. 2 (2018): 181–196.

30. G. Inzelt, "Role of Polymeric Properties in the Electrochemical Behaviour of Redox Polymer-Modified Electrodes," *Electrochimica Acta* 34, no. 2 (1989): 83–91.

31. C. S. Brossia, E. Gileadi, and R. G. Kelly, "The Electochemistry of Iron in Methanolic Solutions and Its Relation to Corrosion," *Corrosion Science* 37, no. 9 (1995): 1455–1471.

32. K. Kanamura, "Anodic Oxidation of Nonaqueous Electrolytes on Cathode Materials and Current Collectors for Rechargeable Lithium Batteries," *Journal of Power Sources* 81–82 (1999): 123–129.

33. W. Schmidt, *Zashchita Metallov* 5 (1970): 529.

34. G. Capobianco, P. Venti, and F. Bellucci, "Influence of Water Content on Corrosion of Iron and Stainless Steels in Organic Solvents," *British Corrosion Journal* 25, no. 2 (1990): 133–135.

35. J. Banas, in *Passivity of Metals and Semiconductors*, ed. M. Froment (London: Elsevier Science, 1983).

36. T. R. Agladze, Y. M. Kolotyrkin, T. G. Malysheva, and O. O. Denisova, *Zashchita Metallov* 22 (1986): 509.

37. V. A. Safonov, L. Y. Komissarov, and O. A. Petril, *Protection of Metals* 22 (1978): 178.

38. R. G. Kelly, P. J. Moran, E. Gileadi, and J. Kruger, "The Passivity of Iron in Mixtures of Propylene Carbonate and Water," *Electrochimica Acta* 34, no. 6 (1989): 823–830.

39. R. G. Kelly, P. J. Moran, and J. Kruger, "Passivity of Fe in Anhydrous Propylene Carbonate," *Journal of the Electrochemical Society* 136, no. 11 (1989): 3262.

40. C. A. Farina, G. Faita, and F. Olivani, *Corrosion Science* 18 (1977): 465.

41. J. F. Scanlon, P. J. Moran, and J. Kruger, *Journal of Power Sources* 54 (1995): 85.

42. F. Bellucci, G. Faita, C. A. Farina, and F. Olivani, *Journal of Applied Electrochemical* 11 (1981): 781.

43. D. A. Shifler, J. Kruger, and P. J. Moran, *Journal of the Electrochemical Society* 145 (1998): 23–96.

44. J. A. Bardwell, G. I. Sproule, and M. J. Graham, "Ex Situ Surface Analysis of Passive Films on Fe-Cr Alloys: When Is It Valid?" *Journal of the Electrochemical Society* 140 (1993): 50.

45. H. D. Speckmann, S. Haupt, and H.-H. Strehblow, "A Quantitative Surface Analytical Study of Electrochemically-Formed Copper Oxides by XPS and X-Ray-Induced Auger Spectroscopy," *Surface and Interface Analysis* 11 (1988): 148.

46. F. Mazza, S. Torchio, and N. Ghislandi, "Anodic Behaviour of Armco Iron and of a Low-Alloyed Steel in Methanolic Environments," *International Congress on Metallic Corrosion* 1 (1984): 102–109.

47. G. Capobianco and G. Faita, *International Congress on Metallic Corrosion* 3 (1984): 532.

48. F. Bellucci, G. Capobianco, G. Faita, et al., *Corrosion Science* 28 (1988): 371.

49. F. Bellucci, L. Nicodemo, and B. Licciardi, "Iron Dissolution in Acid Water-Methanol Mixtures," *Corrosion Science* 27, no. 2 (1987): 1313–1321.

50. R. J. Lewis, *Hazardous Chemicals Desk Reference*, 2nd ed. (New York: Van Nostrand Reinhold, 1991).

51. V. K. Singh and V. B. Singh, "Electrochemical Behaviour of AISI 321 Stainless Steel in Methanol-H2SO4 Mixtures," *Journal of Applied Electrochemistry* 19 (1989): 317–322.

52. J. Banas, *Corrosion Science* 22 (1982): 1.

53. E. Kirowa-Eisner and E. Gileadi, *Electroanalytical Chemistry and Interfacial Electrochemistry* 25 (1970): 481.

54. C. S. Brossia and R. G. Kelly, "A Reference Electrode for Use in Methanol Solutions," *Electrochimica Acta* 41 (1996): 25–79.

55. D. J. G. Ives and G. J. Janz, eds., *Reference Electrodes, Theory and Practice* (New York: Academic Press, 1961).

56. J. O. Breitenbach, T. S. Renck, C. E. F. Kwietniewski, T. R. Strohaecker, G. S. Pimenta, I. P. Baptista, and M. Araujo, "Evaluation of the Notch Influence on the Stress Corrosion Cracking Susceptibility of the API 5L X70 Steel in Ethanol," *Corrosion* 70, no. 9 (2014): 907–914.

57. R. D. Kane and S. Srinivasan, "Influence of Metallurgical Processing, Welding and Surface Treatments on Ethanol SCC of Carbon Steel" (paper presentation, Corrosion/2014, paper 4419, NACE International, San Antonio, TX, March 9–13, 2014).

58. A. Venkatesh, B. Chambers, R. Kane, and K. Kirkham, "Evaluation of Stress Corrosion Cracking Behavior of Steel in Multiple Ethanol Environments" (paper presentation, Corrosion/2010, paper 10077, NACE International, San Antonio, TX, March 14–18, 2010).

59. X. Lou, L. R. Goodman, P. M. Singh, and D. Yang, "Understanding the Stress Corrosion Cracking of X-65 Pipeline Steel in Fuel-Grade Ethanol" (paper presentation, Corrosion/2010, paper 10073, NACE International, San Antonio, TX, March 14–18, 2010).

60. F. Gui, H. Cong, J. A. Beavers, and N. Sridhar, "Inhibition of Carbon Steel Stress Corrosion Cracking in Fuel Grade Ethanol by Chemical Addition or Oxygen Control: A Feasibility Evaluation" (paper presentation, Paper No. 2202, Corrosion/2013, NACE International, Orlando, FL, March 17–21, 2013).

61. R. D. Kane, "Use of NACE TM0111 Slow Strain Rate Test for Evaluation of Ethanol SCC," (paper presentation, Corrosion/2015, paper 5945, NACE International, Dallas, TX, March 15–19, 2015).

62. J. G. Maldonado and N. Sridhar, "SCC of Carbon Steel in Fuel Ethanol Service: Effect of Corrosion Potential and Ethanol Processing Source" (paper presentation, Corrosion/2007, paper 07574, NACE International, Nashville, TN, March 11–15, 2007).

63. A. Dravnieks and H. A. Cataldi, *Corrosion* 10 (1954): 224.

64. A. J. Freedman, E. S. Troscinski, and A. Dravnieks, *Corrosion* 14 (1958): 175.

Materials and Applications

Chapter 17 | Titanium

Ronald W. Schutz[1]

Introduction

Application of titanium and its alloys in aerospace, marine, energy, chemical process, and other industrial sectors continues to expand. This has been motivated, in part, by trends in decreasing cost and increasing commercial availability of titanium mill products, improved designer and user knowledge and familiarity, and titanium's attractive combination of engineering properties. These properties include, but are not limited to, relatively low density and elastic modulus, a wide range of strength, and exceptional corrosion resistance over a wide span of environmental conditions.[1,2]

Growing application of titanium and its alloys has led to increased laboratory and in-process (*in situ*) corrosion testing for the purpose of evaluation and service qualification. Although titanium alloys are evaluated with the same basic test methodologies used for other passive, film-forming corrosion-resistant alloys (CRAs), its unique metallurgy, windows of susceptibility, and properties can require additional consideration of and adjustments in certain testing details. This chapter provides an overview of relevant corrosion test methods and detailed guidelines to ensure proper and meaningful evaluation of titanium alloy corrosion resistance and environmental behavior.

Commercial Titanium Alloys

The designations and nominal compositions of various commercial aerospace and industrial titanium alloys are listed in table 1. The first 11 alloys listed are titanium alloys primarily used in chemical or industrial applications in which corrosion resistance is the main design consideration. These alloys consist of single-alpha phase (hexagonal close-packed crystal structure) or near-alpha alloys containing relatively small amounts of beta phase (body-centered cubic crystal structure) in an alpha-phase matrix. The remaining alloys exhibit significantly higher strength and were developed primarily for aerospace service (except for Grade 29 titanium), although several are finding application in industrial and energy service. Alloy strengthening is achieved through solid-solution alloying and stabilization of two-phase structures. These alpha-beta and beta alloys contain varying amounts of beta phase, which may be heat-treated (aged) by precipitating the fine-alpha phase to achieve higher strength levels. The first 16 alloys listed are typically used in the annealed (nonaged) metallurgical condition. Further details on the metallurgy and mechanical–physical properties of titanium alloys can be found elsewhere.[3–8]

Mechanism of Corrosion Resistance

The excellent corrosion resistance of titanium alloys results from the formation of chemically stable and resistant, highly adherent and continuous, ultra-thin (on the order of 10-nm thick) titanium oxide films on the metal surface. Because titanium metal is highly reactive and has an extremely high affinity for oxygen, these beneficial surface oxide films form spontaneously and instantly when fresh metal surfaces are exposed to air or moisture, or both. In fact, a damaged oxide film generally can reheal itself instantaneously if at least traces (i.e., parts per million) of oxygen or water (moisture) are present in the environment. However, anhydrous conditions in the total absence of a source of oxygen (or water/moisture) may result in titanium corrosion, because the protective film may not be regenerated if damaged.

The nature, composition, and thickness of the protective surface oxides that form on titanium alloys depend on environmental conditions. In most aqueous environments, the oxide is typically and primarily titanium dioxide (TiO_2), but may consist of mixtures of several titanium oxides, including TiO_2, Ti_2O_3, Ti_3O_5, and TiO,[9] depending on exposure conditions. Higher temperature (>500 °C) oxidation in air tends to promote the formation and growth of the chemically resistant, highly crystalline form of TiO_2, known as rutile. Lower temperatures, oxidizing aqueous media, and anodizing favor generation of a less-crystalline form of anatase TiO_2, or a mixture of rutile and anatase.[9,10] These naturally formed films typically are less than 10- to 30-nm thick and are invisible to the eye. The TiO_2 oxide is highly chemical resistant and is attacked by few substances, including hot, concentrated hydrochloric acid (HCl), sulfuric acid (H_2SO_4), sodium hydroxide (NaOH), and (most notably) hydrogen fluoride (HF).

[1]Fellow-Corrosion and Energy Materials, TiCorr LLC, 410 Shadydale Dr., Canfield, OH 44406, USA

DOI: 10.1520/MNL202NDSUP20190027

Copyright © 2022 by ASTM International, 100 Barr Harbor Dr., PO Box C700, West Conshohocken, PA 19428-2959
ASTM International is not responsible, as a body, for the statements and opinions expressed in this chapter. ASTM International does not endorse any products represented in this chapter.

TABLE 1 Various Commercial Titanium Alloys

Common Alloy Designation	UNS Designation	Nominal Composition, wt%	ASTM Grade	Ti Alloy Type
CP Grade 1	R50250	unalloyed titanium (commercially pure)	1	alpha
CP Grade 2	R50400	unalloyed titanium (commercially pure)	2	alpha
CP Grade 3	R50550	unalloyed titanium (commercially pure)	3	alpha
CP Grade 4	R50700	unalloyed titanium (commercially pure)	4	alpha
Ti-Pd	R52400/R52250	Ti-0.15Pd	7/11	alpha
Ti- Lean Pd	R52402/R52252	Ti-0.05Pd	16/17	alpha
Ti-Ru	R52404/R52254	Ti-0.lRu	26/27	alpha
Grade 12	R53400	Ti-0.3Mo-0.8Ni	12	near-alpha
Ti-3-2.5	R56320	Ti-3Al-2.5V	9	near-alpha
Ti-3-2.5-Pd	R56322	Ti-3Al-2.5V-0.05Pd	18	near-alpha
Ti-3-2.5-Ru	R56323	Ti-3Al-2.5V-0.1Ru	28	near-alpha
Ti-6-4	R56400	Ti-6Al-4V	5	alpha-beta
Ti-6-4-ELI	R56407	Ti-6Al-4V (0.13 % O max.)	23	alpha-beta
Ti-6-4-Ru	R56404	Ti-6Al-4V-0.1Ru (0.13 % O max.)	29	alpha-beta
Ti-5-2.5	R54520	Ti-5Al-2.5Sn		alpha
Ti-6-2-4-2 S	R54620	Ti-6Al-2Sn-4Zr-2Mo-0.1Si		near-alpha
Ti-550		Ti-4Al-2Sn-4Mo-0.5Si		alpha-beta
Ti-6-6-2	R56620	Ti-6Al-6V-2Sn-0.6Fe-0.6Cu		alpha-beta
Ti-6-2-4-6	R56260	Ti-6Al-2Sn-4Zr-6Mo		alpha-beta
Ti-6-22-22		Ti-6Al-2Sn-2Zr-2Cr-2Mo-0.15Si		alpha-beta
Ti-10-2-3		Ti-10V-2Fe-3Al		near-beta
Ti-15-3-3-3		Ti-15V-3Sn-3Cr-3Al		beta
Beta-21S	R58210	Ti-15Mo-2.7Nb-3Al-0.2Si	21	beta
Ti-3-8-6-4-4 (Ti Beta-C)	R58640	Ti-3Al-8V-6Cr-4Zr-4Mo	19	beta
Ti-13-11-3		Ti-13V-11Cr-3Al		beta

This thin-surface oxide film is also a highly effective barrier to atomic and molecular hydrogen. With this hard rehealable (ceramic-like) oxide film, titanium alloys exhibit elevated resistance to erosion, erosion-corrosion, and cavitation damage under high-velocity turbulent flow conditions.[1] Note that this titanium surface oxide film also may be substantially thickened for cosmetic or coloration purposes or for enhanced corrosion protection through thermal oxidation (heating of the metal in air at higher temperatures) or by anodizing in certain aqueous salt solution electrolytes at higher positive DC voltage, as described elsewhere.

The TiO_2 film, being an n-type semiconductor, is electronically conductive. As a cathode, titanium permits electrochemical reduction of ions in an aqueous electrolyte. Conversely, high resistance to anodic current flow through the passive oxide film (i.e., significant anodic polarization) can be expected in most aqueous solutions. Elevated anodic pitting (breakdown and repassivation) potentials in aqueous media can be expected with many titanium alloys.

Passivity and good corrosion resistance of titanium can be expected under conditions in which these protective surface oxides are thermodynamically stable. Pourbaix (potential-pH) diagrams for the titanium-water system.[1,11] reveal that oxide film stability occurs over a wide range of potentials, from highly oxidizing to mildly reducing conditions. As a result, titanium alloys can be expected to resist all natural waters (including seawater) and common salt solutions of halides (i.e., chlorides), sulfates, silicates, phosphates, nitrates, and carbonates over the pH range of 3–12. Oxide film breakdown and the resultant corrosion of titanium, however, occurs under moderate to strong reducing acid conditions.

Thus, severe general corrosion is possible in strong uninhibited reducing acids, such as HCl, hydrobromic acid (HBr), H_2SO_4, or phosphoric acid (H_3PO_4) solutions, particularly as acid concentration or temperature, or both, increases.[1,2] Severe attack of titanium occurs in acidic aqueous fluoride (i.e., HF) solutions, even at relatively low concentrations (>10 to 15 ppm free fluorides) and temperatures. If other metallic ions that form stable fluoro-complexes are also present, acidic fluoride attack may be inhibited (i.e., resulting in little or no free fluoride available) and may not occur. Titanium hydride formation is predicted under strongly reducing aqueous conditions (i.e., at highly cathodic or negative potentials) and is dependent on solution pH.

Factors Affecting Passivity in Aqueous Media

The passivation of titanium is favored and can be expanded in aqueous reducing acid media by any factor that shifts the alloy potential in the noble or positive direction (i.e., increased redox potential) where oxide film stability is promoted. This beneficial

ennobling influence may result from several factors including the following:

- an increased surface oxide film thickness by anodizing or thermal oxidation;
- anodic polarization of the alloy by impressed anodic current, or galvanic coupling to a more noble metal (i.e., precious/platinum-group metals);
- the presence of dissolved oxidizing species in the environment acting as cathodic depolarizers; and
- the presence of certain alloying elements in titanium that decreases the cathodic (hydrogen) overvoltage, thereby depolarizing the cathodic process.

The last two factors listed are most commonly encountered and can dramatically influence titanium alloy performance in reducing acid solutions. Dissolved reducible (oxidizing) species in solutions are common in many chemical process streams, whether intentionally added or present as minor background contaminants. Some common oxidizing inhibiting species in reducing acid solutions include iron (Fe^{+3}), copper (Cu^{+2}), nickel (Ni^{+2}), titanium (Ti^{+4}), chromium (Cr^{+6}), oxygen (O_2), chlorine (Cl_2), and nitrate (NO_3^{-2}) ions. For example, it is not uncommon for upstream steel component corrosion to produce ferric corrosion products (i.e., Fe^{+3} ions), which contaminate process streams. Several parts per million concentration or more of any of these species may partially or fully passivate titanium alloys in reducing aqueous media depending on acid concentration and temperature and should be taken into account when evaluating alloy corrosion resistance.

These same oxidizing species can also stimulate and aggravate crevice corrosion of titanium in hot salt solutions. By depolarizing the cathodic process on open-metal surfaces exposed to bulk solution, these oxidants effectively increase the potential difference between creviced and noncreviced metal surfaces, thereby driving the crevice cell.[1,12–14] This explains why hot iron(III) chloride ($FeCl_3$) solutions, Cl_2-saturated solutions, or oxygenated/aerated brines are often selected as test media for accelerated test screening of alloy crevice corrosion resistance. Again, it is vital that these common minor background species be accounted for in any crevice corrosion tests involving simulated laboratory environments.

The last factor addresses certain alloying element additions to titanium that also may enhance passivation in reducing acid solutions through cathodic depolarization (reduced hydrogen overvoltage on metal surfaces). This simultaneously enhances the alloys resistance to crevice corrosion in hot salt solutions, because the solutions within an active crevice are essentially deaerated reducing acids. Alloying elements commonly added to commercial titanium alloys to achieve these improvements include the precious metals (i.e., ≥ 0.04 wt% palladium [Pd] or ≥ 0.08 wt% ruthenium [Ru]), nickel (Ni; ≥ 0.5 wt%), and molybdenum (Mo; ≥ 3.5 wt%). Alloys incorporating these alloying additions for corrosion resistance enhancement in table 1 include titanium Grades 7, 11, 12, 16, 17, 18, 19, 21, 26, 27, 28, and 29, and the Ti-6-2-4-6 alloy.

OTHER METALLURGICAL FACTORS IN AQUEOUS MEDIA

The nature of the oxide film on titanium alloys basically remains unaltered in the presence of minor alloying constituents; thus, small additions (less than 1–2 wt%) of most commercially used alloying elements, or minor variations in interstitials (i.e., oxygen, nitrogen, carbon, hydrogen) or trace alloy impurities (i.e., iron) generally have little effect on the general corrosion resistance of titanium in passivating environments. Under active (nonpassive) conditions (i.e., in strong reducing acids) in which titanium exhibits significant general corrosion, certain alloying elements, such as iron or sulfur, or both, may accelerate corrosion. Thus, minor variations in alloy chemistry may be of significance only under conditions in which the passivity of titanium is borderline or when the metal is fully active. Increasing aluminum content generally diminishes alloy corrosion resistance in strongly reducing or oxidizing acid media. Higher vanadium content also can result in higher corrosion rate in strong oxidizing acids, especially as temperature increases.

Weldments and castings of the first 11 titanium alloys listed in table 1 generally exhibit corrosion resistance similar to that of their unwelded, wrought counterparts.[1] These titanium alloys contain so little alloy content and second phase that metallurgical instability and thermal effects are not substantial. Protected by the same surface oxide film, titanium weldments and associated heat-affected zones will exhibit passive behavior (insignificant corrosion) for the same conditions under which the wrought base metal is passive. However, under marginal or active corrosion conditions (for corrosion rates ≥ 0.10 mm/y, or ≥ 4 mils/y), weldments may experience accelerated corrosion attack relative to the base metal, depending on alloy composition.[15,16] Microstructural and crystallographic texture, which often exists in many commercial titanium products, generally produces little or no effect on general or crevice corrosion test results. Thus, sample orientation or end-on (edge) grain texture effects are generally minor or insignificant in these two test modes. Unlike many metals, the introduction of severe cold work (plastic deformation/damage) has little impact on passivity, and generally it does not alter the basic corrosion resistance of titanium alloys.

Although little effect of heat treatment or annealing is observed with the leaner-alloy industrial titanium alloys (the first 11 listed in table 1), certain heat treatments (e.g., aging) may affect the corrosion resistance of higher strength alpha-beta and beta titanium alloys in reducing acid environments. Evaluation of stress corrosion cracking (SCC) resistance of titanium alloys, in contrast, does require attention to, and can be highly dependent on, alloy composition, heat treatment, microstructure, product processing, crystallographic texture, and orientation. Although the leaner alloyed industrial alloys (the first 11 listed in table 1) are generally SCC resistant in aqueous environments, most higher strength titanium alloys generally exhibit SCC susceptibility in the form of K_{IC} or K_c reduction (i.e., K_{ISCC} or K_{SCC}) or increased environmental crack growth rates. With the exception of a few, unique Ti alloys in sensitized conditions (e.g., Ti-13-11-3), most commercial Ti alloys will not exhibit SCC in stressed smooth or notched samples or component configurations

when exposed to aqueous media. For this reason, aqueous SCC testing of titanium alloys is often conducted through loaded precracked fracture mechanics or slow strain rate to failure tests. Titanium alloying elements that decrease SCC susceptibility include molybdenum, vanadium, niobium, and tantalum, and precious metals (palladium and ruthenium) in high-temperature halide media. Reduced SCC resistance may stem from increasing aluminum (>5 wt%), silicon, chromium, and manganese content in these alloys, as well as oxygen (≥0.2 wt% in unalloyed titanium, or >0.13 wt% in higher strength alloys) and other interstitials. In alloys containing more than 5 wt% aluminum, this SCC susceptibility (typically in aqueous chlorides) may stem from ordering and precipitation of Alpha-2 (Ti_3Al) intermetallic phase, which promotes lower energy planar slip along certain near-basal-oriented alpha grains. The influence of these metallurgical factors on titanium alloy SCC behavior is discussed in detail elsewhere.[1,17–20]

Titanium alloys are generally not susceptible to sulfide stress cracking (SSC) in H_2S- and sulfide-rich or sulfur-containing environments (e.g., sour gas/oil well fluids). This inherent SSC resistance stems from the fact that formation of TiS corrosion products is not thermodynamically favored, such that stability of titanium's protective oxide surface film will prevail even at higher service temperatures. In these cold and hot sour brine service environments, resistance to chloride-induced SCC is a more relevant issue for titanium alloys.

As a rough guide, the corrosion fatigue resistance of titanium alloys generally parallels its relative SCC behavior in a given environment. As such, the first 11 titanium alloys listed in table 1 generally exhibit minimal degradation in S-N and fatigue crack growth resistance (i.e., minimal corrosion fatigue) in most environments where metal passivity occurs. Conversely, environmental knockdown in fatigue life may be expected in situations in which crevice corrosion or SCC are possible.

Because of the protective oxide film, titanium alloys generally exhibit anodic pitting (breakdown and repassivation) potential values that are elevated and well above those of most corrosion engineering metals (i.e., >>+1 V). For example, pitting potentials in sulfate and phosphate solutions exceed +80 V (versus SCE), and are typically in the +2 to + 10 V range in chloride media depending on alloy composition, brine pH, and temperature. As a result, spontaneous pitting of titanium alloys in most aqueous environments does not occur and usually is not of engineering concern in the majority of applications. However, relatively low anodic pitting potential values near or just below +1.0 V, which decrease with increasing temperature and acidity, may be observed in pure bromide or iodide salt solutions. Studies have shown that increasing almost any alloying element reduces anodic repassivation potential values in titanium,[21] whereas molybdenum, niobium, and zirconium generally have neutral or slightly beneficial influences. Unlike the intrinsic, conservative anodic repassivation potential value, the extrinsic anodic breakdown pitting potential is highly dependent on metal surface conditions. Roughened, mechanically damaged, ground, and sandblasted surfaces reduce values, whereas well-pickled, thermally oxidized, and anodized surfaces elevate alloy anodic breakdown potentials.[7]

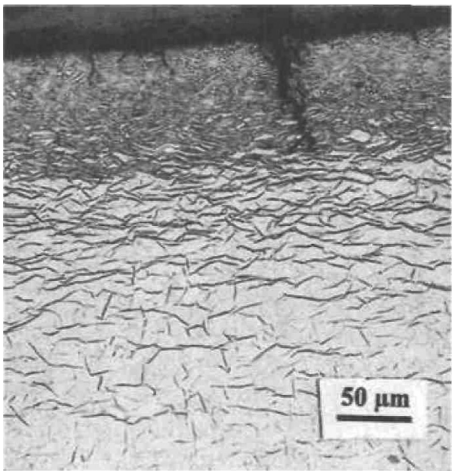
Role of Hydrogen

Titanium alloys are generally highly resistant to penetration by gaseous (diatomic) hydrogen and nascent (atomic) hydrogen because of the surface oxide barrier film. In hydrogen gas exposures, traces of moisture or oxygen are sufficient to maintain this protective film, whereas anhydrous gas can lead to hydrogen absorption, particularly as hydrogen gas pressures and temperature increase. Excessive cathodic charging of atomic hydrogen on titanium metal surfaces through galvanic coupling with active metals or impressed cathodic currents may induce excessive hydrogen uptake, depending on solution pH and temperature. Active corrosion of titanium in reducing acids, within active crevices, or exposure to high-temperature strongly alkaline solutions in which the oxide film is compromised also can result in significant hydrogen pickup. Metallic iron embedded or galled into titanium metal surfaces can provide "windows" for enhanced penetration of hydrogen. Conversely, surface treatments that increase oxide film thickness, such as anodizing and thermal oxidation, tend to thwart hydrogen absorption.

In alpha and alpha-beta alloys, excessive hydrogen uptake can induce the precipitation of the titanium hydride phase in the alpha phase. These acicular-shaped (needle-like) hydrides (fig. 1) when viewed in cross section are actually platelets and are a relatively brittle phase. In most cases, small amounts of hydride precipitates are not detrimental from an engineering standpoint, but they can cause severe reduction in alloy ductility and toughness when present in greater amounts. For example, hydride precipitates can be observed in Grade 2 titanium microstructures at hydrogen concentrations above approximately 40–100 ppm at room temperature, depending on the amount of background beta phase and interstitials present.

These precipitates do not result in gross embrittlement of Grade 2 titanium until hydrogen levels in excess of 500–600 ppm are reached. Because hydrogen solubility increases dramatically with temperature, hydride embrittlement may not be observed at

FIG. 1 Photomicrograph of severely hydride unalloyed titanium at 200×. Note the acicular (needle-like) titanium hydride precipitate.



higher temperatures. If significant absorption has occurred, embrittlement may manifest upon cooling as the hydride phase precipitates. Hydrogen solubility and tolerance generally increase with increasing volume percent beta phase in alpha-beta alloys. In Ti-6Al-4V, for example, hydride precipitates are not formed below approximate hydrogen levels of 600–1,000 ppm, depending on product microstructure.

Although uniaxial tensile properties may experience little effect from increasing hydrogen levels, biaxial or triaxial stress properties, such as bend ductility, cold-drawing limits, and impact toughness in alpha and near-alpha alloys may be sensitive to hydrogen levels.[21–24] In alpha and especially alpha-beta alloys, hydrogen contents above critical levels (i.e., > 80–120 ppm) can result in sustained-load cracking (SLC), which dramatically reduces useful maximum service loads (reduced fracture resistance) in notched or cracked components under slow strain rate or constant tensile load situations,[22–26] Beta titanium alloys have a high solubility for hydrogen and, therefore, high hydrogen tolerance. As such, embrittlement generally is not associated with hydride precipitation. Significant losses in ductility or formability do not occur below hydrogen levels of several thousand parts per million, although the tolerance to hydrogen decreases somewhat in the aged (high-strength) condition where fine alpha phase precipitates are also present. In addition, hydrogen atom diffusivity (mobility) within the beta alloy is typically several orders of magnitude above that in alpha titanium even at room temperature.

Relevant Forms of Titanium Corrosion

It is important to know where titanium might exhibit susceptibility to corrosion attack to establish which corrosion test methods may be applicable or relevant to titanium alloys. Table 2 presents

TABLE 2 Environments in which Corrosion and Environmental Susceptibility of Titanium Alloys Has Been Observed

Environment	Corrosion Mode of Concern	Susceptible Ti Alloys	Conditions Promoting Susceptibility
Strong reducing acids (HCl, HBr, HI, H_2SO_4, H_3PO_4, and especially HF)	general corrosion/etching, and possible by-product hydrogen absorption	all	Dependent on alloy composition, acid concentration, and temperature, and presence of inhibitive oxidizing species.
Higher temperature halide (chloride and bromide) and sulfate solutions	crevice corrosion	Alloys without Pd or Ru, or alloys with <3.5 % Mo or < 0.5 % Ni	Dependent on alloy composition, brine pH and temperature. Requires severe, tight crevices.
Pure bromide/iodide solutions	anodic pitting	all	Dependent on alloy composition and surface, and solution pH and temperature.
High-temperature strongly alkaline solutions	hydrogen absorption	all	Occurs at pH > 12 and >75 °C.
High-temperature sour brine (sulfide/H_2S-rich)	galvanically induced hydrogen absorption	all	Requires galvanic coupling to an active metal/alloy and >75 °C.
Anhydrous hydrogen gas	hydrogen absorption	all	Occurs at higher temperatures, and gas pressures if water- or oxygen-free.
Anhydrous methanol	stress corrosion cracking	all	Occurs when water content is below 2–3 wt%, and is most severe near room temperature.
Red-fuming nitric acid or nitrogen tetroxide	stress corrosion cracking and/or pyrophoric reaction	all	Dependent on water and/or oxygen content.
Halide salt residues at high temperatures (>230°C)	hot salt stress corrosion cracking	Higher strength Ti alloys	Dependent on alloy composition, stress load, temperature, and exposure time.
Chlorinated hydrocarbons	stress corrosion cracking	Higher strength alpha- beta and beta alloys	Dependent on alloy composition and condition.
Halide (chloride, bromide) salt solutions	stress corrosion cracking	Higher strength alpha-beta and beta alloys	Dependent on alloy condition, brine pH and temperature, and test method.
Liquid cadmium and mercury, and solid silver (>230 °C) and cadmium	liquid or solid metal embrittlement	all	Requires direct, intimate contact with fresh unfilmed metal surface under high stress.
Dry chlorine gas	general corrosion and/or ignition/burning	all	Occurs when water content is below 0.5–1.0 wt% depending on temperature.
Pure oxygen gas and liquid oxygen (LOX)	ignition/burning	all	Dependent on alloy composition, component thermal mass, and gas pressure. Ignition in LOX requires impact damage threshold.
Warm alkaline peroxide solutions	general corrosion	all	Dependent on peroxide solution composition, pH, and temperature.
High-temperature air or oxygen-containing gas exposures (>600 °C)	metal oxidation, wastage, and/or embrittlement	all	Dependent on alloy composition, temperature, and exposure time.

a list of specific environments in which some form of corrosion susceptibility has been observed on titanium alloys in laboratory tests or service experience. The table shows the relevant mode of corrosion degradation that can be expected, general scope of titanium alloys susceptible, and comments on critical factors that strongly influence each corrosion phenomenon.

Based on table 2, the general forms of corrosion and corresponding test methods relevant to titanium alloys include the following: general corrosion, crevice corrosion, anodic pitting, SCC, hydrogen absorption or embrittlement, ignition or burning, and oxidation. The following sections will provide methods and guidelines for testing and evaluation of these seven basic forms of titanium alloy corrosion damage.

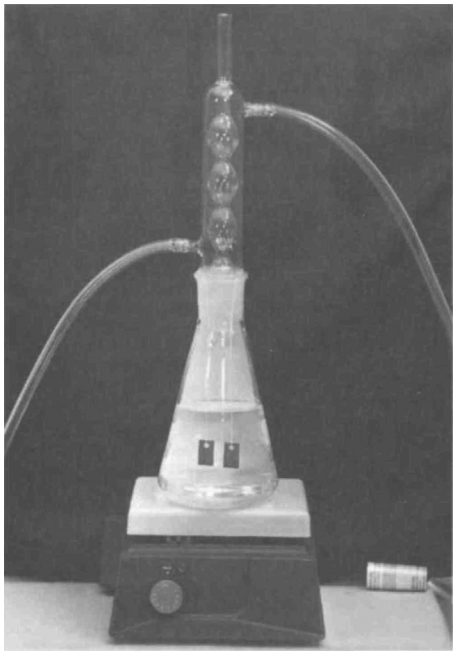
Test Methods for Evaluation of Corrosion Damage

GENERAL CORROSION TESTING

General corrosion rates for titanium alloys can be determined from measurements of changes in component or test coupon mass (i.e., typically weight loss, and sometimes weight gain), dimensional change, or electrochemical methods. Electrochemical anodic and cathodic polarization testing is often used to supplement weight loss testing. Polarization testing can identify whether the alloy is truly fully passive or possibly metastable; this is often not discernible from weight loss tests alone. The immersion test procedures described in ASTM G1, *Standard Practice for Preparing, Cleaning, and Evaluating Corrosion Test Specimens*, and ASTM G31, *Standard Practice for Laboratory Immersion Corrosion Testing of Metals*, apply, provided that several modifications are observed[1,27] These modifications focus on test sample surface preparation and post-test sample-cleaning procedures. A typical laboratory test apparatus for weight-loss immersion testing in acid solutions at or below the boiling point is shown in figure 2.

The type of sample surface finish tested should resemble the one expected in service. For many titanium alloys, depending on product form, this is frequently the pickled finish, although sandblasted, ground, or machined surfaces also are common. The initial degreasing of test samples should avoid chlorinated organic solvents (with higher-strength titanium alloys), anhydrous/neat methanol, or hot alkaline cleaners. Acceptable cleaning solvents include methyl-ethyl ketone (MEK), acetone, most alcohols, benzene or toluene, and most detergent solutions. The pickled finish can be prepared by pickling the metal in a 35 vol% nitric acid (HNO_3) to 5 vol% HF solution (based on 48 wt% HF and 70 wt% HNO_3 stock acid solutions, with the balance being water) at 20–55 °C for 0.5–5 min or more. Typically, 0.005–0.05 mm (0.2–2 mils) of sample surface is removed in this process, depending on surface requirements. More dilute solutions, such as 12 vol% HNO_3 to 1 vol% HF, also can be used if slower pickling rates are desired. In any case, a minimum 7:1 HNO_3 to HF stock acid vol% ratio should be maintained to avoid excessive uptake of hydrogen in titanium alloys during pickling. After pickling, a quick rinse in deionized water and air drying leaves a shiny gray specimen that is ready for weighing. The abraded surface finish can be obtained by wet grinding with fine-grit silicon carbide (SiC), aluminum oxide (Al_2O_3), or zirconium dioxide (ZrO_2) abrasive paper after the cleaning step. A final deionized water rinse and drying would prepare the specimens for weighing and testing. Prepared and weighed titanium samples may be stored in open air before exposure for several days without significantly affecting sample weight.

FIG. 2 Typical Huey test apparatus with water-cooled condenser for conducting sample general corrosion (weight-loss) tests up to the solution boiling point. Samples are typically suspended in the solution by Teflon string or glass rods.



A mechanically abraded or polished coupon surface finish is highly recommended over pickled finishes when corrosion testing titanium alloys containing readily reducible (noble) alloying elements. These alloys include those containing platinum group metals (Pd, Ru, Pt) and other metals (Ni, Cu), which may readily plate back in pure form onto titanium coupon surfaces during the final pickling step. These plated metal residues can ennoble coupon test surfaces and may not represent the most conservative test methodology.

Consideration should be given to the presence of certain test solution contaminants that may significantly affect the corrosion rate. More specifically, contamination of acid media with transition metal ions, such as ferric, nickel, cupric, and chromate ions, and other oxidizing species should be avoided because these ions act as cathodic depolarizers and inhibit corrosion in most acid media. In nitric acid testing, dissolved silicon, Ti^{+4}, Fe^{+3}, and most precious metal ions are fairly effective inhibitors and will lower corrosion rates. In strong nitric acid media, it is best to avoid prolonged testing in glass, and the accumulation of dissolved Ti^{+4} corrosion product, which inhibits corrosion. This

can be counteracted by frequent solution change or refreshment. In most reducing acids, such as HC1, H_2SO_4, or H_3PO_4 (but not HF), testing in glass flasks is acceptable. The Ti^{+3} ion corrosion product normally formed and dissolved in a reducing acid medium has minimal effect on corrosion except at near-saturated concentrations; but the mild oxidizing agents mentioned earlier, such as the transition metal ions (particularly those in higher oxidation states), may inhibit corrosion at concentrations above several parts per million. It is recommended that the solution be constantly refreshed or changed at least every 24 h (or more frequent) in corrosion tests where foreign ions are generated from corrosion processes to minimize their effects. It is also critical that the degree of aeration (dissolved oxygen level) and other background chemistry variables in the test media that influence titanium passivity be taken into account to achieve valid and relevant test results.

The presence of surface corrosion products on titanium after testing depends on the environment to which the titanium was exposed. Removal of these products, when formed, is necessary for obtaining the proper weight loss data, and the correct corrosion rate. In media where the titanium has remained essentially passive, such as near-neutral brines, the original shiny metal luster usually will still exist, and the specimens need only be rinsed in distilled water before their final weighing. Most deposits from the medium that adhere to the specimen surface and are nontitanium corrosion products may be cleaned off in a warm (<65 °C) 25 vol% HNO_3 to 25 vol% HC1 ratio solution or a 50 vol% HNO_3 solution based on stock acids. Other compatible post-test acid cleaning solutions include ≤ 10 wt% HC1 or H_2SO_4 inhibited with a minimum of 1,000 wppm ferric (Fe^{+3}), cupric (Cu^{+2}), chromate (Cr^{+6}), or molybdate (Mo^{+6}) ions heated up to about 70 °C. These are generally oxidizing inhibitor additions that maintain titanium passivity during exposure to these dilute reducing acid cleaning solutions. Traditional filming or adsorption-type acid corrosion inhibitors used for ferrous alloys (e.g., amines, quaternary salts, cyclic imines, aldehydes) generally are not effective for titanium. Siliceous scales may be removed in warm (<65 °C) solutions containing < 20 % NaOH inhibited with 1 wt% sodium nitrate ($NaNO_3$), sodium hypochlorite (NaOCl), sodium dichromate ($Na_2Cr_2O_6$), or sodium molybdate (Na_2MoO_4). The use of strong, uninhibited mineral acids such as HCl, H_2SO_4, H_3PO_4, and especially HF are not recommended for cleaning, because they will corrode the metal samples, which also explains why the electrolytic cleaning method mentioned in ASTM G1 is not used.

In media in which the titanium does have a low but finite corrosion rate and where the dissolved titanium in solution hydrolyzes back onto the surface of the specimen (such as dilute hot-reducing acids) or in strongly oxidizing media (such as boiling concentrated HNO_3), a titanium oxide–hydroxide corrosion product may build up slowly on the surface. This oxide film or deposit is not soluble in common mineral acids and cleaning solutions. The more desirable means of cleaning the specimen of titanium corrosion product or even stubborn nontitanium deposits is a fine-grit- or glass bead-blasting procedure. Tests run in the laboratory suggest that the use of 180-grit or finer silica or alumina sand to lightly grit-blast off titanium surfaces results in acceptably small weight losses in sample coupons. Weight losses in the 10^{-4} g range may be incurred when light sandblasting (<5 s exposure) is used, and these can be corrected for by exposing an untested titanium specimen to the same blasting procedure and correcting for its weight loss. A final rinse in distilled water after sandblasting leaves the dried specimen ready for weighing. Titanium specimens that have been exposed to hot, strong reducing acids in which the corrosion rate is quite high generally exhibit chemically roughened, matte-gray hydride metal surfaces, which may not require surface cleaning.

Immersion testing will generate weight loss (or weight gain) data for corrosion rate determination. Also, corrosion current measurements for corrosion rate calculation can be obtained from standard electrochemical polarization tests (see ASTM G5, *Standard Reference Test Method for Making Potentiostatic and Potentiodynamic Anodic Polarization Measurements*, and the *ASM Metals Handbook*[28]).

Corrosion rates in millimeters per year (mm/y) for titanium alloys can be calculated from sample weight loss data as follows:

$$\text{Corrosion rate (mm/y)} = \frac{(8.76 \times 10^4)(W)}{(d)(A)(t)}, \qquad (1)$$

where:

d = alloy density in g/cm^3,
A = sample surface area in cm^2,
t = exposure time in h,
W = weight change in g.

Corrosion rates in mpy (thousandths of an inch per year) can be derived using the formula:

$$\text{Corrosion rate (mpy)} = \frac{(534{,}700)(W)}{(d)(A)(t)}, \qquad (2)$$

where:

W = weight change in g,
d = alloy density in g/cm^3,
A = sample surface area in in.^{2},
t = exposure time in h.

A list of density values for common commercial titanium alloys is given in Table 3.

TABLE 3 Room Temperature Density Values for Some Common Commercial Titanium Alloys

Alloy	Density, g/cm^1
Ti Gr.l, 2, or 3	4.51
Ti Gr.7, 11, 16, 17, 26, or 27	4.51
Ti Gr.12	4.52
Ti Gr.9, 18, or 28	4.48
Ti Gr.5, 23, or 29	4.42
Ti-6-2-4-6	4.68
Ti-10-2-3	4.64
Ti-15-3-3-3	4.78
Ti-3-8-6-4-4 (Ti Gr.l9)	4.82
Ti Gr.21	4.93

Corrosion rates in mm/y can be calculated from electrochemical measurements by using the formula:

$$\text{Corrosion rate (mm/y)} = \frac{(3.3)(i_{corr})(EW)}{d}, \quad (3)$$

where:

i_{corr} = the measured corrosion current in mA per cm^2,
d = alloy density in g/cm^3
EW = the equivalent weight (atomic weight/valence state) for titanium.

The equivalent weight for titanium is 16 g per equivalent under reducing acid conditions (Ti to Ti^{+3} species), and 12 g per equivalent under oxidizing conditions (Ti to Ti^{+4} species). The corrosion current (i_{corr}) value is typically determined from Tafel slope extrapolation or linear polarization methods.[28–30]

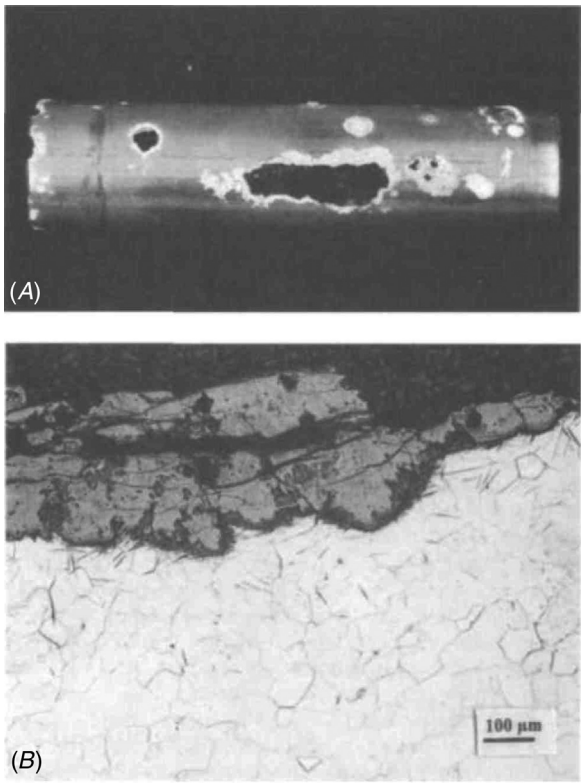
The use of weight loss measurements and the alloy densities cited here assume the standard gravity state at the Earth's surface and should be reconsidered when testing under varying gravity scenarios at other universe locations. In these cases, it may be beneficial to measure changes in test coupon mass using dimensional parameter changes to calculate true corrosion rates. This approach also may provide more accurate corrosion rates in instances in which severe uniform corrosion attack has occurred in the test exposure.

CREVICE CORROSION TESTING

Crevice corrosion is a form of localized attack of titanium alloys that may occur in higher temperature (>70 °C) chloride, bromide, iodide, fluoride, and sulfate-containing solutions; its occurrence is highly dependent on alloy composition, solution pH, and temperature. Crevice attack on titanium requires the presence of large and severe (tight) crevices, such as gasket-to-metal flange joints or seals, tube-to-tube-sheet joints, metal-to-metal joints, or adherent process stream deposit or scale crevice formers found in service. Attack typically takes the form of irregularly shaped craters or pits, with voluminous, off-white, light gray, or sometimes black corrosion product caps, as pictured in figure 3. Metal surfaces adjacent to active crevices may display vivid oxide film coloration from hydrolyzed acidic crevice solutions. The mechanism for titanium alloy crevice corrosion generally is similar to that for stainless steel and nickel alloys, in which oxygen-depleted reducing acid conditions develop within tight crevices as detailed elsewhere.[1,31]

Crevice corrosion testing of titanium alloys generally aims at determining go/no-go performance information. The rate of crevice corrosion is of little practical interest, because crevice attack generally is insidious and rapid and, therefore, cannot be tolerated in any form. Many crevice test assemblies have been used, including the multiple-crevice (serrated) washer (ASTM G78, *Standard Guide for Crevice Corrosion Testing of Iron-Base and Nickel-Base Stainless Alloys in Seawater and Other Chloride-Containing Aqueous Environments*), the Dutchman or spool rack (ASTM G4, *Standard Guide for Conducting Corrosion Coupon Tests in Field Applications*) assembly, and the sheet (or thin-plate) sandwich-type assembly. The multiple-crevice (serrated) washer generally is not a conservative test and is not recommended,

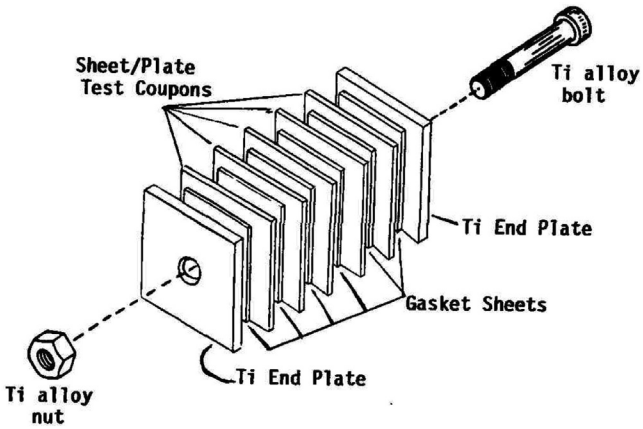
FIG. 3 Typical example of crevice corrosion of titanium in hot chloride brines. (*A*) Irregularly shaped crevice corrosion attack on Grade 2 titanium tubing. (*B*) Photomicrography of cross section through crevice corrosion site in Grade 2 titanium showing the titanium oxide corrosion product cap and irregular attack profile (100 × magnification).



because titanium is highly crevice resistant and requires a relatively large, deep creviced surface area for crevice corrosion initiation. The larger creviced surface area and depth of the sheet/plate coupon sandwich-type assembly, illustrated in figure 4, dramatically increases susceptibility to attack and is most commonly used. This method uses a test assembly in which thin gasket sheets (typically PTFE, FEP, or other polymeric gasket material, or sealant, of interest), or highly polished ceramic wafers, are interspersed between flat metal sheet or plate coupons to produce the desired number of metal-to-metal or metal-to-gasket crevices, or both. Coupons are typically 1 in. by 1 in. (25 mm by 25 mm) or larger to create large, deep creviced surfaces. Each test assembly is fastened together with a centerline titanium bolt and nut and tightened down to a torque of 25 to 90 in.-lb (2.8 to 10.1 m-N) to create tight, severe crevices. The titanium assembly bolts and nuts may be of the same titanium alloy being tested, or covered with an insulating PTFE sleeve or tape wrap to avoid galvanic interferences. Ceramic washers also may be incorporated, if needed, to electrically isolate the assembly bolting.

It is important that coupon surfaces be flat and, especially, as smooth as possible (low root mean square roughness) to minimize crevice gap and volume and, thereby, stimulate initiation. Highly roughened sandblasted or ground surfaces exhibit

FIG. 4 Typical crevice test assembly for crevice corrosion testing of titanium alloy sheet or plate coupons. Sequence of coupons and gasket sheets can be modified to form gasket-to-metal or metal-to-metal crevices.



reduced crevice corrosion susceptibility compared to finer, smoother, and more polished surfaces. Although a 220-grit wet-ground coupon surface finish may be considered a minimum requirement, a 400-grit finish or finer is recommended for most conservative test results. Preparation of crevice test coupons follows the same procedures as that for general corrosion test coupons. It is also vital that only the virgin grade of fluoropolymer gaskets (e.g., PTFE, FEP) be used in these tests, because nonvirgin (reprocessed) grades may release soluble fluorine–fluoride compounds within crevices during test exposures that may falsely stimulate localized attack.

Laboratory crevice testing is usually conducted in glass flasks and vessels, titanium alloy autoclaves, or other CRA autoclaves. The minor presence of background or contaminating metal ion species or other oxidizing species may aggravate crevice attack. Thus, it is also vital that suitable test vessels be selected and that the representative degree of aeration, pH, and other aspects of background solution chemistry be controlled and simulated. Although crevice corrosion can initiate within the first several hours of exposure, a minimum test duration of 30 days is recommended to develop a sufficient degree of attack for detection and measurement purposes.

Post-test evaluation of crevice test coupons may require removal of titanium oxide–hydroxide corrosion products (see figure 3) if crevice attack has occurred. Common mineral acids and reagents will not dissolve these adherent, tenacious deposits. A light (>l20 grit and <5 s) grit-blasting or glass-bead blasting of coupon surfaces will readily remove these scales and facilitate visual examination of pitted surfaces (per ASTM G46, *Standard Guide for Examination and Evaluation of Pitting Corrosion*) and permit sample weighing after water rinsing. Creviced coupon surfaces are often highly colored after hot aqueous exposures, but reveal no visible pits or localized attack after sandblasting. This is indicative of slight growth and thickening of a protective titanium oxide film on creviced surfaces, which is considered quite normal and acceptable from a performance standpoint. Slight coupon weight gain is often measured in this situation. In addition to visual examination and weight change measurements, monitoring of creviced specimen potential[32,33] and current[34] has been used to a limited extent to identify the initiation of crevice corrosion. Examination of polished and etched metallurgical sections through pitted areas of creviced coupons may provide additional information regarding depth and attack mechanism.

PITTING POTENTIAL TESTING

The susceptibility of an alloy to pitting on openly exposed surfaces (in the absence of crevices) in a given solution and fixed temperature is normally assessed by determination of anodic pitting potential values. The two pitting potentials of interest are (1) the extrinsic, surface-dependent anodic breakdown potential (E_b); and (2) the conservative, intrinsic anodic repassivation potential (or protection potential, E_{prot}) that defines the minimum potential at which pitting is possible in the test environment.

The anodic breakdown potential of titanium alloys is typically determined by the potentiodynamic (potential scan) technique (ASTM G3, *Standard Practices for Conventions Applicable to Electrochemical Measurements in Corrosion Testing*, and ASTM G5) at slow scan rates ($\leq$0.5 mV/s). Because this value is sensitive to sample surface condition, it is vital that the representative metal surface anticipated in service be tested. Conversely, titanium alloy repassivation potential may be measured by a galvanostatic method,[35] the constant potential-surface scratch test,[28,30,35] or reverse scan potentiodynamic method. The galvanostatic method is quick, easy, and generally preferred. It involves impressing a constant anodic current density of approximately +200 mA/cm^2 on the specimen for at least several minutes before measuring the sample polarization potential relative to a reference electrode. This potential, once stabilized and corrected for electrolyte IR drop, represents the anodic repassivation potential. The constant potential-scratch method is more tedious and time consuming, involving trial iterations for bracketing the critical potential. Potentiodynamic scan reversal (ASTM G61, *Standard Test Method for Conducting Cyclic Potentiodynamic Polarization Measurements for Localized Corrosion Susceptibility of Iron-, Nickel-, or Cobalt-Based Alloys*) after scanning anodically to induce breakdown pitting may produce ambiguous results with nonreproducible, scan rate–dependent repassivation potential values.

The exceptionally high anodic pitting potentials of titanium alloys in most aqueous solutions means that (1) oxidizing acid solutions, such as $FeCl_3$ or $Fe_2(SO_4)_3$ solutions (ASTM G28, *Standard Test Methods for Detecting Susceptibility to Intergranular Attack in Wrought, Nickel-Rich, Chromium-Bearing Alloys*, and ASTM G48, *Standard Test Methods for Pitting and Crevice Corrosion Resistance of Stainless Steels and Related Alloys by Use of Ferric Chloride Solution*) cannot be used to identify critical pitting parameters; and (2) potential range or power requirements for potentiostats/galvanostats are greater than that for most other common metals and alloys. In chloride solutions, for example, a potentiostat or galvanostat with an impressed sample potential output range as high as +10 to + 12 V may be required for pitting potential determinations. Practical counter-electrodes

for these electrochemical techniques include glassy carbon and platinum wire and mesh.

STRESS CORROSION CRACKING TESTING

SCC test methods commonly used for metals[36] are applicable to titanium alloys, as long as relevant mechanical and physical properties are accounted for. This means selecting applied stresses based on alloy strength or elastic modulus values for the appropriate sample orientation, which is corrected for test temperature when appropriate. The smaller spread between yield and ultimate strength, and the lower plastic strain limits exhibited by titanium alloys compared with most common CRAs also means limiting applied sample stresses values to approximately 105% yield strength in static- or deflection-loaded (e.g., tensile, U-bend, C-ring, bent-beam) tests. Because many titanium alloy products can exhibit significant crystallographic texture depending on alloy type and processing history, it is advisable that SCC susceptibility be evaluated with regard to sample orientation as well. In alpha and alpha-beta titanium alloy mill products, for example, greater susceptibility is often associated with the direction along the hexagonal closed-packed basal plane intensification (e.g., T-L direction in unidirectional processed products).

Test methods to assess the SCC resistance of titanium alloys can be grouped into three basic categories:

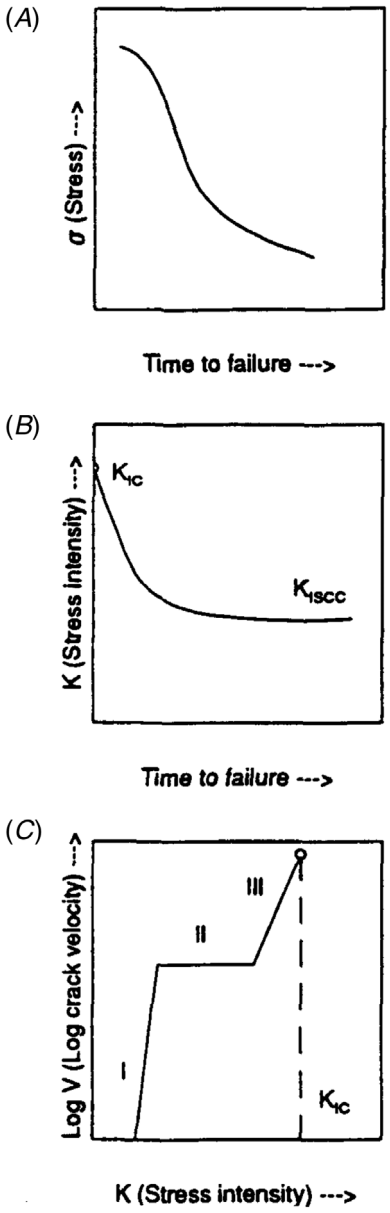
- *Category 1* tests use smooth, statically loaded specimens, such as U-bend, C-ring, bent-beam, and direct-tension test specimens (per ASTM G30, *Standard Practice for Making and Using U-Bend Stress-Corrosion Test Specimens*; ASTM G38, *Standard Practice for Making and Using C-Ring Stress-Corrosion Test Specimens*; ASTM G39, *Standard Practice for Preparation and Use of Bent-Beam Stress-Corrosion Test Specimens*; and ASTM G49 *Standard Practice for Preparation and Use of Direct Tension Stress-Corrosion Test Specimens* (superseded), respectively).
- *Category 2* tests are fracture mechanics tests that use notched and fatigue precracked specimens that are statically or dynamically loaded, such as cantilever beam, compact tension, and double cantilever beam specimens. These tests are conducted per ASTM E399, *Standard Test Method for Linear-Elastic Plane-Strain Fracture Toughness of Metallic Materials*; ASTM E1820, *Standard Test Method for Measurement of Fracture Toughness*; ASTM E1681, *Standard Test Method for Determining Threshold Stress Intensity Factor for Environment-Assisted Cracking of Metallic Materials*; and ASTM G168, *Standard Practice for Making and Using Precracked Double Beam Stress Corrosion Specimens*.
- *Category 3* tests use smooth (or notched, but not precracked) tension specimens that are dynamically axially loaded in tension and strained to failure at very low strain rates. The slow strain rate tensile (SSRT) test is typically conducted in accordance with ASTM G129, *Standard Practice for Slow Strain Rate Testing to Evaluate the Susceptibility of Metallic Materials to Environmentally Assisted Cracking*, or NACE TM0198-2011, *Slow Strain Rate Test Method for Screening Corrosion Resistant Alloys for Stress Corrosion Cracking in Sour Oilfield Service*.

Selection of a suitable SCC test method for titanium alloys is primarily determined by the nature of the stress cracking data or design information desired, and by the chemical nature of the test environment relative to titanium alloy passivation. For simple go/no-go assessment of SCC with no quantitative cracking parameters, the least costly, simpler category 1 tests may be adequate if SCC initiation (incubation) periods are not too long. The data typically are considered in terms of specimen stress level versus time to failure, as shown in figure 5*A*. Category 3 SSRT test results are generally assessed as comparisons or ratios of test sample ductility (total elongation or reduction in area) or time-to-failure values to those from a reference (control) sample (tested in air or inert gas), providing some degree of relative SCC susceptibility. Confirmation of SCC occurrence, however, must entail examination of SSRT specimen post-test fracture surfaces for indications of any SCC (i.e., low-energy fracture mode), such as relative extent of any cleavage, intergranular cracking, or secondary cracking over the total fracture area.

If fracture mechanics design information (i.e., K_{ISCC}, K_{SCC}, J_{IC}, $J_{c,}$ K_J) is sought, then the more sophisticated and costly category 2 fracture tests per ASTM E399 or ASTM E1820 specifications (using compact-tension [C-T] or single-edge notch bend [SENB]-type test specimens) are the preferred choice. As indicated in figures 5*B* and 5*C*, K_{ISCC} results for titanium alloys are stress and time dependent, such that K_{ISCC} values may be plotted as a function of time to failure to reveal true, conservative K_{ISCC} values. These may involve bolt- or wedge-open-loaded fracture specimens (see ASTM E1681 or ASTM G168), which should be tested for at least 24–100 h, or by rising (increasing) load steps applied to fracture specimens as described by ASTM F1624, *Standard Test Method for Measurement of Hydrogen Embrittlement Threshold in Steel by the Incremental Step Loading Technique*. Sufficient hold time at each stress-intensity level (applied load step) tested should be considered relative to load step size to ensure that the plateau shown in figure 5*B* will be reached. Step load hold times on the order of 20 min to 2 h should be considered to manifest SCC effects in aqueous environments. A more practical modified version of the rising step method and ASTM E399 test protocol, which identifies a singular Kscc value from each test specimen, is the continuous rising-K test conducted on these fracture specimens, which involves loading at a slow displacement rate. In aqueous media, specimen loading can be initiated at 15–20 MPa $m^{0.5}$ to reduce testing time, to which a subsequent constant rising-K rate in the typical range of 0.3 to 1.0×10^{-3} MPa $m^{0.5}$ s^{-1} is applied to the specimen. As with other rising-K or K-load testing, the critical K_{SCC} (or threshold K) is derived in cases in which the load curve drops sharply and an increase in CMOD data measurements (i.e., discernable crack growth) coincide.

It is important to recognize that K values derived from the elastic fracture mechanics tests (ASTM E399, ASTM E1681, ASTM G168, and ASTM F1624) will be highly dependent on fracture specimen geometry and type and, especially, specimen thickness. With most relatively plastic titanium alloy materials, plane stress effects (i.e., crack tip blunting) can result in artificially lower Kc and K_{SCC} values. As such, it is highly recommended that all fracture specimen thicknesses (B value) be maximized for the product

FIG. 5 Various types of SCC test data presentation: (*A*) typical for category 1 tests; (*B*) and (*C*) typical for category 2 tests.



form tested so that plane-strain conditions are approached or achieved to obtain more representative K values. Furthermore, ligament size should be maximized where possible, such that C-T and B × 2B-type SENB specimen geometries are preferred over B × B-type SENB specimens where possible. Fracture mechanics parameters derived from elastic-plastic fracture-based testing methods (e.g., J-R testing per ASTM E1820) are less sensitive to this effect and should be considered when component cross-section or specimen thicknesses are relatively small and serious plane stress conditions prevail. In the case of the higher strength (but still reasonably plastic) Ti-6Al-4V alloy, for example, substantial reductions in fracture toughness (K) values measured using elastic fracture mechanics test methods may be observed at test specimen thicknesses below approximately 19–25 mm depending on particular alloy strength and toughness properties and metallurgical condition. Those same specimens measured by elastic-plastic test methods (e.g., J-testing) generally produce significantly higher toughness, with reduced sensitivity to variations in specimen size and thickness.

SSRT testing of smooth specimens (ASTM G129 or NACE TM0198-2011) is a highly sensitive, rapid, most discriminating, and conservative SCC test method for titanium alloys. In some cases, this SCC test may be too conservative from a design or use standpoint because the surface-oxide film is continuously being broken during straining to failure. This method is particularly useful for rapid alloy screening and sorting, and provides a relative or semiquantitative sense of alloy SCC susceptibility. Discriminating strain rates for titanium alloys in aqueous and methanolic solutions lie within the 10^{-5} to 10^{-7} s^{-1} window. A practical strain rate traditionally used effectively in aqueous and methanolic test media is 4×10^{-6} s^{-1}. It is also recommended that specimen test gage sections and diameters be sufficiently large in coarser-grain titanium alloy product forms (e.g., beta annealed alpha-beta alloy condition) to avoid scatter and variability in resultant test strain values.

The selection of an appropriate SCC test method for titanium alloys may be based on the particular type of environment to be tested. In environments in which alloy repassivation (oxide film formation) is favored, and in which stage I subcritical cracking generally is not observed, category 2 and 3 tests are more severe and discriminating than category 1 tests. This is the case for aqueous media, including salt water and brines, and chlorinated organic solvents in which cracking failure of category 1 specimens generally is not observed at near-ambient temperatures. One must provide initial or continued local oxide film breakdown, such as in category 2 and 3 tests, to expeditiously initiate and manifest potential SCC tendencies in these alloys. Exceptions to this rule include those few titanium alloys that may exist in highly sensitized metallurgical conditions. For example, alloys susceptible to SCC in ambient neutral salt water in smooth or notched samples include step-cooled Ti-8Al-lMo-lV and Ti-13V-11Cr-3Al alloys. Highly stressed category 1 test specimens also may be applicable for testing in hot aqueous halides or chlorinated solvents, where higher temperatures may overcome SCC activation barriers in certain alloys after sufficient exposure periods.

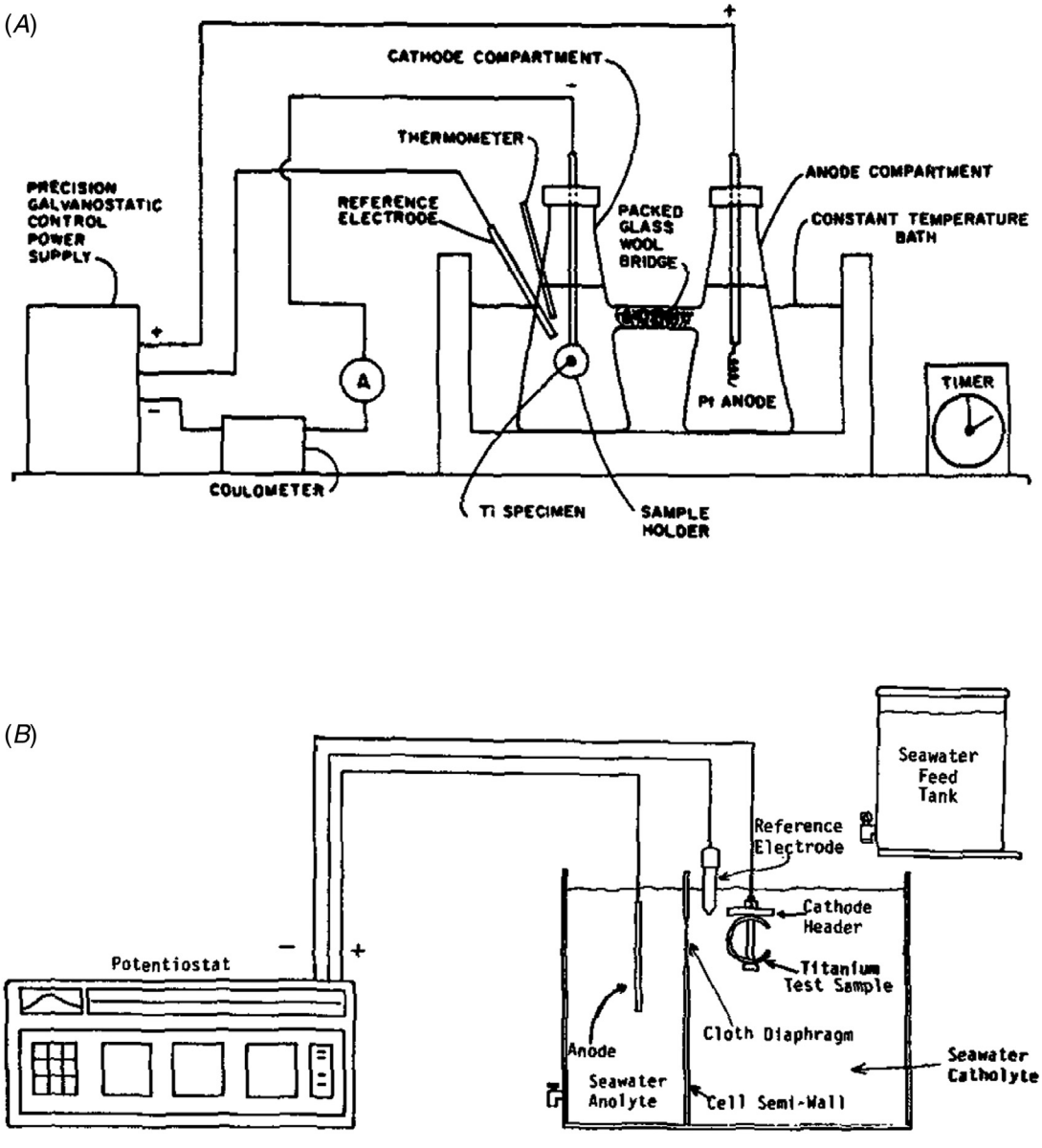
For environments in which stage I subcritical cracking behavior occurs and repassivation is not favored, category 1, and sometimes category 3, testing is generally preferred over category 2 testing for practical reasons. These environments include methanol, red-fuming nitric acid and dinitrogen tetroxide (N_2O_4), certain liquid and solid metals, molten salts, and hot salt, as listed in table 2. Note that category 2 testing is not physically applicable to the evaluation of solid metal embrittlement and hot salt SCC in these alloys. Note also that hot salt SCC testing of titanium should follow the guidelines and procedures provided in ASTM G41, *Standard Practice for Determining Cracking Susceptibility of Metals Exposed under Stress to a Hot Salt Environment*.

HYDROGEN TESTING

Testing to determine the susceptibility of a titanium alloy to hydrogen uptake and embrittlement should simulate conditions expected in service. In hydrogen gas atmospheres, simple coupon exposures for as long as is deemed practical are recommended to ensure significant uptake, if it occurs. The gas atmosphere must duplicate exact gas chemistry, particularly with respect to water and oxygen content. Mere traces of moisture, for example, will effectively inhibit hydrogen absorption by titanium in dry hydrogen gas and possibly cause test interference.

Galvanic coupling tests or cathodic charging tests also can be conducted to evaluate susceptibility to hydrogen uptake. For a given electrolytic media, an active metal (e.g., iron, aluminum) sample is galvanically coupled to the titanium alloy sample, such that a specific anode-to-cathode surface area is tested. Impressed cathodic charging tests are performed in electrolytic cells containing a specific electrolyte. A power supply (potentiostat or galvanostat) impresses a constant potential or current on the cell, such that the titanium is cathodic relative to an inert counter-electrode, such as graphite or platinum. A reference electrode also can be used to control or to measure the polarization potential of the test cathode. There are no standardized test methods or setups for cathodic charging studies; therefore, they are designed to best simulate conditions anticipated in service. Two examples of typical laboratory charging cell setups are depicted in figures 6*A* and 6*B*. Note the presence of a porous diaphragm

FIG. 6 Typical examples of laboratory cell setups for cathodic charging tests on titanium alloys. (*A*) Typical cell setup for short-term cathodic charging of titanium samples at constant current in hot acidic electrolytes. (*B*) Typical cell setup for longer-term cathodic charging of titanium samples at constant potential in seawater and brines.



(e.g., glass wool, sintered glass frits) in these cells to minimize unwanted intermixing of cathode or anode by-products and catholyte contamination. Catholyte refreshment should be considered to maintain representative electrolyte composition and pH, especially if higher current densities and longer charging times are involved.

The surface condition of the test sample is a critical variable in all hydrogen uptake tests. Studies have shown that abraded or sandblasted surfaces absorb hydrogen more readily than as-pickled surfaces.[1] Thickening of the surface oxide film by anodizing or thermal oxidation further retards absorption. The actual surface finish anticipated in service should be evaluated.

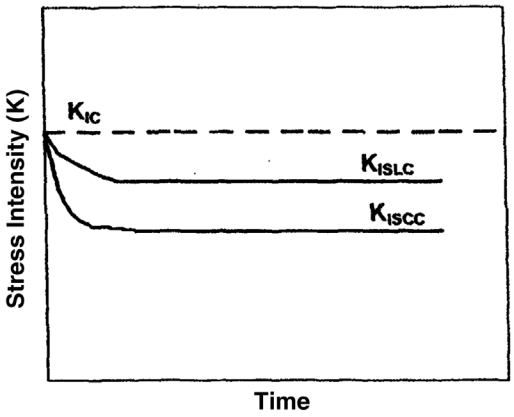
After test exposure, sample evaluation for hydrogen may include smooth or notched tensile, bend, ductility/cold formability, or impact Charpy tests, hydrogen analysis, or cross-sectional microstructural examination. Uniaxial, smooth specimen tension testing is generally of little value in manifesting the subtle embrittling effects of increasing hydrogen content. Titanium alloys tend to exhibit susceptibility under biaxial or triaxial stress states; therefore, bend tests, cup-forming tests, or notched tension tests are generally more sensitive to hydrogen effects. Impact toughness testing can be an especially sensitive indicator of hydrogen effects in alpha alloys, whereas slow strain rate methods are suitable for alpha-beta alloys.[22,23,26] Because hydrogen content has relatively little effect on alloy hardness, macro- or micro- hardness testing is generally of little use.

Some titanium alloys may be susceptible to SLC, also known as delayed cracking. This can occur on alpha, alpha-beta, and aged beta alloys that are highly stressed in tension for sustained periods. SLC susceptibility increases with increasing internal hydrogen content, increasing alloy aluminum or oxygen equivalency, decreasing strain rate, and increasing triaxial tensile stress state and stress intensity.[24,37] Highest susceptibility generally occurs at or somewhat below room temperature[24] and diminishes at higher temperatures.

SLC test severity increases (to the right) according to the following types of test specimens: smooth tensile $<<$ notched tensile $<<$ loaded precracked specimen. For determination of fracture toughness thresholds (K_{SLC}), ASTM F1624 may be useful, whether a specimen is loaded in increasing steps or using a continuous rising load at a slow rising-K rate (e.g., 0.3 to 1.0×10^{-3} MPa $m^{0.5}$ s^{-1}). Typical K_{ISLC} data dependence with test time (i.e., time-to-failure) is depicted in figure 7 with respect to K_{IC} (air) and K_{ISCC} (salt water). Approximate test time scale typically ranges anywhere from several hours to a day.[24,37] Because alloy microstructure and, especially, product crystallographic texture strongly influence SLC susceptibility, it is important to consider the sample orientation of interest for testing. Examination of post-test specimen fracture surfaces should reveal low-energy facets of quasi-cleavage under high-magnification scanning electron microscopy examination if SLC has occurred.

Hydrogen analysis of coupons is performed according to ASTM E1447, *Standard Test Method for Determination of Hydrogen in Titanium and Titanium Alloys by Inert Gas Fusion Thermal Conductivity/Infrared Detection Method*, whereby a small (0.12 g) metal sample extracted from a titanium test coupon is

FIG. 7 Generalized test time dependence of K_{ISLC} values measures for high-strength titanium alloys compared with their K_{IC} and K_{ISCC} values.



fused within a chamber to reversibly release the absorbed hydrogen, which is subsequently measured. LECO hydrogen analyzers offer measurement resolution on the order of ±5 wppm at sample hydrogen levels below 200 wppm. It is critical to note that the analyzed hydrogen content may be directly dependent on the test sample thickness tested if a nonhomogeneous distribution (i.e., hydrogen gradient or surface film) of absorbed hydrogen exists within the sample. If the hydrogen is uniformly distributed or diffused through the sample cross section (which is often not the case), no sample thickness dependence exists, and the hydrogen content may be directly used to predict or correlate with metal behavior and properties.

Because hydrogen chemical analysis only provides the total hydrogen content in a specific localized specimen location, test specimens are often metallurgically cross-sectioned and examined for the titanium-hydride phase to determine the hydrogen distribution. This technique, which is useful only in alpha and near-alpha titanium alloys, where hydrides may precipitate because of limited alpha phase solubility. This procedure involves wet-abrasive wheel- or saw-cutting through the sample cross section, wet-grinding down below any worked or heat-affected metal, and hand-polishing down through abrasive papers and slurry or cloth wheels down to 0.05 µm alumina. Sample edge retention is vital in this hand-polishing technique. Final, very light etching with an HF/HNO_3-type etch (i.e., Kroll), or even a 1 wt% HF acid etch, should reveal the acicular hydride precipitates (fig. 1), if present, which tend to etch out first. Intermediate electropolishing followed by etching also may be employed if sample edge (surface) retention is not critical or of interest. Basic guidelines and procedures for preparation of titanium alloy samples for metallographic examination can be found in *Metallography and Microstructure*.[38] Microscopic examination of hydride phase precipitates is typically conducted at magnifications of 200 to 1,000×, depending on hydride phase size and quantity.

IGNITION TESTING

Titanium alloys can be susceptible to ignition or burning, or both, in few specific gas environments, such as pure gaseous or

liquid oxygen, oxygen-enriched gas mixtures, and dry chlorine gas.[1] These highly exothermic reactions generally increase with increasing gas pressure, concentration, flow rate, and temperature. Normally, the nonreactive, protective surface oxide film on titanium must be removed, damaged, or penetrated for ignition and reaction to occur. In the case of oxygen gas, burning is sustained only if the local metal surface temperature remains at or above the alloy's melting point, above which formation of the protective oxide film is not possible. Any factor that removes local heat generated, such as increased metal thermal conductivity or section thickness (i.e., increased thermal mass), will inhibit or diminish ignition and burning tendencies.

Although no standard metal ignition tests exist, testing traditionally has been aimed at identifying ignition and sustained burning thresholds of a metal as a function of gas pressure, concentration, and temperature. Ignition and burning tests may be categorized as either static or dynamic, depending on whether the reaction gas is nonflowing (static) or continuously flowing past the test sample through a test chamber. Because increased gas flow rate exacerbates metal ignition and burning, the dynamic tests tend to produce more conservative thresholds.

Ignition tests must incorporate a means of breaking or removing the surface oxide film and exposing fresh metal surface on the sample. This can be achieved by a variety of methods,[39] including tensile straining to fracture, puncture, impact, severe surface abrasion or scratching, severe plastic straining, explosive shock, or high-energy beams (i.e., laser)[40] or electric sparks focused on the metal test sample. Although less relevant to high-impact ignition sensitivity in titanium alloys found in LOX,[39] tensile rupture of test samples within pressurized test vessels has been employed most commonly for testing in oxygen-rich gas mixtures[41–43] and dry chlorine gas.[44] A typical ignition test setup using tensile rupture is depicted in figure 8.

Continuous measurement of gas pressure and test sample temperature can provide an indirect means of assessing ignition occurrence. Go/no-go assessment of ignition is usually based on post-test visual examination of sample fracture surfaces for melting or oxide scaling, or both. More sophisticated burn testers may incorporate continuous video monitoring and pyrometers, or other heat sensors to track the ignition or burn event.

Burning or sustained combustion testing of titanium alloys typically involves intentional localized heating of a test sample at one end or location to a temperature above its melting point. This localized focused sample heating can be achieved by laser, electron beam, electric arc, electrical resistance, or plasma arc methods. Once sample ignition is induced, the ignition heating source is removed, and duration and extent of sustained sample burn is measured. A typical burn test has used a 4-in. (102-mm) long, 0.125-in. (3.18-mm) diameter test sample (rod) that is ignited on one end by electric arc.[43] The rod length remaining after the test is measured and used to rate alloy burn susceptibility. Design details and setup of static and flow (dynamic) burn testers are presented in figure 9 and figure 10, and are discussed in more detail in Mcllroy and Zawierucha.[45] Test sample size,

FIG. 8 Typical ignition test setup for titanium samples using tensile rupture.

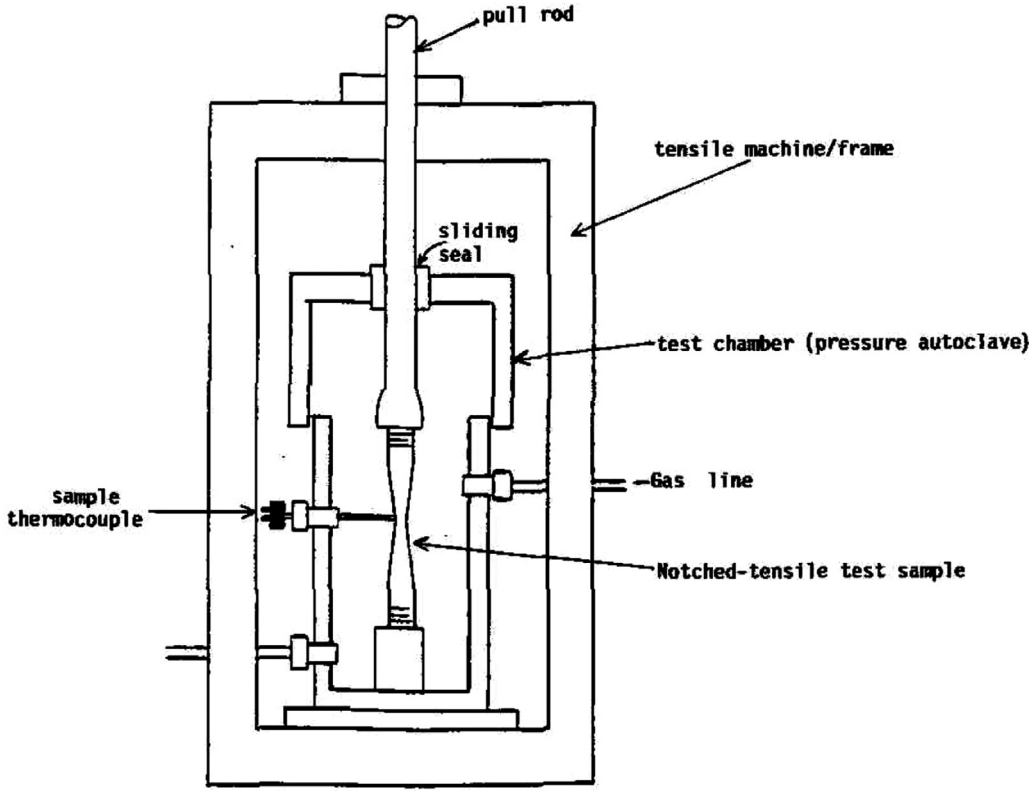
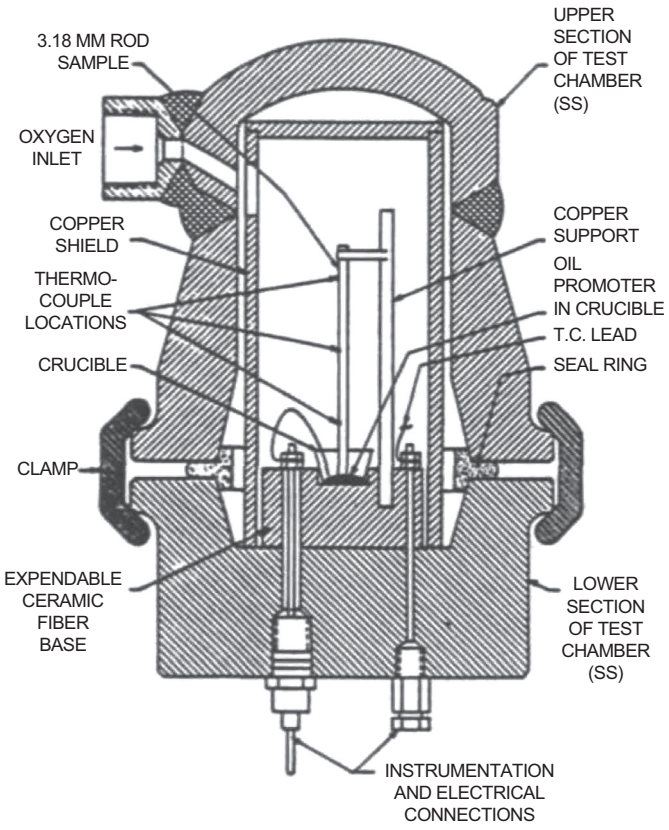


FIG. 9 Static burn testing using promoted metal sample ignition.[43]



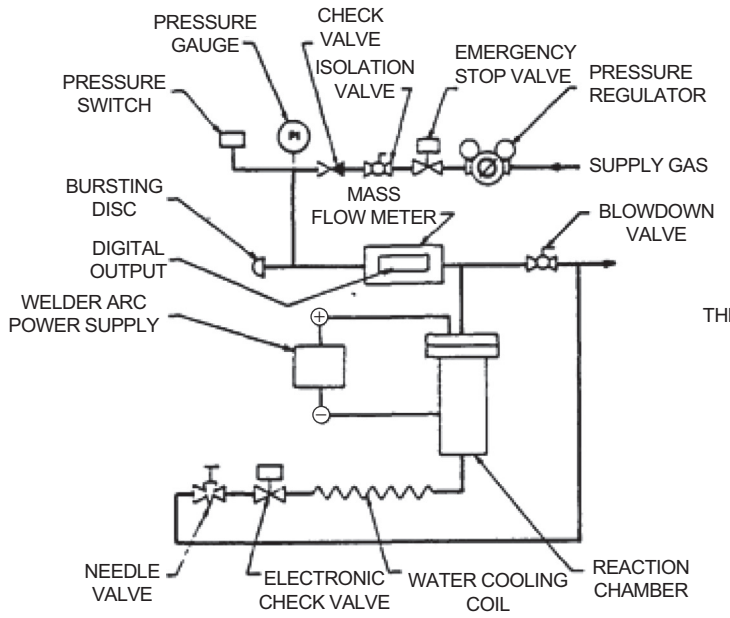
geometry, and section thickness directly influence burn susceptibility and must be standardized for comparative tests and specified in all cases.

OXIDATION TESTS

Although titanium alloys are highly resistant to oxidation up to moderate temperatures, colored protective surface oxide films form in the air at 370–595 °C. Depending on exposure time at temperature and alloy composition, oxide film or scale growth may become excessive and unacceptable for engineering purposes above ~620 °C. In terms of titanium alloy content, increasing vanadium, manganese, and zirconium concentrations are generally detrimental, whereas increasing molybdenum, niobium, silicon, and chromium concentrations tend to retard oxidation. Elevated aluminum content, as in the titanium aluminide intermetallics, markedly enhances oxidation resistance, elevating titanium alloy use windows by several hundred degrees Fahrenheit.

In addition to surface oxide film growth or scale formation when thermomechanically processed or heat-treated in air at elevated temperatures, titanium alloy products can experience oxygen enrichment of metal surfaces beneath the titanium-oxide scale. These hard, brittle metal surface layers, known as the alpha case, represent a diffused-in gradient of interstitial oxygen (and possibly nitrogen or carbon in other exposures) into the metal surface. This diffusion-based time- and temperature-dependent phenomenon becomes significant above ~540–590 °C, depending on alloy type. It severely reduces metal formability, ductility, and, particularly, fatigue life, in particular as metal section thickness is reduced. Typical examples of alpha case formed on an

FIG. 10 Typical dynamic, flowing gas metal burn tester showing (*A*) overall equipment setup and (*B*) details of reaction chamber internals for ignition and burning of metal test specimens.[45]



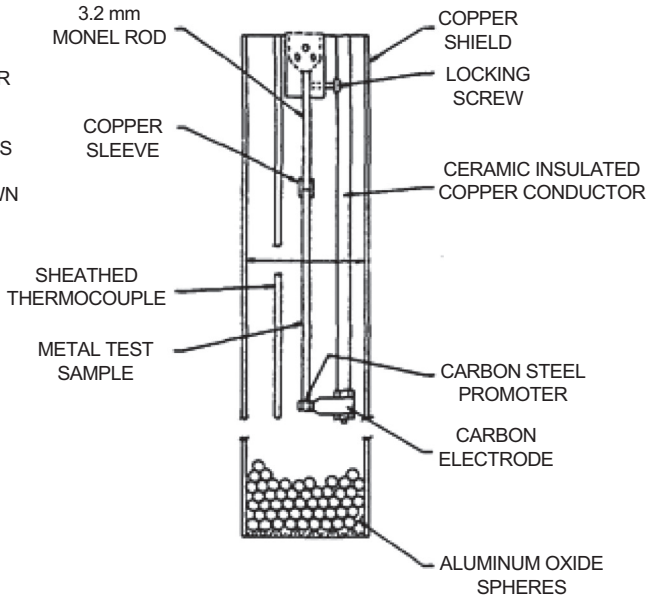
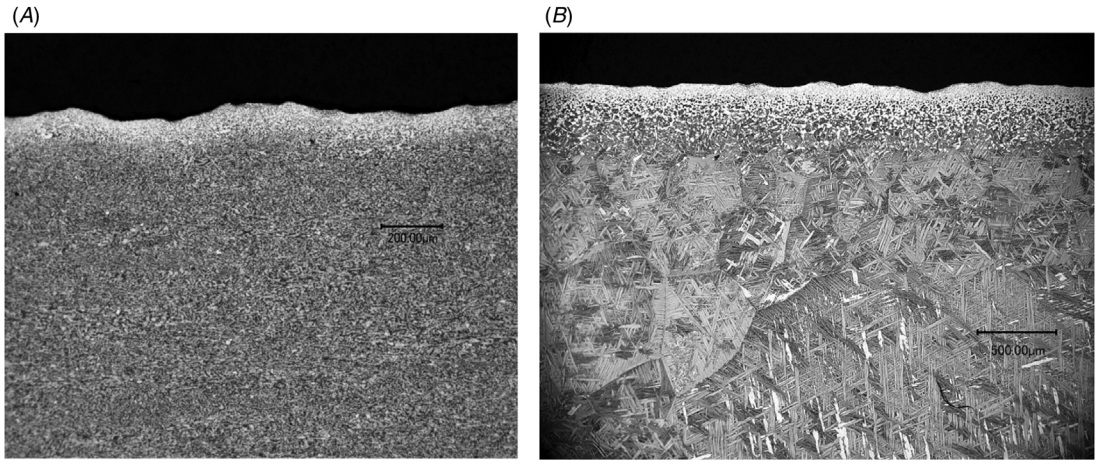


FIG. 11 Cross-sectional photomicrographs showing thin surface layers of alpha case (diffused-in oxygen) on a Ti-6Al-4V wrought product heat-treated in air (*A*) below (200×) and (*B*) above its beta-transus temperature (100×).



alpha-beta titanium alloy surface after heating in air for 1 h just below and above its beta-transus temperature are shown in the magnified cross section in figure 11.

Simple static oxidation testing of titanium alloys can be conducted per ASTM G54, *Standard Practice for Simple Static Oxidation Testing* (withdrawn 2002), with a few distinct considerations relative to post-test evaluation. Descaling of titanium samples after test exposure may employ mechanical scale removal or hot alkaline solution descaling. A light fine sand grit or a glass-bead blast for several seconds are both good mechanical descale methods if a procedure is prequalified to ensure insignificant substrate metal weight loss. Several high-temperature alkaline descale solutions based on concentrated KOH solutions are available commercially for titanium alloys. Again, prequalification of the chemical descale procedure (i.e., exposure time and temperature) is recommended to avoid substrate metal corrosion. Conventional strong reducing acids will not dissolve heavy-oxide films or scales on titanium and will attack the metal substrate and, therefore, should be avoided.

Metallographic examination offers valuable information once the sample is sectioned, mounted, hand-polished, and Kroll etched per recommended procedures outlined in *Metallography and Microstructure*.[38] The remaining metal sample thickness and the alpha-case layer thickness along the sample surface can be determined from the cross-sectioned mount. As revealed in figure 11, alpha-case layers manifest as lighter in appearance when lightly Kroll etched. An oxalic acid etch (2-mL HF stock acid + 98-mL saturated oxalic acid solution) is more sensitive and recommended to discern situations in which only marginal or minimal titanium surface oxygen enrichment (very light diffused-in oxygen zone with no obvious alpha-case layer) exists, but did not appear as an obvious alpha-case layer with the Kroll etch. Note that this alpha-stabilized (alpha-case) layer generally is not visually discernable in alpha-titanium alloys because of the lack of phase contrast after etch, but it should be readily apparent when thicker than several microns in alpha-beta and beta titanium alloys (see fig. 11). Subscale or internal oxidation attack typically is not observed with titanium alloys. Mechanical testing of samples after thermal exposure (i.e., tensile, bends, S-N fatigue testing) may be of interest to assess extent of oxidation wastage and surface diffused-in interstitial embrittlement. Knoop or Vickers microhardness profiles of mounted and polished sample cross sections may be useful in identifying heavy alpha-case layer depth, because these oxygen-rich layers are substantially harder than the metal matrix.

References

1. R. W. Schutz, "Corrosion of Titanium and Titanium Alloys," in *ASM Metals Handbook*, vol. 13B, *Corrosion: Materials* (Metals Park, OH: ASM International, 2005), 252–299.

2. R. W. Schutz, "Titanium," in *Process Industries Corrosion: The Theory and Practice* (Houston, TX: NACE International, 1986), 503–527.

3. M. J. Donachie, Jr., ed., *Titanium: A Technical Guide* (Metals Park, OH: ASM International, 1988).

4. "Titanium and Its Alloys," Course 27, Lesson 3 (Metals Engineering Institute, ASM International, Metals Park, OH, 1968).

5. *Aerospace Structural Metals Handbook* (Washington, DC: Mechanical Properties Data Center, U.S. Department of Defense, 1985).

6. F. Schwartzberg, F. Holden, H. Ogden, and R. Jaffee, "The Properties of Titanium Alloys at Elevated Temperatures" (TML Report 82, Titanium Metallurgical Laboratory, Battelle Memorial Institute, Columbus, OH, September 1957).

7. M. Mote, R. Hooper, and P. Frost, "The Engineering Properties of Commercial Titanium Alloys" (TML Report 92, Titanium Metallurgical Laboratory, Battelle Memorial Institute, Columbus, OH, June 1958).

8. R. A. Wood and R. J. Favor, eds., *Titanium Alloys Handbook*, MCIC-HB-02 (Columbus, OH: Metals and Ceramics Information

Center, Department of Defense Information Analysis Center, December 1972).

9. N. D. Tomashov and P. M. Altovskii, "Corrosion and Protection of Titanium" (Government Scientific-Technical Publication of Machine-Building Literature [Russian translation], 1963).

10. V. V. Andreeva, "Behavior and Nature of Thin Oxide Films on Some Metals in Gaseous Media and in Electrolyte Solutions," *Corrosion* 20, no. 2 (1964): 35t–46t.

11. M. Pourbaix, *Atlas of Electrochemical Equilibria in Aqueous Solutions* (Houston, TX: NACE International, 1974).

12. J. C. Griess, Jr., "Crevice Corrosion of Titanium in Aqueous Salt Solutions," *Corrosion* 24, no. 4 (1968): 96–109.

13. R. W. Schutz, "Understanding and Preventing Crevice Corrosion of Titanium Alloys: Part I," *Materials Performance* (October 1992): 57–62.

14. R. W. Schutz, "Understanding and Preventing Crevice Corrosion of Titanium Alloys: Part II," *Materials Performance* (November 1992): 54–56.

15. R. W. Schutz, J. S. Grauman, and J. S. Hall, "Effect of Solid Solution Iron on the Corrosion Behavior of Titanium," in *Titanium, Science and Technology, Proceedings of the 5th International Conference on Titanium* (Deutsche Gesellschaft fur Metallkunde E.V., 1985), 2617–2624.

16. L. C. Covington and R. W. Schutz, "Effects of Iron on the Corrosion Resistance of Titanium," in *Industrial Applications of Titanium and Zirconium, ASTM STP728* (West Conshohocken, PA: ASTM International, 1981), 163–180.

17. R. W. Schutz, "Stress Corrosion Cracking of Titanium Alloys," in *Stress-Corrosion Cracking, Materials Performance and Evaluation* (Metals Park, OH: ASM International, July 1992), 265–297.

18. R. J. H. Wanhill, "Aqueous Stress Corrosion in Titanium Alloys," *British Corrosion Journal* 10, no. 2 (1975): 69–78.

19. B. F. Brown, *Stress Corrosion Cracking in High Strength Steels and in Titanium and Aluminum Alloys* (Washington, DC: Naval Research Laboratory, 1972).

20. M. J. Blackburn, J. A. Feeney, and T. R. Beck, "State-of-the-Art of Stress-Corrosion Cracking of Titanium Alloys" (Part 4 of Monograph Review, Boeing Company, sponsored by the Advanced Research Projects Agency, ARPA Order No. 878 and NAS7-489, June 1970).

21. R. W. Schutz and J. S. Grauman, "Compositional Effects on Titanium Alloy Repassivation Potential in Chloride Media," in *Advances in Localized Corrosion, Proceedings of the 2nd International Conference on Localized Corrosion* (Houston, TX: NACE International, 1990), 335–337.

22. N. E. Paton and J. C. Williams, "Effect of Hydrogen on Titanium and Its Alloys," in *Titanium and Titanium Alloys: Source Book* (Metals Park, OH: ASM International, 1982), 185–207.

23. G. A. Lenning, J. W. Spretnak, and R. I. Jaffe, "Effect of Hydrogen on Alpha Titanium Alloys," *Transactions of the Metallurgical Society of AIME* 206 (October 1956): 1235–1240.

24. R. R. Boyer and W. F. Spurr, "Characteristics of Sustained-Load Cracking and Hydrogen Effects in Ti-6A1-4V," *Metallurgical Transactions* 9A (January 1978): 23–29.

25. D. A. Meyn, "Effect of Hydrogen on Fracture and Inert-Environment Sustained Load Cracking Resistance of α-β Titanium Alloys," *Metallurgical Transactions* 5 (November 1974): 2405–2414.

26. C. M. Craighead, G. A. Lenning, and R. I. Jaffe, "Hydrogen Embrittlement of Beta-Stabilized Titanium Alloys," *Transactions of the Metallurgical Society of AIME* (August 1956): 923–928.

27. R. W. Schutz and L. C. Covington, "Guidelines for Corrosion Testing of Titanium," in *Industrial Applications of Titanium and Zirconium, ASTM STP728* (West Conshohocken, PA: ASTM International, 1981), 59–70.

28. *ASM Metals Handbook*, 9th ed., vol. 13, *Corrosion* (Metals Park, OH: ASM International, 1987).

29. S. W. Dean, Jr., "Electrochemical Methods of Corrosion Testing," in *Electrochemical Techniques for Corrosion* (Houston, TX: NACE International, 1977), 52–60.

30. E. L. Liening, "Electrochemical Corrosion Testing Techniques," in *Process Industries Corrosion* (Houston, TX: NACE International, 1986), 85–122.

31. M. G. Fontana and N. D. Greene, *Corrosion Engineering* (New York: McGraw-Hill, 1967).

32. D. D. Bergman and J. S. Grauman, "The Detection of Crevice Corrosion in Titanium and Its Alloys Through the Use of Potential Monitoring," in *Titanium '92, Science and Technology* (Warrendale, PA: Minerals, Metals and Materials Society, 1993), 2193–2200.

33. M. Kobayashi, Y. Araya, S. Fujiyama, et al., "Study on Crevice Corrosion of Titanium," in *Titanium '80, Science and Technology*, vol. 4 (New York: American Institute of Mining, Metallurgical, and Petroleum Engineers, 1980), 2613–2622.

34. R. B. Diegle, "Electrochemical Cell for Monitoring Crevice Corrosion in Chemical Plants" (paper presentation, CORROSION/81, paper 154, NACE International, Toronto, Canada, April 1980).

35. L. Szklarska-Smialowska and M. Janik-Czachor, "The Analysis of Electrochemical Methods for the Determination of Characteristic Potentials of Pitting Corrosion," *Corrosion Science* 11 (1971): 901–914.

36. D. O. Sprowls, "Evaluation of Stress-Corrosion Cracking," *Metals Handbook*, 9th ed., vol. 13, *Corrosion* (Metals Park, OH: ASM International, 1987), 245–282.

37. G. R. Yoder, C. A. Griffis, and T. W. Crooker, "Sustained-Load Cracking of Titanium Alloys" (NRL Report 7596, Naval Research Laboratory, Washington, DC, August 1973).

38. *ASM Metals Handbook*, 9th ed., vol. 9, *Metallography and Microstructure* (Metals Park, OH: ASM International, 1985), 458–475.

39. "Reactivity of Metals with Liquid and Gaseous Oxygen" (DMIC Memorandum 163, Defense Metals Information Center, Battelle Memorial Institute, Columbus, OH, January 15, 1963).

40. V. G. Anderson and B .A. Manty, "Titanium Alloy Ignition and Combustion" (Report No. NADC 76083-30, United Technologies Corporation, Pratt & Whitney Aircraft Group, West Palm Beach, FL, January 15, 1978).

41. F. E. Littman, F. M. Church, and E. M. Kinderman, "A Study of Metal Ignitions, I. The Spontaneous Ignition of Titanium," *Journal of the Less-Common Metals* 3 (1961): 367–378.

42. F. E. Littman and F. M. Church, "Reaction of Titanium with Water and Aqueous Solutions" (Final Report, SRI Project No. SD-2116, Stanford Research Institute, Menlo Park, CA, June 1958).

43. P. Krag and R. Henson, "An Ignition Resistant Titanium Alloy for Acid Pressure Oxidation Applications," in *Proceedings of the RANDOL Gold Forum* (Golden, CO: Randol International, 1992), 201–204.

44. E. E. Millaway and M. H. Klineman, "Factors Affecting Water Content Needed to Passivate Titanium in Chlorine," *Corrosion* 23, no. 4 (1972): 88–97.

45. K. McIlroy and R. Zawierucha, "The Effects of Testing Methodology on the Promoted Ignition-Combustion Behavior of Carbon Steel and 316L Stainless Steel in Oxygen Gas Mixture," *Flammability and Sensitivity of Materials in Oxygen-Enriched Atmospheres*, vol. 4, *ASTM STP1040* (West Conshohocken, PA: ASTM International, 1989), 38–53.

Chapter 18 | Corrosion Testing of Nonmetallic Coatings

William L. Mankins[1]

Introduction

A large number of tests exist for establishing the reliability of nonmetallic protective coatings on metal substrates. Definitions, fundamentals, methodology, and practical examples are offered for a better understanding of tests for protective coatings and to demonstrate that well-defined tests alone are not adequate without rational application and interpretation.

FOCUS OF TESTING

Materials tests and standards of nonmetallic organic and inorganic coatings systems on metallic substrates are described. Coating systems may provide many properties in addition to corrosion resistance (e.g., appearance and insulation). Although test methods exist for a wide variety of coatings characteristics, the primary nonmetallic coatings tests addressed herein evaluate corrosion resistance, adhesion, and physical or chemical durability.

NONMETALLIC COATINGS MATERIALS

Two broad groups of nonmetallic coatings materials are considered:

1. *Organic*, including formulations containing dispersed inorganic or metallic materials: Examples include clear coatings, typical paints, metal flake coatings, and organic-based galvanic (zinc-rich) coatings.
2. *Inorganic*, which may be modified by organic and metallic materials. Examples include phosphates, anodic coatings, oxides, carbides, nitrides, borides, silicides, and inorganic-based galvanic (zinc-rich) coatings. Most of these inorganic coatings are applied to the metallic substrates by a combination of thermal or chemical processes. Some, such as anodic coatings, are formed by reactions on the surface.

Additional types of coatings exist, which are hybrids of these groups, and may be appropriately classified as metallic coatings or composite materials.

COATINGS AND COATINGS SYSTEMS

The term "coatings" implies that there is a supporting structure or substrate—an obvious point sometimes overlooked. The failure of otherwise-acceptable coatings may be due to the substrate. The machined, molded, or polished substrate may contain defects or trapped impurities that affect performance of the coatings system. A coatings test may assess the substrate properties. Likewise, the cleaning, surface preparation, and pretreatment methods influence the coatings system performance. Use of the term *coatings system* is intended to emphasize these interdependent properties. Most tests evaluate whole coatings systems, with an emphasis on a particular component or processing step. (Conversely, the term *film* is appropriate when a coatings material can be evaluated independent of the substrate.)

Fundamentals

TESTS/STANDARDS, APPLICATION/SELECTION, AND SPECIFICATIONS

Corrosion inspection programs include those sponsored by the National Association of Corrosion Engineers (NACE International) and the Society for Protective Coatings (SSPC); both societies have training and certification programs aimed at improving quality control. They introduce inspectors, users, blasters, manufacturers, owner's representatives, specifiers, and technical salesmen to the basics of corrosion control, paint inspection, and project management in a way that has resulted in savings of billions of dollars in costly mistakes.

Tests and standards are intended to provide a means for determining the appropriateness of materials for the users' purposes, for example, when a user requires excellent performance at low cost. The requirement must be translated to a set of tests and standards, collectively known as specifications, agreeable to the supplier and user, often on a contractual basis. Achieving an agreement accrues benefits to both supplier and user; an efficient

[1]Metallurgical Services, Inc., 594 Fairwood Rd., Huntington, WV 25705, USA
The author acknowledges the previous author of this chapter, Richard D. Granata, Florida Atlantic University, Boca Raton, FL.

DOI: 10.1520/MNL202NDSUP20190035

Copyright © 2022 by ASTM International, 100 Barr Harbor Dr., PO Box C700, West Conshohocken, PA 19428-2959
ASTM International is not responsible, as a body, for the statements and opinions expressed in this chapter. ASTM International does not endorse any products represented in this chapter.

and effective agreement yields a competitive result. The major specification or objective in the context of corrosion testing is service life. Tests and standards must be selected and applied to satisfy user specifications (service and lifetime requirements). A difficulty is the often-unsatisfactory relationship between long-term field service results to laboratory tests and standards results. Application and interpretation of tests for nonmetallic corrosion protective coatings is a dynamic, evolving process of satisfying specifications, including both short-term tests and long-term service performance. It is important to understand the limitations of tests and standards results.

ELECTROCHEMICAL MECHANISM OF CORROSION

A typical corrosion process, the reaction of iron with hydrochloric acid (HCl) under anaerobic conditions, is represented by the following equation:

$$Fe^{\circ} + 2HCl = FeCl_2 + H_2(g), \quad (1)$$

which indicates that the acid reactant and the ferrous chloride ($FeCl_2$) corrosion product exist largely in the ionic state in aqueous solution. The probability of this reaction occurring by the mechanism implied in the equation is very low because too many species must meet simultaneously. Conceivably, this reaction occurs in two independent steps:

$$\begin{aligned} &\text{Anodic Reaction: } Fe^{\circ} - 2e^{-} = Fe^{++}(aq) \\ &\text{Cathodic Reaction: } 2H^{+}(aq) + 2e^{-} = H_2(g). \end{aligned} \quad (2)$$

In these two reactions, electron loss occurs at one site and electron gain occurs at another with the electrons linking the reactive sites through the conductive metal phase (Fe°) and the ions linking the reactive sites through the aqueous (aq) phase.

The overall reaction takes place at a rate determined by the more difficult of these two steps. This simple concept—that is, independent anodic and cathodic half-reactions—is the basis of the electrochemical mechanism of corrosion. The mechanism has profound effects on the corrosion protective properties of nonmetallic coatings materials. Some tests exploit the electrochemical mechanism to determine specific corrosion susceptibilities of coatings systems, such as cathodic disbondment and pinhole detection. Coatings that are permeable to oxygen may be vulnerable to damage because of the following alternative cathodic reaction:

$$O_2 + 2H_2O + 4e^{-} = 4OH^{-}. \quad (3)$$

This reaction is capable of causing high local pH and chemical degradation of the polymer or adhesive bonds. Thermodynamically, this cathodic (reduction) reaction takes precedence over the hydrogen ion reduction reaction whenever oxygen is present at the cathodic reaction site.

A more accurate representation of the combined corrosion reaction for an oxygen-deprived cathode follows:

$$Fe^{\circ} + 2H^{+}(aq) + 2Cl^{-}(aq) = Fe^{++}(aq) + 2Cl^{-}(aq) + H_2(g). \quad (4)$$

CORROSIVE ENVIRONMENTAL EXPOSURE

Corrosion occurs when all components of the process are present (anode, cathode, electrolyte, and intimate contact of the components) and capable of reaction (see preceding section). Basic test conditions include exposure of the coatings systems to an electrolyte containing reducible species (typically oxygen or hydrogen ion). More sophisticated testing would include closely replicating known corrosive conditions, such as wet–dry cycles and multicomponent and multiphase chemical environments. Immersion, salt spray, and a partial pressure of sulfur dioxide corrosion tests correspond to water tank, marine, and combustion exhaust service environments, respectively. An important relationship exists between the corrosive environment used in the test procedures and the product's intended service use.

CORROSION EFFECTS

Distinction should be made between degradation because of corrosion and other processes. Corrosion can cause loss of coatings adhesion, such as occurs with cathodic disbondment, blistering, or undercutting. Although adequate adhesion is necessary, greater adherence does not correspond to greater corrosion resistance. Exposing a coatings system to water can reduce the adhesion (wet adhesion), which is regained upon drying. Unless permanent damage occurs during the low-adhesion period, no corrosion degradation results. The same may be true for other properties such as flexibility. Initial properties and property changes due to a corrosion environment may relate to corrosion protective properties. Clearly defining the relationship between measured properties and the intended use of the protective coatings is important.

NONCORROSIVE EFFECTS

Many tests for coatings systems provide useful information related to service requirements involving salts, fogs, immersion, scribes, radiation, heat, chemical, cold, and pressure transients. Whether such tests are applicable to the service intended for the coatings must be established, and the test results must be interpreted in the context of corrosion protection performance. Ultraviolet (UV) resistance is not a useful property for the interior of water storage tanks. Long-term 100% relative humidity and water immersion resistances are not necessarily appropriate for outdoor desert or climate-controlled indoor environments. Selecting tests without regard for the coatings' use may be detrimental to the development or qualification of a satisfactory coatings system.

Tests and Standards: Selection, Application, and Interpretation

AVAILABLE TESTS AND STANDARDS

New and existing tests and standards are under continuous development and revision. ASTM is a leader of tests and standards; other contributors, with various emphasis on specifications, are the federal government with Federal Test Method Standard 141C (supersedes 141A and 141B), state government agencies,

NACE International, Society of Automotive Engineers (SAE), Steel Structures Painting Council (SSPC), National Coil Coaters Association (NCCA), International Standards Organization (ISO), and foreign systems (DIN), as well as commercial (e.g., automotive, architectural, electronics), proprietary, and military organizations. A comprehensive listing of these tests and standards is not the intent of this document.

Gaynes[1] and Munger[2] give descriptions and the framework for effective use of tests and standards. Gaynes[1] provides detailed descriptions including photographs, cross-listing ASTM to federal tests and a broader perspective encompassing the federal standard, miscellaneous tests, and some caveats of traditional testing. Munger[2] offers practical material directed toward large structures and provides a listing based on ASTM standards. Altmayer[3] compiled a table of 13 applicable corrosion tests for 30 metallic, inorganic, and organic coating/substrate combinations. The most commonly used tests are salt spray (ASTM B117-19, *Standard Practice for Operating Salt Spray (Fog) Apparatus*), acetic acid salt spray (ASTM G85-19, *Standard Practice for Modified Salt Spray (Fog) Apparatus*, Annex Al [formerly ASTM B287]), and the 100% humidity test (ASTM D2247-15(2020), *Standard Practice for Testing Water Resistance of Coatings in 100% Relative Humidity*). A condensed listing with brief descriptions of tests selected from Altmayer,[3] Mazia,[4] ASM International,[5,6] and others is given in table 1. Additional tests are listed in table 2, which is an edited and revised listing by Munger.[2] Hess[7] provides an important auxiliary reference to aid in identifying the causes of paint film defects.

TABLE 1 Brief Descriptions of Selected Protective Coating Tests for Metal Substrates

Test	Description and Remarks
Salt Spray (ASTM B117-19)	Most widely specified test. Atomized 5% sodium chloride, neutral pH, 35°C*, follow details of ASTM B117-19, Appendix XI. Emphasizes wet surfaces (nondrying), high oxygen availability, neutral pH, and warm conditions. Control or comparative specimens should be run simultaneously. Corrosivity consistency should be checked as described in ASTM B117-19, Appendix X3. Notes: May be the most widely misused test. Requires correlation to service tests for useful results. Do not assume correlation exists. *Note that dissolved CO_2 concentration at 0°C is three times that of concentration at 35°C and can affect corrosion.
100% Relative Humidity (ASTM D2247-15(2020)	Widely used test. Condensing humidity, 100% relative humidity (RH), 38°C. Emphasizes sensitivity to water exposure.
Acetic Acid-Salt Spray (ASTM G85-19, Annex A1 [formerly ASTM B287])	Widely used test. Atomized 5% sodium chloride, pH 3.2 using acetic acid, 35°C. More severe than ASTM B117-19. The lower pH and the presence of acetate affect the solubility of corrosion products on and under the protective coatings.
Sulfur Dioxide-Salt Spray (ASTM G85-19, Annex A4)	Atomized 5% sodium chloride, collected solution pH = 2.5–3.2, 35°C, SO_2 metered (60 min x 35 cm^3/min per m^3 cabinet volume), four times per day.
Copper Accelerated Salt Spray (ASTM B368-09(2014))	Atomized 5% sodium chloride, pH 3.2 with acetic acid, 0.025% cupric chloride-dihydrate, 35°C. Galvanic coupling because of copper salt reduction to copper metal. More severe than ASTM B117-19.
FACT (formerly ASTM B538)	Testing anodized aluminum specimens. Electrolyte as in salt-spray or CASS test. Specimen is made the cathode to generate high pH at defects.
Accelerated Weathering	Exposure of coated specimens to effects of ultraviolet (UV) radiation experienced in outdoor sunlight condition which may be combined with other exposures such as moisture and erosion. Exposure cabinets use carbon arc (ASTM D822/D822M-13(2018)), xenon lamp (ASTM G26-70 [historical version]), or fluorescent lamp (ASTM G53-96).
Lactic Acid	On substrates of brass and copper alloys, determines coatings porosity and resistance to handling (perspiration). Consists of immersion in 85% lactic acid solution, drying and incubating above acetic acid vapors for 20 h to reveal discoloration spots at failure points or delaminations.
Acidified Synthetic Seawater Testing (SWAAT) (ASTM G85-19, Annex A3-01(2019) [formerly ASTM G43])	Atomized synthetic seawater (ASTM D1141-98(2013)) with 10 mL glacial acetic acid per L of solution, pH 2.8 to 3.0, 35°C. More severe than ASTM D117-19. The lower pH and the presence of acetate affect the solubility of corrosion products on and under the protective coatings.
Electrographic and Chemical Porosity Tests	Pores and active defects in nonmetallic coatings can be revealed by color indication or deposit formation. On nickel substrates, dimethylglyoxime, or steel, potassium ferricyanide (ferroxyl test) indicator can be applied to surface on filter paper while substrate is made the anode. Alternatively, a substrate immersed in acidic copper sulfate can be made the cathode to form copper nodules at conductive coatings defects.
Adhesion (ASTM D3359-17)	Knife and fingernail test consists of cutting through the coating with knife or awl and dislodging coating with thumbnail or fingernail (pass/fail). This test consists of "X" scribes or parallel cross-hatches followed by adhesive tape stripping of loosened coating.

(continued)

TABLE 1 (*continued*)

Test	Description and Remarks
T-Bend Adhesion (ASTM D4145-10(2018))	Combined flexibility and adhesion test consists of clamping end of coated flat metal panel in vise or similar tool, bending (convex) through 90°, reclamping to bend through 180° to give "0T" bend (where *"T"* is panel thickness and # (zero, 1, 2, ...) is the number of panel thicknesses). Rebending over the 180° bend gives an "IT" bend. Adhesive tape is pressed down along edge of bend and any loose coating stripped off. Cyclic testing consisting of short salt exposure, short drying period followed by longer period of high humidity. Undercutting from the scribe is also measured.
Exterior Exposure (ASTM D1014-18)	Method for conducting exterior exposure tests of paints on steel. Well-defined exposure setup, not necessarily equivalent to service tests.
Service Test/Data	Performance data of coatings systems under use conditions. Slowest evaluation method: provides tangible results.

TABLE 2 Coatings Tests and Methods Pertinent to Corrosion Protection

Standard	Title of Standard
NACE TM0174-2002	*Laboratory Methods for the Evaluation of Protective Coatings and Lining Materials on Metallic Substrates in Immersion Service*
ASTM B117-19	*Standard Practice for Operating Salt Spray (Fog) Apparatus*
ASTM B368-09(2014)	*Standard Test Method for Copper Accelerated Acetic Acid-Salt Spray (Fog) Testing (CASS Test)*
ASTM B457-67(2018)	*Standard Test Method for Measurement of Impedance of Anodic Coatings on Aluminum*
ASTM C536-83(2018)	*Standard Test Method for Continuity of Coatings in Glassed Steel Equipment by Electrical Testing*
ASTM C743-87(2018)	*Standard Test Method for Continuity of Porcelain Enamel Coatings*
ASTM D522/D522M-17	*Standard Test Methods for Mandrel Bend Test of Attached Organic Coatings*
ASTM D523-14(2018)	*Standard Test Method for Specular Gloss*
ASTM D610-08(2019)	*Standard Practice for Evaluating Degree of Rusting on Painted Steel Surfaces*
ASTM D662-93(2019)	*Standard Test Method for Evaluating Degree of Erosion of Exterior Paints*
ASTM D714-02(2017)	*Standard Test Method for Evaluating Degree of Blistering of Paints*
ASTM D822/D822M-13(2018)	*Standard Practice for Filtered Open-Flame Carbon-Arc Exposures of Paint and Related Coatings*
ASTM D823-18	*Standard Practices for Producing Films of Uniform Thickness of Paint, Varnish, Lacquer, and Related Products on Test Panels*
ASTM D870-15(2020)	*Standard Practice for Testing Water Resistance of Coatings Using Water Immersion*
ASTM D968-17	*Standard Test Methods for Abrasion Resistance of Organic Coatings by Falling Abrasive*
ASTM D1014-18	*Standard Practice for Conducting Exterior Exposure Tests of Paints on Steel on Metal Substrates*
ASTM D1186-01 (withdrawn 2006, replaced by ASTM D7091-20)	*Standard Test Method for Nondestructive Measurement of Dry Film Thickness of Nonmagnetic Coatings Applied to a Ferrous Base (Withdrawn 2006)*
ASTM D1400-00 (withdrawn 2006, replaced by ASTM D7091-20)	*Standard Test Method for Nondestructive Measurement of Dry Film Thickness of Nonconductive Coatings Applied to a Non-Ferrous Metal Base (Withdrawn 2006)*
ASTM D1567-89(1995) (withdrawn, no replacement)	*Standard Test Method for Testing Detergent Cleaners for Evaluation of Corrosive Effects on Certain Porcelain Enamels*
ASTM D1653-13	*Standard Test Methods for Water Vapor Transmission of Organic Coating Films*
ASTM D1654-08(2016)e1	*Standard Test Method for Evaluation of Painted or Coated Specimens Subject to Corrosive Environments*
ASTM D1735-14	*Standard Practice for Testing Water Resistance of Organic Coatings Using Water Fog Apparatus*
ASTM D2197-16	*Standard Test Method for Adhesion of Coatings by Scrape Adhesion*
ASTM D2247-15(2020)	*Standard Practice for Testing Water Resistance of Coatings in 100% Relative Humidity*
ASTM D2248-01a(2018)	*Standard Practice for Detergent Resistance of Organic Finishes*
ASTM D3258-04(2019)	*Standard Test Method for Porosity of White or Near White Paint Films by Staining*
ASTM D3273-16	*Standard Test Method for Resistance to Growth of Mold on the Surface of Interior Coatings in an Environmental Chamber*
ASTM D3276-15e1	*Standard Guide for Painting Inspectors (Metal Substrates)*
ASTM D3359-17	*Standard Test Methods for Rating Adhesion by Tape Test*
ASTM D3361/D3361M-13(2018)	*Standard Practice for Operating Open-Flame Carbon-Arc Exposures of Paint and Related Coatings*
ASTM D3363-20	*Standard Test Method for Film Hardness by Pencil Test*
ASTM D4145-10(2018)	*Standard Test Method for Coating Flexibility of Prepainted Sheet*
ASTM D4585/D4585M-18	*Standard Practice for Testing Water Resistance of Coatings Using Controlled Condensation*

(*continued*)

TABLE 2 (*continued*)

Standard	Title of Standard
ASTM D4587-11(2019)e1	*Standard Practice for Fluorescent UV-Condensation Exposures of Paint and Related Coatings*
ASTM E376-19	*Standard Practice for Measuring Coating Thickness by Magnetic-Field or Eddy Current (Electromagnetic) Test Methods*
ASTM G8-96(2019)	*Standard Test Method for Cathodic Disbonding of Pipeline Coatings*
ASTM G12-07(2013) (withdrawn 2013, replaced by ASTM D7091-20)	*Standard Test Method for Nondestructive Measurement of Film Thickness of Pipeline Coatings on Steel (Withdrawn 2013)*
ASTM G42-11(2019)e1	*Standard Test Methods for Cathodic Disbonding of Pipeline Coatings Subjected to Elevated Temperatures*
ASTM G53-96 (withdrawn, replaced by ASTM G154-16)	*Standard Practice for Operating Light- and Water-Exposure Apparatus (Fluorescent UV-Condensation Type) for Exposure of Nonmetallic Materials (Withdrawn 2000)*
ASTM G60-01(2018)	*Standard Practice for Conducting Cyclic Humidity Exposures*
ASTM G80-07 (withdrawn 2013, replaced by ASTM G8)	*Standard Test Method for Specific Cathodic Disbonding of Pipeline Coatings (Withdrawn 2013)*
ASTM G84-89(2020)	*Standard Practice for Measurement of Time-of-Wetness on Surfaces Exposed to Wetting Conditions as in Atmospheric Corrosion Testing*
ASTM G85-19	*Standard Practice for Modified Salt Spray (Fog) Testing*
ASTM G87-02(2018)	*Standard Practice for Conducting Moist SO_2 Tests*
ASTM G90-17	*Standard Practice for Performing Accelerated Outdoor Weathering of Nonmetallic Materials Using Concentrated Natural Sunlight*
ASTM G92-20	*Standard Practice for Characterization of Atmospheric Test Sites*
SAE J2334_201604	*Laboratory Cyclic Corrosion Test (Stabilized April 2016)*

Source: Revised from Munger, 310.[2]

METHODS SELECTION

The large number of tests and possible test methods makes selection difficult. Suppliers, users, and testers and researchers all have different perspectives to narrow the selection process. Obtaining corrosion-resistance information enables a better focus. To aid in the selection process in which no universal methodology exists, engage one or more from the following sections: (1) survey of practices, (2) specific practice by a successful coatings industry participant, (3) service life testing philosophy, or (4) a useful practical example involving cooperative efforts through better understanding (methodology).

A SPECIFIC PRACTICE

The following tests constitute a generic test plan used by one industrial service company for coated metal in laboratory performance testing. Typical test coupons, 4 in. by 12 in. (10.2 cm by 30.5 cm) are prepared with all surfaces uniformly coated. Before accelerated corrosion testing, use one of the following procedures:

- ASTM B117-19, *Standard Practice for Operating Salt Spray (Fog) Apparatus*
- ASTM G85-19, *Standard Practice for Modified Salt Spray (Fog)*
- ASTM B68/B68M-19, *Standard Specification for Seamless Copper Tube, Bright Annealed*
- ASTM G85-19, A3-10(2019), *Standard Practice for Modified Salt Spray (Fog) Apparatus*

The procedure selected from this list usually is defined from the product specifications.

All coupons are to be "scribed" using the procedures of ASTM D3359-17, *Standard Test Methods for Rating Adhesion by Tape* Test, wherein the coating scratched or compromised through the entire thickness of the coating to expose the unprotected substrate. Exposure times are variable, depending on test and substrate. Additional corrosion tests (unscribed and ASTM D714, *Standard Test Method for Evaluating Degree of Blistering of Paints*) include hot humidity (ASTM D2247-15(2020), *Standard Practice for Testing Water Resistance Coatings in 100% Relative Humidity*; 100°F/100% relative humidity), condensing humidity (ASTM D4585/D4585M-18, *Standard Practice for Testing Water Resistance of Coatings Using Controlled Condensation*), condensing humidity/UV (ASTM G53-96 withdrawn, replaced by ASTM G154), water soak (ASTM D870-15, *Standard Practice for Testing Water Resistance of Coatings Using Water Immersion*), and detergent soak (ASTM D2248-01a(2018), *Standard Practice for Detergent Resistance of Organic Finishes*). Scribed samples are prepared for ASTM D1654-08(2016)e1, *Standard Test Method for Evaluation of Painted or Coated Specimens Subjected to Corrosive Environments*, evaluation by scrape/rinse/dry or by rinse/blow-off tape pull-off. Other noncorrosion tests (mainly adhesion) are also performed including t-bend, wedge bend, conical mandrel, impact (direct/reverse), methyl ethyl ketone solvent rub test, Olsen cup, gravelometer, pencil hardness, cross-hatch, dry film thickness, and loss of gloss. This battery of tests provides generous information about the coatings system, without establishing a direct link to service data. The test battery is necessarily extensive because the intent is to determine possible causes for service problems. A clear relationship between service and test data is necessary for problem resolution. Discussion of each test procedure is beyond the scope of this paper.

SURVEY OF PRACTICES

A survey commissioned by the Federation of Societies for Coatings Technology (FSCT) was performed by Steel Structures Painting Council (SSPC).[8] The full report[9] is available from FSCT and contains useful details, including nonstandard tests and analyses. One portion of the report is particularly relevant to methods selections; a compilation of 102 coatings test users' responses is shown in table 3, from which two conclusions are drawn: (1) most respondents used only one or two tests; and (2) the most prevalent test was salt spray. Salt spray testing is a crude approximation to highway environments involving deicing compounds[9] (see also the section, "Cooperative Practice Yielding Better Understanding") and is more useful for marine systems.[9] Coatings users may approach quality assurance with fewer tests than formulators.[9] Liu[10] presents a discussion describing salt spray test usefulness or uselessness based on years of experience (see chapter 23, "Automotive," in this manual).

SERVICE LIFE TESTING METHODOLOGY

In the previous example, no rationale is given for the selection or application of the tests. Experience provides an important gage for developing a useful set of tests. Dickie[11] suggested that a methodology be developed to provide rational guidance for service life testing and proposed a general framework integrating laboratory experiments, field exposure history, and theoretical and empirical models. The central role of physical and chemical models of degradation processes in service life prediction was examined[11] and represents an important philosophical contribution to coatings testing. The methodology was first presented in a somewhat-different form at an informal meeting of experts discussing coatings failure mechanisms.[12] (Correlation of test results with service life is discussed in several chapters in this manual.)

COOPERATIVE PRACTICE YIELDING BETTER UNDERSTANDING

AISI has taken a leadership role to develop and evaluate a methodology based on laboratory experiments, field exposure history, and theoretical and empirical models.[13–15] An open forum of all interested parties (mainly North American automotive and steel industries) was organized as the Corrosion Task Force of the AISI. This task force developed an improved laboratory-accelerated test for ranking the cosmetic corrosion resistance of coated automotive steel sheet products. This approach serves as a model for methodology development in areas of nonmetallic coatings corrosion testing.

TABLE 3 Compilation of Corrosion Tests and Standards Manual

Survey Results of 102 Users	Responses	Frequently Used Tests
Test		Respondents, %[a]
Salt Spray		52
Immersion		24
Outdoor		22
Ultraviolet/Condensation		20
Accelerated Weathering		14
Humidity/Condensation		10
Cathodic Disbondment		7
Adhesion		7
Atlas Cell Test (NACE TM0174)		4
Other Physical Tests		4
Other Chemical Tests		3
Flexibility		2

[a]Multiple tests used (total greater than 100%).

Summary

- Many tests are available for evaluation of corrosion protective properties necessitating a test selection process.
- Understanding the protective mechanisms of coatings systems aids in developing methodologies for systems having long lives.
- The interpretation of the test results requires adequate correlation to service life data.
- Service results validation is difficult and often requires constrictively long times.
- Successful case histories and experiences provide the best means for useful evaluations until functional methodologies are devised.

References

1. N. I. Gaynes, *Testing of Organic Coatings* (Park Ridge, NJ: Noyes Data Corporation, 1977), 293–312.
2. C. G. Munger and D. V. Vincent, Chapter 12 in *Corrosion Prevention by Protective Coatings*, 2nd ed. (Houston, TX: NACE International, 1999).
3. F. Altmayer, "Choosing an Accelerated Corrosion Test," *Metal Finishing, 69th Guidebook and Directory* 99, no. 1A (January 2001): 579–585.
4. R. D. Athey, "Testing," *Metal Finishing Organic Finishing Guidebook and Directory* 101, no. 10A (October 2003): 438.
5. M. H. Sandier, "Nonmetallic Coating Processes: Painting," in *Metals Handbook*, vol. 5, *Surface Cleaning, Finishing and Coating*, 9th ed. (Metals Park, OH: ASM International, 1990), 489–498, 527–531.
6. F. Mansfeld, "Electrochemical Methods of Corrosion Testing," in *Metals Handbook*, vol. 13A (Metals Park, OH: ASM International, 2003), 446.
7. H. R. Hamburg and W. M. Morgans, eds., *Hess's Paint Film Defects: Their Causes and Cure* (London: Chapman and Hall, 1979).
8. B. R. Appleman, "Survey of Accelerated Test Methods for Anticorrosive Coating Performance," *Journal of Coatings Technology* 62, no. 787 (August 1990): 57–67.
9. B. R. Appleman, *Survey of Accelerated Test Methods for Anti-Corrosive Coating Performance* (monograph prepared for Corrosion Committee of Federation of Societies for Coatings Technology, Blue Bell, PA, June 1990).

10. T. Liu, "Is the Salt Fog Test an Effective Method to Evaluate Corrosion Resistant Coatings?" in *Corrosion Control by Organic Coatings*, ed. H. Leidheiser, Jr. (Houston, TX: NACE International, 1981), 247–254.

11. R. A. Dickie, "Toward a Unified Strategy of Service Life Prediction," *Journal of Coatings Technology* 64, no. 809 (June 1992): 61–64.

12. W. Funke, H. Leidheiser Jr., R. A. Dickie, et al., "Unsolved Problems of Corrosion Protection by Organic Coatings: A Discussion," *Journal of Coatings Technology* 58, no. 741 (October 1986): 79–86.

13. H. E. Townsend, R. D. Granata, D. C. McCune, W. A. Schumacker, and R. J. Neville, *Progress by the Automotive and Steel Industries Towards an Improved Laboratory Cosmetic Corrosion Test, ACAP Conference Proceedings*, SAE P-250 (Warrendale, PA: SAE International, 1991).

14. H. E. Townsend, "Development of an Improved Laboratory Corrosion Test by the Automotive and Steel Industries," in *Advanced Coatings Technology, Proceedings of the 4th Annual ESD Conference* (Ann Arbor, MI: The Engineering Society, 1994).

15. *Cosmetic Corrosion Lab Test*, SAE J2334 (Warrendale, PA: SEA International, 1997).

Chapter 19 | Metal-Matrix Composites

L. H. Hihara[1]

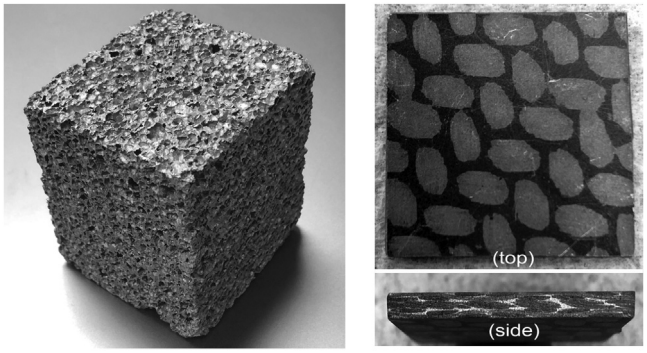
Introduction

Metal-matrix composites (MMCs) are metals that are reinforced with fibers or particles that usually are stiff, strong, and lightweight. The fibers and particles can be metal (e.g., tungsten), nonmetal (e.g., carbon or boron), or ceramic (e.g., silicon carbide (SiC) or alumina (Al_2O_3)). The purpose for reinforcing metals with fibers or particles is to create composites that have properties more useful than that of the individual constituents. For example, fibers and particles are used in MMCs to increase stiffness,[1] strength,[1] and thermal conductivity,[2] and to reduce weight,[1] thermal expansion,[3] friction,[4,5] and wear.[6] Particulate MMCs can even be foamed (fig. 1*A*) resulting in extraordinary properties, such as extremely low density and excellent energy, vibration, and noise absorption, with potential application for impact-absorbing material for blast attenuation, fire-proof walls, and sound barriers. MMCs can even be processed from woven ceramic fabric (fig. 1*B*).

Selection of the matrix metal and reinforcement constituent usually is based on how well the combination interacts to achieve desired properties. Interaction of the MMC with the environment is normally a secondary consideration; therefore, it is not uncommon for MMCs to have low resistance to corrosion. It is also not uncommon for MMCs to have corrosion behavior significantly different from what might be expected based on the normal corrosion behavior of the MMC constituents. The corrosion resistance of the MMC is usually inferior to that of its monolithic matrix alloy for one or more of the following reasons: (1) galvanic coupling of reinforcement constituent and matrix; (2) formation of an interphase between the reinforcement constituent and matrix; (3) microstructural contaminants and processing residuals in the MMC; and (4) microstructural changes caused by the presence of the reinforcement constituents.

The corrosion behavior of aluminum, magnesium, lead, depleted uranium, stainless steel, titanium, copper, and zinc MMCs will be reviewed. Reinforcement constituents used in these MMCs include Al_2O_3, boron, boron carbide (B_4C), calcium compounds, fly ash, graphite, mica, quartz, silicon, SiC, titanium carbide (TiC), tungsten, tungsten carbide (WC), yttria, and zircon. The reinforcement constituents usually range from 10 to 60 vol%. This review focuses on the corrosion properties of bulk MMCs and does not cover corrosion protection of MMCs, surface modification of MMCs, or MMCs used as coatings. Other reviews on corrosion of various types of MMC are available.[7–14] Methods and tests that can be used in a corrosion testing program to assess corrosion damage, determine corrosion mechanisms, and study specific types of corrosion will be discussed.

FIG. 1 Foamed particulate SiC/Al MMC (*A*). Each side of cube is approximately 6 cm. Al_2O_3/Al MMC fabricated from woven Al_2O_3 fabric (*B*). Each side of square coupon is 2.54 cm.



(*A*) (*B*)

Corrosion Susceptibility of MMCs

The effect of different types of reinforcement constituents on MMC corrosion behavior is discussed in this section. Because of the limited amount of information on MMC corrosion behavior, it is not feasible to have separate sections for effects of alloying elements, effects of microstructure, and sensitivity to acidity/alkalinity. MMCs are still relatively new and specialized materials; therefore, only a limited number of corrosion studies have been conducted. Most studies relate the effects of the reinforcement constituents to overall MMC corrosion behavior.

[1]Dept. of Mechanical Engineering, 2540 Dole St., University of Hawaii at Manoa, Honolulu, HI 96822, USA http://orcid.org/0000-0002-4777-4287

DOI: 10.1520/MNL202NDSUP20190037

Copyright © 2022 by ASTM International, 100 Barr Harbor Dr., PO Box C700, West Conshohocken, PA 19428-2959
ASTM International is not responsible, as a body, for the statements and opinions expressed in this chapter. ASTM International does not endorse any products represented in this chapter.

ALUMINUM MMCS

Corrosion research has focused primarily on aluminum MMCs, which is the only type of MMC that has become widely available.[3] Aluminum has relatively good corrosion resistance and is light weight. Its density is 2.7 g/cm^3. Corrosion studies have been conducted on aluminum MMCs reinforced with boron, graphite, SiC, B_4C, silicon, Al_2O_3, mica, and fly ash. Corrosion of diffusion bonds, stress corrosion, and corrosion fatigue will also be discussed.

Effect of Boron

The primary use of boron/aluminum (B/Al) MMCs has been tubular struts in the mid-fuselage structure of the space shuttle. The use of B/Al MMCs instead of aluminum alloys (as planned in the original design) resulted in a 44% savings in weight.[15]

Boron filaments (BFs) consist of polycrystalline boron with a core of tungsten and tungsten borides, which form during processing.[16] B/Al MMCs are usually fabricated by diffusion bonding BFs between aluminum foils.[17] Aluminum borides (i.e., AlB_{12} and AlB_2) have been found at BF-matrix interfaces.[18]

Crystalline boron has good chemical resistance and is not attacked by strong acids and bases even though it is thermodynamically unstable in water.[19] Accordingly, BFs are relatively inert in aqueous solutions. No observable degradation of the BFs was observed after exposure to boiling, saturated, nickel chloride solutions for 16 s,[20] or to 3% sodium chloride (NaCl) solutions containing 0.1% hydrogen peroxide (H_2O_2).[21]

Pure boron (99.999%),[22] as-manufactured (referred to as "virgin") BF with tungsten core shielded,[22,23] virgin BF with tungsten core exposed,[23] and BF extracted from aluminum matrices (not specified if tungsten core exposed)[24] are noble to aluminum in NaCl solutions. Therefore, galvanic corrosion of aluminum coupled to pure boron or BF is thermodynamically possible. Pure boron, however, is an insulator and cannot support electrical currents under normal conditions. Cathodic and anodic currents were unmeasurable on pure boron (99.999%) electrodes in aerated NaCl solutions.[22] The conductivity of BFs is many orders of magnitude greater than that of pure boron because of tungsten and tungsten borides in the core.[16] Galvanic currents, however, were also unmeasurable between virgin BF and 2024 aluminum or 6061 aluminum in 3.5% NaCl solutions.[24] It was not specified whether solutions were aerated or deaerated and whether the tungsten core of the BFs was exposed. Galvanic currents were measurable between the aluminum alloys and BFs that were extracted from the matrix.[24] The extracted BFs were enveloped by a 4-μm-thick layer of aluminum boride, which could not be positively identified as AlB_2 or AlB_{12}. Galvanic currents measured between the aluminum alloys and aluminum boride (boride species not specified) were similar to those between the alloys and the extracted BFs. When the layer of aluminum boride was removed from the extracted BFs, the galvanic current ceased, indicating that the aluminum boride interphase is necessary for galvanic corrosion. In addition, B/Al MMCs were noble to the matrix alloy and active to the extracted BF and aluminum boride, which coincides with the mixed-potential theory. The corrosion rate of B/Al MMCs also increased when the BF content was increased from 18 to 46 vol%, suggesting that corrosion rates increase as aluminum-boride cathodic sites increase. It was also noted that BF-matrix interface regions were preferentially corroded, but it was not determined whether matrix near the interphase or the interphase was attacked. Others have found that diffusion bonds in B/Al MMCs have been major sources of corrosion.[21,22] This is discussed in the subsection "Effect of Diffusion Bonds and Microstructural Contaminants."

Effect of Graphite

Continuous fiber Gr/Al MMCs (fig. 2) are known to have high specific tensile strength and stiffness in the direction of the fiber axis. Limitations of shear, compression, and transverse strengths of the MMCs, however, have restricted their use.[5] Particulate Gr/Al MMCs also have been developed for potential use in tribological applications because of good resistance to wear and seizure.[25,26]

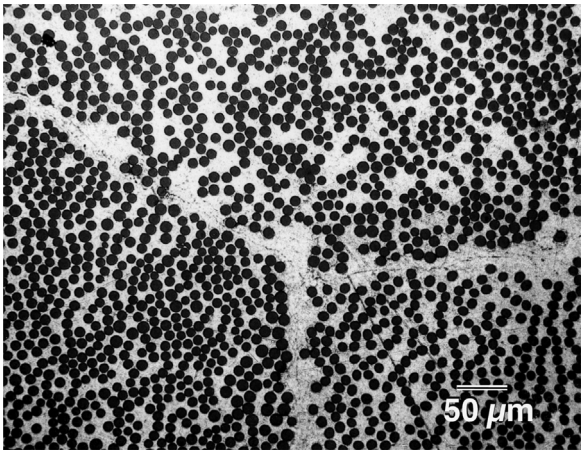
In the presence of water, carbon has a small domain of thermodynamic stability in potential-pH space.[27] At active potentials, it is thermodynamically possible to form methane (CH_4) by the following reaction:

$$C + 4H^+ + 4e = CH_4. \quad (1)$$

This has not been confirmed, however.[27] No CH_4 was detected or visual fiber degradation observed when pitch-based graphite fibers were cathodically polarized.[28] At noble potentials, various carbon compounds may form during carbon oxidation,[27] but carbon dioxide (CO_2) and carbon monoxide (CO) are believed to be the dominant reaction products.[28] During anodic polarization, pitch-based graphite fibers are oxidized to CO_2 and CO with crevice formation.[28] Graphite compounds also form by the intercalation of ions between graphite planes during polarization.[29] In the open-circuit condition or when coupled to aluminum, however, graphite fibers do not usually exhibit visual degradation.

Graphite, which is an electrical conductor, can serve as an efficient cathode during galvanic corrosion in Gr/Al MMCs. Czyrklis[30] and others[31–33] have found that the open-circuit

FIG. 2 Micrograph of Gr/6061-T6 Al MMC. Graphite fiber volume fraction is approximately 50%.



potential of a Gr/Al MMC is noble to the matrix alloy in deaerated NaCl solutions.[30] The open-circuit potential of a particulate Gr/Al MMC, however, was reported to be more active than the matrix material for a case in which the presence of graphite particles caused a large increase in the anodic currents.[33] Dull, Harrigan, and Amateau[34] conducted polarization experiments on various Gr/Al MMCs in NaCl solutions and found that dissolved oxygen greatly increases the corrosion rate, indicating that the main driving force for galvanic corrosion is oxygen rather than proton reduction in aerated solutions. Using the zero-resistance ammeter (ZRA) technique,[35] Dash[36] showed that the galvanic-corrosion current density (i_{GALV}) of a galvanic couple with a 5-to-1 area ratio of pure aluminum to pitch-based graphite fiber increased from less than 1×10^{-8} A/cm^2 in deaerated 3.5 wt% NaCl to 1.5×10^{-6} A/cm^2 in aerated 3.5 wt% NaCl. Hihara and Latanision[37] also found that i_{GALV} of galvanic couples consisting of equal areas of 6061-T6 aluminum and pitch-based graphite fiber was about 60 times greater in aerated 3.15 wt% NaCl solutions compared to deaerated solutions where i_{GALV} was equal to about 3×10^{-6} A/cm^2. The galvanic effect has also been reported in particulate Gr/Al MMCs.[38,39]

Galvanic corrosion between Gr and the aluminum matrix (fig. 3) was also evident in atmospheric corrosion studies of a 50% nickel-coated Gr fiber/pure Al MMC exposed in agricultural, rainforest, marine, industrial, arid, and volcanic (with acid rain) environments.[40] The corrosion damage of the 50% nickel-coated Gr fiber/pure Al MMC is contrasted with that of a 50% Al_2O_3/pure Al MMC exposed at the industrial site for the same exposure period (fig. 3). The annual corrosion rate of the MMC was approximately 500 times higher than that of pure Al at the marine site, and ranged from approximately 30 to 300 times higher in the agricultural, rainforest, industrial, and arid sites. Interestingly, the corrosion rate of the MMC was only approximately 10 times higher than that of pure aluminum at the volcanic site; which was attributed to the dissolution of Ni, which may have had an inhibitive effect on the aluminum matrix in acidic environments.[41] The high corrosion rates of the MMC is likely caused by oxygen reduction on the Gr fibers.

Figure 4 shows the anodic polarization diagrams of ultrapure aluminum (99.999%) and 6061-T6 aluminum in deaerated 3.15 wt% NaCl with the cathodic polarization diagrams of pitch-based graphite fibers in deaerated and aerated 3.15 wt% NaCl. As shown in the figure, proton reduction on graphite will polarize aluminum to noble potentials that are less than the pitting potential E_{PIT}, explaining the negligible galvanic-corrosion rates in deaerated solutions. Oxygen reduction on graphite, however, polarizes aluminum into the pitting regime, which causes high galvanic-corrosion rates in aerated, chloride-containing solutions. Figure 5 shows i_{GALV} of 6061-T6 aluminum and ultrapure aluminum as a function of the area fraction of pitch-based graphite fiber (cross-section exposed) in aerated 3.15 wt% NaCl.[37] Both ultrapure aluminum and 6061-T6 aluminum are represented by the same curve because they have similar galvanic-corrosion behavior. Relatively new, nonequilibrium aluminum alloys containing approximately 20 at% molybdenum or 26 at% tungsten, with marked higher pitting potential (i.e., in excess of 1 V compared with pure aluminum) in chloride solutions have been studied as potential new alloys for Gr/Al MMCs.[42,43] The results have been promising, as graphite fibers in aerated chloride solutions were incapable of polarizing the alloys to their pitting potentials, resulting in galvanic corrosion rates between

FIG. 4 Anodic polarization diagrams of ultrapure aluminum and 6061-T6 aluminum in deaerated 3.15 wt% NaCl plotted with the cathodic polarization diagrams of pitch-based graphite fibers (cross section exposed) in deaerated and aerated 3.15 wt% NaCl at 30°C. Scan rate = 0.1 mV/s.

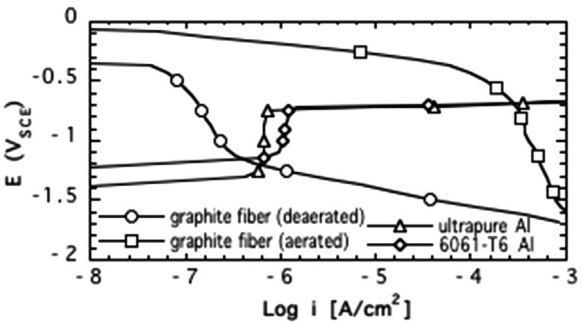
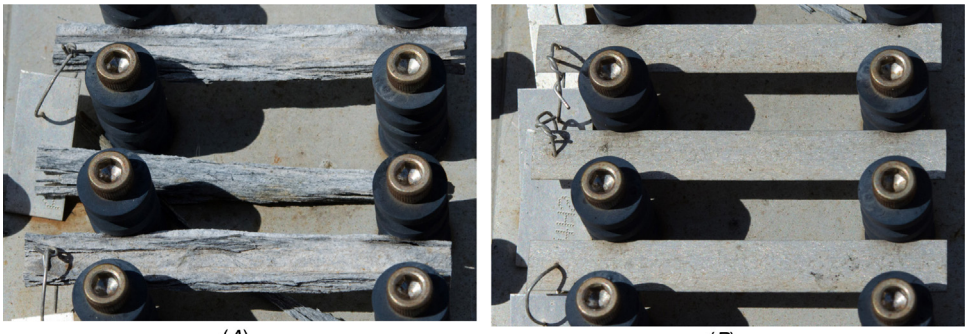
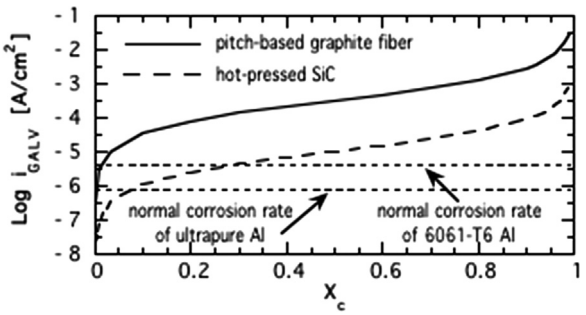


FIG. 3 Corrosion of the 50% nickel-coated Gr fiber/pure Al MMC (*A*) contrasted to 50% Al_2O_3/pure Al MMC (*B*) exposed at industrial site for the same period.



(*A*) (*B*)

FIG. 5 Graphs showing i_{GALV} of ultrapure aluminum and 6061-T6 aluminum as a function of area fraction X_c of graphite fiber and SiC in aerated 3.15 wt% NaCl at 30°C.



the fibers and alloys up to three orders of magnitude lower than that with pure aluminum.[42,43]

Another cause of degradation in Gr/Al MMCs is the presence of aluminum carbide (Al_4C_3). An Al_4C_3 interphase forms by the reaction of aluminum and carbon.[44] In Gr/Al MMCs, the formation of Al_4C_3 becomes substantial during processing at temperatures much higher than the liquidus temperature.[45] Portnoi et al.[46] showed that Al_4C_3 in Gr/Al MMCs readily decomposes in water, producing CH_4 and aluminum hydroxide $Al(OH)_3$:

$$Al_4C_3(s) + 12H_2O(1) = 4A1(OH)_3(s) + 3CH_4(g), \quad (2)$$

The hydrolysis rate of hot-pressed Al_4C_3 (78% theoretical density) was measured to be approximately 1%/h.[47]

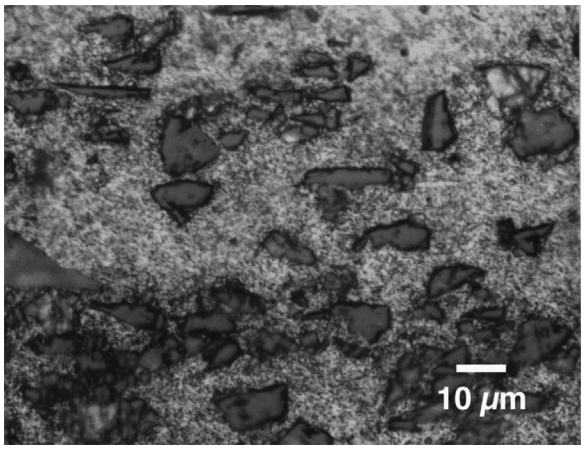
Aylor and Moran,[48] who conducted polarization experiments on Gr/Al MMCs in seawater, also hypothesized that diffusion of carbon into aluminum could lower the integrity of the passive film, rendering it more susceptible to breakdown. Wielage[49] reported that the pitting potentials of various squeeze-cast Gr/Al MMCs were approximately 20 mV more active than that of the pure aluminum matrix material in a chloride solution. Al_4C_3 was found at the Gr fiber-matrix interfaces. Shimizu, Nishimura, and Matsushima,[50] however, found that pitting potentials of a squeeze-cast, short fiber Gr/6061 Al MMC had pitting potentials similar to that of monolithic 6061 Al in a chloride solution.

Effect of Silicon Carbide

The SiC/aluminum (SiC/Al) MMCs are reinforced with SiC particles (P) (fig. 6), whiskers (W), fibers, or monofilament (MF). In 1988, an aluminum tube in the catamaran Stars and Stripes '88 was replaced by a lighter SiC_P/Al MMC tube having a 30.5-cm outer diameter.[3] Lightweight mirrors for telescopes have also been fabricated from SiC_P/Al MMC foam.[51]

SiC is a semiconductor and its electrical resistivity depends on its purity. It ranges from about 10^{13} to 10^5 Ω•cm.[52] Thus, in the unpure state, the resistivity of SiC can be rather low. Some SiC_{MF} also have carbon cores and carbon-rich surfaces,[53] with resistivities on the order of 10^2 Ω•cm.[47] Consequently, in aqueous solutions, SiC can serve as an inert electrode for proton and oxygen reduction. Also, depending on doping and impurity levels, SiC can be a p-type or n-type semiconductor which can induce cathodic or anodic photo-generated currents,

FIG. 6 Micrograph of SiC_P/6061-T6 Al MMC. SiC volume fraction is 13%.



respectively.[54] Therefore, galvanic corrosion between Al and SiC could be possible, but the degree will be highly dependent on the purity level of SiC.

In deaerated, chloride-containing solutions, SiC/Al MMCs and their matrix alloys passivate in the open-circuit condition.[48,55] Proton reduction alone cannot polarize the composites or the matrix alloys to E_{PIT} because oxygen reduction is required for this. Accordingly, in aerated, chloride-containing solutions, the open-circuit potentials of SiC/Al MMCs and their matrix alloys are nearly equal to pitting potentials.[55]

In aerated chloride-containing solutions, the degree of galvanic corrosion is strongly dependent on the type of SiC reinforcement. Figure 7 shows the anodic polarization diagrams of ultrapure aluminum and 6061-T6 aluminum in deaerated 3.15 wt% NaCl with the cathodic polarization diagrams of hot-pressed SiC, SiC_{MF} (configurations with either carbon cores or carbon-rich surface exposed), pitch-based graphite fiber, and 6061-T6 aluminum in aerated 3.15 wt% NaCl. The figure shows that i_{GALV} of 6061-T6 aluminum coupled to hot-pressed SiC (of equal surface area) is about twice the normal corrosion current density (i_{CORR}) of 6061-T6 aluminum. When 6061-T6 aluminum is coupled to SiC_{MF} (of equal surface area), i_{GALV} is about 25 times greater than i_{CORR} of 6061-T6 aluminum. The influence of the carbon core and carbon-rich surface of the SiC_{MF} is clearly seen in figure 7 where the polarization diagram of the SiC_{MF} has a stronger resemblance to that of pitch-based graphite than that of hot-pressed SiC.[47] Galvanic current between Nicalon SiC fibers and an aluminum alloy was also measured in an aerated NaCl solution.[31] The galvanic current was 72 μA (specimen areas not given) and 15% of that between carbon fiber and the aluminum alloy. If the SiC is of the p-type semiconductor, galvanic currents also can increase under illumination. This effect is shown in aerated 0.5 M Na_2SO_4 where the cathodic current density of a 20 vol% SiC/6092-T6Al increased because of photo-generated currents under illumination (fig. 8).[54]

For particulate-reinforced SiC/Al MMCs, the galvanic corrosion behavior is likely to be more accurately represented

FIG. 7 Anodic polarization diagrams of ultrapure aluminum and 6061-T6 aluminum in deaerated 3.15 wt% NaCl plotted with the cathodic polarization diagrams of pitch-based graphite fiber, SiC_{MF}, hot-pressed SiC, and 6061-T6 aluminum in aerated 3.15 wt% NaCl at 30°C. CS = cross section exposed. FS = fiber surface exposed. Scan rate = 0.1 mV/s.

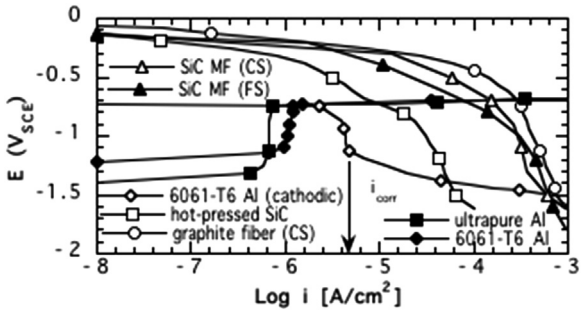
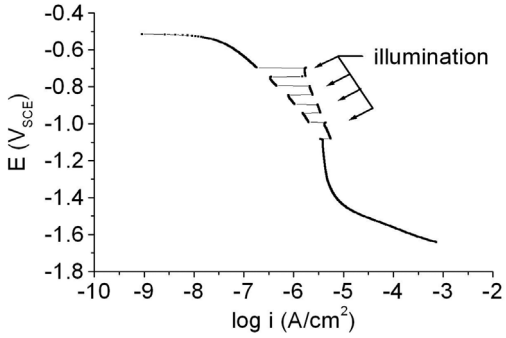


FIG. 8 Cathodic polarization diagram of the 20 v% SiC/6092-T6 Al MMC exposed to air-exposed 0.5 M Na_2SO_4 at 20°C in the dark with four periods of illumination.



by comparison to the hot-pressed SiC data, as opposed to the SiC_{MF} and Nicalon SiC fiber data. From the polarization data in figure 7, galvanic-corrosion rates were calculated for ultrapure aluminum and 6061-T6 aluminum coupled to hot-pressed SiC exposed to aerated 3.15 wt% NaCl.[37] Figure 5 graphically shows i_{GALV} as a function of hot-pressed SiC area fraction. Galvanic corrosion between hot-pressed SiC and 6061-T6 Al would not exceed the normal corrosion rate of 6061-T6 Al in aerated 3.15 wt% NaCl until the SiC volume fraction exceeds approximately 0.3. Hence, based on figure 5, galvanic corrosion of particulate SiC/Al MMCs would increase with SiC content and become relatively noticeable only at higher SiC volume fractions—for example, in the electronic-grade MMCs with 35 to 55 vol% SiC.

Díaz-Ballote et al.[56] showed via electrochemical microscope that SiC_P was electrochemically active and oxygen reduction occurred over SiC_P in an Al alloy (13.5% Si, 9% Mg, balance Al) MMC exposed to aerated 0.1 N NaCl. Experimental results have generally indicated that the corrosion rate of particulate and whisker SiC/Al MMCs increases with SiC content in aerated, chloride-containing environments. Lore and Wolf[57] found that the degree of corrosion in SiC_W/6061 Al MMCs exposed to chloride-containing solutions is proportional to the SiC content. Metzger and Fishman[7] reported the results of DeJarnette and Crowe who exposed 20 vol% SiC_P/2024 Al MMCs and monolithic 2024-T4 Al to aerated 3.5 wt% NaCl. The composite corroded about 40% faster than the matrix alloy. Sun, Koo, and Wheat[58] and Modi et al.[59] also reported that corrosion rates of SiC_P/Al MMCs were higher than that of the matrix alloys. Hawthorn[60] showed that atmospheric corrosion rates (in rainforest and marine environments) of SiC_P/6092 Al MMCs generally increased as the content of black SiC increased from 5, 10, 20, 40, to 55 vol%. The corrosion rate of an SiC_P/6092 Al MMC reinforced with 55 vol% high-purity green SiC was consistently lower than that reinforced with 55 vol% lower-purity black SiC. The high-purity green SiC should have higher electrical resistivity resulting in lower galvanic corrosion compared with the MMC reinforced with the lower purity black SiC.

Griffiths and Turnbull[61] found no evidence of galvanic corrosion in SiC/6061 aluminum MMCs with 20–30 wt% (17–27 vol%, respectively) SiC particles. Rather, they showed that diffusion-limited oxygen reduction on SiC/Al MMCs in an NaCl solution was significantly greater than that of the monolithic alloy, which could not be attributed to the SiC content but could be attributed to the increase in intermetallic particles in the MMC. Hence, it is possible that the increase in corrosion rates of the MMCs in comparison to the monolithic alloys could be the result of oxygen reduction on intermetallics. Aziz and Zhang[62] and Aziz[63] also reported that 17.5% SiC/5A06 Al MMCs corroded faster than the monolithic alloy in aerated 3.5 wt% NaCl, and attributed the higher rates to the high uniform density of cathodic (Al (Mn, Fe)) and anodic (Al (Si, Mg)) intermetallics with respect to the monolithic matrix alloy as well as cervices at SiC-Al interfaces. Qian et al.[64] reported that the corrosion rate of 25 % SiC_P/2124 MMCs in naturally aerated 0.6 M NaCl solution at room temperature were higher when the SiC particles were larger (3 μm vs. 0.7 μm). The formation of intermetallics at the SiC/Al interface was significantly reduced for the smaller 0.7 μm SiC, thus reducing active sites for corrosion initiation. Some observations contrary to these, however, have been made. Sun et al.[58] reported that the degree of corrosion increased with SiC particle content, but the intermetallic content was relatively constant. Cheng et al.[65] showed that the cathodic current density of 15% SiC_P/7075 Al MMC was lower than that of the base alloy in 3.5 wt% NaCl, indicating that oxygen reduction was lower on the MMC compared with the base alloy. The characteristics of the SiC_P or intermetallics, however, were not described.

SiC particles in SiC/Al MMCs have little effect on passive currents. In a chloride-free, sodium tetraborate-boric acid solution of pH 8.4, the passive current of a SiC_W/6061 Al MMC was only slightly greater than that of monolithic 6061 aluminum.[66] In deaerated 0.1 N NaCl, the passive current densities (at potentials less than E_{PIT}) of 20 vol% SiC_W/2024 Al and 20% vol% SiC_W/6061 Al MMCs were actually slightly less than that of their monolithic matrix alloys. The passive current densities were on the order of 10^{-5} A/cm^2.[55]

SiC generally has little effect on E_{PIT},[31,48,50,55,61,67–70] indicating that the presence of SiC particles does not degrade the pitting resistance of passive films on aluminum. In one example, however, the pitting potential of a 20 vol% SiC_W/2024 Al MMC was depressed by about 0.1 V.[55] Contrary to the relatively invariable behavior of E_{PIT}, pit morphology is indirectly affected by the presence of SiC particles. Trzaskoma[71] found that pits on SiC_W/Al MMCs were notably more numerous and much smaller in size compared with pits on wrought and powder-compacted monolithic alloys during anodic polarization in 0.1 N NaCl. The pits nucleated at intermetallic particles (not SiC), which are smaller and more numerous in the MMCs than in the monolithic matrix alloys.[71] Apparently, SiC whiskers[71] and particles[61] enhance the precipitation of the intermetallic phases. The presence of SiC, therefore, may increase the number of intermetallic pit-nucleation sites but does not weaken the resistance of the passive film, as gauged by pitting potentials. Others have also observed pit nucleation at dendrite cores,[70] near eutectic silicon,[69,72] and intermetallic particles[72] in various SiC/Al MMCs.

The corrosion behavior of particulate SiC/Al MMCs is also sensitive to processing. The SiC particles have an indirect effect on corrosion behavior by altering the condition of the matrix metal. Processing conditions and the presence of SiC particles can affect void content,[73] dislocation density,[74] and the precipitation of active phases[75] in aluminum matrices. Paciej and Agarwala[73] found that certain solution heat treatments and high extrusion ratios improved corrosion resistance of a 20% SiC_P/7091 Al MMC. Bhat, Surappa, and Sudhaker Nayak[76] reported that extrusion improved the corrosion resistance of cast MMCs by reducing the amount of pores and agglomerates of SiC particles; and Ahmad and Abdul[77] found that the T4 temper improved corrosion resistance over O and F tempers because of a finer, more homogenous distribution of secondary phases. Dikici and Tekmen,[78] however, observed increasing corrosion rates with increase in cold work from 4–50% reduction in area (before aging) in 10% and 20% SiC/Al (Si-Mg based) MMCs. The effect of the cold working had a greater influence on the corrosion behavior compared to the SiC content (10% vs. 20%). It has been suggested that corrosion near the SiC-Al interface could be caused by high dislocation density because of a mismatch of the coefficient of thermal expansion between SiC and aluminum,[47,69,79] segregation of alloying elements to the SiC-Al interface,[80] or the formation of Al_4C_3, which hydrolyzes in water. SiC reacts with molten aluminum to form Al_4C_3 if the silicon activity is low.[81] Al_4C_3 has been identified as a source of corrosion for MMCs reinforced[82] with particles[83] and SiC Nicalon fibers.[31]

Effect of Boron Carbide

B_4C has low density and relatively high hardness and often used in ballistic armor. B_4C also has good neutron shielding properties and, therefore, B_4C/Al MMCs have found utility in nuclear applications as neutron absorber materials. B_4C is a p-type semiconductor (without deliberate doping) and has high electrical resistivity (i.e., $\approx 10^{10}$ Ω•cm) at room temperature.[82] The electrical resistivity of commercially available hot-pressed or reaction-bonded B_4C, however, has been reported to be relatively low, ranging from 0.1–1,000 Ω•cm.[84] Hence, it is possible that B_4C can serve as cathodic sites and induce galvanic action with the aluminum matrix. In some particulate 20% B_4C/6092-T6 Al MMCs (fig. 9), sporadic graphite particles identified by Raman spectroscopy (fig. 10) have been found to be mixed in with the B_4C particles.[85]

In particulate 16% B_4C/1100 Al MMCs exposed to 0.5 M K_2SO_4, Han, Gallant, and Chen[86] reported that B_4C supported O_2 and/or H_2O reduction, which was verified by the deposition of copper oxides on the B_4C because of the alkalinization of the solution. Han and Chen[87] also showed that the corrosion rate increased with B_4C content and that galvanic currents could be measured between bulk B_4C and 1100 Al in aerated 3.5 wt% NaCl.

Dikici and Tekmen[78] also reported an increase in corrosion rates as the B_4C content was increased from 10% to 30% in particulate B_4C/Al (5% Cu) MMCs exposed to aerated 3.5% NaCl solution, but attributed this increase to the formation of $CuAl_2$ precipitates that served as cathodic sites. The $CuAl_2$ precipitates formed on the B_4C-Al interface.

Relatively large, circular, localized anodic regions formed on particulate 20% B_4C/6092-T6Al MMCs immersed in near-neutral, chloride-free, 0.5 M Na_2SO_4 solution exposed to air at room temperature within 40 h.[88] The localized anodic sites were approximately 300–400 µm in diameter and significantly larger than the reinforcement size (≈10–20 µm). The rapid corrosion of the MMC in the sodium sulfate solution indicated that there was a galvanic coupling effect between the Al matrix and B_4C reinforcement network. The anodic region grew and spread out into the surrounding cathodic regions. Near the center of the localized anodic region, the solution was most acidic with a pH close to 5. The pH rose to approximately 8.5 in the surrounding cathodic regions. It was hypothesized that the localized acidification of the solution is enhanced by the formation of microcrevices created by reinforcement particles left in relief as the matrix corroded. The results do not preclude the possibility of the formation of short-range, microgalvanic cells between individual B_4C particles and the surrounding matrix; however, the formation of macro anodic and cathodic regions seemed to dominate the corrosion process. Because of the amphoteric properties of aluminum, the anodic and cathodic regions flip-flopped with time.

FIG. 9 Particulate B_4C/6092 Al MMC with sporadic graphite particle (arrow) identified by Raman spectroscopy amongst B_4C particles.

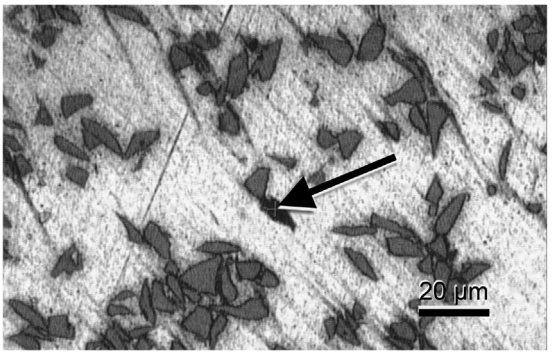
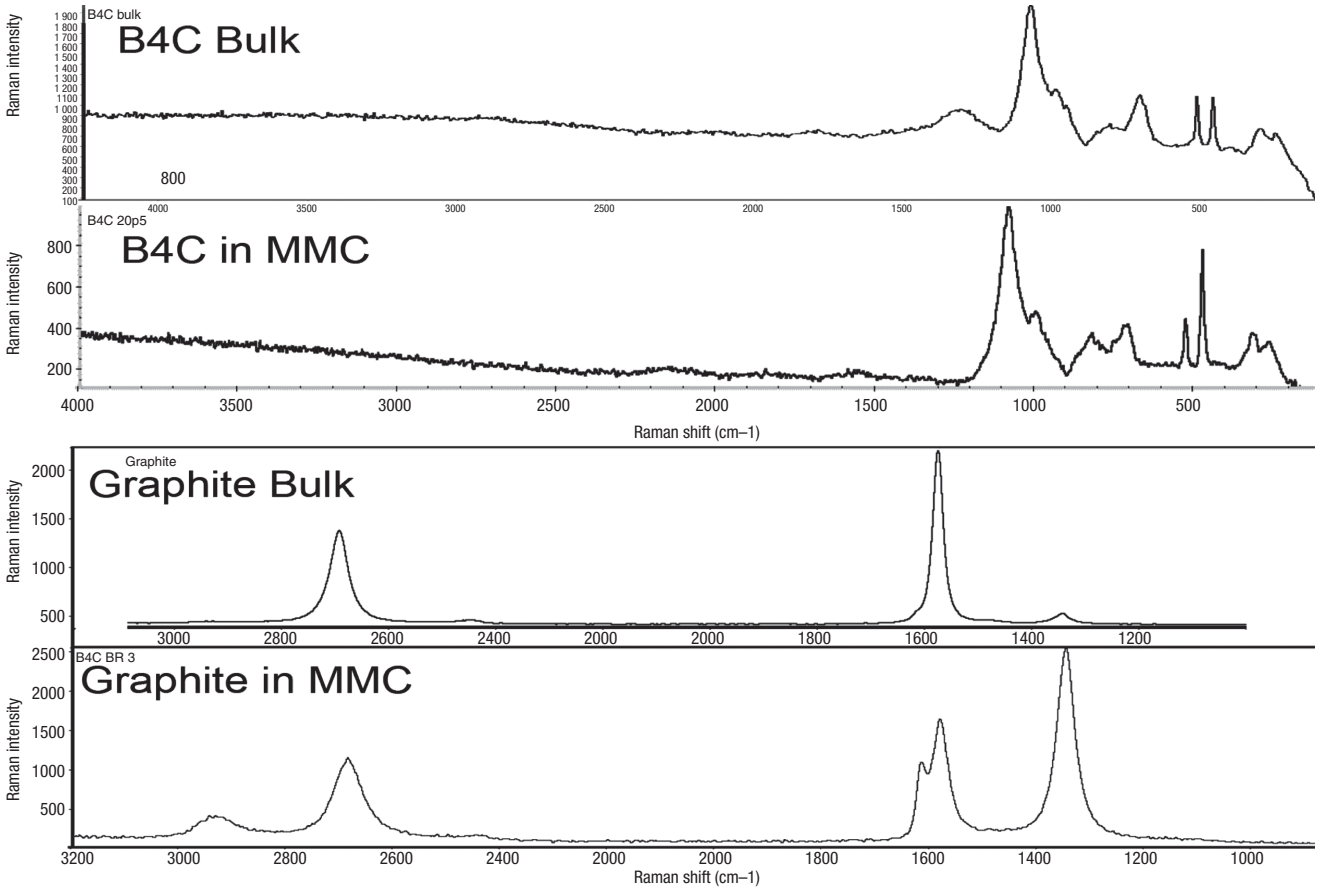


FIG. 10 Raman spectra of bulk B_4C, B_4C particles in B_4C/Al MMC (fig. 9), bulk graphite, and graphite particle in B_4C/Al MMC (fig. 9).



Effect of Silicon

Silicon/aluminum MMCs have been used for electronic packaging materials because of (1) the relative ease of machining compared with other MMCs with harder reinforcements (e.g., SiC), and (2) the relatively low coefficient of thermal expansion compared with monolithic aluminum. The electrical resistivity of pure silicon is 2.3×10^5 Ω•cm, but can be much lower for impure Si (e.g., four to five orders of magnitude lower for boron-doped Si).[89] Hence, galvanic corrosion with Si could be possible depending on the purity.

Open-circuit potential measurement of 40 wt% Si/pure Al MMCs exposed to aerated 3.15 wt% NaCl indicated various degrees of oxygen-reduction activity on the Si/Al MMC specimens.[90] For some specimens, the corrosion potentials indicated that the specimens were not polarized to the aluminum pitting potential by oxygen reduction after 1 h of immersion. Therefore, to further investigate the susceptibility of the Si/Al MMCs to pitting corrosion in aerated 3.15 wt% NaCl, the corrosion potentials were monitored for 120 h, at which time all of the samples equilibrated to that of the aluminum pitting potential. The initial variability of the corrosion potential was likely associated with the amount of iron-containing intermetallic particles contained within the exposed specimen surface, and the degree and amount of Si particles in relief. The iron-containing intermetallic particles were found to serve as effective cathodic sites.[91] Also, as the aluminum matrix corroded, aluminum-doped Si (p-type) surfaces became exposed, which served as efficient cathodic sites in contrast to the lesser-doped interior regions of the Si particles. Hence, with time, as more Si particles were left in relief as the matrix corroded, a large cathodic network formed polarizing the MMC to the aluminum pitting potential. The p-type semiconductor behavior was verified by the observation of instantaneous increases in cathodic currents on partially corroded (to expose the aluminum-doped Si surface) Si/Al MMCs upon illumination.[91]

Effect of Alumina

Particles and both short and continuous Al_2O_3 fibers have been used to reinforce aluminum alloys. A short type of Al_2O_3 fiber has been used to reinforce diesel-engine pistons.[92]

The resistivity of Al_2O_3 (99.7% pure) is greater than about 10^{14} Ω•cm,[93] and therefore galvanic corrosion between Al_2O_3 fibers and aluminum is unlikely. In alkali and acidic solutions, Al_2O_3 is thermodynamically unstable[94]; however, the short type of Al_2O_3 fibers are resistant to hot concentrated alkalis and most hot acids.[95] It can be assumed for practical purposes that Al_2O_3 fibers are inert in aqueous solutions that Al_2O_3/Al MMCs are likely to be exposed.

The Al_2O_3 reinforcements usually do not have significant effects on pitting potentials in chloride solutions,[31,50,67–69,96] although passive current densities below the pitting potential

have been reported to increase with Al_2O_3 content.[96,97] Microbial corrosion was also more significant on particulate MMCs compared with the monolithic alloy, indicating that the Al_2O_3/Al matrix interface may have aided biofilm formation.[98]

Formation of interphases (incorporating aluminum, oxygen, and alloying elements) as well as intermetallics have been observed in some Al_2O_3/Al MMCs. Preferential corrosion near fibers and particles is sometimes noticed.

Continuous Al_2O_3 fibers in an aluminum (2% Li) MMC (containing 50 vol% of fibers)[99] were enveloped by a 2- to 3-μm-thick $Li_2O/5Al_2O_3$ interphase, which formed during processing of the composite.[7] The corrosion resistance of the Al_2O_3/Al (2% Li) MMC was compared to that of 6061-T6 aluminum and 2219-T87 aluminum in eight accelerated-corrosion tests that often are used for wrought aluminum alloys. Most of the test environments contained chlorides. In most cases, weight-loss data showed that the corrosion rate of Al_2O_3/Al (2% Li) MMCs was slightly higher than that of 6061-T6 aluminum, but significantly lower than that of 2219-T87 aluminum. No severe interfacial corrosion was observed.

Continuous fibers in an aluminum (2% magnesium) MMC[100] were enveloped by a thin layer of $MgAl_2O_4$ through which bonding between fiber and matrix was made. Near the fibers, iron was detected and magnesium concentrations reached levels of about 10%, suggesting that Mg_2Al_3 clusters were present. Pits were found near the fibers after the composites were exposed to NaCl solutions containing H_2O_2. Yang and Metzger.[100] attributed the pits to corrosion of Mg_2Al_3, which is rapidly attacked at low potentials. No attack of the $MgAl_2O_4$ interphase was observed.

On a 60% Al_2O_3/Al (2% Cu)-T6 MMC exposed to aerated 3.15 wt% NaCl, corrosion initiated around intermetallic precipitates that formed on the continuous alumina fibers.[97] The precipitates that served as cathodic sites contained on average approximately 60% Al, 10% Fe, and 30% Cu.

Preferential corrosion in the proximity of an unspecified type of Al_2O_3 fiber in a 6061-T6 Al MMC was observed by Agarwala.[101] The MMC was exposed to 3.5 wt% NaCl (deaeration or aeration was not specified) for a 500-h period. No correlation was made between the microstructure and the region of corrosion.

Selective attack in the vicinity of Al_2O_3 particles have been observed during anodic polarization[102] and in the open-circuit condition[69] in chloride solutions.

Effect of Mica

Mica/aluminum (mica/Al) MMCs have been developed for potential use in applications in which good antifriction, seizure resistance, and high-damping capacity are required.[103]

Muscovite ($KAl_3Si_3O_{10}(OH)_2$) mica particles that are less than about 70 μm in size are used in mica MMCs.[104] Galvanic corrosion between aluminum and muscovite should not be a problem since muscovite is an insulator with resistivities that range from about 10^{13} to 10^{17} Ω•cm.[105] Muscovite is insoluble in cold water.[106] It has been reported, however, that muscovite particles have a tendency to absorb moisture and then swell.[107]

Mica particles were cast in various aluminum alloys.[107,108] In 3.5 wt% NaCl solutions, the presence of mica particles depressed pitting potentials by approximately 20 to 30 mV compared with the monolithic matrix alloys, suggesting that the presence of mica particles may slightly weaken the passive aluminum film. Corrosion behavior was affected by the precipitation of secondary phases. In some cases, precipitates were preferentially attacked. Pits around and away from mica particles, interfacial corrosion of the mica-matrix interface, and exfoliation of mica particles also were observed. Values of i_{CORR} (extrapolated from polarization diagrams) for nondeaerated 3.5 wt% NaCl ranged from about 3 to 10 $\mu A/cm^2$, which was slightly less than that of the monolithic matrix alloys. Weight-loss data that were measured over a 32-day period showed that the MMCs corroded at higher rates than that of the alloys, contradicting trends observed in i_{CORR} data. The mica MMCs corroded at rates ranging from approximately 3.0 to 5.5 $mg/dm^{-2}/day^{-1}$, which was approximately 1.5 to 2.0 times that of the monolithic alloys. The discrepancy in the trends of the weight-loss and i_{CORR} data could have resulted from several possibilities. Some of the weight loss could be due to nonelectrochemical reactions, such as the dissolution of dissolvable phases and the exfoliation of mica particles. The values of i_{CORR} were extrapolated from polarization curves that were generated after relatively short exposure times, whereas the weight loss was assessed over a 32-day period.

Effect of Fly Ash

Prototype fly ash MMC castings were developed[109] to combat the relatively high cost of MMCs, which has been a major impediment toward their widespread application. Fly-ash particles are waste by-products of combustion in coal-based power generation,[109] and primarily composed of SiO_2, Al_2O_3, and Fe_2O_3, as well as other oxides. Fly ash, therefore, should be electrically insulating and not promote galvanic corrosion.

Ramachandra[110] exposed 5, 10, and 15 wt% fly ash/Al (12%Si) MMC to ASTM B117, *Standard Practice for Operating Salt Spray (Fog) Apparatus*. The fly ash had an average particle size of 10 μm, and consisted of SiO_2 (30 wt.%), Al_2O_3 (58%), Fe_2O_3 (8%), TiO_2 (3%), and carbon (carbon determined by froth floatation). The form of the carbon was not specified. After 10 days in the ASTM B117 test, the weight loss of the fly ash MMCs was 10% (5 wt% fly ash MMC), 50% (10 wt% fly ash MMC), and 80% (15 wt% fly ash MMC) higher than the base Al (Si 12%) alloy. Corrosion initiated around the fly ash particles.

Effect of Diffusion Bonds and Microstructural Contaminants

B/Al and Gr/Al MMCs have been fabricated using techniques in which aluminum foils, filaments, and precursor wires have been consolidated by diffusion bonding. The diffusion bonds, if of low integrity or if contaminated, may cause severe corrosion damage.

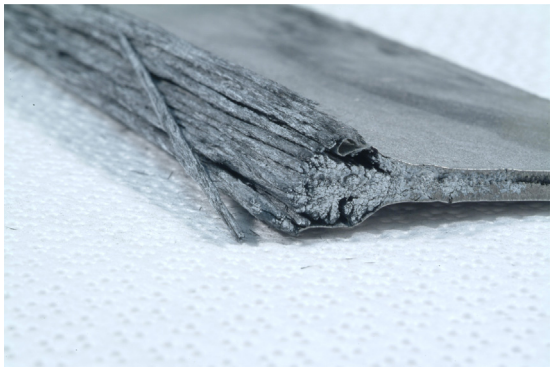
Sedriks, Green, and Novak[22] and Bakulin, Ivanov, and Kuchkin[21] found that E_{CORR} of B/Al MMCs was active to that of their monolithic matrix alloys in aerated NaCl solutions. That behavior does not appear to comply with the mixed-potential theory. Bakulin et al.,[21] however, found that hot-pressed stacks of aluminum foil processed in the same way as the MMC (but without the BFs) have E_{CORR} values that are active to the MMCs. The only difference between the monolithic aluminum and the

hot-pressed stacks of aluminum foil was crevices in the diffusion bonds between adjacent foils. The crevices, which are sources of additional anodic sites, can polarize the stacks to active potentials. Thus, the B/Al MMCs are actually noble to the matrix material processed in the same way, and the E_{CORR} values actually coincide with the mixed-potential theory. Sedriks et al.[22] found that increasing the volume fraction of BF caused anodic current densities (w.r.t. matrix area) to increase. This implies that BF-matrix interfaces, which increase with BF content, were also sources of anodic sites. Evans and Braddick[111] also reported that BF-matrix interface regions were severely attacked in an oxygenated NaCl solution. These reports indicate that the BF-matrix and foil-foil interfaces are major causes of corrosion.

Gr/Al MMCs that were fabricated by the Ti-B vapor deposit method[112] go through a processing sequence where a tow of graphite fibers is infiltrated with molten aluminum and solidified as a precursor composite wire. Bunches of wires are then diffusion bonded to consolidate larger components such as plates and bars. Some of these composites have been susceptible to exfoliation (fig. 11), which is the disbonding of precursor wires and aluminum foils caused by localized corrosion along wire-wire and wire-foil diffusion bonds. This form of corrosion is severe because composite plates can be rendered useless even though corrosion in the bulk of the foils and precursor wires may not be severe. There have been some reports[113,114] of preferential corrosion of diffusion-bonded regions in marine environments. In severe cases of exfoliation, precursor wires are expelled from the sides of MMC plates.[115]

The cause of exfoliation has been attributed[116] to residual microstructural chloride[95] that is trapped in the diffusion-bonded regions. The residual chloride originates from the Ti-B vapor deposit method, which uses titanium tetrachloride ($TiCl_4$) and boron trichloride (BCl_3) gases. The chloride is deposited on the skin of the precursor wires as the wires are extracted from the aluminum melt. Experiments have shown that in sodium sulfate solutions, in which aluminum should be passive, the chloride-contaminated diffusion bonds corrode vigorously[116] (see the subsection "Determination of Dissolution Behavior Using Polarization Techniques").

FIG. 11 Exfoliation of Gr/6061-T6 Al MMC. MMC exposed to indoor environment.



Effect of Reinforcement Constituents on Stress Corrosion in Al MMCs

Stress corrosion studies have been conducted on continuous-fiber reinforced and particle-reinforced Al MMCs.

Studies have been conducted on unidirectional, continuous-fiber Gr/6061 Al,[117] BF/2024 Al,[22] BORSIC/2024 Al, BORSIC/6061 Al,[118] and Nextel (Al_2O_3, SiO_2, B_2O_3)/6061 Al[119] MMCs. Stresses have been applied either parallel or perpendicular to the fiber axis of unnotched specimens. The Gr/6061 Al MMCs were stressed parallel to the fiber axis in natural sea water. At high stresses, failure was stress-dependent and occurred in less than 100 h. At lower stresses, failure was primarily caused by extensive corrosion, and therefore was relatively stress-independent. BF/2024 Al MMCs stressed parallel to the fiber axis at 80% fracture strength in an NaCl solution did not fail in 1000 h, but failed after 500 h when H_2O_2 was added to the NaCl solution. Extensive intergranular matrix corrosion and broken filaments at random sites were observed. The monolithic matrix alloy failed within 10 h under similar conditions. For BF/2024 Al MMCs stressed perpendicular to the fiber axis at 90% yield strength in the NaCl and NaCl with H_2O_2 solutions, failure occurred by intergranular matrix corrosion and separation at diffusion-bonded, fiber-matrix interfaces. Failure times decreased with increasing BF content. BORSIC/Al MMCs were stressed to 689 MPa along the fiber axis by three-point bending and exposed to synthetic sea-salt spray at 95 °C and nearly 100% relative humidity. The 6061 Al MMCs showed general corrosion attack without preference to tensile regions, whereas the 2024 Al MMCs showed about a 2-to-1 depth-of-attack ratio comparing the tensile to the compressive surfaces, which may have been related to specimen orientation. Unlike the 6061 Al MMCs, the corrosion resistance of the 2024 Al MMC was sensitive to heat treatment. In the Nextel fiber MMC, the prevailing mode of failure was attributed to extensive corrosion along the fiber-matrix interface and not to stress-corrosion cracking in a pH 2 NaCl solution.[119]

The stress corrosion behavior of particulate Al_2O_3/2014 Al,[120] SiC_w/6061 Al,[120] SiC_p/6061 Al,[120] and SiC_p/2024 Al.[100,110] MMCs were investigated in NaCl solutions. The Al_2O_3/2014 Al MMC was susceptible to stress corrosion cracking while subjected to three-point beam bending and alternate exposure and continuous immersions in an NaCl solution.[120] Under the same conditions, however, the 6061 Al MMCs reinforced with SiC_p and SiC_w were not susceptible to stress corrosion cracking.[120] Similarly, SiC_p/2024 Al MMCs were not prone to stress-corrosion cracking under constant strain in at 75% of ultimate tensile strength while exposed to an aerated NaCl solution.[121] Slow strain rate tension testing of SiC_p/2024 Al MMCs in an NaCl solution in the open-circuit condition indicated that the MMC lost up to 10% of failure strength compared with exposure in air.[122]

Effect of Reinforcement Constituents on Corrosion Fatigue in Al MMCs

Corrosion-fatigue studies have been conducted on Al MMCs reinforced with graphite fibers,[117] SiC_W,[123–126] and SiC_P.[124,127] Processing conditions and the type of reinforcement affect corrosion-fatigue behavior. Unnotched Gr/6061 Al MMCs were exposed to

natural seawater and stressed parallel to the fiber axis. The MMCs were processed with either silica (SiO_2)-coated or Ti-B-coated graphite fibers. For a given stress amplitude, the Ti-B type MMC had the longest corrosion-fatigue life, followed by the SiO_2 type, and the monolithic matrix alloy. At low stress amplitudes corresponding to longer exposure times, the SiO_2-type MMC suffered premature failure because of extensive corrosion. In SiC/Al MMCs, fatigue crack rates of compact tension specimens usually are higher in NaCl solutions compared with air[123] or argon.[127] Loading frequency affects corrosion-fatigue crack rates,[127] but no consistent trends were observed. Fatigue[123] and corrosion-fatigue[127] crack rates are influenced by loading and extrusion or rolling direction. The nucleation of a crack was also observed at the bottom of a corrosion pit.[105] The shape of the reinforcement constituent also may have significant effects. Jones[125] developed a model based on crack-tip strain rate that is applicable to stress corrosion and corrosion fatigue. The model is relatively insensitive to slight variations in reinforcement volume fraction. The model predicts that crack rates are reduced by increasing the reinforcement constituent length-to-diameter ratio, implying that MMCs reinforced with whiskers are more resistant to stress corrosion and corrosion fatigue than those reinforced with particles. This is in agreement with results of Hasson et al.[124] who found that SiC_W/6061 Al MMCs have longer corrosion-fatigue lives than SiC_P/6061 Al MMCs in salt-ladened moist air.

MAGNESIUM MMCs

Very light composites can be fabricated from magnesium, which is one of the lightest structural metals. Its density is only 1.7 g/cm^3. Magnesium, however, is the most active structural metal in the electromotive series,[128] which means that it has a very high tendency to corrode. Because magnesium is an active metal, it is particularly susceptible to galvanic corrosion when in contact with noble reinforcement constituents. Corrosion studies have been conducted on magnesium MMCs reinforced with BF, graphite fibers, SiC_{MF}, Al_2O_3 fibers, fly ash particles, and calcium compound particles. Stress-corrosion behavior of an Al_2O_3/Mg MMC is included in the Al_2O_3 section.

Effect of Boron

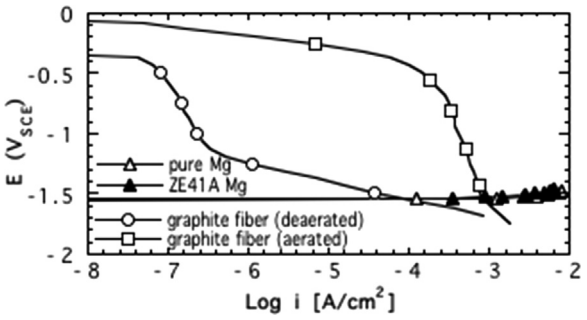
The general properties of BFs given in the subsection "Aluminum MMCs: Effect of Boron Filaments" also apply here. Pure boron is an insulator and a poor cathode. Galvanic currents were unmeasurable between pure boron and magnesium in 0.005 N NaCl solutions[23,129] (it was not specified if solutions were deaerated or aerated). Galvanic currents, however, were measurable between virgin tungsten-core BF (cores either shielded or exposed) coupled to magnesium[129] and an MA2-1 magnesium alloy.[23] Galvanic currents were higher when tungsten cores were exposed.[23,129] This is not unexpected because pure tungsten was shown to be an effective cathode.[23] Because galvanic currents were unmeasurable between magnesium and pure boron, but measurable between magnesium and virgin BF (with tungsten cores shielded), it was suspected that the outer layer of BFs consisted of tungsten boride and not of pure boron.[130] It was also found that BF extracted from the matrix supported cathodic-current densities that were about five times that of virgin BFs.[23] The corrosion rates of actual BF/MA2-1 MMCs in 0.005 N and 0.5 N NaCl solutions were 12.49 g/m^{2}day and 81.72 g/m^{2}day, respectively, which were about six times the values of the monolithic matrix alloy in respective environments.

Effect of Graphite

The general properties of graphite given in the subsection "Aluminum MMCs: Effect of Graphite Fibers" also apply here. Figure 12 shows the cathodic polarization diagrams of pitch-based graphite (cross-section exposed) in deaerated and aerated 3.15 wt% NaCl with the anodic polarization diagrams of pure magnesium and ZE41A magnesium in deaerated 3.15 wt% NaCl. Figure 12 reveals that galvanic-corrosion rates increase in aerated solutions. Note that both anodic and cathodic curves of pure magnesium and ZE41A magnesium are practically insensitive to solution aeration, indicating that normal corrosion rates are virtually unaffected by dissolved oxygen. Figure 12 shows that galvanic corrosion of magnesium is not anodically controlled, and therefore galvanic-corrosion rates should increase with increasing area fraction of cathodic reinforcement material. Trzaskoma[130] showed that galvanic-corrosion current densities increased from about 0.3 to 0.6 mA/cm^2 (based on magnesium area) as the graphite-to-magnesium area ratio was increased from 0.25 to 0.44. The galvanic couples consisted of AZ31B magnesium alloy and pitch-based graphite fiber with fiber ends and circumferential fiber surface exposed to an aerated, borated-boric acid solution of 8.4 pH containing 10,00 ppm NaCl. Actual MMCs immersed in air-exposed 0.001 N NaCl suffered severe degradation within five days. Bakkar[131] also reported galvanic currents between Sigrafil C-40 carbon fibers and AS41 Mg alloy and AS41(with 0.5 wt% Ca) exposed to pH 12, 100 ppm NaCl solution. The galvanic currents were slightly lower for the AS41(0.5Ca) alloy. Accordingly, Sigrafil C-40/ AS41 Mg MMCs were subjected to severe pitting in the pH 12, 100 ppm NaCl solution under open-circuit conditions.

Czyrklis[30] showed electrochemical evidence of galvanic corrosion in actual graphite/magnesium (Gr/Mg) MMCs. He measured open-circuit potentials and calculated corrosion current

FIG. 12 Anodic polarization diagrams of pure magnesium and ZE41A magnesium in deaerated 3.15 wt% NaCl plotted with the cathodic polarization diagrams of pitch-based graphite fiber (cross section exposed) in deaerated and aerated 3.15 wt% NaCl at 30°C. Scan rate = 0.1 mV/s.



densities (by Tafel extrapolation) of a 40% Gr/Mg MMC and its matrix alloy that were exposed to a deaerated 50 ppm chloride solution. The open-circuit potential of the composite (-1.127 V_{SCE}) was about 0.3 V noble to that of the matrix alloy, and i_{CORR} of the composite (178 μA/cm^2) was about 40 times greater than that of the matrix alloy at 25 °C. Czyrklis also reported severe degradation of Gr/AZ91C Mg MMCs that were exposed to 50 ppm chloride solutions and 95% relative humidity atmospheres. Composite degradation was attributed to galvanic corrosion and to selective attack of $Mg_{17}Al_{12}$ precipitates in the magnesium matrix.

Interphase formation of Al_4C_3 was observed in a Gr/Mg (1% aluminum) MMC produced by squeeze casting. The Al_4C_3 formation resulted from heat treatments at 500 °C.[132] Degradation of these MMCs could be accelerated by both galvanic corrosion and Al_4C_3 hydrolysis.

Effect of Silicon Carbide

The general properties of SiC given in the subsection "Aluminum MMCs" also apply here. Galvanic corrosion between magnesium and SiC depends to a large degree on the type of SiC reinforcement and on the presence of dissolved oxygen in solution. Figures 13 and 14 show anodic polarization diagrams of pure magnesium and ZE41A magnesium with cathodic polarization diagrams of hot-pressed SiC, SiC_{MF} (with either carbon core or carbon-rich surface exposed) in deaerated and oxygenated 0.5 M sodium nitrate ($NaNO_3$) solutions, respectively. Galvanic-corrosion rates (as determined by the mixed-potential theory) are greater in oxygenated solutions because of oxygen reduction occurring on the reinforcement materials (compare figs. 13 and 14). Galvanic-corrosion rates are lowest between magnesium and hot-pressed SiC and highest between magnesium and SiC_{MF} (with core exposed).[133] The carbon-core and the carbon-rich surface appear to have a dominant effect on cathodic behavior of the SiC_{MF}. The curves of SiC_{MF} have a stronger resemblance to pitch-based graphite fiber (cross-section exposed) than to hot-pressed SiC (figs. 13 and 14). Similar results were obtained for sodium sulfate (Na_2SO_4) and NaCl solutions.[134] For AZ80A Mg and ZK60A Mg reinforced with 20 vol% SiC particles, the corrosion rates were significantly increased by the chlorides.[135] Corrosion rates for both MMCs were over one order of magnitude higher in air-exposed 1 NaCl compared with 1 N Na_2SO_4.

Nunez-Lopez et al.[136] conducted studies on particulate ZC71 magnesium alloy reinforced with 12 vol% SiC particles ranging in size up to approximately 20 μm. Specimens exposed to salt spray tests did not show signs of galvanic coupling between the matrix and SiC particles. Preferential attack between SiC particles and the matrix was not observed. Instead, macroscopic anodic and cathodic regions developed. Corrosion spread over the MMC surface much more rapidly than on the monolithic alloy, but the local corrosion rates were approximately only three times greater on the MMC. The authors[136] speculated that the higher corrosion rates on the MMCs could have been caused by iron contamination of the magnesium matrix during processing in a steel crucible. Studies on a model MMC consisting of high-purity magnesium and well-separated SiC particles exposed to 3.5 wt% NaCl also did not show evidence of galvanic corrosion between the particles and matrix.[137] Studies[138] on AZ91 Mg reinforced with 0, 5, 10, and 15 vol% alpha-SiC particles showed that cathodic current densities and corrosion rates increased with increasing SiC content in 3.5 wt% NaCl (aeration not specified). The increase in current density was attributed to cathodic activity on the beta phase that formed in the highly strained matrix around the SiC particles. Cathodic currents on hot-pressed alpha-SiC were more than an order of magnitude lower than the cathodic currents on the MMCs, indicating that galvanic action with SiC was negligible.

FIG. 13 Anodic polarization diagrams of pure magnesium and ZE41A magnesium plotted with cathodic polarization diagrams of hot-pressed SiC, SiC_{MF}, and pitch-based graphite fibers in deaerated 0.5 M $NaNO_3$ at 30°C. Scan rate = 0.1 mV/s. CS = cross section exposed. FS = fiber surface exposed.

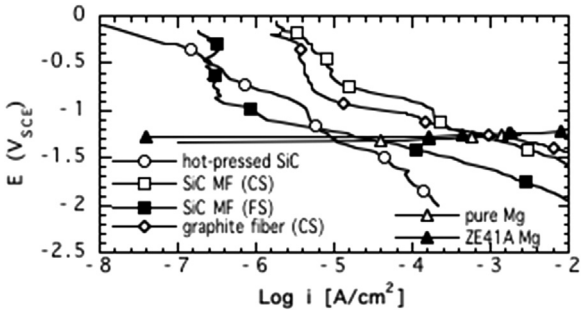
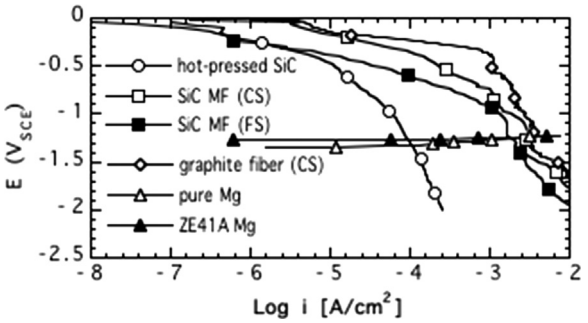


FIG. 14 Specimens and test conditions are similar to figure 13, except the 0.5 M $NaNO_3$ solution is oxygenated.



Effect of Alumina

The general properties given for Al_2O_3 in the subsection "Aluminum MMCs" also apply here. Galvanic corrosion should not be expected in Al_2O_3/magnesium (Al_2O_3/Mg) MMCs since Al_2O_3 is an insulator. However, Levy and Czyrklis[139] found that continuous-fiber Al_2O_3/AZ91C MMCs were much more susceptible to corrosion in chloride-containing solutions compared with the matrix alloy. They did not specify if the solutions were deaerated. In a 50 ppm Cl^- solution at 25 °C, the corrosion rate of the composite was 0.78 mm/y compared with only 0.10 mm/y for the alloy. When the temperature was increased to 66 °C, the

corrosion rate of the composite dramatically increased to about 150 mm/y, whereas that of the alloy increased to only 0.13 mm/y. Corrosion rates were highest in 3.5 wt% NaCl at 25 °C, where the composite corroded at an astronomical rate of about 350 mm/y compared with 3.6 mm/y for the alloy. In chloride-free environments, the composite showed equivalent or greater resistance to corrosion than the alloy. In distilled water at 25 °C and 95% relative-humidity environments at 25 °C and 66 °C, the corrosion rate of the composite and matrix alloy was less than 0.25 mm/y. The tremendously higher corrosion rates of the composites in the chloride-containing environments appear to be caused by the presence of the Al_2O_3 fibers. It is unlikely that galvanic corrosion between the matrix and Al_2O_3 fibers can take place since Al_2O_3 is an insulator. Galvanic corrosion could be possible, however, between the matrix and an interphase or precipitates, which potentially could form because of the presence of the Al_2O_3 fibers. Czyrklis[140] reported that E_{CORR} of 35% continuous-fiber Al_2O_3/AZ91C MMCs was more noble than that of the matrix alloy in 50 ppm Cl^- solutions, indicating that galvanic corrosion is a possibility. It was not specified if the solutions were deaerated.

Evans[141] studied the stress-corrosion behavior of continuous-fiber Al_2O_3/ZE41A Mg MMC in an NaCl-potassium chromate (K_2CrO_4) solution. Unnotched and notched specimens stressed parallel to the fiber axis and exposed for approximately 100 to 1,000 h in the NaCl-K_2CrO_4 solution retained approximately 90% of the strength in air. The matrix alloy and the MMC with the stress aligned perpendicular to the fiber axis retained only approximately 40% to 60% of the strength in air.

Effect of Fly Ash Cordierite

Cordierite ($Mg_2Al_4Si_5O_{18}$) consisting of SiO_2 (45–51 wt.%), Al_2O_3 (32–35%), FeO_3 (2–12%), and MgO (3–35%) was obtained from fly ash and used in the amount of 2 wt% and 4% to fabricate AM60 Mg matrix MMCs.[142] Cordierite is electrically insulating and should not promote galvanic corrosion. Potentiodynamic polarization test were conducted in 3.5 wt% NaCl (aeration not specified, but Mg usually corrodes with proton reduction as the cathodic reaction), and i_{corr} values were used to determine corrosion rates of the MMCs and base AM60 Mg alloy. The MMCs were examined in the as fabricated and heat-treated conditions with two surface finishes (ground with 600-grit or 2,000-grit grinding paper). No clear trends were observed in the corrosion rates, which could not be correlated to the presence of or amount of cordierite.[142] Hence, the cordierite did not significantly affect corrosion behavior, as gauged by the polarization tests.

Effect of Calcium Compounds

Calcium silicate (CS: $CaSiO_3$) was used as a reinforcement in pure (99.9%) Mg MMC.[143] These MMCs were targeted for biodegradable orthopedic implant materials as Mg has an elastic modulus relatively close to bone.[143] The high corrosion rate of Mg, however, can lead to rapid hydrogen gas generation and premature loss of mechanical strength before defect bone can be regenerated.[143] CS is a promising MMC reinforcement for implant material because it has good bioactivity that can enhance bone growth.[143] Powder metallurgical specimens with 0 wt%, 10% , 20%, 30% and 40% CS were sintered. In simulated body fluid (SBF: solution containing NaCl, $NaHCO_3$, KCl, $K_2HPO_4 \bullet 3H_2O$, $MgCl_2 \bullet 6H_2O$, HCl, $CaCl_2$, Na_2SO_4, tromethamine) at 37 °C (likely air-exposed), the corrosion rates decreased as the CS content was increased and reached a minimum corrosion rate at 20% CS. However, at higher CS content, the corrosion rate began to increase at 30% CS and reached a maximum corrosion rate at 40% CS. The CS enhanced the formation of a hydroxyapatite (HA: $Ca_5(PO_4)_3(OH)$) film, which reduced the Mg corrosion rate. The higher corrosion rates at 30% and 40% CS were attributed to incomplete sintering which lead to the ingress of SBF into the bulk MMC.[143]

Tricalcium phosphate (TCP: $Ca_3(PO_4)_2$) powder of 99.89% purity with sizes ranging from 100 to 150 µm was sintered with pure (99.9%) Mg powder ranging in sizes from 53 to 75 µm to produce MMCs.[145] Specimens were fabricated using no TCP or 5 wt% TCP for corrosion studies in SBF. The pure Mg specimens (no TCP) served as a baseline in comparison for corrosion behavior. In immersion studies in the SBF for 72 h at 37 °C (likely air-exposed), the mass loss of the MMC sample was 16.1%, whereas that of the pure Mg was and 20.1%. Potentiodynamic polarization also indicated that the MMC had lower i_{corr} values compared with the pure Mg. The lower corrosion rates of the MMC in comparison to the pure Mg was attributed to the formation of crystalline HA films, which formed only on the MMC. $Mg(OH)_2$ films formed on both the MMC and pure Mg surfaces. It was suggested the TCP/Mg MMC is promising for enhancing bone growth activity.

LEAD MMCs

Lead is a relatively heavy metal with a density of 11.4 g/cm^3. Lead MMCs, therefore, normally are developed for applications in which a combination of its structural, physical, and chemical properties are important. The corrosion behavior of pure lead MMCs in simulated, lead-acid battery environments has been studied to assess the feasibility of using these composites as positive electrode grids in place of conventional lead-based alloy grid materials. Lead can be alloyed with elements such as arsenic, antimony, or calcium to increase strength and stiffness. These elements, however, reduce corrosion resistance. Monolithic pure lead has very good corrosion resistance in lead-acid battery environments (which consists of sulfuric acid solutions) but is heavy and lacks sufficient mechanical strength. Pure lead, therefore, has been reinforced with strong, lightweight fibers in hopes of achieving the goals of increasing strength, reducing weight, and retaining the corrosion resistance of pure lead.[145–147] More recently, a study on the corrosion behavior of particulate lead-antimony alloy MMCs exposed in sodium chloride solutions has been conducted.[148]

Effect of Fibers

To simulate corrosion in lead-acid battery environments, Dacres et al.[145] and others[146,147] anodically polarized test materials at 1.226 V (versus mercury/mercurous sulfate reference electrode) in sulfuric acid solutions (of 1.285 specific gravity) at 50 °C, 60 °C, or 70 °C. At 1.226 V, lead and water are oxidized to lead

dioxide (PbO_2) and molecular oxygen (O_2), respectively.[149,150] About one-third of the total anodic current is consumed in the oxidation of lead under these conditions.[147]

Al_2O_3, carbon, SiC, and glass-quartz fibers of various volume percents have been used in lead MMCs. Fabrication methods as well as fiber type may have significant effects on corrosion resistance. Several types of continuous-fiber Al_2O_3/lead (Al_2O_3/Pb) MMCs.[145,147] were examined. MMCs containing 5%[147] and 7.5%[145] Al_2O_3 fibers showed good corrosion resistance. The 5% Al_2O_3 fiber MMC had gravimetric and Faradaic corrosion rates of 0.033 mm/y and 0.10 mm/y, respectively. Al_2O_3/Pb MMCs having 6%,[145] 10%,[147] 15%,[147] and 25%[145] Al_2O_3 fibers did not have acceptable corrosion resistance. Poor bonding between Al_2O_3 fibers and the matrix allowed the electrolyte to diffuse into fiber-matrix interfaces, leading to accelerated corrosion[145] and swelling of the composite because of corrosion-product buildup.[147]

Composites reinforced with carbon or graphite fiber were not resistant to corrosion.[145,147] Viala, El Morabit, and Bouix[146] reported that the graphite fibers were oxidized. SiC fiber/Pb MMCs also did not have good corrosion resistance.[146,147] Viala et al.[146] reported that composites were destroyed by swelling because of the formation of PbO_2 in the bulk of the composites. The SiC fibers (which do not have carbon cores) were stable. The corrosion resistance of glass-quartz/Pb MMCs having 9.5% fiber was not satisfactory, and gravimetric and Faradaic corrosion rates were 0.24 and 0.62 mm/yr, respectively.[147] Lead alloys containing calcium and tin had gravimetric and Faradaic corrosion rates of 0.49 and 1.35 mm/yr, respectively, also showing unsatisfactory corrosion resistance.[145,147] These studies[145–147] have indicated that the penetration of electrolyte into the bulk of the composites, possibly through poorly bonded fiber-matrix interfaces or by oxidation of fibers, is a major factor governing degradation properties.

Effect of Particles

A commercially available lead (80%)-antimony (20%) alloy was reinforced with 1, 3, and 5 wt% zircon ($ZrSiO_4$) particles[148] and exposed to a 1 N NaCl solution. The particles should not induce galvanic corrosion. Weight loss measurements, made over a 72-h period, showed that weight loss of the lead MMCs increased with increasing zircon content. Heat treatment of the $ZrSiO_4$/Pb-Sn MMC at 200 °C also improved resistance to weight loss.

DEPLETED URANIUM MMCs

Tungsten fiber/depleted uranium (W/DU) MMCs are the antitheses of the lightweight MMCs. W/DU MMCs were developed to create high-density materials. Uranium has a density of 18.9 g/cm^3.

DU corrodes galvanically when coupled to tungsten fibers in air-exposed 3.5 wt% NaCl solutions at room temperature.[151] The open-circuit potential of tungsten fiber ($-0.25\ V_{SCE}$) is noble to that of the DU alloy ($-0.80\ V_{SCE}$). The open-circuit potentials of the W/DU MMC and galvanic couples consisting of tungsten fiber and DU alloy of equal areas are $-0.78\ V_{SCE}$ and $-0.77\ V_{SCE}$, respectively. These potentials fall between those of tungsten fibers and the DU alloy, which is consistent with the mixed-potential theory. The galvanic-corrosion current density measured between equal areas of tungsten fibers and the DU alloy was equal to about 4×10^{-5} A/cm^2. In a 30-day exposure test in the NaCl solution, the W/DU MMC lost 43.56 mg/cm^2, which was about 1.3 times that of the DU alloy.

STAINLESS STEEL MMCs

Sintered, particulate composites consisting of ferritic 434L stainless steel (SS) and Al_2O_3 particles have been developed for potential application in chemical processing plants, turbine blades, and heat exchanger tubes[152,153] Austenitic 316L stainless steels reinforced with Al_2O_3 and Y_2O_3 also have been investigated for enhanced strength and wear resistance.[154]

Effect of Alumina

The corrosion behavior of sintered Al_2O_3/434L SS MMCs and sintered 434L alloy without Al_2O_3 particles was examined.[152,153,155] The volume fraction of Al_2O_3 particles in these materials ranged from 0% to 8%. The effect of small amounts of titanium and niobium alloying elements on corrosion resistance was also investigated. Galvanic corrosion between 434L stainless steel and Al_2O_3 should not occur because the latter is an insulator. Experiments were conducted in 1 N sulfuric acid (H_2SO_4),[152,153] and 5 wt% NaCl[152] solutions at room temperature. It was not mentioned if solutions were deaerated. In 1 N H_2SO_4, [152,153] there was no strong correlation between Al_2O_3 content and corrosion behavior. The E_{CORR} and i_{CORR} values varied between materials, but clear trends relating E_{CORR} and i_{CORR} to Al_2O_3 content or alloy composition were not conspicuous. One of the few generalities that could be made was that passive-like anodic current densities were high and within an order of magnitude of 1 mA/cm^2 for almost all materials. Alloying with titanium and niobium tended to increase anodic current densities. In the 5 wt% NaCl solutions, i_{CORR} of the MMCs was less than 10 μA/cm^2.[152] Upon polarization, all materials displayed active corrosion behavior in the NaCl solutions.

Particulate 316L SS MMCs,[154] fabricated using powder metallurgy, were reinforced with 3, 4, and 5 wt% Al_2O_3 and additions of 2 wt% chromium diboride (B_2Cr) or 1 wt% boron nitride (BN) for sintering aids. The density of the MMCs ranged from 86% to 96% of the theoretical value. Unreinforced 316L specimens were also fabricated using powder metallurgy without sintering aids, resulting in 85% of theoretical density. The test samples were immersed in 10% sulfuric acid (H_2SO_4) at room temperature for 24 h, 1% hydrochloric acid (HCl) at room temperature for 24 h, and boiling 10% nitric acid (HNO_3) for 8 h. The pure, unreinforced 316L specimens passivated in the 10% H_2SO_4 solution, whereas the corrosion rate of the MMC generally increased with increasing Al_2O_3 content to a maximum value of approximately 4 mm/yr. Specimens with the BN sintering aids corroded at higher rates as compared to those with the B_2Cr sintering aids. The authors correlated this behavior to the local depletion of chromium in the matrix due to matrix reactions with BN compared with reactions with chromium-rich B_2Cr. The MMC performed better than the un-reinforced 316L specimen in the 1 wt% HCl solution, but worse than the unreinforced specimen in the boiling nitric acid solution. There was no

strong correlation between Al_2O_3 content in the MMCs and the corrosion rates in 1 wt% HCl and boiling 10 wt% HNO_3 solutions.

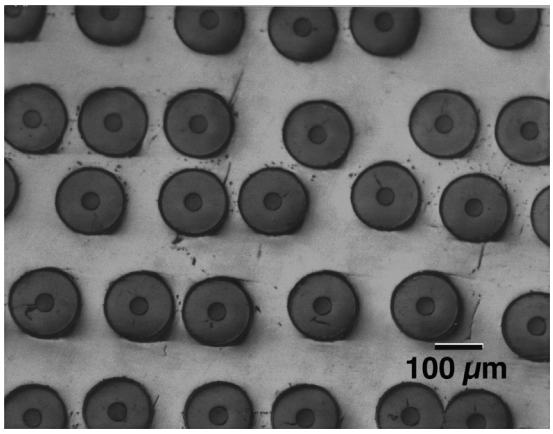
Effect of Yttria

Yttria (Y_2O_3) is an insulator and galvanic effects are not expected. The 316L stainless steel specimens discussed earlier[154] were also reinforced with 3, 4, and 5 wt% Y_2O_3 and additions of 2 wt% chromium diboride (B_2Cr) or 1 wt% BN for sintering aids. In all solutions (i.e., sulfuric, hydrochloric, and nitric acid solutions), the Y_2O_3-reinforced MMCs exhibited reduced corrosion resistance compared with the Al_2O_3-reinforced MMCs. The Y_2O_3 MMCs were sintered to 88–96% of theoretical density, and the Al_2O_3 MMCs were sintered to 86–92% of theoretical density. The Y_2O_3 particles also showed better bonding to the matrix, probably forming a complex $YCrO_3$ oxide, compared with the Al_2O_3 particles. It is possible that the formation of the reaction layer around the Y_2O_3 particles may have depleted chromium from the matrix, resulting in reduced corrosion resistance, compared with the Al_2O_3-reinforced MMCs.

TITANIUM MMCs

Titanium MMCs have been developed for aerospace applications as well as potential surgical implant materials. SiC MF/titanium (SiC_{MF}/Ti) MMCs (fig. 15) have utility in high-temperature applications requiring strong, lightweight materials. Titanium has a density of 4.5 g/cm^3. Structural SiC_{MF}/Ti MMCs have been used in prototype drive shafts, turbine-engine discs, compressor discs, and hollow fan blades and also are candidate materials for the skin of the National Aerospace Plane.[156] Porous, particulate Ti MMCs have potential use as surgical implant materials, owing to the compatibility of titanium and bone growth.[157] Porous titanium is a good surgical implant material because bone growth is enhanced by the relatively low elastic modulus of titanium, and bone ingrowth is allowed by the porous structure. Porous titanium, however, has poor tribological properties and, therefore, MMCs that incorporate graphite to reduce friction and incorporate TiC to improve wear resistance are of interest.[157]

FIG. 15 Micrograph of SiC_{MF}/Ti-15-3-3-3 MMC. Monofilament volume fraction is approximately 40%.



Effect of Graphite

Graphite/porous titanium MMCs were processed and heat treated to fabricate a graphite/TiC/porous titanium MMC.[157] Polarization tests were conducted in 0.9 wt% NaCl and lactated Ringer's solution for *in vitro* use. The E_{CORR} values of the graphite/TiC/porous Ti MMCs were more noble than that of pure Ti, as expected because of the presence of graphite and TiC. The anodic polarization current densities of the MMCs were significantly higher than that of pure monolithic titanium, which passivated. The authors attributed the higher corrosion rates of the graphite/TiC/Ti MMC to its porosity, which may have prevented complete passivation of the titanium matrix. Another possibility for the higher current densities could be the oxidation of graphite particles, and not dissolution of the titanium matrix (see the next subsection).

Effect of Silicon Carbide

Corrosion studies on titanium alloy Ti-15-3-3-3 (15 wt% vanadium, 3 wt% chromium, 3 wt% tin, 3 wt% aluminum, balance titanium)[158] and titanium aluminide α_2Ti_3Al (14 wt% aluminum, 21 wt% niobium, balance titanium)[159] reinforced with SiC_{MF} have been conducted. The corrosion behavior of SiC_{MF}/Ti-15-3-3-3 MMC was investigated in 3.15 wt% NaCl. There was excellent agreement in the polarization diagrams of the actual MMC and that of a model utilizing the polarization diagrams of the individual constituents and the mixed-potential theory (see the subsection "Determination of Dissolution Behavior Using Polarization Techniques"), indicating that the fabrication processing did not affect the dissolution behavior of the MMC constituents. The matrix passivated and the carbon cores and carbon-rich outer surface of the SiC_{MF} oxidized. During anodic polarization, graphite oxidizes to CO_2.[116] ZRA studies showed that galvanic currents between the Ti-15-3-3-3 matrix and SiC_{MF} were negligible. Based on the polarization diagrams, the galvanic current density cannot exceed that of the passive current density of Ti-15-3-3-3. The corrosion behavior of the SiC_{MF}/α_2Ti_3Al[159] was somewhat similar to that of the SiC_{MF}/Ti-15-3-3-3 MMC,[158] with the exception that the α_2Ti_3Al matrix is less resistant to pitting. During anodic polarization, the α_2Ti_3Al/SiC_{MF} pitted at approximately 1 V_{SCE} in 0.5 N NaCl, which was approximately 0.5 V less than that of the monolithic matrix alloy. Some matrix pitting and crevice corrosion around the SiC_{MF} were also observed after anodic polarization. The galvanic current density of the α_2Ti_3Al/SiC_{MF} MMC was negligible and limited to the passive current density of the α_2Ti_3Al matrix.[159]

COPPER MMCs

Copper MMCs have been investigated for use in marine, electronic and thermal applications. Copper is relatively heavy, with a density of 8.96 g/cm^3. Reinforcements typically are chosen to impart strength and stiffness, reduce weight, enhance thermal and electrical properties, improve machinability, and enhance wear resistance. Initial studies[8] were conducted on a wide variety of experimental copper and copper alloy MMCs for marine applications. The MMCs generally showed corrosion behavior that was similar to that of the monolithic alloys, although

corrosion rates were higher for some of the MMCs. More recent corrosion studies have also added additional insight to corrosion mechanisms of copper MMCs.

Effect of Graphite

Copper MMCs have been reinforced with graphite particles and fibers. The particulate MMCs have been developed for sliding electrical contact materials,[160] and improved machinability for lead-free copper alloys.[161] Fiber reinforced MMCs have been developed for applications requiring reduced-weight and high thermal conductivity.[162] Highly graphitized fibers have very high thermal conductivity, exceeding that of silver.[3]

Sun Orth, and Wheat[163] examined the corrosion behavior of pure copper MMCs with 1.2, 5, 15, 25, and 40 vol% graphite particles and fiber-reinforced pure copper MMCs with 50 vol% graphite fibers in deaerated and aerated 3.5 wt% NaCl solutions. The corrosion potential of the particulate reinforced MMCs became more noble with increasing graphite content in both the deaerated and aerated solutions, as would be expected by increasing the content of the noble graphite particles. Polarization resistance generally decreased, with a few exceptions, with increasing graphite content in both dearated and aerated solutions. This indicated that corrosion rates generally increased with graphite content, assuming that cathodic and anodic Tafel slopes remained relatively constant for the different MMC specimens (i.e., 1.2 through 40 vol% graphite). The corrosion rate is a function of both the polarization resistance and Tafel slopes. The 6% porosity of the MMCs may have also been a factor regarding corrosion behavior. The corrosion potential of the fiber-reinforced MMC (50 vol% graphite fiber) was approximately as noble as the particulate MMC with 40 vol% graphite in the aerated solution, but was significantly more active than the particulate composite in the deaerated solution. This finding could be expected if the hydrogen evolution kinetics on the graphite fiber were significantly different from that of the graphite particles.

Rohatgi, Nath, Kim, and Agrawal[161] studied C90300 copper alloy reinforced with approximately 1–10 vol% graphite particles and 1 wt% Ti, added to enhance wettability of the graphite. The corrosion potentials of the MMCs increased with increasing graphite content in an aqueous solution containing ferric chloride, copper sulfate, and hydrochloric acid. Gravimetric measurements were made on specimens immersed for one year in an aqueous solution containing sodium bicarbonate, magnesium chloride, calcium chloride, sodium sulfate, and sodium chloride. The results showed insignificant weight gain (<0.25%), indicating that the MMCs were resistant to corrosion in the test solution.

Effect of Silicon Carbide

Lee, Lee, and Lin[164] examined the corrosion behavior of pure copper MMCs reinforced with 0, 5, 10, and 20 vol% SiC particles in a 5 wt% NaCl solution. The porosity of the materials ranged from 2.2% to 3.5%, and generally increased with increasing SiC content. Corrosion potentials became more active, and corrosion current densities increased with increasing SiC content. The corrosion morphology indicated that there was significant corrosion at SiC-copper interfaces. Voids caused by porosity and SiC-copper interfaces both increased with increasing SiC content. Hence, the decrease in E_{CORR} with increasing SiC content is likely to have been caused by an increase in anodic currents from voids and SiC-copper interfaces. The SiC particles could also serve as cathodes, but because of their relatively high electrical resistivity, they are not as effective, for example, as graphite. Hence, any increases in cathodic currents with the increase in SiC content may not have been sufficient to shift E_{CORR} to positive values and to overcome the effect of the higher anodic currents.

Effect of Alumina

A copper MMC reinforced with 2.7 vol% Al_2O_3 was studied by Sun and Wheat[165] in deaerated and aerated 3.5 wt% NaCl. The corrosion potentials of the MMC were slightly more active (i.e., 0.01 to 0.02 V) than monolithic pure copper. The corrosion rates of the MMCs were comparable to monolithic copper. A galvanic effect with Al_2O_3 was not expected because of its insulative nature.

ZINC MMCs

Zinc MMCs have been developed[166] for potential use as bearing materials. Zinc has a density of 7.14 g/cm^3. An MMC with a ZA-27 zinc alloy matrix was cast with 1, 3, and 5 wt% graphite particles ranging in sizes from 100–150 µm. Zinc alloys are known to have excellent wear and bearing characteristics.[167] Gravimetric corrosion tests were conducted at 23 °C in (1) SAE 40-grade lubricating oil that had been in service for 6 months in an internal combustion engine and (2) 1 N HCl. The MMCs did not corrode in the previously used lubricating oil. Interestingly, in the 1 N HCl, corrosion rates decreased with higher content of graphite, which is a noble conductor that can induce galvanic corrosion. Several hypotheses have been made,[166] such as the presence of the graphite network hindering the reaction between HCl and the matrix. Another possibility is that zinc ions in solution, acting as a cathodic inhibitor,[168] eventually may have precipitated as zinc hydroxide on the cathodic graphite particles if the local pH resided in the correct range. This would also explain the decreasing corrosion rates with time that was observed. Similar behavior was noticed in graphite-aluminum couples in solutions containing zinc chloride.[169]

Methods for Evaluating Corrosion Damage

Tests to evaluate corrosion damage of conventional monolithic alloys are not always applicable to MMCs. Under some circumstances, the reinforcement constituents that are left in relief after matrix corrosion may interfere with measurements. There have been relatively few studies on MMC corrosion in comparison to monolithic metals. Tests that have been more commonly used for MMCs are gravimetric and those that assess loss of mechanical properties. The researcher should be able to use other tests that have been developed for monolithic alloys; however, data must be analyzed carefully to ensure that test results are valid because special problems are sometimes associated with MMCs.

Further details regarding corrosion analysis of MMCs are provided in the next section.

DEPTH OF ATTACK

Depth of attack can be used to assess corrosion damage in MMCs. It may be more difficult, however, to assess the penetration depth in MMCs compared with that in monolithic metals because reinforcement constituents that are left in relief can prevent a depth gage from contacting the matrix surface and thus prevent the true depth of penetration from being measured. In particulate MMCs, the interference may be attenuated because reinforcement particles are free to detach from the matrix as they are undercut by corrosion. When reinforcements interfere with mechanical measurements, depth of penetration can be assessed metallographically. Samples may be mounted and polished, and penetration measurements can be made with a microscope and a calibrated eye piece. Details for determining penetration depth are available in ASTM G46, *Standard Guide for Examination and Evaluation of Pitting Corrosion*.

GRAVIMETRIC

Gravimetric evaluation is often used to assess corrosion damage. Special problems, however, can be encountered when using gravimetric evaluation for MMCs. Results obtained from MMCs can be misleading because corrosion is sometimes accompanied by weight gain. MMC samples can experience weight gain when corrosion products and moisture are trapped in composite microstructures, resulting in swelling of the MMC. Swelling of MMCs appears to be more troublesome with fiber-reinforced composites, as opposed to particulate composites. For details on gravimetric measurements, reference should be made to ASTM G1, *Standard Practice for Preparing, Cleaning, and Evaluating Corrosion Test Specimens*. This standard addresses metal alloys and references should be followed for the matrix alloy in the MMC.

LOSS IN MECHANICAL PROPERTIES

Corrosion damage of MMCs is sometimes assessed by measuring a loss in strength. Changes in strength are measured before and after exposure to corrosion environments. These tests can be useful for assessing corrosion damage in MMCs when corrosion appears to be mild on the surface but penetrates deep into the bulk along diffusion bonds or reinforcement-matrix interfaces. Test specimens may take on various shapes and sizes, depending on the form of the stock material (e.g., wire, sheet, rod). Reference should be made to ASTM G1 (section 7.3.2) and G46 (section 7.5).

Tests for Specific Corrosion Types

Various tests can be performed on MMCs to obtain specific information on corrosion behavior. Tests used for monolithic metals can be applied to MMCs with some success. Because MMCs may have properties significantly different from those of monolithic metals, conventional tests developed for monolithic metals may not always produce sought-after results when used to test MMCs.

DETERMINATION OF DISSOLUTION BEHAVIOR USING POLARIZATION TECHNIQUES

Dissolution behavior of MMCs can be determined by anodic polarization measurements. To ensure that the polarization setup is working properly, it should be checked against ASTM G5, *Standard Reference Test Method for Making Potentiostatic and Potentiodynamic Anodic Polarization Measurements*. The dissolution behavior of MMCs in specific environments can be determined by generating anodic polarization diagrams of the MMC. To determine the extent of matrix dissolution versus that of reinforcement dissolution, polarization diagrams of monolithic matrix metal and reinforcement constituents should be generated separately. The individual diagrams of the MMC constituents are then used to generate a polarization diagram of the MMC (here called a mixed-electrode diagram) using the mixed-potential theory. If good correlation exists between the polarization diagram of the actual MMC and the mixed-electrode diagram, the fraction of dissolution current originating from the matrix and from the reinforcement constituents can be determined. The results can be verified by examining the corrosion morphology of the MMC. For example, the anodic polarization diagrams of an actual 40 vol% SiC_{MF}/Ti-15-3-3-3 MMC and that generated using the MMC constituents and the mixed-potential theory corresponding to a 3.15 wt% NaCl solution were in good agreement (fig. 16). Corrosion morphology studies have confirmed that the high anodic currents measured on the MMC corresponded to oxidation of the carbon cores and carbon-rich surface of the SiC_{MF}.[158]

If there is poor correlation between the polarization diagram of the actual MMC and the mixed-electrode diagram, the discrepancy in dissolution behavior might be caused by formation of interphases or contaminants introduced in the MMC microstructure during processing. For example,[116] figure 17 shows an anodic, mixed-electrode diagram generated from polarization diagrams of graphite fiber and 6061-T6 aluminum exposed to 0.5 M Na_2SO_4. The mixed-electrode diagram shows that 6061-T6

FIG. 16 Anodic polarization diagrams of SiC monofilament (cross section exposed), monolithic Ti-15-3-3-3, and SiC_{MF} (40 vol. %)/Ti-15-3-3-3 MMC exposed to deaerated 3.15 wt% NaCl at 30°C. Scan rate = 0.1 mV/s. A diagram for a composite consisting of 40 vol.% SiC monofilament was generated on the basis of the mixed-potential theory.

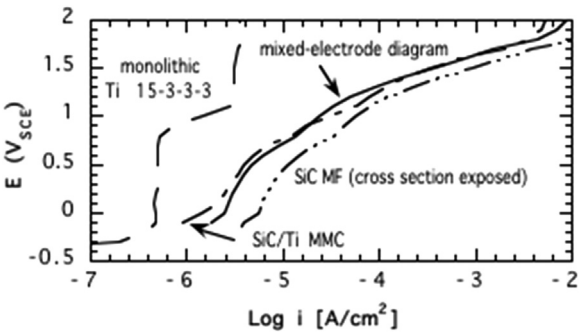
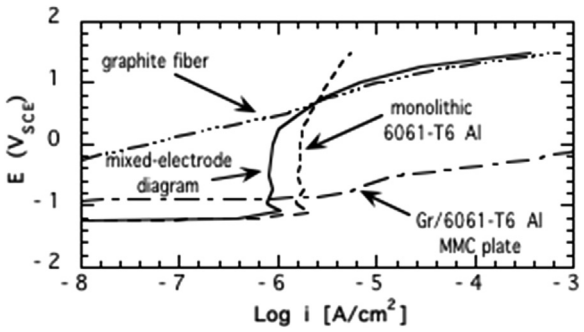


FIG. 17 Anodic polarization diagrams of pitch-based graphite fiber (cross section exposed), monolithic 6061-T6 aluminum, and Gr(50 vol. %)/6061-T6 Al MMC plate exposed to deaerated 0.5 M Na_2SO_4 at 30°C. Scan rate = 0.1 mV/s. A diagram for a composite consisting of 50 vol.% graphite and 6061-T6 aluminum was generated on the basis of the mixed-potential theory.



aluminum passivates during the anodic scan. The anodic polarization diagram of an actual 40 vol% Gr/6061-T6 Al MMC, however, exposed to the same solution shows that pitting is induced at approximately −0.6 V_{SCE} (fig. 17). The unexpected pitting was found to be caused by residual microstructural chloride[116] that was unintentionally introduced into the microstructure during processing.[170] Buonanno[171] later verified that the anodic polarization diagram of chloride-free Gr/Al MMCs traces the mixed-electrode diagram.

GALVANIC CORROSION BETWEEN MATRIX AND REINFORCEMENT CONSTITUENTS UNDER IMMERSED CONDITIONS

Galvanic corrosion between the matrix and reinforcement constituents can be determined by several methods. The mixed-potential theory can be used with polarization data of the matrix metal and reinforcement constituents to estimate galvanic-corrosion currents and potentials. The intersection of the anodic polarization curve of the matrix metal with the cathodic polarization curve of a noble reinforcement constituent gives the galvanic-corrosion current and potential (refer to appendix of ASTM G82, *Standard Guide for Development and Use of a Galvanic Series for Predicting Galvanic Corrosion Performance*). When using this method, note that changes in electrochemical behavior of MMC constituents caused by MMC processing cannot be taken into consideration if virgin MMC constituents are used to obtain polarization data. The behavior predicted using virgin MMC constituents could be quite different compared with that of the actual MMC. Timonova et al.[23] showed that BFs extracted from a magnesium matrix supported cathodic-current densities that were about five times that of virgin BFs (see the subsection "Magnesium MMCs: Effect of Boron").

The galvanic-corrosion rate can also be determined from the open-circuit corrosion current of actual MMCs. To obtain the galvanic-corrosion current density, the local-corrosion current density[172] should be subtracted from the open-circuit current (of the MMC) that has been normalized with respect matrix area. One difficulty would be to obtain an accurate estimation of the local-corrosion current density.

The ZRA technique (ASTM G71, *Standard Guide for Conducting and Evaluating Galvanic Corrosion Tests in Electrolytes*) can be used to measure galvanic-corrosion currents between monolithic pieces of the matrix metal and reinforcement constituents. One advantage of this technique is that galvanic-corrosion currents can be measured over long periods of time. If virgin MMC constituents are used, changes due to processing cannot be accounted for. Pohlman[24] showed that galvanic-corrosion currents between aluminum alloys and BFs extracted from an aluminum MMC were significantly greater than currents between aluminum alloys and virgin BFs. Aluminum borides that formed on the BFs during MMC processing were responsible for increasing galvanic-corrosion currents (see the subsection "Aluminum MMCs: Effect of Boron").

These three methods can be used to estimate galvanic-corrosion behavior. Advantages and disadvantages are associated with each method. Some comparisons between these methods have been made for Gr/Al[37] and SiC/Mg MMCs.[133]

UNIFORM CORROSION

Uniform corrosion of MMC matrices can be expected in environments that attack the matrix metal uniformly. In continuous-fiber MMCs, however, fibers will be left in relief as the matrix corrodes, whereas, in particulate MMCs, reinforcement particles fall free as they are undercut. Uniform corrosion rates of MMCs may be greater than that of the monolithic matrix alloys because of galvanic action between the matrix and reinforcement constituents.

MMCs should be exposed to environments of interest and then inspected. If corrosion is uniform, corrosion rates can be assessed using recommendations in ASTM G1. Electrochemical measurements also can be used to determine uniform corrosion rates. Refer to ASTM G102, *Standard Practice for Calculation of Corrosion Rates and Related Information from Electrochemical Measurements*. Note that when determining matrix corrosion rates, the corrosion current should be normalized with respect to the matrix area if reinforcements are inert.

PITTING CORROSION

MMCs are susceptible to pitting in environments that induce pitting in the matrix metal. These environments usually contain halides and are oxidizing. In MMCs that have noble reinforcement constituents, galvanic corrosion between reinforcement constituent and matrix can accelerate pitting compared with the monolithic matrix alloy. The presence of the reinforcement constituents also may influence pitting by altering MMC microstructures. In SiC_W/Al MMCs, for example, pits were more numerous and much smaller in size compared with pits on monolithic alloys.[71] Apparently, the SiC whiskers enhance the precipitation of the intermetallic particles upon which pits nucleate[71] (see subsection "Aluminum MMCs: Effect of Silicon Carbide").

MMC specimens should be exposed to environments of interest. The degree of pitting can be assessed using ASTM G46. Pitting potentials may be obtained by generating anodic

polarization diagrams of the MMCs. Refer to ASTM G5 to ensure that the electrochemical setup is working properly. Electrochemical impedance spectroscopy also has been used to detect the onset of pitting in some MMCs.[173]

STRESS CORROSION

Studies on stress-corrosion behavior of MMCs have been limited. Results for some aluminum and magnesium MMCs are summarized in the subsections on "Aluminum MMCs: Effect of Reinforcement Constituents on Stress Corrosion," and "Magnesium MMCs: Effect of Al_2O_3," respectively. The type of tests that can be used will depend to some degree on the form in which the MMC is produced and whether or not the MMC can be precracked. Some types of MMCs are produced only in the form of relatively thin panels (e.g., less than about 0.25 cm), whereas other types are available in bars or tubes. It is sometimes impossible to properly precrack unidirectional, continuous-fiber MMCs because cracks do not always grow perpendicular to the direction of applied stress.[174]

A variety of stress-corrosion testing methods, using unnotched, notched, and precracked specimens have been well documented.[175] The following ASTM standards are also helpful in developing a stress-corrosion testing program: ASTM E399, *Standard Test Method for Linear-Elastic Plane-Strain Fracture Toughness of Metallic Materials*; ASTM G30, *Standard Practice for Making and Using U-Bend Stress-Corrosion Test Specimens*; ASTM G38, *Standard Practice for Making and Using C-Ring Stress-Corrosion Test Specimens*; ASTM G39, *Standard Practice for Preparation and Use of Bent-Beam Stress-Corrosion Test Specimens*; and ASTM G49, *Standard Practice for Preparation and Use of Direct Tension Stress-Corrosion Test Specimens*.

CORROSION FATIGUE

Relatively few studies on corrosion fatigue of MMCs have been conducted. Results for Gr/Al and SiC/Al MMCs are summarized in the subsection "Aluminum MMCs: Effect of Reinforcement Constituents on Corrosion Fatigue." An appropriate testing program will depend on the form of the MMC and the ability to precrack specimens, which is a problem in some MMCs. The practices for fatigue testing in section 3, "Metals Test Methods and Analytical Procedures," vol. 03.01, *ASTM Book of Standards*,[176] should be helpful in selecting a testing scheme. Annex A.1 in ASTM E647, *Standard Test Method for Measurement of Fatigue Crack Growth Rates*, is particularly useful when doing corrosion-fatigue tests in aqueous environments.

Comparison of Corrosion Behavior between MMCs

To some degree, the corrosion resistance of MMCs can be ranked based on the intrinsic corrosion resistance of the matrix alloy. Within an MMC group, corrosion resistance can be further ranked based on the type of reinforcement constituent. For example, MMCs reinforced with graphite would have less resistance to corrosion than those reinforced with Al_2O_3, because the degree of galvanic corrosion between the reinforcement and matrix. It should be emphasized, however, that ranking by generalities may be misleading because MMC corrosion properties can be highly sensitive to the effects of processing conditions. The formation of interphases, presence of microstructural contaminants, and microstructural changes in the matrix metal caused by reinforcement constituents may significantly deteriorate corrosion resistance. Two identical types of MMCs, but fabricated by different methods, may have different corrosion resistances.

In the most general terms, titanium MMCs have the best resistance to corrosion because of the general and localized corrosion resistance of titanium. Al MMCs reinforced with semiconductors or insulators (i.e., SiC, Al_2O_3, and mica) were ranked next due to lack of significant galvanic action between reinforcement and matrix. Al MMCs reinforced with conductors (i.e., graphite, carbon-coated SiC_{MF}) are more susceptible to corrosion due to galvanic coupling with the reinforcements. Mg MMCs were ranked the least resistant because of the highly reactive magnesium matrix. However, Mg MMC reinforced with calcium compounds for biodegradable orthopedic implant materials show improved corrosion resistance compared to the monolithic Mg because of the formation of hydroxyapatite films. Lead as well as depleted uranium, stainless steel, copper, and zinc MMCs were not ranked because these MMCs or testing conditions were specialized or limited. This assessment is general and exceptions are likely.

ACKNOWLEDGMENTS

The author is grateful to many people and organizations for support and for funding in the area of MMCs over a number of years. The author acknowledges the following individuals and original affiliations for support: Dr. R. M. Latanision, Massachusetts Institute of Technology; Dr. A. J. Sedriks of the Office of Naval Research; Dr. S. P. Rawal of Martin Marietta Denver Aerospace; Dr. B. A. MacDonald of the National Science Foundation; Dr. Reynold Kagiwada and Mr. Aaron Oki of TRW, Inc.; Mr. M. A. Mittnick of Textron Specialty Materials; Mr. Tom Rodjom of Alcoa Inc.; Dr. Herve Deve of 3M Corporation; Mr. Brian DeForce and Mr. Robert Mason of Concurrent Technologies Corporation; Dr. Joseph Argento, Mr. John Theis, Mr. Robert Zanowicz, and Mr. Donald Skelton of the Army Corrosion Office; Mr. Lance Miyahara, Hawaiian Electric Company; and Mr. Matthew Koch, US Marine Corps, Corrosion Prevention and Control Program.

References

1. J. W. Weeton, D. M. Peters, and K. L. Thomas, *Guide to Composite Materials* (Metals Park, OH: American Society for Metals, 1987.

2. G. B. Park and D. A. Foster, "Metal Coated Fibers for Metal Matrix Composites," in *International Technical Conference Proceedings, SUR/FIN'90* (Boston, MA: American Electroplaters and Surface Finishers Society, 1990), 1349–1360.

3. W. C. J. Harrigan, "*Metal Matrix Composites*," in *Metal Matrix Composites: Processing and Interfaces* (New York: Academic Press, 1991).

4. K. Akutagawa, H. Ohtsuki, J. Hasegawa, and M. Miyazaki, "Reduction of the Friction Coefficient of Metal Matrix Composite under Dry Conditions," SAE Transactions, Vol. 96, Section 2 (1987): 286–293.

5. Y. Liu, P. K. Rohatgi, S. Ray, and T. L. Barr, "Influence of Graphite Shape and Flake Orientation on Friction and Wear Characteristics of Al-50% Graphite Composites," in *Proceedings of the 1991 International Conference on Composite Materials, ICCM/8* (Covina, CA: Society for the Advancement of Material and Process Engineering, 1991), 20H1–20H14.

6. T. Lim, C. S. Lee, Y. H. Kim, and K. S. Ha, "Mechanical Properties at Elevated Temperatures and Wear Behavior of Aluminum Matrix Composite Materials," in *Proceedings of the 1991 International Conference on Composite Materials, ICCM/8* (Covina, CA: Society for the Advancement of Material and Process Engineering, 1991), 20E1–20E14.

7. M. Metzger and S. G. Fishman, "Corrosion of Aluminum-Matrix Composites. Status Report," *Industrial and Engineering Chemistry Product Research and Development* 22 (1983): 296–302.

8. D. M. Aylor, "*Corrosion of Metal Matrix Composites*," in *Metals Handbook*, 9th ed. (Metals Park, OH: ASM International, 1987), 859–863.

9. P. P. Trzaskoma, "Corrosion," in *Metal Matrix Composites: Mechanisms and Properties*, ed. E. R. K. and R. J. Arsenault (New York: Academic Press, 1991), 383–404.

10. A. Turnbull, "Review of Corrosion Studies on Aluminum Metal Matrix Composites," *British Corrosion Journal* 27, no. 1 (1992): 27–35.

11. K. A. Lucas and H. Clarke, *Corrosion of Aluminum-Based Metal Matrix Composites* (New York: Wiley, 1993).

12. L. H. Hihara and R. M. Latanision, "Corrosion of Metal Matrix Composites," *International Materials Review* 39, no. 6 (1994): 245–264.

13. R. H. Jones, "Metal Matrix Composites," in *Environmental Effects on Engineered Materials*, ed. R. H. Jones (Germany: Marcel Dekker, 2001), 379–390.

14. L. H. Hihara, "Corrosion of Metal-Matrix Composites," in *ASM Handbook, vol. 13B, Corrosion: Materials*, ed. S. D. Cramer and B. S. Covino Jr. (Materials Park, OH: ASM International, 2005), 526–542.

15. M. E. Buck and R. J. Suplinskas, "Continuous Boron Fiber MMC's," in *Engineered Metal Handbook: Composites*, vol. 1 (Materials Park, OH: ASM, 1987), 851–857.

16. A. M. Tsirlin, "Boron Filaments," in *Strong Fibres (Handbook of Composites, Vol. 1)*, ed. W. Watt and B. V. Perov (New York: Elsevier Science Publishers, 1985), 155–199.

17. M. M. Schwartz, *Composite Materials Handbook* (New York: McGraw Hill, 1984).

18. W. H. Kim, M. J. Koczak, and A. Lawley, "Interface Reaction and Characterization in B/Al Composites," in *Proceedings of the 1978 International Conference on Composite Materials, ICCM/2* (Toronto, Canada: Metallurgical Society of AIME, 1978): 487–505.

19. N. de Zoubov, E. Deltombe, and M. Pourbaix, "Boron," in *Atlas of Electrochemical Equilibria in Aqueous Solutions*, ed. M. Pourbaix (Houston, TX: NACE International, 1974), 158–167.

20. M. C. Porter and E. G. Wolff, "Corrosion of Boron-Metal Composites" in *Advances in Structural Composites, 12th National Symposium and Exhibit* (Anaheim, CA: Society for the Advancement of Material and Process Engineering, 1967), paper AC-14.

21. A. V. Bakulin, V. V. Ivanov, and V. V. Kuchkin, "Corrosive Behavior of Boron-Aluminum Composite Material," *Zaschita Metallov* 14, no. 1 (1978): 102–104.

22. A. J. Sedriks, J. A. Green, and D. L. Novak, "Corrosion Behavior of Aluminum-Boron Composites in Aqueous Chloride Solutions," *Metallurgical Transactions* 2 (1971): 871–875.

23. M. A. Timonova, G. I. Spiryakina, V. F. Stroganova, and L. A. Zolotarev, "Corrosion Resistance and Electrochemical Properties of a Magnesium Matrix Composite Material," *Mettallovedenie i Termicheskaya Obrabotka Metallov* 11 (1980): 33–35.

24. S. L. Pohlman, "Corrosion and Electrochemical Behavior of Boron/Aluminum Composites," *Corrosion* 34 (1978): 156–159.

25. V. G. Gorbunov, V. D. Parshin, and V. V. Pamin, *Russian Castings Production* (Aug 1974): 348.

26. S. Biswas, A. Shantharam, N. A. P. Rao, K. Narayana Swamy, P. K. Rohatgi, and S. K. Biswas, "Performance of Graphic Aluminium Particulate Composite Materials," *Tribology International* 13, no. 4 (1980): 171–176.

27. J. Van Muylder and M. Pourbaix, "Carbon," in *Atlas of Electrochemical Equilibria in Aqueous Solutions*, ed. M. Pourbaix (Houston, TX: NACE International, 1974), 449–457.

28. L. H. Hihara, *Corrosion of Aluminum-Matrix Composites* (Cambridge, MA; MIT, 1989).

29. K. Kinoshita, *Carbon, Electrochemical and Physiocochemical Properties* (New York: Wiley, 1988).

30. W. F. Czyrklis, "Corrosion Evaluation of Graphite-Aluminum and Graphite-Magnesium Metal-Matrix Composites," in *Conference Proceedings of Corrosion 85* (Boston, MA: NACE International, 1985).

31. S. L. Coleman, V. D. Scott, and B. McEnaney, "Corrosion Behaviour of Aluminium-Based Metal Matrix Composites," *Journal of Materials Science* 29 (1994): 2826–2834.

32. I. Dutta, L. R. Elkin, and J. D. King, "Corrosion Behavior of a P130x Graphite Fiber Reinforced 6063 Aluminum Composite Laminate in Aqueous Environments," *Journal of the Electrochemical Society* 138, no. 11 (1991): 3199–3209.

33. O. P. Modi, M. Saxena, B. K. Prasad, A. K. Jha, and A. H. Yegnesawaran, "Role of Alloy Matrix and Dispersoid on Corrosion Behavior of Cast Aluminum Alloy Composites," *Corrosion* 54, no. 2 (1998): 129–134.

34. D. L. Dull, W. C. J. Harrigan, and M. F. Amateau, *Final Report, The Effect of Matrix and Fiber Composition on Mechanical Strength*

and Corrosion Behavior of Graphite-Aluminum Composites (El Segundo, CA: Aerospace Corporation, 1977).

35. R. H. Brown and R. H. Mears, "The Electrochemistry of Corrosion," *Transactions of the Electrochemical Society* 74 (1938): 495–518.

36. L. C. Dash, *The Mechanisms of Corrosion and Corrosion Control of Aluminum/Graphite Metal Matrix Composites* (Columbus: Ohio State University, 1988).

37. L. H. Hihara and R. M. Latanision, "Galvanic Corrosion of Aluminum-Matrix Composites," *Corrosion* 48, no. 7 (1992): 546–552.

38. M. Saxena, A. K. Jha, and G. S. Upadhyaya, "Corrosion Behaviour of Sintered 6061 Aluminum Alloy-Graphite Particle Composites," *Journal Materials Science* 28 (1993): 4053–4058.

39. M. Saxena, B. K. Prasad, and T. K. Dan, "Corrosion Characteristics of Aluminum Alloy Graphite Particulate Composite in Various Environments," *Journal Materials Science* 27 (1992): 4805–4812.

40. S. Tiwari and L. H. Hihara, "Development of a Corrosion Model to Correlate the Atmospheric Corrosion Rate of a Carbon-Fiber Reinforced Aluminum MMC to Weather and Environmental Parameters," *Journal of The Electrochemical Society* 161, no. 9 (2014): C382–C388.

41. H. Ding and L. H. Hihara, "Corrosion Morphologies of Aluminum-Based Materials in Solutions Containing Nickel or Cobalt Cations," *ECS Transactions* 16, no. 43 (2009): 9–18.

42. T. R. Schrecengost, B. A. Shaw, R. G. Wendt, and W. C. Moshier, "Nonequilibrium Alloying of Graphite-Reinforced Aluminum Metal Matrix Composites," *Corrosion* 49, no. 10 (1993): 842–849.

43. R. G. Wendt, W. C. Moshier, B. Shaw, P. Miller, and D. L. Olson, "Corrosion-Resistant Aluminum Matrix for Graphite-Aluminum Composites," *Corrosion* 40, no. 11 (1994): 819–826.

44. H. J. Becher, "Aluminum Carbide Al_4C_3," in *Handbook of Preparative Inorganic Chemistry*, vol. 1, ed. G. Brauer (New York: Academic Press, 1963), 832.

45. E. G. Kendall, "Development of Metal-Matrix Composites Reinforced with High-Modulus Graphite Fibers," in *Metal Matrix Composites*, ed. K. G. Kreider (New York: Academic Press, 1974), 319–397.

46. K. I. Portnoi, N. I. Timofeeva, A. A. Zabolotskii, V. N. Sakovich, B. F. Trefilov, M. Kh. Levinskaya, and N. N. Polyak, "Dependence of the Properties of a Carbon-Aluminum Composite Material on Its Carbide Phase Content," *Poroshkovaya Metallurgiya* 218, no. 2 (1981): 45–49.

47. L. H. Hihara, "Corrosion of Aluminum-Matrix Composites," *Corrosion Reviews* 15, nos. 3–4 (1997): 361–386.

48. D. M. Aylor and P. J. Moran, "Effect of Reinforcement on Pitting Behavior of Aluminum Based Metal Matrix Composites," *Journal of the Electrochemical Society* 132 (1985): 1277–1281.

49. B. Wielage and A. Dorner, "Corrosion Studies on Aluminum Reinforced with Uncoated and Coated Carbon Fibres," *Composites Science and Technology* 59 (1999): 1239–1245.

50. Y. Shimizu, T. Nishimura, and I. Matsushima, "Corrosion Resistance of Al-Based Metal Matrix Composites," *Materials Science and Engineering A* 198 (1995): 113–118.

51. *Advanced Composite Materials Corporation Stablcel™* SiC/Al MMC Foam, http://web.archive.org/web/20210604101407/https://www.trademarkelite.com/trademark/trademark-detail/74108311/STABLCEL

52. N. Ichinose, *Introduction to Fine Ceramics* (New York: Wiley, 1987).

53. M. Rix, "Development of Silicon Carbide Monofilaments for the Reinforcement of Metal Matrix Composites," in *Mechanical Engineering Science* (Surrey, UK: University of Surrey, 2018).

54. H. Ding and L. H. Hihara, "Galvanic Corrosion in Metal-Matrix Composites Containing Semiconducting Constituents," *Journal of The Electrochemical Society* 156, no. 12 (2009): C422–C427.

55. P. P. Trzaskoma, E. McCafferty, and C. R. Crowe, "Corrosion Behavior of SiC/Al Metal Matrix Composites," *Journal of the Electrochemical Society* 130 (1983): 1804–1809.

56. L. Díaz-Ballote, L. Veleva, M. A. Pech-Canul, M. I. Pech-Canul, and D. O. Wipf, "Activity of SiC Particles in Al-Based Metal Matrix Composites Revealed by SECM," *Journal of The Electrochemical Society* 151, no. 6 (2004): B299–B303.

57. K. D. Lore and J. S. Wolf, "An Investigation of the Aqueous Corrosion of SiC-Aluminum Metal Matrix Composites," in *Extended Abstracts, Vol. 81* (Denver, CO: The Electrochemical Society, 1981): 387–388.

58. H. Sun, E. Y. Koo, and H. G. Wheat, "Corrosion Behavior of SiC_p/6061 Al Metal Matrix Composites," *Corrosion* 47, no. 10 (1991): 741–753.

59. O. P. Modi, M. Saxena, B. K. Prasad, A. H. Yegnesawaran, and M. L. Vaidya, "Corrosion Behaviour of Squeeze-Cast Aluminum Alloy-Silicon Carbide Composites," *Journal of Materials Science* 27 (1992): 3897–3902.

60. G. A. Hawthorn, "Outdoor and Laboratory Corrosion Studies of Aluminum Metal-Matrix Composites," in *Mechanical Engineering* (master's thesis, University of Hawaii at Manoa, 2004).

61. A. J. Griffiths and A. Turnbull, "An Investigation of the Electrochemical Polarisation Behaviour of 6061 Aluminum Metal Matrix Composites," *Corrosion Science* 36, no. 1 (1994): 23–35.

62. I. Aziz and Q. Zhang, "Evaluation of Pitting Corrosion of the SiCp/5A06 Aluminum Metal Composite in 3.5% NaCl Solution by Means of Electrochemical Impedance Spectroscopy (EIS)," *International Journal of Modern Physics B* 23, nos. 6–7 (2009): 1497–1502.

63. I. Aziz, Q. Zhang, Z. Tang, and Z. Jiang, "Electrochemical Behavior and Corrosion Morphology of SiCp/5A06 Aluminum Alloy Composite," *International Journal of Modern Physics B* 24, nos. 15–16 (2010): 2261–2266.

64. D. S. Qian, X. Zhong, T. Hashimoto, and Z. Liu, "Effect of Reinforcements on the Corrosion Behavior of SiCp/AA2124 Metal Matrix Composites," *Corrosion* 71, no. 9 (2015): 1083–1092.

65. Y. L. Cheng, Z. H. Chen, H. L. Wu, and H. M. Wang, "The Corrosion Behaviour of the Aluminum Alloy 7075/SiCp Metal Matrix

Composite Prepared by Spray Deposition," *Materials and Corrosion* 58, no. 4 (2007): 280–284.

66. S. L. Golledge, J. Kruger, and C. M. Dacres, "Effect of Anodic Film Properties on the Corrosion Behaior of SiC/Al Metal Matrix Composites," in *Extended Abstracts*, Abstract No. 146 (Las Vegas, NV: The Electrochemical Society, 1985), 227–228.

67. G. W. Roper and P. A. Attwood, "Corrosion Behaviour of Aluminum Matrix Composites," *Journal Materials Science* 30 (1995): 898–903.

68. C. Monticelli, F. Zucchi, F. Bonollo, G. Brunoro, A. Frignani, and G. Trabanelli, "Application of Electrochemical Noise Analysis to Study the Corrosion Behavior of Aluminum Composites," *Journal of the Electrochemical Society* 145, no. 2 (1995): 405–410.

69. P. C. R. Nunes and L. V. Ramanathan, "Corrosion Behavior of Alumina-Aluminum and Silicon Carbide-Aluminum Metal-Matrix Composites," *Corrosion* 51, no. 8 (1995): 610–617.

70. G. E. Kiourtsidis and S. M. Skolianos, "Corrosion Behavior of Squeeze-Cast Silicon Carbide-2024 Composites in Aerated 3.5 wt.% Sodium Chloride," *Materials Science and Engineering A* 248 (1998): 165–172.

71. P. P. Trzaskoma, "Pit Morphology of Aluminum Alloy and Silicon Carbide/Aluminum Alloy Metal Matrix Composites," *Corrosion* 46 (1990): 402–409.

72. M. M. Buarzaiga and S. J. Thorpe, "Corrosion Behavior of As-Cast, Silicon Carbide Particulate-Aluminum Alloy Metal-Matrix Composites," *Corrosion* 50, no. 3 (1994): 176–185.

73. R. C. Paciej and V. S. Agarwala, "Influence of Processing Variables on the Corrosion Susceptibility of Metal-Matrix Composites," *Corrosion* 44 (1988): 680–684.

74. S. R. Nutt and J. M. Duva, "A Failure Mechanism in Aluminum-Silicon Carbide Composites," *Scripta Metallurgica* 20 (1986): 1055–1058.

75. J. England and I. W. Hall, "On the Effect of the Strength of the Matrix in Metal-Matrix Composites," *Scripta Metallurgica* 20 (1986): 697–700.

76. M. S. Bhat, M. K. Surappa, and H. V. Sudhaker Nayak, "Corrosion Behaviour of Silicon Carbide Particle Reinforced 6061/A1 Alloy Composites," *Journal Materials Science* 26, no. 18 (1991): 4991–4996.

77. Z. Ahmad and B. J. Abdul Aleem, "Effect of Temper on Seawater Corrosion of an Aluminum-Silicon Carbide Composite Alloy," *Corrosion* 52, no. 11 (1996): 857–864.

78. B. Dikici and C. Tekmen, "A Comparative Study: the Combined Effect of the Cold Working and Age Hardening Processes on Pitting Behaviour of Al/SiC Metal Matrix Composites under Saline Environment," *Journal of Composite Materials* 50, no. 4 (2016): 471–480.

79. H.-Y. Yao and R.-Z. Zhu, "Interfacial Preferential Dissolution on Silicon Carbide Particulate/Aluminum Composites," *Corrosion* 54, no. 7 (1998): 499–503.

80. W. N. C. Garrard, "The Corrosion Behaviour of Aluminum-Silicon Carbide Composites in Aerated 3.5% Sodium Chloride," *Corrosion Science* 36, no. 5 (1994): 837–851.

81. T. Iseki, T. Kameda, and T. Maruyama, "Interfacial Reactions between Silicon Carbide (SiC) and Aluminum during Joining," *Journal of Materials Science* 19 (1984): 1692–1698.

82. N. Hong, M. A. Langell, J. Liu, O. Kizilkaya, and S. Adenwalla, "Ni Doping of Semiconducting Boron Carbide," *Journal of Applied Physics* 107 (2010): 024513-1–024513-7.

83. J. K. Park and J. P. Lucas, "Moisture Effect on SiC_p/6061 A1 MMC: Dissolution of Interfacial $A1_4C_3$," *Scripta Materialia* 37, no. 4 (1997): 511–516.

84. CoorsTek, *"Boron Carbide Overview,"* CoorsTek, CoorsTek, Inc., Golden, CO, 11 May 2021, http://web.archive.org/web/20210511074523/https://www.coorstek.com/english/materials/engineered-ceramics/boron-carbide/

85. L. H. Hihara, H. Ding, and Z. L. Lin, "Scanning Electrode Methods for Evaluating Corrosion of Metal Matrix Composites" (paper presentation, *Research in Progress Symposium, NACE Corrosion/2003*, NACE International, San Diego, CA, March 16–20, 2003).

86. Y. Han, D. Gallant, and X.-G. Chen, "Investigation on Corrosion Behavior of the Al-B4C Metal Matrix Composite in a Mildly Oxidizing Aqueous Environment," *Corrosion* 67, no. 11 (2011): 115005-1–115005-11.

87. Y.-M. Han and X.-G. Chen, "Electrochemical Behavior of Al-B_4C Metal Matrix Composites in NaCl Solution," *Materials* 8 (2015): 6455–6470.

88. H. Ding and L. H. Hihara, "Localized Corrosion Currents and pH Profile over B4C, SiC, and Al2O3 Reinforced 6092 Aluminum Composites: I. In 0.5 M Na_2SO_4 Solution," *Journal of the Electrochemical Society* 152, no. 4 (2005): B161–B167.

89. G. Eranna, *Crystal Growth and Evaluation of Silicon for VLSI and ULSI*. (Boca Rotan, FL: CRC Press, 2014).

90. Z. J. Lin and L. H. Hihara. "Corrosion of Silicon/Aluminum Metal-Matrix Composites," (paper presentation, *Sixth Japan International SAMPE Symposium and Exhibition*, Tokyo, Japan, 1999).

91. H. Ding and L. H. Hihara, "Galvanic Corrosion and Localized Degradation of Aluminum-Matrix Composites Reinforced with Silicon Particulates," *Journal of The Electrochemical Society* 155, no. 5 (2008): C266–C233.

92. T. Donomoto, K. Funatani, N. Miura, and N. Miyake, *Ceramic Fiber Reinforced Piston for High Performance Diesel Engines* (Warrendale, PA: Society of Automotive Engineers, 1983).

93. R. E. Bolz and G. L. Tuve, *CRC Handbook of Tables for Applied Engineering Science* (Boca Raton, FL: CRC Press, 1973).

94. E. Deltombe, C. Vanleugenhaghe, and M. Pourbaix, "Aluminum," in *Atlas of Electrochemical Equilibria in Aqueous Solutions*, ed. M. Pourbaix (Houston, TX: NACE International, 1974), 168–176.

95. N. N. Greenwood and A. Earnshaw, *Chemistry of the Elements* (Oxford, UK: Pergamon Press, 1984).

96. C.-K. Fang, C. C. Huang, and T. H. Chuang, "Synergistic Effects of Wear and Corrosion for $A1_20_3$ Particulate-Reinforced 6061 Aluminum Matrix Composites," *Metallurgical and Materials Transactions A* 30A (1999): 643–651.

97. J. Zhu and L. H. Hihara, "Corrosion of Continuous Alumina-Fibre Reinforced Al–2 Wt.% Cu–T6 Metal–Matrix Composite in 3.15 wt.% NaCl Solution," *Corrosion Science* 52 (2010): 406–415.

98. R. U. Vaidya, D. P. Butt, L. E. Hersman and A. K. Zurek, "Effect of Microbiologically Influenced Corrosion on the Tensile Stress-Strain Response of Aluminum and Alumina-Particle Reinforced Aluminum Composite," *Corrosion* 53, no. 2 (1997): 136–141.

99. A. R. Champion, W. H. Krueger, H. S. Harlmann, and A.K . Dhingra, "Fiber FP Reinforced Metal Matrix Composites," in *Proceedings of the 1978 International Conference on Composite Materials, ICCM/2* (Toronto, Canada: Metallurgical Society of AIME, 1978): 883–904.

100. J. Y. Yang and M. Metzger, "Relation between Pitting and Structure in Experimental Al-Mg/Al_2O_3 Composites," Abstract No. 155 in *Extended Abstracts, Vol. 81* (Denver, CO: The Electrochemical Society, 1981): 389–390.

101. V. S. Agarwala, "Corrosion Behavior of Aluminum/Alumina Composite," Abstract No. 15 in *Extended Abstracts* (Montreal, Canada: The Electrochemical Society, 1982): 28.

102. L. Bertolini, M. F. Brunella, and S. Candiani, "Corrosion Behavior of a Particulate Metal-Matrix Composite," *Corrosion* 55, no. 4 (1999): 422–431.

103. P. K. Rohatgi, R. Asthana, and S. Das, "Solidification, Structures, and Properties of Cast Metal-Ceramic Particle Composites," *International Materials Review* 31 (1986): 115–139.

104. D. Nath, R. T. Bhat, and P. K. Rohatgi, "Preparation of Cast Aluminum Alloy-Mica Particle Composites," *Journal of Materials Science* 15 (1980): 1241–1251.

105. H. R. Clauser, *The Encyclopedia of Engineering Materials and Processes* (New York: Reinhold, 1963).

106. R. C. Weast, *CRC Handbook of Chemistry and Physics*, 67th ed. (Boca Rotan, FL: CRC Press, 1986).

107. D. Nath and T. K. G. Namboodhiri, "Corrosion of an Aluminum Alloy-Mica Particulate Composite in 3.5% Sodium Chloride," *Composites* 19 (1988): 237–243.

108. D. Nath and T. K. Namboodhiri, "Some Corrosion Characteristics of Aluminum-Mica Particulate Composites," *Corrosion Science* 29 (1989): 1215–1229.

109. P. K. Rohatgi, "Low-Cost, Fly-Ash-Containing Aluminum-Matrix Composites," *Journal of Metals* 46, no. 11 (1994): 55–59.

110. M. Ramachandra and K. Radhakrishna, "Synthesis-Microstructure-Mechanical Properties-Wear and Corrosion Behavior of an Al-Si (12%)—Flyash Metal Matrix Composite," *Journal of Materials Science* 40 (2005): 5989–5997.

111. J. M. Evans and D. M. Braddick, "Corrosion Behavior of Fiber-Reinforced Aluminum Composites," *Corrosion Science* 11 (1971): 611–614.

112. W. C. J. Harrigan and R. H. Flowers, "Graphite-Metal Composites Titanium-Boron Vapor Deposit Method of Manufacture," in *Failure Modes in Composites IV*, ed. J. A. Cornie and F. W. Crossman (Warrendale, PA: Metallurgical Society of AIME, 1979), 319–335.

113. M. G. Vassilaros, D. A. Davis, G. L. Steckel, and J. P. Gudas, "Marine Corrosion of Graphite/Aluminum Composites," in *Mechanical Behavior of Metal-Matrix Composites*, ed. J. E. Hack and M. F. Amateau (Warrendale, PA: Metallurgical Society of AIME, 1983), 335–352.

114. W. H. Pfeifer, "Corrosion of Graphite/Aluminum," in *Hybrid and Select Metal Matrix Composites: A State-of-the-Art Review*, ed. W. J. Renton (New York: American Institute of Aeronautics and Astronautics, 1977), 159–255.

115. D. M. Aylor and R. M. Kain, "Assessing the Corrosion Resistance of Metal Matrix Composite Materials in Marine Environments," in *Recent Advances in Composites in the United States and Japan*, ed. J. R. Vinson and M. Taya (Philadelphia, PA: ASTM International, 1985), 632–647.

116. L. H. Hihara and R. M. Latanision, "Localized Corrosion Induced in Graphite/Aluminum Metal-Matrix Composites by Residual Microstructural Chloride," *Corrosion* 47, no. 5 (1991): 335–340.

117. D. A. Davis, M. G. Vassilaros, and J. P. Gudas, "Corrosion Fatigue and Stress Corrosion Characteristics of Metal Matrix Composites in Seawater," *Materials Performance*, Vol. 21 (1982): 38–42.

118. L. E. Dardi and K. G. Kreider, "Effect of Salt Water and High-Temperature Exposure on Boron-Aluminum Composites," in *Composite Materials: Testing and Design (Third Conference)* (Philadelphia, PA: ASTM International, 1974), 269–283.

119. D. W. Berkeley, H. E. M. Sallam, and H. Nayeb-Hashemi, "The Effect of pH on the Mechanism of Corrosion and Stress Corrosion and Degradation of Mechanical Properties of AA6061 and Nextel 440 Fiber-Reinforced AA6061 Composites," *Corrosion Science* 40, nos. 2–3 (1998): 141–153.

120. C. Monticelli, F. Zucchi, G. Brunoro, and G. Trabanelli, "Stress Corrosion Cracking Behaviour of Some Aluminum-Based Metal Matrix Composites," *Corrosion Science* 39, nos. 10–11 (1997): 1949–1963.

121. G. E. Kiourtsidis and S. M. Skolianos, "Stress Corrosion Behavior of Aluminum Alloy 2024/Silicon Carbide Particles (SiC_p) Metal Matrix Composites," *Corrosion* 56, no. 6 (2000): 646–653.

122. H.-Y. Yao, "Effect of Particulate Reinforcing on Stress Corrosion Cracking Performance of a SiC_p/2024 Aluminum Matrix Composite," *Journal of Composite Materials* 33, no. 11 (1999): 962–970.

123. S. S. Yau and G. Mayer, "Fatigue of Metal Matrix Composite Materials," *Materials Science and Engineering* 82 (1986): 45–57.

124. D. F. Hasson, C. R. Crowe, J. S. Ahearn and D. C. Cooke, "Fatigue and Corrosion Fatigue of Discontinuous SiC/Al Metal Matrix Composites," in *Failure Mechanisms in High Performance Materials*, ed. J. G. Early, T. R. Shives, and J. H. Smith (Cambridge: Cambridge University Press, 1984), 147–156.

125. R. H. Jones, "Stress Corrosion Cracking of Metal Matrix Composites: Modeling and Experiment," in *Environmental Effects on Advanced Materials*, ed. R. H. Jones and R. E. Ricker (Warrendale, PA: Minerals, Metals and Materials Society, 1991), 283–295.

126. K. Minoshima, I. Nagashima, and K. Komai, "Corrosion Fatigue Fracture Behaviour of a SiC Whisker-Aluminum Matrix Composite under Combined Tension-Torsion Loading," in *Fatigue*

and Fracture of Engineering Materials and Structures 21, no. 12 (1998): 1435–1446.

127. R. F. Buck and A. W. Thompson, "Environmental and Frequency Effects on Fatigue Crack Growth Rates in Aluminum-Silicon Carbide Composites," in *Environmental Effects on Advanced Materials*, ed. R. H. Jones and R. E. Ricker (Warrendale, PA: Minerals, Metals, and Materials Society, 1991), 297–313.

128. H. H. Uhlig and R. W. Revie, *Corrosion and Corrosion Control*, 3rd ed. (New York: Wiley, 1985).

129. V. F. Stroganova and M. A. Timonova, "Mechanical and Corrosion Properties of Composite Material of the Magnesium-Boron System," *Metallovedenie i Termicheskaya Obrabotka Metallov* (1978): 44–46.

130. P. P. Trzaskoma, "Corrosion Behavior of a Graphite Fiber/Magnesium Metal Matrix Composite in Aqueous Chloride Solution," *Corrosion* 42 (1986): 609–613.

131. A. Bakkara and V. Neubert, "Corrosion Behaviour of Carbon Fibres/Magnesium Metal Matrix Composite and Electrochemical Response of Its Constituents," *Electrochimica Acta* 54 (2009): 1597–1606.

132. I. W. Hall, "Corrosion of Carbon-Magnesium Metal Matrix Composites," *Scripta Metallurgica* 21 (1987): 1717–1721.

133. L. H. Hihara and P. K. Kondepudi, "The Galvanic Corrosion of Silicon Carbide Monofilament/ZE41 Magnesium Metal-Matrix Composite in 0.5 M Sodium Nitrate," *Corrosion Science* 34 (1993): 1761–1772.

134. L. H. Hihara and P. K. Kondepudi, "Galvanic Corrosion between SiC Monofilament and Magnesium in NaCl, Na_2SO_4 and $NaNO_3$ Solutions for Application to Metal-Matrix Composites," *Corrosion Science* 36 (1994): 1585–1595.

135. F. Zucchi, G. Trabanelli, V. Grassi, and A. Frignani, "Corrosion Behavior in Sodium Sulfate and Sodium Chloride Solutions of SiCp Reinforced Magnesium Alloy Metal Matrix Composite," *Corrosion* 60, no. 4 (2004): 362–368.

136. C. A. Nunez-Lopez, P. Skeldon, G. E. Thompson, P. Lyon, H. Karimzadeh, and T. E. Wilks, "The Corrosion Behaviour of Mg Alloy ZC71/SiC_p Metal Matrix Composite," *Corrosion Science* 37, no. 5 (1995): 689–708.

137. C. A. Nunez-Lopez, H. Habazaki, P. Skeldon, G. E. Thompson, H. Karimzadeh, P. Lyon, and T. E. Wilks, "An Investigation of Microgalvanic Corrosion Using a Model Magnesium-Silicon Carbide Metal Matrix Composite," *Corrosion Science* 38, no. 10 (1996): 1721–1729.

138. C. Zhang, T. Zhang, Y. Wang, F. Wei, Y. Shao, G. Meng, F. Wang, and K. Wu, "Effect of SiC Particulates on the Corrosion Behavior of Extruded AZ91/SiCp Composites during the Early Stage of Exposure," *Journal of the Electrochemical Society* 162, no. 14 (2015): C754–C766.

139. M. Levy and W. Czyrklis, "Corrosion Behavior of FP/Mg Metal Matrix Composite," Abstract no. 156 in *Extended Abstracts* (Denver, CO: Electrochemical Society, 1981), 391–392.

140. W. F. Czyrklis, "Corrosion Evaluation of Metal Matrix Composite FP/Mg AZ91C," in *1983 Tri-Service Corrosion Conference* (Annapolis, MD: U.S. Naval Academy, 1983), 279–291.

141. J. T. Evans, "Fracture and Subcritical Crack Growth in Alumina-Fiber/Magnesium Composites," *Acta Metallurgica* 34 (1986): 2075–2083.

142. A. Szewczyk-Nykiel, P. Dlugosz, P. Darlak, and M. Hebda, "Corrosion Resistance of Cordierite-Modified Light MMCs," *Journal of Materials Engineering and Performance* 26, no. 6 (2017): 2555–2562.

143. Z. Huan, C. Xu, B. Ma, J. Zhou, and J. Chang, "Substantial Enhancement of Corrosion Resistance and Bioactivity of Magnesium by Incorporating Calcium Silicate Particles," *Royal Society of Chemistry Advances* 6 (2016): 47897–47906.

144. Y. Wang, Z. Wu, H. Zhou, Z. Liao, and H. Zhang, "Corrosion Properties in a Simulated Body Fluid of Mg/β-tcp Composites Prepared by Powder Metallurgy," *International Journal of Minerals, Metallurgy and Materials* 19, no. 11 (2012): 1040–1044.

145. C. M. Dacres, S. M. Reamer, R. A. Sutula and I. A. Angres, "Anodic Corrosion of Fiber Reinforced Lead Composites for Use in Large Lead-Acid Batteries," *Journal of the Electrochemical Society* 128 (1981): 2060–2064.

146. J. C. Viala, M. El Morabit, and J. Bouix, "Mechanical Properties and Corrosion Behavior of Lead-Silicon Carbide Fiber and Lead-Carbon Fiber Composites Made by Electrodeposition," *Materials Chemistry and Physics* 13 (1985): 393–408.

147. C. M. Dacres, R. A. Sutula, and B. F. Larrick, "A Comparison of Procedures Used in Assessing the Anodic Corrosion of Metal Matrix Composites and Lead Alloys for Use in Lead-Acid Batteries," *Journal of the Electrochemical Society* 130 (1983): 981–985.

148. K. H. W. Seah, S. C. Sharma, J. Venkatesh, and B. M. Girish, "Corrosion Behaviour of Lead Alloy/Zircon Particulate Composites," *Corrosion Science* 39, no. 8 (1997): 1443–1449.

149. J. Burbank, "The Anodic Oxides of Lead," *Journal of the Electrochemical Society* 106 (1959): 369–376.

150. J. Burbank, A. C. Simon, and E. Willihnganz, "The Lead-Acid Cell," *Advances in Electrochemistry and Electrochemical Engineering 8* (New York: Wiley Interscience, 1971), 157–251.

151. P. P. Trzaskoma, "Corrosion Rates and Electrochemical Studies of a Depleted Uranium Alloy Tungsten Fiber Metal Matrix Composite," *Journal of the Electrochemical Society* 129 (1982): 1398–1402.

152. S. K. Mukherjee, A. Kumar, and G. S. Upadhyaya, "Anodic Polarization Study of Sintered 434l Ferritic Stainless Steel and Its Particulate Composites," *Powder Metallurgy International* 17 (1985): 172–175.

153. S. K. Mukherjee and G. S. Upadhyaya, "Corrosion Behavior of Sintered 434l Ferritic Stainless Steel-Alumina Composites Containing Early Transition Metals," *Materials Chemistry and Physics* 12 (1985): 419–435.

154. F. Velasco, N. Anton, J. M. Torralba, and J. M. Ruiz-Prieto, "Mechanical and Corrosion Behaviour of Powder Metallurgy Stainless Steel Based Metal Matrix Composites," *Materials Science and Technology* 13, no. 10 (1997): 847–851.

155. S. K. Mukherjee, A. Kumar, and G. S. Upadhyaya, "Effect of Iron Phosphide (Fe2P) Additions on Corrosion Behavior of Ferritic Stainless Steel Composite Compacts Containing 6 Volume % Aluminum Oxide," *British Corrosion Journal* 20 (1985): 41–44.

156. D. Hughes, "Textron Unit Makes Reinforced Titanium, Aluminum Parts," *Aviation Week Space Technology* (November 28, 1988): 90–91.

157. D. J. Blackwood, A. Chua, K. H. W. Seah, and R. Thampuran, "Corrosion Behaviour of Porous Titanium-Graphite Composites Designed for Surgical Implants," *Corrosion Science* 42 (2000): 481–503.

158. L. H. Hihara and C. Tamirisa, "Corrosion of SiC Monofilament/Ti-15-3-3-3 Metal-Matrix Composites in 3.15 wt.% NaC1," *Materials Science and Engineering A* 198 (1995): 119–125.

159. H. M. Saffarian and G. W. Warren, "Aqueous Corrosion Study of α_2-Ti_3A1/SiC Composites," *Corrosion* 54, no. 11 (1998): 877–886.

160. H. L. Marcus, W. F. Weldon, and C. Persad, *High Energy High Rate Pulsed Power Processing of Materials by Powder Consolidation and by Railgun Deposition*, Final Technical Report (Austin, TX: Center for Materials Science and Engineering, University of Texas at Austin, 1987).

161. P. K. Rohatgi, D. Nath, J. K. Kim, and A. N. Agrawal, "Corrosion and Dealloying of Cast Lead-Free Copper Alloy-Graphite Composites," *Corrosion Science* 42 (2000): 1553–1571.

162. R. Taylor and Y. Qunsheng, "Thermal Transport in Carbon Fibre-Copper and Carbon Fibre/Aluminum Composites," in *Proceedings of the 1991 International Conference on Composite Materials, ICCM/8* (Covina, CA: Society for the Advancement of Material and Process Engineering, 1991).

163. H. Sun, J. E. Orth, and H. G. Wheat, "Corrosion Behavior of Copper-Based Metal-Matrix Composites," *Journal of Metals* 45 (1993): 36–41.

164. Y.-F. Lee, S.-L. Lee, and J.-C. Lin, "Wear and Corrosion Behaviors of SiC_p Reinforced Copper Matrix Composite Formed by Hot Pressing," *Scandinavian Journal of Metallurgy* 28 (1999): 9–16.

165. H. Sun and H. G. Wheat, "Corrosion Study of $A1_2O_3$ Dispersion Strengthened Cu Metal Matrix Composites in NaCl Solutions," *Journal of Materials Science* 28 (1993): 5435–5442.

166. K. H. W. Seah, S. C. Sharma, and B. M. Girish, "Corrosion Characteristics of ZA-27-Graphite Particulate Composites," *Corrosion Science* 39, no. 1 (1997): 1–7.

167. W. Smith, *Structure and Properties of Engineering Alloys*, 2nd ed. (New York: McGraw-Hill, 1993).

168. B. P. Boffardi, "*Control of Environmental Variables in Water-Recirculating Systems*," in *Metals Handbook*, vol. 13, 9th ed. (Metals Park, OH: ASM International, 1987).

169. L. H. Hihara and R. M. Latanision, "Suppressing Galvanic Corrosion in Graphite/Aluminum Metal-Matrix Composites," *Corrosion Science* 34, no. 4 (1993): 655–665.

170. L. H. Hihara and R. M. Latanision, "Residual Microstructural Chloride in Graphite-aluminum Metal Matrix Composites," *Materials Science and Engineering: A* (1990): 231–234.

171. M. A. Buonanno, *The Effect of Processing Conditions and Chemistry on the Electrochemistry of Graphite and Aluminum Metal Matrix Composites* (Cambridge, MA: MIT, 1992).

172. W. A. Wesley and R. H. Brown, "Fundamental Behavior of Galvanic Couples," in *The Corrosion Handbook*, ed. H. H. Uhlig (New York: Wiley, 1948), 481–496.

173. F. Mansfeld, S. Lin, S. Kim, and H. F. Shih, "Pitting and Passivation of Aluminum Alloys and Aluminum-Based Metal Matrix Composites," *Journal of the Electrochemical Society* 137, no. 1 (1990): 78–82.

174. K. K. Chawla, "Fatigue of Continuously Reinforced Metal Matrix Composites," in *Metal Matrix Composites: Mechanisms and Properties*, ed. R. K. Everett and R. J. Arsenault (New York Academic Press, 1991), 235–253.

175. A. J. Sedriks, *Stress Corrosion Cracking Test Methods* (Houston, TX: NACE International, 1990).

176. *ASTM Annual Book of Standards* (West Conshohocken, PA: ASTM, 2021).

Chapter 20 | Water Handling Systems

Walter Young[1]

Introduction

Corrosion monitoring is an integral part of any water treatment program. It is used to determine treatment effectiveness and to establish the optimum level of chemical treatment that is most cost effective, but not necessarily the cheapest per pound.

The purpose of corrosion monitoring is to assess or predict corrosion behavior of the system. Basically, there are two objectives to monitoring: (1) to obtain information on the condition of the operational equipment, and (2) to relate this information to the operating variables (i.e., pH, temperature, water quality, chemical treatment, etc.). Meeting these objectives will provide the following results:

- Increased life of the plant.
- Improved quality of the plant's product.
- Prediction of maintenance needs at the plant.
- Reduction in plant's operating costs.

Corrosion monitoring is standard practice in the water treatment industry. The plant engineer can use this information to predict equipment life. Monitoring helps the engineer identify significant factors responsible for corrosion problems and ensures implementation of solutions.

Corrosion monitoring is a diagnostic tool. It provides information for the solution of corrosion problems. Knowledge of corrosion trends can be valuable. Frequently, several variables might appear to be significant, and the ability to correlate corrosion rates with a single variable under specific conditions can be vital. As a logical extension of its diagnostic capabilities, corrosion monitoring is used to assess the effectiveness of a solution to a specific water treatment problem.

[1]Corrpro Companies, Inc., 470 Lapp Rd., Malvern, PA 19355, USA
http://orcid.org/0000-0003-4670-8066

The author acknowledges the previous author of this chapter, Bennett P. Boffardi, Boffardi and Associates, Inc., Pittsburgh, PA. This chapter is a revision of P. Boffardi, "Water Handling System," in *Corrosion Tests and Standards: Application and Interpretation, MNL20*, 2nd ed., ed. R. Baboian, S. W. Dean, H. P. Hack, E. L. Hibner, and J. R. Scully (West Conshohocken, PA: ASTM International, 2005), 826–833.

DOI: 10.1520/MNL202NDSUP20190017

Corrosion monitoring can be used to provide operational information. If corrosion can be controlled by maintaining a single variable (e.g., temperature, pH, chemical treatment) within limits previously determined, then that variable can be used to predict changes in corrosion patterns as the limits are exceeded in both a positive and negative direction. An extension of this technique is to use a monitored variable to control chemical addition directly through automatic feed systems.

The particular corrosion monitoring techniques selected depend on their applicability to the system and the information being sought. Some techniques provide information that is effectively instantaneous. Other techniques provide a measure of corrosion rate. Others measure total corrosion or the remaining metal thickness, while others provide information on the overall system. Most corrosion monitoring techniques are best suited to situations in which corrosion is of a general nature, but some techniques provide at least some information on localized attack, such as pitting.

No one monitoring technique will provide all the necessary data to properly evaluate the efficacy of the treatment program. More than one technique may be necessary to monitor a particular system.

An overview of the various corrosion monitoring techniques used in cooling water systems is shown in tables 1–3. The essential information is listed in table 1, whereas table 2 lists some of the characteristics of the monitoring techniques. table 3 is a summary chart of the various monitoring techniques overall.

Corrosion Coupons

The most obvious method of assessing the corrosivity of a cooling water system to a specific material is to expose a specimen or coupon made of that material for a given time in the flowing water. Coupons are made from specific alloys, which have been cleaned and preweighed with a known surface area. Coupons vary widely in size and shape. Some commonly used coupons are 12.5 mm (1/2 in.) wide, 75 mm (3 in.) in length, and 1.6 mm (1/16 in.) thick, having an approximately 2,155 mm^2 (3.4 $in.^2$) surface area. At selected time intervals, the coupons are removed, cleaned, and reweighed to determine the metal loss.

Copyright © 2022 by ASTM International, 100 Barr Harbor Dr., PO Box C700, West Conshohocken, PA 19428-2959
ASTM International is not responsible, as a body, for the statements and opinions expressed in this chapter. ASTM International does not endorse any products represented in this chapter.

TABLE 1 Corrosion Monitoring

Method	Measures	Applications
Coupon Testing	Average corrosion rate expressed as uniform corrosion in mm/y. Weight change over 30- to 90-day duration.	Most suitable for uniform corrosion under steady conditions. Combined with visual observation, can indicate localized attack (i.e., pitting, underdeposit, galvanic). Coupons made from most engineering alloys.
LPR	Instantaneous corrosion rate is measured by electrochemical polarization of ± 10 mV between two electrode probes. Pitting tendency can be measured.	Suitable for most engineering alloys. Probe must be placed in fluid of sufficient conductivity to provide accurate rate. Alloy multiplier required for materials other than carbon steel.
ER	Metal loss is determined from resistance change of a corroding metal element. Uniform corrosion rates are calculated from resistance reading. Does not measure localized corrosion.	Suitable for measurements in low-conductivity environments, either liquid or vapor. Elements made from most engineering alloys. Element design a function of probe life and sensitivity.
Analytical	Concentrations of dissolved or suspended species in fluid systems including pH and conductivity. Does not measure corrosion.	Determines water quality level of chemical treatment, inhibitory and antagonistic species, dissolved and suspended corrosion by-products.
Heat Transfer Units	Visual observation of corrosion attack on heat transfer surface. Unit can determine corrosion rate from weight loss of heated surface.	Most suitable in simulating conditions in heat exchanger for corrosive attack. Heat transfer tubes can be made from most engineering alloys.
Test Heat Exchanger	Determines the effect of velocity, heat flux, chemical treatment on corrosion, scale, and fouling.	Most suitable in simulating conditions of critical plant heat exchanger. Heat transfer tubes can be made from most engineering alloys.

TABLE 2 Monitoring Technique Characteristics

Method	Time Interval for Measurement	Type of Information	Response to Changing Condition	Plant Environment	Type of Corrosion	Ease of Interpretation
Coupon Testing	Long-term duration, 30 to 90 days	Average uniform corrosion rate	Poor	Any	Uniform and localized attack	Simple
LPR	Instantaneous	Corrosion rate, pitting index	Fast	Conductive	Uniform	Simple
ER	Short duration	Integrated corrosion rate	Moderate	Any	Uniform	Simple
Analytical	Fast	Species influencing corrosive attack	Fast	Any	Not applicable	Moderate
Heat Transfer Units	Long-term duration, 30 to 90 days	Corrosion rate, scale, and fouling	Moderate	Any	Uniform and localized attack besides deposition	Difficult

TABLE 3 Monitoring Devices

Systems	Coupon	LPR ER	Analytical	Test Heat Exchanger
Once-through	X	X X	X	
Cooling				
Closed System	X	X	X	
Cooling				
Open	X	X	X	X
Recirculating Cooling				

The weight loss is converted to overall thickness loss or average corrosion rate expressed in millimeters per year (mm/y) as follows:

$$\text{mm/y} = 3.65(\Delta W)[(A)(d)(D)] \quad (1)$$

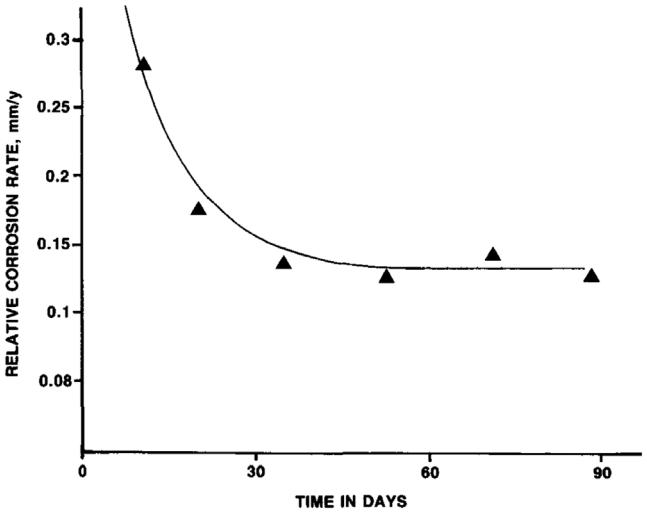
where

ΔW = weight change, mg,
A = coupon surface area, cm^2
d = metal density, g/cm^3, and
D = exposure time, (days).

Conversion to English units, mils per year (mpy), requires that equation (1) be multiplied by 39.4. Corrosion coupons are highly susceptible to initial corrosion because the metal surface is in an "active" state because of surface preparation. Coupons should not be touched during installation and monitoring processes. Use of plastic gloves when handling the coupons is highly recommended. Normally, 30 days is a typical test period for low-corrosivity water (under 0.25 mm/y or 10 mpy). Low-corrosivity water usually contains chemical treatments to stifle corrosion attack. Exposure periods less than 30 days can yield misleading results. Frequently, long-term tests are required, up to 90 days' exposure. During this time frame, three sets of coupons are normally placed in a test rack and changed in sequence of 30-, 60-, and 90-day intervals. Normally, the longer the exposure period, the lower the measured average corrosion rate, and the more closely the coupons will approximate conditions in the system. Figure 1 graphically shows the decrease in corrosion rate with exposure time. Steady state is normally achieved in the 60- to 90-day time frame.

Screws and nuts made of nylon or plastic should be used to hold the coupons to the coupon holder. Mixed metallurgy should be avoided. Copper-base screws and nuts should not be used to

FIG. 1 Relative carbon steel corrosion rate versus elapsed time.



hold carbon steel or stainless steel coupons. Galvanized screws and nuts should never be used.

Coupons having large amounts of deposits or tuberculation may indicate insufficient chemical treatment, unstable water characteristics, or highly corrosive conditions. Alternatively, deposits may have been transported from elsewhere in the system. Heavy, uniform deposits will reduce corrosion rates, because they can act as a protective barrier.

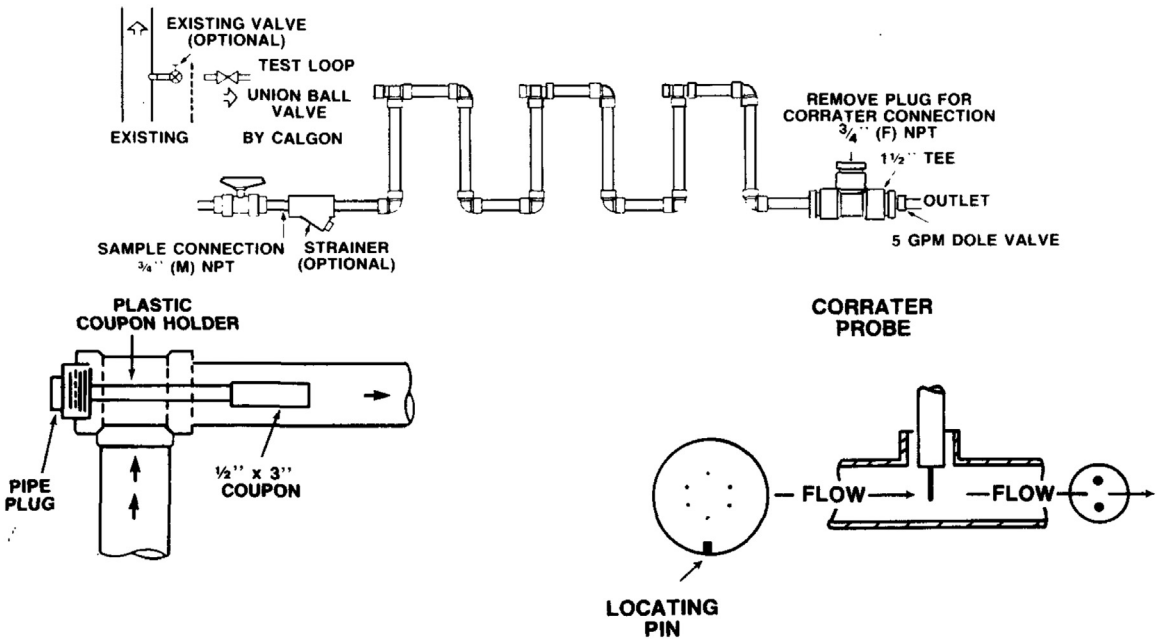
General guidelines for acceptable uniform corrosion depend on the coupon metallurgy. Low-carbon steel (mild steel) corrosion rates less than 0.13 mm/y (5 mpy) are considered good, rates between 0.13 to 0.25 mm/y (5 to 10 mpy) are fair, and rates greater than 0.25 mm/y (10 mpy) are poor. Copper-base alloys, such as admiralty and 90:10 copper nickel, should have rates under 0.013 mm/y (0.5 mpy). Above this value is considered excessive. General classification of corrosion rates is shown in table 4.

Coupon installation should be placed in a coupon test rack shown in figure 2. Note that the broad face of the coupon is vertical to prevent deposits from settling during periods of low flow. It is important that the flow rate through the rack corresponds to the actual service flow rate. Too high a flow rate will keep debris off of the coupons and may initiate erosion attack on copper-base alloys. Low flow rates may result in excessive corrosion and fouling. Normally, flow rates of 1–2 m/s (3 to 5 ft/s) are adequate. The coupon rack should be connected to the return riser to the cooling tower or at the exit of the hottest part of the system using plastic piping or any other material that will not

TABLE 4 Qualitative Classification of Corrosion Rates

Corrosion Rate (mm/y)		
Carbon Steel	Copper-Base Alloys	Description
<0.03	0 to 0.003	Negligible or excellent
0.03 to 0.08	0.003 to 0.006	Mild or very good
0.08 to 0.13	0.006 to 0.009	Good
0.13 to 0.20	0.009 to 0.0125	Moderate to fair
0.20 to 0.25	0.0125 to 0.03	Poor
>0.25	>0.03	Very poor to severe

FIG. 2 Corrosion test rack installation.



influence coupon corrosion rates. For example, do not use galvanized pipe, copper pipe, or brass valves to connect the test loop to the riser.

Note in figure 2 the use of an optional strainer. The strainer should be used in water systems known to have high-suspended solids or assorted foreign matter, or both.

Flow through the coupon rack can be controlled using an orifice control valve, but this valve is subject to plugging. A plugged orifice control valve will have reduced flow or no flow at all, resulting in high coupon corrosion rates. A rotameter valved at the end of the coupon rack will give more flexibility and accuracy in controlling water velocity. A strainer in the system will prevent plugging of the fluid control valve. Cooling water discharge from the rack should go to a sump (e.g., drain, tower basin) and not be plumbed back into the cooling system. The outflow of the rack must be open to the atmosphere.

In a high-rise building the cooling tower is normally placed on the roof and the corrosion rack is in the mechanical room, which are frequently in the basement. In this situation, the corrosion rack is plumbed between the down-comer and the riser. Materials of construction for the corrosion rack should be made of stainless steel to provide rigidity and have minimal influence on the coupons. Use of carbon steel or galvanized steel is not recommended as construction materials. Coupon placement in the rack follows the galvanic series, starting from the active end. That is, aluminum, carbon steel, stainless steel, and then copper-base alloys.

Coupon corrosion studies are simple to perform. This is the most direct method, aside from inspection of the actual plant equipment, to determine the efficacy of a treatment. Coupon evaluation allows simple comparison between different alloys, which provides visual examination for localized attack, such as pitting, crevice attack, dealloying, or any other form of nonuniform attack. There are limitations, however, to coupon evaluation. Coupons provide weight loss determination of corrosion rates. This consists of accumulated loss of material over the period of exposure. Therefore, coupons cannot determine the time or magnitude of corrosion upsets within the exposed time frame. Finally, 30 to 90 days are needed to allow sufficient weight change to be meaningful. This 30- to 90-day exposure can sometimes indicate differences between short-term and long-term corrosion rates.

Linear Polarization-Resistance Meter

The linear polarization-resistance (LPR) technique is the only corrosion monitoring method that allows corrosion rates to be measured in real time. Although limited to electrolytically conducting liquids, the response time and data quality of this technique make it superior, where applicable, to all other forms of corrosion monitoring.

LPR is particularly useful as a method to rapidly identify corrosion upsets and, thus, evaluate remedial action, reducing and minimizing unscheduled downtime, thereby prolonging plant life.

Two LPR devices are presently in use, a three-electrode probe (working, counter, and reference electrodes) and a two-electrode probe. In the author's opinion, the three-electrode system is a better-designed corrosion monitor; however, it accounts for a small percentage of LPRs used to monitor corrosion rates in industrial water treatment systems. The two-electrode LPR device is used by most water treatment vendors and industrial plants. It will be the only LPR device discussed.

The basic operation of the LPR instrument uses two electrodes made of the material of interest (i.e., carbon steel, Admiralty, 90:10 copper nickel). One of the electrodes acts as an anode, the other as a cathode. During the operation of the instrument, a very small voltage of 20 mV is applied across the electrodes. In this region, the polarization curves approach linearity, and hence the term LPR. The applied potential divided by the measured current i_{meas} is a resistance term called polarization resistance, or Rp. The resistance to current flow between the two electrodes of the LPR probe is the sum of polarization resistance values at each electrode and the resistance of the solution between the electrodes (R_s), as follows:

$$\Delta E = i_{meas}(2R_p + R_s). \quad (2)$$

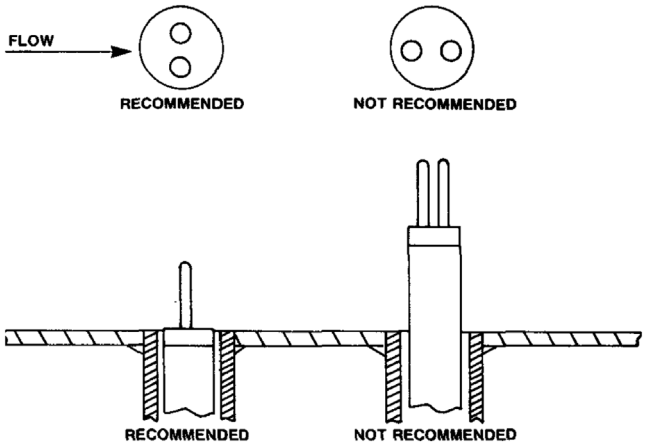
In addition to general or uniform corrosion, localized corrosion (pitting) may occur in a system. A pitting index or imbalance measurement can be obtained from some LPR meters. The electrochemical current generated is a qualitative measurement or index. If the imbalance reading (pitting) is low compared with the corrosion reading, pitting is probably minimal. A high imbalance reading compared to a general corrosion rate can indicate that pitting or crevice corrosion will be the main form of attack. When a general corrosion rate reading is about the same as the imbalance index, then some pitting is indicated, but the pits probably will be broad and shallow. Further information on the pitting index can be found in NACE International Publication 3T199.[1]

The LPR probe should be installed perpendicular to the water flow in a representative water stream which is part of the piping system or at the end of the coupon test rack, as shown in figure 2. The probe must be installed such that water flows between the two electrodes to avoid fouling of the electrodes. An aligning pin at the male cable connector of the probe indicates the electrode position as shown in figure 2. The two electrodes should project into the flowing water, with the probe lead flush with the pipe wall, as shown in figure 3.

Serious errors in corrosion rate measurements may occur in low-conductivity water because of solution resistivity effects. This situation tends to occur at moderate to high corrosion rates and is manifested by indicating lower corrosion rates than actual. The operating range for various LPR instruments can be obtained from the manufacturer.

The LPR probe alloy multiplier should be used when electrodes are made from materials other than carbon steel. The purpose of the multiplier is to convert the built-in constants that are specific for carbon steel to other alloys. Corrosion rate multipliers account for the specific alloy's anodic reactions, the

FIG. 3 Installation of LPR probe.



valency of the anodic reactions, the alloy equivalent weight, and the alloy density. LPR electrodes should be changed periodically and at least annually.

Corrosion rates obtained with LPR instruments provide rate data directly and within a few minutes. This instrument is well suited to applications in which upsets or other accelerated corrosive conditions can be detected quickly so that remedial action can be taken. The corrosion rates obtained with the meter assume uniform corrosion with a tendency to predict pitting attack. Deposits on the electrodes can bias the pitting index value. If the index value is high, the probe should be removed and the electrode visually examined for debris. Bridging the electrodes with conductive deposits will affect both the general corrosion value and the pitting index.

The LPR reading may not agree with the coupon corrosion rate. The LPR data are real time and measure the corrosion rate at the time of measurement. Coupon rates are an accumulated average mass loss, taking into account all corrosion that has occurred during its exposure period. Coupon mass losses are a direct measure of corrosion rate, whereas LPR data are generated from electrical currents, which are influenced by other factors. The main advantage of LPR devices is the rapid detection of sudden changes in system operating parameters or chemical levels.

Details on how to calculate corrosion rates from electrochemical measurements can be obtained from ASTM G102, *Standard Practice for Calculation of Corrosion Rates and Related Information from Electrochemical Measurements.*[2]

Electrical Resistance Meter

The electrical resistance (ER) technique is an online method of monitoring corrosion rates. It is universally applicable to all types of corrosive environments—that is, conductive to poorly or nonconductive media (such as deionized or potable waters) and vapor phase systems (such as steam).

There are many manufacturers of ER instruments. ER meters measure the change in resistance of a metal element as it corrodes. The metal element or probe is usually in the form of a wire, strip, or tube.

When it corrodes uniformly, the change in electrical resistance is proportional to corrosion

$$R = K/A, \tag{3}$$

where:
R = the probe resistance,
A = the cross-sectional area of the metal element, and
K = a constant and a function of probe metallurgy, element length, and resistivity.

As the probe element corrodes, its cross-sectional area is reduced, increasing its electrical resistance. Thus, the measurement of electrical resistance is inversely proportional to the remaining metal in the probe. Therefore, increases in the measured resistance signal increase the metal loss to corrosion. The probe is internally temperature compensated for changes in the probe constant, which is temperature dependent.

The advantage of the ER meters is their ability to measure corrosion in liquids, vapor phases, and in inaccessible locations. The liquid does not have to be conductive or have a minimum conductivity as with the LPR systems. Corrosion rates, however, are not instantaneously determined. The time frame required to determine corrosion rates is a function of probe element and metal loss. The ER probes are suitable only for uniform corrosion. There is no pit index built into the instrument. Any pits developed on the element will cause rapid penetration and indicate excessively high corrosion rates.

Typical probe elements are shown in figure 4. Appropriate response time information for any given probe can be obtained from the manufacturer. The corrosion rate is calculated from the change in dial reading on the instrument.

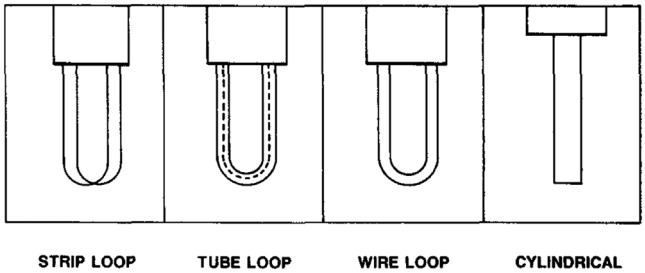
The corrosion rate is calculated from the change in dial reading on the instrument, as follows:

$$\text{Corrosion rate}(\text{mm/y}) = \frac{9.3 \times 10^{-3} \times \Delta D \times PF}{T}, \tag{4}$$

where:
AD = the change in the dial reading,
PF = the probe factor (supplied with each probe), and
T = the elapsed time in days.

ER probes must be allowed to corrode for a period of time before accurate corrosion rate measurements can be made. The

FIG. 4 Electrical resistance element design.



time duration depends on the corrosion rate. The higher the rate, the shorter the time period and vice versa.

Probe placement in the fluid should be similar to LPR electrode placement—that is, the probe element should protrude into the fluid. Flow should pass the element. There is no specific orientation for the probe element.

Figure 5 shows a plot of dial setting or metal loss from the ER meter versus time, which can give an indication of corrosion rates. A large change in slope represents an increase in corrosion, whereas a zero slope indicates no significant increase in corrosion.

Generally, LPR is the preferred technology for online monitoring of corrosion in highly conductive waters such as those in industrial recirculating cooling water systems. The preference is based on two factors: (1) the relative instantaneous nature of the LPR, and (2) the distortional effect that even a single pit has on the ER measurement and reducing the usable life of the ER probe.

Chemical Analysis

Water parameters relevant to the corrosion process can be provided through chemical analysis. This monitoring technique does not directly indicate corrosion rate but provides information on factors that can influence the corrosion process. It measures parameters that are known to be associated with acceptable or unacceptable corrosion processes within a system.

A thorough water analysis is not required of every water sample. Core analyses, however, should be performed to determine the operating state of the system. It is good practice to periodically obtain complete analyses so that seasonal variations in water composition can be tracked.

A "well check" analysis is also advisable. This consists of a thorough analysis when the plant is operating properly and corrosion rates are meeting the objectives. The well check can then be used as base line data when corrosion rates are outside the norm and analyses are being performed to determine the cause.

Parameters to be determined for a thorough analysis and their impact on corrosion/deposit are shown in table 5.

FIG. 5 Electrical resistance meter dial setting versus time: (*A*) a medium corrosion rate, (*B*) essentially no corrosion, and (*C*) high corrosion rate.

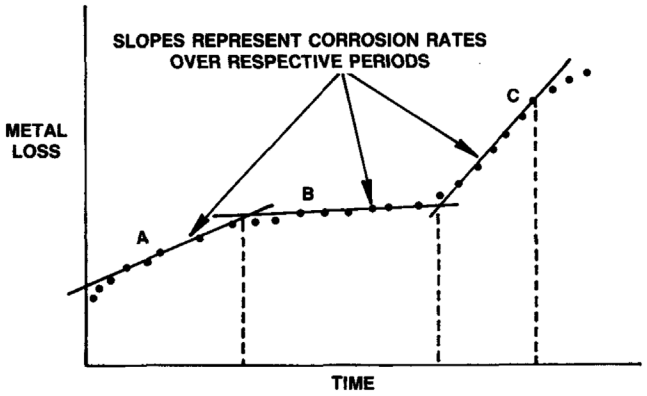


TABLE 5 Analytical Parameters

Species	Impact on Operating System
pH	Corrosion or scale-forming tendency.
P Reading	Monitor buffering capacity, differentiates between CO_3^{-2} and HCO_3^-.
M Reading	Provides data for calculating $CaCO_3$ potential. Includes all hydrogen titratable species (i.e., PO_4^{-3}, SiO_2) polymers. If pH/alkalinity relationship is outside of norm, then additional alkalinity value may be due to other titratable species.
Conductivity	Estimates total dissolved solids.
Suspended Solids	Monitors general water quality or turbidity.
Orthophosphate	Monitors inhibitor concentration and/or reversion.
Polyphosphate	Monitors inhibitor concentration.
Organic Phosphate	Monitors inhibitor concentration.
Total Organic Carbon	Monitors overall water quality.
Calcium, Total	Monitors potential hardness scale deposition.
Calcium, Dissolved	Monitors hardness scale deposition if value is different from calcium, total.
Magnesium, Total	Monitors potential deposition.
Magnesium, Dissolved	Monitors potential silicate or hydroxide deposition if value differs from magnesium, total.
Aluminum, Total	Monitors possible inhibitor adsorption, reducing corrosion protection if concentration >0.1 mg/L.
Aluminum, Dissolved	Monitors possible inhibitor adsorption, if concentration >0.1 mg/L. Loss of 3.5 mg/L of phosphate per 1 mg/L of aluminum.
Copper, Total	Monitors potential copper corrosion reducing steel corrosion protection if concentration >0.1 mg/L.
Copper, Dissolved	Monitors potential copper corrosion. Acceptable level < 0.05 mg/L.
Zinc, Total	Monitors potential zinc scale deposition and level of treatment needed to inhibit/disperse solids.
Zinc, Dissolved	Monitors background levels and active synergist.

Dissolved Oxygen Monitoring

Oxygen is the common cathodic reduction species found in water, which is responsible for continued corrosive attack on some engineering materials, such as low carbon steel. Passive engineering alloys, however, utilize the oxygen to form thin, tenacious, and adherent protective oxide films. Some common alloys with protective films are stainless steels, nickel alloys, copper-base alloys, and aluminum alloys. The oxygen concentration at ambient temperatures and atmospheric pressure is approximately 6–8 mg/L. An increase in temperature decreases oxygen solubility, whereas an increase in pressure increases oxygen solubility.

In open cooling water environments, oxygen cannot be economically removed as an antagonistic species. Appropriate cathodic inhibitors control its impact on corrosion.

In boilers, it is a common practice to remove the oxygen from the water, because it is a major corrodent. Removal is through a combination of physical and chemical means.

Deaerators physically remove the oxygen by purging the boiler feed water with steam, which heats and degases the water. Oxygen content can be reduced to 5–7 ug/L by this method. Further reduction of oxygen is required, and this is achieved through the use of chemical oxygen scavenger. The combination of deaeration and oxygen scavenger can reduces the oxygen content to zero.

Oxygen measurements can be made directly and continuously using online monitors or by wet chemical analysis.

Oxidation Reduction Potential

Oxygen reduction potential (ORP), or redox potential, is the potential of a reversible oxidation-reduction electrode measured with respect to a reference electrode, corrected to the hydrogen electrode, in an electrolyte. It is an online, real-time measurement. In water treatment, ORP is used to control the addition of oxidizing biocides, such as chlorine, chlorine dioxide, bromine, hydrogen peroxide, and ozone. The presence of these chemicals will raise the ORP value. When an ORP probe is placed in the open recirculating cooling water environment in the absence of an oxidant, its value is taken as an initial set point. The addition of an oxidizing biocide increases the ORP value. The actual ORP reading depends on concentration and activity of the oxidant or biocide, temperature of the system, contaminates and nutrients, pH, and other parameters. Usually, at recommended concentrations of oxidizing biocides, the ORP value increases hundreds of millivolts depending on these parameters. Maintaining the recirculating water at the higher oxidizing potential ensures adequate disinfection. ORP measurements are similar to pH measurements. A typical ORP cell uses a platinum surface for measuring the ORP versus a silver-silver chloride reference electrode. Maintenance of an ORP system is similar to that of a pH electrode—that is, the ORP electrode should remain in the water circuit at all times.

Electrodes are replaced approximately every two years. The electrodes are cleaned in 5% hydrochloric acid solution to remove any hard-water deposits that may form and interfere with the reference junction.

Quinhydrone is used to calibrate the ORP electrodes. By placing the quinhydrone in a known pH solution, a standard mV reading is achieved. An ORP value of 87 mV is obtained in a quinhydrone solution at pH 7, and 240 mV at pH 4. Other calibration protocol exists for higher ORP readings in the 600 mV range.

Heat Transfer Systems

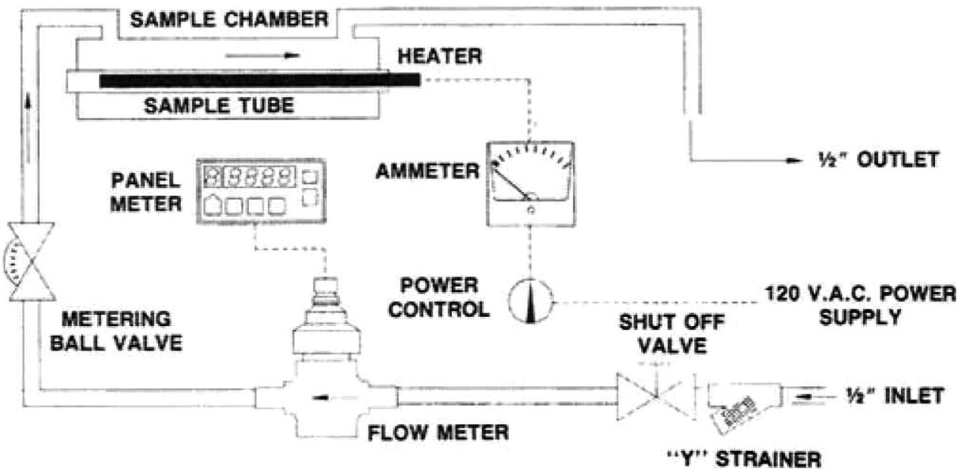
Fouling and deposit monitors are used primarily to track the buildup of scale or deposits on heat transfer surfaces. The heat transfer tube can also be used as a tubular corrosion coupon to monitor corrosion under heat transfer conditions.

These units are designed to simulate heat exchangers under as near actual operating conditions as possible, taking into account ease of use and simplicity in design. Figure 6 shows a simplified schematic. An electric resistance heating element is used to impose a heat load on the tubular metal surface. The metal test specimen is inside a glass outer jacket in which water flows in the annular space. The glass tube makes it possible to visually examine the metal surface for deposit buildup or corrosion attack.

Heat flux (W/m^2), which is the heat transfer rate (W) divided by the exposed metal tube surface area (m^2), is constant as long as no deposits accumulate on the specimen. Deposits coming from hardness salts, corrosion by-products, silt, process contamination, and biomass, however, can form on the heated surface, raising the surface temperature. If the surface temperature becomes excessive, a temperature cutoff switch can protect the device.

It is important to gather as much information about the system using fouling and deposit monitors as possible. Periodic visual inspection of the heat transfer tube is necessary to qualify the buildup of deposit. At the termination of the test, the tube deposit should be collected and chemically analyzed. Photographs of the deposits on the tube can be useful in describing the type of buildup. Also, photographs after the tube has been

FIG. 6 Corrosion deposit test unit.



cleaned can be used to document the type of corrosion attack that has occurred (e.g., uniform, underdeposit, pitting). After the tube has been cleaned, the corrosion rate of the heat transfer tube should be determined. This rate should be compared with nonheat transfer coupons to determine the impact of heat flux.

Test Heat Exchanger

The test heat exchanger is a monitoring tool that evaluates a heat transfer surface for corrosion and deposition. The test heat exchanger is only as good a monitoring or evaluating piece of equipment as its ability to duplicate or represent system conditions. The factors inherent in plant heat exchanger equipment that determine the corrosion and deposition of exchanger surfaces are as follows:

- Product temperature, which determines metal skin temperature.
- Water flow velocity in the tube, which can influence fouling rate. Low velocities of 0–0.6 m/s (0 to < 2 ft/s) can result in more severe fouling. Average velocities of 1–2 m/s (3–5 ft/s) would correspond to normal rate of deposition. High velocities of 2–4 m/s (6–12 ft/s) will result in less fouling.
- Heat flux, a major influence on scale/deposition rate. Corrosion rates will also be influenced but to a lower degree. Heat flux of 0–6,300 W/m^2 (0–2,000 BTU/ft^2-h) are considered low. Heat flux of 6,300–15,800 W/m^2 (2,000–5,000 BTU/tf-h) are average. Heat flux of 15,800–31,500 W/m^2 (5,000–10,000 BTU/ft^2-h) are considered high.
- Cooling water temperature, which accepts heat from the plant exchanger.

To obtain reliable results from a test heat exchanger, these factors must be determined from the plant exchanger in the system that is to be duplicated. Once the plant parameters have been determined, they should be duplicated as nearly as possible in the test unit and held constant. Figure 7 is a schematic of a typical two-tube test heat exchanger. It is used to simulate tube side water conditions in a plant exchanger. Heated water or steam on the shell side is used to heat the tubes.

The flow of cooling water to the tubes must be controlled to maintain system velocity. An inlet water strainer is used to eliminate foreign objects, which can restrict flow. A valve ahead of a flow indicator controls flow.

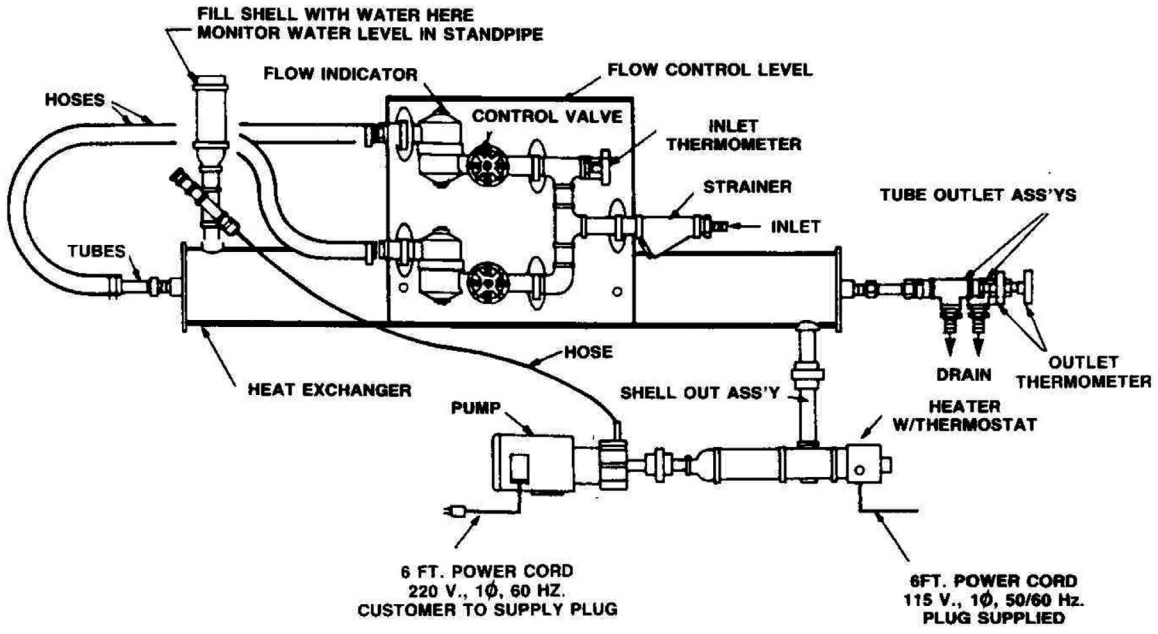
The flow of hot liquid on the shell side is pumped through the exchanger and the temperature is controlled by a thermostat. Thermometers on the inlet and outlet waters are used to determine temperature differential. Once the operating parameters have been selected and established, they should be checked and recorded on a per day or per shift basis.

The two-tube heat exchanger can be used to compare treatment, metallurgy, and the impact of heat flux on deposition by varying the flow in one of the tubes. At the end of the monitoring test period, which is at least 30 days, the heat transfer tubes should be evaluated for scale deposition, fouling, and corrosion. Analysis usually includes the following:

1. Cutting the tubes in half for visual inspection on both the heat transfer and nonheat transfer surfaces (tube extension outside the shell).
2. Scraping the deposits from the tube for analysis.
3. Brushing and chemically cleaning the tube to examine tube surface for general and localized corrosion.

These heat exchanger devices require considerable time and expertise to properly operate. They are not commonly used because of manpower commitment and ancillary expenses.

FIG. 7 Field evaluation test heat exchanger.



Conclusion

A wide range of corrosion monitoring techniques is used in water treatment to systematically measure the corrosion or degradation of equipment and distribution piping. Corrosion monitoring is a viable tool to assess the performance of any chemical treatment program. No one technique is universally applicable. The wide variety of corrosion monitoring tools can be used in any industry, and, although each technique has limitations, they provide a practical means to monitor corrosion behavior. More details on the various monitoring techniques can be found in the technical literature.[3–7]

References

1. *Techniques for Monitoring Corrosion and Related Parameters in Field Applications*, Item No. 24203-SG, NACE Publication 3T199-2012 (Houston, TX: AMPP, 2012).
2. *Standard Practice for Calculation of Corrosion Rates and Related Information from Electrochemical Measurements*, ASTM G102 (West Conshohocken, PA: ASTM International, approved November 1, 2015), http://doi.org/10.1520/G0102-89R15E01
3. W. H. Ailor, *Handbook on Corrosion Testing and Evaluation* (New York: Wiley, 1971).
4. *Standard Test Methods for Corrosivity of Water in the Absence of Heat Transfer (Electrical Methods)*, ASTM D2776 (West Conshohocken, PA: ASTM International [historical version]).
5. *Standard Practice for Online Monitoring of Corrosion in Plant Equipment (Electrical and Electrochemical Methods)*, ASTM G96 (West Conshohocken, PA: ASTM International, approved May 1, 2018), http://doi.org/10.1520/G0096-90R18
6. *Cooling Water Test Units Incorporating Heat Transfer Services*, NACE TM0286 (Houston, TX: NACE International, 2001).
7. *Recommended Practice On-line Monitoring of Cooling Waters*, NACE RP0189 (Houston, TX: NACE International, 1989).

Chapter 21 | Pipeline

Abdelmounam M. El-Sherik[1]

Introduction

In the oil and gas industry, pipelines are the primary economical and safest method for the transportation of high volumes of hydrocarbon fluids at high flow rates over short and long distances (thousands of kilometers). To transport a greater volume of fluids in pipelines, higher operating pressures are required, while also maintaining pipeline network integrity and reliability. This can be achieved through proper corrosion testing strategies that include inspection, *in situ* testing, and monitoring as well as predicting the likelihood of corrosion occurring along the pipe.

Corrosion testing of pipelines is conducted for several reasons. One is to evaluate the pipeline condition to determine whether or not it is safe to operate. If repairs are needed, testing is performed to determine if repair is feasible or if replacement is needed. Testing is performed to track the pipe condition so that repair or replacement can be budgeted. Another reason for testing pipes is to evaluate the effectiveness of corrosion control measures, such as inhibitors for internal pipe surfaces or cathodic protection (CP) and coatings for external pipe surfaces.

The intent of this chapter is to provide an overview of the primary testing techniques and methods most commonly utilized in the field for testing and monitoring of corrosion in buried oil and gas pipelines. Before discussing test techniques, the chapter will discuss briefly pipeline materials, relevant corrosion threats, and corrosion control methods and strategies. This chapter is by no means a detailed text on corrosion and corrosion testing of pipelines, and the reader is encouraged to consult the references for further detail.

Pipeline Materials

CARBON AND LOW-ALLOY STEELS

Carbon and low-alloy steels are probably the most commonly used materials for pipelines transporting hydrocarbon fluids. *ASM Metals Handbook* provides a summary of the different specifications used for pipelines.[1]

Steels such as API 5L X52 and X65 remain the most widely used grades in oil and gas pipelines.[2] In many cases the mechanical properties of these grades are insufficient to meet the increasing demands to transport higher volumes of fluids at higher operating pressures and at lower costs. To meet these industry demands, line pipe steel development has focused on improving the strength and mechanical properties, without reducing toughness and weldability, of pipeline steels. This is achieved through thermo-mechanical treatments and the addition of small amounts (typically less than 1 wt%) of alloying elements (Nb, V, Mo, Ni, Cr, and Zr) in various combinations to achieve the desired properties.[2,3] These efforts led to the development of high-strength low-alloy (HSLA) steels, or microalloyed steels, namely, API 5L 70X, X80, X100, and X120 grades. With increasing tensile strength, the pipe wall thickness required for pressure containment is reduced, leading to lower pipe laying and welding costs.[3] These remarkable improvements in mechanical properties and lower pipeline-laying costs, however, do not come without adverse side effects. HSLA steels are more susceptible to hydrogen damage and embrittlement than the lower-strength API grades in sour service environments.

CORROSION-RESISTANT ALLOYS

Under extreme operating conditions (high pressures and temperatures) and more aggressive environments, such as unprocessed production fluids containing high chloride, hydrogen sulfide (H_2S), and carbon dioxide (CO_2) contents, carbon and low-alloy steels are susceptible to rapid corrosion attacks, such as pitting, crevice, or underdeposit corrosion. This rapid corrosion occurs even when corrosion inhibitors are factored into the design life of the carbon and low-alloy steel pipe. In such extreme service environments, corrosion-resistant alloys (CRAs) are the preferred material design option.[4] CRAs are typically classified into four main material classes: martensitic stainless steels, duplex stainless steels, super-austenitic stainless steels, and nickel-based alloys. Each of these four CRA classes consists of several grades that are compositionally fine-tuned for specific service environment. For several tables showing chemical compositions and

[1]Saudi Aramco, P.O. Box 62, Dhahran 31311, Saudi Arabia http://orcid.org/0000-0002-0863-9576

The author acknowledges the previous author of this chapter, Paul S. Rothman, The Port Authority of New York and New Jersey, New York, NY.

DOI: 10.1520/MNL202NDSUP20190039

Copyright © 2022 by ASTM International, 100 Barr Harbor Dr., PO Box C700, West Conshohocken, PA 19428-2959
ASTM International is not responsible, as a body, for the statements and opinions expressed in this chapter. ASTM International does not endorse any products represented in this chapter.

applications for each of the CRA class material, see Hill and Perez.[4]

CRAs can be employed as solid pipe or as clad product.[5] The first reported application of CRAs dates back to 1975 in flow lines internally clad with 316L stainless steel and also as solid duplex stainless steel lines.[4] Because of the prohibitive cost of CRAs, their application is limited to short distances, such as flow lines carrying aggressive production fluids. The decision whether to use CRA instead of carbon and HSLA steels typically is made during the design phase of a pipeline through the use of corrosion prediction software packages that can predict uniform and pitting corrosion rates in the intended service environment. Although CRAs show superior resistance to localized and uniform corrosion compared with carbon and HSLA steels, even with inhibition, they remain susceptible to environmental cracking corrosion attacks particularly in sour and chloride containing environments.

THERMOPLASTIC LINERS

Thermoplastic liners such as high-density polyethylene and polyamides (PA11 and PA12) are used to internally line carbon steel pipes.[5–10] The final product (a lined steel pipe) is made by the insertion of a solid thermoplastic pipe into a carbon steel host pipe. The thermoplastic liner provides protection to the underneath carbon steel pipe by acting as a barrier between the corrosive production fluids and the steel surface. Lined products are almost always significantly cheaper than CRA clad pipes and therefore provide a cost-effective alternative to clad pipes. Thermoplastic liners have been used successfully for the past several decades in a range of onshore and offshore pipeline applications. For example, a 2013 report issued by Alberta Energy Regulator,[11] indicated that in Alberta, there are approximately 7,900 km of lined steel pipelines. More than 90% of this inventory is in water and multiphase services and the remainder is in gas service.

Some of the drawbacks of using thermoplastic liners are their temperature limitations and permeation by water, H_2S, and CO_2 molecules leading to corrosion of the host carbon steel pipe and pressure buildup at the liner–steel interface (annulus). If the lined pipe is not operated as per standard operating procedures, this pressure buildup in the annulus can cause buckling of the liner.

The following standards provide guidelines for the use of thermoplastic liners in oilfield applications:

- NACE Recommended Practice SP-0304 (latest revision), *Design, Installation, and Operation of Thermoplastic Liners for Oilfield Pipelines*
- Canadian Standards Association (CSA) Z-662, *Oil and Gas Pipeline Systems*, Clause 13

Corrosion Threats

Steel pipes in oil and gas environment tend to corrode by various internal and external corrosion mechanisms.[12,13] Table 1 presents the most common corrosion threats to pipelines and provides a brief synopsis of each threat.[12,13]

The 10 to 2 o'clock and 4 to 8 o'clock orientations in pipelines are typically more prone to internal corrosion attacks as a result of water condensation and precipitation at these locations, respectively. Internal corrosion occurring at the 10 to 2 o'clock orientation is typically termed top-of-the-line corrosion (TLC), whereas corrosion taking place at the 4 to 8 o'clock position termed bottom-of-the-line corrosion (BLC). Internal corrosion in these locations is primarily affected by the composition (e.g., CO_2, H_2S, water cut, salts) of the transported fluids and pipeline operation conditions (temperature, pressure, flow regime, and velocity). CO_2 and H_2S gases in combination with liquid water (condensed or produced) are the main causes of corrosion in oil and gas pipelines. The corrosivity of the water phase is normally enhanced by the presence of dissolved salts naturally occurring in the production fluids. The concentrations of H_2S and CO_2 gases determine the corrosion mechanism (sour, sweet, or mixed), composition of corrosion products, corrosion damage mechanisms (CDM), and the appropriate mitigation strategies. According to Kermani, Martin, and Esaklul,[14] there are three corrosion domains for mixed CO_2/H_2S systems, which can be represented by the ratios of their partial pressures in the system:

$CO_2/H_2S < 20$ Sour corrosion dominates with iron sulfide as the main corrosion product

$20 < CO_2/H_2S < 500$ Mixed regime with both iron sulfide and iron carbonate corrosion products

$CO_2/H_2S > 500$ Sweet corrosion dominates with iron carbonate as the main corrosion product

These ratios are used by corrosion engineers as a general rule of thumb to predict the corrosion mechanism expected to occur. The ratios are based on the original work by Dunlop, Hassell, and Rhodes,[15] published in 1983. More recently, Smith[16,17] investigated the origins of these ratios and reported that these ratios were developed for low-ionic-strength solutions at a temperature of 25°C and are extremely sensitive to the quality of the input thermodynamic data. These key assumptions cover a narrow range of oilfield environments. Smith recalculated these ratios using higher quality thermodynamic input data and a wider temperature range. He proposed that a CO_2/H_2S ratio values of below 1 and above 5,000 are more accurate as cutoff values for sour and sweet corrosion, respectively. Smith continued to state that laboratory testing or thermodynamic modeling is required to determine the corrosion mechanism for ratio values between 1 and 5,000.

Mahajanam[18,19] and Gunaltun[20] provide more information on these types of corrosion.

Internal corrosion protection can be achieved through corrosion inhibitors and biocides, frequent internal cleaning of pipelines, coatings, linings, claddings, design process control, and materials selection.[21]

External corrosion of pipelines can take on different forms depending on whether the pipeline is buried or above ground. Atmospheric corrosion of aboveground pipelines is visible and typically not a serious problem. Corrosion control requirements, however, are still needed. The pipeline must still be protected from atmospheric corrosion through the application and continual

maintenance of corrosion-resistant coatings. A continuing program of visual inspection and maintenance of the coatings must be conducted to prevent the deterioration of the coating and the pipe.[21]

In contrast, external corrosion of buried pipelines can pose a serious integrity risk because of the invisibility of the corrosion attack and the corrosivity of the soil environment. Soils are a complex environment with different chemical-physico-hydro-bio properties that may affect soil corrosivity, the corrosion rate, and the CDM of a buried pipeline.[22–24] Soil properties such as soil resistivity, redox potential, concentrations of soluble salts, pH, bacterial activity, and soil type (rocky, silt, clay, sandy, or a mixture of all or some), as well as particle size, moisture content, aeration, compaction, and organic content, influence soil corrosivity.[22–24] Laboratory and field standard test methods can test these soil properties. Table 2 summarizes the main test methods used to test soil properties affecting corrosion.

Soil properties are strongly interdependent and show variability with time (rainy versus dry seasons) and location (horizontal versus vertical), which further complicate examining the effect of one factor (e.g., resistivity) on the corrosion of a buried pipeline.[22–24] Because of this complexity, soil corrosivity is difficult to quantify for any given soil type (e.g., clay versus silt). No single property (e.g., soil resistivity, redox potential, or soil pH) can be used alone to determine the soil corrosivity of a soil. For this reason, multivariate point scale methods, such as the American Water Works Association (AWWA) C-105 method[25] or Dechema Soil Corrosivity Worksheet,[26] that incorporate many of the key soil parameters are better methods to classify soil corrosivity. As a rule of thumb, however, soil corrosivity increases with increasing moisture, increasing acidity, soluble salts, dissolved oxygen contents in the soil, decreasing redox potential, and presence of sulfate-reducing bacteria (SRB).

TABLE 1 Most Common Pipeline Corrosion Threats, Influencing Factors, and Management Strategies

Corrosion Threat	Internal	External	Description	Influencing Factors	Management Strategies	References
AC Corrosion		✓	A buried pipeline that runs parallel to high-voltage powerlines, develops an induced alternating current (AC) in the pipe as a result of the alternating magnetic field associated with the powerlines. The induced AC escapes the pipe steel surface through holidays in the external coating. These sites then become the sites where AC corrosion initiates and progresses. AC can induce corrosion in coated buried pipelines despite adequate CP protection levels.	– AC density – CP potential level – Coating type and condition – Coating defect size – Soil type and resistivity – Distance from high-power voltage towers and power loads – Electrical grounding of the pipeline – Number of pipelines running parallel to the high-voltage lines	– DC decoupling – Connection to natural drains (e.g., steel casings) – Providing additional grounding – Insertion of isolating joints between pipeline sections – Monitoring of AC potentials and AC densities	27–30
Stray DC Corrosion		✓	Stray DC currents are electrical currents flowing in the soil from external sources, not directly associated with the CP system. A buried pipeline represents a low-resistance current path and therefore is prone to the effects of stray currents. Stray DC currents tend to enter and escape a buried pipeline through defects in the coating. It is where the current escapes the pipeline surface into the soil that severe corrosion can be expected.	– Soil type and resistivity – Coating type and condition – Depth of buried pipeline – Applied CP potential level – Presence of undesirable stray currents sources	– Removal of the stray current source or reduction in its output current – establishment of an electrical connection between the interfering and interfered-with structure – Cathodic shielding – Use of sacrificial anodes – Application of coatings to current pickup areas	31–33
Top of the Line Corrosion (TLC)	✓		TLC occurs primarily in subsea pipelines carrying unprocessed multiphase fluids (sweet or sour) with stratified and stratified-wavy flow regimes. TLC occurs because of water condensation at the 10 to 2 o'clock orientation. The condensed water phase is highly corrosive because of the presence of dissolved acid gases (H_2S and CO_2) and organic acids.	– Temperature gradient between the carried production fluid and the pipeline surface – Flow regime (TLC occurs only in stratified and stratified-wavy flow regimes) – Pipe material	– Providing corrosion allowance to the carbon steel pipe wall thickness during the design phase – Insulation (thermal or concrete) of the pipe to reduce temperature gradient	34–37

(continued)

TABLE 1 (*continued*)

Corrosion Threat	Internal	External	Description	Influencing Factors	Management Strategies	References
			Sour TLC primarily exists as uniform corrosion attack with low corrosion rates. In contrast, sweet TLC leads to localized corrosion attacks with high penetration rates.		– Applying corrosion inhibitors (batch or slug treatment) or vapor phase inhibitors – Using CRA solid pipe or CRA clad material – Using thermoplastics lined pipes	
Hydrogen Damage – Hydrogen embrittlement or loss in ductility (HE) – Hydrogen-assisted cracking (HAC) – Hydrogen-induced blistering (HIB) – Hydrogen-induced cracking (HIC) – Sulfide stress cracking (SSC)	✓	✓ (HE only)	Hydrogen damage causes loss of ductility and reduction in strength and fracture toughness of the pipe steel to a degree that could result in catastrophic failures of the pipe. Hydrogen damage is more dominant in high-strength low-alloy steels (X70, X80, X100, and X120) and CRAs and is most severe in the presence of H_2S because of the inhibition of hydrogen recombination reaction.	– Exposure time – Fluid composition – Operating conditions (temperature and pressure) – Stress level and state (applied or residual) – Hardness, strength, and microstructure of the pipe steel – CP level (in case of HE) – Pipe manufacturing process	– Materials selection via laboratory testing remains the principal approach for qualifying and selecting line pipe steels in applications where hydrogen damage can be a potential damage mechanism. – Use of internal coatings – Fitness-for-Service (FFS) assessment using API 579	38–40
Microbiologically Influenced Corrosion (MIC)	✓	✓	Microbiologically influenced corrosion (MIC) infers to the effect of specific microorganisms on the corrosion processes that take place at the metal surface. MIC typically takes on the form of localized attack. Although sulfate-reducing bacteria (SRB) is the most frequently reported bacteria type causing MIC, other types of bacteria have also been reported to cause MIC.	– Nutrients (must be present) – Water (must be present) – Temperature (<90°C) – Salinity – Fluid velocity and flow regime	– Use of high-performance corrosion inhibitors and biocides coupled with frequent pipeline pigging to remove biofilms and solid deposits – Fluid velocity control (avoid stagnant flow conditions during design stage) – Control fluid quality	41–44
Stress Corrosion Cracking (SCC)		✓	Two types of SCC in buried pipelines have been identified: high-pH SCC (occurs at pH range of 9.6 to 12.3 and is primarily intergranular) and near-neutral pH SCC (occurs at pH ≤7.5 and is primary transgranular). Both types are associated with colonies of microcracks near disbonded coatings. High-pH SCC is more predominant on coal tar or tape coated pipelines, whereas near-neutral pH SCC is more likely to occur on tape or asphalt coated pipelines. SCC has not been report on Fusion bonded epoxy (FBE)-coated pipelines and this is believed to be due to the nonshielding properties of FBE.	– Coating type and condition (e.g., disbondment) – Local environment – CP potential – Operating stresses – Temperature – Pipeline age – Distance from pump station or compressor	Adherence to common industry guidelines stated in ASME Code for pressure piping[49]	45–49
Black Powder	✓		Black powder refers to the blackish material that forms inside internally uncoated cross-country pipelines carrying "dry" sales gas. Black powder is composed mainly of corrosion products mechanically or chemically mixed with impurities, such as sand, metal debris, elementals sulfur, and hydrocarbon liquids. The primary reason for the corrosion in otherwise-"dry"	– Gas not meeting moisture specification is the primary factor – Presence or absence of internal coating – Commissioning practice	Strict adherence to gas moisture content specification coupled with in-pipeline removal methods, such as filtration and pigging, are the primary strategies to mitigate black powder formation and its impacts.	50–55

(continued)

TABLE 1 (*continued*)

Corrosion Threat	Internal	External	Description	Influencing Factors	Management Strategies	References
			sales gas lines is water condensation on the internal surfaces of these lines as a result of deficiencies in gas dehydration process (i.e., process upsets or under design of the dehydration units). Black powder adversely affects pipeline operations and sales gas customers alike.			
Underdeposit Corrosion (UDC)	✓		UDC is most prevalent in dead legs and low-flow/intermittent-flow pipelines. UDC typically takes on the form of localized attack that occurs beneath or around deposits/solids that accumulate and settle at the bottom of the pipeline. The corrosion mechanism and severity of the UDC is influenced by the type of deposit, and therefore an effective mitigation strategy relies on understanding the nature of the deposit that is present.	– Type and concentration of solids in the fluid – Pipe geometry and elevation – Fluid velocity – Pigging frequency	– Improved design of pipelines to avoid locations prone to solids and water accumulation – Improved quality of the fluid (solids management) – Optimization of flow velocity to keep solids entrained – Use of high-performance corrosion inhibitors and biocides coupled with frequent pipeline (pigging).	56–58
Pitting Corrosion	✓	✓	Internal pitting attack is more likely to occur at the 10 to 2 o'clock (sweet TLC) and 4 to 8 o'clock (BLC) orientations as result of water condensation and precipitation at these locations, respectively. Locations along the external surface of buried pipelines that experience coating damage or disbondment are more prone to pitting corrosion.	– Operating conditions (flow, temperature) and fluid composition – Soil type, properties and resistivity – Coating type and condition – CP level at coating defect areas	Chemical inhibitors coupled with periodic pigging, FBE coating, monitoring of coating condition and CP levels using aboveground inspection techniques (to be discussed)	35, 59
Erosion-Corrosion (EC)	✓		EC is typically reported in multiphase pipelines where one of the phases is solids (e.g., sand) and high-fluid velocity. It is believed that the erosion action removes the corrosion protective scale (e.g., $FeCO_3$ and FeS scales on carbon steels pipes and oxide layers on CRAs) exposing the bare metal for corrosion to occur. Typically, the damage caused by EC is higher than the damage incurred by either erosion or corrosion alone. The damage caused by EC is typically localized in locations where high changes in flow are experienced, such as pipeline bends, tees, and pressure control valves.	– Type, concentration, and geometry of solid particles – Fluid velocity – Flow regime – Geometry and diameter of pipe	– Enhanced design by changing flow geometry – Materials selection – Corrosion inhibitors – Solids management – Flow velocity control – Erosion and corrosion Monitoring – Monitoring of eroding particles	60–62
Flow-Induced Localized Corrosion (FILC)	✓		FILC is typically associated with high flow and high turbulence fluids creating hydrodynamic conditions that cause the destruction of the protective corrosion product films and hinder their reformation leading to increased localized corrosion rates. Also, the high shear accelerates the transfer of the corrosive elements (e.g., corrosive gases, salts) to the bare steel pipe surfaces	– Fluid velocity and composition – Flow regime – Temperature and pressure – Geometry and diameter of pipe	– Improved pipeline design to avoid high-turbulence hydrodynamic conditions – High-shear-resistant corrosion inhibitors	63–65

(continued)

TABLE 1 (*continued*)

Corrosion Threat	Internal	External	Description	Influencing Factors	Management Strategies	References
			leading to increased corrosion at these sites. FILC is different than EC in that fluids causing FILC are solid free or do not contain solid particles in sufficient concentrations or sizes to cause erosion.			
Preferential Weld Corrosion (PWC)	✓	✓	Weldments can experience accelerated preferential corrosion attacks compared with the adjacent parent metal even though both areas are exposed to the same environment. This is mainly due to the fact that weldments are not exactly of the same metallurgy and have higher stresses than the rest of the pipe. PWC can exist in various forms, such as pitting, crevice, galvanic, SCC, and different types of hydrogen damage. PWC can initiate and progress from inside (fluid side) or outside (soil side) of the pipe.	Welding Factors – Welding procedure – Choice of filler metal – Weld quality Environmental Factors – Fluid composition and hydrodynamic condition – Soil type and properties – External coating type and condition – CP level – Stress (applied or residual)	– Improved welding procedures and filler metal selection – Corrosion inhibitors – Quality of girth weld coating	2, 66–70

TABLE 2 Test Methods for Testing Soil Properties Affecting Corrosion of Buried Metal Structures

Property	Test Method	F/L
Resistivity	ASTM G57, *Standard Test Method for Measurement of Soil Resistivity Using the Wenner Four-Electrode Method*	F
	ASTM G187, *Standard Test Method for Measurement of Soil Resistivity Using the Two-Electrode Soil Box Method*	L
Moisture Content	ASTM D4959, *Standard Test Method for Determination of Water Content of Soil by Direct Heating*	L
Chloride Content	ASSHTO T291-94, *Standard Method for Test for Determining Water-Soluble Chloride Ion Content in Soil*	L
Sulfate Content	ASSHTO T290-95, *Standard Method for Test for Determining Water-Soluble Sulfate Ion Content in Soil*	L
pH	ASTM G51, *Standard Test Method for Measuring pH of Soil for Use in Corrosion Testing*	F/L
MIC	Accepted laboratory test methods (e.g., quantitative polymerase chain reaction [qPCR] technique)	L
Redox Potential	ASTM G200, *Standard Test Method for Measurement of Oxidation-Reduction Potential (ORP) of Soil*	F/L

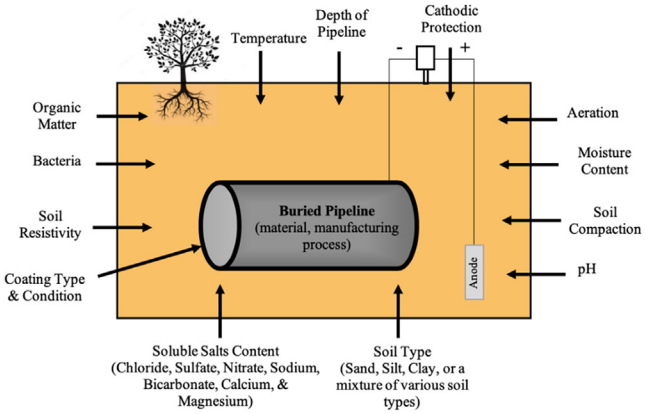
Note: F, Field test method; L, Laboratory test method.

The susceptibility of buried pipelines to different external CDM, such as pitting, stress corrosion cracking (SCC), alternating current (AC), and direct current (DC) corrosion, is further complicated by other non-soil-related factors, such as external coating type and condition, CP levels, distance from compressors or pump stations, and distance from high-power voltage towers. Figure 1 illustrates the complexity of factors affecting external corrosion of buried pipelines in soils.

External corrosion protection of buried pipelines can be achieved through materials selection, selective backfill, barrier coatings, AC and stray DC control, and CP.[21]

In some cases, however, external corrosion of buried pipelines can be eliminated by installing these pipes above grade, rather than burying them. To further safeguard against soil corrosion of the bottom side of the pipe (if the pipe were to be placed immediately on the soil), flow lines typically are raised off the ground on "sleepers," which are typically concrete blocks. This has become a common practice with oil and gas companies operating in the Middle East.

FIG. 1 A schematic representation of the key factors influencing soil corrosivity and external corrosion of pipelines buried in soils.



Corrosion Testing

Pipeline operators and owners resort to different testing strategies to ensure the integrity of their pipelines. These strategies can be categorized into three main time domains: (1) Reactive, which utilizes nondestructive testing (NDT) technologies that reveal corrosion defects that existed in the pipeline before the commencement of NDT (i.e., reveal past conditions); (2) present, which uses testing and monitoring methods and techniques to assess the "current" corrosion performance of the pipeline; and (3) proactive, which employs indirect inspection techniques, modeling, and direct assessment (DA) methods to predict the likelihood of corrosion occurring along the length of a buried pipeline.

Table 3 lists the primary testing techniques and methods that most commonly are used in the field for testing and monitoring corrosion in a pipeline along its life span. The following sections provide a brief overview of each of these testing strategies.

For the entire range of testing, inspection, and corrosion monitoring methods available to oil and gas pipelines operators, see NACE International publications and paper presentations.[71–75]

Reactive Testing Strategies

VISUAL

Field evaluations consist of documenting both visual observations and measurements of corrosion on pipeline sections. Evaluation of the environment also provides valuable information in the analysis of pipe corrosion. Visual methods are difficult to use on underground pipes because the pipeline must be excavated to be examined; however, this is often the best way to evaluate the condition of a pipe. Carefully obtained corrosion measurements can be analyzed using normal probability and extreme value statistics.[21] There are no standards for performing this type of test. It is suggested that the locations for visual evaluations be carefully selected from leak and inspection records, excavation reports, close-interval potential (CIP), alternating current attenuation (ACA), direct current voltage gradient (DCVG), and alternating current voltage gradient (ACVG) surveys results (to be discussed), and soil resistivity. The visual examination and corrosion measurement sites can also be selected through the use of DA methodologies (to be discussed).

It is often difficult to evaluate the condition of a pipe by simple examination in the ditch because of the presence of corrosion products, deposits, and coatings. Cleaning and measuring corrosion on a section of pipe in the ditch provides the most accurate information, and the collected data are used in the statistical analysis. Extending the data from a single pipe section to the entire pipe is not recommended beyond 1,000 ft (305 m) or where the environment is known to vary significantly from that in the excavated section.[21]

Uncoated pipeline should be thoroughly cleaned to remove all corrosion product and foreign matter (as in the evaluation of any corrosion, samples of the corrosion product should be retained for further analysis if the cause of the corrosion is unknown). Irregular surfaces and hard brownish deposits on the pipe are indicators that corrosion has occurred. Black or whitish deposits are indicators of possible anaerobic SRB.

Visual inspection of an uncoated pipe in the ditch before pipe preparation includes the following steps:[21,76]

1. Take macro shots of the excavated pipeline section and close-up photos of the defect areas.
2. Clean the pipe surface to remove loose soil and debris and expose the defect areas.
3. Describe locations of corroded areas (near spiral or seam weld, near girth weld, under heat shrink sleeve [HSS], at bends, clock position).
4. Photograph and describe corrosion product properties (color, smell, dry/wet).
5. Collect corrosion product in well-sealed and clean containers for further laboratory analyses.
6. Take soil samples from the location near the corroded area for further lab analysis.
7. On site, evaluate black or whitish deposits for SRB. A quick qualitative determination can be made using a 10% hydrochloric acid solution in water. Place a drop of the solution on the deposit. An aroma of H_2S (rotten eggs) indicates that SRB are present. Significant corrosion of the pipe might have occurred and further investigation is warranted. Wear safety glasses and gloves when handling the acid and observe all necessary safety precautions. Commercial test kits are available that can provide a quantitative determination of the type and quantity of bacteria present.

TABLE 3 Commonly Used Field Techniques and Methods for Testing and Monitoring of Pipeline Corrosion

Reactive	Present Condition	Proactive
– Visual	– Corrosion Coupons	– Close-Interval Potential (CIP) Survey
– Liquid Penetrant Testing	– ER Probes	– Alternating Current Attenuation (ACA) Survey
– Magnetic Particle Testing	– LPR Probes	– Direct Current Voltage Gradient (DCVG) Survey
– In-Line Inspection (ILI)		– Alternating Current Voltage Gradient (ACVG) Survey
– Handheld Ultrasonic Testing		– Direct Assessment (DA) Methods
– Guided Wave Testing		– Modeling and Prediction

8. Photograph the steel surface beneath the corrosion product (after removal of all corrosion using grit blast) and describe the appearance of exposed steel surface.
9. Describe the steel surface defect (size, spacing, shallowness, elongation) and measure wall thickness loss (e.g., pit depths).
10. Document all observations on data sheets and with photographs.

Coated pipes are somewhat more difficult to evaluate, because corrosion occurs only at coating defects and sometimes under disbonded coating. Visual inspection of coated buried pipelines includes the following steps:[76]

1. Take macro shots of the dugout pipeline section and damaged coating areas.
2. Describe damaged coating locations (near spiral or seam weld, near girth weld, under HSS, at bend, clock position).
3. Extract liquid from any intact coating blisters, measure pH (using litmus paper) and send extracted liquid sample to laboratory for further analysis (CNS, pH). Use safety gloves and glasses when extracting these liquids (pH values as high as 12 of the liquids have been measured).
4. Document color of coating and describe coating properties (brittle, fragments, flexible, tough).
5. Describe any pipe markings/stencils on the underside of coating.
6. Describe any scratches, gouges, or impact marks on the coating.
7. Describe any contamination or adherent corrosion visible on underside of the coating.
8. Measure dry film thickness of damaged coating and adjacent areas.
9. Remove the damaged coating by prying.
10. Describe appearance (rusted, pristine) of exposed steel surface underneath the removed coating and take macro and close up photos.
11. Measure blast profile and identify contamination, if any, on steel surface (abrasive, grease, oil, dust).
12. Determine salt levels using a Bresle patch.

Table 4 shows some of the key field test methods used for external coated buried pipelines. For more information on how to conduct in-ditch examination of uncoated and coated buried pipelines, see El-Sherik, Dakwar, and Byrnes[76] and Zinter.[77]

TABLE 4 Key Field Test Methods Used for External Coated Buried Pipelines

Test	Method	Purpose
Bresle Test (surface salt)	ISO 8502-9, *Preparation of steel substrates before application of paints and related products—Tests for the assessment of surface cleanliness*; Part 9: *Field method for the conductometric determination of water-soluble salts*	Used to determine preexisting contamination. Surface salt on the steel draws in moisture through the film through osmosis, leading to blistering.
Glass Slide Test	ASTM A380 (7.3.1), *Standard Practice for Cleaning, Descaling, and Passivation of Stainless Steel Parts, Equipment, and Systems*	Grease and oil on steel surface are dissolved with a nonpolar solvent, and then evaporated away from a glass slide. The oily film retained is indicative of hydrocarbon contamination.
Tape Test	ISO 8502, Part 3, *Assessment of dust on steel surfaces prepared for painting (pressure-sensitive tape method)*	Tape applied to the steel surface will collect any dust and this can be rated to comment on plant cleanliness. Dust affects film adhesion.
Surface Profile	ASTM D4417, *Standard Test Methods for Field Measurement of Surface Profile of Blast Cleaned Steel*	Coatings bond to steel mechanically, so a minimum profile is needed.

LIQUID PENETRANT AND MAGNETIC PARTICLE TESTING

Liquid penetrant (LP) and magnetic particle (MP) testing techniques are visual methods employed by inspectors to aid in the visual inspection of the external surfaces of pipelines. Removal of external coating as well as cleaning of the pipe steel surface of any corrosion product, rust, dirt, and soil are essential steps before carrying out these testing methods. In the case of a buried pipeline, this also implies excavation of the pipe section to be examined. The advantages of both techniques are their maturity and reliability, low cost, speed of the tests, and simplicity of application and interpretation. By their nature, these techniques are limited to examining the external surfaces of pipelines for surface-breaking and shallow near-surface (in case of MP only) flaws.

When performing LP testing, a liquid penetrant(normally a colored dye or a fluorescent material) is applied to a clean pipe surface. The liquid is allowed time to soak the cleaned pipe surface area and some of this liquid penetrates into any existing cracks that are open to the surface. The excess liquid is then removed (wiped off) from the pipe surface and a developer (normally white in color) is applied to the area. The developer draws out the liquid penetrant from the surface cracks and onto the steel surface to form visible indications. These indications can be observed easily by the naked eye under visible light or, if necessary, using ultraviolet light in case fluorescent penetrant was applied. LP is effective for detection of open-to-surface hairline cracks, such as SCC.

When carrying out MP testing, the surface to be examined is magnetized, inducing a magnetic field in the pipe. Surface or shallow subsurface flaws distort the magnetic field, leading to flux leakage at these distortion sites. To visually identify these flux leakage sites, fine magnetic particles, either dry or in a wet suspension, are applied to the magnetized surface. The fine

particles (normally white or yellow in color) become attracted to the flux leakage sites and take on the shape and size of the imperfections. MP testing is effective in detecting open to surface or shallow subsurface flaws such as SCC and hydrogen-induced cracking (HIC) cracks, respectively. The application of MP technique is limited to ferromagnetic materials, such as iron, nickel, and cobalt, and some of their alloys.

The following standards provide guidelines for conducting LP and MP techniques:

- ASTM E1444/E1444M (latest revision), *Standard Practice for Magnetic Particle Testing for Aerospace*
- ASTM E1417 (latest revision), *Standard Practice for Liquid Penetrant Testing*

IN-LINE INSPECTION

In-line inspection (ILI) of pipelines is carried out using instrumented or "smart pigs" that travel inside the pipeline from one end of the pipe to the other. Only pipelines that are designed with an ILI instrument launcher and receiver ports and have no obstructions, such as sharp bends or changes in diameter, can be tested using ILI technique.[78] These pipelines are normally designated as “piggable” pipelines. “Unpiggable" pipelines can be inspected employing different methods and techniques other than ILI. For several techniques used for inspection of unpiggable pipelines, see Steinvoorte.[79]

ILI instruments are equipped with nondestructive testing tools (probes), such as magnetic flux leakage (MFL), ultrasonic, eddy current, and electromagnetic acoustic transducer (EMAT). These probes can detect and measure different types of defects and anomalies, including pitting, cracks, coating disbondment, dents, and gouges, that exist on the inside and outside surfaces of the pipe wall.

Ultrasonic devices work by measuring the time that it takes a high-frequency sound wave to travel across the pipe thickness and back to the transducer. The instrument is calibrated to measure this time as thickness of the pipe wall. A change in wall thickness or the presence of a crack perpendicular to the UT wave will cause a change in the height of reflected UT echo. Magnetic or eddy current devices work by sensing deviations in a magnetic flux field caused by corrosion pits or other defects that distort the flux field. For more information, consult Holm,[80] Schmidt,[81] and NACE International.[82]

The choice of ILI tool is largely dictated by the purpose of the inspection (e.g., what the pipeline operator/owner is looking for). For example, ILI-MFL, an ILI instrument equipped with MFL probe, is primarily used to detect metal loss caused by general corrosion, pitting, erosion, or mechanically induced metal loss (e.g., gouges).[78] ILI-MFL can be used in gas and crude lines and the MFL sensor comes with different resolutions depending on the required level of detection. ILI-UT is employed primarily for the detection and measurement of cracks along the major access of the pipeline such as HIC and blisters.[78] This method requires that the UT sensors be fully coupled to the pipe wall for the ultra–sound wave to travel through the wall thickness. This implies that the UT sensors and by extension the instrument must be fully immersed in a homogenous fluid. This makes pipelines carrying crude oils and refined products suitable for ILI-UT inspection, whereas gas and multiphase pipelines unsuitable.

A recent advancement in ILI testing is the use of an EMAT tool to detect tight cracks (e.g., SCCs, step-wise cracks), coating damage and disbondment that exist on the inside and outside of the pipe.[83,84] ILI-EMAT uses guided wave acoustics sensors that do not require liquid coupling; therefore, this technology is widely used to test gas pipelines.

ILI instruments also can be equipped with more than one tool to increase their effectiveness of detection and sizing of different defects at a lower cost (one instrument run instead of multiple runs each using a specific ILI tool). For example, ILI-MFL-UT can detect and size various defects more effectively and at a lower cost than running a separate ILI-MFL and following it with an ILI-UT run.

ILI testing of the same pipeline segment is typically repeated every several years (three- to five-year cycles is typical). This repeat test cycles provide corrosion growth rate information of the same reported defects.

The following standards provide general guidelines for performing ILI of pipelines:

- NACE Standard Practice SP0102 (latest revision), *In-Line Inspection of Pipelines*
- NACE Publication 35100, *Inline Non-destructive Inspection of Pipelines*

HANDHELD ULTRASONIC NONDESTRUCTIVE TESTING

Ultrasonic testing (UT) is a nonintrusive NDT technique that uses high-frequency sound waves to detect and measure flaws and dimensional changes. UT operates on the principal of measuring the time that it takes a high-frequency sound waves to travel across the pipe thickness and back to the transducer. The instrument is calibrated to measure this time as thickness of the pipe wall. A change in wall thickness or the presence of a crack perpendicular to the UT wave will cause a change in the height of reflected UT echo. Conventional UT probes use single-element transducer or paired-element transducers, one for transmission of the sound waves and the other for receiving. Phased arrays UT (PAUT) is the latest advancement in handheld UT testing and uses transducers that contain a large number (16 to 256) of elements. The main advantage of PAUT is that it provides improved flaw detection and flaw visualization.[85]

In principle, UT techniques can measure wall thickness losses of 0.025 mm given that the transducer is accurately positioned in contact with the pipe surface.[74] The detection accuracy is strongly affected by several factors, such as variations of sound velocity in different metals, temperature variations in the metal substrate, improper surface preparation, and the ability of the transducer to resolve the different acoustic reflections. Under realistic field conditions, UT can detect wall losses larger than 0.1 mm.[74] Ultrasonic measurements can be used to verify and validate ILI results and to supplement mechanical pit depth measurements and also can be used in areas where the internal

condition of the pipe must be determined.[21] Ultrasonic measurements can be analyzed using the same statistical approach as mechanical measurements.

There are several important considerations relative to ultrasonic measurements. One is the doubling effect of some digital gages when the thickness limitation of the transducer is reached. Another is the effect of coatings on the readings. Most pulse-echo instruments will provide inaccurate information when the tester tries to read through an organic coating on the pipe. Coatings must be removed unless the equipment used compensates for the presence of the coating. The surface roughness of the pipe, both internal and external, plays an important role in the accuracy of the data. The surface must be relatively smooth. Roughness can make it either difficult or impossible to obtain accurate thickness data. It is sometimes necessary to grind the surface just enough to allow the transducer a flat surface. An important consideration is the nature of the internal corrosion. Internal pitting that consists of narrow or widely scattered pits might be difficult to find with handheld UT devices, because the probability of the transducer being immediately above a pit can be low.[21] In that case, a scanning approach should be used to cover the widest area possible. A visual inspection of the pipe is a good idea if at all possible to determine the type of corrosion present.

The following standards provide general guidelines for using UT inspection:

- ASME (4) Boiler and Pressure Vessel Code, Section V, *Nondestructive Examination*
- ANST Recommended Practice No. SNT-TC-1A, *Personnel Qualification and Certification in Non-destructive Testing*
- NACE 3T199, *Techniques for Monitoring Corrosion and Related Parameters in Field Applications*

GUIDED WAVE TESTING

Another technique that is increasingly gaining acceptance with pipeline operators is guided wave testing (GWT). GWT employs ultrasonic waves that propagate through the pipe wall for long distances along the pipe and, as such, GWT has the potential to achieve many meters of inspection using one probe location. GWT sensors are made into a ring that can be installed around the pipe circumference. This ring configuration provides 360° inspection coverage of the inspected pipe length. GWT provides only qualitative information and therefore is used as a rapid screening tool for corrosion detection. Once defect areas are identified by GWT, other corrosion mapping technologies, such as handheld UT, are used to examine these specific areas and collect more in-depth information, such as the size, depth, and type of corrosion defects.

GWT is not suitable for the detection of pits, cracks, and pinholes but is most effective in detecting general internal or external metal loss (normally above 5% wall loss). GWT cannot distinguish whether the wall loss is on the internal or external surface of the pipe. GWT is ideal to inspect inaccessible pipes (under road crossings where excavation is not possible) or difficult-to-inspect pipes (e.g., overhead pipes and pipelines inside casings).

The following standard provides general guidelines for the application of GWT in pipeline inspection:

- NACE Standard Practice SP0313 (latest revision), *Guided Wave Technology for Piping Applications*

Present Condition Testing Strategies

CORROSION COUPONS

Coupons are relatively small pieces of metal, with the same metallurgy as the pipeline being evaluated, that are inserted into the environment to which the pipeline is exposed. Coupons can be buried in the soil next to the pipeline to measure soil corrosivity and CP protection level and to reveal the CDM.[21,86,87] For existing pipelines, coupons should be connected to the pipe to expose them to galvanic and stray currents and to the surrounding soil environment. Coupons can be inserted inside the pipeline and into the carried fluid to measure fluid corrosivity and determine the effectiveness of the inhibition program. Coupons should be inserted at locations where corrosion is expected to be the highest (e.g., 4 to 8 o'clock position) and not at the most convenient location (e.g., 10 to 2 o'clock). Coupons can be evaluated, after immersion in the environment, at predetermined periods of time (typically 90 or 180 days) using mass loss following ASTM G112, *Standard Guide for Conducting Corrosion Tests in Aluminum Alloys*.[88] This method provides general corrosion rate information in terms of thickness loss (in millimeters per year). All coupons should be large enough for pitting to develop and should be evaluated visually after exposure for the presence of corrosion pits. If present, pit depths should be measured after cleaning of coupons surface as per ASTM G112. Simple methods, such as handheld pin micrometer, or more sophisticated automated methods, such as surface profilometry (mechanical or chromatic light) or high-powered digital microscopy, can be used to measure pit depths. Another method for measuring pit depth is to use nondestructive X-ray radiography technique. The latter three methods quantify pitting corrosion both in terms of pit depths and percentage of affected areas. Regardless of which method is used to evaluate pitting, the pitting corrosion rate should be calculated based on the deepest pit.

More information on this topic can be found in the following standards:

- ASTM G46, *Standard Guide for Examination and Evaluation of Pitting Corrosion*
- ASTM G4, *Standard Guide for Conducting Corrosion Tests in Field Applications*
- NACE Technical Committee Report 3T199, *Techniques for Monitoring Corrosion and Related Parameters in Field Applications*
- NACE Standard Recommended Practice SP0775 (latest revision), *Preparation, Installation, Analysis, and Interpretation of Corrosion Coupons in Oilfield Operations*

ELECTRICAL RESISTANCE PROBES

Similar to coupons, electrical resistance (ER) probes can be installed inside the pipeline and into the transported fluid to determine the internal corrosion rate and evaluate the effectiveness of the inhibition program. They can also be installed in the soil next to the pipe to measure soil corrosivity and determine potential CDM. For soil side applications, ER probes are also referred to as soil corrosion probes (SCP).[87] SCP also can be used to evaluate the effectiveness of the CP particularly in high resistivity soils.

All ER probes consist of sensing wires of the same metallurgy as the pipe of interest. The change (increase) in the ER of these sensing wires is due to the reduction in the cross-sectional area as a result of corrosion. This is the basis by which the corrosion rate is calculated,[86,89] per the following formula:

$$R = \sigma_{metal} L/A, \quad (1)$$

where:
R = measured resistance, ohm,
σ_{metal} = resistivity of the metal, ohm-m,
L = length of the sensing wire, m, and
A = cross-sectional area of the sensing wires, m^2.

It is assumed that the reduction in the cross-sectional area of the sensing wire is uniform and therefore ER probes can provide only general corrosion rates. ER probes cannot be used to measure pitting corrosion rates.[86,89] Another important application of ER probes is in the monitor of corrosion under insulation. This is achieved by direct detection of the early corrosion taking place under the insulation.[90]

ER probes do not measure the instantaneous corrosion rate as it takes place but until a certain detectable amount of thinning of the sensing wire occurs over a period of time (this is the reason ER probes are considered near-real-time probes). The response time of ER probes is a function of the corrosion rate and the starting thickness of the sensing wire and can be in the range of hours or days. For example, in one ER probe configuration, response times of 7 h and 30 h for a corrosion rates of 10 mpy and 5 mpy, respectively, were reported.[91] Corrosion rate measurement may be taken periodically using a portable data logger or on a continuous basis using a permanently installed unit.

ER probes can be used in low- or high-conductivity fluids but should be used with caution in sour fluids because of the potential of forming conductive corrosion deposits (FeS) covering the sensing elements leading to short circuiting.[86] Short circuiting can be reduced through the selection of the appropriate wire design configuration (ring, cylinders, flat shaped, flush).

For more information on this topic, see NACE International publications and paper presentations.[71–74]

LINEAR POLARIZATION RESISTANCE PROBES

Linear polarization resistance (LPR) probes also intrusive devices that can be inserted into the pipeline and into the carried fluid to measure fluid corrosivity (and determine the internal corrosion rate) and provide information about the effectiveness of the inhibition treatment.[86–89] Their chief merit is that they provide instantaneous corrosion rates (real-time devices) permitting pipelines operators and owners to react quickly to acquired information (e.g., adjusting inhibitor dosage). To work properly, LPR probes require high-conductivity solutions such as disposal water pipelines but they have poor performance in low conductivity fluids such as crude oil, hydrocarbons etc.

More information on LPR technique can be found in the following NACE and ASTM publications:

- NACE Technical Committee Report 3T199, *Techniques for Monitoring Corrosion and Related Parameters in Field Applications*
- NACE Publication 31014, *Field Monitoring of Corrosion Rates in Oil and Gas Production Environments Using Electrochemical Techniques*
- ASTM G96, *Standard Guide for Online Monitoring of Corrosion in Plan Equipment (Electrical and Electrochemical Methods)*

Proactive Testing Strategies

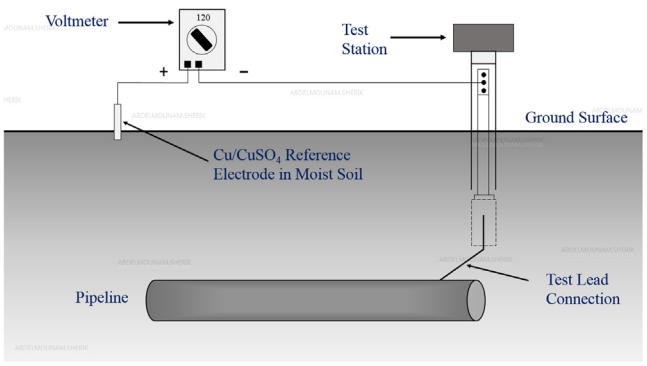
POTENTIAL MEASUREMENTS

Corrosion testing often involves determining the relative level of electrical activity of various structures, such as pipelines in the environment in which they are installed. These environments may be soil or water. The environment in which the structure is installed is the electrolyte that can and will support corrosion activity. Pipeline-to-electrolyte potential measurements may be used at various stages in the corrosion evaluation to determine the existence of corrosion activity. This is accomplished by measuring the "native" or "natural" potential of the pipeline. This involves using the circuit shown in figure 2.

The measurements taken will indicate the electrical characteristics exhibited by the pipeline in its natural state. For example, for a pipeline installed in soil, the potential with respect to the soil by means of a standard reference electrode, taken at regular intervals along the pipeline, will indicate the corrosion patterns affecting the pipeline (described in the next section).

Once the potential pattern has been measured for a structure, potential measurements can be used to evaluate the effects of the application of CP current. While a measured quantity of current is applied to a structure, potential measurements are taken at locations at which the native potential measurements

FIG. 2 Pipe-to-soil potential measurement.



had been taken. The shift in potential as well as polarization effects due to the application of the current can be measured. These data can be used to determine the quantity of current required to achieve CP of the structure.

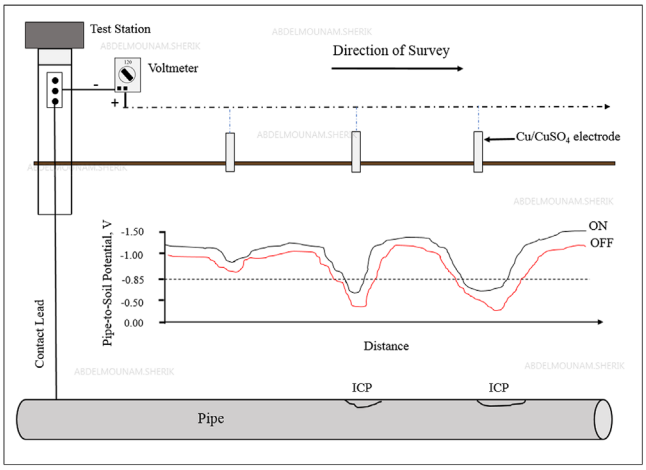
Potential measurements also are used to gauge the effectiveness of a CP system, after it has been installed and is operating, in mitigating the corrosion activity detected by the native potential profile. The pipe-to-soil potential measurement has been established by corrosion engineers as a standard for determining the degree of CP on buried pipelines. Various criteria have been promulgated; the three currently in use for steel structures are as follows:[21] (1) the achievement of a pipe-to-soil potential of −850 mV referenced to a copper-copper sulfate (CSE) electrode with CP current applied considering IR drop, (2) the achievement of a polarized potential of −850 mV (instant-off) versus CSE, and (3) the achievement of a −100 mV shift in potential because of cathodic polarization. Although these are the generally accepted CP criteria, different criteria also can be used to address unique environments (soil types). For example, one company in the Middle East uses −1,000 mV ON versus CSE for pipelines buried in Sabkha areas (Sabkha is a low-resistivity soil found near the sea shores; Sabkha is quite corrosive because it is high in moisture and salt content) and −1,100 mV ON versus CSE for non-Sabkha areas (dry soils).

These potential measurements can be taken at set locations (test station surveys) along a pipeline, or continuously, as in the case of a close interval potential survey (CIPS). Test station surveys do not guarantee that the pipeline segments between these test stations are adequately protected against corrosion. For this reason, CIPSs are more reliable in determining the effectiveness of CP in providing corrosion protection along the entire length of a buried pipeline.

CLOSE-INTERVAL POTENTIAL SURVEY

The CIPS technique measures pipe-to-soil potential to assess the performance of the CP system. CIPS provide both the on-potential and the instant off-potential profiles along the length of the pipeline at the ground surface.[21,92–97] The CIPS is achieved by connecting an insulated electrical wire (typically few kilometers long) to the buried pipeline with the other end of the wire connected to the positive port of a high impedance (10^7 ohms or higher) data logger-voltammeter or multimeter.[92] The positive port of the voltmeter is connected to a reference electrode (typically a CSE electrode). The center line of the pipeline must be located accurately before performing the survey. The surveyor walks over the centerline of the pipeline, unwinds the insulated electrical wire, and places the reference electrode directly above the pipeline at intervals of 1 to 2 m. Both the on- and instant off-potentials between the buried pipeline and the reference electrode are measured. Locations where both potentials are more positive than the established CP protection criteria (see previous section) are sites of inadequate CP protection and therefore are the most probable sites for external corrosion to occur.[21,92–97] Figure 3 is a schematic representation of on-potential and instant off-potential profiles obtained by a CIPS on a buried pipeline. Sites of inadequate CP protection are marked as ICP on the pipeline in figure 3. These locations of inadequate CP protection can further be examined during the direct examination step in the external corrosion direct assessment (ECDA) method (discussed in the following sections).

FIG. 3 A representation of on-potential and instant off-potential profiles obtained by CIPS on buried pipeline. Locations of inadequate CP are marked as (ICP) on the pipe.



Sophisticated computerized data loggers to record the large numbers of potential readings that can be collected during the course of CIPS have been developed and are commercially available. These data loggers along with personal computers can provide a continuous profile of the potential along miles of pipeline traversing all types of terrain. Some instrumentation can be linked to global positioning systems synchronization software.

The following standards provide general guidelines for performing a CIPS for pipelines:

- NACE Recommended Standard Practice SP0207, *Performing Close Interval Potential Surveys and DC Surface Potential Gradient Surveys on Buried or Submerged metallic Pipelines*
- NACE Standard Practice SP0502, *External Corrosion Direct Assessment Methodology (ECDA)*

ALTERNATING CURRENT ATTENUATION SURVEY

ACA technique provides the average coating quality over a pipeline segment typically of 50 to 300 ft in length.[75,92] The ACA survey does not locate coating flaws but instead provides a macro assessment of the coating condition over a given length of buried pipeline.[75,92] It is normally performed to prioritize pipeline segments for subsequent closer indirect inspection using the ACVG technique (discussed in the next section).[75]

The ACA survey is conducted by placing an AC current-transmitter at one end and a receiver (detector) at the other end of the pipe segment to be surveyed. Both transmitter and receiver are placed above the ground surface over the centerline of the pipe section to be surveyed. The transmitter has to be in physical contact with the ground surface and in conductive contact with the pipe, but the detector can be located some

distance off the ground.[92] In carrying out this survey, an AC current signal of low frequency is applied by the transmitter to the buried coated metallic pipe. The AC current flows away from the injection point (transmitter) down the length of the pipe inducing an electromagnetic (EM) field around the pipe. The EM field attenuates (i.e., becomes weaker) as a function of distance from its source (AC transmitter). The principal of the ACA technique is the measurement of the attenuation in the strength of EM field between the transmitter and receiver locations. Figure 4 is a schematic representation depicting the principals of ACA survey.

EM field attenuation is measured in milibells per unit length of pipe (mB/m or mB/ft) allowing comparison of coating quality of different pipeline segments. The rate of attenuation is affected by pipe diameter, wall thickness and depth, AC current frequency, soil resistivity, and coating dielectric constant.[92] For a given set of these parameters, EM field attenuation is affected by the coating quality. For a perfectly coated pipe, the magnitude of the EM field decreases gradually as it flows from the transmitter to the receiver. When a coating contains flaws, however, EM attenuates more rapidly. Comparison of the rate of current attenuation of several pipe segments allows for the ranking of the coating condition on these pipe sections.

The following standard provides guidelines for performing ACA survey:

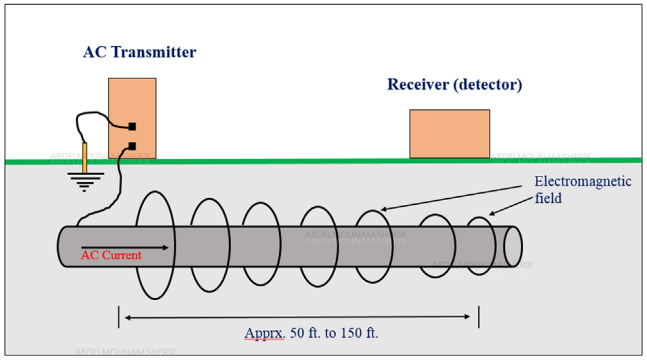
- NACE Standard TM0109, *Above-ground Survey Techniques for the Evaluation of Underground Pipeline Coating Condition*

DIRECT CURRENT VOLTAGE GRADIENT SURVEY

DCVG surveys typically are performed on well-coated pipelines with the goal of locating coating flaws and assess the relative severity of these flaws once found. Locations of coating defects are expected to be the most likely sites for external corrosion to occur.[75,92–97]

DCVG surveys involve soil-to-soil potential difference (voltage gradient) measurements at the ground surface over the pipeline. In CP-protected buried pipelines, DC current flows in the soil from the anode bed to the pipeline polarizing the pipe with respect to the surrounding soil.[92–96] As such a potential gradient exists between the pipe and the surrounding soil where the potential is highest (most negative) at the pipe surface and dropping off rapidly to zero value at a certain distance away from the pipe. In the case of a perfect coating (no holidays), the potential in the vicinity of the pipe at the ground surface over the pipe will be close zero and no potential gradient exists. In the presence of a coating defect, however, the DC current flows primarily into the defect site polarizing the pipe with respect to the surrounding soil and, as such, a voltage gradient is developed.[92–96] This voltage gradient can be measured using two CSE reference electrodes positioned at the bottom of walking cane probes. The two cane probes are connected to a standard voltmeter measuring voltage in mV.

FIG. 4 A schematic representation depicting the principals of ACA survey. EM field lines attenuate as the current flows away from the transmitter.



DCVG survey can be performed in two different ways: perpendicular mode and in-line (or parallel) mode.[97] In both modes, no direct electrical connection is made to the pipeline, and the center line of the pipeline must accurately be located before performing the survey. In the perpendicular mode, the two probes (while electrically connected to the voltmeter) are placed perpendicular to the pipeline direction. One probe is positioned over the centerline of the pipe and the other probe is placed typically 5 ft away from the first probe. With this probe spacing maintained, the surveyor walks down the length of the pipeline placing the probe pair at intervals (typically 5 ft) and measures the potential difference between the two probes at the ground surface.

In the in-line (or parallel) mode, a surveyor walks over the pipe placing the two probes at different locations directly over the centerline of the pipe measuring the potential gradient between the two probes.

In both DCVG survey modes, the voltage gradient increases as the surveyor approaches the defect and decreases moving away from the defect. The maximum voltage gradient measured between the two probes indicates the location of the center of a coating defect.[92] Factors such as soil resistivity, pipe depth and diameter, coating type, clock position of the coating defect (e.g., 12 o'clock versus 6 o'clock), probe contact to the ground surface, and density of coating defects affect the magnitude of the measured voltage gradient. For a given set of these factors, the magnitude of the voltage gradient is directly related to the size of the coating defect.[92,95]

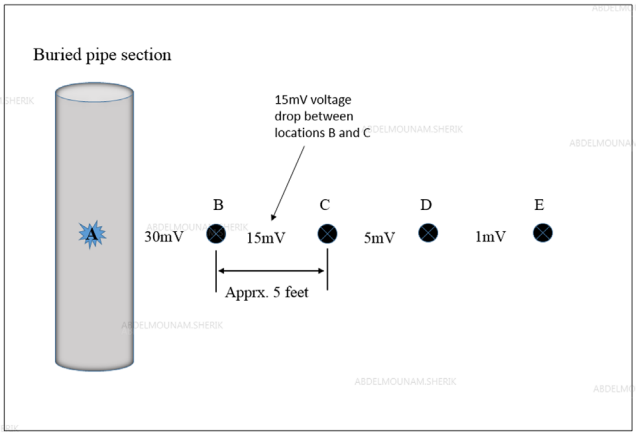
Once a coating defect is located (as discussed previously), the severity of the defect is determined through % IR drop calculation.[96,97] Table 5 provides general guidelines for interpretation of % IR values and recommended actions.

Taking the % IR measurement involves successive lateral measurements of the soil-to-soil potential difference in the perpendicular direction moving away from the defect. Figure 5 is a schematic representation of % IR measurements. The potential measurements are made using a CSE electrode placed on the ground surface at intervals of approximately 5 ft. The measurements are stopped when the potential gradient is equal or less than 1.0 mV. To calculate % IR, the potential gradient of the successive measurements are added and then divided by the IR drop

TABLE 5 % IR Values, Defect Severity, and Recommended Actions

% IR	Defect Severity	Recommended Action
1–15	Very minor	No action; existing CP is assumed to provide adequate protection
16–35	Minor	Monitor; schedule another DCVG in near future
36–60	Moderate	Excavate and examine OR monitor using DCVG
61–100	Severe	Immediate action; excavate and repair coating

FIG. 5 A representation illustrating lateral measurements of % IR.



at the ground surface directly above the coating defect. Details on how to calculate % IR can be found in McKinney.[97]

ALTERNATING CURRENT VOLTAGE GRADIENT SURVEY

ACVG is similar to DCVG in that it is an indirect inspection technique capable of pinpointing coating defects and evaluating their severity.[77,92–97] The ACVG technique utilizes very low AC frequency (typically 3 Hz and 6 Hz or 4 Hz and 8 Hz) to induce an electric current in the pipeline.[95,97] The AC current creates a voltage gradient around coating defects. The produced voltage gradient is measured by a paired reference electrode connected to a monitoring device.

The hardware required to carrying out ACVG has three main components: (1) a transmitter capable of generating low-frequency AC current that is electrically connected to the pipe, (2) a specialized voltmeter that is tuned to the generated AC frequencies and capable of measuring low voltages in decibel μV (dBμV) range, and (3) a paired reference electrode positioned at the bottom of a structure (called A-frame with fixed distance metal poles) connected to the voltmeter.

The ACVG survey is conducted in a similar fashion as the DCVG survey. The voltammeter connected to the A-frame measures the voltage difference, in decibel μV (dBμV) between the two poles.[92] When one of the poles is placed directly above the center of a coating defect (the other pole being remote from the defect), the measured voltage difference between the two poles is at its maximum. McKinney[97] provides the detailed procedure for carrying out ACVG survey.

Factors such as soil resistivity, pipe depth and diameter, coating type, clock position of the coating defect (e.g., 12 o'clock versus 6 o'clock), probe contact to the ground surface, and density of coating defects affect the magnitude of the dBμV indication.[95] For a given set of these factors, the magnitude of the severity of the coating defect is related to the magnitude of the dBμV indication. In general, the larger the dBμV indication, the more sever the coating defect. Normally, a voltage gradient above 30 dBμV indicates the presence of a coating defect.[92]

ACVG, in most instances, is a more sensitive survey technique than DCVG and will provide more information about the overall coating condition. For example, the ACVG technique can identify extremely small areas of coating damage (smaller than 0.01 square inch).[75]

Many operators perform a CIPS simultaneously with DCVG and ACVG or both to obtain the combined benefit of these techniques in identifying high-corrosion-risk areas.[93,95]

The following NACE standards provide guidelines for conducting ACVG and DCVG surveys:

- NACE Standard TM0109, *Above-ground Survey Techniques for the Evaluation of Underground Pipeline Coating Condition*
- NACE Standard Practice SP0502, *External Corrosion Direct Assessment Methodology (ECDA)*
- NACE Standard Practice SP0207, *Performing Close Interval Potential Surveys and DC Surface Potential Gradient Surveys on Buried or Submerged metallic Pipelines*

DIRECT ASSESSMENT METHODS

DA methods are structured processes and procedures that identify areas where corrosion (internal or external) is most likely or unlikely to occur along the length of a buried pipeline as well as detect existing corroded areas. In this way, DA methods are considered proactive techniques in predicting the most probable locations for corrosion on underground pipelines. These methodologies require the presence of qualified personnel who can conduct and interpret the results of these methods.

NACE has developed several DA standard practices for pipelines:

- NACE Standard Practice SP0110 (latest revision), *Wet Gas Internal Corrosion Direct Assessment Methodology (WG-ICDA)*
- NACE Standard Practice SP0206 (latest revision), *Internal Corrosion Direct Assessment Methodology for Pipelines Carrying Normally Dry Natural Gas (DG-ICDA)*
- NACE Standard Practice SP0288 (latest revision), *Internal Corrosion Direct Assessment Methodology for Liquid Petroleum Pipelines (LP-ICDA)*
- NACE Standard Practice SP0116 (latest revision), *Multiphase Flow Internal Corrosion Direct Assessment Methodology for Pipelines (MP-ICDA)*

- NACE Standard Practice SP0502 (latest revision), *External Corrosion Direct Assessment Methodology (ECDA)*
- NACE Standard Practice SP0204 (latest revision), *Stress Corrosion Cracking Direct Assessment Methodology (SCCDA)*

All of these DA methods have four common steps: (1) pre-assessment, (2) indirect inspection, (3) direct examination, and (4) post-assessment.

The objectives of pre-assessment (step 1) is data collection, selection of DA regions, and selection of appropriate indirect examination tools. In case of ICDA projects, the appropriate pipeline flow and internal corrosion models are selected. NACE Publication 21410-SG, *Selection of Pipeline Flow and Internal Corrosion Models*,[98] is required for selection of models for all ICDA methodologies. For ECDA, the appropriate aboveground inspection techniques, such as CIP, ACA, DCVG, or ACVG surveys, or combinations thereof, are identified for indirect inspection (step 2). In this step, at least two of these techniques are applied to gather critical information required to select excavation locations and perform the direct examination (step 3). Gathered data from the direct examination step is then used to predict remaining life and reassessment intervals (step 4).

More information on this topic can be found in Beavers, Bensman, and Kowalski[99] as well as in NACE publications and paper presentations.[98,100–101]

MODELING AND PREDICTION

The primary function of corrosion models is to predict whether a given material is susceptible to a particular CDM in a given environment and to estimate the corrosion rate at which the material would corrode in that environment. Modeling helps the corrosion professionals establish corrosion allowance (i.e., material wall thickness) and decide if additional corrosion control strategies (e.g., chemical treatment, coatings, CP) are required.

Existing corrosion models can be classified as mechanistic (or theoretical), semi-empirical, and empirical (or statistical) models. Mechanistic models are first principal models that are developed from the equations that govern the corrosion phenomenon of interest. The appealing aspect of these models is that a wide range of parameters and conditions can be used as inputs into these types of models; however, they often are extremely difficult to validate especially when modeling complex CDM, such as localized corrosion.

Semi-empirical models are developed from a combination of empirical relationships and mechanistic equations that govern the corrosion phenomenon of interest. These types of models are applicable in situations with similar conditions to that of the experiments used to develop them, but they are more limited than purely mechanistic models. There are also some issues with the validation of semi-empirical models but not as many as mechanistic models.

Empirical or statistical models are based on statistical relationships, which are developed purely from actual data (field or laboratory or both). The strength of these models is that they can easily and reliably be validated, but their weakness is that they are valid only for situations with identical conditions as those in which the relationships were originally developed.

Papavinasam[102,103] presents excellent reviews of internal corrosion models and external corrosion models, respectively.

The reader is also encouraged to consult with the following NACE publications for the selection and use of the various flow and internal corrosion models.

- NACE Technical Committee Report 21413-SG, *Prediction of Internal Corrosion in Oilfield Systems from System Conditions*
- NACE publication 21410-SG, *Selection of Pipeline Flow and Internal Corrosion Models*

STATISTICAL EVALUATION

Corrosion, particularly pitting corrosion, tends to be distributed in a nonuniform manner. The depth of pits on a surface can be described by a normal probability curve. This can be used to advantage when evaluating a pipeline, because it is necessary to measure only a few representative areas and to use statistics to determine the condition of the entire pipe. There are no standard test methods, but ASTM G16, *Standard Guide for Applying Statistics to Analysis of Corrosion Data*,[104] describes statistical approaches to laboratory data, and applicable references can be found in Gumbel,[105] Hawn,[106] and Bushman and Mehalick.[107]

The reader is also encouraged to consult the following standards:

- ISO 11463 (latest revision), *Corrosion of Metals and alloys - Evaluation of Pitting Corrosion*
- ASTM G46 (latest revision), *Standard Guide for Examination and Evaluation of Pitting Corrosion*

The corrosion data collected in ASTM G16 provide information about the samples tested, but not necessarily about the pipe as a whole. Thus, it is important not only to select sampling locations that represent the condition of the pipe run as a whole but also to include the worst-case conditions. Whatever areas are selected, it is possible that more severe corrosion exists. Statistical analysis is a method that uses known data to predict the range of corrosion.

For a statistical analysis to provide useful results, the data must be taken in a systematic fashion. The corrosion measurements for both the field and laboratory evaluation, as described earlier, provide corrosion data at known and consistent intervals along the pipe sample. This provides usable data for the statistical analysis.

The statistical analysis procedure most useful in evaluating corrosion on pipes is the extreme value statistical method. The referenced publications provide details on extreme value statistics and their application to pipeline corrosion. The extreme value statistical approach analyzes the maximum pit depth (or minimum wall thickness) per unit length to estimate the range of corrosion data for the pipe. The results, of course, assume that the pipe run is in the same condition as the sample tested. The more samples tested, the greater the accuracy of the result.

Normal probability and extreme value statistics have already been discussed as means of evaluating corrosion and soil

resistivity. Statistical methods have been applied to determine when steel tanks will fail.[107] Individual soil characteristics, such as resistivity, pH, and soluble salt ion content, are unsatisfactory methods of predicting the corrosion behavior of a structure in a particular soil. The statistical method is based on a regression analysis of all of the soil characteristics that affect corrosion as compared with actual corrosion of structures found in those soils. This method yields a mean time to corrosion failure as opposed to an actual corrosion rate. Its validity for structures other than steel tanks has not been demonstrated.

Conclusion

Buried oil and gas pipelines can experience a variety of corrosion damages that may impact the integrity and reliability of these lines. Corrosion monitoring, inspection and testing of pipelines is conducted for several reasons to ensure the integrity of the pipeline network. One reason is to evaluate the pipeline condition to determine whether or not it is safe to operate. If repairs are needed, inspection and testing are performed to determine if repair is feasible or if replacement is needed. Monitoring and inspection are performed to track the pipe condition so that repairs or replacements can be budgeted. Another reason for monitoring and inspection of pipes is to evaluate the effectiveness of corrosion control measures, such as inhibitors for internal pipe surfaces or cathodic protection (CP) and coatings for external pipe surfaces.

To ensure the integrity of their pipelines, pipeline operators, inspectors and corrosion engineers need to employ a variety of testing strategies coupled with industry standards and best practices in developing and implementing their pipeline integrity management programs.

ACKNOWLEDGMENT

The author would like to thank Saudi Aramco management for their support. Also, I would like to thank the reviewers for their comments and suggestions that improved the chapter.

References

1. ASM International, *ASM Metals Handbook, vol. 1, Properties and Selection: Irons, Steels, and High Performance Alloys*, 10th ed. (Materials Park, OH: ASM International, 1990), 327–336.
2. D. I. Pantelis and T. E. Tsiourva, "Corrosion of Weldments," in *Trends in Oil and Gas Corrosion Research and Technologies: Production and Transmission*, ed. A. M. El-Sherik (Cambridge, MA: Elsevier, 2017), 249–270, https://doi.org/10.1016/B978-0-08-101105-8.00010-3
3. Total Materia, "High-Strength Low Alloy Steels: New Generation," Key to Metals AG, 2007, http://web.archive.org/web/20191031050643/http://www.totalmateria.com/page.aspx?ID=CheckArticle&site=kts&NM=209
4. R. Hill and A. L. Perez, "New Steels and Corrosion-Resistant Alloys," in *Trends in Oil and Gas Corrosion Research and Technologies: Production and Transmission*, ed. A. M. El-Sherik (Cambridge, MA: Elsevier, 2017), 613–626, https://doi.org/10.1016/b978-0-08-101105-8.00026-7
5. S. J. Hall, D. J. Hill, and P. Dang, "Plastic Liners for Hydrocarbon Transport: A Qualified and Cost Efficient Alternative to CRAs" (paper presentation, Offshore Technology Conference 2009, paper no. 19937, Houston, TX, 2009).
6. K. A. Esaklul and J. Mason, "Nonmetallic Applications in Oil and Gas Production (Pipes, Liners, Rehabilitations)" in *Trends in Oil and Gas Corrosion Research and Technologies: Production and Transmission*, ed. A. M. El-Sherik (Cambridge, MA: Elsevier, 2017), 627–657, https://doi.org/10.1016/b978-0-08-101105-8.00027-9
7. J. Mason, "Thermoplastic Liners for Oilfield Pipelines," in *Oil and Gas Pipelines Integrity and Safety Handbook*, ed. Winston Revie (New York: Wiley, 2015), 447–455, https://doi.org/10.1002/9781119019213.ch31
8. J. Mason, A. Ponda, M. Stanley, and D. Demicoli, "Case Study: Engineered Polyamide 12 (PA12) Pipeline Liner for Management of Sour Gas Corrosion at Elevated Temperatures" (paper presentation, Corrosion/2017, paper no. 9592, NACE International, New Orleans, LA, March 26–30, 2017).
9. J. Mason, "Pipe Liners for Corrosive High Temperature Oil and Gas Production Application" (paper presentation, Corrosion/1997, paper no. 80, NACE International, New Orleans, LA, March 1997).
10. B. Bulleri, A. Ticci, M. Genoni, and J. Sutherland, "Engineering Thermoplastic-Liners" (paper presentation, Corrosion/2004, paper no. 04705, NACE International, New Orleans, LA, March 28–April 1, 2004).
11. Alberta Energy Regulator, "Report 2013-B: Pipeline Performance in Alberta, 1990–2012" (2013), http://web.archive.org/web/20210430140207/https://static.aer.ca/prd/documents/reports/R2013-B.pdf
12. S. Papavinasam, "Inspection, Monitoring, Model: Past, Present and Future" (paper presentation, Corrosion/2018, paper no. 10607, NACE International, Phoenix, AZ, April 16–19, 2018).
13. B. Kermani and T. Chevrot, "Pipeline Corrosion Management; A Compendium" (paper presentation, Corrosion/2014, paper no. 3723, NACE International, San Antonio, TX, March 9–13, 2014).
14. B. Kermani, J. Martin, and K. Esaklul, "Materials Design Strategy: Effects of H_2S/CO_2 Corrosion on Materials Selection" (paper presentation, Corrosion/2006, paper no. 06121, NACE International, San Diego, CA, March 12–16, 2006).
15. A. K. Dunlop, H. L. Hassell, and P. R. Rhodes, "Fundamental Considerations in Sweet Gas Well Corrosion" (paper presentation, Corrosion/83, paper no. 46, NACE International, Anaheim, CA, April 18–22, 1983).
16. S. N. Smith, "Discussion of the History and Relevance of the CO_2/H_2S Ratio" (paper presentation, Corrosion/2011, paper no. 11065, NACE International, Houston, TX, March 13–17, 2011).
17. S. N. Smith, "The Carbon Dioxide/Hydrogen Sulfide Ratio—Use and Relevance," *Material Performance* 54, no. 5 (May 2015): 64–67.
18. S. Mahajanam, ed., *CorrCompilation: Mechanism of CO_2 Corrosion*, vol. 1 (Houston, TX: NACE International, 2017).

19. S. Mahajanam, ed., *CorrCompilation: Mechanism of CO_2 Corrosion*, vol. 2 (Houston, TX: NACE International, 2017).

20. Y. Gunaltun, ed., *CorrCompilation: CO_2 and H_2S Metal Loss Corrosion: 10 Year Review* (Houston, TX: NACE International, 2017).

21. S. Dean, P. S. Rothman, and W. T. Young, "Pipeline," in *Corrosion Tests and Standards: Application and Interpretation-Second Edition*, ed. R. Baboian (West Conshohocken, PA: ASTM International, 2005), 696–705, https://doi.org/10.1520/MNL11070M

22. M. Wasim, S. Shoaib, N. M. Mubarak, I. Inamuddin, and A. M. Asiri, "Factors Influencing Corrosion of Metal Pipes in Soils," *Environmental Chemistry Letters* 16, no. 3 (March 2018): 861–879, https://doi.org/10.1007/s10311-018-0731-x

23. H. Castaneda and O. Rosas, "External Corrosion of Pipelines in Soil," in *Oil and Gas Pipelines Integrity and Safety Handbook*, ed. W. Revie (New York: Wiley, 2015), 267–273, https://doi.org/10.1002/9781119019213.ch20

24. L. de Arriba-Rodriguez, J. Villanueva-Balsera, F. Ortega-Fernandez, and F. Rodriguez-Perez, "Methods to Evaluate Corrosion in Buried Steel Structures: A Review," *Metals* 8, no. 5 (May 2018): 334, https://doi.org/10.3390/met8050334

25. *Polyethylene Encasement for Ductile-Iron Pipe Systems* (report ANSI/AWWA 105/21.5-05, AWWA/ANIS 2010, American Water Works Association, Denver, CO, 2010), http://web.archive.org/web/20191226100014/https://www.awwa.org/Store/Product-Details/productId/25362

26. P. R. Roberge, *Corrosion of Steel H-Piles at Nuclear Generating Stations* (report RSP-665.1, prepared for Canadian Nuclear Safety Commission, December 2015), http://web.archive.org/web/20191226100132/http://www.nuclearsafety.gc.ca/eng/pdfs/RSP-665-1-final-report.pdf

27. L. V. Nielsen, "AC Corrosion," in *Oil and Gas Pipelines Integrity and Safety Handbook*, ed. W. Revie (New York: John Wiley, 2015), 363–382, https://doi.org/10.1002/9781119019213.ch26

28. *AC Corrosion State of the Art: Corrosion Rate, Mechanism and Mitigation Requirements*, NACE Technical Committee Report 35110 (Houston, TX: NACE International, 2010).

29. Y. Hosokawa, F. Kajiyama, and Y. Nakamur, "New CP Criteria for Elimination of the Risks and Over protection of Cathodically Protected Pipelines" (paper presentation, Corrosion/2002, paper no. 02111, NACE International, Denver, CO, April 7–11, 2002).

30. C. Baeté, A. Rose, B. Van den Bossche, L. Bortels, D. Lindemuth, and L. Nielsen, "Develop a New Unique AC Corrosion CP Mitigation Criteria" (Final PRCI Report, PR-405-113604-R01, August 23, 2013).

31. *Standard Practice for Determining Rail-to-Earth Resistance*, ASTM G165-99(2017) (West Conshohocken, PA: ASTM International, approved May 1, 2017), http://doi.org/10.1520/G0165-99R17

32. Z. Chen, D. Koleva, and K. van Breugel, "A Review on Stray Current-Induced Steel Corrosion in Infrastructure," *Corrosion Review* 35, no. 6 (November 2017): 397–423, https://doi.org/10.1515/corrrev-2017-0009

33. G. Cui, Z.-L. Li, C. Yang, and M. Wang, "The Influence of DC Stray Current on Pipeline Corrosion," *Petroleum Science* 13, no. 1 (February 2016): 135–145, https://doi.org/10.1007/s12182-015-0064-3

34. M. Singer, "Top-of-the Line Corrosion," in *Trends in Oil and Gas Corrosion Research and Technologies: Production and Transmission*, ed. A. M. El-Sherik (Cambridge, MA: Elsevier, 2017), 383–403, http://dx.doi.org/10.1016/B978-0-08-101105-8.00016-4

35. S. Papavinasam, "Mechanisms," in *Corrosion Control in the Oil and Gas Industry* (Oxford: Elsevier, 2014), 249–298, https://doi.org/10.1016/B978-0-12-397022-0.00005-4

36. G. Svenningsen, "Sour Top of Line Corrosion Testing with Methanol" (paper presentation, Corrosion/2017, paper no. 9337, NACE International, New Orleans, LA, March 26–30, 2017).

37. G. Svenningsen, "Sour Top of Line Corrosion: An Overview" (paper presentation, 16th Nordic Corrosion Congress 2015, paper no. 25, Stavanger, Norway, 2015).

38. K. Esaklul, "Hydrogen Damage," in *Trends in Oil and Gas Corrosion Research and Technologies: Production and Transmission*, ed. A. M. El-Sherik (Cambridge, MA: Elsevier, 2017), 315–336, https://doi.org/10.1016/B978-0-08-101105-8.00013-9

39. *Petroleum and Natural Gas Industries—Materials for Use in H_2S-Containing Environments in Oil and Gas Production, Parts 1, 2, and 3*, NACE Standard MR0175/ISO15156 (Houston, TX: NACE International, 2015).

40. *Standard Test Method for Evaluation of Pipeline and Pressure Vessel Steels for Resistance to Hydrogen-Induced Cracking*, ANSI/NACE TM0284 (2016) (Houston, TX: NACE International, approved 2016), http://web.archive.org/web/20191225095849/https://store.nace.org/ansi-nace-tm0284-2016

41. J. Telegdi, A. Shaban, and L. Trif, "Microbiologically Influenced Corrosion," in *Trends in Oil and Gas Corrosion Research and Technologies: Production and Transmission*, ed. A. M. El-Sherik (Cambridge, MA: Elsevier, 2017), 191–214, https://doi.org/10.1016/B978-0-08-101105-8.00008-5

42. B. J. Little, and J. S. Lee, *Microbiologically Influenced Corrosion* (New York: Wiley, 2006), https://doi.org/10.1002/047011245X

43. B. J. Little, and J. S. Lee, "Microbiologically Influenced Corrosion: An Update," *International Material Review* 59, no. 7 (August 2014): 384–393, https://doi.org/10.1179/1743280414Y.0000000035

44. R. Eckert, ed., *CorrCompilations: Introduction to Corrosion Management of Microbiologically Influenced Corrosion* (Houston, TX: NACE International, 2015).

45. J. A. Beavers, and T. Bubenik, "Stress Corrosion Cracking," in *Trends in Oil and Gas Corrosion Research and Technologies: Production and Transmission*, ed. A. M. El-Sherik (Cambridge, MA: Elsevier, 2017), 295–313, https://doi.org/10.1016/B978-0-08-101105-8.00012-7

46. *Stress Corrosion Cracking Recommended Practices*, 2nd ed. (Canadian Energy Pipeline Association (CEPA), 2007), http://web.archive.org/web/20191226100531/https://www.cepa.com/wp-content/uploads/2011/06/Stress-Corrosion-Cracking-Recommended-Practices-2007.pdf

47. W. Chen, "An Overview of Near-Neutral pH Stress Corrosion Cracking in Pipelines and Mitigation Strategies for Its Initiation and Growth," *Corrosion* 72, no. 7 (July 2016): 962–977, http://dx.doi.org/10.5006/1967

48. J. A. Beavers and R. G. Worthingham, "The Influence of Soil Chemistry on SCC of Underground Pipelines" (paper presentation, International Pipeline Conference, paper no. IPC 02-27146, Calgary, Alberta, 2002).

49. *Managing System Integrity of Gas Pipelines*, ASME Code for Pressure Piping, B31 Supplement to ASME B31.8 (New York: American Society of Mechanical Engineers, October 31, 2016), http://web.archive.org/web/20191226100618/https://law.resource.org/pub/us/cfr/ibr/002/asme.b31.8s.2004.pdf

50. R. M. Baldwin, "Black Powder in the Gas Industry-Sources, Characteristics and Treatment" (GMRC Report No.TA97-4, May 1998).

51. A. M. El-Sherik, J. Perez, S. Jutaily, and A. AbdulHadi, "Composition, Sources and Formation Mechanisms of Black Powder in Gas Transmission Pipelines" (paper presentation, EUROCORR Conference 2007, Freiburg, Germany, 2007).

52. A. M. Sherik, A. Rasheed, and A. Jabran, "Effect of Sales Gas Pipelines Black Powder Sludge on the Corrosion of Carbon Steel" (paper presentation, Corrosion/2011, paper no. 11087, NACE International, Houston, TX, March 13–17, 2011).

53. M. Cowie and A. M. El-Sherik, "Naturally Occurring Radioactive Material and Naturally Occurring Mercury Assessment of Black Powder in Sales Gas Pipelines," *Radiation Protection and Environment* 42, no. 1 (January 2019): 34–39, https://doi.org/10.4103/rpe.RPE_69_18

54. A. M. El-Sherik, "Managing Black Powder in Sales Gas Transmission Pipelines," *Journal of Pipeline Systems Engineering and Practice* 15, no. 3 (March 2016): 19–24.

55. A. M. El-Sherik, "Strategies for Managing Black Powder in Sales Gas Pipelines," *Pipeline and Gas Journal* 245, no. 9 (September 2018): 63–65.

56. A. M. El-Sherik, ed., *CorrCompilation: Underdeposit Corrosion* (Houston, TX: NACE International, 2019).

57. J. R. Vera, D. Daniels, and M. H. Achour, "Under Deposit Corrosion (UDC) in the Oil and Gas Industry: A Review of Mechanisms, Testing and Mitigation" (paper presentation, Corrosion/2012, paper no. 1379, NACE International, Salt Lake City, UT, March 11–15, 2012).

58. N. M. Alanazi, A.M. El-Sherik, A.H. Rasheed, S. H. Amar, M. R. Dossary, and M. N. Alneemai, "Corrosion of Pipeline Steel X-60 under Field-Collected Sludge Deposit in a Simulated Sour Environment," *Corrosion* 71, no. 3 (March 2015): 305–315, https://doi.org/10.5006/1237

59. N. U. Obeyesekere, "Pitting Corrosion," in *Trends in Oil and Gas Corrosion Research and Technologies: Production and Transmission*, ed. A. M. El-Sherik (Cambridge, MA: Elsevier, 2017), 215–248, https://doi.org/10.1016/B978-0-08-101105-8.00009-7

60. S. Hernandez, S. Hassani, and A. Nassef, "Erosion-Corrosion," in *Trends in Oil and Gas Corrosion Research and Technologies: Production and Transmission*, ed. A. M. El-Sherik (Cambridge, MA: Elsevier, 2017), 341–360, https://doi.org/10.1016/B978-0-08-101105-8.00014-0

61. F. Al-Mutahar, G. Aithan, E. Iski, M. Keller, S. Shirazi, and K. P. Roberts, "Mechanistic Modeling of Erosion-Corrosion for Carbon Steel," in *Trends in Oil and Gas Corrosion Research and Technologies: Production and Transmission*, ed. A. M. El-Sherik (Cambridge, MA: Elsevier, 2017), 749–763, https://doi.org/10.1016/B978-0-08-101105-8.00031-0

62. S. Shirazi, B. S. McLaury, J. R. Shadley, K. P. Roberts, E. F. Rybicki, H. R. Rincon, S. Hassani, F. Al-Mutahar, and G. Aithan, "Erosion-Corrosion in Oil and Gas Pipelines," in *Oil and Gas Pipelines Integrity and Safety Handbook*, ed. W. Revie (New York: Wiley, 2015), 399–419, https://doi.org/10.1002/9781119019213.ch28

63. G. Schmitt, C. Bosch, M. Mueller, and G. Siegmund, "A Probabilistic Model for Flow Induced Localized Corrosion" (paper presentation, Corrosion/2000, paper no. 00049, NACE International, Orlando, FL, March 26–31, 2000).

64. A. Chandra, M. Parsi, J. Vera, and P. Sharma, "CFD-Based Flow-Induced Corrosion Modeling" (paper presentation, Corrosion/2017, paper no. 9126, NACE International, New Orleans, LA, March 26–30, 2017).

65. K. D. Efird, "Flow Accelerated Corrosion Testing Basics" (paper presentation, Corrosion/2006 Conference, paper no. 06689, NACE International, San Diego, CA, March 12–16, 2006).

66. M. A. Adegbite, M. J. Robinson, and S. A. Impey, "Evaluation of Flow Enhanced Preferential Weld Corrosion of X65 Pipeline Steel Using a Novel Submerged Impingement Jet," Society of Petroleum Engineers, SPE-184380-MS (Richardson, TX: SPE, 2016).

67. D. McIntyre and M. Achour, *Preferential Weld Corrosion of Caron Steel* (Houston, TX: NACE International, 2016).

68. C.-M. Lee, S. Bond, and P. Woollin, "Preferential Weld Corrosion: Effects of Weldments Microstructure and Composition" (paper presentation, Corrosion/2005, paper no. 05277, NACE International, Houston, TX, April 3–7, 2005).

69. K. Alawadhi and M. J. Robinson, "Preferential Weld Corrosion of X65 Pipeline Steel in Flowing Brines Containing Carbon Dioxide," *Corrosion Engineering, Science and Technology* 46, no. 4 (November 2011): 318–329, https://dx.doi.org/10.1179/147842210X12695149033891

70. R. Case, M. Achour, and J. Daniels, "Evaluation of Preferential Weld Corrosion Susceptibility and Its Mitigation in Slightly Sour Condition" (paper presentation, Corrosion/2015, paper no. 5640, Dallas, TX, March 15–19, 2015).

71. *Techniques for Monitoring Corrosion and Related Parameters in Field Applications*, NACE Publication 3T199 (2013 ed.) (Houston, TX: NACE International, 2013).

72. *Field Monitoring of Corrosion Rates in Oil and Gas Production Environments Using Electrochemical Techniques*, NACE Publication 31014 (2014 ed.) (Houston, TX: NACE International, 2014).

73. T. Pickthall, M. Rivera, M. McConnell, and R. Vezis, "Corrosion Monitoring Equipment, A Review of Application and Techniques" (paper presentation, Corrosion/2007, paper no. 07037, NACE International, Nashville, TN, March 2007).

74. S. Papavinasam, A. Doiron, M. Attard, A. Demoz, and P. Rahimi, "NonIntrusive Techniques to Monitor Internal Corrosion of Oil and Gas Pipelines" (paper presentation, Corrosion/2012, paper no. 1261, NACE International, Salt Lake City, UT, March 11–15, 2012).

75. "Evaluation Technologies to Assess the Condition of Pipe Coating on Line 5" (report to the State of Michigan, Enbridge, June 30, 2018), http://www.web.archive.org/web/20220215052214/https://mipetroleumpipelines.org/sites/mipetroleumpipelines.org/files/document/pdf/SectionD_CoatingTechnologies_Jun2018.pdf

76. A. M. El-Sherik, N. M. Dakwar, and T. Byrnes, "Guidelines for Investigating Failures of External FBE Coatings on Buried Pipelines," *Journal of Pipeline Systems Engineering and Practice* no. 2 (June 2018): 105–115.

77. G. Zinter, "In-The-Ditch Pipeline Inspection," in *Oil and Gas Pipelines Integrity and Safety Handbook*, ed. W. Revie (New York: Wiley, 2015), 557–577, https://doi.org/10.1002/9781119019213.ch38

78. N. I. Uzelac, "In-Line Inspection (ILI) (Intelligent Pigging)," in *Oil and Gas Pipelines Integrity and Safety Handbook*, ed. W. Revie (New York: Wiley, 2015), 515–535, https://doi.org/10.1002/9781119019213.ch35

79. T. Steinvoorte, "Unpiggable Pipelines," in *Oil and Gas Pipelines Integrity and Safety Handbook*, ed. W. Revie (New York: Wiley, 2015), 545–555, https://doi.org/10.1002/9781119019213.ch37

80. W. K. Holm, "Magnetic Inspection Pigging Aids Pipeline Inspection," *Gas Industries* (March 1985): 6–11.

81. J. T. Schmidt, "Magnetic Flux Leakage Inspection of Pipelines—An Operator's Viewpoint," *Materials Performance* 33, no. 7 (July 1994): 53–57.

82. *Corrosion Detection Using Intelligent Pigs* (Houston, TX: NACE International, 2001).

83. R. Norsworthy, G. Grillenberger, S. Brockhaus, and M. Ginten, "EMAT, Pipe Coating, Corrosion Control and Cathodic Protection Shielding" (paper presentation, Corrosion/2013, paper no. 2378, NACE International, Orlando, FL, March 17–21, 2013).

84. W. Krieg, T. Beuker, M. Klann, J. Damaschke, and H. Lindner, "A Novel EMAT Crack Detection and Coating Disbondment (RoCD2) ILI Technology" (paper presentation, Pipeline Technology Conference 2007, Germany, 2007).

85. "Conventional UT vs. Phased Array UT," Patterson Tubular Services, http://web.archive.org/web/20210430140829/http://www.pattersontubular.com/whitepapers/ConventionalvsPhasedArrayUT_technicalwhitepaper.pdf

86. D. E. Powell, "Internal Corrosion Monitoring Using Coupons and ER Probes: A Practical Focus on the Most Commonly Used, Cost-Effective Monitoring Techniques," in *Oil and Gas Pipelines Integrity and Safety Handbook*, ed. W. Revie (New York: Wiley, 2015), 494–513, https://doi.org/10.1002/9781119019213.ch34

87. N. Khan, "Use of CP Coupons and Soil Corrosion Probes in Application of Pipeline Cathodic Protection Criteria" (paper presentation, Corrosion/2007, paper no. 07037, NACE International, Nashville, TN, March 11–15, 2007).

88. *Standard Guide for Conducting Exfoliation Corrosion Tests in Aluminum Alloys*, ASTM G112-92(2015) (West Conshohocken, PA: ASTM International, approved November 1, 2015), http://doi.org/10.1520/G0112-92R15

89. S. Papavinasam, "Monitoring-Internal Corrosion," in *Corrosion Control in the Oil and Gas Industry* (Oxford: Elsevier, 2014), 425–528, https://doi.org/10.1016/B978-0-12-397022-0.00008-X

90. B. Bavarian, B. Samimi, Y. Ikder, and L. Reiner, "Protection Effectiveness of Vapor Corrosion Inhibitor for Corrosion under Insulation" (paper presentation, Corrosion/2015, paper no. 5448, NACE International, Dallas, TX, March 2015).

91. "Electrical Resistance (ER) Monitoring," Metal Samples, http://www.web.archive.org/web/20191031052218/http://www.alspi.com/erintro.htm

92. S. Papavinasam, "Monitoring—External Corrosion," in *Corrosion Control in the Oil and Gas Industry* (Oxford: Elsevier, 2014), 715–750, https://doi.org/10.1016/B978-0-12-397022-0.00011-X

93. P. Nicholson, "Combined CIPS and DCVG Surveys for Improved Data Correlation" (paper presentation, Corrosion/2007, paper no. 07181, NACE International, Nashville, TN, March 2007).

94. P. Nicholson, "Is Your Pipeline Corroding" (paper presentation, Corrosion/2008, paper no. 08123, NACE International, New Orleans, LA, March 16–20, 2008).

95. Jim Walton, "ACVG or DCVG: Does it Matter? Absolutely It Does" (paper presentation, Conference/2017, paper no. 9374, NACE International, New Orleans, LA, March 26–30, 2017).

96. J. P. McKinney, "Evaluation of Above-Ground Potential Measurements for Assessing Pipeline Integrity" (master's thesis, University of Florida, 2006).

97. *Above-Ground Survey Techniques for the Evaluation of Underground Pipeline Coating Condition*, NACE Standard TM0109 (Houston, TX: NACE International, 2014).

98. *Selection of Pipeline Flow and Internal Corrosion Models*, NACE Publication 21410-SG (Houston, TX: NACE International, 2016).

99. J. Beavers, L. A. Bensman, and A. Kowalski, "Direct Assessment," in *Oil and Gas Pipelines Integrity and Safety Handbook*, ed. W. Revie (New York: Wiley, 2015), 487–494, https://doi.org/10.1002/9781119019213.ch33

100. S. Srinivasan, "ICDA: A Quantitative Framework to Prevent Corrosion Failures and Protect Pipelines" (paper presentation, Corrosion/2006, paper no. 06198, NACE International, San Diego, CA, March 12–16, 2006).

101. A. P. Pillai, "Direct Assessment Pipeline Integrity Management" (paper presentation, Corrosion/2011, paper no. 11126, NACE International, Houston, TX, March 13–17, 2011).

102. S. Papavinasam, "Modeling: Internal Corrosion," in *Corrosion Control in the Oil and Gas Industry* (Oxford: Elsevier, 2014), 301–360, https://doi.org/10.1016/B978-0-12-397022-0.00006-6

103. S. Papavinasam, "Modeling: External Corrosion," in *Corrosion Control in the Oil and Gas Industry* (Oxford: Elsevier, 2014), 621–714, https://doi.org/10.1016/B978-0-12-397022-0.00010-8

104. *Standard Guide for Applying Statistics to Analysis of Corrosion Data*, ASTM G16-13(2019) (West Conshohocken,

PA: ASTM International, February 15, approved 2019), http://doi.org/10.1520/G0016-13R19

105. E. J. Gumbel, *Statistics of Extremes* (New York: Columbia University Press, 1958).

106. D. E. Hawn, "Extreme Value Prediction of Maximum Pits on Pipelines," *Materials Performance* 16 (March 1977): 29.

107. J. Bushman and T. E. Mehalick, "Statistical Analysis of Soil Characteristics to Predict Mean Time to Corrosion Failure of Underground Metallic Structures," in *Effects of Soil Characteristics on Corrosion*, ed. V. Chaker and J. Palmer (West Conshohocken, PA: ASTM International, 1989), 107–118, https://doi.org/10.1520/STP19712S

Chapter 22 | Highways, Tunnels, and Bridges

Stephen R. Sharp[1] and Jason T. Provines[1]

Introduction

To counter the effects and high maintenance costs of corrosion on highways, tunnels, and bridges, improvements in materials and testing have been made and many have been implemented. Furthermore, member organizations like American Association of State Highway and Transportation Officials (AASHTO), ASTM, American Welding Society (AWS), Concrete Reinforcing Steel Institute (CRSI), NACE International, National Steel Bridge Alliance (NSBA), American Institute of Steel Construction (AISC), The Society for Protective Coatings (SSPC), and many others have continued to improve specifications, standards, and guidelines that support the effort to mitigating corrosion issues in these vital resources. In addition, some organizations like the Transportation Research Board (TRB) sponsor meetings and research activities, such as the National Cooperative Highway Research Program (NCHRP), so practitioners can pursue issues, discuss challenges, and learn about new transportation-related advancements in corrosion.

One of the challenges in dealing with corrosion of the highway network is that the materials used are exposed to a variety of environments. Some of these environments aide in reducing the corrosion rate, like placing steel in alkaline concrete, whereas others accelerate corrosion, such as steel exposed to salt water. To reduce the chance of unexpected corrosion related maintenance, the design of a transportation structure should incorporate durable materials to ensure that it reaches its expected design life. Although some of these materials have inherent corrosion resistance, like carbon fiber–reinforced polymer (CFRP) strands, for example, other structural materials rely on a second material to mitigate corrosion, for instance, a coating on a mild steel beam. Therefore, it is important to understand how these materials will perform in their environments when specified during the design stage of a project.

[1]Virginia Transportation Research Council, 530 Edgemont Rd., Charlottesville, VA 22903, USA S. R. S. http://orcid.org/0000-0003-1850-6280
The author acknowledges the previous author of this chapter, James B. Bushman, Bushman and Associates, Inc., Medina, OH.

DOI: 10.1520/MNL202NDSUP20190020

Environmental Exposure

Because of the nature of transportation structures, many different exposure conditions can be encountered. This section focuses on five commonly encountered conditions that can have an effect on corrosion performance. These conditions include atmospheric, concrete (alkaline encasement), saltwater, soil, and water. It is also important to highlight that some transportation structures are subjected to a combination, if not all, of these environments.

ATMOSPHERIC EXPOSURE

Because highways, bridges, and tunnels are designed for transporting people and goods along the highway network, most structures are subjected to atmospheric exposure. The atmospheric exposure, however, can be quite different for different types of transportation structures. For example, a complex tunnel might use an exhaust system to remove what otherwise would be trapped exhaust gases, whereas this is not necessary for a bridge. Moreover, the bridge in a bridge-to-tunnel system might also be exposed to small microclimates as it starts on dry land, and then moves over saltwater, before ending on a natural or humanmade island, where it connects to the tunnel structure. This difference in the atmospheric environment between transportation structures, or even between different locations on the same structure, can vary for several factors, including the following:

- time of wetness, with variability because of highway structures having different distances to the water;
- sulfur dioxide, with variability because of the structure's orientation in the vicinity of a source burning fossil fuels; and
- chloride exposure, with variability because of the seasonal use of deicing salts.

All of these factors can strongly alter the corrosiveness of a highway structures environment.

CONCRETE (ALKALINE) EXPOSURE

Reinforced concrete (RC), a system consisting of concrete with embedded steel reinforcement (rebar), is commonly used for

Copyright © 2022 by ASTM International, 100 Barr Harbor Dr., PO Box C700, West Conshohocken, PA 19428-2959
ASTM International is not responsible, as a body, for the statements and opinions expressed in this chapter. ASTM International does not endorse any products represented in this chapter.

transportation structures. In this case, the concrete mitigates steel corrosion by creating a protective barrier and beneficial alkaline environment around the embedded rebar. The protective barrier is created by using concrete mix designs that restrict the movement of ions, especially salts that contain chlorides, through the pore system within the concrete. The barrier is further enhanced by increasing the concrete thickness over the rebar, which is called cover. In Portland cement concrete mixtures, the alkaline environment is a natural outcome of the reaction between the cement and water, which results in an elevated pH value adjacent to the rebar in the hardened concrete.

When uncracked, RC can provide a durable structural system that is highly resistant to rebar corrosion; however, it is important to note that if the concrete mix is not designed properly, cracks in the concrete can form, creating a pathway for moisture and chlorides to reach the rebar and cause corrosion.[1] Concrete cracking can depend on design restraint, weather conditions during placement, concrete mix proportions, cement types, and even cement paste and aggregate content.[2–4] Factors like these can significantly influence the tendency of the concrete to crack, with some of these factors being difficult to control outdoors or when larger RC elements are being cast. Therefore, it is important to consider the effects of concrete cracking when evaluating materials for corrosion resistance. Furthermore, when the cracks occur in bridge decks or tunnel liners, other metal components, whether embedded in concrete or not, then can be subjected to direct contact with water or saltwater that can lead to corrosion.

SALT EXPOSURE

A transportation structure's exposure to salt typically comes from either saltwater or de-icing salts. The location of a structure often dictates if routine exposure to saltwater will occur. This is most obvious when a structure is located close to a body that contains brackish water or saltwater. In certain regions where snow and ice are a concern, however, salt or brine are used to prevent ice forming on the roadway and improve traction for traveling vehicles. The application of de-icing salts can be observed as spreading dry salt, pretreating the road surface before an ice event using a brine solution, or spreading a salt and sand mixture on the road. All of these de-icing treatments generally contain sodium chloride, but other chloride containing salts can be used too.

SOIL EXPOSURE

Other chapters of this book discuss the factors that can influence corrosion in soil. It is important to understand the characteristics of the soil for transportation structures because contact with soil is inevitable. The soils in contact with these structures can exhibit a wide range of characteristics as these structures can have substantial lengths, with some elements also going deeply into the ground. In addition, the structures might not only contact native soils but also fill materials that commonly are used during construction. Ensuring that the fill materials exhibit favorable characteristics to promote corrosion resistance is important to minimize the possibility of corrosion development in the structural elements as well.

WATER EXPOSURE

Many structures are commonly exposed to sources of water, like rivers, rain, groundwater, and even flooding. Furthermore, the amount of time the water remains in contact with a surface can be influential. When carbon steel is directly exposed to water, it will corrode, although at a slower rate than when in contact with saltwater. Moreover, water can provide a mechanism for transporting abrasive materials, for example, through a culvert, which can damage a protective coating and expose the underlying carbon steel, initiating corrosion.

Corrosion Design and Mitigation Techniques

The materials commonly used to construct the highway network include both metallic and nonmetallic materials. Asphalt, aggregate, concrete, steel, cast iron, aluminum, wood, and various polymeric materials are commonly found throughout the network. In addition, composite materials like CFRP and glass fiber–reinforced polymers (GFRP) are also finding use. Although all of these materials are used in highways, tunnels, and bridges, the two primary materials that are most prevalent and susceptible to corrosion damage are steel and concrete. The following sections present some general corrosion design and mitigation techniques for both steel and RC.

STEEL

There are some typical methods for providing corrosion protection to steel plate within the highway system. This section provides background information on each of these corrosion protection systems.

Coatings

Zinc-rich primer paint systems are the most common form of corrosion protection for steel plate used on bridges and generally consist of three coats of paint: primer, intermediate coat, and topcoat. Before being coated, the steel substrate must be blast-cleaned to a surface level of "near white" (SSPC-SP 10) to allow for good bonding with the primer, which is essential for good paint performance.[5] The primers used for bridges are made using either inorganic or organic zinc.[6] Once the primer has been applied, it is typically followed by an intermediate coat, which provides additional barrier protection. After the intermediate coat, the topcoat is applied and provides a first layer of corrosion protection against the environment. The topcoat can have aesthetic requirements depending on the requirements of the bridge owner. For best performance, paint coats must be used as a system, designed by a single manufacturer and used together according to the manufacturer's recommendations. When selecting a zinc-rich primer paint system, other non-corrosion-related items to consider include the drying times, curing times, and slip resistance of the primers being applied to faying surfaces of bolted connections.

Coating Removal and Recoating

Once coated steel has been in service for years, the paint coating can eventually fail and flake off. When this occurs, a decision must be made to either over-coat or recoat the member. If over-coating is performed, it temporarily extends the time before a full coating removal and recoating operation must be applied. If recoating is selected, the failed coating must be removed completely, down to the bare steel, before recoating. The coating removal process is typically done using a metallic blast media. In some regions, depending on agency requirements, all of the removed coating and discarded blast media must be collected and properly disposed of due to environmental concerns. Worker safety also must be considered during this process, especially if the coating being removed contains lead. Once the failed coating has been removed, a new coating can be applied in the field to provide corrosion protection to the steel substrate. The new coating must be applied in the field to the manufacturer's recommendations. It is generally believed that field-applied coatings do not possess the service life that shop-applied coatings do. Coating removal and recoating is an especially common repair technique for steel bridges.

Metallic Coatings

Hot-dip galvanizing (HDG) is another common corrosion protection method for steel. This process begins with dipping steel into a series of surface preparation solutions, including degreasing, pickling, and fluxing. Once the steel is properly cleaned, it is dipped into a bath of molten zinc.[7] Typically these baths are approximately 40 ft long in the United States, but longer baths do exist. When dipped into the molten bath, a chemical bond is formed between the steel and zinc to form a sacrificial zinc layer.[7] The thickness and composition of this zinc layer depends on the steel chemistry. When the silicon content in the steel is either between 0.04 and 0.15 or more than 0.22 percent, the steel is considered "reactive." When reactive steels are hot-dip galvanized, the zinc can grow to excessively thick levels and become brittle, increasing the potential for the zinc to flake off.[8] Nonreactive steels have much more consistent zinc thicknesses after being hot-dipped galvanized. When selecting an HDG protection system, it is important to be cognizant of the length limitations of galvanizing baths for the steel, which can lead to additional splices within structural members.

Thermal spray coating (TSC), also known as metalizing, is the process of heating a metallic feedstock and then spraying it onto a steel plate substrate. The wire or powder feedstock typically used for steel bridges are pure zinc, pure aluminum, or an 85 percent zinc/15 percent aluminum alloy.[9] The feedstock is heated using a flame or an electric arc, and then compressed air is used to spray the molten metal onto the steel. Once the metal hits the steel, it instantly solidifies to form a sacrificial protective coating. Multiple passes are required to achieve the specified thickness for the TSC to perform as intended. Similar to other systems, TSC has both advantages and disadvantages. It is a mobile process that can be performed in the field where HDP would be nearly impossible. There are also no length restrictions like for HDP baths, so longer steel plate members can be coated with a TSC. The process, however, does require specialized equipment and expertise and can be time-consuming. TSC has extensive use in Europe and is slowly continuing to gain traction within the United States.

A duplex coating system, as referred to as in the steel bridge community, is a corrosion protection systems consisting of multiple layers, such as either HDG or TSC acting as the base layer and then a topcoat paint layer to provide enhanced corrosion resistance and aesthetics.[10] Conventional thinking suggests that when predicting the corrosion resistance of a duplex coating system, the predictive life of both coatings can be added together to get the life of the complete system. Observational data suggest that the life of a duplex coating system performs better than the sum of its individual coatings, depending on the severity of the environment.[11] Bridge owners, however, have had mixed results using these systems. Some past issues include HDG or TSC quality, adhesion of the topcoat layer, or insufficient performance leading to required maintenance sooner than expected. There are current research projects within the United States to develop guidelines for the improved usage of duplex coating systems on steel bridges. The use of these systems has had increased success in Europe.

Alloyed Steel

Corrosion-resistant steels have become increasingly common for steel bridges. Within the United States, all bridge steel plates fall under ASTM A709, *Standard Specification for Structural Steel for Bridges*.[12] One corrosion-resistant steel within this specification is Grade 50W, which is essentially identical to ASTM A588, *Standard Specification for High-Strength Low-Alloy Structural Steel, up to 50 ksi [345 MPa] Minimum Yield Point, with Atmospheric Corrosion Resistance*, and commonly is referred to as "weathering steel."[13] The high-performance steels within ASTM A709, such as grades HPS 50W, HPS 70W, and HPS 100W, are also considered weathering grades. Weathering steel provides inherent corrosion resistance by forming a stable oxide layer, which is tightly adherent to the steel substrate. This oxide layer, sometimes referred to as a "patina," forms after many wet and dry cycles. The historical performance of weathering steels within the United States has been successful in some environments, but poor in others. Much of the poor performance of weathering steel was in areas, such as marine coastal environments, areas of prolonged wetness, or industrial areas. This led to a Federal Highway Administration (FHWA) technical advisory in 1989 detailing areas in which uncoated weathering steel is not recommended.[14] The use of weathering steel has continued in the United States because of its inherent corrosion resistance and minimal cost increase when compared with non-weathering bridge steels. In many cases, weathering steel is also painted for use in steel bridges. In some cases, weathering steel beam ends are painted for increased corrosion protection.

Another corrosion-resistant steel plate within ASTM A709 is Grade 50CR, which is nearly identical to ASTM A1010, *Standard Specification for Higher-Strength Martensitic Stainless Steel Plate, Sheet, and Strip*.[12,15] Grade 50CR steel is a dual-phase stainless steel made up of fine-grained ferrite and tempered martensite. It contains 10.5 wt% chromium and 1.5 wt% nickel to provide much

more inherent corrosion resistance than weathering steel. According to accelerated corrosion testing, Grade 50CR can provide approximately 10 times more corrosion resistance compared with weathering steel when placed in the vertical direction and approximately four times more in the horizontal direction, with the difference being attributed to time of wetness.[16] An FHWA-funded research study used lifecycle cost analysis to show that Grade 50CR could be more cost-effective than painted carbon steel after one or two repainting cycles.[17] As of 2019, Grade 50CR has been used in six bridges in the United States and two in Canada.[18] It is expected that provisions for welding Grade 50CR steel are expected to appear in interim editions of the 2020 edition of the AASHTO/AWS D1.5 Bridge Welding Code. Numerous research studies are being conducted on Grade 50CR to increase the knowledge on welding consumables, bolted connections, galvanic corrosion when in contact with other metals, and cost analysis.

A third type of corrosion-resistant steel available for use on steel plate girder bridges is duplex stainless steel. Duplex stainless steels have a two-phase microstructure made up of ferrite and austenite. The most prominent grades of duplex stainless steel for bridge use are likely UNS S32205 (2205), UNS S32304 (2304), and UNS S32101 (2101), although many other types do exist. Duplex stainless steels have excellent inherent corrosion resistance, likely multiple orders of magnitude better than weathering steel or Grade 50CR.[19] Much of this is due to their high chromium, nickel, and molybdenum contents. They also are attractive for steel bridge use because of their high strength and good toughness when compared with austenitic or ferritic stainless steels. Duplex stainless steels have been used on more than 30 vehicular, pedestrian, and rail bridges in Europe and around the world. Within the United States, they have been used either as primary members or specific components on five vehicular and pedestrian bridges. Fabrication and design guides are both available for duplex stainless steels, which is important since guidance on items like the welding parameters need to be sound to ensure corrosion resistance is maintained.[20,21] These steels are expected to cost more than traditional steels, although their use may be warranted when considering a lifecycle cost analysis.

Detailing

In many instances, the corrosion resistance of steel bridges can be improved through detailing during the design stage. One of the ways this can be done is to increase the vertical clearance between an overpass structure and the roadway below. In this example, de-icing salt applied to the roadway below can be splashed up on to the overpass bridge, causing accelerated corrosion of the overpass. There is no current guidance on the minimum clearance that would eliminate this effect; however, the minimum vertical clearance on the United States interstate system has been 16 ft, and this type of corrosion has continued to occur.[13] If increasing the minimum clearance is neither possible nor desirable, another strategy is to apply a corrosion protection system, such as painting, HDG, or the use of corrosion-resistant steel, to the inbound fascia girder of the overpass bridge.

Steel bridge connections should be designed with corrosion in mind. Members should be sloped when possible to prevent ponding of water. Snipes on stiffeners at the stiffener to web and bottom flange connection should be made large enough to allow water to flow and prevent clogging.[8] Drip bars can also be added to redirect the flow of water off of the bottom flange.[11] Welded drip bars should be placed in areas of low stress to prevent unintended fatigue issues related to the resultant welds. Horizontal or built-up members should be limited, but when necessary, they should employ a corrosion protection system, such as painting, HDG, TSC, or alloyed steel. In other cases, the thickness of a member can be increased to allow for some section loss without compromising the structural performance of the member. When existing steel bridge connections experience corrosion damage, the existing corrosion should be thoroughly removed before installing welded or bolted repairs. Once in place, repairs should have a corrosion protection system in place to increase the remaining service life of the susceptible location.

Closed box members should be used sparingly because they can trap moisture and are difficult to inspect. Open members, such as wide flange beams can serve as an alternative, if they are designed with corrosion in mind. If box members must be used, weep holes should be placed at the lowest point practically possible on the member to allow for drainage of water. The inside of box members often are painted with a high-contrast white coating to facilitate easier inspection. Other corrosion protection systems, such as HDG or alloyed steel, also can be used in these instances.

Washing

In some cases, it may be beneficial to wash steel bridges made of weathering steel. Multiple studies have shown that washing can remove debris, loose rust flakes, and surface chlorides that can cause extended periods of wetness; these extended periods of wetness are detrimental to weathering steel because the protective patina cannot form without alternating wet and dry cycles.[22] Some items to consider when washing weathering steel bridges include the water pressure and nozzle spray angle.[23] Location specific agency requirements also must be considered for environmental concerns. In some cases, all water and debris washed off the bridge must be collected and properly disposed of after washing. In some cases, this requirement can significantly increase the cost of bridge washing.

Isolation

In steel bridges where dissimilar metals, such as carbon steel and stainless steel, are used, electrical isolation can be implemented to alleviate galvanic corrosion. Isolation is a common galvanic corrosion mitigation technique in which another material, such as nylon or plastic, is placed in between the two dissimilar metals to prevent the formation of a galvanic cell The concept of using isolation is to prevent the use of a small anode to protect a large cathode from preferentially corroding. Isolation can be challenging to use on large structures such as bridges, because isolation materials typically do not offer adequate structural characteristics for bridge use. For example, using a nylon washer for isolation is not recommended in structural bolted applications because nylon is a compressible material compared with steel, and it use can lead to lower levels of pretension or relaxation in the bolt,

unless additional testing and bolt tightening procedures are developed. As new corrosion-resistant and more noble materials are used for bridges, isolation will need to be considered.

CONCRETE

Similar to steel plate, a few common corrosion protection methods can be employed for concrete structures in the transportation system. These methods can provide corrosion protection to the concrete, reinforcing steel, or both. This section provides information on each of these systems.

Concrete Mix Design

The concrete mix design is vital for ensuring a long service life of the concrete. Service life extension is achieved through low-permeable and low-cracking concrete mix designs. Concretes routinely now use supplementary cementious materials (SCM) to improve durability and make the concrete less permeable to chlorides. SCMs typically used include ground granulated blast furnace slag, fly ash, and silica fume. Low cracking concrete mixes are also now possible by selecting proper admixtures or lightweight aggregates within the concrete mix design.

During the design stage of a concrete element, it should be considered that the cover of concrete over the embedded steel, also called cover depth, could delay the movement of chloride ions and increase the time before corrosion initiation of the steel reinforcement. It is common for designers to increase the cover depth to extend the service life of steel reinforcement within a concrete section.

Consolidation of the concrete also plays a significant role in its durability. Properly consolidated concrete provides a barrier between environmental and salt exposure. When consolidation is inadequate, voids can form in the concrete that can reduce the cover over the steel or, even worse, provide incomplete embedment of the steel. Concrete consolidation is achieved through vibration of fresh concrete at the worksite or fabrication shop. It also can be improved by using a self-consolidating concrete mix design that provides good flow. Improper curing can cause cracks to form that can create voids and nullify the benefit of cover depth.

Concrete Reinforcement

RC members commonly are used in highway network applications to simultaneously use the beneficial properties of both concrete and steel. The reinforcement can be in the form of rebar, strand, rods, welded wire fabric, or fibers. In addition to providing strength, reinforcement is routinely used to overcome concrete's tendency to crack in a brittle manner or minimize the width of the cracks once they form.

One mechanism for improving the corrosion resistance of an RC element is the use of a corrosion-resistant reinforcing material compared with the conventional carbon steel reinforcement. When rebar is used, coatings or corrosion-resistant steel grades can be used. Two of the commonly used coating systems include epoxy- and metallic-coated, such as galvanized, rebar. Combinations of epoxy and zinc have been used to create dual-coated rebar. These types of reinforcement have been used for many years with increased success when compared with carbon steel rebar, at only a slight cost increase.

Similar to steel plate, there are also alloyed solutions for rebar. One such option is ASTM A1035, *Standard Specification for Deformed and Plain, Low-Carbon, Chromium, Steel Bars for Concrete Reinforcement*, Grade CS.[24,25] Rebar meeting these requirements contains 8–10.9 wt% chromium, making it slightly below the minimum level of chromium to qualify as a stainless steel. Nevertheless, it still provides an increased amount of corrosion resistance compared with traditional-grade rebar.[26] Duplex stainless steel rebar also exists and can be specified according to ASTM A955, *Standard Specification for Deformed and Plain Stainless Steel Bars for Concrete Reinforcement*,[25,27] For example, a UNS S3108 rebar has 21–23 wt% chromium and 4.5–6.5 wt% nickel. Other lower-nickel-containing rebar, including UNS S32304 and UNS S32101, also have become more common for use in bridges. The increased alloy content contained in these duplex stainless steels allows it to provide a much higher corrosion resistance than either traditional-grade or ASTM A1035 Grade CS rebar. Overall, alloyed rebar carries an increased cost, but it has excellent corrosion resistance and is capable of providing a long service life.

As a replacement for mild steel reinforcement, composite materials are also available for RC structures. GFRP and CFRP provide a corrosion-free option for bridges. Prestressed and post-tensioned concrete elements also have reinforcement materials available with improved corrosion resistance. The steel used in these elements traditionally has been seven-wire strands with a minimum tensile strength of 250 ksi or 270 ksi. Historically, these strands have been encased in grout with the hope of providing corrosion resistance, but they have experienced increased corrosion damage because of poor grout consolidation from improper construction practices and chloride contamination within grout mixes. Coated steel strands are available, but tensioning them can be more challenging compared with conventional steel strands.

Corrosion-resistant and corrosion-free solutions are also available for seven-wire, high-strength strand, including stainless steel and CFRP. Duplex stainless steel grade 2205 strand has a minimum tensile strength of 250 ksi and has been used by U.S. agencies for prestressed concrete piles. Corrosion-free CFRP seven-wire prestressing strand with a minimum tensile strength of 338 ksi also has been used by several U.S. agencies for both prestressed concrete piles and beams. CFRP also has been used in post-tensioned concrete girder bridge systems.

Fiber RC is another option for increasing corrosion resistance. Research into fibers and how to incorporate them in the concrete mix continues to advance. Metallic and nonmetallic fiber materials have found use in making concrete elements stronger, more ductile, or with tighter crack widths. Fieldwork on bridges has demonstrated the benefits of using fibers to improve strength or reduce crack widths in concrete.[28–30]

Overlays, Sealants, and Coatings

The addition of a barrier, in the form of an overlay, sealant, or coating, can aid in restricting the movement of aggressive species

through the concrete to improve the service life of an RC structure; these barriers are especially helpful where de-icing salt or saltwater are present. Overlays can provide additional protection to a bridge deck, for example, by providing a riding surface that is more impermeable to chloride ions than a standard bare deck. Crack sealants can be used to seal existing cracks to restrict the movement of aggressive ions through the cracks. Concrete sealants and coatings can be used on uncracked concrete to provide increased corrosion protection.

Electrochemical Techniques

Cathodic Protection

Cathodic protection increases the corrosion resistance of an RC structure by incorporating a second metal into the system; the existing reinforcement within the structure then becomes the cathode, and the second metal becomes the anode. Two common types of cathodic protection include galvanic anode cathodic protection (GACP) and impressed current cathodic protection (ICCP). When using GACP, sometimes termed sacrificial anode cathodic protection, the second metal incorporated into the structure is less noble than the reinforcing steel, thus making the second metal sacrificial. Zinc is one of the commonly used sacrificial metals in GACP. ICCP systems use a rectifier that polarizes the reinforcing steel with a negative rectifier pole; once the second metal is incorporated into the structure, it becomes polarized positively, and thus it becomes the anode. Although ICCP systems require monitoring to ensure the applied current and voltage are within tolerances, this has been made easier by the use of remote monitoring systems. NACE International and other similar organizations have standards that cover cathodic protection of RC structures.

Electrochemical Chloride Extraction

Electrochemical chloride extraction (ECE) systems are similar to ICCP in how they are connected to the structure. The systems are different, however, in that they are not a permanent part of the structure, but instead are installed temporarily for a much shorter duration of time. ECE systems are operated at a higher voltage difference and current density than ICCP. NACE International and other organizations have standards that cover the use of ECE systems for RC structures.

Electrochemical Realkalisation

Electrochemical realkalisation (ER) is similar to cathodic protection, but its purpose is to increase the alkalinity around the steel of the carbonated concrete.

Vulnerable Areas and Repair Strategies

The following sections highlight areas that are most vulnerable to corrosion on typical highways, tunnels, and bridges.

HIGHWAYS

On a highway system, some of the elements that are most susceptible to corrosion are not the highways themselves, but rather the surrounding infrastructure. This includes the guardrails, culverts, and ancillary structures. Corrosion vulnerabilities for each of these three elements are discussed in the following sections.

Guardrail

Roadside safety barriers are located relatively close to moving traffic; therefore, these devices can experience high levels of water spray and de-icing salts. Within the United States, the FHWA advises against the use of weathering steel guardrails.[14,31] The concern is that the barrier could experience significant section loss because the patina fails to form as a result of frequent wet cycles and salt exposure. Galvanized steel is acceptable, however, and if aesthetics are important, then powder coated galvanized guardrails are allowed.[31]

In 2008, FHWA sponsored a report, "W-Beam Guardrail Repair: A Guide for Highway and Street Maintenance." This report discusses maintenance of commonly used W-shape beam guardrails and indicates that corrosion-related maintenance is important to ensure the safety barrier perform as expected.[32] Because these types of guardrails are routinely galvanized, W-beam guardrail sections were also evaluated in 2014 to determine whether galvanizing using either a hot-dip batch or a hot-dip continuous process altered the corrosion protection.[32,33] This work concluded that increasing the coating thickness provided a greater corrosion resistance and that its benefit was not sensitive to the type of galvanizing method.[33] It also highlighted that mating metal surfaces could exhibit crevice corrosion.[33]

Although corrosion of guardrails can occur, these structures often are replaced because of vehicular crashes, rather than because of significant corrosion damage. Guardrails are described as "critical safety devices" that reduce the chance of a motorist experiencing a "more severe crash when leaving the roadway."[32] When impacts occur on guardrails, many agencies may require that the guardrail be replaced or upgraded, meaning that the service life of guardrail could be relatively short compared with other steel elements, so replacement because of corrosion is less common.

Culverts

It is important to understand the properties of the soil and water that will be in contact with the culvert. These properties and how they interact with the culvert, possibly because of flow or abrasion, will influence material selection.

In 1986, FHWA published the "Culvert Inspection Manual" supplement to the "Bridge Inspector's Training Manual." It states that damage to the culvert materials used at that time could be the result of corrosion and abrasion.[34] Bushman and Chaker highlight this issue with culverts in the 2005 version of this manual, indicating that commonly used hot-dipped galvanized steel corrugated pipe exhibited higher corrosion rates on the invert section of the pipes. This was attributed to harsh water conditions and higher flow rates.[35]

More recently, the NCHRP sponsored a study to update the 1986 FHWA culvert manual. A more recent study was needed because different materials, such as plastic pipe, now are commonly used but were not addressed in the 1986 FHWA manual. These changes were incorporated in the 2019 manual released by AASHTO.[36]

Ancillary Structures and Luminaires

Ancillary structures, such as signs and luminaires, are subject to corrosion because of the atmosphere and through de-icing salt when they are located close to the roadway. Corrosive soils can affect these structures if they are not encased in concrete at the level of the soil; accelerated corrosion also can occur if the encasing concrete cracks and allows the soil to penetrate to the anchor rods or other connecting elements from the structure to the foundation. Weathering steel has shown poor performance as a light pole material, as noted by a 1989 FHWA Technical Advisory.[14] The FHWA cited section loss or localized structural failure as potential failure modes, likely because of the increased time of wetness associated with these low-lying structures. In a similar fashion, anchor rods can experience accelerated corrosion when encased in grout in between the structure base and foundation. In many instances, common practice has been to encase them in grout to prevent corrosion, but when cracks in the grout do occur, they can retain moisture and salt to cause corrosion damage at an accelerated rate. Similar to the discussion in the section "Concrete," it is important to minimize cracking of the encasing grout.

Many ancillary structures and luminaires are designed with either HDG steel or aluminum to provide increased resistance to corrosion. In many cases, the hardware, including the anchor rods, nuts, and washers, are also HDG. It is recommended to leave a space between the bottom of the structure and the top of the foundation, rather than filling this void with grout. If a gap is left here, it can allow moisture to dry and de-icing salts to be washed away, rather than potentially being encased in grout. Generally, when sign structures and luminaires have significant corrosion, it is recommended that the damaged areas, or the entire structure, be replaced because of the high maintenance cost relative to the cost of the structure.

TUNNELS

The impediment a tunnel must pass through to create a passageway can also vary widely. For example, in the western part of the Commonwealth of Virginia, travelers pass through a mountain using the Big Walker Mountain Tunnel.[37] In the eastern part of the state, however, several tunnels pass under the waterways leading to the Atlantic Ocean.[38] Although the environments through which these tunnels must pass are different, the methods of construction also are different, which can affect the corrosion resistance of the structure.

The FHWA "Tunnel Operations, Maintenance, Inspection, and Evaluation (TOMIE) Manual" discusses some of the common tunnel construction methods and how the method is often selected by the project conditions.[39] As with other civil structures, the amount of damage associated with corrosion is sensitive to exposure time. Time is needed for chlorides to move through concrete or coatings on steel to degrade, which then mitigates the benefit from the original corrosion protection system. In the United States, nearly 70% of the tunnels were built over a 50-year span, between 1922 and 1972, which means this group of tunnels is quickly approaching 50 years old.[40] This trend for the aging tunnel population is similar to the aging bridge population in the United States. Aging bridges require significant maintenance to extend their service lives, and because bridges and tunnels of the same era were built with the same steel and concrete materials, it is likely that tunnels will require significant maintenance as well.[41]

Tunnel Liners

Bushman and Chaker highlighted that, over time, tunnel linings have been constructed using segmental cast iron, steel ribs and wood lagging, fabricated steel, pressed steel plates, and precast concrete.[35] The TOMIE manual suggests that, in recent years, the three most common tunnel lining materials are RC (prefabricated or cast-in-place), cast iron, and steel.[39] One typical corrosion mechanism of tunnel linings is from groundwater, which can deteriorate and corrode the lining from sources of salt, galvanic interactions, and stray currents aggravating the problem.[39] Corrosion damage of linings includes metal section loss, concrete spalling, and damage to electrical systems. If any corrosion damage is observed, repairs should be made to mitigate the damage, and actions should be taken to protect the liner from ongoing corrosion.[39]

Ceiling Panels

In many instances, the ceiling panels, supporting hardware, or hardware for attachments have experienced failures because of corrosion. Many of these cases were due to the materials irregularities resulting from poor fabrication or construction. For example, if corrosion-inducing materials are found within a concrete mix design, they could cause the corrosion-resistant supporting hardware in contact to be more susceptible to stress corrosion cracking. Attachment hardware can be susceptible to corrosion damage if it is not manufactured properly, such as during the casting or sintering process.

Corrosion damage of ceiling panels and adjacent hardware can largely be prevented in the design process by having specifications that ensure that all of the materials are properly manufactured and fabricated. If corrosion damage is discovered on any hardware, it is recommended that the damaged hardware be replaced before reaching a critical state.

Flood Gates

Flood gates are an important element of a tunnel for mitigating corrosion. When tunnels are located in regions where storm surges can occur, flood gates can seal a tunnel and protect the interior of the tunnel from exposure to water. Although the discussion on tunnels has focused mainly on the structural elements and materials, tunnels also can contain other systems sensitive to corrosion, like electrical or mechanical components.[42]

BRIDGES

Bridges often are broken up into three components: deck, superstructure, and substructure. In general, the deck carries the wheel loads from the traffic above and transfers them to the superstructure. The superstructure, typically made from either steel or concrete girders, then transfers the loads to the substructure. Each of these three main components will be discussed in terms of their corrosion vulnerability.

Deck

Steel Decks

Although not extremely common, steel decks, such as open grid or orthotropic decks, can be used in long span bridges, where dead load needs to be minimized. This puts the steel in direct contact with de-icing salts applied to the deck from above. Corrosion-resistant steels can be used in these instances to prevent accelerated corrosion. Improved detailing of the steel deck also can be used to prevent de-icing salt and moisture from collecting in specific areas.

Concrete Decks

A properly designed concrete bridge deck can protect the superstructure below from salt exposure, acting as a first line of defense against corrosion damage. Figure 1*A* shows a photograph of a bridge under construction; figure 1*B* provides a closer view of the deck reinforcement, which is alloyed for corrosion resistance; and figure 1*C* shows the finished concrete surface with cracks. Because the deck typically acts as the primary riding surface, it can be subject to large amounts of de-icing salts in regions that receive snowfall and ice. Concrete decks typically have a minimum cover between the top layer of reinforcing steel and the top of the riding surface; this cover assists in preventing corrosion of the reinforcing steel. If, however, the concrete cracks, the de-icing salt can penetrate through the concrete to the reinforcing steel. If the reinforcement corrodes enough, it can lead to spalling or larger cracks, which can allow water and de-icing salts to penetrate to the superstructure below, causing accelerated corrosion. To mitigate salt movement through the cracks, bridge owners must decide on the appropriate maintenance operation that might include using a crack sealant.

Bridge decks often contain joints to allow for thermal expansion and contraction of the bridge. These joints typically have expected service lives that are much shorter than the decks themselves. Once a joint fails, it can cause leakage of water and de-icing salts onto the bridge girders below; after several years, this leakage can cause significant corrosion because water and de-icing salts can become trapped on the girders. It is important to repair leaking joints in the early stages of failure to prevent future, expensive repairs on the bridge girders. Although more expensive, eliminating a deck joint can lead to significantly better corrosion performance for the deck and the superstructure.

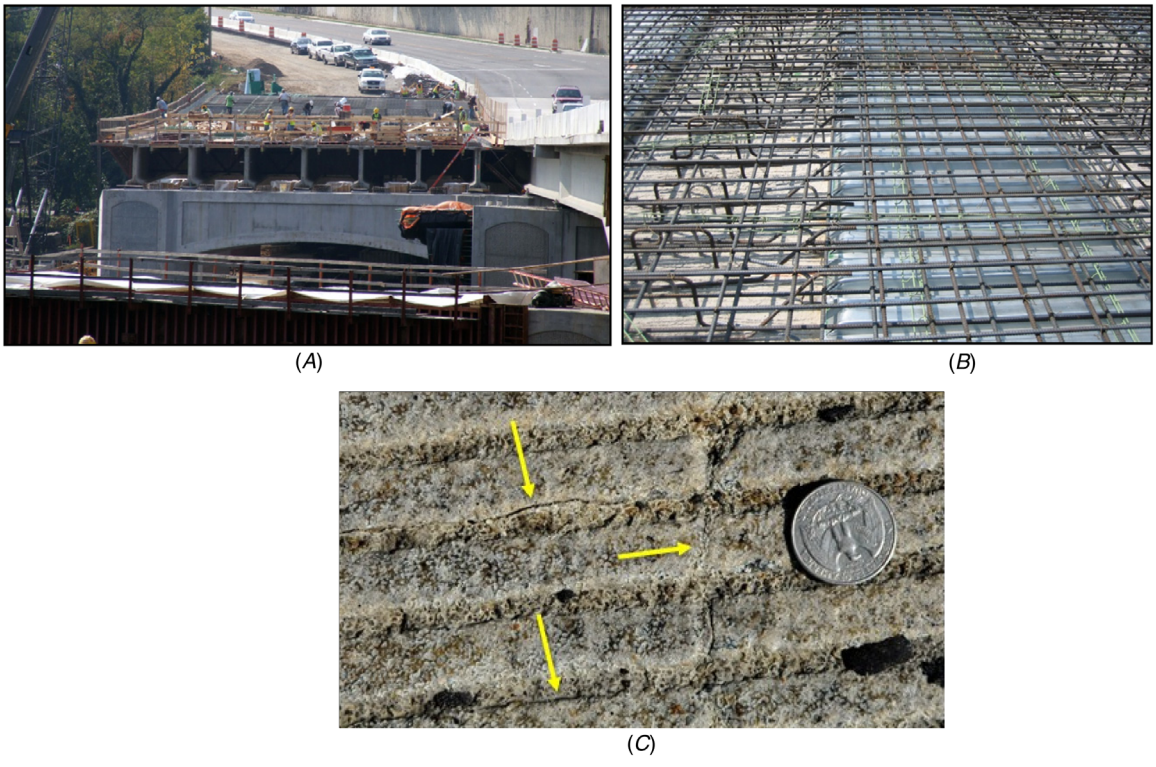
Superstructure

The majority of bridge superstructures are made of either steel or concrete girders. The corrosion deterioration of each type of superstructure is different, so the two types of superstructures will be discussed separately.

Steel Superstructure

The continuous application of chlorides and moisture onto a steel girder under a leaking joint, and subsequent ponding on the bottom flange, can lead to accelerated corrosion and section loss in the web and bottom flange of the steel beam. An example of this is shown in figure 2. Ultimately, the best strategy for repairing

FIG. 1 A bridge deck that is (*A*) under construction with the corrosion-resistant reinforcing steel being placed, (*B*) close-up of the corrosion-resistant reinforcing steel that will be encased in concrete, and (*C*) cracks (yellow arrows) in the concrete bridge deck.



(*A*) (*B*) (*C*)

FIG. 2 Corroded steel beam end.



corrosion damage to steel beam ends is to replace the deck joint above the areas of corrosion. Once the section loss in the steel beam reaches a critical state, however, repairs will need to be made to restore the structural capacity of the beam. If the corrosion damage is severe enough, portions of the beam web and bottom flange may need to be cut out and a new beam portion will need to be welded in its place. Field welding, however, historically has had many challenges and can lead to further complications if not done properly. Another repair strategy is to bolt repair plates to the existing beam to restore the beam's structural capacity. This process is started by cleaning and removing all of the existing corrosion damage. Steel repair plates then can be bolted into place over the once-corroded area. It is important that these repair plates extend into unaffected portions of the steel beam and provide adequate structural capacity. The repair plates should have some form of corrosion protection system, such as painted, TSC, or alloyed steel. Care also should be taken to close the gaps between the existing beam and repair plates using some form of sealant.

Steel bridges also can experience increased corrosion when used as a grade separation between two intersecting traffic routes. This scenario is referred to as a "tunnel effect" in the FHWA Technical Advisory regarding the use of uncoated weathering steel because the bridge acts as the ceiling of the tunnel over the roadway below. In this case, de-icing salts are applied to the roadway below the bridge. As trucks travel on the roadway below, they splash the de-icing salts up onto the bridge above. Many of these de-icing salts come into contact with and stick to the inbound fascia girder to cause accelerated corrosion.

Steel bridge connections, especially those that are oriented horizontally, are susceptible to increased corrosion because they form a natural ponding area for de-icing salt, water, bird guano, and other debris to accumulate. If this corrosion-inducing debris is stagnant and is not able to drain off of the surface naturally, it can lead to localized accelerated corrosion. Many older bridges also contain built-up members, which are made up of individual plates and angles and then are bolted or riveted together to form a structural member. Built-up members are susceptible to crevice corrosion because of the presence of multiple plates for which water or chlorides to penetrate.

Trusses can experience accelerated corrosion because of a multitude of factors. Deck trusses are subject to corrosion from trucks kicking up de-icing salts from the roadway, similar to the tunnel effect described previously. In this case, the de-icing salts are sprayed both upwards and sideways, affecting the diagonals, vertical members, and horizontal members that cross over the roadway. Another case in which trusses can experience increased corrosion is due to the presence of closed box-members. Many trusses have closed members that, if not detailed properly, can prevent drainage. Because it is nearly impossible to completely prevent water and other debris from entering these closed members, the lack of drainage will certainly lead to accelerated corrosion from the inside out. Due to the closed nature of these types of members, inspecting them for the presence of corrosion is also difficult.

Concrete Superstructure

Similar to a concrete bridge deck, concrete used for the superstructure can crack, especially when restrained. These cracks can provide a direct path for corrosive exposure to penetrate to the reinforcing steel and quickly nullify the benefit of mitigation techniques such as SCMs in the mix design and additional concrete cover. Overall, using a good quality concrete, including low permeability and low cracking additives, in conjunction with a corrosion-resistant reinforcement can provide a cost-effective, long-term method of preventing corrosion in a structure. The benefit of this combination is more evident in locations where aggressive environmental conditions increase the probability of corrosion in a structure.

On example of when a concrete superstructure would be more likely to experience accelerated corrosion is if the bridge is located in an area where de-icing salts are applied. This could occur if the concrete deck is a part of the concrete girders, such as in a decked bulb tee or adjacent box girder. In this type of system, the post-tensioning rods between the box girders can corrode, leading to a loss of transverse post-tensioning between the girders. Using a good quality grouting material between the girders and corrosion-resistant steel like Type 2304 is expected to provide a longer service life than conventional carbon steel rebar.[43]

In both examples, salt exposure over time will result in chloride ions diffusing through the concrete, and cracks in the concrete will increase the rate of chloride movement, until a sufficient quantity of chlorides reach the steel, which then causes cracking and spalling of the concrete.

Corrosion related repairs in RC can include starting with trying to minimize the structural damage. Early corrosion prevention methods could include using a barrier method to keep corrosive electrolytes from reaching the steel.

Substructure

The bridge substructure transfers the load from the bridge deck and superstructure to the foundation. In bridges, the superstructure elements are typically referred to as abutments and piers, and can be made out of either steel or concrete.

Steel Substructure

H-piles are a common form of steel substructure used to support pier caps. Because these support the rest of the bridge above, it is

critical they have sufficient durability to match the design life of the structure. These H-piles can be subject to corrosion through aggressive soil or water conditions. One example of H-pile corrosion occurred in 2013, when the piles supporting a bridge in the United States experienced a local failure that caused approximately 2 ft of vertical displacement at the pier.[44] When steel H-piles are used as substructure elements, it is advised that a corrosion protection system be applied to them, such as metallic coatings or alloyed steel.

Concrete Substructure

Piles, drilled shafts, or spread footings are all examples of RC substructure elements. Depending on the bridge location, these elements can be subject to corrosion because of being exposed to aggressive soil conditions or through direct contact with saltwater or brackish water. Using a good quality concrete and corrosion-resistant or corrosion free, like UNS Type 2205 or CFRP, prestressing strands can greatly improve the service life.[45,46] Concerns also have been raised that as utility and light rail share more of the right-of-way with existing bridges, the bridges could be exposed to stray currents that could damage the foundations.

Future Corrosion Related Ventures

LASER ABLATION COATING REMOVAL

Laser ablation coating removal (LACR) is a coating removal technique that uses high-energy light pulses that are directed at the coated surface to vaporize the coating. Then, a vacuum and filtration system is used to collect the coating as it is being removed; in doing this, LACR is expected to reduce the total coating removal time, personnel exposure to hazardous waste, and the amount of hazardous waste generated during the removal process. The process can be used on both steel and concrete coated bridge components. Although this technology is newer to the bridge community, LACR has been used in other industries with positive results. LACR is slower than conventional coating removal methods, but this technique could provide a means for removing coatings from corroded sections while improving capture efficiency of environmental contaminants, and reducing the amount of material requiring disposal.[47]

DISSIMILAR METAL STEEL BRIDGES

Corrosion-resistant steel bridges can be built more cost effectively when dissimilar metals are used. This can be done by using corrosion-resistant alloyed steels in targeted, highly corrosive areas, such as beam ends and areas close to water, and lesser corrosion-resistant or coated steels would be used in benign locations. By doing this, the more durable, but higher cost steels would be used only where truly needed, and the more common, lower cost steels would be used elsewhere. Galvanic corrosion of the dissimilar metal connections, either bolted or welded, would need to be considered before employing such designs.[19]

FLEXIBLE FILLER ALTERNATIVES FOR GROUT IN POST-TENSIONED CONCRETE APPLICATIONS

As mentioned in a previous section, post-tensioning strands encased in grout have experienced increased corrosion because of chloride-infused grout and poor grout consolidation. In the past, segregation of grouts and the formation of soft grout has been a concern that is compounded by the difficulty in detecting these issues using nondestructive methods. One potential solution to this problem is to use a flexible filler, such as wax or grease, in place of the grout. Flexible fillers have been used in the past, but this approach is relatively new to many agencies so it could usher in a new type of corrosion that will have to be addressed when designing and maintaining post-tensioned structures. One of the unique concerns with switching to flexible fillers is that the fill material could support microbiologically influenced corrosion.[48] Fortunately, if this is the case, post-tensioned structures can be designed so that the strands can be replaced if needed.

SEA-LEVEL CHANGE

In the coming years, the sea level is expected to rise along the coastlines and lower elevation inland areas. A large portion of the world's population lives in these areas, which means there is a large amount of transportation infrastructure in these locations. As sea-level rise continues, the risk is greater for corrosion on these highways, tunnels, and bridges because of the influx of saltwater. These systems likely will require maintenance to address corrosion that occurred earlier in their service lives, and new structures in these areas will require more corrosion-resistant designs.

Corrosion-Related Standards for Highways, Tunnels, and Bridges

Although individual transportation departments can use documents that provide corrosion-related guidance when doing work for them, the following documents have been generated for broader use. Some of these documents are referenced in the guidance provided by the individual transportation departments.

ATMOSPHERIC TEST METHODS

- ASTM G33, *Standard Practice for Recording Data from Atmospheric Corrosion Tests of Metallic-Coated Steel Specimens*
- ASTM G50, *Standard Practice for Conducting Atmospheric Corrosion Tests on Metals*
- ASTM G84, *Standard Practice for Measurement of Time-of-Wetness on Surfaces Exposed to Wetting Conditions as in Atmospheric Corrosion Testing*
- ASTM G87, *Standard Practice for Conducting Moist SO_2 Tests*
- ASTM G91, *Standard Practice for Monitoring Atmospheric SO_2 Deposition Rate for Atmospheric Corrosivity Evaluation*
- ASTM G101, *Standard Guide for Estimating the Atmospheric Corrosion Resistance of Low-Alloy Steels*
- ASTM G116 (replaced ASTM G104), *Standard Practice for Conducting Wire-on-Blot Test for Atmospheric Galvanic Corrosion*

SALTWATER TEST METHODS

- ASTM G52, *Standard Practice for Exposing and Evaluating Metals and Alloys in Surface Seawater*
- ASTM G78, *Standard Guide for Crevice Corrosion Testing of Iron-Base and Nickel-Base Stainless Alloys in Seawater and Other Chloride-Containing Aqueous Environments*

SOIL TEST METHODS

- ASTM G51, *Standard Test Method for Measuring pH of Soil for Use in Corrosion Testing*
- ASTM G57, *Standard Reference Test Method for Measurement of Soil Resistivity Using the Wenner Four-Electrode Method*

STEEL TEST METHODS

- ASTM G46, *Standard Guide for Examination and Evaluation of Pitting Corrosion*
- ASTM G61, *Standard Test Method for Conducting Cyclic Potentiodynamic Polarization Measurements for Localized Corrosion Susceptibility of Iron-, Nickel-, or Cobalt-Based Alloys*

REINFORCED CONCRETE TEST METHODS

- ASTM C876, *Standard Test Method for Corrosion Potentials in Uncoated Reinforced Steel in Concrete*
- ASTM G109, *Standard Test Method for Determining Effects of Chemical Admixtures on Corrosion of Embedded Steel Reinforcement in Concrete Exposed to Chloride Environments*
- ASTM G180, *Standard Test Method for Corrosion Inhibiting Admixtures for Steel in Concrete by Polarization Resistance in Cementitious Slurries*
- AASHTO T 373, *Linear Polarization Resistance and Potentiodynamic Polarization Test*
- AASHTO T 374, *Tombstone Test*
- AASHTO T 376, *Macrocell Slab Chloride Threshold*
- Bureau of Reclamation M-82, *Time-to-Corrosion Slabs*
- FHWA-RD-98-153, *Southern Exposure Time-to-Corrosion Slabs*

HIGHWAY GUIDANCE

Guardrail, Culverts, and Ancillary Structures and Luminaires

- See the "Structural Steel" section for ASTM Standards on Galvanizing.

TUNNEL GUIDANCE

- FHWA, "Tunnel Operations Maintenance, Inspection, and Evaluation (TOMIE) Manual"
- FHWA and Federal Transit Administration, "Highway and Rail Transit Tunnel Maintenance and Rehabilitation Manual", 2005
- FHWA and Federal Transit Administration, "Highway and Rail Transit Tunnel Inspection Manual", 2005
- FHWA, "Underground Transportation Systems in Europe: Safety, Operations, and Emergency Response," International Technology Scanning Program, June 2006
- NCHRP, "Best Practices for Implementing Quality Control and Quality Assurance for Tunnel Inspection," NCHRP Project 20-07/Task 261, Transportation Research Board, October 2009
- NCHRP, "Best Practices for Roadway Tunnel Design, Construction, Maintenance, Inspection, and Operations," Domestic Scan 09-05, NCHRP Project 20-68A, Transportation Research Board, April 2011
- NCHRP, "Development of Guidelines for Rehabilitation of Existing Highway and Rail Transit Tunnels," NCHRP Project 20-07/Task 276, Transportation Research Board, July 2010

BRIDGE GUIDANCE

General

- AASHTO, *Manual for Bridge Evaluation*, 2011
- AASHTO, *Guide Manual for Bridge Element Inspection*, 2011
- ACI 301, *Specifications for Structural Concrete*

Structural Steel Plate

- ASTM A709, *Standard Specification for Structural Steel for Bridges*
- ASTM A588, *Standard Specification for High-Strength Low-Alloy Structural Steel, up to 50 ksi [345 MPa] Minimum Yield Point, with Atmospheric Corrosion Resistance*
- ASTM A780, *Standard Practice for Repair of Damaged and Uncoated Areas of Hot-Dip Galvanized Coatings*
- ASTM A1010, *Standard Specification for Higher-Strength Martensitic Stainless Steel Plate, Sheet, and Strip*
- ASTM A123, *Standard Specification for Zinc (Hot-Dip Galvanized) Coatings on Iron and Steel Products*
- ASTM A153, *Standard Specification for Zinc Coating (Hot-Dip) on Iron and Steel Hardware*
- ASTM A385, *Standard Practice for Providing High-Quality Zinc Coatings (Hot-Dip)*
- ASTM B6, *Standard Specification for Zinc*
- ASTM D6386, *Standard Practice for Preparation of Zinc (Hot-Dip Galvanized) Coated Iron and Steel Product and Hardware Surfaces for Painting*
- AASHTO/SSPC-PA 18/NSBA S 8.2, *Specification for the Application of Thermal Spray Coatings to Steel Bridges*

Grade 60 to Grade 100 Reinforcing Bars

- ASTM A615, *Standard Specification for Deformed and Plain Carbon-Steel Bars for Concrete Reinforcement*
- ASTM A706, *Standard Specification for Deformed and Plain Low-Alloy Steel Bars for Concrete Reinforcement*
- ASTM A767, *Standard Specification for Zinc-Coated (Galvanized) Steel Bars for Concrete Reinforcement*

- ASTM A775, *Standard Specification for Epoxy-Coated Steel Reinforcing Bars*
- ASTM A934, *Standard Specification for Epoxy-Coated Prefabricated Steel Reinforcing Bars*
- ASTM A955, *Standard Specification for Deformed and Plain Stainless Steel Bars for Concrete Reinforcement*
- ASTM A1035, *Standard Specification for Deformed and Plain, Low-carbon, Chromium, Steel Bars for Concrete Reinforcement*
- AASHTO M284, *Standard Specification for Epoxy-Coated Reinforcing Bars: Materials and Coating Requirements*
- AASHTO M 334M/M 334-17, *Specification for Uncoated Corrosion-Resistant, Deformed and Plain Alloy, Billet-Steel Bars for Concrete Reinforcement and Dowels*
- AWS D1.4/D1.4M, *Structural Welding Code—Reinforcing Steel*
- ANSI/CRSI, CG1.1-2016, *Epoxy Coating Plant: Straight Bar Lines*
- CRSI, CG1.2-2016, *Epoxy-Coated Facilities: Custom Lines*
- ANSI/CRSI, CG2.1-2016, *Epoxy-Coated Steel Reinforcing Bar Fabrication Facilities*
- ANSI/CRSI, IPG4.1-2016, *Stainless Steel Reinforcing Bar Fabrication Facilities*
- CRSI, *Corrosion Resistant Steel Reinforcement: Summary of Test Methods*, Report WJE No. 2016.1849, October 13, 2016

High-Strength Strand Reinforcement

- ASTM A416, *Standard Specification for Low-Relaxation, Seven-Wire Steel Strand for Prestressed Concrete*
- ASTM E1356, *Standard Test Method for Assignment of the Glass Transition Temperatures by Differential Scanning Calorimetry*
- ASTM D7028, *Standard Test Method for Glass Transition Temperature (DMA Tg) of Polymer Matrix Composites by Dynamic Mechanical Analysis (DMA)*
- ASTM D7913, *Standard Test Method for Bond Strength of Fiber-Reinforced Polymer Matrix Composite Bars to Concrete by Pullout Testing*
- ASTM D7205, *Standard Test Method for Tensile Properties of Fiber Reinforced Polymer Matrix Composite Bars*
- ASTM D7337, *Standard Test Method for Tensile Creep Rupture of Fiber Reinforced Polymer Matrix Composite Bars*
- ASTM D7705, *Standard Test Method for Alkali Resistance of Fiber Reinforced Polymer (FRP) Matrix Composite Bars Used in Concrete Construction*
- ACI 440.3R, *Guide Test Methods for Fiber-Reinforced Polymers (FRPs) for Reinforcing or Strengthening Concrete Structures*, Method B.3

Corrosion Mitigation Techniques

- NACE RP 0187-2005, *Standard Recommended Practice, Design Considerations for Corrosion Control of Reinforcing Steel in Concrete*
- NACE RP0281-2004, *Standard Recommended Practice, Method for Conducting Coating (Paint) Panel Evaluation Testing in Atmospheric Exposures*
- NACE RP0287-2002, *Field Measurement of Surface Profile of Abrasive Blast-Cleaned Steel Surfaces Using a Replica Tape*
- NACE RP0290-2000, *Impressed Current Cathodic Protection of Reinforcing Steel in Atmospherically Exposed Concrete Structures*
- NACE SP21427-2019, *Detection and Mitigation of Stray-Current Corrosion of Reinforced and Prestressed Concrete Structures*

References

1. S. S. G. Balakumaran, R. E. Weyers, and M. C. Brown, *Linear Cracking in Bridge Decks*, Final Report VTRC 18-R13, (Charlottesville, VA: Virginia Transportation Research Council, March 2018), https://web.archive.org/web/20220215221715/https://www.virginiadot.org/vtrc/main/online_reports/pdf/18-r13.pdf
2. P. D. Krauss and E. A. Rogalla, *Transverse Cracking in Newly Constructed Bridge Decks*, NCHRP Report 380 (Washington, DC: Transportation Research Board, National Academy Press, 1996).
3. TRB, *Control of Cracking in Concrete, State of the Art*, TR Circular E-C107 (Washington, DC: Transportation Research Board, 2006).
4. D. Darwin, J. Browning, W. Lindquist, H. A. K. McLeod, J. Yuan, M. Toledo, and D. Reynolds, "Low-Cracking, High-Performance Concrete Bridge Decks Case Studies over First 6 Years," *Transportation Research Record*, no. 2202 (2010): 61–69.
5. *Systems and Specifications: SSPC Painting Manual*, vol. 2, 2012 ed. (Pittsburgh, PA: Society for Protective Coatings, 2012).
6. *Guide Specification for Application of Coating Systems with Zinc-Rich Primers to Steel Bridges*, S 8.1-2014, SSPC-PA Guide 13 (Pittsburgh, PA: American Association of State Highway and Transportation Officials, National Steel Bridge Alliance, Society for Protective Coatings, 2014).
7. *Hot-Dip Galvanizing for Corrosion Protection: A Specifier's Guide* (Centennial, CO: American Galvanizers Association, 2012).
8. A. Azizinamini, E. H. Power, G. F. Myers, H. C. Ozyildirim, E. Kline, D. W. Whitmore, and D. R. Mertz, *Design Guide for Bridges for Service Life*, SHRP 2 Report S2-R19A-RW2 (Washington, DC: Transportation Research Board, 2014).
9. *Specification for Application of Thermal Spray Coating Systems to Steel Bridges*, S8.2-2017/SSPC-PA 18 (Pittsburgh, PA: American Association of State Highway and Transportation Officials, National Steel Bridge Alliance, Society for Protective Coatings, 2017).
10. J. F. H. Van Eijnsbergen, *Duplex Systems: Hot-Dip Galvanizing Plus Painting* (Amsterdam, Netherlands: Elsevier, 1994).
11. R. Kogler. *Steel Bridge Design Handbook: Corrosion Protection of Steel Bridges*, FHWA-HIF-16-002, vol. 19 (Washington, DC: Federal Highway Administration, Washington, DC, 2015).
12. *Standard Specification for Structural Steel for Bridges*, ASTM A709/A709M-17 (West Conshohocken, PA: ASTM International, approved September 1, 2017), http://doi.org/10.1520/A0709_A0709M-17

13. *Standard Specification for High-Strength Low-Alloy Structural Steel, up to 50 ksi [345 MPa] Minimum Yield Point, with Atmospheric Corrosion Resistance* ASTM A588/A588M-15 (West Conshohocken, PA: ASTM International, approved March 1, 2015), http://doi.org/10.1520/A0588_A0588M-15

14. FHWA, *Uncoated Weathering Steel in Structures*, Technical Advisory 5140.22 (Washington, DC: Federal Highway Administration, October 3, 1989).

15. *Standard Specification for Higher-Strength Martensitic Stainless Steel Plate, Sheet, and Strip*, ASTM A1010/A1010M-13 (West Conshohocken, PA: ASTM International, approved October 1, 2013), http://doi.org/10.1520/A1010_A1010M-13

16. I. G. Groshek, *Corrosion Behavior of ASTM A1010 Stainless Steel for Applicaitions in Bridge Components* (Blacksburg, VA: Virginia Tech, 2017).

17. F. B. Fletcher, *Improved Corrosion-Resistant Steel for Highway Bridge Construction*, FHWA Report FHWA-HRT-11-062 (Washington, DC: Federal Highway Administration, 2011).

18. S. R. Sharp, J. T. Provines, A. K. Moruza, W. F. Via, and K. N. Harrop, "Design, Fabrication, Construction, and Cost Assessment of Virginia's First Corrosion Resistant ASTM A1010 Plate Girder Bridge," *Transportation Research Record* 2672, no. 26 (2018): 68–76.

19. J. T. Provines and S. R. Sharp, "Corrosion Resistant Alloyed Steel for Low Maintenance Steel Bridges" (paper presentation, *World Steel Bridge Symposium*, St. Louis, MO, April 3–5, 2019).

20. N. Baddoo, *AISC Design Guide 27: Structural Stainless Steel* (Chicago, IL: American Institute of Steel Construction, 2013).

21. *Practical Guidelines for the Fabrication of Duplex Stainless Steels*, 3rd ed. (London, UK: International Molybdenum Association, 2014).

22. D. D. Crampton, K. P. Holloway, and J. Fraczek, *Assessment of Weathering Steel Bridge Performance in Iowa and Development of Inspection and Maintenance Techniques*, Final Report SPR-90-00-RB17-012 (Ames, IA: Iowa Department of Transportation, Office of Bridges and Structures, February 21, 2013).

23. K. Alland, J. M. Vandenbossche, R. Vidic, and X. Ma, *Evaluation of Bridge Cleaning Methods on Steel Bridges*, Report No. FHWA-PA-2013-007-PIT WO 2 (Washington, DC: Federal Highway Administration, 2013).

24. *Standard Specification for Deformed and Plain, Low-Carbon, Chromium, Steel Bars for Concrete Reinforcement*, ASTM A1035/A1035M-16 (West Conshohocken, PA: ASTM International, approved January 15, 2016), http://doi.org/10.1520/A1035_A1035M-16

25. *Specification for Uncoated Corrosion-Resistant, Deformed and Plain Alloy, Billet-Steel Bars for Concrete Reinforcement and Dowels*, AASHTO, M 334M/M 334 -17 (Washington, DC: American Association of State Highway and Transportation Officials, 2017).

26. J. R. Scully and M. F. Hurley, *Investigation of the Corrosion Propagation Characteristics of New Metallic Reinforcing Bars*, VTRC Report No. 07-CR9 (Charlottesville, VA: Virginia Transportation Research Council, February 2007).

27. *Standard Specification for Deformed and Plain Stainless Steel Bars for Concrete Reinforcement*, ASTM A955/A955M-18 (West Conshohocken, PA: ASTM International, approved January 1, 2018), http://doi.org/10.1520/A0955_A0955M-18

28. H. C. Ozyildirim, *Evaluation of Ultra-High-Performance Fiber-Reinforced Concrete*, VTRC Report No. 12-R1, (Charlottesville, VA: Virginia Transportation Research Council, August 2011).

29. E. Khakimova and H. C. Ozyildirim, *Investigation of Properties of High-Performance Fiber-Reinforced Concrete: Very Early Strength, Toughness, Permeability, and Fiber Distribution*, VTRC Report No. 17-R3 (Charlottesville, VA: Virginia Transportation Research Council, January 2017).

30. H. C. Ozyildirim and H. Nair, *Low Cracking Concretes for the Closure Pours and Overlays of the Dunlap Creek Bridge*, VTRC Report No. 18-R10 (Charlottesville, VA: Virginia Transportation Research Council, October 2017).

31. "Frequently Asked Questions: Barriers, Terminals, Transitions, Attenuators, and Bridge Railings," Federal Highway Administration, https://web.archive.org/web/20211215090628/https://safety.fhwa.dot.gov/roadway_dept/countermeasures/faqs/qa_bttabr.cfm

32. W. J. Fitzgerald, *W-Beam Guardrail Repair: A Guide for Highway and Street Maintenance Personnel*, Report No. FHWA-SA-08-002 (Washington, DC: Federal Highway Administration, November 2008).

33. Elzly Technology Corporation, *Comparing the Corrosion Protection of Hot Dip Batch versus Hot Dip Continuously Galvanized W-Beam Guardrail Sections Project*, NCHRP Final Report No. 20-07/Task 333 Task 16 (Washington, DC: National Academies of Science, Engineering, and Medicine, November 2014).

34. J. D. Arnoult, *Culvert Inspection Manual, supplement to the Bridge Inspector's Training Manual*, Report No. FHWA -IP-86-2 (McLean, VA: Federal Highway Administration, July 1986).

35. S. W. Dean, J. B. Bushman, and V. Choker, "Highways, Tunnels, and Bridges," in *Corrosion Tests and Standards: Application and Interpretation—Second Edition*, ed. R. Baboian (West Conshohocken, PA: ASTM International, January 2005), 706–715, https://doi.org/10.1520/MNL11071M

36. J. L. Beaver and M. C. Richie, *Culvert and Storm Drain System Inspection Manual*, NCHRP Final Report No. 14-26 (Washington, DC: National Academies of Science, Engineering, and Medicine, May 2016), https://web.archive.org/web/20220119234421/https://onlinepubs.trb.org/onlinepubs/nchrp/docs/NCHRP14-26_FR.pdf

37. R. Longfellow, "Highway History—Back in Time: The Big Walker and East River Mountain Tunnels," Federal Highway Administration, June 27, 2017, https://web.archive.org/web/20220215231536/https://www.fhwa.dot.gov/infrastructure/back0705.cfm

38. "Bored Method Selected for Hampton Roads Bridge-Tunnel Project," Tunnel Business Magazine, August 2, 2018, https://web.archive.org/web/20220215232554/https://tunnelingonline.com/bored-method-selected-hampton-roads-bridge-tunnel-project/

39. W. Bergeson and S. Ernst, *Tunnel Operations, Maintenance, Inspection, and Evaluation (TOMIE) Manual*, Report No. FHWA-HIF-15-005 (Washington, DC: Federal Highway Administration, July 2015).

40. C. Allen, M. Averso, C. Hargraves, and S. McNeil, *Guide for the Preservation of Highway Tunnel Systems*, NCHRP Report No. 816 (Washington, DC: National Academies of Sciences, Engineering, and Medicine, 2015), https://doi.org/10.17226/21903

41. NACE International, "Corrosion Control Plan for Bridges" (white paper, NACE International, Houston, TX, November 2012).

42. E. Rosenthal, "Hurricane Exposed Flaws in Protection of Tunnels," *New York Times*, November 9, 2012, https://web.archive.org/web/20220215234509/https://www.nytimes.com/2012/11/10/nyregion/hurricane-sandy-showed-vulnerability-of-citys-tunnels.html

43. "Instructional and Informational Memorandum: Corrosion Resistant Reinforcing Steels (CRR)," Virginia Department of Transportation, October 15, 2018, https://web.archive.org/web/20220119042335/https://www.virginiadot.org/business/resources/bridge/Manuals/IIM/SBIIM81.8.pdf

44. Wisconsin DOT (WisDOT), *I-43 Leo Frigo Memorial Bridge Investigation Report*, Executive Summary, Report No. ID 1220-15-01 (Wisconsin Rapids, WI: Wisconsin DOT (WisDOT), May 2015), https://web.archive.org/web/20211227212148/https://wisconsindot.gov/Documents/projects/by-region/ne/Leo%20Frigo%20Executive%20Summary%20Final.pdf

45. S. R. Sharp, H. C. Ozyildrim, and A. K. Moruza, *Corrosion-Free Carbon Fiber Reinforced Polymer for Prestressed Piles*, Final Report VTRC 19-R13 (Charlottesville, VA: Virginia Transportation Research Council, February 2019).

46. A. Paul, L. F. Kahn, and K. E. Kurtis, *Corrosion-Free Precast Prestressed Concrete Piles Made with Stainless Steel Reinforcement: Construction, Test and Evaluation*, Report No. FHWA-GA-15-1134, (Washington, DC: Federal Highway Administration, March 2015).

47. J. M. Fitz-Gerald, S. R. Agnew, W. Moffat, S. R. Sharp, J. Gillespie, D. R. Becker, R. Liu, and A. Runion, *Innovative Coating Removal Techniques for Coated Bridge Steel*, VTRC 20-R2, (Charlottesville, VA: Virginia Transportation Research Council, August 2019), https://web.archive.org/web/20210616155506/http://www.virginiadot.org/vtrc/main/online_reports/pdf/20-R1.pdf

48. F. J. Presuel-Moreno, C. F. Castaneda, I. Santillan, A. Kaxemi, and F. Tang, *Corrosion Prevention of Bridge Tendons Using Flexible Filler Materials*, FDOT Report No. BDV27-977-10 (Tallahassee, FL: Florida Department of Transportation Research, November 2018).

Chapter 23 | Automotive

Niamh Hosking[1]

Introduction

The automotive industry is one of the key sectors of the economy throughout the world. It drives a significant percentage of research in engineering and science, totaling $125 billion globally in 2018, and supports around 5% of private-sector employment in the United States, contributing at least 3% of America's total gross domestic product.[1] The automotive industry is a prime sector for the deployment of emerging technologies in robotics, connectivity and data analytics, and artificial intelligence, which are pillars of the newest industrial revolution, known as Industry 4.0.[2] Despite the transformation and disruption of much of the industry's traditional manufacturing methods and materials, high- and medium-volume passenger car production continues to rely on the use of metallic construction materials. Corrosion management, including testing, of those metallic structures remains a priority for the automotive engineer and across the industry generally.

Vehicle production starts with the input of sheet metal, typically steel or aluminum in coil form. The metal is cut and formed into 300–500 pieces, which are joined together to form the vehicle body in the bodyshop of the automotive factory. Castings, extrusions, and rolled frames also may be incorporated into the body structure. The assembled vehicle body passes to the paint line where corrosion protection coatings, sealants, and paint are applied. The final trim, chassis, and powertrain components (e.g., seats, carpets glass, engines, transmissions, suspensions, electrics, wheels, tires, and brakes) are fitted in the final assembly line to produce the finished vehicle.

Since the early 1980s, strategies to improve fuel economy and environmental impact, as well as vehicle quality and reliability, while also reducing manufacturing costs and increasing profit margins, have brought about considerable change in the industry. New designs and powertrains, improved processing, and new or improved materials and components have been developed to meet these challenges. The resulting improvements in corrosion resistance have led to extended warranties, which are typically 6–12 years for perforation and 3–5 years for cosmetic corrosion. Corrosion testing, of both components in the laboratory and full vehicles at the test track, has played a major role in the development of corrosion-resistant vehicles. The cost of conducting a corrosion test track study depends primarily on the duration and complexity of the test, which varies considerably from manufacturer to manufacturer as described by Ström.[3] Estimates for the test range between $100,000 and $200,000 per vehicle, excluding the vehicle cost. Therefore, there is strong interest in the industry to use alternative (i.e., quicker and cheaper) assessment methods to determine performance characteristics of vehicles and components in service environments. This chapter addresses the testing technology used in the development of corrosion-resistant vehicles and highlights some emerging trends for future corrosion testing.

Automotive Materials

The automobile has evolved into a complex, multi-material system that is exposed to a highly aggressive and variable environment. Its design includes highly finished external body panels and structural materials; hardware, such as trim, bumpers, and brackets; engine and batteries; drive train; exhaust systems; electrical systems; systems incorporating liquid passages and reservoirs, such as heat exchangers, hydraulic brake lines, fuel lines, and tanks; and oil and transmission fluid reservoirs. Nontraditional powertrains, such as hybrid electric, battery electric, and fuel cell–powered vehicles, present novel corrosion challenges. Thus, the variety of materials used is extremely large. Some of the metallic materials used in various automotive systems are listed in table 1. The most significant change in automotive materials in the 1980–2000 period was the transition from bare steel to precoated sheet steels, such as galvanized steel, which enabled gage reductions of the sheet steel. More recent material changes include the increased use of high-strength and ultra-high-strength steels, aluminum and magnesium alloys, plastics, and plastic composites. High-strength steels have found several applications in the vehicle body structure, particularly for load-bearing and energy-absorbing features (i.e., the crash structure)

[1]Ford Motor Company, Research and Advanced Engineering, 2101 Village Rd., Dearborn, MI 48124, USA https://orcid.org/0000-0002-7774-3967
The author acknowledges the previous author of this chapter, Robert Baboian, RB Corrosion Service, Greenville, RI.

DOI: 10.1520/MNL202NDSUP20190022

Copyright © 2022 by ASTM International, 100 Barr Harbor Dr., PO Box C700, West Conshohocken, PA 19428-2959
ASTM International is not responsible, as a body, for the statements and opinions expressed in this chapter. ASTM International does not endorse any products represented in this chapter.

TABLE 1 Metallic Materials Used in Automotive Vehicle Systems

System/Component	Materials
Body panels and structure	Steel, high-strength-low-alloy (HSLA) steel, coated steel (zinc, zinc-iron, zinc-nickel, zinc-aluminum, zinc-aluminum-magnesium, aluminum), high- and ultra-high strength steels, aluminum alloys, magnesium alloys
Chassis	Steel, HSLA steel, coated steel (zinc, zinc-aluminum, aluminum), aluminum alloys, magnesium alloys
Trim and hardware	Chrome-plated steel, stainless steel, aluminum, chrome plated zinc, stainless steel, clad aluminum (bimetal), magnesium
Exhaust system	Steel, coated steel (zinc, zinc-aluminum, aluminum), stainless steel, Monel
Engine and components	Iron, steel, aluminum, magnesium
Transmission	Steel, stainless steels, copper and alloys, nickel and alloys, aluminum
Fasteners	Steel, coated steel (wide range of metallic and nonmetallic coatings), aluminum
Cooling system	Copper and alloys, aluminum alloys, cast iron, steel, stainless steel, solder (lead-tin, tin, zinc) braze alloy (aluminum, copper), brass
Fuel system	Steel, coated steel (zinc, zinc-aluminum, zinc-nickel, aluminum, lead-tin, tin)
Brake system	Steel, coated steel (zinc, zinc-aluminum, zinc-nickel, lead-tin, tin), stainless steel, cupro-nickel alloy
Electrical and electronics	Aluminum, copper and alloys, coated steel (cadmium, chromium, nickel, copper, tin, lead), solder, beryllium, gold, silver stainless steels, magnesium

of the vehicle body.[4–6] The use of aluminum has expanded from hang-on parts, such as hoods and decklids dating back to the 1970s and earlier in some models,[7] to a much broader range of applications and structures in almost every system of the vehicle.[8]

Magnesium alloys, typically in cast form, also have found applications in vehicles, with different alloys developed depending on their mechanical properties and service conditions.[9] Their unfavorable and fluctuating material cost, among other factors, however, has limited their application compared with aluminum alloys. Joost and Krajewski[6] reported in 2017 that magnesium makes up less than 0.5% of the weight of the average vehicle. Carbon fiber–reinforced plastics (CFRP) also suffer from unfavorable material costs compared with aluminum and steel alternatives; nonetheless, some components for lower-volume vehicles have been produced from CFRP,[6,10–12] allowing for significant weight reductions compared with steel components.

Metallic and nonmetallic coatings used in the automotive industry are listed in table 2. Improvements in the corrosion resistance of galvanized steel continue with the development of alloyed coatings of zinc-aluminum, zinc-magnesium, and zinc-aluminum-magnesium, variants of which are commercially available at large volumes, suitable for the mass production of automobiles. The quest for further enhancements in corrosion

TABLE 2 Coatings Used in the Automotive Industry

Precoated Steels	
Hot Dip	Zinc, zinc-iron, aluminum, aluminum (55%)-zinc, zinc-aluminum (5%), zinc-aluminum-magnesium, terne (lead-tin), nickel terne (nickel/lead-tin)
Electroplated	Zinc, zinc-iron, zinc-nickel, tin plate, tin free (chrome)
Organic/Precoat	Zinc-rich organic primer, magnesium-rich organic primer
Post-Applied (Protective and Decorative)	
Metallic	Cadmium, zinc, lead, copper, copper/nickel/chromium, nickel/chromium, chromium (micro-discontinuous), chrome flash, hard chromium, nickel-iron
Chemical Conversion Coatings	
Inorganic	Zinc phosphate, manganese phosphate, iron phosphate, zirconium oxide, silanes, black oxide, anodic oxide (aluminum), oxide/chromate, magnesium oxide, zirconium oxide, organophosphate
Organic Primers and Topcoats	
Organic Base	Epoxies, epoxy esters, polyesters, alkyds, vinyls, acrylics, oils, urethanes, cellulosics
Pigments	Molybdates, lead, zinc, coloring
Other Organics	
Sealers	Asphaltic, rubber, vinyl, hot melts

resistance for the next generation of galvanized steel was highlighted in a 2016 study by Prosek et al.,[13] which reported corrosion benefits through the addition of a fourth alloying element to Zn-Al-Mg coatings on steel.

Some coatings are applied on individual components or raw materials before assembly. For example, metallic precoatings for steels and organophosphate treatments for aluminum alloys are applied to coils of sheet materials at the rolling mills, or are batch applied to components or preformed parts before delivery to the original equipment manufacturer or bodyshop. Chemical conversion coatings develop a controlled surface suitable for subsequent painting, and the conversion coating along with the organic primer form the basis of the corrosion protection of the substrate by the paint system.[14] These processes may be applied both at the component level, before vehicle assembly, and to the assembled vehicle body, as described in the following section.

The selection of a specific material and the appropriate coatings from the wide range available is made through consideration of the mechanical, processing, cost, weight, and service environment of the target component within the overall vehicle system. In all cases, consideration also must be given to the corrosion prevention strategies required. Corrosion management of the vehicle system is particularly important when the vehicle design includes combinations of dissimilar materials.

Processing

Automotive manufacturing processes evolve continuously, and significant changes and new processes have been introduced to vehicle factories in recent years. Quality and efficiency are two of

the prime drivers of innovation in automotive manufacturing. In addition, the increasing use of mixed materials in contemporary vehicles has required the development of new joining methods and approaches, with, for example, an increased use of adhesives, rivets and novel welding techniques, at high rates, in body construction. Environmental legislation has stimulated innovation in automotive processing, particularly in the paintshop processes that traditionally consumed significant amounts of water and electricity and previously may have involved the use of restricted or controlled materials. The paintshop processes that contribute to the final vehicle corrosion resistance include the pre-treatment system, electrocoat primer (E-coat) application, sealing, painting, and wax augmentation coating of the body structure.

The vehicle manufacturer's pretreatment system of the assembled body includes three main steps: (1) a cleaning stage to remove oils and contamination from the assembled body, (2) deposition of a pretreatment layer through a chemical conversion process, and (3) rinsing the vehicle body of the pretreatment chemicals.[14,15] The pretreatment imparts a relatively inert, chemically resistant finish to the metal substrates and delivers a consistent surface, enhancing the adhesion of the E-coat and providing the foundation for visually appealing paint finish. Strong adhesion of the E-coat is required to establish and maintain an effective barrier to corrosion upon exposure of the vehicle to the corrosive environment.

Pretreatment and paint suppliers, in partnership with vehicle manufacturers, continuously enhance established processes and materials to deliver improvements in quality, efficiency, effectiveness, and robustness, leading to many variants of these processes and chemical systems across the industry. In addition, an entirely new conversion coating system, based on zirconium oxide chemistry, has been introduced to the automotive industry in recent years, such that vehicle manufacturers currently have more options in their selection of a pretreatment type and variant.[14,16,17] The zirconium-based pretreatments are thin films, about 100 times thinner than the traditional zinc phosphate systems, and they are more compatible with aluminum-intensive than ferrous-dominant body structures. The zirconium thin film pretreatment process offers advantages in water consumption, energy costs, and waste generation compared with the zinc phosphate process.

Design

Design improvements have played a major role in the development of corrosion-resistant vehicles. Areas of entrapment, where salt, poultice, or liquids may accumulate and generate a corrosive environment, have been eliminated to enhance corrosion resistance in vehicles. For example, wheel wells are designed to have a sloping configuration so that corrosives can be washed or will drain out. Drain holes have been incorporated in the lowest points of cavities that might become wet and sealers and baffles are used to exclude contaminants and moisture from cavities that are designed to be dry in vehicle service. Adhesives and sealers between and outside joints effectively eliminate crevices and joints, thereby preventing corrosion within flanges. Isolation or separation strategies have been implemented to reduce galvanic corrosion at mixed-material interfaces.

Automotive Environment

The automotive environment can be categorized as (1) external exposure, (2) internal combustion exposure, and (3) internal functional liquids. Of these, the most complicated and the most highly investigated environment is external exposure.

EXTERNAL EXPOSURE

The severity of external automotive corrosion varies considerably around the world, because of differences in the chemistry of the environment. The most severe corrosion environments are in the snowbelt areas where deicing salts are used, and along coastal areas where warm, humid, salty atmospheres exist. To design automobiles for corrosion resistance, it is necessary to understand the nature of the environment and how materials react in that environment. Rain and snow are important to provide moisture to the environment. Atmospheric moisture and the conditions that produce fog and dew are also important. Extensive studies and historic data, however, have shown that moisture alone does not cause serious corrosion problems on automobiles. Aggressive corrosive constituents include chlorides and pollutants. Marine environments are corrosive because of dissolved chlorides. A typical seawater composition has a sodium chloride (NaCl) content of about 3.5 wt%, although this content will vary depending on location, such as that near tidal rivers or oceans. Splash and spray, which cause the atmospheric redistribution of seawater, are extremely important in marine environments. Larger seawater droplets fall out rapidly closer to the source. Smaller droplets distribute over a wide area while evaporating to an equilibrium size and deposit according to local weather conditions. Slamova et al.[18] mapped the global corrosivity of coastal regions using models for airborne salinity, relative humidity (RH) levels, and atmospheric sulfur dioxide (SO_2) levels and a Geographical Information System (see fig. 1). Florida was identified as having the most severe coastal corrosion in the United States.

Salts applied to roadways for winter weather treatments are the other major source of corrosive chlorides encountered by vehicles in service. The use of NaCl as a deicing agent for U.S. roadways was first trialed in New Hampshire in 1938,[19] with an application of approximately 5,000 tons of rock salt. A concept termed "bare pavement," under which motorists could expect snow- and ice-free pavements shortly after storms, became a policy in most cities and suburbs starting from the 1950s, resulting in a marked increase in salt use, from around 1 million tons in 1955 to approximately 8 million tons by 1975.[20–22] The application of salt remains the primary mechanism for clearing ice- and snow-covered roads today, and the amount of salt applied each winter has continued to increase, with on average 2.5-times more salt used on roads annually in the 2010–2019 decade compared with 1980–1989,[19,21,23] as illustrated in figure 2.

Year-to-year changes in the amount of salt applied are due to variations in the severity and number of winter weather events.[26]

FIG. 1 Distribution of atmospheric corrosivity on the global map. *Source*: Reproduced from Slamova et al.[18] with permission.

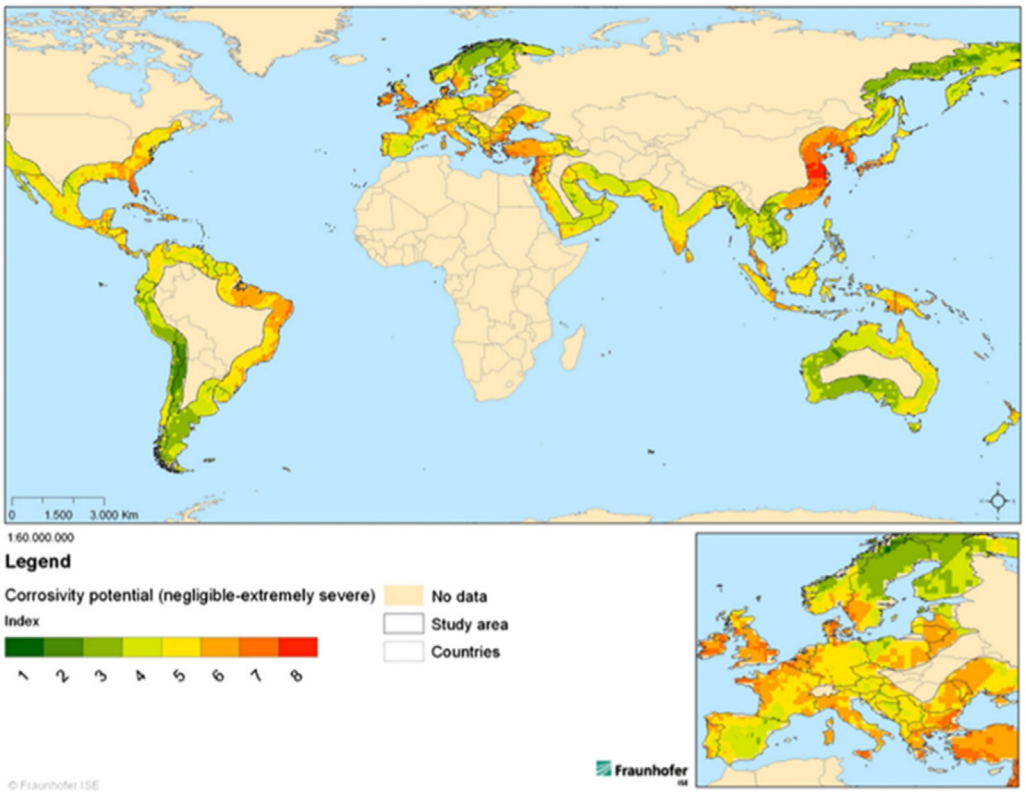
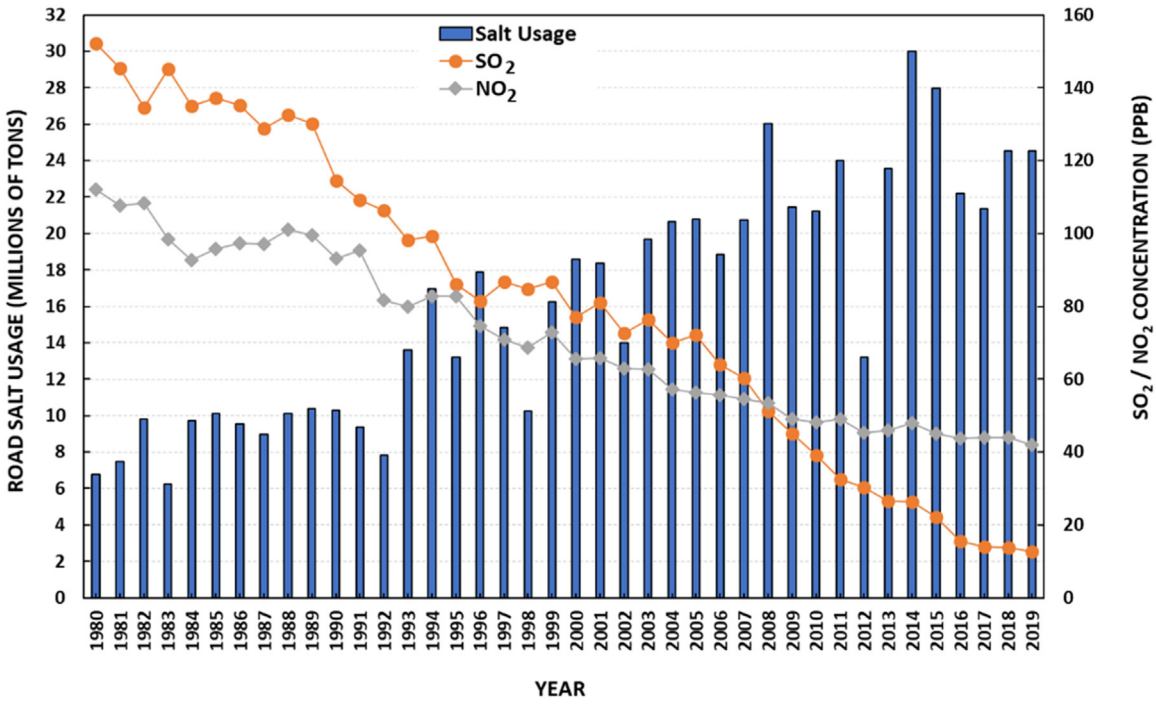


FIG. 2 Road salt usage[21,23] and average annual emissions[24,25] in the United States, 1980–2019.



For example, the 2011–2012 winter was relatively mild nationwide, leading to a decrease in the use of road salt in 2012,[27] whereas much colder temperatures and a greater number of frozen precipitation and winter weather events in the 2013–2014 winter, even in some southern U.S. states, led to a peak in road salt usage of 30 million tons in calendar year 2014.[28]

The number of types, as well as the total amount, of road salts has increased significantly.[20] Different agents may be required depending on the road condition: the use of NaCl is not effective if the pavement temperature is below -10°C. In such cases, a more expensive chloride or acetate treatment is required to prevent or remove ice formation on the road. Some general properties of the deicing agents summarized by the Western Transportation Institute[29] and with cost data taken from Kelting and Laxson[30] are shown in table 3.

The various treatment agents may be applied to roadways in dry or wet form, as indicated in figure 3. Salt brines may be used as anti-icing agents when sprayed to the roadways before a winter storm, or used as a deicing agent when they are sprayed onto deicing salts as a prewetting process. Equally, dry agents can be applied to the roads before or after a winter storm. Many brines are a blend of different chlorides and the quantities shown in figure 3*B* are based on the primary agent in the brine—that is, NaCl brine also may contain some amount of magnesium or calcium chloride and vice versa. Composition of the enhanced brines shown in figure 3*B* was not given in the Clear Roads report,[20] but it is likely a blend of salts—for example, the data sheet for one particular enhanced brine deicer reported 13% NaCl, 8% calcium chloride, and 2% magnesium chloride content.[30]

A 2007 study by Prosek et al.[33] found that the type of chloride used affected the corrosion rates for steel and zinc substrates. The effect of the cations (Na^+, Mg^{2+} or Ca^{2+}) was stronger for the zinc substrate under the test conditions used and the corrosivity effects of the chlorides on zinc increased in the order of $MgCl_2 < CaCl_2 < NaCl$. This finding was later corroborated by a study at the Swedish Corrosion Institute,[34] which reported a similar effect of chloride cations on zinc corrosion rates in both a laboratory cyclic corrosion test and an outdoor exposure with weekly spray by pollutants. The order of corrosivity was different for steel substrates compared to zinc substrates in both studies, with $NaCl < CaCl_2 < MgCl_2$. The reversal of the trend of chloride corrosivity between zinc and steel was attributed to the hydrolyzation of the bivalent cations Mg^{2+} and Ca^{2+}, leading to an overall reduction in pH in the surface electrolyte, which tends to promote steel corrosion but inhibit zinc corrosion under atmospheric conditions. These findings highlight the importance of the interactions of the chloride cations with the electrolyte and, subsequently, with the substrate material.

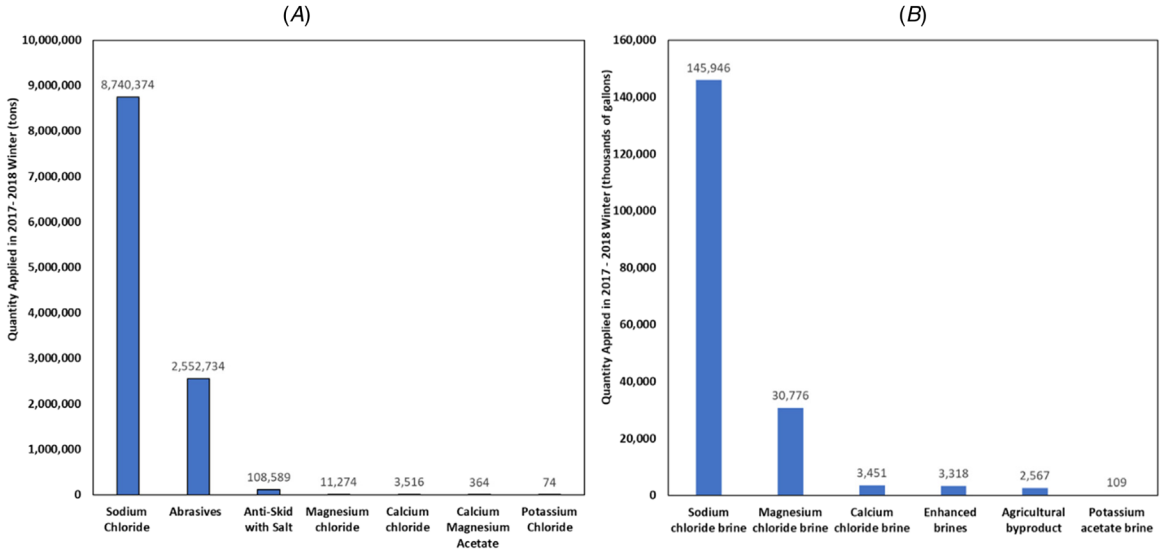
The various chlorides also have different characteristics in terms of their capacity to absorb water vapor at different atmospheric conditions (e.g., RH and temperature). Magnesium and calcium chloride absorb water and form a liquid over a much broader range of RH conditions (RH > 30%) than NaCl

TABLE 3 Summary of Road Treatment Agent Properties

Agent Type	Formula	Lower Functional Temperature	Cost per Ton[a]
Sodium chloride	NaCl	−9°C (15°F)	$42
Magnesium chloride	$MgCl_2$	−21°C (-5°F)	$111
Calcium chloride	$CaCl_2$	−26°C (-15°F)	$140
Potassium acetate	KAc	−32°C (-26°F)	$1,166
Calcium magnesium acetate	CMA	−18°C (0°F)	$1,492

[a]Costs reported in 2010, relevant for comparison purposes only.
Source: Adapted from Western Transportation Institute,[29] and with cost information from Kelting and Laxson.[30]

FIG. 3 Types and amounts of (*A*) dry, and (*B*) liquid, treatment agents used on U.S. roadways over the 2018–2019 winter season. *Source*: Data taken from Clear Roads and New Jersey Department of Transportation.[20,32]



(RH > 75%), leading to greater opportunity for electrolyte film formation and corrosion reactions to occur under different atmospheric exposures.[33–35] In the experiments performed by Prosek et al.,[33] water absorption was not found to be higher for zinc samples dosed with $MgCl_2$ and $CaCl_2$ compared with NaCl, and the authors concluded that an important interaction of the cations with the substrates controlled the corrosion dynamics.

The influence of sugars, as found in agricultural byproducts, mixed with salts was also investigated by Jönsson.[34] The influence of the sugar additives in laboratory cyclic corrosion test was not observed, but reduced corrosion rates (50% and 25%, respectively) were observed for steel and zinc with sugar-salt blends exposed in the outdoor corrosion test. The benefit of the sugar additive on the corrosion performance was attributed to the ability of the sugar to block the metal surface from the corrosive environment. This blocking was not effective in the laboratory cyclic corrosion test because the sugar-dosing of the surface occurred only once at the start of the test and was not replenished during the exposure. The importance of the exposure conditions, and indeed the duration of the exposure for the slow kinetics that can be associated with corrosion processes and corrosion product formation and transformation, is highlighted by these observations.

A 2006 study by Blücher, Svensson, and Johansson[35] investigated the effects of aluminum, magnesium, and sodium chlorides on high-purity aluminum under controlled atmospheres with and without carbon dioxide. In the carbon dioxide–free (<1 ppm) atmosphere, the corrosivity of the chloride salts increased in the order $MgCl_2.6H_2O < AlCl_3.6H_2O <$ NaCl. When the experiment was repeated with approximately ambient levels of carbon dioxide (350 ppm), strong inhibition of corrosion by NaCl was observed, and similar aluminum corrosion rates were found for all three chloride types. The authors concluded that the availability of carbon dioxide to form carbonates on the corroding aluminum surface tended to inhibit corrosion activity at high pH sites and attenuate overall corrosion rates. This important effect of carbon dioxide also has been reported for zinc and magnesium, and laboratory tests that do not account for these atmospheric influences may lead to false predictions of corrosion rates in the field. At the same time, the lack of access to atmospheric carbon dioxide, oxygen, and drying cycles can occur on a vehicle in service—for example, underpaint corrosion of a galvanized steel or aluminum body panel or crevice corrosion within a weld flange or under an adhesive bead. The general studies published in the literature highlight a need for further specific research on the effects of different road treatment agents, including acetates, on automotive vehicle construction materials, joint configurations, and painted substrates.

Atmospheric pollutants, including sulfur dioxide, nitrogen oxides, hydrogen sulfide, ammonia, ozone (SO_2, NO_x, H_2S, NH_3, O_3 respectively), and particulate matter, are known to influence the corrosion of metals. Leygraf and Graedel[36] reported that steel and zinc have high sensitivity, and aluminum has moderate sensitivity, to corrosion because of the presence of SO_2 and SO_4. Fossil fuel consumption is a major source of atmospheric SO_2[36] and the levels of SO_2 pollution in a given region tend to reflect both the level of industrialization and the impact of air-pollution controls. The data in figure 2 show the marked decrease in the average SO_2 concentration measured at 37 sites across the United States, as reported by the Environmental Protection Agency.[25] The presence of SO_2 in the atmosphere and its effect on corrosion has been studied extensively. The complex reaction involves the SO_2 molecule striking a metal surface and converting to sulfuric acid as a result of oxidation and hydrolysis. This introduces reactive ions, increased conductivity, and a lower pH. The presence of hygroscopic sulfate corrosion products also lowers the critical humidity for corrosion reaction.

Nitrous oxides, NO and NO_2 (collectively known as NO_x), are produced by fossil fuel consumption and their concentration in the atmosphere reflects the level of industrialization, as well as the density of gasoline and diesel-fueled vehicles, in a given region. NO from tailpipe emissions is rapidly converted to NO_2 in the air[37] and measurements of NO_2 in the atmosphere are chiefly influenced by vehicle emissions. Significant progress has been made in reducing the levels of NO_x emissions from vehicles, with a 25-factor reduction in median NO_x emissions measured for newer (around 2 years in service) versus older (up to 28 years in service) gasoline-fueled vehicles in a 2014 study by May et al.[38] Reduction of NO_x emissions from diesel-fueled vehicles is more challenging,[39,40] although a 50% reduction measured by May et al. for newer versus older heavy-duty diesel vehicles[38] indicated some progress toward that aim. Technical challenges, possibly compounded by older vehicle fleets, heavy congestion, and greater numbers of vehicles on the roads, have resulted in a more modest reduction in NO_2 pollution compared with SO_2 over the past few decades (see fig. 2). This has led to an increase in the relative NO_2/SO_2 molar ratio over time.[41] Laboratory tests have shown a synergistic effect of the corrosiveness of SO_2 to steel,[41] zinc,[42,43] and nickel,[44] but not aluminum,[45] in the presence of NO_2 and high RH. The marked influence of NO_2 on SO_2 corrosivity to those metals measured in controlled laboratory exposures has not been observed in outdoor exposures,[36,44,46] presumably because of the more complicated and varying chemistry, temperature, and RH of the outdoor environment.

The combined effect of chloride (a film disruptor on metals) and acids formed from atmospheric pollutants (which provide reducible hydrogen ions) can be much worse than the added separate effects. Thus, geographic areas that are subjected to both road or marine salts and acid deposition are likely to be the most corrosive to automobiles. The external environment in which vehicles operate has become increasingly complex and varies considerably from region to region. The general corrosivity categories of rural, industrial, and marine considered in atmospheric corrosion studies and defined by ISO standard 9223[47] may not consider the very high seasonal chloride contamination of vehicles driving on salt-treated roads. Therefore, the automotive engineer must pay attention to this significant and automotive-specific corrosive environment. Another important factor in the external environment that is specific to vehicles is the highly localized and corrosive environment produced by the accumulation of dirt, vegetation, and other debris in metallic entrapment areas.[48] These areas remain wet almost continuously because of

the presence of this poultice and produce a stationary electrolyte environment. The result is a concentrating effect of the corrosive species, similar to the phenomena observed in crevices. When metals are exposed to this poultice environment, the corrosion process may become autocatalytic, leading to rapid deterioration.

INTERNAL COMBUSTION EXPOSURE

Internal combustion produces water vapor and exhaust gases, which can condense in internal areas such as the exhaust system of automobiles.[49–51] This condensate chemistry includes sulfate, sulfite, nitrate, ammonium, carbonate, bicarbonate, and chloride ions. The acidity of the condensate is high because of the presence of nitric, hydrochloric, sulfuric, and sulfurous acids. Nitric acid is formed from atmospheric nitrogen, which is converted to oxides in the engine and then to the acid. Sulfuric and sulfurous acids are formed because fuels and lubricating oils contain sulfur, which converts to SO_2 and then reacts with water vapor to form these acids. In addition, catalytic converters are designed to convert SO_2 to SO_3 yielding acids. Chloride additives to fuels yield hydrochloric acid.

The temperature of the system has a great impact on the environment within the exhaust system. If the system does not become hot enough (above the dew point), the condensate remains and concentrates. Thus, vehicles that are driven for short distances are more susceptible to corrosion by exhaust gas condensates, sometimes referred to as cold-condensate corrosion.[49] The inclusion of drain holes at strategic locations in the exhaust system helps to avoid the accumulation of these corrodents.[51] Deterioration is also accelerated by stress (both cyclic and static) and by design configurations (such as at joints and welds).

Direct exhaust-gas impingement (erosion corrosion) can occur because of the high-velocity exhaust gas stream on the internal surfaces of the exhaust system. This effect is important at sharp bends and surfaces normal to the gas flow. The combination of particulate matter with hot corrosive gas produces this type of attack.

High-temperature oxidation of exhaust system components is governed mainly by the temperature encountered, as well as the exhaust gas composition. Temperatures measured near the exhaust-manifold typically range up to 800°C and the skin temperature of metal components in this area can reach 600°C.

INTERNAL FUNCTIONAL LIQUIDS

The vehicle includes many internal functional liquids, such as engine coolants, engine oil, transmission fluid, hydraulic brake line fluid, and fuels. The function of engine coolants is to transfer heat from the engine to the radiator where it is dissipated and used to provide heat to the passenger compartment. Properties must include high specific heat, good thermal conductivity, low freezing point, high boiling point, chemical stability, and noncorrosivity. The coolant system includes many different metals, as noted in table 1. Glycols remain the principal component of modern coolants,[52,53] and ethylene glycol diluted to a 50 vol% solution with water provides boiling point protection to 130°C and freezing point protection to -37°C.[54] Additives to the dilute glycol are required to impart corrosion inhibition, pH buffering or neutralizer, foam suppression, and identification color to the coolant. The selection of the coolant package depends on the materials and operating conditions of the cooling system. Coolant systems up to around 1995 typically were of dilute ethylene glycol with corrosion inhibitors based on inorganic compounds, such as silicates, phosphates, and nitrites.[55] These inhibitors operate effectively for vehicles with cast iron engine blocks and heads, and copper or brass in the heat exchangers. Their mode of corrosion protection, however, depletes the inhibitor content at a rate that requires their replenishment, or replacement of the coolant, within 2–3 years of operation.[55] A testing and replenishment strategy may be feasible within heavy truck fleets but a better solution for light-duty vehicles emerged in 1995, when General Motors introduced a long-life coolant, which used organic acid technology (OAT) or hybrid organic acid technology (HOAT) corrosion inhibition systems.[55] instead of inorganic inhibitors. OAT- or HOAT-inhibitor coolants have a 5-year or 150,000-mile projected service life, because of their slower inhibitor-depletion rate compared to inorganic inhibitors. Coolants for vehicles with aluminum blocks and heads also may be configured with lower pH control than coolants for vehicles with cast iron blocks and heads to enhance the corrosion protection of the former. Further developments in coolant technology have targeted longer service life, or greater tolerance to nonideal operating conditions, such as coolant makeup with chloride-containing water or excessive temperatures or pressures within the cooling system.

The functions of engine oil are manifold, including the dissipation of heat, reduction of friction and wear, detergency, sealing of critical areas, and separation of water.[56] The composition of the oil is about 75–90% base stock (such as mineral oil) and 10–25% chemical additives, such as viscosity index (VI) improvers, antioxidants, corrosion inhibitors, detergents, dispersants, and antifoam agents. The performance of engine oil depends on the blend of these chemically active and chemically inert additives. The aging of engine oil, as determined by the type of driving and exposure to contaminants,[57] can result in an aggressive liquid. Examples include oxidized oil resulting from exposure to heat and oxygen, loss of buffer when it is used up in neutralizing acids, and contamination by coolant, gasoline, and engine exhaust gases. Prolonged use of aged engine oil can lead to general corrosion, pitting, fretting, and erosion corrosion.

Automatic transmission fluid (ATF) performs many functions, including cooling and lubrication, and it also must maintain the friction-speed characteristics that prevent shudder.[58] ATF consists of a base mineral (paraffinic, naphthenic, and aromatic hydrocarbons) or synthetic base oils and an additive package. The additives prevent fluid oxidation, corrosion, loss of lubricity, and foaming. Even though antioxidants, inhibitors, and stabilizers are added to the ATF, the base oil can react with oxygen to form organic acids. The acidity is quantitatively measured as the total acid number (TAN). In addition, some additives, such as organothiophosphates, are reactive to some metals.

Hydraulic brake line fluids are usually glycols, and commercial brake fluids are hygroscopic and absorb moisture when

exposed to humid atmosphere. Water contamination also can occur from atmospheric condensation. The result of this water contamination is a liquid with various degrees of corrosivity toward brake cylinders, the master cylinder, hydraulic brake line tubing, and other brake system components.[59]

Corrosion Mechanisms

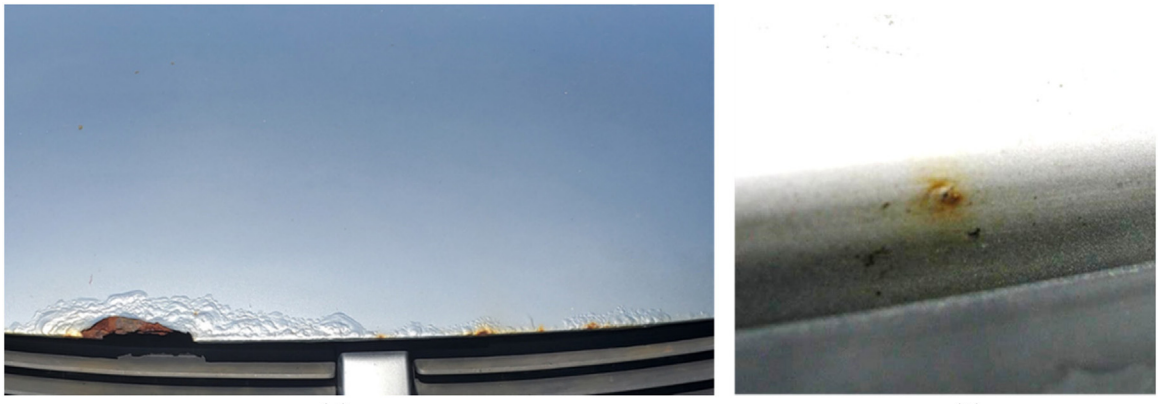
The occurrences and modes of corrosion on automobiles depend on such factors as physical and chemical properties of the environment, vehicle construction materials, and the specific application. A summary of corrosion mechanisms according to different applications is given in table 4. Although they have many modes in common, different forms of corrosion may occur for ferrous versus nonferrous metals, particularly for painted body panels, as noted in table 4.

Corrosion degradation generally is classified into structural (inside-out) and cosmetic (outside-in) corrosion. Structural corrosion in the auto-body may lead to perforation of the panel, generally from the inside out, as shown in figure 4. Cosmetic corrosion eventually may lead to perforation, from outside to inside, if repair or remedial actions are not implemented. Structural corrosion is most likely to occur at crevices, such as weld flanges, hem flanges, and other entrapment areas where poultice can build up and moisture can accumulate. The most visible part of the automobile is the exterior body panel structure and cosmetic corrosion usually is associated with these high-visibility, painted, outer-body panels. The quality and nature of the paint–metal interface is important to avoid premature cosmetic corrosion. Paint coating failure can initiate at thin, missing, or damaged paint associated with the cut edges of panels, fretting effects, abrasion from sand, or chips from gravel impingement. Propagation of corrosion under the paint can be stimulated by a wide range of mechanisms, including

TABLE 4 Corrosion Mechanisms in Automobile Applications

System/Component	Ferrous	Nonferrous
Body Panels, Structural	Uniform, pitting, crevice, fretting, poultice, coating failure, stress cracking, galvanic	Pitting, intergranular, galvanic, exfoliation, crevice, stress cracking, galvanic
Body Panels, Cosmetic	Paint blistering, paint delamination, perforation, galvanic, fretting	Filiform, paint blistering, paint delamination, perforation, galvanic, fretting
Chassis	Uniform, pitting, crevice, fretting, stress cracking, coating failure, poultice, galvanic	Pitting, intergranular, crevice, fretting, stress cracking, coating failure, poultice, galvanic
Trim and Hardware	Uniform, pitting, intergranular, crevice, galvanic, dealloying, fretting, stress cracking, coating failure, poultice	
Engine and Components	Uniform, pitting, crevice, galvanic, dealloying, fretting, intergranular, stress cracking, high temperature oxidation	
Transmission	Uniform, crevice, galvanic, fretting	
Fasteners	Uniform, pitting, crevice, galvanic, fretting, stress cracking, coating failure	
Cooling System	Uniform, pitting, crevice, galvanic, dealloying, erosion, cavitation, intergranular	
Fuel System	Pitting, crevice, coating failure	
Brake System	Pitting, crevice, galvanic, fretting, coating failure	
Electrical and Electronics	Fretting, uniform, pitting, crevice, galvanic, dealloying, stress cracking, coating failure, corrosion product creep	
Exhaust System	Uniform, pitting, crevice, dealloying, erosion, fretting, intergranular, stress cracking, coating failure, high-temperature oxidation	

FIG. 4 Ferrous corrosion examples, with (*A*) structural corrosion (inside-out perforation) at the leading edge of the steel hood and (*B*) cosmetic corrosion (outside-in) on a roof panel where the paint was damaged by stone impingement.



(*A*) (*B*)

differential cells, cathodic disbondment, anodic undermining, filiform corrosion, galvanic (bimetallic) effects, and fretting. Examples of these corrosion modes are shown in figures 4–6.

Galvanic corrosion can occur if two dissimilar materials are joined and exposed to the corrosive environment; the more anodic of the two materials will corrode at a high rate, which may lead to perforation within the lifetime of the vehicle. Galvanic corrosion is avoided by careful management of dissimilar material interfaces, including the use of isolation or separation components and robust barrier coatings and moisture exclusion strategies. CFRP and stainless steel are two of the most noble materials used in automotive construction, and any materials joined to these materials are prone to galvanic corrosion attack.[12] Aluminum is frequently joined to galvanized steel in vehicle structures with optimized strength-to-weight designs, and aluminum alloys may suffer increased pitting attack when a galvanic cell is established between steel (e.g., at a cut edge or where the zinc coating has previously corroded) and the aluminum.[60] Pitting corrosion of an aluminum heat shield because of the installation of a steel fastener and the exposure of both to the road environment, can lead to the perforation of the thin sheet component, as shown in figure 6.

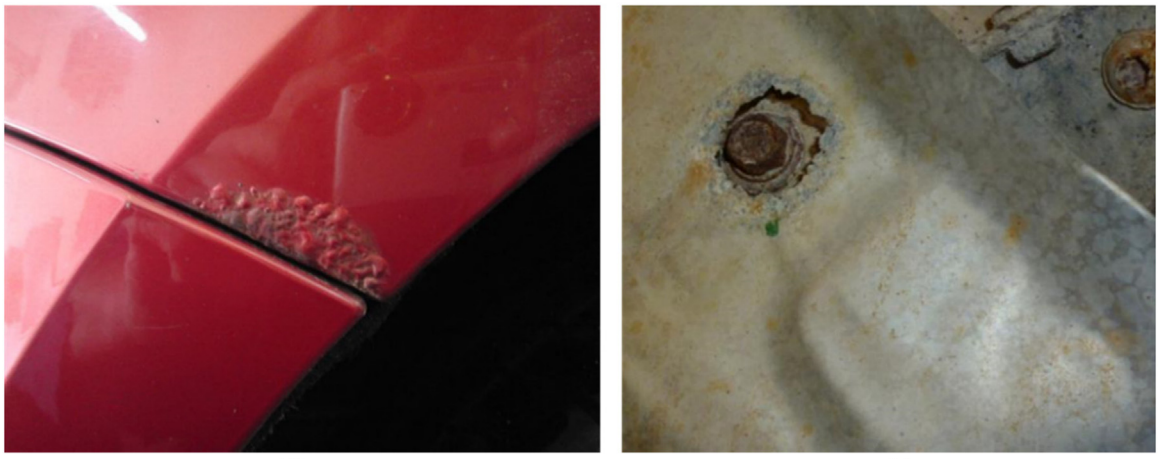
The chassis and vehicle underbody are susceptible to mechanical damage of coatings due to dirt, sand, and stone impingements and seasonal dousing in salty water because of their proximity to external road conditions. Coatings failure can enhance deterioration, as can poultice that is built up in entrapment areas. The vehicle underbody may be considered to be "low visibility" and therefore not subject to stringent requirements for cosmetic corrosion resistance, depending on the customer usage profile in a given market; however, the safety-critical chassis and structural components in the underbody must have adequate corrosion resistance to avoid functional degradation for the entire life of the vehicle, typically considered to be at least 15 years.

FIG. 5 Cosmetic corrosion on painted aluminum panels: (*A*) paint blistering and delamination and (*B*) paint blistering and filiform corrosion.



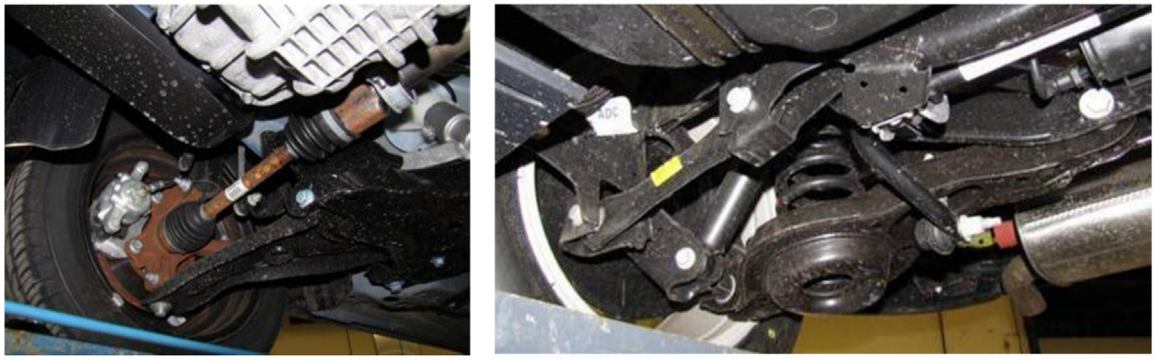
(*A*) (*B*)

FIG. 6 Corrosion associated with (*A*) fretting action between rear bumper panel and bodyside panel and (*B*) galvanic corrosion of aluminum heat shield with ferrous fastener.



(*A*) (*B*)

FIG. 7 Assessments of underbody corrosion resistance showing: (*A*) superficial rust of uncoated chassis components, and (*B*) coated components showing no corrosion attack. *Source*: Photos courtesy of Ford Motor Company.



(*A*) (*B*)

Trim and hardware are used for several reasons, including styling, hiding of joints and welds, and protection from mechanical damage. Underbody shields may offer dual-functionality with both aerodynamic and corrosion resistance benefits through air flow control and protection of the underlying vehicle structures from stones, sand, and water splashed up by the tires. Trim materials, such as stainless steel and anodized aluminum, are susceptible to pitting, crevice corrosion, and discoloration. Stainless steel and chromed trim materials can cause galvanic corrosion of painted auto-body steel and aluminum panels. Conversely, some trim materials such as aluminum and zinc die cast are anodic to auto-body steel and corrode sacrificially.

The exhaust system and engine are exposed to a dual (external and exhaust gas) environment. Therefore, the materials must be chosen to perform in more complex service conditions. High temperatures are important along with the chemistry of the exhaust gas condensate. Corrosion mechanisms include those normal in the external environment with the additional temperature factor.[49,61]

Electrical and electronic systems are extremely susceptible to corrosion caused by the aggressive automobile environment. This susceptibility has only increased with the development of much smaller electronic units in recent times.[62] Fretting, pitting, crevice, and galvanic corrosion, and corrosion product creep are all important mechanisms. In many cases, these mechanisms are accelerated by leakage currents, which impose a potential bias on the materials.

Controlling Automotive Corrosion

This section discusses strategies to avoid, manage, and control automotive corrosion for vehicle systems exposed to the exterior and internal combustion environments. It also presents considerations for liquid passages and reservoirs, and electrical and electronic systems.

EXTERIOR EXPOSURE

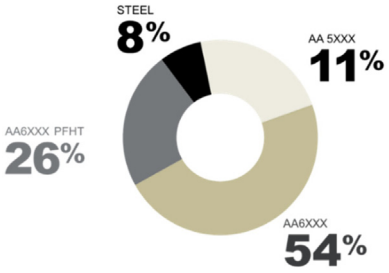
The severe corrosivity of the automobile environment resulting from road salts, atmospheric salts, and acid deposition has made it necessary for the industry to improve corrosion protection through (1) proper design, (2) choice of corrosion-resistant materials, (3) use of coatings and sealants, and (4) proper consumer maintenance.[63–66]

Proper design has been recognized as an important aspect of automobile corrosion resistance.[65,66] Thus, elimination of entrapment areas where moisture and poultice can collect, minimization of crevice configurations, elimination of unnecessary holes in body panels, provision of drainage holes, access for complete pretreatment and primer coverage, and elimination of dissimilar metal crevices are common practices in the design of automobiles.

The development of automotive construction materials with enhanced corrosion resistance (compared with bare steel) is one of the most important factors in the development of corrosion-resistant automobiles. The use of precoated steel is typical for all automobile body and chassis parts exposed to the external environment. A wide range of materials is used as coatings, including hot dip and electrodeposited zinc, zinc-iron, zinc-aluminum, zinc-aluminum-magnesium, zinc-nickel, and zinc-nickel/organic composite-coated steel. Other materials include aluminum- and aluminum-zinc-coated steels, stainless steels for exhaust systems, terne- (tin-lead) coated steel for fuel tanks, and tin-coated steel.[67]

New alloys have been introduced for specific automobile applications, including type 434 stainless steel for exterior trim, type 409 and 430 stainless steels for exhaust systems, and aluminum alloys from the 5XXX, 6XXX with and without post-form heat treatment (PFHT), and 7XXX series for auto-body and structural parts. The use of aluminum for body panels such as hoods and decklids has prompted the development of new processing and corrosion protection techniques for this material. Today, many vehicle bodies are almost completely constructed from aluminum alloys, pioneered by the Audi A8 and implemented on the Tesla Model S, Jaguar XJ and Honda NSZ, among others. The highest-volume enterprise in the use of aluminum-intensive body structures is the Ford F150 truck body (see the material details in fig. 8).[68] Many other advanced body structures utilize a mixed-material strategy, with targeted applications of aluminum alloys in sheet, extrusion, and cast form, along with

FIG. 8 Materials used in the Ford F150 truck body.[68]



advanced and ultra-high-strength steels, exemplified in the Cadillac CT6 and Chevrolet Malibu.[69]

A wide range of inorganic and organic coatings and sealants is used to provide supplemental corrosion protection to automobiles.[64,70] Conversion coatings formed by the interaction of the metal surface with constituents in solution to form an inert inorganic film may be used for components supplied to the automotive manufacturer. Examples of pretreatments used in the automotive industry are phosphate, zirconium, chromate, and various anodized and oxide coatings. Organic coatings also are used extensively, and they function as a barrier between the metal surface and the environment. These include primers, waxes, seam sealers, shields to mechanical damage, and petroleum-based rust preventives.

The automobile paint system involves several different process steps and coating layers.[64,70] The first stage of the paintshop line includes cleaning and a conversion coating, such as phosphate or zirconium, to improve corrosion protection and ensure good adhesion of the paint to the assembled body. Then, an epoxy primer is applied by cathodic electrocoating, whereby the assembled body is negatively charged and is immersed in an aqueous bath where it is coated with a positively charged organic primer under the influence of an electric field. The advantages of this process, known as E-coating, include uniform coverage, edge protection, penetration into enclosed areas, and full automation. The next step is a primer surfacer, which offers protection against stone-chipping, provides adhesion to the topcoat and prevents ultraviolet (UV) light from reaching the UV-sensitive E-coat layer.[64] Finally, the topcoat is applied, usually in two or more steps, including a base coat and a clear coat. These are generally enamels and urethanes. The performance of these complex painted auto-body materials in the aggressive automobile environment is understandably dependent on a number of factors. Photographs of the paint stages are shown in figure 9 and typical thicknesses and functions of the paint layers are noted in figure 10.

Sealers play an important role in automobile corrosion protection by preventing water and contaminants from entering crevices and joints. Examples of the different types of additional coatings and sealers that may be applied to vehicles and their functions are shown in figure 11. These protective materials may be applied to the E-coated body (and under topcoat) and to the underbody. The choice depends on the specific application, such as at door hem flanges, brackets, fasteners, and body joints. Structural adhesives also are used to bond assemblies, such as doors, decklids, and hoods, thereby sealing crevices and eliminating welds.

Consumer maintenance is an important part of automobile corrosion protection. Automobile manufacturers have provided

FIG. 9 Photographs of a car body in different stages of the paintshop: (*A*) E-coat, (*B*) primer, (*C*) basecoat, and (*D*) clearcoat applications. *Source*: Photos courtesy of Ford Motor Company.



FIG. 10 Automotive paint layers, including typical thicknesses and functions. *Source*: Reproduced from Akafuah et al.,[70] with permission.

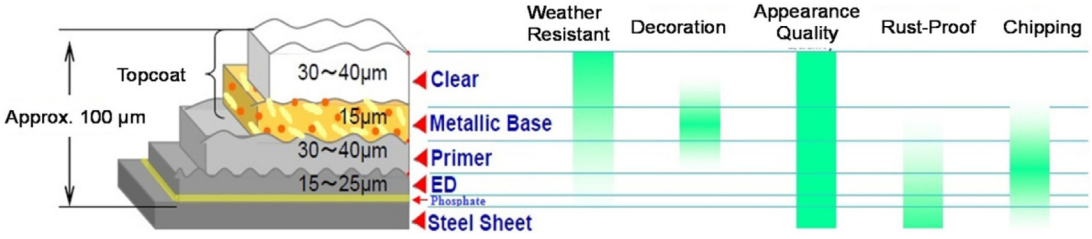
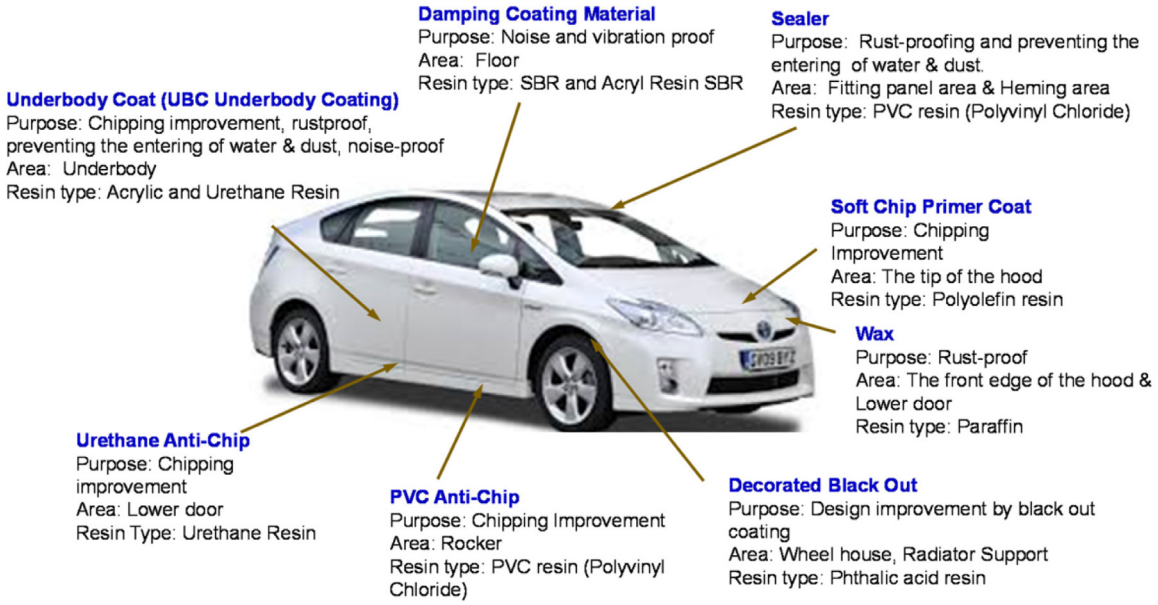


FIG. 11 Coatings and sealers that may be applied to the vehicle body, and their functions. *Source*: Figure reproduced from Akafuah et al.,[70] with permission.



recommendations for maintenance to prevent deterioration from corrosion. The first defense is regular washing to remove road salts and other corrosive agents, and poultice. The procedure should ensure that mud and dirt is removed from entrapment areas underneath the vehicle. Drain holes should be cleaned out. The second defense includes repair of paint damage to avoid propagation of corrosion in these areas. Precautions should be taken to exclude corrosive agents from the interior, such as driving in or splashing seawater or road deicing salt puddles on the vehicle, although many customers may choose to use their vehicles in such off-road scenarios. The corrosion engineer should consider the customer usage profile for any new vehicle design.

INTERNAL COMBUSTION

The service life of exhaust systems has been greatly extended through the use of more corrosion-resistant materials, most notable ferritic 400-series stainless alloys.[51] The use of catalytic converters presents some special problems because of the catalyzed oxidation reactions that take place in the exhaust gas stream. The converter itself must be highly corrosion resistant because of its location near the exhaust manifold and the reaction to form acids such as sulfuric acid. Therefore, stainless steel is used widely for the catalytic converter canister. More corrosion-resistant materials also are being used downstream from the converter.

LIQUID PASSAGES AND RESERVOIRS

Internal functional liquids generally have inhibitors in the formulation to minimize degradation caused by corrosion. These inhibitors provide the necessary protection as long as they are present in the required concentration. Inhibitor depletion and acidity buildup due to the decomposition of base organics can occur, however, depending on the nature of vehicle use and maintenance practice. For example, engine coolant formulations contain a complex inhibitor package providing protection to component metals, such as copper, steel, aluminum, and solder.[54] When inhibitor depletion occurs, failure of an aluminum water pump due to corrosion can result, but this component is easily replaced. When a transmission component fails due to corrosion, replacement is more costly and therefore more corrosion-resistant materials generally are used. For example, copper and brass may corrode in used ATF, whereas steels and stainless steels are generally resistant in that environment. The development of long-life coolant systems and a proper maintenance schedule of replacement of these fluids are very important in maintaining corrosion protection within liquid passages and reservoirs.[55]

ELECTRICAL AND ELECTRONIC SYSTEMS

The use of electrical and electronic components on automobiles has increased dramatically in recent years, such that electronic systems are now an integral part of all types of vehicles with more than 400 connectors and 3,000 electrical contacts on board a single vehicle.[71] Electronic sensors are primed for deployment in self-driving cars, and it has been predicted that electronic devices will constitute 50% of total vehicle cost by 2030.[72] These devices and systems enable new functions and capability for the automotive engineer, and offer enhanced safety, convenience, and comfort to the vehicle driver. The primary method for corrosion protection of these systems is to minimize exposure to the environment by locating wiring and other components within the passenger compartment, by shielding or providing good drainage, and by sealing and coating.[73] Proper design,

manufacturing, and quality are a precursor. Electrical connectors allow electronic devices and components to be installed and maintained individually, or in chunks, within the full vehicle electrical system. Such an architecture enables efficiency and flexibility in individual vehicle configurations, as well as lower-cost part replacement, upgrades and service.[74] The use of noble metals, notably gold, for electrical contacts provides corrosion resistance, but their cost prohibits their use in the automotive industry with the exception of high-performance race cars.[71]

Copper alloys generally are used for automotive electrical contacts and contact failure can occur through a fretting corrosion mechanism. The damage to the contacts' surfaces from the vibrational fretting action leads to wear particles, which are oxidized in air. The presence of the resultant corrosion products increases the electrical resistance between two parts of electrical contact, resulting in contact failure.[72] Automobile printed circuit boards (PCBs) are sensitive to a specific corrosion mechanism known as corrosion product creep, whereby moisture adsorbed on the surface of the PCB and exposed to atmospheric pollutants leads to the growth of copper- or tin-containing corrosion products.[71] Various organic and inorganic coatings are used to exclude air, moisture, and chemical contaminants and to increase lubricity and reduce thermal degradation within the electrical system. These include paint, primer, varnish, resin, silicone compounds, oil, and greases. A wide range of sealed connectors has been developed for use on automobiles because even the best selection of base materials and plating cannot provide the necessary termination protection in the severe automotive environment. The problems associated with leakage currents (bias) have been addressed by ensuring that proper barrier coatings, sealing, and design are used.

Test Methods

Corrosion testing has played a major role in the development of corrosion-resistant automobiles. These tests generally are classified as laboratory tests or field tests. The difference involves the nature of the environment and the duration of the test. Laboratory tests simulate the environment and accelerate corrosion processes, whereas field tests are conducted in the natural environment usually without additional acceleration factors. Some tests combine a simulated environment and the natural environment. Although laboratory test results are obtained in shorter times, field test results are more reliable because they are conducted in the actual environment. The design and interpretation of laboratory tests are important to obtain data for material selection, process approval, and joint designs for corrosion-resistant vehicles.

Test parameters are categorized according to their chemical and physical effects. Chemical parameters involve the composition of the environment, such as the concentration of constituents, pH, and dissolved gases. The complexity of the automobile environment was described earlier in this chapter. The physical conditions include temperature, static or flowing solution or vapor, liquid or atmospheric volume, and mechanical factors such as stress and impingement. Finally, the duration of the test and exposure periods must be chosen carefully so that under- or over-exposure is avoided, and the degree of corrosion developed gives a reasonable prediction of the real, in-service scenario. Some methods and guidelines that are used in the automobile industry for design and interpretation of corrosion tests are listed in table 5.

TABLE 5 Test Methods and Guidelines for the Design and Interpretation of Corrosion Tests

Test Method or Guideline	Organization
Standard Practice for Rating of Electroplated Panels Subjected to Atmospheric Exposure	ASTM B537
Standard Practice for Preparation of Cold-Rolled Steel Panels for Testing Paint, Varnish, Conversion Coatings, and Related Coating Products	ASTM D609
Standard Practice for Evaluating Degree of Rusting on Painted Steel Surfaces	ASTM D610
Standard Test Method for Evaluation of Painted or Coated Specimens Subjected to Corrosive Environments	ASTM D1654
Standard Guide for Testing Filiform Corrosion Resistance of Organic Coatings on Metal	ASTM D2803
Standard Practice for Preparing, Cleaning, and Evaluating Corrosion Test Specimens	ASTM G1/ ISO 8407
Standard Practice for Conventions Applicable to Electrochemical Measurements in Corrosion Testing	ASTM G3
Standard Guide for Applying Statistics to Analysis of Corrosion Data	ASTM G16
Standard Guide for Laboratory Immersion Corrosion Testing of Metals	ASTM G31
Standard Practice for Recording Data from Atmospheric Corrosion Tests of Metallic-Coated Steel Specimens	ASTM G33
Standard Guide for Examination and Evaluation of Pitting Corrosion	ASTM G46
Standard Guide for Conducting and Evaluating Galvanic Corrosion Tests in Electrolytes	ASTM G71
Standard Guide for Development and Use of a Galvanic Series for Predicting Galvanic Corrosion Performance	ASTM G82
Standard Practice for Calculation of Corrosion Rates and Related Information from Electrochemical Measurements	ASTM G102
Standard Guide for Conducting Exfoliation Corrosion Tests in Aluminum Alloys	ASTM G112
Standard Terminology and Acronyms Relating to Corrosion	ASTM G193/ ISO 8044
Corrosion Tests in Artificial Atmosphere—General Requirements	ISO 7384
Methods for Corrosion Testing of Metallic and Other Inorganic Coatings on Metallic Substrates—Rating of Test Specimens and Manufactured Articles Subjected to Corrosion Tests	ISO 10289
Guidelines for the Introduction of Scribe Marks through Coatings on Metallic Panels for Corrosion Testing	ISO/DIS 17872
Direct Calculations of Economic Appraisals of Corrosion Control Measures	NACE RP0272

LABORATORY TESTS: EXTERNAL EXPOSURE

Categories of laboratory tests are as follows: electrochemical, immersion, chamber, cyclic, and proving grounds. These accelerated tests require (1) selection of environmental and physical conditions representative of service exposure, (2) accelerated corrosion rates without a change in the mechanism, (3) reproducibility of results, and (4) acceleration factors which relate to service performance.

Electrochemical tests are rapid techniques to determine mechanisms, determine the effect of various parameters on corrosion rate, and screen out a large number of materials.[75] They usually involve measurement of corrosion potentials, corrosion currents, polarization curves, and electrochemical impedance. They are used to evaluate metals and alloys and the behavior of metallic, inorganic, and organic coatings. The simplest test involves the measurement of the corrosion potential and its use in conjunction with other measurements. A zero-resistance ammeter (ZRA) is used to measure corrosion currents between dissimilar metals and alloys. Controlled potential tests and anodic and cathodic polarization curves using potentiostats are the most commonly used electrochemical tests. These are powerful tools for investigating the effect of various parameters on corrosion behavior. Cyclic polarization and polarization resistance tests are used to probe localized corrosion and the corrosion rate of material surfaces. Electrochemical tests used for corrosion tests in the automobile industry are listed in table 6.

Immersion tests, whereby specimens are immersed in a fluid of interest, that might be used in the automotive industry are listed in table 7. Variations of the test can be used to enhance certain types of exposure such as partial immersion to create oxygen concentration cells, and alternate (cyclic) immersion to produce wetting and drying effects. The latter test, along with the ferric chloride spot test, is used to determine the behavior of exterior stainless steel trim materials.

TABLE 6 Common Electrochemical Tests Used on Automotive Materials

Test Method	Organization
Standard Reference Test Method for Making Potentiodynamic Anodic Polarization Measurements	ASTM G5
Standard Test Method for Conducting Potentiodynamic Polarization Resistance Measurements	ASTM G59
Standard Test Method for Conducting Cyclic Potentiodynamic Polarization Measurements for Localized Corrosion Susceptibility of Iron, Nickel, or Cobalt-Based Alloys	ASTM G61
Standard Test Method for Measurement of Corrosion Potentials of Aluminum Alloys	ASTM G69
Standard Test Method for Conducting Cyclic Galvanostaircase Polarization	ASTM G100
Standard Practice for Verification of Algorithm and Equipment for Electrochemical Impedance Measurements	ASTM G106
Standard Test Method for Electrochemical Reactivation (EPR) for Detecting Sensitization of AISI Type 304 and 304L Stainless Steels	ASTM G108
Standard Test Method for Electrochemical Critical Pitting Temperature of Stainless Steels and Related Alloys	ASTM G150

TABLE 7 Standard Immersion Tests Used on Automotive Materials

Test Method	Organization
Standard Test Methods for Evaluating the Corrosion Resistance of Stainless Steel Powder Metallurgy (PM) Parts/Specimens by Immersion in a Sodium Chloride Solution	ASTM B895
Standard Test Method for Exfoliation Corrosion Susceptibility in 2XXX and 7XXX Series Aluminum Alloys (EXCO Test)	ASTM G34
Standard Practice for Exposure of Metals and Alloys by Alternate Immersion in Neutral 3.5% Sodium Chloride Solution	ASTM G44
Standard Test Method for Pitting and Crevice Corrosion Resistance of Stainless Steels and Related Alloys by the Use of Ferric Chloride Solution	ASTM G48
Standard Test Method for Visual Assessment of Exfoliation Corrosion Susceptibility of 5XXX Series Aluminum Alloys (ASSET Test)	ASTM G66
Standard Test Method for Determining the Susceptibility to Intergranular Corrosion of 5XXX Series Aluminum Alloys by Mass Loss after Exposure to Nitric Acid (NAMLT Test)	ASTM G67
Standard Practice for Evaluating Intergranular Corrosion Resistance of Heat Treatable Aluminum Alloys by Immersion in Sodium Chloride+Hydrogen Peroxide Solution	ASTM G110/ ISO 11846

Environmental or corrosion test chambers enable the corrosion engineer to approximate a desired environment under controlled conditions. A list of tests that typically require such chambers is given in table 8. The simplest of these tests is the humidity test, whereby the temperature and RH within a chamber are controlled. A condensing humidity chamber, which operates at 100% RH and 38°C, provides an environment whereby condensation occurs continuously on the specimens. The moist SO_2 test (the Kesternich test; ASTM G87, *Standard Practice for Conducting Moist SO_2 Tests*) is a modification of the humidity test but is much more aggressive because of the presence of SO_2, which converts to sulfuric acid. Another modification commonly referred to as the mixed flowing gas test (ASTM B827, *Standard Practice for Conducting Mixed Flowing Gas (MFG) Environmental Tests*) uses extremely low quantities of pollutants, such as H_2S, SO_2, NO_x, Cl_2, and HCl, with humidity to duplicate environments within the passenger compartment. This test is especially useful for electrical and electronic systems.[76]

The automotive industry has a long history and deep experience of using steel for automotive body construction. Neutral salt spray (NSS) testing according to ASTM B117, *Standard Practice for Operating Salt Spray (Fog) Apparatus*, was first released in 1939 and was the traditional and preferred method of assessing material and vehicle corrosion resistance for many decades. The increased use of galvanized steel in the automotive industry

TABLE 8 Standard Chamber Corrosion Tests Used for Automotive Materials

Test Method	Organization
Standard Practice for Operating Salt Spray (Fog) Apparatus	ASTM B117/ ISO 9227/ JIS Z2371
Standard Test Method for Copper-Accelerated Acetic Acid-Salt Spray (Fog) Testing (CASS Test)	ASTM B368/ JISH8681-2
Standard Test Method for Corrosion Testing of Decorative Electrodeposited Coatings by the Corrodkote Procedure	ASTM B380
Standard Practice for Conducting Mixed Flowing Gas (MFG) Environmental Tests	ASTM B827
Standard Practice for Testing Water Resistance of Coatings Using Water Fog Apparatus	ASTM D1735
Standard Test Method for Rust Protection by Metal Preservatives in the Humidity Cabinet	ASTM D1748
Standard Practice for Testing Water Resistance of Coatings in 100% Relative Humidity	ASTM D2247
Standard Practice for Testing Water Resistance of Coatings Using Controlled Condensation	ASTM D4585
Standard Practice for Conducting Cyclic Humidity Exposures	ASTM G60
Standard Practice for Modified Salt Spray (Fog) Testing	ASTM G85
Standard Practice for Conducting Moist SO_2 Tests	ASTM G87/ DIN 50018
Corrosion Tests in Artificial Atmosphere at Very Low Concentrations of Polluting Gases	ISO 10062
Determination of Resistance to Cyclic Corrosion Conditions	ISO 11997
Chip Resistance of Surface Coatings	SAE J400
Accelerated Exposure of Automotive Exterior Materials Using a Fluorescent UV and Condensation Apparatus	SAE J2020
Laboratory Cyclic Corrosion Test	SAE J2334
Cyclic Corrosion Testing of Materials and Components in Automotive Construction	VDA 233-102/ DIN 55635

highlighted the shortcomings of ASTM B117, and the equivalent ISO standard ISO 9227, in predicting the corrosion behavior and rates of these materials in their actual service environment.[77,78] The automotive manufacturers, suppliers, test standard, and research institutions have invested significant effort to develop cyclic corrosion tests that correlate better to vehicle service conditions and that give realistic corrosion rates for nonferrous construction materials.[79–81] Cyclic corrosion tests are by nature more challenging to run in a controlled manner than static tests, and expensive test chambers and rigorous maintenance may be required to ensure the test protocol is followed with integrity. This may be one of the reasons for the persistence of the relatively simple and cheap salt spray test in the industry. Modifications to the salt spray test have emerged as ASTM G85, *Standard Practice for Modified Salt Spray (Fog) Testing*, which now includes five variations: acetic acid-salt spray test; cyclic acidified salt spray test; cyclic seawater acidified test (SWAAT); cyclic SO_2 salt spray; and dilute electrolyte cyclic fog dry test (see ASTM G85, Annex 1–5, respectively). The ISO standard for cyclic corrosion testing (ISO 11997-1) also includes different variations based on alternative methods; for example, Annex A is based on Japanese Automobile Standards (JASO) M609 and M610, and Annex B is a test cycle based on the German Automobile Association method VDA 621-415. Some of the standard methods for static and cyclic corrosion tests that are used for automotive materials, and typically require a test chamber, are listed in table 8.

In addition to the standard methods listed in table 8, many automotive manufacturers have developed their unique and custom corrosion test procedures independently,[79,82] despite the efforts of cross-functional team to develop standard methods, such as SAE J2334 and VDA 233. This in-house development by the automakers has led to a proliferation of cyclic corrosion test procedures across the industry,[79] with each vehicle manufacturer typically preferring their own test method. Examples of automotive manufacturers' cyclic corrosion test methods and some of the principal test parameters are given in table 9. Note that Volvo test method ACT-2 is the same as Ford test method L-467.

Automotive manufacturers typically use standard or custom cyclic corrosion tests (see table 8 and table 9, respectively) for the assessment of construction materials, components, and smaller subassemblies that are exposed to the external environment. The lack of a single, standard test procedure for corrosion assessment of automotive materials and designs means that research scientists and suppliers to the industry may be required to assess their products and technologies using a different corrosion test for each automotive customer. Even accelerated laboratory tests typically run for 6–12 weeks, and with several replicates usually required, a full corrosion qualification test plan for several automakers can easily become costly and time consuming,[79,83,84] with the possibility of conflicting outcomes in terms of corrosion performance. It is obvious that the adoption of a single standard corrosion test method would be beneficial to the automotive

TABLE 9 Example Cyclic Corrosion Test Methods Developed by Automakers, Including Some Test Parameters for Each[79,82]

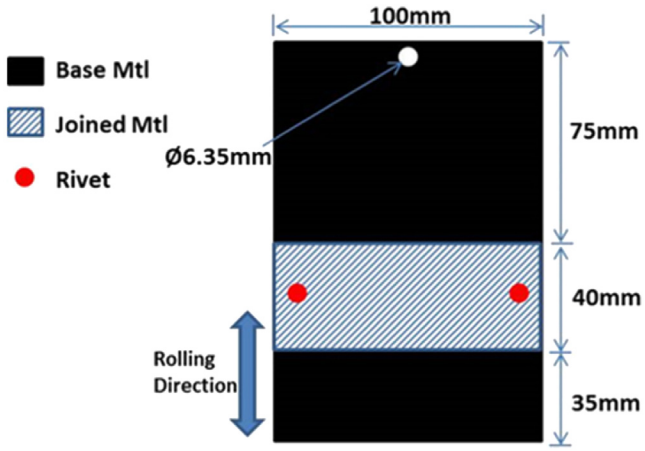
Manufacturer	Test Method	Corrodent (wt%)	T Set Points (°C)	RH Set Points (%)
Daimler-Chrysler	KWT-DC	1% NaCl, pH 6.5–7.2	−15 & 50	50 & 100
Ford / Volvo	CETP L-467 / VCS 1027,1449 (ACT-2)	0.5% NaCl, pH unadjusted	25 & 50	70 & 95
General Motors	GMW 14872	0.9% NaCl + 0.1% $CaCl_2$ + 0.075% $NaHCO_3$	25, 49 & 60	≤ 30, 45, 100
Renault	D172028 (ECC 1)	1% NaCl, pH 4	35	20, 55 & 90
Volvo	STD423-0014 (ACT-1)	1% NaCl	35 & 45	50 & 95
Volkswagen	PV1210	1% NaCl, pH 6.5–7.2	23 & 40	50 & 100

industry generally; however, there may be resistance from the automakers to abandon a test approach with which they have developed numerous data and mechanistic understanding, with reasonable correlation to field experience, and to "start over" with a new test. Even among the standard bodies, several different corrosion test methods have been proposed, as discussed previously and indicated by the number of tests (excluding annexes) listed in table 8.

In addition to making a judicious choice of test method, the corrosion engineer must also select or design a suitable test object. The corrosion resistance of bare panels of steel or galvanized steel can be assessed by recording the time or number of corrosion cycles until the formation of red rust is observed.[85] Painted panels, with a deliberate scribe cut in through the paint, commonly are used to assess the resistance of the panel substrate (which may be ferrous or nonferrous), and the paint system, to corrosion propagation from a controlled defect.[3,86–88] Photographs of diagonally scribed painted steel and aluminum panels following corrosion exposure are shown in figures 12*A* and 12*B*, and digital images for analysis of creep-back and paint blistering are shown in figures 12*C* and 12*D*.

Acceptance criteria, based on the extent of creep-back or length of filaments after a certain corrosion exposure, are set by the automotive manufacturer and typically are benchmarked versus a well-tested system of known corrosion performance. Scribe creep panels are one of the simplest test objects used in automotive corrosion testing, and yet there is no standard agreement among automakers on panel size or panel orientation in the test chamber; scribe location, orientation, cutting method, shape, or width; or scribe creep-back measurement procedure.[89] Overlapping coupons that simulate a hem flange, weld flange or crevice configuration,[3,90] and mixed-material coupons with different joining elements[60,91] are frequently custom-designed for a given joint and material configuration of interest. Reference coupons with known corrosion rates (e.g., mass loss) in laboratory and outdoor exposures frequently are used to give context to test objects of unknown performance.

FIG. 13 Example design of an overlapping coupon that also could be used as a mixed-material coupon for galvanic corrosion studies.



The proving ground (PG) test allows the entire vehicle to be exposed, with materials, processes, and geometries representative of fully assembled vehicles.[55] Much like the laboratory tests listed in table 9, the PG test procedure varies between automakers. It is desirable that the automaker's laboratory test correlates with the automaker's PG test. PG tests generally include a driving schedule over various roads, including highway travel, salt highway, gravel road, mud trough, and salt trough (see fig. 14), and significant time under controlled temperature and relative humidity conditions in large environmental chambers. Exposure to rain, snow, drying, elevated temperature, freezing temperatures, and UV also may be included. The period required to complete one set of exposure is termed a cycle and usually a number of cycles is related to a set number of years of automotive service. SAE standard J1950 describes PG vehicle corrosion testing with details of the cycles at four U.S. proving grounds. Note, however,

FIG. 12 Scribe creep panels after corrosion exposure: diagonally scribed paint on (*A*) steel, and (*B*) aluminum alloy; digital images of creep-back from (*C*) steel and (*D*) aluminum alloy, with scribes cut perpendicularly to the rolling direction.

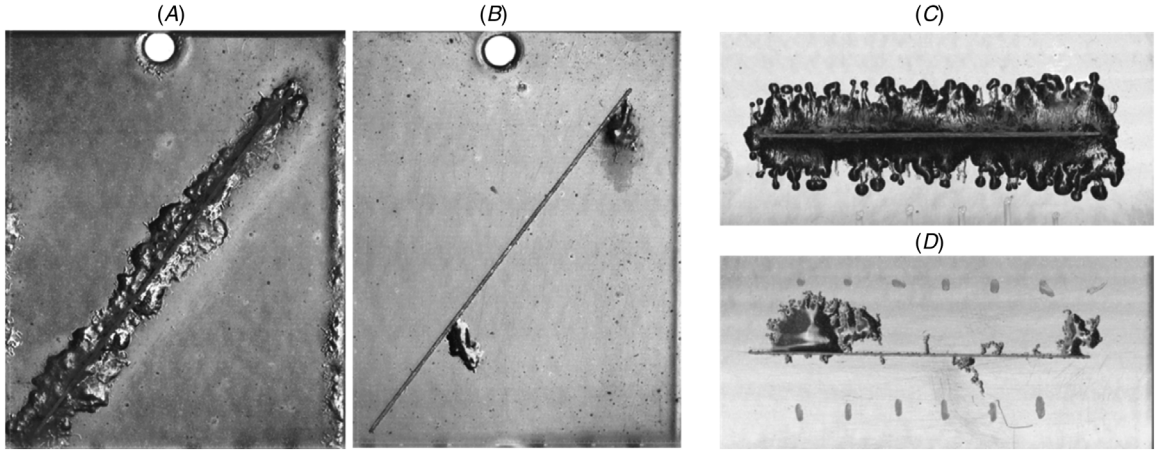


FIG. 14 Environmental loading on test vehicle at the proving ground: (*A*) mud splash, (*B*) salt highway, and (*C*) gravel road. *Source*: Photos courtesy of Ford Motor Company.



(*A*) (*B*) (*C*)

that the tests described are not recent—for example, the current Ford PG test method does not match the cycles presented in SAE J1950.[92]

One method to provide comparison to previous and future tests, as well as to service performance is by the use of coupons with known field behavior mounted on the test vehicle, as illustrated in figure 15. Reference coupons are routinely used in automotive corrosion testing to ensure that the corrosion exposure is running as expected and, in some methods, to adjust the exposure period accordingly. Typically, these reference coupons are of mild steel, such as that shown in figure 15*B*, and corrosion rates are checked by mass loss or gage loss measurements. As noted by Ström,[3] however, open steel faces corrode at a rather stable and consistent rate over a rather broad range of corrosive conditions, and zinc is a more sensitive indicator of corrosion rates. Because these tests simulate service exposure but still represent accelerated conditions, considerable expertise is required for evaluation and interpretation of results. Fuller discussion of the advantages and limitations of automotive proving ground corrosion testing can be found in Ström.[3]

FIELD TESTS—EXTERNAL EXPOSURE

When products or materials are exposed to the natural environment, they are considered field or service tests. Included in this category are atmospheric exposure, mobile test racks, fleet tests, and field surveys. Atmospheric exposure consists of placing specimens, such as coupons, parts, and components, on racks at stationary test sites. The nature of the site varies depending on geographic area and specific location within an area. Factors such as environmental chemistry (e.g., chlorides, pollutants), time of wetness, temperature, humidity, hours of sunlight, and seasonal changes have an important effect on the corrosion rate and mechanism. The most useful field tests include measurements of these important parameters so that corrosion rates can be understood within the context of the environment, and similarities and differences between different exposure sites and accelerated test methods can be clarified.[93,96]

Mobile test racks or plates are mounted on vehicles or trailers that are subjected to normal driving conditions. They are mounted on various locations on vehicles, such as the underbody, as described in SAE J1293.[97] These racks or plates, however, also may be mounted on bumpers, grilles, and truck trailers. Panels, coupons, parts, and components are attached to these racks and are exposed to driving conditions in the natural environment. Direct comparisons therefore can be made on the corrosion behavior of these materials. As with static atmospheric exposures, measurements of the relevant environmental conditions and the inclusion of reference materials yield a richer dataset than exposure of test panels alone. A truck used for mobile exposure of a variety of corrosion test coupons is shown in figure 16. Sensors for time of wetness, temperature, and relative humidity were co-located with the test panels.

FIG. 15 Proving ground test preparations showing: (*A*) test vehicle with coupons attached to the door lowers, (*B*) close-up of a reference coupon, and (*C*) close-up of a mixed-material test coupon showing E-coat blistering on the base panel. The reference and test coupons are carried through the corrosion test by the vehicle. *Source*: Photos courtesy of Ford Motor Company.



(*A*) (*B*) (*C*)

FIG. 16 Test coupons and sensors mounted on racks, fixed to the underbody of a truck driving in the Montreal region of Canada. *Source*: Photo courtesy of Dr. Danick Gallant, National Research Council Canada.



Fleet tests are extremely valuable in providing direct information on corrosion behavior in specific geographic locations. Groups of cars that typically are used for these tests are taxicabs, rental cars, municipally owned cars, and sales fleet cars. Because the operating parameters can be recorded through fleet recordkeeping, this type of test is probably the most reliable of all for automobile corrosion performance.

Field surveys are valuable because of the large number of vehicles that can be inspected visually over a short period of time. In general, a location and time of year is chosen and a team of evaluators inspect vehicles in parking lots, on streets, and at dealerships with survey sheets. Therefore, corrosion performance is based on inspection and evaluation of actual standard production vehicles exposed to natural environments and normal operating conditions. Some drawbacks to field surveys are that actual driving conditions and history (e.g., crashes and repairs) for each vehicle cannot be determined unless each owner is interrogated, and the survey typically is restricted to visible body panel corrosion.[98,99] More in-depth analysis of the entire vehicle's long-term corrosion performance can be undertaken by the purchase of a vehicle, ideally with known driving history, that has been in use for a useful period, typically several years. Such studies are informative to the automaker, particularly for corroboration of accelerated laboratory and PG tests. Besides the long waiting period for such data, another disadvantage of this approach is the uncertainty of how representative the selected vehicle might be of the fleet in general.

TESTING—INTERNAL COMBUSTION

The complex exhaust system environment including internal condensate corrosion, high-temperature oxidation, and exhaust-gas impingement makes it difficult to obtain meaningful accelerated corrosion test results. Laboratory tests generally are based on exposure to exhaust gas condensate. The condensate may be delivered to the test parts as gas flow through alternate immersion, or through liquid condensate injection through the system with air flow.[100,101] Various test temperatures, immersion times, and condensate chemistries are used, depending on the specific component and manufacturers' requirements. Controlled engine laboratory tests are valuable for evaluating internal exhaust system deterioration. These tests are conducted with actual engines to produce the exhaust gas, which is directed through the appropriate materials to be tested. This can be a coupon exposed to the exhaust stream or an actual exhaust system, depending on the test design. The dew point temperature can be controlled such that condensation occurs within a temperature range. This control provides an acceleration factor for the test. Each of these approaches has advantages and disadvantages, as discussed by Garcia,[100] but it is difficult to find an optimum balance of corrosion stimulation and the simulation of realistic in-service scenarios. Although corrosion vehicles tested at the proving ground do include driving cycles, it has been observed that the relatively short driving times are not sufficient to stimulate long-term exhaust system corrosion mechanisms. Therefore, various laboratory bench and dynamometer tests are required to ensure corrosion performance. In general, the widespread use of stainless steels together with sound design principles, as discussed by Douthett,[51] ensures adequate corrosion resistance.

TESTING—LIQUID PASSAGES AND RESERVOIRS

Laboratory tests to determine the behavior of materials and corrosivity of automotive fluids, such as engine coolants, engine oils, and ATFs, and fuels involve exposure to the actual fluid as close to operating conditions as possible. In most cases, aging of the fluids due to their functional use produces a more corrosive liquid; therefore, it is important that the test be conducted on used or pre-aged liquids or that the aging of the fluid occurs *in situ*. Simple immersion tests can be used if chemical and physical environmental effects are introduced. This is not always possible and therefore simulated service tests have been developed. These laboratory bench tests simulate more closely actual service conditions by using a model of a particular automobile function. Field service tests are the most reliable but also the most time consuming and costly.

Corrosion testing of engine coolants is the most advanced in this group. These are divided into three categories, including (1) laboratory tests, (2) engine tests, and (3) field service tests. Tests under these categories are listed in table 10. Laboratory tests have been the primary means for evaluating the corrosive effects of engine coolants and the effectiveness of the coolant inhibitor formulation. The most important of these is ASTM D1384, *Standard Test Method for Corrosion Test for Engine Coolants in Glassware*. A wide range of other tests is used, including electrochemical techniques. ASTM D2570, *Standard Test Method for Simulated Service Corrosion Testing of Engine Coolants*, is also used quite widely and includes the use of a pump, radiator, thermostat housing, and a large pot to house test coupons. An extension of this test includes an actual operating engine, which is referred to as a no-load engine test (ASTM D2758, *Standard Test Method for Engine Coolants by Engine Dynamometer*). Field service tests evaluate materials and inhibitor systems under actual vehicle operating conditions and are the most reliable. The test is described in ASTM D2847, *Standard Practice for Testing Engine Coolants in Car and Light Truck Service*. The ASTM specifications for engine coolants (e.g., ASTM

TABLE 10 Standard Tests and Specifications for Engine Coolants

Test Method or Specification	Organization
Standard Test Method for Boiling Point of Engine Coolants	ASTM D1120
Standard Test Method for Reserve Alkalinity of Engine Coolants and Antirusts	ASTM D1121
Standard Test Methods for Water in Engine Coolant Concentrate by the Karl Fischer Reagent Method	ASTM D1123
Standard Test Method for Corrosion Test for Engine Coolants in Glassware	ASTM D1384
Standard Test Method for Simulated Service Corrosion Testing of Engine Coolants	ASTM D2570
Standard Test Method for Engine Coolants by Engine Dynamometer	ASTM D2758
Standard Test Methods for Cavitation Corrosion and Erosion-Corrosion Characteristics of Aluminum Pumps with Engine Coolants	ASTM D2809
Standard Practice for Testing Engine Coolants in Car and Light Truck Service	ASTM D2847
Standard Specification for Glycol Base Engine Coolant for Automobile and Light-Duty Service	ASTM D3306
Standard Specification for ASTM Reference Coolant for Coolant Tests	ASTM D3585
Standard Test Method for Corrosion of Cast Aluminum Alloys in Engine Coolants Under Heat-Rejecting Conditions	ASTM D4340
Coolants for Internal Combustion Engines	SAE J814
Automotive and Light Truck Engine Coolant Concentrate	SAE J1034
Principles of Engine Cooling Systems and Maintenance	SAE HS-40

D3306, *Standard Specification for Glycol Base Engine Coolant for Automobile and Light-Duty Service*) include performance requirements on corrosion resistance according to the test methods. Additional specifications not listed in table 10 are available specifically for heavy-duty engines, which may require pre-charging and re-charging with inhibitors during vehicle service.

The behavior of ATF and its effect on materials has also been investigated through several different test approaches, as listed in table 11. The most commonly used are bench tests, laboratory motor-driven transmission tests, and field service tests. Laboratory tests for ATF include the copper corrosion test (ASTM D130, *Standard Test Method for Corrosiveness to Copper from Petroleum Products by Copper Strip Test*), rust test (ASTM D665, *Standard Test Method for Rust-Preventing Characteristics of Inhibited Mineral Oil in the Presence of Water*), and a variety of glassware oxidation tests. Various bench tests, such as Ford's Aluminum Beaker Oxidation Test and Japanese Industrial Standard JIS K2514, are used by manufacturers to determine ATF oxidation stability.[102] General Motor's ATF fluid specification includes oxidation testing with the use of transmissions mounted on test beds. These tests are designed to deliberately oxidize the ATF under controlled conditions so that the extent of oxidation and the effects on materials can be measured. The behavior of copper wire, strip, or components frequently is used as a standard for corrosion resistance in the tests. Visual examination of copper

TABLE 11 Tests and Specifications for ATF

Test Method or Specification	Organization
Standard Test Method for Corrosiveness to Copper from Petroleum Products by Copper Strip Test	ASTM D130/ ISO 2160
Standard Test Method for Rust-Preventing Characteristics of Inhibited Mineral Oil in the Presence of Water	ASTM D665
Ford Aluminum Beaker Oxidation Test (ABOT)	FLTM BJ110-04
General Motors DEXRON®-III Automatic Transmission Fluid Specification	GM-6297M
Testing Methods for Oxidation Stability of Lubricating Oils	JIS K2514
Oxidation Stability of Lubricating Oils Used in Automotive Transmissions by Artificial Ageing	CEC L-48-00

content and in-depth surface analysis of deposits on tested parts[58] are methods used for evaluation of ATF performance.

A laboratory immersion test for corrosion in hydraulic brake line fluid is described in Motor Vehicle Brake Fluid Standard SAE J1703. This test includes the use of standard metal coupons for mass change and visual examination after immersion at 100°C in the brake fluid. Other tests are used to evaluate specific components in the braking system, such as that described in SAE J1047 for hydraulic brake line tubing. Internal corrosion is not considered to be as important as external corrosion of the braking system and therefore only simple tests are used outside of on-vehicle service tests.

Corrosion tests for hydraulic brake line fluid, as well as for motor oil, grease, and lubricants are listed in table 12. In addition, the interactions of various fuels on materials have been important because of the effect of small amounts of water, which can become trapped in areas, such as the fuel tank. Various additives to fuels can prevent corrosion effects and include inhibitor packages and small amounts of alcohol and aromatics. Corrosion of metals within the fuel system can occur if the fuel is contaminated with water and chlorides. Corrosion testing of bio-based fuels and mixtures, such as ethanol blended with gasoline, has been of interest because ethanol has both higher affinity for water and significantly higher conductance than gasoline,[103] increasing the likelihood of biofuel-system corrosion issues compared with gasoline alone. Corrosion resistance of steel and aluminum alloys in the fuel system depends on fuel contamination, conductance, and temperature; ferrous materials have been reported to have higher corrosion rates in water-contaminated fuel blends than in water-free or dry fuel, whereas the opposite trend was observed for aluminum alloy.[104,105] Tests for fuels include electrochemical polarization, electrochemical impedance spectroscopy, and immersion tests.

TESTING—ELECTRICAL AND ELECTRONIC SYSTEMS

Corrosion testing of electrical and electronic systems has generally followed the guidelines used for testing in external environments. A large degree of evaluation is performed in the standard tests used for external exposure (tables 5–8). Proving grounds and field tests are the most reliable, but these are lengthy and costly procedures and are not practical for rapid innovation. At the same time, microelectronics perform critical vehicle

TABLE 12 Standard Tests for Automotive Fluids

Brake Fluid	Organization
Motor Vehicle Brake Fluid	SAE J1703
Motor Vehicle Brake Fluid Based Upon Glycols, Glycol Ethers, and the Corresponding Borates	SAE J1704
Low Water Tolerant Brake Fluids	SAE J1705
Specification of Non-Petroleum Based Brake Fluids for Hydraulic Systems	ISO DIS 4925
Standard Test Method for Detection of Copper Corrosion from Petroleum Products by the Copper Strip Test	ASTM D130
Standard Test Method for Corrosiveness and Oxidation Stability of Hydraulic Oils, Aircraft Turbine Engine Lubricants, and Other Highly Refined Oils	ASTM D4636
Motor Oil, Grease, Lubricants	
Standard Test Method for Evaluation of Rust Preventive Characteristics of Automotive Engine Oils	ASTM D6557
Standard Test Method for Corrosiveness to Copper from Petroleum Products by Copper Strip Test/Standard Test Method for Copper Strip Corrosion by Industrial Aromatic Hydrocarbons	ASTM D130/ ASTM D849
Standard Test Method for Determining Corrosion Preventive Properties of Lubricating Greases	ASTM D1743
Standard Test Method for Corrosion Characteristics of Solid Film Lubricants	ASTM D2649
Fuels	
Standard Test Method for Rust-Preventing Characteristics of Inhibited Mineral Oil in the Presence of Water	ASTM D665
Standard Test Method for Detection of Copper Corrosion from Petroleum Products by the Copper Strip Test	ASTM D130

operational and safety functions, such as the deployment of airbags during traffic accidents,[62] and so corrosion avoidance for these systems is essential. The emergence of the battery electric vehicle (BEV), which does not require a traditional internal combustion engine (ICE) or transmission system, offers the opportunity to reconfigure the vehicle architecture.[69] Battery packs for BEV are rather large and heavy, and their mounting location has a significant impact on weight distribution and crash performance. In the case of the Tesla Model S, the battery pack is integrated with the chassis; this underbody location is more exposed to a severe external environment than the ICE underhood location. As noted by Liu et al.,[69] future designs for BEVs are likely to include electric motors at or integrated into the vehicle wheels, where they would be exposed to the most corrosion-severe environment. These comments highlight the systems engineering approach required for the development of robust corrosion strategies for electrical and electronic systems. The type and duration of the corrosion test most appropriate for the system under test depends on the installation condition, mounting location, and in-service environmental exposure. The ISO standards listed in table 13 distinguish between electrical and electronic equipment that are installed within the vehicle from equipment that is exposed to the external environment. Judicious choice of testing approach and the generation of field data are required to ensure safety in these novel systems.

TABLE 13 Tests for Automotive Electrical and Electronic Systems

Test Method	Organization
Environmental Conditions and Testing for Electrical and Electronic Equipment	ISO 16750
Corrosion Preventive Compound for Connectors	MIL-C-81309 and 16173
Environmental Testing of Electronic and Associated Equipment	MIL-T-5422
Environmental Conditions & Testing for Electrical & Electronic Equipment for Drive System of Electric Propulsion vehicles	ISO 19453
Electric and Hybrid Electric Vehicle Rechargeable Energy Storage System (RESS) Safety & Abuse Testing	SAE J2464

Test Standards

Automobiles consist of a wide range of materials fabricated into various components and exposed to complex environments, including external driving conditions, functional internal fluids, and exhaust gas. Therefore, a wide range of corrosion tests is required to ensure corrosion resistance of the vehicles in service. Corrosion standards are developed to ensure that results are reproducible and consistent. The wide range of standards used in the automobile industry is demonstrated by the long lists for corrosion testing of body, chassis, trim, and hardware materials given in the previous sections. In addition to the ASTM, SAE, ISO, VDA, and JISO (and others globally) standard methods, automakers have developed further corrosion test methods. In some cases, these methods have been considered proprietary. The long service life expected for today's vehicles; the emergence of innovative materials, technologies, and powertrains; and the increasing corrosivity of the road environment because of high levels or road salts (see fig. 1) highlight the need for consistent approaches in corrosion standards across the automakers to innovate safely at a rapid pace. Opportunities to rationalize test methods, where appropriate, should be considered.

Automotive Corrosion Testing: Outlook

The scientific research that underpins corrosion testing for automotive vehicles has led to much greater corrosion resistance of vehicles and has enabled the automotive sector to embrace new materials, technologies, and processes; to extend vehicle life and service intervals; and to enhance the customer experience. Despite the establishment of many standard tests that claim to have good correlation to in-service conditions, challenges in repeatability and reproducibility of corrosion tests persist.[106,107] Round-robin tests have highlighted differences in interpretations of a test method, idiosyncratic behaviors of test chambers or laboratories, and varying approaches to test object preparations and corrosion measurements. Variations in materials and processes that might be unknown to the corrosion test engineer—for

example, the rolling direction and thermal history of a heat-treatable aluminum alloy, or the presence of micro-defects in a coating sublayer—can influence and even control corrosion rates for a painted scribed panel.

An approach with controlled test objects and known environments offers a path toward the establishment of the fundamental interactions of the test material and that environment. For painted or adhesive-covered panels, the substrate microstructure, pretreatment chemistry and morphology, and coating or adhesive performance must be treated as an interacting system. The establishment of a known environment in the laboratory is more complex than temperature and RH control within a test chamber; the real environment of interest is the electrolyte formed on the test material's surface. The use of corrosion rate sensors, along with localized temperature, RH, time of wetness, and electrolyte impedance sensors, and in test chamber with high levels of control, gives *in situ*, quasi-instantaneous data on material-environment interactions.[67,108–110] Such data are necessary to clarify corrosion mechanisms and rates under the different conditions likely to be encountered in service.

Corrosion is one of the few vehicle attributes that is not simulated with computer-aided engineering. There is a strong desire for accurate prediction of the corrosion rates of vehicles in service, as well as structures generally, to avoid failure modes, implement timely service, and reduce the amount of physical testing required to achieve these ends. Much research is focused on providing numerical solutions to these problems.[111–113] Simulation of atmospheric corrosion is a complex problem and the development of models is currently in its early stages, with many researchers focused on simplified test samples under controlled laboratory electrolyte films. Simple setups, such as galvanic couples of two well-characterized materials, turn out to be complicated systems because of the dynamic nature of atmospheric corrosion and the complex interactions occurring for today's highly engineered construction materials.[113] Even if reliable predictive models for atmospheric corrosion are a long-term prospect, the value offered by such models, and the insight to be gained from the research into these questions, ensure that this corrosion research area will be pursued actively over many years to come.

References

1. Alliance of Automobile Manufacturers, "America's Automobile Industry Is One of the Most Powerful Engines Driving the U.S. Economy," 2020, http://web.archive.org/web/20210509190303/https://www.autosinnovate.org/initiatives/the-industry
2. M. Ebrahimi, A. Baboli, and E. Rother, "The Evolution of World Class Manufacturing toward Industry 4.0: A Case Study in the Automotive Industry," *IFAC-PapersOnLine* 52, no. 10 (2019): 188–194.
3. M. Ström, "Automotive Proving Ground Corrosion Testing," in *Corrosion: Environments and Industries*, vol. 13C, ed. S. D. Cramer and B. S. Covino, Jr. (Materials Park, OH: ASM International, 2006), 538–544.
4. K. Olsson and J.-O. Sperle, "New Advanced Ultra-High Strength Steels for the Automotive Industry," *AutoTechnology* 6, (2006): 46–49.
5. O. Bouaziz, H. Zurob, and M. Huang, "Driving Force and Logic of Development of Advanced High Strength Steels for Automotive Applications," *Steel Research International* 84, no. 10 (2013): 937–947.
6. W. J. Joost and P. E. Krajewski, "Towards Magnesium Alloys for High-Volume Automotive Applications," *Scripta Materialia* 128 (2017): 107–112, https://doi.org/10.1016/j.scriptamat.2016.07.035
7. K. R. Brown, R. A. Woods, W. Springer, C. Fujikura, M. Nabae, Y. Bekki, R. Macé, J. C. Ehrstrom, and T. Warner, *The Corrosion Performance of Aluminum Automotive Body Panels in Service*, Technical Paper Series No. 980460 (Warrendale, PA: SAE International, 1998).
8. J. Hirsch, "Recent Development in Aluminium for Automotive Applications," *Transactions of Nonferrous Metals Society of China* 24, no. 7 (2014): 1995–2002.
9. M. K. Kulekci, "Magnesium and Its Alloys Applications in Automotive Industry," *International Journal of Advanced Manufacturing Technology* 39, nos. 9–10 (2008): 851–865.
10. M. Wayland, "Carbon Fiber Truck Bed Just a Beginning," *Automotive News*, April 29, 2019, http://web.archive.org/web/20210509191523/https://www.autonews.com/manufacturing/carbon-fiber-truck-bed-just-beginning
11. R. Miel, "Toyota Says Carbon Fiber Goes beyond Lightweighting," *Automotive News*, July 31, 2017, http://web.archive.org/web/20210509193815/https://www.autonews.com/article/20170731/OEM01/170739914/toyota-says-carbon-fiber-goes-beyond-lightweighting
12. B. Reinhold, D. Blücher, and M. Korte, "Herausforderungen an Füge- und Oberflächentechnik für Zukünftige Leichtbaukonstruktionen im Automobilbau," *Materialwissenschaft und Werkstofftechnik* 44, no. 1 (2013): 58–69.
13. T. Prosek, A. Nazarov, F. Goodwin, J. Serák, and D. Thierry, "Improving Corrosion Stability of ZnAlMg by Alloying for Protection of Car Bodies," *Surface and Coatings Technology* 306 (2016): 439–447.
14. S. J. Simko, B. Schneider, J. L. Tardiff, M. Jagner, and A. Drews, *Characterization of Zirconium Oxide-Based Pretreatment Coatings, Part 1: Variability in Coating Deposition on Different Metal Substrates*, Technical Paper Series No. 2009-01-0890 (Warrendale, PA: SAE International, 2009).
15. A. Amirudin and D. Thierry, "Corrosion Mechanisms of Phosphated Zinc Layers on Steel as Substrates for Automotive Coatings," *Progress in Organic Coatings* 28, no. 1 (1996): 59–75.
16. I. Milošev and G. S. Frankel, "Review—Conversion Coatings Based on Zirconium and/or Titanium," *Journal of The Electrochemical Society* 165, no. 3 (2018): C127–C144.
17. B. Schneider, A. Drews, M. Jagner, S. J. Simko, and J. L. Tardiff, *Characterization of Zirconium Oxide-Based Pretreatment Coatings, Part 2: Challenges in Coating Aluminum Body Panels*, Technical Paper Series No. 2009-01-0892, (Warrendale, PA: SAE International, 2009).

18. K. Slamova, C. Schill, S. Wiesmeier, M. Köhl, and R. Glaser, "Mapping Atmospheric Corrosion in Coastal Regions: Methods and Results," *Journal of Photonics for Energy* 2, no. 1 (2012): 1–12.

19. V. R. Kelly, S. E. G. Findlay, W. H. Schlesinger, K. Menking, and A. M. Chatrchyan, "Road Salt: Moving toward the Solution" (Millbrook, NY: Cary Institute of Ecosystem Studies, 2010).

20. "Annual Survey of State Winter Maintenance Data," Clear Roads, http://web.archive.org/web/20210509194224/https://clearroads.org/winter-maintenance-survey/

21. T. D. Kelly and G. R. Matos, "Salt End-Use Statistics," in *Historical Statistics for Mineral and Mateiral Commodities in the United States* (Reston, VA: U.S. Geological Society, 2014), http://web.archive.org/web/20210509194657/https://s3-us-west-2.amazonaws.com/prd-wret/assets/palladium/production/mineral-pubs/historical-statistics/salt-use.pdf

22. R. Baboian, "Successes in Automotive Engineering," *Materials Performance* 48, no. 2 (2009): 16–17.

23. "Salt," in *Mineral Commodity Summaries"* (Reston, VA: U.S. Geological Society, 2020), http://web.archive.org/web/20210509194759/https://pubs.er.usgs.gov/publication/mcs2020

24. "Nitrogen Dioxide Trends," Environmental Protection Agency, 2019, http://web.archive.org/web/20210509194933/https://www.epa.gov/air-trends/nitrogen-dioxide-trends

25. "Sulfur Dioxide Trends," Environmental Protection Agency, 2019, http://web.archive.org/web/20210509195037/https://www.epa.gov/air-trends/sulfur-dioxide-trends

26. W. P. Bolen, "Salt," in *2016 Minerals Yearbook* (Reston, VA: U.S. Geological Society, 2016), http://web.archive.org/web/20210509195208/https://prd-wret.s3-us-west-2.amazonaws.com/assets/palladium/production/atoms/files/myb1-2016-salt.pdf

27. "Salt," in *Mineral Commodity Summaries* (Reston, VA: U.S. Geological Society, 2013), http://web.archive.org/web/20210509195331/https://s3-us-west-2.amazonaws.com/prd-wret/assets/palladium/production/mineral-pubs/mcs/mcs2013.pdf

28. "Salt," in *Mineral Commodity Summaries* (Reston, VA: U.S. Geological Survey, 2015), http://web.archive.org/web/20210509195432/https://s3-us-west-2.amazonaws.com/prd-wret/assets/palladium/production/mineral-pubs/salt/mcs-2015-salt.pdf

29. "Field Usage of Alternative Deicers for Snow and Ice Control," *Transportation Research Synthesis*, TRS 1706 (2017), http://web.archive.org/web/20210509195508/http://dot.state.mn.us/research/TRS/2017/TRS1706.pdf

30. D. L. Kelting and C. L. Laxson, "Review of Effects and Costs of Road De-icing with Recommendations for Winter Road Management in the Adirondack Park" (Report No. AWI2010-01, Adirondack Watershed Institute, Paul Smiths, NY, 2010), http://web.archive.org/web/20210509195613/http://www.protectadks.org/wp-content/uploads/2010/12/Road_Deicing-1.pdf

31. "Enhanced Salt Brine: Liquid Deicer" (Report No. DEICE-1115, Cargill Deicing Technology, North Olmsted, OH, April 11, 2018), http://web.archive.org/web/20210509195708/https://www.cargill.com/doc/1432076034989/enhanced-salt-brine-sell-sheet.pdf

32. "Overview," New Jersey Department of Transportation," http://web.archive.org/web/20210509195902/https://www.state.nj.us/transportation/about/winter/

33. T. Prosek, D. Thierry, C. Taxén, and J. Maixner, "Effect of Cations on Corrosion of Zinc and Carbon Steel Covered with Chloride Deposits under Atmospheric Conditions," *Corrosion Science* 49, no. 6 (2007): 2676–2693.

34. M. Jönsson, "Investigation of the Corrosivity of De-Icing Materials" (KIMAB-2012-554, swerea KIMAB, MRC Automotive Corrosion Member Program, Borås, Sweden, 2012).

35. D. Bengtsson Blücher, J.-E. Svensson, and L. G. Johansson, "The Influence of CO_2, $AlCl_3.6H_2O$, $MgCl_2.6H_2O$, Na_2SO_4 and NaCl on the Atmospheric Corrosion of Aluminum," *Corrosion Science* 48 (2006): 1848–1866.

36. C. Leygraf and T. E. Graedel, "Atmospheric Corrosion Gases and Their Involvement in Corrosion," in *Atmospheric Corrosion* (Hoboken, NJ: Wiley, 2000), 37–53.

37. C. Leygraf, "Atmospheric Corrosion," in *Corrosion Mechanisms in Theory and Practice* (Boca Rotan, FL: CRC Press, 2012), 681–716.

38. A. A. May, N. T. Nguyen, A. A. Presto, T. D. Gordon, E. M. Lipsky, M. Karve, A. Gutierrez, et al., "Gas- and Particle-Phase Primary Emissions from In-Use, On-Road Gasoline and Diesel Vehicles," *Atmospheric Environment* 88 (2014): 247–260.

39. "Nitrogen Oxides (NOx), Why and How They Are Controlled" (EPA-456/F-99-006R, U.S. Environmental Protection Agency, Washington, DC, 1999), http://web.archive.org/web/20210509200017/https://www3.epa.gov/ttncatc1/dir1/fnoxdoc.pdf

40. V. Praveena and M. L. J. Martin, "A Review on Various after Treatment Techniques to Reduce NOx Emissions in a CI Engine," *Journal of the Energy Institute* 91, no. 5 (2018): 704–720.

41. C. Arroyave and M. Morcillo, "The Effect of Nitrogen Oxides in Atmospheric Corrosion of Metals," *Corrosion Science* 37, no. 2 (1995): 293–305.

42. L. A. Farrow, T. E. Graedel, and C. Leygraf, "Gildes Model Studies of Aqueous Chemistry, II: The Corrosion of Zinc in Gaseous Exposure Chambers," *Corrosion Science* 38, no. 12 (1996): 2181–2199.

43. J. G. Castaño, C. Arroyave, and M. Morcillo, "Characterization of Atmospheric Corrosion Products of Zinc Exposed to SO_2 and NO_2 Using XPS and GIXD," *Journal of Materials Science* 42, no. 23 (2007): 9654–9662.

44. C. Leygraf and T. E. Graedel, "Corrosion in Outdoor Exposures," in *Atmospheric Corrosion*, (Hoboken, NJ: Wiley, 2000), 91–108.

45. D. Bengtsson Blücher, J.-E. Svensson, and L. G. Johansson, "Influence of ppb Levels of SO2 on the Atmospheric Corrosion of Aluminum in the Presence of NaCl," *Journal of The Electrochemical Society Journal* 152, no. 10 (2005): B397–B404.

46. S. Oesch and M. Faller, "Environmental Effects on Materials: The Effect of the Air Pollutants SO2, NO2, NO and O3 on the

Corrosion of Copper, Zinc, and Aluminium. A Short Literature Survey and Results of Laboratory Exposures," *Corrosion Science* 39, no. 9 (1997): 1505–1530.

47. *Corrosion of Metals and Alloys—Corrosivity of Atmospheres—Classification, Determination and Estimation*, ISO Standard No. 9223 (Geneva, Switzerland: International Organization for Standarization, 2012).

48. R. Baboian and R. C. Turcotte, "Development of Poultice Corrosion Tests for Automobiles," *Materials Performance* 24, no. 12 (1985): 13–17.

49. W. R. Patterson, "Materials, Design and Corrosion Effects on Exhaust-System Life," *SAE Transactions* 87 (1978): 3294–3329.

50. S. N. Thakur, J. R. McMillen, M. L. Holly, and P. K. Samal, *High Temperature Oxidation/Corrosion Performance of Various Materials for Exhaust System Applications*, Technical Paper Series, (Warrendale, PA: SAE International, 2006).

51. J. Douthett, "Automotive Exhaust System Corrosion," in *Corrosion: Environments and Industries*, vol. 13C, ed. S. D. Cramer and B. S. Covino, Jr. (Materials Park, OH: ASM International, 2006), 519–530.

52. L. C. Rowl, "Automotive Engine Coolants: A Review of Their Requirements and Methods of Evaluation," in *Engine Coolant Testing: State of the Art* (West Conshohocken, PA: ASTM International, 1980), 3–23.

53. E. Beynon, N. R. Cooper, and H. J. Hannigan, "Cooling System Corrosion in Relation to Design and Materials," in *Designing for Automotive Corrosion Prevention* (Warrendale, PA: SAE International, 1978), 3285–3293.

54. A. V. Gershun and P. M. Woyciesjes, "Engine Coolants and Coolant System Corrosion," in *Corrosion: Environments and Industries*, vol. 13C, ed. S. D. Cramer and B. S. Covino, Jr. (Materials Park, OH: ASM International, 2006), 531–537.

55. C. A. Mesa, *Engine Coolants* (Livonia, MI: Technology Transfer Systems, 2002).

56. H. Z. Abou-Ziyan, "Heat Transfer Characteristics of Some Oils Used for Engine Cooling," *Energy Conversion and Management* 45, no. 15 (2004): 2553–2569.

57. C. Besser, K. Steinschütz, N. Dörr, F. Novotny-Farkas, and G. Allmaier, "Impact of Engine Oil Degradation on Wear and Corrosion Caused by Acetic Acid Evaluated by Chassis Dynamometer Bench Tests," *Wear* 317, no. 1 (2014): 64–76.

58. N. Fatima, I. Minami, A. Holmgren, P. Marklund, and R. Larsson, "Surface Chemistry of Wet Clutch Influenced by Water Contamination in Automatic Transmission Fluids," *Tribology International* 96 (2016): 395–401.

59. T. E. Ryan and T. Hinz, *Analysis of Water Content in Brake Fluid. Part I. Method Comparison: Karl Fisher Titration versus Refractive Index*, Technical Paper Series (Warrendale, PA: SAE International, 1997).

60. B. Kannan, S. Fraley, M. Pollum, R. Fleischauer, and M. L. Lim, "Galvanic Corrosion of Automotive Mixed Metal Substrates: Fundamental Understanding," *ECS Meeting Abstracts* MA2019-02 (2019): 785.

61. R. L. Chance and R. G. Ceselli, *Corrosiveness of Exhaust Gas Condensates*, Technical Paper Series No. 830585 (Warrendale, PA: SAE International, 1983).

62. G. L. Badilla and J. M. T. Gaynor, "Corrosion Analysis in Automotive Electronics," *Materials Performance* 5, no. 4 (2020), http://web.archive.org/web/20210509200120/https://www.materialsperformance.com/articles/material-selection-design/2017/06/corrosion-analysis-in-automotive-electronics

63. L. L. Piepho, L. Singer, and M. R. Ostermiller, "Advancements in Automotive Corrosion Resistance," in *Proceedings of the Corrosion/91 Symposium: Automotive Corrosion and Prevention*, ed. R. Baboian (Houston, TX, NACE International, 1993), 20-1–20-21.

64. D. L. Jordan and J. L. Tardiff, "Automotive Body Corrosion," in *Corrosion: Environments and Industries*, vol. 13C, ed. S. D. Cramer and B. S. Covino, Jr. (Materials Park, OH: ASM International, 2006), 515–518.

65. G. Courval, "Corrosion of Aluminum Components in the Automotive Industry," in *Corrosion: Environments and Industries*, vol. 13C, ed. S. D. Cramer and B. S. Covino, Jr. (Materials Park, OH: ASM International, 2006), 545–547.

66. *Prevention of Corrosion of Motor Vehicle Body and Chassis Components*, J447A_196409 (Warrendale, PA: SAE International, 2016).

67. D. Ellicks, F. Friedersdorf, M. Merrill, and P. Kramer, "Continuous Monitoring of Atmospheric Corrosion and Coating Degradation" (paper presentation, Corrosion/2017, NACE International, New Orleans, LA, April 27, 2017).

68. M. Keller and D. Wagner, "Ford F150" (paper presentation, EuroCarBody 2015 Conference, Bad Nauheim, Germany, Ocrober 21, 2015).

69. M. Liu, Y. Guo, J. Wang, and M. Yergin, "Corrosion Avoidance in Lightweight Materials for Automotive Applications," *NPJ Materials Degradation* 2, no. 1 (2018): 1–4.

70. N. K. Akafuah, S. Poozesh, A. Salaimeh, G. Patrick, K. Lawler, and K. Saito, "Evolution of the Automotive Body Coating Process: A Review," *Coatings* 6, no. 2 (2016): 1–22.

71. T. W. Liskiewicz, K. J. Kubiak, D. L. Mann, and T. G. Mathia, "Analysis of Surface Roughness Morphology with TRIZ Methodology in Automotive Electrical Contacts: Design against Third Body Fretting-Corrosion," *Tribology International* 143 (2020): 106019.

72. T.-H. Tseng and A. T. Wu, "Corrosion on Automobile Printed Circuit Broad," *Microelectronics Reliability* 98 (2019): 19–23.

73. J. H. Payer, "Effect of Environmental Stress of Reliability of Automotive Electronics," in *Proceedings of the Corrosion/91 Symposium: Automotive Corrosion and Prevention*, ed. R. Baboian (Houston, TX: NACE International, 1993), 11-1–11-8.

74. Y.-Z. Lam, C. Maul, and J. W. McBride, "Temperature, Humidity and Pressure Measurement on Automotive Connectors," *IEEE Transactions on Components and Packaging Technologies* 29, no. 2 (2006): 333–340.

75. R. Baboian, *Electrochemical Techniques for Corrosion Engineering* (Houston, TX: NACE International, 1987.

76. W. H. Abbott, "Field vs Laboratory Experience in the Evaluation of Electronic Components and Materials," *Materials Performance* 24, no. 8 (1985): 46–50.

77. S. B. Lyon, G. E. Thompson, and J. B. Johnson, "Materials Evaluation Using Wet-Dry Mixed Salt Spray Tests," in *New Methods for Corrosion Testing of Aluminum Alloys*, ed. V. S. Agarwala and G. M. Ugiansky (Philadelphia, PA: ASTM International, 1992), 20–31.

78. T. S. Doppke and A. W. Bryant, *The Salt Spray Test—Past, Present, and Future*, Technical Paper Series No. 831815 (Warrendale, PA: SAE International, 1983).

79. N. LeBozec, N. Blandin, and D. Thierry, "Accelerated Corrosion Tests in the Automotive Industry: A Comparison of the Performance towards Cosmetic Corrosion," *Materials and Corrosion* 59, no. 11 (2008): 889–894.

80. "Corrosion under Control," Voestalpine Stahl GmbH, 2018, http://web.archive.org/web/20210509200928/https://www.voestalpine.com/ultralights/en/Newsletter/All-Automotive-Notes-articles/Corrosion-under-control

81. J. Hagler and H. Rudolph, "The Influence of Scribing and Evaluation on the Repeatability and Reproducibility of the New Standardized Corrosion Test DIN 55636 (Statistical Analysis of an Interlaboratory Study)," (paper presentation, EUROCORR 2019, Seville, Spain, September 9-13, 2019).

82. N. Van Den Steen, H. Simillion, D. Thierry, H. Terryn, and J. Deconinck, "Comparing Modeled and Experimental Accelerated Corrosion Tests on Steel," *Journal of The Electrochemical Society* 164, no. 9 (2017): C554–C562.

83. S. Ramamurthy, R. D. Davidson, N. S. McIntyre, G. Courval, and J. Allin, "Corrosion Product Analysis of Aluminum Closure Panels" (paper presentation, SAE 2005 World Congress and Exhibition, Detroit, MI, April 11–14, 2005).

84. T. Nakayama, H. Shige, L. Vega, and E. Colvin, *Correlation between Accelerated Laboratory Tests and Field Tests for Filiform Corrosion of Painted Aluminum Alloy Sheets for Automobiles*, Technical Paper Series (Warrendale, PA: SAE International, 2003).

85. N. C. Hosking, M. A. Ström, P. H. Shipway, and C. D. Rudd, "Corrosion Resistance of Zinc–Magnesium Coated Steel," *Corrosion Science* 49, no. 9 (2007): 3669–3695.

86. J. L. Delplancke, S. Berger, X. Lefèbvre, D. Maetens, A. Pourbaix, and N. Heymans, "Filiform Corrosion: Interactions between Electrochemistry and Mechanical Properties of the Paints," *Progress in Organic Coatings* 43, nos. 1–3 (2001): 64–74.

87. N. LeBozec, D. Persson, D. Thierry, and S. B. Axelsen, "Effect of Climatic Parameters on Filiform Corrosion of Coated Aluminum Aloys," *Corrosion* 60, no. 6 (2004): 584–593.

88. P. Visser, Y. Liu, X. Zhou, T. Hashimoto, G. E. Thompson, S. Lyon, L. van der Ven, J. M. C. Mol, and H. Terryn, "The Corrosion Protection of AA 2024-T3 Aluminium Alloy by Leaching of Lithium-Containing Salts from Organic Coatings," *Faraday Discussions* 180 (2015): 511–526.

89. N. Hosking and M. E. Nichols, *Corrosion Testing of Multi-Material Lightweight Vehicle (MMLV) Body Structure*, Ford Research Laboratory Technical Report SRR-2015-0187, (Dearborn, MI: Ford Motor Company, 2015).

90. N. LeBozec and D. Thierry, "Influence of Climatic Factors in Cyclic Accelerated Corrosion Test towards the Development of a Reliable and Repeatable Accelerated Corrosion Test for the Automotive Industry," *Materials and Corrosion* 61, no. 10 (2010): 845–851.

91. N. LeBozec, A. LeGac, and D. Thierry, "Corrosion Performance and Mechanical Properties of Joined Automotive Materials," *Materials and Corrosion* 63, no. 5 (2012): 408–415.

92. *Proving Ground Vehicle Corrosion Testing*, J1950_198905 (Warrendale, PA: SAE International, 2016).

93. R. J. Santucci, M. D. Holleman, and J. R. Scully, "Laboratory Accelerated and Field Exposure Testing of MgRP and MgORP on AA2024-T351: Chemical and Electrochemical Protection Effects," *Surface and Coatings Technology* 383 (2020): 125245.

94. D. Thierry, D. Persson, G. Luckeneder, and K.-H. Stellnberger, "Atmospheric Corrosion of ZnAlMg Coated Steel during Long Term Atmospheric Weathering at Different Worldwide Exposure Sites," *Corrosion Science* 148 (2019): 338–354.

95. W. D. Ganther, D. A. Paterson, C. Lewis, P. Isaacs, S. Galea, C. Meunier, G. Mangeon, and I. S. Cole, "Monitoring Aircraft Microclimate and Corrosion," *Procedia Engineering* 188 (2017): 369–376.

96. I. S. Cole, W. D. Ganther, S. A. Furman, T. H. Muster, and A. K. Neufeld, "Pitting of Zinc: Observations on Atmospheric Corrosion in Tropical Countries," *Corrosion Science* 52, no. 3 (2010): 848–858.

97. *Undervehicle Coupon Corrosion Tests*, J1293_201604 (Warrendale, PA: SAE International, 2016), https://doi.org/10.4271/J1293_201604

98. A. W. Bryant, *1985 Body Corrosion Field Survey: 5 and 6 Year Old Vehicles*, Technical Paper Series No. 862025, (Warrendale, PA: SAE International, 1986).

99. A. C. Tiburcio and M. J. Yergin, *U.S. Automotive Corrosion Trends: 1998 SAE (ACAP) Automotive Body Corrosion Survey Results*, Technical Paper Series No. 2003-01-1244 (Warrendale, PA: SAE International 2003).

100. J. J. Garcia, *Exhaust Gas Condensate Corrosion Test on Low Pressure Cooling System of Aluminum Brazed EGR, ACAC and WCAC*, Technical Paper Series No. 2012-01-1947 (Warrendale, PA: SAE International, 2012).

101. J. Hirasawa, T. Ujiro, S. Satoh, and O. Furukimi, *Development of High Corrosion Resistant Stainless Steels for Automotive Mufflers Based on Condensate Corrosion Test and Field Investigation*, Technical Paper Series No. 2001-01-0640 (Warrendale, PA: SAE International, 2001).

102. H. Ohtani, P. A. Willermet, J. W. Sprys, J. L. Linden, J. E. Flaherty, T. E. King, M. Kagawa, et al., *Oxidation Stability of Automatic Transmission Fluids: A Study by the International Lubricants Standardization and Approval Committee (ILSAC) ATF Subcommittee*, Technical Paper Series No. 2001-01-1991 (Warrendale, PA: SAE International, 2001).

103. J. K. Thomson, S. J. Pawel, and D. F. Wilson, "Susceptibility of Aluminum Alloys to Corrosion in Simulated Fuel Blends Containing Ethanol," *Fuel* 111 (2013): 592–597.

104. H. Jafari, M. H. Idris, A. Ourdjini, H. Rahimi, and B. Ghobadian, "EIS Study of Corrosion Behavior of Metallic Materials in Ethanol Blended Gasoline Containing Water as a Contaminant," *Fuel* 90, no. 3 (2011): 1181–1187.

105. M. S. Thomson and G. S. Frankel, "Atmospheric Pitting Corrosion Studies of AA7075-T6 under Electrolyte Droplets: Part I. Effects of Droplet Size, Concentration, Composition, and Sample Aging," *Journal of The Electrochemical Society* 164, no. 12 (2017): C653–C663.

106. N. LeBozec, L. Bougon, J. Carter, T. Scholz, O. Oystein Knudsen, and A. Flogard, "Round-Robin Evaluation of ISO 20340 Annex a Test Method" (paper presentation, Corrosion/2016, Vancouver, BC, Canada, March 6–10, 2016).

107. H. E. Townsend and D. C. McCune, "Round-Robin Evaluation of a New Standard Laboratory Test for Cosmetic Corrosion" (paper presentation, SAE International Congress and Exposition, Detroit, MI, February 24, 1997).

108. E. Diler, F. Lédan, N. LeBozec, and D. Thierry, "Real-Time Monitoring of the Degradation of Metallic and Organic Coatings Using Electrical Resistance Sensors," *Materials and Corrosion* 68, no. 12 (2017): 1365–1376.

109. M. E. Parker and R. G. Kelly, "Improved Atmospheric Corrosion Testing for Aluminum Alloys, Part I: Deconstructing ASTM G85-A2," *Corrosion* 76, no. 1 (2020): 39–50.

110. M. E. Parker and R. G. Kelly, "Improved Atmospheric Corrosion Testing for Aluminum Alloys, Part II: Developing Improved Testing Protocol," *Corrosion* 76, no. 1 (2020): 51–62.

111. N. Van den Steen, H. Simillion, O. Dolgikh, H. Terryn, and J. Deconinck, "An Integrated Modeling Approach for Atmospheric Corrosion in Presence of a Varying Electrolyte Film," *Electrochimica Acta* 187 (2016): 714–723, http://doi.org/10.1016/j.electacta.2015.11.010

112. M. Mandel and L. Krüger, "Determination of Pitting Sensitivity of the Aluminium Alloy EN AW-6060-T6 in a Carbon-Fibre Reinforced Plastic/Aluminium Rivet Joint by Finite Element Simulation of the Galvanic Corrosion Process," *Corrosion Science* 73 (2013): 172–180.

113. S. Palani, T. Hack, J. Deconinck, and H. Lohner, "Validation of Predictive Model for Galvanic Corrosion under Thin Electrolyte Layers: An Application to Aluminium 2024-CFRP Material Combination," *Corrosion Science* 78 (2014): 89–100.

Chapter 24 | Commercial Aircraft

Edward L. Colvin[1]

Introduction

Corrosion of aircraft structures has plagued the airline industry since the first use of metals in aircraft manufacture. It is costly both in unscheduled downtime and maintenance. The International Air Transport Association (IATA) reported in 1983 that corrosion costs the airlines between $8 and $20 per flight hour.[1] These numbers did not reflect the unscheduled downtime, both at the main bases and route stations, nor the additional corrosion inspections of aging airplanes recently mandated by the regulatory agencies. In fact, unlike fatigue damage, corrosion is extremely difficult to predict (i.e., when and where it will start, how fast it will progress, or how much damage it will cause). Because of this unpredictability, corrosion inspections are an integral part of an airline's maintenance program and make up a significant part of its cost.

Corrosion problems on commercial aircraft are the result of combinations of factors whose causes can be found in the basic design, manufacturing, materials interactions and operations of the aircraft. Some of these factors are summarized in table 1 (manufacturer) and table 2 (operator and service environment). These present unique problems to the manufacturer who must make the best design, materials, and process choices that are compatible with structural requirements and the economics of building and operating an airplane. To achieve these ends, deliberate and comprehensive corrosion evaluations and risk assessments must be conducted before establishing requirements for design, structural materials and compatible finish systems, as well as the numerous manufacturing protocols, interior materials, and operational maintenance fluids that will ensure the structural integrity of the aircraft during its useful life.

In addition, anticipation and consideration of factors whose presence may at times be accidental in the operation of the airplane is necessary to the selection of the appropriate standardized corrosion tests. Sometimes test modifications, which account for these factors, are necessary, and it is especially important to recognize that no one accelerated, laboratory corrosion test can possibly simulate all situations that a fleet of airplanes may experience during service. With over 60 years of service history on commercial jet aircraft, corrosion problems continue to be addressed systematically and evaluated with deliberate processes and intent around the world and in many adjacent applications.[2] Many improvements that are being incorporated into today's new aircraft would not have been possible without laboratory and outdoor corrosion tests.

TABLE 1 Contributing Causes of Corrosion—Manufacturer Related

Causes	Factors
Basic Design	• Anticipated operating environments • Materials selection • Dissimilar metals • Finish system • Drainage • Crevices • Pockets and cavities • Access to structure • Process selection • Maintenance schedules and protocols
Manufacturing	• Assembly and residual stresses • Metal finishing process control • Bonding process control • Inspection
Processing	• Assembly quality and misfits • Handling of parts and structures • Storage of parts and structures

Service Environments

Environmental conditions inside and outside an airplane vary considerably from one operator to another. Factors that influence environments include airplane interior configuration, an airline's geographic location, route structure, and world climatic conditions. The commercial jet airplane is designed to be a self-contained

[1]HELM Technology, LLC , 1423 Simmonsville Rd., Newport, VA 24128, USA
The author acknowledges the previous authors of this chapter, A. A. Adjorlolo and J. A. Marceau, The Boeing Company, Seattle, WA.

DOI: 10.1520/MNL202NDSUP20190033

Copyright © 2022 by ASTM International, 100 Barr Harbor Dr., PO Box C700, West Conshohocken, PA 19428-2959
ASTM International is not responsible, as a body, for the statements and opinions expressed in this chapter. ASTM International does not endorse any products represented in this chapter.

TABLE 2 Contributing Causes of Corrosion—Service Related

Causes	Factors
Finish Deterioration	• Chipping • Scratches • Breaks around fasteners • Abrasion • Deposits • Age
Environmental Conditions within Airplane	• Skydrol (hydraulic fluid) • Condensation • Animals (cargo) • Fish (cargo) • Microbial growth
Accidental Contamination	• Lavatory spills • Galley spills • Cargo spills • Chemical spills • Mercury • Fire smoke and extinguisher residues
Operational Environment	• Seacoast • Tropical environment • Humidity • Industrial environment • Ground-air ground cycle
Maintenance Problem Areas	• Neglect • Improper repairs • Inadequate corrosion control program or lack of implementation • Inadequate training • Ignorance of corrosion • Plugged drain systems

pressurized vessel that creates a comfortable living environment for flight durations of less than 0.5 min to longer than 12 h. Inside the fuselage, the air is conditioned for the comfort of passengers. Galleys (food stations) are provided for food and drink, and lavatories are provided for the needs of passengers.

Creating these passenger comforts directly results in localized environments that are unique, and if the structural components are not properly protected, these environments can be aggressive to structural components. Aqueous solutions form the essential basis for corrosion of many metallic materials, such as aluminum alloys, steels, and bimetallic structures. For instance, fluids from food and drink spillage drain under floor panels. Trapped in crevices between the floor panels and the underlying structure, these fluids fester and become a corrosive solution for the structural components. The same is true for lavatory fluids, which can leak and become trapped between the flooring and floor structure; excess fluids from galleys and lavatories will flow to the bilge; and entryways (e.g., passenger, service, and cargo) are exposed to the weather and occasional spills, which all combine to generate a corrosive environment that also flows beneath the floor structure to the bilge.

The rest of the fuselage interior is regularly exposed to condensing humidity caused by colder temperatures that result from the ground-air-ground flight cycle. Although this condensate is initially fairly benign compared with the fluids encountered under galleys and lavatories, it can absorb other chemical species and accelerate corrosion and structural damage processes, such as fatigue and fatigue crack growth.

The exterior surfaces of airplanes are always exposed to the elements, and hence, are affected by world and local climatic conditions, including rain, humidity, airborne industrial pollutants, hot and/or cold temperatures, dust, runway dirt, and spray from the oceans and seas. Corrosive contaminants trapped in exterior cavities and cove areas (e.g., wheel wells, wing front and rear spar cove areas, and fairing areas) are not washed off by rain in contrast to aerodynamic surfaces, thereby compounding potential corrosion problems.

Techniques Used to Control Corrosion

The primary defenses for corrosion control of the airplane structure are proper design, material selection, finishing systems, and maintenance protocols. For the first three, which are built into the airplane, intelligent corrosion evaluation of metals, assemblies, and compatible finish systems must inform their selection. The tests for evaluating these materials, assemblies, and finishes depend on the function and the anticipated environmental exposure of the component parts. Finishes that will be used during repairs must have been demonstrated that they can be applied locally over surface preparations accomplished in the field under less-than-optimum conditions. Techniques available to the airlines for controlling corrosion involve (1) maintaining drain holes open for proper drainage of condensed moisture, (2) restoring the finish, and (3) using corrosion inhibiting compounds to protect the paint in problem areas and to drive trapped moisture from joints and crevices.

Many of the corrosion tests described in the section "Use of Test Methods to Evaluate Corrosion" are used routinely in the materials and aircraft industries to evaluate materials, components, and finish systems. The tests specifically aim to assess expected performance during long-term service, usually relative to an incumbent material, finish, or process with well-established in-service capability. It is essential that interactions among the material, finish, and processing be considered in the testing protocol, including specimen design. Because laboratory tests represent relatively short-term exposures compared with the lives of airplanes, and cannot always simulate the inherent variability in-service airplanes experience, the rationale used to establish test duration and protocols must be relevant. It may be necessary to use multiple predictive tests to account for these various service conditions. To provide context for the accelerated tests, various organizations, industry, government, and independent laboratories have devoted extensive resources to long-term testing in natural and service environments, such as seacoast and industrial sites.[3,4]

IN-SERVICE MONITORING

Despite the obvious economic advantage of allowing airlines the ability to disassemble a structure for repairs only when corrosion is known to exist in certain areas, *in situ* monitoring of corrosion is not practiced in the industry. The resulting monitoring system's complexity, added weight, and future certification issues are certainly negative factors. The authors are aware of only one instance of experimentation with sensors in U.S. commercial aviation to detect the presence of moisture in certain areas prone to corrosion, such as floor support structure. A system using an optical fiber-based sensor and data acquisition system is being field-tested. This system was described at an Aging Aircraft 2000 Conference.[5]

Currently, in-service monitoring of corrosion on commercial airplanes is accomplished by inspection during routine maintenance checks. Although most airlines have corrosion control programs implemented in their maintenance programs, the regulatory agencies recently have required mandatory corrosion inspections based on calendar time rather than airplanes' cumulative flight hours, as well as defining the specific areas to be inspected and at what frequency. For instance, a known problem area, such as the fuselage bilge, is inspected much more frequently than the crown (ceiling) area. These directed inspections, such as FAA-mandated Corrosion Prevention and Control Program (CPCP), assign levels of 1, 2, and 3 to corrosion findings. These levels relate to the amount of material blend-out required to remove the corrosion occurring between repeat inspections (level 1 or 2) and identify whether airworthiness concerns exist (level 3) with specific corrosion findings.

INSPECTION

Inspection for corrosion is conducted primarily by visual methods, requiring very good access to the structure and the ability to recognize various forms of corrosion, their early signs in different metallic structures, or conditions leading to corrosion, such as finish damage and blocked drains. Other difficult-to-access areas may require borescope inspection. In some cases of hidden structure, such as lap joints, nondestructive inspection (NDI) techniques, such as eddy current or X-ray (radiography), may be used. Ultrasonic inspection has the advantage of detecting small cracks that may appear in corroded locations. Because some of these techniques may require significant amounts of material loss for detection, are complex, and require high technician skills, visual observation of a partially opened lap joint is necessary to determine the full extent of the corrosion.

Specific Problem Areas

Most corrosion problems on commercial aircraft are associated with aluminum alloys in part because material selection has focused on maximizing mechanical and damage-tolerant properties, such as fracture toughness, thus sacrificing the better corrosion resistance of lower strength alloy systems used in marine, building, industrial, and transportation applications. For these high-strength alloy systems used in aerospace, tempers such as 2xxx-T8X and 7xxx-T7X have been developed to improve resistance to intergranular forms of corrosion such as intergranular, exfoliation, and stress-corrosion cracking,[6] for which specific ratings are listed in ASTM G64, *Standard Classification of Resistance to Stress-Corrosion Cracking of Heat-Treatable Aluminum Alloys*. To varying degrees, all of the high-strength alloys used are susceptible to corrosion and must be protected appropriately; protection systems have become especially important in multimaterial structures that utilize increasing amounts of carbon-fiber reinforced composites and titanium, both of which are galvanically cathodic to aluminum alloys requiring appropriate protection systems for the aluminum, especially systems that will electrically isolate aluminum from the other materials.

Corrosion protection of the aluminum alloys relies primarily on alloy-temper selection and the protection systems used. Anodic, or sacrificial, protection can be used in specific situations. The largest use is aluminum cladding applied to aluminum sheet used for fuselage skins; the Alclad layer consists of a relatively pure aluminum alloy that protects the high strength core. Plated, thermal, and vapor-deposed coatings also have been used, especially for fasteners that often have metallic coatings that provide sacrificial protection. Barrier protection systems, including anodizing, conversion coatings, primers, sealants, etc., typically fail at joints, faying surfaces, or crevices where water and aggressive electrolytes can become trapped for long periods of time. Crevices can be created by many conditions, (e.g., joints, poorly adhering paint, insulation blankets against structure in wet areas, etc.). Although coatings are helpful, control of certain forms of corrosion, such as stress corrosion cracking (SCC) and exfoliation, should focus on material selection, because once a barrier coating has been breached, the environment will propagate with the corrosion to the interior of the metal.[7]

When corrosion problems exist in the highly susceptible areas described in the previous section, they are greatly compounded. Other potentially corrosive conditions would include dissimilar metal couples—for example, an aluminum-nickel-bronze bushing in an aluminum alloy housing or an aluminum hinge fitting attached to a carbon fiber–reinforced plastic control surface (e.g., elevator, aileron, etc.). Some of these conditions are unavoidable; therefore, it is extremely important that the proper finish protection schemes be incorporated.

Use of Test Methods to Evaluate Corrosion

The foregoing discussions on airplane corrosion problems, service environments, techniques for corrosion control, and problem areas underscore the need for comprehensive corrosion testing, including sound rationale and methods. Table 3 summarizes the corrosion tests used in the commercial airplane industry, including names of the tests, how they are used, the type of information sought, and the type of comparative control used. These tests primarily address alloys, coatings, manufacturing aids or process evaluation, and also service conditions. The tests, particularly those from ASTM, lend themselves to multiple applications (e.g., there are many uses of the salt spray test—ASTM B117, *Standard*

TABLE 3 Corrosion Tests Conducted in the Commercial Airplane Industry

General Test Name	Where Used (Alternate Test Name)	Information Sought	Control
EXCO Test (ASTM G34, *Standard Test Method for Exfoliation Corrosion Susceptibility in 2XXX and 7XXX Series Aluminum Alloys (EXCO Test)*)	Alloy evaluation	Resistance to exfoliation corrosion after 48 to 96 h immersion in test solution	Conventional alloy and/or thermomechanical treatment
Modified ASTM Acetic Acid Salt Intermittent Spray-MASTMAASIS (ASTM G85, *Standard Practice for Modified Salt Spray (Fog) Testing*)	Alloy evaluation	Resistance to exfoliation corrosion after 14 to 28 days exposure	Conventional alloy and Al-Li treatment
3.5% NaCl Alternate Immersion (ASTM G44, *Standard Practice for Exposure of Metals and Alloys by Alternate Immersion in Neutral 3.5% Sodium Chloride Solution*)	Alloy evaluation	SCC resistance per ASTM G47 Resistance to pitting of unstressed specimens	Conventional alloy
Double Cantilever Beam (ASTM G168, *Standard Practice for Making and Using Precracked Double Bean Stress Corrosion Specimens*)	Alloy evaluation	SCC growth rate, threshold K1scc	Conventional alloy
Electrochemical Tests	Alloy evaluation. Paint/coating evaluation	Passivation characteristics (ASTM G5) Corrosion rates Pitting/protection potentials (ASTM G61, *Standard Test Method for Conducting Cyclic Potentiodynamic Polarization Measurements for Localized Corrosion Susceptibility of Iron-, Nickel-, or Cobalt-Based Alloys*) Corrosion potential (ASTM G69, *Standard Test Method for Measurement of Corrosion Potentials of Aluminum Alloys*) Polarization resistance Galvanic corrosion Impedance spectrum (ASTM G106, *Standard Practice for Verification of Algorithm and Equipment for Electrochemical Impedance Measurements*)	Conventional alloy Conventional paint/coating
Notched Tension Test (ASTM F519, *Standard Test Method for Mechanical Hydrogen Embrittlement Testing of Plating/Coating Processes and Service Environments*)	Alloy evaluation	Resistance to hydrogen embrittlement	Conventional alloy
	Maintenance fluid evaluation	Potential to cause hydrogen embrittlement on AISI4340 steel per ASTM F519, *Standard Test Method for Mechanical Hydrogen Embrittlement Evaluation of Plating/Coating Processes and Service Environments*, Section 7.2	Conventional fluid
	Plating process evaluation	Resistance to hydrogen embrittlement of plated AISI 4340 per ASTM F519, Section 7.3	Specification requirement per ASTM F519, Section 7.3
Intergranular Attack/End Grain Pitting (IGA/EGP) (ASTM G110, *Standard Practice for Evaluating Intergranular Corrosion Resistance of Heat Treatable Aluminum Alloys by Immersion in Sodium Chloride + Hydrogen Peroxide Solution*)	Process assessment and quality control evaluation (deoxidizer/cleaner)	Potential to cause end grain pitting or intergranular attack in excess of recommended limits	Aluminum alloys 2x24-T3, 7178-T6X, 7075-T65X
Filiform Corrosion Test (ASTM D2803, *Standard Guide for Testing Filiform Corrosion Resistance of Organic Coatings on Metal*)	Metal surface preparation processes and paint evaluation	Resistance to filiform corrosion *Vi* in. (3.2 mm) beyond line scribed on a painted panel specimen pre-exposed to HC1 vapor and held at 104 °F at 80 % RH for 1,000 h	Conventional organic coatings
Salt (Fog) Spray (ASTM B117, *Standard Practice for Operating Salt Spray (Fog) Apparatus*)	Alloy evaluation	General corrosion, pitting resistance after 30 days, 90 days, or one-year exposure	Conventional alloy
Modified Salt Spray (Fog) Test (ASTM G85, *Standard Practice for Modified Salt Spray (Fog) Testing*)	Chemical conversion coating/process evaluation	Resistance to pitting after 168 h exposure period (ASTM G117 only per specification)	Conventional chemical coating/qualified process
Outdoor Environmental Exposures	Anodizing/process evaluation Paint/alloy evaluation (scribed line test)	Resistance to pitting after 336 h exposure period (ASTM B117 only per specification) Resistance of scribed line to corrosion after predetermined exposure period; loss of adhesion; blistering	Conventional chemical coating/qualified process Paint over conventional alloys or conventional paint over alloy

(continued)

TABLE 3 (*continued*)

General Test Name	Where Used (Alternate Test Name)	Information Sought	Control
	Paint/alloy evaluation (fastener insulation test)	Resistance to corrosion around fastener heads; rating per ASTM D1654, *Standard Test Method for Evaluation of Painted or Coated Specimens Subjected to Corrosive Environments*	Paint over conventional alloys or conventional paint over alloy
	Paint/alloy evaluation (Al/CRES or CFRP coupling)	Resistance to corrosion aided by galvanic coupling; rating per ASTM D1654	Paint over conventional alloys or conventional paint over alloy
	All adhesive bonding process evaluation (metal/metal) (Lap Shear Corrosion Test)	Reduction in lap shear strength after exposure for predetermined period	Qualified adhesive/primer over recommended surface preparation
	All adhesive bonding process evaluation (metal/metal) (Wedge Corrosion Test)	Crack growth rate after exposure to salt spray for 30, 60, and 90 days, or longer	Same as above
All adhesive bonding process evaluation (metal/metal) (Double Cantilever Test)	Crack growth after exposure to neutral salt spray for one year or longer; resistance to galvanic corrosion	Same as above	
Titanium Compatibility Test	Manufacturing aids evaluation (lubricants/coolant)	Potential of fluid considered to cause pitting, cracking, or rough etching on titanium	Currently qualified material
Evaporation Corrosion Test	Manufacturing aids evaluation (lubricants/coolant)	Potential for pitting caused by fluid left to evaporate on machined alloy after 7 days	Currently qualified fluid
	Interior materials (silicone rubber-coated fabric, floor covering, carpet and underlay, thermal/ acoustical insulation, flame-resistant polymer-coated fabric, Nomex felt, etc.)	Assessment of the corrosivity of water-leachable species from tested materials left to evaporate on 2024-T3 aluminum after 7 days	Deionized or distilled water
	R&D (evaluation of corrosion inhibitors; maintenance fluids, and various extracts)	General corrosivity and pitting caused by water soluble extract from material of interest left to evaporate on 2024-T3 aluminum after 7 days	Deionized, 3.5% NaCl, or distilled water
	Manufacturing aids evaluation (lubricants and coolants)	Resistance to general corrosion or staining caused by fluid entrapment on 7075-T6, 2024-T3 bare or clad Al alloys	Deionized, distilled water, or conventional fluid
	Maintenance fluids evaluation	Resistance to general corrosion or staining caused by fluid entrapment on 7075-T6, 2024-T3 bare or clad Al alloys	Deionized, distilled water, or conventional fluid
Immersion Test (ASTM F483, *Standard Practice for Total Immersion Corrosion Test for Aircraft Maintenance Chemicals*)	Manufacturing aids (lubricants and coolants) evaluation	Resistance to weight loss of AISI 4130 and 2024-T3, 7075-T6 Al alloys in fluid of interest	None—Allowable weight loss table
	Maintenance fluids evaluation	Resistance of selected aerospace aluminum, steel, titanium, and magnesium alloys, cadmium plate, to weight loss in fluid of interest; Resistance to galvanic corrosion	None—Allowable weight loss table
Galvanic Entrapment	Manufacturing aids (cuttings fluids and greases) evaluation	Resistance to crevice corrosion caused by test fluid entrapment between drilled and fastened Al/Cad plated steel/Ti stackup	Deionized water, conventional fluid
Stress Corrosion Test	Manufacturing aids evaluation (lubricants and coolants)	Resistance to corrosion crack growth, pitting on precracked, 50 ksi$\sqrt{\text{in}}$ prestressed specimens immersed for 24 h in test fluid, and in ambient environment for 76 h minimum	Conventional fluid
Drip Test	Titanium/coating evaluation	Resistance to hydraulic fluid of coating and substrate at various temperatures (usually 450 °F)	Bare 6A1-4V titanium specimen

Practicing for Operating Salt Spray (Fog) Apparatus). Alternately, multiple tests are available to evaluate a particular corrosion issue (e.g., pitting can be evaluated using many different tests).

The following detailed discussion explains why some of these tests are used in the selection of materials and processes. Importantly, no single laboratory test method, or even natural environmental exposure, can simulate all possible environments that the materials and structures of an in-service aircraft may see over 20 to 50 years of service. To the extent possible, designers and those making material selections must anticipate the service conditions and evaluate design choices using a menu of tests for various corrosion morphologies, such as exfoliation, SCC, pitting, intergranular, etc., as well as assembly conditions, such as galvanic cells, sealants, and coatings.

MATERIALS SELECTION

The desirability of light structures for increasing payloads in commercial aircraft design dictates the use of materials with high strength-to-weight ratios. High-strength aluminum alloys, 7xxx- and 2xxx-series, and their tempers, are evaluated for their integrity in environments likely to cause exfoliation and SCC. Steels must demonstrate that they are no more susceptible to hydrogen embrittlement and SCC than conventional high-strength, low-alloy (HSLA) steels. These represent the most commonly used ferous alloys and also are the most susceptible to hydrogen embrittlement.

ALUMINUM ALLOY/HEAT-TREAT EVALUATION

Exfoliation corrosion is the flake-like degradation of high-strength aluminum alloys caused by corrosion product forming along the elongated grain boundaries of sheet, plate, forgings, or extrusions, which act as propagation paths for corrosion processes. Susceptibility to exfoliation corrosion is predicted by testing in accordance with ASTM G34, *Standard Test Method for Exfoliation Corrosion Susceptibility in 2XXX and 7XXX Series Aluminum Alloys (EXCO Test)*, and ASTM G85, *Standard Practice for Modified Salt Spray (Fog) Testing*, Annex A2. Proper choice of exfoliation corrosion test varies by alloy type; a very good discussion of the proper test environment by alloy forms the core of ASTM G112, *Standard Guide for Conducting Exfoliation Corrosion Tests in Aluminum Alloys*. For example, ASTM G85 (i.e., the MASTMAASIS test with Dry Bottom conditions) has been demonstrated to more accurately predict seacoast performance of aluminum-lithium (Al-Li) alloys and certain 2xxx alloy-tempers than EXCO. This and other environmental factors responsible for exfoliation are difficult to integrate into one laboratory test, and ideally, one would like to expose the materials in outdoors for two or more years depending on severity of the local environment.

Several test methods currently are used for the testing of SCC in aluminum alloys, including ASTM G47, *Standard Test Method for Determining Susceptibility to Stress-Corrosion Cracking of 2XXX and 7XXX Aluminum Alloy Products*, in conjunction with ASTM G44, *Standard Practice for Exposure of Metals and Alloys by Alternate Immersion in Neutral Sodium Chloride Solution*. The double-cantilever beam test per ASTM G168, *Standard Practice for Making and Using Precracked Double Bean Stress Corrosion Specimens*,[5] and the breaking load test per ASTM G139, *Standard Test Method for Determining Stress-Corrosion Cracking Resistance of Heat-Treatable Aluminum Alloy Products Using Breaking Load Method*, also have been used to that effect. The contrasting performance of SCC-resistant 7075-T73X and 7075-T74X aluminum products, against that of 7079-T6, replaced by the more SCC-resistant alloys in the 1960s and 1970s, is a reflection of the implementation of these two test methods.

Note that for certain tempers, with somewhat improved exfoliation or SCC resistance, the material may take longer to exhibit attack and the performance of the material may be more variable. The precision and bias statement in ASTM G47 describes just such a situation for a laboratory temper with intermediate SCC resistance.

TESTING OF HIGH-STRENGTH STEELS

Because most high-strength steels have requirements for chromium, low-embrittlement cadmium, or cadmium-titanium plating, their selection is dictated by their ability to be processed in a way that avoids the hydrogen-embrittling effects of these processes. Requirements for avoiding hydrogen embrittlement in AISI 4340 steel establish a baseline that must be met by any new alloy. A notch tensile test generally is performed using AISI 4340 as control material and evaluated according to ASTM F519, *Standard Test Method for Mechanical Hydrogen Embrittlement Evaluation of Plating/Coating Processes and Service Environments*.

PAINT EVALUATION

Paints are used on a wide variety of materials and parts as a means to protect the underlying metal and generally are the first line of defense. The paint itself must adhere to the substrate under dry, humid, or wet conditions, a requirement that underscores the critical nature of a base surface preparation. The ability of the paint to protect against corrosion is evaluated using ASTM G85 and ASTM B117 for a test duration of 1,000–3,000 h on scribed surfaces, with fasteners installed, or on specimens galvanically coupled to a more noble metal. These tests are designed to simulate accidental scratch marks, corrosion-prone areas, or conditions that accelerate corrosion.

SURFACE FINISHES EVALUATION

ASTM B117 is the standard test typically used for evaluating the corrosion resistance of unpainted aluminum alloy surfaces when treated by anodizing, conversion coating, and plating processes aluminum surfaces, which are anodized and then sealed for corrosion protection. These surfaces must be able to resist the salt spray environment for at least 336 h without pitting. Conversion-coated surfaces must resist the salt spray environment for at least 168 h. Cadmium plate on ferrous or copper alloys must also resist this environment for 96 h without showing base metal or cadmium corrosion. Although it is generally agreed in industry that the salt spray test is used too broadly, individual pass/fail criteria developed for each process have helped detect and monitor process problems. For example, ASTM G85 has

been shown to be useful for coated aluminum.[8] Alternate testing methods (e.g., electrochemical tests) are under development and have found limited use to aid in the evaluation of alloys and finishes.

Conclusion

The multiplicity of external environments, the unpredictability of various spillage inside an airplane, the influence of environmental and loading cycles on material and finishes, and the long design life of an airplane account for the main difficulties encountered in selecting and conducting the most appropriate laboratory corrosion tests to evaluate commercial airplane. As a large amount of data from the commercial airplane fleet has become available, service history has emerged as the most important criterion in validating design choices, modifying the corrosion tests, and developing better test acceptance criteria. Materials with improved corrosion resistance, such as Al-Li alloys, which have been demonstrated to perform well in severe environments, can improve durability.[9]

The history of airplane corrosion testing includes many successful tests that are now performed routinely (e.g., ASTM **G85** Annex A2, and ASTM **G44**). Some other successful tests, such as the wedge test (ASTM **D3762**, *Standard Test Method for Adhesive-Bonded Surface Durability of Aluminum [Wedge Test] [Withdrawn 2019]*), discovered as a result of bond line corrosion problems on airplanes, are not described here because they are not strictly corrosion tests. Many of the tests described here are current ASTM standards. As discussed previously in this chapter, addressing specific circumstances, including environment, structure, and dissimilar metals, may require refinements to these standard tests and even may require completely different, dedicated test protocols designed to address specific applications. As the industry progresses, improved understanding of the fundamental interaction between environmental factors and dynamic loads will take the airplane industry closer to the ultimate goal of minimizing corrosion costs and failures in aircraft.

References

1. International Air Transport Association (IATA), *Guidance Material on Design and Maintenance against Corrosion of Aircraft Structures*, DOC GEN/2637A, Issue 2 (Montreal, Canada: IATA, November 1983).
2. R. Wanhill and M. Wisndisch, *Corrosion and Stress Corrosion Testing of Aerospace Vehicle Structural Alloys*, Briefs in Applied Sciences and Technology (Cham, Switzerland: Springer, 2018).
3. J. J. Thompson, "Exfoliation Corrosion Testing of Aluminum Lithium Alloys," in *New Methods for Corrosion Testing of Aluminum Alloys*, ed. V. S. Agarwala and G. M. Ugiansky (Philadelphia, PA: ASTM International, 1992), 70–81.
4. S. Dean and W. Anthony, "Atmospheric Corrosion of Wrought Aluminum Alloys during a Ten-Year Period," in *Degradation of Metals in the Atmosphere*, ed. S. Dean and T. Lee (West Conshohocken, PA: ASTM International, 1987), 191–205.
5. J. L. Elster, A. Trego, M. Jones, P. Tulou, B. Fitzpatrick, and I. Perez, "Corrosion Monitoring in Aging Aircraft Using Optical Fiber-Based Chemical Sensors" (paper presentation, DOD/NASA/AFRL Aging Aircraft 2000 Conference, St. Louis, KS, May 15–18, 2000).
6. J. E. Hatch, ed., *Aluminum Properties and Physical Metallurgy* (Metals Park, OH: ASM International, 1984).
7. D. O. Sprowls and R. H. Brown, "What Every Engineer Should Know about Stress-Corrosion Cracking of Aluminum Alloys," *Metal Progress* 81, no. 4 (1962): 77–83, 118–122.
8. E. L. Colvin, L. F. Vega, T. Nakayama, K. Ikeda, H. Shige, T. Ueda, M. W. Egbert, and M. Inman, *Filiform Corrosion of Aluminum Auto Body Sheet in Accelerated and Outdoor Environments*, Technical Paper Series No. 970735, (Warrendale, PA: SAE International, 1997).
9. J. P. Moran, F. S. Bovard, J. D. Chrzan, R. J. Rioja, and E. L. Colvin, "Improvements in Corrosion Resistance Offered by Newer Generation 2x99 Aluminum-Lithium Alloys for Aerospace Applications," in *Proceedings of the 12th International Conference on Aluminum Alloys* (Yokohama, Japan: Japan Institute of Light Metals, 2010), 1492–1497.

Chapter 25 | Military Aircraft and Associated Equipment

Diane Buhrmaster[1] and Nicholas Wilson[1]

Introduction

This chapter discusses the typical corrosion tests used to verify the performance of military equipment, from basic components to fully mission-capable ordinance, aircraft, space vehicles, and supporting equipment. For military operations, corrosion is defined as the deterioration of a material or its properties because of a reaction of that material with its chemical environment. Military aircraft, ordinance, space equipment, and supporting equipment must be designed to operate for long periods of time in extreme environments. This includes from the Arctic Circle to the equator, desert to the coast, urban to remote areas, and ground units to space assets. This chapter defines ground temperatures from very cold (−70°F [−57°C]) to very hot (136°F [58°C]) and relative humidity from near zero to near saturated. Extreme environments also can have high levels of ozone (O_3), sodium chloride (NaCl), sodium carbonates (Na_2CO_3), sulfur oxides (e.g., SO, SO_2, SO_3), sodium sulfates (Na_2SO_4), and sodium bicarbonate ($NaHCO_3$), in addition to reactive dust or sand particles and volcanic ash dust (as small as 140 µm in diameter).

Military equipment must be designed to operate in these various exposure conditions, because these conditions could be experienced during the life cycle of the item. This includes manufacturing, transportation, storage, mission theater, forward operating base deployment, and depot refurbishment. Military aircraft can spend time at ground bases outside, under tents, in hangars, packaged for transportation, shipped on cargo vehicles, and of course flying. With these many environments, test programs must be designed around the corrosion resistance of the base materials (traditional aluminum and newer polymeric composites) as well as the assembled component systems (avionics, propulsion, hydraulics, and ordinance). Careful planning is required to ensure that the final product, whether it is a small drone, ordinance, large aircraft, or mobile communications unit, has the ability to perform as intended in extreme environments.

[1]Materials and Manufacturing Directorate, Air Force Research Laboratory, 2179 12th St., Building 652, Wright-Patterson AFB, OH 45433, USA

The authors acknowledge the previous author of this chapter, Harvey S. Rosenberg, Guild Associates, Hilliard, OH.

DOI: 10.1520/MNL202NDSUP20190028

Storage, Transportation, and Deployment of Equipment

During these phases of the military equipment life cycle, it generally is assumed that the asset is packaged as carefully as possible, perhaps even partially disassembled, and then transported by truck, rail, airplane, or ship. In some cases, however, the military equipment is flown to the operating location. With each method of transportation, the equipment is exposed to some temperature and humidity fluctuation, and sometimes to pressure changes. These fluctuations and exposures can still occur even when using packaging that attempts to provide environmental control or protection. Mechanical wear (i.e., rubbing or abrasion) can occur on equipment transported in shipping containers. Equipment might be stored in environmentally controlled warehouses when possible (i.e., office and computer equipment) or in unimproved temporary storage locations at forward operating bases (i.e., temporary buildings or mobile operating structures). In these variable environments, military equipment may experience diurnal cycling with both high and low humidity, high and low temperature, and often direct sunlight. These environments may be experienced for days, weeks, or months. Operational environments also may experience chemical attack, which requires potentially corrosive decontamination processes. Transportation and storage limitations must be part of the corrosion prevention and mitigation planning, because there is wide variability in military equipment size, use, and expected life cycle. Appropriate testing and references covering these phases are described later.

The Military Mission

During its mission, military equipment will be exposed to various weather conditions, including fully wet conditions in rain and condensing humidity from dew; blowing and settling sand or dust and debris; and salt spray in coastal areas. Additionally, mission threats will expose military equipment to chemical and biological attack agents, explosive ordinance, and live fire. Various military specifications and standards provide guidance for these latter military-specific exposures, but planning for future

Copyright © 2022 by ASTM International, 100 Barr Harbor Dr., PO Box C700, West Conshohocken, PA 19428-2959
ASTM International is not responsible, as a body, for the statements and opinions expressed in this chapter. ASTM International does not endorse any products represented in this chapter.

corrosion protection of equipment can have a beneficial impact on protection from other mission-related exposures.

Environmental Testing

Testing involves basic materials testing to ensure that the equipment or military article will withstand the mission environment. This includes testing the components that are made from those materials and testing the final product that contains the individual components. These tests do not have the same rigidity, and a materials test may be more focused on lifetime and endurance, whereas a component test may focus on operational functionality.

Many of the general military corrosion test standards from MIL-STD-810, *Environmental Engineering Considerations and Laboratory Tests*,[1] now include the phrase "tailoring is essential." The majority of the test methods should not be called out in a blanket fashion nor applied as unalterable routines, but rather should be selected and tailored to generate the most relevant test data possible. Many military equipment requirements documents for new acquisition now cite MIL-STD-1568, *Department of Defense Design Criteria Standard, Materials and Processes for Corrosion Prevention and Control in Aerospace Weapons* Systems.[2] This military standard is specifically designed for aerospace weapon systems, whereas MIL-STD-810 is generic and provides guidance on hundreds of test areas. The corrosion scientist or engineer must evaluate the appropriate testing guidance and design protocols that ensure that the data provides confidence in the longevity of the military equipment.

HUMIDITY TESTING

Military aerospace equipment require verification that the corrosion control design is sufficient for components and subsystems. Testing from MIL-STD-1568 includes ASTM D2247-15(2020), *Standard Practice for Testing Water Resistance of Coatings in 100% Relative Humidity*.[3] This is a 30-day humidity test to verify that the sealants, coatings, and other protective layers on the test article will prevent moisture ingress. Test articles must have no blistering, softening, loss of adhesion, or other notable damage to the corrosion protection layers.

General testing for other military hardware, such as ground vehicles, may include one or more of the MIL-STD-810 humidity tests. These vary between simulating diurnal solar radiation and high humidity of tropical environments, severe dew point changes in the Persian Gulf and Red Sea area, and induced storage and transit cycles. The appropriate testing is dictated by the materials, components, subsystems, and final equipment or hardware. As stated previously, these test methods must be tailored to capture the suitable life-cycle expectations for the test article. There is no one-size-fits-all test for components and subsystems. The corrosion scientist or engineer must select appropriate testing to reduce risk.

THERMAL SHOCK

In the context of corrosion testing, thermal degradation evaluates physical damage or deterioration in performance of the component, or subsystem with a sudden air temperature change greater than 18°F (10°C) per minute. In the context of MIL-STD-810, this method is designed around tracked and wheeled vehicles, such as ground support equipment, in a mission environment. This method focuses on surface changes following air delivery or air drop from high altitude/low temperature to ground level, or transfer of an item from very high temperature areas in a desert to a cold air-conditioned enclosure. Several variations are listed in MIL-STD-810, but the most frequently cited procedure has three cycles between low- and high-temperature extremes. When testing a component or subsystem, the test article starts at ambient temperature and is placed at the extreme low (e.g., for a military application, −70°F [−57°C]) and held there for a long enough period of time for the article to equilibrate to that temperature. This could be 1 h or several hours, depending on the thermal capacitance and heat transfer rate of the component or subsystem in test. Once the test article has equilibrated, it is transferred to a different test chamber set to very hot (e.g., for a military application, 136°F [58°C]) and again left to equilibrate for 1 h or several hours. This represents one cycle. After three cycles, the test article is visually evaluated for damage. Further postexposure testing may be warranted if the test article shows cracks or failure of the corrosion protection system. Typically, this would evaluate that the component or subsystem operates as intended after testing.

MICROBIAL-INFLUENCED CORROSION

Microbial-influenced corrosion (MIC) is a potentially major contributor to corrosion that affects aircraft structures and fuel systems. Over time, mold, mildew, fungi, bacteria, and other organic contaminants can build up on aircraft structures. Some produce acids and enzymes that contribute to corrosion on aircraft surfaces. Other microbes can cause illness and become a health hazard for military personnel. Still others simply have an unsightly appearance and need to be removed before new components can be installed on an aircraft or before new coating materials can be applied.

One area of high interest is fuel systems. Biofuels are particularly conducive to microbial growth because they serve as a nutrient source for the microbes.[4] Some biofuels are from processed vegetable oils and animal fats, substances in which microbes can thrive. Few predictive measures are in place that allow for the systematic evaluation of the susceptibility of emerging fuels to microbial contamination or evaluation of their ability to contribute to corrosion. Fuel components are investigated for compatibility with an aircraft fuel system, and additives are investigated for interactions with materials in those fuel systems. Because of the risk of biocontamination, similar evaluations need to be performed in which biologically derived fuels are used or could be used. Once identified, the impact of that contamination must be understood and mitigated. General guidance is available in MIL-STD-810 to determine the susceptibility of materials to fungal growth. Additional guidance can be found in MIL-STD-1568.

SALT SPRAY

Multiple ASTM standard practices can be employed to evaluate the corrosion protection system against salt sprays, sea water

mist, and industrial pollutants in salt mist. For many decades, the baseline has been ASTM B117-19, *Standard Practice for Operating Salt Spray (Fog) Apparatus*.[5] Salt spray testing in a continuous fog of 5 wt% NaCl at 95°F (35°C) has been used to evaluate basic barrier properties. It often is used to extrapolate corrosion inhibition performance in a marine or coastal environment but cannot be directly correlated to field exposure results. Some military operations require resistance to industrial chemicals in salt spray, and ASTM G85-19, *Standard Practice for Modified Salt Spray (Fog) Testing*,[6] Annex 4 salt spray with SO_2 is used for that verification. Additionally, in ASTM G85, Annex 5, the dilute electrolyte cyclic fog/dry test is used to rapidly evaluate both the barrier and the inhibitor performance of aerospace aluminum corrosion protection systems. To date, there is no accelerated test that correlates with field exposure, and this topic continues to be of high interest in the Department of Defense (DoD) and commercial aviation world.

LOW-PRESSURE DEGRADATION

Low-pressure degradation occurs when an aerospace component, subcomponent, or system is transported or operated in unpressurized areas of an aircraft. This includes scenarios of "on-wing" ordinance that is rapidly taken from ground to operational altitude attached to the wing of the aircraft. MIL-STD-810 provides a baseline test for aircraft and missiles that will operate below 70,000 feet. With rapid loss of pressure, test articles can experience deformation of sealed areas and leakage of gases or fluids, which may cause components to fail. A typical test is MIL-STD-810, Method 500, which requires altitude changes at 32.8 ft/s (10 m/s) or lower. In full military power takeoff, military transport aircraft have an average altitude change of 25 ft/s (7.6 m/s), so using the 32.8 ft/s change rate provides sufficient information to determine whether sealed areas or corrosion protection systems on test articles will be deformed, allowing for moisture, chemicals, or other contaminants to damage the component. Typically, after a low-pressure test cycle, an operational check on the military component or subsystem will be performed to verify that the item still performs as intended. There is no blanket performance test for all components or subsystems, so the corrosion scientist or engineer must collaborate with other materials and process engineers to determine the best test cycle for the item in question.

SOLAR RADIATION

Military equipment will be exposed to solar radiation during its life cycle. As with any accelerated test method, there are limitations to solar radiation tests because they do not correlate to the effects of a natural environment. For this reason, test method tailoring is essential to determine the best procedures that reduce risk and provide confidence in the life cycle of the test article. At high elevations, solar radiation contains more ultraviolet-B radiation than at sea level. Solar radiation also can be absorbed by some military corrosion protection systems, causing oxidation and degradation of those systems.

A common test procedure for worldwide deployment of military equipment utilizes ASTM G155-13, *Standard Practice for Operating Xenon Arc Light Apparatus for Exposure of Non-Metallic* Materials,[7] Cycle 1, which is 102 min of irradiance at 0.35 W/(m^2·nm) at 340 nm and a black panel temperature of 145.4°F (63°C), followed by 18 min of irradiance only and water spray (air temperature not controlled). This method often is run continuously, and the test article may be exposed for a few days to many weeks, depending on the intended mission requirements. Post-test materials evaluation determines whether the corrosion protection system has degraded by loss of color, adhesion, or visual deformation, such as cracking, crazing, peeling, or other damage. Post-test component or subsystem evaluation also requires that the test article be verified for performance.

RAIN

There are two scenarios for rain exposure testing. One is for military equipment that will be outside, either at a runway or in a storage area. The other scenario is for the military equipment that will be flying or be on-wing of an aircraft. After either of these scenarios, the materials, components, or subsystems are evaluated for loss of key properties or reduced functionality.

In the first scenario, the test article is exposed to simulated wind and blowing rainfall as if it were stored outside or sitting on the runway. If the test article has already been tested for resistance to water immersion, there is no need to perform the blowing rain test. The test article is exposed to droplets that predominantly are 500 µm with some up to 4,500 µm, and with rain rates of 4 in./h (1.7 mm/min). Simulated wind velocity is 40 mph (18 m/s). The test duration can be as short as an hour to as long as several hours, simulating continual rain and storms.

In the second scenario, the test article is exposed to simulated rain particle damage during flight. Typical areas of degradation are optical windows, radomes, leading edges on wings, flaps, and rudders, as well as damage to the protective coatings and sealants. Liquid impingement erosion and cavitation is well-described in ASTM G73-17, *Standard test Method for Liquid Impingement Erosion Using Rotating* Apparatus,[8] along with methods for testing certain situations. Military applications also will use the description from AMS-C-83231, *Coatings, Polyurethane, Rain Erosion Resistant for Exterior Aircraft and Missile Parts*.[9] This method uses airfoils, coupon testing, or other sample configurations that are coated with a rain erosion–resistant material and placed on a double-blade whirling arm. The test article is accelerated to 500 mph and exposed to simulated natural rainfall with an average droplet size of 0.08 inches (2 mm) and a rainfall rate of 1 in./h. Test duration can be a few minutes to more than 2 h, depending on the intended use of the material.

After either of these test scenarios, the materials, components, or subsystems are evaluated for loss of key properties or reduced functionality.

SAND AND DUST PARTICLES

Sand or dust particles exist in nearly every military operational environment. Not all sand and dust particles are created equal. Particles collected from southwestern United States have different mineral chemistry, angularity, and size distribution than those collected from the United Arab Emirates. Particles

collected from soil in Hawaii have substantial volcanic ash, but particles in the Iraq Peninsula are course and glassy with clay grains. The damage expected by sand and dust is directly related to aerospace vehicle velocity and altitude. Larger particles are closer to ground level altitude below 10,000 ft, whereas lighter dust particles reach higher altitudes.

Sand particles cause erosive corrosion damage because they impinge on surfaces and ablate corrosion protection systems. The damaged, unprotected surfaces collect ambient chemicals, such as industrial pollutants and salts, which can cause corrosion when dew or other moisture comes into contact with those surfaces. Sand and dust particles will enter air intakes on engines, erode at the protective high-temperature resistant coatings on blades and stators, and cause premature failure of the engine (hot corrosion damage) in extreme cases.

Effective methods to design for hot corrosion are still in development, but methods for evaluating sand or dust impingement of leading edges has been developed in MIL-STD-3033, *Particle/Sand Erosion Testing of Rotor Blade Protective* Materials.[10] This military standard uses the apparatus in ASTM F1864, *Standard Test Method for Dust Erosion Resistance of Optical and Infrared Transparent Materials and* Coatings,[11] and focuses on evaluating exterior surfaces of rotor blades for helicopters and other rotary-driven aircraft that could be located in hot arid regions. Particles are sieved to between 240 µm and 550 µm, which is comparable to the particles that have been found on aircraft in desert hover or low-level flight testing. Particle velocity is controlled to 730 ft/s with a mass loading between 30 and 50 g/cm^2 for the test. The impingement angle is between 20° and 90° depending on the life cycle and use of the military equipment. This method has been used for the design and sustainment of various helicopters and low-altitude hover vehicles. Post-test evaluation requires mass loss, visual examination, and metallographic analysis to determine if the material has sufficient durability. Testing can be tailored for components and smaller subsystems, particularly when sand or dust encroachment may cause electrical or hydraulic failure of a military component. As with all accelerated or simulation testing, corrosion scientists and engineers must plan select and design testing that reduces improves likelihood that the military equipment will function as intended in extreme environments.

ACCELERATED AND COMBINED EFFECTS CORROSION TESTS

The DoD corrosion community has long recognized the need to expose materials to a simultaneous mix of two or more environmental variables during development and to consider the interaction of autonomous materials during validation, verification, and ultimately operation. Such environmental factors include, but are not limited to, electrolytes (salt spray), temperature and humidity cycles, insolation, background gases, solar exposure, acoustic loading, sand or rain exposure, and dynamic loading. The DoD has been taking aggressive steps toward the development of advanced accelerated test methodologies that will allow testing for true material performance in relevant service environments. Such an approach has clear potential to change the way engineers test and select materials across all engineering disciplines. Advanced materials degradation tests will require new innovative protocols for better prediction of materials performance and service life. Once developed, these methods will provide materials developers with realistic and reliable data that correlate to real-world operation for materials selection, with an eye toward corrosion prevention in the military equipment design.

Standards and Specifications

Military specifications have undergone many changes over the past decade. In the early- to mid-20th century, when aerospace was largely the purview of militaries and governments, military specifications existed for materials formulas, properties, fluids, fuels, test methods, and complete design criteria. In the mid-1990s, the DoD revised numerous military specifications with the goal to replace them with existing industrial specifications such as ASTM International, the International Organization for Standardization (ISO), the Society for Automatic Engineers (now SAE International), and others. This led to reliance on the industrial base to provide specifications that would meet both commercial and military needs. In many cases, these dual-purpose standards were appropriate. In other cases, it became clear that the industry and commercial use of aircraft was not always close enough to that of the military. In the early 21st century, there has been a greater push for reapproval of military standards and the development of new standards and specifications that focus on military needs.

MIL-STD-1530, *Aircraft Structural Integrity Program* (ASIP),[12] requires materials, components, and subsystems to be tested for durability in operational environments. Design analysis and development testing requirements in that standard provide guidance on how corrosion tests should be conducted. The standard emphasizes that corrosion protection systems should be tested on representative structures in relevant and operational environments.

There are several ways to locate military standards and specifications related to corrosion prevention and control. One website is the Acquisition Streamlining and Standardization Information System (ASSIST) operated by the Defense Standardization Program (DSP) and managed by the Defense Logistics Agency (DLA) Document Service.[13] Additional standardization information can be found at the Defense Standardization Program website.[14]

Conclusion

Military aircraft and equipment are exposed to all climates and conditions. Unlike commercial aviation, there are cases where the military equipment is required to perform a mission that could expose that equipment to chemicals or environmental stresses that have an unknown effect on service life. Various military and industry standards attempt to address the underlying failure mechanisms and to reduce the risk that the equipment could be damaged. The extensive DoD systems engineering process exists to design, integrate, test, validate, and verify new military capabilities. The DoD Corrosion Policy and Oversight

Office published the Corrosion Prevention and Mitigation Strategic Plan in 2011, providing policy, strategy, objectives, and plans to address corrosion prevention in the planning and development phase of acquisition. Instead of looking at corrosion control as a "find and fix" approach many years after military equipment has been deployed, corrosion design strategy now focuses on "prevent, predict, detect, and manage." Specific military corrosion policy and strategies can be found at either the Defense Acquisition University website,[15] or the DoD Corrosion Policy and Oversight Office website.[16]

References

1. *Environmental Engineering Considerations and Laboratory Tests*, MIL-STD-810 (Arlington, VA: Department of Defense, January 2019).
2. *Department of Defense Design Criteria Standard, Materials and Processes for Corrosion Prevention and Control in Aerospace Weapons Systems*, MIL-STD-1568 (Arlington, VA: Department of Defense, August 2015).
3. *Standard Practice for Testing Water Resistance of Coatings in 100% Relative Humidity*, ASTM D2247-15(2020) (West Conshohocken, PA: ASTM International, approved June 1, 2020), http://doi.org/10.1520/D2247-15R20
4. E. Mansfield, J. Sowards, W. Crookes-Goodson, "Findings and Recommendations from the NIST Workshop on Alternative Fuels and Materials: Biocorrosion," *Journal of Research NIST* 120 (March 2015): 28–36, http://doi.org/10.6028/jres.120.003
5. *Standard Practice for Operating Salt Spray (Fog) Apparatus*, ASTM B117-19 (West Conshohocken, PA: ASTM International, approved November 1, 2019), http://doi.org/10.1520/B0117-19
6. *Standard Practice for Modified Salt Spray (Fog) Testing*, ASTM G85-19 (West Conshohocken, PA: ASTM International, approved November 1, 2019), http://doi.org/10.1520/G0085-19
7. *Standard Practice for Operating Xenon Arc Light Apparatus for Exposure of Non-Metallic Materials*, ASTM G155-13 (West Conshohocken, PA: ASTM International, approved June 1, 2013), http://doi.org/10.1520/G0155-13
8. *Standard Test Method for Liquid Impingement Erosion Using Rotating Apparatus*, ASTM G73-10(2017) (West Conshohocken, PA: ASTM International, approved July 15, 2017), http://doi.org/10.1520/G0073-10R17
9. *Coatings, Polyurethane, Rain Erosion Resistant for Exterior Aircraft and Missile Parts*, AMS-C-83231 (Warrendale, PA: Aerospace Material Specifications, SAE International, 2001).
10. *Particle/Sand Erosion Testing of Rotor Blade Protective Materials*, MIL-STD-3033 (Arlington, VA: Department of Defense, 2010).
11. *Standard Test Method for Dust Erosion Resistance of Optical and Infrared Transparent Materials and Coatings*, ASTM F1864-16 (West Conshohocken, PA: ASTM International, approved April 1, 2016), http://doi.org/10.1520/F1864-16
12. *Department of Defense Standard Practice, Aircraft Structural Integrity Program (ASIP)*, MIL-STD-1530 (Arlington, VA: Department of Defense, October 2016).
13. Acquisition Streamlining and Standardization Information System (ASSIST), Defense Standardization Program (DSP), Defense Logistics Agency (DLA) Document Service, http://web.archive.org/web/20210505141209/https://assist.dla.mil/
14. Defense Standardization Program, http://web.archive.org/web/20210505142139/https://www.dsp.dla.mil/
15. Defense Acquisition University, http://web.archive.org/web/20210505144319/https://www.dau.edu/
16. DoD Corrosion Policy and Oversight Office, http://web.archive.org/web/20210505153437/https://www.dau.edu/cop/cpc/Pages/Default.aspx

Chapter 26 | Industrial Chemicals: Manufacture and Usage

Sheldon W. Dean, Jr.[1]

Introduction

Industrial chemicals are usually relatively pure chemical compounds that are manufactured for use in a variety of applications.[1] In some cases, they are mixtures of compounds. In other cases, they are blended with other materials to make products. They constitute a major class of industrial products that are used in commerce. These materials are produced in large volumes and, in many cases, are corrosive, toxic, or flammable. As a result, the manufacture, storage, and transportation of these materials must be handled with care. Leaks or other releases to the environment can result in substantial damage and present hazards to both workers and others in the vicinity.[2]

Standards are used in the design, production, transportation, and storage of industrial chemicals and in the inspection of equipment exposed to these materials to ensure safe operation, containment, and protection of the environment. Corrosion damage can result in leaks and other releases to the environment. Corrosion also can cause contamination of chemical products. Corrosion standards are a significant source of information that is used to prevent, minimize, or manage issues resulting from corrosion processes. A number of different organizations write standards that are used in the chemical process industries to deal with corrosion issues. Several of these organizations are listed in table 1. ASTM International, NACE International, and the International Organization for Standardization (ISO) produce standards directly relating to corrosion testing and best practices associated with corrosion issues. The other organizations shown in table 1 address specific issues that result from corrosion damage.

TABLE 1 Organizations That Write Standards Used by the CPI

Organization	Types of Standards
ASTM International	Tests, practices, guides, specifications, nomenclature, classifications
NACE International	Tests, practices, guides, nomenclature
International Organization for Standardization (ISO)	Tests, practices, nomenclature
American Society of Mechanical Engineers (ASME)	Practices, specifications
American Petroleum Institute (API)	Practices
American Society for Non-Destructive Testing (ASNT)	Certification

Corrosion Testing for Industrial Chemicals Manufacturing

The subject of manufacturing industrial chemicals covers the design of the process, construction of the facility, operating the equipment, maintenance of the facility, and inspection and repair of the facility. Storage and shipment of the chemical products are also covered. Corrosion of the materials of construction is a significant damage mechanism that can lead to release of the chemical products with all of the issues that can result. Corrosion testing is used to establish the suitability of the materials for construction and to determine inspection intervals.

Corrosion damage occurs in several characteristic forms. Many of the most common forms are listed in table 2. It is important to recognize that these forms can occur, and each one has specific characteristics. Understanding these characteristics can aid in planning a corrosion test program and will be important in analyzing the results of the program. For example, a test program that is solely designed to determine general corrosion rates may not detect stress corrosion cracking, thereby missing a critical failure mechanism.

When designing a test program, a review the existing references on the possible materials of construction and the environments that may be encountered can be helpful. Such information may be available from material suppliers, academic sources, professional society papers, and publications from organizations such as NACE International, the Materials Technology Institute (MTI), and ASTM International.

[1]Dean Corrosion Technology, Inc., 306 Marshall Landing, Glen Mills, PA 19342, USA
http://orcid.org/0000-0003-0611-7384
The author acknowledges the previous author of this chapter, Robert B. Puyear, Chesterfield, MO.

DOI: 10.1520/MNL202NDSUP20190019

Copyright © 2022 by ASTM International, 100 Barr Harbor Dr., PO Box C700, West Conshohocken, PA 19428-2959
ASTM International is not responsible, as a body, for the statements and opinions expressed in this chapter. ASTM International does not endorse any products represented in this chapter.

TABLE 2 Forms of Corrosion Damage

Type	Characteristics
General	Uniform attack, constant rate
Pitting	Local areas of accelerated attack
Under Deposit	Pitting under solid deposits
Crevice	Accelerated attack in occluded areas
Stress Corrosion Cracking	Cracking from corrosion in areas under tensile stress
Liquid Metal Embrittlement	Cracking in areas under tensile stress from liquid metal
Hydrogen Embrittlement	Cracking in tensile stressed areas from hydrogen permeation
Corrosion Fatigue	Cracking resulting from corrosion and cyclic tensile stressing
Galvanic Corrosion	Accelerated attack from electrical contact with a more noble material
Fluid Flow Accelerated	Accelerated attack from flowing liquid or turbulence
Intergranular	Localized corrosion at grain boundaries

PROCESS DESIGN

The selection of materials of construction for a process is an important issue in the design phase of the project. In cases in which the process has been used previously, the selection usually retains the materials from the previous design if the performance of those materials was satisfactory. In some cases, newer alloys may be available that offer benefits in terms of cost, ability to be fabricated, or performance. In such cases, it might be important to run laboratory tests to obtain actual data on the performance of the newer material as compared with the material previously used. Table 3 shows a number of ASTM standard laboratory tests methods and procedures for metals and alloys. These different standards are used to test for the various forms of corrosion damage that might occur.

LABORATORY TESTING

The most widely used laboratory test procedure for immersion testing is the NACE TM01-69/ASTM G31-12A, *Standard Guide for Laboratory Immersion Corrosion Testing of Metals (Historical Version)*.[3] This guide was developed independently by both ASTM Committee G01 and NACE International. Subsequently,

TABLE 3 ASTM Laboratory Corrosion Test Procedures

Type	ASTM No.	Title	Metal
General Corrosion	G31	*Standard Guide for Laboratory Immersion Corrosion Testing of Metals*	All
Pitting	G46	*Standard Guide for Examination and Evaluation of Pitting Corrosion*	All
	G48	*Standard Test Method for Pitting and Crevice Corrosion of Stainless Steels and Related Alloys by Use of Ferric Chloride Solution*	SS
	G61	*Standard Test Method for Conducting Cyclic Potentiodynamic Polarization Measurements for Localized Corrosion Susceptibility of Iron-, Nickel-, or Cobalt-Based Alloys*	SS
	G150	*Standard Test Method for Electrochemical Critical Pitting Temperature Testing of Stainless Steels and Related Alloys*	SS
Crevice Corrosion	G48	*Standard Test Method for Pitting and Crevice Corrosion Resistance of Stainless Steels and Related Alloys Solution by Use of Ferric Chloride Solution*	SS
	G78	*Standard Guide for Crevice Corrosion Testing of Iron-Base and Nickel-Base Stainless Alloys in Seawater and Other Chloride Containing Aqueous Environments*	SS
Galvanic Corrosion	G71	*Standard Guide for Conducting and Evaluating Galvanic Corrosion Tests in Electrolytes*	All
	G82	*Standard Guide for Development and Use of a Galvanic Series for Predicting Corrosion Performance*	All
High-Temperature, High-Pressure Testing	G111	*Standard Guide for Corrosion Tests in High Temperature or High Pressure Environment, or Both*	All
	G142	*Standard Test Method for Determination of Susceptibility of Metals to Embrittlement in Hydrogen Containing Environments at High Pressure, High Temperature, or Both*	All
Flow Accelerated Corrosion	G184	*Standard Practice for Evaluating and Qualifying Oil Field and Refinery Corrosion Inhibitors Using Rotating Cage*	CS
	G185	*Standard Practice for Evaluating and Qualifying Oil Field and Refinery Corrosion Inhibitors Using the Rotating Cylinder Electrode*	CS
	G202	*Standard Test Method for Using Atmospheric Pressure Rotating Cage*	CS
	G208	*Standard Practice for Evaluating and Qualifying Oilfield and Refinery Corrosion Inhibitors Using Jet Impingement Apparatus*	CS
Intergranular Corrosion	A262	*Standard Practices for Detecting Susceptibility to Intergranular Attack in Austenitic Stainless Steels*	SS
	G28	*Standard Test Methods for Detecting Susceptibility to Intergranular Corrosion in Wrought, Nickel-Rich, Chromium-Bearing Alloys*	SS
	G108	*Standard Test Method for Electrochemical Reactivation (EPR) for Detecting Sensitization of AISI Type 304 and 304L Stainless Steels*	304

(continued)

TABLE 3 (*continued*)

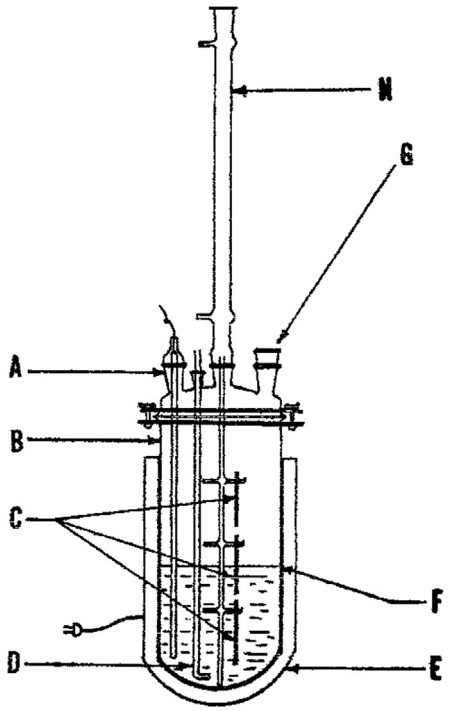
Type	ASTM No.	Title	Metal
Stress-Corrosion Cracking and Hydrogen Embrittlement from Corrosion	G30	*Standard Practice for Making and Using U-Bend Stress-Corrosion Test Specimens*	All
	G35	*Standard Practice for Determining Susceptibility of Stainless Steels and Related Nickel-Chromium-Iron Alloys to Stress-Corrosion Cracking in Polythionic Acids*	SS
	G36	*Standard Practice for Evaluating Stress-Corrosion-Cracking Resistance of Metals and Alloys in Boiling Magnesium Chloride Solution*	SS
	G37	*Standard Practice for Use of Mattsson's Solution of pH 7.2 to Evaluate the Stress-Corrosion Cracking Susceptibility of Copper-Zinc Alloys*	Brass
	G38	*Standard Practice for Making and Using C-Ring Stress-Corrosion Test Specimens*	All
	G39	*Standard Practice for Preparation and Use of Bent-Beam Stress-Corrosion Test Specimens*	All
	G41	*Standard Practice for Determining Cracking Susceptibility of Metals Exposed under Stress to a Hot Salt Environment*	All
	G44	*Standard Practice for Exposure of Metals and Alloys by Alternate Immersion in Neutral 3.5% Sodium Chloride Solution*	All
	G49	*Standard Practice for Preparation and Use of Direct Tension Stress-Corrosion Test Specimens*	All
	G58	*Standard Practice for Preparation of Stress-Corrosion Test Specimens for Weldments*	All
	G123	*Standard Test Method for Evaluating Stress-Corrosion Cracking of Stainless Alloys with Different Nickel Content in Boiling Acidified Sodium Chloride Solution*	SS
	G129	*Standard Practice for Slow Strain Rate Testing to Evaluate Susceptibility of Metallic Materials to Environmentally Assisted Cracking*	All
	G168	*Standard Practice for Making and Using Precracked Double Beam Stress Corrosion Specimens*	All

the two documents were merged into a joint standard. The test vessel used to hold the specimens is shown in figure 1. This approach is most often used for mass loss rate determinations, but it also has been used to study other forms of corrosion damage, depending on the specimen design. A modification of this approach is shown in figure 2. In this case, the setup can simultaneously expose specimens to boiling liquid, vapor, and hot condensate.

One laboratory mass loss corrosion study determined the corrosion mechanism on the top tray of a vacuum distillation column used to purify toluene diamine (TDA).[1] This column had an internal condenser at the top of the column to minimize the pressure drop. The column used valve trays and was constructed of carbon steel. There was no reason to expect corrosion of the carbon steel in this case. It was noted that the gas exiting the column through the vacuum system was a mixture of water vapor and carbon dioxide.

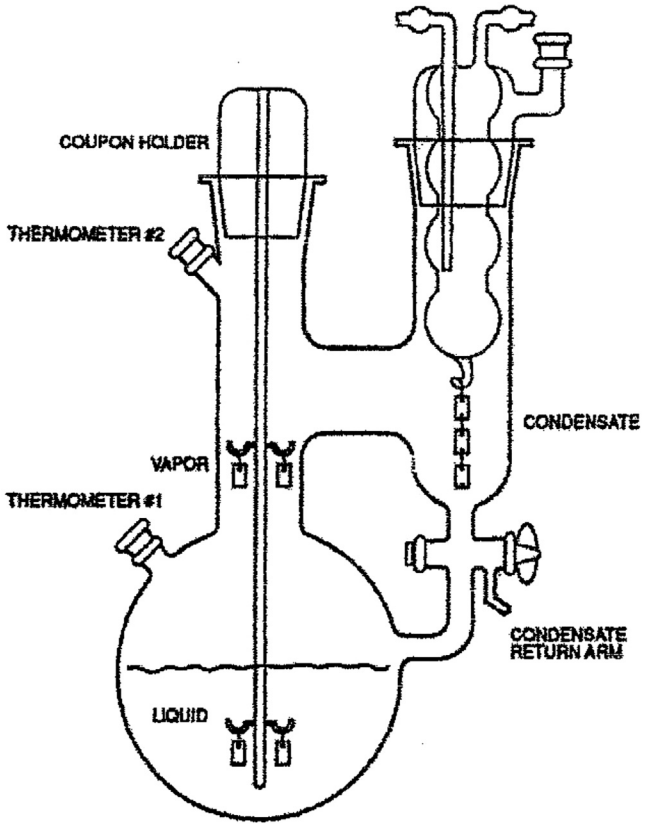
A test was set up using the ASTM G31 flask assembly with TDA liquid held at the temperature at the top of the column. A nitrogen gas stream was sparged through the liquid to maintain an oxygen-free environment and to provide a flow of condensate that contacted the specimens. Carbon steel coupons showed no corrosion after one week of exposure. Then the test was repeated with a gas mixture containing 10% by volume carbon dioxide. Again, no corrosion was found after a one week of exposure. This test was repeated again after saturating the gas with water vapor at ambient temperature, and again no corrosion was noted. Finally, an addition was made to the TDA of cyclohexyl amine at about 0.1%, and the test was repeated using the gas mixture. In this case, the carbon steel coupons showed a corrosion rate of about 20 mpy. This was believed to have resulted from the formation of cyclohexyl amine carbamic acid, which is

FIG. 1 Typical resin reaction flask used for laboratory immersion testing (see NACE TM0169/G31).



NOTE 1—The flask can be used as a versatile and convenient apparatus to conduct simple immersion tests. Configuration of top to flask is such that more sophisticated apparatus can be added as required by the specific test being conducted. *A* = thermowell, *B* = resin flask, *C* = specimens hung on supporting device, *D* = air inlet, *E* = heating mantle, *F* = liquid interface, *G* = opening in flask for additional apparatus that may be required, and *H* = reflux condenser.

FIG. 2 Modified flask system for multiple exposure of coupons to boiling liquid, vapor, and condensate.[1]



about as acidic as an acetic acid. Although this compound will decompose spontaneously in hot TDA, its presence is sufficient to cause the corrosion damage noted. A similar amine can be generated during the hydrogenation of dinitro-toluene if the hydrogenation catalyst is too active. A test with coupons of type 304L stainless steel showed no corrosion, so it was decided to line the column top with this alloy and use it for the top tray. In this case, ASTM G31 provided guidance that enabled the successful completion of this test program. Thereafter, no corrosion problems have been noted with this column.

PILOT PLANT TESTING

In the case of a new process in which a pilot plant test program has been set up, the inclusion of corrosion specimens of various candidate materials is usually a desirable procedure.[4] The pilot plant operation can create conditions that are difficult or impossible to simulate in a laboratory test. In such situations, ASTM G4, *Standard Guide for Conducting Corrosion Tests in Field Applications*, provides several designs of coupon holders that may be appropriate for a pilot plant situation. Three different types of specimen holders are shown in figures 3, 4 and 5. In these cases, the coupons are used for corrosion rate determination by means of mass loss measurement. Stressed coupons, bimetallic specimens, welded coupons, or crevice assemblies also can be included, if desired.

FIG. 3 Spool corrosion rack for use in vessels (see ASTM G4).

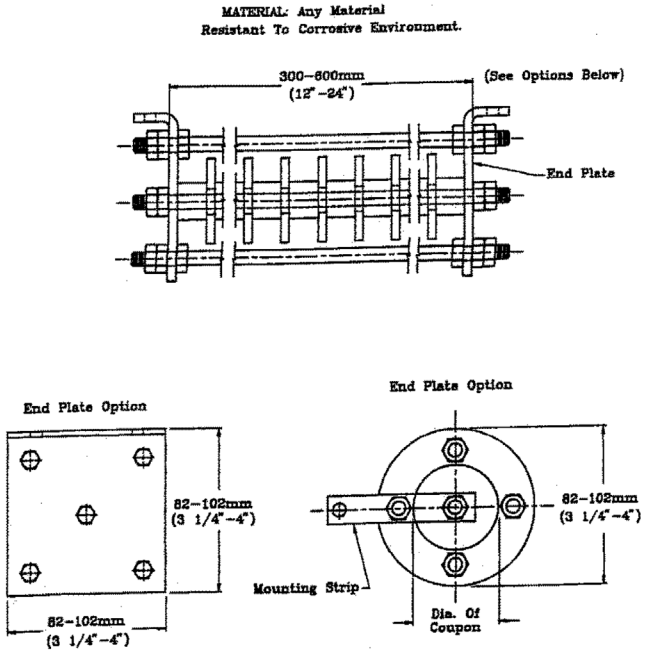


FIG. 4 Pipe insertion rack (see ASTM G4).

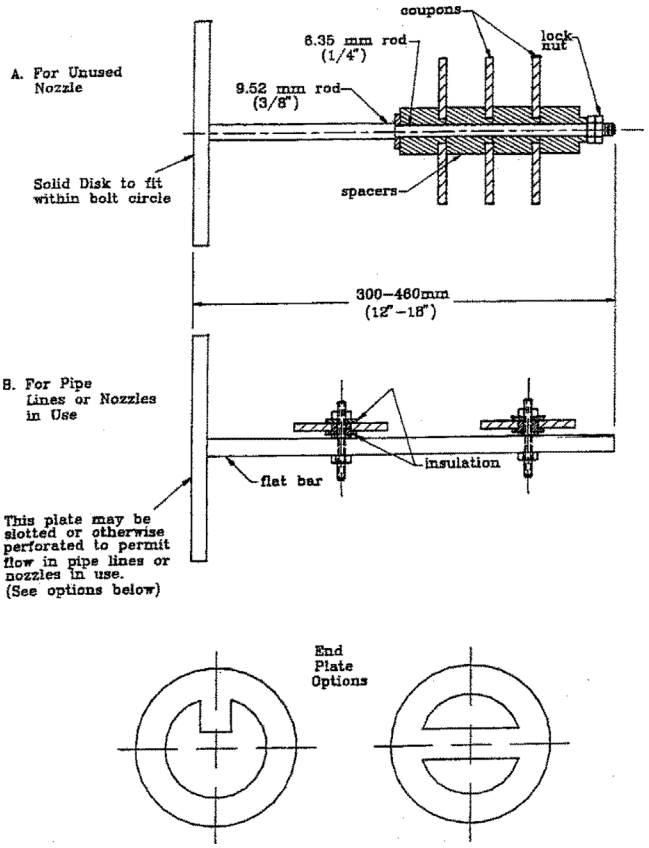
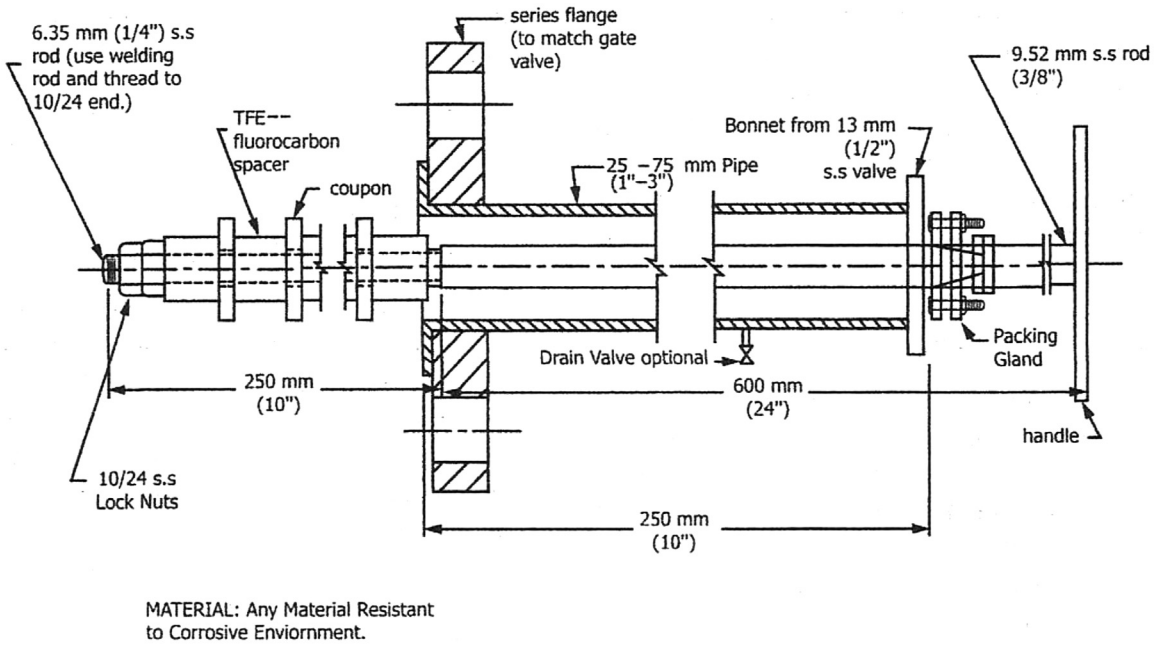
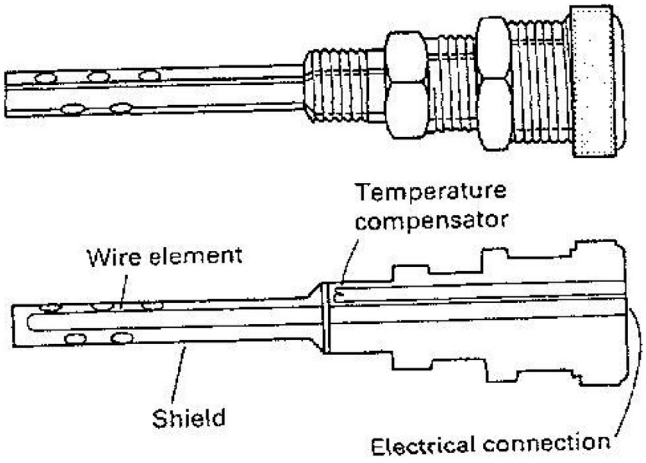


FIG. 5 Retractable "slip-in" specimen holder (see ASTM G4).



Electrical resistance probes or electrochemical probes provide the possibility of obtaining corrosion rate information without the necessity of removing and analyzing specimens. ASTM G96, *Standard Guide for Online Monitoring of Corrosion in Plant Equipment (Electrical and Electrochemical Methods)*, provides guidance on the design and use of both electrical resistance and electrochemical probes. These approaches are particularly helpful in cases in which the same apparatus is being used to produce a number of different chemicals in a campaign mode, or in cases in which the process conditions are being varied, and it is desired to understand how the changing conditions affect the corrosion behavior of the metal being tested. Figure 6 shows a typical electrical resistance probe assembly. This concept is based on the fact that the electrical resistance of a rod is inversely proportional to its cross-sectional area. Corrosion reduces this cross section, so the measurement of the resistance of the rod provides a way to monitor the extent of any corrosion that is occurring.

FIG. 6 Typical electrical resistance probe (see ASTM G96).

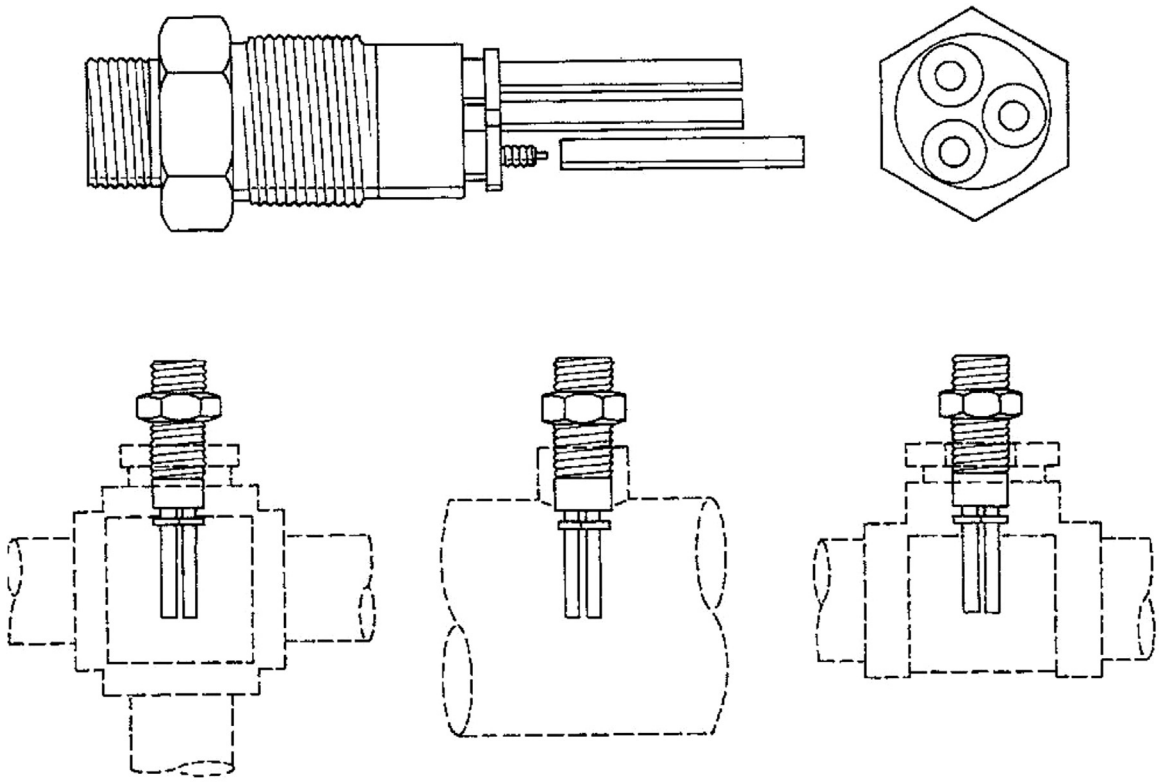


Electrochemical probes are based on the concept that the polarization resistance of an electrode is inversely proportional to the corrosion rate that is occurring. Polarization resistance is the slope of the electrode potential versus current density curve at the corrosion potential.[5] The electrochemical probes consist of two or three identical electrodes that are placed into the environment. The measurement process consists of applying either 20 mV for the two electrode system or 10 mV relative to the reference electrode for the three-electrode system. In either case, the resulting current that flows between the working electrodes is measured and converted to a corrosion rate by the apparatus. Figure 7 shows a typical three-electrode system.

TESTING IN OPERATING PLANTS

In operating plants corrosion, testing is carried out from time to time for a variety of reasons. Such testing can be helpful in investigating the performance of new materials. In cases in which a significant change in the process is being evaluated, it is important to include corrosion testing as part of the evaluation. In plants that operate in a campaign mode where different products are manufactured using the same equipment, running corrosion tests during each campaign can help pinpoint which campaigns are responsible for the problems that are occurring. In cases in which impurities are observed in the product, corrosion testing can assist in determining if corrosion of the metals in the system is the source of the contamination. In these cases, ASTM G4 coupon holders and procedures are used if mass loss measurements are carried out. The decisions regarding specimen size and shape are based on the type of holder used and the space available.

FIG. 7 Three electrode polarization resistance probe design and installation (see ASTM G96).



Special designs are required if the specimens are to be inserted and removed while the plant is operating. In addition, a safety evaluation is necessary in this case to ensure that the procedures will not result in a hazardous situation. If the procedure results in removing some of the process stream along with the coupon rack, this material must be recovered and discarded appropriately. Figure 5 shows a slip-in rack assembly that allows the specimens to be withdrawn without shutting the operation down. High-pressure systems pose particular risks because of the force they exert on the withdrawal devices.

Electrical resistance and electrochemical probes are also used in operating plants. They offer the possibility of obtaining data without the need to remove the probe from service. They have been used in cooling water service to monitor the performance of corrosion inhibitors in these systems. This was especially important when the use of chromates was ended, and new inhibitor systems were instituted. ASTM G96 provides important operating information on these devices.

Electrode potential measurements have also been used to monitor passivity in process systems. ASTM G215, *Standard Guide for Electrode Potential Measurement*, provides information in this type of measurement. This approach is helpful when an inhibitor is added to the system to maintain the surfaces in a passive condition. It is necessary to install a reference electrode to obtain the electrode potential measurement. Reference electrodes are widely used in laboratory testing, but in plant environments it is necessary to use robust designs that are not as susceptible to contamination or mechanical damage. In the case of a system that is showing marginal passivity, it may be important to increase the inhibitor addition or investigate why the change has occurred.

Specialized Testing

CORROSION UNDER THERMAL INSULATION

Thermal insulation is widely used in chemical manufacturing facilities. Traditionally, thermal insulation is applied after the facility construction is completed, usually without any protective coatings applied to the metal surfaces. Thermal insulation is used to minimize heat loss from the item, and to protect workers from exposure to hot metal surfaces. A variety of different types of insulation is used depending on the temperature of the surface, the degree of insulation required, and other factors. In most cases, a metallic covering is added after the insulation is installed. The covering is intended to protect the insulation from rain or other water exposure. In many cases, however, the covers are damaged or breached during normal operation, or when modifications are made to the facility, and repairs usually are postponed or not carried out. As a result, water penetrates through the insulation and causes corrosion of the metal. Carbon steel is the most widely used construction material in chemical plants,

and it is most susceptible to corrosion damage from being exposed to water permeating through insulation. Generally, soluble electrolytes in the insulation are extracted during the water permeation, and they accelerate the corrosion of the steel.[6] Such damage can be discovered only by removing the insulation, but that step is seldom carried out unless there is evidence of damage.[7,8]

In a related situation, insulation with soluble chloride–containing compounds was discovered to be responsible for stress corrosion cracking of stainless steel components. In this case, the insulation could be checked to verify that it did not contain damaging chloride levels by exposing stressed stainless steel to the wet insulation while heating the stainless steel above the boiling point for an extended period. If the stainless steel item was cracked at the end of the exposure the insulation would not be used (see ASTM C795, *Standard Specification for Thermal Insulation for Use in Contact with Austenitic Stainless Steel*).

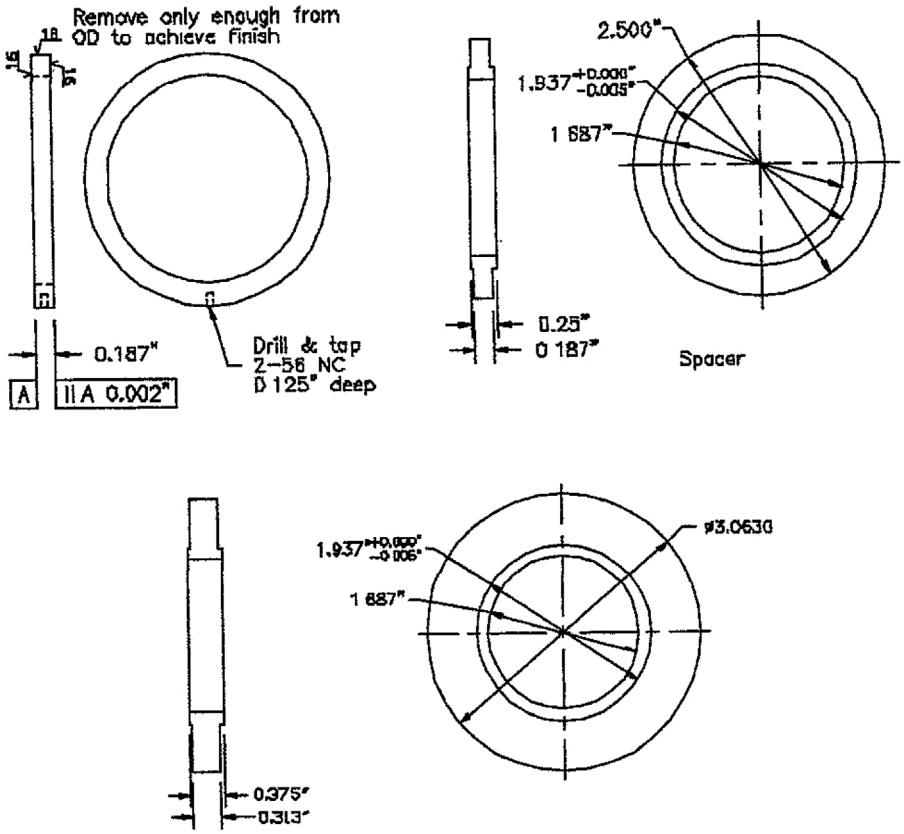
Note that this problem occurs in many industries other than in chemical processing. For example, problems have been noted in power plants. Because of the breadth of this problem, many standards have been developed to deal with it by several organizations, including ASTM International, NACE International, American Petroleum Institute (API), and others. This is covered in more detail elsewhere in this manual.

A test procedure was also developed to simulate the corrosion process that occurs under thermal insulation. This procedure, ASTM G189, *Standard Guide for Laboratory Simulation of Corrosion under Insulation*, uses carbon steel ring specimens that are heated internally using a heat transfer fluid, while an aqueous solution flows over them under the insulation being tested. Figure 8 shows the specimen design and the nonconductive spacer design, figure 9 shows the insulation orientation, and figure 10 shows the dimensions of insulation pieces. Figure 11 shows the assembly. This approach can be used to evaluate inhibitor systems for insulation or to evaluate coatings.

LEAK DETECTION FLUIDS

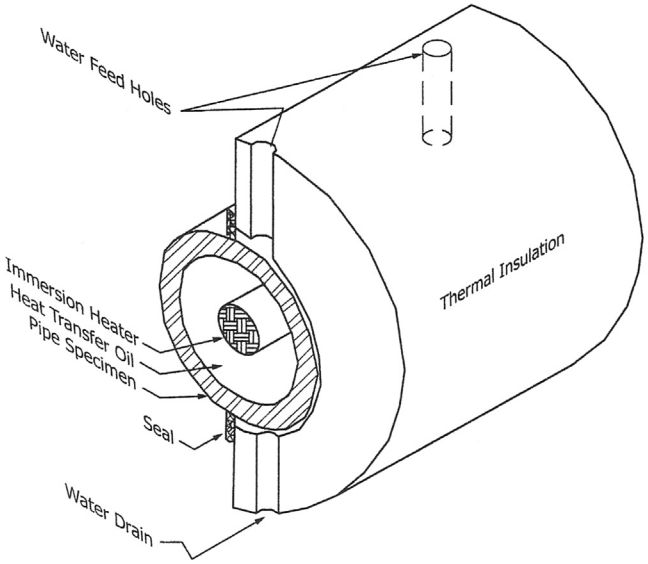
Industrial gas suppliers and users regularly employ a number of devices manufactured from brass. Brass components have given excellent service because they provide leak tight connections, and they are resistant to degradation both from the atmospheres where they are used and the gases that are flowing through them. It is usually necessary, however, to verify that a connection is leak tight after the system is pressurized by applying a leak detection fluid (LDF) to the joint. If a leak is present, bubbles will form to reveal the leak. The problem that has been observed is that occasionally the LDF has caused the brass components to

FIG. 8 Ring specimen and nonconductive spacer for corrosion under insulation (CUI) cells (see ASTM G189).



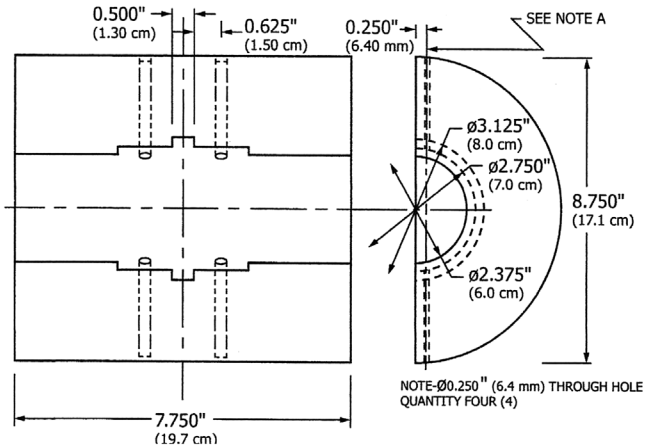
Top Left—Configuration of the ring specimen.
Top Right—Nonconductive spacer.
Bottom—Nonconductive large spacer (dam) located between the two sides of the CUI-Cell.

FIG. 9 Cross section of CUI cell showing orientation of thermal insulation (see ASTM G189).



develop cracks resulting from a stress corrosion cracking process. Test method ASTM G186, *Standard Test Method for Determining Whether Gas-Leak-Detector Fluid Solutions Can Cause Stress Corrosion Cracking of Brass Alloys*, was developed to demonstrate that an LDF was not capable of causing brass to stress corrosion crack. This method uses hard drawn brass (UNS C27200)

FIG. 10 Dimensions of thermal insulation for CUI cell (see ASTM G189).



C-ring specimens exposed to the LDF for 15 wet-dry cycles. Figure 12 shows the C-ring design for this test method. If no cracks are found at the end of this exposure the LDF is judged to be acceptable. ASTM G188, *Standard Specification for Leak Detector Solutions Intended for Use on Brasses and Other Copper Alloys*, is a standard specification requiring the ASTM G186 test method be carried out on LDFs. Purchasers can use this specification to obtain products that will not cause brass components to crack from stress corrosion cracking.

FIG. 11 Schematic diagram of the CUI cell.

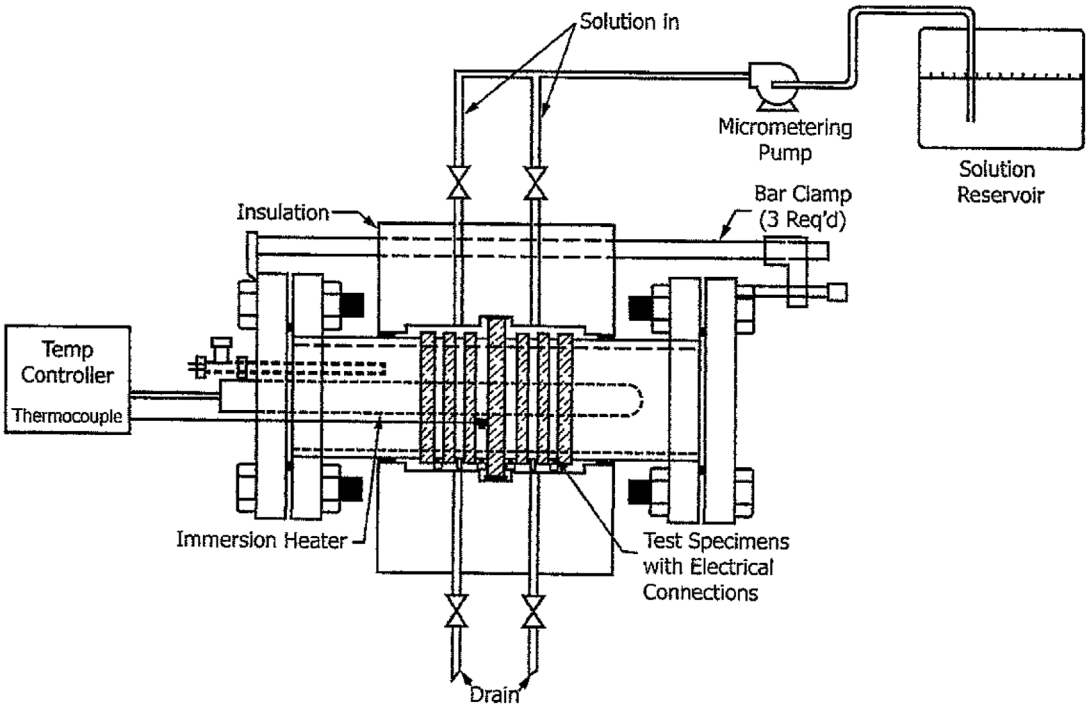
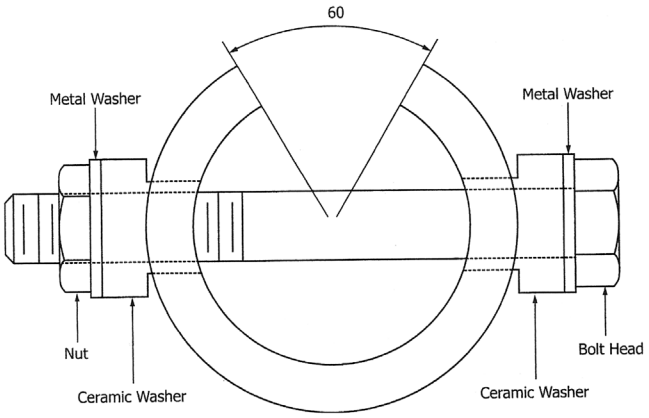


FIG. 12 C-ring specimen for LDF test (see ASTM G186).



STANDARDIZED CORROSION TESTS FOR ALLOYS FOR CHEMICAL MANUFACTURERS

Alloy producers have developed newer products that could offer significant improvements over the traditional corrosion-resistant alloys. The problem for corrosion engineers is to determine if these alloys are improvements for the processes that they are evaluating. Ultimately, specific corrosion tests would be necessary for each process for such an evaluation to be made, but it is helpful if the performance of new alloys in a range of typical environments could be available. The problem is determining which environments should be tested. MTI instituted a project to create a list of tests that alloy producers could use to evaluate their alloys. The advantage to this approach is that because the tests are standardized, it is possible to compare the results from different laboratories on different alloys without having to include all of the alloys in a single program.

The MTI program was developed by Treseder and Degnan, and their report became the basis for ASTM G157, *Standard Guide for Evaluating Corrosion Properties of Wrought Iron- and Nickel-Based Corrosion Resistant Alloys for Chemical Process Industries*.[9–11] The various test environments are shown in table 4. ASTM G157 also recommends that welded specimens be included. Crevice coupons and ASTM G30, *Standard Practice for Making and Using U-Bend Stress-Corrosion Test Specimens*, U-bend stressed specimens also are included. The concept for mass loss corrosion rate evaluations is to determine the lowest temperature at which the corrosion rate exceeds 0.13 mm/yr. Tests are carried out at 30°C, 50°C, 70°C, 90°C, 110°C, and 130°C, or if the normal boiling temperature is lower than 130°C, at the boiling point. The tests are run for 96 h. If a specimen shows a corrosion rate in excess of 0.13 mm/yr, tests at higher temperatures are not necessary. The crevice corrosion test uses the acidified ferric chloride solution specified in ASTM G48, *Standard Test Methods for Pitting and Crevice Corrosion Resistance of Stainless Steels and Related Alloys by Use of Ferric Chloride Solution*, to determine the critical crevice corrosion temperature. The chloride stress corrosion cracking testing is done according to the acidified sodium chloride solution in ASTM G123, *Standard Test Method for Evaluating Stress-Corrosion Cracking of Stainless Alloys with Different Nickel Content in Boiling Acidified Sodium Chloride Solution*, and is run for 1,000 h. If an alloy does not crack in the ASTM G123 environment, a second round of testing is conducted for 30 days in boiling magnesium chloride solution, as proposed in ASTM G36, *Standard Practice for Evaluating Stress-Corrosion-Cracking Resistance of Metals and Alloys in a Boiling Magnesium Chloride Solution*.

TABLE 4 Fourteen Environments for Evaluating General Corrosion Resistance of Alloys for Use in Chemical Manufacturing Facilities

Test Environment	Formula	Concentrations, mass %[a]
Hydrochloric acid	HCl	0.2, 1.0, 5.0
Sulfuric acid	H_2SO_4	10, 60, 96[b]
Nitric acid	HNO_3	10, 70[b]
Phosphoric acid	H_3PO_4	85
Formic acid	HCOOH	50
Acetic acid	CH_3COOH	80
Sodium hydroxide	NaOH	50
Hydrochloric acid+ ferric chloride	$HCl+FeCl_3$	1.0 HCl+0.3 $FeCl_3$[c]
Acetic acid+acetic anhydride	$CH_3COOH+(CH_3CO)_2$	50/50

[a]All aqueous solutions are to be prepared with purified water.
[b]Undiluted reagent grade acids may be used.
[c]Ferric chloride concentration based on anhydrous reagent.

The results of this program provide a reasonable selection of environments that can be used to determine if an alloy might have application in a new process. Additional testing can be carried out if an alloy looks promising, but this group of results should provide a good basis for determining which alloys would be candidates for that testing.

References

1. S. W. Dean, Jr., *Laboratory Corrosion Testing of Metals and Alloys* (St. Louis, MO: Materials Technology Institute, 2014).

2. S. W. Dean, Jr., *Field Testing of Metals and Alloys* (St. Louis, MO: Materials Technology Institute, 2018).

3. B. S. Covino, Jr., "Introduction to Corrosion Testing and Evaluation," in *ASM Handbook, vol. 13A, Corrosion: Fundamentals, Testing, and Protection*, ed. S. D. Cramer and B. S. Covino, Jr. (Metals Park, OH: ASM International, 2003), 419.

4. R. B. Puyear, "Industrial Chemicals," in *Corrosion Tests and Standards: Application and Interpretation*, 2nd ed., ed. R. Baboian (West Conshohocken, PA: ASTM International, 2005), 418-424.

5. F. Mansfeld, "Electrochemical Methods of Corrosion Testing," in *ASM Handbook, vol. 13A, Corrosion: Fundamentals, Testing, and Protection*, ed. S. D. Cramer and B. S. Covino, Jr. (Metals Park, OH: 2003), 446–462.

6. P. Elliot, "Designing to Minimize Corrosion," in *ASM Handbook, vol. 13A, Corrosion: Fundamentals, Testing, and Protection*,

ed. S. D. Cramer and B. S. Covino, Jr. (Metals Park, OH: ASM International, 2003), 929–939.

7. W. G. Ashbaugh and T. F. Laundrie, "A Study of Corrosion of Steel under A Variety of Thermal Insulations," in *Corrosion of Metals under Thermal Insulation*, ed. B. J. Moniz and W. I. Pollock (West Conshohocken, PA: ASTM International, 1985), 121–131.

8. P. Elliot, "Materials Selection for Corrosion Control," in *ASM Handbook, vol. 13A, Corrosion: Fundamentals, Testing, and Protection*, ed. S. D. Cramer and B. S. Covino, Jr. (Metals Park, OH: ASM International, 2003), 909–928.

9. R. S. Treseder and E. A. Kachik, "MTI Corrosion Tests for Iron- and Nickel-Base Corrosion Resistant Alloys," in *Laboratory Tests and Standards*, ed. G. S. Haynes and R. Baboian (West Conshohocken, PA: ASTM International, 1985), 373–399.

10. R. S. Treseder and T. F. Degnan, *Corrosion Testing of Iron- and Nickel-Base Alloys, Part I: Test Methods* (Revised), MTI vol. 46 (St. Louis, MO: Materials Technology Institute, 1995).

11. T. F. Degnan, *Corrosion Testing of Iron- and Nickel-Base Alloys, Part II: Test Data*, MTI vol. 46 (St. Louis, MO: Materials Technology Institute, 1995).

Chapter 27 | Flue Gas Desulfurization

James R. Crum[1] and Ralph W. Ross [2]

Description of Materials of Construction Used and Selection Criteria

A variety of construction materials has been used in flue gas desulfurization (FGD) systems on utility boilers. They can all be classified into three major categories: metals, organics, and nonmetallic inorganics.

METALS

Metals ranging from carbon steel to stainless steels and nickel-based alloys have been used in most components of FGD systems. Unlined carbon steel is used in cases in which the flue gas is above the acid dewpoint or in which alkaline conditions are maintained, such as most of the components of spray-dryer FGD systems, inlet ducts upstream of the wet/dry interface of all FGD systems, lime/limestone storage silos, and fresh lime/limestone storage tanks and piping. Under acidic conditions, the carbon steel must be protected by a lining or by other corrosion-control techniques. Alternatively, corrosion-resistant alloys are used under these conditions. Stainless steels (e.g., type 316L, 317L, 317LMN, duplex 2205 and 2507, Ferralium 255, Zeron 100, 904L, 254 SMO, 25-6MO, 1925 hMo, and AL6XN) and nickel-based alloys (e.g., G-3, G-30, 625, C-276, C-22, 622, 686, and 59) have been used in FGD system components, such as prescrubbers, absorbers, spray nozzles, reheaters, and dampers. In critical locations with more aggressive environments, such as reheaters, outlet dampers, outlet ducts, and gas mixing zones, nickel-based alloys (e.g., alloys 625, G-3, C-276, C-22, 622, 686, and 59) and titanium (grades 2 and 7) have been used.

Because of the relatively high cost of nickel-based and titanium alloys, a significant cost savings can be realized by using thin claddings of these alloys over carbon steel plates, rather than solid alloy plates, for absorbers, dampers, ductwork, and stack liners. Clad plate can be manufactured by hot rolling, explosive bonding, or welding the cladding and base plate together.[1,2] However, these methods are generally applicable only to new or replacement FGD components, because existing systems already have the substrate (e.g., carbon steel) in place. A method that is applicable to both new and retrofit construction is called "wallpapering" (NACE SP-0292, *Installation of Thin Metallic Wallpaper Lining in Air Pollution Control Equipment and Other Process Equipment*).[3,4] This method, which has been used in the chemical industry for many years, involves welding thin sheets, usually 1.6 mm (1/16 in.) thick, of an alloy, such as C-276, C-22, 622, 686, or 59 to the carbon steel substrate. The clad plate method is discussed in NACE SP-0199, *Installation of Stainless Chromium-Nickel Steel and Nickel-Alloy Roll-Bonded and Explosion-Bonded Clad Plate in Air Pollution Control Equipment*.[5] Both methods offer guidance for an excellent means of providing protection using thin corrosion-resistant materials.

The most frequently reported failures for alloys in FGD components are pitting and crevice corrosion (especially under scale-deposits), weld heat-affected-zone (HAZ), and weld attack. General corrosion, erosion-corrosion, or stress corrosion cracking (SCC) can also occur. Many environmental factors are responsible for the failures, but high levels of chloride combined with low pH and elevated temperatures play a major role.[6] Fluoride also can be a factor, but its role is complex. For example, acid fluorides are especially corrosive to certain metals, such as titanium.[7] Fluoride forms complex ions with species such as aluminum, magnesium, and silicon, which are typically present in fly ash. Corrosion failure analysis studies have shown that the fluoride ion is interacting with the chloride ion in limestone-based FGD systems to cause severe crevice and pitting corrosion.[8,9] Elevated temperatures, such as those encountered in prescrubbers and reheaters, increase SCC susceptibility, whereas erosive particulates play a role in influencing erosion-corrosion in prescrubbers.[10]

ORGANICS LININGS

Organics linings have been used extensively in various FGD components, including prescrubbers, absorbers, tanks, outlet ducts, and stacks. These linings include polyesters, vinyl esters,

[1]Alloy Consulting LLC, 20 Quail Dr., Ona, WV 25545, USA
[2]Nickel Institute, 77 Keeneland Dr., Huntington, WV 25705, USA
The authors acknowledge the previous authors of this chapter, Harvey S. Rosenberg, Guild Associates, Hilliard, OH and Eldon R. Dille, Specialists in Solutions, Inc., Highland, IN.

DOI: 10.1520/MNL202NDSUP20190021

Copyright © 2022 by ASTM International, 100 Barr Harbor Dr., PO Box C700, West Conshohocken, PA 19428-2959
ASTM International is not responsible, as a body, for the statements and opinions expressed in this chapter. ASTM International does not endorse any products represented in this chapter.

epoxies, novolac epoxy, novolac phenolic epoxy, fluoroelastomers, and rubber. Organic linings are attractive because they can provide the low initial cost for many of these components, but they may have higher maintenance costs. The linings generally are applied in liquid form by brushing, rolling, spraying, or troweling. To provide an effective barrier, the organic linings used in FGD systems are often applied in several layers. This decreases the probability of through-thickness pinholes and achieves a greater permeation thickness than typical coatings. Moreover, the polyester, vinyl ester, epoxy, novolac epoxy, and novolac phenolic epoxy linings often contain a mica flake or glass flake filler that further decreases the permeability and provides reinforcement. Mica flake-filled linings generally are not as abrasion resistant as glass flake-filled linings.

In components for which high abrasion resistance is required, linings reinforced with glass cloth or inert matting along with abrasion-resistant pigments silicon dioxide, aluminum oxide, and tungsten carbide have been used. Although rubber is an organic lining, it is often placed in a separate category because it is applied in sheet rather than liquid form. Three types of sheet rubber have been used for lining absorbers: natural (gum), neoprene, and chlorobutyl. Of these, the rubber industry generally considers chlorobutyl to be the preferred material for this application. Chlorobutyl rubber has low moisture permeability.

Failure of organic linings can occur by blistering, disbonding, and wear from abrasive slurries.[11] Blistering of organic linings immersed in liquids is greatly increased when a thermal gradient is present.[12] Excursions to hot flue gas temperatures can damage or destroy organic linings. Fluoroelastomer linings can withstand excursions up to 260°C (500°F) and are resistant to chemical attack and abrasion. They are relatively permeable to moisture, however, and with the use of scrubbed flue gas in the outlet duct, less-than-desirable coating life has been obtained. In addition, fluoroelastomer coatings generally are more expensive than other types of organic linings. Rubber sheet linings offer excellent resistance to abrasion, but rubber is a flammable material, so care must be taken to prevent ignition of these sheet linings by external sources, such as welding on the steel side. It is good practice to label the external surfaces of rubber sheet-lined absorbers to indicate the presence of a rubber lining. Close attention to product specification and application is required to prevent short life and inconsistent performance of rubber linings.[13]

Fluoroelastomer, fluoropolymer, and fluorinated elastoplastic materials, as well as rubber, are used in expansion joints, typically with fabric reinforcement. The cost of the fluorine-containing materials may be an order of magnitude higher than that of rubber materials, but longer life expectancy, higher temperature tolerance, and better overall operating performance can easily offset the higher installed cost. Mixing reprocessed fluoroelastomer scrap with virgin fluoroelastomer can reduce the cost of the material, but physical properties critical to the performance of expansion joints are impaired. The causes of failure of fluoroelastomer expansion joints include thermal degradation induced by temperature excursions or thermal cycling, acid attack, and mechanical damage.

Fiberglass-reinforced plastic (FRP, also known as glass-reinforced plastic [GRP or GFRP] in Europe) is used to fabricate mist eliminators, piping and spray headers, and stack liners. Various polymeric resins are used, including polyester, vinyl ester, and novolac vinyl ester. The typical operating maximum temperature range of the FRP structures is 82°C (180°F) to 177°C (350°F). FRP also is a flammable material that must be protected against ignition from external sources. The types of FRP failures include mechanical damage, laminate degradation, physical damage, and fire. The causes of failure include inadequate engineering, poor fabrication quality, abrasion, temperature excursions, and, depending on the resin, chemical attack (e.g., acid hydrolysis of polyester).

INORGANIC LININGS

Nonmetallic inorganic materials are used in prescrubbers, spray nozzles, slurry pumps, outlet ducts, and stacks. The materials include prefired bricks and shapes, ceramic tiles, borosilicate foamed-glass blocks, hydraulically bonded concretes and mortars, and chemically bonded concretes and mortars, all of which are used as lining materials in cases in which temperature resistance, chemical resistance, or abrasion resistance are required. Acid-resistant bricks commonly are used as construction materials for stack liners. A potential failure cause of these bricks is mechanical stress from dimensional changes during service. Also, several free-standing brick flues have been found to lean toward the outer concrete shell. This problem appears to be associated with mixing bypassed gas and scrubbed gas in the stack, thus creating temperature and moisture gradients that cause one side of the flue to expand more than the other side. A freestanding brick flue that is constantly wet with scrubbed FGD gas does not lean.[14]

Borosilicate foamed-glass blocks bonded with urethane-modified asphaltic mastic have been used to line outlet ducts and stacks. The combination of these two materials results in a lining that is resistant to permeation by aggressive condensate and can handle continuous temperatures to 205°C (400°F) and excursions to 370°C (700°F). The urethane-modified asphaltic mastic has a temperature limit of 82°C (180°F). As the mastic between the bricks is reduced to char by high temperatures, however, the char provides insulation for the remaining mastic. Moreover, the thermal insulating properties of the glass block and the flexibility of the membrane material contribute to the good performance of the lining. The foamed borosilicate glass can be mechanically damaged easily, and failures can occur as a result of abrasion, puncturing, and cracking. Also, scale that forms on the lining cannot be removed easily. These problems can be minimized by applying a topcoat of chemically bonded mortar over the borosilicate foamed-glass blocks.

Hydraulic-setting, cement-bonded concretes (hydraulic concretes) are used as linings for prescrubbers, outlet ducts, and stacks. These concretes contain aluminate to withstand temperatures of 260°C (500°F) without strength degradation. In sulfuric acid solutions (pH < 4), however, the cement is attacked because of the dissolution of the calcium aluminate. This dissolution of the bond results in loosening of the aggregate and erosive wear of the lining.[15]

Chemically bonded mortars are commonly used to bond acid-resistant brick stack liners. Chemically bonded concrete mixes also can be used as linings. These materials generally contain siliceous aggregates, a sodium silicate, potassium silicate, or colloidal silica bond phase, and a silicofluoride, phosphate, or organic bond gelling agent. They also may contain potassium fluoride. Because chemically bonded concretes can withstand hot, acidic environments, they offer an abrasion-resistant alternative to organic linings. They do have a higher permeability than most organic linings and are subject to cracking, so that any condensed acid will reach the substrates to which they are applied. In many cases, an organic membrane is used under a chemically bonded concrete lining to provide additional protection to the carbon steel substrate. Although this measure increases the time for acidic condensate to reach the substrate, it can complicate repair procedures. When the membrane fails because of permeation by acidic species, the concrete must be removed to repair or replace the membrane.[16]

COST CONSIDERATIONS

The prime objective in selecting construction materials for FGD systems is to choose the most cost-effective or optimum material for each component—that is, the one meeting the design requirements at the least cost over the life of the facility. Even though a more corrosion-resistant material may cost twice as much as a less corrosion-resistant material, the effect of the materials cost may be a small percentage on the total construction cost. A reduction in cost can result if the labor costs involved in the installation are significant compared with the difference in the cost of the materials. In addition to installed cost, it is necessary to consider repair or replacement cost over the 20- to 30-year design life of the plant when specifying the most economical materials available for the intended service conditions. Certain materials, such as organic linings, cannot be expected to last the plant lifetime without periodic maintenance touchup, repair, or replacement.

Description of Corrosion Environments Encountered

The environment in an FGD system depends on three factors: temperature, chemistry, and abrasiveness. ASTM has identified three levels of severity, from 1 (mild) to 3 (severe), for classifying these three environmental factors (see table 1).[17] Figure 1 is a schematic diagram of environmental severity levels in the major components of a wet FGD system. In all three digit codes shown, the first digit represents temperature, the second digit represents chemistry, and the third digit represents abrasiveness. (A code of zero for a given environmental factor denotes that the factor does not exist or is not applicable for a specific operating condition.) For example, the mildest condition encountered can be coded 1-1-1 and represents a temperature below 60°C (140°F), a pH greater than 3 with low concentrations of chloride and fluoride (as defined in table 1), and low-velocity fluid flow with no direct impingement by particulates. An example of this mild condition is a mist eliminator (see fig. 1). By contrast, the most severe condition can be coded 3-3-3 and represents a temperature above 93°C (200°F), an acid concentration greater than 15% with high concentrations of chloride and fluoride, and very high-velocity fluid flow with impingement by entrained particulates.

TABLE 1 ASTM Classification System for Environmental Factors in FGD Systems[13]

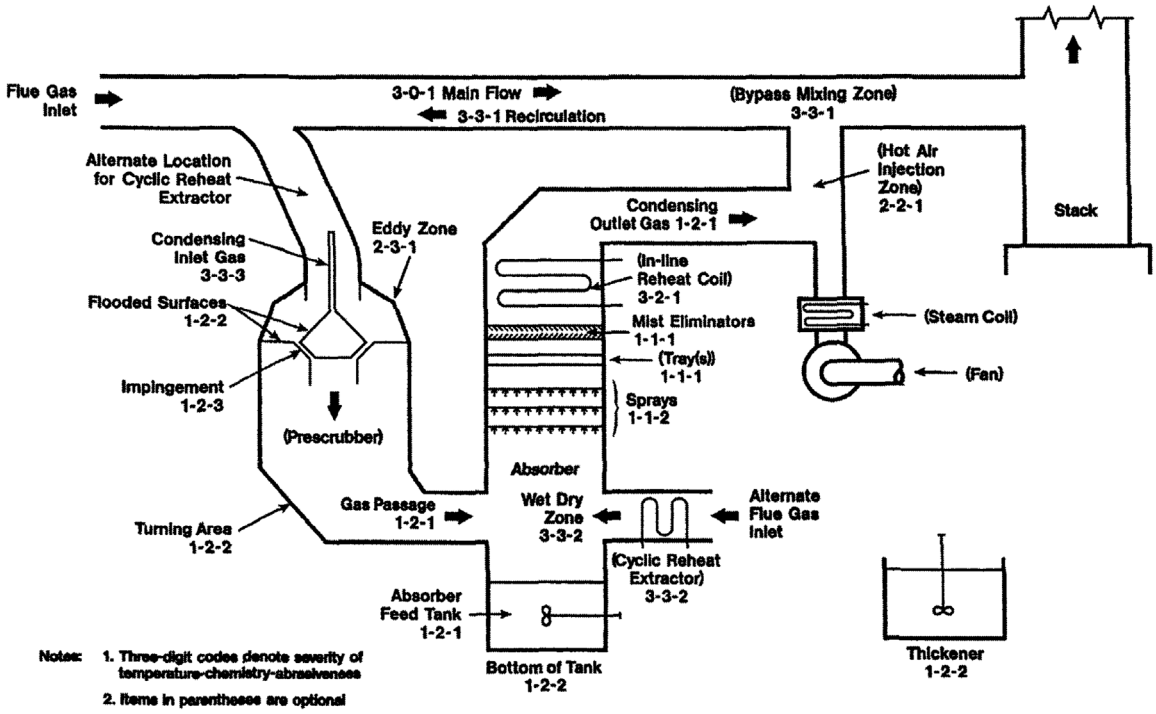
Level of Severity	Temperature	Chemistry	Abrasiveness
1	Ambient to 60°C (140°F)	pH > 3 with < 100 ppm F^- and < 1,000 ppm Cl^-	Low-velocity fluid flow with no direct impingement of particulates (e.g., duct wall)
2	60°C (140°F)–93°C (200°F)	pH 0.1 to 6 with 100 to 1,000 ppm F^- and 1,000 to 10,000 ppm Cl^-, or saturated flue gas	High-velocity fluid flow, spray impingement, or strong agitation (e.g., absorber spray zone)
3	Above 93°C (200°F)	Greater than 15% acid with >1,000 ppm F^- and >10,000 ppm Cl^-, or intermittent wet/dry zones	Very high-velocity fluid flow with impingement of entrained particulates (e.g., venturi throat)

An example of this severe condition is the inlet of a venturi prescrubber. Several species in solution have been found to affect the corrosion of alloys in FGD systems. Most of these species, however, are considered trace elements in scrubbing liquors. Notable exceptions are chlorine and fluorine, both of which are present in coal. Depending on the source, the makeup water can also contribute chlorides, fluorides, and oxidizing species (e.g., ferric and/or manganate ions) to the FGD system. When the water balance is tightly closed, dissolved ionic species, such as chlorides, become highly concentrated. Chloride ions cause localized corrosion in alloys. The corrosion rate for a given alloy is a function of chloride concentration, pH, temperature, and, in many instances, the concentrations of trace elements present at levels below 2,000 ppm (e.g., aluminum, copper, and iron).[18,19] Uncomplexed fluoride ions can cause localized attack in the HAZ of welded austenitic and duplex stainless steels and can be catastrophic to titanium. In addition to having its own effect on corrosion rates, aluminum, dissolved from fly ash, can react with fluorides to form the complex ions AlF_2^{+1} and AlF^{+2}. If there is enough aluminum, free fluoride will not be available.

Techniques Used for Controlling Corrosion and Materials Degradation

To avoid materials problems, it is important to ensure that the selected material has adequate corrosion-resistance to give

FIG. 1 Schematic diagram of environmental severity levels in wet FGD systems.[13]



satisfactory service in a well-defined environment. The applicability of an alloy in the temperature range of a wet FGD environment is mainly a function of pH, chloride concentration, and oxidizing ions (e.g., ferric). Because the condensate in an outlet duct or flue can have a pH of 2.5 or lower, a more corrosion-resistant alloy should be used for these components than for an absorber, where the pH of the scrubbing liquor is typically above 5.0. (Under upset conditions, however, the pH may drop to 2.0 or lower). The chloride concentration in the scrubbing liquor depends primarily on the type of coal burned in the boiler. In addition, chlorides are provided by the water balance and the type of makeup water. If there is carryover of scrubbing liquor from the mist eliminator, the chloride concentration in the outlet duct can increase because of the evaporation of water during periods of bypass of the absorber. Stainless steel Types 316L, 317LMN, 904L, 254SMO, 25-6MO, and AL6XN have been used successfully in the absorber vessels when the chloride concentration is within the applicable range for these alloys.

In some FGD reaction tank vessels, for example, an electrochemical potential adjustment protection (PAP) system has been used successfully to control thiosulfate pitting, chloride/fluoride pitting, crevice corrosion, and general corrosion of all submerged stainless steels Types 317L, 317LMN, and 904L. This combination of stainless steels with the PAP system allows for the use of an alternative cost-effective technique for corrosion control in FGD reaction tanks made of otherwise-susceptible materials.[20] In outlet ducts exposed to both scrubbed flue gas and untreated flue gas, the use of a highly corrosion-resistant alloy, such as alloys C-276, C-22, 622, 686, or 59, generally is required to prevent corrosion.[21]

In certain cases, it may be possible to modify the environment, that is, temperature, chemistry, or abrasiveness, to extend the useful life of a material. Temperature modifications in an FGD system can be accomplished only by a limited number of practical methods. These practical methods include (1) water sprays to protect against thermal excursions, and (2) insulation to reduce thermal gradients. The scrubbed flue gas can be reheated by a variety of methods to prevent, for example, formation of acidic condensate on the floor of the outlet duct or to downstream fans in wet FGD systems. Most reheat methods, however, increase the capital and operating costs of an FGD system, increase the energy consumption of the system, and create materials problems of their own. Bypass reheat can avoid an increase in energy consumption, but it also creates an extremely aggressive environment in the mixing zone of the bypassed gas and the scrubbed gas. Therefore, bypass to the outlet duct or stack for reheat or emergencies should be avoided, if possible.

The process chemistry can be modified by using additives or by minimizing the chloride and fluoride concentrations in the scrubbing liquor. The use of additives that inhibit oxidation of sulfite to sulfate reduces gypsum deposition, which, in turn, can reduce crevice corrosion that tends to occur under deposits. The use of additives that buffer the pH of the scrubbing liquor may prevent pH excursions that can cause failure of alloys.

Several methods are available for minimizing the chloride and fluoride concentrations in the scrubbing liquor. These include using a separate quench loop, operating the FGD system with an open water balance, or using sludge stabilization with fly ash and lime so that a considerable amount of water can be purged with the scrubber effluent. A minor reduction of chloride

and fluoride concentrations also can be achieved by using river water or well water, rather than cooling tower blowdown, for makeup. Because the chloride and fluoride ions are primarily products of coal combustion, these non-coal-related methods for reducing chloride and fluoride result in only minor reductions.

The abrasive effects of fly ash on downstream FGD components also can be minimized by using a separate quench loop, but in conjunction with a venturi prescrubber. Alternatively, a high-efficiency particulate collection device can be used upstream of a wet FGD system.

Aside from the use of linings, other corrosion protection techniques include cathodic protection (CP) and corrosion inhibitors. Impressed current cathodic protection technology is attractive because it avoids the use of expensive alloys. The Electric Power Research Institute (EPRI) has developed a system that allows CP to be applied to duct walls having thin films of condensate, rather than immersed in a liquid.[22] EPRI also has evaluated the performance of several inhibitors on the corrosion behavior of alloys in a pilot-scale scrubber. The data suggest that the use of corrosion inhibitors in FGD systems is possible, but the results from this study were not very encouraging.[23]

Another electrochemical technique, PAP, was patented by the Pulp and Paper Research Institute of Canada.[24] PAP is an electrochemical corrosion protection technique that is used to protect stainless steel in oxidizing chloride environments. The technique uses a DC current source to move the electrochemical potential of the protected surface in the negative direction. This technique is not CP in the traditional sense. Although both CP and PAP move the potential in the electronegative direction, CP requires the set potential to be in the immunity region as depicted by the Pourbaix diagrams. In contrast, PAP takes advantage of the passive film available in stainless steel/oxidizing environment and the set potential is in the passive zone. Some of the economic advantages of PAP versus CP are smaller current source requirements and lower anode consumption. This method has now been used on 14 FGD stainless steel reaction tanks.[25]

Another technique for avoiding corrosion is the use of FRP (GRP in Europe) for FGD components, such as absorbers and tanks. FRP vessels as large as 30 m (100 ft) in diameter can be fabricated on site by using a spinning process to produce multiple layers of material.[26] After an initial 3-m-high (10 ft) cylindrical section is spun, it is hoisted to the top of the mandrel and another 3 m (10 ft) section is wound, overlapping the first. The overall height of the structure is limited by the mechanical properties of the composite unless external support is provided. A potential problem is abrasion from spray impingement and from highly agitated slurries. The interior surface of an FRP component can be lined with an abrasion-resistant lining, thus providing additional vessel life.

Specific Problem Areas

WELDING

The quality of the welding is critical in FGD components constructed of stainless steels, nickel alloys, and titanium. Achieving a high level of quality in alloy welding requires stringent specifications, qualified fabricators, and installation contractors, as well as thorough inspection and nondestructive testing of the welds.[27] A great deal of care must be taken to avoid iron contamination during fabrication (e.g., using stainless steel tools and ceramic abrasives). To prevent rust blooms, any embedded iron must be removed by an acid pickling treatment. Heat input should be minimized using small-diameter welding electrodes and stringer passes to avoid carbide precipitation and hot cracking. Welding defects (poor fit-ups, lack of penetration, weld spatter, pencil markings, heat tint oxides) should be avoided or removed by grinding. If the proper alloy and welding electrodes have been selected for the service environment, the quality of the welds is the next most critical item. Leaking welds can cause discharges of process fluids, which, in turn, can deteriorate external equipment. Corrosion of welds can cause a loss of structural integrity of the welded component (e.g., ductwork, absorbers, and internal supports).

Thin metallic linings require good welding procedures and inspections to achieve leak-tight welds. Improper welding results in flaws and pinholes in the seal welds between the overlapped alloy sheets. Because of these flaws, liquid can get behind the sheets and cause corrosion of the substrate. Also, during plug welding of the alloy sheets to the substrate, the proper welding material and care must be used to ensure that iron dilution does not adversely affect the corrosion resistance of the weld. One approach is to cover the plug weld with a seal-welded patch of the alloy lining.

FIRE PROTECTION

In cases in which combustible linings are used, fire protection should be provided by an automatic water spray system.[28] The system should be designed so that the spray patterns are not obstructed, and the lining is completely covered by the spray. The spray nozzles should include corrosion-resistant blow-off caps to prevent plugging. The scrubbing liquor spray nozzles are not suitable for fire protection in prescrubbers or absorbers. There have been a few costly and fatal fires in FGD systems where the ignition source has been linked to cutting and welding operations during maintenance procedures. Absorbers can contain a large quantity of combustible materials, including plastic mist eliminators and packing, as well as flammable linings. For example, the plastic materials may be as much as 1.2 m (4 ft) in height and 15 m (50 ft) in diameter. The fire hazard is most prevalent when the unit is down for periodic maintenance. Typically, the access hatches are open, allowing for a high volume of air movement; the fire loading may be increased because of the presence of combustible scaffolding; and ignition sources may be present because of cutting and welding activities.

The National Fire Protection Association (NFPA), in Report No. NFPA 850, has recognized the fire hazard associated with FGD systems during outage and construction activities.[29] The NFPA committee responsible for this document is considering a revision to enhance guidance. The proposed revision will include identification of hazards for combustible-lined equipment and will suggest closing the outlet damper during cutting and welding operations to reduce airflow through the equipment.[28]

Use of Test Methods to Evaluate Corrosion and Degradation

Continuous, online corrosion monitoring may be used to detect active corrosion of FGD systems; however, this technique is not widely utilized. Conventional corrosion monitors are designed for use in bulk liquids and do not function satisfactorily in the thin condensate films that form on the surfaces of FGD ducts. EPRI has used an advanced electrochemical method of corrosion surveillance developed by the Corrosion and Protection Centre Industrial Services (CAPCIS) in England.[30] This method allows for online monitoring of corrosion activity in either thin condensate films or bulk liquids. EPRI sponsored demonstration tests of the CAPCIS system at several U.S. electric utility plants in 1985.

An electrochemical monitoring system that tracks the rate and depth of permeation of aggressive chemicals in the walls of FRP or other nonmetallic vessels is also available.[31] The system uses a set of conductivity probes mounted at various depths in the wall of an FRP component. The probes can be attached during fabrication, before final installation, or as a retrofit for equipment already installed.

Methods to evaluate materials performance are used both for materials selection and for failure analysis. Materials selection can be based on prior service history, corrosion tests in operating commercial units, or in the laboratory.[21] Field corrosion testing provides long-term performance results from actual FGD environments, but the environmental conditions usually are not well-defined or constant. Laboratory tests with simulated flue gas may not be representative of actual service conditions and may yield misleading results.

Failure analysis involves documentation of environmental conditions, inspection of the failed component, collection of samples of the failed material, any deposits on the material, and any liquids that condensed on or had contact with the material, and appropriate laboratory analyses of the collected samples. The background information and laboratory results are analyzed to identify the failure mechanism or the failure cause.[32] The results then lead to a plan to prevent a reoccurrence of the failure

TEST METHOD APPROACH

Coal contains many of the elements in the periodic table, even in trace amounts, which makes it difficult to simulate the environment of an FGD system. The scrubbed flue gas from coal-fired power plants typically contains nitrogen, carbon dioxide (CO_2), oxygen, water vapor (H_2O), sulfur dioxide (SO_2), sulfur trioxide (SO_3), nitric oxide (NO), nitrogen dioxide (NO_2), hydrogen chloride (HCl), hydrogen fluoride (HF), trace organics, fly ash, and solids carried over from the absorber slurry. The concentration of species such as HCl and HF are very low in the scrubbed gas, but can be significant if some flue gas is bypassed for reheat. In one of the early FGD units with bypass reheated flue gas in the outlet ducts, the scale that formed on the walls of the duct was 10% potassium fluoride (KF).[8]

If gas cylinders are used to prepare simulated flue gas for exposure testing, many cylinders may be required to run long exposure periods. If a combustion source is used to supply flue gas, it is difficult to match the composition of flue gas from a large pulverized coal-fired boiler. Maintaining the proper ratio of NO to NO_2 is a special problem because NO oxidation to NO_2 is a function of the temperature, the initial NO concentration, the oxygen concentration, and the gas residence time in the exposure chamber. The usual procedure is to use simulated flue gas with the same SO_2 concentration as actual flue gas, but with different concentrations of other species. This procedure can produce erroneous results.

Many species are typically present at various concentrations in FGD outlet duct condensate.[15] Those typically present at concentrations greater than 100 mg/L include the following: aluminum, calcium, iron, potassium, magnesium, sodium, chlorine, fluorine, sulfate, borate, and phosphate. Species present in the range of 10–100 mg/L include the following: manganese, selenium, silicon, tin, titanium, vanadium, zinc, and nitrate. Several species, including barium, beryllium, cadmium, lead, and antimony, are present at concentrations less than 10 mg/L. The pH ranges from less than 1.0 to about 2.5, depending on the FGD system operating parameters.

In preparing solutions for corrosion testing, solubility problems need to be considered. If precipitation occurs in a solution, the composition changes. If some species typically present in FGD condensate are omitted from the test environment, the results can be erroneous. As previously mentioned, trace elements can affect corrosion rates.

Many of the exposure tests in commercial units have involved the use of spools or racks of different materials placed in various locations inside an FGD system.[33] When using several corrosion racks, at many locations inside an FGD system, the probability is good that one or more of the corrosion racks will be exposed to the environment causing the failure. The environment in the bulk gas stream, in which the specimens are usually placed, is not the same as at a duct wall, where condensation can occur. In some field tests, the specimens were directly mounted on the duct wall so that they experienced the same conditions as the wall.[34] Test coupons were mounted using bolts of the same alloy as the duct wall, and in another method, sheets or plates were welded onto the vessel wall. To avoid galvanic corrosion of alloy coupons, the coupons were insulated from the bolts and the substrate with fluoropolymer film and washers.

METHODS USED

Some laboratory exposure tests are conducted in chambers like that described in ASTM B117, *Standard Practice for Operating Salt Spray (Fog) Apparatus*. Because the environment is more corrosive than the salt fog described in ASTM B117, the variations described in ASTM G85, *Standard Practice for Modified Salt Spray (Fog) Testing*, are often used. Some investigators have used a modified procedure in which the test coupons are mounted over holes on the outside wall of the exposure chamber so that they can be subjected to a thermal gradient.[35] Outside mounting of the coupons also affords the opportunity to conduct *in situ* electrochemical impedance measurements.

Electrochemical impedance spectroscopy (EIS) is an AC technique used to determine the components of an analog

electric circuit that represents an electrochemical process.[36] Electrochemical impedance is the ratio of the change in potential to the change in current (ΔE/ΔI) and is determined from the applied potential and the response current as a function of frequency (co) in an electrochemical cell, when potential and current are linearly related. The impedance, Z, is a complex number incorporating both the magnitude of ΔE/ΔI and the phase shift between E and I. EIS can give valuable mechanistic information for analyzing the corrosion behavior of alloys[37] and the performance of coatings.[38]

Two ASTM test methods are particularly useful for characterizing organic resin linings and bricks, respectively. These methods include ASTM D1653, *Standard Test Methods for Water Vapor Transmission of Organic Coating Films*; and ASTM C20, *Standard Test Methods for Apparent Porosity, Water Absorption, Apparent Specific Gravity, and Bulk Density of Burned Refractory Brick and Shapes by Boiling Water*.

Two additional test methods regarding bricks are worthy of mention. One is a laboratory test in which the moisture expansion that occurred in service is recovered as a shrinkage during heating of a brick sample in a dilatometer. The dilatometer measures thermal expansion as a function of temperature. Shrinkage causes a hysteresis in the thermal expansion curve so that the heating and cooling curves do not coincide. The shrinkage is determined from the difference in the curves at room temperature.

The other method is a field test to document the amount of lean in a free-standing brick flue. A laser beam is used to project a target onto the interior surface of a flue in four compass directions spaced 90° apart. In each direction, the target is tracked at predetermined incremental elevations for the entire height of the stack. The precise position of the target is determined by a triangulation method using two Kern electronic theodolites (precision optical tooling instruments) and a computerized data acquisition system. The data from each compass direction provide a profile of the interior surface of the flue. Opposing wall profiles are used to calculate centerline profiles, which give the amount of lean as a function of height.[14]

Standard laboratory techniques are used to characterize samples for a failure analysis. These techniques include metallography, scanning electron microscopy, electron probe microanalysis, X-ray diffraction, Fourier transform-infrared analysis, and analytical chemistry.

Marine Scrubbers

In 1997, the International Convention for the Prevention of Pollution from Ships Committee of the International Maritime Organization (IMO) began setting limits of emissions of sulfur oxides and particulates from exhaust from ships burning heavy diesel fuel oil.[39] The global shipping industry responded by using wet scrubber systems similar in design and operation to the land-based FGD units described earlier. As of 2022, more than 5,000 ships are utilizing wet scrubber systems. By 2050, thousands of ships may be fitted with marine scrubber systems.

The primary difference between land-based versus shipboard FGD systems is that marine scrubbers may use seawater as the scrubber slurry. Obviously, this environment, consisting of 19,000 ppm chlorides, will be aggressive for most materials of construction. Three types of scrubbers are used. Open-loop or once-through scrubbers use seawater with enough alkalinity to remove the sulfur oxides from the engine exhaust. The resulting waste is discharged back into the ocean. Closed-loop systems use seawater or fresh water mixed with chemicals, such as caustic soda, to provide the alkalinity of the scrubber liquor to neutralize the sulfur oxides. The scrubber liquor is recirculated through the system with no discharge. Hybrid systems operate in open- or closed-loop mode depending on the discharge regulations of the area. They can operate as a once-through (open-loop) system using seawater, or in the closed-loop system using fresh water mixed with caustic soda, which is less corrosive if there is little contamination by chlorides.[39]

Marine scrubbers operate at up to 80°C (176°F), whereas land-based FGD typically operate at 54°C (130°F). The higher operating temperature makes the marine scrubbers more susceptible to crevice corrosion and SCC. Unlike land-based scrubbers, marine scrubber exhaust gas temperatures can reach 300–450°C (572–842°F) when operating in dry mode. Such high operating temperatures will eliminate coatings and plastics and may increase the risk of embrittlement of duplex stainless steels. A typical marine scrubber system is similar to the design shown in figure 1. Like land-based FGD units, some shipboard scrubbers also may be designed without venturi sections.

The marine scrubber components are generally stainless steels and nickel alloys, like the land-based FGD units. Slurry piping systems, which operate at lower temperatures and are not exposed to hot exhaust gas, are GFRP or FRP (also known as GRP), and nickel alloys/stainless steels depending on scrubber slurry chemistry and the ship owners' preference. The C-family of alloys (primarily alloys C-276, 686, and 59) with 55-59% nickel, 16–22% chromium, and 14–16% molybdenum (Mo) generally are required for optimum corrosion resistance if seawater is used to scrub the exhaust gas. Some scrubbers are reportedly using 6–7% Mo super-austenitic and duplex stainless steel alloys, but little information is available on their service performance. In fact, no detailed information is available in the open literature on corrosion performance of any marine scrubber system. In 2018, NACE International initiated Task Group 575 to determine corrosion performance of marine scrubbers and to prepare an industry white paper report.[40] In some cases, this industry appears to be following the materials selection history of the land-based electric power plant's experience.

It is extremely important to identify shop or field fabrication and welding pitfalls (precautions) that may induce corrosion—for example, scratches (micro-crevices), weld heat tints, and iron contamination on the metal surface. The 6–7% Mo super-austenitic and duplex stainless steel alloys are especially susceptible to these surface defects and contamination.

Seventy very large, land-based FGD units made of alloy 2205 duplex stainless steels failed between 2009 and 2011.[41] The reason for the failures was crevice corrosion (under-deposit attack) under heavy deposits of scale, especially in cases in which high-heat-input welding lead to severe corrosion of welded

seams in the absorber sump walls. Although alloy 2205 failed in land-based units, it may be appropriate for shipboard closed-loop scrubbers using caustic soda slurries containing less than 1,000 mg/L (ppm) chlorides.

References

1. S. L. Morse and C. E. Stevens, "Alloy C-276 Clad Steel Plate for Handling Scrubbed Flue Gases," paper no. 9 in *Proceedings of the 1990 Air Pollution Seminar* (Houston, TX: NACE International, 1990).
2. M. X. Cerny and C. G. Dormer, "Resista-Clad Plate in Flue Gas Desulfurization Units," paper no. 21 in *Proceedings of the 1987 Air Pollution Seminar* (Houston, TX: NACE International, 1987).
3. R. L. Richard, "Economics of a C-276 Outlet Duct Wallpaper Retrofit at Public Service Indiana Gibson #5," paper no. 4 in *Proceedings of the 1987 Air Pollution Seminar* (Houston, TX: NACE International, 1987).
4. *Installation of Thin Metallic Wallpaper Lining in Air Pollution Control and Other Process Equipment*, SP0292-2018 (Houston, TX: NACE International, 2018).
5. *Installation of Stainless Chromium-Nickel Steel and Nickel-Alloy Roll-Bonded and Explosion-Bonded Clad Plate in Air Pollution Control Equipment*, RP0199-HD1999 (Houston, TX: NACE International, 1999).
6. G. H. Koch and J. A. Beavers, "Laboratory and Field Evaluation of Materials for Flue Gas Sulfurization Systems," paper no. 2D in *Proceedings of the Seventh Symposium on Flue Gas Desulfurization* (Research Triangle Park, NC: U.S. Environmental Protection Agency, 1982).
7. G. H. Koch, J. A. Beavers, and T. K. Christman, *Materials Testing in Synthetic FGD Environments*, Report CS-2740 (Palo Alto, CA: Electric Power Research Institute, 1984).
8. E. R. Dille and T. Lemke, "FGD Corrosion at the R. D. Morrow, Sr. Generating Plant" (paper presentation, Solving Corrosion Problems in Air Pollution Equipment Seminar, PCA-IGCI-NACE, Denver, CO, 1981).
9. E. R. Dille, "Tame the Latest FGD-System Corrosion Pest: Fluorides," *Power Magazine*, August 1983.
10. J. A. Beavers and G. H. Koch, *"Review of Corrosion Related Failures in Flue Gas Desulfurization Systems"* (paper presentation, Corrosion/82, paper no. 202, NACE International, Houston, TX, March 22–26, 1982).
11. H. Leidheiser, Jr., M. L. White, R. D. Granata, and H. L. Vedage, *Mechanisms of Failure of Coatings Used in Flue Gas Desulfurization Systems*, Report CS-4546, Palo Alto, CA: Electric Power Research Institute, 1986).
12. J. F. Montle, *"Unexplained Coating Phenomena with Some Partially Baked Answers"* (paper presentation, Corrosion/71, paper no. 53, NACE International, Chicago, IL, March 25, 1971).
13. P. F. Ellis and P. Cassidy, *Specification Guidelines for Flue Gas Desulfurization Rubber*, Report CS-5528 (Palo Alto, CA: Electric Power Research Institute, 1987).
14. H. S. Rosenberg, C. W. Kistler Jr., F. W. Brust, E. R. Dille, et al., *Leaning Brick Stack Liners*, Report GS-6520 (Palo Alto, CA: Electric Power Research Institute, 1989).
15. H. S. Rosenberg, G. H. Koch, M. L. Meadows, and D. A. Stewart, "Materials for Outlet Ducts in Wet FGD Systems," *Materials Performance* 25, no. 2 (February 1986): 41–55.
16. H. S. Rosenberg, G. H. Koch, C. W. Kistler, Jr., et al., "Performance of Linings in FGD Systems," paper no. 9C-4 in *Proceedings: First Combined Flue Gas Desulfurization and Dry SO_2 Control Symposium* (Palo Alto, CA: Electric Power Research Institute, 1988).
17. J. I. Accortt, et al., *Manual of Protective Linings for Flue Gas Desulfurization Systems*, (West Conshohocken, PA: ASTM International, 1984).
18. G. H. Koch, N. G. Thompson, and J. L. Means, *Effects of Trace Elements in Flue Gas Desulfurization Environments on the Corrosion of Alloys—A Literature Review*, Report CS-4347 (Palo Alto, CA: Electric Power Research Institute, 1986).
19. F. Mansfeld, *The Effects of SO_2 Scrubber Chemistry on Corrosion*, Report CS-4847 (Palo Alto, CA: Electric Power Research Institute).
20. E. R. Dille, *"Using Electrochemical Protection to Prolong Service Life of Scrubbers and Associated Equipment"* (paper presentation, AIR-POL, update/98, Corrosion/98, NACE International, San Diego, CA, March 1998).
21. H. S. Rosenberg, B. Hindin, and P. T. Radcliffe, "Guidelines for FGD Materials Selection and Corrosion Protection," in *Proceedings of the 1992 Air Pollution Seminar*, (Houston, TX: NACE International, 1992).
22. G. H. Koch, S. P. Pednekar, E. H. Patterson, and B. C. Syrett, "Corrosion Control by Impressed Current Cathodic Protection in the Outlet Duct of a Pilot Wet Scrubber," paper no. 4B-5 in *Proceedings of the 1990 SO_2 Control Symposium* (Palo Alto, CA: Electric Power Research Institute, 1990).
23. B. S. Phull, T. S. Lee, N. H. Martin, and B. C. Syrett, "Corrosion Inhibitors for Flue Gas Desulfurization Systems," *Materials Performance*, 27, no. 2 (February 1988): 12–20.
24. A. Garner, Monitor assembly for electrochemical corrosion protection of stainless steel bleach plant washers, US Patent 4,285,232, issued August 25, 1981.
25. E. R. Dille and W. Shim, "Electrochemical Protection of Flue Gas Desulfurization Reaction Tanks" (paper presentation, Corrosion/2000, paper no. 0580, NACE International, Orlando, FL, March 26–31, 2000).
26. J. Selley and J. Kamody, "Build a Durable FGD System with FRP," *Chemical Engineering Progress* 87, no. 9 (September 1991): 86–92.
27. G. Cantrell, C. B. Pickett, D. A. Froelich, and D. C. Pattison, "Quality Control of Alloy Welding in Flue Gas Desulfurization Installations," paper no. 12 in *Proceedings of the 1990 Air Pollution Seminar* (Houston, TX: NACE International, 1990).
28. R. C. Adcock, J. B. Biggins, R. E. Fringeli, et al., "Clean Air Act Amendments: Overview of Gas and Electric Utility Fire Protection" (draft report, M&M Protection Consultants, Chicago, IL, 1991).

29. *Recommended Practice for Fire Protection for Fossil-Fueled Steam and Combustion Turbine Electric Generating Plants*, Report No. NFPA 850 (Quincy, MA: National Fire Protection Association, 1990).

30. D. Gearey and W. M. Cox, *Multitechnique Corrosion Monitoring in Flue Gas Desulfurization Systems: Phase I*, Report CS-5605 (Palo Alto, CA: Electric Power Research Institute, 1988).

31. "Conductivity Probe Guards against FRP Degradation," *Chemical Engineering* 98, no. 7 (July 1991): 163.

32. H. S. Rosenberg, *Performance Analysis of Materials in Wet FGD System Components*, report (Palo Alto, CA: Electric Power Research Institute, 1994).

33. E. C. Hoxie and G. W. Tuffnell, "A Summary of INCO Corrosion Tests in Power Plant Flue Gas Scrubbing Systems," in *Resolving Corrosion Problems in Air Pollution Control Equipment* (Houston, TX: NACE International, 1976), 65–71.

34. G. H. Koch, C. Kistler, and W. Mirick, *Evaluation of Flue Gas Desulfurization Materials in the Mixing Zone: R. D. Morrow Sr. Generating Station*, Report CS-5476, (Palo Alto, CA: Electric Power Research Institute, 1987).

35. H. S. Rosenberg and J. M. Spangler, *Effect of Environmental Parameters on the Performance of Coatings in FGD Ductwork*, Report TR-102162 (Palo Alto, CA: Electric Power Research Institute, 1993).

36. C. Gabrielli, *Identification of Electrochemical Processes by Frequency Response Analysis*, Issue 2, Technical Report/83 (Burlington, MA: Solartron Instrumentation Group, 1984).

37. M. W. Kendig and F. Mansfeld, "Corrosion Rates from Impedance Measurements: An Improved Approach for Rapid Automatic Analysis," *Corrosion* 39, no. 11 (November 1983): 466–467.

38. M. Kendig and J. Scully, "Basic Aspects of the Application of Electrochemical Impedance for the Life Prediction of Organic Coatings on Metals" (paper presentation, Corrosion/89, paper no. 32, NACE International, New Orleans, LA, April 17–21, 1989).

39. *ABS Advisory on Exhaust Gas Scrubber Systems* (Spring, TX: ABS Corporate Technology, July 2018).

40. *Corrosion Control and Prevention for Marine Scrubbers*, TR21448-2021 (Houston, TX: Association for Materials and Protection), September 2021).

41. R. W. Ross, B. Phull, and E. R. Dille, "Recent Failures of 2205 Duplex Stainless Steel in FGD Scrubbers: Could They Have Been Avoided?" (paper presentation, Corrosion/2017, paper no. 9747, NACE International, New Orleans, LA, March 26–30, 2017).

Chapter 28 | Nuclear Power

Barry M. Gordon[1] and George J. Licina[1]

Introduction

Minimizing corrosion is a primary objective of nuclear power plant design.[1] Such plants use corrosion-resistant alloys and high-purity (e.g., fleet average of ~0.07 μS/cm water conductivity in boiling water reactors [BWRs]) and well-controlled water chemistries in critical systems to achieve that objective. Despite such measures, nuclear plants have experienced various forms of corrosion in several plant components. These corrosion events have had significant ramifications on plant operability because of the extremely stringent requirements on component reliability and containment of radio-nuclides. Standards devoted to assessing susceptibility to localized corrosion, such as stress-corrosion cracking (SCC), have been used to qualify materials and remedial countermeasures. In many cases, the evolution of nuclear plant designs has required development of new standards.

Nuclear power plants convert heat energy from the fission of uranium (^{235}U) into high-quality steam. The steam is used to turn steam turbines and generate electricity. Large amounts of electric power can be produced inexpensively with long refueling intervals (nominally 18 to 24 months) and small operating staffs. These typically large plants (600–1400 MWe) are an excellent source for providing "base load" electricity; however, their large size and the long time from design to commercial operation represent a significant investment of time and resources.

The total quantity of fuel material used, and the volume of wastes generated by a nuclear plant per kW is very small; however, the radioactive nature of much of the waste requires that they be contained and closely monitored well beyond the life of the plant. The potential dangers of radioactivity to operating personnel, the public, and other living creatures dictate designs with multiple barriers to the release of fission and activation products. The reliability of each barrier must meet exacting standards to ensure that releases to the environment, including leaks to the air or water supply, do not occur.

Corrosion problems in nuclear plants have almost always been associated with both general corrosion and a few forms of localized corrosion. For example, steam generator tubes in pressurized water reactors (PWRs) have experienced general corrosion, SCC, intergranular attack (IGA), pitting corrosion, and "denting" of support plates because of crevice corrosion. PWRs have suffered extensive primary water stress-corrosion cracking (PWSCC) of alloy 600 and its weld metal, alloy 182. In BWRs, recirculation system piping has been degraded by intergranular stress-corrosion cracking (IGSCC), especially adjacent to weldments because of weld sensitization. Irradiation-assisted stress corrosion cracking (IASCC) has degraded reactor internal structural components in both BWRs and PWRs. The zirconium alloys used for fuel cladding have been subject to hydriding, SCC, under-deposit corrosion (e.g., under crud), and nodular corrosion. The occurrence of rapid general corrosion, pitting corrosion, under-deposit corrosion, and microbiologically influenced corrosion (MIC) have prompted increased attention to nuclear service water systems.

Materials of Construction and Specific Concerns

GENERAL

Reliability is the major concern with components in nuclear power plants. Component reliability must be ensured for plant safety and to protect the investment in the plant. The stringent regulations related to release of radioactivity to the environment drive much of the materials selection, environmental controls, and inspection requirements of nuclear plants. Unlike fossil-fueled plants, where repairs of leaking or flawed components are a routine fact of life, the availability of diverse and redundant systems for containment of radioactivity requires a far greater reliability of systems and components in nuclear systems.

MATERIALS OF CONSTRUCTION

Primary Systems

Both BWRs and PWRs presently use zirconium alloys for fuel cladding. The "neutron economy" afforded by low cross-sectional materials, such as zirconium, is critical for efficient operation of the reactor's core. Zirconium alloys also exhibit good resistance

[1]Structural Integrity Associates, Inc., San Jose, CA 95138, USA
The author acknowledges the previous author of this chapter, George J. Licina.

DOI: 10.1520/MNL202NDSUP20180005

Copyright © 2022 by ASTM International, 100 Barr Harbor Dr., PO Box C700, West Conshohocken, PA 19428-2959
ASTM International is not responsible, as a body, for the statements and opinions expressed in this chapter. ASTM International does not endorse any products represented in this chapter.

to corrosion in water–steam environments as well as to the high-temperature fission products (the fission of the uranium produces iodine, cesium, and cadmium). The fuel cladding thus represents the first containment barrier to radioactive products. Fuel cladding is also subject to high heat fluxes. The effects of heat flux and neutron and gamma irradiation can be synergistic with the aggressiveness of the high-temperature water environment, producing corrosion effects that are more severe than those encountered out-of-reactor or in non-heat-transfer applications. Currently, several projects are under way to replace zirconium alloy cladding with more accident-resistant alloys, such as high chromium ferritic steels[2] or silicon carbide.[3]

Corrosion Tests and Standards Manual

Reactor internals include both fixed and movable components. Examples of such components are control rods (movable), in-core instrumentation (fixed and movable), the core shroud, core plate, jet pumps, top guide, and steam separators and steam dryers (all fixed). Austenitic stainless steels are used for most of these components for their general corrosion resistance. In other specific applications, such as in the control rod drives and jet pumps, precipitation-hardened nickel-base alloys (e.g., alloy X-750, UNS N07750) are used where greater corrosion resistance and strength are required.

REACTOR COOLANT SYSTEMS

Heat transport system piping in most PWRs (fig. 1) is fabricated from carbon steel and low-alloy steels, for strength and economy, and often clad with roll-bonded or weld-deposited corrosion-resistant cladding (either stainless steel or high-nickel alloys).[4] Nickel-base alloys are used extensively as weld fillers for cladding and for joints between alloy steels and stainless steels for their superior corrosion resistance.

The primary coolant in PWRs is circulated through the core, through the reactor coolant piping, and to the steam generators where it transfers its heat to a second, high-purity water loop. The water in the secondary loop is heated to steam. That steam is expanded in the turbine where the thermal energy is converted to mechanical energy to generate electricity.

The piping arrangement in a BWR is different from that of a PWR. In the BWR, only a single coolant loop is used (fig. 2).[4] The same water that is heated in the core to produce steam is expanded in the turbine. The water is further cooled in the condenser and is returned to the core as feed-water. Water is rapidly recirculated through the core at about 7–10 times the mass flow rate of steam, most often using jet pumps. Flow from the recirculation pumps "drives" the jet pumps, which have no moving parts. About a third of the flow from the vessel is returned to the recirculation loop. Water in the recirculation loop is pumped through a header, through riser pipes, and discharged to the jet pumps, providing the jet pumps' driving flow. In the jet pumps, water in the down comer region is

FIG. 1 PWR components and alloys.[4]

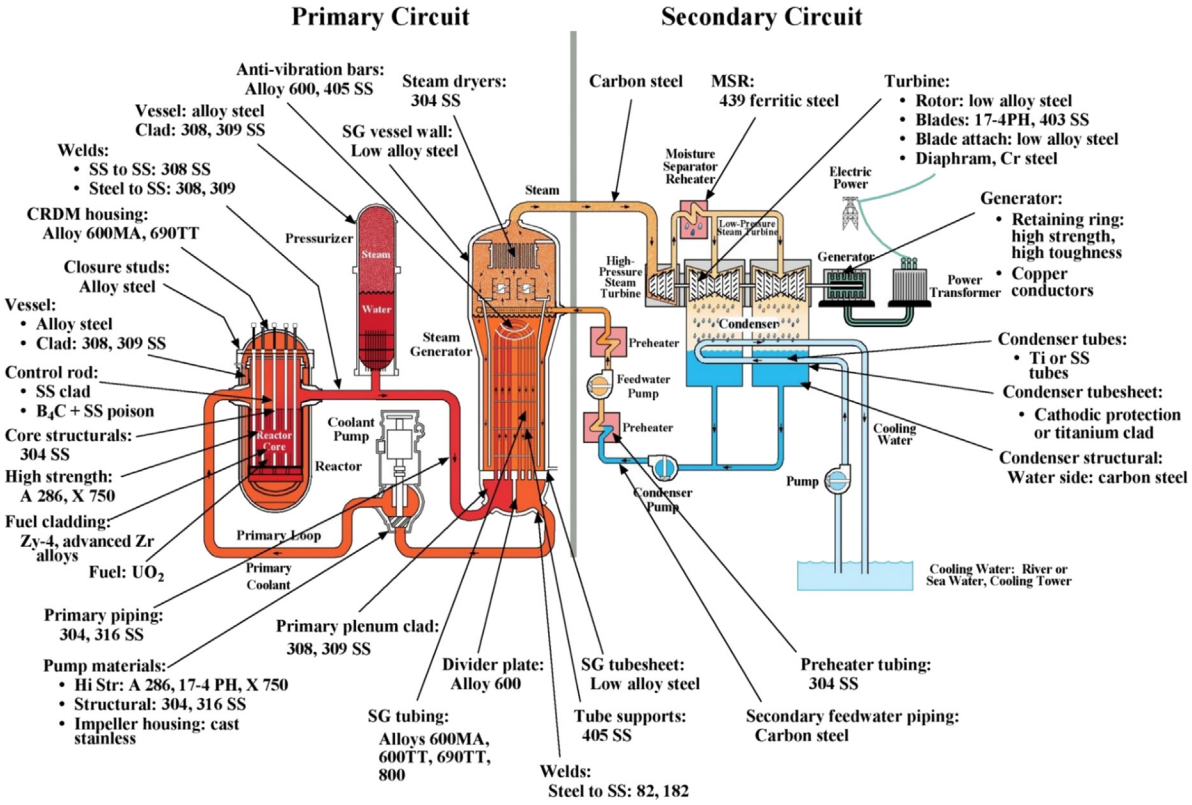
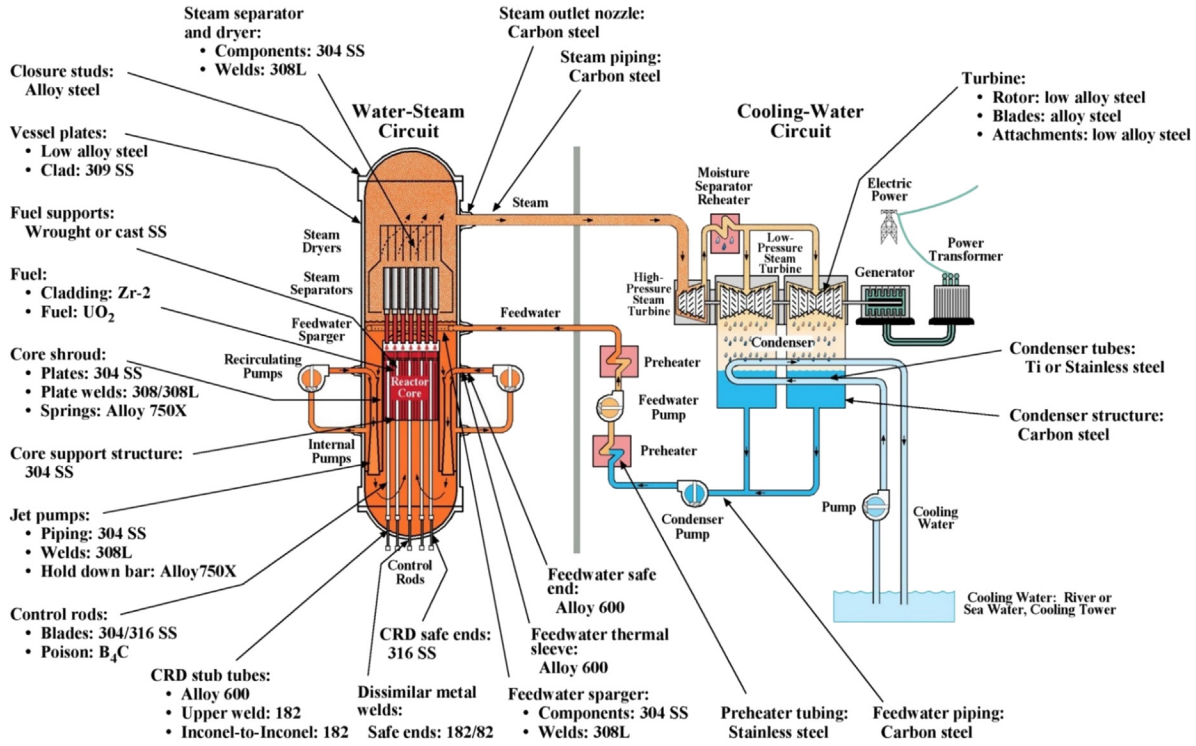


FIG. 2 BWR components and alloys.[4]



accelerated through the jet pump, and then discharged into the lower core plenum.

Flow proceeds from the lower plenum through the core. The steam and water are separated; the steam is then dried and passed to the turbine. Other flow returns to the recirculation system. Feedwater is introduced to the annulus between the core shroud and reactor vessel. The recirculation system piping is a primary pressure boundary for the high-pressure, high-temperature reactor coolant. Type 304 stainless steel was selected for recirculation system piping and numerous other auxiliary systems (such as the reactor water cleanup system, residual heat removal system, core spray, and other emergency core cooling systems) for its corrosion resistance and adequate mechanical properties. Failures of weld heat-affected zones (HAZs) by IGSCC in the oxidizing environment resulting from water radiolysis in the core have shown the selection of these stainless steels, at least grades with carbon contents of 0.04% and above, to have been a poor choice. Remedies, implemented in the most recent designs and in some retrofits, involved the use of special grades with very low carbon contents to avoid sensitization (and higher nitrogen to compensate for decreased mechanical strength), special welding procedures to minimize sensitization, and other remedial procedures to reduce residual stresses at welds. Decreasing the oxidizing power of the high-temperature water environment also has been implemented. This is accomplished by injecting hydrogen into the feedwater to recombine with the oxygen produced by radiolysis.

The BWR also uses some carbon steel and low-alloy steel for steam and other piping (to avoid IGSCC, when corrosion resistance is adequate) and a limited number of nickel-base alloys (e.g., for reactor vessel and piping safe ends).

Pressure Vessels and Heat Transfer Components

The key pressure vessels in the PWR system were discussed in the section "Reactor Coolant Systems." PWR vessels, including the reactor vessel, steam generator shells, and pressurizer, operate at pressures of approximately 2,000 psi (13.8 MPa) and temperatures of up to 625 °F (330 °C). These vessels are fabricated from low-alloy steels (e.g., ASME SA-302, Grade B; SA-533, Grade B; SA-508, Classes 1, 2, and 3; UNS K12022, K12359, K12042, and K12766) and clad (usually weld clad) with stainless steels or nickel-base alloys. The alloy steel provides adequate strength at a reasonable cost for the thick-walled vessels. The stainless steel cladding provides corrosion resistance.

BWR reactor pressure vessels operate at much lower internal pressures than those of a PWR such as 1,000 psi (6.89 MPa) at 550 °F (288 °C). As a result, BWR reactor vessels can be much larger than those of PWRs, which permits much of the equipment (such as jet pumps, steam driers, and steam separators) to be contained within the vessel. These pressure vessels are fabricated from low-alloy steels (SA-533, Grade B; SA-508, Class 2; UNS K12539, K12766) for strength and economy and weld clad with stainless steel for corrosion resistance.

The steam generators in PWRs provide the boundary between the primary (radioactive) and the secondary (nonradioactive) systems. Service experience has proven the steam generator to be a key, if not the key, piece of equipment for PWRs.

Corrosion problems in the steam generators have been the principal cause of PWR downtime.

Nickel-base alloys (alloys 600, 690, and 800; UNS N06600, N06690, and N08800) are most commonly selected for steam generator tubes for their good heat transfer properties and resistance to general corrosion. Because of its numerous corrosion problems, alloy 600 has been universally been replaced with higher chromium containing and more PWSCC-resistant alloy 690.

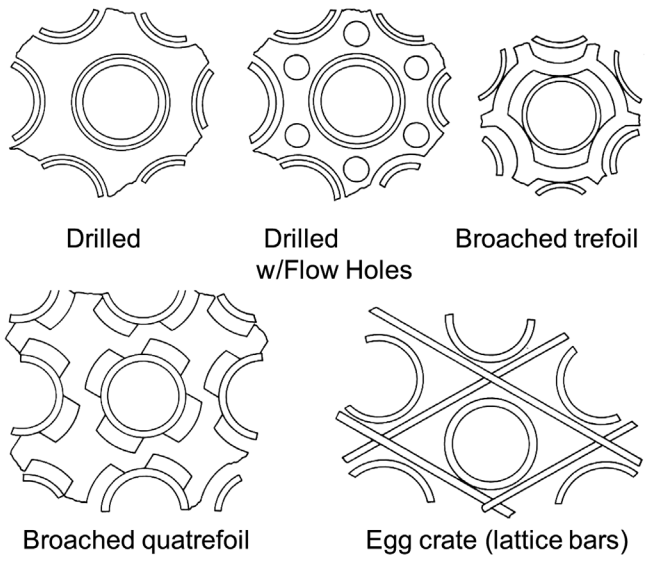
Like the steam generator shell, tubesheets are fabricated from low-alloy steels for their strength and economy. In some designs, the tubesheets are clad with stainless steel or nickel-base alloys for corrosion resistance during shutdowns.

On the secondary side of the steam generator (i.e., where the steam is generated), carbon steel tube support plates initially were used (fig. 3). This selection was based on economics because the support plates have minimal structural function and represent a relatively small area exposed to the coolant; the amount of iron released to the system from corrosion of the spacers can easily be accommodated by the cleanup system. Selection of carbon steel support plates (e.g., SA-515, Grade 6; UNS K02401) proved to be a poor choice. Corrosion of the support plates, especially those with drilled holes, resulted in a thick, adherent magnetite corrosion product. The magnetite buildup caused a notable change in support plate dimensions (a decrease in the size of the holes), producing stresses that were sufficient to deform (i.e., dent) the steam generator tubes. Ferritic or martensitic stainless steel tube support plates are used in newer designs.

Power Conversion and Auxiliary Systems

The power conversion system and the balance of plant components for nuclear plants are like those for fossil plants with a few significant differences. First, fossil plants are generally much smaller than nuclear plants; hence, many of the key components in the power conversion system are smaller. Second, fossil plants generally operate at significantly higher temperatures—that is, steam may be superheated from a few degrees to hundreds of degrees. The requirements on the power conversion system are, therefore, much different. The great emphasis on reliability of nuclear units often affects design and materials selection of power conversion or balance of plant components. Finally, the "diverse and redundant" design philosophy inherent in the design of nuclear plants requires greater numbers of heat exchangers, pumps, and valves, and far more piping in the balance of the plant than in a fossil-fired unit of comparable power output. Many of these systems operate infrequently. The most common operational conditions for many of these systems is a monthly or quarterly demonstration of their operability to ensure that they are functional in the event of an accident.

FIG. 3 Steam generator tubing support plate designs.



Nuclear units use all the commonly used condenser materials including brass (particularly Admiralty and aluminum brass), copper-nickel (90-10 and 70-30), stainless steels, and titanium tubes, and Muntz metal and stainless steel tubesheets. Many retubed condensers have used specialty alloys, such as titanium or the so-called super-ferritic (high chromium; very low carbon; molybdenum contents to 4%), super-austenitic (basically 20% Cr-25 %Ni and up to 6 %Mo) or duplex stainless steels, to eliminate pitting, SCC, and MIC. Tube replacements, with titanium or super stainless steels, have been performed most often in saline cooling waters; however, the critical nature of some heat exchangers and the insidious nature of under-deposit corrosion and MIC have prompted the use of such alloys in freshwater-cooled systems.

Carbon and low-alloy steels are most commonly used in the condensate system for economy and their adequate resistance to corrosion. Austenitic stainless steels also have been used in some systems and in key components. Copper alloys also have been used in some locations, although much less frequently.

Copper alloys (Admiralty, copper-nickel) and austenitic stainless steels are the most commonly used materials for feedwater heater tubing based on their resistance to general and localized corrosion, erosion-corrosion, and SCC, as well as their adequate heat transfer performance.[5,6] Carbon and low-alloy steels are most often used for the shells of such heaters for economy and availability.

Much of the materials selection for service water systems and closed cooling water systems is dictated by the water source (e.g., carbon steel for fresh waters; coated or lined steel, copper alloys, or stainless steels for saline waters). Coatings, linings, copper alloys, stainless steels, super-austenitic stainless steels, super-ferritic stainless steels, and titanium have been used for replacements.

FAILURE MODES

Fine cracks or localized regions of attack, resulting from SCC, corrosion fatigue, or localized corrosion, are the most common corrosion failure modes in nuclear facilities. Small leaks can be a major concern in nuclear power plants where the release of radioactive products to the environment or leakage of extremely expensive materials, such as heavy water from Canadian Deuterium Uranium (CANDU) plants must be avoided. CANDU plants are a type of heavy water-moderated process using natural uranium. The other major concern with small cracks or fine pits

is their potential to act as initiation sites for cracks that could lead to large leaks or unstable cracking and loss of coolant events. Almost without exception, the toughness of the alloys used for piping and vessels is sufficiently high that nuclear piping and vessels are structurally stable, even with such flaws present. This assurance of "leak-before-break" is a critical criterion of nuclear plant reliability.

Radiation buildup, the result of general metal loss to the heat transport system and the deposition of activated corrosion products on metal surfaces, can represent a serious corrosion concern unique to nuclear plants, as radiation levels can limit worker exposure and hinder maintenance. The dissolution of metal and subsequent loss of the metal to the system also has other potential ramifications as maintenance activities, such as refueling operations, depend on a high degree of water clarity. Nuclear plants are designed with minimal corrosion allowance on heat transfer surfaces, unlike the large fireside corrosion allowance designed into fossil-fueled plants. The relatively low operating temperatures, high-purity water, and the extensive use of corrosion-resistant alloys permit the waterside corrosion allowances to be minimized. This reduction is driven by requirements for water clarity and radiation buildup. Because much of the in-vessel maintenance must be performed using water for shielding, the clarity of the water is extremely important.

Typical Environments, Metallurgical Conditions, and Corrosion Problems

The PWR primary system operates over a range of temperatures averaging approximately 617 °F (325 °C) and 2,000 psi (13.8 MPa), with a pH of 6.8 to 7.4 at operating temperatures and a hydrogen overpressure (e.g., > 35 cc/kg) to suppress radiolysis and PWSCC. Boric acid is added for reactivity control—that is, higher concentrations early in a fuel cycle, and progressively lower concentrations as the enriched uranium is depleted. Lithium hydroxide (LiOH) is added for pH control in U.S. PWRs. Some components, particularly steam generators and control rod drive mechanism penetrations, have experienced PWSCC, a phenomenon first discovered by Coriou et al. in 1959.[7] Cracking is intergranular and was not associated with any particular metallurgical anomaly. The major concerns with PWSCC are radioactive contamination of the nonradioactive water or steam environment (e.g., from steam generator leaks) or the potential for a loss of coolant event from cracking in control rod drive mechanism attachments to the reactor vessel head.

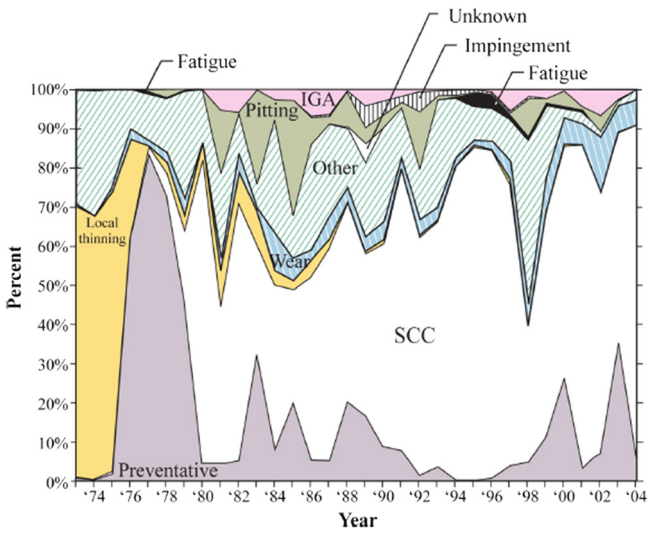
PWR steam generators are exposed to a hydrogen-rich primary water environment on the tube side (inner side) and deoxygenated water on the secondary side. The method for corrosion control in the secondary circuit has evolved from a coordinated phosphate treatment to the all-volatile treatment (AVT). Different AVT treatments have included hydrazine and ammonia, hydrazine and morpholine, and the use of alternate amines. Crevices on the secondary side, where impurities can concentrate, and other locations where deposits develop thermal gradients that enhance the concentration of impurities, have produced aggressive local environments (e.g., oxygen concentration cells, both acidic and caustic pH excursions) that have led to pitting corrosion, IGA, and SCC.[5,6,8] Figure 4 summarizes the history of steam generator failure from 1974 to 2004.[9]

Single-cycle BWRs currently use very high-purity water (e.g., conductivity < 0.1 μS/cm) at a neutral pH. More recent experience has shown that control to levels far less than 0.1 μS/cm can be achieved in large operating plants. The radiolytic decomposition of water in the BWR core, however, produces dissolved oxidizing species (oxygen and hydrogen peroxide) that make the environment far more aggressive, particularly to the HAZs of stainless steel welds. All of these factors produce an oxidizing environment that, in concert with the sensitized microstructure and tensile stress, produce IGSCC of austenitic stainless steel, SCC of nickel-base alloys, and earlier onset of IASCC.

In both PWRs and BWRs, the carbon steel feedwater train can be susceptible to flow-assisted corrosion and erosion-corrosion effects, especially at extremely low oxygen concentrations. Thinning of this piping, generally at areas of high turbulence, depends on temperature, pH, and oxygen content. Oxygen additions are made to some feedwater lines in BWRs to support the formation of a protective magnetite film.

The main heat removal system (e.g., the main condenser and associated equipment) and service water systems, which provide cooling for auxiliary equipment, such as pumps, room coolers, chillers, fire protection, and reactor heat removal systems used under accident and other shutdown conditions, for both BWRs and PWRs are exposed to environments that are controlled by the site's water source—that is, the cooling water may be seawater, brackish water, or a fresh water (lake, river, or pond). Fresh waters may range from the acidic to the highly alkaline. The pH and concentration of dissolved minerals (particularly calcium and magnesium salts) or metals (manganese or iron) can have a strong influence on the corrosivity of the water. Corrosion under deposits and MIC can result in a variety of such environments. Oxygen and flow rate are key factors in determining the aggressiveness of

FIG. 4 Steam generator failure history.[9]



the environment. Very high flow rates produce flow-assisted corrosion and, eventually, erosion-corrosion, especially on copper alloys and carbon steels. Low flow rates encourage deposition and under-deposit corrosion and MIC.

The importance of corrosion in these balance-of-plant (BOP) systems increased tremendously for nuclear plant owners in the 1980s. Leakage and functional failures in safety-related and non-safety-related cooling systems as a result of general corrosion, localized corrosion (especially under-deposit corrosion), and MIC became critical issues. Several plants in the United States have completely replaced service water system piping, others have initiated planning for such a replacement, and the remainder have been faced with the need for local repairs, often on buried piping that is essentially inaccessible. Utilities are in the process of learning the importance of monitoring for corrosion and deposition and the necessity for early detection and actions to mitigate corrosion. The phenomenon of MIC is even more complex because the presence of living organisms makes it extremely dynamic. Many of the standard approaches to monitoring and control are not applicable. Similarly, the toxicity of many of the standard water treatments for biological control have significant environmental and administrative ramifications for storage and discharge. Most of the methods for testing MIC susceptibility in the laboratory or in service remain under development.

Testing for Corrosion

PURPOSE OF TESTING AND TYPES OF TESTS

Corrosion tests are performed for the selection or qualification of materials (including materials to be used for repairs or replacements), for monitoring (to assess corrosion or to track process controls such as water treatments), or to supplement and assist with failure analyses.

Streicher[10] identified the following five categories of corrosion test methods:

1. Plant service (i.e., how components behave in actual service)
2. Tests in process streams or cooling waters
3. Laboratory tests in plant solutions
4. Laboratory tests with reagent chemicals in place of plant solutions
5. Mechanism tests

Test types 1 or 2 are most useful for monitoring performance in existing facilities, in particular for evaluating the performance of existing or candidate replacement materials or for monitoring mitigation treatments. Type 2 tests may include immersion or electrochemical tests. Corrosion (or SCC) may be accelerated by loading the specimen, forming a crevice (using a washer or other means), or increasing the temperature. Test types 3 and 4 have been used and continue to be used to qualify materials for various service environments, including those in which general corrosion, localized corrosion, or SCC are concerns. The corrosive conditions may be enhanced by using more concentrated electrolyte, higher temperature, greater aeration or acidity, creviced conditions, applied electrochemical potentials, or stress. Mechanism test type 5 often incorporates environments or loading conditions that have little correspondence to plant conditions; however, they have been formulated to provide a useful indication of a particular characteristic that may be correlated with long-term service exposure. For example, the pitting corrosion resistance of stainless steels and nickel-base alloys may be compared by using a ferric chloride solution to determine the critical temperature above which pitting or crevice corrosion occurs (ASTM G48, *Standard Test Methods for Pitting and Crevice Corrosion Resistance of Stainless Steels and Related Alloys by Use of Ferric Chloride Solution*), by determining the key corrosion potentials for pit initiation and pit growth (hysteresis loop) in chloride solutions (ASTM G61, *Standard Test Method for Conducting Cyclic Potentiodynamic Polarization Measurements for Localized Corrosion Susceptibility of Iron-, Nickel-, or Cobalt-Based Alloys*; and ASTM G192, *Standard Test Method for Determining the Crevice Repassivation Potential of Corrosion-Resistant Alloys Using a Potentiodynamic-Galvanostatic-Potentiostatic Technique*) or using the electrochemical technique for determining the critical pitting temperature (ASTM G150, *Standard Test Method for Electrochemical Critical Pitting Temperature of Stainless Steels and Related Alloys*).[11,12] These values are not directly applicable to plant service but provide a useful basis for comparing different alloys.

Similarly, ASTM A262, *Standard Practices for Detecting Susceptibility to Intergranular Attack in Austenitic Stainless Steels*, is a mechanism test used to screen alloys for their resistance to IGA associated with the precipitation of chromium carbides. This standard has been used to rank alloys and treatments for their relative degree of sensitization and to infer their resistance to IGSCC. ASTM A262 provides a method for evaluating the sensitization of stainless steels. Both IGA and IGSCC have been shown to strongly depend on sensitization.

TEST METHODS

Most of the corrosion testing performed for the initial qualification of materials in the environments encountered in nuclear power plants was based on the predominant materials in fossil-fueled power plants and nuclear-powered submarines in which water is the heat transfer fluid. The extensive use of corrosion-resistant alloys, the lower temperatures used in nuclear plants, and the carefully controlled or high-purity environments of nuclear plants suggested that corrosion problems should be at a minimum. Early work to qualify materials for the first generation of reactors indicated that localized corrosion and SCC would not be expected in BWR or PWR environments. Those tests showed that control of chlorides and other aggressive anions would avoid corrosion problems. Those tests did not include some of the subtle environmental effects produced in the nuclear plants, such as the radiolytic decomposition of water in the BWR core to produce hydrogen peroxide and oxygen or the aggressive under-deposit environment in PWR steam generators. Many of the tests used to evaluate SCC resistance of material–environment pairs used deformation-controlled loading conditions (U-bends

or C-rings) and test times on the order of thousands of hours. Such methods include the following:

- ASTM G30, *Standard Practice for Making and Using U-Bend Stress-Corrosion Test Specimens*
- ASTM G38, *Standard Practices for Making and Using C-Ring Stress-Corrosion Test Specimens*
- ASTM G39, *Standard Practice for Preparation and Use of Bent-Beam Stress-Corrosion Test Specimens*
- ASTM G49, *Standard Practice for Preparation and Use of Direct Tension Stress-Corrosion Test Specimens*
- ASTM G58, *Standard Practice for Preparation of Stress-Corrosion Test Specimens for Weldments*

The constant deflection methods, in many cases, were inadequate to predict the corrosion effects that would be encountered in long-term service in the various reactor and coolant systems. For example, in constant deflection tests, load relaxation at temperature results in a much lower stress level in the specimen and a less aggressive test.

The constant extension rate testing (CERT) or the identical slow strain rate test (SSRT) was developed to overcome the deficiencies of deformation-controlled SCC initiation tests. Experience with turbine rotor steels had revealed that U-bends, C-rings, and the like might not crack in environments that would produce cracking in long-term service. Even constant load tests (actively loaded specimens exposed to aggressive environments) would under predict SCC susceptibility when tests were run for times on the order of (only) thousands of hours. In the CERT/SSRT, a tension specimen is actively loaded at a slow, nearly constant, strain rate in the environment of interest. That environment may be the actual plant environment or may be accelerated by using a higher concentration of the species responsible for the attack (e.g., oxygen, chloride, hydroxide) or an applied potential. The slow and continuous strain rate produces deformation at the crack tip that maximizes the interaction of the corrosion and the crack tip strain. That method initiates cracks and causes film rupture events at the tips of existing cracks. Under proper conditions, the bare metal surfaces (continue to) interact with the environment, resulting in crack advance. Considerable development work has been devoted to establishing optimum strain rates for the test. The CERT/SSRT has been used extensively for investigating the cause of IGSCC in BWRs and continues to be used for selection and qualification of replacement materials and remediation processes.

The test produces results that look like those from a tensile stress-strain curve. Like a tension test, the test always produces a failure. Typical test times are of the order of weeks to a month when extension rates from 10^{-8} to 10^{-6} /s are used. The interpretation of the test results may be compared with the results for the same material exposed to an environment where little or no environmental degradation occurs based on one or more of the tensile test parameters (e.g., maximum stress, elongation to failure, reduction of area). The standardized version of this test, ASTM G129, *Standard Practice for Slow Strain Rate Testing to Evaluate the Susceptibility of Metallic Materials to Environmentally Assisted Cracking*, is useful for identifying materials that are susceptible to SCC, but assessing the degree of susceptibility to be expected in service is far more difficult.

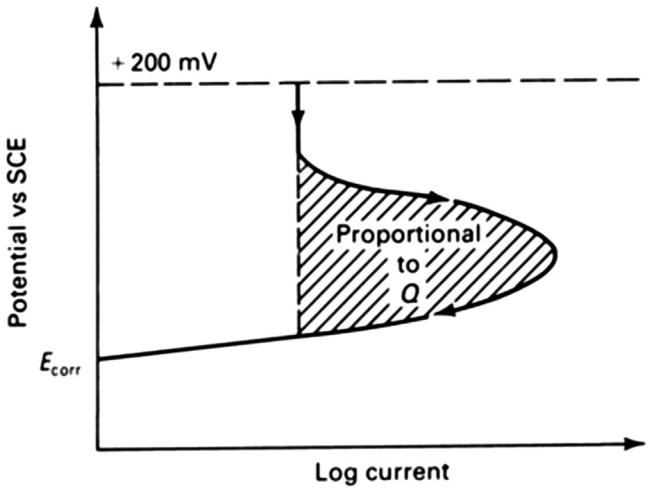
This test, however, presents only those alloy-environment systems in which SCC can occur. CERT/SSRT is also known to be overly conservative in some instances and nonconservative/insensitive in other cases in which the test standards provide no guidance or insight on this issue. CERT/SSRT inherently masks most material effects that affect sustained dynamic deformation by inducing a forced strain rate.

ASTM A262 was probably the most commonly used mechanism (type 5) test for corrosion testing in support of nuclear reactor materials. It provides a qualitative measure of the degree of sensitization (DOS). The electrochemical potentiokinetic reactivation (EPR) test[13] provides a rapid method for generating a more quantitative measure of DOS. This test (see ASTM G108, *Standard Test Method for Electrochemical Potentiokinetic Reactivation [EPR] for Detecting Sensitization of AISI Type 304 and 304L Stainless Steels*[1]) involves polarizing a polished sample (including pipe work in the field) at a controlled rate, and then reversing the direction of polarization and returning to the open circuit potential. The area under the curve, normalized for the grain boundary area exposed (fig. 5), provides a quantitative measure of the DOS as the width of the chromium-depleted grain boundary. The "double-loop" method is similar but is less critical regarding specimen preparation and provides the quantitative measure as a relative peak height by measuring the ratio of ir:ia (fig 6).

Other methods that have been, and continue to be, used are as follows:

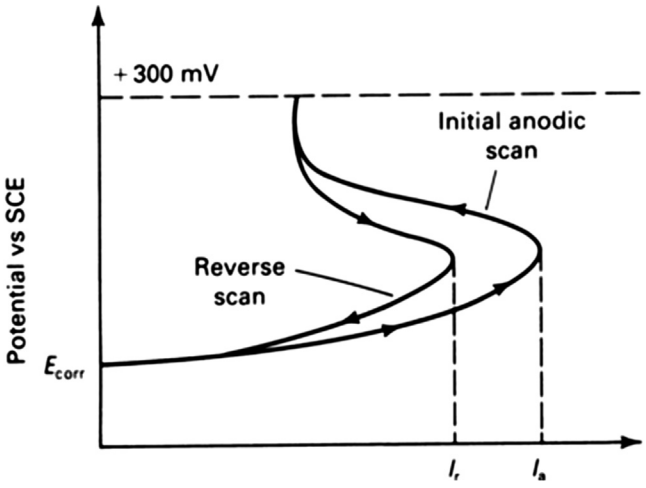
- ASTM G1, *Standard Practice for Preparing, Cleaning, and Evaluating Corrosion Test Specimens*

FIG. 5 Plot of single-loop EPR test.



[1]ASTM is working on incorporating the double-loop test into ASTM G108

FIG. 6 Plot of double-loop EPR test.



- ASTM G2, *Standard Test Method for Corrosion Testing of Zirconium, Hafnium, and Their Alloys at 680 °F (360 °C) or in Steam at 750 °F (400 °C)*
- ASTM G4, *Standard Method for Conducting Corrosion Coupon Tests in Field Applications*
- ASTM G5, *Standard Reference Test Method for Making Potentiostatic and Potentiodynamic Anodic Polarization Measurements*
- ASTM G46, *Standard Guide for Examination and Evaluation of Pitting Corrosion*
- ASTM G31, *Standard Guide for Laboratory Immersion Corrosion Testing of Metals*
- ASTM G61, *Standard Test Method for Conducting Cyclic Potentiodynamic Polarization Measurements for Localized Corrosion Susceptibility of Iron-, Nickel-, or Cobalt-Based Alloys*
- ASTM G96, *Standard Guide for Online Monitoring of Corrosion in Plant Equipment (Electrical and Electrochemical Methods)*
- ASTM G102, *Standard Practice for Calculation of Corrosion Rates and Related Information from Electrochemical Methods*
- ASTM G106, *Standard Practice for Verification of Algorithm and Equipment for Electrochemical Impedance Measurements*
- ASTM G111, *Standard Guide for Corrosion Tests in High Temperature or High Pressure Environment, or Both*

The test technique most commonly used in the nuclear power industry is the reversing DC potential drop (DCPD) technique for measuring real-time crack growth rates in compact tension fracture mechanics specimens, ASTM E647-00, *Standard Test Method for Measurement of Fatigue Crack Growth Rates (Historical Version)*. Although this method is titled for fatigue testing, it is mainly used for SCC propagation measurements in cases in which after the potentials are measured, the DC current is reversed, and the process is repeated. The ratio of the two active and reference probe sets are then considered to be a single potential measurement. The current reversal method, and the use of the potential amplitude compensates for long-term signal drift, which thereby increases the stability and sensitivity of the technique. Hundreds of potential measurements are collected over the collection interval. At the end of the collection interval, the active and reference potentials are averaged, ratioed, and compared with the initial potentials collected at time zero (i.e., the start of the test). This results in a calculated change in crack length that, when added to the initial crack length at time zero, provides an average crack length for the collection interval. This method provides precise crack-length measurements (5 μm/0.0002 in.) on a real-time basis.

Future Outlook

Several unresolved issues remain in corrosion testing for nuclear power plants. These include the following:

- The SCC of austenitic stainless steels in PWR environments.
- IASCC in BWR environments has been observed in highly irradiated components. Threshold levels of irradiation and methods to assess susceptibility and mitigate IASCC have been defined but require standardization.[14]
- Standard test methods are also required to qualify alternative approaches to environmental controls, such as hydrogen water chemistry (HWC) with and without noble metal injections. HWC has been shown to be effective for protection of recirculation system piping against IGSCC (at the expense of higher radiation levels); however, the higher levels of hydrogen injection required to protect components in the reactor vessel may not be tolerable from a radiation dose (^{16}N carryover in steam) perspective. Therefore, noble metals are injected to catalyze the recombination of dissolved oxygen and dissolved hydrogen peroxide with hydrogen.
- PWSCC has been observed in PWR steam generator tubing, control rod drive mechanism penetrations, and bolting materials. Methods to evaluate susceptibility of components and mechanisms and methods to quantify alternate materials for resistance to this specific form of IGSCC are required, such as higher chromium-containing nickel alloys and weld metals.
- The nuclear industry has learned the value of online monitoring to provide an early warning of corrosion problems. Standard methods for automated and online methods (including measurements made at reactor system temperatures and pressures) need to be developed.
- The importance of corrosion effects in BOP components in nuclear plants increased dramatically in the 1980s. BOP problems, such as MIC, pitting, and under-deposit corrosion, had a dramatic effect on plant performance. Methods for monitoring and for selecting materials for resistance to pitting and crevice corrosion exist. Additional standard methods for MIC testing are under development.[15]

- Because of defense, depth design, and operating features, materials degradation issues, such as SCC of piping and core internals, in current BWR and PWR designs do not increase significantly a plant's baseline core-damage frequency (CDF) or large energy release frequency (LERF).[16,17] Without question, however, such failures have a marked negative impact on both the economy of plant operation and the public perception of nuclear reactor safety. Thus, the resolution of such problems is essential, especially with changes in the plants' licensing basis associated with, for example, life extension and license renewal and power uprates that may affect environment-associated cracking susceptibility.
- The corrosion challenges for the future will be governed by changes in operating and regulatory conditions.[16] For instance, in the United States there is a steady movement toward regulations that are not only performance-based but also risk-informed. This development emphasizes decision-making that takes into account the relative importance of various maintenance, in-service inspection, and procurement activities in terms of their impact on plant safety (e.g., CDF, LERF; U.S. NRC Reg. Guides 1.174, 1.175, 1.176, 1.177, and 1.178). To date, time-dependent materials degradation phenomena have not been included in the probabilistic risk assessments and the associated event- and fault-trees that address, for instance, either the accident initiation frequency or the reliability of components that play a role in subsequent accident mitigation. Thus, the near-term challenge in materials-degradation technology is to extend the current deterministic and mechanism-informed understanding of the cracking phenomena to cover the uncertainties associated with the random crack initiation processes as well as the uncertainties associated with the propagation rate data and models.
- Another operational driver that presents challenges is the constant desire for longer fuel cycles and the resultant increase in time between component inspections and more than 60 years of plant operation.[16] This puts a premium on defining the kinetics of damage accumulation and the development of inspection techniques that have adequate resolution and probability of detection capabilities for the particular system at risk.
- Note, finally, that this industry has experienced a long series of surprises with essentially all being only partially (or mostly) addressed, coupled with a subsequent erroneous perspective that there would be few future problems. Several disconnects exist between past and future performance in plants, including lack of inspection, highly nonlinear development of cracks, increasing susceptibility with time (e.g., IASCC), and sequential phenomena (e.g., alloy 182 attachment pads must crack before the underlying reactor pressure vessel can).

References

1. B. M. Gordon, "Corrosion and Corrosion Control in Light Water Reactors," *Journal of Metals* 65, no. 8 (August 2013): 1043–1056.
2. P. L. Andresen, R. B. Rebak, and E. Dolley, "SCC Growth Rate of Irradiated and Unirradiated High Cr Ferritic Steels" (paper presentation, 17th International Symposium on Environmental Degradation of Materials in Nuclear Power Systems—Water Reactors, Ottawa, Ontario, Canada, August 9–13, 2015).
3. T. Koyanagi, Y. Katoh, G. Singh, and M. Snead, *SiC/SiC Cladding Materials Properties Handbook*, ORNL/TM-2017/385, (Washington, DC: U.S. Department of Energy, Nuclear Technology Research and Development Advanced Fuel Campaign, August 2017).
4. X. Ru and R. W. Staehle, "Historical Experience Providing Bases for Predicting Corrosion and Stress Corrosion in Emerging Supercritical Water Nuclear Technology: Part 1—Review," *Corrosion* 69, no. 3 (2013): 211–229.
5. P. Cohen, ed., *The ASME Handbook on Water Technology for Thermal Power Systems* (New York: American Society of Mechanical Engineers, 1989).
6. J. C. Danko, "Corrosion in the Nuclear Power Industry," in *Metals Handbook, 9th ed., vol. 13, Corrosion* (Metals Park, OH: ASM International, 1987), 927–937.
7. H. Coriou, L. Grail, M. LeGall, and S. Vettier, *Third Colloque de Metallurgie, Corrosion* (Amsterdam: North Holland, 1959), 161–169.
8. C. S. Welty Jr. and J. C. Blomgren, "Steam Generator Issues," in *Proceedings of the Fourth International Symposium on Environmental Degradation of Materials in Nuclear Power Systems—Water Reactors*, ed. D. Cubicciotti (Houston, TX: NACE International, 1990), 1-27–1-36.
9. X. Ru and R. W. Staehle, "Historical Experience Providing Bases for Predicting Corrosion and Stress Corrosion in Emerging Supercritical Water Nuclear Technology: Part 3—Review," *Corrosion* 69, no. 5 (2013): 423–447.
10. M. A. Streicher, *"Classification and Application of Corrosion Tests"* (paper presentation, ASTM Symposium on Application of Accelerated Corrosion Tests to Service Life Prediction of Materials, Miami, FL, November 16–17, 1992).
11. A. Garner, "Materials Selection for Bleached Pulp Washers," *Pulp and Paper Canada* 82 (1981): T414.
12. J. Kolts and N. Sridhar, "Temperature Effects in Localized Corrosion," in *Corrosion of Nickel-Base Alloys* (Metals Park, OH: ASM International, 1985), 289–311.
13. W. L. Clarke, *The EPR Technique for the Detection of Sensitization in Stainless Steels*, NUREG/CR-1095 (Washington, DC: U.S. Nuclear Regulatory Commission, 1981).
14. P. L. Andresen, F. P. Ford, S. M. Murphy, and J. M. Perks, "State of Knowledge of Radiation Effects on Environmental Cracking in Light Water Reactor Core Materials," in *Proceedings of Fourth International Symposium on Environmental Degradation of Materials in Nuclear Power Systems—Water Reactors*, ed. D. Cubicciotti (Houston, TX: NACE International, 1990), 1-83-1-121.
15. J. R. Kearns and B. J. Little, eds., *Microbiologically Influenced Corrosion Testing* (West Conshohocken, PA: ASTM International, 1994).

16. F. P. Ford, B. M. Gordon, and R. M. Horn, "Intergranular Stress Corrosion Cracking (IGSCC) in Boiling Water Reactor (BWRs)," in *Nuclear Corrosion Science and Engineering*, ed. Damien Féron (Cambridge, UK: Woodhead, 2012), 548–580.

17. D. G. Ware, D. K. Morton, M. E. Nitzel, and S. A. Eide, *Evaluation of Risk Associated with Intergranular Stress Corrosion Cracking in Boiling Water Reactor Internals*, NUREG/CR-6677, INEEL/EXT-2000-00888 (Washington, DC: U.S. Regulatory Commission, July 2000).

Chapter 29 | Food and Beverage

Dipak Negandhi[1]

Materials of Construction Used and Selection Criteria

In the food and beverage industry, the workhorse materials are the "300 series" austenitic stainless steels (i.e., S30400, S30403, S31600, and S31603). S30100 and 30200 are used but less frequently. The 300 series alloys are used because they resist corrosion attack by most environments in the industry, are easily fabricated, do not cause contamination of the products, and are readily sanitized.[1–3] As with any industry, many other unique materials also are used. In neutral or slightly acid environments in which chlorides are significant, chloride-resistant stainless steel or other high-alloy materials are used.[4] Duplex stainless steels are being used more and more frequently.[5,6] In some services like fats and edible oil, copper or copper-containing alloys should be avoided. Complying materials with U.S. Food and Drug Administration (FDA) and U.S. Department of Agriculture (USDA) regulations for contact with foods and beverages during manufacture, processing, and handling is a significant issue. Users should be cautious about generic claims of materials being "FDA approved."

Another unique factor in the food and beverage industry is that the finish and polish of the equipment is often a consideration. There are concerns about microbial sterility on the inside of process equipment.[2,7,8] Of concern are both the type of surface finish on the material and the assurance that fabrication and welding practices prevent cracks or crevices. Surface finish is a valid consideration to cleanability. Eliminating crevices is an important concern to maintaining cleanliness. Many plants want the outside of the equipment to be "gleaming stainless steel" to give the appearance of purity and high quality to both visitors of the plant as well as to plant personnel. Although this is not directly related to process needs, it is a frequent consideration.

Much of the equipment is frequently sterilized and must resist modest cleaning with various kinds of antibacterial solutions.[4] The most common method is hot water with a low concentration of hypochlorite. Most of the common stainless steels will handle this type of cleaning without significant problems, as long as the cleaning cycle is not too long and there are no serious problems with residue buildup or leaving the cleaning solution in the equipment afterward. Steam cleaning is frequently a part of the cleaning cycle. Quality of cleaning water should properly be maintained to prevent chloride buildup and other contaminants. Connolly[3] describes cleaning solutions typically used in wine, brewery, and sugar industries.

In some environments, the iron contamination of stainless steel during fabrication must be removed before operation. This is done most often with nitric acid or nitric-hydrofluoric acid rinsing. The 300 series stainless steels and other high alloys can be beneficial in avoiding loss of flavor, taste, color, or bouquet.

Worldwide this industry cans large quantities of foods and beverages for storage and distribution. Common canning materials used are steel, aluminum, and glass.[9] In addition, any water used for sanitation or for human consumption in the beverage industry must comply with U.S. Safe Drinking Water Act of 1974 and the 2018 Amendments. Additionally, particular attention is placed on brasses and copper-based alloys used in the industry.[10,11]

The food service industry encompasses hotels, restaurants, fast food kitchens, and institutional kitchens, such as cruise and navy ships, schools and colleges, military bases, hospitals, and prisons. The facilities utilize storage hot water heaters for their cooking, washing, and sanitation requirements. Potable water from public water source is stored; however, it has corrosive components, such as chlorides, ammonia (chloramine), and sulfides. Many of these establishments pretreat incoming water to remove corrosive and fouling chemicals. Storage water heaters have steel tanks lined with porcelain enamel lining for corrosion protection. Because of the high fusion temperatures of the enamel coating to steel, the porcelain tends to pull away from sharp corners and radii, leaving exposed metal. Additionally, during the fusion process, reactions occur that involve the coating components and gassing of the steel substrate. These form bubbles in the coating, exposing metal. These water heaters use cathodic protection (CP) to minimize corrosion. CP provides a

[1]A O Smith Corp–Commercial Engineering, 25731 US Hwy 1, McBee, SC 29101, USA
http://orcid.org/0000-0002-9221-6292
The author acknowledges the previous authors of this chapter, W. E. Clayton and B. Tholke, The Proctor & Gamble Company, Cincinnati, OH.

DOI: 10.1520/MNL202NDSUP20190030

Copyright © 2022 by ASTM International, 100 Barr Harbor Dr., PO Box C700, West Conshohocken, PA 19428-2959
ASTM International is not responsible, as a body, for the statements and opinions expressed in this chapter. ASTM International does not endorse any products represented in this chapter.

current to an area that otherwise would corrode in the presence of an electrolyte (water, in this case). Current is supplied by electrochemical reaction at the anode surface. The anode electrochemical reaction is normally provided by an externally impressed potential on an inert electrode, or by the galvanic potential of a sacrificial anode material. The sacrificial anode material has a higher electrochemical driving force to oxidize than the metal to be protected. Thus, it corrodes (sacrifices itself by oxidizing) in favor of the tank.[12]

Typical Corrosive Environments Encountered

No single or small group of appropriate environments adequately describes the "food and beverage industry." The industry, however, handles aqueous-based solutions that frequently contain acidic chlorides.[4] When the chloride-containing aqueous solutions are modest in temperature, they are typically handled with the S30400/S31600 type stainless steels. At higher temperatures, however, more chloride-resistant alloys are needed and must be used. The authors' experience is that in most food and beverage services, pitting of S30400/S31600 stainless steel usually occurs only over 60°C and usually the temperature must be over 70°C for stress-corrosion cracking (SCC). The temperature to have pitting or SCC can vary widely because of pH, inhibitor effect of other ingredients, or the many other factors well known about chloride corrosion of stainless steel.[13] Pitting and stress corrosion can occur at temperatures much lower than 60°C to 70°C.[14]

Typical examples of chloride corrosion of stainless steel in the food and beverage industries have been described by Richardson and Godwin[4] and Page.[15] Many food environments are multiphase. Even if the overall chloride level is low, chlorides can be very high in an aqueous phase and can be highly corrosive.

Other parts of the industry may be based on fats and edible oils, which typically are not corrosive to even carbon steels as long as the carbon steel equipment can stand the cleaning cycles. The author's experience is that carbon steels are widely used for fats and oils and typically resist corrosive attack well up to 90°C. When fatty acids are present in hot fats and edible oils, stainless steel must be used over 90°C. Also, copper or iron pickup can cause rancidity.

S30400 and S31600 are widely used in the brewery and wine industry,[16–19] although stress corrosion-resistant alloys are needed at high chloride levels.[20] Typical corrosion environments and materials used in the brewery and wine industry are described by Dreyman[21] and Connolly.[3] The 300 stainless series alloys are widely used in the dairy[3,22,23] and citrus juice[24] industries. S44400 has been reported[5,17] to be effective in brewery, meat processing, hot water tanks, and similar services in which chlorides are present. The 300 series stainless steels are commonly used for vegetable processing.[25]

Some foods require heating to moderately high temperatures during processing to sterilize the product. The specific composition of the solution and temperature governs whether or not the environment is highly corrosive.[3] In some food services, wear and abrasion of moving parts and processing equipment can be significant. The wear and abrasion resistance becomes the dominant factor rather than corrosion. Materials often used to eliminate wear and abrasion include hard-faced cobalt or nickel-based alloys for cutting, scraping, conveying, mincing, and atomizing.[26] Electroless nickel plating is sometimes used on carbon steel parts.[27] S44400 has been used for conveyor parts where corrosion resistance similar to S30400 is needed.[28] The author's experience is that precipitation hardenable stainless steel alloys like SI7400 are surprisingly successful for mechanical process equipment when corrosion resistance similar to S30400 is needed but galling must be avoided.

As mentioned earlier, it is common to clean food processing equipment with sanitizing solutions. For example, in fats and oils processing equipment, the equipment must be cleaned with caustic to remove organics. Steam cleaning is a common requirement. Almost all equipment is sanitized at some frequency and this often involves chloride environments.[4,7] Clean-in-place systems are usually used. Steel used in canning industry is subjected to corrosive action with chlorides and sulfides being the most aggressive.[9] Austenitic stainless steels are subject to intergranular or galvanic corrosions and oxidation. Appropriate preventive measures include alloying and annealing (for intergranular corrosion), proper material selection to minimize electrolysis (galvanic corrosion), and appropriate preventive techniques following welding (oxidation corrosion).[29]

Because SCC is related to nickel content, 316 stainless steel offers no advantage over 304 SS with regard to this type of corrosion. Duplex (e.g., 2205) and superduplex stainless steel, however, both offer excellent resistance to SCC. Resistance to SCC also can be achieved by annealing processes and by using techniques that apply compressive stress to the surface (e.g., shot peening).[30]

Contact corrosion combines elements of galvanic and pitting corrosion, which occurs when small particles of foreign matter (especially carbon) are left on a stainless steel surface as a result of poor manufacturing techniques. Good manufacturing practices and specific standard operating procedures should be followed during fabrication and installation to prevent cross-contamination of stainless steel materials with mild steels, embedded iron particles (caused by ferrous grinding), high-carbon "tramp" steel, and machine lubricants as well as other oils, crayon, paint, and other markings or shop dirt. If not adequately removed, these contaminants could lead to pitting, rusting, and crevice or crack formation. Most important, the grinding, sanding, or polishing tool used for stainless steel should be segregated and should not be used for mild steels.[30] A regularly scheduled preventive maintenance and sanitizing plan will reduce the occurrence of corrosion and will remove mild corrosion that may have been initiated.[30]

Passivation is done to maintain the passive (nonreactive) oxide film to enhance the chrome content on the stainless steel surface and to protect the surface from corrosion. This is accomplished by exposing the surface to a solution of nitric acid at an appropriate concentration and time. Passivation of stainless steel food contact surfaces is recommended after any surface repair, polishing, or rework. Detailed procedures for cleaning and

passivation using nitric acid and other acids are provided under ASTM A380, *Standard Practice for Cleaning, Descaling, and Passivation of Stainless Steel Parts, Equipment, and Systems*.[30]

Techniques Used to Control Corrosion and Materials Degradation

In the food and beverage industry, the most common approach for controlling corrosion is to use resistant alloys. Because of concerns over product contamination, it is not as common to use other approaches for corrosion control. Linings and coatings, however, are used for shipping by truck, barge, or rail.

Another significant criterion in selecting materials is that they must comply with FDA/USDA regulations for contact with foods and beverages for the specific service.[7,8] Many people do not understand or recognize the process for obtaining such approval. The two possible methods or directions of approval to consider are (1) external FDA/USDA approval and (2) internal FDA/USDA approval.

In the case of external FDA/USDA approval, the approval is obtained from the manufacturer or supplier of the material and generally cannot be established or determined by the user company. It is common practice to request that an officer of the company supplying the construction material sign a statement on their company letterhead that the material complies with FDA or USDA regulations for food and beverage contact and include the basis for such approval. Caution should be used when using notes in product catalogues that refer to a material being FDA or USDA approved. In the case of internal FDA/USDA approval, the user needs to evaluate their own manufacturing, processing, or handling process to ensure that corrosion products or chemicals leached from organic materials do not contaminate the product. With the extensive use of austenitic stainless steel, FDA/USDA concerns exist mostly with nonmetals.

In the canning industry, steel cans generally are coated with tin or plastic. The layer of tin provides a discontinuous structure, because of their porosity and mechanical damage or defects resulting from handling the can. Plastic coatings have good resistance to compression, and the resistance to corrosion is better than the tin coating. Plastic coatings (e.g., oleoresins, phenolic, epoxy, vinyl, acrylic, polyester) should be per FDA-approved formulations.[9] Lead-free brass is used for plumbing components to eliminate lead contamination.[9]

Cooking, storage, and preparation equipment used by the food service industry (equipment used for cooking in hotels, restaurants, fast food kitchens, and institutional kitchens, such as cruise and navy ships, schools and colleges, military bases, hospitals, and prisons) is manufactured to comply with and approved to the applicable National Sanitation Foundation (NSF)/ANSI Standard. FDA or USDA approval for this equipment is not required.[31]

In the United States, the NSF is best known for its role in the development of standards for equipment, primarily in the food service area. The NSF's materials and finishes guide refers to three zones: the food zone, the splash zone, and the non-food zone. The NSF stipulates that in the food zone, "surface materials shall be smooth, corrosion resistant, non-toxic, stable and non-absorbent under use conditions. They shall not impart odor, color or taste, nor contribute to the adulteration of the food. Exposed surfaces shall be easily cleaned."[31,32]

Equipment manufactured with a finely polished stainless steel surface tends to have a better corrosion resistance relative to nonpolished stainless steel surface, and it is easier to clean and maintain. Stainless steel sanitary tubing and pipelines intended for use in the food industry should have special surface finishes, as specified by ASTM A270, *Standard Specification for Seamless and Welded Austenitic and Ferritic/Austenitic Stainless Steel Sanitary Tubing*. In addition to the mechanically rolled and polished finishes, other finishes achieved by chemical, electrochemical, or thermal treatment aid sanitation. These techniques also are applied for rehabilitation or rework of damaged stainless steel surfaces.[32]

Materials scientists at the University of Birmingham, United Kingdom, made stainless steel surfaces resistant to bacteria in a project funded by the Engineering and Physical Sciences Research Council. By introducing silver or copper into the steel surface (rather than coating it on to the surface), researchers developed a technique that not only kills bacteria but also has a surface that is very hard and resistant to wear and tear during cleaning. This type of modified steel could be used in the food industry and kitchens.[32]

Under conditions of hot or boiling liquids, the environment turns more aggressive because of the higher temperature and the depletion of the oxygen content. This inconvenience is solved by the choice of a more strongly passivating stainless steel. For example, S31600 is used for equipment, such as mash tuns, whirlpool separators, and heat exchanger plates in the wort cooler.[32]

For hot water storage tanks, an impressed current (IC) system is used. In an IC system, the output from the rectifier supplying the anode current is typically adjusted for the specific water characteristics. The anodes used for IC cathode protection in water heaters are typically mixed metal-oxide anodes. These are noble metal oxides on a titanium substrate. Power is obtained from an alternating current (AC) source and a direct current (DC) rectifier to deliver DC voltage to the anodes.[12,33]

Specific Problem Areas

Chloride corrosion is a major corrosion problem. Another major problem area requires ensuring that the materials used comply with FDA/USDA regulations for contact with foods or beverages during manufacture, processing, and handling.[2,7]

Material selection and processing requirements to ensure cleanliness and sterility are critical. For example, welding to ensure that crevices are not present at a level that would allow microbial growth in service is a significant consideration. Some overly zealous people, however, often specify mirror finishes or flush ground welds as a requirement. Usually this extreme is not necessary. Modest surface finishes as well as welds on the inside of equipment that are ground smooth, but not flush, to a 150 silicon carbide grit (30 to 35 rms) finish with fabrication consistent

with 3-A Sanitary Standard[34] usually are adequate in most services. Care should be taken that the grinding and polishing operation does not cause contaminants, usually steel, to be imbedded into the surface. Austenitic stainless steel has been shown to sanitize easily even when the surface has been abraded.[2,35] As mentioned earlier, external appearance of a shiny polished stainless steel is a frequent consideration.

Microbiological-induced corrosion (specifically bacteria, fungi, and algae) is another problem area. These microorganisms are not corrosives by themselves, but because of the impossibility to produce their nutrients by photosynthesis, they must metabolize organic content present in the media, producing other substances that are returned to the solution. Bacteria are diverse and can live in extreme conditions, such as a high concentration of chlorides (halophilic) or at higher temperatures (thermophilic), or to realize different chemical transformations. Bacteria can participate in corrosion processes in different ways: changing the environment by replacing a substance with another, covering partially the metallic surface with their biofilms creating local corrosion cells, or inducing the corrosion process by depolarization of hydrogen at the metal.[32]

The Use of Test Methods to Evaluate Corrosion

Several standard corrosion test methods are used, including immersion,[36,37] intergranular,[38] and electrochemical[39] (for aqueous solution) methods. Any of the specialized test methods described by Sprowls[40] might be used for special testing conditions.

Steel cans exposed to indoor conditions have been tested according to ASTM G1, *Standard Practice for Preparing, Cleaning, and Evaluating Corrosion Test Specimens*; ASTM G4, *Standard Guide for Conducting Corrosion Tests in Field Applications*; and ASTM G31, *Standard Guide for Laboratory Immersion Corrosion Testing of Metals*. The concentration levels of SO_X (sulfur monoxide, dioxide, trioxide, and disulfer monoxide) and chlorine (for corrosion testing) were evaluated with the sulfation technique plate (SPT) and wet candle method (WCM); see ASTM G91-97(2010), *Standard Practice for Monitoring Atmospheric SO2 Using the Sulfation Plate Technique (superseded)*; and ASTM G140-02(2008), *Standard Test Method for Determining Atmospheric Chloride Deposition Rate by Wet Candle Method (Historical Version)*.[9]

Corrosion resistance of materials is tested per ASTM B117, *Standard Practice for Operating Salt Spray (Fog) Apparatus*, Section 8.1.[31]

New Materials Selection

Several standard laboratory immersion tests described in the previous section are used for new materials selection. U-bend stress corrosion tests[13,41] and multiple crevice washer tests for crevice corrosion[42] are used to evaluate localized corrosion.

High-temperature chlorides can require unique chloride resistance testing.[13] In aqueous solutions, it is common to use electrochemical testing to evaluate pitting potential or crevice corrosion. In nonaqueous base solutions, this usually is evaluated by in-service tests in pilot plants or in existing process equipment.

Wear-related or abrasion-related problems can be determined only by actually testing hardware in full-scale service. Accelerated tests have not proven to be successful in reflecting most service and performance.

IN-SERVICE MONITORING

In-service monitoring is seldom used in the food and beverage industry except in testing alternatives for known problem areas.

FAILURE ANALYSES

Normal "after-the-fact" failure analysis can be used,[43] but there is no standard approach for simulating field failures, and lab simulation is used infrequently.

TEST METHOD APPROACH

Materials normally are evaluated by using field sample racks in pilot plant or full-scale equipment. Electrochemical tests are sometimes used in aqueous solutions to evaluate the likelihood or propensity for localized corrosion caused by pitting or crevice corrosion.

METHODS USED

Industry standard field or laboratory immersion tests described earlier are common and adequate for most food and beverage service applications. Single-sided tests for linings and coatings[44] also are used.

Food service equipment that complies with NSF/ANSI requirements use materials specified in NSF/ANSI Standard 51. Materials selected are corrosion resistant in the intended end-use environment. Conforming coatings may be applied to render a material corrosion resistant. Materials that are worked (e.g., bent, cut, sheared, extruded, drawn) during equipment manufacture may require additional treatment (i.e., passivation) following fabrication to render them corrosion resistant. Brass, bronze, copper, and copper alloys used in areas they may contact food are rendered corrosion resistant.[31]

Special formulations of austenitic stainless steels such as 17% chrome and 4% nickel are used to counteract SCC. This formulation of stainless steel requires heat treatment and annealing at specific values to achieve optimum resistance to SCC. The author has personal experience with this approach to extend the life of stainless steel equipment used by food industry.[45]

Polished finish (No. 3) is a ground (80- to 100-grit abrasive) finish and is used extensively for food contact surfaces. The No. 4 ground finish (80- to 150-grit abrasive) is the most commonly used general purpose stainless steel for food contact surfaces. Buffed finishes (Nos. 5, 6, 7, 8) are generally more expensive and thus are not used extensively in the food industry.[30]

The 3-A Sanitary Standard, as well as USDA guidelines, specify that all surfaces, including fabricated, welded, and soldered joints, shall be at least as smooth as a No. 4 (150 grit) finish and shall be free of pits, folds, crevices, cracks, and misalignments in the final fabricated form.[30]

Additional Comments and Discussion

Problems in the food and beverage industry are unique to specific services within those industries. Many of the chloride-resistant stainless steels, duplex stainless steels,[5] and high-alloy materials have been used in specific applications with good success.[3]

One of the problem areas for food and beverage equipment that is often neglected has to do with the use of jacketed heating and cooling vessels. Sometimes there is a process need to alternately heat a batch process with steam in a jacket and then use cooling water in the same jacket. If chlorides are present in the cooling water, this often can lead to chloride SCC in the jacketed system. Alternative processing methods or chloride-resistant materials must be used in these cases.

Conclusion

Most food and beverage services are handled with the 300 series stainless steels. The issues relating to complying with FDA and USDA regulations for contact with foods and beverages during manufacture, processing, and handling must be carefully evaluated, especially for nonmetallic materials. With few exceptions, however, most of the problems in the industry relate to design and construction according to FDA and USDA codes or NSF standards, to microbes, or to chloride corrosion. The bulk of the equipment used in the industry is S30400, S30403, S31600, and S31603 stainless steel and works quite satisfactorily.

References

1. R. B. Puyear, "To Process Food, 200,000 Tonnes of Stainless," *Nickel* 8, no. 2 (December 1992): 9.
2. J. T. Holah and R. H. Thorpe, "Cleanability in Relation to Bacterial Retention on Unused and Abraded Domestic Sink Materials," *Journal of Applied Bacteriology* 69 (1990): 599–608.
3. B. J. Connolly, "The Use of Stainless Steel and Nickel Alloys to Combat Corrosion in the Brewing, Dairy, Wine and Food Industries," *British Corrosion Journal* 5 (September 1970): 209–216.
4. J. A. Richardson and A. W. Godwin, "Localized Corrosion of Stainless Steel during Food Processing," *British Corrosion Journal* 8 (November 1973): 258–263.
5. J. D. Redmond, "Solving Brewery Stress Corrosion Cracking Problems," *MBAA Technical Quarterly* 21, no. 1 (1984): 1–7.
6. F. F. Lyle, "Stress Corrosion Cracking Susceptibility of Weldments in Duplex Stainless Steels," in *MTI Publication No. 33* (Houston, TX: National Association of Corrosion Engineers, 1989), 1.
7. M. O. Pearce and J. S. Pettibone, "Stainless Steel and Hygiene" (paper presentation, 2nd National Stainless Steel Fair, Sao Paulo, Brazil, July 15–17, 1987).
8. J. S. Pettibone, "Burgers, Fries, Coke and Stainless Steel," in *Proceedings, Nickel Metallurgy, vol. 2. Industrial Applications of Nickel*, Canadian Institute of Mining and Metallurgy and Nickel Development Institute, NiDi Technical Series No. 10009, 1986), 1–6.
9. G. L. Badilla, B. Valdez Salas, and M. Schorr Wiener, *Scientific, Health and Social Aspects of the Food Industry*, ed. B. Valdez (InTech, 2012).
10. *Safe Drinking Water Act* (Title XIV of Public Health Service Act, chapter 373, 78th Congress, approved July, 1944, 58 Stat. 682; amended P.L. 115–270, enacted October 23, 2018).
11. A. A. Estelle, "Drinking Water Lead Regulations: Impact on the Brass Value Chain," *Materials Science and Technology* 32, no. 17 (2016): 1763–1770.
12. NACE International, "A State-of-the-Art Report on the Internal Corrosion of Residential Water Heating Systems" (NACE Technical Committee Report, TG 147, Publication 11114 (Houston, TX: NACE International, 2008).
13. D. R. McIntyre and C. P. Dillon, "Guidelines for Preventing Stress Corrosion Cracking in the Chemical Process Industries," in *MTI Publication No. 15* (Houston, TX: National Association of Corrosion Engineers, 1989), 111–145.
14. D. R. McIntyre, "Environmental Cracking," in *Process Industries Corrosion—Theory and Practice*, ed. B. J. Moniz and W. I. Pollock (Houston, TX: National Association of Corrosion Engineers, 1986), 26.
15. G. C. Page, "Corrosion Failures of Types 304 and 316 Stainless Steels in the Food Industry," *Materials Performance* (July 1989): 58–63.
16. G. Tachis, "Linguistic Purity, World-Famous Wine and Maintenance-Free Tanks," *Nickel* 2, no. 2 (December 1986): 8–9.
17. "Fermenter Tanks for Canada's Two Big Brewers in Ni Stainless," *Nickel* 6, no. 2 (December 1990), 6.
18. D. M. Chorley, "Depend Heavily on Nickel Stainless for Microbrewery Process Equipment," *Nickel* 6, no. 3 (March 1991): 12.
19. J. Ribeca, "Umbrian Makers of Olive Oil, Wine Prompt Tank Manufacturing Business," *Nickel* 8, no. 3 (March 1993): 12.
20. D. W. Rahoi, "The Stress-Cracking Limitations and Corrosion Resistance of Austenitic Stainless Steels and Nu ELI-T 18-2 in Brewery and Related Applications" (paper presentation, Corrosion/84, paper no. 106, NACE International, New Orleans, LA, April 1–6, 1984).
21. E. W. Dreyman, "Corrosion in the Brewery Industry," in *Metals Handbook*, 9th ed., vol. 13 (Metals Park, OH: ASM International, 1979), 1221–1225.
22. "Producing Yogurt or Ice Cream? Nickel Stainless Means Hygiene," *Nickel* 3, no. 2 (December 1987): 8.
23. I. G. de Caprio, "How Stainless Steels Help to Combat Famine in the World," *Nickel* 1, no. 1 (September 1985), 6.
24. "Take a Reefer. Gut it and Add Stainless Tanks. Presto! A New Orange Juice Ship," *Nickel* 3, no. 2 (December 1987): 12.
25. C. A. Smith, "Stainless Steel in the Food Processing Industry," *Anti-Corrosion* (April 1984): 7–8.
26. R. W. Kirchner, P. Crook, and A. I. Asphahani, "Wear/Corrosion-Resistant, High Performance Alloys for the Food Industries" (paper presentation, Corrosion/84, paper no. 102, NACE International, New Orleans, LA, April 1–6, 1984).

27. R. N. Duncan and T. L. Arney, "Performance of Electroless Nickel Coatings in Food Products" (paper presentation, CORROSION/84, paper no. 101, NACE International, New Orleans, LA, April 1–6, 1984).

28. H. J. Dundas, A. P. Bond, and H. Watanaabe, "Corrosion Behavior of Type 304 and 444 Stainless Steel in Food and Beverage Environments" (paper presentation, Corrosion/84, paper no. 104, NACE International, New Orleans, LA, April 1–6, 1984).

29. *Proceedings of Materials and Finishes Seminar, Relative to Food Service Equipment* (Ann Arbor, MI: National Sanitation Foundation, March 1979).

30. R. H. Schmidt, D. J. Erickson, S. Sims, and P. Wolff, "Characteristics of Food Contact Surface Materials: Stainless Steel," *Food Protection Trends* 32, no. 10 (2012): 574–584.

31. *Food Equipment Materials*, NSF/ANSI 51-2017 (Ann Arbor, MI: National Sanitation Foundation, 2017).

32. B. Valdez Salas, M. Schorr Wiener, M. Stoytcheva, R. Zlatev, and M. Carrillo Beltran, *Corrosion in the Food Industry and Its Control*, ed. Benjamin Valdez (InTech, 2012).

33. R. A. Knoeppel, T. G. Van Sistine, and M. A. Murphy, Water storage device having a powdered anode, U.S. Patent 7,372,005, issued May 13, 2008.

34. *Accepted Practices for Permanently Installed Sanitary Product-Pipelines and Cleaning Systems*, 3-A Sanitary Standard, No. 605-04 (McLean, VA: International Association of Milk, Food and Environmental Sanitarians, U.S. Public Health Service, The Daily Industry Committee, 1992).

35. J. T. Holah, "Tests Show Stainless Offers Better Cleanability," *Nickel* 8, no. 3 (March 1993): 2.

36. D. O. Sprowls, "Immersion Tests," in *Metals Handbook*, 9th ed., vol. 13 (Metals Park, OH: ASM International, 1979), 220–224.

37. C. A. Natalie, "Evaluation of Uniform Corrosion," in *Metals Handbook*, 9th ed., vol. 13 (Metals Park, OH: ASM International, 1979), 229–230.

38. R. A. Corbett and B. J. Saldanha, "Evaluation of Intergranular Corrosion," in *Metals Handbook*, 9th ed., vol. 13 (Metals Park, OH: ASM International, 1979), 229–230.

39. J. R. Scully, "Electrochemical Methods of Corrosion Testing," in *Metals Handbook*, 9th ed., vol. 13 (Metals Park, OH: ASM International, 1979), 216–219.

40. D. O. Sprowls, "Corrosion Testing and Evaluation," in *Metals Handbook*, 9th ed., vol. 13 (Metals Park, OH: ASM International, 1979), 191–317.

41. D. O. Sprowls, "Evaluation of Stress Corrosion Cracking," in *Metals Handbook*, 9th ed., vol. 13 (Metals Park, OH: ASM International, 1979), 220–224.

42. R. M. Kain, "Evaluation of Crevice Corrosion," in *Metals Handbook*, 9th ed., vol. 13 (Metals Park, OH: ASM International, 1979), 305–308.

43. L. M. Wyatt, D. S. Bagley, and M. A. Moore, "An Atlas of Corrosion and Related Failures," in *MTI Publication No. 18* (Houston, TX: NACE International, 1989).

44. *Laboratory Methods for the Evaluation of Protective Coatings Used as Lining Materials in Immersion Service—Item No. 53023*, JTM0174-74 (Houston, TX: NACE International, 1991).

45. Product Data Bulletin, 17-4 PH Stainless Steel, No. UNS S17400 (West Chester, OH: AK Steel Corporation, 2018).

Index

A

accelerated tests, for military aircraft, 396
acceptance testing, 148
acid-producing bacteria (APB), 74
acids/acidity
  automobiles and, 364
  in freshwater, 179
  hydrogen and, 60
  organic liquids and, 255–256
adenosine phosphosulfate reductase (APS), 224
adenosine triphosphate photometry (ATP), 224
aeration
  organic fluids and, 253
  of soils, 221
aircraft. *See* commercial aircraft; military aircraft
alkalinity
  aluminum and, 129
  crevice corrosion and, 15
  in freshwater, 181
  on RC, 345–346
alloys. *See also specific types*
  for galvanic corrosion computational models, 51–52
  galvanic corrosion of, 52
  HE of, 127
  industrial chemicals and, 407, 407 (table)
  in petroleum chemistry, 249
  in seawater, 197
  sensitization of, 128–129, 129 (figure)
  SVET for, 120–121
  tribocorrosion of, 81
alternating current (AC)
  EFM and, 117–118
  electrochemical impedance and, 115–117, 115 (figure)
  FGD and, 414–415
  food and beverage and, 431
  pipelines and, 327 (table), 330, 331
  uniform corrosion and, 181
alternating current attenuation (ACA), 336–337, 337 (figure)
alternating current voltage gradient survey (ACVG), 338
aluminum and aluminum alloys
  atmospheric corrosion of, 153, 154, 154 (table), 155, 158 (table), 159 (table), 163
  for automobiles, 360, 364
  in commercial aircraft, 387, 390
  critical potentials for, 124
  EIS for, 130–131, 130 (figure), 131 (figure)
  FACT for, 129
  FGD and, 411
  in freshwater, 179, 181 (table)
  galvanostatic methods for, 123
  immersion testing for, 144
  MMCs of, 292–300, 292 (figure), 297 (figure), 299 (figure), 300 (figure), 308
  organic fluids and, 253, 253 (figure)
  pitting electrochemical tests for, 10
  pitting of, 4
  potentiodynamic polarization for, 123
  in seawater, 208, 209
  sodium hydroxide and, 144
  TSA, 172
  in water handling systems, 320 (table)
aluminum/copper MMCs, 305
aluminum/magnesium MMCs, 301–302
aluminum/stainless steel MMCs, 303–304
ammonia
  automobiles and, 364
  food and beverage and, 429
  immersion testing and, 143
  SCC and, 192
  in seawater, 192
AMPP SP0198, 169
anions, 222–223
anode-cathode area ratio, 43, 44 (figure), 46, 47 (figure)
anodes, 224
anodic polarization curve, 46
anodic reactions
  electrochemical impedance and, 116
  in galvanic corrosion, 41, 42, 52, 119
  polarization resistance and, 114
  in seawater, 192
API 510, 174, 174 (table)
API 570, 174 (table), 175
API 574, 175
API 653, 174 (table), 175
API RP571, 175
API RP572, 174
API RP575, 175
API RP580, 175
API RP581, 175
API RP583, 169
apparent specific gravity index, 219
asperity, 85–86, 85 (figure), 90
ASTM A123, 354
ASTM A153, 354
ASTM A242, 154
ASTM A262, 129, 147 (table), 148, 185, 400 (table), 424, 425
ASTM A270, 431
ASTM A385, 354
ASTM A416, 356
ASTM A480, 15
ASTM A588, 154, 354
ASTM A615, 354

ASTM A674, 222
ASTM A706, 354
ASTM A709, 347, 354
ASTM A763, 147 (table)
ASTM A767, 354
ASTM A775, 356
ASTM A923, 28
ASTM A934, 356
ASTM A955, 356
ASTM A1010, 347, 354
ASTM A1035, 356
ASTM B6, 354
ASTM B68, 287
ASTM B85, 414
ASTM B117, 3, 199, 199 (figure), 207, 285, 285 (table), 286 (table), 287, 298, 331, 372, 373 (table), 375, 387, 388 (table), 390, 395, 414, 432
ASTM B287, 285, 285 (table)
ASTM B368, 200, 285 (table), 286 (table), 373 (table)
ASTM B380, 373 (table)
ASTM B457, 130, 286 (table)
ASTM B537, 371 (table)
ASTM B538, 129, 285 (table)
ASTM B627, 130
ASTM B827, 372
ASTM B895, 372 (table)
ASTM C20, 415
ASTM C461, 172
ASTM C533, 173 (table)
ASTM C534, 173 (table)
ASTM C536, 286 (table)
ASTM C552, 173 (table)
ASTM C553, 173 (table)
ASTM C578, 173 (table)
ASTM C591, 173 (table)
ASTM C610, 173 (table)
ASTM C647, 172
ASTM C692, 147 (table), 171, 172
ASTM C743, 286 (table)
ASTM C795, 171, 405
ASTM C871, 171, 172
ASTM C876, 354
ASTM C892, 173 (table)
ASTM C929, 171, 172
ASTM C1029, 173 (table)
ASTM C1126, 173 (table)
ASTM C1617, 172
ASTM C1728, 173 (table)
ASTM D130, 377
ASTM D512, 223
ASTM D522, 286 (table)
ASTM D523, 286 (table)
ASTM D609, 371 (table)
ASTM D610, 286 (table)
ASTM D662, 286 (table)
ASTM D665, 377
ASTM D714, 286 (table), 287
ASTM D822, 286 (table)
ASTM D823, 286 (table)
ASTM D870, 286 (table), 287
ASTM D968, 286 (table)
ASTM D1014, 286 (table)
ASTM D1120, 377 (table)
ASTM D1123, 377 (table)
ASTM D1141, 27, 198, 206
ASTM D1186, 286 (table)
ASTM D1193, 143
ASTM D1384, 143, 147 (table), 377 (table)
ASTM D1400, 286 (table)
ASTM D1653, 286 (table), 415
ASTM D1654, 286 (table), 287, 371 (table), 389 (table)
ASTM D1735, 286 (table), 373 (table)
ASTM D1748, 373 (table)
ASTM D2010, 156
ASTM D2197, 286 (table)
ASTM D2216, 218
ASTM D2247, 285, 285 (table), 286 (table), 287, 373 (table), 394
ASTM D2248, 286 (table), 287
ASTM D2434, 219
ASTM D2488, 217
ASTM D2570, 143, 147 (table), 377 (table)
ASTM D2688, 182 (table)
ASTM D2758, 377 (table)
ASTM D2803, 371 (table), 388 (table)
ASTM D2809, 377 (table)
ASTM D2847, 377 (table)
ASTM D2980, 219
ASTM D3258, 286 (table)
ASTM D3273, 286 (table)
ASTM D3276, 286 (table)
ASTM D3306, 377, 377 (table)
ASTM D3359, 285 (table), 286 (table), 287
ASTM D3361, 286 (table)
ASTM D3363, 286 (table)
ASTM D3585, 377 (table)
ASTM D3762, 391
ASTM D4145, 286 (table)
ASTM D4340, 377 (table)
ASTM D4585, 286 (table), 287, 373 (table)
ASTM D4587, 287 (table)
ASTM D4959, 330 (table)
ASTM D5894, 200, 206
ASTM D6386, 354
ASTM D7028, 356
ASTM D7091, 286 (table), 287 (table)
ASTM D7205, 356
ASTM D7337, 356
ASTM D7705, 356
ASTM D7913, 356
ASTM E3, 103, 185, 185 (table)
ASTM E45, 101
ASTM E80, 185
ASTM E112, 101, 129
ASTM E203, 260
ASTM E399, 68, 69, 274
ASTM E407, 185, 185 (table)
ASTM E466, 205
ASTM E562, 101
ASTM E606, 205, 206
ASTM E647, 205, 206, 426

ASTM E1049, 206
ASTM E1064, 260
ASTM E1122, 101
ASTM E1351, 101
ASTM E1356, 356
ASTM E1382, 101
ASTM E1447, 277
ASTM E1524, 206
ASTM E1681, 67, 205, 206, 274
ASTM E1820, 68, 69, 274, 275
ASTM F326, 65
ASTM F483, 389 (table)
ASTM F519, 66, 69, 388 (table), 390
ASTM F519-18, 66
ASTM F746, 21 (figure), 30–31, 31 (figure), 123, 183, 183 (table), 184 (table)
ASTM F897, 185, 186 (table)
ASTM F1113, 65
ASTM F1459, 66, 67
ASTM F1624, 69, 79, 205, 274, 277
ASTM F1864, 396
ASTM F1940, 66, 69
ASTM F2129, 147 (table)
ASTM F3044, 47, 147 (table)
ASTM G1, 1, 52, 147 (table), 182 (table), 207, 260, 270, 307, 371 (table), 432
ASTM G3, 143 (table), 147 (table), 182 (table), 207, 229, 371 (table)
ASTM G4, 1, 147 (table), 182 (table), 207, 246, 261, 334, 402, 403 (figure), 432
ASTM G5, 35, 111, 142 (table), 147 (table), 207, 229, 246, 260, 306, 308, 372 (table)
ASTM G8, 287 (table)
ASTM G12, 287 (table)
ASTM G15, 180
ASTM G16, 2, 183 (table), 207, 339
ASTM G28, 147 (table), 400 (table)
ASTM G30, 55, 164 (table), 184, 185 (table), 207, 234, 260, 274, 401 (table), 407, 425
ASTM G31, 142 (table), 143 (table), 146, 147 (table), 182 (table), 198, 207, 237, 246, 260, 371 (table), 400, 400 (table), 402, 432
ASTM G32, 184, 185 (table), 203, 207
ASTM G33, 47, 163, 164, 164 (table), 208, 354, 371 (table)
ASTM G34, 147 (table), 372 (table), 388 (table), 390
ASTM G35, 142 (table), 147 (table), 401 (table)
ASTM G36, 142 (table), 147 (table), 204, 401 (table), 407
ASTM G37, 401 (table)
ASTM G38, 164 (table), 184, 185 (table), 207, 234, 260, 274, 401 (table), 425
ASTM G39, 164 (table), 184, 185 (table), 260, 274, 401 (table), 425
ASTM G40, 184 (table)
ASTM G41, 275, 401 (table)
ASTM G42, 287 (table)
ASTM G43, 285 (table)
ASTM G44, 147 (table), 198–199, 204, 206, 372 (table), 388 (table), 390, 391, 401 (table)
ASTM G46, 2, 25, 26, 52, 103, 183 (table), 207, 229, 234, 246, 334, 339, 354, 371 (table), 400 (table)
ASTM G47, 184, 185 (table), 207, 388 (table), 390
ASTM G48, 2, 19, 20 (table), 24–26, 25 (figure), 28, 31, 142 (table), 147 (table), 149, 183, 184 (table), 372 (table), 400 (table), 407, 424
ASTM G49, 147 (table), 164 (table), 185, 185 (table), 204, 207, 274, 401 (table), 425
ASTM G50, 47, 49, 147 (table), 163 (figure), 164, 164 (table), 208, 354
ASTM G51, 222, 330 (table), 354
ASTM G52, 206, 354
ASTM G53, 287 (table)
ASTM G54, 280
ASTM G57, 219, 220, 237, 330 (table), 354
ASTM G58, 164 (table), 185, 185 (table), 401 (table), 425
ASTM G59, 111, 113, 113 (figure), 182 (table), 207, 229, 236, 260, 372 (table)
ASTM G60, 147 (table), 148, 287 (table), 373 (table)
ASTM G61, 6, 22 (table), 31–33, 35, 122, 147 (table), 183, 183 (table), 184 (table), 185, 186 (table), 201, 202, 207, 229, 246, 260, 354, 372 (table), 400 (table), 424
ASTM G64, 185, 185 (table), 387
ASTM G66, 372 (table)
ASTM G67, 372 (table)
ASTM G69, 4, 207, 372 (table), 388 (table)
ASTM G71, 28, 52, 55, 142 (table), 143 (table), 147 (table), 184, 184 (table), 207, 229, 371 (table), 400 (table)
ASTM G73, 184, 184 (table), 203, 207, 395
ASTM G75, 142 (table), 147 (table)
ASTM G78, 20 (table), 21 (table), 24, 28, 31, 142 (table), 147 (table), 183, 184 (table), 207, 354, 400 (table)
ASTM G80, 287 (table)
ASTM G82, 43 (figure), 48, 52, 55, 119, 183, 184, 184 (table), 207, 307, 371 (table), 400 (table)
ASTM G84, 49, 155, 164 (table), 208, 287 (table)
ASTM G85, 3, 199, 199 (figure), 200, 285, 285 (table), 287, 287 (table), 373 (table), 388 (table), 390, 391, 395
ASTM G87, 287 (table), 354, 372
ASTM G90, 287 (table)
ASTM G91, 156, 156 (figure), 164 (table), 208, 354, 432
ASTM G92, 47, 163, 164 (table), 287 (table)
ASTM G96, 113, 182 (table), 246, 403, 404, 404 (figure)
ASTM G97, 48
ASTM G100, 8, 123, 207, 260, 372 (table)
ASTM G101, 153, 154, 164 (table), 354
ASTM G102, 53, 111, 182 (table), 207, 229, 237, 246, 260, 307, 371 (table)
ASTM G106, 115, 142 (table), 147 (table), 229, 246, 372 (table), 388 (table)
ASTM G107, 207
ASTM G108, 142 (table), 147 (table), 185, 186 (table), 372 (table), 400 (table), 425, 425 (figure)
ASTM G109, 354
ASTM G110, 372 (table)
ASTM G111, 246, 400 (table)
ASTM G112, 334, 371 (table), 390
ASTM G116, 49–50, 51 (figure), 160, 161, 164 (table), 354
ASTM G123, 401 (table), 407
ASTM G129, 66, 67, 204, 207, 260, 275, 401 (table), 425
ASTM G134, 203
ASTM G139, 204, 207, 390
ASTM G140, 156, 208, 432
ASTM G142, 66, 67, 400 (table)
ASTM G148, 126, 229
ASTM G149, 50, 160, 164 (table)
ASTM G150, 10, 22 (table), 31, 31 (figure), 124, 142 (table), 202, 207, 372 (table), 400 (table), 424

ASTM G154, 287, 287 (table)
ASTM G155, 395
ASTM G157, 147 (table), 407
ASTM G158, 230
ASTM G162, 147 (table), 229
ASTM G168, 204, 260, 274, 388 (table), 390, 401 (table)
ASTM G168-17, 67
ASTM G170, 147 (table)
ASTM G180, 354
ASTM G185, 400 (table)
ASTM G186, 406, 407 (figure)
ASTM G187, 220, 221 (figure), 330 (table)
ASTM G188, 406
ASTM G189, 147 (table)
ASTM G189, 172
ASTM G189, 172, 406 (figure)
ASTM G192, 22 (table), 23 (table), 33, 202, 261, 424
ASTM G193, 15, 29, 207, 224, 371 (table)
ASTM G199, 11, 30, 202, 207
ASTM G200, 246, 330 (table)
ASTM G202, 400 (table)
ASTM G205, 147 (table)
ASTM G208, 400 (table)
ASTM G210, 147 (table)
ASTM G215, 47, 404
ASTM G217, 55
atmospheric corrosion
  classification of, 157–158, 158 (table), 159 (table)
  exposure standards for, 164–165, 164 (table), 165 (table)
  exposure types for, 155
  indoor, 158–159, 159 (table), 163
  kinetics of, 153–155, 154 (table)
  monitoring variables for, 155–157, 156 (figure), 157 (figure)
  outdoor exposure to, 162–163, 162 (figure)
  seawater and, 188, 188 (table)
  site monitoring and evaluation of, 163–164
atmospheric tests, 159–164
  exposure program for, 159–160
  for galvanic corrosion, 49–50, 50 (figure), 51 (figure), 55
  program development for, 159, 159 (table)
  specimen preparation for, 160–162, 160 (figure), 161 (figure), 162 (table)
automatic transmission fluid (ATF), 365, 377
automobiles, 359–379
  coatings for, 360, 360 (table)
  corrosion control for, 368–371, 370 (figure), 371 (figure)
  corrosion tests for, 371–379, 371 (table), 372 (table), 373 (table), 374 (figure), 376 (figure), 377 (table), 378 (table)
  corrosive mechanisms of, 366–368, 366 (table), 366–368 (figure)
  design, 361
  electrochemical tests for, 272 (table), 372
  external exposure of, 361–365, 362 (figure), 363 (figure), 363 (table)
  immersion testing for, 272 (table), 372
  internal combustion exposure in, 365
  internal functional liquids of, 365–366
  materials, 359–360, 360 (table)
  processes for, 360–361

B

bacteria. *See* microbiologically influenced corrosion
barnacle electrode, 127
beverage. *See* food and beverage
bicarbonates
  in freshwater, 179
  military aircraft and, 393
  in soils, 222
biofilms
  from MIC, 74
  in seawater, 192, 197
biopotentiostat, 121
Boltzmann superposition, 85–86, 86 (figure)
boron/aluminum MMCs, 292
boron carbide/aluminum MMCs, 295, 295 (figure), 296 (figure)
boron/magnesium MMCs, 300
bottom-of-the-line corrosion (BLC), 326
boundary element analysis, for galvanic corrosion, 51
brass, 103–104, 104 (figure)
  atmospheric corrosion of, 155
  in freshwater, 181 (table)
  LDF and, 405
  for nuclear power, 422
bridges
  coatings for, 346–347, 349–350
  concrete for, 349–350
  corrosion resistance for, 354
  corrosion standards for, 354–356
  CP for, 350
  electrochemical tests for, 350
  LACR for, 354
  RC for, 345–346, 349
  salt exposure of, 346
  sea-level change and, 354
  steel for, 346–349
  vulnerable areas of, 352–354, 353 (figure)
  water exposure of, 346
bright-field illumination (BF), 100
bronze, 181 (table)
butane, 242, 242 (table)

C

cadmium, 390
calcium
  in freshwater, 179
  in seawater, 187 (table)
  in water handling systems, 320 (table)
capillary water, 219
carbonates
  in freshwater, 179
  in seawater, 192
  in soils, 222
carbon dioxide
  automobiles and, 364
  in freshwater, 179, 181
  immersion testing and, 143
  MIC and, 75
  in petroleum chemistry, 241–243, 242 (table)
carbon steel
  CUI of, 170, 172
  for food and beverage, 430

for nuclear power, 422
for pipelines, 325
in seawater, 208
seawater temperature and, 190, 191 (figure)
in soils, 228
in water handling systems, 317, 317 (figure)
cast iron
dealloying of, 103–104
in freshwater, 181 (table)
cathodes, 224
cathodic protection (CP), 236–237
for FGD, 413
for food and beverage, 429–430
for highways, bridges, and tunnels, 350
for pipelines, 325, 340
cathodic reactions
electrochemical impedance and, 116
in galvanic corrosion, 41, 42, 43, 44, 46, 47 (figure), 52, 119
polarization resistance and, 114
in seawater, 192
cations, 222–223
cavitation
in freshwater, 184, 185 (table)
in seawater, 196
ceiling panels, of tunnels, 351
chemical microbially influenced corrosion (CMIC), 74
chloride
atmospheric corrosion from, 156–157, 158 (table)
automobiles and, 361, 363–364
crevice corrosion and, 16, 19, 24, 29
CUI from, 172
ECE for, 350
FGD and, 411, 415
food and beverage and, 429, 431, 432
in freshwater, 179, 180, 181
MIC and, 75
in nuclear power, 425
in seawater, 187 (table)
in soils, 222–223
titanium and, 267
chromium
electrolytic corrosion test and, 129–130
in freshwater, 180
MIC and, 75
in nuclear power, 424
SCC of, 102–103, 103 (figure)
tribocorrosion and, 84
chromium-nickel-iron alloys, 104–105
closed-system boundary condition, 62–63
close-interval potential survey (CIPS), 336, 336 (figure)
coatings
atmospheric tests for, 161
for automobiles, 360, 360 (table)
in commercial aircraft, 387
CUI and, 172–173, 173 (figure)
descriptions of, 285 (table), 286 (table)
effects of corrosion on, 284
EIS for, 130–131, 130 (figure), 131 (figure)
electrochemical tests for, 129–130
EN for, 131
environmental corrosive exposure of, 284
for highways, bridges, and tunnels, 346–347, 349–350
noncorrosive effects of, 284
for nuclear power, 422
for pipelines, 332
SECM for, 121–122, 122 (figure)
service life testing for, 288
SKPFM for, 132–133, 132 (figure)
SKP for, 132–133, 132 (figure)
in soils, 228
standards for, 172–173
testing of, 283–288, 286 (table), 287 (table), 288 (table)
cobalt, in soils, 228
cobalt-chromium alloys, 81, 84, 87 (figure), 90
coefficient of friction (COF), 85, 89, 90
commercial aircraft, 385–391, 385 (table)
aluminum in, 387, 390
corrosion control for, 386–387
corrosion tests for, 387–391, 388 (table), 389 (table)
in-service testing for, 387
inspection of, 387
paints for, 390
service environments of, 385–386, 386 (table)
surface finish of, 390–391
concentration cell corrosion, 180, 183
concrete. *See also* reinforced concrete
for highways, bridges, and tunnels, 349–350
pressure pipe, in soils, 228
constant extension rate testing (CERT), 425
constant phase elements (CPE), 116–117
copper and copper alloys
atmospheric corrosion of, 153, 154, 154 (table), 155, 158 (table), 159 (table), 163
for commercial aircraft, 390
for food and beverage, 430
in freshwater, 179, 180, 181 (table)
MIC of, 78
MMCs, 304–305
for nuclear power, 422
SCC of, 192
in seawater, 196, 208–209
in soils, 228, 229, 235, 235 (table)
titanium and, 267
in water handling systems, 320 (table)
copper-nickel alloys
atmospheric corrosion of, 155
in freshwater, 180
MIC and, 77
for nuclear power, 422
in seawater, 209
copper-zinc brass, 103–104, 104 (figure)
corrosion fatigue
of Al MMCs, 299–300, 308
of industrial chemicals, 400 (table)
in nuclear power, 422
in seawater, 196
corrosion potential
in crevice corrosion, 21 (table)
in electrochemical tests, 110
in galvanic corrosion, 45–46, 46 (figure)
corrosion rates
for commercial aircraft, 385

electrochemical tests for, 110–111, 110 (figure)
for FGD, 411
for galvanic corrosion, 120
immersion testing and, 143, 144–145
penetration rate and, 111
in petroleum chemistry, 249
polarization resistance and, 114
in seawater, 195–196
in soils, 236
Tafel extrapolation for, 112
for titanium, 271–272
in water handling systems, 317, 317 (figure), 319
corrosion resistance
to atmospheric corrosion, 154
in automobiles, 361
for bridges, 354
of crevice corrosion, 19–20, 20 (table), 23 (table)
in food and beverage, 432
to pitting, 24
of titanium, 265–266
corrosion-resistant alloys (CRAs)
crevice corrosion of, 26, 28
FGD and, 409
for pipelines, 325–326
of steel, 347–348
of titanium, 265
corrosion under insulation (CUI), 169–175, 404–405, 405 (figure), 406 (figure)
coatings and, 172–173, 173 (figure)
incidents of, 170
inspection planning for, 174–175, 174 (table)
insulation materials in, 172, 173 (table)
laboratory tests for, 171–172
mechanisms of, 170
moisture entry sources for, 170–171, 171 (figure)
susceptible temperatures for, 170
coupled multi-electrode arrays (CMEAs), 125–126, 126 (figure)
coupon testing
for organic liquids, 259
for pipelines, 334
for pitting, 1–4, 3 (figure)
for water handling systems, 315–318, 316 (figure), 316 (table), 317 (figure), 317 (table)
crack growth resistance curve, 65, 65 (figure)
crevice corrosion, 15–35. *See also* fretting corrosion
atmospheric corrosion and, 154
CCS for, 16–17, 19, 35
CCT for, 25–26, 27 (table)
CMEAs and, 125
in commercial aircraft, 387
corrosion potential in, 21 (table)
corrosion resistance of, 19–20, 20 (table), 23 (table)
CPT in, 19
of CRAs, 26, 28
critical acidification model for, 17–18, 17 (figure), 18 (figure)
critical potentials for, 124
electrochemical tests for, 27–35, 28 (figure), 32 (figure), 34 (figure), 35 (figure)
EN for, 21 (table)
in food and beverage, 429, 432
in freshwater, 183, 184 (table)
geometry of, 15, 16 (figure)
immersion testing for, 141, 142 (table), 146
of industrial chemicals, 400 (table)
mechanisms of, 16–18, 17 (figure), 18 (figure)
of nickel alloys, 17, 24
nonelectrochemical tests for, 23–27, 25 (figure), 27 (table)
in nuclear power, 423
ohmic potential drop in, 18–19
pitting and, 4–6, 17, 24, 30–31, 31 (figure)
potentiodynamic polarization and, 123
in seawater, 195
stages of, 19
of stainless steel, 2–3, 16, 17, 24, 27
test methods for, 19–20, 20 (table), 23 (table)
of titanium, 272–273, 272 (figure), 273 (figure)
uniform corrosion and, 181
critical acidification model, 17–18, 17 (figure), 18 (figure)
critical crevice solution (CCS), 16–17, 19, 35
critical crevice temperature (CCT), 25–26, 27 (table)
critical pitting temperatures (CPT)
CCT and, 26, 27 (table)
in crevice corrosion, 19
in pitting electrochemical tests, 10
seawater and, 202
crude oil, 243–245, 243 (figure), 245 (figure), 243 (table), 244 (table)
corrosion tests for, 247, 248 (figure)
CSA CHMC1, 67
culverts, 350
current
CMEAs and, 125
in galvanic corrosion, 44–46, 45 (figure), 46 (figure)
polarization resistance and, 114
in soils, 226–227, 226 (figure), 227 (figure)
SVET and, 120
tribocorrosion and, 81, 83, 86, 88
uniform corrosion and, 182
cyclic potentiodynamic polarization
complications of, 123
for crevice corrosion electrochemical tests, 29
for localized corrosion, 122–123, 122 (figure)
in pitting electrochemical tests, 6–8, 7 (figure), 8 (figure)
for saltwater, 201, 201 (figure)
cyclic tests, 148

D

dark-field illumination (DF), 99, 100
dealloying
in freshwater, 185
immersion testing for, 142 (table)
metallographic analysis of, 103–104, 104 (figure)
in seawater, 195
decks, of bridges, 352, 352 (figure)
deep ocean, seawater in, 189, 189 (figure)
depth of attack, on MMCs, 306
differential interference contrast microscopy, 100
differential variable reluctance transducers (DVRTs), 88 (figure), 89
dilatometer, 415
Dimension and Conductivity Scaling (DACS), 48
direct assessment (DA), of pipelines, 338–339

direct current (DC)
for EIS, 130
food and beverage and, 431
pipelines and, 327 (table), 330
polarization resistance and, 114
for seawater, 202–203
uniform corrosion and, 182
direct current voltage gradient survey, 337–338, 338 (figure), 338 (table)
disc spring multiple crevice assembly (DSMCA), 23, 24 (table)
disk pressure tests, 67
dissolved oxygen
in seawater, 190–191, 191 (table)
in water handling systems, 320–321
DNA analysis, for MIC, 76
double cantilever beam (DCB), 67–68, 68 (figure)
ductile iron
in freshwater, 181 (table)
in soils, 228

E

EFC-55, 170
elastic modulus, 64
electrical microbially influenced corrosion (EMIC), 74
electrical resistance (ER) probes
for industrial chemicals, 403, 403 (figure)
for pipelines, 335
for seawater, 206
for water handling systems, 316 (table), 319–320, 319 (figure), 320 (figure)
electric resistance welded (ERW), 180
electrochemical cells, 224
electrochemical chloride extraction (ECE), 350
electrochemical frequency modulation (EFM), 117–119, 117 (table)
electrochemical impedance, 115–117, 115 (figure), 115 (table)
electrochemical impedance spectroscopy (EIS)
for aluminum, 130–131, 130 (figure), 131 (figure)
for coatings, 130–131, 130 (figure), 131 (figure)
for FGD, 414–415
for organic fluids, 253
for seawater, 202
for soils, 229, 237
for uniform corrosion, 182
electrochemical noise (EN)
for coatings, 131
for crevice corrosion, 21 (table)
EFM and, 117–118
in pitting electrochemical tests, 10–11
for SCC, 125
seawater and, 202
in ZRA for crevice corrosion, 21 (table), 28–29
electrochemical polarization, for soils, 235–236, 235 (figure), 236 (figure)
electrochemical realkalisation (ER), 350
electrochemical tests, 109–133
for alloy sensitization, 128–129, 129 (figure)
for automobiles, 272 (table), 372
for coatings, 129–130
for corrosion rates, 110–111, 110 (figure)
for crevice corrosion, 22 (table), 23 (table), 27–35, 28 (figure), 32 (figure), 34 (figure), 35 (figure)
electrochemical impedance and, 115–117
electrode reaction thermodynamics and kinetics and, 109–111, 110 (figure)
frequency modulation and, 117–119, 117 (table)
for galvanic corrosion, 48–49, 53, 119–120, 119 (figure)
for highways, bridges, and tunnels, 350
immersion testing and, 146
for industrial chemicals, 403–404, 404 (figure)
for localized corrosion, 122–124, 122 (figure), 124 (figure)
for MIC, 78
for organic liquids, 252–255, 252 (figure), 255 (figure), 259–261
for pitting, 4–11, 5 (figure), 10 (figure)
polarization methods in, 111–117, 113 (figure), 115 (figure)
potential probe methods in, 120–133
for SCC, 126–129, 128 (figure), 129 (figure)
for seawater, 200–203
for soils, 229–230, 230 (figure)
for tribocorrosion, 87–89, 88 (figure), 90
electrode potential, 81–82, 84
electrolytes, 224
in commercial aircraft, 387
in freshwater, 181
organic liquids and, 255–256
electrolytic corrosion test, 129–130
electron microprobe analyzer (EMPA), 100
energy dispersive spectrometer (EDS)
for dealloying, 185
for metallographic analysis, 100
for soils, 237
epifluorescent microscopy, 224
erosion corrosion (EC)
in freshwater, 184, 185 (table)
immersion testing for, 142 (table)
of pipelines, 329 (table)
in seawater, 196
ER probes, 236, 237 (figure)
ethane, 242, 242 (table)
external chloride stress corrosion cracking (ECSCC), 169, 170, 171–172
external corrosion direct assessment (ECDA), 237–238
extracellular DNA (e-DNA), 76
extracellular electron transfer MIC (EET-MIC), 74
extracellular polymeric substances (EPS), 74

F

Faraday's constant, 83, 109
Faraday's law, 90, 111
ferric chloride ($FeCL_3$)
crevice corrosion and, 24
pitting and, 2–3
titanium and, 267
Fick's first law, 60, 112
film creep, 159
finite difference analysis, 51
finite element analysis, 51, 52
flood gates, of tunnels, 351
flow-induced localized corrosion (FILC), 329 (table), 330 (table)
flow rate, in galvanic corrosion, 43–44, 44 (figure), 45 (figure)
flue gas desulfurization (FGD)
corrosion control for, 411–413, 412 (figure)
corrosion environments of, 411, 411 (table)

corrosion testing for, 413–415
fire protection for, 413
inorganic linings for, 410–411
marine scrubbers and, 415–416
organic linings for, 409–410
welding and, 413
fluorescence *in situ* hybridization (FISH), 76
fly ash/aluminum, 298, 411
fly ash/magnesium MMCs, 302
food and beverage, 429–433
corrosion control for, 431
corrosion testing for, 432
corrosive environments of, 430–431
in-service testing for, 432
materials of construction for, 429–430
new materials selection for, 432
specific problem areas in, 431–432
Ford anodized aluminum corrosion test (FACT), 129
freshwater, 179–185
biological factors of, 180
cavitation in, 184, 185 (table)
chemistry of, 179–180
concentration cell corrosion in, 180, 183
crevice corrosion in, 183, 184 (table)
dealloying in, 185
electrolytes in, 181
erosion corrosion in, 184, 185 (table)
fretting corrosion in, 185, 186
intergranular corrosion in, 185, 186 (table)
metallurgy of, 180
pitting in, 183, 184 (table)
process conditions of, 180
SCC in, 184–185, 185 (figure)
test methods for, 180–185, 181 (table), 186 (table)
uniform corrosion in, 181–182, 182 (table)
fretting corrosion
in freshwater, 185, 186
tribocorrosion and, 89, 89 (figure)

G

galvanic anode cathodic protection (GACP), 350
galvanic corrosion
anode-cathode area ratio in, 43, 44 (figure), 46
atmospheric tests for, 49–50, 50 (figure), 51 (figure), 55
in automobiles, 367
computational modeling for, 50–52
corrosion potential in, 45–46, 46 (figure)
corrosion rates for, 120
current in, 44–46, 45 (figure), 46 (figure)
electrochemical reactions in, 41, 42 (figure)
electrochemical tests for, 48–49, 53, 119–120, 119 (figure)
factors in, 46, 47 (figure)
flow rate in, 43–44, 44 (figure), 45 (figure)
in freshwater, 184 (table), 183–184
galvanic couples and, 46–48, 52, 119–120, 119 (figure)
immersion testing for, 141, 143 (table), 146
of industrial chemicals, 400 (table)
mixed potential theory for, 42–43, 43 (figure), 119–120
of MMCs, 307
from oxidation, 41
polarization curve for, 53
in seawater, 195
in soils, 237
SVET for, 52, 53–55, 53 (figure), 55 (figure), 120
test results evaluation for, 52–55
tests for, 46–52, 50 (figure), 51 (figure)
galvanic couples, 46–48, 52, 119–120, 119 (figure)
galvanic series, 41–42, 42 (figure), 43 (figure), 48
galvanostaircase technique, 29
galvanostatic methods
for crevice corrosion electrochemical tests, 29
for localized corrosion, 122 (figure), 123
for pitting electrochemical tests, 8
galvanostep technique, 29
global positioning satellite (GPS), 231
glucose oxidase (GOD), 27
grain-boundary area (GBA), 129, 195
graphite/aluminum (Gr/Al) MMCs, 292–294, 292 (figure), 294 (figure)
graphite/copper MMCs, 305
graphite/magnesium MMCs, 300–301, 300 (figure)
gravimetric evaluation, of MMCs, 306
gravitational water, 218
guardrails, for highways, 350
guided wave testing (GWT), 334

H

half-cell reactions, 109–110, 116
harmonic frequency modulation, 117–119, 117 (table)
heat-affected zone (HAZ)
FGD and, 409
nuclear power and, 421
heat transfer
for nuclear power, 422
in water handling systems, 316 (table), 321–322, 321 (figure)
heavy metals
in freshwater, 181
in seawater, 194
high-strength low-alloys (HSLA)
for commercial aircraft, 390
for pipelines, 325
high velocity flow tests, for seawater, 203
highways, 345–356
ancillary structures of, 351
coatings for, 346–347, 349–350
concrete for, 349–350
corrosion standards for, 354–356
CP for, 350
culverts for, 350
electrochemical tests for, 350
guardrails for, 350
LACR for, 354
luminaires of, 351
RC for, 345–346, 349
salt exposure of, 346
sea-level change and, 354
steel for, 346–349
vulnerable areas of, 350
water exposure of, 346
hot-dip galvanizing (HDG), 347

humidity tests
for automobiles, 372
for coatings, 285
for military aircraft, 394
hybrid organic acid technology (HOAT), 365
hydraulic brake fluid, 365–366, 377
hydrogen, 59–70
barnacle electrode for, 127
crack growth resistance curve and, 65, 65 (figure)
disk pressure tests for, 67
in galvanic corrosion, 41
MIC and, 75
in nuclear power, 423
permeation method for, 127–128, 128 (figure)
quantitative measurements for, 66–70, 68 (figure), 69 (figure)
rising displacement test for, 69–70
in soils, 224
strain localization and, 63–65, 64 (figure)
stress and, 60–65, 64 (figure)
sustained load test for, 67–68, 68 (figure)
tensile testing for, 66–67
testing for failures with, 65–66
threshold stress intensity factor and, 67–70, 68 (figure), 69 (figure)
trapping of, 61, 61 (figure)
uptake of, 59–60
hydrogen embrittlement (HE), 62–65, 64 (figure), 65 (figure)
of alloys, 127
of industrial chemicals, 400 (table)
of pipelines, 328 (table)
SCC and, 126
in seawater, 196–197
of titanium, 268–269, 276–277, 276 (figure), 277 (figure)
hydrogen sulfide
atmospheric corrosion from, 159
automobiles and, 364
immersion testing and, 143
MIC and, 77
in petroleum chemistry, 241
in soils, 223

I

ignition testing, for titanium, 277–279, 278 (figure), 279 (figure)
immersion testing, 141–150, 142 (table), 143 (table)
for automobiles, 272 (table), 372
physical parameters for, 144–145, 145 (table)
precautions and validity of results of, 150–151
for seawater, 198–199
test conditions for, 143
types of, 146–148, 147 (table), 148
impressed current cathodic protection (ICCP), 350
for food and beverage, 431
incremental step loading (ISL), hydrogen and, 66
industrial chemicals, 399–407, 399 (table)
alloys and, 407, 407 (table)
corrosion testing for, 399–404, 400 (table), 401 (table), 401 (figure), 404 (figure)
CUI with, 404–405, 405 (figure), 406 (figure)
electrochemical tests for, 403–404, 404 (figure)
pilot plant tests for, 402–403, 402 (figure), 403 (figure)
specialized testing for, 404–407, 405 (figure), 407 (figure)
in-line inspection (ILI), for pipelines, 333
inorganic linings, for FGD, 410–411
in seawater, 196
in-service testing
for commercial aircraft, 387
for food and beverage, 432
of seawater, 205–206
intergranular attack/corrosion (IGA)
in food and beverage, 430
in freshwater, 185, 186 (table)
immersion testing for, 142 (table)
of industrial chemicals, 400 (table)
in nuclear power, 419, 423, 424
intergranular stress corrosion cracking (IGSCC), 102–103
iron and iron alloys. *See also* cast iron; ductile iron
coatings and, 284
in freshwater, 179
galvanic corrosion of, 41, 42 (figure)
MIC of, 74, 75, 77
in nuclear power, 423
titanium and, 267, 268
iron-chromium alloys, 104–105, 104 (figure)
iron-chromium-zinc alloys, 124
ISO 45-40, 165 (table)
ISO 45-42, 165 (table)
ISO 1462, 207
ISO 4540, 207
ISO 4623, 206
ISO 7384, 206, 371 (table)
ISO7441, 49
ISO 7441, 165 (table)
ISO 7539, 207
ISO 8565, 165 (table)
ISO 8993, 207
ISO 8994, 165 (table), 207
ISO 9223, 153, 165 (table)
ISO 9224, 165 (table)
ISO 9225, 165 (table)
ISO 9226, 165 (table)
ISO 9227, 199–200, 373 (table)
ISO 9591, 207
ISO 10062, 373 (table)
ISO 10289, 371 (table)
ISO 11303, 165 (table)
ISO 11306, 207
ISO 11463, 207, 339
ISO 11782-2, 207
ISO 11845, 207
ISO 11997, 373 (table)
ISO 15156, 241
ISO 16539, 206
ISO 23226, 206
ISO DTR 10783, 66
ISO TCI56/WG4, 153

K

Kohler principle, 99, 99 (figure)

L

laser ablation coating removal (LACR), 354
lead and lead alloys
  in freshwater, 179
  MMCs, 302–303
  in soils, 228–229
leak detection fluid (LDF), 405, 407 (figure)
light optical microscope (LOM), 100
linear polarization-resistance (LPR) probes
  for pipelines, 335
  for water handling systems, 316 (table), 317 (figure), 318–319, 318 (figure)
liquid metal embrittlement (LME), 105, 105 (figure), 105 (table)
liquid penetrant (LP), for pipelines, 332–333
lithium perchlorate, 255
localized corrosion
  electrochemical tests for, 122–124, 122 (figure), 124 (figure)
  in nuclear power, 422–423
low-pressure degradation, of military aircraft, 395
LPR probes, 236
luminaires, of highways, 351

M

macrofouling organisms, in seawater, 193
magnesium and magnesium alloys
  for automobiles, 360, 364
  in freshwater, 179
  MMCs, 300–302
  in seawater, 187 (table), 209
  in water handling systems, 320 (table)
magnesium rich primer (MgRP), 52
magnetic particle (MP), 332–333
manganese
  atmospheric corrosion of, 154
  in freshwater, 179, 180, 181
  MIC and, 75
  in nuclear power, 423
marine scrubbers, 415–416
mass balance, 82–84, 83 (figure)
mass loss electrochemical tests, 111
mass transport-controlled corrosion, 196
metabolite MIC (M-MIC), 74
metabolomics, 76–77
metallographic analysis, 93–107
  of chromium-nickel-iron alloys, 104–105
  of dealloying, 103–104, 104 (figure)
  etching for, 97–99, 97 (figure), 98 (table)
  grinding for, 95–96, 95 (figure)
  interpretation of, 99–101
  of iron-chromium alloys, 104–105, 104 (figure)
  of LME, 105, 105 (figure), 105 (table)
  NDT for, 101–102, 101 (figure)
  of pitting, 103, 103 (figure), 104 (figure)
  polishing for, 96–97, 96 (table), 97 (figure)
  quantitative, 100–101
  sample selection for, 93
  for SCC, 102–103, 102 (figure), 103 (figure)
  sectioning for, 93
  specimen preparation for, 93–95, 95 (figure)
  of stainless steel, 104–105, 104 (figure)
  of sulfidation, 105
  of TBC, 106–107, 106 (figure)
metal-matrix composites (MMCs), 291 (figure)
  of aluminum, 292–300, 292 (figure), 297 (figure), 299 (figure), 300 (figure)
  aluminum/copper, 305
  aluminum/magnesium, 301–302
  aluminum/stainless steel, 303–304
  boron/aluminum, 292
  boron carbide/aluminum, 295, 295 (figure), 296 (figure)
  boron/magnesium, 300
  copper, 304–305
  corrosion evaluation for, 305–306
  corrosion susceptibility of, 291–305
  depth of attack on, 306
  fly ash/aluminum, 298
  fly ash/magnesium, 302
  galvanic corrosion of, 307
  graphite/aluminum, 292–294, 292 (figure), 294 (figure)
  graphite/copper, 305
  graphite/magnesium, 300–301, 300 (figure)
  gravimetric evaluation of, 306
  lead, 302–303
  magnesium, 300–302
  mica/aluminum, 298
  pitting of, 307–308
  silicon/aluminum, 297
  silicon carbide/aluminum, 294–296, 294 (figure), 295 (figure)
  silicon carbide/copper, 305
  silicon carbide/magnesium, 301, 301 (figure)
  silicon carbide/titanium, 305
  stainless steel, 303–304
  stress on, 308
  testing for, 306–308, 306 (figure), 307 (figure)
  titanium, 304, 304 (figure)
  uniform corrosion in, 307
  uranium, 303
  yttria/stainless steel, 304
  zinc, 305
  ZRA for, 307
methane, 242, 242 (table)
mica/aluminum MMCs, 298
microbiologically influenced corrosion (MIC), 73–78
  corrosion mechanisms of, 73–75
  diagnosis of, 76–77
  electrochemical tests for, 78
  in food and beverage, 432
  on military aircraft, 394
  monitoring of, 77–78
  in nuclear power, 419, 422, 423–424
  of pipelines, 328 (table)
  scope of problem with, 73
  in soils, 223–224, 237
  soils oxidation-reduction potential and, 222
  standards for, 75–76
micro-electrode (ME), 121–122
microfouling organisms, 193
MIL-C-81309, 378 (table)

military aircraft, 393–397
accelerated tests for, 396
environmental testing for, 394–396
humidity tests for, 394
low-pressure degradation of, 395
MIC on, 394
mission of, 393–394
rain exposure testing for, 395
salt spray testing for, 394–395
sand and dust testing for, 395–396
solar radiation on, 395
standards and specifications for, 396
storage, transportation, and deployment of equipment for, 393
thermal shock on, 394
MIL-STD-810, 394, 395
MIL-STD-1530, 396
MIL-STD-1568, 394
MIL-STD-3033, 396
MIL-T-5422, 378 (table)
mixed potential theory, 110–111, 110 (figure), 113 (figure)
for galvanic corrosion, 42–43, 43 (figure), 119–120
for seawater, 200–201
molecular microbiological methods (MMMs), for MIC, 76, 77, 224
molybdenum
atmospheric corrosion of, 154
crevice corrosion of, 15
MIC, 73
for nuclear power, 422
in soils, 228
MTI1, 148 (table)
MTI2, 148 (table)
MTI3, 148 (table)
MTI4, 148 (table)
MTI5, 148 (table)
mud, seawater in, 188 (figure), 190
multiple-crevice assembly (MCA), 19, 23, 24 (table), 33

N

NACE RP0172-72, 165 (table)
NACE RP0173-73, 207
NACE RP0174, 234
NACE RP0176-83, 165 (table)
NACE RP0177, 234
NACE RP0187-2005, 356
NACE RP0194, 234
NACE RP0274, 234
NACE RP0281-86, 165 (table)
NACE RP0281-2004, 356
NACE RP0285, 234
NACE RP0286, 234
NACE RP0287, 356
NACE RP0290, 356
NACE RP0375, 234
NACE RP0502, 234, 238
NACE RP0692-92, 165 (table)
NACE RP0775-87, 182 (table)
NACE RPO272, 371 (table)
NACE SP024, 339
NACE SP104, 234
NACE SP0116, 338
NACE SP0169, 234
NACE SP0206, 338
NACE SP0207, 234
NACE SP0288, 338
NACE SP0502, 338, 339
NACE SP21427, 356
NACE TM0106, 76
NACE TM0109, 338
NACE TM0169, 147 (table), 182 (table)
NACE TM0170-70, 165 (table)
NACE TM0171, 182 (table)
NACE TM0174, 147 (table)
NACE TM0175-75, 165 (table)
NACE TM0177, 147 (table), 148
NACE TM0196, 147 (table)
NACE TM0212, 76
NACE TM0274, 182 (table)
NACE TM0284, 147 (table), 148
NACE TM0286, 147 (table)
NACE TM0416, 49, 147 (table)
NACE TM0497, 234
Nernst equation, 109–110
neutral salt spray (NSS), 372–373
nickel and nickel alloys
atmospheric corrosion of, 154
crevice corrosion of, 17, 24
electrolytic corrosion test and, 129–130
FGD and, 409
for nuclear power, 422
potentiodynamic polarization for, 123
in seawater, 208
in soils, 228
titanium and, 267
nickel-chromium-molybdenum, 208
nickel silvers, atmospheric corrosion of, 155
niobium, atmospheric corrosion of, 154
nitrate
in freshwater, 179, 181
MIC and, 75
in soils, 222
titanium and, 267
nitric oxide
automobiles and, 364
FGD and, 414
nitrogen
atmospheric corrosion and, 154
immersion testing and, 143
nondestructive examination (NDE), of CUI, 174
nondestructive testing (NDT)
for CUI, 169
for metallographic analysis, 101–102, 101 (figure)
for pipelines, 331–334, 331 (table)
nuclear power, 419–427
corrosion tests for, 420–426, 420 (figure), 423 (figure), 425 (figure)
environments, metallurgical conditions, and corrosion problems of, 423–424
failure modes of, 422–423, 423 (figure)
materials of construction for, 419–420

O

ohmic potential drop, 18–19
oil and gas industry. *See* pipelines
oils
  for automobiles, 365
  specimen preparation for, 231–233, 232 (figure)
open-circuit corrosion rate, 42
open-circuit potential (OCP), 111
  galvanic corrosion and, 120
  polarization resistance and, 114
  Tafel extrapolation and, 112
open-system boundary condition, for hydrogen, 62
organic acid technology (OAT), 365
organic liquids
  ASTM standards for, 260–261
  classification of, 251
  corrosion types with, 252
  coupon testing for, 259
  electrochemical tests for, 252–255, 252 (figure), 255 (figure), 259–261
  environmental factors with, 255–259, 256 (figure), 258 (figure), 256 (table)
  field tests for, 261–262
  laboratory tests for, 259–261, 260 (figure), 261 (figure)
  SCC with, 253, 256, 256 (figure), 260, 260 (figure)
oxidation
  galvanic corrosion from, 41
  metallographic analysis of, 105–106
  from MIC, 73, 74
  Nernst equation for, 109–110
  of titanium, 265, 279–280, 280 (figure)
  tribocorrosion and, 81–82, 84
oxidation-reduction potential (ORP)
  in soils, 221–222, 222 (table)
  in water handling systems, 321
oxygen. *See also* dissolved oxygen
  in nuclear power, 423–424
  organic fluids and, 253, 253 (figure)
  in soils, 221, 225, 225 (figure)
  titanium and, 267

P

paint adhesion on scribed surface test, 130
paints
  for commercial aircraft, 390
  for steel, atmospheric corrosion of, 155
passivation
  in food and beverage, 430–431
  of titanium, 266–267
penetration rate, corrosion rates and, 111
pentane, in petroleum chemistry, 242, 242 (table)
permeation method, for hydrogen, 127–128, 128 (figure)
petroleum chemistry, 241–249
  in crude oil phase, 243–245, 243 (figure), 245 (figure), 243 (table), 244 (table)
  in gas and gas condensate phases, 241, 241 (table)
  laboratory corrosion tests for, 245–248
  in liquid water phase, 242–243, 243 (table)
  new production corrosion tests for, 248–249, 248 (figure), 249 (table)
  temperatures and pressures with, 242, 242 (figure)
pH
  in nuclear power, 423
  of seawater, 192
  of soils, 222
  titanium and, 268
pickling, 24
pilot plant tests, for industrial chemicals, 402–403, 402 (figure), 403 (figure)
pipelines
  ACA for, 336–337, 337 (figure)
  ACVG for, 338
  carbon steel for, 325
  CIPS for, 336, 336 (figure)
  coatings for, 332
  corrosion threats to, 326–330, 327 (table), 330 (figure)
  coupon testing for, 334
  CRAs for, 325–326
  DA of, 338–339
  DCVG for, 337–338, 338 (figure), 338 (table)
  ER for, 335
  GWT for, 334
  ILI for, 333
  LP for, 332–333
  LPR for, 335
  materials for, 325–326
  modeling and predictions for, 339
  MP for, 332–333
  NDT for, 331–334, 331 (table)
  potential measurement for, 335–336, 335 (figure)
  present condition testing of, 334–335
  proactive testing for, 335–340, 335 (figure), 338 (figure), 338 (table)
  in soils, 326–330, 327 (table), 330 (figure)
  statistical evaluation of, 339–340
  thermoplastic liners for, 326
  visual inspection of, 331–332, 332 (table)
piping
  CUI from, 170–171
  freshwater in, 180
  for nuclear power, 429–430
  in soils, 225, 225 (figure), 227–229, 227 (figure), 237–238
  in water handling systems, 315–318, 316 (figure), 316 (table), 317 (figure), 317 (table)
pitting, 1–12
  of aluminum alloys, 4
  CMEAs and, 125
  corrosion resistance to, 24
  coupon testing for, 1–4, 3 (figure)
  crevice corrosion and, 4–6, 17, 24, 30–31, 31 (figure)
  critical potentials for, 124
  cyclic potentiodynamic polarization and, 123
  electrochemical tests for, 4–11, 5 (figure), 10 (figure)
  in freshwater, 183, 184 (table)
  immersion testing for, 141, 142 (table)
  of industrial chemicals, 400 (table)
  metallographic analysis of, 103, 103 (figure), 104 (figure)
  of MMCs, 307–308
  in nuclear power, 422–423
  of pipelines, 329 (table), 330
  potentiodynamic polarization and, 123
  predictive capabilities with, 11–12

in seawater, 195
in soils, 227–228, 227 (figure)
of titanium, 273–274
uniform corrosion and, 181
pitting resistance equivalence number (PREN), 183, 208
polarization curve, for galvanic corrosion, 53
polarization methods
concentration effects with, 112–113, 113 (figure)
in electrochemical tests, 111–117, 113 (figure), 115 (figure)
polarization resistance, 113–114, 113 (figure)
uniform corrosion and, 182
polarized light (PL), 100
polychlorotrifluoroethylene (PCTFE), 19
polymerase chain reaction (PCR), 76
polytetrafluoroethylene (PTFE), 2, 5, 5 (figure), 19, 30, 33, 95
polyvinylidene difluoride (PVDF), 19, 23
potential measurement
in electrochemical tests, 120–133
for pipelines, 335–336, 335 (figure)
for soils, 234–235
potentiodynamic galvanostatic-potentiodynamic technique (PD-GS-PD), 33–35, 34 (figure), 35 (figure)
potentiodynamic polarization
for crevice corrosion electrochemical tests, 29, 31–35, 32 (figure), 35 (figure), 43 (figure)
for galvanic corrosion electrochemical tests, 48
immersion testing and, 146
for localized corrosion, 123
for SCC, 126–127
potentiokinetic polarization, 29
potentiostaircase technique, 29
potentiostatic methods
for crevice corrosion electrochemical tests, 30–31, 30 (figure), 31 (figure)
for galvanic corrosion electrochemical tests, 48
for localized corrosion, 122 (figure), 123
for pitting electrochemical tests, 8–10, 9 (figure)
for tribocorrosion, 87–89, 88 (figure)
potentiostatic polarization, 29
potentiostep technique, 29
preferential weld corrosion (PWC), 330 (table)
probes. *See also* electrical resistance; linear polarization-resistance
for galvanic corrosion tests, 49
for soils, 236, 237, 237 (figure)
propane, 242, 242 (table)
pyrite, 77

Q

quantitative PCR (qPCR), 76

R

rain exposure testing, for military aircraft, 395
reinforced concrete (RC), for highways, bridges, and tunnels, 345–346, 349
remote crevice assembly, 28
repassivation potential
in crevice corrosion electrochemical tests, 32
in pitting electrochemical tests, 9–10, 10 (figure)
potentiodynamic polarization and, 123
tribocorrosion and, 82–83, 84
rising displacement test, for hydrogen, 69–70
risk-based inspection (RBI), for CUI, 175
RNA analysis, 76

S

SAE J400, 373 (table)
SAE J1703, 377
SAE J2020, 373 (table)
SAE J2334, 373 (table)
salinity, of seawater, 191–192, 191 (table)
salts
automobiles and, 361–363, 362 (figure), 363 (table)
immersion testing and, 146
in soils, 218
salt spray (fog) testing
for commercial aircraft, 390
for military aircraft, 394–395
for pitting, 3–4, 3 (figure)
for seawater, 199–200, 199 (figure)
saltwater. *See* seawater
sand and dust testing, for military aircraft, 395–396
saturated calomel electrode (SCE), 129
seawater and, 201
scanning electrochemical microscopy (SECM), 121–122, 122 (figure)
for pitting electrochemical tests, 11
scanning electron microscope (SEM)
for metallographic analysis, 100
for soils, 237
scanning Kelvin probe (SKP)
for coatings, 132–133, 132 (figure)
for pitting electrochemical tests, 11
scanning Kelvin probe force microscopy (SKPFM)
for coatings, 132–133, 132 (figure)
for pitting electrochemical tests, 11
scanning vibrating electrochemical technique (SVET), 120–121, 121 (figure)
for galvanic corrosion, 52, 53–55, 53 (figure), 55 (figure), 120
for pitting electrochemical tests, 11
scratch tests
for localized corrosion, 124, 124 (figure)
for pitting electrochemical tests, 8–9, 9 (figure)
for SCC, 126
sea-level change, highways, bridges, and tunnels and, 354
seawater, 187–209
atmospheric corrosion and, 188, 188 (table)
automobiles and, 361
biological organisms in, 192–193
carbonates in, 192
composition of, 187–188, 187 (table)
corrosion mechanisms of, 194–197, 197 (figure)
corrosion testing of, 197–205
crevice corrosion in, 26–27
cyclic potentiodynamic polarization for, 201, 201 (figure)
DC for, 202–203
in deep ocean, 189, 189 (figure)
dissolved oxygen in, 190–191, 191 (table)
EIS for, 202
electrochemical tests for, 200–203
EN and, 202
environmental zones of, 188–190, 188 (figure), 188 (table), 189 (figure)
flow velocity of, 193–194, 193 (figure)

heavy metals in, 194
high velocity flow tests for, 203
immersion testing for, 198–199
in-service testing of, 205–206
laboratory evaluation of, 195–196
MIC and, 78
mixed potential theory for, 200–201
in mud, 188 (figure), 190
pH of, 192
salinity of, 191–192, 191 (table)
salt spray testing for, 199–200, 199 (figure)
SCC in, 196, 203–205
small-specimen testing for, 205–206
splash-spray zone of, 188 (figure), 189
standards for, 206–207
in submerged/shallow ocean, 189, 189 (figure)
sulfides in, 192, 194, 194 (table)
temperature of, 190, 190 (table)
tidal zone of, 189, 189 (figure)
uniqueness of, 190
service life testing, for coatings, 288
σ-phase metallographic analysis, 104–105, 104 (figure)
silicon/aluminum MMCs, 297
silicon carbide/aluminum (SiC/Al) MMCs, 294–296, 294 (figure), 295 (figure)
silicon carbide/copper MMCs, 305
silicon carbide/magnesium MMCs, 301, 301 (figure)
silicon carbide/titanium MMCs, 305
simulated service testing, 148
for seawater, 206
slow strain rate test (SSRT), for nuclear power, 425
small-specimen testing, for seawater, 205–206
soil box corrosion testing, 229
soils, 217–238
aeration of, 221
anions in, 222–223
carbon steel in, 228
cations in, 222–223
coatings in, 228
concrete pressure pipe in, 228
copper and copper alloys in, 229, 235, 235 (table)
corrosion in, 224–229
corrosion monitoring in, 234–238, 235 (figure), 237 (figure), 235 (table)
definition and classification of, 217–218, 217 (figure), 218 (table)
disturbance of, 224
ductile iron in, 228
electrochemical polarization for, 235–236, 235 (figure), 236 (figure)
electrochemical tests for, 229–230, 230 (figure)
field corrosion tests for, 229–234, 232 (figure), 233 (figure)
galvanic corrosion in, 237
laboratory corrosion tests for, 229–230, 229 (figure), 230 (figure)
lead in, 228–229
MIC in, 223–224, 237
moisture in, 218–219
oxidation-reduction potential in, 221–222, 222 (table)
oxygen in, 221, 225, 225 (figure)
pH of, 222
pipelines in, 326–330, 327 (table), 330 (figure)
piping in, 225, 225 (figure), 227–229, 227 (figure), 237–238
pitting in, 227–228, 227 (figure)
probes for, 236, 237, 237 (figure)
resistivity of, 219–220, 219 (figure), 221 (figure), 220 (table)
SRB in, 223–224, 223 (figure)
stainless steel in, 228
stray current corrosion in, 226–227, 226 (figure), 227 (figure)
solar radiation, on military aircraft, 395
solution resistance
polarization methods and, 112
polarization resistance and, 114
specimen preparation
for atmospheric tests, 160–162, 160 (figure), 161 (figure), 162 (table)
for immersion testing, 144, 148–150, 149 (figure)
for metallographic analysis, 93–95, 95 (figure)
for pitting electrochemical tests, 4–5
for soils, 231–233
splash-spray zone
automobiles and, 361
of seawater, 188 (figure), 189
stainless steel
atmospheric corrosion of, 153–155, 154 (table), 159 (table)
crevice corrosion of, 2–3, 16, 17, 24, 27
critical potentials for, 124
cyclic potentiodynamic polarization for, 122
ECSCC of, 170, 171–172
electrolytic corrosion test and, 129–130
FGD and, 409, 411
for food and beverage, 430
in freshwater, 181 (table)
galvanic corrosion of, 52
immersion testing for, 146
metallographic analysis of, 104–105, 104 (figure)
MMCs, 303–304
for nuclear power, 422
for pipelines, 325
pitting electrochemical tests for, 5–6, 5 (figure), 7 (figure)
polarization resistance and, 113
potentiodynamic polarization for, 123
SCC of, 102
soil pH and, 222
in soils, 228
tribocorrosion of, 81
steel. *See also* high-strength low-alloys; stainless steel
in freshwater, 181 (table)
for highways, bridges, and tunnels, 346–349
for nuclear power, 419–420
strain
hydrogen and, 63–65, 64 (figure)
tribocorrosion and, 81
stray current corrosion, in soils, 226–227, 226 (figure), 227 (figure)
stress
hydrogen and, 60–65, 64 (figure)
on MMCs, 308
in soils, 234
tribocorrosion and, 81
stress corrosion cracking (SCC)
ammonia and, 192
of commercial aircraft, 390

of copper and copper alloys, 192
electrochemical tests for, 126–129, 128 (figure), 129 (figure)
EN for, 125
FGD and, 409
in food and beverage, 430
in freshwater, 184–185, 185 (figure)
immersion testing for, 142 (table), 146
industrial chemicals and, 400 (table), 406
metallographic analysis for, 102–103, 102 (figure), 103 (figure)
in nuclear power, 419, 422–423
with organic liquids, 253, 256, 256 (figure), 260, 260 (figure)
in petroleum chemistry, 249
of pipelines, 328 (table), 330
in seawater, 196, 203–205
in soils, 227–228, 234
of titanium, 268, 270, 274–275, 275 (figure)
uniform corrosion and, 181
submerged/shallow ocean, seawater in, 189, 189 (figure)
substructure, of bridges, 353–354
sugars, automobiles and, 364
sulfate
atmospheric corrosion from, 156–157, 158 (table)
in freshwater, 179, 180
MIC and, 75
in soils, 222
sulfate-reducing bacteria (SRB)
MIC from, 74, 77
soil pH and, 222
in soils, 223–224, 223 (figure)
soils oxidation-reduction potential and, 222
sulfide-producing prokaryotes (SPP), 74, 75
sulfides
food and beverage and, 429
in seawater, 192, 194, 194 (table)
sulphate-reducing bacteria (SRB), 197
super-duplex stainless steels (SDSS), crevice corrosion of, 27
superstructure, of bridges, 352–353, 353 (figure)
sustained-load cracking (SCL), 269, 277
sustained load test, for hydrogen, 67–68, 68 (figure)

T

Tafel extrapolation
for corrosion rates, 112
for seawater, 201, 202–203
uniform corrosion and, 181, 182
Tafel parameters, for EFM, 117
Tafel slope
in galvanic corrosion, 43
in polarization methods, 111
in tribocorrosion, 83
uniform corrosion and, 182
tensile testing, for hydrogen, 66–67
test heat exchanger, for water handling systems, 322, 322 (figure)
thermal barrier coatings (TBC), 106–107, 106 (figure)
thermally grown oxide (TGO), 107
thermal shock, on military aircraft, 394
thermal spray aluminum (TSA), 172
thermal spray coating (TSC), 347
thermoplastic liners, for pipelines, 326
threshold stress intensity factor, hydrogen and, 67–70, 68 (figure), 69 (figure)
tidal zone, of seawater, 189, 189 (figure)
tin, atmospheric corrosion of, 154
titanium, 266 (table)
atmospheric corrosion of, 154
corrosion forms of, 269–270, 269 (table)
corrosion resistance of, 265–266
corrosion testing for, 270–280, 270 (figure), 271 (table), 272 (figure), 273 (figure), 275 (figure), 280 (figure)
crevice corrosion of, 272–273, 272 (figure), 273 (figure)
HE of, 268–269, 276–277, 276 (figure), 277 (figure)
ignition testing for, 277–279, 278 (figure), 279 (figure)
MMCs, 304, 304 (figure)
for nuclear power, 422
oxidation of, 265, 279–280, 280 (figure)
passivation of, 266–267
pitting of, 273–274
SCC of, 268, 270, 274–275, 275 (figure)
SCL of, 269, 277
in seawater, 208, 209
in soils, 228
tribocorrosion of, 81, 83, 84
titanium and titanium alloys, 265–280
toluene diamine (TDA), 401–402
top-of-the-line corrosion (TLC), of pipelines, 326, 327 (table)
transgranular stress corrosion cracking (TGSCC), 102–103
transmission electron microscope (TEM), 100
tribocorrosion
asperity and, 85–86, 85 (figure), 90
Boltzmann superposition for, 85–86, 86 (figure)
contact mechanics and, 84–87, 85 (figure)
electrochemical tests for, 87–89, 88 (figure), 90
electrode potential in, 81–82, 84
fretting corrosion and, 89, 89 (figure)
maps of, 90
mass balance in, 82–84, 83 (figure)
material characterization in post-testing of, 89–90
mechanisms of, 81–82
potentiostatic methods for, 87–89, 88 (figure)
repassivation potential and, 84
testing of, 87–89, 88 (figure)
tunnels
coatings for, 346–347, 349–350
concrete for, 349–350
corrosion standards for, 354–356
CP for, 350
electrochemical tests for, 350
LACR for, 354
RC for, 345–346, 349
salt exposure of, 346
sea-level change and, 354
steel for, 346–349
vulnerable areas of, 351
water exposure of, 346

U

ultrasound (UT)
for pipelines, 333–334
for seawater, 206
underdeposit corrosion (UDC)

of nuclear power, 422
of pipelines, 329 (table)
uniform corrosion
in freshwater, 181–182, 182 (table)
in MMCs, 307
in seawater, 195
uranium. *See also* nuclear power
MMCs, 303

V

vanadium, atmospheric corrosion of, 154

W

wallpapering, 409
water handling systems, 315–323
chemical analysis of, 320, 320 (table)
corrosion rates in, 317, 317 (figure)
coupon testing for, 315–318, 316 (figure), 316 (table), 317 (figure), 317 (table)
dissolved oxygen in, 320–321
ER for, 316 (table), 319–320, 319 (figure), 320 (figure)
heat transfer in, 316 (table), 321–322, 321 (figure)
LPR for, 316 (table), 317 (figure), 318–319, 318 (figure)
ORP in, 321
test heat exchanger for, 322, 322 (figure)
wavelength-dispersive spectrometer (WDS)
for dealloying, 185
for metallographic analysis, 100
welding, FGD and, 413

X

X-ray diffraction, for MIC, 77

Y

yield strength, hydrogen and, 63
yield stress
hydrogen and, 64, 68 (figure)
SCC and, 196
yttria/stainless steel MMCs, 304

Z

zero resistance amperometry (ZRA), 109
for crevice corrosion, 21 (table), 28–29, 29 (figure)
EFM and, 117–118
EN and, 131
galvanic corrosion and, 120
for MMCs, 307
for pitting electrochemical tests, 10
zinc and zinc alloys
atmospheric corrosion of, 153, 154 (table), 155, 158 (table), 159 (table), 163
for automobiles, 360
electrolytic corrosion test and, 129–130
in freshwater, 179, 180
MMCs, 305
in water handling systems, 320 (table)
zirconium, for nuclear power, 419–420



EDWARD L. HIBNER is a Metallurgical and Corrosion consultant. He was most recently with Haynes International as a Senior Metallurgical Consultant and prior to that a Code Manager at Special Metals Corporation, formerly Inco Alloys International, in Huntington, West Virginia. He received his BS in Chemistry from Marshall University and in Metallurgy from the University of Cincinnati. He is the recipient of the ASTM Award of Merit, the ASTM Committee G01 Francis L. LaQue Memorial Award, the ASTM Committee G01 Certificate of Appreciation, and the NACE Fellow Award, and is currently Vice-Chairman and the Editorial Review Chairman of ASTM Committee G01 on Corrosion of Metals. He has served as Chairman and as Trustee of the West Virginia Section of NACE International and is currently serving on the NACE MR0175/ ISO 15156 Maintenance Panel. He has extensive experience in alloy development for chemical process, flue gas desulfurization, marine, and oil field applications. He has written widely on materials applications and corrosion topics in these fields and has four patents and 60 publications. In addition to ASTM International, he is a member of the International Desalination Association, the Society for Petroleum Engineers, ASME International, SAE International, NACE International, and the Naval Submarine League.



HARVEY P. HACK Dr. Hack is a Northrop Grumman Fellow for Northrop Grumman Corporation, where he does materials selection and corrosion control for underwater vehicles and systems for the Department of Defense. He received his B.S. and M.S. from Carnegie-Mellon University, and his Ph.D. in Metallurgy from The Pennsylvania State University. He is the recipient of the ASTM International Award of Merit and is past Chairman of the Board of Directors of ASTM International. Dr. Hack has received the Distinguished Service Award from NACE International (now AMPP), the Francis L. LaQue Memorial Award from ASTM Committee G-1 on Corrosion of Metals, and the Francis L. LaQue Award from the Sea Horse Institute. He is a Past President of NACE International, a NACE Corrosion Specialist, Cathodic Protection Specialist, and Coatings Inspector, a Fellow of NACE International, ASTM International, the Washington Academy of Sciences, and the Institute of Corrosion in the United Kingdom. Dr. Hack was the Associate Editor for the Materials Performance and Characterization section of the Journal of ASTM International (JAI) and is a past President of the Council of Engineering and Scientific Specialty Boards. Dr. Hack has approximately 100 publications and is the author, editor, or major contributor to five books.



JOHN R. SCULLY received his B.S, M.S., and Ph.D. in Materials Science and Engineering from Johns Hopkins University. While pursuing his Ph.D., he worked at David Taylor Naval Ship R&D Center in Annapolis, Maryland in the Marine Corrosion Branch. He then joined Sandia National Laboratory after a term as a Visiting Scientist at AT&T Bell Laboratories. In 1990, he joined the faculty of the Department of Materials Science and Engineering at the University of Virginia and is now the Charles Henderson Chaired Professor of Materials Science and Engineering, Department Chair of MSE and co-directs the Center for Electrochemical Science and Engineering. He is the technical editor of CORROSION. Professor Scully has received numerous awards for corrosion research and education of the next generation of corrosion professionals. Professor Scully has published over 300 technical papers, given invited talks around the world, and edited several books on corrosion.

www.astm.org

ISBN: 978-0-8031-7134-3
Stock #: MNL20-2ND-SUP

ISBN-EB: 978-0-8031-7135-0
Stock #: MNL20-2ND-SUP-EB

Copyright by ASTM Int'l (all rights reserved) Tue Aug 22 19:35:07 GMT 2023